AGARD-CP-586

AGARD

ADVISORY GROUP FOR AEROSPACE RESEARCH & DEVELOPMENT
7 RUE ANCELLE, 92200 NEUILLY-SUR-SEINE, FRANCE

AGARD CONFERENCE PROCEEDINGS 586

Service Life of Solid Propellant Systems

(la Durée de vie des systèmes à ergols solides)

Papers presented at a Symposium held in Athens, Greece, 10-14 May 1996.

DISTRIBUTION STATEMENT A
Approved for public release;
Distribution Unlimited

NORTH ATLANTIC TREATY ORGANIZATION

DTIC QUALITY INSPECTED 2

Published May 1997

Distribution and Availability on Back Cover

AGARD-CP-586

AGARD

ADVISORY GROUP FOR AEROSPACE RESEARCH & DEVELOPMENT
7 RUE ANCELLE, 92200 NEUILLY-SUR-SEINE, FRANCE

AGARD CONFERENCE PROCEEDINGS 586

Service Life of Solid Propellant Systems

(la Durée de vie des systèmes à ergols solides)

Papers presented at a Symposium held in Athens, Greece, 10-14 May 1996.

DISTRIBUTION STATEMENT A
Approved for public release;
Distribution Unlimited

19971016 167

North Atlantic Treaty Organization
Organisation du Traité de l'Atlantique Nord

The Mission of AGARD

According to its Charter, the mission of AGARD is to bring together the leading personalities of the NATO nations in the fields of science and technology relating to aerospace for the following purposes:

- Recommending effective ways for the member nations to use their research and development capabilities for the common benefit of the NATO community;
- Providing scientific and technical advice and assistance to the Military Committee in the field of aerospace research and development (with particular regard to its military application);
- Continuously stimulating advances in the aerospace sciences relevant to strengthening the common defence posture;
- Improving the co-operation among member nations in aerospace research and development;
- Exchange of scientific and technical information;
- Providing assistance to member nations for the purpose of increasing their scientific and technical potential;
- Rendering scientific and technical assistance, as requested, to other NATO bodies and to member nations in connection with research and development problems in the aerospace field.

The highest authority within AGARD is the National Delegates Board consisting of officially appointed senior representatives from each member nation. The mission of AGARD is carried out through the Panels which are composed of experts appointed by the National Delegates, the Consultant and Exchange Programme and the Aerospace Applications Studies Programme. The results of AGARD work are reported to the member nations and the NATO Authorities through the AGARD series of publications of which this is one.

Participation in AGARD activities is by invitation only and is normally limited to citizens of the NATO nations.

The content of this publication has been reproduced
directly from material supplied by AGARD or the authors.

Published May 1997

Copyright © AGARD 1997
All Rights Reserved

ISBN 92-836-0036-3



Printed by Canada Communication Group Inc.
(A St. Joseph Corporation Company)
45 Sacré-Cœur Blvd., Hull (Québec), Canada K1A 0S7

Service Life of Solid Propellant Systems

(AGARD CP-586)

Executive Summary

Solid propellant systems for rockets, gas generators and guns are designed to function within narrow performance boundaries after an increasingly extended shelf life. In order to guarantee these performances we must be able to predict and extend their life cycle, as well as determine their residual life span after the system has been subject to handling and storage under varying conditions which are not always recorded. This type of approach would also improve system reliability, as well as safety and cost.

Service life assessment begins in the development phase and monitoring programs must be developed and implemented during the life span of the system. The complexity of the operational cycles makes this a very difficult task. A full understanding of the technical field known as "Service Life" is therefore essential and the AGARD PEP Panel considered that it was important to look at all aspects of the question during the course of a Symposium.

This symposium brought together more than 160 people from different backgrounds (industry, government departments, scientific bodies, etc...), all concerned at different levels by weapon system service life problems. A total of 43 papers were presented out of the 46 announced. The high level of the participants, the quality of the presentations and the interest of the discussions all combined to make this a highly successful symposium.

All aspects of service life issues for both solid rocket motor and gun propellant systems were addressed, including chemical and physical aging mechanisms, methodology and techniques for determining service life, application of the service life methodology and techniques to systems and non-destructive test methods.

Advances highlighted during the Symposium, both for solid propellant systems and gun propellants, included:

— demonstration of the importance of environmental conditions;

— test methods used on in-service or prototype mock-up motors;

— improved chemical and physical analysis methods;

— better simulation of the stabilizer consumption mechanism;

— improvement of stress measurement in motors;

— improved mechanical codes;

— improvement of fault probability analysis methodologies.

These advances will help to improve the design of solid propellant systems for rockets and guns under optimum conditions of safety, reliability and cost. They will also enable the definition of handling and storage procedures aimed at longer service life for these propellant systems.

La durée de vie des systèmes à ergols solides

(AGARD CP-586)

Synthèse

Les systèmes à propergols solides pour les fusées, les générateurs de gaz et les canons sont conçus pour fonctionner selon des critères de performances très précis après une durée de vie toujours plus importante. Pour garantir ces performances, il est indispensable de pouvoir prédire et prolonger leur cycle de vie, ainsi que de pouvoir déterminer la durée de vie résiduelle suite aux différentes opérations de manutention et de stockage qui se font dans des conditions très variées dont il ne reste parfois pas de trace. Ce type d'étude permet également d'améliorer la fiabilité et la sécurité des systèmes ainsi que d'abaisser leur coût. L'évaluation de la durée de vie commence dès la phase de développement et il est nécessaire de prévoir des programmes de contrôle qui seront exécutés tout au long de la vie du système. La complexité des cycles opérationnels rend cette tâche très difficile.

Le domaine technique "durée de vie" est ainsi essentiel à maîtriser et le panel PEP de l'AGARD avait estimé qu'il était important de l'aborder dans sa globalité à l'occasion d'une symposium.

Ce symposium a rassemblé plus de 160 personnes d'origines diverses (industriels, services officiels, scientifiques...) toutes préoccupées à leur niveau par les problèmes de durée de vie des systèmes d'armes. 43 papiers sur les 46 prévus ont été présentés. Le haut niveau des participants, la qualité des présentations et des discussions ont fait de ce symposium un succès.

Les présentations ont traité de tous les aspects de la durée de vie des systèmes à propergol solide des moteurs fusée et des canons y compris les mécanismes de vieillissement physiques et chimiques, les méthodologies et les techniques permettant de déterminer la durée de vie, l'application de ces méthodologies et techniques au niveau des systèmes, et les méthodes d'essais non destructifs.

Les progrès enregistrés au cours de ce symposium tant pour les moteurs à propergol solide que pour les poudres pour armes à tube incluent :

— la mise en évidence de l'importance des conditions d'environnement;

— les méthodes d'essai sur moteur réel ou maquette améliorées;

— les méthodes d'analyses chimiques et physiques améliorées;

— la meilleure simulation du mécanisme de consommation des stabilisants;

— l'amélioration des mesures de contraintes dans les moteurs;

— l'amélioration des codes mécaniques;

— l'amélioration des méthodologies d'analyse de probabilité d'apparition de défauts.

Ces progrès contribuent à améliorer la conception des systèmes à propergol solide pour fusées et canons dans les meilleures conditions de sécurité, de fiabilité et de coût. Ils permettent également de bien définir les procédures de manutention et de stockage en vue du prolongement de la durée de vie de ces systèmes propulsifs.

Contents

	Page
Executive Summary	iii
Synthèse	iv
Recent Publications of PEP	ix
Theme\Thème	xi
Propulsion and Energetics Panel	xii
	Reference
Technical Evaluation Report by J. Bennett	T
Keynote Address by G. Hooper	K
SESSION I: CHEMICAL AND PHYSICAL AGING MECHANISMS	
Development of Methods for Aging and Analyzing Propellants Containing Nitrate Ester Stabilized with MNA and 2-NDPA by P.S. Carpenter, A. Atwood, C.J. Meade, N. Carey and A. Paiz	1
Methods and Kinetic Models for the Lifetime Assessment of Solid Propellants by M.A. Bohn	2
Caractérisation et modélisation du vieillissement des propergols solides by C. Perut, S. Chevalier and L. Minguet	3
Hazard Testing of Ferrocene Propellant in the SRAM-A Motor by M. Swett	4
Paper 5 withdrawn	
Ageing Behaviour of Composite Propellants by G. Jenaro, F. Rey, E. de la Cruz and V. Pérez	6
Microstructural Damage and Crack Growth Behavior in a Composite Solid Propellant by C.T. Liu	7
Ageing and Life Prediction of Composite Propellant Motors by A.V. Cunliffe, A. Davis and D. Tod	8
Life Time Assessment and Stability of AN/GAP Propellants by M.A. Bohn, J. Böhnlein-Mauß and K. Menke	9
Characterization of the Degradation of the Polymer Binder in GAP-based Propellants by S. Désilets and F. Perreault	10

SESSION II: NON-DESTRUCTIVE TEST METHODS

Applicabilité de quelques méthodes globables au CND des petits propulseurs à propergol solide 11
by A. Déom, F. Lepoutre, J.C. Krapez, C. Masson, F. Christophe and D.L. Balageas

The Penetrometer: Non-Destructive Testing of Composite Propellant Rocket Motor Grains to Determine Ageing Characteristics 12
by G.S. Faulkner, A.W. Thompson and H.J. Buswell

Thermographic Detection of Bond Defects within Models of Solid Propellant Motors 13
by H. Schneider and N. Eisenreich

The Role of NDE in Service Life Prediction of Solid Rocket Propellant 14
by L.H. Pearson, T.E. Doyle, R.S. Hamilton and I.L. Davis

Estimation de la durée de vie des systèmes propulsifs à propergol solide: Perspectives offertes par l'utilisation de la tomographie haute énergie 15
by P. Lamarque and J.M. Tauzia

Ultrasonic Evaluation of Small Rocket Motor Grains 16
by L.M. Glowacki

SESSION III: GUN PROPELLANTS

Overview of the United States Army and Navy Gun Propellant Safety Surveillance Programs 17
by D.D. Lee, G.Y. Stine, D.G. Robertson and W.F. Ark

Former and Modern Methods for the Determination of the Service Life of Rocket Propellants 18
by G. Holl, S. Wilker, M. Kaiser and P. Guillaume

Corrélation entre les résultats de stabilité de poudres pour armes obtenus après vieillissement articificiel à 50°C et ceux obtenus en vieillissement naturel 19
by O. Ruault and C. Bales

Ageing Behaviour of Propellants Determined by Mass Loss, Heat Generation, Stabilizer Consumption and Molar Mass Decrease 20
by F. Volk and M.A. Bohn

LOVA Propellant Aging: Effect of Residual Solvent 21
by R.A. Pesce-Rodriguez and R.A. Fifer

Evaluation comparée de la durée de vie de poudres composites et simple base 22
by M. Rat

The Canadian Gun Propellant Surveillance Program 23
by L.S. Lussier and H. Gagnon

SESSION IV: METHODOLOGIES AND TECHNIQUES FOR DETERMINING SERVICE LIFE

Service Life Prediction Methodologies Aspects of the TTCP KTA-14 UK Programme 24
by G.S. Faulkner and D. Tod

Miniature Sensor for Measuring Solid Grain Rocket Motor Case Bond Stress 25
by H. Chelner and J. Buswell

Verification of the Swanson Nonlinear Thermo-Viscoelastic Model using Stress Gage Technology 26
by F.C. Wong, A. Firmin and Y.C. Liu

Improvements in Rocket Motor Service Life Prediction 27
by E.C. Francis and H.J. Buswell

Instrumented Service Life Program for the Pictor Rocket Motor 28
by S.Y. Ho, K. Ide and P. Macdowell

Solid Rocket Motor Service Life Prediction using Nonlinear Viscoelastic Analysis and a Probabilistic Approach 29
by G.A. Collingwood, M.D. Dixon, L.M. Clark and E.B. Becker

Paper 30 withdrawn 30

Intrinsic Strength of Solid Propellant Bond Systems 31
Stress-Strain Behavior of Rectangular Bit-in-Tension with Rubber Materials
by S.H. Slivinsky, H.P. Kugler and H. Drude

Structural Service Lifetime Modelling for Solid Propellant Rocket Motors 32
by H.L.J. Keizers and J.R. Miedema

Aging Studies on HTPB Propellants by Dynamic Mechanical Analysis 33
by C. Schüller and J.L. de la Fuente

Probabilistic Service Life Prediction for Solid Propellant Motors Subjected to Environmental Thermal Loads 34
by R.A. Heller, S. Thangjitham and I.M. Janajreh

Methodology and Techniques for Determining Service Life of Solid Rocket Motors 35
by R.K. McCamey and E.K.S. Liu

SESSION V: APPLICATION OF THE SERVICE LIFE METHODOLOGY AND TECHNIQUES TO ROCKET MOTOR SYSTEMS

Service Life Prediction of Solid Propellant Motors Stored in a Random Thermal Environment 36
by J. Margetson and F.C. Wong

Paper 37 withdrawn

Prediction of the Shelf Life of Munitions: Ballistic and Chemical Properties 38
by G. Jenaro de Mencos and J. Hernandez Tamayo

Environmental Data for Rocket Motor Service Life Assessment 39
by I.H. Maxey

Evaluation de la durée de vie des moteurs tactiques 40
by B. Herran and J.C. Nugeyre

Service Life Determination of Rocket Motors by Comprehensive Property Analysis of Propellant Grains 41
by H. Schubert and K. Menke

Structural/Ballistic Instability Ageout Mechanism in the Sparrow Mark 52 SRM 42
by D.I. Thrasher and P.R. Empleo

Chemical Safe Life Predictions for Cast Double Base Rocket Propellants 43
by M.P. Sloan, S.J. Salsbury and G.M. Keeton

Contraintes opérationelles et durée de vie des systèmes propulsifs pour missiles tactiques 44
Particularités des propulseurs à structure composite
by N. Laurençon

Programme général d'essais de vieillissement 45
Application à un missile Air-Sol
by A. Chevalier and J.M. Laurent

Service Life Assessment for Space Launch Vehicles 46
by W.L. Hufferd

Recent Publications of the Propulsion and Energetics Panel

CONFERENCE PROCEEDINGS (CP)

Interior Ballistics of Guns
AGARD CP 392, January 1986

Advanced Instrumentation for Aero Engine Components
AGARD CP 399, November 1986

Engine Response to Distorted Inflow Conditions
AGARD CP 400, March 1987

Transonic and Supersonic Phenomena in Turbomachines
AGARD CP 401, March 1987

Advanced Technology for Aero Engine Components
AGARD CP 421, September 1987

Combustion and Fuels in Gas Turbine Engines
AGARD CP 422, June 1988

Engine Condition Monitoring — Technology and Experience
AGARD CP 448, October 1988

Application of Advanced Material for Turbomachinery and Rocket Propulsion
AGARD CP 449, March 1989

Combustion Instabilities in Liquid-Fuelled Propulsion Systems
AGARD CP 450, April 1989

Aircraft Fire Safety
AGARD CP 467, October 1989

Unsteady Aerodynamic Phenomena in Turbomachines
AGARD CP 468, February 1990

Secondary Flows in Turbomachines
AGARD CP 469, February 1990

Hypersonic Combined Cycle Propulsion
AGARD CP 479, December 1990

Low Temperature Environment Operations of Turboengines (Design and User's Problems)
AGARD CP 480, May 1991

CFD Techniques for Propulsion Applications
AGARD CP 510, February 1992

Insensitive Munitions
AGARD CP 511, July 1992

Combat Aircraft Noise
AGARD CP 512, April 1992

Airbreathing Propulsion for Missiles and Projectiles
AGARD CP 526, September 1992

Heat Transfer and Cooling in Gas Turbines
AGARD CP 527, February 1993

Fuels and Combustion Technology for Advanced Aircraft Engines
AGARD CP 536, September 1993

Technology Requirements for Small Gas Turbines
AGARD CP 537, March 1994

Erosion, Corrosion and Foreign Object Damage Effects in Gas Turbines
AGARD CP 558, February 1995

Environmental Aspects of Rocket and Gun Propulsion
AGARD CP 559, February 1995

Loss Mechanisms and Unsteady Flows in Turbomachines
AGARD CP 571, January 1996

Advanced Aero-Engine Concepts and Controls
AGARD CP 572, June 1996

ADVISORY REPORTS (AR)

Producibility and Cost Studies of Aviation Kerosines *(Results of Working Group 16)*
AGARD AR 227, June 1985

Performance of Rocket Motors with Metallized Propellants *(Results of Working Group 17)*
AGARD AR 230, September 1986

Recommended Practices for Measurement of Gas Path Pressures and Temperatures for Performance Assessment of Aircraft Turbine Engines and Components *(Results of Working Group 19)*
AGARD AR 245, June 1990

The Uniform Engine Test Programme *(Results of Working Group 15)*
AGARD AR 248, February 1990

Test Cases for Computation of Internal Flows in Aero Engine Components *(Results of Working Group 18)*
AGARD AR 275, July 1990

Test Cases for Engine Life Assessment Technology *(Results of Working Group 20)*
AGARD AR 308, September 1992

Terminology and Assessment Methods of Solid Propellant Rocket Exhaust Signatures *(Results of Working Group 21)*
AGARD AR 287, February 1993

Guide to the Measurement of the Transient Performance of Aircraft Turbine Engines and Components *(Results of Working Group 23)*
AGARD AR 320, March 1994

Experimental and Analytical Methods for the Determination of Connected — Pipe Ramjet and Ducted Rocket Internal Performance *(Results of Working Group 22)*
AGARD AR 323, July 1994

Recommended Practices for the Assessment of the Effects of Atmospheric Water Ingestion on the Performance and Operability of Gas Turbine Engines *(Results of Working Group 24)*
AGARD AR 332, September 1995

LECTURE SERIES (LS)

Design Methods Used in Solid Rocket Motors
AGARD LS 150, April 1987
AGARD LS 150 (Revised), April 1988

Blading Design for Axial Turbomachines
AGARD LS 167, June 1989

Comparative Engine Performance Measurements
AGARD LS 169, May 1990

Combustion of Solid Propellants
AGARD LS 180, July 1991

Steady and Transient Performance Prediction of Gas Turbine Engines
AGARD LS 183, May 1992

Rocket Motor Plume Technology
AGARD LS 188, June 1993

Research and Development of Ram/Scramjets and Turboramjets in Russia
AGARD LS 194, December 1993

Turbomachinery Design Using CFD
AGARD LS 195, May 1994

Mathematical Models of Gas Turbine Engines and their Components
AGARD LS 198, December 1994

AGARDOGRAPHS (AG)

Measurement Uncertainty within the Uniform Engine Test Programme
AGARD AG 307, May 1989

Hazard Studies for Solid Propellant Rocket Motors
AGARD AG 316, September 1990

Advanced Methods for Cascade Testing
AGARD AG 328, August 1993

REPORTS (R)

Rotorcraft Drivetrain Life Safety and Reliability
AGARD R 775, June 1990

Impact Study on the use of JET A Fuel in Military Aircraft during Operations in Europe
AGARD R 801, January 1997

The Single Fuel Concept and Operation Desert Shield/Storm
AGARD R 810, January 1997 (*NATO Unclassified*)

Propulsion and Energy Issues for the 21st Century
AGARD R 824, March 1997

Theme

Solid propellant systems for rockets, gas generators and guns are designed to function within narrow performance boundaries after an increasingly extended shelf life. In order to guarantee these performances we must be able to predict and extend their life cycle, as well as determine their residual life span after the system has been subject to handling and storage under varying conditions which are not always recorded. This type of approach would also improve system reliability, as well as safety and cost.

Service life assessment begins in the development phase and monitoring programs must be developed and implemented during the life span of the system. The complexity of the operational cycles makes this a very difficult task.

All aspects of service life issues for both solid rocket motor and gun propellant systems will be addressed including chemical and physical aging mechanisms, methodology and techniques for determining service life, application of the service life methodology and techniques to systems and non-destructive test methods.

This defence-specific symposium aims at having a complete presentation by military and industry of the most advanced work in the area of service life. It will help industry in designing improved solid propellant systems for rocket and guns under reliable safety and cost conditions including recommendations for improved handling and storage procedures aimed at longer service life. The military user will benefit from a more precise determination of the usable life span, thereby improving reliability as well as life cycle cost.

Thème

Les systèmes à propergols solides pour les fusées, les générateurs de gaz et les canons sont conçus pour fonctionner selon des critères de performances très précis après une durée de vie toujours plus importante. Pour garantir ces performances, il est indispensable de pouvoir prédire et prolonger leur cycle de durée de vie, ainsi que de pouvoir déterminer la durée de vie résiduelle suite aux différentes opérations de manutention et de stockage qui se font dans des conditions très variées dont il ne reste parfois pas de trace. Ce type d'étude permet également d'améliorer la fiabilité et la sécurité des systèmes ainsi que d'abaisser leur coût.

L'évaluation de la durée de vie commence dès la phase développement et il est nécessaire de prévoir des programmes de contrôle qui seront exécutés tout au long de la vie du système. La complexité des cycles opérationnels rend cette tâche très difficile.

Tous les aspects de la durée de vie des systèmes à propergol solide des moteurs fusée et des canons seront examinés, y compris les mécanismes de vieillissement physiques et chimiques, les méthodologies et les techniques permettant de déterminer la durée de vie, l'application de ces méthodologies et techniques au niveau des systèmes, et les méthodes d'essais non destructifs.

Ce symposium orienté défense a pour ambition la présentation, par les spécialistes militaires et civils, des travaux les plus avancés dans le domaine de la durée de vie des systèmes à propergols solides. Il doit apporter une aide à l'industrie, permettant d'améliorer la conception des systèmes à propergols solides pour fusées et canons dans les meilleurs conditions de sécurité, de fiabilité et de coût. Il doit en résulter des recommandations pour l'amélioration des procédures de manutention et de stockage en vue du prolongement de la durée de vie. L'utilisateur militaire bénéficiera d'une définition plus précise de durée de vie de ces systèmes, ainsi qu'une meilleur fiabilité et un coût d'utilisation réduit.

Propulsion and Energetics Panel

Chairman: Prof. Dr. D.K. HENNECKE
Fachgebiet Gasturbinen und Flugantriebe
Technische Hochschule Darmstadt
Petersenstrasse 30
64287 DARMSTADT, Germany

Deputy Chairman: Prof. R.S. FLETCHER
Deputy Vice Chancellor
Cranfield Institute of Technology
Cranfield, BEDFORD MK43 0AL,
United Kingdom

PROGRAMME COMMITTEE

L'Ingénieur en Chef de l'Armement
P. LUSSEYRAN (Chairman)
DGA – Direction des Missiles
et de l'Espace
0046 Armées, France

Dipl.-Ing. H.-L. BESSER
Bayern-Chemie GmbH
Werk Ottobrunn
Abteilung BCE
Postfach 10 47
85501 Ottobrunn, Germany

Mr. R. COUTURIER
Chef des Recherches de la Division
Defense Espace du SNPE
Centre de Recherches du Bouchet
BP 2 - 91710 Vert le Petit, France

Prof. D. DINI
Director, Dipartimento di Energetica
Universita di Pisa
via Diotisalvi 2
56126 Pisa, Italy

Mr. B. JONES
British Aerospace Limited
P.O. Box 874
660 Berry Street
Winnipeg, Manitoba, R3C 2S4, Canada

Mr. E. INGER
ROKETSAN
Ankara-Samsun Karayolu 40
P.K. 30 Elmadag
Ankara, Turkey

Prof. Dr. P. KOTSIOPOULOS
Hellenic Air Force Academy
Chair of Propulsion Systems
Dekelia, Attiki, Greece

Dr. I. W. MAY
Chief, Propulsion and Flight Division
Weapons Technology Directorate
Army Research Laboratory
Aberdeen Proving Ground
MD 21005-5066, US

Mr. L.G. MEYER
Deputy Director, Propulsion Directorate
OL-AC PL/RK
5 Pollux Drive
Edwards AFB, CA 93524-7084, US

Prof. M.N.R. NINA
CTAMFUL
Instituto Superior Tecnico
Avenida Rovisco Pais
1096 Lisboa Codex, Portugal

Prof. J. J. SALVA MONFORT
Catedratuci de Universidad
Dpt. de Motorpropulsion y
Termofluidodinamica ETSIA
Plaza Cardenal Cisneros
28040 Madrid, Spain

Mr. I. SOLLIEN
Norwegian Defence Research Establishment
P.O. Box 25
N-2007 Kjeller, Norway

Mr. A. WHITEHOUSE
Manager, Design Section
Royal Ordnance plc
Rocket Motors Division
Summerfield, Kidderminster
Worcestershire DV11 7RZ, United Kingdom

HOST NATION COORDINATOR

Professor Dr. P. KOTSIOPOULOS

PANEL EXECUTIVE OFFICE

From Europe:
PEP, AGARD-OTAN
7, rue Ancelle
92200 Neuilly-sur-Seine
France

From US & Canada:
PEP, AGARD-NATO
PSC 116
APO AE 09777

Tel: 33 (1) 55 61 22 85
Telex: 610176 (France)
Telefax: 33 (1) 55 61 22 98

TECHNICAL EVALUATION REPORT for the 87th SYMPOSIUM of the PROPULSION AND ENERGETICS PANEL on SERVICE LIFE OF SOLID PROPELLANT SYSTEMS

by

J. Bennett
554 North 300 East
Brigham City, Utah 84302, USA

1.0 INTRODUCTION:

The goal of service life assessment is to provide the most reliable and most accurate prediction of service life possible in support of assuring safety, mission performance, and effective cost. In striving to attain this goal for solid propellant systems (rocket motor and gun propellants), it is essential to understand the factors which affect their service life.

Papers presented at the Propulsion and Energetics Panel (PEP) 87th Symposium on Service Life of Solid Propellant Systems, identified that the important factors governing service life are:

First-The design and processing of the system
Second-The environment to which the system is subjected
Third-The response of the system to its environment
Fourth-The length of time for the system to reach a prescribed safe life limit or to reach a critical design condition (potential for ballistic/structural failure or for sub-mission performance) under real life conditions.

Figure 1 displays a typical Service Life Prediction flow. Materials, structural configuration and manufacturing processes are selected during system design (first factor affecting service life). These selections determine how the system will respond to subsequent environmental exposures and what the life limiting modes may be (i.e., energy loss, stabilizer depletion, bore cracking, bondline separation, etc.). A Failure Modes and Effects Analysis (FMEA) or similar evaluation is conducted which shows a positive margin of safety. A preliminary service life estimate is made which meets a minimum service life requirement.

Two parallel paths are generally followed for a continuing assessment of service life. One path is analytical which assesses the rate of material aging, the effect of material aging on the system (i.e., stability, performance, structural integrity, etc.) and the statistical probability of system failure with age life. The principal advantage of the analytical path is that it provides a prediction of anticipated events with sufficient lead time to take any necessary action that will provide safe, reliable, cost effective use of the system.

The second path is one of system surveillance (monitoring) which includes system observation and system trend analysis. The principal advantage of this path is that it assesses the actual condition of the system as it ages. These two paths interact iteratively to produce current service life estimates at various age times throughout the life of the system. The service life estimate may predict a minimum service life (safe interval) that will likely be extended on testing at a later period (Papers 17,

35) or the estimate may predict an absolute age-out of the system (Paper 4).

The final step in service life assessment is dispositioning the system (i.e., extend the service life through an updated service life estimate, prioritize use of aging system assets, withdraw the system assets from the inventory, etc.).

2.0 ENVIRONMENT

The second factor contributing to the chemical and mechanical changes taking place with aging, is the environment to which the as-built Solid Propellant System is subjected. One is impressed with the significant effect the environment may have on service life. Elevated temperature accelerates the rate of chemical degradation and of chemical aging reactions, as well as the migration of chemical species. High relative humidity may induce specie migration and propellant softening. Changes in temperature from the stress (strain) free temperature induce stresses and strains in the propellant grain of a rocket motor including in the grain-to-case bondlines. Shock and vibration loads may induce damage in the grain as does diurnal and annual thermal cycling of the system.

While a moderate storage environment may have little effect on the service life of a system over a short period of time, extremes of temperature and temperature cycling may have a significant effect in a much shorter period of time. Paper 8, Tables 2 and 3 show that similar motors aged in London and in Dhahran have relative lives of 100 and 10 respectively. This dramatic effect of environment on propellant strength and service life is further illustrated where the effect of thermal cycling is considered (Paper 34, Figures 5 and 6 and Papers 24, 28, 36). The significant extension of service life expected from a protective inert nitrogen atmosphere is illustrated in Paper 40, Figures 12 and 13.

Accurate service life analysis requires a knowledge of the environmental history of a system from manufacture-to-target. This kind of information is seldom available (Papers 41, 43). For expediency and treatment of systems by groups, the world is categorized into regions (Paper 39, Figure 1) which makes service life estimation by region tractable. Only certain regions experience the extremes of temperature, reducing the number of systems which must be evaluated for these extremes. Experimental testing and system analysis can be more narrowly focused for other regions. Progressively more national and international environmental history data are being accumulated, making service life analysis more precise. Environmental data are, however, yet incomplete, particularly with respect to individual motor data and to mission induced loads. I. H. Maxey in Paper 39, astutely

observes that "recording and feedback of environmental data with established aging and damage models, could rapidly -------give enhanced confidence in the safe life of service motors."

The third factor affecting service life is the response of the system (chemical change, altered performance, mechanical response, material damage, etc.) to the environmentally imposed loads (chemical, thermal, and mechanical) and the effect these responses have on the service life of the system. This factor is the focus of the technical discussion of this report and of the majority of the papers presented during the symposium.

3.0 ANALYTIC PATH

The analytic approach uses measured material property data accompanied by chemical, ballistic, structural and statistical analyses to arrive at a deterministic estimate of service life (Papers 36, 46) or a probability of motor failure estimate (Papers 29, 34, 36, 40).

3.1 Material Aging

Chemical and physical changes occur as solid propellants age, altering their stability, performance, and structural properties. The rate of property change depends on the specific material and on the environment to which it is exposed. Considerable progress has been made in the techniques to measure these property changes (Papers 10, 18, 22, 23, 31, 33) and in the estimation of properties after extended periods of age life.

3.1.1 Composite Propellants

For this report, composite propellants are those propellants having a CTPB, HTPB or GAP matrix. Change in the ballistic response of a CTPB/AP/Al propellant subjected to 266 days of accelerated aging at 65°C after five years of age was minuscule from that of the baseline five year old motor (Paper 6, Figure 11). The service life of such a propellant system is not likely driven by ballistic changes.

Changes in mechanical properties are routinely measured on almost all solid propellant systems. Using the measured data, a projection of properties at a future time provides an estimate of properties on which a service life analysis is based. Several papers (3, 6, 10, 32, 33, 36) report the use of the Layton model to assess the effect of chemical aging on the mechanical properties of composite propellants. Figure 2a shows the ease of extrapolating data using the Layton model. Figure 2b shows the advantage of testing the material frequently in the early age life while the rate of property change is highest. This, however, is not often done and too often original and early life data are

not available for conducting service life analyses (Papers 41, 43).

The slow rate of property change at long age times results in the long service life experienced with solid propellant systems containing composite propellants. However, the small change in properties over long periods of time makes determination of an absolute service life a difficult challenge. It is for this reason that many service life projections provide an estimation of a minimum viable service life (safe interval) with periodic updates (Papers 17, 35). This slow rate of change also points out the need for a more precise measure of strain-at-maximum-stress, a critical parameter for bore cracking analysis, to reduce the test variability of this parameter.

In addition to the cross-linking (network formation) reactions on which the Layton model is based, there are also surface oxidation reactions (Papers 8, 32, 33), humidity effects (Papers 1, 35), and chemical specie migration (Papers 3, 4, 20, 21, 32, 33, 38, etc). These effects create chemical gradients near interfaces which can be chemically analyzed and changes with age can be evaluated (Paper 3, Figure 4). These chemical gradients can be modeled using diffusion equations and reaction kinetics (paper 35, Figures 3,4,5,6). Corresponding gradients in mechanical properties can be measured (Paper 14, Figure 7). However, there is no theoretical basis for transposing the chemical gradients to the corresponding mechanical properties.

Though the aging ratio of propellant (aged to unaged property ratio) is often determined from strain-at-maximum-stress data measured at 75° F and 2 inches per minute crosshead displacement, this parameter measured at these condition is not used for structural analysis. Paper 46, Figures 10 and 11 show the rate of propellant aging for the uniaxial strain endurance, a parameter used directly in the structural analysis. This approach should be considered when determining an aging factor.

3.1.2 Nitrate Ester Propellants

For this report, nitrate ester propellants are either gun or rocket motor propellants containing energetic nitrate ester plasticizers and incorporating various stabilizers. Change in the ballistic properties of a nitrate ester plasticized propellant can be significant (Paper 38, Figure 4). The change illustrated is attributed to nitroglycerine or other nitrate ester migration and is most pronounced in the increase of the ignition spike.

The primary life limiting change for this type of propellant is stabilizer depletion. Remarkable progress has been made in the stability testing of nitrate ester propellants (Papers 1, 18, 20, 23, 43). Even field testing of propellant has become a reality through use of a mobile laboratory (Paper 17). An excellent

summary of available test methods with their advantages and disadvantages is presented in Paper 18, Table 2.

The rate of stabilizer depletion is strongly temperature dependent as illustrated in Paper 20, Figure 8. Corresponding behavior is observed when measuring the decrease in molar mass M_w (Paper 20, Figure 14). The knee in the Arrhenius plot near 60° C was observed years ago and was conjectured to possibly stem from two or more competing reactions. Today, with the improved methods of stability testing and chemical identification of species, a whole array of related daughter compounds have been identified (Paper 23, Tables 1 and 2). The mechanism of the reactions, though subject to discussion, is reasonably well understood (Papers 1, 2, 17, 20, 23, 43). With this knowledge, can the service (safe) life of the propellant be predicted, i.e. when the stabilizer content reaches a prescribed level? The knee in the curve complicates the analysis and interferes with a precise prediction. The effect of temperature on the change in reaction products and rates of reaction through the transition region are almost impossible to consider other than globally. And elevated temperatures above the knee are not representative of natural aging (Paper 19). Similarly, the level of stabilizer prescribed as life limiting is somewhat arbitrary (Paper 18) and may depend on the propellant formulation, but also on specific material characteristics; i.e. safety, evolution, ballistic behavior.

Paper 2, Figures 5 and 6 show the necessity of a viable predictive model, if a reasonable life estimate is to be made. The exponential model does not fit the data of Figure 5 at long times. The polynomial equations in Figure 6 fit the data, but provide grossly erroneous predictions of behavior outside of the data. The proposed equation 20 combining zero and first order kinetics fits the data and provides a reasonable prediction. This is an encouraging result for making realistic predictions for the service life of nitrate ester propellants.

3.1.3 Bond systems

Measuring the mechanical interaction of multiple materials across bondlines, may be made possible through a multi-path laser system that can detect displacement at individual interfaces (Paper 31, Figures 1 and 9). Measuring the chemical composition of material gradients and measuring the mechanical properties of microtomed layers of propellant have been possible (Paper 33). Being able to observe the relative displacement of individual materials and calculate the relative stiffness across gradients in as-built bondlines is exciting. This technique can have application to both the evaluation of bond strength and to the fracture resistance of bond systems, such as is being done for cohesive fracture (Paper 7).

Other bond separations have been experienced as possible failure

sites (Papers 35, 41). These separations are important in conducting the FMEA and in the surveillance of systems.

3.2 Structural Analysis

The service life of solid rocket motors may be terminated by structural failure through a combination of chemical aging of the propellant and of damage induced by thermal storage, thermal cycling, ignition and mission loads. The primary failure modes are bore cracking and bondline separation.

Considerable progress has been made in the structural evaluation of service life. The nonlinear stress-strain behavior of solid propellants is universally recognized. Applicable nonlinear constitutive relations have become available. Computer codes make nonlinear viscoelastic (NLVE) analyses computationally feasible (Papers 26, 28, 29).

A much needed comparative evaluation of different approaches to NLVE is presented in Paper 29. A definitive two step biaxial test was conducted to generate the experimental data. Hyperelastic models did not match the functional form of the data from the second step. Constitutive models having a damage function were required to produce the functional form of the data. Chemical aging is accounted for through a fit of the capability and response properties of the propellant. Damage to the propellant is accounted for in the NLVE 3D structural analysis of the motor.

Linear viscoelastic analysis underpredicts bondline stresses as measured in instrumented motors using stress gages (Papers 24, 26, 29). The nonlinear analysis correctly predicts bondline stress for thermo-mechanical coupling induced through multiple step cooling, Figure 3. This analysis places NLVE on a firm basis for motor analysis and for further development of nonlinear constitutive models.

Stress gage technology has advanced to a state where instrumented motors provide reliable data (Papers 25, 27, 28, 29, 36). Measured stress (force) in the grain of a motor can now be used for comparing analytically calculated stresses with measured stresses to validate constitutive expressions and structural analyses (Papers 26, 29, 36). The TTCP KTA-14 involving the UK, Canada, Australia and the US has made commendable progress in such effort (Paper 24).

Thermal cyclic loading induces damage in the propellant causing a decrease in stress capability (Paper 24, Figure 8). This figure also shows the repeatability one can expect using current stress gages to measure bond stresses (UK and Canadian normalized data comparison). The degradation of stress with repeated loading is further illustrated in Paper 28, Figure 3. A cumulative damage function is often applied to model propellant damage (Papers 32,

34, 36). This function is based on the principle that the sum of the proportional stresses, i.e. time of applied stress divided by the time to failure at the applied stress, is equal to unity at failure. Using this function, the stress capability is determined. Failure is predicted at the time when the stress capability decreases to the level of the applied stress (Paper 32, Figure 10).

3.3 Statistical Analysis

The fourth factor affecting service life is the length of time to reach a life limiting condition. Evaluation requires both a definition of the life limit condition and an estimate of when the condition will be reached. Using a deterministic approach, the appropriate viscoelastic property (failure boundary) is determined as a function of time. Corrections are applied for the statistical variability and for the aging of the material. When the adjusted property decays to the corresponding calculated grain value, onset of failure is predicted (Papers 36, 46).

Using a probabilistic approach, the length of time to reach a prescribed life limit (allowed probability of failure) is determined. The properties of propellant and bondlines are statistically variable. The distribution of properties about the mean is determined from experimental data. As the property decreases in capability (through viscoelastic relaxation, chemical aging or damage), the distribution of capability and the distribution of induced stress or strain overlap (Paper 34 Figure 3). The probability of failure is a function of the interference of the two distributions and can be calculated as a function of age life. Excellent treatises of the statistical analysis and calculation of probability of failure are presented in Papers 29, 34, 36, 40.

A comparison of the probabilistic approach to service life prediction and the deterministic approach is illustrated in Paper 36, Figures 3.5 and 3.6. Both methods indicate a service life of about 12 years for the motor.

Table 1 is a summary of three methods for conducting a service life prediction. Method 1 is a comprehensive nonlinear viscoelastic (NLVE) strain criterion method which includes both chemical aging and propellant damage in the probability of failure analysis of a solid rocket motor (Paper 29). Method 2 is a thorough linear viscoelastic (LVE) stress criterion method using properties adjusted for chemical aging (aging model) and damage (cumulative damage function) in the probability of failure analysis of a solid rocket motor (Papers 34, 36). Method 3 is a chemical criterion method using chemical or physical tests for measuring the stabilizer concentration or decomposition of nitrate ester propellants (Papers 17, 18, 19, 20, 21, 23).

A fourth method for conducting service life prediction is termed simulated natural aging (Papers 40, 44, 45) where "the evaluation of aging effects on physical properties and performance of rocket motors is performed through specific short time aging programs, simulating long term storage and field conditions." The simulation tests may be conducted on rocket motors or on analogs. Advantages and disadvantages of accelerated aging, simulated natural aging and natural aging are presented.

4.0 SURVEILLANCE PATH

4.1 Motor Observation

Probably the most significant criteria of solid propellant system service life are: the physical and chemical condition of the system and 2) a critical decrease in performance of the system. Bore cracking and other surface conditions may be detected by visual observation (Papers 32, 41). Significant advances are being made in on-site hardness measurements (Paper 12) and in field laboratory testing of propellants (Paper 17). Non-destructive testing provides means of detecting debonds and other visually unobservable conditions (Papers 11, 13, 14, 15, 16). Non-invasive NDE methods may be used for motor health monitoring. Motor sampling and micro-testing (mechanical and chemical) are now feasible on individual motors without sacrificing the motor (Paper 33). Individual motors can be instrumented with stress gages to measure property degradation and the occurrence of grain separations (Papers 24, 25, 27, 36). Some of these methods have been implemented while other methods are on the threshold of application.

Nor should we forget the effective, yet simple methods of the past (Paper 41). "For the test a silver coin was used and the sound was acoustically observed by the tester. It was a surprise that all separations (case and liner) apart from small improper bindings, were found by this rather simple method", H. Schubert. More sophisticated ultrasound methods (Paper 14, Figures 3, 4, 5) capable of detecting and measuring the degree of porosity (damage) in a propellant have been demonstrated in the laboratory. Such methods have potential for the unobtrusive health monitoring of rocket motors.

A surprisingly good correlation is obtained between propellant capability properties and the slope of an indentation curve (Paper 12, Figures 7 and 8). These data suggest that by measuring the propellant hardness of a motor grain, the capability of the propellant can be assessed. A unique device has been demonstrated to make feasible such hardness measurements in motors (Paper 12, Figure 9). This instrument conceptually can be used for the field testing of a variety of motors and of individual motors.

Non-destructive testing has become indispensable for the inspection of solid rocket motors. Computed tomography is capable of detecting bond separations on the order of 100 microns (Paper 15) and is used extensively for motor inspection. Thermography has opened new vistas of debond detection. Detection of separations as small as 0.05 mm show clear patterns (Paper 13, Figures 5a and 5b). Thermography has application to full scale motors as demonstrated on analog motors (Paper 11, Figures 7, 10). The exciting capability of thermography is that it not only detects bond separations but that it can distinguish between a case-to-insulation debond and an insulation-to-propellant debond. The question was asked, "With thermography, how do you distinguish between a case-to-liner disbond and a propellant-to-liner disbond?" Answer: We can easily distinguish between a case-to-liner disbond and a propellant-to-liner disbond (Paper 11). This capability is a significant step forward in the detection and evaluation of debonds. With additional development, the thermographic method will find extensive use with real motors (Paper 13, Figure 5)

4.2 Trend Analysis

Data storage and statistical treatment of data have improved to a point where individual motor or munition data can be recorded and analyzed. Trends due to aging may appear for motor or munition systems such as a decrease in energy, heat generation, the discoloration or softening of propellant, a greater tendency to fume, the appearance of grain separations, etc. Analysis of such trends often suffers from lack of valid models for predicting future behavior and from lack of well defined failure or age-out criteria.

Such trend analysis for existing systems is an indispensable tool for establishing when a system may be approaching age-out and for establishing the frequency for service life testing.

This significant area of service life assessment was not extensively discussed in this symposium. Particularly lacking was information correlating aging trends of existing systems with the behavior predicted from the service life assessments.

5.0 EXTENSION OF SERVICE LIFE

Methods of extending service life as a cost effective use of assets and as a retention of inventory were suggested (Papers 8, 22, 32, 34, 35, 42). These methods may include improving the antioxidant, reducing the storage temperature, lowering the original crosslink density of the propellant and reducing the oxygen access to the propellant. They may also include reformulating the propellant (Paper 22), sealing the motors, improving the analytic life estimate, reducing the test

variability of property measurement. Some of these methods are in current use. However, the potential of service life extension should be a primary consideration as solid propellant systems are formulated and designed, as well as when service life analyses are conducted.

6.0 INVENTORY DISPOSITION

The final step in service life prediction is inventory disposition. Safety (low risk) and cost effective use or replacement of a system are primary considerations in dispositioning aging solid propellant systems. Both risk and cost can be strongly affected by the accuracy of the service life prediction. Conservative life estimates or safe intervals are often used so that solid propellant system performance is assured, though shortened service life of systems may result. Papers presented in this symposium identify considerable progress in service life assessment for providing better predictions on which to base inventory disposition.

7.0 CONCLUSIONS

Progress is being made toward measuring, monitoring and controlling factors that determine the service life of solid propellant systems.

The technical community continues to influence the service life of solid propellant systems by defining conditions which extend service life during design and during deployment, by providing better definition of environmental loads to which the systems are subjected, and by providing more accurate and reliable service life estimates.

Progress reported in this symposium for influencing the service life of solid propellant systems, both gun propellants and rocket motors, include:

- Recognition of environmental impact on service life and the recording of environments to which systems are exposed
- Improved methods of rocket motor and analog simulation testing
- Improved methods of chemical and physical analysis including the field testing of systems
- Better definition of the mechanism of stabilizer depletion in nitrate ester propellants and better predictions of the rate of depletion
- Improved measurement of motor response to imposed loads through the development of reliable stress gages and their application in instrumented motor testing
- Improved methods of structural analysis including rigorous

3D nonlinear viscoelastic analysis
- Improved non-destructive methods for determining chemical and physical conditions in a motor and potentially to monitor motor health
- Better defined methodology for conducting probability of failure analyses

8.0 RECOMMENDATIONS

Recommendations for future work and for continuing work are dispersed throughout sections 3.0, 4.0, 5.0, in the context of work being reported. The following recommendations, listed in possible order of importance, address accurate analytic predictions and sensitive surveillance methods that support system safety, mission performance, and effective cost.

Recommendation 1: The goal of having a standardized method for conducting a service life prediction (possibly one for gun propellants and one for rocket motors) would focus the work of different investigators toward a common goal and ultimately make service life predictions more precise and the results easier to interpret.

Certain test methods and analytic procedures have been standardized or recognized so that results can be compared on a common basis and also can be comparatively verified across systems. Service life prediction could benefit from a similar common effort, resulting in greater confidence for making operational decisions.

Recommendation 2: The work of TTCP KTA-14 and similar cooperative programs should continue for the express purpose of comparing system behavior with analytic calculations.

The KTA-14 program and similar cooperative programs could be an initiatory step toward recommendation 1. With the advent of trusted stress (force) gages, the validity of structural analyses can be assessed, and analytic and material test methods improved specifically where and as needed. The KTA-14 program allows comparison of results across systems, minimizing the development of system specific procedures. The results of this program and similar cooperative programs can aid in bringing into coincidence analytic procedures and system behavior for improved service life predictions.

Recommendation 3: Combined activity of scientists and engineers working together would be synergistic and should be fostered.

The aging of solid propellant systems results from chemical and physical changes that affect the performance, safety and structural integrity of the system. Only when the interaction of

the chemistry, physical behavior, ballistic performance and structural effects are understood collectively can valid system life predictions be made. This collective understanding is enhanced through the combined efforts of multiple disciplines.

Recommendation 4: areas for future work are embodied in the following seven suggestions:

- Improved definition and modeling of induced environmental loads

  An essential requirement for making an accurate service life assessment is to define the loads and material aging experienced by the system. The impact the environmental exposure has on service life is receiving progressively more recognition. However, too often, the system history is not well documented nor is it adequately modeled for service life prediction. For some conditions, the induced loads are unknown. With improved definition and modeling of induced environmental loads, service life predictions will be more accurate, improved methods for system protection from environmental exposure can be developed and system service life can be extended while premature system rejection can be minimized.

- Reliable service life prediction for individual solid propellant systems based on chemical and physical changes and on the rigorous conversion of these changes to ballistic and mechanical properties.

  Health monitoring of individual solid propellant systems requires the surveillance of chemical and physical changes. This surveillance is often most easily done through chemical and physical measurements, especially in regions of material gradients. However, there is presently no rigorous theoretical basis for conversion of the measured chemical and physical changes to the corresponding ballistic and mechanical properties. Such conversions will allow the accuracy and versatility of chemical and physical measurements to be used with greater precision for assessing system performance, safety and structural integrity with age time.

- Sensitive NDE methods and stress gages for direct non-invasive measurement of grain chemical or physical changes, and of local grain structural response

  Closely related to the preceding recommendation is the development of sensitive non-invasive NDE methods to measure the chemical and physical changes occurring with age time and, in the case of imbedded stress (force) gages, to measure

grain response to induced loads or to grain separations. This is a necessary step toward assessing and predicting the performance, integrity, and service life of individual solid propellant systems.

- Improved NDE methods for supporting defect criticality analysis

  NDE methods are employed to inspect for physical changes and defects in solid propellant systems. When a physical change or defect is observed in a system, NDE resolution is sometimes marginal for assessing the criticality of the change or defect. With improved NDE methods, the criticality of the physical change or defect can be better assessed and the system can be dispositioned with greater confidence.

- Improved constitutive expressions for the mechanical behavior of propellant based on the mapping of macro-material changes under material deformation

  Solid propellants are both nonlinear and time dependent in mechanical behavior. This complex behavior stems from macro-material changes under material deformation. Constitutive relations based on these macro-material changes (i.e. viscoelastic polymer behavior, solids/polymer interactions, solids packing, etc.) have the potential of improving and generalizing the modeling of mechanical behavior resulting in more accurate structural analyses.

- Greater focus of grain structural design and system service life on cost reduction without sacrificing safety or reliability

  Methods for extending the life of solid propellant systems and reducing system costs should be further developed and implemented both in the design of new systems and in making safe life estimates.

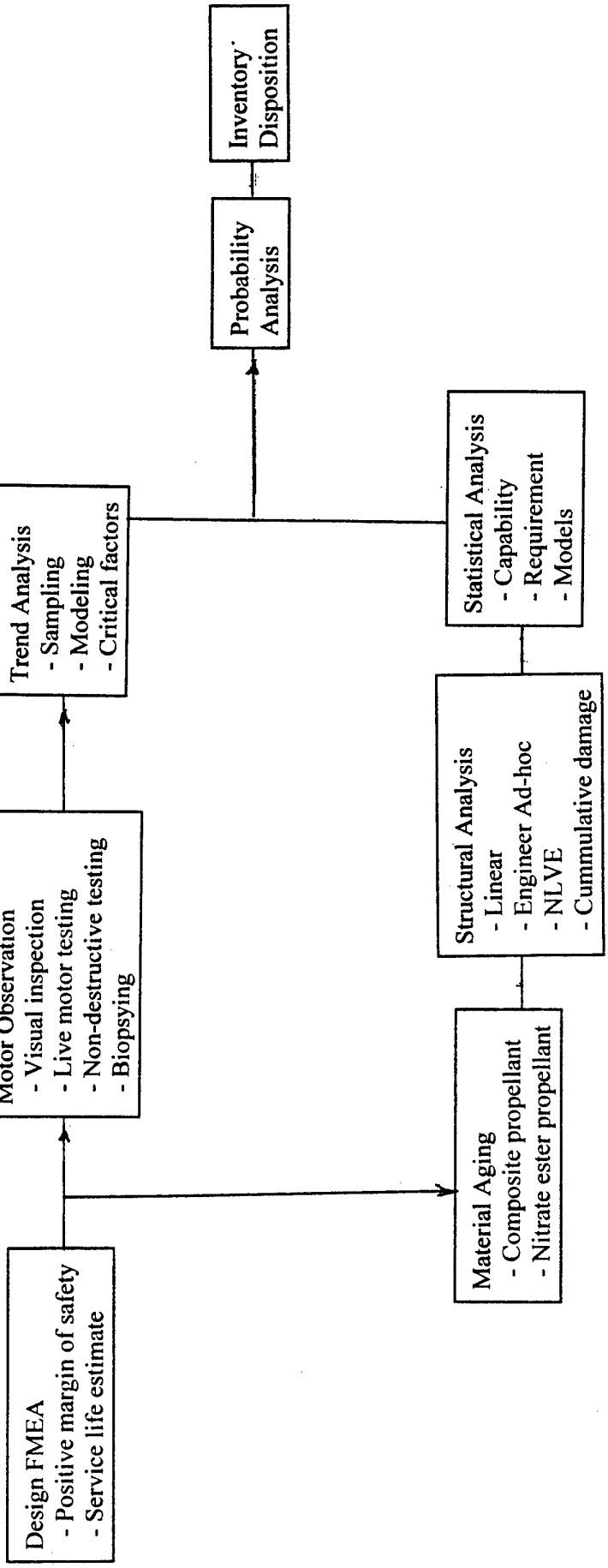
- Rigorous prediction and verification of growth in a burning crack

  The criticality of a defect may depend on whether or not the flame precedes a crack extension. Such criticality may affect the safety of the system. In addition, this issue is often crucial in reconstructing and correcting the cause of a system failure.

TABLE 1 EXCELLENT DESCRIPTIONS OF METHODS FOR CONDUCTING SLP

	Method 1	**Method 2**	**Method 3**
Material testing	Mechanical tests Aging trends Data for NLVE Predictive equations	Mechanical tests Aging trends Cumulative damage constants Predictive equations Dynamic material properties	Chemical tests Stabilizer depletion Decrease in molar mass
Induced loads/analysis	Storage load Operational loads NLVE analysis	Thermally induced (cyclic) Temperature environment model Heat conduction analysis Elastic-viscoelastic correspondence Stress analysis	
Probability analysis	Statistical model - Induced strain (calculated) - Strain capability (measured) - Standard deviations - Equation $P_f = P(\epsilon_{cap} < \epsilon_{ind})$	Statistical model - Induced stress (calculated) - Reduced strength adjusted for damage and aging (R) (measured/calculated) - Equation $P_f = P[R \leq S]$	
Failure criterion	Prescribed level of probability	Prescribed level of probability	Stabilizer concentration reduced to prescribed level

FIGURE 1 SLP FLOW CHART



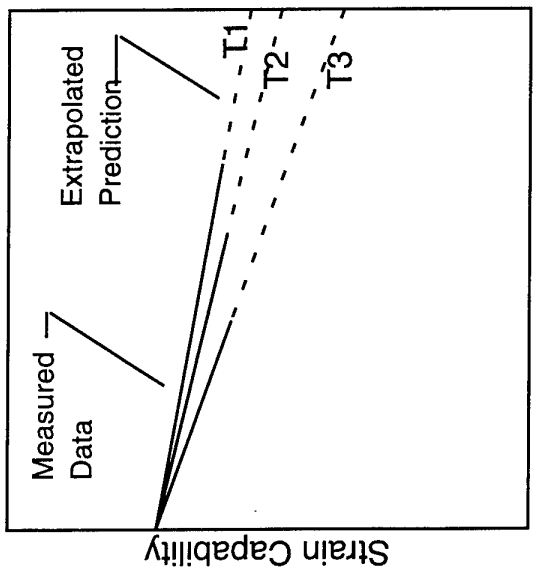


Figure 2a

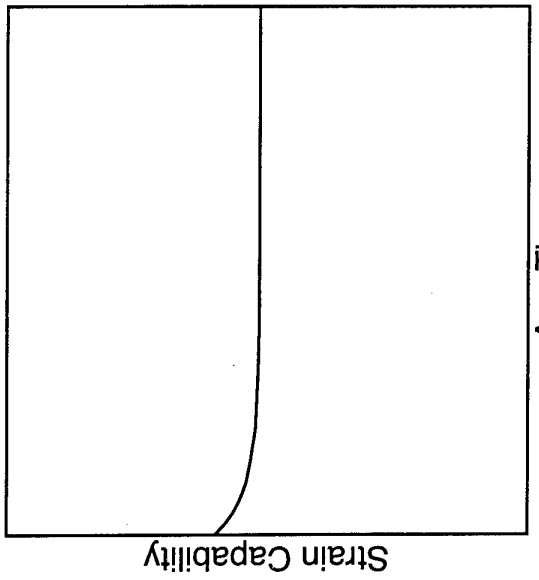


Figure 2b

Figure 2. Layton Model of Aging

Subscale Motor Analysis for Model Verification

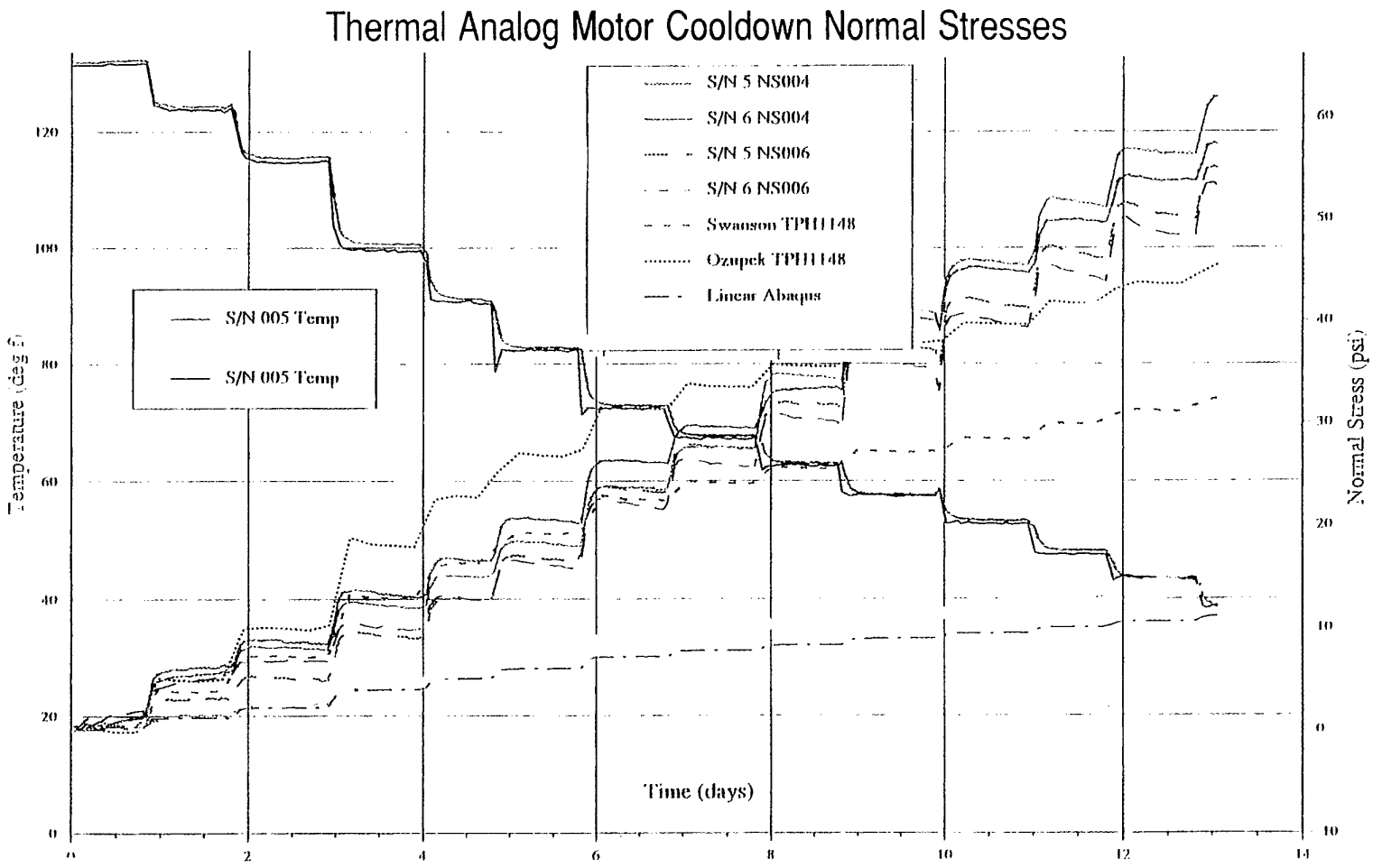


FIGURE 3

G A Collingwood

SERVICE LIFE OF SOLID PROPELLANT SYSTEMS - MAY 1996

KEYNOTE ADDRESS

by
Dr. G. Hooper, Vice-President (Safety and Support)
United Kingdom Ordnance Board, Ministry of Defence
Empress State Building, Lillie Road
London SW6 1TR, United Kingdom

INTRODUCTION

1. Good morning ladies and gentlemen and welcome to this Symposium of the Propulsion and Energetics Panel on Service Life of Solid Propellant Systems. For those of you not familiar with the UK Ordnance Board let me explain that it is a joint service, Army, Navy, Air Force and Civilian body whose purpose it is to provide an impartial appraisal of the safety and suitability for service of weapons used by the UK armed forces.

2. The Ordnance Board was formed in 1415 by Henry V and has been in existence in one form or another virtually continuously ever since. Our coat of arms was granted at the beginning of the 1800's, and members of an organisation with such a long history tend to have a passing interest in history generally. Therefore I will start by looking back in history to early UK work on service life assessment of solid propellant systems.

3. A review of historical archives leads to 1787 and William Congreve who was the first Comptroller of the Royal Laboratory at Woolwich. He was the first person in the UK to put real science into the production of gunpowder and in that year took into government ownership the principal production base. Some twenty years later, having done much work to improve the production process, he demonstrated to the government of the day what he had achieved. He took gunpowder from the mills that he had modernised and conducted comparative trials with powder from other sources. His powder clearly had superior performance. He went on to show that if the powder was properly stored it would not deteriorate after many years of storage and also that the effect on service life of the compatibility between gunpowder and the barrels in which it was stored could be significant.

4. His son, another William Congreve, also became comptroller at Woolwich and followed in his father's footsteps in technical innovation. He invented the Congreve rocket which although having terror and incendiary value as its main quality rather than accuracy or lethality, was extensively used in the land and sea battle scenario. It was used in Boulogne in 1806, Copenhagen in 1807, Leipzig in 1813 and Waterloo in 1815. Its use against Fort McHenry in 1814 is commemorated by the wording "the rockets' red glare" in the US National Anthem. William Congreve junior did much to refine the process technology for gun and rocket applications, and to improve gunpowder service life by attention to the granulation and propellant coating process.

5. The environments in which solid propellant systems are required to operate are becoming more taxing. Guided weapons are required to have a greater range, to be stealthy and agile to defeat countermeasures, while at the same time carrying greater warhead payloads to improve lethality. Certainly in the UK, and I know that the same is true for other nations, we have moved away from a clearly defined threat concentrated in eastern Europe to a world-wide one calling for extensive out-of-area operations, with stores seeing transport by land, sea and air and all this entails.

6. There is a general international push towards requiring Insensitive Munition characteristics for our stores, and environmental legislation is becoming an increasingly important issue; it will, I suspect, dominate our thinking in the next century. Shrinking defence budgets in most nations are dictating reduced whole life costs, that is the total cost from concept to use or disposal, and all of these factors mean that we must extend the life of our existing inventories and assure longer lives for new weapon systems. To give you an example of the former point, the UK purchased Polaris from the United States in the 1960's with an initial 3 year guarantee. It is only now, in the mid 1990's, being phased out in favour of a new system.

7. So what are the key issues that we must consider if we are to effectively determine the safe life of a store:

- Firstly, the environment which the weapon has seen or will see throughout its life;
- Secondly, a detailed and comprehensive understanding of the physical and chemical processes that are involved in the ageing process;
- Thirdly, an appreciation of the consequences of the ageing process: does it matter that the store has aged, will it fail safe, will its performance be unacceptably degraded?

SERVICE ENVIRONMENT

8. It is very important that we understand the real environment that the store will see, and I am very pleased to see contributions on the symposium agenda from the USA, from France, from Canada and from the UK on the important subject of defining the environment. Service life covers both storage, including standby, and operational use. Storage occurs mostly

Paper presented at the AGARD PEP Symposium on "Service Life of Solid Propellant Systems" held in Athens, Greece, 10-14 May 1996, and published in CP-586.

under controlled conditions but can be subject to statistically varying thermal environments with diurnal and seasonal variations. Standby conditions subject munitions to widely varying environments, whilst operational use generates conditions that are often practically difficult to quantify and may not be what the designer envisaged.

9. As I said earlier, our principal threat used to lie in eastern Europe, and hence our equipment was expected to see service in moderate climates. The Gulf War, however, was in an A1 climatic region, that is extremely hot and dry. Before the conflict we put a great deal of our inventory through climatic chambers to assure ourselves that the stores could tolerate the heat. What we were not prepared for, however, was the scene at the bomb dump at Dhahran immediately before the conflict. It was not just muddy but pouring with rain. We did, fortunately get a good record of the environment that the bombs had seen by the tide marks on them.

10. I think the lesson is obvious; it emphasises the imperative that we acquire and analyse real service life data and not rely on what we think the stores should experience. It is for this reason that at the Ordnance Board we seek to encourage a regular rotation of service officers with recent front-line experience into our key posts so that we know what does happen rather than what should happen.

11. Next I would like to take a look at the consequences of the ageing process. Most of you who have been in the rocketry business for some time will have seen scenes such as a rocket proof stand where the rocket motor is in several pieces and a sadly dilapidated experimental facility has resulted. I would like to illustrate my talk with a number of video clips, the first shows what has happened to a number of rocket motors that have been subjected to artificial ageing and then proof fired. As you would expect, all does not go well. I would like you to take note of the violence of the events and imagine the effect on the launch platform or the immediate environment. If we now look at a firing of a Blowpipe missile it shows a slightly different failure mode. What happens is the delay line between boost and sustain did not delay with unfortunate consequences to the operator. Fortunately this was during training; the operator was wearing protective clothing, and he survived relatively unscathed. The final example is of a missile that technically failed safe, but in doing so put the launch platform and the servicemen at risk. The scene was a warship in the Gulf region. The warship from which the missile was to be fired was warning off an aggressor who had ignored advice to get out of certain territorial waters and who had started to fire at the warship. The aggressor ignores the warning and is engaged with unfortunate consequences when the missile motor fails to ignite.

PHYSICAL AND CHEMICAL PROCESSES

12. Physical and chemical properties of the store are set by the initial design of the propellant. Due to the intrinsically unstable nature of propellants it is essential that life requirements are considered at every stage in the design, from the molecular level, through the formulation and production process, and into the charge design. Starting at the molecular level, techniques are now becoming available to predict the properties of energetic molecules from the basic atomic parameters and with no *a-priori* assumptions. The performance, likely decomposition route, intrinsic sensitiveness and properties in combination with other molecules can now be predicted with a greater or lesser degree of accuracy.

13. For example, if we look at the polycyclic nitramine hexa-nitrhexa-aza-isowurtzatane, or CL20, it has of course been widely synthesised and evaluated. However the molecular modelling technique may help us in future to weed out undesirable candidate molecules life-wise at an early stage, and to home in on those which have the desired performance and are intrinsically of adequate resistance to degradation. Another example is gas cracking in a colloidal propellant, where the instability inherent in the presence of the fuel and oxidiser in the same molecule has caused an obvious end to the service life of the grain.

14. Research must continue, even for traditional propellants, into the second aspect that I mentioned earlier; establishing the degradation of the material properties and the physical damage to the propellant charge that occurs in the life cycle. Here is an extreme example of a Carboxy-terminated Polybutadiene binder being hydrolysed by moisture intrusion. The motor has been subject to 8 years storage in hot-wet conditions with poor sealing. It highlights the need to identify the real culprit in the ageing process, be it heat, moisture or oxygen, and to mitigate its effect. There are many useful papers being presented here on this aspect which I hope will continue to receive proper attention in the future.

15. Another extremely important element in the overall equation is processing. We are generally not dealing with ideal materials, in that the end product is process dependant as well as composition dependant. We continue to see considerable batch-to-batch variations and we need to understand the effect on service life. Attention also needs to be paid to the impact on service life of the filling or casting techniques that are used. The aim must be to provide a propellant grain with adequately uniform physical properties and with the minimum residual stress or damage. When service life analysis is conducted on a grain most methods consider the charge as flaw free; this we know not to be the case in practice and flaw criticality should be given greater attention in future analysis. Here we see a cracked HTPB grain where stress raisers built in at the design stage have caused the problem, but, equally, poor processing can cause defect sites resulting in similar cracks. Other parts of the system, such as liners, insulators and bonding materials play an important role and must also be considered.

16. Organisations concerned with service life have considered for many years the various methodologies used to perform a detailed service life assessment of

solid rocket motors. Selection of the most appropriate methods will primarily depend on the precision in the estimate required to be made at a particular stage in the motor's life cycle. This in turn will be affected by the consequences of failure and the length of service life being predicted. Generally it has been necessary to determine if a motor will last a set number of years in the future, typically 5 to 10 years, but it may be required to determine the absolute value of the motor's life; indeed for credible whole-life costings this is vital. The selected method will then most likely be determined by whether chemical ageing will be the predominant driver for the end of life or whether loss of grain structural integrity is more likely to be the failure mechanism. There is almost certain however to be a degree of interdependence, with many aspects to be considered in such a process, and it is vital that a systematic approach is taken to select the most suitable method.

17. Each of the methods can provide, to a greater or lesser extent, an estimation of the service life for the motor. These estimates can be used in a Risk Assessment exercise to determine that an adequate confidence level has been reached in the prediction. Further refinement of marginal estimates can then be undertaken until a sufficiently robust prediction can be made.

18. Traditionally service life has been established by experimentally-based methods. The three most often used to date, generally in combination, are:

a. Accelerated Ageing. This approach is the basis of the method used by the UK Ordnance Board to give an initial service life estimate prior to introduction to service and it is also used in the US Navy's Type Life programmes. Underwriting this of course is the work on chemical and physical ageing that we will hear in Sessions 1 and 2;

b. Destructive Testing/Surveillance. This is a traditional method used by many countries to develop critical ageing trends for in-service motors;

c. Non-Destructive Evaluation. This involves surveillance by using imaging techniques or by non-destructive propellant sampling methods to assess the condition of motors aged in the field or under a controlled environment. This approach is receiving much support with contributions in Session 2, from both contractors and governments in US, UK, France and Germany.

19. Analytical methods such as the Cumulative Damage/Probabilistic Approach, Empirical-Modelling of Ageing versus Failure Criteria and Probability of Failure Approach are increasingly coming to the fore. These methods have progressed as developments take place based on a better understanding of the material properties and behaviour laws involved in propellants and with improved modelling of the thermal and mechanical loads applied to the charge. These have become possible with the increased computational power now available cheaply and readily.

20. To be useful, these approaches must consider the combined and variable loading environments in the service life cycle, the effects of chemical and mechanical degradation and the inherent variability in the material properties across the population. For these reasons the probabilistic approach is becoming the favoured method for the determination of service life, as it takes into account the variability of the chemical and mechanical properties of the propellant and the deployment temperature of the motor.

21. Increasing financial constraints generate a need to use more accurate models to reduce the end-to-end testing of full systems. Whilst full life cycle testing will remain necessary in the foreseeable future, a more certain indication of failure modes and reduction in uncertainties will be needed before embarking on expensive tests.

22. The assessment of structural integrity remains a challenging area. It is a key discipline that governs performance, reliability and life. I am pleased to see good representation from the TTCP nations in Sessions IV and V on these aspects.

To conclude, in my view, the way ahead for us is to formulate a service life strategy for the future as follows:

1. Pursue the various technologies on a broad front;

2. Identify critical deficiencies in the technologies. Any service life model is only as good as the weakest link in the prediction chain;

3. Continue to develop advanced data capture and analysis techniques to monitor the environment experienced by real in-service motors;

4. Increase emphasis on modelling and small-scale testing.

Finally, we are all working in an environment where resources are increasingly limited and this makes it all the more important to pool our efforts to achieve the common goal. This makes the work of this AGARD Panel particularly relevant and I look forward to what promises to be a very valuable and stimulating meeting.

Development of Methods for Aging and Analyzing Propellants Containing Nitrate Ester Stabilized With MNA and 2-NDPA

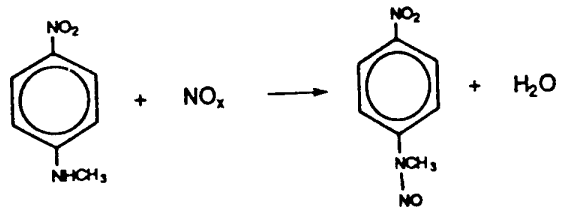
P.S. Carpenter, A. Atwood, C.J. Meade, N. Carey and A. Paiz
Naval Air Warfare Center Weapons Division, Code 47340D
China Lake, CA 93555,USA

ABSTRACT

The objective of this work was to develop a reliable and safe method, for the accelerated aging, of propellants at different known relative humidities. Safety testing, nitrate ester content, and stabilizer levels were monitored. The safety testing was completed to ensure that all of the samples were safe to handle and store and to determine if aging had any effect on the propellants sensitivity to impact, friction and electrostatic discharge.

INTRODUCTION

Missile propellants containing nitrate esters must have stabilizers present to prevent self heating and ignition. As the nitrate esters age, they produce NOx's and these NOx's promote the decomposition of more nitrate ester. The stabilizers work by scavenging the NOx produced and slowing down the decomposition. The two stabilizers used in this study were MNA and 2-NDPA. The MNA was the primary stabilizer and the 2-NDPA was there as a backup stabilizer. As MNA reacts with the NOx it produces N-Nitroso-N-methyl-p-nitroanaline (NOMNA). By tracking the amount of MNA loss and the amount of NOMNA formation over time at different temperatures an Arrenhius plot can be generated to estimate the safe life of the propellant.



MNA NOMNA

During this testing it was observed that at temperatures above 100°F and after several weeks of aging the mass balance of MNA and NOMNA no longer added up to one. This meant that we were either not extracting all of the materials or that another reaction was taking place. Upon close examination of the spectra it was determined that other reactions were taking place. We were able to track the growth of two other peaks in the High Performance Liquid Chromatography (HPLC) spectra over time. Presently, investigation into the identity of these new reaction products is under way.

If NOMNA also scavenges NOx's, then it may also serve as a stabilizer and the safe life predictions can be extended. This would be important since our existing inventories would not have to be replaced as soon. If these new reaction products are from a different reaction with MNA, then we will need to further examine the mechanism of how MNA works as a stabilizer.

Another variable in this study was the Relative Humidity (RH). Samples were prepared and aged in various RH's to determine the effect of %RH on the propellant. This is important information since we can, to some extent, control the conditions that motors containing these propellants are stored at.

EXPERIMENTAL APPROACH

Test Plan:

Two propellants containing a nitrate ester, 0.5% MNA and 0.2% 2-NDPA were aged and analyzed. These propellants were aged at 75, 100, 120, and 140°F with the RH varied from 11%,33% and 54%. Also, the samples were aged in either a wrapped or unwrapped condition. The following tables show the test matrix used in this study.

TEST PLAN AND STATUS

75 F (33% RH ONLY)

TIME (WKS)	0	104	156	208	260
WRAPPED	•	•		•	
UNWRAPPED	•	•	•	•	

100 F (ALL 3 RH'S)

TIME (WKS)	0	35	64	86	128	160
WRAPPED	•	•	•	•	•	•
UNWRAPPED	•		•		•	

120 F (ALL 3 RH'S)

TIME (WKS)	0	16	32	48	64	80	96
WRAPPED	•	•	•	•	•	•	•
UNWRAPPED	•		•		•		•

140 F (ALL 3 RH'S)

TIME (WKS)	0	8	16	24	32	40	48
WRAPPED	•	•	•	•	•	•	•
UNWRAPPED	•				•		•

160F (33% RH ONLY)

TIME (WKS)	0	3	11

Paper presented at the AGARD PEP Symposium on "Service Life of Solid Propellant Systems" held in Athens, Greece, 10-14 May 1996, and published in CP-586.

Sample Preparation and Aging:

The samples were prepared for aging by taking a slab of propellant, 1500g, and slicing it into 1 cm thick strips. Each strip was then perstamped into dogbones and reassembled into the original slab configuration. The unwrapped samples were then placed into an expanded metal tray as seen in Fig. 1. The wrapped samples were tightly wrapped in aluminum foil and then vacuume sealed in the Flexcan. Prior to wrapping all of the samples were equilibrated at the appropriate RH for 30 days. The sample slab sizes were kept relatively small due to the length of time it takes to reach equilibrium in the RH's. The larger the sample the longer it takes. The saturated salt solutions were made of lithium chloride for the 11%RH, magnesium chloride for the 33%RH and sodium bromide for the 54%RH.

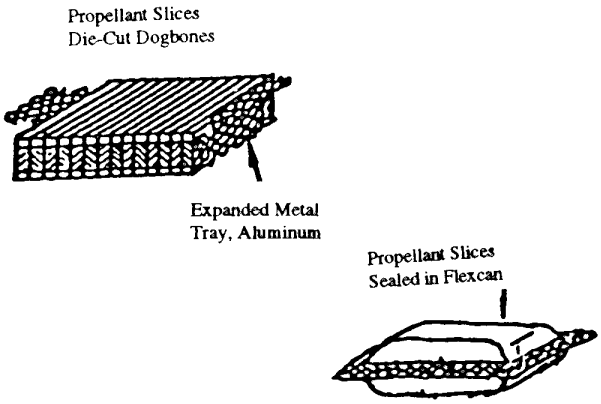


Figure 1. Sample Configuration

The wrapped and unwrapped samples were then placed in the dissectors, with saturated salt solutions, and the dissectors placed in the ovens Fig. 2. At the end of each aging interval a sample was removed from the oven and tested for mechanical properties, burning rate, stabilizer depletion and safety testing. This paper will only cover testing methods and safety testing. Other papers are being prepared that look into how the stabilizer depletion relates to mechanical properties and burning rates. The samples used for the stabilizer depletion and safety testing were taken from a slice of propellant in the middle of the slab. The outside 1/4" was cut away so that the samples tested were from the bulk of the propellant.

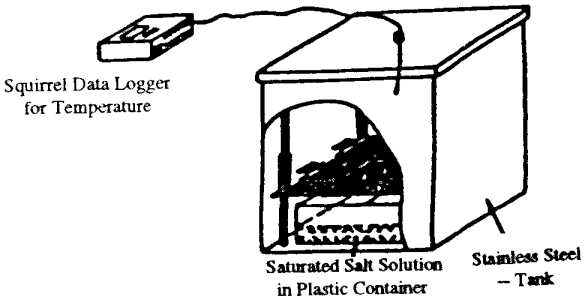


Figure 2. Aging Ovens

Safety Testing:

Impact, Friction and electrostatic Discharge (ESD) sensitivity testing was completed on each sample to ensure that the samples were safe to handle and store. Also, we wanted to see if there were any trend in sensitivity with aging.

The impact sensitivity testing was done following MIL-STD-650, Method 505.1. The Naval Air Warfare Center uses an ERL Model machine with a 2.5kg drop weight and type 12 tools. Figure 3 shows the assemble of the test elements to be used, which consists of a free-falling weight, tooling to hold the energetic sample, and a supporting frame. The procedure consists of weighing out 35+/- 2mg samples of energetic material onto garnet sandpaper. The sand paper and the sample are then placed in the center of the anvil and the striker is lowered to rest on top of the sample. The 2.5kg drop weight is raised to the desired height, dropped, and the results observed. A positive test is detected by a smudge on the sandpaper, the observance of smoke, a spark. odor, or a brisk response. After each drop, the test sample is discarded and a fresh sample used for the next drop. If the test was determined to be positive, then the next sample was tested at the next lower level. If the result was determined to be negative, then the next sample was tested at the next higher level. This was continued for a total of 20 samples. From that data the 50% point was determined (the level at which 50% of the time the sample will fire). The "Low Fire" point is also recorded since it has been determined to be the level at which 10% of the time the sample will fire. A complete description of the up-and-down method can be found in Introduction to Statistical Analysis, by W.J. Dixion and I.M. Massey.

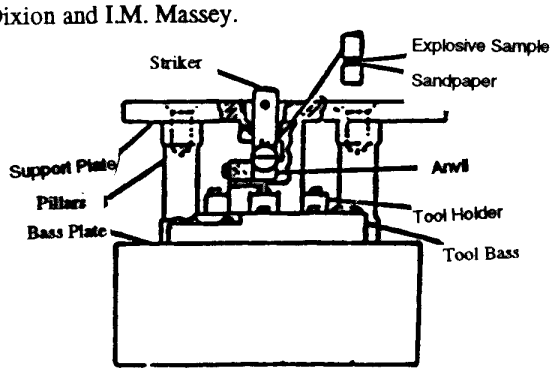


Figure 3. Impact Tester

Friction sensitivity was determined using an Allegheny Ballistics Laboratory (ABL) sliding friction apparatus. The test was conducted using a pendulum drop angle of 90 degrees. This imparts an initial velocity of 8ft per second to the sliding steel platen. A 50 mg sample was placed on the platen and the edge of

a 1/8 inch wide steel disc was pressed down on the sample with a selected force. Fig. 4 illustrates the placement of the sample and the friction force. The platen was free to move exactly 1 inch after being struck by the pendulum, and the sample arranged on the platen so that it is carried between the sliding metal surfaces. Fig.5 gives the overall view of the ABL friction apparatus. A positive test is detected by a smudge on the sandpaper, the observance of smoke, a spark. odor, or a brisk response. If the test was determined to be positive, then the next sample was tested at the next lower level. If the result was determined to be negative, then the next sample was tested at the next higher level. This was continued for a total of 20 samples. From that data the 50% point was determined (the level at which 50% of the time the sample will fire). The "Low Fire" point is also recorded since it has been determined to be the level at which 10% of the time the sample will fire. A complete description of this test method can be found in OD44811.

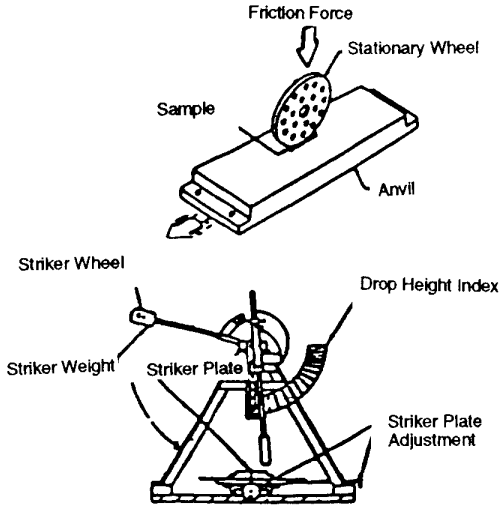


Figure 4. ABL Friction Tester

ESD sensitivity tested was designed to simulate an electrostaticlly charged person or object discharging through a thin layer of sample to a grounded conductive surface. A sample of approximately 50mg was placed on a grounded steel button. A capacitor, in this case a 0.02 micro farad, was charged to a selected voltage by means of a high voltage power supply. The positive side of the capacitor was brought into contact with the sample by means of a steel phonograph needle on the end of a probe and so discharged through the sample to the steel button. Samples were tested at 0.25 joules. A total of 10 trials for each sample were run.

Stabilizer Depletion:

The concentrations of the stabilizers were determined using a HPLC equipped with a UV/VIS detector. The HPLC conditions were as follows:

Mobil Phase	30%1,2 -Dimethoxyether / 70% Heptane
Flow Rate	2.00 ml/ min
Column	Normal Phase Silica Gel, 4.6mm X 25cm
Wavelength	360 nm
InjectVolume	20 ul

The sample were prepared by chopping the propellant into very small pieces (1/16" x 1/16") using a razor blade. 250mg of the sample were then weighed into the end of a pencil column. The pencil column were made by placing a small amount of glass wool into the tip of a pasture pipette and then filling the pipette three fourths of the way up with silica gel. Glass wool was then placed on top of the silica gel and the sample placed on top of the glass wool. The stabilizers were extracted with approximately 4 ml of 1,2-Dimethoxyether (Glyme). The Glyme was added slowly to the top of the pencil column and allowed to flush through the sample and the silica gel then into a 25ml volumetric flask containing 20 ml of Heptane. The flask was then brought to volume with Glyme. Each sample was prepared in duplicate and then analyzed in duplicate.

Nitrate Ester Content

The nitrate ester content was also tracked during this aging study. This was done using the same HPLC but at a different wavelength and reverse phase instead of normal phase. The HPLC conditions were as follows:

Mobil Phase	50% Acetonitrile/ 50% water
Flow Rate	1.2 ml/ min
Column	ReversePhase, C-18, 4.6mm X 25cm
Wavelength	219nm
InjectVolume	20 ul

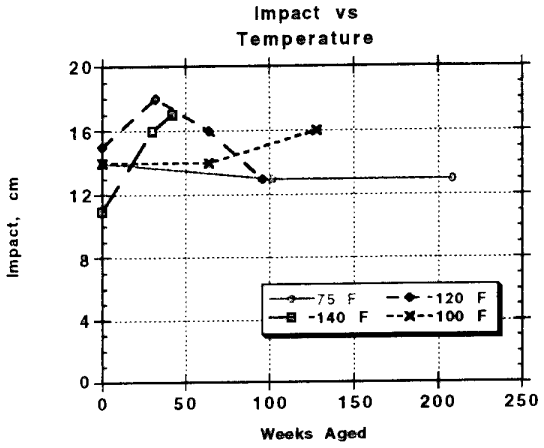
The samples were prepared by cuting the propellant int very small pieces (1/16" x 1/16"). 250 mg of the sample were then weighed into a 125 ml flask and 25 ml of acetonitrile was added. The flask was shaken and then allowed to sit overnight to extract out the nitrate ester. The mixture was then filtered through a cintered glass filter equiped with GF/C filter paper. The filtrate was then quantitately transfered into a 50 ml volumetric flask and brought to volume with acetonitrile. All of the samples were prepared in duplicate and analyzed in duplicate.

EXPERIMENTAL RESULTS

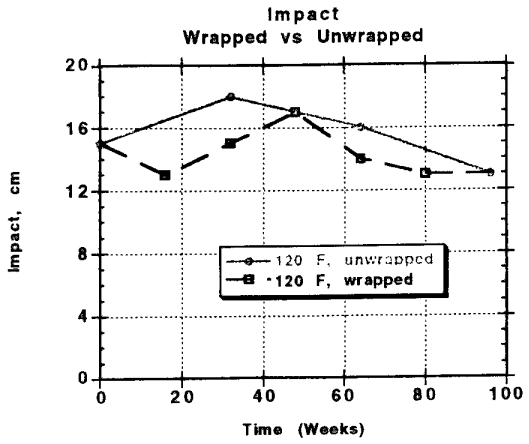
Two different propellants were analyzed with the results for both propellant showing the same trends. It was noted that as the propellants aged one got softer while the other one got rubbery and very hard to cut. This was also seen in the modulus data for the aged propellants.

IMPACT:

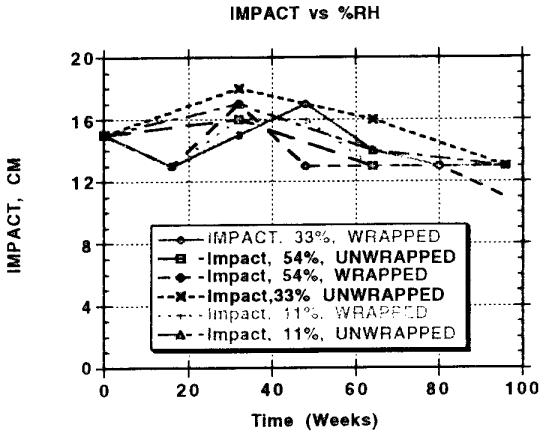
There were no clear trend with impact sensitivity vs. aging temperature. . It should be noted that RDX impact sensitivity on NAWC's equipment was 12-15 cm. None of these samples were more impact sensitive than RDX.



There was virtually no difference in impact sensitivity of the wrapped samples vs. the unwrapped samples. The variation in the data was typical of what can be expected for the test method. This test is very sensitive to changes in room temperature and percent relative humidity. The toom temperature and percent RH are closely monitored. The room temperature must be between 70 and 80 F and the percent relative humidity must be below 50 percent for the test to be run. Standards of RDX and PETN are ran at the same time as the sample to monitor the variation in the test data. It is not uncommon for the RDX impact senssitivty to vary from 12 to 15 cm depending on the day it was tested.



If you look at all of the samples, both wrapped and unwrapped and all three RH's there is little difference in the data. All of the samples seemed to be getting slightly more sensitive but are still within the range we found for RDX.

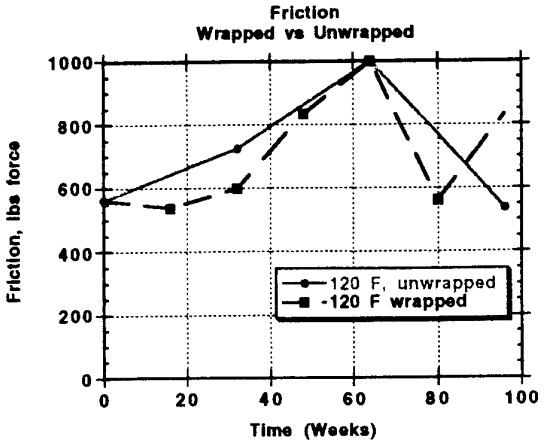


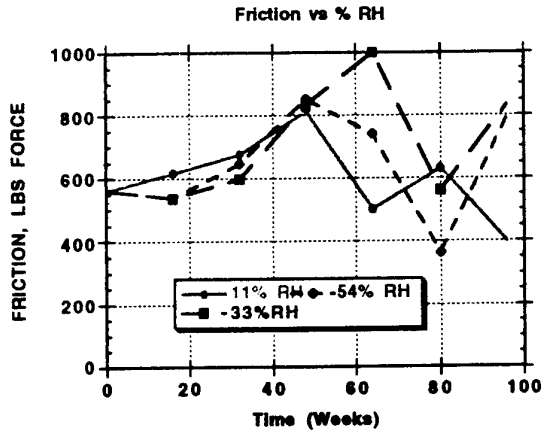
FRICTION:

There is a lot of variation in the friction test. This test is also very sensitive to the room temperature and relative humidity. The 140 and 120 F samples look to be on a downward swing but we were unable to age them any longer since the samples were pulled from aging. It is difficult to say which way the data would have gone. From looking at all of the data sets the overall trend was for the samples to become less friction sensitive as they aged. When the testing ended the friction data for the aged samples was still as good for the aged samples as it was for the unaged samples.

Our cut off for friction sensitivity is 50 lbs and all of the samples were well above that threshold.

There was no dependency on RH or wrapping condition vs. friction sensitivity. The samples became less sensitive with aging.



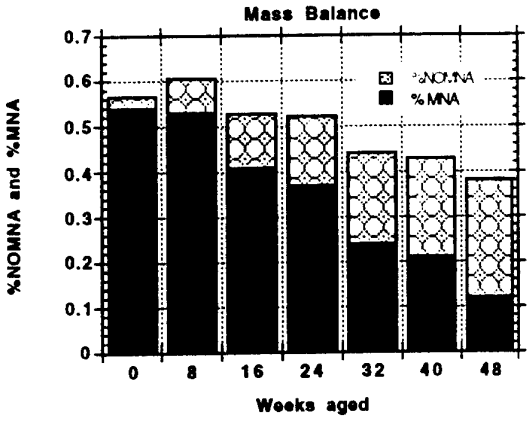


ESD:

All samples were determined to be insensitive to ESD. That is that all samples were 10 out of 10 no fires at 0.25 joules.

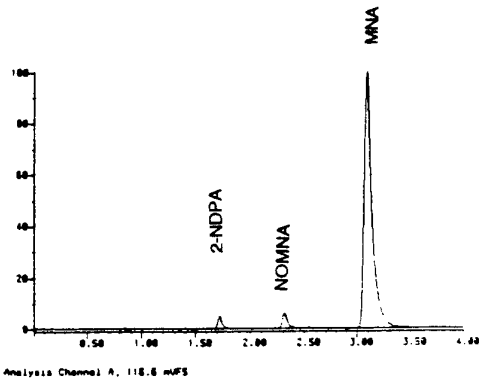
Stabilizer Depletion

As mentioned earlier after several weeks of aging at temperatures above 100 F the mass balance for MNA and NOMNA no longer equals one.



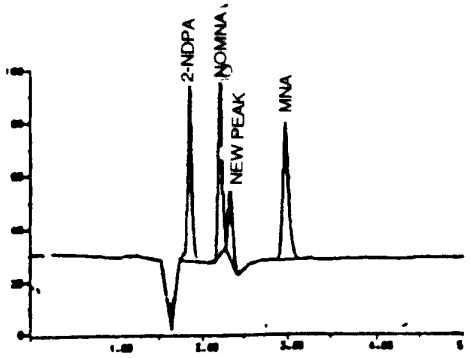
In fact there is a considerable loss of mass of about one third of the material after 48 weeks. The first chromatography shows the peaks we would expect to see in an unaged sample. There are three nice sharp peaks.

MNA and 2-NDPA unaged



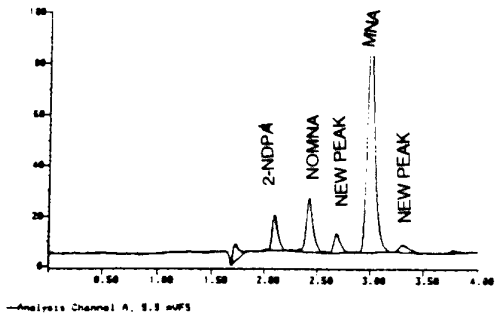
The second chromatograph shows the new peak we see after aging at high temperature. This chromatograph only shows one new peak but we have seen a second peak that is very broad that comes out late in the chromatogram. These peaks grow as the mass balance goes down. Presently, we are in the process of identifying these compounds so that we can better understand what is going on. These new peaks may not be important since they are only seen at temperatures over 100 F but, until we identify them and understand the mechanisms involved we will not be sure.

MNA and 2-NDPA 120 F aged sample

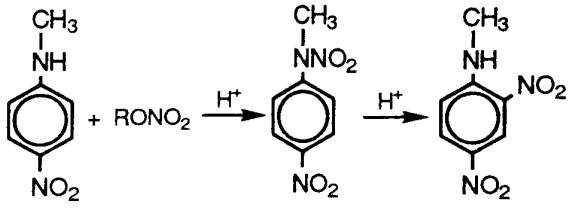


We wanted to see if this was true for the other nitrate esters we use so we aged butane triol trinitrate (BTTN) and trimethylolethane trinitrate (TMETN) with 1% MNA at 100, 120, and 140 F. We observed the same thing happen where the mass balance no longer added up to one and the same two new peaks. It was interesting to note that the rate of growth for the new peaks was a lot faster for the TMETN than for the BTTN. The TMETN samples developed three additional peaks in the chromatogram. Also, TMETN depleted the MNA at a much faster rate, up to five times faster at 160 F, than the BTTN. This may help give some insight into the reaction mechanism once we have the new compounds identified.

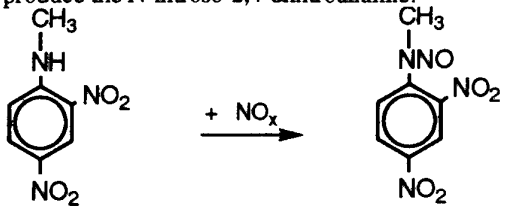
TMETN 4weeks at 160F



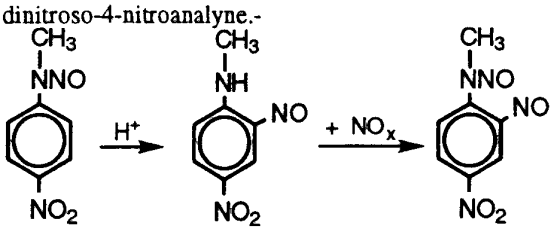
We have looked at some possible other reactions for both the MNA and the NOMNA. MNA can react with the nitrate ester in the presence of acid or a metal catalyst to produce N-methyl-N,4-dinitroanaline. That can then in the presence of acid rearange adding a nitro group to the meta position forming N-methyl-2,4-dinitroanaline.



The dinitro compound can then react with more NOx to produce the N-nitroso-2,4-dinitroanaline.



The NOMNA can also rearrange in the presence of acid or a metal catalyst which can then react with nore NOx to form the N-methyl-N,2-dinitroso-4-nitroanalyne.-



These are just a few of the possible reactions possible. The extracted samples cantaining the additional compound are being analyzed by Liquid Chromotography / Mass Specoscopy to determine the identity of the other compounds.

SUMMARY

We feel that we have developed a safe and accurate way to age propellants at different %RH and temperatures. The analysis data can only be as good as the samples being tested so being able to age the propellants at a known %RH and wrapped or unwrapped conditions is critical. The time that the samples equilibrate to RH is very important. The larger the sample the longer the time it will take to equilibrate the samples.

The analysis technique for determining Stabilizer levels was very reproducible and easy to use. We would recommend it to anyone testing MNA and 2-NDPA in propellants containing nitrate esters. With one extraction procedure all of the stabilizers can be determined. The analytical procedure for determining the nitrate ester content is also very reproducable and accutate sine it takes advantage of the UV maximum for the nitrate ester you are looking for.

The two propellants that were aged became slightly more impact sensitive with aging but less friction sensitive. All of the samples were still within NAWC's acceptable range for handleing and storage.

Finally, once we determine the identity of the new peaks in the HPLC then we will have a better understanding of the mechanisms for using MNA as a stabilizer.

Methods and Kinetic Models for the Lifetime Assessment of Solid Propellants

Manfred A. Bohn

Fraunhofer-Institut für Chemische Technologie (ICT)
Postfach 1240, D-76318 Pfinztal
Fax: +49-721-4640-111
e-mail: bo@ict.fhg.de

1. ABSTRACT

The relatively low bond energy of the energetic groups of explosives, typical values are between 150 kJ/mol and 250 kJ/mol, together with frequently occurring low values of the activation energies, between 90 kJ/mol and 200 kJ/mol, lead to an increase in the rate of ageing in the case of energetic substances when compared to chemical substances such as toluene and heptane, which are more stable. The activation energies for physical and physical-chemical ageing can be even lower, typical values for the migration of plasticizers, phlegmatizers (deterrents), and burning catalysts are about 50 kJ/mol to 100 kJ/mol.

The ageing of gun propellants (GPs) and solid rocket propellants (RPs) expresses itself in many quantities and properties: in chemical properties such as mean molar masses of polymers, degree of cross-linking, content of stabilizers, antioxidants and plasticizers, in mechanical properties such as tensile strength, strain at break, compressive strength, elasticity and shear modulus, glass transition temperature and embrittlement temperature, in "composite values" such as specific impulse, burning rate, ignition delay, vivacity and muzzle velocity. As ageing can only be slowed down by means of stabilizers and not really stopped, the specified properties of GPs and RPs are altered with time-temperature stresses. This makes the substances dangerous whilst in storage and when in use. The hazards are known as spontaneous ignition, breech blow and motor explosion. But also the designed performance data of a gun or a rocket are changed, which expresses itself in a lowering of the muzzle velocity, bad target picture and in the case of RP in a non-controlled burning rate.

Therefore it is necessary to quantify ageing processes in order to be able to specify after what time-temperature stresses the properties required still lie within the range of tolerance that means to make a reliable prediction. The quantification is done using mathematical descriptions of the changes in the values of properties, which are connected to the relevant ageing processes, as a function of time and temperature. If necessary also further variables such as humidity and oxygen are included. The description must achieve a separation between time and temperature so that a prediction for other time-temperature values becomes possible. This procedure will be described using a number of examples: migration of burning catalysts, decrease in the mean molar masses Mn, Mw and Mz of nitrocellulose in the propellants, stabilizer consumption, decrease of mechanical properties, mass loss, and heat generation, the latter two also with autocatalysis.

Empirical descriptions as well as those based on kinetic models are possible for good predictions. The deciding factors are that the extrapolation ability of the description for the measurements in the direction of the time axis is good and that the correct parameterization of temperature dependence is made. This will be shown in examples for the GP A5020 and of the RP RLC 470/6A. One example also shows that a purely empirical description can lead to a wrong assessment. A description of the ageing with models based on mechanistic concepts mitigates this danger.

2. INTRODUCTION

Like other explosives, gun propellants (GP) and solid rocket propellants (RP) are substances with so-called energetic groups. The most common ones are shown in Table 1. The bond energy B for the weakest chemical bond has also been given for the individual groups. One can find other values, usually lower ones caused by catalytic effects. For instance, in the case of the possibility of hydrogen transfer to the NO_2 group, smaller values apply for the nitro group, as low as given in brackets /1, (determined as activation energy) /.This is valid also for the nitramine group. The bond energy values of these groups are relatively low, typical values of C - H bonds are 415 kJ/mol and of C - C bonds 344 kJ/mol. The nitro group is the most stable energetic group. Bonds with these low

Presented on the 87th Symp. of the Propulsion and Energetics Panel of the AGARD, Athens, Greece, 1996.

bond energies can easily be split thermally (thermolysis). The NO_2 radical is split off from the nitric acid ester group already at moderate high temperatures (≥30°C - 40°C). The azide group gives off easily molecular nitrogen.

Table 1: Energetic groups with their bond energies and weakest bonds.

		B [kJ/mol]	weakest bond	Ea[kJ/mol]
nitric acid ester group:	$C - ONO_2$	155 - 163	$CO - NO_2$	90-150
azide group:	$C - N_3$	170	$CN - NN$	140-170
nitramine group:	$N - NO_2$	193	$N - NO_2$	?
nitro group (aromatic):	$C - NO_2$	297 (152)	$C - NO_2$	150-290
nitro group:	$CH_3 - NO_2$	250	$C - NO_2$	?

The activation energy for the decomposition of the energetic groups is usually between about 90 kJ/mol and 200 kJ/mol, some of the ranges of the values are given. These low values for bond energy and activation energy lead to an increase in the rate of ageing of energetic substances. The formation of NO_2 usually leads to an autocatalytic decomposition. Especially in the case of the nitric acid ester group, the ageing of GPs and RPs does not only lead to performance losses, but also to spontaneous ignition due to an increase in decomposition triggered by autocatalysis.The ageing cannot be prevented directly. Its effect can be largely reduced with stabilizers such as those used for nitrocellulose and for blasting oils. Stabilizers to catch reactive molecules, which would otherwise increase the decomposition, such as e.g. NO_2 or oxygen. The decomposition of energetic groups and substances is an exothermic reaction, i.e. it releases heat. Mostly it is connected also with the splitting off of gases.

Apart from ageing due to chemical reactions, there are also ageing processes due to physical and physical-chemical processes. This includes migration and evaporation of low molecular mass components such as energetic plasticizers, phlegmatizers, deterrents, and burning catalysts. Examples are the migration of the substances mentioned from the propellant into the insulation or the diffusion of a surface treatment agent from the surface of a GP grain to its interior. These processes change the ballistic behaviour, so this is also referred to as ballistic ageing.The adherence to and the constancy of the mechanical properties of GPs and RPs is important for the safe use but also for an operation in accordance with the design. Ageing of the propellant due to chemical reactions as well as physical-chemical ageing changes the mechanical quantities such as tensile strength, strain at break, elasticity modulus, shear modulus and thermo-mechanical properties such as glass transition temperature and embrittlement temperature. This can result in dangerous failures in the form of breech blow and rocket motor explosion.

If the propellants are used in areas of the world with differing climatic conditions (hot, cold and humid areas), they are subjected to increased stresses. The exact knowledge of the ageing process is required for safe and cost saving use of ammunition containing GPs and RPs. An accurate mathematical description of the ageing processes using chemical-kinetic and physical as well as physical-chemical models makes a more reliable prediction of ageing possible and therefore also of safe storage time and safe service life. In order to do this, better data in form of temperature - time profiles are necessary. Inaccurate data or estimates about the temperature stress in service /2/ can only provide a rough prediction. This can lead to a removal of ammunition, which could still be used (costs) or it can lead to a dangerous misjudgement about the service life (safety).

3. DETERMINATION OF AGEING

3.1. Methods

Ageing means the change in one or more quantities determining operation and/or safety as a function of time and temperature, if necessary also as a function of other variables such as humidity and oxygen. The problem is to determine the data within acceptable times. In order to do this, the ageing process is accelerated by increasing the temperature. From the data gained at increased temperatures, a prediction for the ageing at ambient temperatures must be made. This is a reliable method only, when the ageing mechanism for a change of a property is independent of temperature, that means that only the rates are a function of temperature. This is a condition, which is not given from the start, it must be proved. When selecting the range of temperatures and other storage conditions, care must be taken not to trigger artificial ageing, which would not occur during service. Transferring existing methods can lead to false evaluations, e.g. if the methods used for nitric acid ester propellants were to be used for HTPB bound propellants.

Many test methods have been developed to assess the stability ot GPs and RPs, among these are:

- Bergmann-Junk test
- Vacuum stability (reactivity) test
- Abel test

- Autoignition test
- Dutch mass loss test (at 105°C and 110°C)
- Heat storage test (time to NO_X formation)
- Mass loss test at different temperatures (75°C, 90°C)
- Methyl violett test
- Differential thermal analysis
- Heat flow test
- Cube cracking test

A full list of all tests applied by the NATO member states can be found in /3/.

All these tests assess the momentary stability and quality of GPs and RPs. They allow not a real prediction of the lifetime. For this, measurements at different temperatures over long enough time periods have to be made. Only with time-temperature data of suitable quantities a real prediction can be made. If one has for some formulations all the necessary data established to assess the ageing, than one may estimate with the above test methods that the stability may be of such a grade that a certain lifetime can be reached. But one has not a full guarantee that the ageing will not be faster during the service life of the propellant. This is of high importance for new formulations. Here only little experience is available on the ageing. It must therefore be adviced to make comprehensive investigations on the ageing processes in order to be able to make a real substantiated and responsible prediction of the lifetime and to develop reliable 'momentary' test methods.

3.2 Suitable quantities and properties to predict lifetime

According to the chemical, physical and physical-chemical reactions and processes in GPs and RPs, ageing is expressed in the following quantities, Table 2:

Table 2: Properties and quantities, which can be used to investigate the ageing behaviour of propellants.

quantity	method of measurement
mean molar masses	GPC (gel permeation chromatography)
stabilizer content	HPLC, IR, IR microscopy
antioxidant content	HPLC, IR, IR microscopy
blasting oil content	HPLC, IR
plasticizer content	HPLC, GC, IR
burning catalyst content	HPLC, GC, AAS, AES
phlegmatizer content	HPLC, GC, IR, IR microscopy
mass loss	scales, TGA
gas generation	GC, MS, chemical luminescence (NO_X), IR
adiabatic selfheating	adiabatic calorimetric analysis (ARC apparatus)
heat generation	microcalorimeter
energy content	DSC, calorimetric bomb
tensile stress and strain	tensile test
compressive stress and strain	tensile test
elasticity modulus	DMA (dynamic mechanical analysis), tensile test
shear modulus	torsion-DMA
adhesion between binder matrix and energetic particles	tensile test (Poisson ratio $\mu=\varepsilon_o/\varepsilon_l$)
glass transition temperature T_G	DMA
embrittlement temperature T_B	high speed pressure impact, high speed tearing machine
cross-link density	swelling behaviour

This list can be extended to include quantites such as diffusion coefficient, which determines the migration rate of blasting oils, catalysts and phlegmatizers as well as thermal conductivity, mass density and specific heat, which determine the critical storage temperatures according to Frank-Kamenetzki. One must consider also: ageing of the coating of an energetic particle, ageing of the catalyst effect.

Some of the quantities listed influence each other interactively or basic quantities influence "composite" ones. Cross-link density, glass transition temperature, embrittlement temperature, shear modulus, elasticity modulus and antioxidant concentration are connected together in HTPB bound propellants. In the case of GPs and RPs based on

nitrocellulose, the decrease of mean molar masses, the stabilizer content, gas generation, heat generation, and mass loss are connected, whereby the decrease in mean molar masses also has an effect on glass transition temperature and embrittlement temperature.

3.3 Quantitative description of ageing

3.3.1 Description using rate equations

In order to make a prediction, the change of the value of a quantity must be described quantitatively as a function of time and temperature, i.e. in a mathematical form. The data received are always like a system of curves, if looked at as a function of time and with temperature as a parameter. The description is made in two steps:

- description of each individual curve as a function of time
- introduction of a time-independent but temperature dependent parameter, the rate constant.

This separates the two variables time and temperature. With the additional variables humidity and oxygen a multidimensional space is spanned up for the investigated quantity. A number of these descriptions are known from chemical kinetics. They can be applied directly, if the change of the quantity is coupled to a chemical reaction. In the following equations, which have been kept quite general, P stands for one of the above mentioned properties. The general rate expression for P is given in eq.(1).

$$(1) \quad \left(\frac{dP(t,T)}{dt}\right)_T = Vp = S \cdot k_P(T) \cdot f\left[P(t,T); g(t,T)\right]$$

$\left(\frac{dP(t,T)}{dt}\right)_T$	rate of change of the property P(t,T)
$k_P(T)$	rate constant, only a function of temperature
$g(t,T)$	parameters and quantities, which influence Vp
$f\left[P(t,T); g(t,T)\right]$	specification of the kinetic formulation
S	= +1: P increases with time = - 1: P decreases with time

The temperature dependency of k_P is represented by the known Arrhenius equation for chemical reactions, eq.(2).

$$(2) \quad k_P(T) = Z_P \cdot \exp(-Ea_P/RT)$$

The Arrhenius parameters Z_P (preexponential factor) and Ea_P (activation energy) are determined from the experimental k_P - values with eq.(2). The temperature ranges for the investigation of the ageing are so small that Z_P and Ea_P are not dependent on temperature, if there are no mechanistic changes in the course of the reaction. The rate constants can be calculated for any storage temperature using the data from this evaluation. Together with the integrated form of eq.(1), the storage times can be determined. The best way of achieving this is by defining the safe service life and storage time using so-called degrees of degradation or degrees of change y_P for the property P.

$$(3) \quad y_P = \frac{\text{limit value for P}}{\text{original value of P}} = \frac{P_L}{P(0)} = \frac{P(ty_P(T))}{P(0)}$$

The $ty_P(T)$ are the times at temperature T after which the limit value P_L is achieved. These $ty_P(T)$ are the desired storage times at temperature T. P(0) is the value of P after manufacture or at the beginning of the ageing. The value of y_P depends on the property P, the accuracy of the measured data and the safety factor. In the most cases the integrated form of eq.(1) is used. There are methods which measure directly the rate dP(t,T)/dt, for example heat generation measured by heat flow microcalorimetry or NO_x-production measured in a flow technique. One can also define such degrees of change for the rate, $y_{dP/dt}$. At the time there is only little experience for the application of $y_{dP/dt}$. But each quantity can be transformed mathematically from P to dP/dt and vice versa. The method using y_P can be extended immediately for different time-temperature stresses, if the time and temperature data have been determined. A good prediction is obtainable only by fulfilling the following conditions:

- the suitable properties P must be selected
- the properties P must be measured with high accuracy
- the description according to eq.(1) must reproduce the measured data very well
- the description according to eq.(1) must extrapolate the data very well in the time axis
- the appropriate temperature dependence of $k_P(T)$ must be found
- the right temperature range must be used.

As an example for eq.(1) and eq.(3) a reaction of first order is given.

(4) $$A \xrightarrow{k_A} B$$

(5) $$\frac{dA(t,T)}{dt} = -k_A(T) \cdot A(t,T) \qquad \text{and} \qquad A(t,T) = A(0) \cdot \exp(-k_A(T) \cdot t)$$

(6) $$y_A = \frac{A_L}{A(0)} = \exp(-k_A(T) \cdot ty_A(T)) \quad \text{and} \quad ty_A = \frac{1}{k_A(T)} \cdot \ln\frac{1}{y_A}$$

The usual kinetic formulations do not contain the variable time on the right hand side in the differential equation. There are ageing processes, which can be described using such modified formulations. However, the rate expressions given below are more of an empirical nature. Layton /4/ found that the mechanical properties like tensile strength and strain at break can be described using the following formulation:

(7) $$\frac{dP(t,T)}{dt} = -k_P(T) \cdot \frac{1}{t} \qquad \text{and} \qquad P(t,T) - P(t_0) = -k_P(T) \cdot \ln\frac{t}{t_0}$$

The change of P is logarithmically in time. In the case of this formulation, a reference time $t_0 \neq 0$ must be selected.

Another formulation, which was found for the migration of burning catalysts /5/, states the following:

(8) $$\frac{d\left(P(t,T) - P(\infty)\right)}{dt} = -k'_P(T) \cdot \frac{P(t,T) - P(\infty)}{\sqrt{t}}$$

and in the integrated form:

(9) $$P(t,T) - P(\infty) = \left(P(0) - P(\infty)\right) \cdot \exp\left(-k_P(T) \cdot \sqrt{t}\right) \qquad \text{with} \quad k_P(T) = 2 \cdot k'_P(T)$$

P(0) may be equal to zero. This equation can start at t = 0 and has a similar characteristic as a logarithmic dependency. However, $P(\infty)$ must be known. If it is not, it must be determined from the data per numeric fitting. Again the constant $k_P(T)$ in both formulations represents the rate constant dependent only on temperature, but $k_P(T)$ may be a composite quantity. Fig. 1 shows an application of eq.(9) for the migration of ferrocene-type burning catalysts at 70°C /5/. As a means of prediction, these empirical rate equations are equivalent to those which are build upon a model in so far as they are able to extrapolate the data in the right manner along the time axis.

3.3.2 Description using the "time until the set degree of change has been reached"

A further method, which must be considered as pragmatical, is to determine the time up to a given change in a quantity P, e.g. the time to achieve a decrease down to say 30% of the initial value of the quantity P. This is also a time $ty_P(T)$. But the rate equation associated with the change of P is unknown. According to this method no rate constants are determined. If one needs a mathematical function to describe the data, one uses for example the spline fitting. The reciprocal time to achieve the given limit is proportional to a reaction rate constant, but only if k and t are coupled linearly in the rate expression on which the change of the quantity is based upon.This is shown for a reaction of first order, eq.(6) and the eq.(9) for the migration. From eq.(6) one obtains with $y_P = 0.3$, eq.(10),

(10) $$\frac{1}{t_{0.3}(T)} = k_P(T) \cdot \frac{1}{\ln\frac{1}{0.3}}$$

In the case of a reaction of the 2nd order, there exists also a simple proportionality between $k_P(T)$ and $1/ty_P(T)$. However this is no longer valid with the equation for the migration, if Arrhenius behaviour is assumed for $k_P(T)$. From eq.(9) one gets:

$$(11)\quad \ln\left(\frac{0.3\cdot P(0)-P(\infty)}{P(0)-P(\infty)}\right) = -k_P(T)\cdot\sqrt{t_{0.3}(T)} = C$$

In this case $\sqrt{t_{0.3}}$ must be taken. If $t_{0.3}$ is used, the following results:

$$(12)\quad \frac{1}{t_{0.3}(T)} = \frac{1}{C^2}\cdot(k_P(T))^2 = \frac{1}{C^2}\cdot Z_P{}^2\cdot\exp(-2\cdot Ea_P/RT)$$

One would determine twice the activation energy. It can be seen that purely empirical procedures conceil the danger of resulting in faulty evaluations, if one uses the value of the activation energy as an assessment parameter. Therefore special care must be taken when starting ageing studies with unknown systems and materials. The method outlined here also demands for a good prediction more experimental data than a model-based evaluation.

4. KINETIC MODELS

4.1 Molar mass decrease

A kinetic model is given, which is based on the statistical chain splitting of a polymer by the decomposition of chain elements /6/. It is independent of the polymer type. The polymer sample consists of n chains, in which the chain elements E (monomer units) with mass m have been numbered from 1 to N. The number of monomer units decrease according to a reaction of first order. A detailed formulation of the model can be found in /6/ and /7/. The result is, eq.(13),

$$(13)\quad \ln\left(1+\frac{m}{Mn(t,T)}\right) = \ln\left(1+\frac{m}{Mn(0)}\right) + k_M(T)\cdot t$$

Mn is the so-called absolute number averaged mean molar mass. Gel permeation chromatography (GPC) usually only determines the relative mean molar masses, i.e. relative to narrow distributed polymer standards with which the equipment has been calibrated and the relation between the molar mass and the retention volume of the chromatograms has been established. By comparing the Mn values from GPC and osmometry, which is an absolute method, one arrives at a factor An for the conversion of the relative Mn values into absolute Mn values.

(14) Mn (absolute) = An · Mn (relative)

This factor is an apparatus constant and cannot be transferred to other equipment or conditions of measurement. A better method is the use of detectors which are sensitive to the size of the polymer particles. In this case a relationship between molar mass and retention volume is created at each measurement and the apparatus is calibrated in this manner. This type of detector can be e.g. a low angle laser light scattering photometer or a viscosity measuring bridge.

Using eq.(14) and the polydispersity D, eq.(15),

$$(15)\quad D(\text{relative}) = \frac{Mw(\text{relative})}{Mn(\text{relative})}$$

one can formulate eq.(13) with the relative mass averaged mean molar mass Mw and relative D values:

$$(16)\quad \ln\left(1+\frac{m\cdot D(t,T)}{An\cdot Mw(t,T)}\right) = \ln\left(1+\frac{m\cdot D(0)}{An\cdot Mw(0)}\right) + k_M(T)\cdot t$$

With the introduction of the degree of degradation y_{Mn}, whereby y_{Mn} is equal to y_{Mw} as long as $Mw(t)/Mw(0) \geq 0.4$, (this value should not be reached with GPs and RPs, because the grains are then already very brittle), eq.(17),

$$(17)\quad y_{Mn} = \frac{Mn_L}{Mn(0)} = \frac{Mn(ty_{Mn}(T))}{Mn(0)} \approx y_{Mw}$$

the times $ty_{Mn}(T) \approx ty_{Mw}(T)$ can be obtained by eq.(18).

$$(18)\quad ty_{Mn}(T) = \frac{1}{k_M(T)} \cdot \ln\left(\frac{\frac{1}{y_{Mn}} + \frac{An \cdot Mw(0)}{m \cdot D(0)}}{1 + \frac{An \cdot Mw(0)}{m \cdot D(0)}} \right)$$

An, m, Mw(0), D(0) are values which have been measured or are known, y_{Mn} is given, $k_M(T)$ was determined from the measured data with eq.(16).

An evaluation with this model for the decrease of the mean molar mass of NC in the doublebase RP RLC 470/20/TM5 is shown in Fig. 2. The lines drawn through are the Mw(t) values, which were calculated from the logarithmic expression, eq.(16). The model has a good inherent extrapolation ability for the measurements, which is one of the conditions required to predict storage times precisely. Fig. 3 shows the decrease in Mw for the GP A5020 at 80°C. The solid curve was obtained using all measured data for a storage time between 0 and 60 days, the broken curve was determined using only the values between 0 and 30 days. Both curves are identical up to a degree of degradation $y_{Mw} = 0.4$.

4.2. Stabilizer consumption

The literature refers to a number of formulations, from a reaction of zero order to the evaluation without a relation to reaction kinetics. The molecular processes which cause stabilizer consumption are very complex /8,9/. They do not have to be viewed in detail here as the decrease in stabilizer is needed as a function of temperature and time. A reaction of first order seems suitable for the way in which the stabilizer content S(t,T) decreases, eq.(19).

$$(19)\quad S(t,T) = S(0) \cdot \exp(-k_S(T) \cdot t) \qquad \text{and} \qquad ty_S = \frac{1}{k_S(T)} \cdot \ln\frac{1}{y_S}$$

This model is called "model 1" or the "exponential model" below. An evaluation thereof can be seen in Fig. 4. with the broken curves. The measured data marked with small arrows could not be taken into consideration, as they deviate too much from the exponential behaviour. This model only makes sense for a degree of degradation $y_S \geq 0.3$.

A formal combination of the reactions of first and zero order should represent the stabilizer decrease better, as S(t,T) = zero can be achieved in a finite time using this formulation, eq.(20), in integrated form eq.(21). A detailed description of this kinetic model is given in /10/. The solid curves in Fig. 4 show an evaluation with this formulation, called "model 2" or "exponential + linear model". All measured data are included now in the evaluation, the reproduction of the data is very good.

$$(20)\quad \frac{dS(t,T)}{dt} = -k_S^1(T) \cdot S(t,T) - k_S^2(T)$$

$$(21)\quad S(t,T) = \left(S(0) + \frac{k_S^2(T)}{k_S^1(T)} \right) \cdot \exp\left(-k_S^1(T) \cdot t\right) - \frac{k_S^2(T)}{k_S^1(T)}$$

$k_S^1(T)$ has the dimension of the reciprocal time, $k_S^2(T)$ that of the stabilizer content devided by time. The times $ty_S(T)$ are to be calculated using eq.(22).

$$(22)\quad ty_S(T) = \frac{1}{k_S^1(T)} \cdot \ln\left(\frac{1 + \frac{k_S^2(T)}{S(0) \cdot k_S^1(T)}}{y_S + \frac{k_S^2(T)}{S(0) \cdot k_S^1(T)}} \right)$$

For $k_S^2(T) = 0$ the equation for $ty_S(T)$ corresponding to eq.(19) results. With $y_S = 0$ the times $t_0(T)$ are obtainable by eq.(22). The function according to eq.(21) shows a simple behaviour. It starts at S(0) (the same for all temperatures) and decreases monotonously to the limit " $-k_S^2/k_S^1$ ". This is the reason for the good inherent extrapolation ability of this equation. It is not necessary to measure the stabilizer content until it is nearly zero. The extrapolation of the stabilizer consumption is good as from $S(t,T)/S(0) \cong 0.5$ on. But how far one must measure towards zero is also a question of the accuracy of the measurements. Eq.(21) is applicable also with temperature - time profiles, which is described in /10/ and in the paper of 'F. Volk and M.A. Bohn' on this AGARD-symposium /11/.

4.3 Mass loss

For a long time now mass loss (ML) measurements with GPs and RPs have been standardised and are performed in laboratory glass tubes with loosely inserted ground glass stoppers. This permits gas exchange to take place so that there is always oxygen above the sample. In the case of singlebase and doublebase GPs and doublebase RPs, a nearly linear increase in mass loss can be observed, as shown in Fig. 5 for plasticized NC, after an initial fast increase due to humidity loss and loss of residual solvents. This linear increase is then followed by an increasing rate of mass loss accompanied by the formation of NOx. This is referred to as autocatalysis. Autocatalysis means that a reaction product fosters its formation. A linear increase in mass loss is equivalent with a reaction of zero order for the decrease of the sample mass M(t). The relationship can be represented by a kinetic scheme, eq.(23).

$$(23)\quad A \xrightarrow{k_1} B + C \qquad \text{and} \qquad \frac{dA(t,T)}{dt} = -k_1(T)$$

C is a volatile product. In the case of autocatalysis, the reaction product B reacts with the starting substance, and the following applies for the total decrease in A(t), eq.(24),

$$(24)\quad A + B \xrightarrow{k_2} 2\,B + C \quad \text{and} \quad \frac{dA(t,T)}{dt} = -k_1(T) - k_2(T)\cdot B(t,T)\cdot A(t,T)$$

This must now be applied to the mass loss whereby in eq.(23) and eq.(24) the relative mass decrease $M_{rA}(t) = M_A(t)/M_A(0)$ is used for A(t). The formation of B(t) equals to A(0)-A(t) and the relative mass is $M_{rB}(t) = M_B(t)/M_A(0)$. With the assumption that the mass of B(t) is much smaller than that of A(t) follows $M_r(t) \approx M_{rA}(t)$ and eq.(25) results.

$$(25)\quad \frac{dM_r(t,T)}{dt} = -k_1(T) - k_2(T)\cdot M_r(t,T)\cdot\left(1 - M_r(t,T)\right)$$

Integrating this differential equation of Riccati type using the starting condition $M_r(0) = 1$ gives (omitting variable T) eq.(26).

$$(26)\quad M_r(t) = \frac{1}{2} + \frac{a}{2k_2}\cdot\frac{(a+k_2)\cdot\exp(-at) - (a-k_2)}{(a+k_2)\cdot\exp(-at) + (a-k_2)} \qquad \text{with} \quad a = \sqrt{k_2(4k_1 + k_2)}$$

For $t \to \infty$ one has $M_r(\infty) = \frac{1}{2} - \frac{a}{2k_2} \approx 0$ if $k_1 << k_2$, which is the case for GPs, RPs, NC, see Fig. 6 and /11/.

In general, nitrocellulose does not decompose into 100% volatile components, a black residue remains and the mass loss levels off. In this case eq.(27) can be applied.

$$(27)\quad ML(t,T) = O + (100\% - L)\cdot\left(1 - M_r(t,T)\right)$$

The constant O can be zero or an offset is taken into consideration, the plateau level is given by (100% - L). The fitting parameters are the reaction rate constants k_1 and k_2, and also L, if the plateau value has not been reached completely. It is often the case that the products react further according to a reaction of first or second order so that eq.(26) does not provide a good fit, as the course of the data is not symmetrical, whereas eq.(26) runs a nearly symmetrical course around the inflexion point. An equation will be stated below without further discussion, which gives a good description of the course of mass loss, eq.(28),

$$(28)\quad \frac{dM_r(t,T)}{dt} = -k_1 - k_2\cdot M_r^n(t,T)\cdot\left(1 - M_r^n(t,T)\right)$$

where n is a formal reaction order. The differential eq.(28) cannot be integrated analytically, the parameters n, k_1 and k_2 are obtained by a combination of numeric integration and non-linear fitting. An example is shown in Fig. 6 for plasticized nitrocellulose. The values for n, k_1 and k_2 are given in Fig. 6.

Eq.(23) can be used for the usual mass loss measurements. First of all the k-values are determined from the measurements at isothermal storage temperatures and these were then parameterized according to Arrhenius. Also the times up to a mass loss of say 2% can be used according to this method, whereby the reciprocal "time to 2% ML" is proportional to a reaction rate constant. Frequently NO_X is formed around this mass loss value, so that the time up to NO_X formation can also be used. Usually the accelerated rate of ML starts at this point in the case of GPs and RPs based on nitric acid esters. Examples for the evaluations can be found in /12/ and /13/. In /13/ a further example for the linear increase in mass loss is given. In this case batches of 380g of plasticized nitrocellulose were stored in cardboard containers at 70°C, 80°C and 90°C. Even at 90°C no acceleration of the rate of mass loss was found until 7% ML. In the parallel investigations carried out in laboratory glass tubes, the increase of the rate of mass loss always started at 2% ML. The permeability of the cardboard material for the decomposition products is a plausible explanation for the non-autocatalytic behaviour of plasticized NC in cardboard containers.

These results support the description above, which assumes that the first step in the decomposition, eq.(23) is a reaction of zero order, more precise it is apparently a reaction of zero order. If one takes a reaction of first order for the first step, the rate equation is a differential equation of Bernoulli type and the integration gives

$$M_r(t,T) = \frac{k_1(T)+k_2(T)}{k_2(T)+k_1(T)\cdot\exp\left(\left(k_1(T)+k_2(T)\right)\cdot t\right)}$$

Sometimes the approximation $k_2(T) = E \cdot k_1(T)$ with $E \neq f(T)$ is used. This may give an acceptable description, if the autocatalytic reaction is just at the beginning.

To determine the service life of GAP (glycidyle azide polymer), mass loss is a suitable quantity, then it is caused nearly completely by nitrogen loss from the azide groups, which means an energy loss respectively. More about this in paper /11/. In the interesting time periods the mass loss is linear and can be given as:

uncured GAP: ML(t,T) = ML(offset) + 8.64 E+16 [%/d]·exp(-134.0 kJ/mol/R/T) ·t

cured GAP: ML(t,T) = ML(offset) + 7.02 E+17 [%/d]·exp(-141.7 kJ/mol/R/T) ·t.

The ML(offset) depends on the sample and is about 1% to 1.5 %. The time t is in days. The splitting off of nitrogen from the azide group produces a nitrene, which stabilizes itself by insertion reactions. Therefore intermolecular N-C-bonds are formed, the crosslink density increases and the glass transition shifts to higher temperatures, see section 5.

4.4 Heat generation

The following basic equation applies to heat generation (HG):

$$(29) \quad \frac{dQ(t,T)}{dt} \equiv \dot{q}(t,T) = -\frac{dA(t,T)}{dt}\cdot(-\Delta H_R)$$

$(-\Delta H_R)$ is the reaction heat (enthalpy) per unit amount. A(t) is the amount of substance A at time t. The units may be: mol, mass%, mol/l, mass or others. By inserting the rate expressions for first order in eq.(29), one arrives at the following equation for the heat generation, eq.(30).

$$(30) \quad \frac{dQ(t,T)}{dt} = k_A(T)\cdot(-\Delta H_R)\cdot A(0)\cdot\exp(-k_A(T)\cdot t)$$

If all of the substance A has been converted after the time te, the heat $Q(te) = A(0)\cdot(-\Delta H_R)$ has been released. An acceleration of the rate with autocatalytic decomposition of the substance, e.g. in the case of nitrocellulose, can also be seen in heat generation. In contrast to mass loss as an integral quantity, the derivative dQ/dt is measured here, which is direct proportional to the reaction rate. With autocatalysis a peak-type heat generation is obtained, see Fig. 7. By integrating dQ/dt, a curve is arrived at, which is analogous to that of the mass loss. In this form the eq.(26) from section 4.3 can be taken over directly and used in eq.(31).

$$(31)\quad \frac{Q(t,T)}{Q(te)} = Q_r(t,T) \;\hat{=}\; 1 - \frac{M(t,T)}{M(0)} = 1 - M_r(t,T)$$

Fig. 8 shows the Q(t) values of the measurements from Fig. 7 and the fit using eq.(31) and (26). As Q(t) levels off on a plateau, Q(te) can be determined as the final value of the plateau. Due to the possible "asymmetry" of the Q(t) curves already discussed in section 4.3, the fit is quantitativly not very good. By introducing a consecutive reaction for the product C, now not volatile, to volatile D, in addition to eq.(24), as a reaction of first order and by a separation of the two reactions, the autocatalytic reactions and the subsequent reaction, according to eq.(32),

$$(32)\quad Q_r(t,T) = 1 - f(t,T) - \left(1 - f(t,T)\right) \cdot \exp(-k_3(T) \cdot t)$$

whereby f(t,T) stands for the right hand side of eq.(26), the measurements can be fitted and parameterized very well. The rate constants have the values (in 1/h):

k_{Q1} = 1.596 E-5
k_{Q2} = 1.020 E-1
k_{Q3} = 1.087 E-2

In terms of the reaction mechanism, it must be pointed out that eq.(32) is only an approximation for the complete reaction scheme.

During the normal ageing condition with sufficient stabilizer content, GPs and RPs (based on NC) show a constant heat generation. This means a reaction of zero order. The HG $\dot{q}(t,T)$ is determined at several temperatures, e.g. between 50°C and 90°C and in each case one waits long enough until a constant HG is achieved. This may take up to several weeks with newly weighed-in samples and only one to two days if the 'equilibration' has been completed already. The dQ(t,T)/dt data are parameterized according to Arrhenius, eq.(33).

$$(33)\quad \ln\left(\dot{q}(t,T)\right) = \ln Z_Q - Ea_Q / RT$$

With this, the times after which the propellant has lost what amount of energy at a given temperature can be calculated, eq.(34).

$$(34)\quad Q(t,T) = \int_0^t \dot{q}(t,T) \cdot dt = \dot{q}(t,T) \cdot t$$

However, this assumes that $dQ(t,T)/dt = k_Q(T) \cdot (-\Delta H_R)$ does not change with ageing. This is not true, which can be seen from the data in Table 3.

Table 3: Measured heat generation $\dot{q}$ of some doublebase RPs /14/, the corresponding Arrhenius parameters and the calculated values at 30°C.

temp. [°C]	$\dot{q}$ [µW/g] HV5 not aged 12 years old	HV5 aged at 60°C, 6 yrs.	DB-RP2 acardite II	DB-RP3 2-NO_2-DPA
80	33.9	133.5	30.3	29.4
70	10.9	54.4	10.5	8.1
60	3.5	15.8	2.6	2.0
50	1.0	-	-	-
Ea_Q [kJ/mol]	111.1	105.2	120.2	131.5
Z_Q [µW/g]	8.637 E+17	5.239 E+17	1.925 E+19	8.269 E+20
30°C (calc.)	0.06	0.39	0.04	0.02

Typical values at 30°C of doublebase propellants are about 0.07µW/g, for newly produced propellants they are even lower. The activation energy is between 120 and 130 kJ/mol. Both, activation energy and Z-factor decrease with ageing, but the heat generation values increase significantly. Table 3 shows a few examples. The HV5 propellant, which was stabilized with 2-nitro-diphenylamine (2-NO_2-DPA), and which has been aged for 6 years at 60°C generates four to five times as much heat as the sample, which has not been aged and was approximately 12 years old at the time of the investigation. RP2 with stabilizer acardite II and RP3 with 2-NO_2-DPA as stabilizer have been newly produced propellants. The values at 30°C were calculated from the measurements using the Arrhenius parameters.

Another method of thermal analysis determines the adiabatic selfheating of the samples /15/. The self heat rate and the onset temperature are very sensitive to chemical composition and the formation of autocatalysts or decomposition catalysts, which are produced by ageing.

5. INFLUENCE OF MOLAR MASS DECREASE ON MECHANICAL PROPERTIES OF PROPELLANTS

The degradation of nitrocellulose (NC) in a propellant due to ageing must also be found in the degradation of mechanical quantities such as strain at break ε_R and tensile strength σ_R /16/. The decrease in Mw of the NC of the doublebase RP DBE 44/36 with storage time and at temperatures of 60°C, 70°C, 80°C and 90°C is shown in Fig. 9. The times necessary to reduce the mean molar mass Mw by a certain percentage are shown in a small table. The decrease in tensile strength σ_R with storage time at the same temperatures are shown in Fig. 10, Fig. 11 shows the strain at break ε_R. The course of the mechanical properties is analogously to that of the decrease in molar mass Mw.

The yield stress σ_Y and the brittle stress σ_B and their dependence on the mean molar mass Mn or Mw determines the transition between brittle and ductile behaviour. This is of great importance with propellants. Fig. 12 shows the dependence on mean molar mass Mw of the brittle-ductile transition. The intersection between $\sigma_B = f(T)$ and $\sigma_Y = f(T)$ defines the brittle-ductile transition /17/. Because the small chain decomposition products act as plasticizers, the yield stress curve is shifted back somewhat to lower temperatures. The Fig. 12 shows the situation, if one would have a polymer with lower Mw - value, but without the additional plasticizer effect of the chain decomposition products. Below the transition temperature, the sample breaks in a brittle manner if it is stressed, the surface increases. In the case of high load (strain) rates, the propellant grains even can be shattered . Above the transition temperature, the material is tough and flows away, it is visco-elastic and the surface increases only moderately. This behaviour is very important for the ignition process of a gun propellant. If the surface is increased by the brittle fracture of the grains, triggered by the pressure the grains excert on each other, a dangerous situation can arise where the propellant burns up with increasing rate, and the accompanying pressure waves can lead to a breech blow. This hazard is known. The keyword is "low temperature embrittlement of propellant grains". It is pointed out here that the shift of the brittle-ductile-transition to higher temperature with a decrease in the mean molar mass Mw of the NC of a gun propellant is due to the decrease of the compressive strength σ_B, which is due to the decrease in chain length of the NC molecules.

With DMA (dynamic mechanical analysis) the glass transition temperature T_G can be determined as function of temperature and frequency (strain rate). If the sample shows a systematic shift with frequency ν, one can apply the Williams - Landel - Ferry 'time - temperature - shift principle' (WLF - equation), eq.(35) /17/.

$$(35)\quad \lg\left(a(T,T_0)\right) \equiv -\frac{C_1\cdot(T-T_0)}{C_2+(T-T_0)} = \lg\left(\frac{\nu_0}{\nu}\right) \qquad \text{or} \qquad \frac{T-T_0}{\lg\left(\frac{\nu}{\nu_0}\right)} = \frac{C_2}{C_1}+\frac{T-T_0}{C_1}$$

T_0 and ν_0 are freely selectable reference values of the measured T_G - ν data. The constants C_1 and C_2 are determined from the measurements, than one can extrapolate T_G to higher frequencies, say 5000Hz. This is in the time scale of the ignition of the propellant in the charge chamber of a tank gun. In this way one can predict the T_G values of the propellant grains at the high strain rates during the ignition process. The embrittlement temperatures are even somewhat above the glass transition temperatures /18/. The reason is that for the prevention of brittle fracture longer molecular chain elements must have enough free volume to move than for the movement during the glass transition. These larger free volumes are only available at somewhat higher temperatures than the T_G values. The WLF - equation is applicable to describe the ageing of cured GAP /19/.

6. SUMMERY

Ageing processes in gun propellants (GPs) and solid rocket propellants (RPs) change important properties such as plasticizer content, phlegmatizer content, and stabilizer content, the mean molar masses Mn, Mw, Mz, cross-linking density, mechanical properties like tensile strength, strain at break, elasticity modulus, shear modulus, glass transition temperature and embrittlement temperature. Therefore the ageing processes limit the safe storage time, the safe use time (safe service life) and also change the design data such as maximum pressure, vivacity, muzzle velocity and specific impulse.

Ageing processes must be investigated in order to be able to predict after what time - temperature stress the limits of tolerance will not have been surpassed. In order to do this, quantities connected to the ageing processes must be measured as a function of time and temperature and the measurements must be described in such a way that a separation of the dependence on time and temperature can be achieved. The dependence on temperature is then given as a purely temperature dependent coefficient, called the rate constant and the complete mathematical expression is a rate equation. Examples were given for migration, changes in mechanical properties, decrease in mean molar masses, stabilizer consumption, mass loss and heat generation. For the last two methods also autocatalytic decomposition models have been discussed. By defining the degree of change (degradation) for each quantity, the times can be calculated, at which the given degree of change has been reached. These are the searched for lifetimes. In order to make good predictions, the mathematical descriptions must not only reproduce the measured data accurately, but also must be able to extrapolate them correctly along the time axis. The dependence on temperature of the rate constants must be parameterized in the right way. In doing so, checks must be made if there are different temperature dependencies of the rate constants at the temperatures of investigation and at the temperatures in service. Such differences in temperature dependence are expressed in different Arrhenius parameters. If this is not considered seriously the predictions are wrong especially at low storage temperatures. The model for stabilizer consumption, based on a combination of reactions of first and zero order as well as the model for molar mass decrease, based on a statistical chain splitting process by monomer decomposition, are able to describe and extrapolate the data accurately. They can be used to make reliable predictions.

The mean molar masses of polymers also determine their mechanical properties. The results for molar mass decrease, tensile strength and strain at break of a doublebase RP have shown that the dependence on time and temperature of these three quantities is of a similar type. The decrease of the mean molar mass of nitrocellulose causes a decrease of the compressive strength in the propellant grain, which shifts the brittle-ductile-transition temperature to higher values. In the case of gun propellants this can lead to a dangerous increase of burning rate with the formation of pressure waves, which can destroy the gun by breech blow.

7. REFERENCES

/1/ J.C. Oxley, J.L. Smith, W. Wang, *J. Phys. Chem. 98, 3893 (1994) and 98,3901 (1994).*

/2/ STANAG 2895. "*Extreme climatic conditions and derived conditions for use in defining design and test criteria for NATO forces material.*" NATO - HQ, Bruxelles.

/3/ Allied Ordnance Publication AOP-7. NATO - HQ, Bruxelles.

/4/ L.H. Layton, *Techn. Report AFRPL-TR-75-13, 1975.*

/5/ J. Böhnlein-Mauß, M.A. Bohn, K.-P. Brehler, a.o., *Paper 105,* Proceed. 25th Internat. Annual Conference of ICT, 1994. Fraunhofer-Institut für Chemische Technologie.

/6/ A.Pfeil, H.H. Krause, N.Eisenreich, *Thermochim. Acta 85, 395 (1985).*

/7/ M.A. Bohn, F. Volk, *Proceed. ADPA Predictive Technology Symp., 22-24 June 1993, Orlando, FL, USA.* US Army ARDEC, Picatinny Arsenal.

/8/ F. Volk, *Propell. Expl. (Pyrot.) 1, 90 (1976).*

/9/ N.J. Curtis, *Propell. Expl. Pyrot. 15, 222 (1990).*

/10/ M.A. Bohn, *Propell. Expl. Pyrot. 19, 266 (1994).*

/11/ F.Volk, M.A. Bohn, „*Ageing Behaviour of Propellants Determined by Mass Loss, Heat Generation, Stabilizer Consumption and Molar Mass Decrease*", Proceed. 87th Symp. of the Propulsion and Energetics Panel of the AGARD, Athens, Greece, 1996.

/12/ F. Volk, *Propell. Expl. (Pyrot.) 1, 59 (1976).*

/13/ M.A. Bohn, F.Volk, *"Determination of the Safe Lifetime of a Plasticized Nitrocellulose"*, Proceed. 21st Internat. Pyrotechnics Seminar, 1995, Moscow, Russia.

/14/ M.A. Bohn, F.Volk, *Propell. Expl. Pyrot.17, 171 (1992).*

/15/ M.A. Bohn, F.Volk, *"Adiabatische Selbstaufheizung bei Treib- und Sprengstoffen",Paper 8*, Proceed. 24th Internat. Annual Conference of ICT, 1993. Fraunhofer-Institut für Chemische Technologie.

/16/ M.A. Bohn, F.Volk, G. Wunsch, *Propell. Expl. Pyrot.12, 81 (1987).*

/17/ I.M. Ward, *"Mechanical Properties of Solid Polymers"*, John Wiley, Chichester, 1983.

/18/ H. Schubert, D. Schmitt, *"Embrittlement of gun propellants"*. Proceed. Internat. Symp. on Gun Propellants, 1973, Picatinny Arsenal.

/19/ M.A. Bohn, P. Elsner, „*Torsions - DMA - Glasübergang von GAP/N100 - und HTPB/IPDI - Elastomeren als Funktion der Alterung", Paper 120*, Proceed. 27th Internat. Annual Conference of ICT, 1996. Fraunhofer-Institut für Chemische Technologie.

8. FIGURES

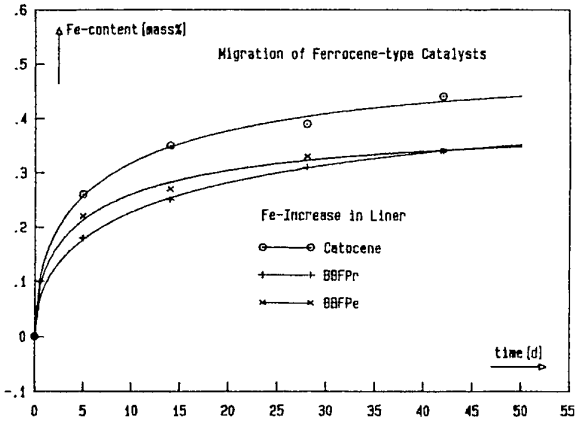


Fig. 1: Migration of ferrocene-type burning catalysts from the propellant into the liner. Lines are the description with eq.(9), /5/.

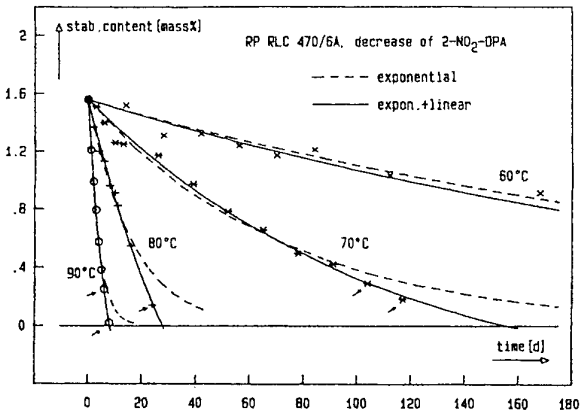


Fig. 4: Description of stabilizer consumption with model 1 (expon.) and model 2 (expon.+lin.).

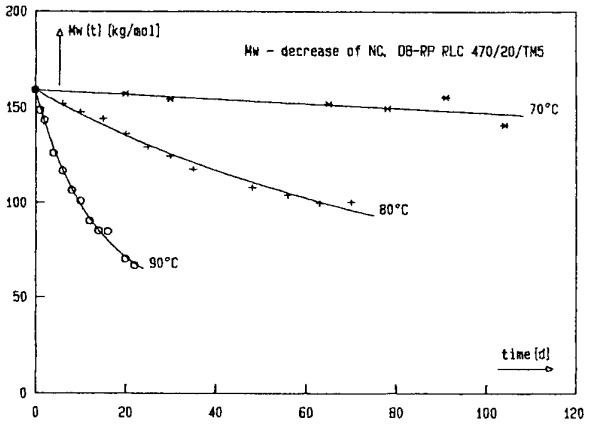


Fig. 2: Reproduction of the measured Mw-data of a RP with the model for molar mass decrease, eq.(16).

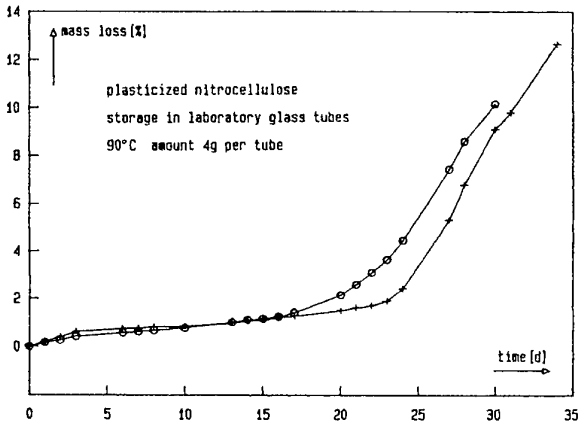


Fig.5: Typical mass loss curves of NC and nitric acid ester based propellants. An autocatalytic increase in mass loss rate follows a linear part.

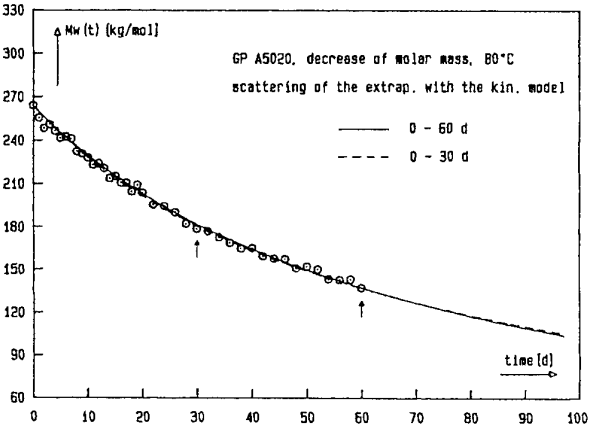


Fig. 3: Extrapolation ability of the model for molar mass decrease, eq.(16).

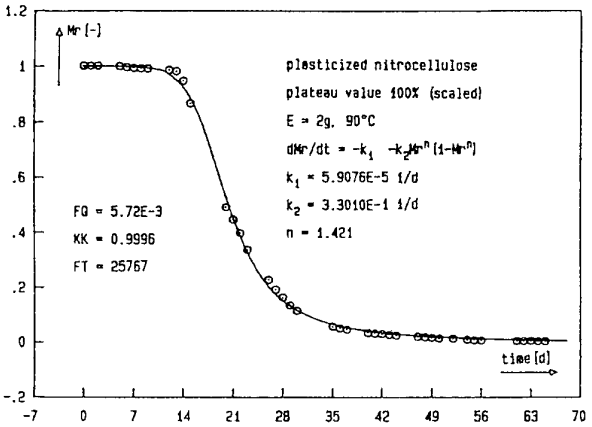


Fig. 6: Description of the mass loss data according to eq.(28). The plateau value of 50.3% is scaled to 100%. M_r = 1 - ML/100%

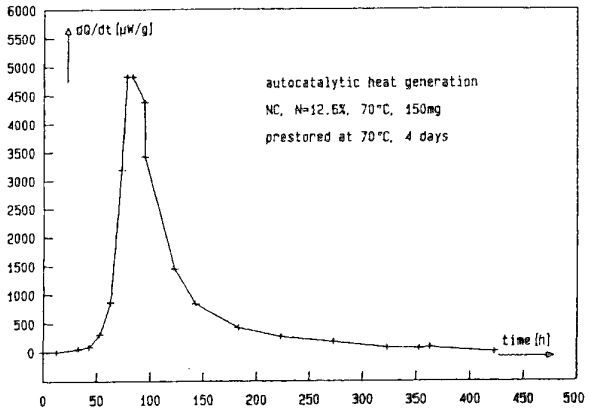


Fig. 7: Heat generation of a NC sample with autocatalytic acceleration.

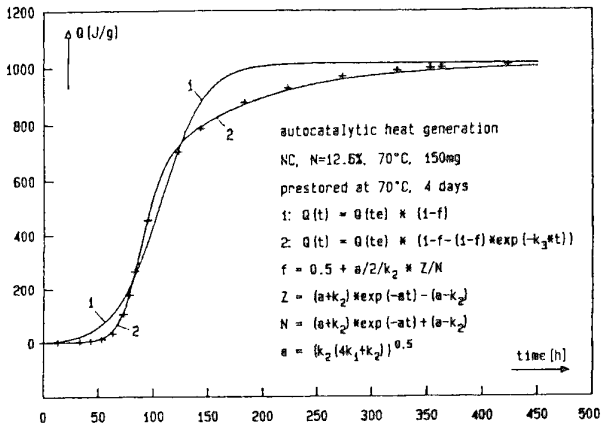


Fig. 8: Description of the heat generation of Fig. 7 with an autocatalytic model based on eq.(26), curve 1, and eq.(32), curve 2. The crosses are the measured data.

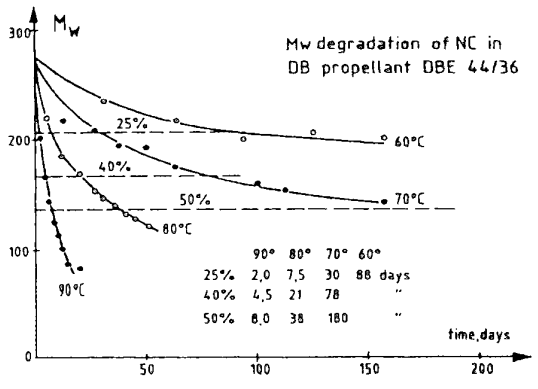


Fig. 9: Decrease of mean molar mass Mw (mass average, from GPC) of double base RP DBE 44/36. The unit of Mw is kg/mol.

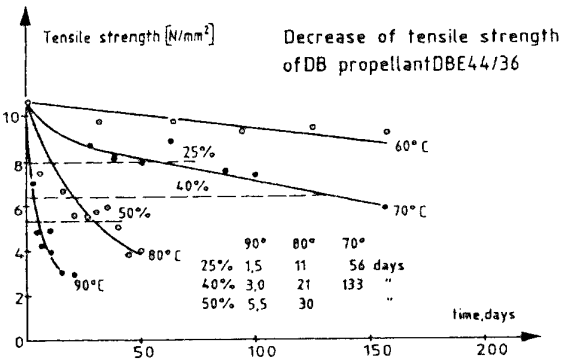


Fig. 10: Decrease of tensile strength of double base RP DBE 44/36 with decreasing molar mass Mw.

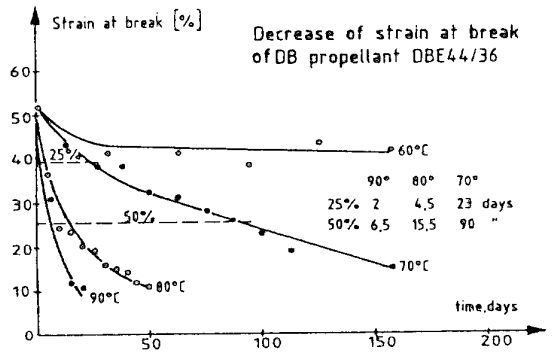


Fig. 11: Decrease of strain at break of double base RP DBE 44/36 with decreasing molar mas Mw.

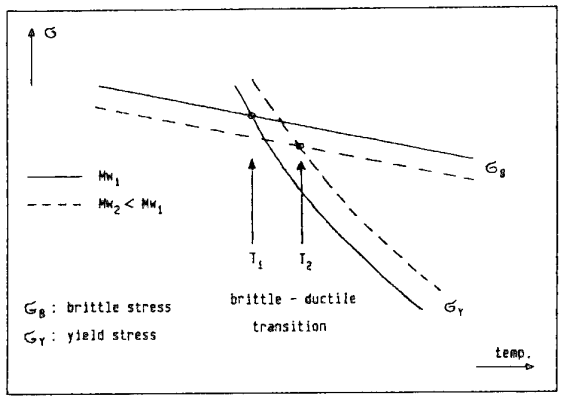


Fig. 12: Shift of the brittle - ductile transition (intersection of brittle and yield stress) with decreasing molar mass Mw.

Caractérisation et modélisation du vieillissement des propergols solides

C. PERUT, S. CHEVALIER, L. MINGUET

S.N.P.E
Division Propulsion

Centre de Recherches du Bouchet - BP n° 2
91710 VERT LE PETIT

FRANCE

RESUME

La méthodologie des études de vieillissement est associée aux études de formulation, de la mise au point du propergol au stade laboratoire jusqu'à sa caractérisation sur site industriel, afin d'intégrer la préoccupation durée de vie dès la conception d'une composition.

La caractérisation des compositions nouvelles est réalisée sur des maquettes moulées-collées qui sont soumises à un conditionnement isotherme ou à un cyclage thermique représentatif de missions aéroportées. Les expertises réalisées fournissent les éléments nécessaires à l'évaluation de la durée de vie d'un chargement moulé-collé réalisé avec le propergol caractérisé sur maquette [1]. Les résultats obtenus sur une composition à fumée réduite catalysée par du Butacène ® a permis de montrer son bon comportement en vieillissement, ainsi que pour les matériaux d'aménagement interne associés, après un cyclage thermique représentatif de 6 ans de vie opérationnelle.
Ces expérimentations permettent également de préciser, dans des conditions d'ambiance et de sollicitations mécaniques représentatives de celles prévalant dans un chargement, les phénomènes de migration et les gradients de propriétés mécaniques.

ABSTRACT

The aging study methodology is joined to the propellant formulation researches from the aging behavior optimisation at laboratory scale to the characterization.
The characterizations are realized on case - bonded mock-ups which are subjected to thermal cycles designed to accelerate the aging produced by environment incountered in airborne applications. 2 months cycle is expected to simulate 1 year of service life. The mock-ups are dissected after 1 or 2 years. The testing are mainly directed at looking at changes in propellant and bonding mechanical properties. The results may be used to assess the service life of a rocket motor loaded with the propellant tested [1].
The experimentations conducted during 1 year on a reduced - smoke propellant containing Butacene ® as burn rate catalyst show the good aging behavior of this composition.

1 - INTRODUCTION.

La connaissance de la durée de vie des moteurs à propergol solide est une donnée essentielle pour l'utilisateur. Elle passe par le calcul de l'évolution de la fiabilité au cours du temps. Celui-ci intègre le comportement du chargement au cours des sollicitations thermo-mécaniques intervenant lors du stockage et des phases opérationnelles et lors de la mise en pression rapide résultant du tir ; les défaillances les plus fréquemment redoutées sont la fissuration du chargement et le décollement du bloc de la structure. Il nécessite la connaissance précise de l'évolution des propriétés du propergol et des assemblages associés.

Paper presented at the AGARD PEP Symposium on "Service Life of Solid Propellant Systems" held in Athens, Greece, 10-14 May 1996, and published in CP-586.

En raison de l'importance du comportement en vieillissement, la méthodologie utilisée dans ce domaine doit être étroitement associée aux études de formulation, de la mise au point jusqu'à la caractérisation des matériaux. Elle se déroule en plusieurs phases : la recherche des constituants des propergols les mieux adaptés (ex : antioxydant), l'étude des mécanismes physico-chimiques intervenant au cours du vieillissement et la caractérisation des nouveaux matériaux, propergol et matériaux d'aménagement interne. Cette méthodologie s'applique aux propergols à liant actif et aux propergols composites à liant inerte avec toutefois des spécificités. Il ne sera présenté ici que l'aspect correspondant au 2ème type de composition. La partie caractérisation sera particulièrement développée. Elle a principalement pour objectif de déterminer l'évolution des matériaux dans des conditions d'ambiance et de sollicitations représentatives de celles prévalant dans un chargement. Les données sont en particulier destinées à être utilisées par le motoriste pour évaluer la durée de vie d'un moteur utilisant les compositions testées. Ceci est illustré par l'article présenté par B. HERRAN et J.C. NUGEYRE [1]

2 - MECANISMES DE VIEILLISSEMENT.

Au cours du temps, les propergols sont susceptibles de subir des modifications chimiques qui sont de nature à modifier leurs propriétés, en particulier mécaniques. Pour les propergols composites dont le liant est formulé à partir d'un polybutadiène, l'évolution la plus fréquemment citée est le durcissement [2.3]. Celui-ci est lié à l'augmentation de la densité de réticulation qui résulte de réactions chimiques en chaîne de type radicalaire faisant intervenir les doubles liaisons du polymère. Les réactions mises en jeu sont fortement accélérées par la température. Les effets sont fortement amplifiés lorsque l'ambiance régnant au dessus du propergol est de l'air. Le processus est alors gouverné par les échanges qui s'établissent avec l'atmosphère, le degré d'oxydation au sein du propergol n'est pas uniforme et il apparaît un gradient de propriétés mécaniques qui s'amplifie au cours du temps. Ce phénomène peut être activé lorsque des catalyseurs de combustion contenant des métaux de transition sont incorporés dans le propergol.
L'influence de l'humidité dépend fortement de la nature du prépolymère utilisé. Les propergols à base de polybutadiène carboxytéléchélique sont le siège d'une réaction d'hydrolyse qui conduit à la rupture des ponts formés lors de la réaction de réticulation. Ce phénomène, de nature irréversible, conduit à un affaiblissement des propriétés mécaniques [4]. L'utilisation du polybutadiène hydroxytéléchélique permet de l'éviter.
D'autres éléments sont à prendre en compte telle que la migration des plastifiants dans les matériaux d'aménagement interne ce qui peut provoquer un durcissement du propergol près de l'interface et modifier le comportement mécanique des collages [5-6]. L'appauvrissement de cette zone en plastifiant peut également conduire à une augmentation locale de la vitesse de combustion. La répercussion sur le comportement balistique du chargement dépend fortement de sa géométrie. Elle est particulièrement importante pour les blocs à combustion frontale.
Les catalyseurs ferrocéniques liquides sont également susceptibles de migrer dans le lieur et la protection thermique et à la surface libre. Dans ce dernier cas, il peut s'en suivre une augmentation de la sensibilité du propergol en surface. Ceci peut être évité en utilisant le Butacène ® qui est un polybutadiène hydroxytéléchélique sur lequel sont greffés des groupements ferrocéniques par réaction d'un silane sur les vinyles [7-8].
Pour les propergols à liant actif, il y a lieu de prendre en compte le vieillissement fissurant qui résulte de la dégradation dans le temps des esters nitriques. Ils sont par contre moins sujet au vieillissement durcissant que les compositions à liant inerte à base de polybutadiène. Le présent article ne porte que sur les propergols composites à liant inerte.

3 - METHODOLOGIE DES ETUDES DE VIEILLISSEMENT.

La méthodologie des études de vieillissement prend en compte les propergols et les assemblages associés. Pour un type de matériau donné, elle se déroule en trois phases qui accompagnent les études de formulation, de la mise au point du matériau au stade laboratoire jusqu'à la caractérisation sur le site industriel en passant par l'étude des mécanismes mis en jeu lors du vieillissement.

Phase 1 : sélection des ingrédients et étude comparative.
L'objectif de cette première phase est de donner des éléments pour orienter les études de formulation. Elle porte sur la sélection de certains constituants (ex : antioxydant) et consiste à effectuer une évaluation du vieillissement à coeur du matériau et à réaliser une comparaison entre les compositions, en ce qui concerne la tenue au vieillissement sous air.

Elle est réalisée :

- sur des mélanges simplifiés d'ingrédients (ex : polymère + catalyseur + antioxydant) en utilisant des méthodes telle que l'analyse thermique différentielle,
- sur propergol, dans ce cas, il s'agit de suivre l'évolution des propriétés mécaniques en fonction du temps. Les essais sont réalisés sur deux types d'échantillon, des éprouvettes de traction mécanique et des pavés de 250 g de propergol [9].

Phase 2 : étude des mécanismes et première caractérisation.
Les objectifs de cette phase d'évaluation sont :

- d'identifier les phénomènes mis en jeu et d'évaluer leurs conséquences sur les propriétés mécaniques et les caractéristiques de sécurité,
- d'effectuer une première évaluation en prenant en compte, dans des conditions représentatives, les phénomènes d'oxydation superficielle en présence d'air.

Les conditions retenues actuellement sont les suivantes :

- restitution de l'effet de masse, épaisseur de propergol de 60 mm,
- conditionnement en boîte étanche,
- atmosphère : air (ou éventuellement azote),
- température : 60°C,
- durée : 2 ans

La température de 60° C a été retenue pour ces essais parce qu'elle paraît actuellement présenter le meilleur compromis, accélération des phénomènes de vieillissement et représentativité.

Les mesures réalisées portent sur :

- les propriétés mécaniques du propergol et des assemblages,
- le taux des ingrédients pour quantifier les phénomènes de migration des espèces mobiles ou pour évaluer la disparition ou la modification de certains produits (ex : antioxydant).
- le comportement aux épreuves de sécurité.

Phase 3 : caractérisation du vieillissement des propergols et des assemblages.

L'objectif est de caractériser le comportement en vieillissement des propergols et des assemblages associés pour des conditions d'ambiance et de sollicitations représentatives de celles régnant dans les chargements. Les expérimentations sont réalisées sur bloc et sur maquette.

Les blocs, de forme cylindrique et d'une masse d'environ 1,5 kg, présentent, sur une de leurs faces, un empilement protection thermique - lieur. Ils sont mis dans des boîtes étanches en laissant un volume libre dans la partie supérieure d'environ 20 % du volume total et sont conditionnés sous air ou sous azote à 20°C, 40°C et 50°C pour des durées respectives de 15 ans, 4 ans ou 2 ans. Les évaluations portent sur les points suivants :

- propriétés mécaniques des assemblages, traction et pelage,
- concentrations locales des espèces migrantes (plastifiant, catalyseur ferrocénique liquide) ou ayant réagies au cours du vieillissement (antioxydant),
- comportement sécuritaire.

Les résultats sont utilisés directement pour évaluer la durée de vie, lorsque l'application prévue est en bloc libre[1]. Par contre, lorsque la configuration envisagée est de type moulé-collé, les caractéristiques précédantes sont complétées, pour les nouveaux types de propergols, par des expérimentations sur maquette. Celles-ci sont moulé-collées dans une structure acier de 160 mm de diamètre et de 600 mm de long. Le tube métallique est garni intérieurement par une protection thermique sur la moitié de sa longueur.
La totalité du tube est enduit d'un lieur dont la fonction est d'assurer la cohésion du propergol à la structure. Le canal central est de forme étoilée (figure n° 1). Les maquettes sont fermées étanches sous air ou sous azote. Elles sont conditionnées en isotherme ou subissent un cyclage thermique. Celui qui a été présentement retenu, correspond à une mission aéroportée et associe des conditions relatives au stockage et des sollicitations thermiques représentatives d'une mission opérationnelle (figure n° 2) [1]. 2 mois de cyclage représentent 1 an de vieillissement opérationnel. Les maquettes sont radiographiées après chaque cycle pour vérifier leur intégrité. Elles sont expertisées au temps initial et après différentes conditions de vieillissement qui figurent dans le tableau n° 1.

TABLEAU N° 1

MAQUETTE
CONDITIONS DE VIEILLISSEMENT

Température	Ambiance	Durée an
Cyclage	Air	1
"	"	2
"	azote	2
40°C	air	3

Les expérimentations portent sur les propriétés mécaniques du propergol et des assemblages, et sur la concentration des espèces chimiques (tableau n° 2) ceci a conduit à définir le plan de découpe et de prélèvement qui est représenté sur la figure n° 3.

4 - EXPERTISE DES MAQUETTES DE VIEILLISSEMENT.

Les résultats qui sont présentement décrits sont relatifs à un propergol à fumée réduite catalysé par du Butacène ® qui présente une vitesse de combustion à 7 MPa de 33 mm/s. Les expertises ont porté sur les propriétés mécaniques du propergol et des assemblages, les caractéristiques cinétiques et sur la composition chimique locale.

TABLEAU N° 2

Maquette - Expertise

Matériau Domaine d'intérêt	Assemblage	Propergol
- Propriétés mécaniques	Traction sur éprouvettes cubiques - Acier/lieur/propergol - Acier/PT/lieur/propergol	- Courbes maîtresses à coeur du propergol Traction éprouvette JANNAF - Gradient près interfaces - Traction éprouvette H2 - Dureté
- Migration - consommation des antioxydants - Balistique	- Analyse chimique	- Analyse chimique Vitesse de combustion par la méthode ultrasonore

Elles ont été réalisées avant mise en vieillissement et après 1 an de vieillissement accéléré correspondant à 6 ans de vieillissement opérationnel. Les expérimenta-tions se poursuivent pour les points à 2 ans et à 3 ans.

contrôle par radiographie X.

Le contrôle par radiographie X qui est réalisé après chaque cycle de 2 mois n'a pas mis en évidence de défaut après 1 an de vieillissement tant pour la maquette qui a été expertisée que pour les 2 autres qui sont encore en vieillissement.

Propriétés mécaniques du propergol.

Les valeurs obtenues sur les éprouvettes H2 provenant des différents endroits de prélèvement mettent en évidence une bonne homogénéité des propriétés mécaniques à coeur du propergol. Ceci a permis de définir d'une façon satisfaisante les courbes maîtresses à partir des prélèvements d'éprouvettes JANNAF. La comparaison des grandeurs obtenues avant et après vieillissement fait apparaître une faible évolution des propriétés mécaniques qui se caractérise par un léger durcissement (figure n° 4). Les épreuves de traction réalisées sur les éprouvettes H2 mettent en évidence (figure n° 5) :

- l'absence, avant vieillissement, de gradient de propriétés mécaniques au voisinage des interfaces ou de la surface libre,
- après vieillissement, un durcissement du propergol apparaît au voisinage des interfaces, celui-ci résulte, comme en atteste les résulats d'analyse chimique, d'un appauvrissement en plastifiant suite à la migration dans les matériaux d'aménagement interne,
- un durcissement près de la surface libre qui est dû à l'accélération du durcissement en présence de l'air.

Propriétés mécaniques des assemblages.

L'évolution des propriétés mécaniques des assemblages est très satisfaisante. La tenue en traction augmente avec le vieillissement ; la rupture ayant lieu dans la grande majorité des cas dans le propergol, cette évolution s'explique par le durcissement du proprergol au voisinage de l'interface (tableau n° 3).

Analyses chimiques.

Les mesures chimiques réalisées précédemment ayant montré qu'il n'y a pas, pour les propergols au Butacène ®, d'enrichississement en fer de la surface libre, il n'y a pas eu d'analyse concernant cet élément [10]. Les expérimentations ont porté sur le taux de plastifiant et des deux antioxydants. Ces éléments sont extraits du propergol par un solvant. Le dosage est réalisé sur la fraction soluble par chromatographie en phase gazeuse (tableau n° 4).

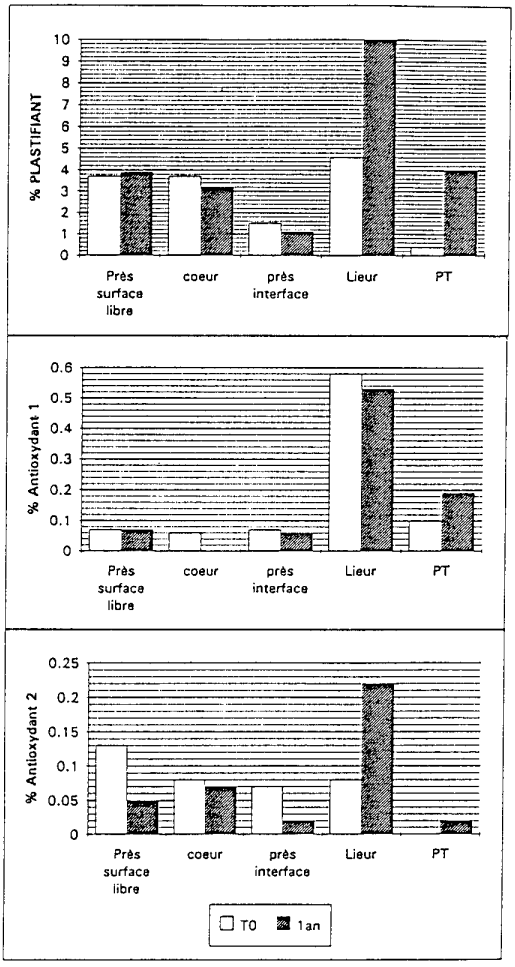
TABLEAU N° 3

EXPERTISE DES MAQUETTES DE VIEILLISSEMENT
EVOLUTION DES PROPRIETES MECANIQUES DES ASSEMBLAGES
EPREUVE DE TRACTION SUR EPROUVETTES CUBIQUES
(SM - MPa)

Cond. traction / Cond. vieillissement	- 50°C 50 mm/mn	+ 20°C 50 mm/mn	+ 60°C 5 mm/mn
- Lieur			
To	3,2	0,78	0,33
1 an de cyclage	4,9	0,91	0,47
PT + Lieur			
To	3	0,79	0,43
1 an de cyclage	3,8	0,93	0,41

TABLEAU N° 4

EXPERTISE DES MAQUETTES DE VIEILLISSEMENT
ANALYSES CHIMIQUES



Plastifiant

Les analyses montrent qu'il y a migration du plastifiant dans le lieur et la protection thermique. Les taux dans ces deux matériaux augmentent avec le vieillissement. Il s'en suit un déficit du propergol en plastifiant près de l'interface. Ce phénomène est responsable du durcissement du propergol au voisinage des matériaux d'aménagement interne.
Il n'y a pas de modification de la concentration près de la suface libre.

Antioxydant 1.

L'antioxydant n° 1 est incorporé dans les trois éléments, propergol, lieur et protection thermique. La consommation au cours du vieillissement est très faible.

Antioxydant 2.

L'antioxydant n° 2 n'est introduit que dans la formulation du propergol. Ce produit migre rapidement dans le lieur et au cours du vieillissement dans la protection thermique. Une consommation importante est à noter au voisinage de la surface libre. Elle est beaucoup plus rapide que celle de l'oxydant n° 1. Ce résultat confirme ceux obtenus sur pavé de propergol qui mettent en évidence une cinétique de consommation environ 2 fois plus rapide pour le produit 1 que pour le produit 2.

Propriétés balistiques.

La mesure de la vitesse de combustion a été réalisée par la méthode ultrasonore dans une large plage de pression. Les résultats obtenus montrent qu'un an de cyclage thermique, correspondant à 6 ans de vie opérationnelle, n'introduit aucune modification de la vitesse de combustion (figure n° 6).

5 - CONCLUSIONS

La méthodologie des études de vieillissement a pour objet l'optimisation du comportement des propergols et des matériaux d'aménagement interne et ensuite de les caractériser. La caractérisation est réalisée sur des maquettes qui sont soumises à des sollicitations mécaniques et thermiques représentatives de celles prévalant dans un chargement et qui sont ensuite disséquées pour expertise. Comme le montre l'article de B. HERRAN et J.C. NUGEYRE [1], les données obtenues peuvent être utilisées par le motoriste pour prévoir la durée de vie d'un moteur utilisant les matériaux testés. Les résultats de ces travaux peuvent également constituer un moyen de validation des simulations numériques de dimensionnement des chargements.

Les expérimentations présentement décrites ont porté sur une composition à fumée réduite catalysée par du Butacène ® ayant subi un vieillissement accéléré représentatif de 6 ans de vie opérationnelle. Elles ont mis en évidence le bon comportement de cette formulation et des matériaux d'aménagement interne.

REFERENCES

[1] - Evaluation de la durée de vie des moteurs tactiques
NUGEYRE J.C.et HERRAN B.
Symposium AGARD n° 87 " Durée de vie des systèmes à propergol solide" ATHENES - Mai 96

[2] - HTPB propellant aging
CHRISTIANSEN A.G. LAYTON L.H and CARPENTIER R.L.
I. Spacecraft Rockets 18 (3) p 211 - 215, 1981.

[3] - Oxidative aging of composite propellant
CUNLIFFE A.V, DAVIS A, and KIRBY F.A
Congres RARDE p 185 - 191, 1989.

[4] - The chemical kinetic approach to service life prediction of propellant systmes
BILLS K.W. , DEPREE D.O., Mc CAMEY R.K. and SMITH R.H.
AIAA 79 - 1243, 1979

[5] - Analysis of DOA migration in HTPB/AP composite propellant
BENNET S.Y and CARPENTIER R.L.
Migration at interfaces
JANNAF Propulsion Meeting, Vol 2, p 53-66, 1983.

[6] - Analysis of DOA migration in HTPB/AP composite propellants
GOTTLIEB L.
Int. Annu. conf ICT, 90/1 - 90/12, 1994.

[7] - Safety and insensitivity improvement by using Butacene ®, a ferrocene grafted HTPB.
B. FINCK, C. PERUT and J. BRUNET
Technology Symposium ADPA, 15 - 18 june 1992
WILLIAMSBURG, V.A. USA

[8] - The maturity of Butacene ® based composite propellants
FOMBLANC G and HERRAN B
AIAA 94 - 3194, 1994.

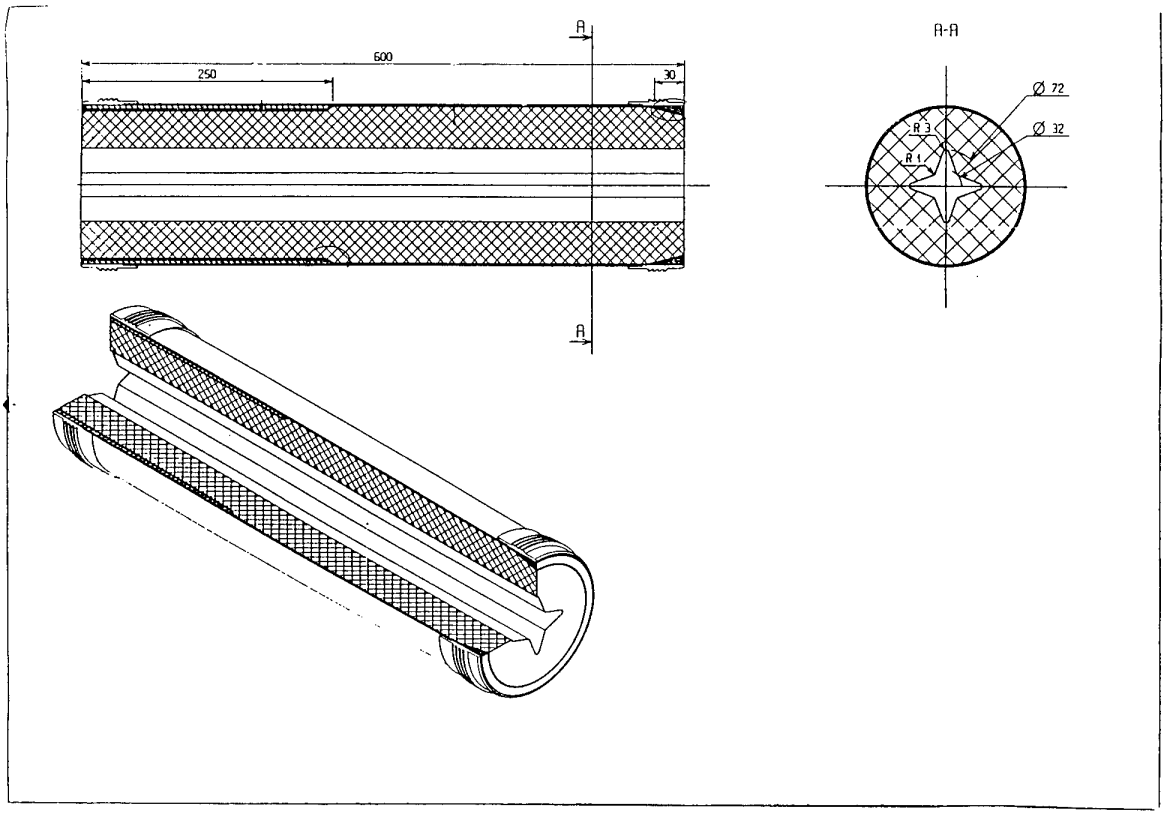


Figure n° 1 : Maquette de vieillissement

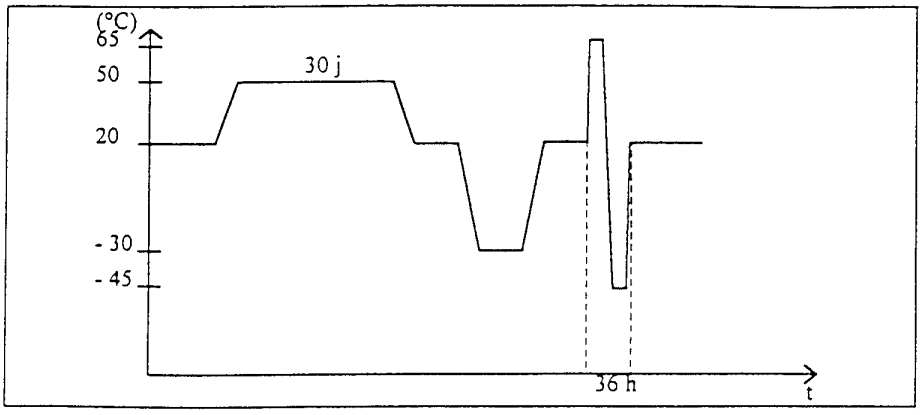


Figure n° 2 : Maquette de vieillissement cycle thermique

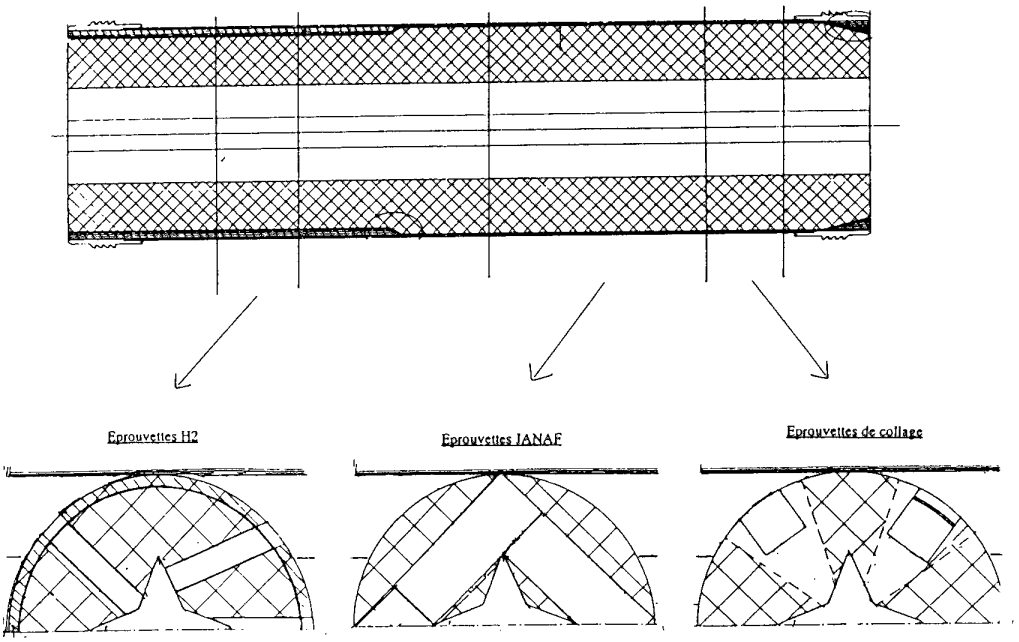


Figure n° 3 : Maquette de vieillissement
Schéma de prélèvement des éprouvettes

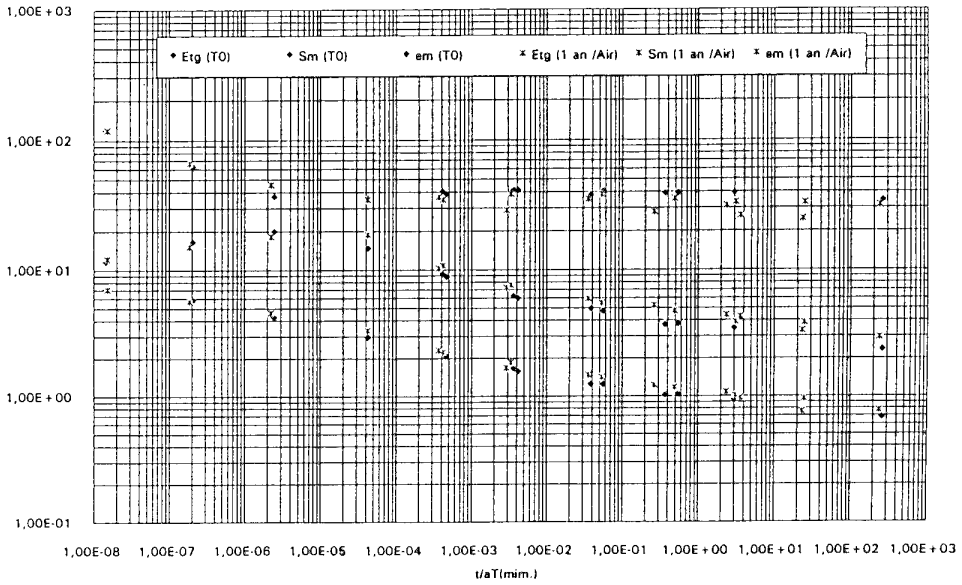


Figure n° 4 : Expertise des maquettes de vieillissement
Propriétés mécaniques du propergol - courbes maitresses

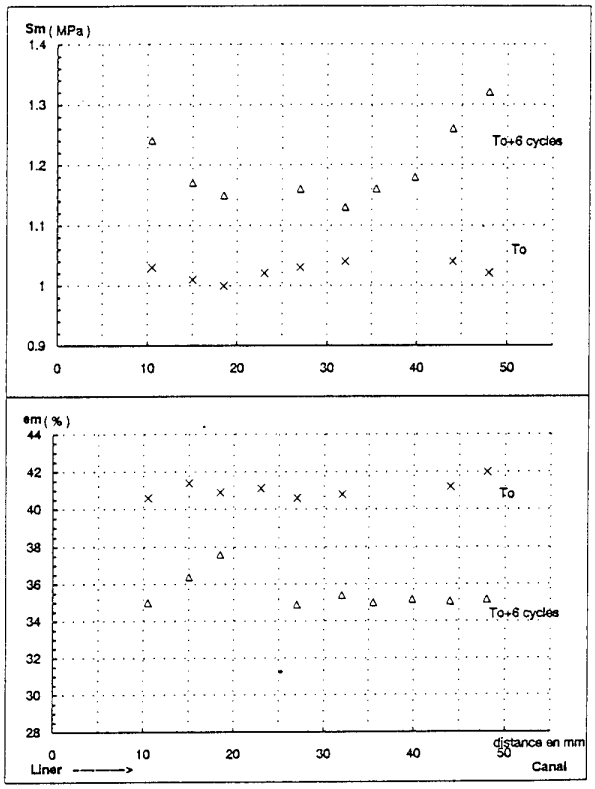


Figure n° 5 : Expertise des maquettes de vieillissement
Evolution des propriétés mécaniques du propergol de
l'interface avec le lieur à la surface libre

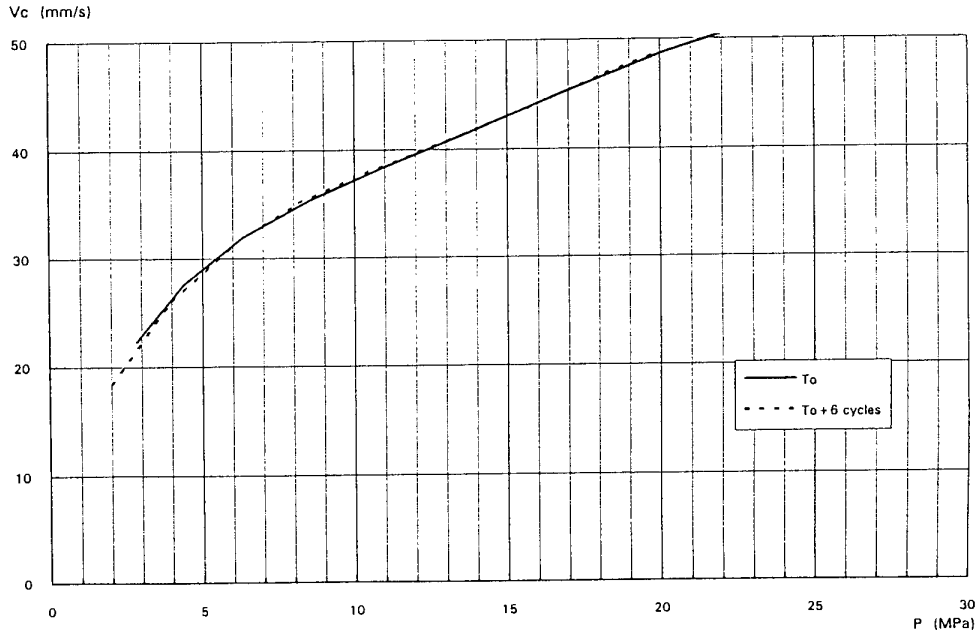


Figure n° 6 : Expertise des maquettes de vieillissement
Vitesse de combustion - Méthode ultrasonore

Paper Number: 3
Discussor's Name: D. I. Thrasher
Responder's Name: C. Perut

Question: Have you done any theoretical work to relate plasticizer migration and chemical changes to the mechanical property changes observed in the analog motors?

Answer: L'approche est principalement experimentale; elle a permis d'etablir des relations:
--pour la migration des plastifiants dans les materiaux d'amenagement interne, entre conditions de viellissement--taux local de plastifiant et, d'une part, les proprietes mecaniques au voisinage de l'interface.
--pour la migration des catalyseurs feroceniques liquides a la surface, entre conditions de viellissement--taux de fer et sensibilite a certaines sollicitations--en fonction de l'augmentation du taux de fer, qui assiste a la diminution de la temperature d'autoinflammation et a une augmentation de l'inflammabilite.

Answer : The approach is primarily experimental, enabling the establishment of the following relationships :

In the case of plasticizer migration in internally structured materials, the relationship is between the local level of plasticizer, (which depends on the aging conditions), and, on the one hand, the mechanical properties and, on the other hand, the overspeed.

In the case of migration of liquid ferrocene type catalysts to the free surface, it is between the iron content at the surface, which is influenced by the aging conditions, and the sensitivity to certain stresses. The increase in iron content is, in fact, accompanied by a decrease in the self-ignition temperature and an increase in inflammability.

Hazard Testing of Ferrocene Propellant in the SRAM-A Motor

Mark Swett
Naval Air Warfare Center Weapons Division
1 Administration Circle
China Lake, California 93555-6001
United States

1. SUMMARY

In June of 1990, the United States Secretary of Defense banned Short Range Attack Missile-A (SRAM-A) from being loaded aboard the B-52, B-1, and F111 bombers. He was concerned that the ferrocene-containing rocket motors could inadvertently detonate and spread plutonium dust over large areas. Tests were conducted to ascertain that the motors were safe enough to be shipped to a facility where they could be properly disposed. The data and methods used to handle the propellant are described herein and may be of interest to anyone contemplating the handling, storing, or formulating of ferrocene-based propellants.

2. NOMENCLATURE

ABL	Allegany Ballistics Laboratory
AP	ammonium perchlorate
CAT	computerized axial tomography
ESD	electrostatic discharge
HPLC	high performance liquid chromatography
HTPB	hydroxyl-terminated polybutadiene
JANNAF	Joint Army, Navy, NASA, and Air Force
RDX	cyclotrimethylenetrinitramine
SRAM-A	Short Range Attack Missile-A
E	Young's modulus, psi
Eo	initial modulus, psi
ε_b	elongation at break, %
ε_m	elongation at maximum tensile stress, %
ε_{tm}	elongation at true maximum tensile stress, %
σ_m	maximum stress, psi
σ_{tm}	true maximum stress, psi

3. INTRODUCTION

The SRAM-A is a 200-inch missile with a nuclear warhead. Its end-burner motor is 83 inches long with a 17.7-inch diameter. Its igniters are placed in the middle and at the aft end, so that the motor can operate as a two-pulse motor. The motor is pressurized with nitrogen gas to ensure the integrity of the weather seal on the aft closure and keep oxygen away from the propellant grain. The propellant grain consists of hydroxyl-terminated polybutadiene (HTPB) with ammonium perchlorate (AP), aluminum, and about 2% n-butylferrocene. N-butylferrocene was used in these motors to increase the burn rate (mass flow) without adversely affecting the slope of the burn rate versus the pressure curve. (High slopes on the burn rate versus the pressure curve require heavier rocket motor cases to contain the pressures developed by the motor. Also, any cracks in the grain of a high slope propellant increase the susceptibility of that motor to initiation or detonation.)

The standard protocol for storing the missile required a check of the nitrogen pressure on the motors every 180 days. From these checks, the Air Force discovered that a number of SRAM-A motors had lost their nitrogen charge. Some of the motors may have been without the nitrogen charge for up to a year or longer. It was estimated that as many as 100 of the motors may have lost their charge at one time or another. There was considerable concern that the lack of nitrogen pressure on the motors would allow oxygen to deteriorate the ferrocene propellant making it very sensitive and, thus, capable of inadvertently initiating or detonating. Two motors had detonated already during surveillance motor firings. One of the motors had been without its nitrogen charge for four years while the other motor for 179 days. Fifteen hundred of these missiles had been built by Lockheed between 1970 and 1975 and a sizable number of them was still deployed across the country at the time of these incidents.

Concern over the SRAM-A ferrocene propellant was high due to the involvement of similar ferrocene-containing propellants in a couple of fatal incidents just a few years prior to the discovery of the depleted nitrogen charge in the SRAM-A motors. These fatalities all involved a ferrocene-type propellant that had been exposed to air. The normal safety tests that had been run on the ferrocene propellants that had caused the fatalities showed that the propellant should not have been as sensitive as it apparently was.

In response to these concerns, the Air Force asked investigators at the Naval Air Warfare Center Weapons Division (formerly Naval Weapons Center), China Lake, to evaluate and test the ferrocene-containing propellant in the SRAM-A motors. At the same time, Boeing Missile Division was investigating all of the historical trends from the rocket motor firings.

4. AGING AND SAFETY STUDIES

A SRAM-A rocket motor that had never lost its nitrogen charge was selected for the China Lake study. The case of the motor was etched off at Hill Air Force Base. Large sections of the propellant were placed in aluminum pressure cookers, purged, pressurized with nitrogen, and sent to the Naval Air Warfare Center Weapons Division, China Lake, for testing.

Approved for public release; distribution unlimited.

Paper presented at the AGARD PEP Symposium on "Service Life of Solid Propellant Systems" held in Athens, Greece, 10-14 May 1996, and published in CP-586.

4.1 Aging Studies

Test specimens were cut out of the propellant blocks and aged. The samples were aged in steel pipes that had one end welded closed with an end plate. The pipes were strong enough to protect the operator from hazards as long as the open end was pointed away from the operator. Great care was taken, while handling the pipes, to never get in front of the open end. A piece of metal screen was placed in the pipes to keep the propellant off the walls. Aluminum foil was placed over the open end of the pipe but was not tightly sealed. Propellant liner from the motor was placed on the inside walls of the pipe to provide a ferrocene rich environment. It had been found earlier that ferrocene can easily migrate; and, indeed, the ferrocene did migrate into the liner changing the burning rate curve. In this fashion, the conditions of the motors were simulated.

The pipes containing the propellant were placed into incubators. The doors of the incubators were removed, and Styrofoam blow-out doors were taped over the openings to the incubators. If there were to be an initiation during testing, the doors would easily blow off and the pipes would provide sufficient separation to prevent any massive detonation effects.

(Ferrocene and AP make a very friction sensitive compound. Since AP is soluble in water, if the propellant were allowed to get wet, the AP would easily dissolve and later precipitate out on the ferrocene causing a very sensitive compound. Any propellant scrap from the sample preparation or completed tests was placed in steel cans containing water soluble oil.)

The aging study was set up to evaluate the propellant with respect to time and temperature. The time intervals were to be 0, 30, 60, 100, 200, 300, and 400 days. One set of specimens was aged at 77°F, while another set was aged at 120°F. (At 135°F, the ferrocene evaporates out of the propellant.) It was estimated that, for every 18 degrees above ambient temperature, the reaction rate would double. (There is some question as to whether this rule of thumb holds true for all HTPB propellants.) Much of the sample preparation was done at the beginning of the aging study to minimize the time that the test operators would be in contact with the aged propellant.

4.2 Hazard Sensitivity and Mechanical Properties Studies

Six tests were selected to evaluate the propellant's safety and handling characteristics. These tests included the following: electrostatic discharge (ESD) test, Allegany Ballistic Laboratory (ABL) sliding friction test, 2.5-kg Bureau of Mines impact test, an experimental laser initiation test, JANNAF Class C dogbone tensile test, and chemical analysis by high performance liquid chromatography (HPLC).

The ESD test normally shocks the specimen with 0.25 joules of energy. This energy is developed with 5000 volts and a 0.25-microfarad capacitor. The voltage level can be lowered until a point is found where 50% of the specimens will ignite. Specimens were also tested to 10,000 volts, which yielded a 1.0 joule spark. RDX was tested in parallel as a known reference. No specimens from the initial sample group ignited during the electrostatic testing.

The ABL friction test is an industry standard. The test uses two sliding metal surfaces with the test specimen between them. The force that is used to push the two metal surfaces is the variable that is measured. For these tests the variable was reported in pounds. This test also aims at finding the level at which 50% of the specimens will ignite. The test gives the operators some confidence that the material tested can be cut, processed, machined or mixed without inadvertent initiation. For RDX, typical numbers for this test are from 450 to 570 pounds. Other HTPB propellants yield numbers between 680 and 1000 pounds or higher. Above 1000 pounds, the test material is smashed so much that it cannot be tested reliably.

The impact test uses a 2.5-kg weight dropped from a known height. In this test, height is the measured variable. RDX is the reference standard. RDX typically yields numbers between 16 and 23 cm. Initial test specimens of the SRAM-A propellant ignited at 11.2 cm.

The laser initiation tests were experimental and were set up to see if any sensitivity changes in the aged propellant could be discerned when variable power from a laser was used to initiate the samples. Attenuating lenses were placed in the beam path to vary the amount of energy illuminating the specimen at any one time. A detector was used to quantify the amount of laser energy that passed through the attenuating lenses. Some problems were encountered getting this test setup to work. In the end, no real conclusions were drawn nor confidence was gained in this method of testing for sensitivity changes.

The JANNAF Class C dogbones are tensile specimens used to measure elongation, stress, strain, and initial modulus. The specimens were tested at 75°F at two rates, 0.1 inches per minute and 1.0 inches per minute. The next group of samples was cooled to -45°F and pulled apart at 1.0 inches per minute and then at 10 inches per minute. The tensile test data for the unaged specimens are presented in Table 1.

The last series of tests was designed to look for ferrocene migration to the surface, changes in ferrocene content, or degradation products as a function of age. Small blocks of propellant measuring 0.5 x 0.5 x 3 inches were cut. These blocks were placed in glass vials that were embedded with epoxy glue in steel pipes. The steel pipes were to contain the glass in the event of an inadvertent initiation. The propellant blocks in their glass-lined containers were placed in 120°F and 77°F aging chambers. At the prescribed interval, the blocks of propellant were removed from the ovens and the exposed edges of the propellant were shaved off the blocks. These propellant slivers were immersed into methanol; ultrasound waves were then applied to dissolve the ferrocene in the methanol. The ferrocene extract was injected into an HPLC C-18 column using 50% methanol and 50% acetonitrile. The wavelength of the ultraviolet detector was set to 254 nanometers.

5. EXPERIMENTAL RESULTS AND DISCUSSION

At the 100-day interval, visual changes in the 120°F aged propellant were noted. The propellant pieces that were closest to the opening in the pipes were turning dark brown; initially, they were a light yellow. Of this aged propellant, the specimens that underwent tensile testing exhibited more strength and less elasticity than the original specimens. At the 100-day mark, the specimens that were aged at 77°F were also getting a little darker, but not nearly as much as the specimens that were being aged at 120°F. This trend continued throughout the entire study. The 400-day final specimens were black, hard, and brittle. When undergoing tensile testing, they yielded the results shown in Table 2. In the meantime, Boeing Missile Division was tracking the test results and looking for correlations. Their correlation graphs are shown in Figures 1 and 2. The results show a peak in brittleness and stiffness and a loss of elasticity at the 200-day interval for the 120°F aged dogbones.

Table 3 provides a summary of the safety data. The safety tests confirmed what was suspected of ferrocene propellants—although they pass the safety tests, they are not safe (i.e., unexpected incidents occur). As the specimens were aged they became somewhat harder to ignite, but once ignited, they would be consumed completely in the test. Some of the aged specimens burned fast enough to become propulsive. Occasionally, unaged specimens would only partially burn. The propellant specimens aged at 77°F and 120°F for 400 days were harder to ignite than the original propellant.

The HPLC analyses were done to explore the hypothesis that ferrocene migrates toward the surface, changes the concentration, and becomes more sensitive locally on the surface. After 300 days, the HPLC studies revealed changes in the surface of both the specimens aged at 120°F and those aged at 77°F. The degradation product was di-n-butylferrocene. The sample aged at 77°F had a 0.18% di-n-butylferrocene content and the one aged at 120°F had a 0.22% di-n-butylferrocene content. The butylferrocene content for the 300-day interval was 2.17% for the samples aged at 77°F and 2.11% for those aged at 120°F. The initial sample had 2.19% butylferrocene. Only one sample exhibited as high a concentration of butylferrocene as the initial sample; all of the others showed slightly lower concentrations. Visual observation of the surface of the aged propellant and the HPLC results suggest that species other than butylferrocene and di-n-butylferrocene may have been forming on the surface. Also, ferrocene may have been migrating to the surface to replenish the ferrocene that was being changed into some other unidentified species. The scope of the tests did not include looking for other degradation or oxidation products. If ferrocene is to be used in any new system, this area should be further explored.

As stated earlier, Boeing Missile Division was also tracking motor firings and burning rates for the test motors that were in the Air Force aging surveillance program. A couple of interesting observations were made by Boeing's researchers and the surveillance group at Hill Air Force Base. As the inventory of SRAM-A motors aged, the burn rate and peak pressure of the motors increased (Figures 3 and 4). The pressure limit of the motor case is a limiting factor for all motors, and the SRAM-A motors were developing pressures that were approaching the case limit design pressure as they aged. Also, a change in the production line occurred when Lockheed built the motors (Figure 5). The motors built late in the production run had higher burn rates than the initial motor production run. Once this trend was uncovered, the subsequent information regarding burn rates and peak pressure with respect to the age of the motor made sense. Another anomaly discovered was that the motors that had spent a lot of time flying under the wing of a B-52 had higher burn rates and peak pressures than the motors of the same age that had been carried inside the bombers.

6. CONCLUSIONS AND CONSEQUENT RESULTS

From the studies conducted by the Naval Air Warfare Center Weapons Division, China Lake, and Boeing, it was determined that the SRAM-A motors could be safely shipped to Hill Air Force Base for destruction and motors that had seen loss of nitrogen pressure for a prolonged period would be taken out of service. Hill Air Force Base continued with its program to conduct computerized axial tomography (CAT) scans and surveillance motor firing for the next couple of years. The system was eventually decommissioned and taken out of service. The SRAM-A was a successful missile that served as a deterrent to nuclear war for almost a quarter of a century.

TABLE 1. Initial Mechanical Properties of SRAM-A Propellant Before Aging.*

Temperature (°F)	Strain Rate (in/min)	Eo (psi)	σ_m (psi)	ε_m (%)	ε_b (%)	σ_{tm} (psi)	ε_{tm} (%)
75	1.0	1025	161.5	20.6	22.8	195.8	21.4
75		1158	164.7	19.4	22.0	198.1	21.2
75		1142	167.0	19.7	22.1	200.7	20.5
75	0.1	963	144.6	20.2	22.3	174.7	21.5
75		956	143.1	19.9	21.6	172.4	20.7
74		905	143.1	20.4	21.2	172.2	20.4
-45	1.0	3824	413.2	19.3	26.9	497.4	21.9
-45		3747	403.3	19.4	26.6	485.4	21.9
-45		3741	419.9	19.5	28.9	509.8	23.4
-45	10.0	9217	598.1	14.3	23.6	694.2	18.0
-46		9292	589.1	14.5	25.4	685.5	18.4
-45		9020	602.0	14.5	23.6	699.4	18.1

* Standard JANNAF tensile specimen.

TABLE 2. Mechanical Properties of SRAM-A Propellant After 400-Day Aging.*

Temperature (°F)	Strain Rate (in/min)	Eo (psi)	σ_m (psi)	ε_m (%)	ε_b (%)	σ_{tm} (psi)	ε_{tm} (%)
75	1.0	1403	183.8	18.6	21.2	219.0	19.6
75		1054	154.1	18.9	19.7	183.5	19.3
75		1006	155.3	20.9	21.7	187.6	20.9
75	0.1	1026	148.1	19.8	21.0	177.7	20.1
75		1222	162.6	18.4	20.5	193.0	19.0
74		837	136.3	22.8	23.8	167.8	23.4
-45	1.0	4535	421.9	16.8	25.0	499.2	19.1
-45		4987	431.1	16.1	20.9	504.0	18.1
-45		5474	433.8	14.7	19.4	502.1	16.5
-45	10.0	9325	576.6	13.1	17.9	657.4	14.8
-46		6458	528.6	17.9	27.2	630.5	20.7
-45		6454	541.2	18.1	23.4	644.4	20.1

* Standard JANNAF tensile specimen.

TABLE 3. Safety Properties of SRAM-A Propellant.

Sample	Average Impact Sensitivity (50%, 2.5 kg, cm)	Impact Sensitivity at Low Fire (2.5 kg, cm)	Average ABL Friction Sensitivity (50%, lbs)	ABL Friction Sensitivity at Low Fire (lbs)	Electrostatic Sensitivity (1 J @ 10,000 V)
Unaged sample	11.2	10.0	417	316	No fire
Sample after 400-day aging at 77°F	13.0	12.5	512	398	No fire
Sample after 400-day aging at 120°F	13.0	10.0	676	501	No fire

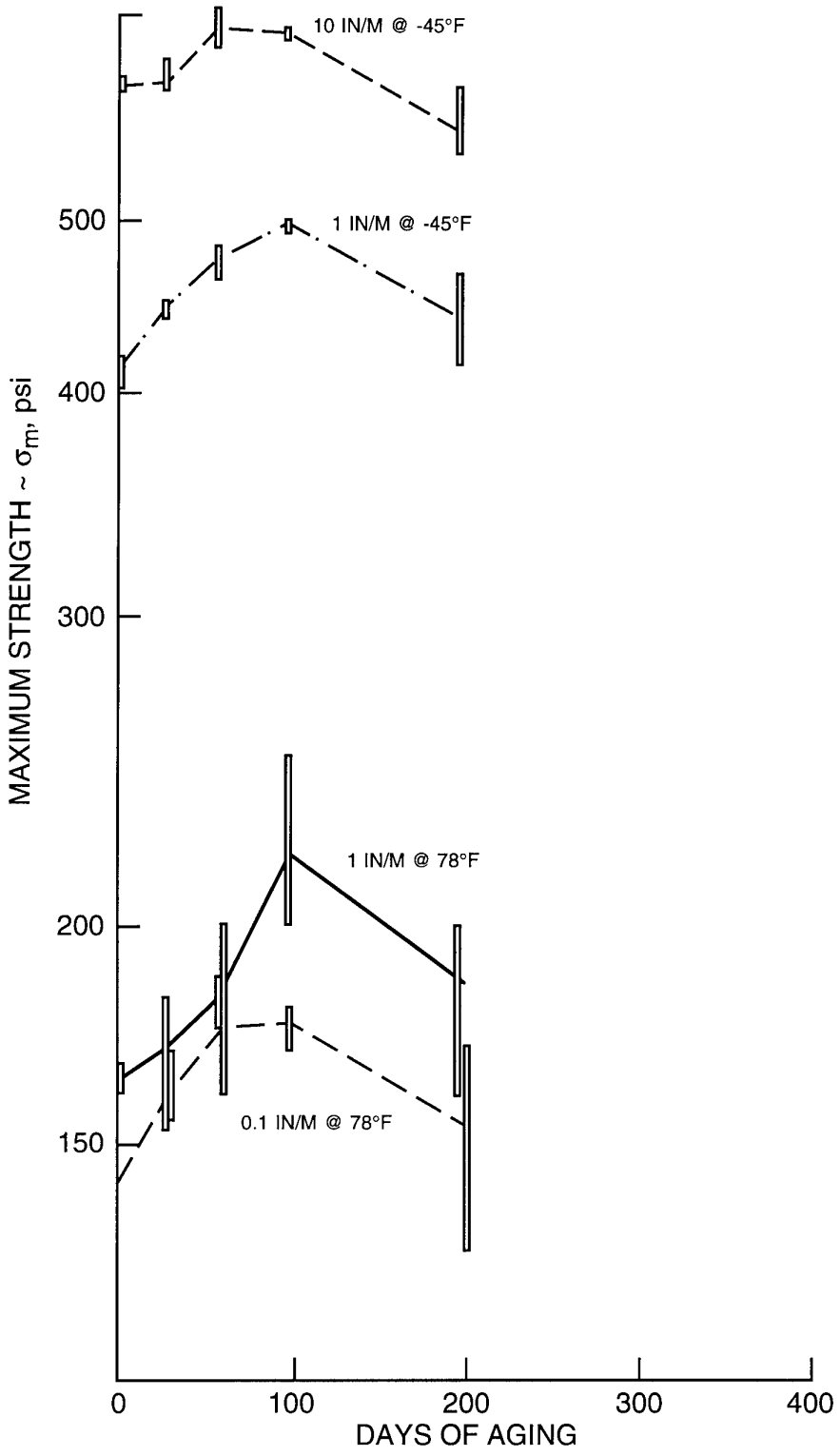


FIGURE 1. Maximum Strength of SRAM-A Propellant After 200 Days of Aging.

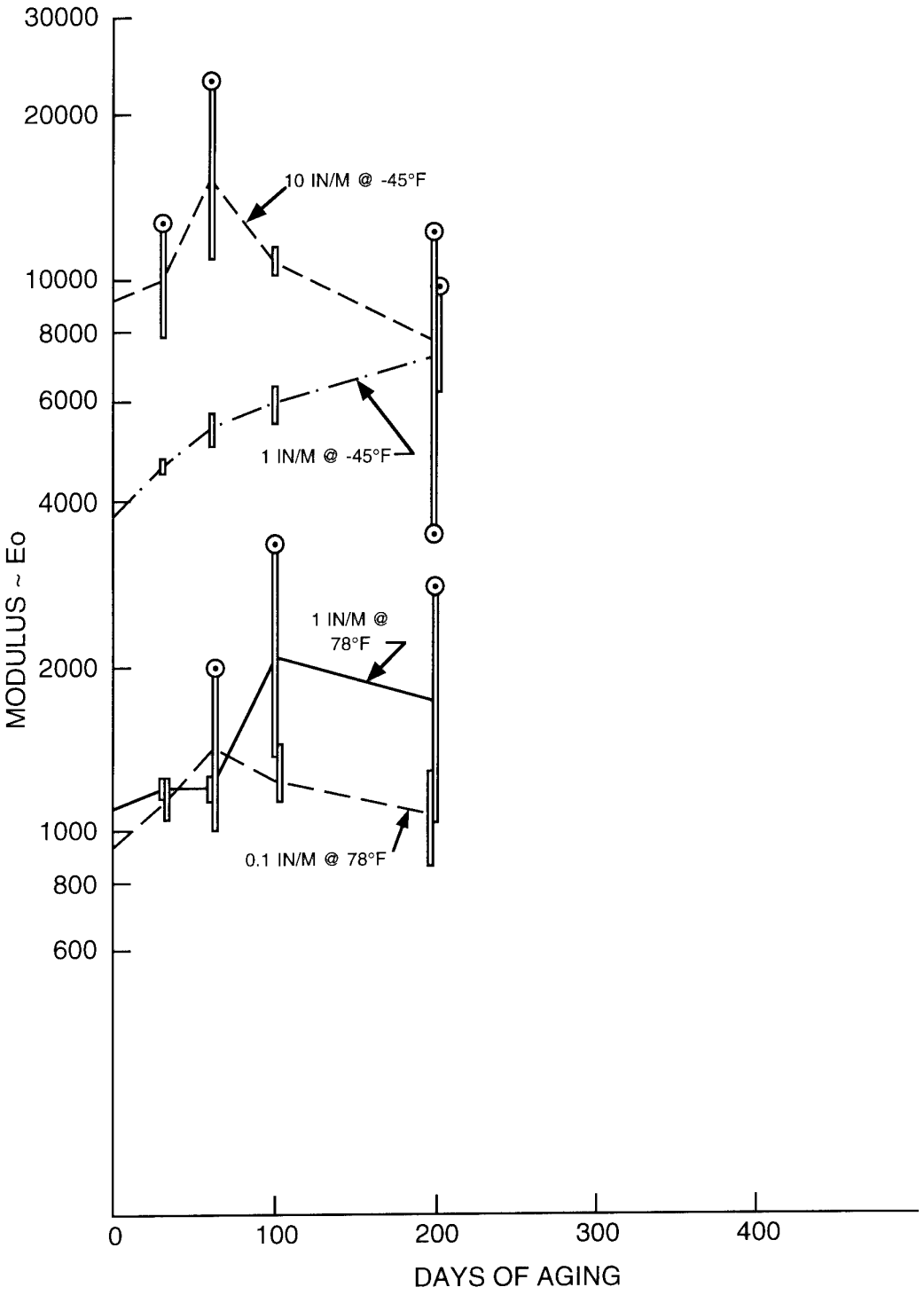


FIGURE 2. Initial Modulus of SRAM-A Propellant at 200 Days.

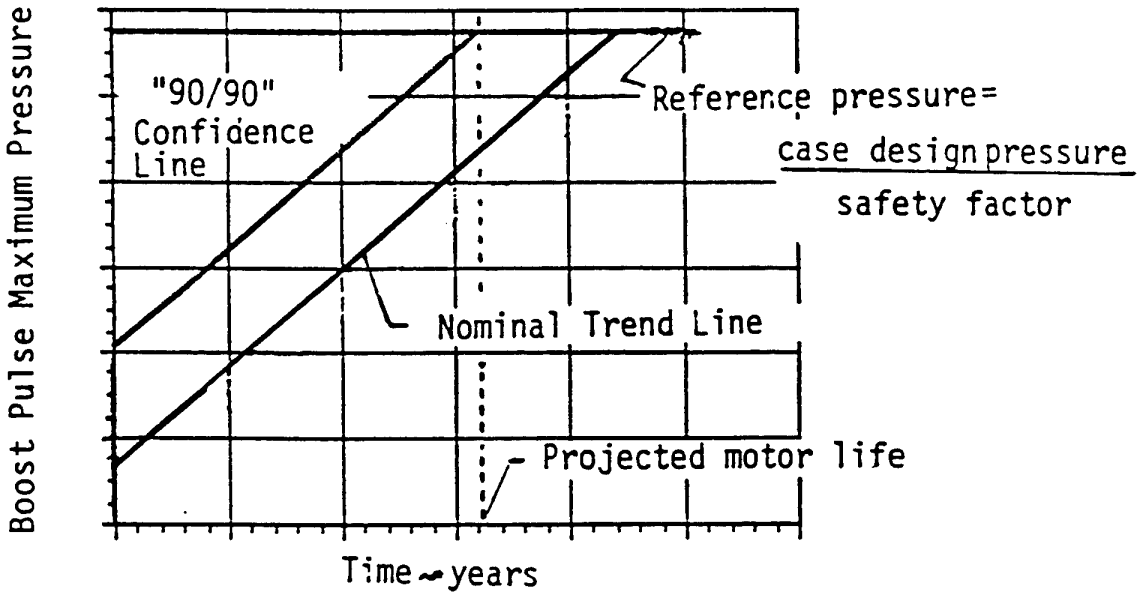


FIGURE 3. Motor Life Projection Method.

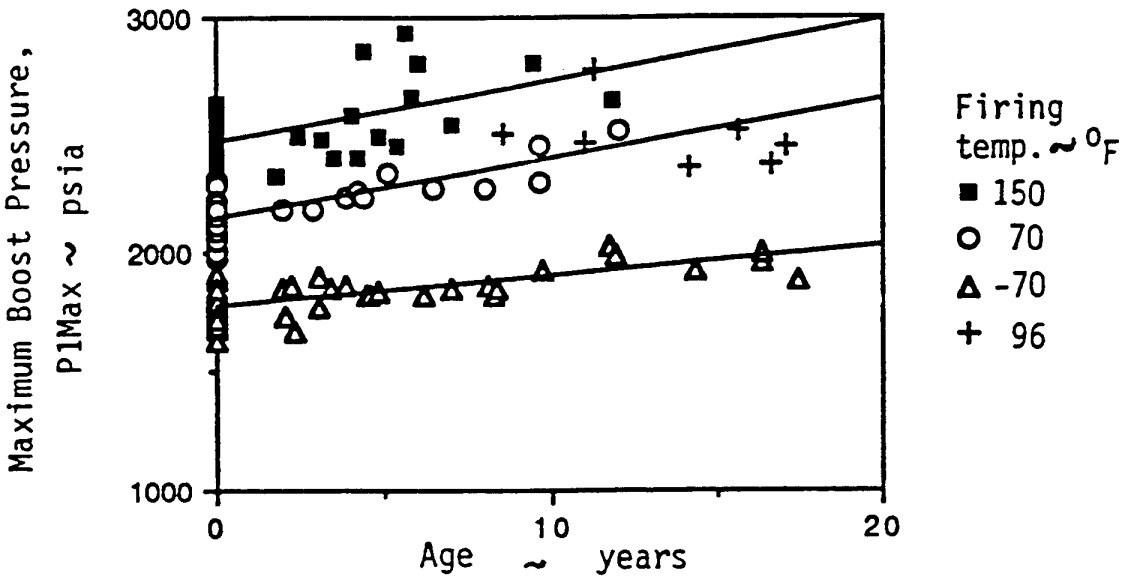


FIGURE 4. Boost Pulse Maximum Pressure.

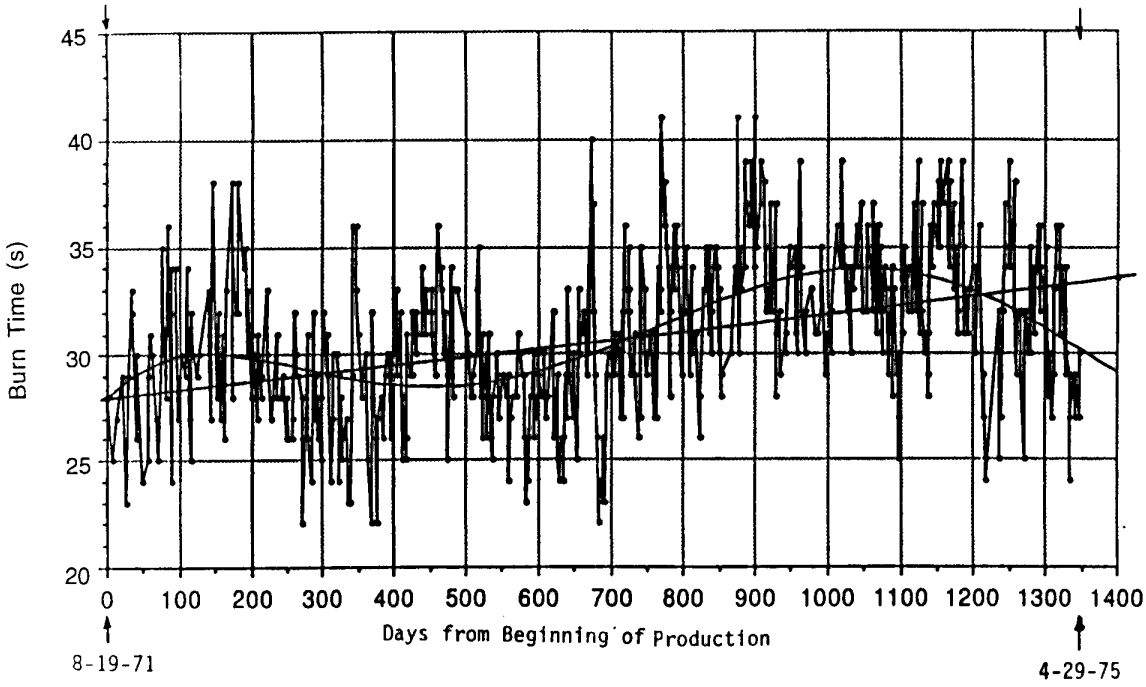


FIGURE 5. Motor Burning Rate Distribution vs. Production Run.

AGEING BEHAVIOUR OF COMPOSITE PROPELLANTS

Jenaro, G.; Rey, F.; de la Cruz, E.; Pérez, V.

Laboratorio Químico Central de Armamento LQCA
Department of Ballistic
P.O. Box 1105, 28080 Madrid, Spain

1. SUMMARY

A study has been conducted to know the effect of ageing over mechanical and ballistic properties of composite propellants.

Natural ageing tests and accelerated ageing tests at elevated temperatures have been performed for five different formulations of rocket propellants; the ageing process has an effect on mechanical, chemical and ballistic properties.

Measurements of tensile, viscoelastic and ballistic properties are reported. A relationship between shore A hardness and tensile properties has been established.

Application of a theoretical prediction model has permitted conclusions to be drawn about service life, effect of environmental conditions and propellant mechanical requirements.

An ageing test and a stability criterium are proposed.

2. INTRODUCTION

Service life of solid rocket motors can be limited by several causes: i.e.deterioration of material mechanical properties, changes in ballistic characteristics and failure in the igniter, propellant or inhibitor.

Several authors [1,2,3] have defined shelf life and distinguished between chemical, physico-mechanical and ballistic shelf life, depending on the aspect studied. Each one of these can limit the service life of a solid rocket motor.

With regard to composite propellants, parameters affecting ageing are: temperature, humidity and thermal fatigue cycles; and parameters affected by ageing are: mechanical -tensile and viscoelastic-, chemical and ballistic properties.

It is necessary to understand the mechanisms of the propellant ageing processes at various storage temperatures. These processes are usually chemical reactions and physical changes in the propellant, and may be different at different temperatures.

The ageing of the propellants at low temperatures is often due to physical processes such as ingredient migration or particle dewetting. At higher temperatures other mechanisms are possible. Among these the typical chemical ageing reactions are: chain scission in the propellant binders, and oxidation process[4].

For this reason it is not always possible to apply artificial ageing data, at elevated temperatures, to natural ageing.

Composite propellants are elastomers containing solid particles and, as in many polimeric applications failure occurs after repeated thermal cycling, in this case cumulative damage must be taken into account. Cumulative damage is attributed to the gradual development and propagation of microscopic tearing or molecular breakdown, following material failure at conditions below expected [5].

Chemical and physical processes bring about changes in mechanical properties and perhaps in the ballistic behaviour; it is interesting for us to know something about the relations between chemical or physical degradation and ballistic properties. Ballistic tests of ammunition give information about the state of the motor, but it is very difficult to make a reliable life time prediction only from this test. This paper wishes to illustrate the effect of ageing over mechanical and ballistic properties and its implication in the service life of solid rocket motors.

3. THEORETICAL BACKGROUND

A solid fuel rocket motor consists of a center perforated elastomeric cylinder (propellant) externally bonded to a metal casing (motor case) with an igniter in aft or bottom position. Both the propellant and the igniter have undergone the same environmental conditions. In this paper we do not study the effect of ageing over pyrothecnic compositions.

Typical behaviour of composite propellants is viscoelastic. Despite this, linear elastic analysis is usually used to predict service life through structural requirements.

Tensile properties

In practice the propellant grain is subjected to mechanical loads from daily temperature cycling; the loss in the strain capability of the propellant is the consequence of chemical ageing combined with cumulative damage, and can lead to overpressure and perhaps explosion in the motor during

Paper presented at the AGARD PEP Symposium on "Service Life of Solid Propellant Systems" held in Athens, Greece, 10-14 May 1996, and published in CP-586.

working conditions. This is a consequence of cracking and may occur when the strain level is close to the strain capability of the propellant.

Evolution of tensile properties has been studied by several authors [7, 8, 9, 10].The knowledge of these properties and the evolution with ageing are both required to predict the service life of rocket motors.

Given the difficulty of obtaining samples from service rocket motors, it is interesting to perform non-destructive tests enlightening their relationship with tensile or viscoelastic properties. As regards tensile properties: i. e. strain capability and Young's Modulus, there seems to be a correlation between them and hardness. G.S.Faulkner [6] has developed a specialized instrument: the penetrometer.

Viscoelastic properties

Since propellants are usually viscoelastic we may consider the stress to consist of two components: one in phase with the strain and the other ninety degrees out of phase with the strain.

The ratio of each component of the stress to the maximum strain ε_0 are the two respective components of the modulus.

The former is the dynamic storage modulus (G') or the amount of energy stored elastically upon deformation and recovered per cycle. The latter is the dynamic loss modulus (G") or the amount of energy lost to viscous dissipation. The ratio of energy lost to energy stored is called the damping factor or loss tangent.In the same way complex Young's modulus can be separated in real (E') and imaginary (E") parts.

Ageing usually affects the dynamic modulus and this change implies a loss of the material strain capability.

It is interesting for us to know these properties and their consequences over service life. Husband [4], Stacer [5] and Tod [11] have measured and studied the viscoelastic behaviour of propellants.

Ballistic properties

Mechanical and chemical changes have influence over ballistic properties: thrust level and burning time. Chemical changes in the propellant have been studied by Chevalier [12]. Ballistic properties can limit the service life, therefore we have defined a test program to discover the real effect of ageing over ballistic characteristics.

4. EXPERIMENTAL PROCEDURE AND EQUIPMENT

4.1. Propellant characteristics

Five propellant formulations have been produced by UEE (Union Española de Explosivos. SPAIN). Their composition are in Table I.

Table I: Propellants composition

WEIGHT PERCENTAGE					
INGREDIENT	AS	SE	C1	C2	BB
AP	80	75	67	67	73
HTPB	15	--	13	13	21
CTPB	--	15	--	--	--
AL	4	9	18	18	-
OTHERS	1	1	2	2	.6
CATALIZER	-	-	NO	YES	--

Propellant C1 and C2 are identical except in a combustion catalizer.To establish the effect of chemical ageing on mechanical and ballistic properties an accelerated ageing program was set up.

4.2 Measurement of tensile properties

Tensile properties were measured using the Zwick 1384 testing machine with a cross-head of 50 mm/min and a tensile force of 500 N.

Samples were cut into test specimen according to the ASTM-D638 specifications and aged thermally under dessicant at 65°C; the ageing period was 350 days.

Maximum stress, strain at maximum stress, strain at break and Young's modulus were measured at 20°C and different ageing times. The Young's modulus has been obtained as the modulus related with a strain of 5%.

4.3 Measurement of viscoelastic properties

Measurements of dynamic mechanical properties by Dynamic Mechanical Thermal Analyzer (DMTA) yield the master dynamic against frecuency curve at the reference temperature, and the shift factor curve.

Propellant rectangular slab samples with a width of 2.2 mm, a thickness of 0.5 mm and a length of 25 mm were tested in the DMTA from PL Thermal Sciences (courtesy of the "Instituto de Polímeros", C.S.I.C., Madrid).

4.4 Measurement of hardness

Shore A hardness was measured with the Baxlo tester according to DIN-53505 specifications. Samples underwent the same ageing program as tensile samples.

4.5 Measurement of ballistic properties

The objetive was to fire standard mini-motors under the same conditions with different levels of ageing and compare the results.

We have used our static test stand facilities; typical ballistic properties: (a) pressure, (b) burning time and (c) pressure-time integral, have been measured during the test of several solid rocket mini-motors.

Propellant grains belonging to the same lots were subjected to an ageing program at 65° C during a one year period. All of them had a previous natural ageing of 5 years.

5. RESULTS AND DISCUSSION

5.1 Effect of ageing on hardness

Results of the measurement of initial shore A hardness are reported in Table II.

Figure 5 shows the change in shore A hardness in three of these propellants as a function of time.

Hardness of propellants SE, C1 and BB has slight variations in the ageing time. Hardness of propellant C2 has clearly augmented.

Table II: hardness of samples without ageing at 20°C

Propellant	C1	C2	BB	AS	SE
Hardness	79	77	74	65	55

5.2 Tensile properties versus ageing time

Results obtained in the tensile mechanical test are reported in Table III and Figures 1 to 4. The examination of figures shows the following:

Maximum stress (Figure 1)

Maximum stress and hardness (Figure 5) in these propellants have identical tendencies.

Strain (Figures 2 and 3)

As regards strain at break and strain at maximum stress, in propellant C1 these remain constant, in propellant BB they diminish slightly and in propellant C2 they increase.

Young's modulus (Figure 4)

Young's modulus of propellants C1 and BB remains aproximately constant, however in propellant C2 increases exponentially with time.

An increase in stiffness and strength, and a decrease in strain capability are usually due to oxidation of the polymer backbone [13]. But it can be seen that the behaviour of the propellants is not always the same, and the results are heterogeneous; therefore the effect of chemical ageing does not always show an identical tendency.

Table III: Tensile mechanical properties of samples without ageing at 20°C

TENSILE MECHANICAL PROPERTIES			
	C1	C2	BB
σ_M (MPA)	1.06	1.11	0.95
ε_M(%)	29.2	32.9	34.6
σ_B(MPa)	1.06	1.11	0.90
ε_B (%)	29.9	32.9	44.5
E(MPa)	7.9	6.9	9.2

5.3. Viscoelastic properties

The dynamic mechanical properties of linear viscoelastic materials are time and temperature dependent, and are usually described as a master stress relaxation modulus against the time curve at a reference temperature, and a shift factor against the temperature curve. These properties were measured in AS propellant.

Storage modulus and damping (tan δ) have been measured at several frequencies (3, 10, and 30 Hz) and over a temperature range from -50 to +10°C. Both, E' and damping increase in a regular fashion with increasing frecuency or decreasing temperature over the temperature range considered. The curves at the highest temperature indicate an equilibrium modulus.

Figures 9, 10 and 11 show the dynamic storage modulus E', the loss tangent and the master curve of AS propellant . It may be seen that the obtained values and general trends are similar to those of references 4 and 7.

Figure 11 was obtained by horizontallly superimposing modulus data at different temperatures on to a master frecuency curve. The horizontal shift factors used to superimpose the data were described using the WLF equation. Figure 12 shows the storage and loss modulus versus frecuency.

5.4 Effect of ageing on ballistic properties

Ballistic properties of small solid rocket motors with different levels of ageing were measured, the results are given in Figures 13 and 14. Notice that maximum pressure, burning time and pressure-time integral of the motors are almost identical between them; the unique effect is a slight

difference in the burning rate and hence in the pressure level. All the motors were previously examined and there is no evidence of cracks. This propellant has shown very small variations in hardness with ageing time.

A second experiment consisted in keeping one full dimension motor (1.5 m lenght and 140 mm diameter) at 65°C and 40% HRC during a period of 600 hours. Results of firing in rocket motor test stand have been good and differences with regard to nominal values are irrelevant.

5.5 Analysis

All the samples exhibit properties in the typical ranges of these propellants; moreover mechanical properties -hardness, maximum stress, strain and Young's modulus- change with ageing time in accordance with Layton's formula [21] (the exception is propellant C2):

$$P = P_o + k \log [t/t_o]$$

where P is the property at any time of ageing, P_o is the property at the end of curing, k is the rate of change of property, t is the ageing time and t_o is the time at the end of curing.

Nevertheless the evolution of tensile properties versus ageing time is not homogeneous: for example in propellant C2, maximum stress and Young's modulus increase; whereas in the propellant C1, the same properties diminish slightly. Shore A hardness follows the same trend as the modulus.

Therefore, the evolution of propellant C2 is towards a more brittle material. The behaviour of propellant BB is different, the trace of strain at break (Figure 6) shows that the trend is towards a ductile material.

Although humidity has not been taken into account -samples were subjected to thermal ageing without humidity-, Miedema [13], Wu [14] and Beckwith [15] have shown that mechanical properties are not significantly affected if based-HTPB propellants are subjected to relative humidities up to 60%; exceptions depend on the type of oxidizer.

It seems possible to establish a correlation between hardness and other properties, as for example Young's modulus, maximum stress and strain, see Figures 6,7 and 8. This result is very interesting because it allows us to predict the tensile properties with only the measurement of the shore A hardness.

Ageing effect over viscoelastic properties was not measured. Ballistic properties have not changed either during the natural ageing period of 5 years or in the following artificial ageing period (aproximately 1 year) at 65°C; it seems that the effect of ageing on ballistic properties is small. It would be of interest to obtain more experimental data.

The results of the tensile mechanical tests have shown that changes in Young's modulus E allow a good indication of the chemical stability of the propellant, therefore we propose an ageing test and relative stability criterium based on the variations of E with ageing time(see Figure 18).

The test consists of the exposure at 65°C during a period of 2 months and thus, depending on the evolution of the Young's modulus E, we can classify the propellant in Type I (good stability) or Types II, III or IV. The result of this test gives an estimation of the future behaviour of the propellant.

6. THEORETICAL PREDICTION OF SHELF LIFE

In a series of papers [17,18,19,20] a basic methodology for the calculation of storage life of rocket motors using several reliability techniques has been published. The motor is supposed to be long hollow elastic cylindrical shells surrounded by a layer of insulation and filled with a viscoelastic propellant. We have developed a mathematical model based on the same methodology.

Other authors have studied this problem with a similar approach [5, 16].

Motors are usually stored in a depot and are subjected to thermal changes depending on the time of the year (summer or winter) and day-night conditions. This thermal cycling results in significant stresses due to thermal shrinkage and to the large difference in thermal expansion coefficients between the polymer (propellant and inhibitor) and the metal casing. As the propellant is subjected to chemical ageing and stress-dependent cumulative damage, the strength is diminished and failure occurs when internal stresses or strains are larger than strength or strain capability of the material.

Of course, the best possible simulation of the environmental conditions is required if the future behaviour of the propellant is to be accurately predicted.

We have applied this method to several motors and results seem to be good, see Figures 15 through to 17. Figure 15 shows the cumulative damage and Figure 16 the reliability curve, hence a service life of about twenty five years is predicted.

Figure 15 includes two curves depending on the inclusion or not of the chemical ageing in the dynamic modulus. Figure 16 presents the reliability curve taking into account or not the aged dynamic modulus. Figure 17 shows the tangential thermal stresses(including the effect of the aged dynamic modulus) and the degraded strength. The evolution of the strength with time is presented in three possibilities: (a) the relaxation strength without ageing, (b) the strength with the effect of chemical ageing and (c) the strength including the effect of chemical ageing, cumulative damage and aged dynamic modulus.

7. CONCLUSIONS

This paper has described the effect of ageing over mechanical and ballistic properties of composite propellants. It has been shown that it is possible to establish a correlation between hardness and other mechanical properties.

Ballistic properties have not changed with ageing time.

We have proposed a criterium for the relative stability of the composite propellants.
Application of the theoretical method for the calculation of storage life seems to give good results, although more experimental data are necessary.

In particular in Spain the following criteria will be applied in the future: First, application of the ageing test and stability criterium in the evaluation of new propellants; second, measurement of shore A hardness or other equivalent non destructive tests during the surveillance program of solid motors and finally the prediction of shelf life using the theoretical method.

8. REFERENCES

[1] C. Forsgren and D. Taylor; "Shelf Life Design Work, A Description of a New Swedish Defence Standard (FSD 0223)"; paper 30, 20th International Annual Conference of ICT, June 27-30, 1989, Karlsruhe, Germany.

[2] Dr.Rudolf Amman, "Ballistic Shelf Life Prediction of the Geewehrpatrone 90 (GP90)"8th Symposium on Chemical Problems connected with Stability of Explosives; Sweden 1988.

[3] Bronniman, E.; Sopranetti, A.; "A Universal Test Procedure to Predict the Shelf Life of Propellants"; 7th Symposium on Chemical Problems connected with Stability of Explosives; Sweden 1985.

[4] D. Mark Husband; "Use of Dynamic Mechanical Measurements to Determine the Ageing Behavior of Solid Propellant"; Propellants, explosives and pyrothecnics, 17, 196-201, 1992.

[5] R. G. Stacer and F. N. Kelley; Systems "Approach for the Design of Polymeric Structures"; paper 11, 20th International Annual Conference of ICT, June 27-30, 1989, Karlsruhe, Germany.

[6] G. S. Faulkner; "The Penetrometer: A Technique for Monitoring Composite Propellant Ageing Characteristics"; paper 45, 20th International Annual Conference of ICT, June 27-30, 1989, Karlsruhe, Germany.

[7] F. W. M. Zee; "Chemical and Physical Ageing of Rocket Propellants"; International Jahrestagung 1983, ICT, Karlsruhe, Germany, June 29-July 1, 1983.

[8] B. Nilsson and R. Sanden; "Accelerated Ageing of HTPB-based Composite Propellants and Liners"; FOA Rapport C-20405-D1 April 1981; Sweden.

[9] A. A. Amer and M. H. Moeen; "Effect of Thermal Ageing on some Properties of C.T.P.B. Solid Rocket Propellants"; paper 103, 25th International Annual Conference of ICT, June 28-July 1, 1994, Karlsruhe, Germany.

[10] E. Sbriccoli, R. Saltarelli and S. Martinucci; "Comparison Between Accelerated and Natural Ageing in HTPB Composite Propellants"; paper 15, 20th International Annual Conference of ICT, June 27-30, 1989, Karlsruhe, Germany.

[11] D. A. Tod; "Ageing of Elastomer Modified Cast Double Base Propellants"; paper 19, 20th International Annual Conference of ICT, June 27-30, 1989, Karlsruhe, Germany.

[12] S. Chevalier, C. Perut, L. Billon and M. Grevin; "Antioxidant Selection Methodology for Hidroxiterminated Polybutadiene Type Solid Propellants", paper 12, 25th International Jahrestagung, June 28-July 1, 1994, Karlsruhe, Germany.

[13] J. R. Miedema, F. W. M. Zee and J. J. Meulenbrugge; "Some Aspects of Ageing of Ammonium-Nitrate Based Composite Rocket Propellants"; paper 13, 20th International Annual Conference of ICT, June 27-30, 1989, Karlsruhe, Germany.

[14] M. T. Wu, S. I. Chen, B. H. Wu and F. Liu; "A Comparative Ageing Study of Nitramine PBX"; paper 14, 20th International Annual Conference of ICT, June 27-30, 1989, Karlsruhe, Germany.

[15] S. W. Beckwith and R. J. Baczuk, "High Solids Content HTPB Propellant Aging, Temperature and Moisture Aging", JANNAF structures and Mechanical Behaviour Subcommitee Meeting, Utah 1982.

[16] G. Francis and J. Buswell; "Service Life Prediction and Testing of Composite Propellant Rocket Motors"; paper 12, 20th International Annual Conference of ICT, June 27-30, 1989, Karlsruhe, Germany.

[17] Janajreh, I.; Heller, R. A. and Thangjitham, S., "Safety Index Approach to Predicting the Storage Life of Rocket Motors"; Journal of Spacecraft and Rockets, Vol. 31, No. 6, Novembre-Decembre 1994, p. 1072-1078.

[18] Zibdeh, H. S. and Heller, R. A.; "Rocket Motor Service Life Calculations Based on the First-Passage Method"; Journal of Spacecraft, Vol. 26, No. 4, July-August, 1989, pp. 279-284.

[19] Heller, R. A. and Singh, M. P.; "Thermal Storage Life of Solid-Propellant Motors"; Journal of Spacecraft, Vol. 20, No. 2, March-April, 1983, p. 144-149.

[20] Heller, R. A.; Kamat, M. P. and Singh, M. P.; "Probability of Solid Propellant Motor Failure Due to Environmental Temperatures"; Journal of Spacecraft, Vol. 16, No. 3, May-June, 1979, p. 140-146.

[21] A. G. Cristiansen, L. H. Layton and R. L. Carpenter, "HTPB Propellants Ageing", J. Spacecraft, Vol. 18, No. 3, May-June 1981.

Figure 1: Max. Stress vs Ageing Time

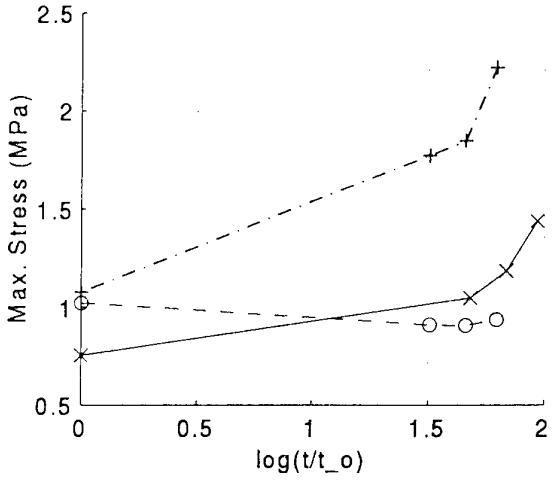


Figure 2:Strain (Max. Stress) vs Ageing Time

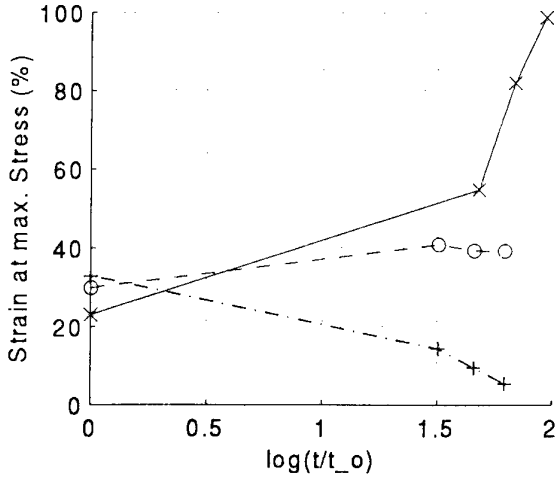


Figure 3: Strain at Break vs Ag. Time

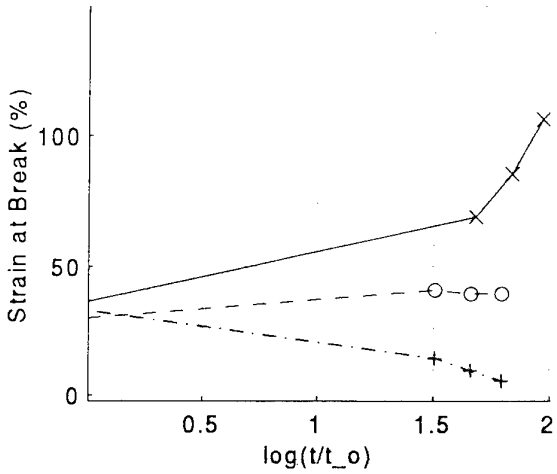


Figure 4: Young Modulus vs Ageing Time

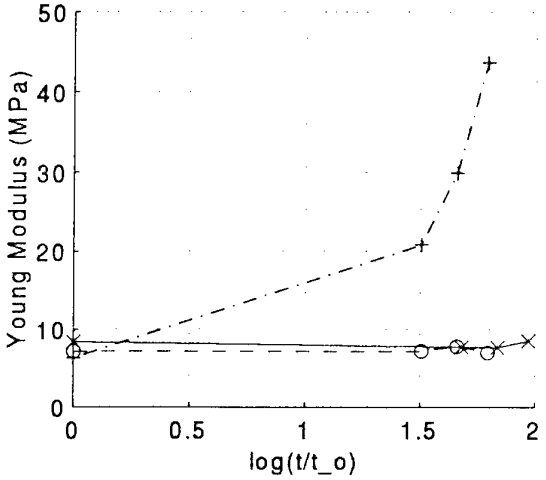


Figure 5: Hardness vs Ageing Time

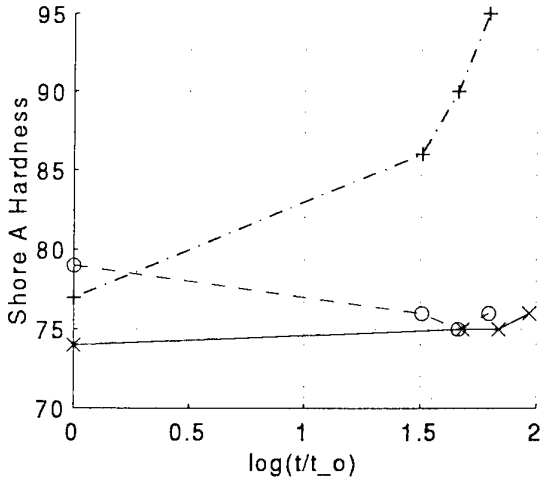
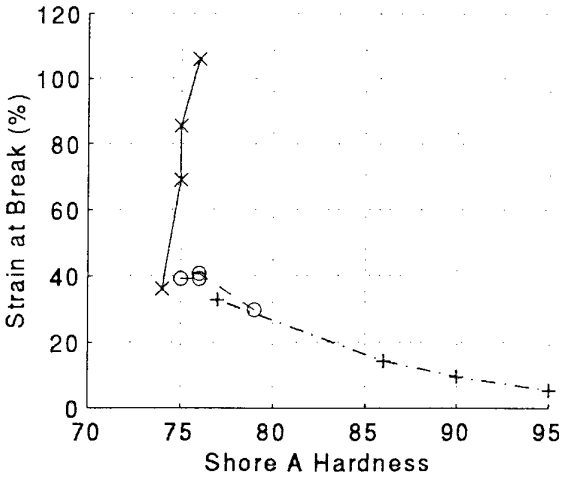


Figure 6: Strain at Break vs Hardness



BB-x- C1 --o-- C2 --.+.--

Figure 7: E vs Hardness

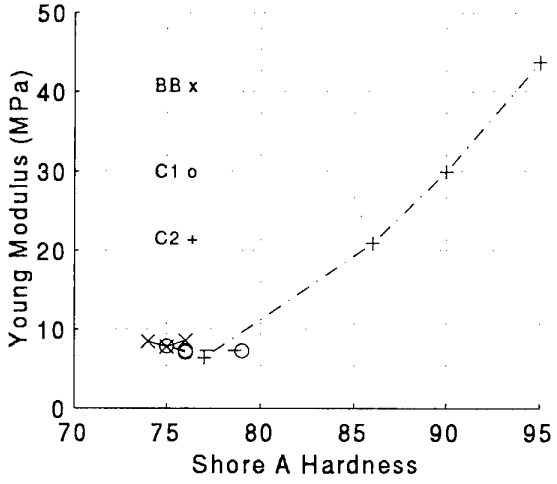


Figure 8: Max. Stress vs Hardness

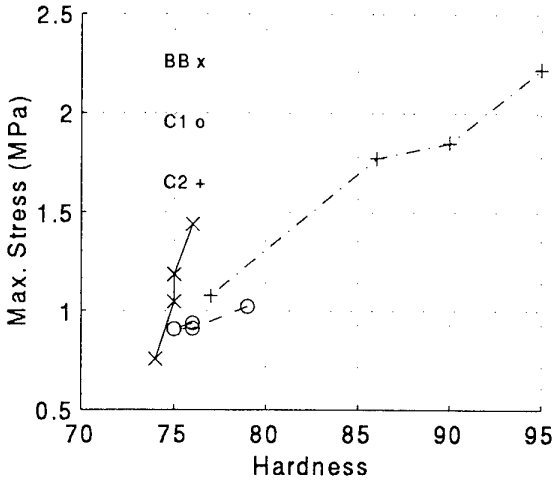


Figure 9:E´vs Temp.

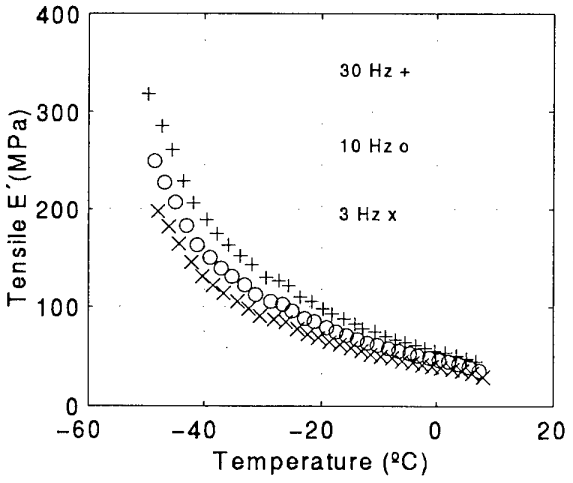


Figure 10: Loss Tangent vs Temp.

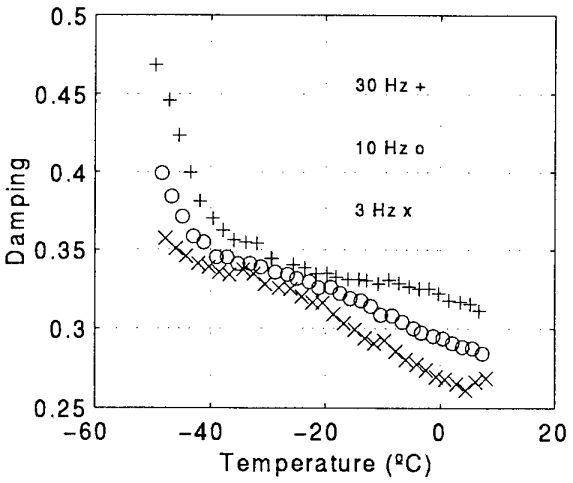


Figure 11: Master Curve T_o=238.96K

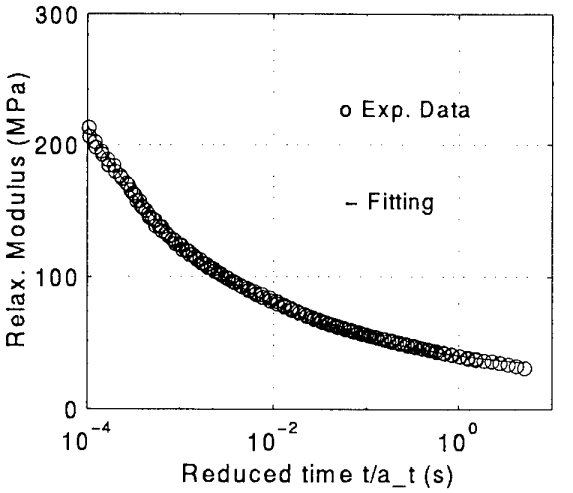


Figure 12: Storage/Dissipation Mod.

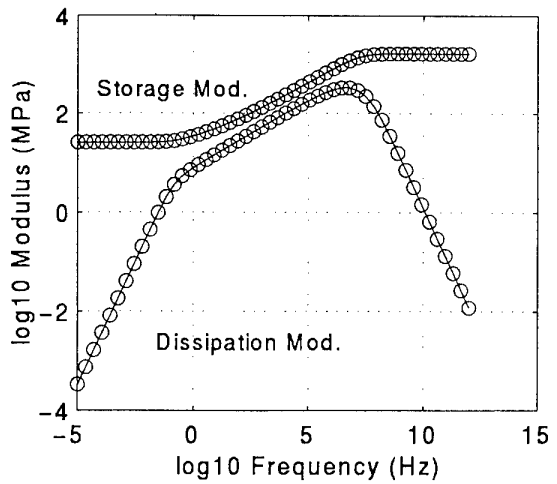
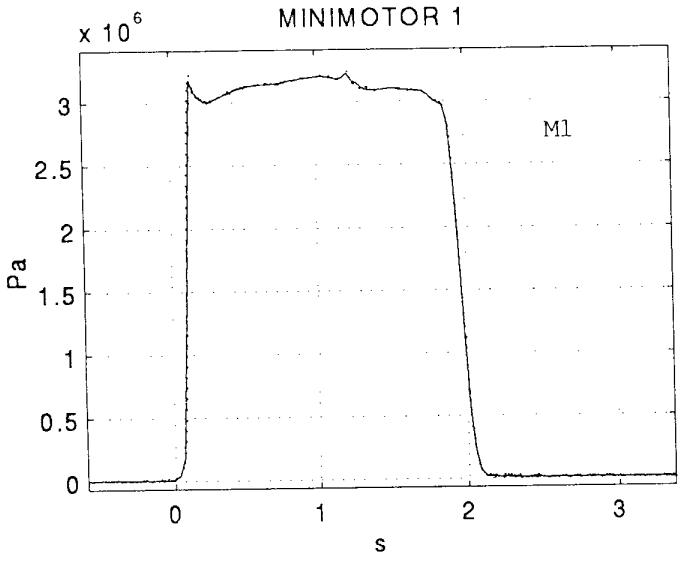
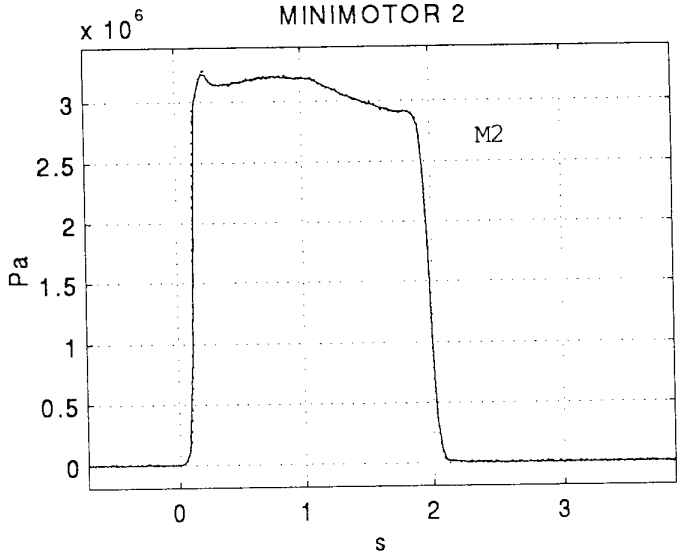


Figure 13. Effect of ageing time in ballistic properties





Material: CTPB/AP/AL (LOT 1)

Property: Pressure vs time

Ageing Data: M1/M2

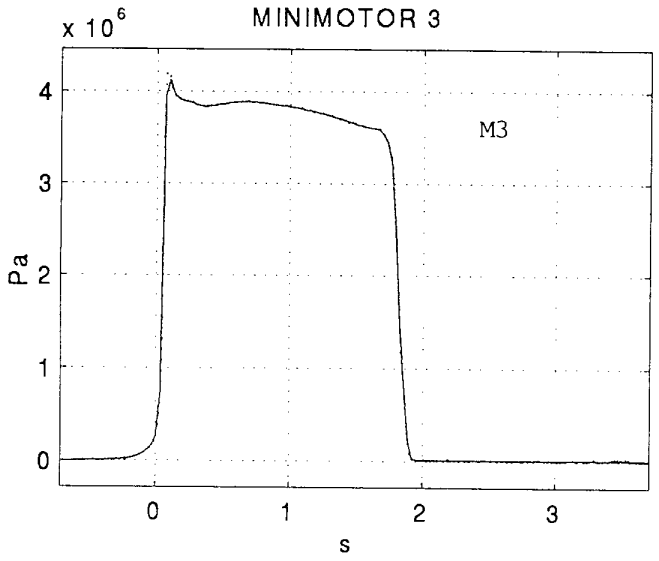
Conditions:

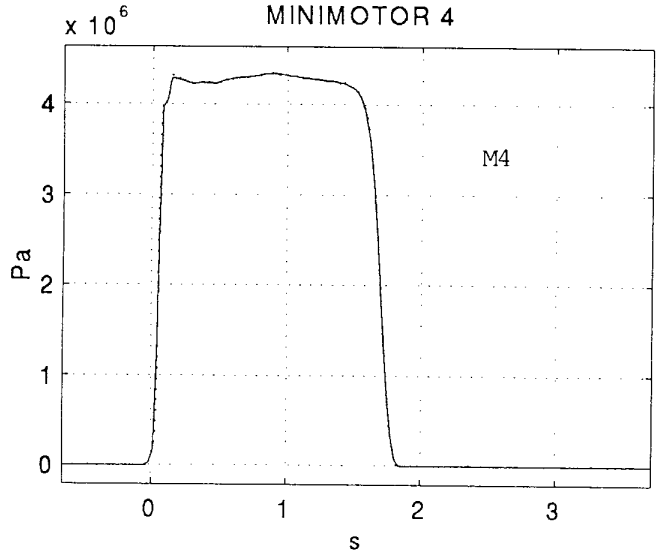
M1: five years of natural ageing

M2: M1 + 266 days at 65ºC

Results:	minimotor nº 1	minimotor nº 2
Burning rate (mm/s);	7.19	6.92
Max. Pressure (MPa);	3.25	3.30
Mean Pressure (MPa);	3.11	3.07
∫P.dt (MPa.s);	5.8	5.75
burning time(s)	1.86	1.87
Shore A Hardness;	60	56

Figure 14: Effect of ageing time in ballistic properties





Material CTPB/AP/AL (LOT 2)

Property: Pressure vs time

Ageing Data: M3/M4

Conditions:

M3: M1 + 328 days at 65ºC

M4: M1 + 385 days at 65ºC

Results:	minimotor nº 3	minimotor nº 4
Burning rate (mm/s);	6.66	7.2
Max Pressure (MPa);	4.25	4.37
Mean Pressure (MPa);	3.8	4.2
$\int P\,dt$ (MPa.s);	6.67	6.88
burning time(s);	1.86	1.73
Shore A Hardness;	60	60

Figure 15: Cumulative Damage

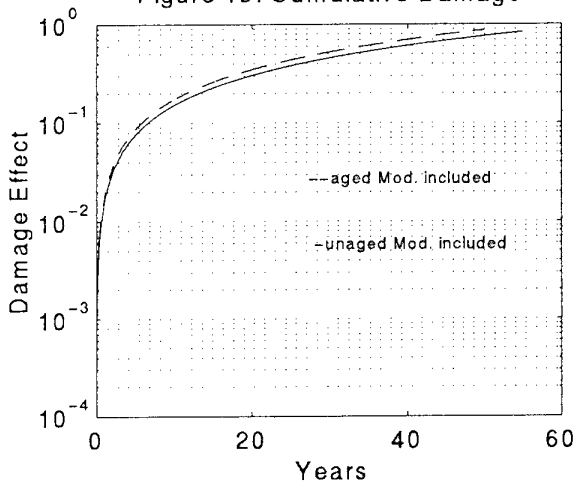


Figure 16: Reliability vs Time

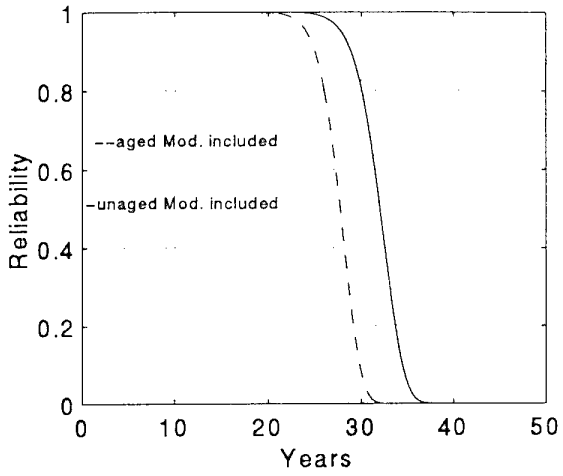


Figure 17: Core Strength and Stress at the bore

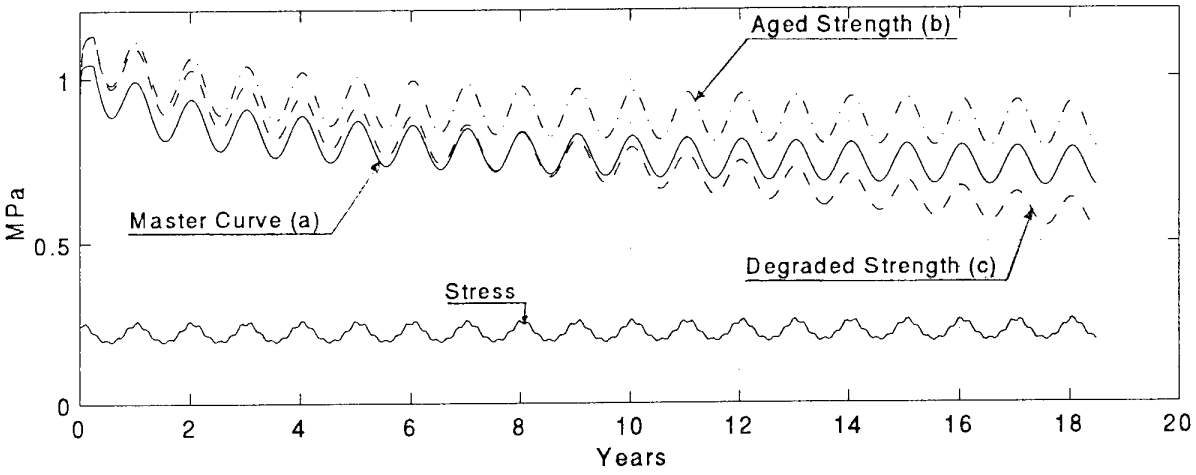
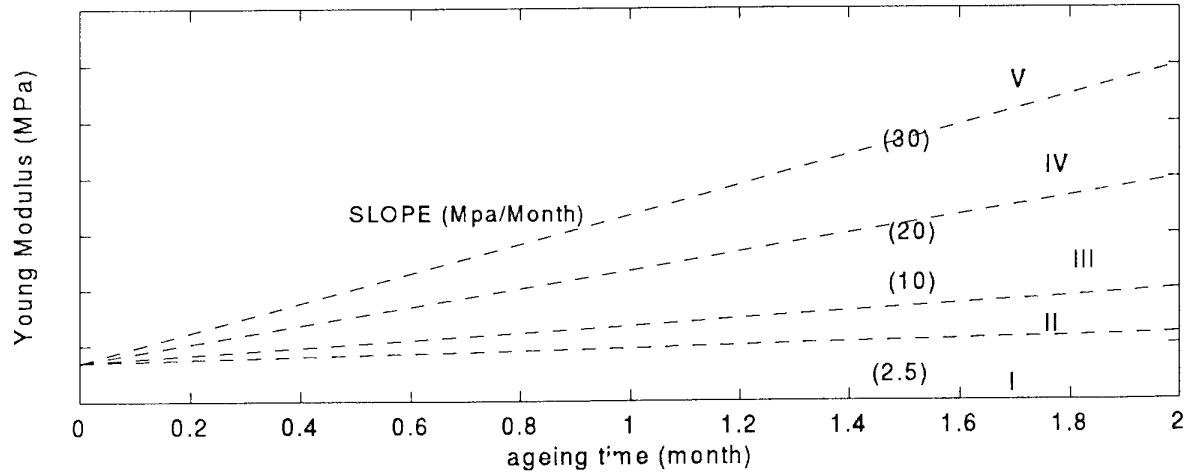


Figure 18: Ageing Test and Stability Criterium



Microstructural Damage and Crack Growth Behavior in a Composite Solid Propellant

C.T. Liu
Phillips Laboratory
OL-AC PL/RKS
10 E. Saturn Blvd.
Edwards AFB CA 93524-7680
USA

1. SUMMARY

The effects of temperature and crosshead speed on the local damage near the crack tip and the crack growth behavior in a composite solid propellant were investigated. In this study, three temperatures (165°F, 72°F and -65°F) and two crosshead speeds (2.54 mm/min and 12.7 mm/min) were considered. The experimental data were analyzed and the results are discussed.

2. INTRODUCTION

An important engineering problem in rocket motor structural design is evaluating structural strength and reliability. It is well known that structural strength may be degraded during its design life due to various aging mechanisms, such as mechanical aging, chemical aging, and the combination of these two aging mechanisms. Depending on the structural design, material type, service loading and environmental condition, the cause and degree of strength degradation due to the different aging mechanisms would differ. One of the common causes of strength degradation is the result of crack development in the structure. According to current failure initiation criteria used for small size rocket motor structural design and service life prediction, failure occurs when a crack is predicted or detected. It is based on the assumption that a small crack will propagate to a catastrophic size with a very high speed. Therefore, based on the failure initiation criterion, the rocket motor's service life is terminated when a crack is initiated regardless of the size of the crack. Past experience indicates that rocket motors with structural flaws, such as propellant cracking and unbonds between grain and case, have been static fired without experiencing catastrophic failure or unacceptable ballistic performance conditions. This implies that structural design and service life prediction based on the failure initiation criteria does not adequately define the condition which limits rocket motor service life. Therefore, in an attempt to determine the ultimate capacity or the ultimate service life as well as to increase reliability and decrease the replacement costs of rocket motors, the failure criteria should include the crack propagation aspect of localized failure. To achieve this goal, a detailed knowledge of both crack growth behavior and methodologies for predicting crack growth are indispensable.

In recent years, a considerable amount of work has been done in studying local behavior near the crack tip in solid propellant [1-6]. It is well known that the mechanical behavior of such materials depends on the strain rate and temperature. Therefore, to provide some insight into the near tip mechanisms which are associated with crack opening and growth, and how they may be affected by changes in strain rate and temperature, a series of experiments was conducted. The experimental data are analyzed to determine the local behavior near the crack tip and the results are discussed.

3. THE EXPERIMENTS

In this study, the effects of temperature and loading rate on the strain distributions and local behavior near the crack tip were investigated using sheet specimens. The specimens were made of a composite solid propellant and the geometry of the specimen is shown in Fig. 1. Since the specimens were quite soft, a special grating had to be developed from which displacements near the crack tip could be measured without affecting the stiffness of the specimen. A coarse grating consisting of squares of 0.2 mm on each side (approximately 1/2 of the largest size of the hard particle) and which had a thickness of less than 2.5×10^{-2} mm was deposited in the neighborhood of the crack tip. The procedure to print the grid on the surface of the specimen was to cover an area of about 5.08 by 5.08 cm with a very thin layer of mixed silicone grease. Then a mesh of 5 lines per millimeter was placed on that area. The grid was pressed gently onto the specimen and

Paper presented at the AGARD PEP Symposium on "Service Life of Solid Propellant Systems" held in Athens, Greece, 10-14 May 1996, and published in CP-586.

the excess grease mixture removed. Then a white colored titanium oxide powder was sprinkled on the specimen surface. When the mesh was removed, a grating showed on the specimen surface.

Prior to testing, the specimens were conditioned at the test temperature for an hour and were then tested at a constant crosshead speed until the specimen fractured. In this study, three temperatures (165°F, 72°F, and 65°F) and two crosshead speeds (2.54 mm/min and 12.7 mm/min) were considered. During the tests, photographs of the grid region were taken at various time intervals and they were used to determine the displacement fields near the crack tip. The procedure to determine the displacement and strain fields is discussed in the following paragraph.

4. RESULTS AND DISCUSSION

It is well known that, on the microscopic scale, a solid propellant can be considered a nonhomogeneous material. When this material is stretched, various forms of damage can be developed, depending upon the cohesive strength of the binder material, the adhesive strength at the interface between the binder and the filler particle, and the magnitude of the local stress in the material. The damage developed in the material may be in the form of dewetting between the binder and the filler particle. The growth of the damage in the material may take place by material tearing or by successive nucleation and coalescence of the microcracks. These damage processes are time-dependent and are the main factor responsible for the time-sensitivity of the strength degradation as well as fracture behavior of the material. Experimental evidence reveals that these basic damage mechanisms take place in the range of temperature considered in this study and they are used to explain some of the local behavior near the crack tip and crack growth phenomena observed experimentally.

Typical sets of photographs showing the crack surface profile and local damage near the crack tip are shown in Fig. 2. The local behavior shown can be regarded as typical for the material investigated and the two crosshead speeds considered in this study. Figures 2 and 3 depict the crack opening and growth which consisted of a blunt-growth-blunt-growth process. Figures 2 and 3 also reveal that voids are formed in a highly damaged zone, known as the failure process zone, ahead of the crack tip during blunting following by growth during which the crack resharpened. As the crack propagates, due to the random nature of the damage developed at the crack tip, the crack path was locally an undulating path. However, in a global sense, the crack grew in a plane normal to the direction of the applied load. Figure 4 shows the crack profile at -65°F. At -65°F, the void development was strongly suppressed. It is conjectured that a transverse constraint is developed which led to the classic brittle fracture.

Typical near tip displacement contours are shown in Fig. 5. The regularity of the displacement field suggests that this material may be described by continuum theory. Typical plots of normal strain ε_y distributions under different temperatures and crosshead rates are shown in Figs. 6 and 7. These figures show that the contour lines are not smooth but irregular. It is believed that a portion of the irregularities may stem from the method of data collection and reduction, but they are mainly due to the inhomogeneity of the material. It is known that, dependent upon the level of interest, micro or macro, the material's microstructure can have a significant effect on the strain fields. Experimental data reveal that, on the macro level, the effect of the material's inhomogeneity on the distributions of the strain near the crack tip becomes small when the applied strain level is large. In addition, when the magnitude of the applied strain is small, the large normal strain occurs in small zones, or the intense strain zones, which are immediately ahead of the crack tip.

From Figs. 6 and 7, it is seen that, for a given temperature, the effect of changing the crosshead speed by a factor of 5 alters the strain fields but the iso-strain contours are of this same general form. Moreover, for a given crosshead speed, the shapes of iso-strain contours are similar. It seems that the intense strain zone size decreases with decreasing testing temperature.

The crack growth behavior in the material was investigated based on the crack growth resistance (K_I Vs Δa-curve) approach. The results of the data analysis were plotted as Mode I stress intensity factor K_I versus the crack extension, $\Delta a = a - a_0$ where a_0 is the initial

crack length, and are shown in Figs. 8 and 9. In general, these figures have three regions. In the first region, defined as the crack tip blunt stage, experimental data showed that the crack tip radius continually enlarged with increasingly applied load. When the critical load reached a critical value for crack growth, the crack started to propagate, which defined the onset of the second region of the K_I Vs Δa-curve. In this region, crack growth was stable under an increasing load. The stable crack growth implied that after the first increment of crack growth, an additional increment of applied load was needed for further crack growth. At a certain value of crack length, the transition from Region 2 to Region 3 was completed. A careful examination of the experimental data revealed that the transition region was located approximately near the value of maximum applied load. This implied that Region 3 was characterized by a continual decrease in the applied load with a continual increase in the crack length and a relatively constant value of the stress intensity factor, K_I. However, the crack was not driven at constant velocity, but instead it propagated at an accelerating rate, indicating unstable crack growth. It should be pointed out that due to the material's brittle nature at low temperature, the times corresponding to unstable crack growth and fracture of specimens at -65°F are much shorter than those at 72°F and 165°F Figures 8 and 9 also show that the crack growth resistance curves at -65°F is significantly different from that at 72°F and 165°F, and the effect of the two crosshead speeds considered in this study on the crack growth resistance curve is relatively small.

The crack growth rate da/dt versus the Mode I stress intensity factor K_I are shown in Figs. 10 and 11. From these figures, it can be seen that a power law relationship exists between K_I and da/dt. Mathematically, it can be written as

$$da/dt = C_1 K_I^{C_2}$$

in which C_1 and C_2 are constants. Figures 10 and 11 also reveal that the crack growth is much faster at -65°F and the higher crosshead speed exhibits higher crack growth rate.

5. CONCLUSIONS

The principal conclusions which can be derived from the results of this work are:

(1) At 165°F and 72°F, a considerable amount of stable crack growth occurs before the onset of unstable crack growth.

(2) At 165°F and 72°F, the basic crack growth behavior consists of a blunt-growth-blunt phenomenon.

(3) At -65°F, the crack growth behavior is significantly different from that at 165°F and 72°F.

(4) A ductile-brittle transition occurs somewhere between -65°F and 72°F.

(5) For the testing conditions considered, the effect of crosshead speed on crack growth behavior is considerably small relative to that of temperature.

(6) Power law relationships exist between the crack growth rate and the Mode I stress intensity factor.

6. REFERENCES

1. Beckwith, S. W. And Wang, D. T., "Crack Propagation in Double-Base Propellants", AIAA Paper 78-170, 1978.

2. Liu, C. T., "Variability in Crack Growth in a Composite Propellant", AIAA Paper 83-1015, 1983

3. Liu, C. T., "Crack Growth Behavior in a Composite Propellant with Strain Gradients", AIAA/ASME/ ASEE/SAE 20th Joint Propulsion Conference, 1984.

4. Liu, C. T., "Crack Growth Behavior in a Composite Propellant with Strain Gradients - Part II", *Journal of Spacecraft and Rockets*, Vol. 27, No. 6, pp. 647-652, 1990.

5. Liu, C. T., "Crack Propagation in a Composite Solid Propellant", *Proc. Society of Experimental, Spring Conf.*, pp. 614-620, 1990.

6. Smith, C. W., Wang, L., Mouille, H., and Liu, C. T., 'Near Tip Behavior of Particulate Composite Material Containing Cracks at Ambient and Elevated Temperatures", ASTM STP 1189, pp. 775-787, 1993.

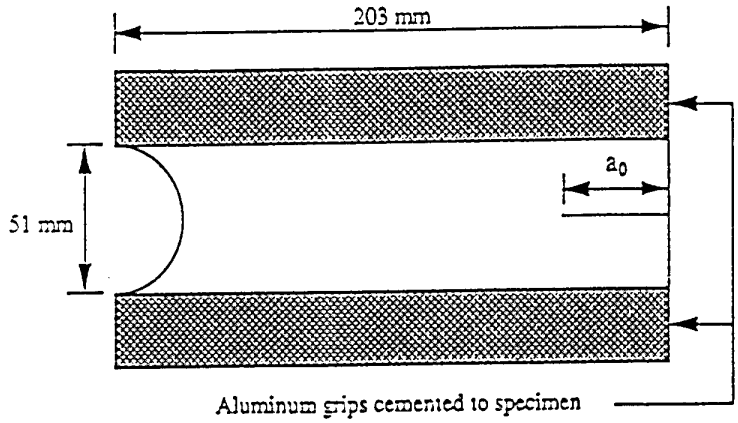


Fig. 1. Specimen geometry

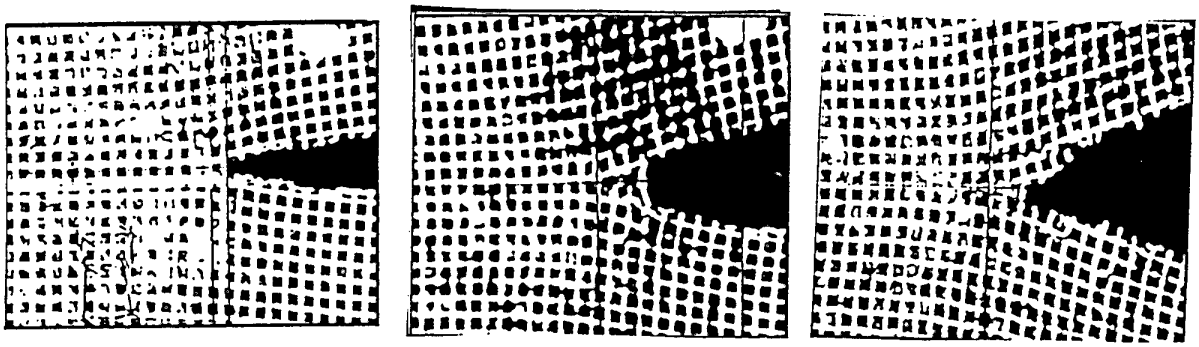


Fig. 2. Crack tip profiles at 72°F and crosshead speed = 2.54 mm/min

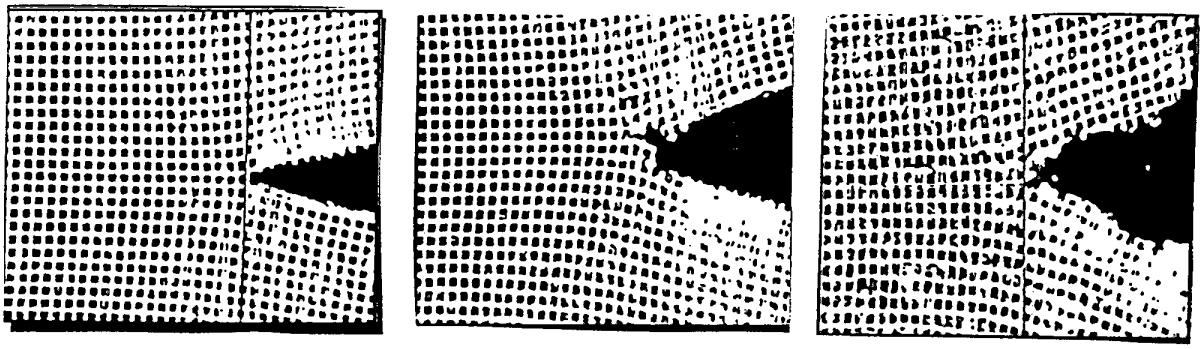


Fig. 3. Crack tip profiles at 165°F and crosshead speed = 2.54 mm/min

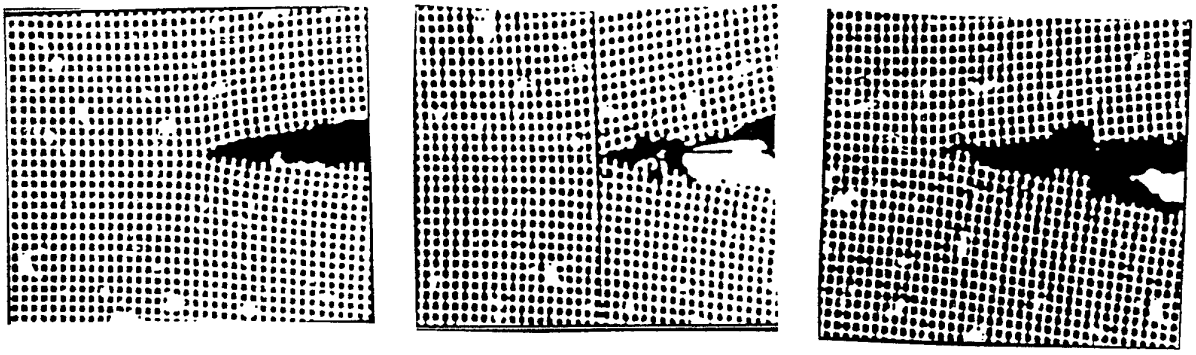


Fig. 4. Crack tip profiles at -65°F and crosshead speed = 2.54 mm/min

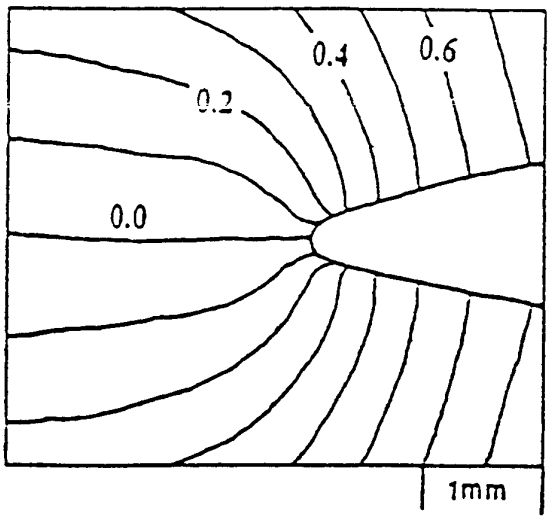
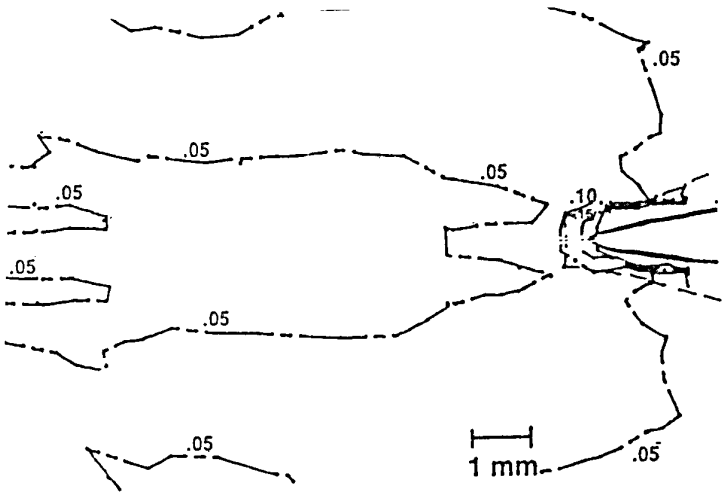
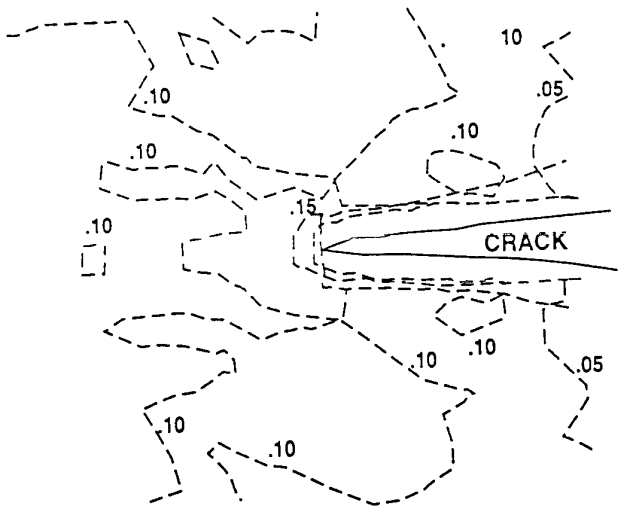


Fig. 5. Near tip contour maps of displacement at 72°F and crosshead speed = 2.54 mm/min

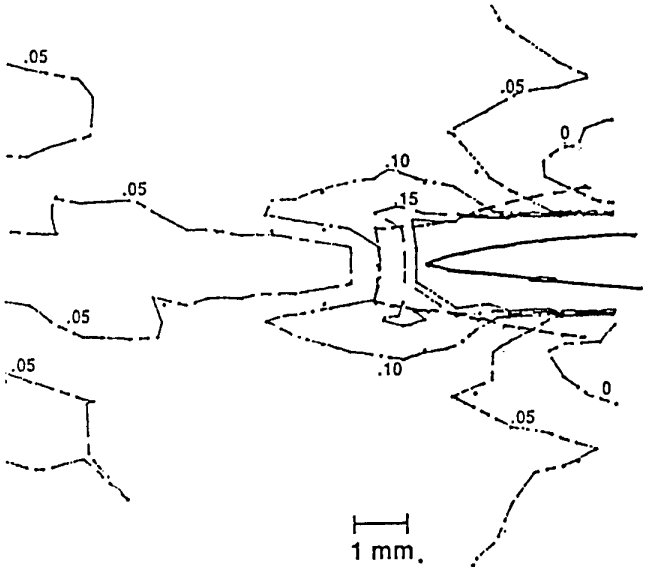


(a) crosshead speed = 2.54 mm/min

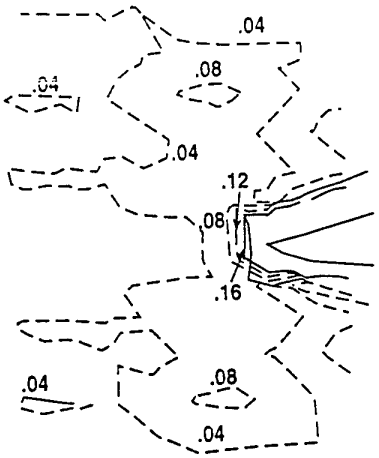


(b) crosshead speed = 12.7 mm/min

Fig. 6. Near tip contour maps of normal strain at 165°F.



(a) crosshead speed = 2.54 mm/min



(b) crosshead speed = 12.7 mm/min

Fig. 7. Near tip contour maps of normal strain at -65°F

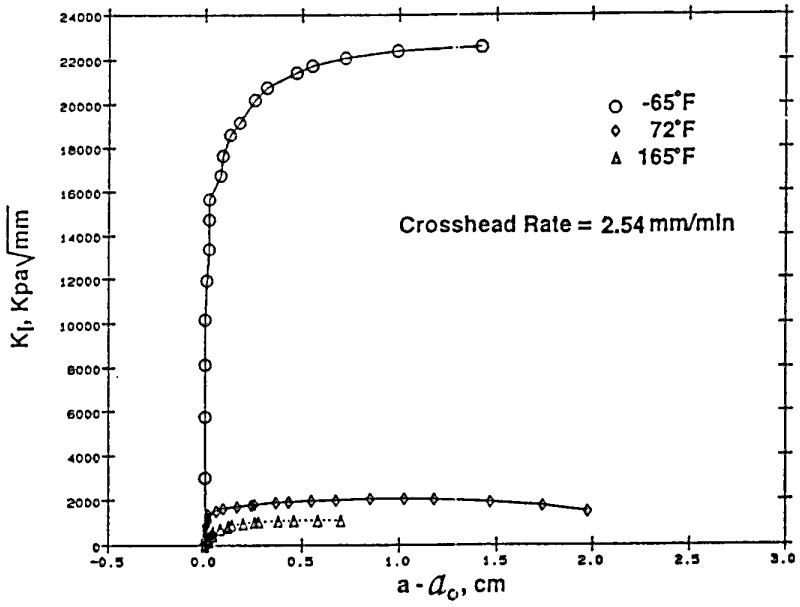


Fig. 8. Crack growth resistance curves at different temperatures (crosshead speed = 2.54 mm/min)

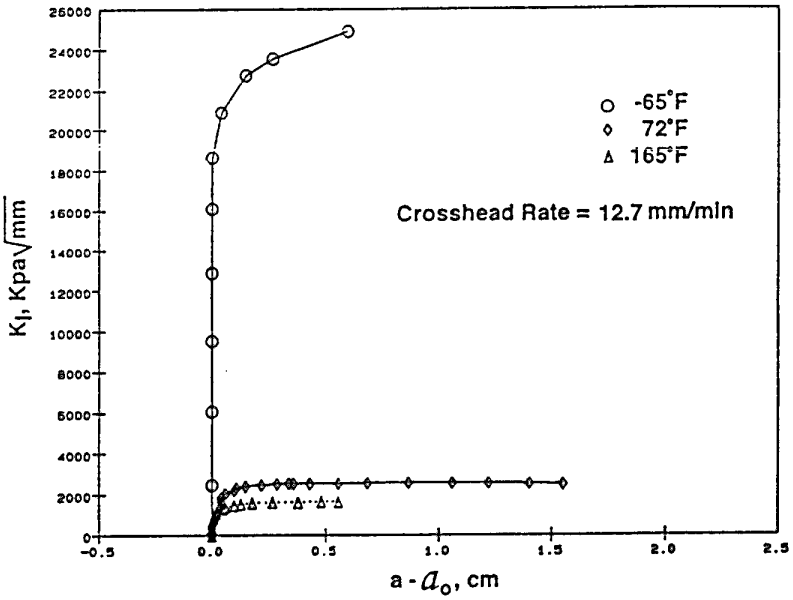


Fig. 9. Crack growth resistance curves at different temperatures (crosshead speed = 12.7 mm/min)

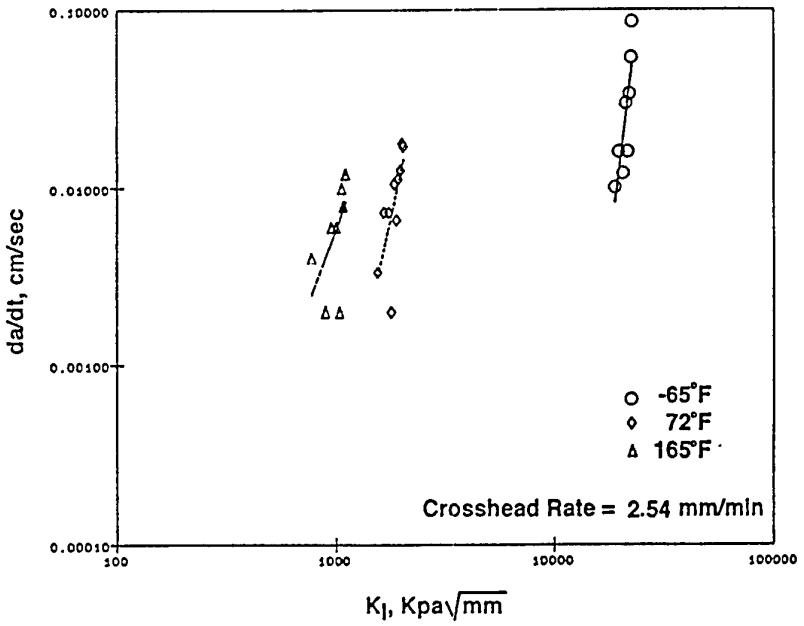


Fig. 10. Crack growth rate versus Mode I stress intensity factor (crosshead speed = 2.54 mm/min)

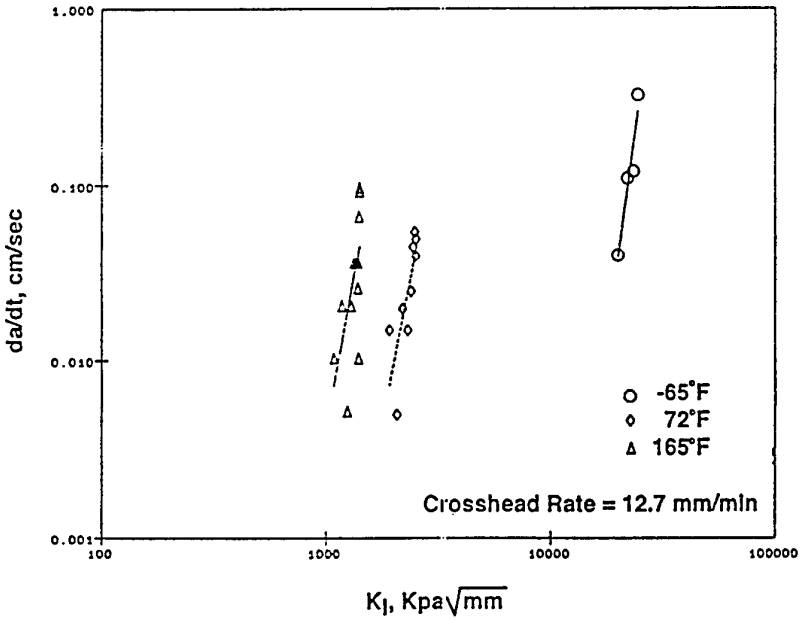


Fig. 11. Crack growth rate versus Mode I stress intensity factor (crosshead speed = 12.7 mm/min)

Ageing and Life Prediction of Composite Propellant Motors

A V Cunliffe*
A Davis
D Tod
Defence Research Agency
Fort Halstead
Sevenoaks
Kent TN14 7BP
UK

1. SUMMARY

The factors which need to be considered in the ageing, life prediction and life extension of composite propellant motors are considered. The chemical and physical changes which can occur are described, with particular reference to compositions based on hydroxy-terminated polybutadiene binders. The importance of atmospheric oxygen in the process is emphasised, and the factors determining the rate of the critical ageing processes are discussed. Accelerated ageing experiments are described, and the information necessary for extrapolation of such data to service temperatures is considered. In order to discuss service lifetimes,it is necessary to have reliable data describing the service environment. The effect of environment, such as temperature, on propellant ageing is considered. The importance of motor design, and its tolerance to changes due to ageing, is discussed, and simple measures which can be taken to extend motor service life are described.

2. INTRODUCTION

Ordnance stores need to have a long service life even although many contain energetic materials which degrade with time. This means that their service life needs to be constantly reviewed. Recent events in SW Asia have highlighted this need and the importance of being able to predict the rate of ageing and the remaining life of ordnance stores. The UK forces had weapons in the Gulf which, in summer months, saw temperatures which would have caused them to age twenty times faster than in Europe. At another level, the rethink which is underway in the west as a result of the changes in Eastern Europe reinforces the importance of predicting and extending the life of ordnance stores. If, for example, the life of a rocket motor can be more accurately predicted or better still extended, then decisions need not be hurried and options can be left open without loss of capability.

One decision which has been made is that the amount spent on defence will decrease. It therefore makes economic and operational sense to extend the life of current systems. We have developed a methodology for predicting the service life of a composite propellant motor which grew out of our core programme on the characterisation and ageing of composite propellant.

Composite propellants were developed because they offered improved properties over double base systems; for example they can be highly loaded, they have good mechanical properties at low temperatures and they can be case bonded at low temperatures. These qualities are directly related to the rubbery properties of the binder which in current composite propellants is polybutadiene. Unfortunately, the unsaturation of the polymer chain, which gives polybutadiene its good rubbery properties also makes it prone to oxidative crosslinking even with an antioxidant present. This crosslinking eventually causes the propellant to harden and loose its flexibility.

Although the general features of this process are common knowledge, little information is available to enable its importance in the ageing of a composite motor charge to be assessed.

In this paper the nature of our predictive methodology and the background research on which it is based will be considered.

3. PREDICTION INPUTS

Three factors need to be known to predict the lifetime of a composite propellant in a motor:-

(a) critical ageing process and its rate expression
(b) service environment
(c) design limits of the motor as they relate to the critical ageing process.

From our work, we have identified three ageing processes in composite propellants

(a) moisture hardening
(b) migration of additives
(c) binder oxidation

Moisture hardening is probably the result of agglomeration of crystals of ammonium perchlorate and can be a potential problem if micronised ammonium perchlorate is used to increase the burning rate.

As with double base propellants, migration of volatile additives, such as plasticisers and some organometallic burning rate catalysts, can be a problem in composite propellants.

The prime ageing process in composite propellant is oxidative crosslinking of the binder which causes the propellant to harden.

Table 1 shows the changes in tensile properties and antioxidant and sol values for a composite propellant, as a result of ageing at 80°C in air and in vacuum.

As the propellant ages in air, the elongation of the propellant decreases and the modulus increases.

Paper presented at the AGARD PEP Symposium on "Service Life of Solid Propellant Systems" held in Athens, Greece, 10-14 May 1996, and published in CP-586.

Table 1 Ageing of composite propellant at 80°C

Sample	Time days	Sol %	AO^ %	e_t %	Ec+ MPa
Control	-	5.76	0.19	13.9	20.9
In air	31	3.83	0.17	12.6	31.5
--	59	2.80	0.13	9.8	35.8
--	99	2.14	0.09	8.0	56.5
In vacuum	113	5.30	0.20	13.5	24.4

The antioxidant concentration is halved after 99 days at 80°C and over the same period the sol fraction is more than halved.

With no air present there is only a small change in the properties of the propellant, even after 113 days at 80°C. This shows that oxidation is sustained by atmospheric oxygen and not from the breakdown of the ammonium perchlorate as has been suggested. Knowing the sol fraction, the relative crosslink density of the binder can be estimated from this modified version of the Charlesby-Pinner equation:-

$$\text{Crosslink density} = \frac{(1 - S)[2 - (S + \sqrt{S})]}{(S + \sqrt{S})}$$

A linear increase in crosslink density with time was found for a range of temperatures from 25 to 80°C which allowed an Arrhenius expression (1) to be derived for the rate of crosslinking.

$$\text{Rate of crosslinking} = 1.75 * 10^{11} e^{-21000/RT} \text{ arbitrary units}$$

Expression (1) is for a conventional aluminised composite propellant free of additives which might accelerate oxidative crosslinking.

Some composite propellants contain transitional metal additives to give particular ballistic properties. As it is known transition metal compounds can catalyse the oxidation, it is important to determine their effect on the ageing process at service temperatures of interest. Figure 1 shows the effect of two such transition metal compounds on the rate of oxidation as a function of temperature. It is seen that while they both accelerate the oxidation process their accelerating behaviour is not identical.

The accelerating effect of additive A varies with temperature; at temperatures below about 50°C it shows no catalytic effect. Additive B on the other hand shows a constant accelerating factor over the whole temperature range.

These examples demonstrate the necessity of determining the effect of an additive over a comprehensive temperature range if correct extrapolation to behaviour at service temperatures is to be made.

Ageing Profiles

Because the oxidation process is sustained by atmospheric oxygen, the degree of oxidation through the propellant is not uniform. That is, we observe a profile in propellant which has been aged (figure 2).

The faster the rate of oxidation the closer the reaction zone moves to the surface and the steeper the profile. Steep profiles are therefore observed at high temperatures.

We have found that if an additive has a catalytic effect on the ageing of the binder it also has an effect on the ageing profile of the propellant. For example figure 3 shows the effect on the ageing profile of a transitional metal compound which accelerates the oxidation process. Thus, increasing the rate of oxidation either by raising the temperature or by the presence of a catalytic additive has the effect of moving the reaction zone towards the exposed surface.

The profile observed is a result of the interdependence of the rate of oxygen consumption and the rate of diffusion of oxygen through the sample.

A mathematical model has been developed which gives good agreement with experimentally measured profiles through blocks and through propellant charges. In other systems, different ageing processes may be critical. For example, the service life of a motor with double base propellant may be determined by the level of the stabiliser added to prevent the exothermic decomposition of the nitrate ester components and gas cracking of the propellant charge.

Migration of nitroglycerine into the inhibitor layer is another process which can fix the life of a double base motor.

Whereas the activation energy of nitrate ester decomposition is of the order 30kcal/mole, the activation energy for the diffusion processes such as the migration of plasticiser, is generally about half this value. One cannot be categorical about whether it is advantageous as regards the life of a motor, whether the critical process has alow or a high activation energy; it depends on the system and the circumstances. Both situations can lead to problems in unfavourable cases. If the critical process has a high activation energy, then the associated rate increases rapidly with temperature, so that a system which has an acceptable lifetime at moderate temperatures may cause problems when used in very hot climates. Conversely, a low activation energy may result in problems in assessing accelerated ageing data, by underestimating the rate of a process. Thus, a process may appear to be relatively slow at 60°C, but if this rate does not reduce significantly on lowering the temperature, then the process may be critical at lower temperatures. It is clearly important to obtain as accurate values as possible for the activation energies, and also to assess carefully both the service temperatures and the temperatures at which the original data was obtained.

4. SERVICE ENVIRONMENT

From data already shown, an Arrhenius expression for the rate of oxidative crosslinking can be derived which allows the rate to be determined for a particular temperature. To estimate the life of a propellant, the time/temperature profile of the propellant in service needs to be known. In addition to the

storage temperature profile it may be necessary to make allowance for the operational temperature/time profile if this is a significant portion of the motor's life in terms of ageing.

The Meteorological Office in the UK has temperature data records for many locations throughout the world and we have made use of these to estimate and compare the ageing rat of composite propellant for representative locations. For example, table 2 shows the average monthly temperature obtained from the Met Office for a number of sites of interest.

Table 2 Average monthly air temperatures for selected locations

Location	J	F	M	A	M	J	J	A	S	O	N	D
London	4.6	4.7	6.2	8.4	12.3	15.1	17.1	16.8	14.4	10.7	6.5	5.2
Dhahran	15.1	16.4	20.3	25.6	31.2	34.3	35.5	34.7	32.1	27.9	22.5	17.1
Jeddah	23.3	23.5	25.6	28.1	30.1	30.9	32.3	31.2	31.3	29.5	27.2	24.8

Taking the average temperature for the year for each location the relative life of the propellant can be estimated by applying the rate expression for the ageing process eg expression 1. Such a comparison is shown in table 3 for a propellant which contains an accelerating transition metal compound. Table 3 also shows the temperatures of two RAF stores in the UK which demonstrate the relative gains to be made in service life by reducing the temperature even in a temperate climate.

Table 3 Average temperature and relative composite propellant life for selected sites

Location	Average Annual T°C	Relative Life
London	10.2	100
Wattisham(part heated)	15.0	50
Leuchars(heated)	20.0	25
Dhahran	26.6	10
Dhahran*	35.5	3
Dhahran+	15.1	49
Jeddah	28.4	8

* highest month, + lowest month

Of particular interest is the wide range of ageing rates for Dhahran as indicated by the relative lives for the hottest and coolest months.

Such considerations are essential for those many stores which have been returned to the UK and for which estimates of remaining service life have to be made.

Temperature Monitoring of Service Stores

As already indicated, the estimates for the Saudi locations given in table 3 are based on air temperature data.

In view of the pronounced dependence of predicted life on temperature and the wide range of conditions in service, the actual temperature profile of the store is needed in order to improve the accuracy of the predictions. A number of programmes have been initiated by various UK agencies to make temperature measurements in the Gulf.

The measurement of temperatures of the Cluster Bomb unit (CBU755) and of the Dispenser (JP233) are two of these exercises which will be described in this paper.

Data Logger

The data logger used was the 1200 series Grant Squirrel which is a small, 1808*120*60mm, 500g, battery driven unit. It has 12 bit resolution, a data storage capacity of 42000 readings of temperature, voltage, current, pulse count or digital state. Eight channels are available for temperature measurement, eight for current voltage, two for pulse rate count or count and one for digital state. The thermistors have a range of -50 to 150°C and a resolution of 0.05°C. The accuracy in the range used in this work was 0.2°C. Data can be down loaded from the logger either by using the manufacturer's program or a spread-sheet.

Logger Configuration

After initial trials at Waltham Abbey it was decided that only five channels would be used for temperature measurement. Four were placed on or in the store and the fifth (T5) was placed in the plastic box used to protect the logger. Uncertainty of how the batteries (6 AA Duracells) would last and how long it would take to recover the loggers from the operational area guided the decision to set the loggers to record from the 3 May to 1 August 1991.

Logger Placement

The Squirrels were prepared for use. One was put onto a Cluster Bomb Unit and another onto a JP233 Dispenser.

Thermistor Placement

The positions of the thermistors on the CBU 755 and the JP233 are indicated in figures 4 and 5 respectively. In each case T1 was on the underside skin of the weapon, in shade, T2 was on top of the weapon and under the environmental cover whereas T3 was above the cover. T4 was inside the steel mesh box for the CBU 755, and protected from direct sunlight, whereas T4 for the JP233 was strapped to a supporting pole, in the shade. T5 was inside the logger container which was itself housed in a polyethylene box lined with aluminium foil and filled with a moisture cured PU foam.

Results

The loggers were positioned on 7 May 1991 and the stores were moved on 19 June; the CBUs onto a ship bound for Germany and the JP233s to a Barraini Defence Force Storage Site.

Figure 6 is an example of the data obtained for the JP33.

Three distinct regions can be seen; the initial low temperature whilst the unit was in transit, the high service temperature while the item was in the field, and the uniform temperature region when it was in storage.

A preliminary analysis of the data for the period 8 May to 18 June is given in table 4.

Table 4 Temperature data, °C, for a CBU and a JP233 in service use in SW Asia

Thermistor	T1	T2	T3	T4	T5
CBU					
Max temp	45.5	52.7	69.4	55.7	45.3
Min "	22.6	21.3	17.9	19.1	21.1
Mean "	31.7	32.9	33.6	31.7	31.3
Std distribution	4.4	6.7	11.6	7.8	5.3
JP233					
Max temp	60.2	59.4	60.2	62.9	50.5
Min "	22.0	20.5	20.5	21.1	22.5
Mean "	31.3	31.8	31.5	30.3	30.7
Std distribution	5.8	7.0	6.7	5.7	4.5

5. DESIGN LIMITS

So far, we have seen that predictions of rates of ageing for propellants are sensitive to the values obtained for the rates and activation energies of the critical process. However, even if accurate values are available for the rate and activation energies for a given propellant, these are not in themselves sufficient to estimate service lifetimes for a particular system. It is important to distinguish here between properties of the propellant and of the whole motor. Rate of oxidation, oxygen diffusion, plasticiser migration, moisture diffusion etc are properties of the propellant. However, the service lifetime is a property of the whole motor. Motors with the same composite propellant can have quite different lifetime.s

A critical failure mechanism for composite motors is cracking of the propellant, caused by hardening of the propellant by oxidation. The propellant will fail when a certain crosslink density is reached, such that the propellant no longer has sufficient extensibility to withstand the thermal and mechanical stresses. However, the critical crosslink density, or extensibility, is dependent on the design of the motor. This is particularly relevant with new designs, where attempts may be made to obtain improvements in performance by pushing established propellants nearer to design limits, for example in motors with high loading densities. In order to obtain estimates of service lifetimes from ageing data, it is necessary to know the acceptable range of crosslink densities for the propellant. We require the initial properties of the propellant as made, and the properties for which cracking will just occur. This information is often difficult to obtain, and can cause great uncertainty in trying to estimate service life. One way of estimating the critical mechanical properties is by design considerations, for example using finite element analysis. Another way, which we have used in a number of cases, is by causing actual failure of a motor by accelerated ageing. If the failure mode can definitely be established, then it may be possible to define the critical propellant properties for failure. Once this information is known, then the experimental data for propellant ageing allows estimation of lifetimes for any particular environmental scenario. In practice, it is usually found that the estimate of the failure point is only approximate (eg 30 weeks accelerated ageing - no failure, 40 weeks ageing - failure).

Knowing the limits for the critical property, for example propellant elongation, the permitted change in crosslink density which can be entertained, can be estimated and thus, knowing the increase in crosslink density which can be allowed and the rate of crosslinking for the service environment, the service life can be estimated.

6. EXTENSION OF SERVICE LIFE

In view of the benefits to be gained by extending the service life of a composite propellant charge, methods of achieving this goal have been investigated.

Four approaches have been considered:

- improving the antioxidant
- reducing the storage temperature
- lowering the original crosslink density of propellant
- reducing oxygen access.

Improving the effectiveness of the antioxidant is an approach which seems to offer a ready solution. However, the isocyanate cure is a limitation on the type and the quantity of antioxidant which can be used. We are currently evaluating alternative antioxidant systems for composite propellants.

As the rat of oxidation increases with temperature a significant decrease in rate an be achieved by lowering the average storage temperature by a few degrees. For example, lowering the storage temperature from 20°C to 15°C will reduce the rate of oxidative crosslinking by about a factor of two for typical HTPB composite propellant.

The third approach is to extend the amount of oxidation which can be permitted by lowering the crosslink density of the propellant as made; that is, increasing the initial extensibility of the propellant however, there is only limited scope for this, since the propellant must not become too soft, or problems of distortion, slumping etc may occur, particularly at the highest operational temperatures, for example, during high speed air carriage.

The fourth approach is to cut off the supply of oxygen; that is seal the motor. We have shown from measurements of the oxygen up-take of propellant, that sealed motors do not contain enough oxygen to oxidise the propellant significantly.

By a combination of lowering the storage temperature, decreasing as much as possible the original crosslink density of the propellant and excluding oxygen, the propellant will effectively last indefinitely and some other failure mechanism other than ageing of the propellant will determine the life of the motor.

7. CONCLUSIONS

In order to predict accurately the service life of a composite propellant in a motor, it is necessary to know several pieces of information. These are often difficult to obtain, but the benefits of achieving accurate information are considerable in terms of reducing costs and increasing capability. Often simple measures can be taken to extend the service life of motors if the ageing mechanisms are properly understood. The main

factors in service life prediction of composite motors may be summarised as follows.

1 Three parameters need to be known to predict the lifetime:

   (a) the critical ageing process and its rate expression
   (b) the service environments
   (c) the design limits of the motor as they relate to the critical ageing processes.

2 Potential failure modes should be identified and their relationship with the underlying chemical or physical processes established.

3 Rate expressions for the underlying chemical or physical processes should be derived, with the help of accelerated test procedures.

4 Without going to academic extremes, degradation mechanisms need to be known if the approach is to be systematic and well founded.

5 An understanding of the temperature dependence of the various critical processes is essential if accurate life prediction is to be made.

6 It should be appreciated that the accuracy of any prediction is very dependent on how accurately the service environment is described. For example, an error in temperature of about 5 degrees can cause an error of 100% in the prediction.

7 If the critical ageing process is well understood, then a number of benefits accrue. Firstly service lifetimes can often be extended by relatively simple means, for example, by defining optimum storage conditions. Secondly, better test procedures can be defined, so that more accurate predictions can be made.

8 With foresight, and an understanding of the main ageing processes, there should be ample time for long term as opposed to accelerated testing.

9 Surveillance testing is an essential part of any prediction program as it allows confirmation and refinement of predictions.

10 Effective life prediction an improve capability and save money.

© British Crown Copyright 1996/DERA
Published with the permission of the controller of Her Britannic Majesty's Stationary Office.

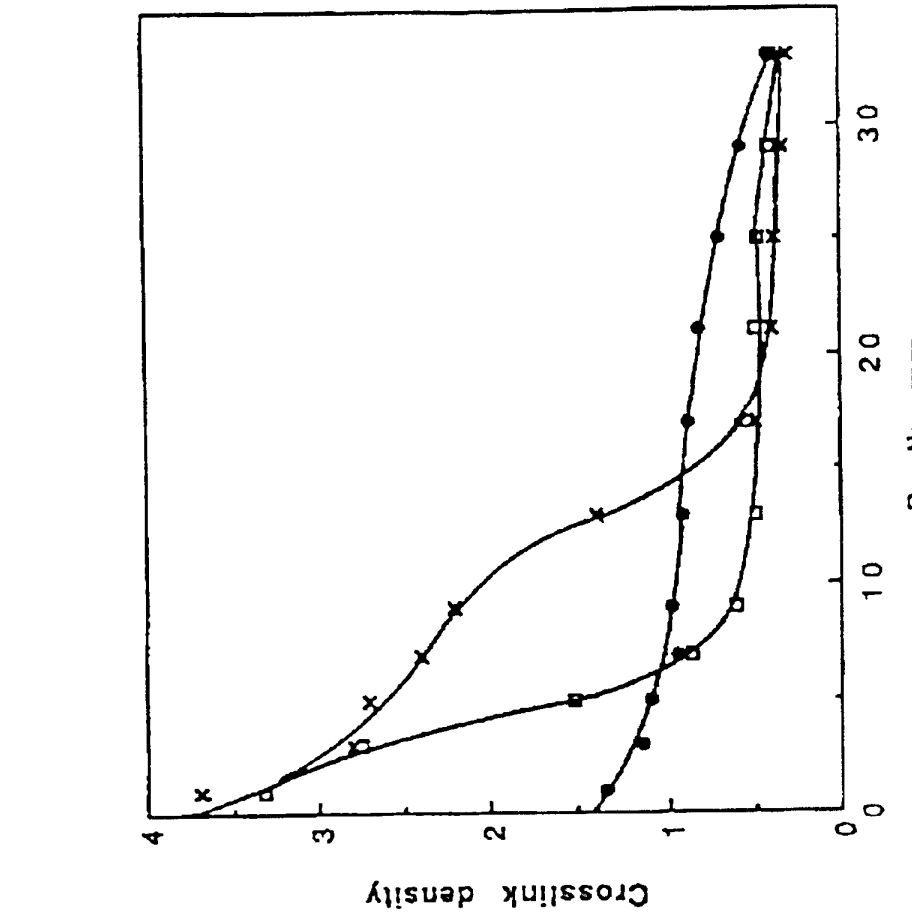


Figure 2 Effect of time and temperature on the ageing profile of composite propellant (□ - 8wks 80°C, x - 64 wks 60°C and ● 167 wks 40°C)

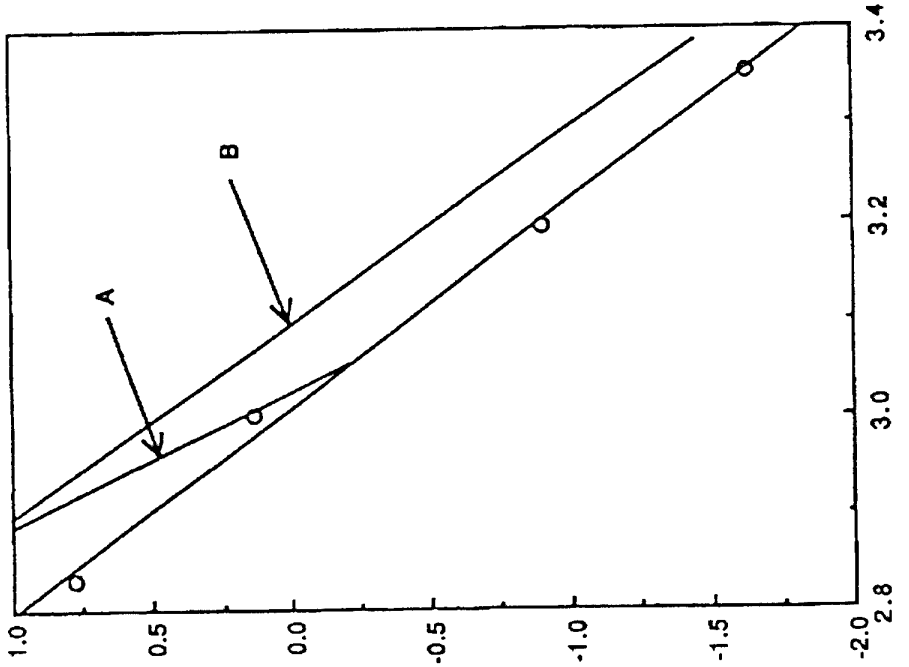


Figure 1 Effect of temperature and additives, A and B, on the rate of oxidative ageing of composite propellant

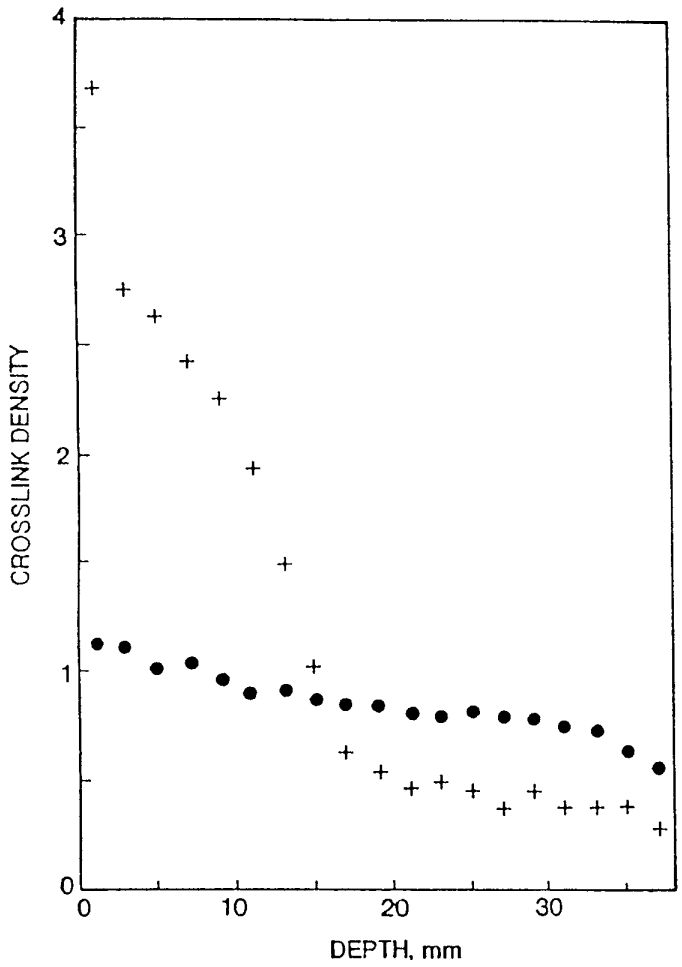


FIG.3 EFFECT OF CATALYTIC ADDITIVE ON THE AGEING OF COMPOSITE PROPELLANT AFTER 64 wks AT 60°C (● NO ADDITIVE, + ADDITIVE)

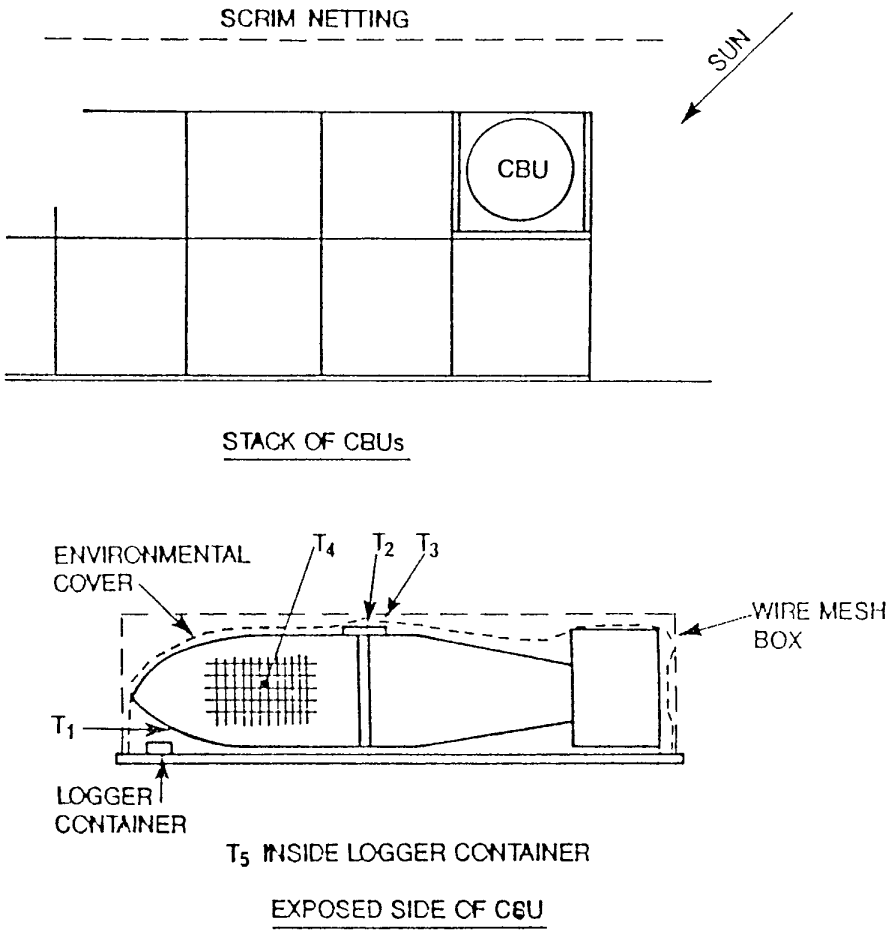


FIG.4 LOCATION OF CLUSTER BOMB UNIT AND THERMISTORS, T_1 – T_4

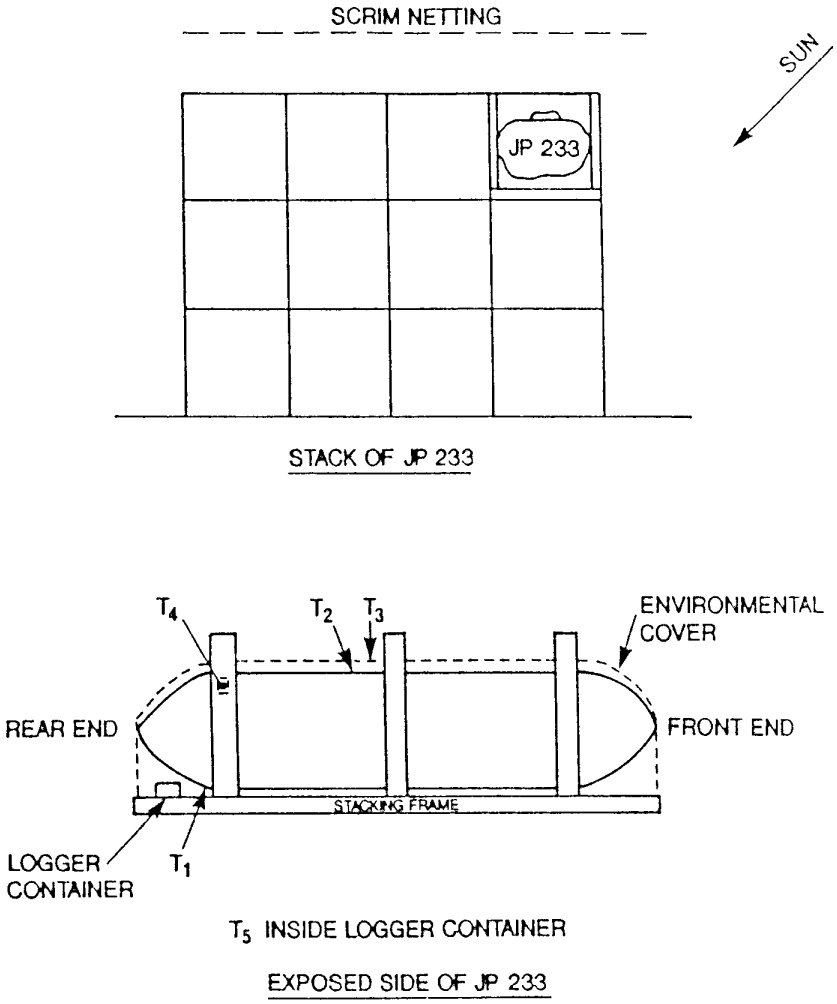


FIG.5 LOCATION OF JP 233 AND THERMISTORS T_1 - T_4

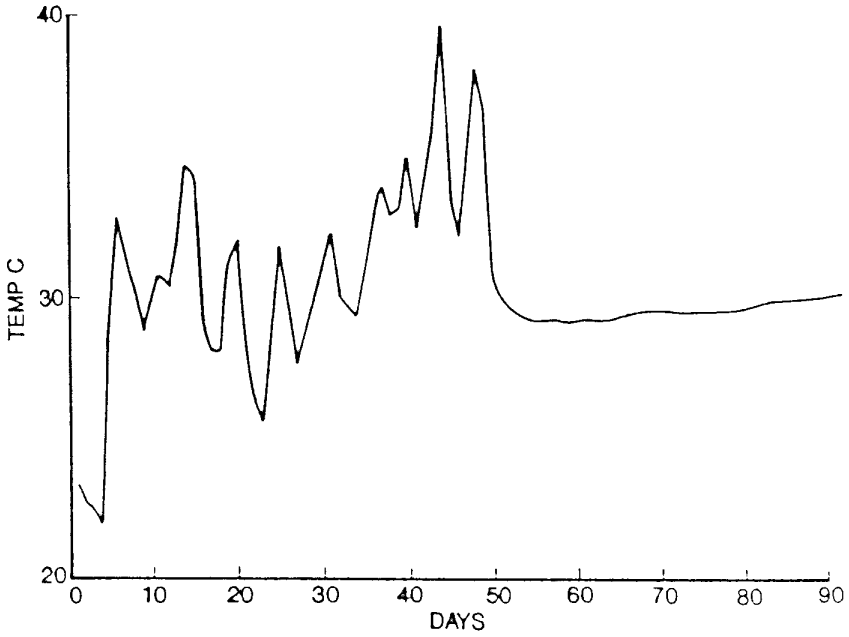


FIG.6 AVERAGE DAILY TEMPERATURES FOR JP 233, THERMISTOR T1 FROM 3rd May to 1st August 1991

Life Time Assessment and Stability of AN/GAP Propellants

Dr. Manfred A. Bohn
Dr. Jutta Böhnlein-Mauß
Dr. Klaus Menke

Fraunhofer-Institut für Chemische Technologie - ICT
Joseph-von-Fraunhofer-Straße 7
D-76327 Pfinztal-Berghausen
Germany

1. Abstract

If the ingredients and their chemical properties are considered, propellants based on ammonium nitrate, GAP binder and nitrate ester plasticizers are a challenge to achieve good chemical stability and a sufficient life time. This contribution gives a short overview about the chemical stability of propellant formulations with pure AN (so-called SCAN with less than 0.04 mass% water content) and phase stabilized AN (PSAN) in AN/GAP/TMETN/BTTN-based formulations and with a new burn rate modifier based on mixed molybdenum/vanadium oxides called MOVO. Stabilizer consumption, mass loss, cube crack thermal cycling and other aging tests were performed with distinctive formulations. It is shown that phase stabilizing metal complexes for AN as well as BTTN deteriorate the chemical stability and shorten the life time of the propellants. DPA and a mixture of MNA/2NDPA prove to be suitable stabilizers. Stabilizer consumption is described with an improved kinetic formulation based on a combination of the reactions of first and zero order. For the prediction of life times with mass loss as function of time and temperature an autocatalytic rate equation is used. As a result of the development a propellant formulation was found with medium performance (I_{SP} = 229 s at 7 MPa) based on pure AN in AN/GAP/TMETN with MOVO burn rate modifier, which has satisfying values for chemical stability and a sufficient life time. The propellant will meet the applicational profiles of a temperate climate.

2. List of Symbols and Abbreviations

I_{SP}	specific impulse
GAP	glycidyl azido polymer
N100	trifunct. isocyanate
IPDI	isophorone diisocyanate
AN	ammonium nitrate
SCAN	spray crystallized AN
PSAN	phase stabilized AN
Ni-, Cu-, Zn-PSAN	with Ni-, Cu- or Zn-complexes phase stabilized AN
TMETN	trimethylolethane trinitrate
BTTN	1,2,4-butanetriol trinitrate
NE	nitrate ester plasticizer
RDX	cyclo-1,3,5-trimethylene-2,4,6-trinitramine, hexogen
DPA	diphenylamine
2NDPA	2-nitrodiphenylamine
MNA	N-methyl-p-nitroaniline
CuPc	copper phthalocyanate
MOVO	mixed molybdenum/vanadium oxides
mps	mean particle size
adp	adhesion promoter

3. Introduction and Objective

Propellants based on ammonium nitrate and energetic binders are regarded as suitable candidates for less sensitive, high energetic, signature free minimum smoke rocket propellants. The development of these systems started in 1986 or even earlier in several propellant laboratories all over the world. Some of the results about propellants based on AN/GAP and PSAN/GAP and nitrate ester plasticizers have been published recently /1, 2/.

Other formulations using NiPSAN/GAP with BDNPF/A and PSAN with nitramine binders appeared in AGARD and AIAA proceedings a few years ago /3, 4/.

For propellants based on AN/GAP/BTTN and TMETN the following properties have been developed at ICT:

Paper presented at the AGARD PEP Symposium on "Service Life of Solid Propellant Systems" held in Athens, Greece, 10-14 May 1996, and published in CP-586.

* a medium to high specific impulse in the range of 226-238 s at 7 MPa, if a high content of energetic plasticizer is used in the formulation

* burn rates r between 6 and 8 mm/s at 7 MPa with pressure exponents n between 0.50 and 0.70, dependent on the applied burn rate modifier

* suitable processing and mechanical properties

* low detonation sensitivity, particularly if high energetic nitramines like RDX or HMX are applied only in a few percent.

So far this type of AN-propellants has been shown to extend the class of minimum smoke propellants. The potential was demonstrated for their use as high energetic non polluting propellants, which are really less sensitive and exhibit smokeless burning /1, 2/.

But the development revealed also some crucial problems of the AN/GAP-propellant system. The most severe ones proved to be a bad combustion behaviour and/or a problematical chemical and aging stability. If the ingredients and their chemical properties are considered, the propellant system based on AN/GAP/NE must be a challenge to achieve a good chemical stability and a sufficient life time.

Several drawbacks are connected with the use of ammonium nitrate. Besides its low energy and low reactivity in combustion reactions there are trends for chemical hydrolysis and the thermal splitting into ammonia and nitric acid, phase and volume changes of the crystal structure and a high hygroscopicity /5, 6/.

GAP contributes to the stability problems by thermal or catalytic cleavage of the azido group and the nitrate esters TMETN and BTTN are known for the thermal splitting of the CO-NO_2 bond and autocatalytic decomposition caused by NO_2. The reduction of NO_2 may lead to nitrous acid, which forms with ammonium nitrogen and water.

Therefore the objective of our work concerns:

* the determination of factors, which influence the stability of AN/GAP/NE and PSAN/GAP/NE propellants

* the determination of chemical ingredients, which can be used in a propellant formulation to achieve
  - high performance
  - acceptable combustion behaviour
  - satisfying chemical stability

* the determination of suitable stabilization agents

* the determination of the degree of stabilizer consumption from storage between 60°C and 90°C

* the life time assessment of distinctive high energetic AN/GAP/NE-propellants.

4. Propellant Ingredients

Basis of the propellants, which were examined in this work, are pure AN (in this work this means always SCAN) and phase stabilized AN products, which were made at ICT by spray atomization (spray crystallization) from the melt. The AN and PSAN are characterized by small particle sizes, spherical particle shape and low water content. Four types have been used for the propellant formulations, which were tested on chemical and aging stability:

AN - SCAN = pure AN
water content: 0.02-0.04 %

Ni - PSAN = made from AN + 3.0 % Ni_2O_3
with the stabilizing complex
$Ni(NH_3)_2(NO_3)_2$
water content: 0.1 - 0.2 %

Cu - PSAN = made from AN + 3.0 % CuO
with the stabilizing complex
$Cu(NH_3)_2(NO_3)_2$
water content: 0.1 - 0.2 %

Zn - PSAN = made from AN + 3.0 % ZnO
with the stabilizing complex:
$Zn(NH_3)_2(NO_3)_2$
water content: 0.1 - 0.2 %

All AN- and PSAN-types were used as bimodal mixtures with the particle sizes of 160 µm and 55 µm. To prevent caking they were coated with 0.5 % Aerosil (SiO_2).

GAP was purchased from SNPE (France) Hydroxy di- and trifunctional versions were used with an equivalent mass of 1200 - 1330 g and an average molecular mass of 2000 - 2500 g/mol. They were cured with the trifunctional isocyanate N100 from Bayer AG (Germany) and with mixtures of N100 and IPDI, the last

one from Hüls AG (Germany). BTTN was received from Wasag Sythen (Germany), TMETN was made at ICT. The molybdenum/vanadium-oxides (MOVO), which were used for burn rate modification, were made at ICT by sintering and grinding from the pure oxides MoO_3 and V_2O_5.

5. Methods and Tests

To determine stability and life time a number of short time stability tests and extended aging tests were performed.

For a screening-type determination of the chemical stability Dutch test and vacuum stability test were applied to small samples of the propellants. For the Dutch test a 2.0 g sample was heated in a stoppered tube for 72 h at 105°C. No more than 2.0%, maximum 3.0 %, mass loss should occur from 8 to 72 h heating at 105°C. To determine vacuum stability a 2.5 g sample was heated in an evacuated standardized apparatus for 40 h at 100°C or 80°C. At 100°C no more than 5 ml gas evolution, at 80°C no more than 1 ml gas evolution should originate from the propellant.

Storage of 50 mm cubes for 15 d at 80°C together with the temperature cycling tests of 60 mm cubes for 80 cycles from -30°C to +70°C, 1 cycle per day, may be regarded more close to service conditions than the tests with smaller samples. For temperature cycling the 60 mm cubes and smaller sample specimen were kept for 6 h at -30°C and 6 h at +70°C level, which were 'connected' with a 6 h increase and 6 h decrease in temperature.

For the 50 mm and 60 mm cubes the days of storage at 80°C and the number of cycles from -30°C to +70°C untill cracks occured in the cubes were determined by X-ray analysis. During the cube crack test at 80 °C the cubes were examined every day. During the temperature cycling test the 60 mm cubes were examined after 5, 10, 20, 40 and 80 cycles. Additionally, tensile strength, elongation (strain) at break and elasticity modulus at 20°C with a drawing speed of 50 mm/min were determined. The relative humidity was kept at 30 % during the tensile tests.

Long term aging tests were performed on 2 g propellant samples at 70°C, 80°C and 90°C storage temperature by mass loss determination. The data were described with an autocatalytic kinetic model for the mass loss, already discussed in Paper 2 on this AGARD-symposium /7/. The life time up to 2 % mass loss of some propellant formulations were calculated.

Stabilizer consumption is investigated between 60°C and 90°C for DPA and MNA/2NDPA stabilizer systems. The stabilizer concentration was determined by HPLC. The decrease of stabilizer concentration is reproduced well by an improved kinetic formulation, based on a combination of the reactions of first and zero order, disussed in /7, 8/.

6. Results

6.1 Short Time Stability Tests

Dutch test and vacuum stability were used for screening tests on AN(=SCAN)/GAP, NiPSAN/, CuPSAN/ and ZnPSAN/GAP-formulations. The results are pointed out in Table 1 and Fig. 1 and Fig. 2. First of all, SCAN/GAP, NiPSAN/, CuPSAN/ and ZnPSAN/GAP-formulations were tested without nitrate esters and without stabilizers. The data in Table 1 indicate that all kinds of PSAN/GAP-formulations are not stable under these conditions. Several stabilizer systems have been tested in SCAN/ and NiPSAN/GAP/TMETN-formulations. Some of the results are outlined in Table 1 and Fig. 1. Again stability is only indicated for SCAN/GAP/TMETN-formulations with DPA as stabilizer. For NiPSAN-formulations DPA also proves to be the best solitary stabilizer, but the mixture of MNA/2NDPA originates the best vacuum stability. The vacuum stability tests at 80°C indicate stability for NiPSAN- and ZnPSAN-formulations. These types failed at 100°C, however. A comparison of the values of Dutch test and vacuum stability test for SCAN/, NiPSAN/, CuPSAN/ and ZnPSAN/GAP/TMETN-formulations is outlined in Fig. 2.

Propellant formulations with SCAN/GAP/TMETN and MOVO burn rate modifier are stable with DPA as stabilizer. Formulations of SCAN/GAP/TMETN and BTTN seem better stabilized with a mixture of MNA/2NDPA, however. The incorporation of BTTN, which increases the specific impulse, deteriorates the stability of the propellant formulations to a certain extent. According to the first results, MOVO burn rate modifier seems to have no influence on stability.

6.2 Cube Crack and Temperature Cycling Tests

With cube crack tests and temperature cycling tests a comparison was made between

'equalized' SCAN/, NiPSAN/ and CuPSAN/GAP-formulations, see Table 2, with TMETN, 5 µm mps RDX and MOVO burn rate modifier. One goal of these tests was the examination of phase stability and thermal cycling behaviour of the pure AN (=SCAN) with less than 0.04% water content incorporated in a propellant formulation. Another goal was the examination of SCAN/GAP-propellants with about 1% copper phthalocyanate as a burn rate modifier which shows a promising synergistic effect to MOVO burn rate modification /9/.

The formulations of the described propellants are outlined in Table 2. The results of these tests are shown in the Fig. 3 to 7.

Fig. 3 shows the results of the cube crack test for a 15 days storage of 50 mm cubes at 80°C. The length of the bars marks the storage time after which cracks have been detected in the cubes, except for the SCAN/GAP-propellants AN 140 and AN 164 with 2.5 % and 2.0 % MOVO catalyst, they did not show any cracks after 15 days storage time. Cracks occur, however, in NiPSAN/ and CuPSAN/GAP as well as in AN + CuPc/MOVO propellant cubes already after a short storage time.

During temperature cycling no cracks occurred in the SCAN/ and NiPSAN/GAP propellant cubes, Fig. 4. The CuPSAN/GAP-propellant No. 110 and the SCAN/GAP-propellant No. 149a with CuPc/MOVO burn rate modifier, showed cracks and instability after a comparatively small number of cycles. The change of mechanical properties during temperature cycling was examinded by taking out two samples for the uniaxial tensile test on an Instron machine after 5, 10, 20, 40 and 80 cycles. The results are presented in Fig. 5, 6 and 7. The tested SCAN-, CuPSAN- and NiPSAN-propellants AN 140, AN 110 and AN 134 were derived from the same basic formulation, keeping the binder system and other ingredients constant.

Tensile strength, elasticity modulus and elongation at break of propellants No. 110, 134 and 140 showed no significant changes. After 80 cycles a decrease in elongation at break is observed together with an increase of elasticity modulus for all three formulations. The reason might be an additional crosslinking of the GAP-binder during aging. It is remarkable that no decrease of the mechanical properties of the SCAN/GAP-propellant No. 140 is observed.

6.3 Determination of Life Time with Mass Loss and Stabilizer Consumption

According to the results of short time stability, cube crack and temperature cycling tests it was obvious that only SCAN/GAP-propellants are worth-while for a further examination of the long term stability that means time-temperature stability. For this, mass loss and stabilizer consumption are measured with selected formulations.

Table 3 shows the particular formulations which were chosen for a more detailed investigation. They enable a comparison of SCAN/GAP-formulations: with TMETN and TMETN/BTTN-plasticizer (AN 164 and AN 178), with and without MOVO burn rate modifier (AN 212 and AN 213), with DPA and MNA/2NDPA-stabilizer (AN 212 and AN 221). AN 178 and AN 212 differ in the adhesion promoter, which is not outlined here.

The determined values of flash point (auto-ignition temperature), Dutch test and vacuum stability are written beneath the formulations. The effects can be summerized as follows:

* BTTN originates less favorable values of Dutch test and vacuum stability
* MOVO burn rate modifier have a slight deteriorating effect on the stability
* MNA/2NDPA seems to have a better stabilizing efficiency on AN/GAP/BTTN/TMETN-formulations than DPA.

The mass loss (ML) of samples with 2g was determined from the five propellant formulations of Table 3 between 60°C and 90°C. In Fig. 8 the curves according to eq.(3) with incorporated eq.(2) are to see together with the measured data at 70°C, 80°C and 90°C for the two types AN 212 and AN 221. The data are described quite well. The mass loss start nearly at the beginning of the storage with steadily increasing mass loss (reaction) rate. This is a typical autocatalytic decomposition behaviour, which is also found with gun propellants (GP), for example with the triple base GP KN6540 /10/. Eq.(1) shows the rate equation for an autocatalytic mass loss, written with the relative mass M_r. In this formulation the two rate constants have the

dimension 1/time. This kinetic formulation is presented more extensive in /7, 10/

The times to reach a preset degree of mass loss y_{ML} are the sought for life times. In Table 4 the times to reach y_{ML}=0.02 (2% ML) at temperatures between 20°C and 100°C are listed, together with the Arrhenius parameters of the two rate constants. For comparison the corresponding times of the GP KN6540 are given also. The formulation AN 164 without BTTN has the longest times $ty_{ML}(T)$. The addition of BTTN in AN 178 reduces the values considerably. AN 212 differs from AN 178 in the used MOVO type and has an adhesion promotor. The ty_{ML} at 80°C and 90°C are the smallest of all five formulations. The greater difference at lower temperatures is probably caused by a scattering in the data at 70°C. The collection of mass loss data is continued also at 60°C. AN 221 is the same formulation as AN 212 except for the stabilizer. In AN 221 a MNA/ 2NDPA mixture is used, which gives an improvement compared to DPA in AN 212.

Mass loss

$$(1)\quad \frac{dM_r(t,T)}{dt} = -k^1_{ML}(T) - k^2_{ML}(T)\cdot M_r(t,T)\cdot\left(1-M_r(t,T)\right) \quad \text{with} \quad M_r(t,T) = 1-M(t,T)/M(0)$$

$$(2)\quad M_r(t,T) = \frac{1}{2} + \frac{a}{2k^2_{ML}(T)}\cdot\frac{\left(a+k^2_{ML}(T)\right)\cdot\exp(-a\cdot t)-\left(a-k^2_{ML}(T)\right)}{\left(a+k^2_{ML}(T)\right)\cdot\exp(-a\cdot t)+\left(a-k^2_{ML}(T)\right)} \quad \text{with} \quad a=\sqrt{k^2_{ML}(T)\left(4k^1_{ML}(T)+k^2_{ML}(T)\right)}$$

$$(3)\quad ML(t,T) = O+100\%\cdot\left(1-M_r(t,T)\right) \quad \text{and} \quad ty_{ML}(T) = f\left(k^1_{ML}(T),k^2_{ML}(T)\right)$$

Stabilizer consumption

$$(4)\quad \frac{dS(t,T)}{dt} = -k^1_S(T)\cdot S(t,T) - k^2_S(T)$$

$$(5)\quad S(t,T) = \left(S(0)+\frac{k^2_S(T)}{k^1_S(T)}\right)\cdot\exp\left(-k^1_S(T)\cdot t\right)-\frac{k^2_S(T)}{k^1_S(T)}$$

$$(6)\quad ty_S(T) = \frac{1}{k^1_S(T)}\cdot\ln\left(\frac{1+\dfrac{k^2_S(T)}{S(0)\,k^1_S(T)}}{y_S+\dfrac{k^2_S(T)}{S(0)\,k^1_S(T)}}\right)$$

The times for KN6540 are all longer, but the range of the ty_{ML}-values of the best formulations AN 164 and AN 221 is comparable with the values of KN6540.

A first impression of the stabilizer consumption in the two formulations AN 212 and AN 221 gives Fig. 9. The curves are eq.(5), which has been discussed already in /7, 8/ and examples can be found in /10/. With eq.(6) one can calculate the times $ty_S(T)$ to reach a preset degree of stabilizer consumption y_S. DPA in AN 212 is consumed quite fast. At 90°C the MNA depletion takes more time compared to the DPA decrease. The 2-NDPA is consumed not before the MNA is consumed nearly completly. But to judge the life time of AN 212 correctly with stabilizer decrease, the consumption of the consecutive DPA products N-NO-DPA, 2-NO_2-DPA and 4-NO_2-DPA should be considered also. The investigation of the stabilizer decrease on these propellants is continued. In Table 5 first data of the reaction rate constants of the DPA and MNA decrease are given.

The calculated life times at ambient temperatures are for all formulations and for the GP KN6540 long, several 100 years to more than 1000 years. The reasons for such long life times are discussed in Paper 20 on this symposium /10/. The method applied here is correct in itself. At lower temperatures the values must be used relatively. To get absolute values one must determine the change of the properties, mass loss and stabilizer consumption, also at somewhat lower temperatures, which needs more time to get the data. The task of a prediction method at the point of development encountered here is, to assess for the first time the time-temperature stability of the formulations. This has to be considered as a part of the total development of a new propellant formulation.

7. Conclusion

According to the results of the short time stability tests and aging tests the chemical stability and the life time of AN/GAP/NE-propellants is critically dependent on phase stabilizing metal complexes of the applied ammonium nitrate, on types and specifications of burn rate modifiers and on the stability of the applied nitrate esters.
NiPSAN/, CuPSAN/ and ZnPSAN/GAP/NE-propellants have not fulfilled the requirements for Dutch test and vacuum stability. They failed in the cube crack test and could not be stabilized efficiently up to now.

Propellants with SCAN (=pure AN with a water content < 0.04 mass%), GAP, TMETN, MOVO burn rate modifier and DPA as stabilizer are moderately stable according to Dutch test, vacuum stability test, cube crack and temperature cycling test. If they contain only TMETN as plasticizer, they have a somewhat lower energy (I_S = 229 s at 7 MPa for AN 164) but significantly better stability and service life than those with BTTN but higher energy (AN 178, 212, 221, I_{SP} = 234 - 235 s at 7 Mpa).

The applied kinetic formulations for stabilizer consumption and autocatalytic mass loss are suitable for the assessment of the life time. All together, the stability and the life time of AN/GAP/NE-propellants appear to be not to far from those of a high energetic double base rocket propellant. They will meet the applicational profiles of a temperate climate, but not those of the hot zones.

Acknowledgement

The authors thank the Bundesministerium für Verteidigung (German MOD) for financial support of this work

8. References

/1/ Y. Longevialle et.al.; *„Low Vulnerability Minimum Smoke Rocket Propellants"*, ADPA-Conf. on Energ. Mat., T.M. 680, p 125 ff, Phoenix, Arizona (1995).

/2/ K. Menke et.al.; *„Development of Less Polluting Propellants"*, AGARD-CP-559, 84th PEP Symp. Alesund, Norway (1994).

/3/ P. Lesard et.al.; *„Development of a Minimum Smoke Propellant based on GAP and AN"*, AGARD-CP-511, 78th Spec. Meeting, Bonn, Germany (1991).

/4/ R.L. Bivin et.al.; *„Development of a Class 1.3 Minimum Smoke Propellant"*, 28th AIAA J. Prop. Conf. Nashville, Tennessy (1992).

/5/ W. Engel et.al.; *„Ammonium Nitrate - a Less Polluting Oxidizer"*, 24th Internat. Annual Conference of ICT, 1993, Karlsruhe, Germany.

/6/ J.C. Oxley et.al.; *„Thermal stability and compatibility of AN explosives on a small and a large scale"*, Thermochim. Acta 212, 77-85 (1992).

/7/ M.A. Bohn, *„Methods and Kinetic Models for the Lifetime Assessment of Solid Propellants"*, 87th AGARD-PEP Symp., Athens, Greece 1996.

/8/ M.A. Bohn, Propell., Expl. Pyrot. 19, 266 (1994).

/9/ K. Menke a.o., *„Characteristic Properties of AN/GAP Propellants"*, Propell., Expl., Pyrot. 21, 1-7 (1996).

/10/ F. Volk, M.A. Bohn, *„Ageing Behaviour of Propellants Determined by Mass Loss, Heat Generation, Stabilizer Consumption and Molar Mass Decrease"*, 87th AGARD-PEP Symp., Athens, Greece 1996.

Table 1: Values of flash point (autoignition temp.), Dutch test and vacuum stability of AN(=SCAN)/GAP and PSAN/GAP formulations.

SCAN (%)	PSAN NiO (%)	PSAN CuO (%)	PSAN ZnO (%)	GAP N100 (%)	TMETN (%)	BTTN (%)	RDX (%)	MOVO Cat. (%)	Stabilizer	%	flash point 20°C/min (°C)	Dutch test 8-72h/105° (% m.loss)	vac. stab. 40h/80°C (ml/2.5g)	vac. stab. 40h/100°C (ml/2.5g)	remarks
70				30							212	1.33	0.80	3.26	stable
	70			30							208	2.52	2.23	16.2	--
		70		30							206	1.77	2.39	10.1	--
			70	30							209	1.74	2.47	11.4	--
50				19	30				NDPA	1	186	3.22	0.68	6.39	--
50				19	30				DPA	1	182	2.76	0.36	3.71	stable
	50			19	30				NDPA	1	184	2.73	0.86	15.6	--
	50			19	30				MNA	1	181	5.59	0.37	12.7	--
	50			19	30				DPA	1	181	3.30	0.35	9.67	--
	50			18.5	30				MNA NDPA	1 0.5	179	3.00	0.36	6.47	--
60				19.5	10		10		DPA	0.5	184	0.37		1.54	stable
		60		19.5	10		10		DPA	0.5	181	3.00	2.01	16.2	--
			60	19.5	10		10		DPA	0.5	186	2.09	0.57	13.6	--
64				13	20			2.0	DPA	0.6	184	2.86		2.82	stable
65				13.5	9.5	9.5		2.4	DPA	0.5	183	4.70	0.22	5.41	--
65				13.5	19			2.4	DPA	0.5	182	3.05		1.86	stable
64				11	11	11		2.0	MNA NDPA	0.5 0.5	180	3.62		2.63	stable

Table 2: Propellant formulations for cube crack and temperature cycling tests.

ingredients	AN 110	AN 134	AN 140	AN 149a	AN 164
Cu-PSAN 160 µm	22	-	-	-	-
Cu-PSAN 55 µm	33	-	-	-	-
Ni-PSAN 160 µm	-	22	-	-	-
Ni-PSAN 55 µm	-	33	-	-	-
SCAN 160 µm	-	-	22	25.6	25.6
SCAN 55 µm	-	-	33	38.4	38.4
RDX 5 µm	10	10	10	-	-
GAP + adp	13.9	13.7	13.9	11.2	11.2
N 100 + IPDI	2.1	2.3	2.1	2.0	2.0
TMETN	15.5	15.5	15.5	19.8	19.8
DPA	0.5	0.5	0.5	0.6	0.6
MOVO	2.5	2.5	2.5	1.0	2.0
CuPc	-	-	-	1.0	-
carbon black	0.5	0.5	0.5	0.4	0.4

Table 3: AN/GAP-formulations, which were examined for aging behaviour with stabilizer consumption and mass loss for the calculation of life times.

ingredients	AN 164	AN 178	AN 212	AN 213	AN 221
AN 160/55µm	64	64	64	66	64
GAP + adp.	11.46	9.41	9.69	9.50	9.50
N100/IPDI	1.74	1.59	1.31	1.50	1.50
TMETN	19.8	11	11	11	10.8
BTTN	---	11	11	11	10.8
DPA	0.6	0.6	0.6	0.6	---
MNA	---	---	---	---	0.5
2NDPA	---	---	---	---	0.5
MOVO	2.0	2.0	2.0	---	2.0
carbon	0.4	0.4	0.4	0.4	0.4
flash point 20°/min , (°C)	183/185	182/183	183/185	182/183	179/180
Dutch test mass loss (%)	2.89/2.84	3.41/3.51	3.92/3.97	2.45/2.46	3.52/3.73
vacuum stability					
40h/80°C (ml/2.5g)	---	---	---	---	---
40h/100°C (ml/2.5g)	2.77/2.87	3.98/3.98	5.14/5.15	3.96/4.00	2.74/2.53

Table 4: Time to 2% mass loss (ML) for AN/GAP rocket propellants calculated according to eq.(3). For comparison the data of GP KN6540 are included.

temp.	AN 164		AN 178		AN 212		AN 213		AN 221		GP KN6540	
[°C]	[d]	[a]	[d]	[a]	[d]	[a]	[d]	[a]	[d]	[a]	[d]	[a]
20		1224		251		990		369		998		1795
30		244		63		173		84		178		309
40		52		17		34		21		36		59
50		11.6		4.5		7.2		5.3		7.8		12.6
60	998	2.7	474	1.3	613	1.7	534	1.5	680	1.9	1066	2.9
70	249		143		156		155		177		269	
80	66		45		43		48		50		73	
90	18.3		14.9		12.5		15.3		15.0		21.5	
100	5.4		5.2		3.9		5.2		4.8		6.7	
Ea^1_{ML} [kJ/mol]	110.7		93.3		122.3		100.5		135.0		135.8	
Z^1_{ML} [1 / d]	1.953 E+12		7.301 E+9		1.439 E+14		9.155 E+10		5.737 E+15		1.555 E+16	
Ea^2_{ML} [kJ/mol]	151.9		132.6		135.7		133.9		124.7		125.4	
Z^2_{ML} [1 / d]	9.998 E+20		2.086 E+18		6.502 E+18		2.822 E+18		1.704 E+17		6.630 E+16	

Table 5: Kinetic data of the stabilizer consumption in two AN/GAP rocket propellants evaluated according to eq.(5) for the rate constants and eq.(6) for t_0 (with y_S=0).

temp.	AN 212, DPA decrease			AN 221, MNA decrese		
	k^1_S	k^2_S	t_0	k^1_S	k^2_S	t_0
[°C]	[1/d]	[mass%/s]	[d]	[1/d]	[mass%/s]	[d]
90	1.3655 E-0	1.0034 E-2	2.94	3.4243 E-1	1.6855 E-2	6.71
80	3.8884 E-1	5.6206 E-3	8.62	-	-	-

Stability of AN- or Ni-PSAN/GAP/TMETN formulations

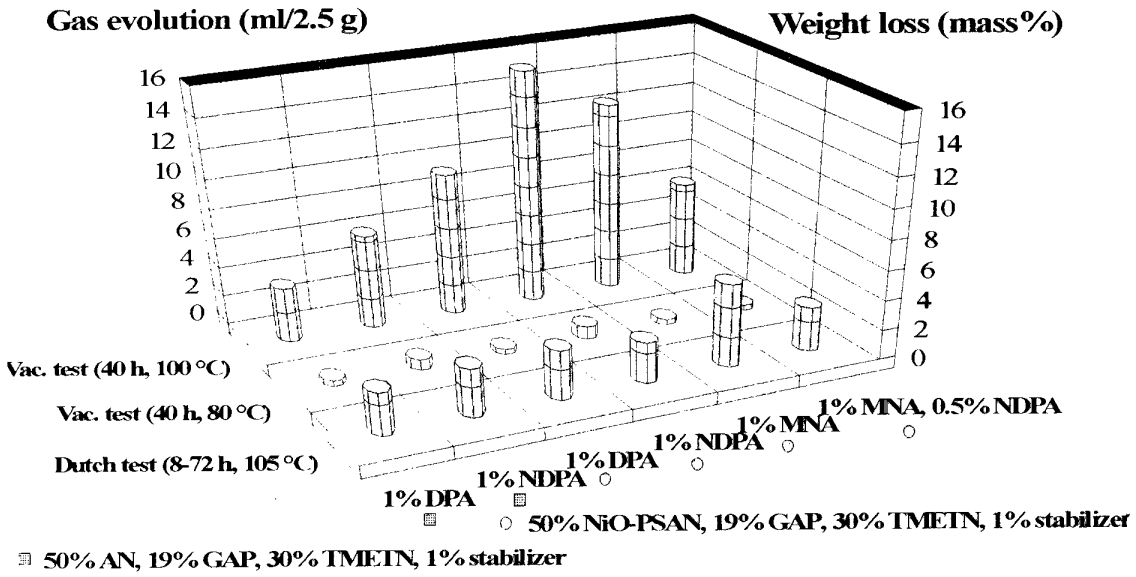
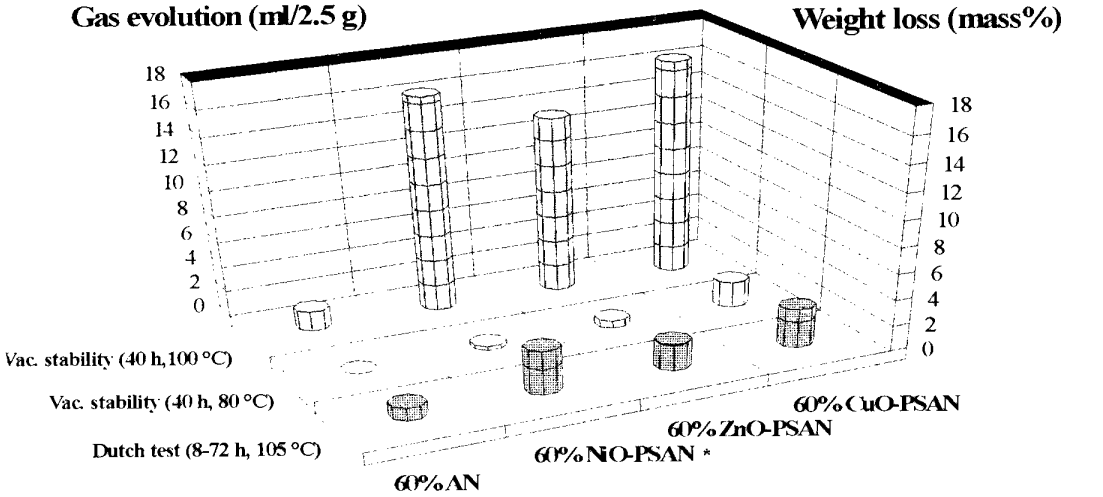


Fig. 1: Values of Dutch test and vacuum stability of basic AN(=SCAN) and NiPSAN/GAP-formulations with different stabilizers.

Stability of AN- or PSAN/GAP/TMETN/RDX formulations



60% AN or PSAN, 19.5% GAP/N100, 10% RDX, 10% TMETN, 0.5 % DPA

Fig. 2: Values of Dutch test and vacuum stability of basic AN(=SCAN) and PSAN/GAP propellant formulations with DPA and 2NDPA stabilizer.

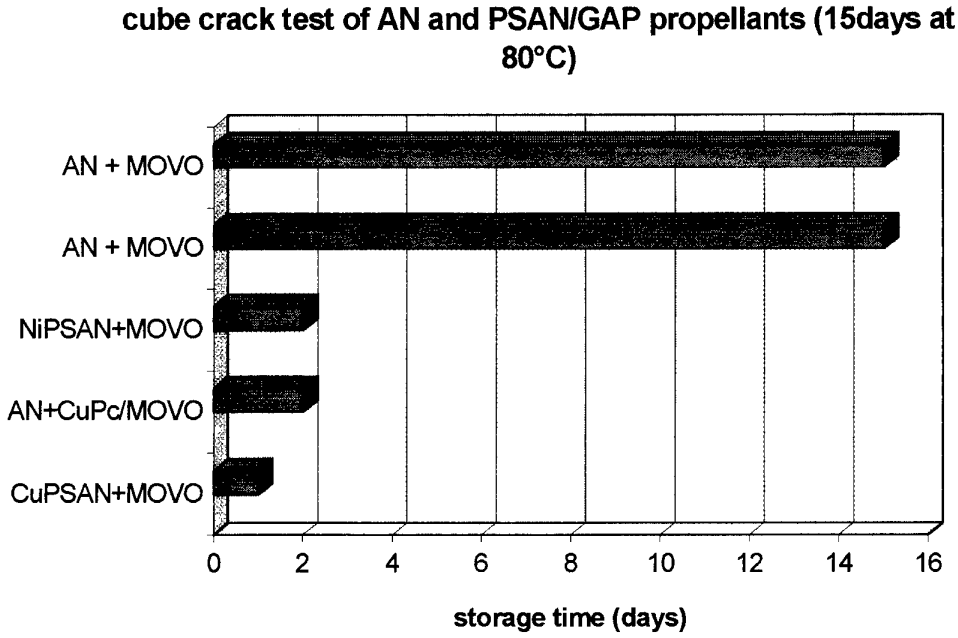


Fig. 3: Storage time till crack formation in 50 mm cubes of AN/ and PSAN/GAP propellants during cube crack test at 80°C.

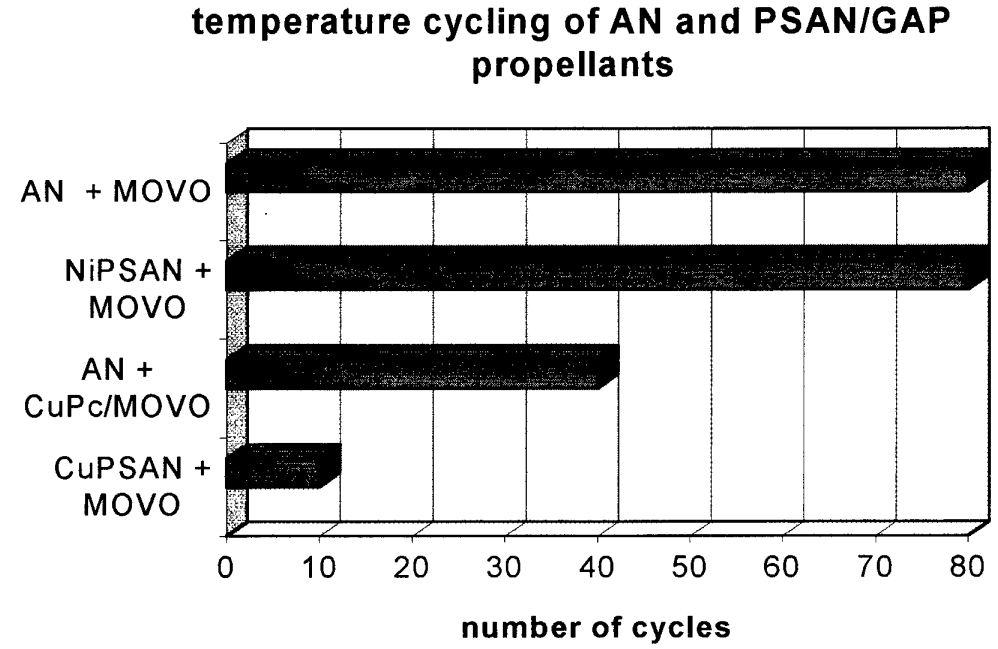


Fig. 4: Number of cycles till crack formation in 60 mm cubes of AN/ and PSAN/GAP propellants during temperature cycling test from -30° to +70°C.

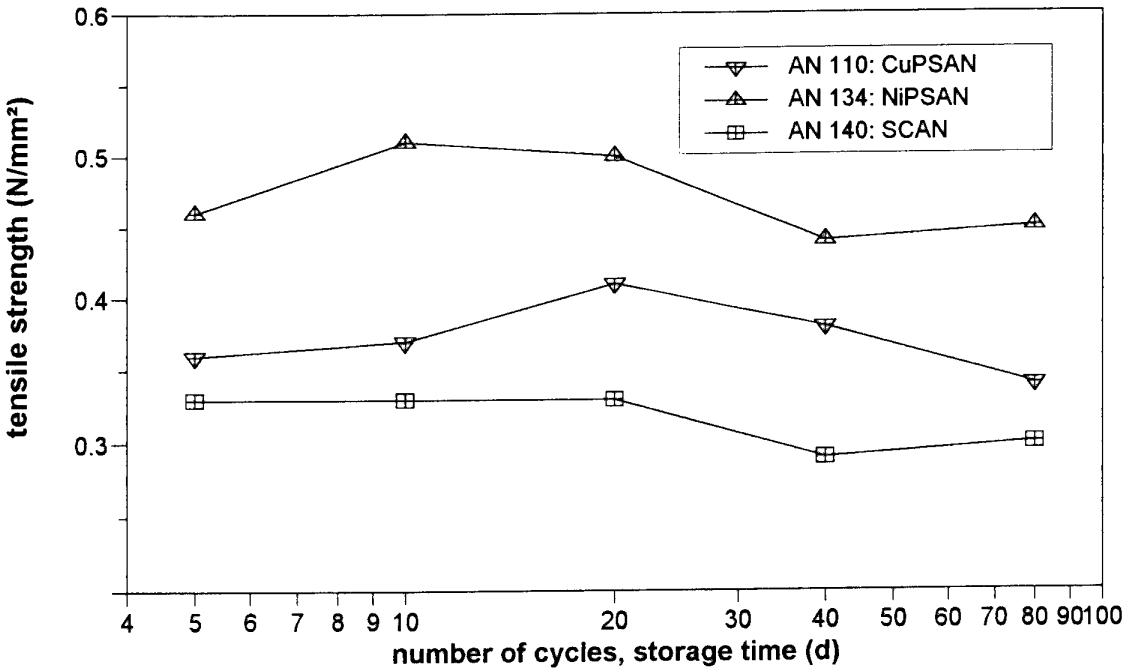


Fig. 5: Change of tensile strength of SCAN/, CuPSAN/ and NiPSAN/GAP propellant samples during temperature cycling test from -30° to +70°C.

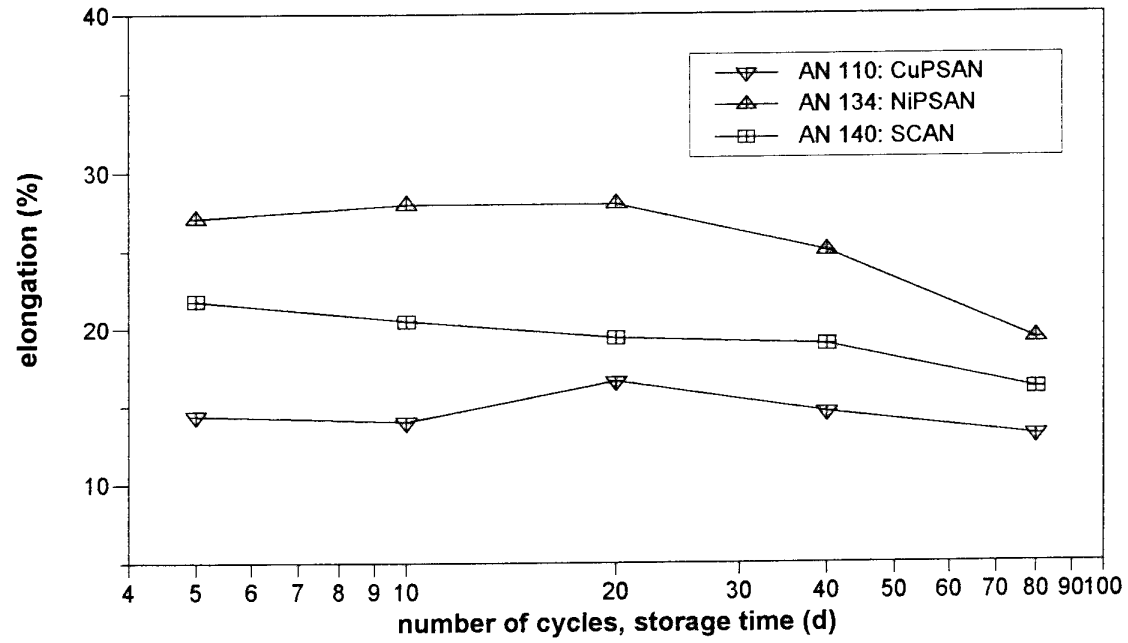


Fig. 6: Change of elongation at break of SCAN/, CuPSAN/ and NiPSAN/GAP propellant samples during temperature cycling test from -30° to +70°C.

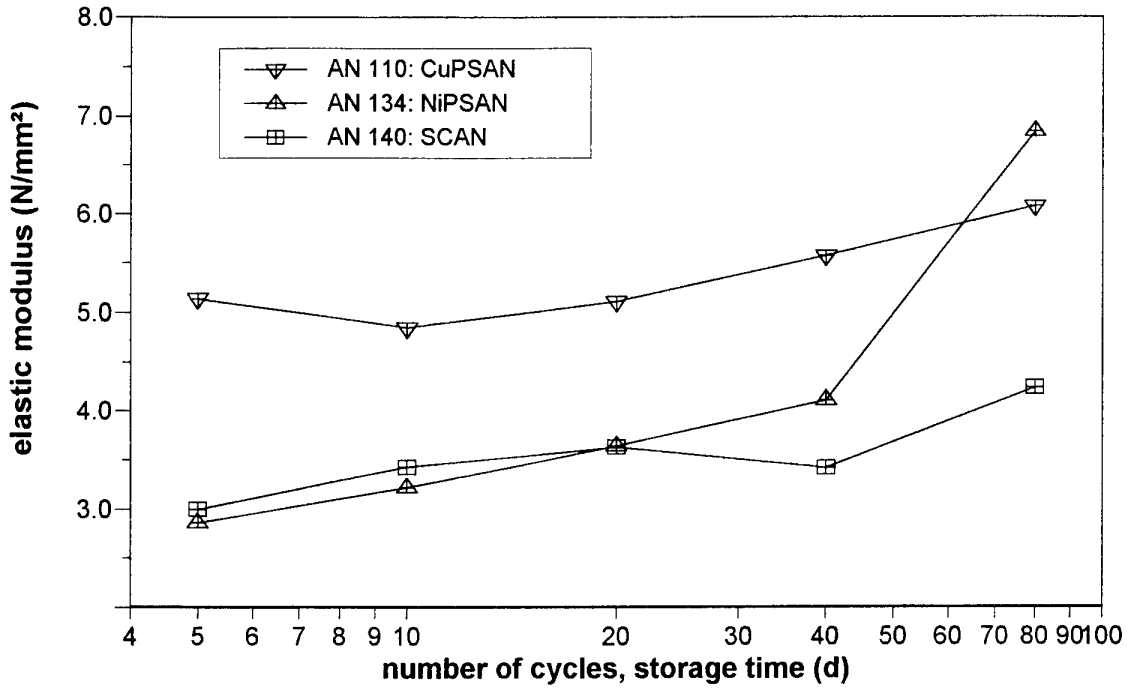


Fig. 7: Change of the elastic modulus of SCAN/, CuPSAN/ and NiPSAN/GAP propellant samples during temperature cycling test from -30° to +70°C.

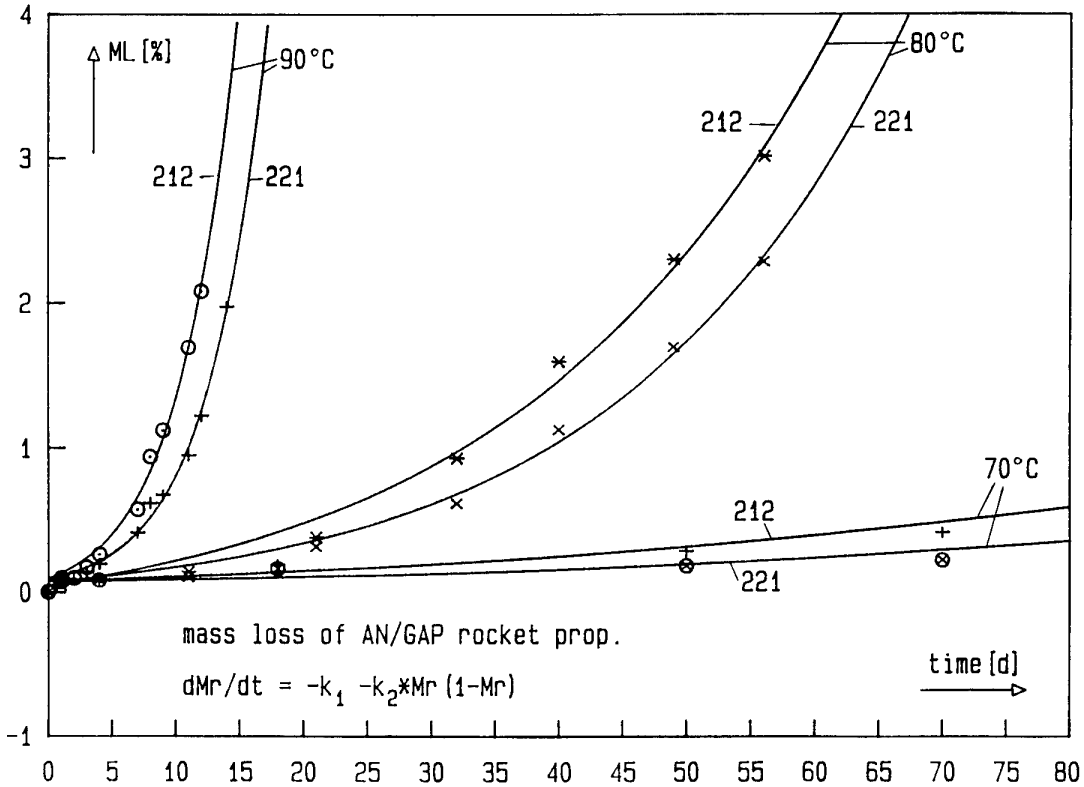


Fig. 8: Mass loss data of AN 212 and AN 221 formulation at 70°C, 80°C and 90°C. The Curves are the autocatalytic kinetic model, eq.(3) with eq.(2).

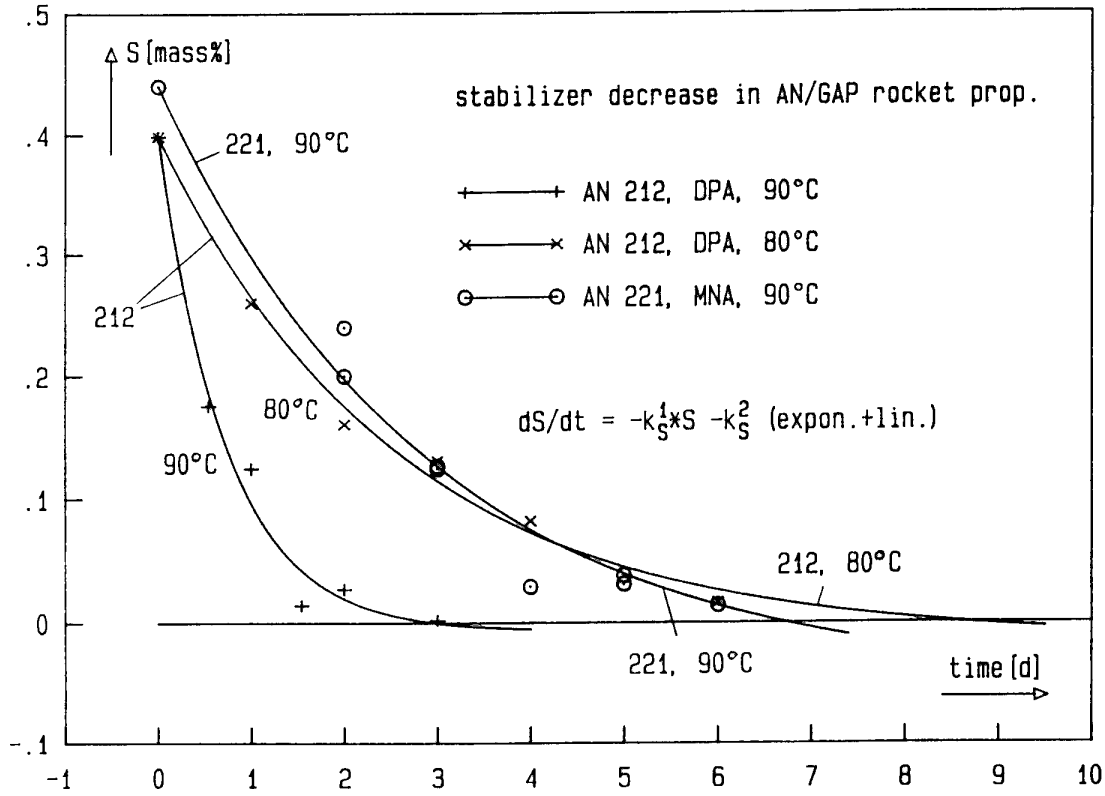


Fig. 9: Decrease of stabilizer DPA in AN 212 and stabilizer MNA in AN 221 formulation at 80°C and 90°C. The Curves are the kinetic model for stabilizer consumption, eq.(5).

Paper Number: 9
Discussor's Name: Dr. H. L. J. Keizers
Responder's Name: Dr. M. A. Bohn

Question: Did you see changes in the mechanical properties after accelerated aging?

Answer: The mechanical properties tensile strength, strain at break and elasticity modulus have been determined with the stressed samples for the cube crack test in temperature cycling (results now included in the paper). There are some changes for the PSAN/GAP formulations in strain at break and modulus. The data of SCAN/GAP did not change significantly. Further effects of accelerated aging on mechanical properties have not yet been investigated.

Characterization of the Degradation of the Polymer Binder in GAP-based propellants.

S. DÉSILETS and **F. PERREAULT,**
Defence Research Establishment Valcartier,
Weapon System Division
2459 Pie XI, North (P.O. Box 8800)
Courcelette, Québec, G0A 1R0
Canada

SYNOPSIS

Reliability assessment for composite propellants call for effective shelf-life predicting tools, implying the existence of appropriate accelerated aging procedures and of quantitative methods for the characterization of the degradation process. Ideally, one would like to investigate stabilizer depletion as well as the mechanical integrity of the polymeric network used as the binder. There are many available methods that can be combined to achieve this goal. In the present work, a comparative study of two of these methods has been performed. The first procedure makes use of FTIR spectroscopy to characterize the binder's degradation and of HPLC to follow stabilizer depletion. The other method based on ^{1}H NMR spectroscopy allows the measurement of the polymer network degradation, the depletion of the stabilizer and the loss of plasticizer in a single step. Finally, the pros and cons of both procedures have been evaluated from the analysis of experimental data related to the accelerated aging at 40, 60 and 80°C of GAP-based composite propellant formulations.

INTRODUCTION

Various methods have been proposed for the determination of propellant shelf-life. The most popular one is based on a stabilizer depletion technique [1,2], but other possible methods make use of heat generation and decrease of the mean molecular weight of the polymer [2], of gas evolution [3,4], or of the deterioration of the mechanical properties [5,6,7]. For composite propellants using a cross-linked polymer network as the binder, reliability is very dependent on mechanical integrity. In such a case, determining the extent of degradation of the polymeric binder upon aging appears to be a particularly good choice for shelf-life predictions.

Polyurethane networks are commonly used as the binder in propellant formulations. These insoluble, very high molecular weight cross-linked structures can not be easily characterized and indirect means of investigation are generally required. One possible way to monitor the binder's degradation is by measuring its sol fraction. As a matter of fact, apart from the sol fraction observed before aging which is a result of incomplete cross-linking, any extra soluble polymer appearing upon aging can only be the result of chain scission in the network. Precise determination of the increase in sol fraction can therefore be related to binder degradation.

Sol fraction of the polymer binder can be quantified by different means. One popular method uses Fourier Transform Infrared Spectroscopy (FTIR) to measure the change in the transmittance of a characteristic band related to a functional group exclusive to the polymer binder [8]. In fact, any analytical method allowing the identification and quantification of the polymer chains present in the sol fraction could be used. For example, it should be possible to proceed through proton Nuclear Magnetic Resonance (^{1}H NMR) if the peaks associated to the polymer are well isolated in the spectra obtained for the extracted solutions.

This work presents the development of such a NMR method applied to the characterization of a propellant binder based on Glycidyl Azide Polymer (GAP). Accelerated aging behaviour results obtained at three different temperatures for a typical propellant formulation are also used for a comparative evaluation of this new method against the more classical FTIR procedure, allowing the presentation of the pros and cons of the two methods investigated.

EXPERIMENTAL

Materials

The binder was based on a mixture of di and trifunctional GAP polymers purchased from Rocketdyne, California. A hydroxyl equivalent weight of 1210 g/eq. OH was determined for both these polymers by FTIR spectroscopy. A 50/50 mixture of bis-(2,2-dinitropropyl) acetal/formal

Paper presented at the AGARD PEP Symposium on "Service Life of Solid Propellant Systems" held in Athens, Greece, 10-14 May 1996, and published in CP-586.

(BDNPA/F), obtained from Aerojet Ltd, was used as a plasticizer. Isophorone diisocyanate (IPDI) from Huels Corp. and N-100 from Bayer Canada were used as the isocyanates, while di-butyltin dilaureate (DBTDL) from Aldrich Chemicals was added as a cure catalyst. The oxidizer was ammonium nitrate (AN), phase stabilized with 3% wt of ZnO, purchased from Wickman. The stabilizer diphenylamine (DPA) was obtained from BDH Inc. Additives like Carbon Black from Cancarb Ltd, magnesium oxide (MgO) from Anachemia, Tepanol surface agent from 3M and boron carbide from Aldrich were also used. Dichloromethane (CH_2Cl_2) from Anachemia was the solvent used for the extractions.

Formulations

The binder was based on a mixture of di and trifunctionnal GAP cured by a mixture IPDI and N-100. The system was plasticized at a plasticizer/polymer ratio of 2/1. The oxidizer consisted of 73% wt of phase stabilized AN and all formulations included 1% of DPA. Formulation 2969 contained no other additives, while 2970 included MgO and 2971 MgO and Tepanol, both of them accounting for less than 0.5% of the total formulation.

Sample preparation and aging

The ingredients were blended at 60°C, under dynamic vacuum in a 8CV Helicone Mixer from Atlantic Research. Moulded blocks were cured at 50°C until their hardness remained constant. The propellant blocks were cut into 6-mm thick slices before they were placed at 40, 60 and 80°C for various periods of time for aging. An unaged sample of the propellant was also kept at room temperature for comparison. A detailed presentation of the aging schedules can be found in Table I.

Table I. - Aging Schedule at 40, 60 and 80°C.

Temperature(°C)	Aging periods (days)
40	14,28,56,84,112
60	14,28,56,84,112
80	7,14,28,56

Extraction procedure

Soxhlet extractions were performed with dichloromethane for 18 hours on finely cut pieces (of aproximately 5 g) of the propellant mixtures. Dichloromethane was then removed under vacuum. The extracted material was weighed for calculation of the % GAP extracted and for the depletion of DPA. Only DPA, BDNPA/F and free polymer chains not attached to the binder network were extractable from the propellants. The network itself can be swollen but not dissolved, and the solubility of the solid ingredients is very low in organic solvents. This particularity provides us with a convenient method to quantify the degradation of the binder. As a matter of fact, an increase in the extractable part of a propellant as compared to what is observed for non-aged samples indicates more labile polymer chains, most probably explained by the degradation of the polymer network.

FTIR-HPLC analytical method

Characterization of the propellant's aging behaviour by FTIR spectroscopy alone was not possible. A combination of two analytical methods was therefore required. While Fourier Transform Infrared Spectroscopy is used to quantify the cross-linked binder's degradation, a chromatographic procedure was necessary for the characterization of the stabilizer's depletion.

FTIR spectroscopy

The extracted solutions were completed to 100 ml and analyzed using a Bomem spectrometer (Model M-110). From transmittance spectra, the GAP concentration in the solutions was determined using the intensity of the azide band at 2110 cm^{-1}. The samples were compared to a calibration curve obtained from GAP solutions of known concentrations. The percentage of GAP extracted from the propellant mixture as a function of aging has been calculated from these measurements.

High Performance Liquid Chromatography (HPLC)

The concentration of stabilizer as a function of aging time was determined using High Performance Liquid Chromatography (HPLC). The experimental set-up used is composed of a model 590 Waters pump system, a CSC-spherisorb column (ODS 2, 5 μm) and a Hewlett Packard multiple wavelength detector (series 1050) at λ = 254 nm. Integration of the peak corresponding to diphenylamine (DPA) was performed on spectra of extracted solutions from aged propellant blocks. A 70/30 methanol-water mixture was used as the mobile phase with a 1.0 ml/min flow rate.

NMR analytical method

^1H NMR spectra of the extracted material (DPA, BDNPA/F, GAP) were acquired with a Bruker WP-200 spectrometer. 10-30 mg of polymer samples were dissolved in

$CDCl_3$ in a 5 mm NMR tube. For each sample, 400-1000 scans were made with a relaxation delay of 20 s between each acquisition. The ^1H NMR spectra had peaks between 3.2-3.8 ppm for the GAP, 1.3, 2.2, 4.3 and 4.8 ppm for BDNPA/F and peaks between 6.8-7.4 ppm for DPA stabilizer. Calculation of the percentage of GAP in mixtures were determined by the integration of the surfaces of representative peaks according to equation 1. For this calculation, the peak at 2.2 ppm was chosen for BDNPA/F, while peaks at 3.2-3.8 ppm and at 6.8-7.4 ppm were used for GAP and DPA respectively. The % of GAP extracted from the formulations was then deduced using equation 2 given that the total weight of the extractable material(see Extraction procedure) and the initial weight of GAP in the sample used for the extraction are known.

Equation 1

$$\%GAP = \frac{\left(\frac{I_{GAP}}{5} \times MW_{GAP}\right)}{\left(\frac{I_{GAP}}{5} \times MW_{GAP}\right) + \left(\frac{I_{BDNPAF}}{6} \times MW_{BDNPAF}\right) + \left(\frac{I_{DPA}}{10} \times MW_{DPA}\right)}$$

MW_{GAP} = Molecular weight of GAP (99.1)

MW_{BDNPAF} = Average molecular weight of BDNPA/F (319.2). From a mixture of 50% BDNPA (326.2) and 50% BDNPF (312.2)

MW_{DPA} = Molecular weight of DPA (169.2)

I_{Gap} = Surface of the GAP peaks between 3.2-3.8 ppm

I_{BDNPAF} = Surface of the BDNPAF peak at 2.2 ppm

I_{DPA} = Surface of DPA peaks between 6.8-7.4 ppm

Equation 2.

$$\%GAP_{extracted} = \frac{\%GAP\,(W_e)}{W_{Gap}}$$

%GAP = Percentage of GAP in the extracted mixture as determined by equation 1.

W_c = Weight of the extracted mixture (GAP, + DPA + BDNPAF)

W_{GAP} = Weight of GAP in the sample before the extraction (known from the formulation).

RESULTS AND DISCUSSION

In Figures 1 and 1b, the increase of the extractable % of GAP polymer with time measured by FTIR and NMR spectroscopy is attributed to the degradation behaviour of the polyurethane network. As can be seen, both techniques (NMR spectroscopy and FTIR spectroscopy) shows similar results. This type of measurement can be readily used to characterised the degree of stability and the evolution of the network in various formulations. Some conclusions can be drawn, for example : In Figure 1a, it was concluded from the curve 2971 that the formulation with tepanol and MgO showed the best resistance to degradation.

Also, the FTIR and NMR techniques were compared at various aging temperatures from 40° to 80°C. The results from the most stable formulation containing Tepanol and MgO is shown for FTIR and NMR techniques on Figure 2a, 2b and 2c. Slight differences in the FTIR and NMR results are due to the precision of the measurements. In Figure 2c, the gentle slope in the curve measured at 40°C show the potential for FTIR and NMR techniques to detect even slight decomposition of the binder. In future work, the decomposition state of the binder measured by spectroscopy will be related to the shelf life of the propellant.

The depletion of DPA stabiliser was also measured by NMR and compared with the standard HPLC technique. As shown in Figure 3, curves obtained from both methods are similar. It is interesting to note here that for the formulations investigated, no trace of any major nitro derivatives of DPA has been detected on the NMR spectra or HPLC chromatograms of the degradaded propellants. This suggests that the DPA depletion is a results of evaporation from the sample during aging and not of stabilizer consumption. Even if both methods allow such an observation, characterization of the nitro derivatives can be more readily done using the HPLC technique.

The major advantage of the NMR technique is that it allows the characterization of all components of the extractable part of the propellants in a single operation. Given this, the BDNPA/F content upon degradation could be checked with this method while extra measurements would have been necessary using the FTIR technique. In all cases investigated in this study, no significative change in the BDNPA/F content has been observed during the aging process.

CONCLUSIONS

In a single step, the NMR technique has allowed the measurement of the polymer network degradation, the depletion of the stabiliser, and the loss of plasticizer . The degradation curves were in agreement with combined results from FTIR and HPLC. Contrary to FTIR and HPLC, the NMR technique does not need calibration curves, and gives an evaluation of all the ingredients at the same time.

In the development of rocket propellants, NMR can be used to select the formulations with the highest potential for long shelf life. This technique could also be used for to characterised the state of degradation of the polymer network in solid rocket propellants, again useful for shelf life determination.

References

1- M. A. Bohn, *Prop. Expl. Pyro.*, **19**, 266 (1994).
2- M. A. Bohn, F. Volk, *Prop. Expl. Pyro.*, **17**, 171 (1992)
3- M. Benchabane, *J. Energetics Mat.*, **11**, 119 (1993).
4- P. Bunyan, A.V. Cunliffe, A. Davis, F.A. Kirby, *Defense Research Agency, Military Division*, Report 7/92.
5- E. Sbriccoli, R. Saltarelli, S. Martinucci, 20th Int. Annu. Conf. ICT 1989: "Environ. Test. 90's", pp 15-1 to 15-19.
6- K. Suzuki, I. Omura, T. Iizuka, T. Harada, *Kogyokayaka*, **30**, 126 (1969).
7- A.G. Christiansen, L.H. Layton, R.L. Carpenter, J. Spacecraft, **18** (3), 211-215 (1981).
8- F. Perreault, M. Benchabane, Propellants, Explos.,Pyrotech., Under Press (1996).

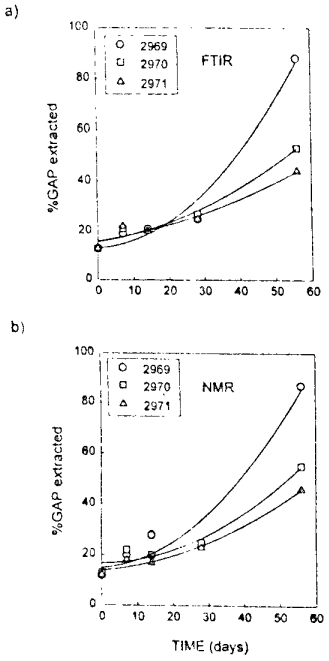


Figure 1 Extractable fraction of the GAP polymer as a function of aging time at 80°C for formulations 2969, 2970 and 2971 as measured by a) FTIR and b) NMR method.

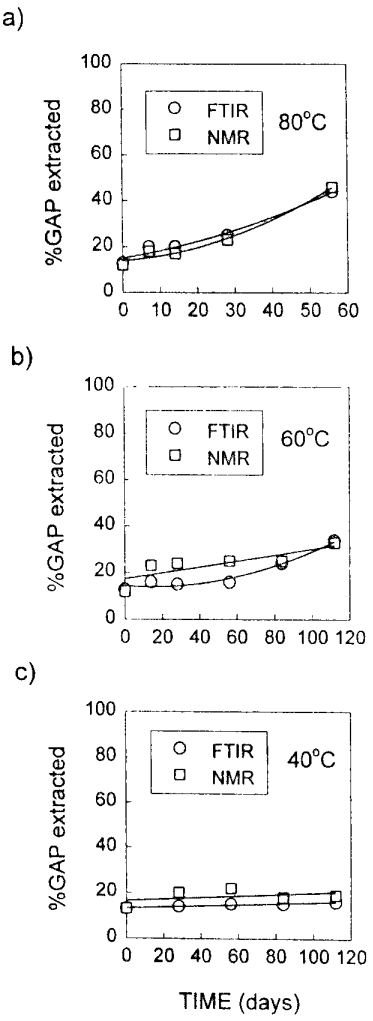


Figure 2 Extractable fraction of the GAP polymer as a function of aging time at a) 80°C, b) 60°C and c) 40°C for formulation 2971 using both analytical methods.

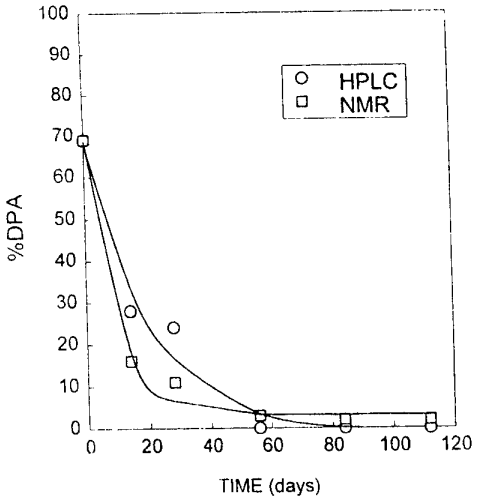


Figure 3 DPA depletion as a function of aging time at 60°C for formulation 2971 as measured by HPLC and NMR methods.

Paper Number: 10
Discussor's Name: Dr. A. Davenas
Responder's Name: S. Desilets

Question: Would your NMR technique work with other stabilizers like MNA or 2-NDPA?

Answer: For MNA, the depletion of the stabilizer and appearance of the main decomposition product (N-Nitro MNA) could be observed and determined by the NMR technique. For 2-NDPA, the various decomposition products (N-Nitroso - 2-NDPA, 2,4-NDPA, 2,4'-NDPA, 2,2'-NDPA) are mostly superposed in the NMR spectra and more difficult to evaluate precisely. Consequently, the HPLC is considered the method of choice for a complete decomposition study of all derivatives of 2-NDPA.

Applicabilité de quelques méthodes globales au CND des petits propulseurs à propergol solide

A. Déom°, F. Lepoutre°, J.C. Krapez°, C. Masson*, F. Christophe+ and D.L. Balageas°

° Laboratoire L3C de la Direction de la Physique, * Direction de l'Energétique à Palaiseau, + CERT DERMO Toulouse
ONERA OP/L3C, 29 Avenue de la Division Leclerc, BP 72
F92322 Châtillon Cedex, FRANCE

1. SUMMARY

After manufacturing, missiles may precociously be aged due to bad storage conditions or/and thermal cycling i.e. repetitive captive flights. This precocious aging can generate disbonds at the various interfaces of the rocket structure or modification of the mechanical properties of the propellant. This defects or modification can be dangerous for the plane when firing the missile. A study began to build a system usable on site which allows to know if the missile can be fired or not. The present paper gives the status of work of this study.

RESUME

Nous nous intéresserons particulièrement au cas des missiles air-air. Après fabrication, un vieillissement prématuré de ces missiles peut survenir, causé par exemple par un stockage dans de mauvaises conditions ou de trop nombreux vols en emport sans tir. Les conséquences du vieillissement peuvent prendre différentes formes : apparition de décollements localisés entre les différentes couches du propulseur ou/et modifications des propriétés mécaniques du propergol. Ces décollements ou ces modifications de propriétés peuvent être dangereuses pour l'avion au moment de la mise à feu du missile. Une étude a été commencée afin de définir un système utilisable sur le terrain qui permette de dire si le missile peut être tiré ou non. Le présent article fait un point sur l'avancement de cette étude.

2. INTRODUCTION

Après fabrication, les missiles peuvent être stockés pendant de nombreuses années ou voler en emport de nombreuses fois sans être tirés. Le stockage, parfois effectué dans des conditions climatiques (chaleur, humidité...) préjudiciables et la répétition des vols en emport peuvent prématurément vieillir le moteur du missile. Ce vieillissement peut se traduire de différentes façons : apparition par exemple de décollements aux interfaces entre les différentes couches du propulseur ou/et modification des propriétés mécaniques du propergol. Ces décollements ou cette modification du propergol peuvent être dangereuses pour le missile et pour l'avion porteur au moment de la mise à feu du missile. La détection de ce vieillissement est donc de première importance.

A la demande de la Direction des Engins (DGA/DEN), le laboratoire L3C a donc entrepris une étude visant à définir un système de contrôle, utilisable sur site, permettant de statuer sur l'état de santé d'un missile.

3. CONSTITUTION TYPE DES MISSILES

Nous nous intéresserons particulièrement au cas des missiles air-air. Ceux-ci sont constitués d'une enveloppe extérieure métallique ou composite de 1,5 à 3 mm d'épaisseur, d'une Protection Thermique Interne (PTI) constituée d'un élastomère à haute masse molaire collé ou vulcanisé, de 1 à 10 mm d'épaisseur, d'un inhibiteur constitué d'un élastomère à faible masse molaire, d'épaisseur 0,2 à 1,5 mm et du propergol. Nous nous intéresserons particulièrement au cas des propergols PBHT (polybutadienne hydroxylé) de type butalane.

Deux types d'architecture apparaissent : les chargements moulés-collés et les chargements libres. Pour les premiers, les couches successives décrites ci-dessus sont bien liées les unes aux autres, alors que pour les seconds, il y a discontinuité mécanique entre la PTI et le propergol. Le contrôle des couches internes des blocs libres par l'extérieur du missile sera donc impossible par toutes les méthodes nécessitant une continuité mécanique aux interfaces.

4. ACCESSIBILITE DES CONSTITUANTS DES MOTEURS A PROPERGOLS SOLIDES

Il faut noter que l'accessibilité aux chargements de propergol s'avère de plus en plus limitée pour les missiles modernes. Pour les missiles récents à structure bobinée il n'est pas de démontage possible des fonds du moteur. Pour d'autres, le chargement est moulé-collé, puis les structures soudées à l'avant et à l'arrière. Dans ces deux cas de figure, le seul accès à l'intérieur du canal, pour examen endoscopique ou passage d'une sonde, est celui de l'emplacement de l'allumeur situé en avant du missile, c'est à dire dans une zone qui permet un démontage du missile.

Pour un contrôle sur le terrain, le démontage étant exclu, il semble possible de détecter les défauts de type décollements enveloppe extérieure-PTI-liner-propergol pour les chargements moulés-collés à partir d'une analyse de la peau du missile. Les méthodes thermiques ou optiques peuvent être envisagées. Pour les propulseurs à structure bobinée, des méthodes ultrasonores ou hyperfréquences peuvent être également mises à l'étude. Il devient plus difficile de traiter le cas des chargements libres de même que toutes les zones de peau décollée (avant ou arrière). Il semble que ces zones ne pourront être inspectées que par une approche radicalement différente qui consiste à intégrer des détecteurs dans le propulseur dès la fabrication ou par tomographie X. La solution capteurs intégrés est probablement également la voie à explorer pour tester le plus facilement la dégradation des propriétés mécaniques des propergols au cours du temps.

Paper presented at the AGARD PEP Symposium on "Service Life of Solid Propellant Systems" held in Athens, Greece, 10-14 May 1996, and published in CP-586.

5. METHODES DE CND ACTUELLEMENT UTILISEES DANS L'INDUSTRIE FRANCAISE DES MISSILES

Il n'existe pas à notre connaissance de méthode de Contrôle Non Destructif des missiles qui soit utilisée directement sur le terrain. Les contrôles se font donc essentiellement au niveau de la fabrication des divers éléments du missile et de leur assemblage. En ce qui concerne les moteurs et leur environnement immédiat, les contrôles suivants peuvent être réalisés en usine :

- contrôle du canal du propulseur par endoscopie. Il permet d'observer les anomalies de surface et de contrôler les dimensions du canal;
- contrôle dans la masse du propergol par radiographie X. Il permet d'apprécier l'homogénéité interne du chargement (absence de fissures ou de cavités);
- contrôle des liaisons généralement réalisé par radiographie ou radioscopie. On contrôle les liaisons entre les différents éléments (enveloppe extérieure-PTI-liner-propergol). Pour les chargements moulés-collés, les liaisons étant plus proches de la surface externe, certaines méthodes locales sont parfois appliquées : ultrasons, rétrodiffusion Compton.

Il apparaît que la plupart de ces méthodes sont lourdes et coûteuses et qu'aucune ne peut répondre de manière satisfaisante au problème de contrôle sur le terrain des missiles opérationnels. De plus, elles sont mal adaptées au contrôle de l'évolution des caractéristiques mécaniques du propergol.

6. INVENTAIRE ET ANALYSE DES METHODES THERMIQUES POUR LA DETECTION DES DOMMAGES DANS LES PROPULSEURS

Les méthodes thermiques de CND reposent sur la détection d'une éventuelle perturbation du champ thermique qui apparaîtrait lorsque dans la structure à inspecter est induit un échauffement permanent ou transitoire. La perturbation est due à une altération locale ou globale des propriétés thermiques relativement à la répartition nominale. Cette altération peut être le fruit d'une modification physico-chimique d'un des constituants (effet de vieillissement), ou la conséquence de l'apparition d'un corps étranger : inclusion introduite accidentellement, décollement ou délaminage associés à l'apparition d'un interstice. Il est à noter qu'une absence d'adhésion sans décollement entre deux couches ne peut pas être détectée par une méthode thermique pure.

Pour des questions de vitesse d'inspection, une méthode globale sera préférée à une méthode ponctuelle, au risque éventuellement de perdre en sensibilité pour la détection de certain type de défauts. Ces considérations, alliées à l'analyse des paramètres thermiques et dimensionnels du système (notamment le fait que le temps de diffusion thermique à travers chacune des couches formant la structure des moteurs est de l'ordre de la seconde) font opter pour la thermographie infrarouge stimulée comme moyen possible de contrôle.

La thermographie infrarouge stimulée consiste à chauffer rapidement la surface de la partie à inspecter (usuellement au moyen de lampes infrarouges ou de flashs), et à enregistrer l'évolution subséquente de la température superficielle à l'aide d'une caméra infrarouge.

Au droit d'un défaut qui se comporte généralement comme une barrière thermique, le refroidissement est plus lent qu'au-dessus d'une zone saine (inversement, au droit d'un bon conducteur de la chaleur, le refroidissement sera plus rapide). L'existence de tels contrastes permet de localiser les défauts puis l'exploitation de leur évolution temporelle permet la caractérisation de ces défauts (détermination de leur profondeur et de leur résistance équivalente) et au besoin leur discrimination vis à vis des artefacts de l'émissivité de la surface, artefacts qui peuvent générer des contrastes équivoques.

Avec la configuration expérimentale habituelle, la thermographie stimulée est bien adaptée pour la détection des barrières ou puits thermiques orientés perpendiculairement au flux nominal, c'est à dire parallèlement à la surface du missile. Des fissures ou inclusions perpendiculaires à la surface ne pourront pas être détectées par cette méthode globale. Seule une approche avec balayage de la surface (faisceau laser ou toute autre source concentrée de flux) et donc diffusion tridimensionnelle de la chaleur permettrait de pallier cet handicap.

Il est nécessaire qu'il y ait continuité thermique entre l'enveloppe extérieure et la barrière à détecter. Ainsi les défauts sous-jacents à un défaut détecté ne le seront, eux, généralement pas (effet de masquage) et l'inspection thermographique des blocs libres ne sera pas possible plus en profondeur que la couche de PTI.

Simulation numérique

Avant d'effectuer des tests sur des échantillons, nous avons voulu, par simulation numérique, quantifier les dimensions (épaisseur et diamètre) limites d'une lame d'air pour qu'elle soit détectable par thermographie stimulée. Nous avons considéré successivement le cas d'une structure avec une enveloppe d'acier de 1 mm d'épaisseur et celui d'une structure avec enveloppe de carbone-époxy de 3 mm d'épaisseur. Dans le modèle nous avons placé le film d'air successivement à l'interface enveloppe/PTI et PTI/liner.

Les résultats d'une analyse monodimensionnelle (1D) du transfert thermique sont résumés dans le tableau suivant (en supposant une densité de flux de l'ordre du W/cm^2).

enveloppe	interface	épaisseur d'air minimum détectable
acier 1mm	env/PTI	2 µm
"	PTI/liner	10 µm
graphite-époxy 3mm	env/PTI	5 µm
"	PTI/liner	10 µm

Nous avons également adapté les résultats d'une analyse 2D du transfert thermique dans un bicouche afin de quantifier l'incidence des dimensions latérales du défaut sur sa détectabilité.

Il est à remarquer que les limites de détectabilité apparaissant dans le tableau ci-après ont été définies pour que le contraste sur une trame de la caméra soit au minimum égal à 0,2°C. Compte-tenu que le contraste met plusieurs dizaines de secondes à se développer, voire plusieurs minutes, alors que la caméra délivre 25 trames par seconde, il est tout à fait envisageable d'effectuer des moyennes de trames et d'augmenter ainsi le rapport signal sur bruit. On

peut donc espérer avoir une détectabilité encore meilleure des défauts.

enveloppe	interface	diamètre minimum détectable pour 100 µm d'air
acier 1mm	env/PTI	2 mm
"	PTI/liner	30 mm
graphite-époxy 3mm	env/PTI	7 mm
"	PTI/liner	23 mm

D'autres modélisations montrent que le vieillissement du propergol en tant que tel ne pourra être décelé par thermographie que si l'effusivité thermique de celui-ci varie d'au moins 10 à 20%. Des mesures de propriétés thermophysiques sur des échantillons vieillis ont été réalisées.

7. CND PAR HYPERFREQUENCES DU CHARGEMENT DES PROPULSEURS

Comme nous l'avons vu, deux types de structures externes existent pour les propulseurs : l'une composite, l'autre métallique. Dans le premier cas, un contrôle par ondes électromagnétiques pourrait être réalisé par l'extérieur alors que, dans le second cas, celui-ci devra être réalisé par l'intérieur. Toutefois, pour certaines structures composites, un feuillard métallique est intercalé entre l'enveloppe extérieure et la PTI qui rend impossible le contrôle par l'extérieur.

D'autres raisons vont à l'encontre d'un contrôle par l'extérieur: les difficultés prévisibles à traverser une structure bobinée, la non-circularité du canal de combustion (profil étoilé, bi-étoilé...) rendant difficile l'interprétation des signaux de retour. Le diamètre de l'orifice laissé libre par l'allumeur varie entre 20 et 60 mm suivant les missiles, cela devant être suffisant pour introduire une sonde hyperfréquence.

Deux méthodes hyperfréquences sont possibles : une imagerie interne en ondes millimétriques et une méthode d'intéraction globale.

Imagerie interne du propulseur en ondes millimétriques

L'imagerie interne d'un propulseur peut être envisagée, en introduisant dans le canal de combustion, via l'orifice laissé libre par l'allumeur, un capteur millimétrique fixé à l'extrémité d'un guide d'onde. La mesure de l'énergie électromagnétique rediffusée par la structure doit permettre de détecter défauts et vieillissement.

Les deux points critiques de cette méthode sont le dimensionnement du capteur fixé en extrémité de guide d'onde et la modélisation de la propagation dans le canal de combustion s'il n'est pas circulaire, ainsi que la connaissance de la signature des défauts recherchés, connaissance obtenue soit par modélisation, soit par apprentissage sur éprouvettes témoins.

Méthode d'intéraction globale

On classe sous cette appellation les solutions fondées sur la mesure d'un effet global, intégrant la totalité du propulseur, contrairement aux méthodes d'imageries décrites précédemment. Deux méthodes peuvent être utilisées : les mesures en cavité résonante et les mesures d'impédance par réflectométrie.

Pour les mesures en cavité, le résonateur est constitué par l'enveloppe métallique du propergol (structure externe métallique du propulseur ou feuillard métallique du propergol dans le cas d'un propulseur en matériau composite). Le propergol et les couches plus externes constituent le diélectrique à caractériser. Deux informations sont utilisables : la variation de la fréquence de résonance et celle du coefficient de surtension de la cavité.

Dans la méthode réflectométrique, le propulseur chargé est considéré comme modifiant l'impédance d'une sonde hyperfréquence dont on va examiner le coefficient de réflexion sur une bande de fréquence donnée.

8. CND PAR VOIE OPTIQUE

Principe général

Lorsque l'on applique un champ de contraintes à un corps élastique (par un moyen qui peut ne pas être mécanique), il se produit une déformation de la surface. La mesure de cette déformation est à la base de nombreuses méthodes de CND.

Nous distinguerons les trois types fondamentaux de mises en contrainte, classés suivant que l'on s'intéresse à des effets statiques, dynamiques stationnaires (mise en résonance) ou dynamiques instationnaires (propagation d'une vibration).

Quand la détection est effectuée par l'observation d'interférences lumineuses entre deux faisceaux de lumière cohérente, dont l'un au moins est réfléchi par la surface, on parle de méthodes optiques. La déformation induite par les contraintes appliquées modifie localement la figure d'interférences.

Nous serons amenés à faire une distinction entre méthodes globales et locales. Les premières, pour lesquelles le champ de contraintes créé et la surface déformée observée sont étendues, permettent des contrôles rapides. Elles sont donc en principe préférables pour le contrôle de relativement grandes structures comme les propulseurs, mais elles n'offrent pas toujours la possibilité de l'hétérodynage.

Modes d'excitation de la structure

Nous les avons classés suivant leur régime temporel (statique, dynamiques stationnaire et instationnaire).

Concernant le régime statique, on peut considérer le système comme formé de milieux homogènes stratifiés et y représenter un délaminage par une lame d'air. La contrainte la plus fréquemment utilisée pour effectuer des contrôles est la pressurisation/dépressurisation. Le calcul montre que, pour une dépressurisation de l'ordre de 500 mbars appliquée sur la surface extérieure, une lame d'air d'épaisseur micronique placée entre moins de 2 mm de métal (ou moins de 6 mm de composite type carbone) et 10 mm de protection thermique produit une déformation de quelques microns. Une autre possibilité d'application des contraintes est la voie thermique, mais selon la littérature, les déformations obtenues semblent plus faibles que par dépressurisation. En ce qui concerne le propergol lui-même, nous n'avons pas trouvé d'étude décrivant le contrôle d'un tel matériau par déformation statique. Il semble que son comportement visco-élastique rende difficile toute interprétation simple des mesures.

La méthode dynamique stationnaire consiste à exciter mécaniquement un mode de résonance de la structure et à

observer, soit les perturbations apportées par la présence d'un défaut, soit, plus fréquemment, à produire une résonance propre au défaut lui-même. Ce type d'excitation doit donc être soit périodique à fréquence variable, soit pulsé de façon à rechercher les modes fondamentaux des défauts. Dans ce dernier cas, les fréquences de résonance sont proportionnelles à la profondeur à laquelle est situé le défaut sous la surface et inversement proportionnelles à la surface du défaut.

La dimension minimum des défauts sera de l'ordre de quelques épaisseurs de la couche considérée de la structure. Malgré cette restriction, le mode résonant paraît plus adapté à la détection des décollements aux interfaces que le mode statique dans la mesure où l'effet de résonance et la faible absorption liée à l'usage de très faibles fréquences permettent d'espérer des signaux beaucoup plus forts, même avec une excitation piézoélectrique.

Concernant le régime dynamique instationnaire on aborde le domaine des ultrasons. Ceux-ci semblent bien adaptés pour fournir des informations quantitatives sur la qualité des différents collages de l'enveloppe du propergol, mais il subsiste deux difficultés technologiques. La première provient de ce que ce mode de mise sous contraintes génère de faibles déformations seulement détectables par hétérodynage. La technique de détection optique à mettre en oeuvre est donc plus délicate. La deuxième difficulté est liée à la structure et aux matériaux constitutifs des propulseurs qui peuvent produire des barrières difficiles, voire impossible, à franchir par les ultrasons :

- le cas le plus grave est celui des chargements libres; il est alors impossible de tester ces propulseurs au delà de l'interface enveloppe/PTI;
- les matériaux constitutifs des propulseurs sont très hétérogènes ou visco-élastiques et il faut prendre en compte l'absorption des ultrasons.

Dans la PTI, l'amortissement est essentiellement produit par la viscosité. Le coefficient d'absorption croît comme le carré de la fréquence ultrasonore. Pour visualiser des interfaces situées au delà de la PTI, il est donc intéressant de travailler à des fréquences aussi basses que possible, ce qui se traduit en CND ultrasonore par capteurs piézoélectriques par une perte de résolution spatiale.

Dans le propergol, qui est un assemblage de grains enrobés par un élastomère, des études antérieures ont révélé une absorption qui croît fortement aux fréquences supérieures à 100 kHz, puis devient indépendante de la fréquence au delà de 500 kHz où elle atteint à peu près le même niveau que celui de la PTI. Ceci rend donc difficile l'analyse ultrasonore locale de défauts internes au propergol par les échos renvoyés vers la surface.

L'amortissement ultrasonore du propergol doit être sensible à son vieillissement. Il est envisageable d'étudier l'évolution au cours du vieillissement du propergol de l'amplitude des échos sur l'interface PTI/propergol qui dépend des caractéristiques du propergol. Cette analyse pour être suffisamment sensible devrait être réalisée soit en fonction de l'incidence, soit en fonction de la fréquence ultrasonore. Elle n'est bien sûr pas possible avec les chargements libres.

Détections optiques

Nous distinguerons les méthodes locales et les méthodes globales.

Les méthodes locales permettent de faire plus facilement de la détection hétérodynée. Une sonde commercialisée est capable de détecter des déplacements inférieurs à l'angström avec une résolution spatiale de l'ordre de 100 μm^2.

Nous distinguerons dans les méthodes globales l'holographie et la shearographie.

Nous ne reviendrons pas sur le principe de l'holographie, technique connue depuis de nombreuses années et utilisée dans l'industrie. Nous signalerons uniquement un de ses principaux inconvénients : sa sensibilité importante aux vibrations qui ne peut être annihilée qu'en utilisant une source d'éclairement impulsionnel.

La shearographie fait partie des techniques d'interférométrie de speckle. Son principe consiste à illuminer l'échantillon avec une lumière cohérente et à faire interférer le front d'onde réfléchi avec ce même front d'onde légèrement décalé. On a un cisaillement d'image ou "shear" en anglais. On fait l'acquisition de cette figure d'interférences pour deux états donnés de la structure à contrôler (par exemple au repos puis sous contrainte). La soustraction de ces deux images donne une figure de moiré représentative de la déformation de l'objet. La présence d'un défaut modifie localement la déformation de la structure contrôlée. On peut utiliser une excitation vibratoire et visualiser les interférences en temps réel. Dans ce cas, la présence d'un défaut aura pour effet de modifier localement les franges représentatives du mode de vibration de l'objet. Cette mesure est qualitative. Par contre une mise sous contrainte thermique (par exemple par l'intermédiaire d'un flash), permet de calculer le déphasage entre les fronts d'onde issus de la stucture avant et après mise sous contrainte et donc d'obtenir la valeur de la déformation au droit du défaut.

9. EPROUVETTES UTILISEES POUR TESTER LES DIFFERENTES METHODES DE CND

Nous avons utilisé d'une part, des éprouvettes prêtées par la SNPE, d'autre part des éprouvettes réalisées à la Direction de l'Energétique de l'ONERA.

Eprouvette A

Echantillon à enveloppe métallique de dimensions 140x80x11 mm, constitué de trois couches : tôle d'acier de 1 mm, couche de liner de 2 mm et couche d'élastomère de 8 mm simulant un propergol. Le liner et l'élastomère sont transparents dans le visible. Des défauts de collage circulaires ont été réalisés à l'interface métal/liner (voir figure 1).

Eprouvette B

Echantillon à enveloppe métallique de dimensions 245x125x42 mm, constitué de quatre couches : acier, PTI, liner et propergol inerte. Des défauts artificiels constitués de pastilles carrées de 0,5 mm d'épaisseur et de dimension latérale variable ont été placés à sa fabrication à l'interface acier/PTI et liner/propergol (voir figure 2).

Eprouvette C

Cylindre d'acier de 165 mm de diamètre et d'épaisseur 2 mm contenant une couche de PTI, une couche de liner et un cœur creux de propergol inerte. Lors de la mise en forme, des inserts de 25 µm de Kapton et de Teflon ont été introduits entre la couche de liner et le propergol en cinq points de la circonférence et à trois positions différentes : au centre et aux deux extrémités du cylindre (figure 3). De plus, certains

des inserts des extrémités ont été retirés, laissant ainsi un délaminage plus ou moins épais, suivant le retrait des matériaux polymériques au voisinage.

Eprouvette D

Plaque plane constituée d'une peau de 2 mm d'acier, de 4,4 mm de PTI, de 1,5 mm de liner et 34,5 mm de propergol, découpée suivant le schéma de la figure 4. Cette découpe est destinée en particulier à la mesure des vitesses des ondes ultrasonores dans les différents matériaux constituant un propulseur.

Eprouvette E

Echantillon à enveloppe composite de dimensions 477x307x34 mm, constitué de quatre couches : kevlar-époxy d'épaisseur 13 mm, PTI+ liner d'épaisseur 2 mm et propergol inerte d'épaisseur 19 mm. Des défauts artificiels de différentes dimensions ont été insérés à la fabrication (voir figure 5).

10. RESULTATS EXPERIMENTAUX CONCERNANT LE CND DES PROPULSEURS

Détection de défauts parallèles à la surface du propulseur

Trois types d'essais ont été réalisés sur les différentes éprouvettes : des essais thermographiques, des essais ultrasonores et des essais shearographiques.

Essais thermographiques

On peut voir figure 6 le dispositif expérimental de la Thermographie Infrarouge Stimulée (TIS) utilisé pour les essais thermographiques. La source radiative impulsionnelle qui a été utilisée pour les essais est composée de deux radiateurs de douze lampes continues de 2 kW électriques. L'impulsion est donnée par un volet tournant commandé par deux électro-aimants contrarotatifs. La caméra infrarouge enregistre l'évolution de la température de la face avant de l'échantillon pendant des périodes de 1 à 9 min après l'impulsion. Le signal vidéo venant de la caméra est numérisé par des cartes CEDIP implantées dans un microrordinateur compatible, ordinateur qui sert également au traitement des données. Pour les essais sur éprouvette cylindrique on a utilisé le dispositif expérimental de la figure 7. Le principe de la mesure consiste à placer le tronçon de cylindre sur un plateau tournant et à analyser le refroidissement le long d'un méridien à l'aide d'une caméra infrarouge, pendant que celui qui lui est diamètralement opposé est chauffé par un tube quartz (puissance électrique 2 kW). La caméra utilisée est une AGEMA 880 LW fonctionnant en mode ligne. Le méridien à analyser étant vertical et le balayage de la caméra horizontal, un dispositif optique comprenant deux miroirs a été utilisé.

On peut voir figure 8 les résultats d'un essai de l'éprouvette B en TIS. Il s'agit d'une image en effusivité apparente, inverse du contraste thermique. On distingue trois régions d'effusivité inférieure à la normale (taches bleues de niveau voisin de 3100, inférieur au niveau nominal arbitraire de 3500). Le plus gros défaut détecté aurait des dimensions d'environ 45x60 mm, alors que les deux autres auraient des diamètres équivalents de 30 mm. L'analyse temporelle des courbes d'effusivité permet de conclure que les défauts détectés sont situés à la première interface, c'est-à-dire entre entre l'acier et la protection thermique. Les défauts situés à l'interface PTI/liner-propergol n'ont pas été détectés.

On peut voir figure 9 les résultats d'un essai de l'éprouvette E en TIS. Il s'agit ici d'une image en profondeur de défauts. La profondeur des défauts détectés varie entre quelques mm et 8 mm environ. Ils sont tous dans la première couche de kevlar-époxy.

Quant à l'éprouvette C, on a utilisé pour le CND par thermographie infrarouge le montage avec mise en rotation de l'éprouvette. La figure 10 illustre les résultats obtenus. Il s'agit de l'image infrarouge de la développée de l'enveloppe cylindrique de l'éprouvette. Les deux taches bleues en haut correspondent à des repères métalliques. On remarque très nettement sur le bord droit de l'image, et plus faiblement sur le bord gauche, les contrastes induits par les inserts de Kapton. Par contre, les inserts de Téflon situés au centre n'ont pu être détectés par la méthode thermographique. Des délaminages localisés entre le liner et le propergol peuvent donc être détectés dans cette structure par thermographie, à condition qu'ils représentent une résistance thermique aussi élevée que celle des inserts de Kapton utilisés pour l'expérience correspondant à une épaisseur d'air de quelques microns.

Essais ultrasonores

L'éprouvette B a été testée en immersion et par réflexion. Les essais réalisés avec un capteur focalisé travaillant à 5 MHz ont permis d'analyser l'interface peau-PTI sur la totalité de la surface de l'éprouvette. On peut voir figure 11 le contrôle effectué sur le quart gauche de l'éprouvette. L'image révèle les inserts de téflon qui ont été placés à cette interface. On y observe assez facilement un insert de 30x30 mm (en bas à droite) et un insert de 15x15 mm (en haut). Cependant, les échos correspondant à ces défauts artificiels sont souvent noyés au milieu de nombreux échos provoqués par des défauts "naturels" situés à la même profondeur. Ces défauts produisent des réflexions suffisamment importantes pour que l'on puisse penser qu'il s'agit en fait d'une multitude de petits décollements. Nous avons attribué ces défauts à la dégradation de l'échantillon au cours de son immersion prolongée dans la cuve d'essais.

Essais holographiques et shearographiques

Le laboratoire ne possédant pas au début de cette étude de shearographe, des campagnes d'essais ont été entreprises chez la société Steinbichler et à Holo 3. La méthode optique choisie pour faire l'inspection a été essentiellement la shearographie, c'est à dire l'interférométrie de speckle à cisaillement vidéo. Deux séries de mesures ont également été entreprises en faisant appel à une technique d'interférométrie de speckle plus classique : la TV-holography ou ESPI (electronic speckle pattern interferometry). Les sollicitations pour mettre l'éprouvette en contrainte et ainsi révéler les défauts internes par une déformation anormale de la surface ont été :

- de type thermique : pour ce faire, une lampe infrarouge de 250 W a été utilisée pour chauffer, soit la face arrière de l'éprouvette pendant que la caméra visualisait les déformations de la face avant, soit cette même face avant (figure 12);
- de type dépression : pour ce faire, l'éprouvette était placée dans une enceinte à vide où se trouvaient également une extrémité de la fibre d'éclairage laser et la caméra de shearographie, puis une dépression de quelques fractions d'atmosphère était appliquée.

Les essais de l'éprouvette A n'ont pas donné de bons résultats avec la sollicitation de type thermique mais par contre de bons résultats avec la dépression. Pour une dépression de seulement 20 mbar les défauts de collage sont apparus : le disque de diamètre 22 mm et les deux disques de 15 mm amalgamés en un seul défaut apparaissent (figure 13). Ces deux derniers défauts étaient trop près l'un de l'autre pour que la technique de contrôle puisse les discerner. Ils se sont donc manifestés comme un unique défaut étendu. Des essais effectués avec une dépression supérieure (90 mbar) ou avec l'approche shearographique sont venus confirmer que les méthodes interférométriques envisagées, alliées à une contrainte de dépression, permettaient de détecter sans équivoque, mais avec une résolution limitée, les délaminages à l'interface métal/PTI.

L'éprouvette B a également été testée par ESPI et shearographie à Holo 3. Lorsque la contrainte choisie est la mise en dépression, seul l'un des trois défauts à l'interface acier-PTI/liner est révélé sur les franges d'interférence pour une expérience de ESPI avec 55 mbar de dépression et pour une expérience de shearographie avec 190 mbar de dépression (figure 14). On peut en conclure que seul ce défaut est accompagné d'une lame d'air non débouchante. En effet, soit les deux autres inserts sont accompagnés d'une lame d'air débouchante, soit ces deux défauts sont constitués des seuls inserts de polystyrène, en l'absence de toute poche d'air. Les défauts situés à l'interface PTI/liner-propergol sont eux-mêmes soit exempts de lame d'air, soit trop peu étendus pour que les niveaux de dépression considérés aient pu entraîner une déformation suffisante de la plaque métallique.

L'éprouvette C a été testée par TV-holographie (ou ESPI) avec une mise en contrainte thermique et par dépressurisation ainsi que par shearographie avec dépressurisation. Aucun des défauts n'a pu être mis en évidence. On peut conclure que l'enveloppe métallique est trop rigide pour que les déformations qu'on y induit puissent être localement modifiées par les défauts sous-jacents.

L'éprouvette E a été testée en shearographie. La figure 15 montre les figures d'interférences obtenues sur quelques-uns des défauts contenus dans l'échantillon. Il est intéressant de remarquer que les formes des franges et des inserts semblent liées.

Détection de défauts internes dans le propergol par méthode hyperfréquence

La méthode utilisée est la réflectométrie dans laquelle le propulseur chargé est considéré comme une impédance qui se modifie en présence de défauts. Deux solutions avaient été retenues : celle du cornet circulaire et celle de la sonde coaxiale. La première solution a été abandonnée, la mauvaise fixation du cornet dans la tuyère conduisant à un manque de répétitivité des réponses observées. Parmi les deux voies d'analyse possibles : le domaine fréquentiel et le domaine temporel, ce dernier a été retenu car il permet de séparer les contributions de certaines discontinuités. On peut voir figure 16 le dispositif expérimental utilisé. La figure 17 représente les différences observées dans les réponses du propulseur chargé, sans défaut et avec un cylindre métallique de diamètre environ 8 mm et de longueur 20 mm placé sur le propergol. On observe qu'un défaut très conséquent dans le propergol produit une petite variation de la réponse. Cette solution est d'autre part limitée dans la pratique par l'accessibilité au canal central sur les missiles récents.

11. CARACTERISATION DU VIEILLISSEMENT DU PROPERGOL

Mesures sur échantillons de propergol vieilli naturellement

Echantillons de propergol vieilli naturellement

La SNPE a fourni à l'ONERA une première série de pavés de butalane non vieillie, vieillie 1 an et vieillie 2 ans, correspondant en fait à trois coulées réalisées en 1993, fin 1991 et début 1991 respectivement. Ces pavés ont été usinés sous la forme apparaissant figure 18 pour répondre aux besoins des méthodes de mesure thermique, ultrasonore et capacitive. Une deuxième série de pavés, de dimensions plus importantes, provenant des trois coulées précédentes mais également d'une coulée de 1989, a été fournie à l'ONERA en vue de réaliser des mesures hyperfréquences.

Mesures thermiques

La propriété thermique du propergol qui a été mesurée et dont les éventuelles variations pourraient être corrélées à un vieillissement du matériau est l'effusivité thermique b, définie de la façon suivante : $b = (k\rho C)^{1/2}$ avec k la conductivité, ρ la densité et C la chaleur massique. Dans cette optique, les trois échantillons de propergol ainsi qu'un échantillon de plexiglas ont été soumis à une impulsion radiative brève sur l'une de leurs faces et nous avons enregistré l'évolution de la température de celle-ci afin d'en déduire l'effusivité des échantillons. Il en est ressorti que le rapport entre l'effusivité des échantillons et celle du plexiglas ne dépendait pas du vieillissement des échantillons.

Mesures ultrasonores

Le principe de la mesure consiste à appliquer par pression un capteur piézoélectrique sur l'une des faces de l'échantillon et à mesurer le temps de vol de l'écho provenant de la face arrière. Les mesures ont été faites en incidence normale avec des ondes de compression, à 500 kHz et à 1 MHz. Cinq échantillons par état de vieillissement (référence, vieilli 1 an et vieilli 2 ans) ont été caractérisés. Il n'a pas été détecté de différence entre les différents stades de vieillissement des échantillons et la vitesse moyenne trouvée est de 1630 m/s. Il n'a pas été possible de faire des mesures d'absorption fiables et reproductibles sur les échantillons de faible épaisseur dont nous disposions.

Mesures hyperfréquences

La méthode retenue pour mesurer la constante diélectrique des échantillons de propergol en hyperfréquence est la méthode du court-circuit dans laquelle l'échantillon à mesurer est placé à l'extrémité d'un guide d'onde rectangulaire. Deux bandes de fréquences ont été retenues : la bande 5,85-8,20 GHz et la bande 8,2-12,4 GHz. Les mesures réalisées sur le banc du CERT/DERMO ont donné des résultats qui se sont révélés dépendre de l'épaisseur de l'échantillon pour une coulée donnée. Ce phénomène, inattendu, peut être soit lié au procédé de mise en place des échantillons dans le guide d'ondes, qui ne permet pas d'assurer une parfaite planéité de la surface de l'échantillon exposée à l'onde incidente, soit plus vraisemblablement dû

aux hétérogénéités du propergol d'un échantillon à l'autre pour une même coulée. On constate entre les échantillons non vieillis et les échantillons vieillis 4 ans une petite tendance à la diminution de la permittivité ε'.

Mesures capacitives

Le principe est de mesurer avec un impédancemètre la tangente de l'angle de perte et la résistivité des échantillons de propergol à différents états de vieillissement. Pour cela, les échantillons sont placés entre deux plaques de circuit imprimé constituant les électrodes reliées à l'impédancemètre. Les mesures de tg δ ne révèlent aucune influence du vieillissement. La résistivité a été trouvée différente suivant les échantillons mais sans corrélation avec le vieillissement.

En conclusion, les mesures thermiques, ultrasonores et capacitives n'ont pas permis de détecter une évolution de propriété physique corrélée avec l'état de vieillissement. Seul la mesure hyperfréquence, qui a pu être réalisée sur des échantillons vieillis 4 ans, a semblé montré pour ces derniers une légère variation de permittivité.

Mesures sur échantillons de propergol vieillis artificiellement

Echantillons de propergol

Des échantillons de propergol ont été réalisés à l'Office et mis en vieillissement accéléré en étuve sous atmosphère sèche à 60°C. Il a été estimé que deux mois d'un tel vieillissement étaient équivalents à un an de vieillissement réel.

Les échantillons réalisés sont:

- des plaques carrées de 100 mm de coté avec une coupe en marche d'escalier dont les épaisseurs sont égales à 5 mm et 2,5 mm (figure 19);
- des cylindres de 100 mm de diamètre dans lesquels sont intégrés des éléments capteurs constitués de diabolos circulaires permettant d'une part, une mesure de capacité entre les faces internes conductrices des deux disques, d'autre part une mesure ultrasonore, chacun des disques étant pourvu d'une céramique piézoélectrique (figure 20);
- des éprouvettes de type haltère pour réaliser des mesures mécaniques;
- des cylindres de 30 mm de diamètre et 30 mm de hauteur.

Vitesse de combustion des échantillons

Celle-ci a été mesurée par méthode ultasonore sur les cylindres de 30 mm de diamètre vieillis pendant sept mois à 60°C. On peut voir dans le tableau qui suit une diminution sensible de la vitesse de combustion avec le vieillissement du propergol.

P (MPa)	Vitesse de combustion (mm/s)	
	non vieilli	vieilli 7 mois
4	9	/
5	9,5	9,05
6	10,2	9,50
8	11,3	10,28
10	12,5	/

Propriétés mécaniques des échantillons

Les propriétés ont été évaluées en traction selon un mode opératoire normalisé. On a caractérisé d'une part, des éprouvettes tirées dans deux lots de propergol non vieilli, d'autre part des éprouvettes tirées dans un gros cylindre de propergol vieilli 7 mois à 60°C et des éprouvettes directement vieillis 7 mois. On peut voir dans le tableau ci-dessous les résultats des mesures réalisées.

Propergol	E (MPa)	σm (Mpa)	δm %	σr (MPa)	δr (%)
t=0					
bloc 1	10	1,3	22,6	1,20	27,5
bloc 2	9,83	1,32	22,1	1,21	27,6
t=7 mois bloc 2	10,5	1,38	26,2	1,3	33
t=7 mois épr.	167	1,36	1,43	0,3	3,4

notations utilisées: E module d'Young, σm contrainte maximale, δm allongement à la contrainte maximale, σr contrainte à la rupture, δr allongement à la rupture.

On note que la seule caractéristique mécanique ayant évolué avec le vieillissement à la fois dans le gros bloc et dans les éprouvettes, et pour une variation dans un même sens, est le module d'Young. Les éprouvettes vieillies sont devenues cassantes. Les essais de traction réalisés sur les éprouvettes vieillies ne sont pas significatifs du vieillissement réel d'un bloc de propergol. En effet, dans ces éprouvettes de faible épaisseur, l'oxygène de l'air diffuse facilement au coeur de celle-ci, pouvant conduire entre autre à une oxydation des doubles liaisons du polymère. Les éprouvettes découpées dans le bloc vieilli, ont été prélevées au cœur de celui-ci de façon à s'affranchir des modifications chimiques superficielles.

Caractéristiques ultrasonores des échantillons

Les plaques carrées de 100 mm ont été caractérisées en vitesse de transmission des ondes longitudinales, transversales et en amortissement. Le vieillissement de ces plaques 7 mois à 60°C n'a pas permis de mettre en évidence de variation nette de célérité ou d'amortissement, mesurés en utilisant des capteurs ultrasonores à 1 MHz et 2,25 MHz.

De même, les mesures réalisées avec les céramiques placées sur les diabolos dans des cylindres n'ont pas mis en évidence de variation ultrasonore corrélable avec un vieillissement des cylindres.

Caractérisation thermique des échantillons

Une fois encore, ce sont les plaques carrées de 100 mm dont on a mesuré l'effusivité thermique après vieillissement de 7 mois à 60°C. Une variation non significative (4%) de l'effusivité a été mesurée.

Propriétés électriques des échantillons

Les mesures réalisées sur les plaques carrées de 100 mm et avec les diabolos n'ont pas mis en évidence de variation sensible ni de capacité, ni de tangente de l'angle de perte avec le vieillissement du propergol.

Mesures optiques sur éprouvettes cylindriques simulant un propulseur chargé avec un propergol ayant vieilli

Pour tester les méthodes optiques, il y a nécessité de simuler un empilement peau extérieur-propergol tout en restant dans une géométrie cylindrique représentative d'un propulseur

réel. Le vieillissement se traduisant par un durcissement ou un ramolissement du propergol, on a, pour tester les méthodes optiques, réalisé deux cylindres en acier de 2 mm d'épaisseur, de 165 mm de diamètre et 185 mm de longueur, pourvus d'un noyau creux réalisé avec deux araldites de dureté différente. Les cylindres pouvaient recevoir des couvercles permettant de mettre l'intérieur en surpression ou en dépression.

Des essais d'interférométrie de speckle (ESPI) réalisés à Holo 3 n'ont pas permis de mettre en évidence de différence entre les deux cylindres.

Des essais ont été aussi réalisés en vibrométrie laser. Cet instrument permet de mesurer sans contact la vitesse et le déplacement de la surface au point visé dans une gamme de fréquences allant du continu à 1,5 MHz. Le cylindre à étudier était soumis à un choc à mi-hauteur à l'aide d'une masselotte et un vibromètre pointait à trois hauteurs différentes sur le méridien à l'opposé du point d'impact (figure 21). On peut voir figure 22 les oscillogrammes obtenus à mi-hauteur de cylindre. La courbe CH1 correspond au signal de vitesse, la courbe CH2 au signal de déplacement. Des courbes obtenues, il ressort pour les trois positions de percussion que le déplacement et la vitesse sont nettement plus importants dans le cas du noyau mou. Cette technique simple a donc permis de faire la distinction entre des matériaux de rigidité différente bien que ceux-ci soient placés derrière une enveloppe d'acier.

12. CONCLUSIONS

Le problème posé est celui de la détection "sur le terrain" du vieillissement des petits propulseurs des missiles tactiques et en particulier des missiles air-air. Après rencontre des industriels concernés, il est apparu deux besoins : le premier est celui de la détection des décollements pouvant se produire aux interfaces entre les différentes couches du propulseur, le second est celui de la détection d'une modification des propriétés du propergol.

Pour la détection des décollements aux interfaces plusieurs méthodes ont été testées : la thermographie infrarouge, les ultrasons et la shearographie. Pour cela on a utilisé des éprouvettes représentatives d'empilements de type propulseur à propergol solide (peau extérieure métallique ou composite, protection thermique, liner, propergol), planes ou cylindriques, afin de se rapprocher dans ce dernier cas de la structure d'un missile. La méthode thermographique permet, que l'on utilise une éprouvette plane ou cylindrique, de détecter un décollement à l'interface peau extérieure-protection thermique, et liner-propergol pour certaines éprouvettes. Les ultrasons permettent bien aussi de détecter un décollement à l'interface peau extérieure métallique/protection thermique. La shearographie a permis de détecter des décollements à l'interface peau extérieure métallique/protection thermique uniquement dans le cas des éprouvettes planes et en utilisant une mise en dépression des éprouvettes. On voit que plusieurs méthodes semblent possibles pour détecter des décollements au niveau de l'interface peau externe-protection thermique, par l'extérieur du missile.

Les études de détection du vieillissement du propergol ont consisté, d'une part, à identifier la ou les propriétés du propergol évoluant le plus avec le vieillissement et, d'autre part, à définir la méthode de CND ou le capteur sensible à cette propriété. Pour cela on a utilisé, d'une part, des échantillons de propergol vieillis naturellement 1, 2 et 4 ans, d'autre part, des échantillons de propergol vieillis artificiellement de manière accéléré. Le vieillissement artificiel consiste à exposer le propergol à une température de 60°C. La règle est que deux mois de vieillissement accéléré seraient équivalents à 1 an de vieillissement naturel. Les essais réalisés sur propergol vieilli naturellement n'ont pas permis de mettre en évidence de variation, ni de propriété thermique, ni de propriété ultrasonore. Seule une petite variation de propriété électromagnétique (permittivité) a pu être décelée.

Concernant les échantillons de propergol vieilli en accéléré, il a été réalisé des échantillons de butalane sous forme de plaques de quelques mm d'épaisseur, de cylindres de 30 et 100 mm de diamètre, d'haltères pour des essais de traction. Les plaques, après vieillissement à l'air libre, ont montré un durcissement très important. Des mesures sur ces plaques vieillies n'ont mis en évidence ni de variation de propriété thermique, ni de variation ultrasonore, mais par contre une variation très importante de module d'Young et d'allongement. Les cylindres vieillis de 30 mm, utilisés pour des mesures de vitesse de combustion, ont mis en évidence une diminution sensible de la vitesse de combustion avec le vieillissement. Des mesures ultrasonores et capacitives réalisées à l'aide de capteurs intégrés dans les cylindres de 100 mm de diamètre n'ont pas mis en évidence de variation de propriété ultrasonore et capacitive après vieillissement. Les essais de traction réalisés sur des plaques tirées dans des cylindres vieillis ont mis en évidence une légère augmentation de module d'Young. Les essais réalisés sur les plaques vieillies en accéléré ne sont certes pas représentatifs d'un vieillissement en volume. Ils montrent toutefois que seul parmi les propriétés mesurées, les propriétés mécaniques : module d'Young et allongement ont sensiblement évolués. L'évolution du module est aussi confirmée sur des échantillons vieillis plus massifs . On note aussi la conséquence du vieillissement du propergol se traduisant par une évolution sensible de la vitesse de combustion. La détection du vieillissement du propergol doit donc se faire par une détection de l'évolution de son module d'Young. Une expérimentation sur deux cylindres représentatifs, l'un contenant un élastomère mou, l'autre un élastomère dur, en utilisant la vibrométrie laser, a montré qu'une variation de rigidité du propergol pourrait être détectée de l'extérieur du cylindre. Reste qu'il faut pouvoir avoir accès à l'enveloppe du missile, ce qui n'est pas possible quand les missiles sont en container, et qu'il faut veiller à ce que la sensibilité du sytème de mesure soit suffisante. La détection de la variation du module d'Young du propergol par des capteurs intégrés dans le missile peut être une solution. Les capteurs pourraient être soit des jauges de contrainte, soit des éléments piézoélectriques, soit des fibres optiques travaillant en jauge extensométrique, ces derniers éléments étant des plus séduisants parce que petits (typiquement 100 µm de diamètre), neutres chimiquement et non perturbants électriquement.

REMERCIEMENTS

Le Service Technique des Systèmes de Missiles Tactiques de la Direction des Missiles et de l'Espace de la Direction Générale pour l'Armement est vivement remercié du soutien financier et technique qu'il a donné à cette étude.

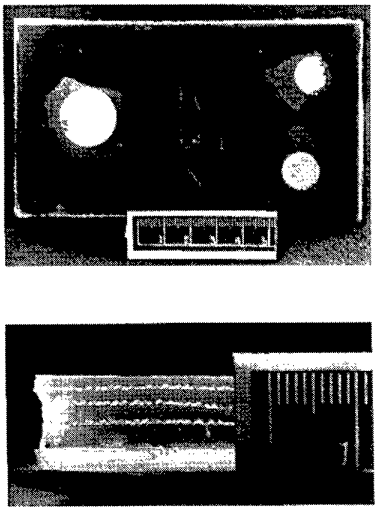


Fig 1 : Eprouvette A - Photographies des vues de dessus et de profil

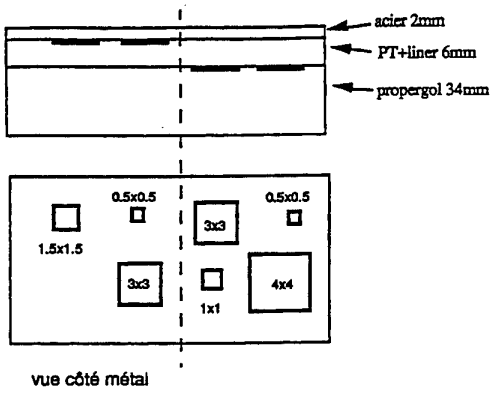


Fig 2 : Eprouvette B - Schéma d'implantation des défauts artificiels - haut : coupe; bas : vue de dessus

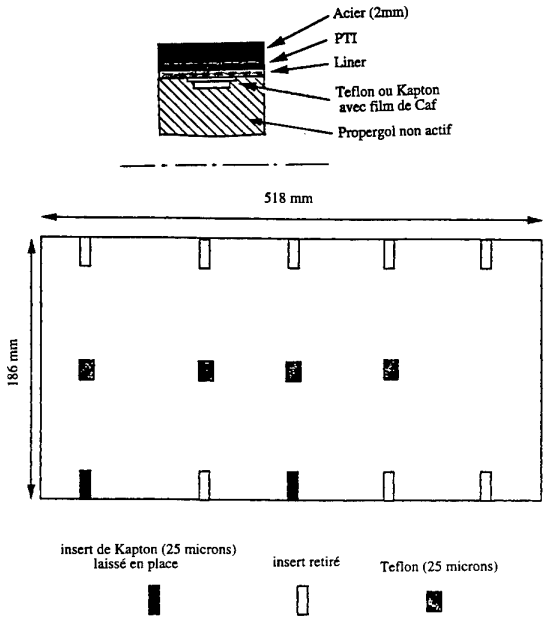


Fig 3 : Eprouvette C - Schéma d'implantation des défauts artificiels - haut : coupe; bas : développée du cylindre

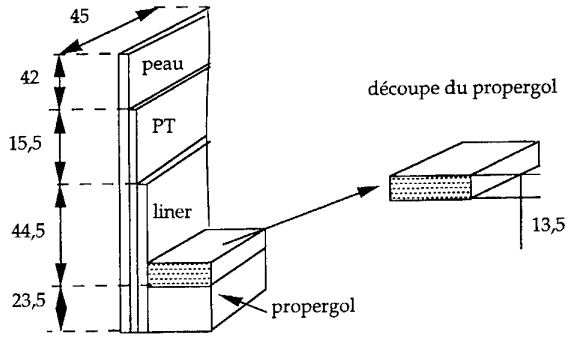


Fig 4 : Eprouvette D - Schéma descriptif

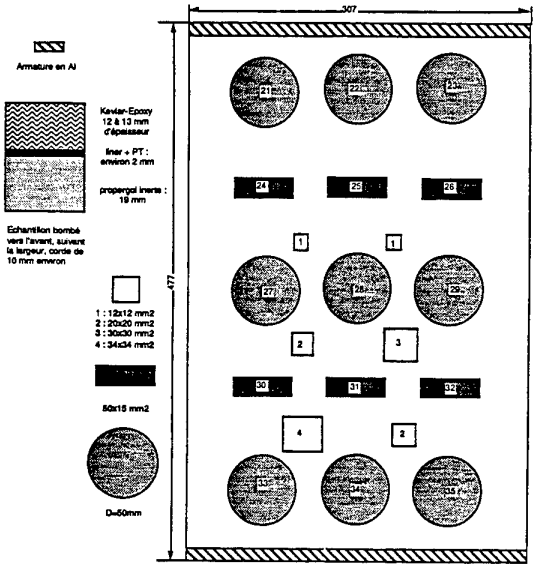


Fig 5 : Eprouvette E - Schéma d'implantation des défauts artificiels

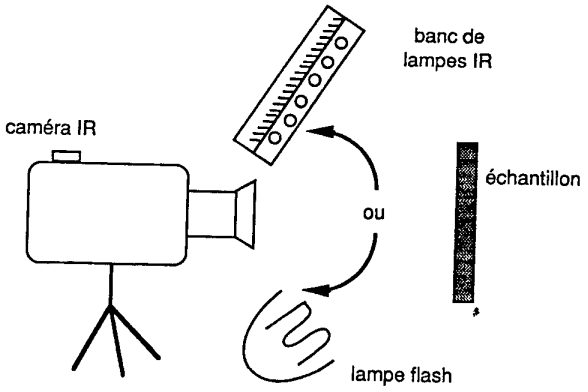


Fig : 6 Schéma du dispositif expérimental pour la thermographie infrarouge stimulée avec configuration en réflexion

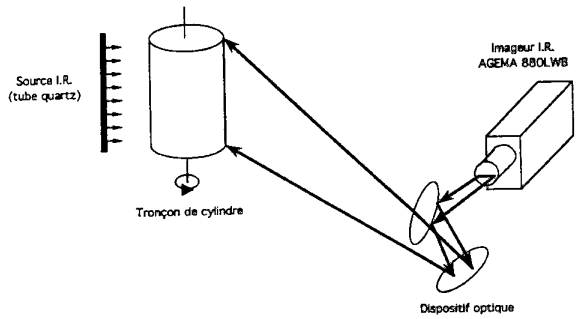


Fig 7 : Configuration expérimentale adoptée pour le contrôle par thermographie infrarouge de l'éprouvette C

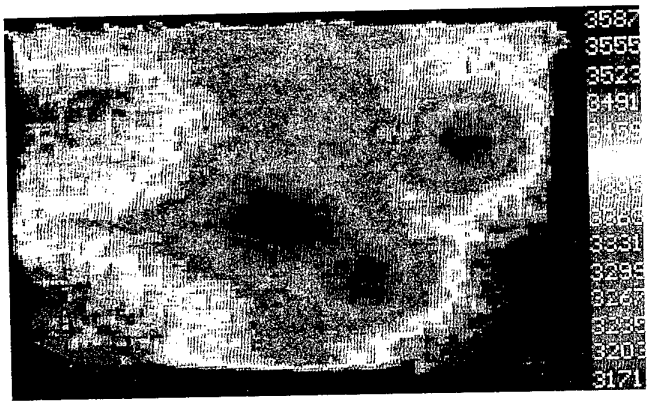


Fig 8 : Eprouvette B - Image en effusivité apparente obtenue après la fin d'une impulsion de chauffage de 7 s

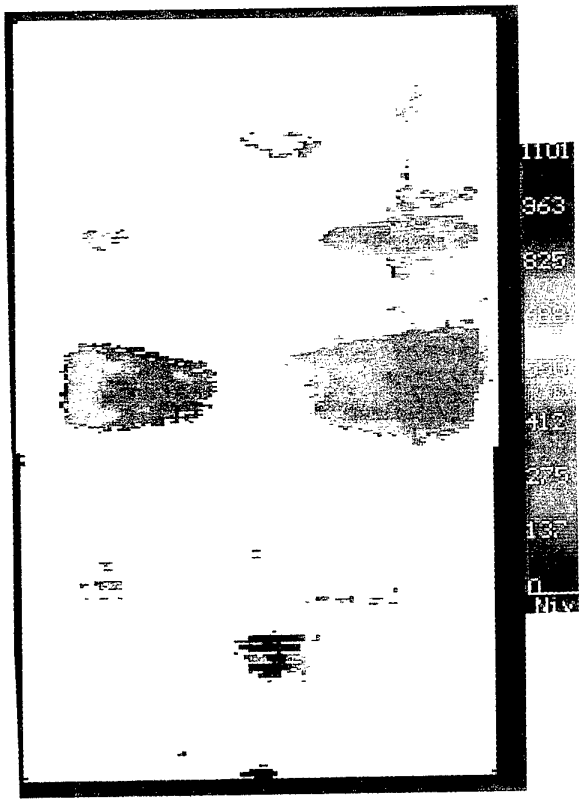


Fig 9 : Eprouvette E - Image en profondeur (exprimée en dizaines de microns) obtenue après contrôle par thermographie infrarouge stimulée



Fig 10 : Eprouvette C - Image infrarouge obtenue par thermographie infrarouge active. Les défauts apparaissent sous forme de taches allant du jaune au rouge suivant leur importance

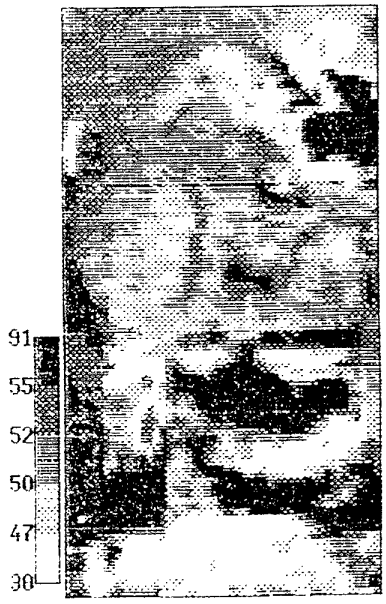


Fig 11 : Eprouvette E - Image ultrasonore partielle

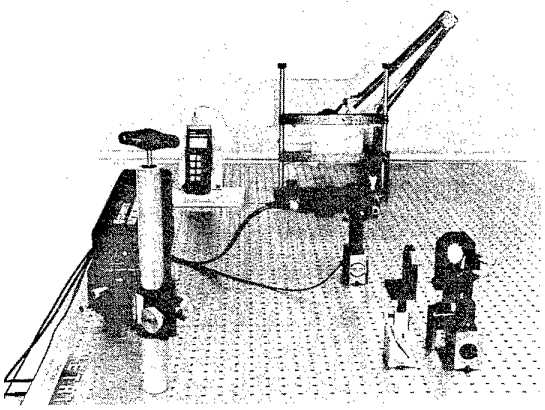


Fig 12 : Montage expérimental utilisé chez Steinbichler
pour les tests de shearographie
avec sollicitation thermique

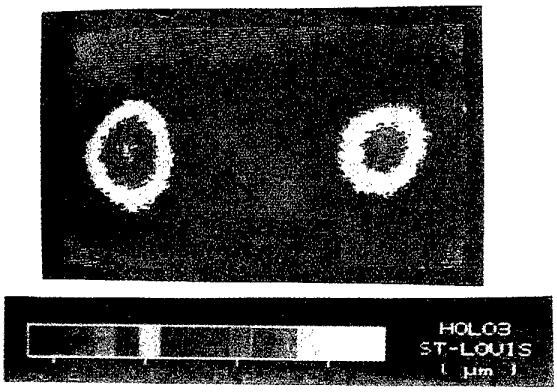


Fig 13 : Eprouvette A - TV holographie avec
contrainte par dépression (Δp = 20 mbar)

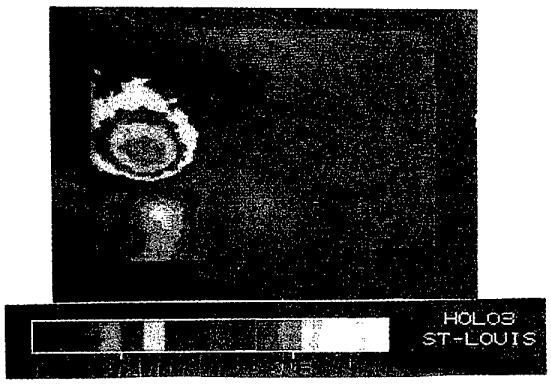


Fig 14 : Eprouvette B -Shearographie
avec Δp =190 mbar

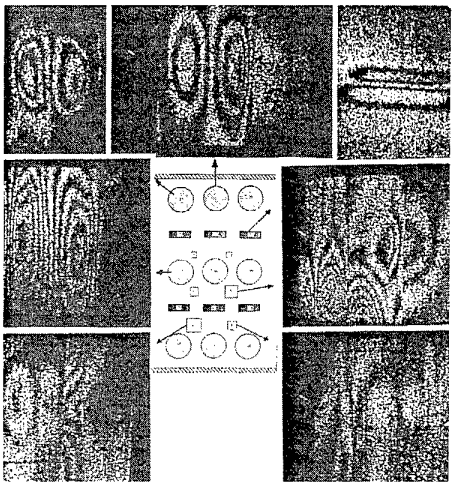


Fig 15 : Eprouvette E - Essai shearographique
Le schéma central rappelle la position des défauts
dont les figures d'interférence sont données

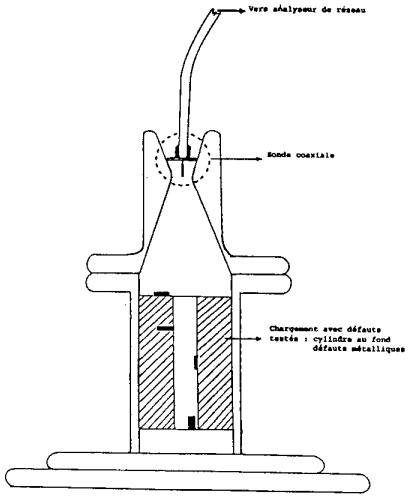


Fig 16 : Réflectométrie micro-onde coaxiale
dispositif expérimental dans un propulseur

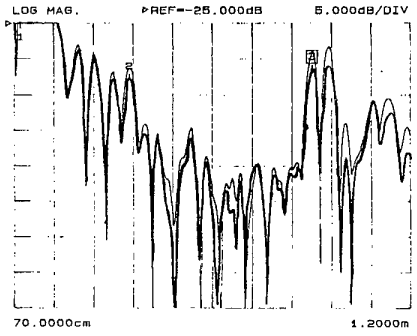


Fig 17 : Réflectométrie micro-onde coaxiale
différences entre le propulseur chargé sans défaut
et avec un cylindre métallique sur le propergol

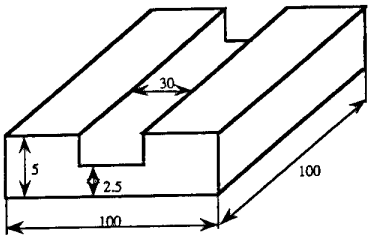


Fig 18 : Schéma de principe des éprouvettes fournies par la SNPE, de propergol vieilli naturellement, après usinage,

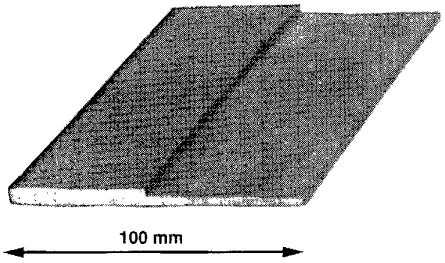


Fig 19 : Photographie de l'une des plaques de propergol préparées à l'Office

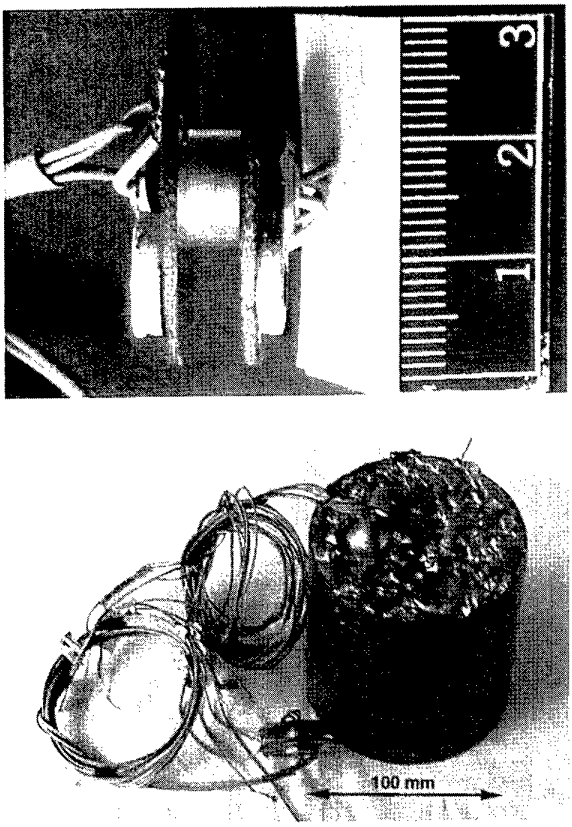


Fig 20 : Photographies d'un diabolo et d'un bloc de propergol contenant un diabolo

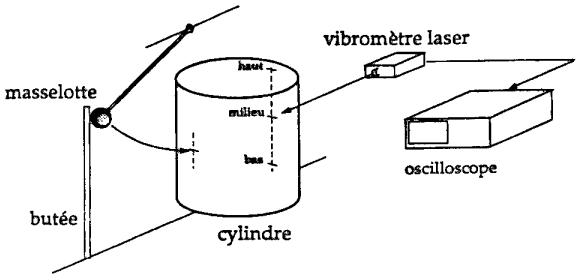
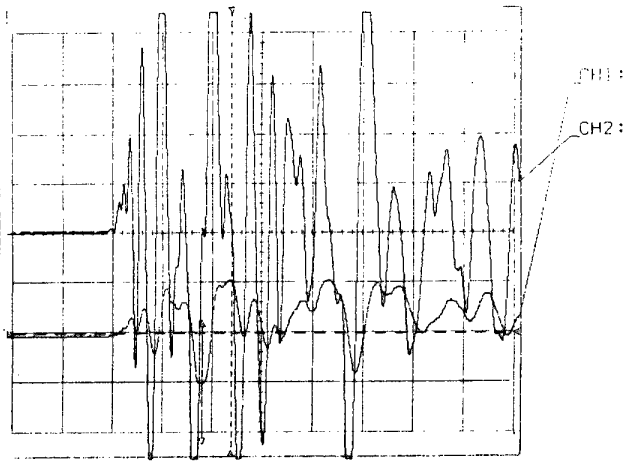
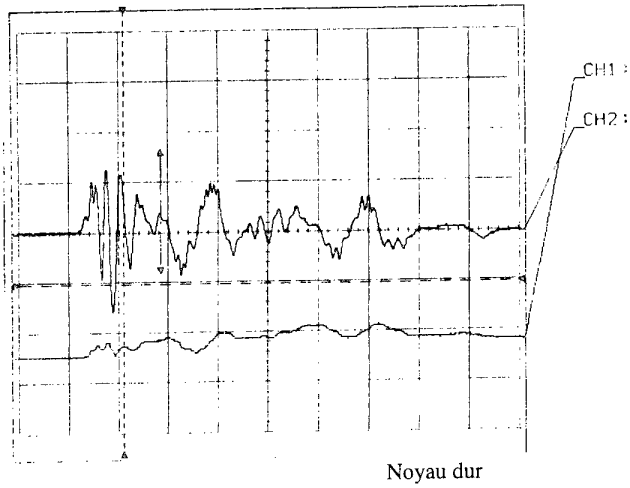


Fig 21 : Schéma de principe du dispositif expérimental de détection de variation des propriétés mécaniques du propergol par vibrométrie laser



Noyau mou



Noyau dur

Fig 22 : Comparaison des réponses du vibromètre pour deux duretés de noyau

Paper Number: 11
Discussor's Name: Professor D. Dini
Responder's Name: A. A. Deom

Question: As a conclusion, what non-destructive global test method are you suggesting to be most reliable in order to know if the missile can be fired or not?

Answer: There is no one non-destructive method affording the best reliability in all the configurations of rockets. I think that taking into account the variety of missiles, it is a system using two, eventually three, methods mounted on the same mechanical system, which will be the most reliable. The building of such a multiple system is presently in progress in our laboratory.

Paper Number: 11
Discussor's Name: D. I. Thrasher
Responders's Name: A. A. Deom

Question: With thermography, how do you distinguish between a case-to-liner disbond and a propellant-to-liner disbond? With shearography/holography, how do you determine which interface contains the disbond?

Answer: Thermography is now a quantitative NDT method. We can easily distinguish between a case-to-liner disbond and a propellant-to-liner disbond by the fact that each disbond produces a bump in the temperature decrease curve at a different time; the thermal diffusion time from the surface to the disbond being different in the two cases. On the other hand, with shearography/holography it is very difficult, up to now, to determine which interface contains the disbonds. Maybe some development of mathematical models will allow the determination of the depth of the detected defects.

The Penetrometer : Non-Destructive Testing of Composite Propellant Rocket Motor Grains To Determine Ageing Characteristics.

G.S. Faulkner & A.W. Thompson
British Aerospace Defence
Royal Ordnance Rocket Motors
Kidderminster, Worcs. DY11 7RZ
ENGLAND

H.J. Buswell
DRA Fort Halstead
Sevenoaks,
Kent TN14 7BP
ENGLAND

1. SUMMARY

It is essential that the mechanical properties of a propellant grain are assessed during its service life to ensure that the grain has an adequate margin of safety to survive future deployment loads. The physical properties of the propellant should also be sufficient to withstand the final loading, motor pressurisation on ignition. Each propellant grain can be considered unique by virtue of its manufacturing processing and its subsequent service history. In the past, it was practice to treat the population of a particular type of motor as being uniform in properties and, as such, individual motors were dissected to determine the physical properties.

The obvious disadvantage to this method was that the rocket motor grain was destroyed. What was realised, however, was that the motor that had been dissected may not have been truly representative of the group to which it belonged. This dilemma was resolved by the introduction of a non-destructive test which could be applied to all the motors in the group. The Penetrometer and its usage is described within this paper.

2. INTRODUCTION

The mechanical properties of solid rocket motor propellant grain are known to change throughout its service life. The mechanism by which these changes occur are dependent on the particular propellant and the mode of deployment of the missile system. There is a need to characterise the extent of the change in order to establish the anticipated mode of failure and, more importantly, to determine when it will occur. The cost savings accrued due to the extension of the service life of a rocket motor can be considerable, as can be the cost that is incurred when an un-anticipated failure arises. Unfortunately, each rocket motor is unique by virtue of the processing conditions of the propellant and also its deployment in service use. Hence, a particular rocket motor which has been deployed (perhaps overseas) and then subsequently returned to magazine storage may have mechanical properties which are somewhat different by comparison to a 'sister' propellant grain which has remained in storage. This naturally lead to problems regarding the sentencing of rocket motors. What was needed was a tool which could assess each motor on an individual basis to ensure that the propellant properties have not deteriorated to such an extent that failure is imminent. This report concentrates on the ageing behaviour of a rubbery-type (H.T.P.B) propellant but the technique is applicable to other propellant systems.

Composite propellant ingredients comprise mainly of a fuel, an oxidiser and a binder. In the case of Hydroxyl-terminated Polybutadiene (H.T.P.B) propellants the Butadiene binder can age mechanically, chemically and physically, leading to a reduction in the binder's strain capability.

Usually solid rocket motors based on this system are case-bonded that is, the propellant is cast into the pressure vessel which is fabricated of High Strength Aluminium or steel. The cast and cure temperature for the motor is around 60°C. A typical value for the linear coefficient of thermal expansion of HTPB based propellants is 9.0E-05 per Kelvin. This value is an order of magnitude different to that of steel and hence large thermal strains can be generated as the motor is cooled to a temperature that is lower than that of the cure. Military applications require that many solid rocket motors function at temperatures as low as -54°C. In practice the propellant charge is subjected to mechanical loads from diurnal temperature cycling combined with chemical ageing due to the presence of Oxygen in the atmosphere. It is for this reason that the U.K. Ordnance Board dictate trials for each type of service motor. Chemical ageing can be restricted by removing atmospheric oxygen by replacing the internal free volume with, for instance, Nitrogen. However , maintenance of this atmosphere requires a seal such as a desiccant pack. However the desiccant packs are not 100% air-tight and degradation in the strain capability of the propellant occurs which can possibly lead to charge cracking. The surface area generated by the newly exposed propellant can lead to an over-pressure situation and a possible case pressure burst when the charge is ignited. For this reason limits are placed on the material properties specifications, both on unaged propellant and also on the critical value at which possible cracking may occur on thermal cooldown.

In the past, the assessment of the mechanical properties of a large number of motors necessitated the random selection of a small number of motors which were subsequently dissected to obtain propellant samples for testing. This method has three main drawbacks:

(i) The rocket motors are destroyed by the dissection.

(ii) The process is expensive in terms of time required for the dissection work and subsequent testing.

Paper presented at the AGARD PEP Symposium on "Service Life of Solid Propellant Systems" held in Athens, Greece, 10-14 May 1996, and published in CP-586.

(iii) The particular motors chosen may not be representative of the group.

Indeed , members of the group may not have all seen the same number of sorties or environmental conditions. A much better technique to assess the remaining service life of the individual charge would be to test each and every motor in a non-destructive manner.

3. BACKGROUND

In the laboratory, a converted Instron tensile tester was being used to investigate the ageing behaviour of HTPB composite propellants. Conventional tensile tests were carried out on fresh and aged specimens. Compression tests were also carried out using a hemi-spherical indenter.

The background to the development of the test came from the field of conventional engineering where such tests as that of Vickers hardness are used to indicate the properties of the material being tested . Laboratory scale tests using a converted Instron tensile test machine indicated a strong relationship between the load required to indent a propellant sample and its modulus. The compression test apparatus is shown schematically in Figure 1. A propellant sample is placed on a platten and the indenter is moved at a fixed cross-head speed into the propellant surface. The indenter compresses the propellant surface to the depth of a few millimetres. It was found for HTPB propellants the optimum speed was 5 mm/min using an indenter of 1.5mm in diameter. For HTPB propellants a load cell rated at 5 Kg full scale load was used with a chart speed of 100 mm/min. All characterisation tests were thus carried out, relating uniaxial data at a cross-head speed of 50mm/min to indentation tests at a rate of 5mm/min. A typical load-strain curve for a H.T.P.B. propellant tested in uniaxial tension is shown in Figure 2. The test was conducted at 20°C with a cross-head speed of 50 mm/min.

Figure 3 shows a load-displacement trace for the same propellant tested in compression. This compression test inadvertantly became known as a 'Penetrometer' test and the name was coined. On reflection, a more appropriate term might be 'Indentometer' test since the propellant surface is merely indented and not penetrated as the term may suggest. Both traces show an initial linear response which is a characteristic of the propellant. As the propellant ages it becomes less compliant with a resulting loss in srain capability. This phenomenon is reflected in the increasing gradient of the linear region of the load-displacement curve between points A and B in Figure 3. The result from the compression test on a specimen is then compared to the mechanical properties from the tensile test. Compression tests are normally carried out first, on a domino of propellant from which the tensile test specimen is subsequently die-cut as shown in Figure 4. The method of Penetrometer calibration for use in determining the propellants ageing characteristics is given below. Under ambient storage conditions the propellant ages relatively slowly. To condense the time-frame, accelerated ageing trials at 60°C have been carried out. "Domino" shaped propellant blocks (dimensions 70x40x10 mm) are used for the Penetrometer calibration .

1: Propellant dominoes from the motor casting are tested using the Penetrometer and also in uniaxial tension. This gives the initial unaged propellant data i.e. a Penetrometer Slope Value and physical property measurements of the modulus, tensile strength and strain capability.

2: Dominoes are then subjected to an accelerated ageing programme.

3: Periodically dominoes are removed for testing .

4: Penetrometer test results are recorded and averaged (six tests) as are the mechanical properties resulting from tensile tests.

The gradient of the initial linear region of the curve in Figure 3 is referred to as the 'Penetrometer Slope Value' (P.S.V) which has units of N/mm. The P.S.V has been empirically related to the propellant mechanical properties by the simple test methods described above by comparing the P.S.V. to the results from the Instron data. The Penetrometer Slope Value as measured by the Instron/Load cage method, is calculated using equation 1

$$\text{P.S.V.} = \frac{\text{FSL} * 9.81 * \text{CS}}{\text{XHS} * \text{X}} \qquad \text{..... (1)}$$

where

FSL = full scale load
CS = chart speed:
XHS = cross-head speed
X = Horizontal distance (in mm) from point A to B

Experiments in the laboratory indicated that there was a minimum thickness of propellant required such that the supporting platten surface did not influence the PSV reading. Figure 5 shows that a minimum propellant thickness of ~ 15mm is required.

Also investigated was the effect that the angle of indentation to the surface has on the PSV reading . It was determined that each degree off from the normal to the surface decreased the PSV by 0.2 units. The results are presented graphically in Figure 6.

The effect of indenter speed was known to be a factor due to the viscoelastic nature of the propellant. Hence a rate of 5mm/min cross head speed was decided upon since the test could be carried out in a more controlled manner than if the cross head speed was 50mm/min.

Figures 7 and 8 show some data determined for a particular HTPB propellant. Figure 7 indicates the relationship between PSV and strain capability whilst Figure 8 relates PSV to propellant strength.

The determination of the modulus, strength and strain capability from this simple indentation test lead to the development of a portable, non destructive test equipment called the 'Penetrometer'. The Penetrometer was designed to address the following problems associated with

measurements made using other techniques such as the Shore hardness meter, these being :

(i) The variability between operators using the equipment

(ii) The need to control the rate at which the load is applied

(iii) The ability to test motors in inaccessible places (such as in the middle of the charge)

(iv) The need to hold the measuring device perpendicular to the propellant surface.

To carry out this task requires that the test method was standardised since the response of propellant to an applied load is strongly rate and temperature dependent.

The development of the Penetrometer has been carried out by Royal Ordnance Rocket Motors to assess the service life of several designs of motor, some in current military use and also structural test motors. The Penetrometer can also be used to monitor each charge as it rolls off the production line and has, therefore, a second role in as much as it can be used as a quality testing device.

4.THE PENETROMETER

The Penetrometer is a self-contained unit which can be used in Service magazines to monitor the degradation of solid rocket motor fuel and hence life the charge. The control unit contains two sets of rechargeable batteries , one set being spare to obviate the need to return to base and stop work to recharge batteries. A general view of the Penetrometer is shown in Figure 9. Located at the end of the probe unit is a 1.5 mm in diameter stainless steel hemisphere which has been bonded to a strain-gauged shank . Also at the end of the probe are two thermocouples which are used to monitor both air and probe temperature.

The probe shaft is graduated in increments of 20 mm and there is a bezel which records the angle at which the indenter is with respect to a reference mark on the charge. Hence both depth and orientation can be recorded. A depth stop prevents the end of the probe from contacting any igniter present at the head-end of the charge.

It was decided at the onset of the construction of the prototype Penetrometer that it should be capable of being used on the many grain designs that give the solid rocket motor the desired ballistic performance. That is, it should be a useful tool for service life work on as many motors as possible . Hence a system was devised where the air bag was used to locate the probe in a specific rocket motor as shown in Figure 10. The air bag is detachable and can quickly be changed for a different design and the operator can then proceed to test other motor types in the magazine. The air-bag unit provides a measured reaction force for the indenter. The air pressure in the air-bag is displayed on the screen of the Husky Hunter. When a pre-set level is reached , the Hunter issues an audible signal. The air-pressure level depends on the motor type , hence the operator is requested to select which motor type is being tested and the computer software sets the correct reference air pressure level.

To guide the air-bag down the conduit a soft former is used. The former is cast from 'silcoset'and matches the grain design. The probe is introduced into the rocket motor via the nozzle end and can be locked in place by utilising the desiccant pack mounting ring where fitted. The probe is supported by a tripod enabling operation of the Penetrometer at different heights. Earthing points are provided on the control unit and Zener barriers are used for cabling that passes down the central probe conduit. Once in position, a strain-gauged identer is driven by a stepper motor at the rear of the probe unit. The indenter depresses the grain surface by up to1.5mm. The load required to do this is measured by the strain gauge. This operation is carried out in a region of low strain, such as the tip of a spline of the grain. The indentation is small and the localised deformation soon recovers.

The information obtained from the test is displayed graphically on the microcomputer, analysed and stored. Stored data is then downloaded via an RS232 serial interface to a database on a personal computer. Changes in the elastic response of the grain can thus be related to changes in mechanical properties. The determination of the mechanical properties of the charge is derived from previous calibration work on the propellant, carried out in the laboratory.

4.1 THE CONTROL UNIT

The control unit is essentially the power pack for the Penetrometer stepper motor. It is connected to the probe unit via Zener barriers. It also acts as a temporary data storage area for onward transmission to the Husky Hunter microcomputer. The unit houses two E.P.R.O.M.s that control the stepper motor and communicate with the Husky Hunter. The Microcomputer, a Husky Hunter model 144K was chosen since it is a robust instrument. The Hunter contains the code which controls the Penetrometer operation. The other function of the Hunter is to analyse the data received from the control unit and store it for subsequent downloading to a computer database on an IBM PC. This procedure is fully automated, utilising the serial ports on both Hunter and I.B.M. The data for up to 80 motors can stored before downloading is necessary. This figure is limited by the Hunters memory. However larger memory Hunters are available. The Hunter computer has an internal battery as well as the four main batteries which drive the screen and port. The software on the Hunter instructs the operator at each stage of the reading. The type of information stored consists of the motor serial number, date of reading, calibration data, the four Penetrometer Slope Values with associated regression and correlation data. The motors location is not recorded by the computer for security reasons.

Typically it takes 20 minutes to test each motor. The test involves taking four readings in the motor and then determining an average value for the P.S.V. Calibration is performed by mounting the Penetrometer on it's carrying case. The stepper motor is driven forward by a fixed number of steps and a dial gauge records the displacement. The load calibration consists of lifting two 1 Kg weights to

obtain readings for one and two Kilograms. The 1Kg reading is stored as one calibration figure and is then subtracted from the 2 Kg reading. After subtraction , the reading is stored as a second calibration figure. The two (effectively both 1 Kg) readings are then compared to check linearity and also to ensure that the probe is functioning correctly. The battery supply levels are displayed on the computer screen and a system status check is carried out.

The operator will be informed if the Penetrometer has passed or failed the calibration checks. After the Penetrometer has been used to take a reading, the microcomputer displays the load versus indentation depth (number of motor steps) trace on the screen .

The operator can select the relevant linear portion of the curve by adjusting movable cursors. The P.S.V. value for the Pentrometer is calculated from equation (2) below:

$$\text{P.S.V.} = \frac{\text{R.C.} * 9.81 * \text{cal 1}}{\text{cal 2}} \qquad \text{..... (2)}$$

Where

R.C. = regression coefficient of the linear region between selected points on the load-displacement graph on the computer screen

cal 1 = displacement calibration value from the 1Kg lift.

cal 2 = load calibration values (average of 1 and 2 Kg)

The regression coefficient and correlation coefficient as well as the P.S.V. are calculated by the Hunter software from the data points selected between the two cursors.

5. TESTS ON ROCKET MOTORS

Figure 11 shows penetrometer measurements made on a group of 36 motors. The motors were filled from the same pre-cure but filled in batches of 6 motors at a time. The PSV values indicate an average PSV reading of 14.2 N/mm .

Figure 12 shows the ageing trend for a proportion of motors from a particular rocket motor grain. The trend shows that all the motors are gradually ageing. The strain capability of the grain is reducing with time. Outlying motors to the general ageing trend can be detected and investigated in more detail.

If a result from the Penetrometer is 'suspect' then, since the test is non-destructive, it can be repeated to confirm the reading.

6. CONCLUSION

The Penetrometer has been developed to monitor the ageing of solid rocket motor propellants . The advantage that the technique has is that each individual motor can be tested rapidly. The ageing of a particular motor or group can be assessed. The ability to monitor motors on an individual basis is important since each motor will have a different deployment profile and, hence, its own service life. To date, four Penetrometers have been manufactured for use in the non-destructive testing of motors.

ACKNOWLEDGEMENT

This paper was supported by Defence Research Agency (DRA) Fort Halstead contract WSFH/E2096C - Service Life Studies.

Figure 12 reprinted by permission of Defence Research Consultancy and DRA Fort Halstead.

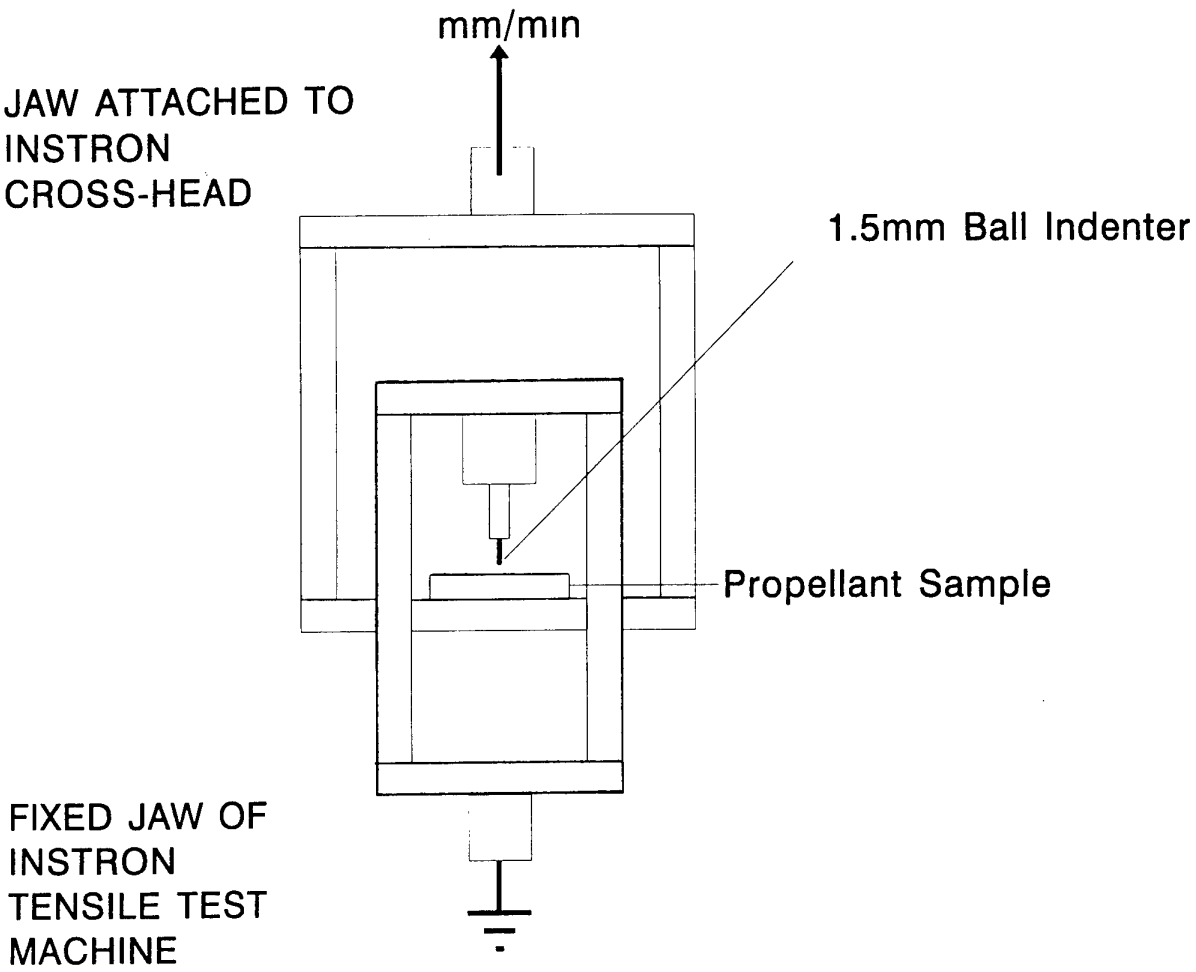


FIGURE 1 : LABORATORY PENETROMETER TEST EQUIPMENT

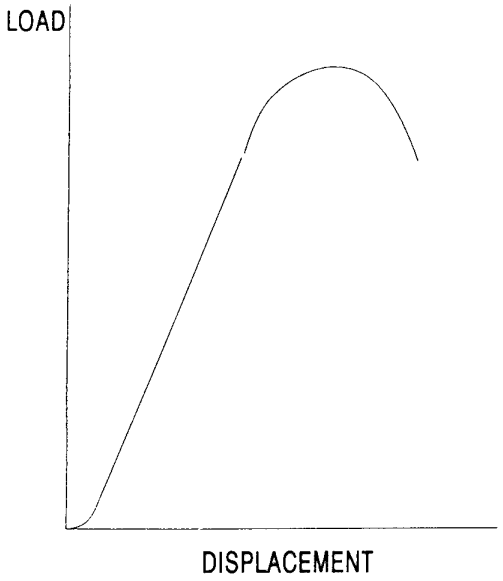


FIGURE 2 LOAD-DISPLACEMENT CURVE FOR AN HTPB PROPELLANT (SCHEMATIC) IN UNIAXIAL TENSION

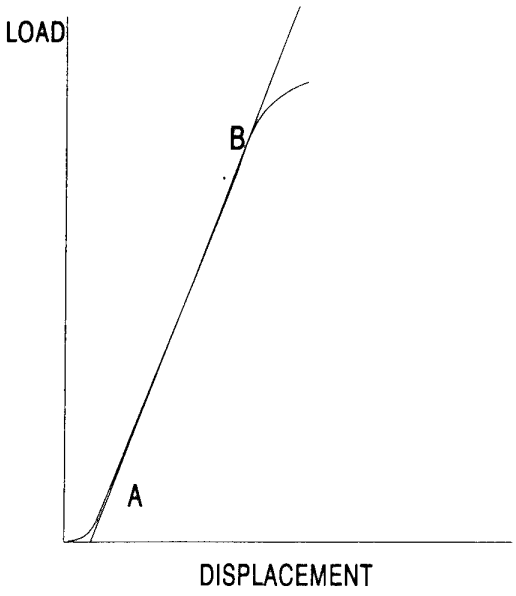


FIGURE 3 LOAD-DISPLACEMENT CURVE FOR AN HTPB PROPELLANT (SCHEMATIC) IN COMPRESSION

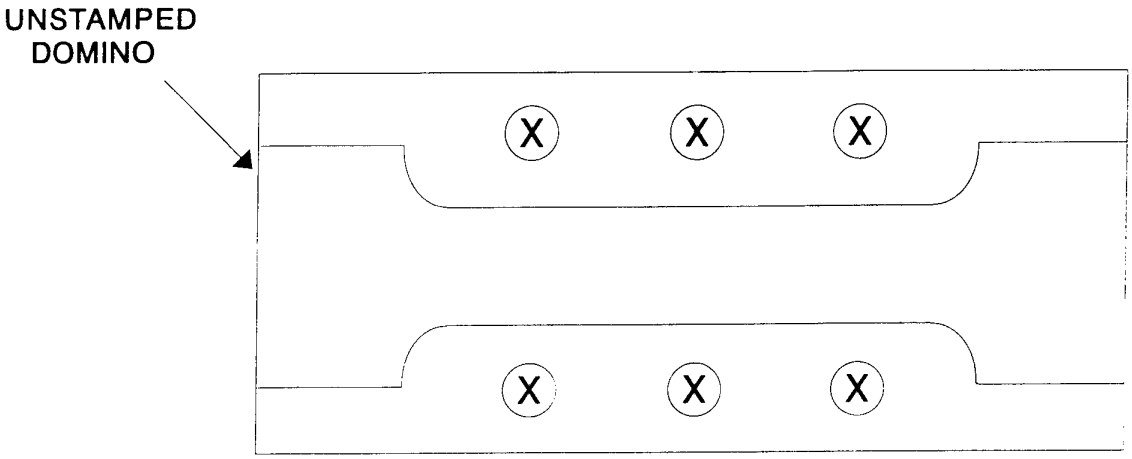


FIGURE 4 PROPELLANT DOMINO SHOWING LOCATION OF PENETROMETER TESTS PRIOR TO BEING DIE-CUT

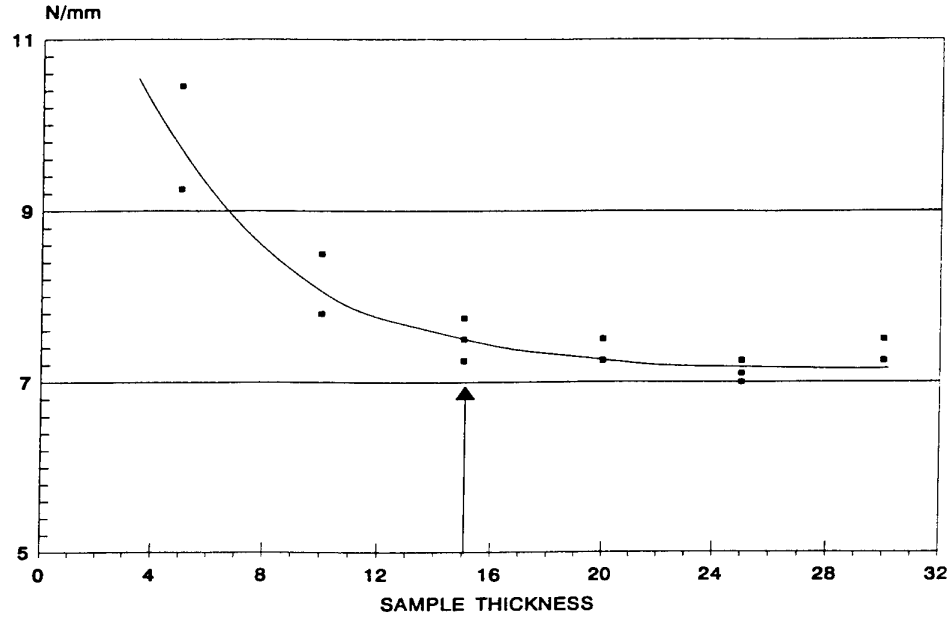


FIGURE 5 . THE EFFECT OF SAMPLE THICKNESS ON INITIAL SLOPE VALUE

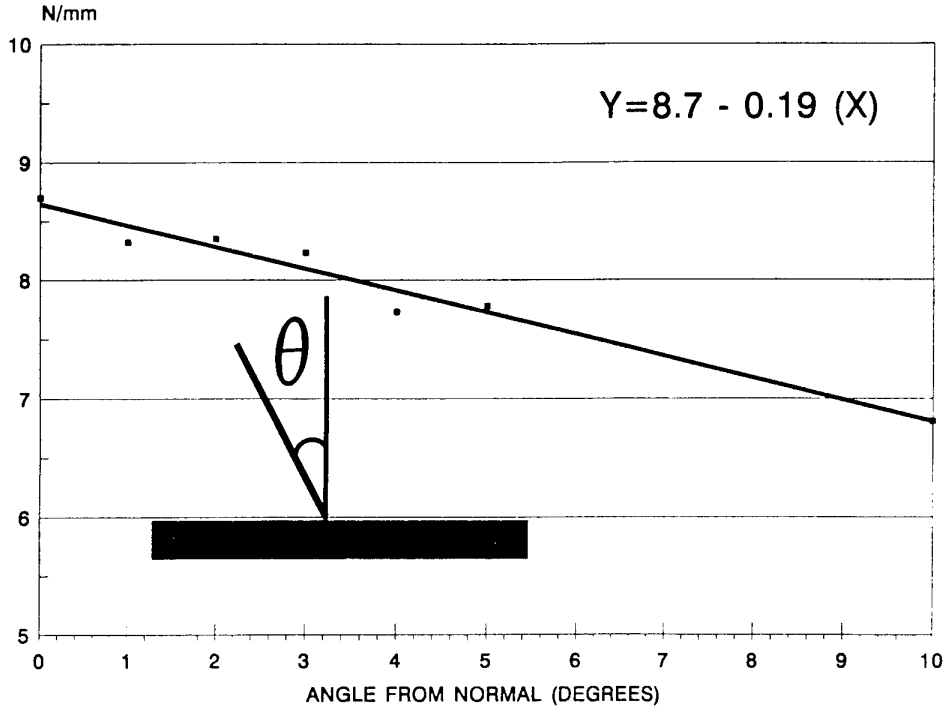


FIGURE 6. THE EFFECT OF ANGLE OF THE INDENTER RELATIVE TO THE SAMPLE NORMAL

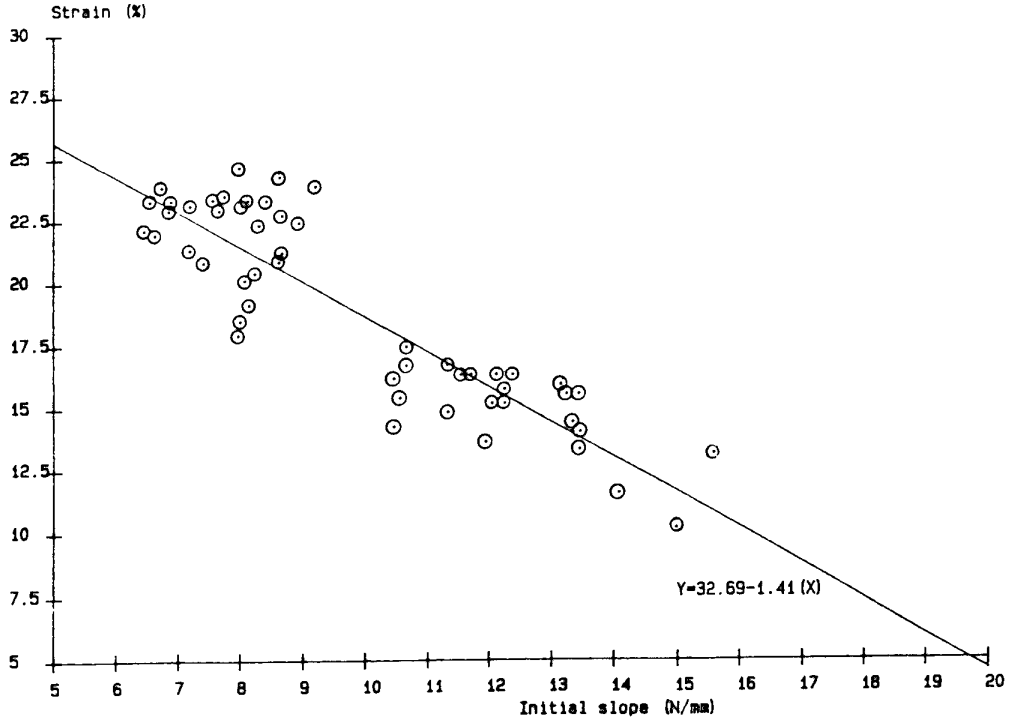


FIGURE 7 LABORATORY PENETROMETER MEASUREMENTS FOR PROPELLANT STRAIN CAPABILITY

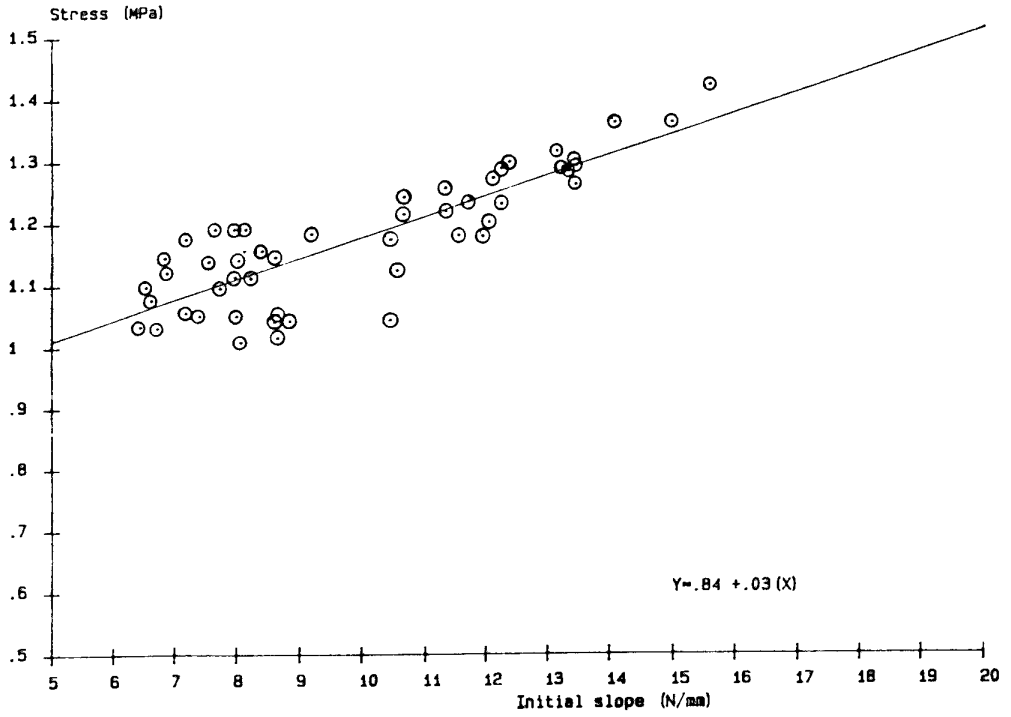


FIGURE 8 LABORATORY PENETROMETER MEASUREMENTS FOR PROPELLANT STRENGTH

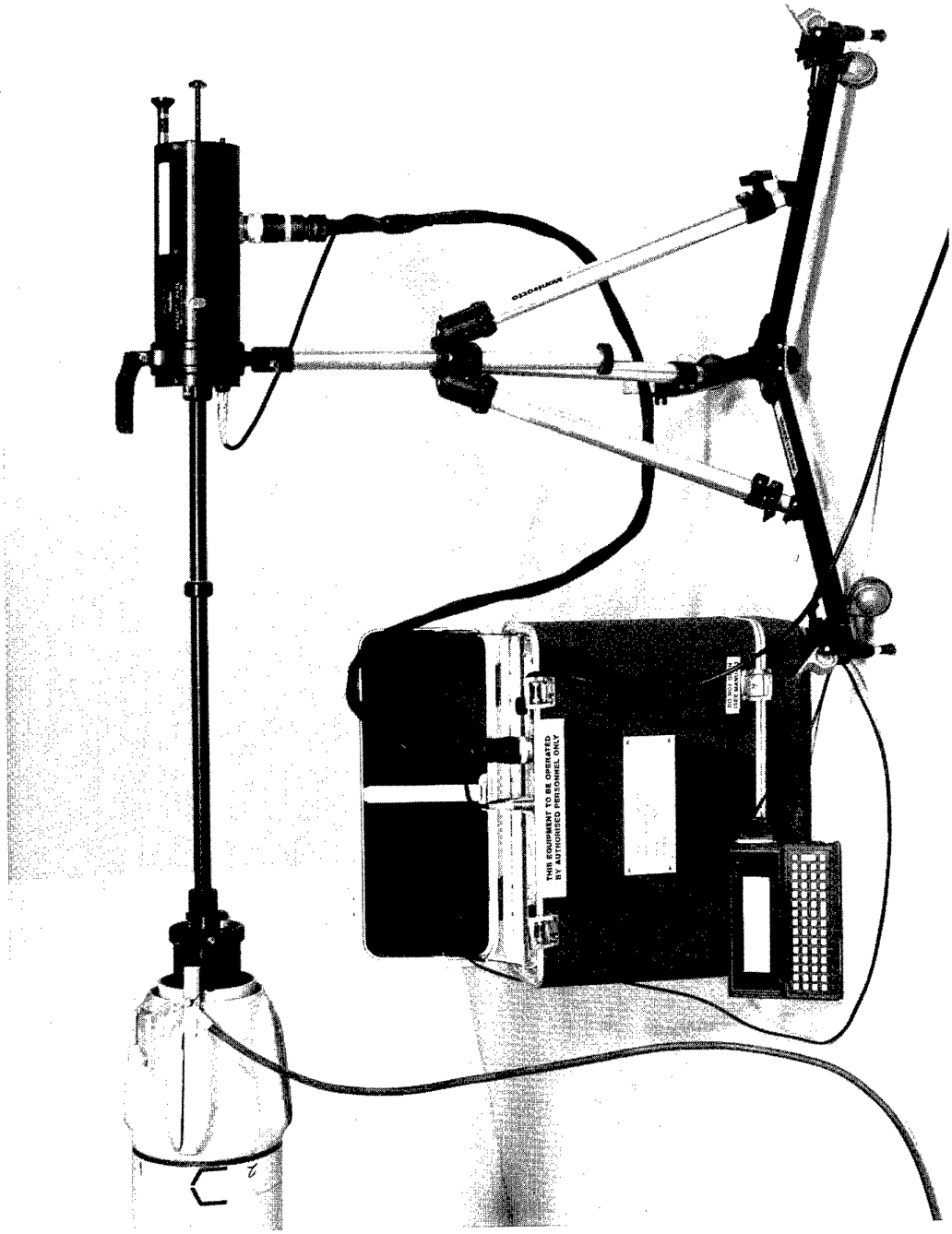


FIGURE 9 GENERAL VIEW OF THE PENETROMETER AND TEST MOTOR

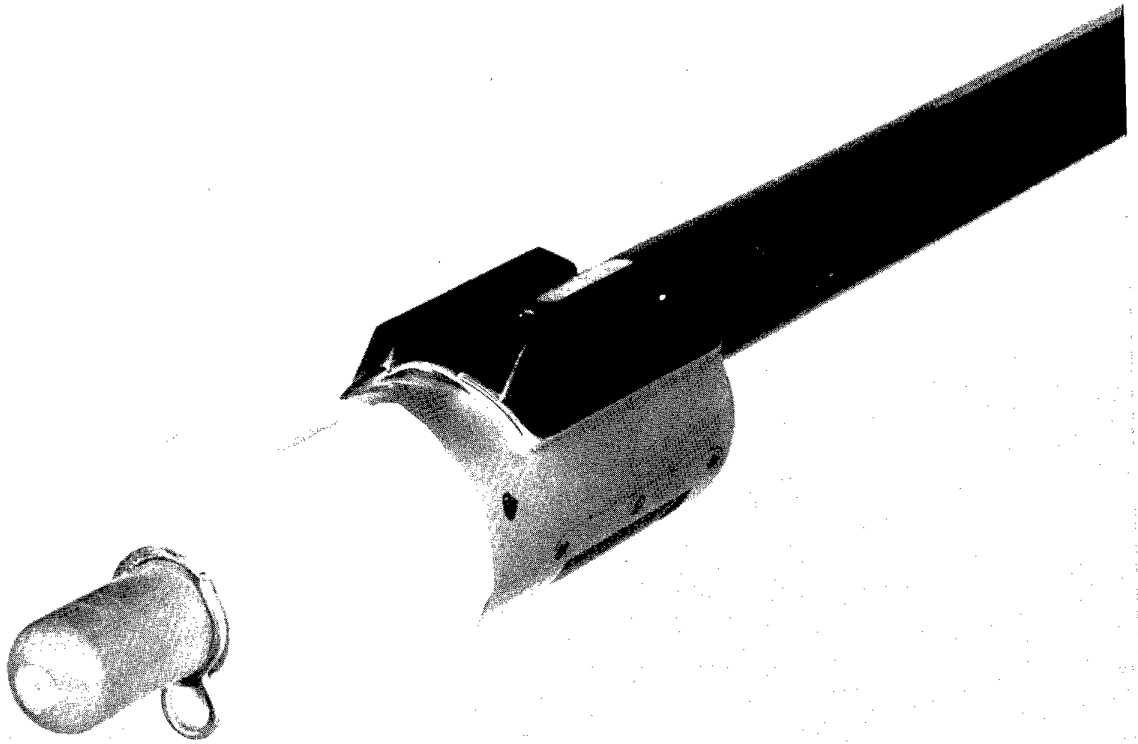


FIGURE 10 PENETROMETER AIR-BAG AND SOFT GUIDE (BOTH REMOVABLE)

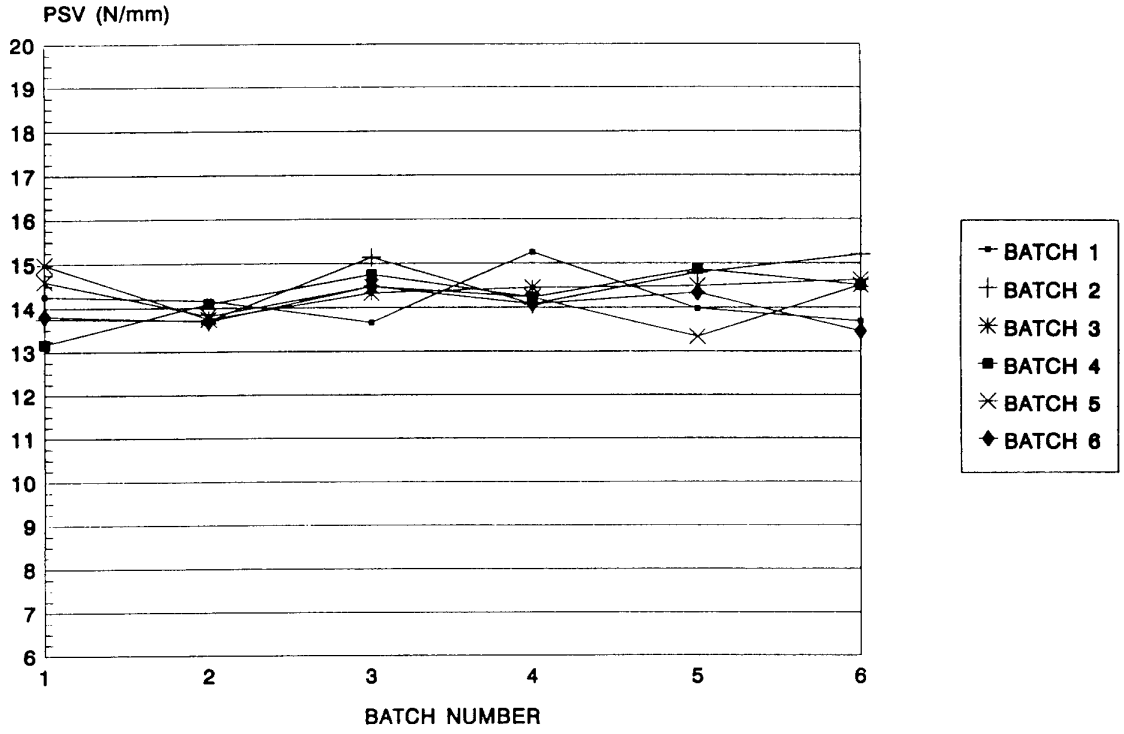


FIGURE 11. PENETROMETER READINGS ON 36 MOTORS FILLED IN GROUPS OF 6

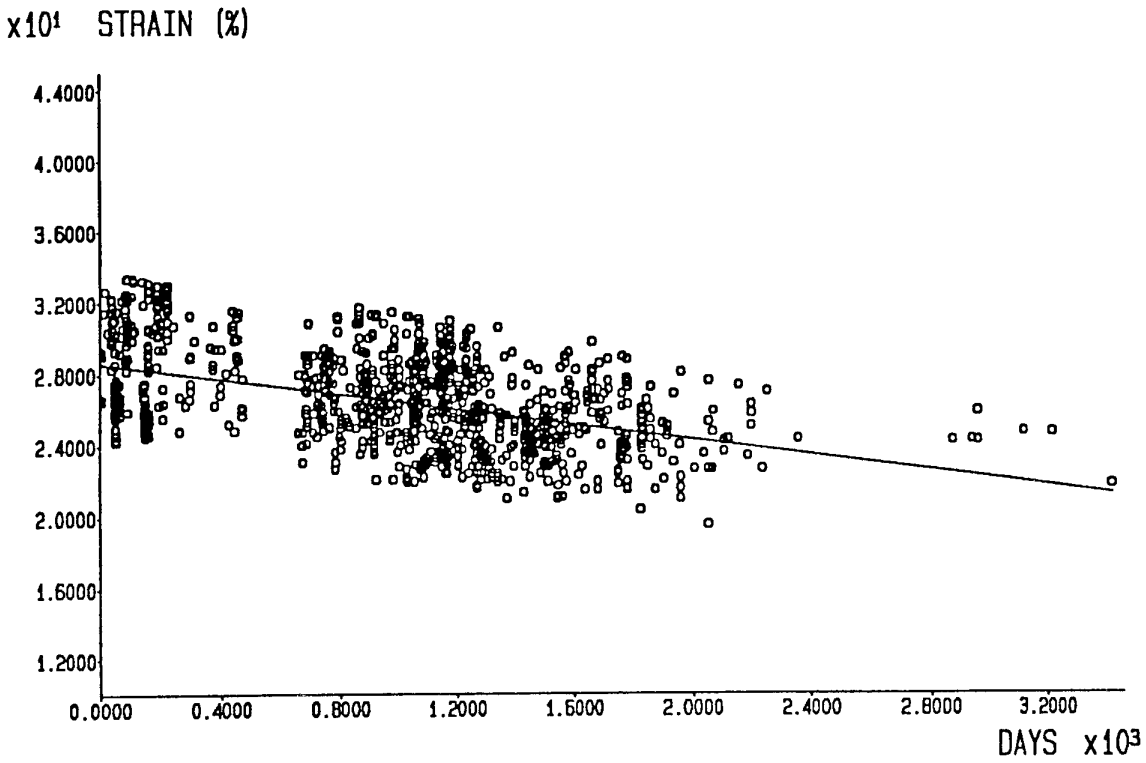


FIGURE 12 AGEING TREND FOR TESTED MOTORS SHOWS A GRADUAL DECREASE IN PROPELLANT STRAIN CAPABILITY WITH AGE

Paper Number: 12
Discussor's Name: Professor D. Dini
Responder's Name: G. S. Faulkner

Question: How can you use the penetrometer when you are afraid that the propellant properties are deteriorated to such an extent that failure may be imminent?

Answer: When we conduct penetrometer tests it is primarily to detect and measure motors up to the point where failure is imminent, hence we can maximize service life. We test the propellant grain in regions of low strain (along the vanes of the grain) hence we are unlikely to precipitate failure. Indeed, for the penetrometer to be a useful tool, it has been necessary to age motors artificially such that failure by grain cracking occurs. Hence, we thus establish the critical penetrometer measurement values.

THERMOGRAPHIC DETECTION OF BOND DEFECTS WITHIN MODELS OF SOLID PROPELLANT MOTORS

H. Schneider, N. Eisenreich
Fraunhofer Institut für Chemische Technologie
Joseph von Fraunhofer Straße 7
D - 76327 Pfinztal
Federal Republic of Germany

1. SUMMARY

Within solid propellant rocket motors there sometimes exist separations or bond defects between case and liner (insulation made of elastic polymer) or between liner and propellant. This paper demonstrates that separations or bond defects can be detected by thermography. Till now the smallest defects that could be detected had a diameter of 20 mm and a separation of 0.05 mm.

2. INTRODUCTION

Solid propellant rocket motors usually consist of a case of metal which is coated inside with the liner which is an elastic polymer. The propellant is casted in this system. The motors may be exposed to mechanical stress and extreme temperature variations during storage and transport. As a consequence motor case and liner or liner and propellant may be separated at some places. In the first case the motor case may be subjected to high temperature combustion gases during operation and may be destroyed by excessive localized heating. In the second case an increase of combustion chamber pressure can also cause the destruction of the rocket motor. Therefore the investigation of rocket motors with respect to such separations is important.

Several years ago, during a comprehensive property analysis of the HAWK motor after long standing troop employment, which was performed at our Institute there was a need for non destructive testing (NDT) methods (A review of the results of the whole HAWK-project will be presented in paper No.41 of this meeting /1/). In parallel to the application of the conventional NDT methods like x-rays, ultrasonic and „coin" inspection to the HAWK motors we made our first experiments with the thermographic testing method.

3. PRINCIPLE OF THE METHOD

The physical basis for the thermographic detection of separations like flaws or bond defects is the fact that these discontinuities interpose a resistance to heat flow. Under proper conditions this causes temperature gradients to appear on the surface of the object. Therefore the detection of separations within the object means to determine the distribution of the surface temperature. Since the temperature difference at the surface due to defects inside is very small, a very sensitive detector is necessary. In thermographic measurements the temperature distribution at the surface of the object is determined by the measurement of the IR - radiation. The principle of the method was applied in this field in USA in the sixties already /2, 3/.

There are two methods of producing useful temperature patterns at the surface of the test object: The heat soaking or passive method consists of placing the motor in a conditioning box (oven or refrigerator) at a temperature significantly different from ambient. The motor remains in the conditioning box until the entire motor mass reaches temperature equilibrium, after which the motor is removed to ambient conditions. During the cooling-down or warming-up process the surface temperature of the motor case is measured.

In the transient heating or active method the motor case is irradiated by an IR-source, i.e. the motor case and the components underneath of the case will be penetrated by a heat flow. Again, any discontinuities within the system will distort the heat flow with the result that the surface temperature above the defect will be somewhat higher than in neighbouring areas. In the transient heating method a key parameter is the time delay between heating and temperature measurement. This parameter controls the penetration depth of the test. Long delays allow the applied heat to penetrate deeply into the part before the surface temperature is measured. This would be required for materials with low heat conductivity such as nonmetallics or for defects deep in a part. Short delays allow only shallow penetration, as would be required for near surface defects or for materials that rapidly conduct heat such as metals.

4. EXPERIMENTAL STUDIES

During the HAWK test program we applied the heat soaking method to the HAWK motor: the motor was stored in a climate chamber for about 48 hours at a temperature of 52 C. After removing the motor to ambient conditions (20 C) and during the cooling down phase the IR-radiation emitted from the surface of the motor was detected by means of a thermocamera type 680 from AGA. The object could be seen on a monitor, where different grey scales corresponded to different temperature ranges. During the inspection the surface temperature of the motor was between 37 C and 32 C. The detected defects appeared on the monitor as dark areas (i.e. cold) with a light (i.e. warm) background. For a confirmation of the results the motor was stored in a climate chamber again for 48 hours at a temperature of - 24 C and then the measuring procedure was repeated at ambient conditions; the surface temperature during the measurement was between - 4 C and +1 C. In this case the defects were light (warm) with a dark (cold) background. Most of the defects which had been detected with the other methods could be found.

Paper presented at the AGARD PEP Symposium on "Service Life of Solid Propellant Systems" held in Athens, Greece, 10-14 May 1996, and published in CP-586.

For a more systematic study of the possibilities of the thermographic detection method we decided to investigate dummy propellant motor cases with the transient heating method. As in earlier studies /2/ the test set up was constructed in such a way that the motor case rotated around its axis at a uniform speed, adjustable between 0.3 and 300 revolutions/minute. The motor case was irradiated by means of a linear, rod-shaped infrared source which was oriented parallel to the motor axis (Figure 1). The IR-source was installed within a water cooled shielding in such a way that only a defined section of the case was irradiated and the surrounding was not heated by the IR-source. To get a uniform irradiation of the case during one revolution, it was necessary that the distance between case and IR-source was kept constant. Since the investigated tubes didn't have completely circular cross sections, the second set of wheels was mounted at the shielding.

An IR-camera type 782 from AGEMA was looking on the surface of the case from the opposite side of the IR-source. Normally, the area of the case which was monitored by the camera was 10 cm x 8 cm. With this arrangement it was possible to detect the thermal radiation from the case with the camera after a predetermined and constant time delay after the irradiation. The camera has a resolution of 0.1 degree and is sensitive in the region between 2 and 5 microns. The pictures were recorded at a frequency of 25 Hz and could be seen on a monitor. They were stored on video-tape and could be transferred to a microcomputer. It was possible to assign to different temperature intervals different colours.

In contrast to the tests which were made in the past - where thermocameras were not yet available - and where in a time consuming line-scanning process only small areas of the motor case could be detected, our procedure would have the advantage to be much faster.

The recorded radiation intensity is not only a function of surface temperature but also of emissivity. Since the emissivity is dependent on the surface structure (roughness, paint) and real rocket motors are often painted with letters or symbols etc. or have scratches, it is advantageous to produce a uniform surface prior to the measurement. For this purpose a liquid black lacquer has been developped. The dummy-motor was immersed into the liquid lacquer to get a homogeneous coating. After the drying of the lacquer in the open air and after the measurement it could easily be removed from the case like a skin .

In Figures 2 and 3 the dimensions of the test object and the dimensions and arrangement of the built-in separations are shown. The separations between case and liner and between liner and dummy-propellant were produced by use of steel 'feeler' stock stripes of various thickness which were arranged parallel to the case axis. After the curing of the liner and the propellant respectively the stripes were pulled from between the case and insulation and from between the insulation and propellant. This left separated regions of known dimensions.

Another kind of defects - so-called bond defects - were also built-in in another model (Figure 3). Circular areas with diameters of 50 mm and 30 mm were coated with substances that prevent the materials (case/liner and liner/propellant) from being bonded. The thickness of the coating was less than 0.05 mm.

5. RESULTS

Figure 4a shows a thermogram of a case without any defects. The picture was taken from the middle section of the case and corresponds to a region with dimensions 10 cm x 8 cm. There is a temperature gradient in the horizontal as well as in the vertical direction of the thermogramm. The main cause for the horizontal gradient is probably due to the heat radiation and heat loss at both ends of the case. The cause for the vertical gradient (Figure 4b) is the cooling of the case. The case rotated from 'top' to 'bottom'; this means that the lower region of the case has more cooled since the time of irradiation than the upper one.

Figure 5a shows a thermogram of the case surface during the passage of a separation located between liner and propellant ('thickness' 0.05 mm, 20 mm wide: see Figure 2). Figure 5b shows the corresponding vertical temperature distribution. The gradient of this distribution is clearly much stronger than in the case without any separation.

For the detection of the so - called bond defects a sequence of thermograms was recorded. Figure 6 shows these thermograms which were taken from the rotating case with a frequency of 1 picture/sec. The rotational speed of the case was 4 revol/min. The case contained the bond defects shown in Figure 3. At first the large bond defect (50 mm diameter) is visible which gradually disappears in the lower left-hand side of the picture; then on the upper righthand side of the picture the smaller bond defect appears. Finally in the last two pictures the first bond defect appears again.

The best results in detecting the separations were achieved for rotational speeds of the motor case of between 4 and 15 revol./min; this corresponds to 2.6 cm/sec and 9.8 cm/sec respectively.

6. CONCLUSIONS

Within models of solid propellant motors separations between case and liner as well as between liner and propellant could be detected down to a 'thickness' of 0.05 mm (20 mm wide) by thermographic inspection.

The same holds for bond defects with circular dimensions down to a diameter of 30 mm.

The minimum size of separations which could be detected by this method is an open question; the answer will also depend on the thickness of the different materials.

7. REFERENCES

1. Schubert, H., Menke, K.: Service Life Determination of Rocket Motors by Comprehensive Property Analysis of Propellant Grains, Proceed. 87th Symp. of the Propulsion and Energetics Panel of the AGARD, Athens, Greece (1996).
2. Gericke O.R., Vogel P.E.J.: Infrared Bond Defect Detection System, Materials Evaluation, Feb. (1964).
3. St. Clair J.C.: An Infrared Method of Rocket Motor Inspection, Materials Evaluation, Aug. (1966).

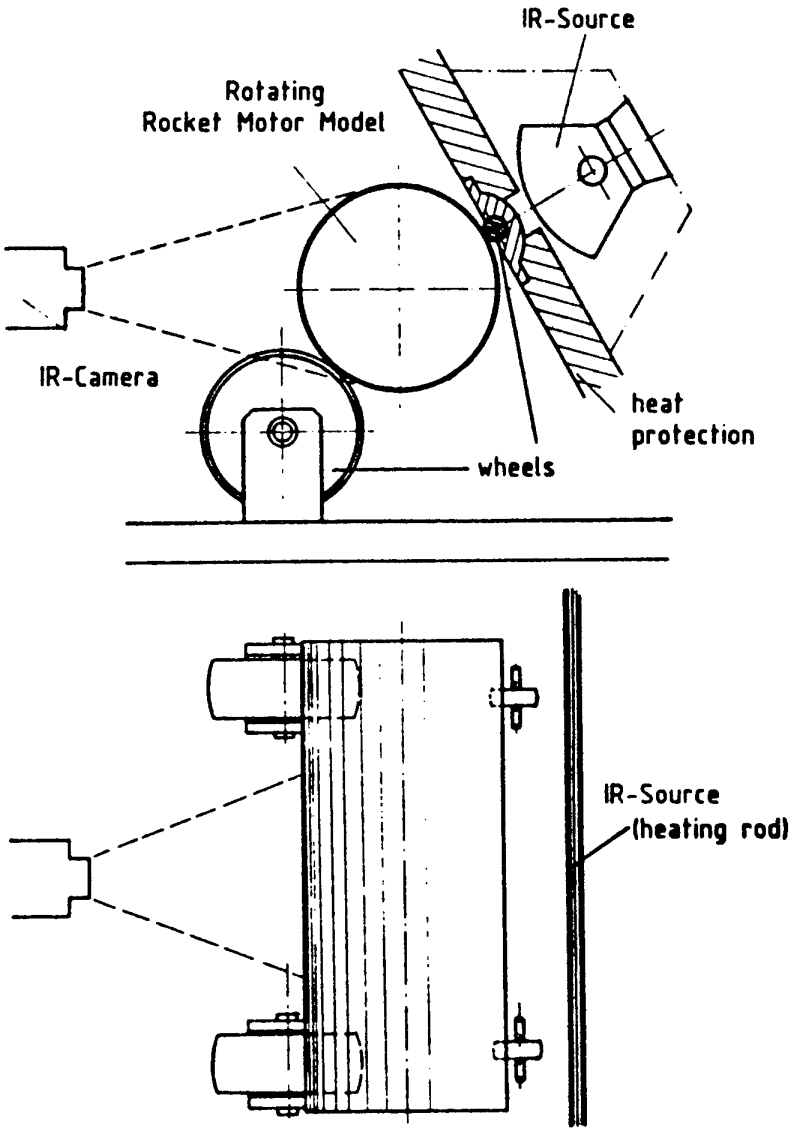


Fig.1: Test set up: side view and top view

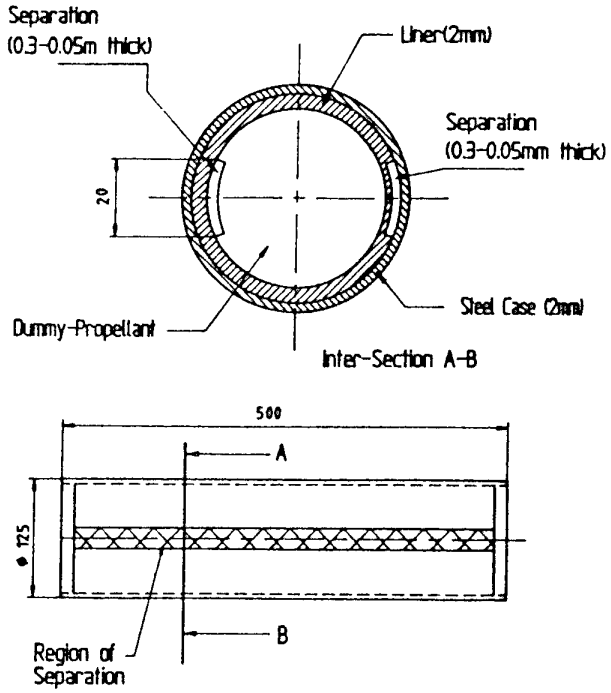


Fig.2: Built-in strip-shaped separations between case and liner and liner and propellant

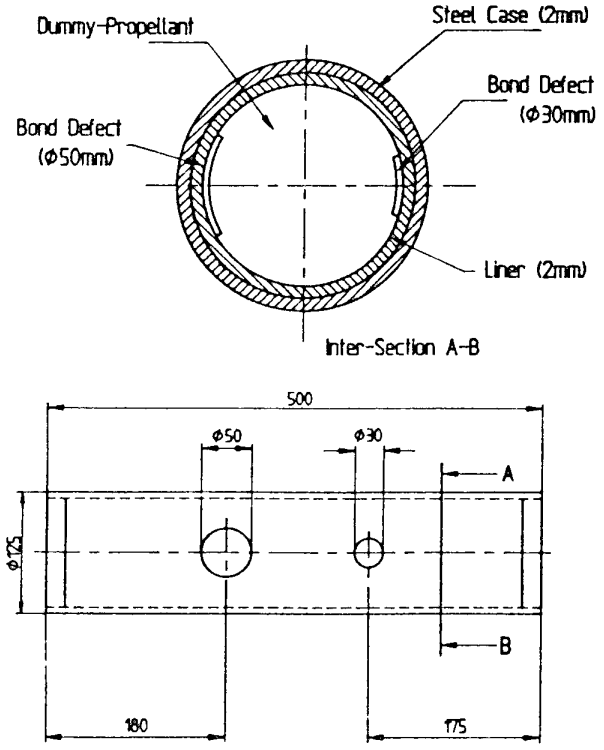


Fig.3: Circular-shaped bond defects between liner and propellant

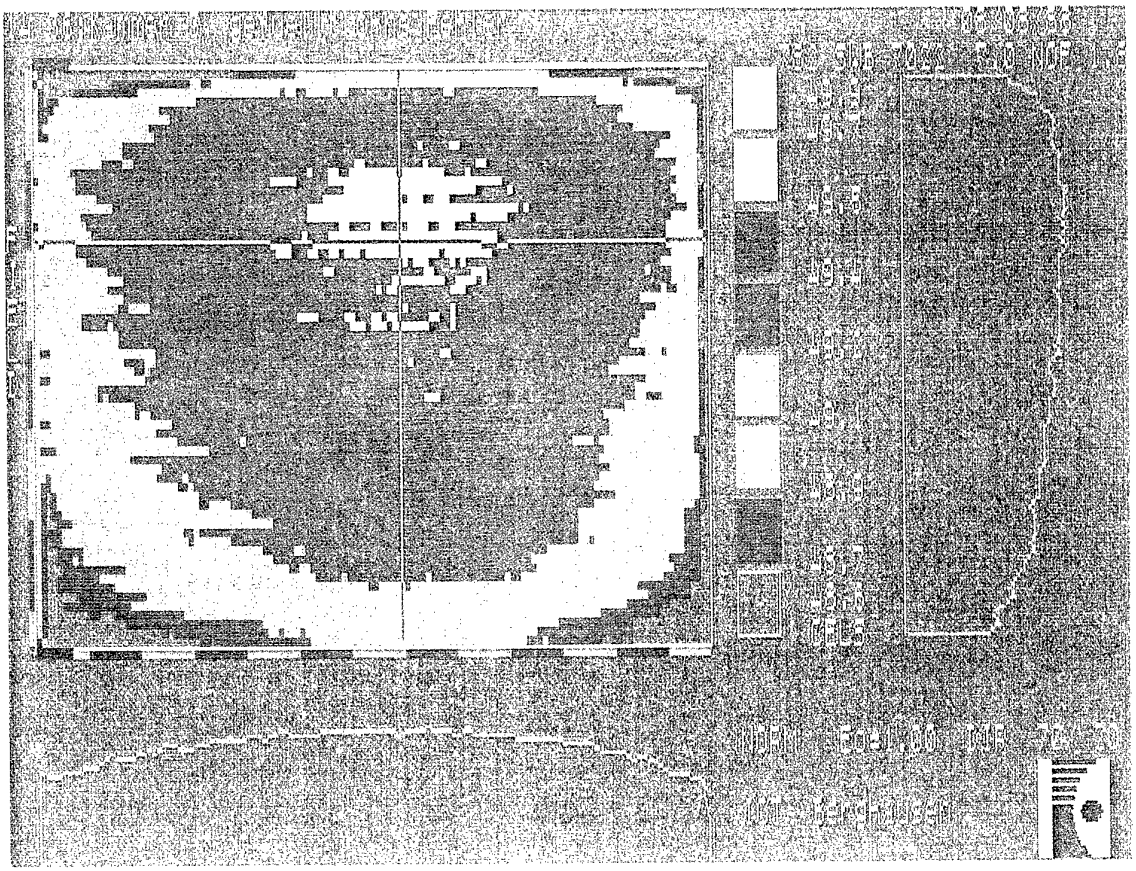


Fig. 4a: Thermogram of a case without separations or bond defects

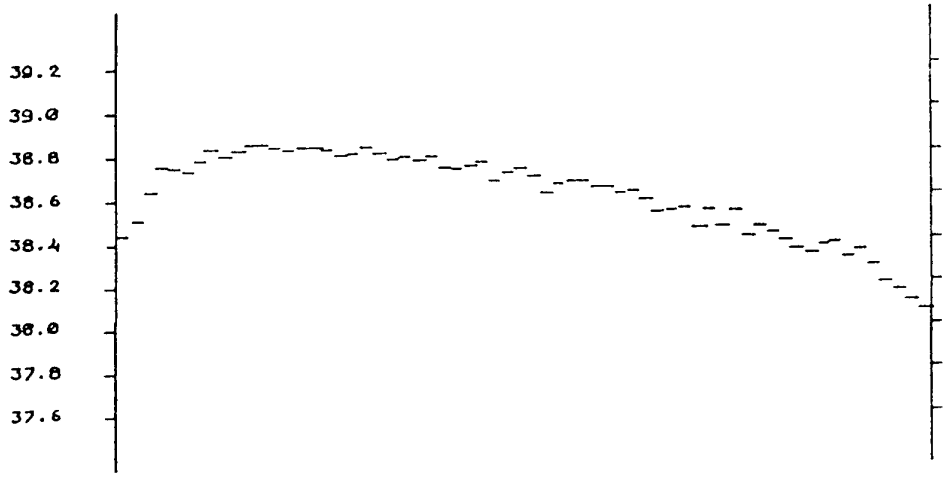


Fig. 4b: Temperature profile of the thermogram of Figure 4a in vertical direction

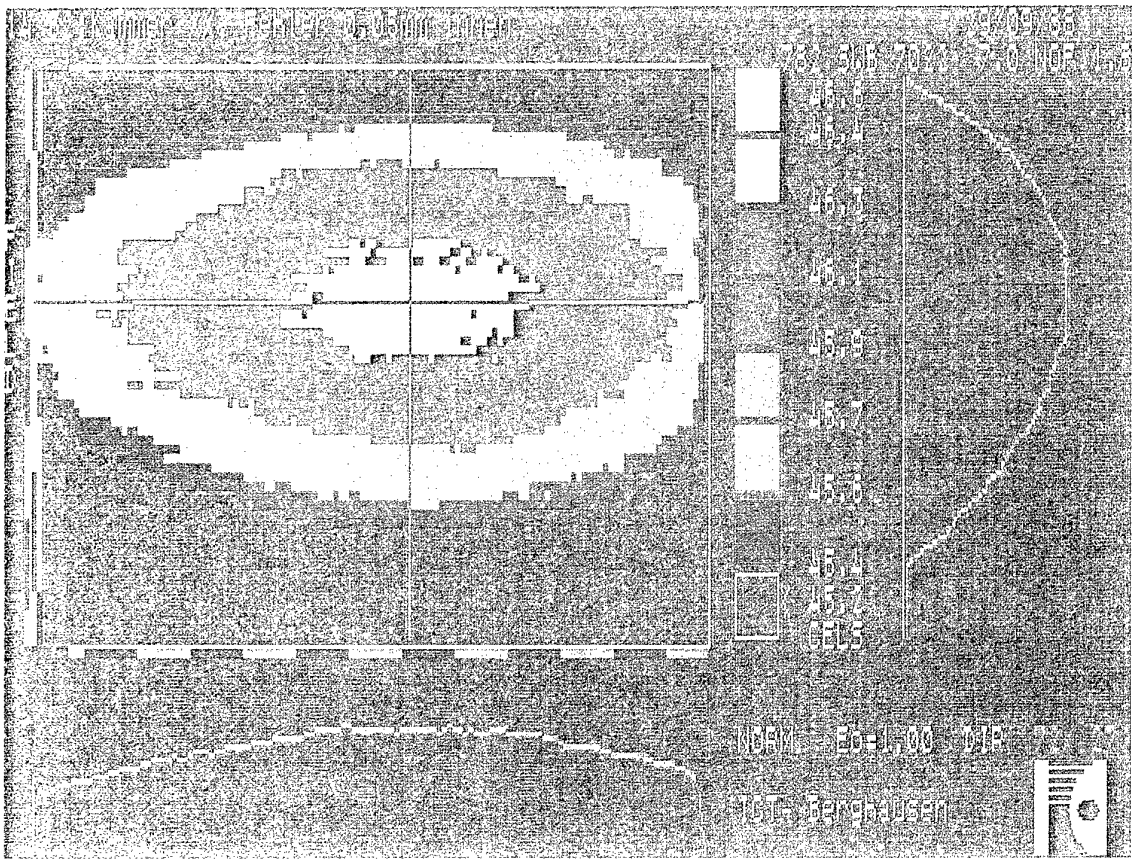


Fig. 5a: Thermogram of a case with a separation between liner and propellant (0.05 mm thick, *see* Fig.2)

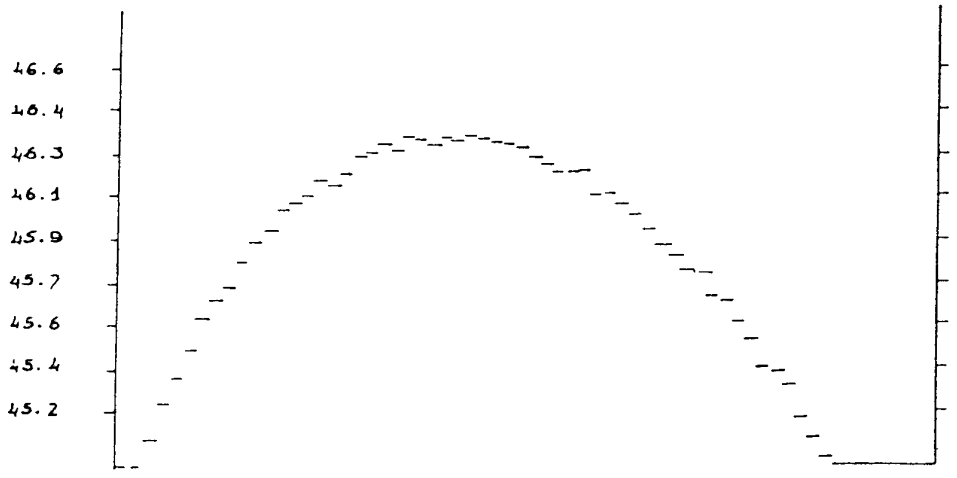


Fig. 5b: Temperature profile of the thermogram of Fig. 5a in vertical direction

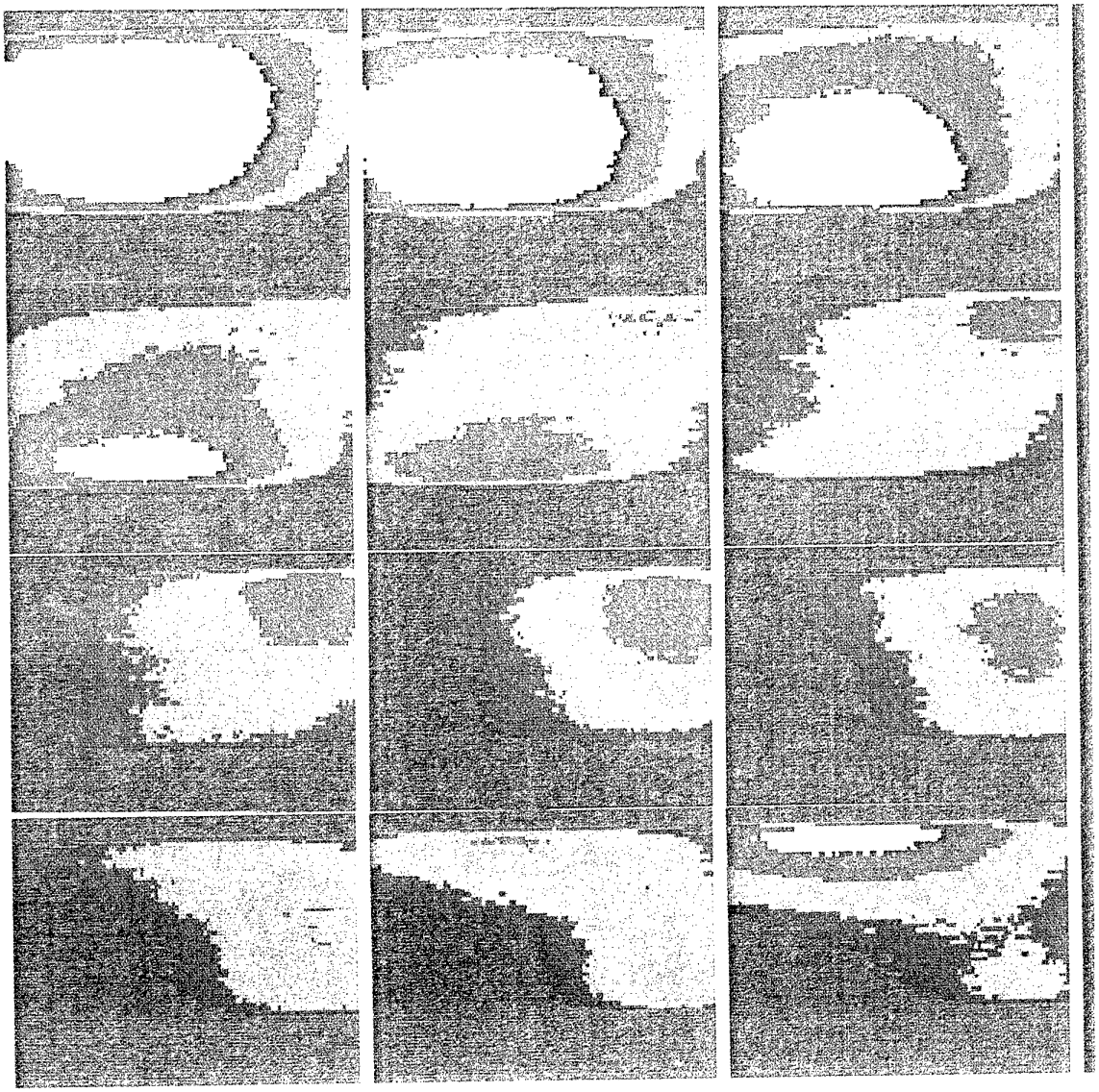


Fig. 6: Thermograms of a rotating case with two circular bond defects between liner and propellant (*see* Fig.3); 1 picture/sec; 4 revolutions/min

Paper Number: 13
Discussor's Name: Professor D. Dini
Responder's Name: Dr. H. Schneider

Question: How might your thermographic detection method be used for real rocket motor evaluation?

Answer: Basically the method might be applied also to real rocket motors, at least for those whose dimensions (diameter, thickness of the motor components) are similar to the dimensions of the dummy motor. The smallest detectable size of defect is still an open question. A drawback of the method is that normally no uniform surface exists on real rocket motors because of paints or scratches and therefore prior to the measurement the surface would have to be prepared with a lacquer, for example. The "phase sensitive modulated thermography" which has recently been developed at the institute for Kunststoffprufung und Kunststoffkunde in Stuttgart is a refined thermographic method where this drawback is eliminated; but so far as I know this method has not yet been applied to rocket motors.

The Role of NDE in Service Life Prediction of Solid Rocket Propellant

L. H. Pearson, T. E. Doyle, R. S. Hamilton, and I. L. Davis
Thiokol Corporation
Mail Stop 244, P.O. Box 707
Brigham City, Utah 84302-0707, USA

1. SUMMARY

Mechanical and chemical properties of a particle filled elastomeric polymer, such as a solid rocket propellant, may change with age and contribute to the degradation of motor performance. Nondestructive evaluation (NDE) methods have been developed and tested to characterize changes in materials caused by chemical aging processes. Ultrasonic methods have been evaluated for monitoring changes in bulk propellant properties including particle dewet strength and bulk elastic properties. Theory of operation and test results for each method are reported. Some methods are applicable to full-scale rocket motors and others are intended for laboratory use to provide data for calibration and understanding.

2. INTRODUCTION

The mechanical properties of a filled polymer such as a solid rocket propellant are significantly affected by the particulate fillers. The non-linear stress/strain behavior of propellants is contributed to by the viscoelastic binder polymer, the particle pack, and the particle/binder interaction. In aging propellants, the particle dewet strength and the binder elastic properties can change with time. In some propellants, the particle pack may also change because the particulates are soluble in the binder chemical environment. In other propellants, the degradation of the bulk mechanical properties may be dominated by changes in the binder modulus and the particle dewet strength. Diffusion of curatives, mobile plasticizers, stabilizers, reinforcing agents, and water into and out of the propellant at or near boundaries, such as the bore surface or the propellant/liner/insulator/case bond region, can contribute to hardening or softening of the elastic properties or degrade bond strength. In addition, damage accumulation from dewetting caused by handling, thermal, and other environmentally induced stresses can play a role in performance degradation of propellants.

Means for directly or indirectly monitoring age induced changes in propellants are needed to provide data essential for predicting service life. This paper focuses on NDE methods that can provide quantitative data relating to propellant damage and elastic properties. The following sections of this paper describe the role of NDE in service life prediction and give examples of ultrasonic techniques applicable to characterization of aging propellant.

3. ROLE OF NDE IN SERVICE LIFE PREDICTION

A general-purpose service life program should include, along with NDE, the components identified in Figure 1. The role that NDE plays is crucial in solid rocket motor service life prediction. The primary function of NDE is to provide a time-line of data showing the history of the rocket motor health up to the present. This time-line is used to monitor trends in properties and to calibrate the chemical/mechanical models to ensure they are "on track" so that service life estimates can be made with some confidence. NDE methods that are quantitative in the sense that they directly measure material properties or measure quantities that relate directly to the current material condition, are most useful because this data provide input for analysis and service life predictions.

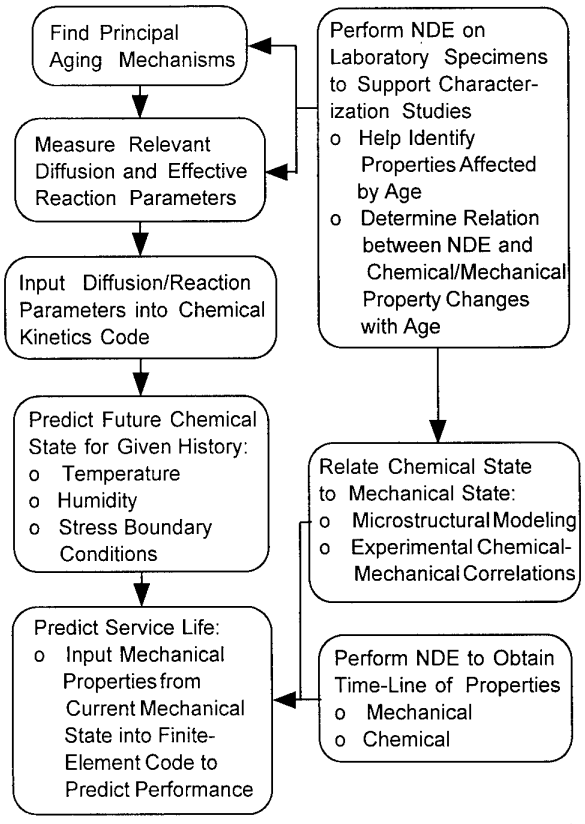


Figure 1. Diagram Showing Components of a General-Purpose Predictive Aging Program.

Paper presented at the AGARD PEP Symposium on "Service Life of Solid Propellant Systems" held in Athens, Greece, 10-14 May 1996, and published in CP-586.

For example, NDE can provide a time-line of properties such as the bulk and shear moduli, or parameters which relate to void volume from cumulative dewetting damage, or parameters which are related to the concentration of diffusing chemical constituents.

4. NDE METHODS

4.1 Introduction

Because ultrasonic wave propagation in solid materials is known to be sensitive to particulate fillers, voids, and elastic properties of materials, ultrasonic methods have been employed as an effective tool for monitoring changes in aging propellants[1-4]. A survey of ultrasonic NDE methods which show promise in monitoring important properties of aging propellants is given in the following subsections. Methods for directly measuring chemical changes in propellant are not presented in this paper but are discussed in reference 1.

4.2 Simultaneous ultrasonic and mechanical testing

The intent of using ultrasonics in the manner described in this section is to provide a means to aid in the understanding of aging mechanisms relating to the particle dewet strength and Young's modulus of the propellant. Simultaneous ultrasonic and mechanical testing provides data which will allow a direct correlation of mechanical properties with ultrasonic wavespeed and attenuation properties which, in turn, are related to the microstructure of the propellant. Further insight into material aging mechanisms is obtainable through chemical analyses such as high resolution NMR spectroscopy which can provide information about the concentrations of various chemical species[5]. The combination of NDE, mechanical test data, and NMR chemical analysis provides data to calibrate and understand the meaning of the ultrasonic NDE data.

The methodology employed allows simultaneous ultrasonic and mechanical tensile testing of propellant specimens. To accomplish the task, a small liquid tight tank was designed to attach to an Instron mechanical testing system allowing the tensile specimen to be immersed in an inert fluid (such as 3M FC-43 Fluorinert) to permit coupling of ultrasonic energy into the sample in a manner that does not interfere with the tensile testing. The experimental setup is shown in Figure 2. (See Reference 6 for a further discussion.)

Referring to Figure 2, one transducer is used in a transmit/receive (T/R) mode, and the facing transducer is used as a transmitter (T) only. A reference ultrasonic waveform is transmitted from the T-transducer through the fluid without the sample present and received by the T/R-transducer, then digitized and stored on computer disk. The propellant tensile specimen is then placed between the transducers and in the Instron grips so that transmitting and reflecting ultrasonic waves are introduced into the sample at normal incidence to its front and back surfaces. The T/R-transducer is pulsed simultaneously with the T-transducer and receives back the reflected waveform which is combined with the transmitted waveform from the T-transducer. The resultant waveform is, then, a combination of transmitted and reflected (pulse-echo) waveforms. The combined waveform is obtained at regular time intervals while the specimen is being strained and each waveform is digitized and stored on the computer disk. Each waveform is signal processed using the reference waveform for normalization to allow computation of wavespeed, attenuation coefficient, and sample thickness (if necessary).

For testing reported in this paper, waveforms were collected at rates of either one waveform per second or one waveform every two seconds during tensile loading. The strain rate for all tests was chosen to be 2 inches/minute to conform with existing data bases.

Sample specimens were dogbone shaped and were modified from the standard JANNAF C tensile specimen

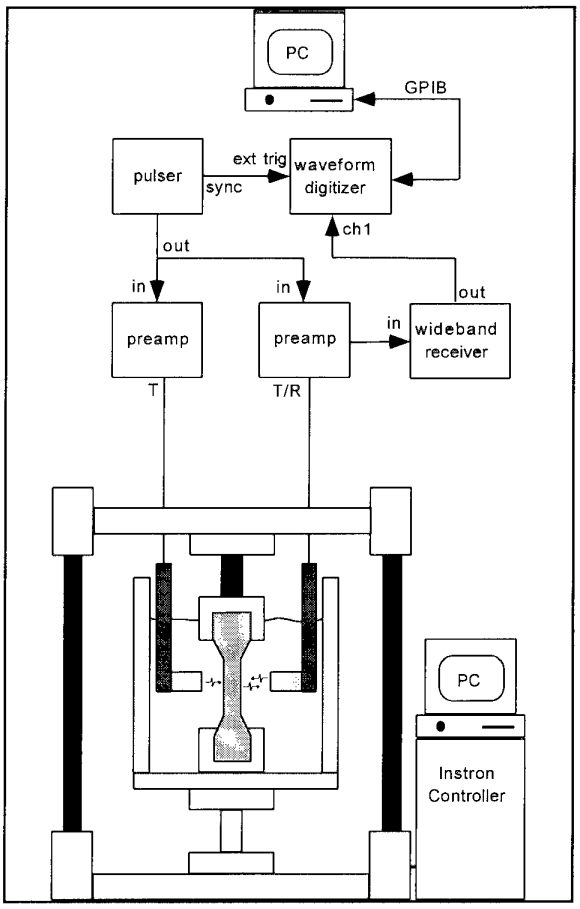


Figure 2. Schematic Diagram of Test Apparatus for Simultaneous Ultrasonic and Mechanical Testing.

by increasing the width from 0.5 inch to 1.0 inch. The increased width was needed to assure that there was no diffraction of the ultrasonic beam around the edges of the sample. The 0.375 inch thickness is adequate to insure separation of multiple reflections within the dogbone in the 500 kilohertz (kHz) center frequency transmitted and reflected waveforms.

Load-time data is acquired simultaneously with the ultrasonic waveforms using separate data acquisition hardware which is integrated into the Instron mechanical test system. This data is stored on a floppy disk and is reduced to stress-strain data and then integrated into a computer spread sheet with the reduced ultrasonic data.

NMR test results are obtained using the procedure described in reference 5. This procedure, in essence, is a sol extraction analysis used to determine the relative concentrations of propellant binder polymer and stabilizers. A microtome is used to cut samples to provide uniformity in sample thickness. The samples were soaked overnight in deuterated chloroform $CDCl_3$ with a known amount of tetrachloroethane (TCE) added as an internal standard. Proton (H^1) NMR spectra were obtained on the material that was extracted which includes the binder polymer. Knowing the original sample weight, the weight of the TCE, and the mole ratio of the TCE to binder polymer obtained from the NMR spectra, relative amounts of extracted binder polymer in units of moles per gram of sample were determined.

Figure 3 shows stress as a function of time during 2.0 inches/minute strain rate tests of 1 year and 9 year aged low solids propellant which were prepared in cartons and aged under ambient conditions. About 15 seconds into the test, it is seen that there is a slope change occurring in each propellant sample in the 50 to 60 pounds per square inch (psi) range which is believed to be caused by softening of the propellant from the onset of dewetting. (Note that stress versus time plots have the identical shape as stress versus strain plots for a constant strain rate test and hence stress-strain curves are not shown.) The corresponding attenuation coefficient versus time data in Figure 4 shows an increase in attenuation growth rate after 15 seconds which correlates with the change in the stress-time data in Figure 3. (The strain curve is also shown in Figure 4.) The attenuation coefficient data corroborates the theory that dewetting is accelerating since the only reasonable cause for an increase in attenuation coefficient is the growth in void volume resulting from dewetting of particles from the binder. Combining the data in Figures 3 and 4 and plotting stress versus attenuation coefficient may be a more instructive way to view the data. This is done in Figure 5 which shows that the attenuation coefficient increases very rapidly at stresses greater than about 55

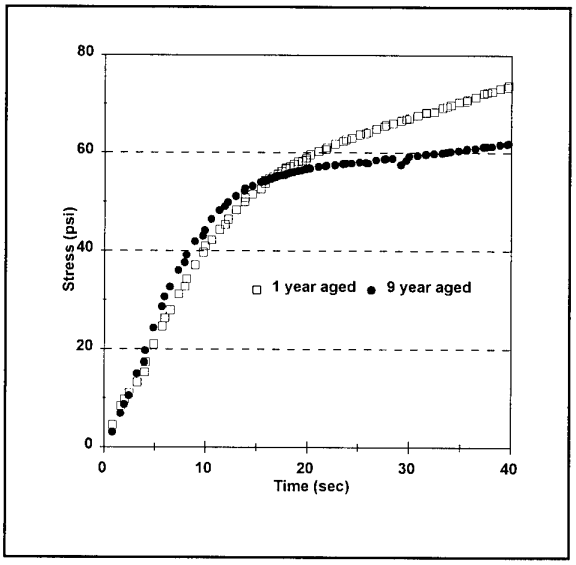


Figure 3. Graph of Stress Versus Time for a 2.0 in/min Test of Carton Propellant.

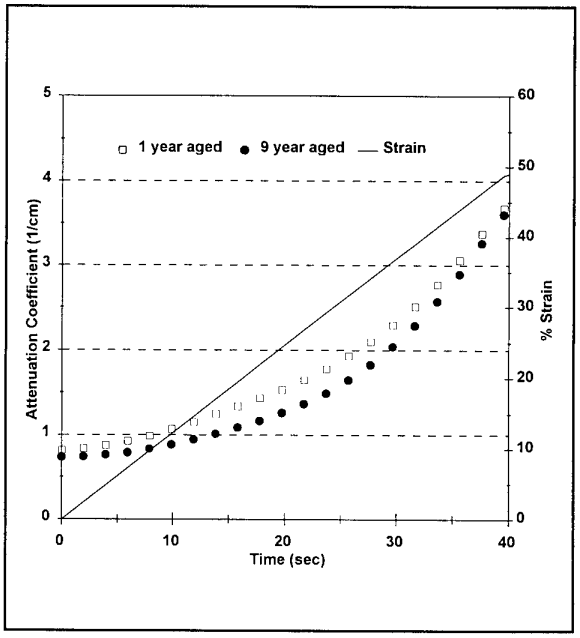


Figure 4. Graph of Attenuation Coefficient for Same Test as Figure 3.

psi. This data indicates that a threshold stress seems to exist which, if exceeded, will cause significant dewetting damage in the propellant. Plotting the data in the format of Figure 5 accentuates the difference between the 1 year and 9 year aged materials. It is seen that the new propellant has a higher stress capability than the older propellant and that the old propellant fails more abruptly than the new.

Along with characterization of aging materials with respect to time, data from experimental methods

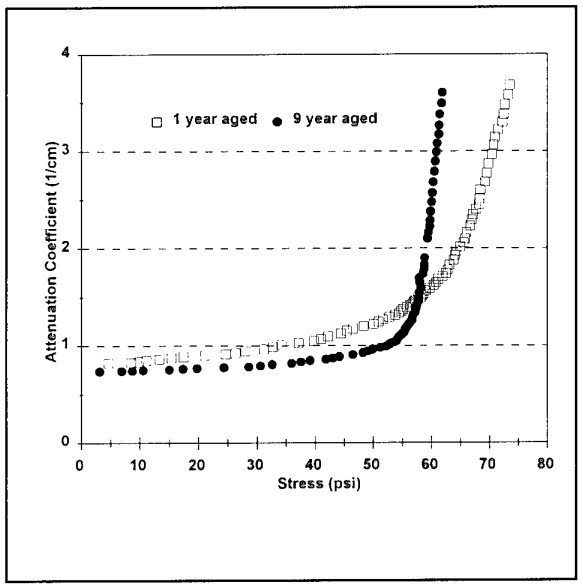


Figure 5. Graph of Stress Versus Attenuation Coefficient for Data in Figures 3 and 4.

described in this paper can be used to detect spacial gradients in material properties caused by aging. For example, within a given rocket motor that has aged under conditions where migration of moisture and other chemical species in the propellant grain has occurred, it is likely that gradients in the mechanical and chemical properties will be present. These gradients may be both radially and axially dependent in the propellant grain. In looking at an aged solid rocket motor with a propellant formulation similar to the previously analyzed carton propellant, such gradients were found. A coin slice was taken from the mid section of a motor from which dogbone tensile specimens were machined. The samples were cut so that their long direction (tensile loading direction) was in the axial direction of the motor. Seven samples were machined from the coin at radial positions ranging from 1.25 inches to 10.25 inches from the bore surface. Each sample was subjected to mechanical/ultrasonic and NMR sol extraction tests. Average Young's modulus was measured for each sample from stress-strain data at stresses below the characteristic slope change where the onset of significant dewetting occurs (see Figure 3). The ultrasonic attenuation coefficient was computed from waveforms acquired during tensile loading. NMR tests were performed on fragments cut from the dogbones from which relative amounts of binder polymer were determined.

Figure 6 shows plots of Young's modulus and the relative amount of binder polymer extracted from each sample as a function of radial position (relative to the bore surface) in the motor. Note that there is a strong inverse correlation between these quantities. Figure 7 shows the corresponding attenuation coefficient versus stress curves for each specimen. It is seen that the dewet stress (bend in curve) increases with distance from the bore surface and appears to inversely correlate with the amount of extracted binder polymer. This indicates, for these samples, that if there is a smaller amount of binder polymer extracted, there is a higher dewet stress. These sets of data (Figures 6 and 7) when interpreted together indicate that less extracted binder polymer (which implies a higher cross-link density) results in a higher Young's modulus and a higher stress capability which is an intuitive conclusion. Figure 8 shows a linear relationship between the zero-strain attenuation coefficient and the measured Young's modulus. The linear regression correlation coefficient (R^2) is about 0.6 which provides confidence that these quantities can be correlated. The zero-strain attenuation coefficient is measurable directly from the motor in-situ if contact methods are used on the propellant bore-surface. Section 4.4 describes contact methods in more detail.

4.3 Embedded Ultrasonic Sensors

In the effort reported in this section, ultrasonic techniques that provide quantitative measurement of ultrasonic wavespeeds and attenuation coefficients have been developed for in-situ characterization of aging propellant. Because of the increased compliance of elastomeric materials, it is difficult to obtain reproducible hand contact ultrasonic measurements from their surfaces. This limitation has provided the impetus for developing alternate methods for making ultrasonic

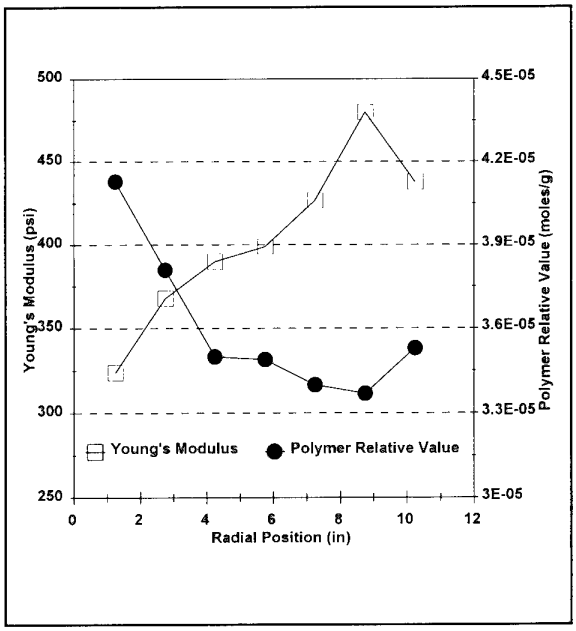


Figure 6. Young's Modulus and Binder Polymer Relative Value Plotted as a Function of Radial Position Relative to Bore Surface.

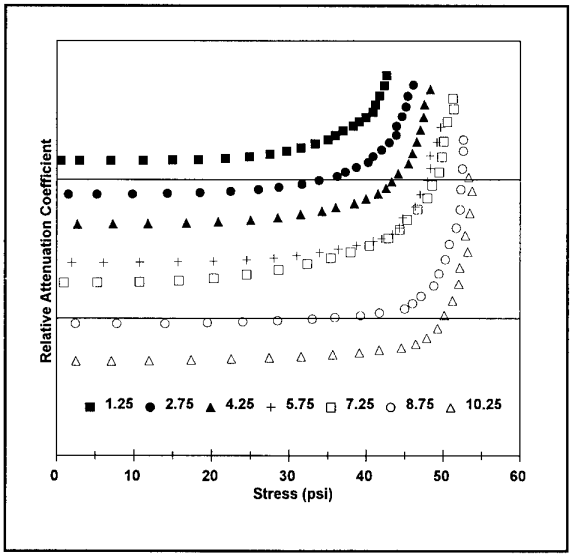


Figure 7. Attenuation Coefficient Plotted Versus Stress Curves for Propellant Taken from Different Radial Locations.

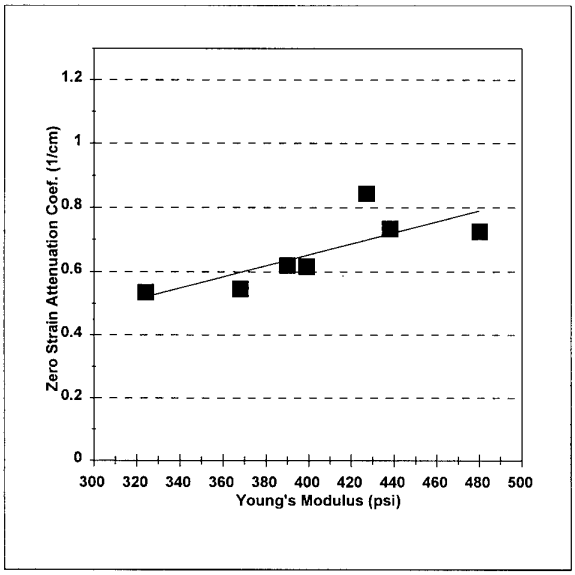


Figure 8. Plot Showing Linear Relationship between Zero-Strain Attenuation Coefficient and Young's Modulus.

measurements. An ultrasonic method is presented in this section which is based on the embedding of polyvinylidene fluoride (PVF_2 or PVDF) sensors[7] in propellant samples for the purpose of detecting externally generated ultrasonic waves. Figure 9 shows an experimental setup for monitoring sub-scale test specimens of propellant. An external, large diameter transducer (relative to the PVDF sensor size) is used as a sound source and is contact coupled to the surface of the sample. It generates a wave that passes through the sample and thus through the PVDF sensors which are separated by a known distance and are centered on the axis of the source beam. Waveforms acquired by this method are used to determine the frequency dependence of the wavespeed and attenuation coefficient. By acquiring two waveforms, one from each sensor, sensitivity to transducer coupling inconsistencies can be eliminated because the same variabilities are present in each waveform and are divided out when the second waveform is properly normalized by the first. The method provides measurements for the same volume of material each time data is acquired which eliminates variability in the measurement due to material inhomogeneity and allows monitoring of only age dependent changes.

To demonstrate the embedded PVDF sensor method, the following experiment was performed. Sensors were constructed in a the manner illustrated in Figure 9 and embedded in an inert propellant mix and cured at 135 degrees Fahrenheit (deg F) for about 3 days. (PVDF can be heated to 212 deg F before it looses its piezoelectric properties.) An external contact transducer was used which produced a wide band wave pulse with center frequency of approximately 500 kHz. Two methods for measuring phase velocity and attenuation

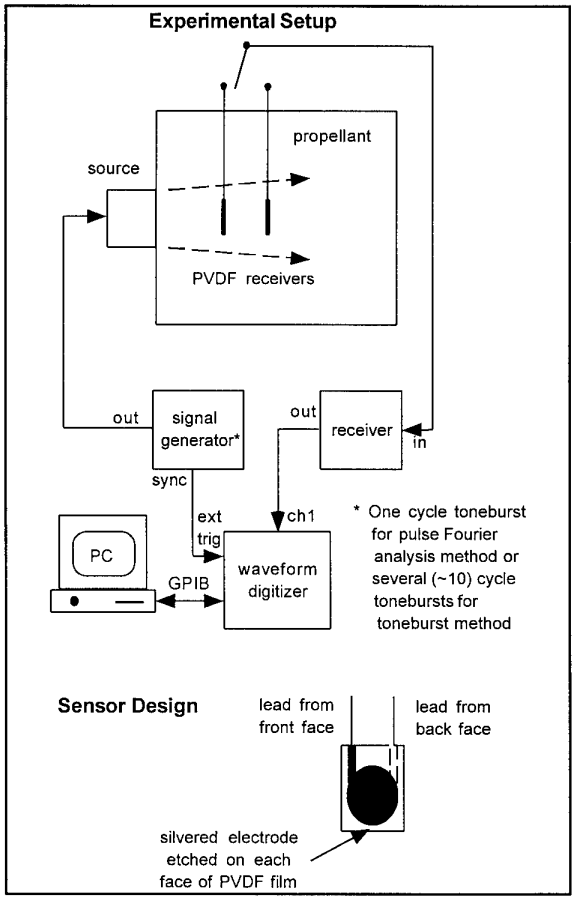


Figure 9. Experimental Setup and PVDF Sensor Design for Testing Propellant Samples with Embedded Sensors.

coefficient were employed. The first involves a Fourier analysis approach to analyzing the two wave pulses obtained from the two receivers from which phase velocity and attenuation coefficient spectra are calculated. This is done by acquiring, digitally, the waveforms detected by each PVDF receiver element. Each waveform is transformed into frequency domain via a fast Fourier transform (FFT) . The frequency domain representation of each measured signal is:

$$S_1(\omega) = p_1(\omega) e^{(i\phi_1)} \quad (1)$$

and

$$S_2(\omega) = p_2(\omega) e^{(i\phi_2)} \quad (2)$$

where $p_n(\omega)$ are the frequency domain magnitudes, $\phi_n(\omega)$ are the phases (n=1,2 corresponding to the two receivers, with 1 being closest to the source and 2 being farthest from the source), and ω is the angular frequency ($\omega = 2\pi f$). The theoretical expression for $S_1(\omega)$ is given by:

$$S_1(\omega) = p_0(\omega) \quad (3)$$

where $p_o(\omega)$ is the combined response function of the electronics and the transducer, and the expression for $S_2(\omega)$ can be shown to be give by[9]:

$$S_2(\omega) = p_0(\omega) e^{-\alpha(\omega)h} e^{\frac{i\omega h}{c(\omega)}} \quad (4)$$

where h is the known separation distance between each receiver element. Substituting equation (1) into (3) and equation (2) into (4) and dividing the resultant equations allows for normalization, that is, the elimination of the electronics and transducer transfer function $p_o(\omega)$. Separating the normalized equation into is real and imaginary components allows for the determination of the wavespeed, $c(\omega)$, and attenuation coefficient, $\alpha(\omega)$, spectra which are given by:

$$c(\omega) = -\frac{\omega h}{\phi_2(\omega) - \phi_1(\omega)} \quad (5)$$

and

$$\alpha(\omega) = \frac{1}{h} Ln[p_1(\omega)/p_2(\omega)] \quad (6)$$

The second method for determining these quantities requires measuring amplitudes and times-of-flight of tone-burst waveforms, over a range of frequencies, received by the two PVDF sensors from which phase velocity and attenuation coefficient are computed for a series of frequencies using the following expressions:

$$c = \frac{h}{\Delta t} \quad (7)$$

and

$$\alpha = \frac{1}{h} Ln\left(\frac{p_1}{p_2}\right) \quad (8)$$

where Δt is the time-of-flight between receiver elements and p_1 and p_2 are the amplitudes of the corresponding waveform peaks at each receiver. This second method proved to be more accurate but requires more time and effort to get results. For applications requiring acquisition of a high volume of data, the Fourier analysis method may be best. Typical results for the toneburst method are shown in Figure 10. The wavespeed spectrum show a slight negative slope relative to frequency which seems to be typical for filled rubber materials in this frequency range. The attenuation coefficient curve is nearly linear with a positive slope.

Data obtained during cure of the low solids inert propellant sample are shown in Figure 11. In this figure it is seen that for this material the attenuation coefficient

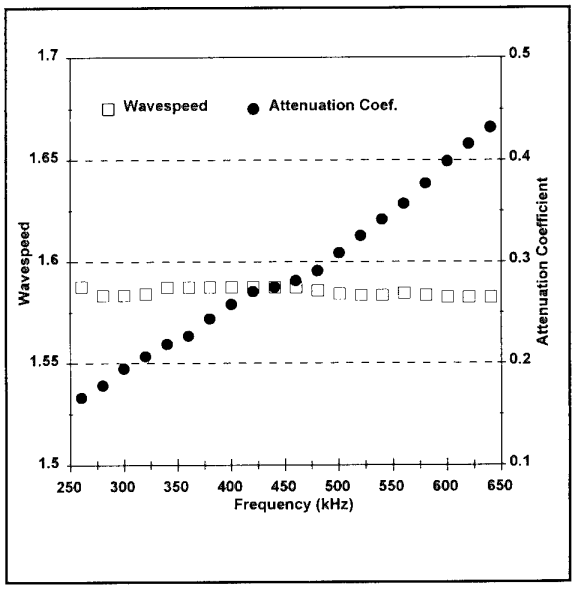


Figure 10. Wavespeed and Attenuation Coefficient Spectra for Inert Propellant Formulation Using Tone Burst Method.

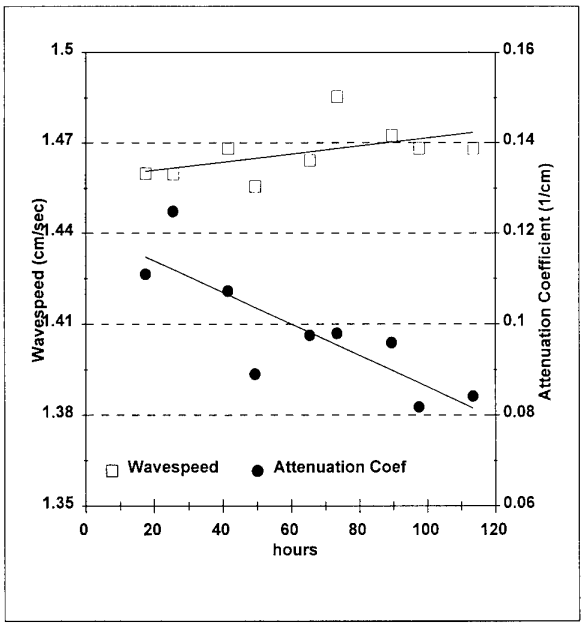


Figure 11. Wavespeed and Attenuation Coefficient During Cure of Inert Propellant Mix Measured with PVDF Sensors.

is more sensitive to chemical changes occurring during cure than is the wavespeed. Figure 12 shows plots of one frequency component (about 500 kHz) of the wavespeed and the attenuation coefficient spectra, calculated from equation (6), as a function of time during an ambient (75 deg F) aging study of a high solids propellant. These plots also show that the attenuation coefficient is more sensitive to the changes than is the longitudinal wavespeed.

Some observations can be made about the embedded ultrasonic sensors. First, ultrasonic longitudinal wavespeed and attenuation coefficient can be measured with good reproducibility, however, accuracy depends on correct knowledge of the spacing between the two embedded sensors. At time zero (the day the propellant is manufactured) the spacing between transducer elements can be obtained from time-of-flight measurements using the known wavespeed obtained from same batch propellant samples using standard contact or immersion methods. The embedded PVDF transducer spacing is then assumed to be constant in the aging propellant. If some doubt arises about actual spacing between transducer elements, film x-ray methods can be employed to provide the actual spacing. Finally, the attenuation coefficient seems to be more sensitive to aging or cure induced changes in the propellants studied in this section.

4.4 Surface Contact Ultrasonic Methods for Measuring Bulk Modulus and Shear Modulus

Section 4.2 discusses an ultrasonic NDE method that can only be applied to mechanical test specimens and hence is not a true NDE technique, but is a technique that provides insight into material aging mechanisms in laboratory studies. Section 4.3 discusses methods that require embedding ultrasonic sensors. In many cases, this may prove to be impractical or not allowed in the particular motor system. Hence, methods that are truly nondestructive must be used. Contact ultrasonics can be applied to rocket motors to assess the condition of the propellant grain and the propellant related bondlines. The case/propellant bondlines are most easily accessible from the external case surface, and the bulk propellant aging is most easily characterized by accessing the internal exposed propellant surfaces. Two different wave modes are generally produced, depending upon the transducer arrangement: bulk longitudinal waves and Rayleigh (surface) waves. Shear waves are attenuated so rapidly in rubber material that it is impractical to try to generate and detect this mode of propagation and Lamb (plate) wave modes are most often not generated because of geometrical constraints.

Contacting a surface with an ultrasonic transducer in the manner shown in Figure 13 will cause a bulk longitudinal wave to be generated and detected in the usual pulse-echo manner. In order to quantitatively interpret and relate pulse-echo measurements to wavespeeds and attenuation coefficients for the material layers involved may require modeling the pulse-echo waveform using a reflection model for layered media[10]. Once the longitudinal wavespeed is obtained, however, the bulk modulus can be calculated from the following mathematics. The wavespeed can be expressed as a function of the Lame' constants, λ and μ, (μ is also the

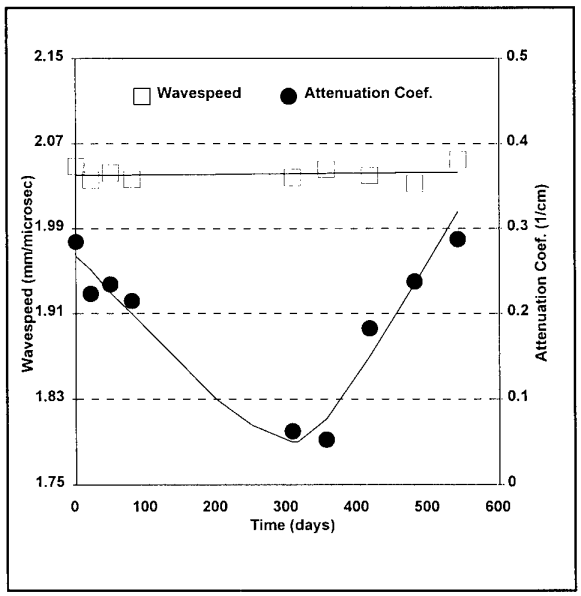


Figure 12. Longitudinal Wavespeed and Attenuation Coefficient Dependence on Time During Aging of Propellant Samples.

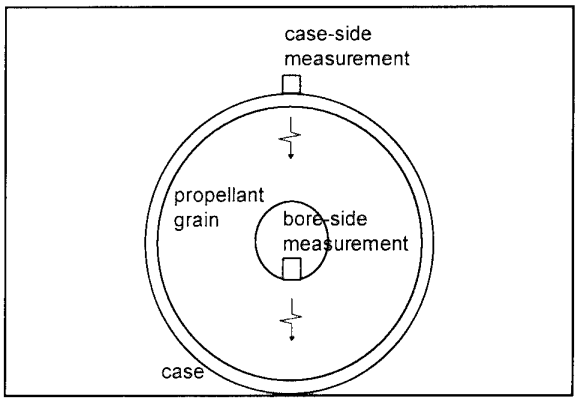


Figure 13. Diagram Showing Case-Side and Bore-Side Measurements.

shear modulus), and the material density, ρ:

$$(9) \qquad c_L = \sqrt{\frac{\lambda + 2\mu}{\rho}}$$

The bulk modulus is related to the Lame' constants by:

$$(10) \qquad B = \lambda + \frac{2\mu}{3}$$

For rubber-type materials such as a solid rocket propellant, μ is much smaller than λ, thus equation (10) reduces to:

$$(11) \qquad B \approx \lambda$$

Substituting equation (11) into (9) and using the small μ assumption again, leads to the following expression for calculating the bulk modulus:

$$(12) \qquad B = c_L^2 \rho$$

Contacting a surface with two ultrasonic transducers in the manner shown in Figure 14 where one is the source of ultrasound and the other is a receiver, will, generally, produce a surface wave if the material depth (or thickness of the material layer) is large compared to a wavelength.

The surface wavespeed is obtained by finding the appropriate real root of the following equation:

$$(13) \qquad c_R^3 \left(\frac{\rho}{\mu}\right)^3 - 8 c_R^2 \left(\frac{\rho}{\mu}\right)^2 + \left(24 - 16\frac{\mu}{\lambda + 2\mu}\right) c_R \left(\frac{\rho}{\mu}\right) + \left(\frac{\mu}{\lambda + 2\mu} - 1\right) 16 = 0$$

Again, if the shear modulus, μ, is much smaller than the Lame' constant, λ, the equation for the wavespeed reduces to a form that only depends on μ:

$$(14) \qquad c_R^3 \left(\frac{\rho}{\mu}\right)^3 - 8 c_R^2 \left(\frac{\rho}{\mu}\right)^2 + 24 c_R \left(\frac{\rho}{\mu}\right) - 16 = 0$$

The shear modulus is obtained from the appropriate root, (ρ/μ), of equation (14).

It should be noted that for rubber-type materials, it is found experimentally that unless very low frequencies are used, a "fast" surface wave mode will unexpectedly be generated which has a wavespeed about the same as the bulk longitudinal wave[11]. If low enough frequencies are used (less than 50 kHz), the Rayleigh wave mode will be established and its wavespeed can be measured from which the shear modulus is calculated using equation (14) above.

It is seen from the above theoretical expressions, that the shear and bulk moduli can be quite directly determined from wavespeed measurements. This allows a quantitative means for monitoring age induced changes in the mechanical properties of propellants.

Bulk modulus measurements, determined from longitudinal wavespeed, and attenuation coefficient were obtained for a low solids aging propellant, using a bore-side method, are shown in Figure 15. (Measurements were made with 500 kHz center frequency transducers.)

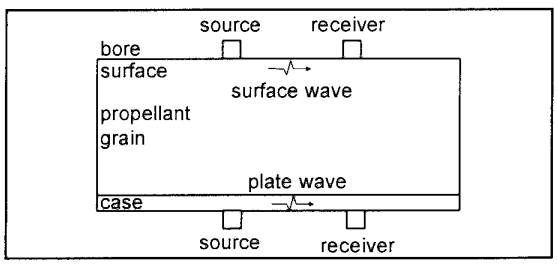


Figure 14. Diagram Showing Surface and Plate wave Measurements.

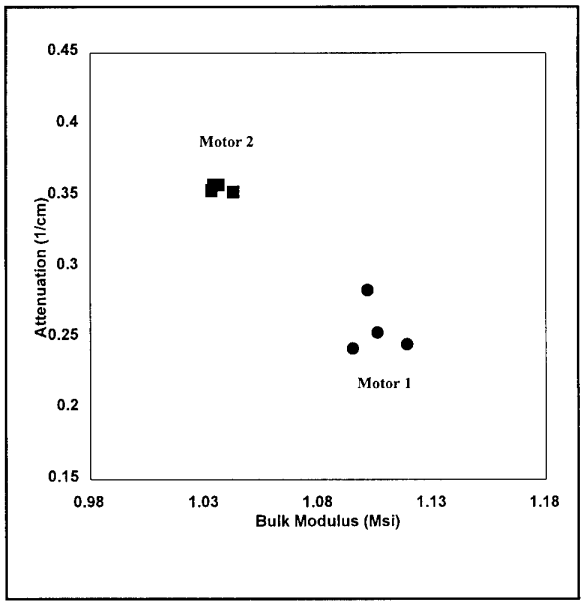


Figure 15. Graph of Ultrasonically Measured Bulk Modulus Versus Attenuation Coefficient for Motors of Similar Age But Aged in Different Environment.

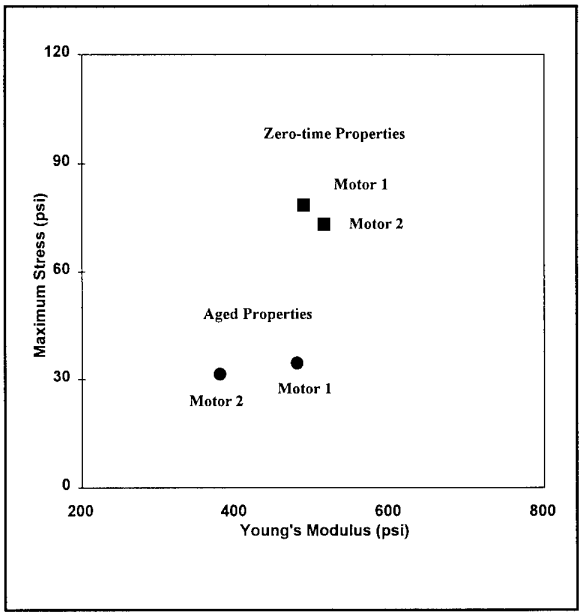


Figure 16. Graph of Young's Modulus Versus Maximum Stress Showing Aged and Zero-Time Properties for Same Motors as in Figure 15.

The bulk modulus is plotted with respect to the ultrasonic attenuation coefficient. Data is collected from motors that are approximately the same age but motor 1 was in a controlled environment while motor 2 was in a more harsh service environment. Displaying the data in this manner allows visualization of motor propellant differences in two properties simultaneously. It is seen that for this type of propellant that the bulk modulus is less for the motor aged in the service environment while the attenuation is greater, as might be expected. For comparison, properties measured by mechanical tensile testing of propellant dogbone samples are plotted in Figure 16. Young's modulus is plotted with respect to the maximum stress (peak in stress-strain curve) for the aged motors. The corresponding measurements for zero-time carton propellant samples, taken from the same batch of propellant as the motors, are also shown. It is noted that the zero-time and aged maximum stresses and Young's moduli are quite different. It is also seen that the Young's modulus is notably different for the two motors after aging. This might be expected because of the difference seen in the ultrasonically measured bulk moduli.

This ability to measure mechanical properties using ultrasonics provides a means to monitor properties of intuitive importance to the engineering analist responsible for service life prediction.

5. CONCLUSIONS

The purpose or role that NDE performs in a service life prediction program has been explained and a number of ultrasonic NDE methods that show promise for monitoring changes in aging solid rocket motor propellant have been discussed. These methods range from methods that are primarily for laboratory applications to methods that can be used in the field. Laboratory methods are designed for aiding in understanding aging mechanisms and for calibrating the field applicable NDE methods. An embedded sensor method was explored that shows promise for monitoring aging propellant in motors where they would be permissible.

NDE methods reported are quantitative in the sense that they provide a measure of elastic properties such as the propellant bulk and shear moduli or relate to propellant microstructure, and chemical changes occurring during aging and cure. The attenuation coefficient of longitudinal waves was found to correlate with changes in both mechanical and chemical properties. The mathematics for converting wavespeeds of longitudinal and surface wave modes to the bulk and shear moduli, respectively were presented. Changes in the bulk modulus were shown to relate to different aging conditions of motors.

6. REFERENCES

1. R. P. Graham, T. E. Doyle, R. S. Hamilton, K. L. Laheru, L. H. Pearson, and A. S. Allen "Extended Service Life Prediction Program", Final Report, PL-TR-94, Contract No. F29601-91-C-0002, January 1994.

2. G. C. Knollman, R. H. Martinson, and J. L. Bellin, "Ultrasonic Assessment of Cumulative Internal Damage in Filled Polymers," J. Appl. Phys., 50(1):111-120, 1979.

3. G. C. Knollman and R. H. Martinson, "Nonlinear Elastic Effects in the Ultrasonic Assessment of Cumulative Internal Damage in Filled Polymers," J. Appl. Phys., 50(12):8034-8037, 1979.

4. C. T. Liu and J. L. Bellin, "Effect of Load History on the Cumulative Damage in a Composite Solid Propellant," Proceedings of AIAA/ASME/ASCE/AHS 27th Structures, Structural Dynamics, and Materials Conference, May 1986.

5. L. F. Cannizzo, "Combination of Microtomy and NMR Spectroscopy to Probe the Variation in Horizontal Layers of Bondlines," Ind. Eng. Chem. Res. 30(8):1945-1949, 1991.

6. L. H. Pearson and T. E. Doyle, "Ultrasonic Method for In-Situ Monitoring of Filled Polymeric Materials During Tensile Loading," Proceedings 1994 JANNAF Nondestructive Evaluation Subcommittee and Structures and Mechanical Behavior Subcommittee Joint Meeting, 24-28 October 1994.

7. G. R. Harris, "Piezoelectric Polymer Probe for Ultrasonic Applications," J. Acoust. Soc. Am., 69(3:853-859, 1981.

8. A. Kline, "Measurement of attenuation and dispersion using an ultrasonic spectroscopy technique," J. Acoust. Soc. Am., 76(2):498, 1984.

9 W. Sachse and Y. H. Pao, "On the Determination of Phase and Group Velocities of Dispersive Waves in Solids," J. Appl. Phys., 49(8):4320-4327, 1978.

10. H. D. Collins, "Acoustical Chirp Frequency and Computer Correlation Technique for Debond Inspection in Solid Rocket Motor Sections," NBS Special Publ. 596, Ultrasonic Materials Characterization, H. Berger and M. Linzer, eds., Proceedings of the First International Symposium on Ultrasonic Materials Characterization held at NBS, Gaithersburg, Md., June 1978. Issued November 1980.

11. J. C. Couchman and J. R. Bell, "Prediction, Detection and Characterization of a Fast Surface Wave Produced Near the First Critical Angle," Ultrasonics, 16(6):241-243, 1978.

Paper Number: 14
Discussor's Name: Dr. G. Hooper
Responder's Name: Dr. L. H. Pearson

Question: Your final vugraph noted that rocket motors of the same age, but having seen different service environments, gave different ultrasonic characteristics. Have you been able to obtain any information from physical inspection, say photomicrographs, to explain this difference and which might relate physical damage of the propellant structure to the ultrasonic characteristics?

Answer: To date we have not. But extensive chemical and physical property data are available from the specific motors referred to in my presentation. We intend to further evaluate the data and hope to answer the intent of your question.

Paper Number: 14
Discussor's Name: Professor D. Dini
Responder's Name: Dr. L. H. Pearson

Question: As you reported, mechanical and chemical properties of particle filled elastomeric polymers may degrade with age. What ultrasonic methods are you suggesting for application to a full-scale rocket motor?

Answer: The answer depends on the results of laboratory studies which determine the principal aging mechanisms and the corresponding mechanical properties affected. The ultrasonic method chosen should be sensitive to the mechanical property(ies) most affected by age.

Paper Number: 14
Discussor's Name: Professor H. Schubert
Responder's Name: Dr. L. H. Pearson

Question: Have you correlated your dewetting measurements with Poisson's ratio?

Answer: No. Poisson's ratio is generally quite difficult to measure in rubber type materials because its value is near 0.5 where a singularity occurs in the equations relating Poisson's ratio to the measurement. The presence of this singularity results in small differences in Poisson's ratio when relatively large errors are present in the measurements. Hence, we do not have a lot of confidence in correlating NDE measurements with Poisson's ratio.

I should note, however, that we developed an ultrasonic method some time ago where two independent measurements, longitudinal wavespeed and plate (lamb) wavespeed, were measured from which the Lame' constants, λ and μ, were determined. Then from λ and μ, Poisson's ratio was calculated and for the inert propellant formulation we were looking at, we obtained values of about 0.47 or 0.48.

Paper Number: 14
Discussor's Name: Dr. A. Davenas
Responder's Name: Dr. L. H. Pearson

Question: The ultimate goal, probably, besides obtaining a measurement of the modulus, is to get an estimation of the rupture properties of the propellant inside an aged motor without intrusion. Do you think your ultrasound techniques plus the correlation of the signal with the elongation properties of propellant until dewetting, as you reported, could help provide this estimation of the rupture properties of propellant? And how?

Answer: For many years, we, and the rest of the NDE community, have desired to measure material strength properties such as maximum stress or strain at maximum stress. We would like to do this with NDE methods. This pursuit has generally been unsuccessful unless the causes for material fracture are understood. For example, if excessive porosity is the cause, then NDE can be used to search for regions of excessive porosity. With propellants, we are measuring the material strength properties along with other chemical, physical, and elastic properties. In addition, we are making NDE measurements and searching for relationships among these measurements that will lead to reaching the goal of indirectly inferring propellant strength with NDE.

Paper Number: 14
Discussor's Name: D. I. Thrasher
Responder's Name: Dr. L. H. Pearson

Question: What is your assessment of the potential for directly predicting mechanical properties from changes in chemical properties?

Answer: There are two approaches to relating mechanical properties to chemical properties. The first is through extensive measurements of chemical properties and mechanical properties, then identifying the corresponding correlations. The second is through micro-constitutive theory, based on first principles, that mathematically relates chemical and mechanical properties. Such theories are currently under development at Thiokol Corporation by my colleague and co-author of this paper, Dr. I. Lee Davis.

NDE has the role of measuring both chemical and mechanical properties separately to determine the current state of the motor. NDE alone, however, cannot determine the relationship between these two sets of properties.

ESTIMATION DE LA DUREE DE VIE DES SYSTEMES PROPULSIFS A PROPERGOL SOLIDE:

PERSPECTIVES OFFERTES PAR L'UTILISATION DE LA TOMOGRAPHIE HAUTE ENERGIE .

P. LAMARQUE - JM . TAUZIA
S.N.P.E.
BP 57
33 166 - SAINT MEDARD EN JALLES (FRANCE)

SUMMARY

The assessment of the safe and nominal operability of solid rocket motors after a long period in storage or in operational carriers is a constant concern of users.

Whilst numerous techniques have been proposed for that purpose, none has proved to be fully satisfactory. Traditional X-ray analysis provides useful, but insufficient results.

High density computed tomography, a powerful non-invasive means of investigation, has become over the last decade, thanks to its unique performance, the major tool for shelf life assessment, especially in the U.S.A.

DOD sponsored research has been carried out in this field in France.

This paper summarizes the results obtained regarding the specific equipment (sensors, measurements) and the performances measured.

From the results available, tomographic images can be considered as providing an identity card of the motor, enabling its monitoring in time.

RESUME

L'estimation de la durée de vie des moteurs à propergol solide ainsi que l'appréciation de l'état des "munitions" au cours de leur cycle opérationnel pose un problème aujourd'hui encore mal résolu.

L'utilisation de moyens de contrôle non destructifs à base de RX fournit une partie de la réponse. Ainsi l'avènement récent de la tomodensitométrie à haute énergie marque un progrès important.

Dans le présent document les résultats obtenus en France, dans ce domaine sont présentés.

INTRODUCTION

PARTICULARITE DE LA PROPULSION PAR PROPERGOLS SOLIDES.

Une caractéristique unique de la propulsion par propergols solides, souvent soulignés, réside dans l'impossibilité d'essayer le moteur avant usage et l'image du fonctionnement d'une allumette s'impose à tous.

Ainsi, les performances réelles d'un missile ne peuvent être vérifiées qu'à l'occasion d'un unique tir ce qui pose le problème de la conformité du moteur aux spécifications de recette et à l'estimation de la durée pendant laquelle, en dépit des contraintes de stockage ou opérationnelles le missile restera apte à remplir les tâches qui lui sont dévolues.

Cependant l'industriel se doit d'apprécier la durée de vie des produits qu'il fabrique tandis que l'utilisateur cherche à remplir sa mission avec le maximum de sécurité.

LE PROBLEME DE LA DUREE DE VIE

Le problème ainsi posé n'est pas simple à résoudre, il rejoint le domaine plus vaste de la surveillance de la "santé" des munitions, de tous types.

La garantie du bon fonctionnement d'un moteur débute chez l'industriel constructeur par un programme de développement rigoureux comprenant des essais durcis ce qui permet

Paper presented at the AGARD PEP Symposium on "Service Life of Solid Propellant Systems" held in Athens, Greece, 10-14 May 1996, and published in CP-586.

d'évaluer les marges de sécurité et d'obtenir une estimation de la durée de vie.

Au niveau des programmes de fabrication les paramètres dégagés lors du développement se traduirait par un choix étroit et sévère des matières premières et par l'application stricte d'un processus de mise en oeuvre éprouvé.

A l'évidence tout cela laisse des insatisfactions notoires qu'il est utile d'essayer de résorber.

COMMENT MESURER LA SANTE D'UN MOTEUR A PROPULSION PAR UN PROPERGOL SOLIDE ?

En simplifiant à l'extrême on pourrait dire qu'il faut pour le moins, remplir deux conditions :

-s'assurer de l'intégrité géométrique des organes du moteur,

-s'assurer de l'intégrité des caractéristiques mécaniques du propergol.

INTEGRITE DE LA GEOMETRIE DU PROPULSEUR

Traditionnellement la conformité géométrique des propulseurs ainsi que l'absence de défauts internes intolérables est obtenue par examen radioscopique. Cependant les images obtenues, constituées par une projection plane d'un objet tridimensionnel, sont complexes et leur interprétation reste l'apanage de spécialistes avertis.

APPRECIATION DES CARACTERISTIQUES MECANIQUES DU PROPERGOL

Usuellement l'appréciation de l'état du propergol se résume à un examen visuel complet quand cela est possible par des essais simples comme une mesure de dureté.

Cependant les propulseurs modernes possèdent parfois des moteurs indémontables (amélioration de la rigidité) ou sont enfermés dans des conteneurs lanceurs scellés de sorte que l'examen direct devient impossible.

Dans la suite de ce document le problème qui vient d'être présenté sera examiné principalement sous l'angle de l'application à la propulsion solide des récents développements des techniques industrielles des rayons X (tomodensitométrie) en raison des progrès réalisés depuis une décennie dans ces technologies.

Le contrôle In situ (à l'aide de capteurs spécifiques embarqués) des caractéristiques mécaniques des propergols qui en est encore à ses débuts ne sera pas abordé ici.

CHOIX D'UNE TECHNIQUE DE CONTROLE NON DESTRUCTIF

Les différentes problèmes exposés ci dessus nécessitent si on désire les résoudre de disposer de techniques permettant d'obtenir les informations nécessaires au travers des différents obstacles que représentent la structure, les divers interfaces et éventuellement un conteneur .

Après avoir fait le choix des rayons X on peut encore hésiter entre les diverses formes de la radiographie, la radioscopie et la tomodensitométrie numérique .

La radiographie projette sur un plan l'ensemble des formes et des défauts contenus dans un volume. Lorsque le volume est simple et lorsque la finesse du défaut recherché n'est pas excessive, la préférence va à la radiographie à cause de son moindre coût, y compris en version directe numérisée telle que la radioscopie .

La tomographie numérique, plus onéreuse parce que nécessitant des moyens informatiques importants pour la formation de l'image et d'un système mécanique précis, permet d'isoler une tranche de l'objet à contrôler ; par ce seul effet, elle bénéficie dès le départ d'une supériorité, d'une clarification de l'analyse par rapport à la radiographie .

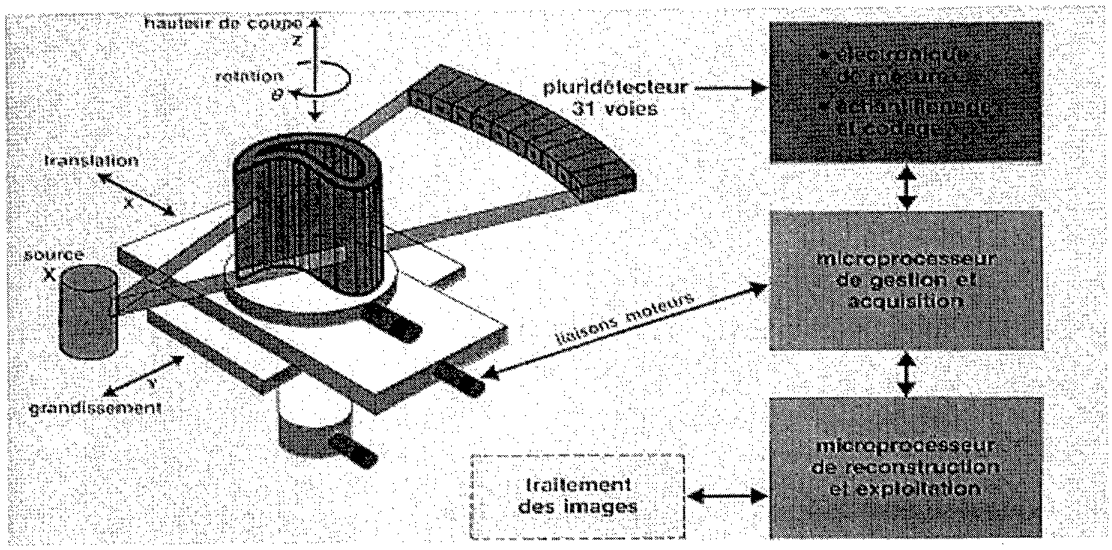
Les principes de base de la tomographie numérique par transmission de rayons X conduisent à l'obtention de la valeur de la densité du matériau analysé dans l'élément de surface de la matrice de reconstruction, que l'on peut aussi appeler pixel image .
C'est pourquoi, l'appellation la mieux appropriée de cette technique est : tomodensitométrie .

PRINCIPE DE LA TOMODENSITOMETRIE NUMERISEE

Le but de la tomodensitométrie est de restituer dans un plan image, la matrice des paramètres physiques qui caractérisent l'interaction rayonnement X - matière d'un grand nombre de faisceaux de rayonnement X balayant le plan de coupe de l'objet à analyser.

Si l'on souhaite que l'atténuation soit essentiellement proportionnelle à la densité des matériaux traversés (ce qui est essentiel si l'on souhaite mettre en évidence de faibles variations de densité représentatives par exemple de migrations chimiques consécutives par exemple à un vieillissement des matériaux) il est nécessaire de se situer dans un domaine d'énergie élevé de 1 Mev à quelques Mev .
Pour cette raison la tomodensitométrie à haute énergie devient nécessaire . De plus l'utilisation de rayons X de forte énergie, du fait de leur fort pouvoir de pénétration, permet en outre l'examen d'objets fortement absorbants tels que les propulseurs à propergol solide.
Dans cette optique nous avons développé avec le concours du Centre d'études nucléaires de Grenoble et son laboratoire des techniques industrielles (LETI) un tomographe haute énergie.

Le principe est représenté sur le schéma ci après .
On mesure l'atténuation RX à travers l'objet pour un grand nombre de direction, l'ensemble des mesures réparties sur 360° forme un fichier de données appelé sinogramme.



TOMOGRAPHE A HAUTE ENERGIE PROTOTYPE UTILISE

Le tomographe du LETI est en service depuis 1990.

Le programme de travail élaboré par les différentes parties a porté notamment :
- sur la mise au point de capteurs très sensibles et résistants au vieillissement,
- sur le développement d'une électronique de mesure à forte dynamique (5 décades permettant de préserver et de traiter toute l'étendue des informations acquises...)
- sur le développement de logiciels spécifiques à la géométrie des propulseurs.

SOURCE RX

La source utilisée est un accélérateur linéaire LINATRON 2000 dont l'énergie maximum des photons est de 8 Mev avec une dose d'émission de l'ordre de 15 Grays par minutes à 1 mètre . Le rayonnement X est pulsé à une fréquence maximum de 300 Hz en synchronisation avec le déplacement en translation de la mécanique.

DETECTEUR

L'ensemble de détection est composé de 25 cellules indépendantes à base de semi-conducteur Chaque cellule est collimaté par du plomb pour minimiser le rayonnement diffusé et la diaphonie entre voies . L'efficacité de détection est de l'ordre de 40 %.

ELECTRONIQUE D'ACQUISITION ET DE REFORMATION

L'électronique d'acquisition intègre le signal issu des détecteurs en synchronisation avec les tirs de l'accélérateur et le déplacement de l'objet. Chaque valeur est codée sur 16 bits . Ceci permet d'avoir

des mesures significatives sur au moins 5 décades d'atténuation du signal . Les valeurs codées sont ensuite transmises par fibres optiques à un calculateur Microvax .
Les données sont traitées par le calculateur puis envoyées à un processeur spécialisé qui applique les algorithmes classiques de la tomographie.

PARAMETRES D'ACQUISITION ET DE REFORMATION

Les paramètres usuels sont les suivants :

- Dimension maximum de l'objet : 600 mm de diamètre
- Poids de l'objet inférieur à 100 Kg
- Pas d'acquisition en translation : de 100 à 600 microns
- Nombre de projections : 562, 1125, 3375, 5625
- Hauteur de coupe : 1, 3, 7, 15 mm
- Reconstruction de 1 à 8 zones en parallèle avec l'acquisition
- Les filtres sont choisis en fonction du type de défauts recherchés (variation de densité, délaminages ou métrologie)

La durée d'une acquisition peut varier suivant le choix des paramètres ou la taille de l'objet entre 10 minutes et 1 heure.

En faisant varier les différents paramètres nous avons établi les valeurs du bruit au centre de l'image, cette valeur est directement liée au niveau de résolution que l'on peut obtenir . Le choix des paramètres d'acquisition et de reformation permet de privilégier la résolution en densité, la résolution géométrique ou le temps d'acquisition.

RESULTATS EXPERIMENTAUX OBTENUS

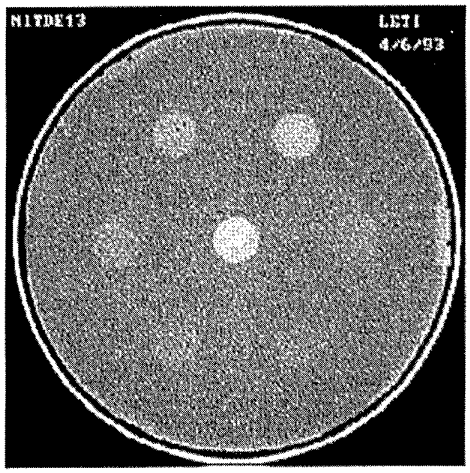
SUR MAQUETTES

Pour cette étude expérimentale une maquette de propulseur à propergol solide a été réalisée. Cette maquette intègre des défauts ou anomalies représentatives de ce qu'il est susceptible d'exister sur un propulseur présentant des signes de vieillissement :

- variation de densité locale (une variation de densité locale de 1% correspond à une variation du taux de liant d'environ 1 point . Ceci est également vrai au niveaux des collages).

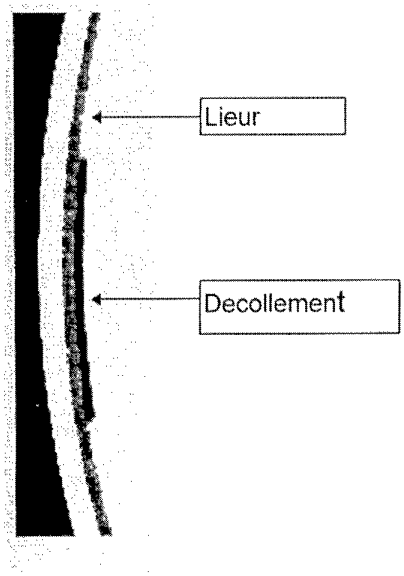
- Décollements aux interfaces

Un exemple d'image réalisé est présenté ci-après. Tous les inserts sont détectés sans ambiguïté. Il s'agit d'une acquisition fine avec un pas d'acquisition en translation de 100 microns.



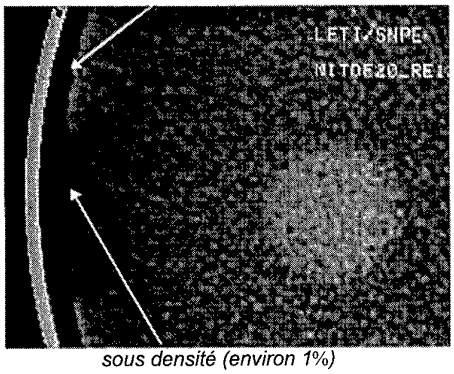
Tous les inserts présentant des variations de densité locale par rapport à la matrice (0,3% à 5%) sont visibles, aussi bien dans la masse du propergol qu'au voisinage des collages .
Tous les décollements de bâillement 0,3 mm et 0,5 mm sont également visibles.

L'image suivante présente un zoom au niveau d'un défaut de collage de 0,3 mm.



L'image suivante présente un zoom de la partie gauche de l'image complète.

sur densité d'environ 1 %



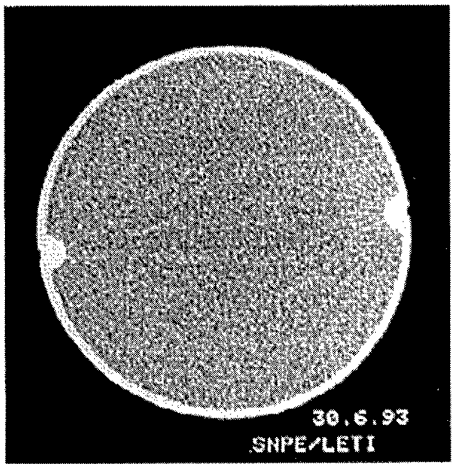
sous densité (environ 1%)

Cette image met en évidence les migrations chimiques de composant (liant) au niveau des interfaces de collage qui se traduisent par des sous densité pour les liaisons non collées et par des sur densité pour les liaisons bien collées.

Ce résultat ouvre des possibilités par cette mesure fine du gradient de densité à l'interface de mise en évidence de décollements jointifs.

SUR PROPULSEUR REEL

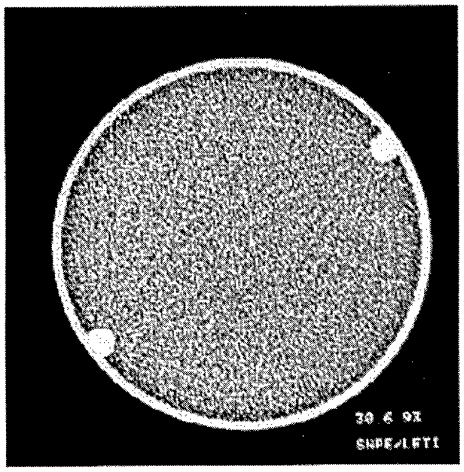
Les images suivantes présentent les résultats obtenus sur des chargements réels.
Il faut noter que ces images ont étés obtenues alors que les propulseurs étaient dans leurs containers.



Cette image montre un propergol de densité homogène sur l'ensemble de la coupe, y compris au niveau des liaisons.

En tir le fonctionnement de ce propulseur est nominal

L'image suivante montre un propergol non homogène avec des variations de densité au niveaux des interfaces, (liseré noir prés de l'interface révélant une sous densité représentative d'un excès de liant.)



Ce propulseur en tir présente une défaillance

Ces images d'un propulseur fournissent une réponse possible, encore que partielle, pour l'estimation de la durée de vie.

Ainsi on peut raisonnablement conjecturer qu'un ensemble de coupes situées dans des zones judicieusement choisies du moteur constituent, à l'issue du cycle de fabrication la carte d'identité du moteur (figers print).

Dès lors il s'agit de mesurer périodiquement l'évolution des images et de les comparer aux situations (déformations du canal, fermeture des systèmes de relâchement de contraintes, fissures, décollements) dont le programme de développement aura défini la limite acceptable.

Le propulseur étant jugé inutilisable dés lors qu'un défaut critique sera détecté.

LE CONTROLE DES MISSILES OPERATIONNELS

La méthodologie développée ci-dessus fait intervenir des équipements de tomodensitométrie tels que ceux que l'on peut trouver chez les industriels constructeurs, néanmoins les progrès récents de cette technique ouvrent la perspective de réalisation d'un équipement de diagnostic mobile (par exemple en conteneur standard)

pouvant être utilisé dans des zones dédiées des sites opérationnels.

Naturellement il ne s'agit ici que de perspectives et un important travail de développement et de validation reste à faire.

CONCLUSION

L'appréciation de la durée de vie des organes des missiles (et surtout du moteur) ainsi que du degré de vieillissement ou d'endommagement reste un problème complexe dont aucune technique prise séparément ne fournit de réponse satisfaisante.

Parmi les techniques les plus prometteuses la tomodensitométrie fournit un outil de choix dont la diffusion est freinée par le coût des investissements correspondants.

Néanmoins la tomodensitométrie est utilisée dans ce rôle aux USA dans les bases de l'Air Force et il est probable qu'il en sera de même en Europe dans un futur proche.

REFERENCES

-Séminaire Tomographie Grenoble, 28-29 mars 1988, Intercontrole

-Special issue on Computed Tomographie, Material Evaluation, May 1990 Volume 48

-Density Measurement by X rays Computed Tomography, C V. Kropas, Material Evaluation April 1991

-Super voltage Computed Tomography for SRM, P. Tonner, Material Evaluation December 1992

-CND des Moteurs à Propergol Solide par Tomographie X, F. Glasser, P. Lamarque,
6° ECNDT Nice 1994

IMMERSION ULTRASONIC ANALYSIS OF EXTRUDED ROCKET MOTORS

Leon M. Glowacki
Senior Materials Engineer
NAVAL SURFACE WARFARE CENTER
INDIAN HEAD DIVISION, Code 310D1
Indian Head, Md. 20640 U.S.A.

BACKGROUND

The Indian Head Division of the Naval Surface Warfare Center, in Indian Head, Maryland, U.S.A., has an ultrasonic system capable of volumetrically evaluating small diameter rocket motor propellant grains. The ultrasonic system and the evaluation technique described in this paper are used to inspect a specific weapon system component. With minor modifications the system and technique can be used to inspect a wide variety of extruded rocket motor propellant grains.

In this evaluation the propellant grains are extruded and tape wrapped prior to inspection. The grains may be evaluated however, in an as extruded condition.

The grains are approximately 2.6" in diameter, approximately 3 feet in length and contain an eight point star bore. The star bore, formed during the extrusion process, is made by forcing a propellant blank or carpet roll through a cross shaped center stake support. The center stake support sections the blank into four quadrants. With a combination of pressure, speed, vacuum and temperature the four quadrants are extruded down onto the eight pointed star shaped center stake. The extrusion process parameters are very critical and any variation in temperature, speed, pressure or vacuum can result in the introduction of discontinuities.

DISCONTINUITIES

Discontinuities detected during the ultrasonic evaluation may come from the base material (carpet rolls), may be produced during the extrusion process or may be introduced after manufacturing.

A typical base material discontinuity is foreign material. A lead/copper compound is the most frequently detected base material discontinuity, however, other types of materials may be detected.

Discontinuities, typical to this extrusion process are fissures, poor consolidation, poor consolidation with voids and poor consolidation with bursts.

Fissures are typically planer indications with an axial component, a circumferential component and minimal radial thickness. Fissures are analogous to laminations in rolled plate.

Poor consolidation, caused by the failure of the propellant quadrants to completely re-consolidate or weld during the extrusion process, is characterized by indications with a large axial and radial component and a small thickness component. Poor consolidation indications are analogous to lack of fusion indications on the side wall of weldments. Poor consolidation indications typically appear as two (2) or more axially orientated linear indications at 90 degree intervals. The 90 degree intervals are due to the placement of the four center stake support me Poor consolidation with voids is similar to poor consolidation except the thickness of the indication is greatly increased. A poor consolidation indication may have a thickness of 0.001" to 0.005", while the void indications may have a thickness of 0.085" or greater.

Poor consolidation with burst is characterized by a linear indication with an axial orientation. This discontinuity is cylindrical with no preferential orientation except along the axis of the grain. This discontinuity typically has randomly located disk shaped anomalies along the length of the cylindrical sections. These disk shaped anomalies resemble forging bursts.

Cracks are the only type of post-manufacturing discontinuity detected with ultrasonics.

ULTRASONIC SYSTEM

The IHD-NSWC's ultrasonic system was custom made by Sonix Inc. to our specifications. The ultrasonic system is made up of four major sub-systems, the tank, the grain positioner/rotator, the transducer fixture/positioner and the computer controller. The tank is constructed of stainless steel and is large enough to allow a full length 36" scan. The tank also has a couplant circulating and filtering system.

The grain positioner/rotator securely centers the grain between the transducer assemblies and rotates the grain at a predetermined velocity. The transducer fixture/positioner allows for independent alignment of each of the six possible transducers. It also secures the transducers in position and moves the transducer fixture down the length of the grain during inspection.

The computer controls the axis motors, the four channel pulser/ receivers, the a/d converters and the various memory and display functions. The computer is a 486 DX, 33 mhz with a 150 mhz removable bernoulli disc drive.

Paper presented at the AGARD PEP Symposium on "Service Life of Solid Propellant Systems" held in Athens, Greece, 10-14 May 1996, and published in CP-586.

SYSTEM OPERATION

With this system, the grains are manually loaded into the positioner. After loading and when cued by the ultrasonic inspector, the system automatically inspects the grain to a pre-determined scan plan. A real time "A" AND "C" scan image is displayed during the scan and an enhancible "A", "B" or "C" scan image is available after the scan is complete.

The system can be configured as four pulse-echo channels, three thru-transmission channels or various pulse-echo/thru-transmission combinations.

The acoustic properties of the test material, dictated the use of relatively low frequency, large diameter transducers. (see table 1)

Acoustic Properties

Material velocity - 1.8575 cm/sec x 10^5
Acoustic impedance - 2.99 g/cm^{2}sec x 10^5
Attenuation @ 1.0 MHz - 6-8 db/cm
Attenuation @ 2.25 MHz - 18-20 db/cm

Table 1

The following is our present scan plan and test parameters:
Scan length - 360 degrees
Scan velocity - 2400 degrees/sec.
Scan data - Eight data points (one peak amplitude, one time of flight per channel x 4 channels) every 3.6 degrees or 800 points/revolution/step.
Scan index - 0.080" per step, 425 steps per grain
Total data - 340,000 data points per grain.

Inspection mode
- Channel 1 - pulse-echo, angled into the web. Gated from the outside to bore
- Channel 2 - pulse-echo, aligned at the bore.
- Channel 3 - thru-transmission, thru the center of the grain.
- Channel 4 - pulse-echo, angled into the web. Gated from the center of the web to past the bore.

Pulse repetition frequency - 1000-2000
Transducer pulsing voltage - 375 volt spike

Transducers
- Channel 1,2,4 - 1.0 MHz, 3/4" diameter, cylindrically focussed to 2" in water.
- Channel 3 - 1.0 MHz, 3/4" diameter, spot focussed to 2" in water.

Calibration
- Pulse echo - 90-100 % indication from a 3/4" long, 1/16" diameter, side drilled hole in the live grain standard.
- Thru-transmission - 90-100% thru wall indication in a defect free area.

Inspection time - 1 1/2-2 minutes per grain

TYPICAL INSPECTION RESULTS

"C" scan images from various discontinuities found and displayed with our ultrasonic system. (following text)

a) Fissures

b) Poor consolidation

c) Crack

SYSTEM EVALUATION:

- The system is able to detect and display the various discontinuity types in a relatively easy to interpret format.

- The automatic scan and rotate feature allows for the gathering of a large amount of data on each grain.

- The inspection times are fairly short.

- The grain handler still needs to manually load and unload the grain

- All grain information is manually entered.

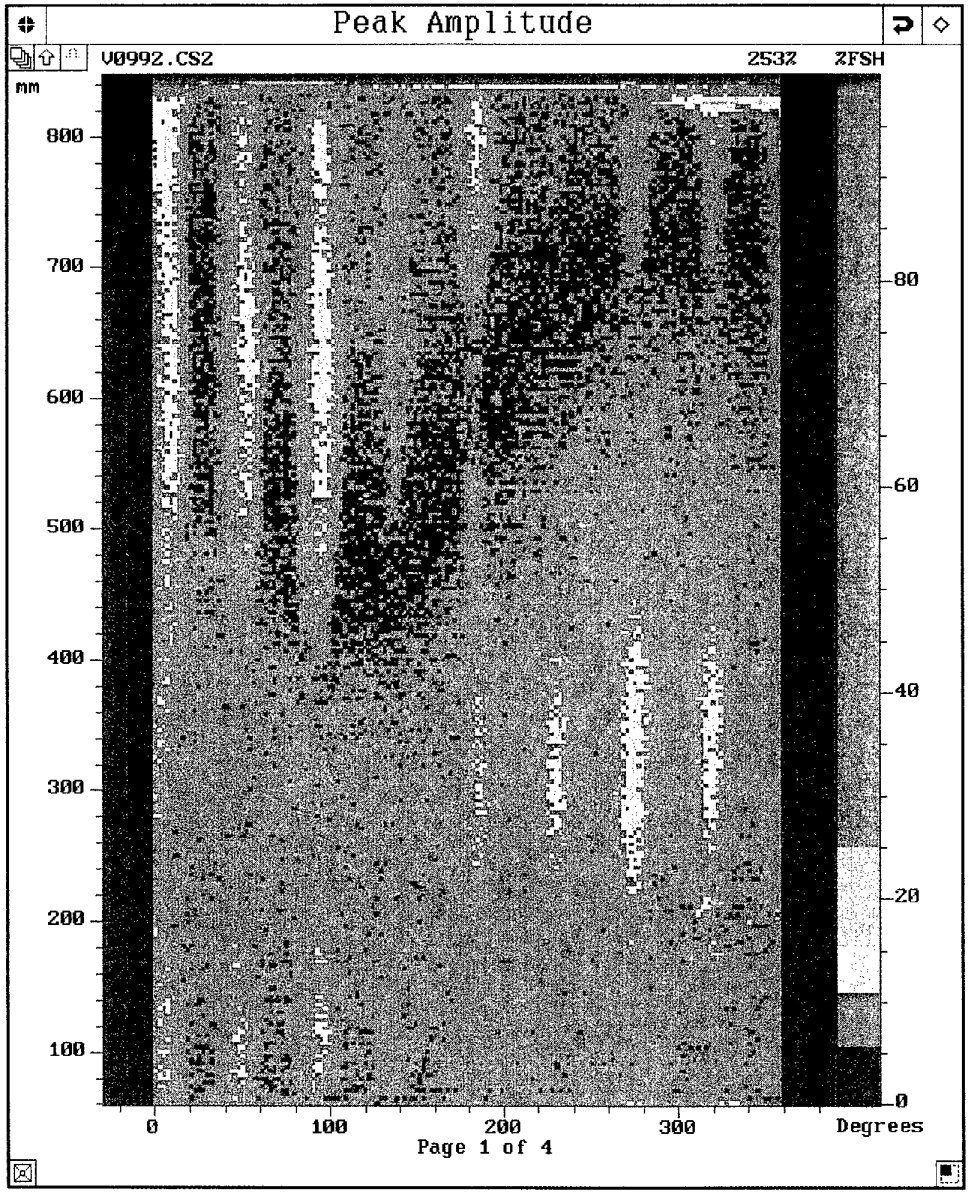
ULTRASONIC/RADIOLOGICAL COMPARISON

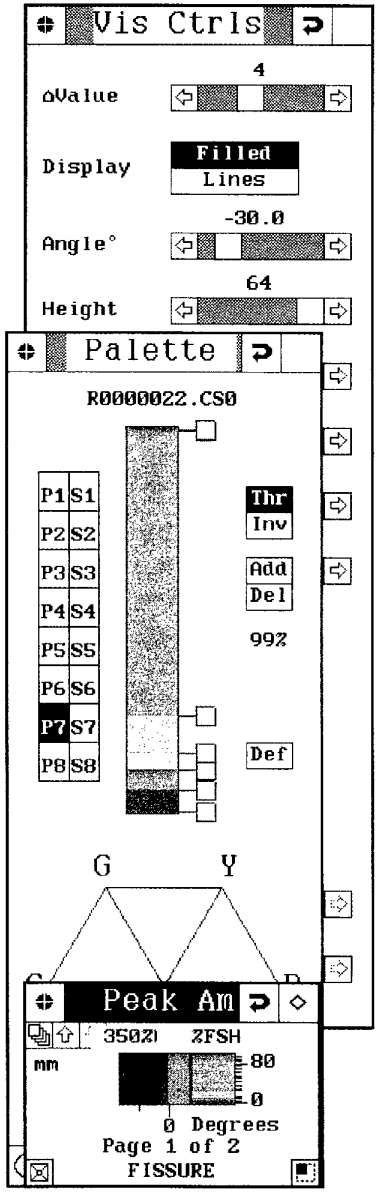
The ultrasonic system was part of an extensive evaluation involving approximately 1000 grains. Part of the evaluation compared the ultrasonic data to real-time radiography (RTR) data. The final evaluation is not complete and additional destructive and nondestructive test need to be performed. The preliminary results show that virtually all the real defects detected with RTR were detected by ultrasonic.

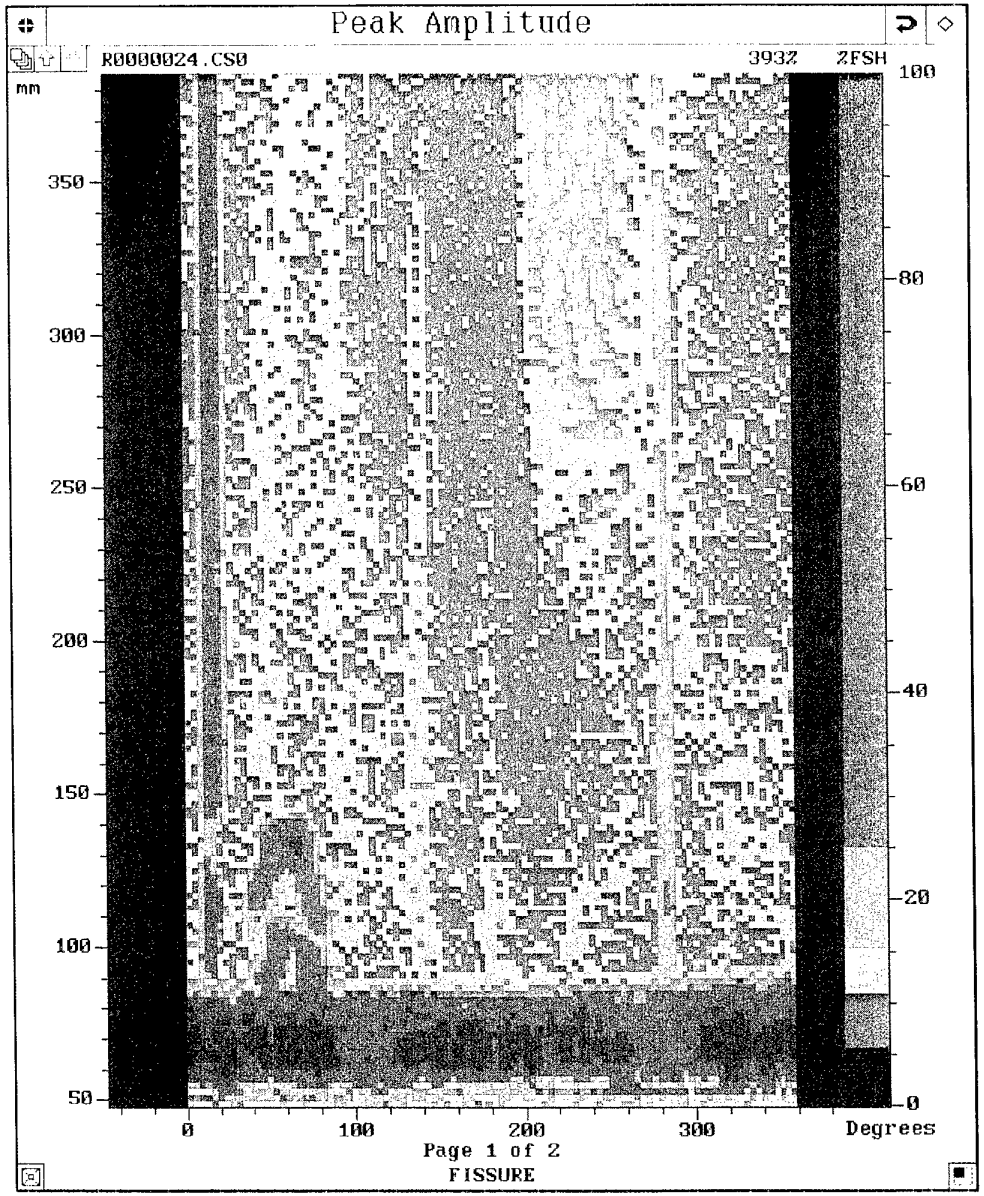
CONCLUSION

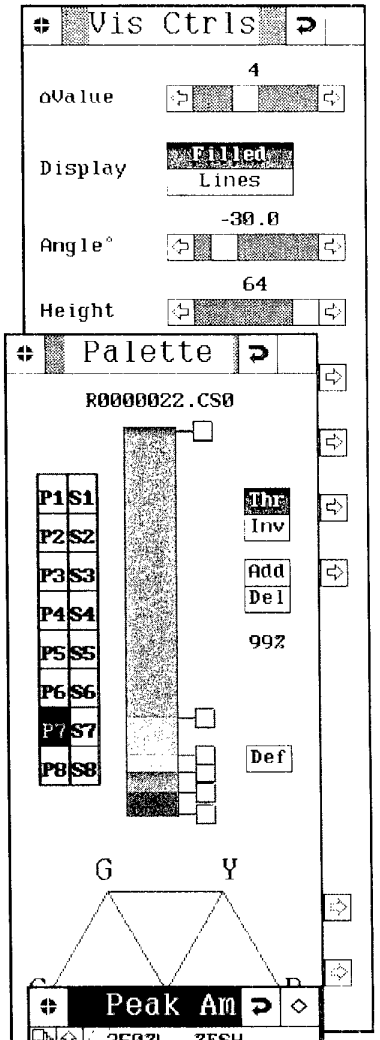
The semi-automated system now at the IHD-NSWC has shown that ultrasonic data can be displayed in a relatively easy to understand and interpret manner and that the inspection can be performed at near production speeds. Ultrasonic appears to by more sensitive than RTR to certain material anomalies and additional studies will show if these anomalies are true defects and a cause for concern.

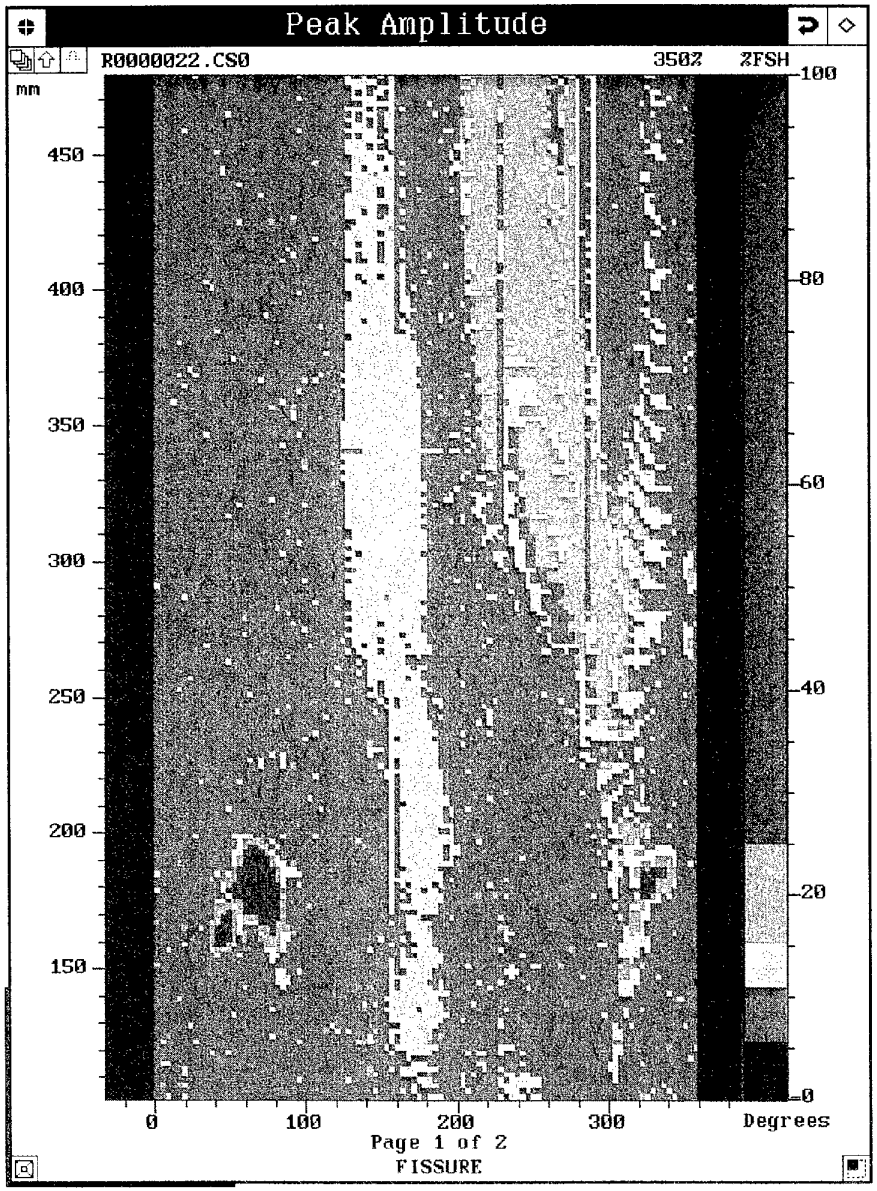
The next generation ultrasonic system will have automatic loading into the tank, automatic accept/reject and the ability to physically separate acceptable grains from rejectable ones.

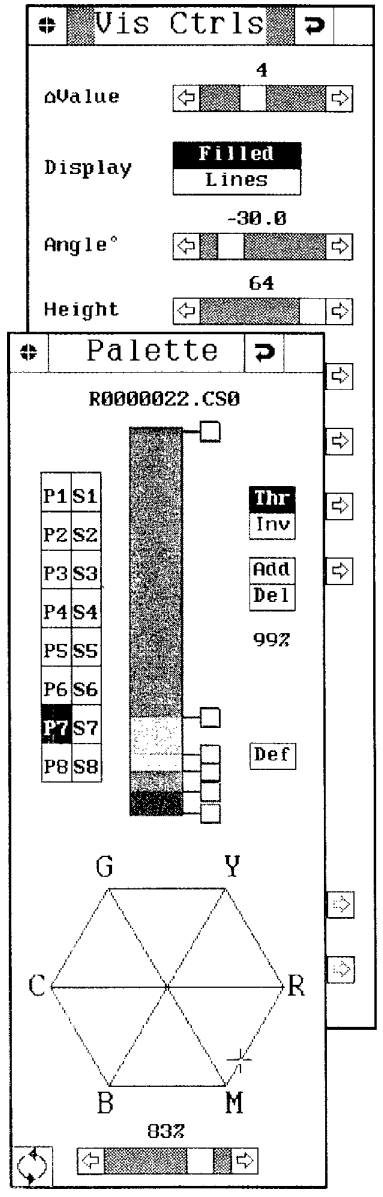

Peak Amplitude
V0992.CS2
253%
ZFSH
mm
800
700
600
500
400
300
200
100
80
60
40
20
0
0
100
200
300
Degrees
Page 1 of 4

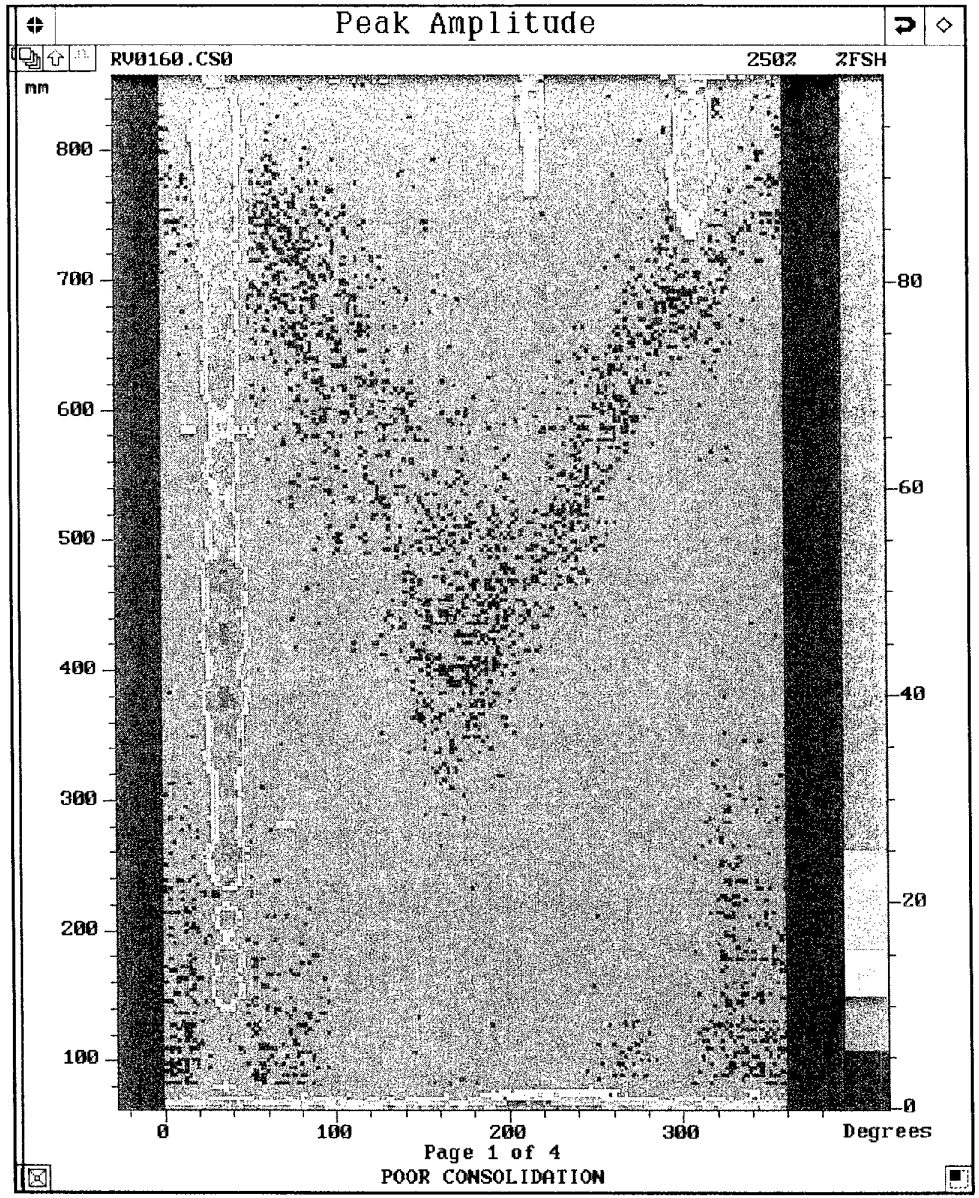

Vis Ctrls
4
ΔValue
Display
Filled
Lines
-30.0
Angle°
64
Height
Palette
R0000022.CS0
P1 S1
P2 S2
P3 S3
P4 S4
P5 S5
P6 S6
P7 S7
P8 S8
Thr
Inv
Add
Del
99%
Def
G
Y
Peak Am
350% ZFSH
mm
80
0
0 Degrees
Page 1 of 2
FISSURE

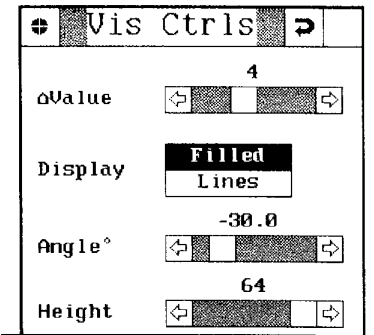

Peak Amplitude
R0000024.CS0
393Z
ZFSH
mm
350
300
250
200
150
100
50
100
80
60
40
20
0
0
100
200
300
Degrees
Page 1 of 2
FISSURE

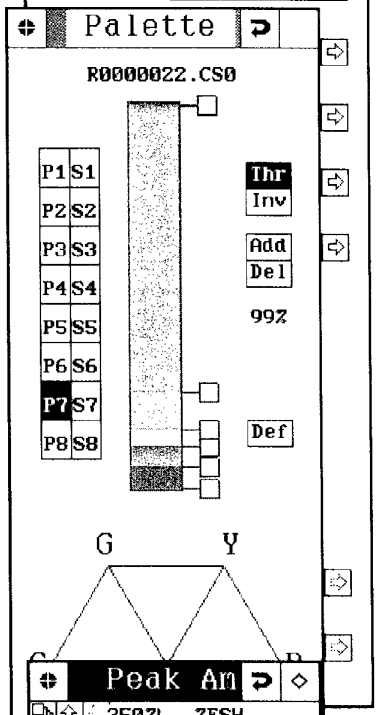

Vis Ctrls
oValue
4
Display
Filled
Lines
Angle°
-30.0
Height
64
Palette
R0000022.CS0
P1 S1
P2 S2
P3 S3
P4 S4
P5 S5
P6 S6
P7 S7
P8 S8
Thr
Inv
Add
Del
99%
Def
G
Y
Peak Am
350ZI
ZFSH
mm
80
0
0 Degrees
Page 1 of 2
FISSURE

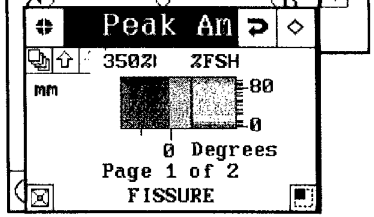

Peak Amplitude
R0000022.CS0
350Z
ZFSH
mm
450
400
350
300
250
200
150
100
80
60
40
20
0
0
100
200
300
Degrees
Page 1 of 2
FISSURE

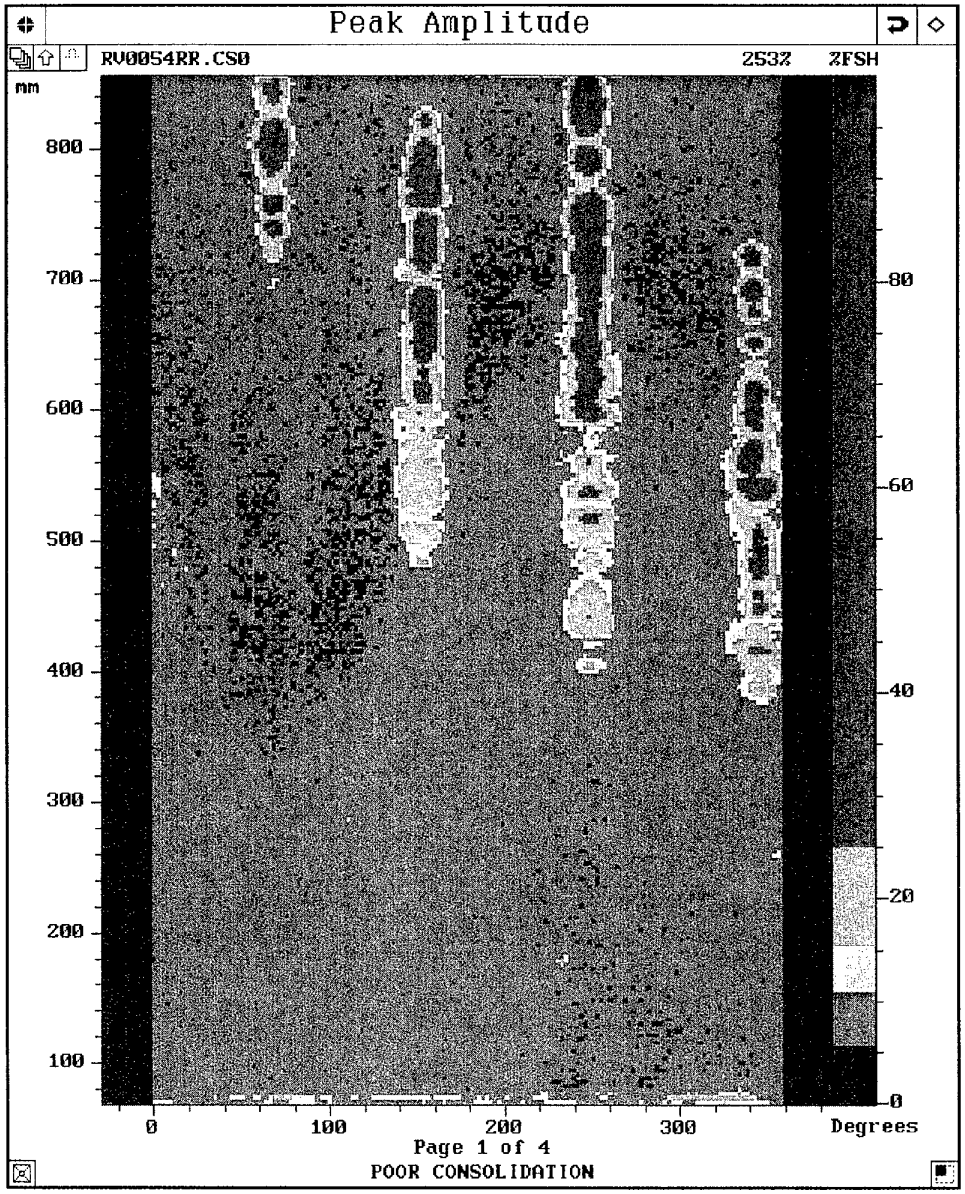

Vis Ctrls
4
ΔValue
Display
Filled
Lines
-30.0
Angle°
64
Height
Palette
R0000022.CS0
P1 S1
P2 S2
P3 S3
P4 S4
P5 S5
P6 S6
P7 S7
P8 S8
Thr
Inv
Add
Del
99Z
Def
G
Y
C
R
B
M
83Z

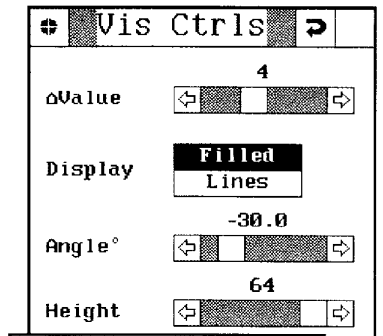

Peak Amplitude
RV0160.CS0
250Z
ZFSH
mm
800
700
600
500
400
300
200
100
0
100
200
300
Degrees
80
60
40
20
0
Page 1 of 4
POOR CONSOLIDATION

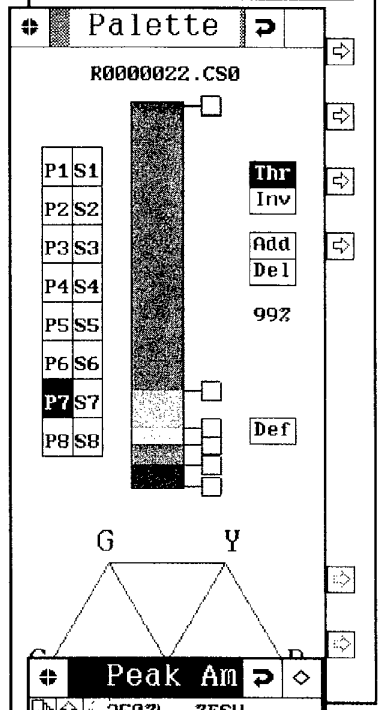

Vis Ctrls
4
ΔValue
Display
Filled
Lines
-30.0
Angle°
64
Height

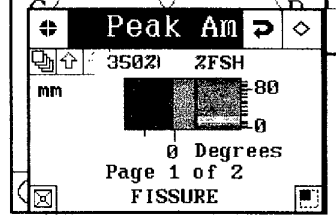

Palette
R0000022.CS0
P1 S1
P2 S2
P3 S3
P4 S4
P5 S5
P6 S6
P7 S7
P8 S8
Thr
Inv
Add
Del
99Z
Def
G
Y

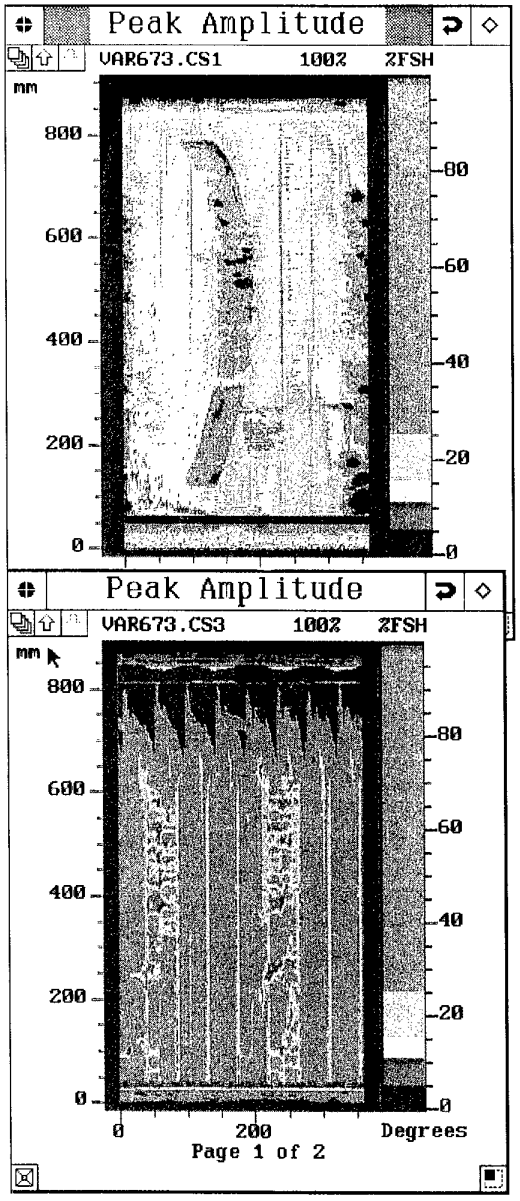

Peak Am
350Z
ZFSH
mm
80
0
0 Degrees
Page 1 of 2
FISSURE

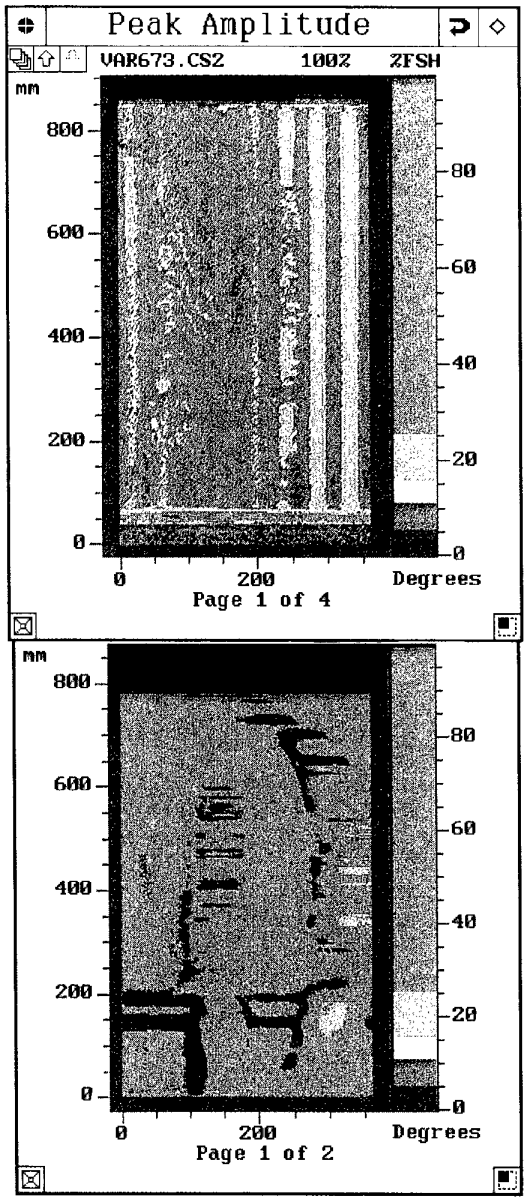

Peak Amplitude
RV0054RR.CS0
253Z
ZFSH
mm
800
700
600
500
400
300
200
100
80
60
40
20
0
0
100
200
300
Degrees
Page 1 of 4
POOR CONSOLIDATION

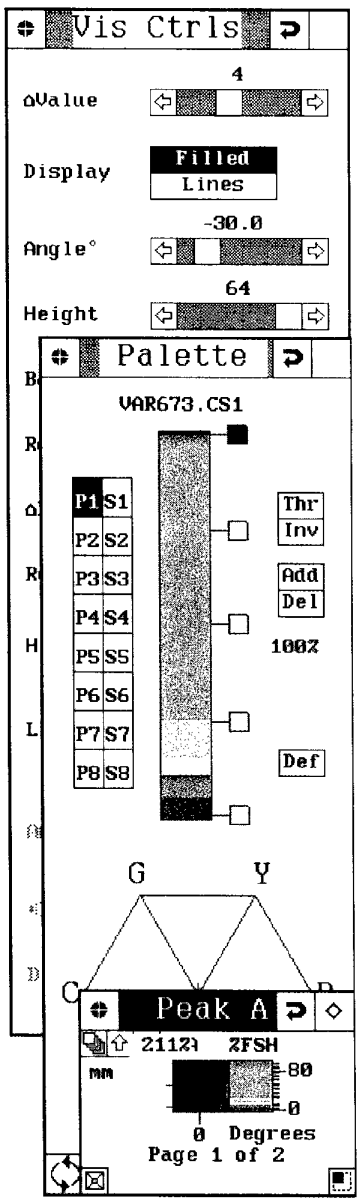

Vis Ctrls
4
ΔValue
Display
Filled
Lines
-30.0
Angle°
64
Height

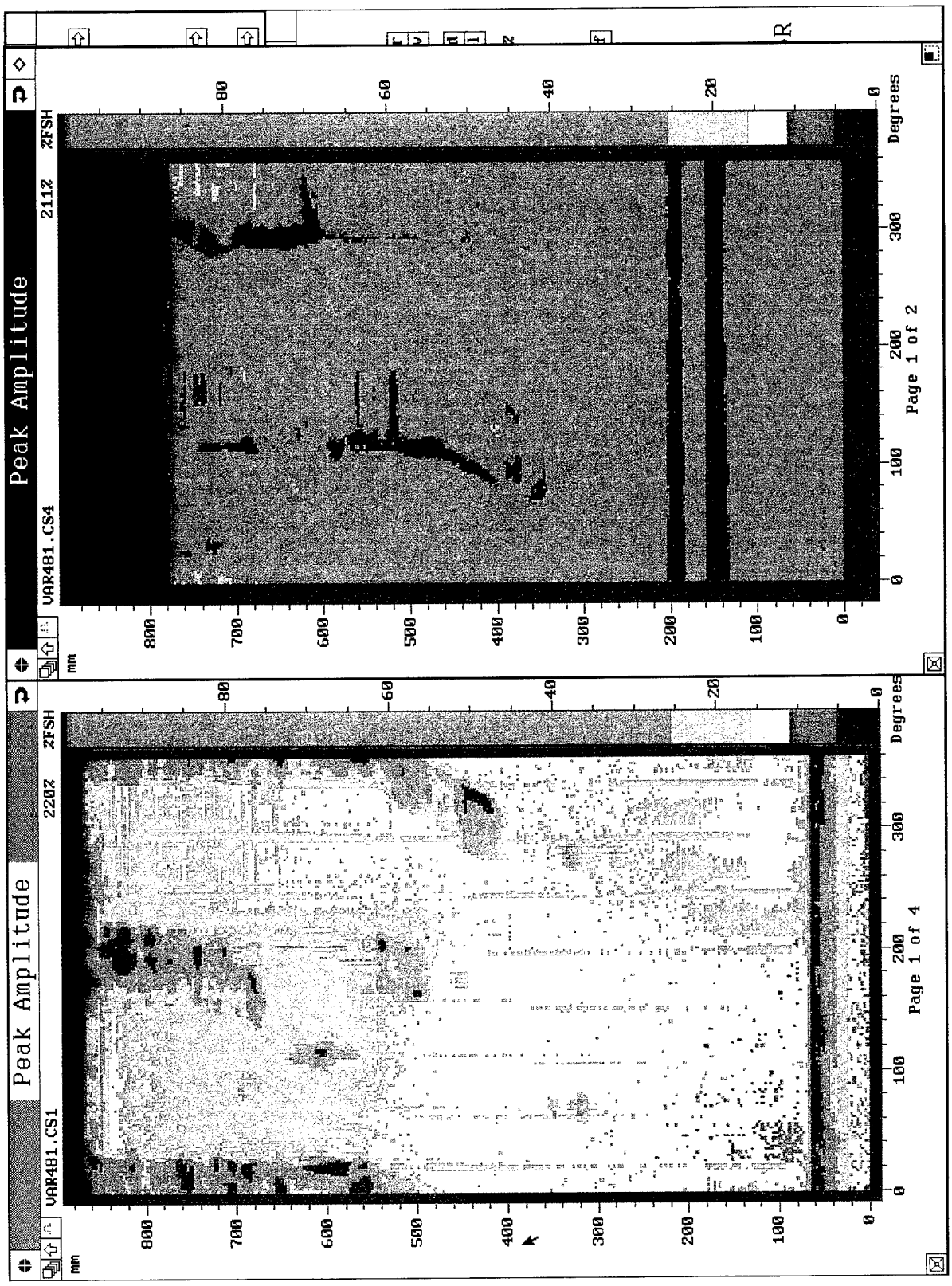

Palette
R0000022.CS0
P1 S1
P2 S2
P3 S3
P4 S4
P5 S5
P6 S6
P7 S7
P8 S8
Thr
Inv
Add
Del
99Z
Def
G
Y


Peak Am
3502I
ZFSH
mm
80
0
0 Degrees
Page 1 of 2
FISSURE


Peak Amplitude
VAR673.CS1 100% ZFSH
mm
800
600
400
200
0
80
60
40
20
0
Peak Amplitude
VAR673.CS3 100% ZFSH
mm
800
600
400
200
0
80
60
40
20
0
0
200
Degrees
Page 1 of 2


Peak Amplitude
VAR673.CS2 100% ZFSH
mm
800
600
400
200
0
80
60
40
20
0
0
200
Degrees
Page 1 of 4
mm
800
600
400
200
0
80
60
40
20
0
0
200
Degrees
Page 1 of 2


Vis Ctrls
4
ΔValue
Display
Filled
Lines
-30.0
Angle°
64
Height
Palette
VAR673.CS1
P1 S1
P2 S2
P3 S3
P4 S4
P5 S5
P6 S6
P7 S7
P8 S8
Thr
Inv
Add
Del
100%
Def
G
Y
C
D
Peak A
211% ZFSH
mm
80
0
0 Degrees
Page 1 of 2


Peak Amplitude
VAR4B1.CS1
2202
ZFSH
mm
Degrees
Page 1 of 4
Peak Amplitude
VAR4B1.CS4
2112
ZFSH
mm
Degrees
Page 1 of 2

OVERVIEW OF THE UNITED STATES ARMY AND NAVY GUN PROPELLANT SAFETY SURVEILLANCE PROGRAMS

D. D. Lee (e-mail: 6210F@WPNENGR.IH.NAVY.MIL)
and G. Y. Stine (330@TESTEVAL.IH.NAVY.MIL)
US Naval Surface Warfare Center
Indian Head Division
101 Strauss Avenue, Indian Head
MD 20640, USA, Att. Code 6210F

D. G. Robertson (e-mail: DROBERTS@PICA.ARMY.MIL)
and W. F. Ark (FARK@PICA.ARMY.MIL)
US Army ARDEC
AMSTA-AR-AEE-WE
Picatinny Arsenal, NJ 07806-5000, USA

1. SUMMARY

The United States Army, the U. S. Navy, and the U. S. Marine Corps each conduct safety surveillance programs to monitor the stability of their gun propellants that are nitrate ester-based. This paper provides an overview of the efforts from those programs. The paper discusses the rationale behind current test programs and test techniques. The paper provides some "lessons learned" from previous techniques and provides some information on the efforts of the programs during the past five years.

2. INTRODUCTION

The primary objective is to assure the storage and handling safety of the propellant and ammunition of each service. In addition to "routine" testing, analysis, and program administration, the programs a) provide technical expertise for investigations where there are concerns about propellant stability, b) advance the scientific understanding of propellant stabilization and decomposition, and c) improve the quality and productivity of surveillance techniques.

3. BACKGROUND

Army and Navy safety surveillance began formally in the 1920's as a joint program. The Army's efforts are now centered at Picatinny Arsenal in New Jersey at the Armament Research, Development and Engineering Center (ARDEC). Navy efforts are now centered at Indian Head, Maryland, at the Indian Head Division of the Naval Surface Warfare Center (IHDIV). Over the years, the United States Marine Corps (USMC) has developed its own separate surveillance program to address the unique needs of their mission. That effort is now coordinated by the Marine Corps Programs Department (MCPD) at Fallbrook, California, although they often use ARDEC and IHDIV for test support and technical guidance.

These surveillance programs face many challenges: a) large quantities of propellant to monitor, b) wide varieties of propellant, c) a broad spectrum of environmental conditions to consider, d) logistic concerns, e) funding constraints, and f) constraints from Federal and State regulatory agencies.

Since the military services have a wide variety of ammunition types and need to stockpile large quantities of ammunition, the surveillance activities must monitor large quantities of many varieties of propellant types. Those propellants are used in gun applications for calibers ranging from 5.56mm to 16" (406mm). Every propellant lot that is manufactured is monitored until it is loaded into ammunition. After that, each propellant lot is monitored for ammunition above 0.50 caliber (12.7mm).

The propellant formulations under surveillance fall into three broad categories – single-base, double-base, and triple-base formulations – indicating the nitrate ester composition. Within each category, there are also a number of different formulations and physical configurations (granulations). Propellant configurations range from particles 2mm in size to wafers to right-circular cylinders with multiple perforations to slotted stick propellants.

The services attempt to take into account a wide variety of environments that the propellant and ammunition might encounter during their service – from arctic to tropical environments; from shipboard storage to storage atop airfields in the desert.

Currently, ARDEC and IHDIV each have over 6,000 "Master" samples whose stability they monitor continuously (see section 3.1). Additionally, each year ARDEC and IHDIV test hundreds of propellant samples from worldwide locations. The MCPD monitors over 6,500 lots of propellant that they have in their ammunition inventories, leading to hundreds of field sample tests, annually.

In addition to these challenges, the surveillance organizations are faced with ever-increasing budgetary constraints. In light of the various challenges, the programs must be pragmatic and cost effective, with no compromise to the goal of assuring the storage safety of the services gun propellants and gun ammunition.

Programmatically, both the Army and the Navy maintain two types of surveillance test programs: a Master Sample program, and a field return program.

3.1 Master Sample Program

Both services rely heavily on Master Sample programs to assess the stability of the gun propellants that they have. Whenever a manufacturer makes a propellant lot, a 2 to 5 pound (0.9 to 2.3 kg) sample is sent to the appropriate organization (ARDEC or IHDIV) where it becomes the surveillance Master Sample* for that lot. The surveillance organization maintains control of each sample and tests it continuously to monitor its stability throughout its safe life. The

* The surveillance Master Sample should not be confused with the ballistic master lot.

Paper presented at the AGARD PEP Symposium on "Service Life of Solid Propellant Systems" held in Athens, Greece, 10-14 May 1996, and published in CP-586.

collections of master samples, along with the testing, data analyses and reports constitute the Master Sample programs. The services use the master sample to assessing the safety of the fielded inventory by stressing the master sample so it ages more rapidly than a fielded sample, and applying a stability criteria that is conservative with respect to safety.

3.2 Field Sample Program

In addition to the Master Sample program, the services take a disciplined approach to testing samples from the field. The Army's test program is known as its Stockpile Surveillance Program (SSP). The Navy's is known as the Fleet Return Program. The USMC has a number of programs under which they test propellants for stability -- Quality Evaluation (QE) program, Safety program, and Maritime Preposition (MPF) program.

Field samples are taken for the following reasons: a) some field inventories may have encountered adverse environments to the degree that they are a stability concern, b) field samples serve as a practical check on the effectiveness of the Master Sample program, c) field samples provide increased lot representation to smooth potential effects of heterogeneity, d) field samples can alert us to situations where there may be chemical interactions with components of the storage configuration that could cause significantly different propellant decomposition than the Master sample, or e) a combination of any of these.

For the Navy, past field sampling has shown that the corresponding Master sample usually ages more quickly than field samples. It has been suggested that the environment and repeated handling of the Master samples at Indian Head promotes aging more-so than storage conditions at depots or aboard ship. There have been some rare occasions where a field sample will be more aged than the master sample.

The Army and the USMC, however, have experienced more frequent incidences where the field sample is more aged than the Master sample. This probably is due to storage and handling conditions that can be more adverse than the conditions that Navy propellant encounters. It may also be due to the different types of ammunition and ammunition packaging that are used.

3.2.1 Mobile Lab

One concern has been the lack of control of the field sample as it was transported to ARDEC or IHDIV from a site that was outside the continental United States (OCONUS). It is not uncommon for OCONUS samples to be in transit for over a year, during which the environmental conditions are not well defined. This led to concerns about how well a sample represents its original storage conditions because the conditions and time of transit age the sample differently than its original population. In 1992, the Navy implemented a Mobile Lab to perform stability testing. The Mobile Lab is essentially a small lab with a HPLC built into a 20-foot by 12-foot (6.1m x 3.7m) trailer van. To date, the Navy has used the Mobile Lab successfully in Japan, Guam, Hawaii, the Caribbean, and in Spain.

4. THERMAL STABILITY TEST TECHNIQUES

A variety of thermal stability tests are available, including newer test techniques such as microcalorimetery or accelerating rate calorimetery. However, the services continue to use the basic Fume Test, a test developed in the mid-1910s as their primary method for assessing thermal stability. Alternate techniques have not been easily adapted to the high volume of testing required in the U.S.

4.1 Fume Test

This is also known as the 65.5°C Oven Test or Surveillance Test. This test is used with single-base and double-base propellants. Triple-base propellants are not tested in the fume test because fumes are not detectable visually.

For many years, the typical technique was to place a 45 gram sample in a specially designed 8 ounce (240cc) glass, stoppered bottle. The sample is then placed in an oven at 65.5°C where it can be visually monitored. It is checked visually at least once each day until it becomes unstable, as evidenced by the test technician seeing the reddish brown nitrogen dioxide fumes. The test result is usually the number of days that the sample takes to fume (days to fume, DTF). As part of its implementation of the Safe Interval Prediction (SIP) test ARDEC has made a number of modifications. The test is applied in more of a pass/fail approach where the sample may be held up to 365 at 65.5°C and removed from the test if it has not fumed by that time. Additionally, the sample size is reduced to 12 grams, with a corresponding decrease in the volume of the container. See section 6.1 for more details.

If the propellants are kept at 65.5°C until they fume a typical single-base propellant would take over 1,000 DTF when new. New double-base propellants would take 500 to 1,000 DTF. As the propellant ages, the number of days to fume decreases. Then, at some point, the fume time would fall below a level that would signal the services to destroy all of their assets that contained that propellant lot. The failure criteria should allow the services a "reasonable" amount of time to safely destroy those assets. In the past, different failure criteria have been used. In 1992, the Army and Navy standardized the criteria to a single criterion: if a sample fumes in 30 days or less, it fails the stability test.

Ideally, as the oven data is monitored over time, it would present a trend that could be analyzed and safe life predictions could be made. As recently as 1995, some Navy data was reviewed by Sohn[1] where the author was able to identify definite trends and make safe life estimates for 5"/54 NACO propellant manufactured by Badger Ordnance Works. However, Ark, et. al.,[2] performed an extensive statistical analysis of ARDEC's database of oven test results for a number of propellant types: M5 (both flake and single-perf), M10 (flake, single- and multi-perf) and M28 (a rocket propellant). They concluded that a) the variability of the fume data were high, b) fume data could not be used reliably for predictive analysis and, c) the fume test should only be used to provide a pass/fail indication of propellant stability.

The advantages of the fume test are a) the test method has proven successful by over 70 years of use, b) the method uses a significantly larger amount of propellant than any of the other thermal stability tests, and c) it is currently the least expensive of the methods. The disadvantages of the fume test are a) it is not very instructive about the chemistry of propellant degradation, b) it may not yield data that can be used for predictive analysis, c) it cannot be used with triple-base propellants, and d) additional safety precautions must be used because of the quantities of propellant, high temperatures to which personnel are exposed, and noxious gases to which test personnel may be exposed.

4.1.1 Improvement Using Pressure Transducers

In the late 1980s, ARDEC undertook an effort to improve their 65.5°C test by monitoring the samples with pressure transducers. The improved method would provide pressure versus time data that might help elucidate the decomposition chemistry for the various propellant types and would make detection better quantified and more systematic. Trials with prototype equipment showed that the method would be useful. Eventually, the method was not implemented on a routine basis because a) start-up costs were estimated to be over 4 million dollars, b) a statistical failure analysis of the equipment showed that maintaining the system would be very costly for a system testing over 6,000 samples, and c) the test could generally only give a pass/fail result. As a result, ARDEC developed the SIP test method that would be more cost effective and provide more useful data.

4.1.2 Improvement Using IR Detection

In 1994 IHDIV initiated an effort to use an IR detector to improve the fume test. The goals are to make the fume test more quantifiable and systematic, and to further elucidate the chemistry of propellant decomposition. As of February 1996, equipment has been obtained and installed and preliminary data gathering is underway.

4.2 Other Thermal Stability Test Techniques

As previously mentioned, there are numerous thermal stability test techniques that are available. These include Differential Thermal Analysis (DTA), Differential Scanning Calorimetry (DSC), Thermogravimetric Analysis (TGA), heat tests involving methyl violet paper, and Microcalorimetry. These techniques are not used routinely either because the method is primarily for short-term stability (test temperatures are considered too high), or they are too costly, or both.

5. STABILIZER TEST TECHNIQUES

Over the years, there have been a number of improvements in the test techniques for determining the stabilizer concentration in propellants.

For many years, the techniques for measuring stabilizer concentration relied on some form of steam distillation extraction combined with a gravimetric, titration or spectrophotometric detection method. Over the years, improvements were made to try to overcome a variety of disadvantages associated with these techniques. The old techniques a) were very labor intensive, involving many steps in the procedure, b) generated a large amount of hazardous waste, and c) could not distinguish between different stabilizer daughter compounds (actually, the high temperatures involved in the method would have affected some of the compounds, ultimately obscuring the value of knowing what they were).

In the late seventies, ARDEC performed extraction efficiency studies for propellants using HPLC. Eventually, in the 1980's, the HPLC method was established at ARDEC as a routine method for assessing propellant stability and was later adopted by IHDIV. Today, the HPLC method has been accepted world-wide as a standard for determining stabilizer.

5.1 Extraction

The stabilizer compounds are extracted from the propellant by dissolving the propellant in a solvent, either a mixture of acetonitrile (ACN) and water or methanol and water. Usually magnetic stirrers are used to aid dissolution. Dissolution times typically take one to three days, depending upon the size and formulation of the propellant. After the propellant has been dissolved a portion of the solution is filtered through a 0.45-μm filter. Since the early 1990s, IHDIV has used equipment from Zymark to automate much of the extraction and filtration process.

Sonication can also be used to hasten extraction and this is often used. However, ARDEC found that, under some conditions, sonication can cause some of the stabilizer compounds to breakdown. Grinding the propellant can also hasten extraction, however this is rarely used. Depending upon the grinding conditions, the process of grinding can change the stabilizer derivative concentrations because of the heat from the work added by the grinding.

The recovery of stabilizer compounds is very good for new propellants. However, when propellants reach an advanced age, where numerous nitrated and nitrosated compounds are present, the recovery drops. In the past, part of this has been due to not quantifying the more heavily nitrated/nitrosated daughter compounds. Both ARDEC and IHDIV have undertaken efforts to try to improve recoveries; some are mentioned in the following sections.

5.1.1 Supercritical Fluid Extraction (SFE)

In 1991 IHDIV initiated efforts to develop SFE extraction techniques. The advantages of SFE are that the methods involve significantly less solvent waste, extraction times could be greatly reduced, and the process is less labor intensive than the current method of solvent extraction, particularly when an autosampler is used with the SFE. Thomas[3] used supercritical carbon dioxide and equipment from Hewlett-Packard and Dionex to obtain recoveries over 80% for a Navy 20mm propellant. Current work involves improving recoveries, and developing methods for larger caliber propellants.

5.2 Chromatography

ARDEC and IHDIV have successfully used HPLC equipment from a variety of instrument manufacturers: Waters, Hewlett-Packard, and Shimadzu. A typical system would also employ a quaternary pump, autosampler, a C-18 column, and a UV detector set at 254 nm. A guard column is also usually used. The HPLC is operated in reverse phase. Although normal phase HPLC methods exist, reverse phase chromatography is used exclusively in the U.S. The advantages of reverse phase HPLC are a) it uses less organic solvents, b) it provides much greater column stability than normal phase HPLC, and c) it larger number of tests per column. Costs are saved by producing less organic hazardous wastes, saving time by not having to equilibrate columns, and not having to replace columns as frequently.

5.2.1 Chromatographic Improvements

Over the years there have been continual improvements in chromatography. ARDEC and IHDIV have made improvements in the areas of a) separating and detecting different compounds, and b) quality and productivity.

Separation and detection improvements have been achieved by carefully screening the efficiency of columns, adjusting mobile phase composition to achieve good baseline separation for the stabilizer daughter products, and using improved detectors. Most recently, a mobile phase modifier has been added that has greatly increased the precision for determining diphenylamine (DPA). The additive triethylamine (TEA) prevents DPA absorption on the column. Modern detectors have assured excellent linearity and sensitivity. Some of the detectors used are able to identify one of four wavelengths for a particular peak using the wavelength that is most responsive to the compound being viewed. More recently, photodiode array (PDA) ultraviolet detection has become a routine tool for propellant surveillance. HPLC peaks can be observed using a wide spectrum of ultraviolet energy. The entire spectrum is recorded, allowing for measurements of peak purity and confirmation of peak identity.

Improvements in equipment have led to most of the improvements in quality and productivity. Modern HPLC equipment is highly automated, allowing overnight operation and a very high sample throughput. Improvements in pump flow stability and detector stability have provided increasing precision for the analytical results. Also, it has become general practice to use column heaters adjusted to about 10°C above ambient. This provides a constant environment that improves column chemistry and mobile phase flow.

5.2.2 Stabilizer Compounds

The use of chromatography created new opportunities for understanding the stabilizer chemistry in propellants, but also created a need for standards for the various daughter compounds of the stabilizers. Steroids, Ltd., through its association with the Navy, documented or developed methods for synthesizing 90 of the DPA and EC daughter compounds.[4] Additionally, ARDEC synthesizes most of the initial stabilizer daughter products and is able to provide them on a commercial basis. Both ARDEC and IHDIV now monitor DPA and 7 or more of its nitrated/nitrosated compounds. Both monitor ethylcentralite (EC) and 3 or more if its nitrated/nitrosated compounds. Both monitor Akardite.

5.2.3 Quality Control

Quality control is maintained by a disciplined use of internal and external controls. A number of HPLC tests are usually performed in series using an autosampler. A control solution is tested during each run at a frequency of every 10th injection or more frequently. Additionally, each propellant extract is spiked with an simulant standard of dimethylphthalate (DMP). Also, the use of the PDA is a powerful tool in assuring that chromatographic peaks are pure. HPLC standards and controls allow the labs to achieve less than two percent relative standard deviation for the stabilizer analyses.

HPLC columns degrade over time and must be monitored carefully. The labs have encountered different responses from columns of the same catalog number from the same manufacturer, thus replacement columns must also be checked and calibrated. Generally, columns within the same production lot behave consistently. ARDEC and IHDIV have had success with columns from a selected number of manufacturers.

5.3 Other Detection Techniques

In the mid-1980s, IHDIV explored the use of gas chromatography (GC) as a technique for measuring stabilizer compounds. The GC was later abandoned because the technique lead to denitrosation of nitroso- stabilizer compounds and because of difficulties resolving some of the peaks where compounds co-eluted.

ARDEC and IHDIV have used a wide variety of techniques to observe degradation chemistry and kinetic mechanisms. These have included nuclear magnetic resonance spectroscopy,[5] GC-mass spectroscopy and Fourier transform infrared (FTIR). Additionally, ARDEC has applied chemiluminescence techniques to observe off gassing rates and degradation kinetics. In 1994 IHDIV also initiated efforts to develop test methods using Capillary Electrophoresis (CE) and Supercritical Fluid Chromatography (SFC).

5.4 Stabilizer Data Analysis

As chromatographic techniques provided improved information about the nitrated and nitrosated stabilizer compounds, questions were raised as to which ones should be counted as effective stabilizers. Of prime concern was the stabilizing role of N-nitroso-diphenylamine (NNODPA).

All organizations recognize that NNODPA was an important compound in the series of reactions involving stabilizers. IHDIV has advocated that NNODPA be counted as effective because of its important role in the stabilizer chemistry and because recent work indicates that NNODPA converts rapidly to mononitro-DPAs.[6,7] However, ARDEC has advocated that NNODPA not be considered an effective stabilizer.

ARDEC is reluctant to count NNODPA as an effective stabilizer because a) they believed there was insufficient evidence

to prove that it reacted directly to capture a NO/NO_2 in gun propellant, b) NNODPA is thermally labile[8], and c) then-recent studies from Australia concluded that there was no evidence to support any stabilizing contribution from NNODPA.[9] For many propellant formulations, especially IMR and WC compositions, ARDEC has observed that the level of NNODPA builds to a peak at the time that about 80% of the DPA is consumed. The level of NNODPA then decreases slowly over time, converting mostly to the mononitro-DPAs. This process can span a significant portion of the safe life of the propellant. Mononitro-DPAs are counted as effective stabilizers as they are formed. While this process occurs, there is a risk for thermal denitrosation of the NNODPA if the propellant sees a rise in storage temperature. This denitrosation is very efficient and the resulting nitration potential can effect the stability of the nitrate esters present. Recent observations of a 2NDPA-stabilized double base propellant indicates that at 65.5°C the initial decrease in stabilizer may be due to dissolved nitrogen oxides and possibly to the presence of meta-stable nitroso compounds. After a period of initial stabilization, the rate of stabilizer consumption slows. Ultimately, excluding NNODPA results in a more conservative approach to assesing stabilizer data.

To try to resolve the differences an analogy has been developed: if we think of propellant decomposition as being like a house with a roof that leaks, an effective stabilizer, like diphenylamine (DPA) would be like a container that captures rain water to prevent it from further damaging the house. NNODPA would be like a container that is temporarily covered. As NNODPA converts to a mono-nitrodiphenylamine, it becomes uncovered, so it is again counted as effective.

This has led to summarizing stabilizer data using two stability indicators: Effective Stabilizer (ES) and Percent Capacity (%CAP). ES excludes NNODPA, and would correspond to the number of containers that are open and able to capture water. ES is the summed concentration of "effective stabilizers," expressed in terms of the equivalent weight percent of virgin stabilizer. %CAP, which includes NNODPA, would be a measure of how much empty capacity remains in all the cups, covered or uncovered. %CAP incorporates factors to account for the effective functionality of each stabilizer compound, then is divided by the nominal concentration of stabilizer for the formulation (also adjusted to reflect its effective functionality).

To date, the services have agreed upon a stability failure criterion for ES: a propellant sample fails the stability test when ES falls below 0.20.[10] Additionally, there are criteria using ES to help set test intervals and manage inventories.[11,12] The calculation of %CAP is a relatively recent development (owing to the advent of chromatographic techniques that measure daughter stabilizer compounds). There has not yet been an attempt to establish agreements on stability criteria for %CAP.

Currently, none of the daughter compounds of EC and Akardite are counted as "effective stabilizers," although some work on EC using HPLC has been performed.[13,14,15] ARDEC and IHDIV are collecting data for possible reevaluation in the future.

6. STABILIZER TESTING PLUS ACCELERATED AGING

ARDEC and IHDIV have also been coupling stabilizer testing with accelerated aging. Typically, propellant samples are aged at 65.5°C and tested at routine intervals to measure the rate of stabilizer depletion. The NATO STANAG 4117 test is one technique that uses this approach. In 1992 ARDEC began developing an approach for using stabilizer testing coupled with accelerated aging as a means for improving its Master Sample program. Initial work was presented as early as April 1993[16]. After many refinements, they are near to finalizing their method, which they have named the Safe Interval Prediction (SIP) test.

6.1. SIP Test

The basic laboratory approach is similar to the STANAG 4117 in the equipment and sample size. Unlike STANAG 4117, it applies to double and triple-base propellants as well as single-base propellants. Like the STANAG 4117 test, the SIP test ages propellant samples at 65.5°C. Stabilizer concentrations are determined (using HPLC) at 4 or more intervals during the aging (including time = 0). Aging intervals vary depending upon the propellant formulation. Typically, single-base and double-base propellants are tested at 14 day intervals; triple-base propellants at 56 day intervals.

Analysis of the accelerated aging data leads to a prediction of the interval of time that can be safely waited until the next test. The data are analyzed by looking only at the virgin stabilizer and applying zero-order kinetics to predict when the concentration will fall to zero. Zero order is selected because the loss in virgin stabilizer is linear with time over the concentration range observed. The resulting time interval is adjusted to account for the effective functionality of the virgin stabilizer and a conservative estimate the difference in rate of reaction between 65.5°C and "ambient." If the resultant "safe interval" is greater than 15 years, 15 years is assigned as the next test interval.

As a master sample gets older and the virgin stabilizer is converted to nitrated and nitrosated stabilizer compounds, those daughter compounds may be involved with stabilizing reactions that compete with the virgin stabilizer. This could undermine the analysis that uses only the virgin stabilizer, possibly rendering an overly optimistic test interval. The SIP test protocol addresses this by switching to more frequent testing of the ambiently stored master sample instead of performing accelerated aging and stabilizer testing. This switch would occur when the ES value for ambiently stored master sample falls below 0.30.

The SIP test also has implicit and explicit components that relate it to the 65.5°C oven test. Implicitly, the SIP test checks to see that the propellant passes the 30 days-to-fume criteria of the oven test since it requires aging the samples

for at least 30 days. Explicitly, the SIP test protocol requires that a) Master samples from new manufacture continue to be aged until they fume or have been in the oven for 365 days, and b) when the accelerated aging portion of the protocol is no longer used, a sample is aged at 65.5°C for at least 45 days (which tests for the 30 days-to-fume failure criteria) whenever the propellant is re-tested to determine stabilizer concentration.

To date, ARDEC has performed SIP tests on over 2,000 propellant lots covering 30 different propellant types. Some examples include: re-test predictions of 13 and 14 years for recently manufactured M1 propellant (a single-base propellant), 6 year re-test predictions for AHH propellant manufactured in the 1980s, and 15 year re-test intervals for some double- and triple-base propellants (DIGL-RP, M28, M31A1 and M31A1E1) whose initially calculated re-test intervals were over 20 years. In the future, there will be additional refinements to the SIP test as additional data and experience are gained.

7. ADDITIONAL INFORMATION AND HIGHLIGHTS

In addition to the items previously mentioned, the different surveillance organizations have been involved in other activities worth mentioning.

7.1 81mm Mortar Propellants

A number of the most recent designs of the propelling charges for 81mm mortars use an increment holder that is shaped like a horseshoe and is also combustible (it is close to 80% nitrocellulose). U.S. designed propelling charges called for loading increment holders with either M10 flake propellant or M38 Ball Powder© manufactured in the U.S.. The USMC also had similar 81mm mortar rounds manufactured by the U.K. that contained Ball Powder© manufactured in Belgium. During routine surveillance testing of 81mm mortar propellants, the MCPD noted that many of these increments were badly discolored (various shades of green instead of beige). Stability tests indicated that stabilizer concentrations were lower than might have been expected, raising many questions about whether the propellant was aging prematurely, and, if so, how it could be prevented in the future and how it would effect managing inventories in the future.

Further investigation determined that the increments from the U.K. rounds were not discolored, despite often being older. This also seemed to absolve the combustible increment holder from culpability since some lots of increment holders had been used on both U.S. and U.K. rounds. Stability testing by ARDEC and IHDIV determined that M38 propellant from mortar rounds were aging more rapidly than the corresponding master samples, implying that there were some environmental conditions related to the loaded configuration that caused premature degradation, rather than the M38 propellant alone.

There were subsequent investigations that attempted to identify the conditions that caused premature propellant degradation, including a) reviews of the different designs, b) reviews of the different facilities where the components were stored or assembled, c) reviews of storage conditions where the ammunition had been (some had been in the Persian Gulf region during Operation Desert Storm), and d) accelerated aging testing on various components. The different efforts have led to measures to a) better control the environment during manufacture, b) improve packaging design, c) improve the design of the M38 propellant, d) prioritize inventories for use during training, and e) increase scrutiny of 60mm mortar ammunition that employ combustible increment holders.

7.2 M55 Rocket Motor

ARDEC Surveillance in the mid 1980's became involved in the M55 Chemical Rocket Program when the ARMY made a decision to demilitarize its chemical munitions inventory. It was soon apparent that the destroying of the chemical rockets would be a long and potentially controversial program. There was a need to properly assess the safe life of the M28 propellant contained in the M55 rocket motor. Under study by Hercules, directed by ARDEC, the chemical degradation kinetics for M28 propellant was established. Subsequently, ARDEC identified an incompatibility with a chemical agent simulant which has led to further studies by the chemical demil community. Currently, ARDEC is applying its chemical kinetic SIP procedures to establish accelerated aging rates for these munitions to support an assessment of their safe storage life.

7.3 Desert Storm

After the Desert Storm conflict, ARDEC, MCPD and IHDIV became heavily involved in efforts to assess the effect of short and long term storage of munitions stored under severe desert conditions. ARDEC performed hundreds of stability assessments on samples from Desert Storm. To date, ARDEC has observed only small effects on stabilizer depletion for ammunition exposed to short durations of desert storage conditions. Continued support by ARDEC Surveillance will allow a more comprehensive understanding of the long term effect on the desert-stored munitions and will promote economic use of these unique assets.

The USMC, because of the nature of their mission and their inventories, needed to know that the ammunition that was returned to their ships would be safe to store for a number of years. MCPD and IHDIV personnel worked together to assemble a field lab in the deserts of Saudi Arabia. There, they overcame adverse environmental conditions (heat, tent accommodations, and very fine sand everywhere) to perform tests and obtain data on over 500 ammunition lots.[17] The MCPD continues to closely monitor assets that had been involved with Operation Desert Storm.

7.4 New IHDIV Laboratory Facility

In 1994 and 1995 IHDIV constructed a new laboratory, replacing some of the buildings (some which were originally barracks and classrooms) with modern facilities. The Elizabeth Luster Whitman laboratory provides many test functions in addition to testing for gun propellant safety surveillance.

7.5 ARDEC Operations and New Surveillance Facility

Over the past few years, ARDEC has made a concerted effort to apply total quality management concepts to its operations. They have implemented a computer-based tracking system to control the sample from the time it is received from the field, through storage and testing and final reporting. With the help of the laboratory management's minicomputer, approximately eight to nine thousand samples are subjected to analysis annually. With the advent of new computerized data management techniques, ARDEC is now making efforts to provide their customers with "on-line" access to surveillance information over the Internet. In addition to many "incremental" process improvements, ARDEC is also in the process of implementing a new surveillance facility.

In 1995 ARDEC broke ground on its new surveillance facility. In addition to providing modern lab facilities, it consolidates surveillance functions that have been dispersed throughout the ARDEC facilities. This facility will be devoted to gun propellant safety surveillance and has been designed to improve efficiency and for future automation of the SIP test. ARDEC anticipates it will be in full operation some time in 1996.

7.6 The Wider Surveillance Community

Although the focus of this paper has been on safety surveillance of gun propellants, ARDEC, IHDIV and MCPD are also involved with life cycle performance surveillance for many types of military ordnance, including rockets, missiles, explosives, cartridge actuated devices, propellant actuated devices, etc. Additionally, ARDEC and IHDIV have been very active in providing technical support to a wide range of demilitarization efforts to both military and contractors. Both labs provide active support for establishing analytical procedures for propellant testing, including on-site training and consultation.

MCPD, IHDIV, ARDEC and the Industrial Operations Command (IOC), at Rock Island, Illinois, serve on the Joint Propellant Safety Surveillance Board, which is under the auspices of the Quality Assurance Sub-Group of the Joint Ordnance Commanders Group (JOCG). This panel was established to address propellant safety assessment concerns on a national level and to provide technical review of methods and criteria.

MCPD, IHDIV, ARDEC and the IOC are a part of the larger surveillance community that, for the Army and Navy, includes: the Aberdeen Proving Ground at Aberdeen, Maryland, the Army Missile Command (MICOM) at Huntsville, Alabama, Lake City Army Ammunition Plant at Independence, Missouri, the Naval Ordnance Center (NOC) at Indian Head, Maryland, the Weapons Quality Engineering Center (WQEC) at Concord, California, the NSWC/Crane Division at Crane, Indiana, and the Naval Air Warfare Center (NAWC) at China Lake, California.

---

[1] Sohn, S.Y., "Shelf-life Estimation of Gun Propellant Stockpile," *Reliability Engineering and System Safety*, **49** (1995), 37-46.

[2] Ark, W. F., C. Eccles, and D. Robertson, "Statistical Analysis of ARDEC's Fume Data Base," 1993 JANNAF PDCS Meeting, 153-162.

[3] Thomas, B. P. and T. R. Willson, "Evaluation of Supercritical Carbon Dioxide as an Extraction Media for Gun Propellants," 1994 JANNAF PDCS Meeting, 81-90.

[4] Moriarty, R.M., "Synthesis of Propellant Stabilizers: Nitrodiphenylamines, N-Nitroso-Nitrodiphenylamines, Nitrocentralites, and Labelled Derivatives," IHCR 95-48, May 95.

[5] Bulusu, S., et. al., "Role of N-nitrosodiphenylamine in the Stabilization of Nitrocellulose-based Propellants: A Preliminary Study Using ^{15}N-NMR Spectroscopy," ADPA 5th Int Gun Propellant & Propulsion Symp., 498-508 (1991).

[6] Moriarty, R.M., et.al., "Reaction of Diphenylamine (DPA) and N-Nitroso Diphenylamine (N-NO-DPA) with NO_2 in Cellulose," ADPA 5th Int Gun Propellant & Propulsion Symp., 481-497 (1991).

[7] Lussier, L.S., and H. Gagnon, "Stability Evaluation of DPA-Stabilized Gun Propellants," ADPA 6th Int Gun Propellant & Propulsion Symp., 16pp (1994).

[8] ibid 5.

[9] Curtis, N.J., "Isomer Distribution of Nitro Derivatives of Diphenylamine in Gun Propellants: Nitrosamine Chemistry," *PEP **15***, 222-230 (1990).

[10] "Propellant Safe Storage Life Criteria," DOD 5160.65-J, Appendix J (1/94).

[11] "Propellant and Propelling Charges: Ammunition Surveillance Procedures," Army SB 742-1300-94-895 (3/95).

[12] "Marine Corps Gun Propellant Surveillance Criteria," Dec. 93.

[13] Drew, W.T., "Characterization of Ethyl Centralite Derivatives," 1994 JANNAF PDCS Meeting, 91-100.

[14] Curtis, N.J., and P. Berry, "Derivatives of Ethyl Centralite in Australian Gun Propellants," *PEP **14***, 260-265 (1989).

[15] Druet, L. and J. Angers, "LC/MS Studies of Ethyl Centralite Stabilized Propellants," *PEP **13***, 87-94 (1988).

[16] Ark, W.F., and D.G. Robertson, "Treatment of Accelerated Aging Data Using First Order Reaction Equations," 1993 JANNAF PDCS Meeting, 163-172.

[17] Stine, G.Y., "Have LC Lab, Will Travel: Testing Propellant Stability after Operation Desert Storm," *Analytical Chemistry*, **64**, no. 7, Apr 92.

Paper Number: 17
Discussor's Name: O. Ruault
Responder's Name: D. Lee

Question: Pourriez-vous rexpliquer la notion de % de capacite et nous indiquer comment vous l'expliquez?

Question: Can you explain the notion of % capacity and indicate how you use it?

Answer: REVIEW OF STABILITY INDICATORS FROM STABILIZER TEST DATA

1.0 OBJECTIVE: The objective of these notes is to provide a review of how stabilizer test data can be, and are being assessed by the U. S. Navy and Army.

2.0 BACKGROUND: Currently, the Navy and the Army use High Performance Liquid Chromatography for determining stabilizer concentration in gun propellants with nitrate esters. For the Navy, we calculate the following stability indicators based upon the data:

a. Effective Stabilizer (ES)
b. Effective Stabilizer plus N-nitrosodiphenylamine (ESNNO)
c. Estimated Percent Capacity (%CAP)

Additionally, the Army has used another stability indicator for some evaluations:

d. Addition of Functional Groups (F)

The calculations for each of these stability indicators is provided in later sections, with additional comments about the stability indicator. Here is an excerpt from the AGARD paper to provide an analogy of how they might be viewed.

To try to resolve the differences an analogy has been developed: if we think of propellant decomposition as being like a house with a roof that leaks, an effective stabilizer, like diphenylamine (DPA) would be like a container that captures rain water to prevent it from further damaging the house. NNODPA would be like a container that is temporarily covered. As NNODPA converts to a mono-nitrodiphenylamine, it becomes uncovered, so it is again counted as effective.

This has led to summarizing stabilizer data using two stability indicators: Effective Stabilizer (ES) and Percent Capacity (%CAP). ES excludes NNODPA, and would correspond to the number of containers that are open and able to capture water. ES is the summed concentration of "effective stabilizers", expressed in terms of the equivalent weight percent of virgin stabilizer. %CAP, which includes NNODPA, would be a measure of how much empty capacity

remains in all the cups, covered or uncovered. %CAP incorporates factors to account for the effective functionality of each stabilizer compound, then is divided by the nominal concentration of stabilizer for the formulation (also adjusted to reflect its effective functionality).

Incidentally, in the leaky roof analogy, Addition of Functional Groups (F), would be like the total amount of water captured.

3.0 EFFECTIVE STABILIZER (ES)

3.1 Calculation of ES: The calculation of ES varies depending upon the stabilizer.

3.1.1 Calculation of ES for DPA-stabilized propellants

ES=DPA+(a/b)*(mononitroDPA)+(a/c)*(dinitroDPA)

DPA,mononitroDPAs & dinitroDPAs are expressed in terms of weight percent of the compound present

a=molecular weight of DPA

b=molecular weight of mononitroDPAs

c=molecular weight of dinitroDPAs

The ratios of the molecular weights are used to correct the DPA daughter products to be expressed as DPA-equivalents

3.1.2 ES Calculation for propellant stabilized with 2-NDPA

ES=2NDPA+(b/c)*(dinitroDPAs)

2-NDPA & dinitroDPAs are expressed in terms of weight percent of the compound present

b=molecular weight of 2-NDPA

c=molecular weight of dinitroDPAs

The ratios of the molecular weights are used to correct the 2-NDPA daughter products to be expressed as 2-NDPA equivalents

3.1.3 ES Calculation for EC, Akardite or EC+Akardite stabilized propellants

ES=EC+Akardite

Ethylcentralite (EC) and Akardite are expressed in terms of weight percent of the compound present

3.2 Comments about ES: To a certain extent, ES is a carry-over from when titration techniques (e.g. bromination) were used to determine stabilizer concentration. Those techniques usually did not determine the concentrations of each of the stabilizer compounds but, instead, yielded a single number. With the use of chromatographic techniques, we have been able to accurately measure the nitrated and nitrosated species of stabilizer compounds. This has led to a great deal of discussion and experimentation to try to determine how the "daughter" compounds effect the stability of

propellants. The value, ES, is the summation of the stabilizer compounds that both the Army and Navy agree are "effective" stabilizers (expressed in terms of the weight percent of the original stabilizer). None of the nitrosated daughter compounds are included, although the Navy believes N-nitroso-DPA should be considered an effective stabilizer. At this time, we are gathering test data for daughter compounds for ethylcentralite and akardite.

The two services have agreed that propellant that has an ES level of 0.2, or below, can be considered a good candidate for demil due to stability concerns. The 0.2 value is based on a mixture of assessing available data, logistic concerns, and administrative expediency. Some of the logistic concerns are: a) how long it would take for the various facilities to actually demil the propellant and ammunition, and b) how representative the sample actually is for the inventory it is supposed to represent. Ideally, we would be able to characterize the rate of decomposition of each propellant type to determine failure criteria that are based more on kinetics.

4.0 EFFECTIVE STABILIZER PLUS N-NITROSODIPHENYLAMINE (ES+NNO)

4.1 Calculation of ES+NNO

ES+NNO=ES+(a/d)*NNODPA

N-nitroso-DPA is expressed in terms of weight percent of the compound present

a=molecular weight of DPA

d=molecular weight of NNODPA

The ratios of the molecular weights are used to correct the DPA daughter products to be expressed as DPA-equivalents

4.2 Comments. This stability indicator is only relevant for propellants stabilized with DPA. Neither service really uses this stability indicator any more. It can serve as a rough estimate of the "recovery" of stabilizer compounds for DPA-stabilized propellants. We are trying to improve our processes to get better recovery of the stabilizer compounds for older propellants (it is not uncommon for recovery to be less that 50% for propellants that are over 40 years old). Partial recovery is due to a combination of the following: a) we do not quantify for all of the stabilizer daughter products, b) we might not be getting 100% extraction, and c) some of the stabilizer might be migrating outside the propellant grain (particularly for propellants with nitroglycerine, which is relatively mobile).

5.0 ESTIMATED PERCENT CAPACITY (%CAP)

5.1 Calculation of %CAP. The calculation for %CAP varies depending upon which stabilizer is used.

5.1.1 Calculation of %CAP for DPA-stabilized propellants

$$\%CAP = 100 * \frac{3*DPA + 2*[(a/b)*mononitroDPA_t + (a/d)*NNODPA_o] + (a/c)*dinitroDPA_t) + (a/e)*(NNO\text{-}mononitroDPA_t)}{3*DPA_o + 2*[(a/b)*mononitroDPAs_o + (a/d)*NNODPA_o] + (a/c)*(dinitroDPA_o + (a/e)*(NNO\text{-}mononitroDPA_o)}$$

Stabilizer compounds are expressed in terms of weight percent of the compound present at time=t for the numerator, or time=0 for the denominator.
a=molecular weight of DPA
b=molecular weight of mononitroDPAs
c=molecular weight of dinitroDPAs
d=molecular weight of NNODPA
e=molecular weight of N-nitroso, mono-nitroDPAs

5.1.2 %CAP Calculation for propellant stabilized with 2-NDPA

$$\%CAP = 100 * \frac{2*2NDPA_t + (b/c)*(dinitroDPA_t) + (b/e)*NNO) - 2NDPA_t}{2*2NDPA_o + (b/c)*(dinitroDPA_o) + (b/e)*NNO - 2NDPA_o}$$

Stabilizer compounds are expressed in terms of weight percent of the compound present at time=t for the numerator, or time=0 for the denominator.
b=molecular weight of 2-NDPA
c=molecular weight of dinitroDPAs
e=molecular weight of N-nitroso, 2-nitrodiphenylamine

5.1.3 %CAP Calculation for EC, Akardite or EC+Akardite stabilized propellants:

$$\%CAP = 100 * \frac{EC_t + Akardite_t}{EC_o + Akardite_o}$$

Stabilizer compounds are expressed in terms of weight percent of the compound present at time=t for the numerator, or time=0 for the denominator.

5.2 Comments on %CAP. For propellants stabilized with DPA or 2-NDPA, %CAP is based upon the idea that the DPA compounds lose their effectiveness once they have 3 nitro/nitroso groups attached. Thus, dinitroDPA and NNO-mononitroDPAs would have a stabilizing

capacity of 1 since they only have one remaining site before losing their effectiveness. NNODPA and mononitroDPAs would have a stabilizing capacity of 2 since they have two remaining sites; DPA molecule would have a stabilizing capacity of 3. Since HPLC data are rendered in terms of weight percent, we adjust the daughter products by the ratio of molecular weights.

For propellants stabilized with EC and/or Akardite, we currently view them as having a stabilizing capacity of 1. In our limited studies of EC, we have seen where some of the EC daughter products will further nitrate or nitrosate, but we have not decided whether to include them as effective stabilizers.

One of the nice features about %CAP is that it normalizes stabilizing capacity. Theoretically, this should make it easier to comprehend the test result and to compare rates of stabilizer consumption when comparing different types of propellant. Currently, there are no criteria for %CAP for assessing stability, so these calculations are made mainly for informational purposes.

One of the shortcomings of %CAP is that the values of the stabilizer compounds at time=0 are not always known. In practice, we assign the nominal value of the compounds when known values are not available.

6.0 ADDITION OF FUNCTIONAL GROUPS (F). F is essentially a count of the number of nitro or nitroso groups that have been captured by the stabilizer compounds.

6.1 Calculation of F. F expresses the number of nitro/nitroso groups in terms of weight percent of the original stabilizer. The calculation of F varies depending upon the primary stabilizer used. I have only listed the calculation for DPA-stabilized compounds. I think the reader will be able to develop the calculation of F for other stabilizer compounds.

F_{DPA} = (a/b)*(mononitroDPA)+(a/d)*NNODPA
+2*[(a/c)*dinitroDPA)+(a/e)*(NNOmononitroDPA)]
+3*[(a/f)*(trinitroDPA)+(a/g)*(NNOdinitroDPA)]
+4*[(a/h)*(tetranitroDPA)+(a/k)*(NNOtrinotroDPA)]
+5*[(a/m)*(pentanitroDPA)+(a/n)*(NNOtetranitroDPA)
+6*[(a/p)*(hexanitroDPA)+(A/q)*(NNOpentanitroDPA)]
+7*[(a/r)*(NNO-hexanitroDPA

6.2 Comments about F. In the few instances where F has been used, it has been used as a technique for evaluating data from accelerated aging tests. It is

used to assess the rate of decomposition of the nitrate ester as much as being used as a way to measure the rate of stabilizer consumption. one concern about getting data for F is that one would need to obtain complete extraction of the stabilizer compounds. In our experience, this becomes more difficult (perhaps impossible) for very old propellants. Also, one would need to have analytical standards for the various daughter compounds and would need to have analytical procedures set up to be able to distinguish between the different compounds on the chromatogram. In practice, the propellants are usually destroyed long before it becomes highly nitrated/nitrosated.

7.0 MISCELLANEOUS COMMENTS

One of the shortcomings of ES is that it does not value the stabilizing potential of DPA molecules differently than nitrated DPA molecules. I think we would all expect gun propellant with 0.5 wt% DPA to be stable longer than gun propellant with 0.766 wt% dinitroDPA (the same number of stabilizer molecules as the 0.5 wt% DPA), assuming all other aspects of the propellant are the same. %CAP tries to remedy this shortcoming. In practice, the Navy looks at both of these stability indicators and also at the results of thermal stability tests (oven tests) in making stability assessments.

None of the previous calculations overtly addresses rates of reaction. The assumption is that the chemical reactions in question happen relatively quickly in comparison to the rate of decomposition (denitration or denitrosation) of the nitrate ester. If the rate of decomposition of the nitrate ester were faster than the rate of stabilization of a given compound, the compound(s) would not really be an effective stabilizer. NNO compounds are a little different in that recent research indicated that NNO compounds must first be converted to a nitro compound (without the nitroso group) before it can act as a stabilizer. In this case, the assumption is that this conversion process takes place at a quick enough rate such that the nitro compounds are available when they are needed. We do not know the process(es) for this conversion with certainty. In the past, others have speculated that it might be a Fisher-Hepps rearrangement or perhaps a free radical reaction. Perhaps there are a variety of reactions that might take place, and that might take place at different stages of propellant decomposition/stabilization. Currently, we do not have the funding to perform the research to investigate these questions.

None of the previous calculations are currently being used in the Army's Safe Interval Prediction (SIP) test. The SIP test considers only the concentrations of original stabilizer, which it applies in calculations based upon zero-order kinetics.

Former and modern methods for the determination of the service life of rocket propellants

G. Holl*, S. Wilker*, M. Kaiser*, P. Guillaume #

* Bundesinstitut für chemisch-technische Untersuchungen beim BWB (BICT)
Großes Cent, D-53913 Swisttal, Germany

PB Clermont S.A., Rue de Clermont 176, B-4480 Engis, Belgium

Abstract

Different methods that are nowadays used to determine the service life of a propellant are briefly introduced and discussed. In the second part selected results of classical high temperature tests, heat flow calorimetry, stabilizer consumption and molecular mass depletion as well as NMR experiments are presented. In summary it can be stated, that only a combination of many different methods allow to make predictions of the ballistic life time of a propellant. To do this still a huge amount of experiments must be done to define the „allowable" limits of energy loss, of stabilizer consumption, of migration processes or changes in mechanical properties.

1 Introduction

The service life of rocket propellants is - besides ballistic performance, low signature and low vulnerability - one of the most important factors that describe their usability [1]. On the one hand there is the (theoretical) possibility of self-ignition, leading to a disastrous destruction of the surroundings, which can be described by the term „**chemical stability**". This is generally fulfilled with new propellants. On the other hand there is a slight loss of the energy content (due to slow chemical decomposition reactions) which leads to a change of the interior ballistic behaviour and probably to a decrease of the mechanical properties [2]. This problem can be collected under the item „**ballistic stability**", which usually is much shorter than the chemical stability and thus of much greater importance. A third way a propellant can be ageing is the diffusion of e.g. nitroglycerine from or to the surface of the propellant which leads to a change in ballistic behaviour which makes it also become a part of the ballistic stability. Although these migration processes may play an important role in the „ballistic service life" of a propellant (they even might be the limiting factor if one thinks about the ingredients of the isolation of double base rocket propellants [2b]), they are not discussed in this paper.

It is very important to calculate the service life of rocket propellants after their production, but it is rather a hard job to do it, because the ageing of the propellant has in most cases to be simulated at elevated temperatures and afterwards extrapolated onto ambient temperatures [3]. As mentioned before, chemical ageing can be accompanied by a loss of energy because e.g. nitrocellulose is slowly generating NO_2 or by changing of the mechanical properties due to reactions of binders (e.g. reaction of the double bonds in HTPB with oxygen [4]). In this paper we present former and modern methods which are used to determine the stability of propellants (especially double base rocket propellants), although with most of them no exact determination of the life time can be made at all.

Paper presented at the AGARD PEP Symposium on "Service Life of Solid Propellant Systems" held in Athens, Greece, 10-14 May 1996, and published in CP-586.

2 High temperature tests

One of the oldest high temperature test is the Dutch weight test [5], which can be performed within 72 hours. The principle of this test is the measurement of the weight loss at elevated temperatures (105°C for double base propellants). The weight loss is determined by subtracting the first eight hours' weight loss (this is due to the evaporation of volatiles) from the total weight loss. Typical results for highly-nitrated Nc/40 % nitroglycerine mixtures are 1.2 - 1.6 %. The test is performed in stoppered glass vessels, the amount of propellant needed is 4 g.

Another test at elevated temperatures is the Bergmann-Junk-Test [6]. The sample is heated to 115°C for 16 hours (double-base propellants) and the nitrogen oxides are dissolved in a H_2O_2 solution and afterwards determined by titration with NaOH. Typical results are about 10 - 15 ml n/100 NaOH/g.

The third high temperature test that is usually performed in the BICT is the weight loss test at 90°C [7]. Compared with the other two tests described above it has two little advantages. The first is the temperature (which is a bit lower than the temperature of the other tests), the second is that the run of the experiment is recorded for about 3 weeks so that the beginning of autocatalysis can be relatively exactly determined. For double base propellants it should not begin within the first 18 days.

But all three tests don't give you sufficient information of the chemical or the service life of the propellants because for a kinetic approach at least 3 different values at 3 different temperatures have to be recorded. In addition, for all 3 tests the test temperature is too high to make a correct calculation for ambient storage temperatures (normally below 30°C). By comparing the results from the 3 tests it can mostly be found, that there is no good correlation between them [8].

Table 1 gives a small impression of the limit values of the classical high temperature tests for double base propellants in Germany today. As can be seen there is no correlation between the different tests and even no dependence on the nitroglycerine content of the propellants. Most of the values are grown historically by transferring the data from one propellant to a newer one.

Table 1: Comparison of limit values of different double base propellants at different high temperature tests

propellant type	Ngl-/DEGN-content	Bergmann-Junk	time	Dutch weight test	weight loss at 90°C; 3%
	[%]	[ml]	[h]	[%]	[days]
GK 5030-13	9,0/-	10	16	0,8	> 18
HK 5250-13	9,5/-	10	16	_·_	_·_
GK 5640-13	12,5/-	12,5	16	2,0	_·_
K 5140-13	18,0/-	10	16	1,5	_·_
K 6210-13	20,0/-	12,5	16	1,2	_·_
NPP 10	21,5/-	12,5	16	2,0	> 18
F 5600-33	25,0/-	6,5	8	_·_	info > 10
K 5310-13	26,0/-	15	16	1,5	_·_
I 5420-12	-/36,7	_·_	_·_	1,0	> 18

Table 1 (continued)

propellant type	Ngl-/DEGN-content	Bergmann-Junk	time	Dutch weight test	weight loss at 90°C; 3%
	[%]	[ml]	[h]	[%]	[days]
F 5410-12	39,2/-	12,5	16	2,0	_·_
F 5410-25	39,2/-	12,5	16	2,0	_·_
F 5620-25	39,2/-	_·_	_·_	2,0	> 18
L 5460-12	14,9/24,8	_·_	_·_	1,0	> 18
F 6510-31	40,0/-	6,5	8	2,0	> 16
H 5540	40,6/-	12,5	16	2,0	> 18
H 5720	41,0/-	12,5	16	2,0	_·_
D 7170	41,7/-	12	16	2,0	_·_
H 6110	44,0/-	6,5	8	_·_	_·_
H 6120	44,0/-	6,5	8	_·_	_·_
FH 6140	44,0/-	6,5	8	_·_	_·_
H 5180-12	44,8/-	_·_	_·_	1,3	_·_

_·_: no criteria defined
info: value only informative

Surveillance test (65.5°C)

The German Army performs this test [9] to evaluate the exact life time of propellants at the WTD 91 at Meppen. The propellants are stored under ambient conditions (21°C) and a sample of 45 g of each lot is transferred into an oven that is heated to 65.5°C. The time until yellow fumes are observed is then recorded. When the time until the yellow fumes appear decreases significantly, then this propellant lot is said to be less stable; the ammunition which contains this propellant lot is then used up preferably or destroyed for safety reasons.
Stable propellant lots normally show NO_x-generation at 65.5°C after 300 - 600 days so this test cannot be used for rapid analysis purposes. So if these stable propellants are stored at 21°C a rapid decrease in the time until the yellow fumes appear can be expected after 10 - 30 years.

3 Fundamental Stability Tests

3.1 DSC

Differential Scanning Calorimetry (DSC) is a technique in which the heat generation of a sample is measured as a function of temperature [8]. The sample and a reference material are facing the same ambient temperature. With increasing temperature decomposition reactions start which can then be recorded as exothermic or endothermic signals. In the BICT DSC technique is not used for the evaluation of safe storage times but the possibility of getting the decomposition temperature and -energy is widely used.

3.2 Heat flow calorimetry

Heat flow calorimetry (or microcalorimetry) is one of the most useful techniques in the field of prediction of the service life of

(rocket) propellants [10, 11]. It has three advantages:

a) The temperature at which the measurements are conducted (80-30°C) are much lower than those of the „classical" stability tests;
b) The sensitivity of modern calorimeters is very high, so that heat flows at or even below 1 µW can be measured reproduceably;
c) The fundamental principle that all chemical or physical reactions, which produce heat are recorded during the whole measuring time.

If the kinetics of decomposition is known (normally there is a zero order kinetics), then the activation energy and the preexponential factor of the decomposition reaction can be calculated. It can be observed that normally a change in the activation energy and the preexponential factor occurs at about 60°C.

Although the kinetics of the decomposition reaction can be calculated very precisely it is difficult to evaluate the ballistic life time from these data, because one has to know the maximum loss of energy of the rocket propellant that still delivers an acceptable ballistic behaviour. For gun propellants normally a value of 3 % energy loss is estimated [12] but there is much work to do to make exact estimations if it is ever possible.

Heat flow calorimetry is not always applicable with composite rocket propellants or double base propellants containing HTPB or comparable binders (CMCDB propellants), because of heat generating reactions within the binder materials that might cover the heat generation due to the decomposition of the propellant.

In future it is also planned to combine heat flow measurements with pressure measurements using special pressure measuring cells.

3.3 Stabilizer consumption (HPLC)

The decomposition reaction of propellants normally produces NO resp. NO_2 which are absorbed by aromatic amines to give nitro derivatives [13]. Much work has been done in this field [14]. The propellant is heated for a period of time at elevated temperatures (normally between 50°C and 80°C) and the consumption of stabilizers is recorded as a function of time. If the kinetics of this process is known then activation energies and preexponential factors can be calculated. Whereas this method is quite easy to be carried out since HPLC techniques are well-established it has the disadvantage that it lasts too long (about 3-4 months below the kinetics change at 60°C) so that it cannot be used for routine controls in production sites.

A standardized procedure for the determination of the activation energy from stabilizer consumption data has been developed by the STANAG 4527 (formerly 4480) working group [15].

3.4 Molecular mass depletion (GPC)

The depletion of the average molecular mass of nitrocellulose is accompanying the stabilizer consumption because the same decomposition (primarily the generation of NO_2) are enforcing both phenomena [16]. Because GPC methods are not as well worked out as HPLC techniques and the standard deviation in GPC is much higher than in HPLC small changes in molecular weight cannot be detected accurately. Up to now there is no generally accepted limit value to which the molecular weight of the nitrocellulose may be reduced until their performance is no more acceptable.
This method is not useful for HTPB or GAP containing propellants.

Table 2: Comparison between different selected methods for stability testing of propellants

Name of test	temperature [°C]	amount [g]	duration [d]	advantages	disadvantages
Dutch weight test	105	4	4	can be readily done;	only a decision between „good" and „bad" pro-
Bergmann-Junk-test	115	5	1	introduced for a very long time	bably depending on surface agent (cf. chapter 4).
Weight loss test	90	5	20	no big costs	No exact estimation of life time possible
Surveillance test	65.5	45	300-600[a)] 10-50 yrs	control of the real life time of a propellant; storage under ambient conditions	lasts too long, no calculation of kinetics possible, only visible control (NO_x-generation)
DSC	50-250	< 1	1	makes estimations about decomposition temperature and -energy possible	not used for life time calculations; not very sensitive
heat flow calorimetry	40-80	2-3	15-30	Exact determination of kinetical factors; very sensitive method; calculation of life time possible	mostly used for Nc-based propellants; apparatus very expensive; no knowledge about the dependence between energy loss and ballistic behaviour
stabilizer consumption	50-80	> 20	15-500	Exact determination of kinetical factors possible if measured <60°C; method well-worked out	Needs too long time to give exact results. Not very sensitive if the stabilizer consumption just starts
molecular mass deptetion	50-80	> 20	15-500	Determination of kinetical factors, probably possible direct observation of the NC chain cleavage	Method is not very sensitive. Needs too long to give good results. No dependence between molecular mass depletion and ballistic behaviour known.
chemiluminescence	25-150	depends on sample preparation and system used		direct observation of nitrogen oxides in dependence of the temperature	Apparatus expensive; no direct correlation between NO_x production and ballistic behaviour known. Must do other experiments (e.g. stabilizer consumption)
thermogravimetry	100-300	< 1	1	very sensitive method to determine activation energies by different heating rates	Temperature range too high for propellants; apparatus quite expensive; not useful for DB-propellants

a) for each test at 65.5°C

3.5 Chemiluminescence

This technique has the advantage that the primary decomposition product (NO_x) can easily be detected in dependence of the temperature of the sample and the atmosphere around it [17]. But it is not very widely used, probably due to the high cost of these apparatus.

3.6 Thermogravimetry

Thermogravimetry is one of the most sensitive techniques in thermoanalysis if used in isothermal experiments. Weight losses of about 0,1 µg can reproduceably be detected. A variety of new methods has been developed to calculate kinetic data of is widely decomposition reactions of explosives [18]. Whereas it used for stability analyses of primers and high explosives it is only rarely applied to propellants, because problems may arise from volatile compounds like DEGN or nitroglycerine.

Table 2 shows a comparison of all described tests for their usefulness to determine the ballistic service life.

4 Results

4.1 Classical tests

Within a series of different double base propellants containing different amounts of surface agents all classical tests are conducted and a markedly dependence of the results from the nature of the surface agent could be observed (table 3). So there is a big difference in test results only depending from the surface agents - because all propellants were made from the same batch!

Table 3: Classical tests results of double base propellant K 6210[1]

TLP\surface agent	with DPA in surface			with N-NO-DPA in surface			without DPA/N-NO-DPA in surface		
Test	1	2	3	1	2	3	1	2	3
without KNO_3	0.6 %	**52 d**	*8.2 ml*	1.1 %	**20 d**	*7.3 ml*	0.6 %	**21 d**	*8.6 ml*
with KNO_3 Lot 219:	2.0 % -	**15 d**	*12.5 ml*	1.4 % -	**22 d**	*8.0 ml*	1.5 % 1.2 %	**17 d** **13 d**	*12.1 ml* *13.0 ml*

1 Dutch-weight-loss-test at 105°C - limit value 1.2 %

2 **90°C-weight loss test - limit value 18 days**

3 *Bergmann-Junk-test at 115°C - limit value 12.5 ml*

There seems to be a negative interaction between KNO_3 and DPA, but not between KNO_3 and N-NO-DPA. Only the classical tests showed this extreme pattern. In heat flow calorimetry the samples containing KNO_3 and DPA were acceptably stable (ballistic life time calculation > 15 years at 30°C).

The full report about these and more investigations in this field will be presented at the forthcoming (27.) ICT Conference in July 1996 by Dr. Guillaume [19].

[1] All propellants are stabilized with 0.9% DPA/N-NO-DPA. Underlined = limit value reached

4.2 Heat flow calorimetry

Several double base rocket and gun propellants had been studied in the isothermal heat flow calorimetry at the BICT. The values of constant heat production rates are taken for the calculation of the activation energy and the preexponential factor by using a zero order Arrhenius kinetics (1) [10].

$$q = A * e^{-\frac{E_a}{R*T}} \qquad (1)$$

The calculation of ballistic service life follows equation (2).

$$t_{30} = \frac{0.03 * Q_{ex}}{q_{303} * 86400 * 365.25} \qquad (2)$$

The following table 4 gives an overview of the microcalorimetric results [20].

Table 4: Heat flow calorimetry of double base propellants

Propellant	NG-content	Specific heat production rate [µW/g]				
	[%]	80°C	70°C	60°C	50°C	40°C
78 CDB 923 [a]	/	69	28	8,0	2,4	0,68
91 DBE 490 [a]	/	18	3,8	0,7	[c]	[c]
Nike Herkules [a]	25	15	4,1	1,7	0,8	0,43
D 7030 [a]	36	19	3,5	1,6	1,0	0,56
GK 5640 [b]	12	16	4,8	2,4	1,2	0,63
K 6210 [b]	20	70	23	6,9	2,1	0,61

a) BICT-calorimeter b) TAM-calorimeter c) heat production rate too small to be measured

From these data all kinetic data including the time until at loss of 3 % of the energy content at 30°C occurs can be calculated (table 5).

Table 5: Kinetic results of heat flow calorimetry

Propellant	activation energy [kJ/mol]		preexponential factor [W/kg]		ballistic
	higher [a]	lower [a]	higher [a]	lower [a]	service life
	temperature range		temperature range		[years]
78 CDB 923 [b]	109		$9{,}8 \cdot 10^{14}$		28
91 DBE 490	190	[c]	$1{,}9 \cdot 10^{26}$	[c]	approx. 100
Nike Herkules	153	70	$6{,}3 \cdot 10^{20}$	$3{,}6 \cdot 10^{6}$	16
D 7030	170	44	$3{,}0 \cdot 10^{23}$	$1{,}2 \cdot 10^{4}$	10
GK 5640 [d]	122	70	$1{,}7 \cdot 10^{16}$	$2{,}7 \cdot 10^{8}$	16
K 6210 [e]	116	105	$1{,}0 \cdot 10^{16}$	$2{,}5 \cdot 10^{14}$	25

a) above or below 60°C, respectively b) no change in activation energy
c) no values available d) lot 11 e) lot 219

In all cases except the second a change in the kinetics at about 60°C degrees could be observed which divides the plots in a higher and a lower temperature range. **The impossibility of obtaining data below 60°C** with the propellant 91 DBE **leads to a „wrong" life-time calculation.**

Generally the error in life time calculation depends on the correctness of the measurement of the specific heat production rates. If you have errors in recording the heat production rates at lower temperatures, which can easily happen if you don't wait long enough with the calibration, your room temperature is not constant or you have slight changes in your sample preparation, then you can easily calculate different data for the ballistic service life.

The following is an example, where you can see, how little changes in double measurements of 11% (which are quite common at 60 or 40°C) can affect the value of ballistic life time.

Table 6a. Experimental heat flow values at lower temperatures (DB-propellant)

temperature	lower value 1 [µW/g]	aver. value 2 [µW/g]	upper value 3 [µW/g]	stand. deviation
40°C	0.48	0.54	0.60	11 %
50°C	1.75	1.88	2.01	7 %
60°C	6.16	6.73	7.32	9 %

Table 6b. Calculated kinetic results at lower temperatures from table 6a

selection	E_a [kJ/mol]	preexp. factor [W/kg]	KK [a]	ballistic life time [b] [yrs]	difference [c]	
all values	**109**	**$9.5 \cdot 10^{14}$**	**0.997**	**7.4/29.5**		
60°C value 3, 40°C value 1	118	$2.3 \cdot 10^{16}$	0.999	8.2/34.0	+11%	
60°C value 1, 40°C value 3	101	$3.9 \cdot 10^{13}$	0.999	6.6/23.7	-11%	-20%

a) correlation coefficient b) time until 3% energy loss at **40°C/30°C** occurs c) values for 40°C

As you can see, an experimental error of 11% at 40°C can lead to an error of 20% for the calculation of the ballistic service life at 40°C and of 30% at 30°C. You can minimize this error by doing multiple experiments or (better) calculate the ballistic service life at 40°C because the experimental errors here are much smaller than at 30°C. So nowadays we calculate the energy loss at 40°C storage time to minimize the error by extrapolation, because normally only at 40°C or above reproduceable heat flows can be observed [24].

In most cases detailed studies - dependent on the nature of the propellant - have to be undertaken to be sure to get the optimal sample preparation and measuring conditions.

4.3 Stabilizer consumption

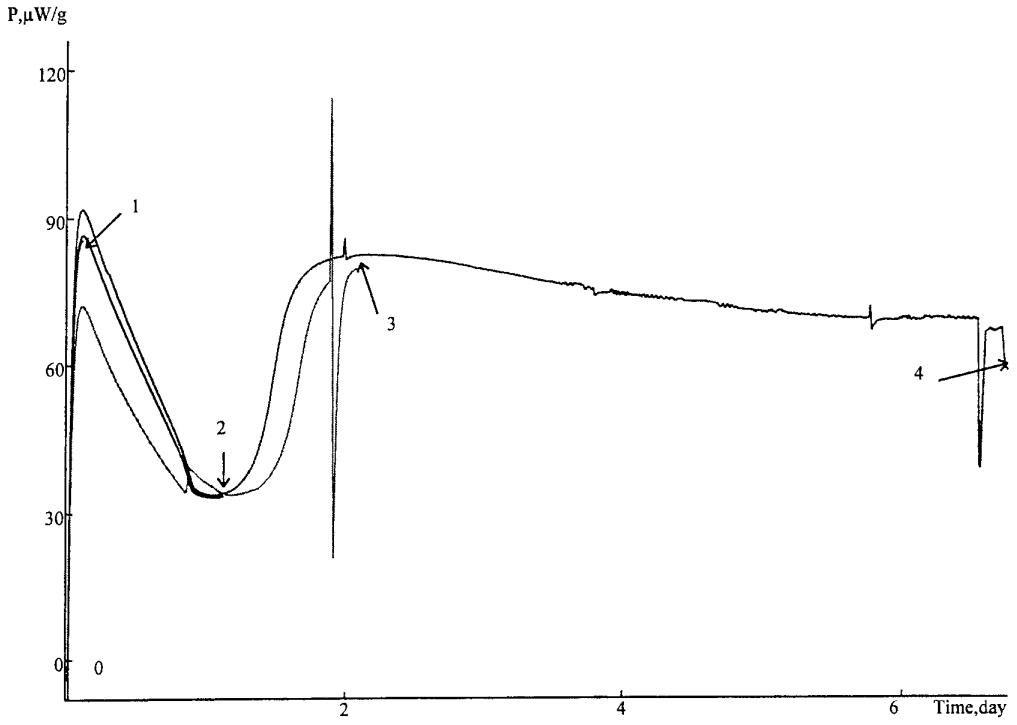
Very extensive studies of stabilizer consumption kinetics of double base rocket propellants were done by different authors [14]. Also correlations between stabilizer consumption and molecular mass depletion have

been worked out [16] so that a detailed study of this matter will not be presented here.
A rather rare result is the correlation between stabilizer consumption and heat production rate [7] (the double base ball powder K 6210 was used for these investigations).

Table 7: Stabilizer consumption at different stages of heat flow calorimetry

sample	N°	DPA	N-NO-DPA	2-N-DPA	4-N-DPA	2,2'-DN-DPA
		[%]	[%]	[%]	[%]	[%]
before	0	45.9	48.7	2.7	2.7	0.0
1. Maximum	1	32.4	61.9	3.0	2.7	0.0
1. Minimum	2	4.1	89.6	3.5	2.8	0.0
2. Maximum	3	0.6	96.8	1.8	0.8	0.0
End of meas.	4	0.0	97.1	0.0	1.4	1.5

Figure 1. Heat flow calorimetry curves of double base propellant at 80°C



As can be seen, between the first maximum and the minimum most of the DPA has been converted into N-NO-DPA, while the nitro derivatives remained constant. This conversion was completed at the second maximum. After several days at 80°C the mono nitro derivatives begin to be converted into the dinitro compounds. When this propellant is heated for about 18 days much of the N-NO-DPA will also be reacting with further NO_2 to give mono-, di-, and trinitro derivatives of DPA.

4.4 GPC

With the GPC it is possible to take a closer look to the molecular mass distribution of the nitrocellulose. If a double base propellant is thermally stressed, the NO_2 generated can lead to chain cracks in the nitrocellulose and so the average molecular weight is reduced. Table 7 gives the results for a double base propellant which has been heated up to 70°C for several weeks.

Table 7. Molecular mass depletion of a double base propellant heated up to 70°C

time	$\overline{M}_n$ [a)]	$\overline{M}_w$ [b)]	M_p [c)]	D [d)]
[days]	[kg/mol]			$[\overline{M}_w/\overline{M}_n]$
0	82	203	191	2,48
15	54	144	121	2,67
30	30	96	110	3,20
60	22	81	62	3,68

a) mass by numerical average b) mass by mass average c) mass at peak maximum d) polydispersity

As long as there are no limit values known, down to which nitrocellulose could be defined as functionable[2] it makes no sense to calculate the ballistic service life of propellants by molecular mass degradation.

4.5 NMR experiments

NMR is rather an unusual technique to determine stability of propellants, but it has some advantages. Especially solid-state-NMR provides you a lot of information about the mechanical properties of nitrocellulose- or HTPB-based propellants.

In the first example a single base propellant (A 5020) was analyzed by broad-line low dissolving solid state NMR. This technique is widely used in polymer technology for the analysis of the motion characteristics of polymer chains [21]. The thinner the line widths are the bigger is the flexibility of a polymer chain. A correlation with the E-module of the polymer can easily be drawn. There is also a correlation with the bullet impact experiments of plastic bonded high explosives [22]. The results are presented in figure 2.

The change in the decomposition kinetics of propellants at about 60°C that is usually observed with heat flow calorimetry techniques can also be correlated with NMR experiments. In this temperature area a „softening" (which means higher molecular motion of the matrix) of the propellant can be detected with solid state proton NMR spectroscopy [23] (figure 3). The detected effects are usually so small, that they cannot be observed by thermoanalytical methods (e.g. DSC).

[2] see [2a]

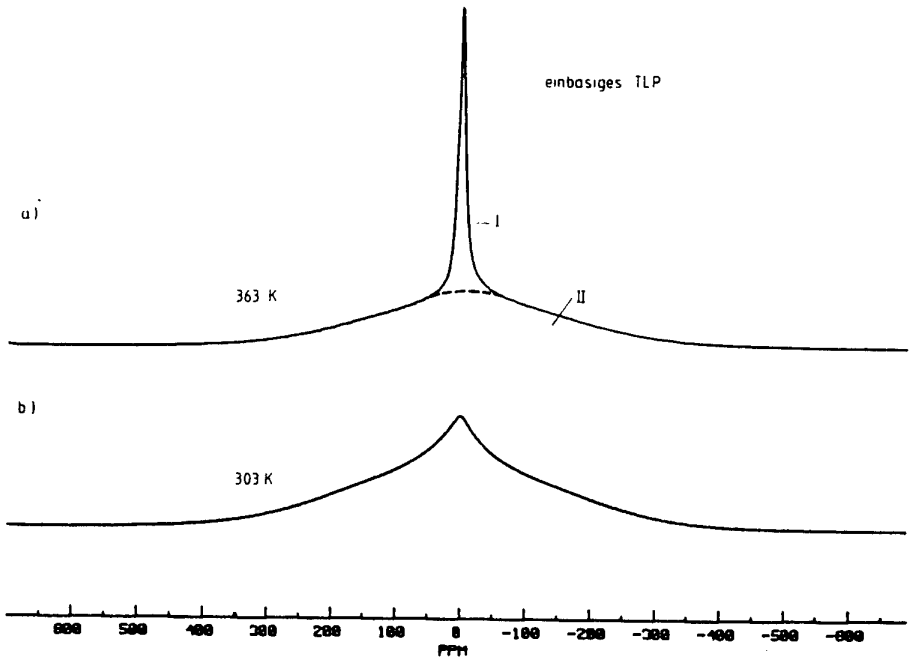


Figure 2. temperature dependent proton NMR spectra of a single base propellant

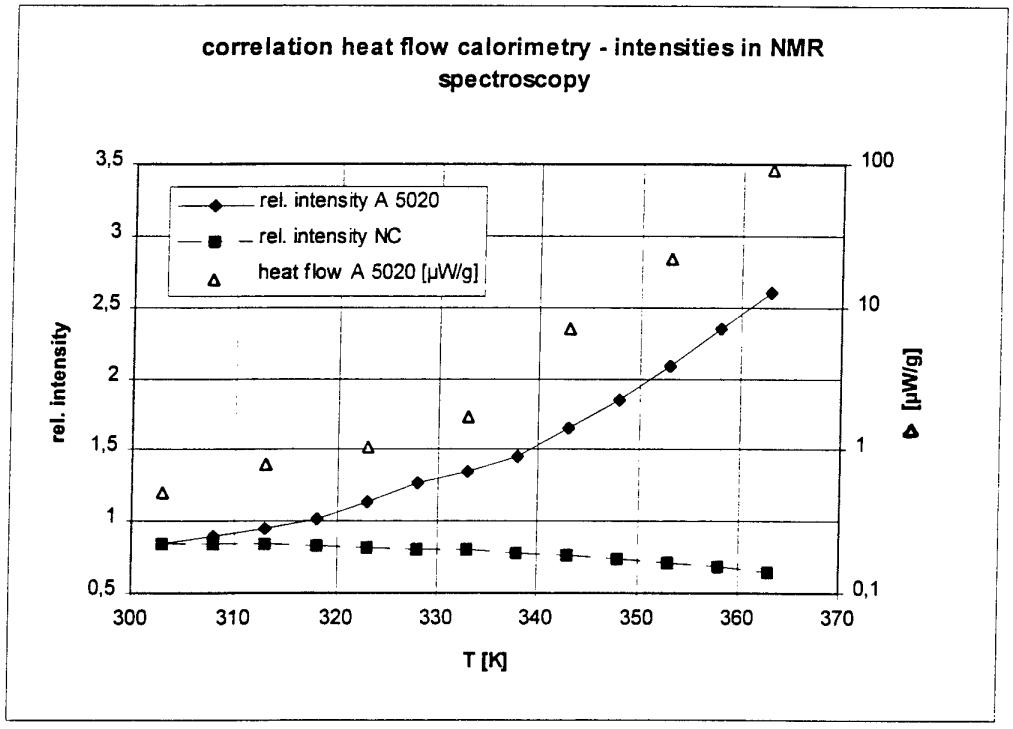


Figure 3. temperature dependent solid state NMR spectra of the single base propellant A 5020 and comparison with heat flow calorimetry

Another possible use for NMR spectroscopy in the field of stability predictions can be the identification of reaction products of explosives or propellants. This might be useful for the determination of the chemical reactions that occur in the propellant. The use of this is limited by the fact that trace analyses with NMR are only possible to a concentration of about 1-3 µg/ml.

5 Conclusions

In this paper we discussed a wide variety of different methods that are used for the determination of the ballistic service life of a propellant. The classical tests are widely used, others are more or less „extravagant". But none of these tests alone allows a substancial prediction of the ballistic service life of propellants. The classical tests only determine whether the chemical stability is given or not (and even here additional effects, e.g. surface agents greatly affect the results). They can only roughly give an impression about the chemical stability, but not about the ballistic service life because there is no possibility to make kinetic calculations from these data. One advantage of these tests is, that they are widely used and a huge amount of test results are available for comparison purposes.
The other tests presented in this paper don't allow a calculation of life time as well independently. But if you combine for example heat flow calorimetry results which give you the speed with which the reaction is going forward **and** stabilizer consumption or molar mass degradation experiments that define the actual stage of the decomposition reaction then it is possible to calculate the ballistic stability. For this purpose all limiting factors must be known, e.g. the „allowed" loss of energy, the „allowed" consumption of stabilizers or the „allowed" loss in average molecular weight. For double base propellants in general all migration processes of nitroglycerine must be taken into account additionally. For double base rocket propellants in special also changes in the mechanical properties have to be looked at, which possibly can be determined either by classical mechanical tests or by NMR spectroscopy. Overall, only the surveillance test can give you a overview of the service life, but this test doesn't allow to make predictions, because the results are only available **after** the propellant has lost its chemical stability.

In the future much more effort is necessary to know more about the influence of each chemical or physical reaction in the propellant on the ballistic behaviour. Only with this knowledge (and it can only be obtained by a multi-method analysis of the propellants) a good and reliable prediction of the ballistic life is possible.

6 References

[1] J.S. Dodds, „Current UK procedures for propellant shelf-life determination", *Symp.Chem.Probl.Conn. Stabil.Explos.* **9,** 247-258 (1992); I.L.C. van Geel, „Self-Ignition Hazard of Nitrate Ester Propellants", *Dissertation TH Delft* (**1969**).

[2] a. B. Vogelsanger, R. Sopranetti, „Sicherheits-, Stabilitäts- und Lebensdaueruntersuchungen im Lebenszyklus von Treibladungspulvern", *Vortrag Mikrokalorimetrie-/Thermoanalyse-Workshop BICT*, p. 27-43 (**1995**);
b. E. Brönnimann, Ch. Herren, A. Sopranetti, „Migration problems and ballistic shelf life of mortar propelling charges", *Symp.Chem.Probl.Conn.Stabil.Explos.* **9**, 215-231 (1992);

[3] J. Tranchant, „Internal mechanism of the chemical evolution of nitrocellulose propellants: Hypotheses and consequences", *Symp.Chem.Probl.Conn.Stabil.Explos.* **6**, 1-20 (1982).

[4] H. Schubert, „Lebensdauer von Raketenfesttreibstoffen", *Wehrtechnik* **2/69**, 62-67.

[5] *TL 1376-0600, Method 2.21.1,* „Holland-Test", Page 27 (**1976**).

[6] *TL 1376-0600, Method 2.22.1,* „Quantitative Prüfung", Page 28 (**1976**).

[7] *TL 1376-0600, Method 2.31.1,* „Bestimmung der chemischen Beständigkeit", Page 22 (**1976**).

[8] W. Verbeek, „Comparative investigation of stability tests for nitrate ester propellants", *TNO Report Ass. K3093-III* (**1974**); T.L. Boggs and R.L. Derr (eds.), „Hazard Studies for Solid Propellant Rocket Motors", *AGARDograph N° 316* (**1990**).

[9] *TL 1376-0600, Method 2.41.1,* „Überwachungstest bei 65.5°C", Page 30 (**1976**).

[10] *TL 1376-0600, Method 2.51.1,* „Wärmeflußkalorimetrie", Page 30a (**1992**).

[11] C.J. Elmqvist, P.E. Lagerkvist, L.G. Svensson, „Stability and Compatibility Testing Using a Microcalorimetric Method", *J.Haz.Mat.* **7**, 281-285 (1983); L.G. Svensson, C.K. Forsgren, P.O. Backman, „Microcalorimetric Methods in Shelf Life Technology", *Proc. ADPA Symp. on Compatibility of Plastics and Other Materials with Explosives, Propellants and Pyrotechnics*, New Orleans **1988**, p. 132-137; S. Wilker, G. Pantel, U. Ticmanis, „Wärmeflußkalorimetrische Untersuchungen an Anzündhütchen", *Proc.Int.Annu.Conf. ICT* **26**, 84 (1995).

[12] H.P.J. Jongeneelen, „Investigation into the ballistic stability of nitrate ester propellants", *TNO Report Ass. TL 7980-II* (1971).

[13] N.J. Curtis, „Isomer Distribution of Nitro Derivatives of DPA in Gun Propellants: Nitrosamine Chemistry", *Propellants, Explosives, Pyrotechnics* **15**, 222-230 (1990);

[14] J.M. Bellerby, M.H. Sammour, „Stabilizer Reactions in Cast Double Base Rocket Propellants I", *Propellants, Explosives, Pyrotechnics* **16**, 235-239 (1991); J.M. Bellerby, M.H. Sammour, „Stabilizer Reactions in Cast Double Base Rocket Propellants II", *Propellants, Explosives, Pyrotechnics* **16**, 273-278 (1991); J.M. Bellerby, M.H. Sammour, "Stabilizer Reactions in Cast Double Base Rocket Propellants III", *Propellants, Explosives, Pyrotechnics* **18**, 46-50 (1993); A.J. Bellamy, M.H. Sammour, J.M. Bellerby, "Stabilizer Reactions in Cast Double Base Rocket Propellants IV", *Propellants, Explosives, Pyrotechnics* **18**, 223-229 (1993); M.H. Sammour, „Stabilizer Reactions in Cast Double Base Rocket Propellants V. Prediction of Propellant Safe Life", *Propellants, Explosives, Pyrotechnics* **19**, 82-86 (1994); J.O. Doali, A.A. Juhasz, „Determination of 2-NDPA in a composite modified double-base propellant by HPLC", *Anal.Chem.* **48**, 1859-1860 (1976); J. Haberman, „HPLC analyses of propellants I. Analysis of M1, M6, and M10 propellants", *Tech. Rep. ARAED-TR-86017* (**1986**); D.A. Wiegand, „Diffusion in the thermal degradation of NC base propellants", *Tech.Rep. ARAED-TR-89035* (**1990**); D. Robertson, L. Kansas, „Analysis of stabilizer content by HPLC", *Tech. Rep. ARAED-TR-90020* (**1990**).

[15] STANAG 4527 (formerly 4480) - AC310 (SG1) - Final Draft (**1994**).

[16] F. Volk, K.M. Bucerius, G. Wunsch, „Ermittlung von Einflußgrößen auf die Genauigkeit von GPC-Messungen", *Symp.Chem.Probl.Conn.Stabil.Explos.* **7**, 197-216 (1985); M.Marx-Figini, O. Soubelet, „Size Exclusion Chromatography of Cellulose Nitrate", *Polymer Bull.* **11**, 281-286 (1984); R.A. Sjöbom, H.G. Oresten, „Separation and Quantitation of Nitrocellulose, Nitroglycerine, Diethylphthalate, and Centralite in a Double-base Powder", *Propellants and Explosives* **5**, 105-110 (1980); M.A. Bohn, „Voraussage der Lagerzeit von Treibmitteln mit Stabilisatorverbrauch und Molmassenabbau", *Vortrag 18. Symp. Innenballistik* (**1993**).

[17] J. Kimura, „Chemiluminescence Study on Thermal Decomposition of Nitrate Esters (PETN and NC)", *Propellants, Explosives, Pyrotechnics* **14**, 89-92 (1989); H.N. Volltrauer, A. Fontijn, „Low-Temperature Pyrolysis Studies by Chemiluminescence Techniques Real-Time Nitrocellulose and PBX 9404 Decomposition", *Combustion and Flame* **41**, 313-324 (1981).

[18] U. Ticmanis, „Kinetik der Zersetzung von TLP während der Langzeitlagerung", *BICT Bericht* 330/7873/89; A. Pfeil, N. Eisenreich, „TGA-, DTA-, IR- und Raman-Methoden für die Untersuchung der thermischen Zersetzung von Nitrocellulose", *Proc.Int.Annu. Conf.ICT* **11**, 335-354 (1980).

[19] P. Guillaume, A. Fantin, M. Rat, S. Wilker, G. Pantel, „Stability studies of spherical propellants", *Proc.Int.Annu.Conf.ICT* **27**, 16-1 - 16-12 (1996).

[20] M. Frey, G. Pantel, *BICT Bericht* 1.1-2/6186/83; S. Wilker, G. Pantel, *BICT Berichte* 110/12662/93, 110/13155/93, and 110/13652/94; S. Wilker, G. Pantel, P. Guillaume, *BICT Bericht* 110/15292/95 (all unpublished).

[21] M. Kaiser, „Festkörper-NMR-Spektroskopie zur Beurteilung von Kunststoffen für kunststoffgebundene Sprengstoffe", *Vortrag 13. Sprengstoffgespräch* (**1989**).

[22] M. Kaiser, „Untersuchungen an verpreßbaren, kunststoffgebundenen Sprengstoffen", *Vortrag 14. Sprengstoffgespräch* (**1990**).

[23] M. Kaiser, G. Holl, „Simulation von Alterungsprozessen beim einbasigen Pulver A 5020", *Proc.Int.Annu. Conf.ICT* **20**, 58 (1989); M. Frey, G. Pantel, „Prüfung der Stabilität des TLP A 5020", *BICT Bericht* 1.1/7040/86 (unpublished).

[24] K. Kupzik, „Stabilitätsuntersuchungen beim TLP K6210", *Vortrag im BICT* am 18.01.1996 (unpublished).

Paper Number: 18
Discussor's Name: Dr. M. A. Bohn
Responder's Name: Dr. S. Wilker

Question: Your method of predicting the service life of gun propellants with heat generation (=heat flow) is based upon the constancy of the heat generation during the predicted period of time. Is this assumption already verified?

Answer: As we assume a degradation of 3% corresponding to the heat of explosion for the calculation of the ballistic service life, we are quite sure that the heat flow is constant until this state of degradation. We measured the heat flow of different propellants at 80° C for about two weeks and have found constant values for the whole period of time (after the initial effects of equilibration) until strong gas evolution took place. The total energy released within that period was more than 1.5%, so we think that it is true for the first 3%.

This assumption of constant heat flow is wrong, when you have strong autocatalytic reactions, e.g., when measuring unstabilized nitrocellulose, but then you need other methods of evaluation for the ballistic service life.

Another comment with regard to the measuring program has to be made:
We measure the heat flow with a descending temperature program with a slight pre-aging at 80° C and afterwards at 70° C, 60° C and so on, with the same state of degradation of the propellant.

Additional comments of the discussor

Comment with regard to mass loss:
Mass loss can be used as a method of predication, if one determines the mass loss at several temperatures, makes a description with an appropriate rate equation and extrapolates the time to reach a preset value of mass loss, for example 2% or 3%, for storage temperature.

Comment with regard to mean molar (molecular) mass decrease of NC:
Molar mass degradation of NC must be considered also as a quantity, which determines service life. With decreasing mean molar mass Mn (number average) or Mw (mass weight average) the compressive strength for propellant grains decreases, which can lead to brittle fracture during ignition. For double base rocket propellants we have also made investigations, which show that with decreasing mean molar mass Mw (or Mn) the strain at break and the tensile strength at break are reduced analogously to the reduction of Mw. Some of the results can be found in one of our papers for the symposium.

CORRELATION ENTRE LES RESULTATS DE STABILITE DE POUDRES POUR ARMES OBTENUS APRES VIEILLISSEMENT ARTIFICIEL A 50°C ET CEUX OBTENUS EN VIEILLISSEMENT NATUREL

O. RUAULT - C. BALES

DSTI Etablissement Technique de Bourges
Laboratoire Poudres et Explosifs
Route de Guerry, BP 712
18015 Bourges Cedex
France

RESUME

Corrélation entre les résultats de stabilité de poudres pour armes obtenus après vieillissement artificiel à 50°C et ceux obtenus en vieillissement naturel.

La France a mis au point en 1975 une épreuve de consommation de stabilisant à 50°C destinée à établir, au temps zéro, si une poudre présentera de bonne garantie de conservation.
Cette épreuve a maintenant 20 ans et il nous est donc possible de prouver, par corrélation avec le vieillissement naturel, la validité de cette épreuve pour des poudres pour armes stabilisées à la DPA et de montrer que des tests basés sur des vieillissements à températures plus élevées ne sont pas représentatifs.

ABSTRACT

Correlation between stability results of gun propellants obtained after artificial ageing at 50°C and natural ageing

France has devised in 1975 a stability test based on decrease of stabilizer after 6 weeks at 50°C. The aim of this test is to predict if a new propellant will give a good guarantee of conservation.
The test has been used for 20 years on single base propellants made with diphenylamine.
Now it's possible to prove the validity of this test by studiing the results obtained after natural ageing and results obtained with this test.
We can also show that tests, based on artificial ageing at higher temperatures, are not representative.

1.- INTRODUCTION

Un des problèmes fondamentaux liés à la stabilité chimique des poudres pour armes est d'estimer l'aptitude d'une poudre à bien se conserver dans le temps.
Les poudres à base de nitrocellulose voient leur stabilité chimique se dégrader au cours du temps.
Afin de prévoir la durée de vie de ces poudres ou leur aptitude à bien se conserver dans le temps, il est nécessaire de disposer de tests fiables et représentatifs.
De nombreux tests, basés sur des vieillissements artificiels réalisés en température afin d'accélérer le phénomène de dégradation pour pouvoir le mesurer dans un temps assez court, ont été utilisés.
Les premiers tests ont tous été, quel que soit leur pays d'origine, effectués à températures très élevées (90-100-108,5-120-134,5°C...).
Ces températures ayant été jugées beaucoup trop élevées pour être représentatives des mécanismes de dégradation observés en vieillissement naturel, d'autres tests réalisés à des températures moyennes ont vu le jour dans les années 70.

La France a mis au point en 1975 une épreuve de consommation du stabilisant à 50°C [1] basée sur un principe similaire à celui du STANAG 4117 (épreuve réalisée après vieillissement à 65,5°C).

Cette épreuve est utilisée depuis maintenant 20 ans et ce papier présente, pour 37 lots de différents types de poudres à simple base, stabilisées à la diphénylamine, une comparaison des résultats obtenus à l'épreuve de consommation de stabilisant à 50°C et des taux de stabilisant résiduel mesurés après vieillissement naturel.

Une seconde comparaison a été effectuée sur 5 types de poudres ayant subi un vieillissement naturel à différents taux d'humidité.
Enfin, des résultats de consommation de stabilisant obtenus par vieillissement artificiel à 50°C pendant 6 semaines et suivant le STANAG 4117 (vieillissement pendant 60 j à 65,5°C) ont été comparés au vieillissement naturel sur 25 lots d'un même type de poudre, afin de mettre en évidence la méthode la plus représentative.

Paper presented at the AGARD PEP Symposium on "Service Life of Solid Propellant Systems" held in Athens, Greece, 10-14 May 1996, and published in CP-586.

2.- CORRELATION ENTRE LES RESULTATS OBTENUS APRÈS VIEILLISSEMENT ARTIFICIEL À 50°C ET VIEILLISSEMENT NATUREL SUR POUDRE SIMPLE BASE

L'épreuve de consommation de stabilisant à 50°C consiste à maintenir un échantillon de poudre à 50°C pendant 6 semaines en tube étanche, à un taux d'humidité défini puis à doser le stabilisant résiduel par chromatographie en phase gazeuse, comparativement avec la même poudre maintenue à 20°C.

Cette épreuve est réalisée, en France, lors des contrôles d'acceptation des poudres, depuis 1975. L'expérience acquise les 5 premières années a permis de considérer que les échantillons présentent une stabilité satisfaisante lorsque la consommation de stabilisant (Δ) mesurée est inférieure ou égale à 0,20 pour des poudres B stabilisées à la diphénylamine. En France, le taux de stabilisant initial de ces poudres est généralement de 1 à 1,2%.

Pour le vieillissement naturel, notre établissement dispose d'échantillons de tous les lots de poudres chargés dans les munitions utilisées par les Etats Majors Français depuis 1945. Ces échantillons d'environ 4 à 5 Kg sont répartis dans des bocaux de verre stockés dans une "poudrière" isotherme à une température voisine de 15°C. Ils sont contrôlés régulièrement, en moyenne tous les 4 ans ou plus fréquemment si cela s'impose au vu de l'avancement de leur dégradation.

Les tableaux et les courbes ci-après donnent, par type de poudre et année de fabrication, la consommation de stabilisant à 50°C pendant 6 semaines et l'évolution du taux de stabilisant en vieillissement naturel jusqu'à 15 ou 18 ans selon les lots.

Remarque : La comparaison avec le vieillissement en munition a été recherchée mais n'a pas pu être établie en raison des différences de conditions de stockage des munitions selon les régions et les types de magasins.

2.1. - POUDRE SIMPLE BASE MULTITUBULAIRE POUR MOYEN CALIBRE FABRIQUEE EN 1975

Le cas étudié ici est celui d'une poudre multitubulaire à fort potentiel fabriquée en 1975 et stabilisée avec environ 1% de diphénylamine. Nous disposons de 5 lots pour lesquels nous avons suffisamment de données pour effectuer une comparaison entre le vieillissement naturel et celui à 50°C.

Les consommations à 50°C sont comprises entre 0,11 et 0,55 % et nous disposons de données au bout de 10, 16 et 18 ans en vieillissement naturel.

L'ensemble des résultats est fourni dans le tableau 1 et les courbes d'évolution du stabilisant sont représentées sur la figure 1.

LOT	Consommation de DPA en % 6 semaines à 50°C	Taux de DPA en vieillissement naturel en %			
		0	10 ans	16 ans	18 ans
13	0,55	0,94	0,89	0,22	0,20
11	0,47	0,94	0,88	0,25	0,23
18	0,40	0,98	0,88	0,31	0,18
519	0,23	1,15	1,08	1,13	1,11
512	0,11	1,15	1,14	1,14	1,15

TABLEAU 1

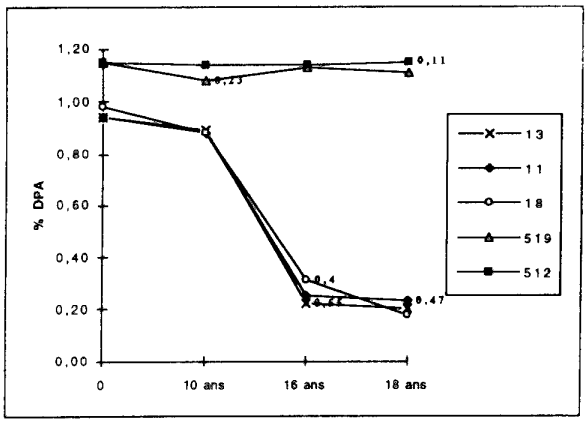


FIGURE 1

L'examen de ces données montre très nettement que les 3 lots présentant des valeurs de consommation de stabilisant anormalement élevées, se sont fortement dégradés lors du vieillissement naturel, alors que les 2 lots présentant des valeurs de $\Delta_{50°C}$ correctes n'ont pas évolué, même au bout de 18 ans de vieillissement naturel.

2.2.- POUDRE SIMPLE BASE MULTITUBULAIRE POUR MOYEN CALIBRE FABRIQUEE EN 1976

Les quatre lots testés sont du même type que la poudre du cas précédent. Le paramètre qui diffère est l'année de fabrication : 1976 au lieu de 1975.
Les consommations à 50°C sont comprises entre 0,23 et 0,56 %.
L'ensemble des résultats est donné dans le tableau 2 . Les courbes d'évolution du stabilisant sont représentées sur la figure 2.

LOT	Consommation de DPA en % 6 semaines à 50°C	Taux de DPA en vieillissement naturel en %			
		0	10 ans	16 ans	18 ans
2	0,56	1,01	0,69	0,18	0,15
25	0,43	1,00	0,95	ne	0,27
6	0,39	1,07	1,05	0,39	0,23
10	0,23	1,10	1,12	1,12	0,81

TABLEAU 2

ne = non effectué

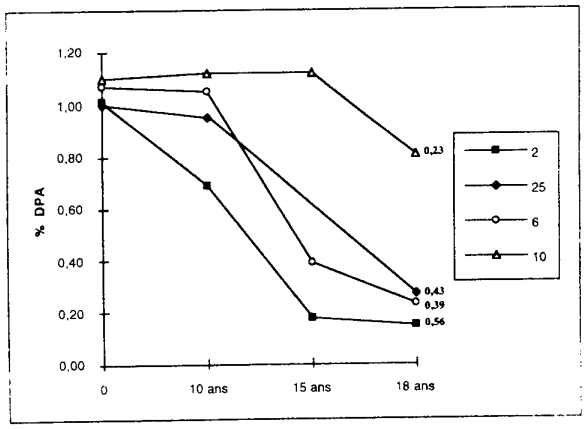


FIGURE 2

Comme dans le cas précédent, les 3 lots présentant des consommations de stabilisant à 50°C anormalement élevées, se sont rapidement dégradés en vieillissement naturel, alors que le lot n°10 présentant un $\Delta_{50°C}$ de 0,23 n'a pas évolué en 15 ans.

2.3.- POUDRE SIMPLE BASE MULTITUBULAIRE POUR MOYEN CALIBRE FABRIQUEE EN 1980

Il s'agit du même type de poudre que dans les deux cas précédents mais leur fabrication date de 1980. Dans cet exemple, les comparaisons ont pu être réalisées sur 9 lots présentant des consommations de stabilisant à 50°C très différentes (entre 0,24 et 0,52 %).
Le tableau 3 présente les résultats et la figure 3, l'évolution du taux de diphénylamine au bout de 14 ans.

LOT	Consommation de DPA en % 6 semaines à 50°C	Taux de DPA en vieillissement naturel en %	
		0	14 ans
40	0,58	1,02	0,37
17	0,49	1,00	0,76
5	0,45	1,08	0,64
13	0,45	1,01	0,70
15	0,44	1,01	0,79
23	0,40	1,03	0,91
19	0,39	1,07	0,89
27	0,32	1,09	1,05
28	0,24	1,08	1,07

TABLEAU 3

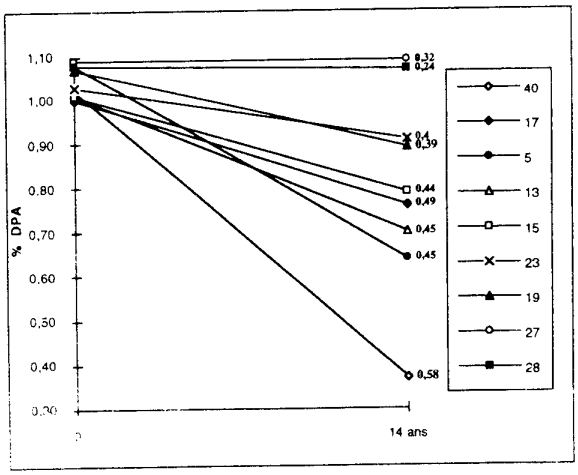


FIGURE 3

Les lots étudiés dans ce tableau étant plus récents que dans les deux cas précédents, les corrélations ne sont pas aussi nettes. Cependant, on note bien que les lots présentant les Δ 50°C les plus élevés se dégradent en vieillissement naturel, alors que les deux lots présentant les Δ 50°C les plus faibles, n'ont absolument pas évolué.

2.4.-POUDRE TUBULAIRE LISSÉE AU CAMPHRE POUR MOYEN CALIBRE FABRIQUEE EN 1977

Dans cet exemple, 5 lots d'une poudre de composition différente des cas précédents ont été testés. Il s'agit d'une petite poudre au camphre pour munitions de moyen calibre. Ces lots ont été fabriqués en 1977. Les consommations de stabilisant obtenues lors des épreuves d'acceptation étaient comprises entre 0,42 et 0,19 %.
L'ensemble des résultats est donné dans le tableau 4 et les courbes d'évolution sont présentées sur la figure 4.

LOT	Consommation de DPA en % 6 semaines à 50°C	Taux de DPA en vieillissement naturel en %		
		0	12 ans	18 ans
6	0,42	0,98	0,67	0,28
2	0,38	1,03	0,52	0,33
33	0,34	1,02	0,96	0,81
9	0,22	1,01	0,91	0,38
18	0,19	1,00	0,97	0,85

TABLEAU 4

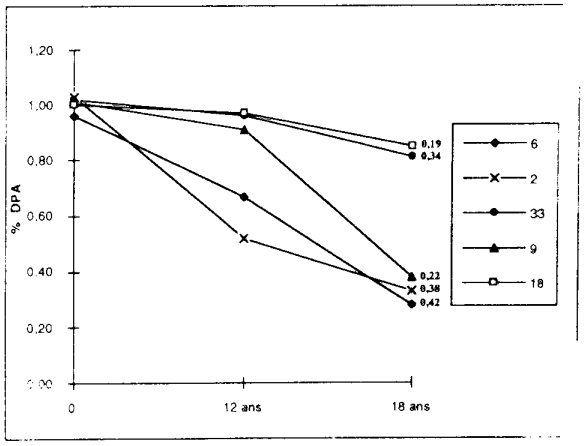


FIGURE 4

Mis à part le lot 33, qui présente un bon comportement en vieillissement naturel malgré son Δ 50°C élevé, on note une bonne corrélation entre le comportement à 50°C et celui en vieillissement naturel.

2.5.-POUDRE HEPTATUBULAIRE LISSÉE AU CAMPHRE POUR MOYEN CALIBRE FABRIQUEE EN 1975 et 1976

Dans cet exemple, nous avons deux lots de poudre de petites dimensions, lissée au camphre et de valeur moyenne en énergie.
Ces deux lots présentaient des consommations élevées lors des épreuves d'acceptation.
Le faible nombre de données présentées dans ce cas s'explique par le fait que ce type de poudre a été très peu fabriqué avant 1980.

LOT	Consommation de DPA en % 6 semaines à 50°C	Taux de DPA en vieillissement naturel en %		
		0	10 ans	15 ans
501/75	0,49	1,05	0,83	0,41

TABLEAU 5

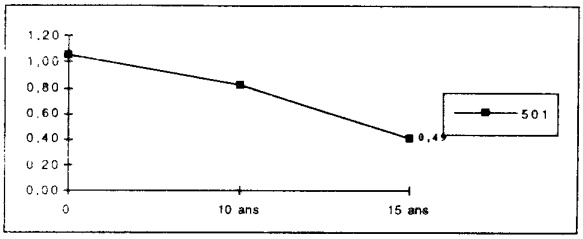


FIGURE 5

LOT	Consommation de DPA en % 6 semaines à 50°C	Taux de DPA en vieillissement naturel en %		
		0	14 ans	18 ans
13 /76	0,38	1,05	0,61	0,36

TABLEAU 6

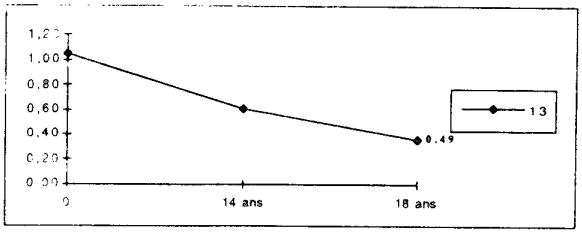


FIGURE 6

Ces deux lots avec des $\Delta_{50°C}$ anormalement élevés présentent une dégradation rapide lors du vieillissement naturel.

2.6. - POUDRE B EN PAILLETTES FABRIQUEE EN 1976

Dans cet exemple, nous disposons de deux lots d'une poudre en paillettes stabilisée à la diphénylamine mais contenant également de la centralite.
Ces lots fabriqués en 1976, présentaient tous les deux à l'époque des consommations de stabilisant à 50°C très élevées.
Les résultats obtenus sont détaillés dans le tableau 7 et les courbes d'évolution du stabilisant sont représentées par la figure 7.

LOT	Consommation de DPA en % 6 semaines à 50°C	Taux de DPA en vieillissement naturel en % 0	10 ans	15 ans	18 ans
3	0,54	1,02	0,35	0,20	détruite (*)
17	0,54	1,02	0,35	0,27	0,27

TABLEAU 7

*poudre détruite en raison de son faible taux de stabilisant

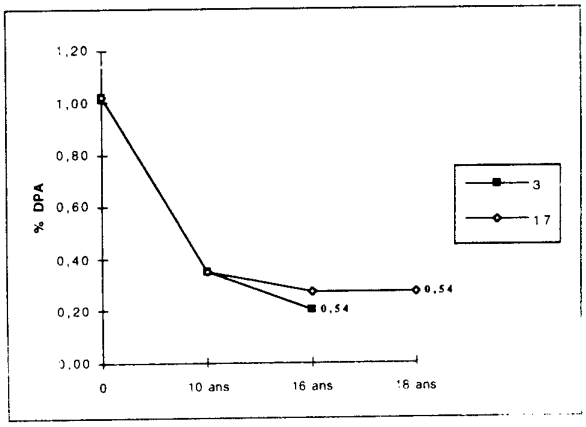


FIGURE 7

Cet exemple montre aussi que le mauvais comportement à l'épreuve à 50°C reflète bien la forte dégradation en vieillissement naturel. L'évolution a même été particulièrement rapide, puisqu'au bout de 10 ans, les lots n'avaient plus que le tiers de leur taux de stabilisant initial.

2.7. - POUDRE D'ARTILLERIE MULTITUBULAIRE FABRIQUEE EN 1976

Les dix lots étudiés dans ce cas correspondent à une poudre d'artillerie, de forte énergie et de grandes dimensions, fabriquée en 1976 et stabilisée avec environ 1,05 % de diphénylamine.

Les consommations obtenues en 1976 étaient comprises entre 0,10 et 0,30 % et elles sont comparées avec des résultats obtenus au bout de 10 et 15 ans de vieillissement naturel.

LOT	Consommation de DPA en % 6 semaines à 50°C	Taux de DPA en vieillissement naturel en % 0	10 ans	15 ans
61	0,30	0,96	0,87	0,74
64	0,28	1,00	0,83	0,58
60	0,26	0,97	0,88	0,72
71	0,23	0,93	0,93	0,79
20	0,19	1,02	1,00	0,84
4	0,18	1,02	0,82	0,69
44	0,18	1,04	1,09	0,92
34	0,17	1,05	1,03	0,93
46	0,10	1,04	1,07	0,89
50	0,10	1,02	1,01	0,93

TABLEAU 8

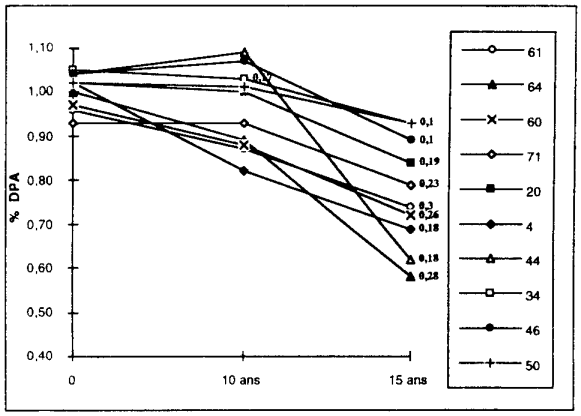


FIGURE 8

Mis à part le lot 4, qui se dégrade malgré une valeur de $\Delta 50°C$ satisfaisante, on observe ici aussi que les lots présentant les plus fortes valeurs de $\Delta 50°C$ ont plus évolué en vieillissement naturel que ceux présentant des $\Delta 50°C$ satisfaisants.

3. - CORRELATION ENTRE LE VIEILLISSEMENT NATUREL SEVERE (à différents taux d'humidité) ET LE VIEILLISSEMENT ARTIFICIEL À 50°C

Cette étude a porté sur 5 poudres de compositions différentes et présentant des consommations de stabilisant à 50°C variant de 0,07 à 0,42. Par rapport à l'étude précédente, nous avons fait varier les conditions de vieillissement naturel :
- Conditionnement préalable à 3 humidités relatives : 35, 63 et 92% HR puis en flacons étanches (75 g).
- Vieillissement dans un abri léger dont la température varie de -10°C en hiver à + 35°C en été.
- Analyse de la poudre après 1, 2 et 4 ans en prélevant à chaque fois des flacons différents.

Les résultats détaillés de cette étude ont fait l'objet d'une communication à Karlsruhe [2]. Dans le tableau ci-dessous, seuls les résultats de taux de stabilisants au bout de 4 ans ont été repris.

N° POUDRES	1	2	3	4	5
Δ50°C	0,07	0,09	0,15	0,35	0,42
Δ en 4 ans à 35 % HR	Pas d'évolution				
Δ en 4 ans à 63 % HR	0,00	0,04	0,00	0,22	0,31
Δ en 4 ans à 92 % HR	0,08	0,02	0,15	0,26	0,68

TABLEAU 9

Ces résultats montrent que :

- Les poudres présentant des $\Delta_{50°C}$ faibles n'évoluent pas ou peu en 4 ans.
- L'humidité de la poudre accélère fortement la dégradation de la poudre, si sa stabilité est moyenne ou faible.

Nous obtenons des classements similaires, à la précision de l'analyse près, avec l'épreuve à 50°C et au bout de 4 ans à 92% HR à température ambiante.

4. - COMPARAISON DES RESULTATS OBTENUS AVEC LE STANAG 4117, À L'ÉPREUVE À 50°C ET APRES 9 ANS DE VIEILLISSEMENT NATUREL

Cette étude a été effectuée sur 25 lots d'un même type de poudre propulsive simple base multitubulaire fabriquée entre 1975 et 1979 avec environ 1,05 % de diphénylamine.

Ces poudres ont subi comparativement 3 tests :
- dès leur fabrication, l'épreuve de consommation de stabilisant à 50°C pendant 6 semaines,
- dès leur fabrication, le STANAG 4117 qui est une épreuve de mesure de consommation du taux de stabilisant après 60 jours de vieillissement artificiel à 65,5°C en tube non étanche, et mesure du taux de stabilisant dans l'Ultra-Violet après saponification de l'échantillon,
- 9 ans de vieillissement naturel.

Les résultats obtenus avec ces trois épreuves sont donnés dans le tableau 10. Les échantillons ont été classés par consommation à 50°C décroissante.

LOT	DPA initial en %	Δ DPA 42 jours à 50°C	Δ DPA 60 jours à 65,5°C Stanag	VIEILLISSEMENT NATUREL (9 ans)	
				% DPA	Δ DPA*
Z	1,02	0,65	0,49	0,21	0,81
S	1,08	0,57	0,46	0,58	0,50
V	1,06	0,55	0,45	0,26	0,80
X	1,08	0,55	0,53	0,87	0,31
B	1,05	0,55	0,48	0,34	0,71
W	1,10	0,55	**0,54**	0,70	0,40
U	1,09	0,54	0,52	0,18	0,91
T	1,08	0,53	**0,54**	0,19	0,89

***ΔDPA = % DPA Initial - %DPA au bout de 9 ans**

LOT	DPA Initial en %	Δ DPA 42 jours à 50°C	Δ DPA 60 jours à 65,5°C Stanag	VIEILLISSEMENT NATUREL (9 ans)	
				% DPA	Δ DPA*
A	1,05	0,47	0,50	0,43	0,62
E	1,08	0,43	0,45	0,24	0,84
C	0,99	0,40	0,50	0,31	0,68
F	1,08	0,39	0,50	0,54	0,54
G	1,06	0,38	0,49	0,99	0,07
O	1,12	0,29	0,50	0,89	0,23
M	1,07	0,28	0,46	0,85	0,22
R	1,09	0,28	0,49	0,93	0,16
Y	1,09	0,27	0,48	1,00	0,09
L	1,10	0,25	0,51	0,98	0,12
P	1,10	0,25	0,51	0,81	0,29
N	1,11	0,24	0,53	1,04	0,07
H	1,10	0,23	0,46	1,03	0,08
I	1,14	0,22	0,54	1,08	0,06
J	1,10	0,22	0,41	1,04	0,06
Q	1,11	0,20	0,57	0,98	0,13
K	1,09	0,12	0,45	1,00	0,09

TABLEAU 10

L'examen de ces résultats montre que :

- L'épreuve à 65,5°C ne permet pas de discriminer les différents lots : les résultats de consommation de stabilisant sont tous voisins de 0,5 (maxi à 0,54 et mini à 0,41) alors que l'épreuve à 50°C permet un classement des 25 lots : les $\Delta_{50°C}$ sont régulièrement répartis entre 0,65 et 0,12.

- Les 25 lots se comportent très différemment les uns des autres en vieillissement naturel et le classement obtenu dans ce cas est, à part deux exceptions (lots X, W), très voisin de celui obtenu après l'épreuve à 50°C.

- Il n'y a aucune corrélation entre les résultats du STANAG et ceux obtenus après vieillissement naturel.

5. - CONCLUSION

L'ensemble des résultats présentés ici, permet de confirmer la validité préétablie [3 et 4] de l'épreuve à 50°C. Avec le recul de 20 ans d'utilisation, on peut affirmer qu'il y a une très bonne corrélation entre les résultats obtenus à l'épreuve de consommation de stabilisant à 50°C et ceux obtenus après vieillissement naturel, alors que cette corrélation n'est pas établie avec le STANAG 4117.
Ceci montre que l'épreuve à 50°C, appliquée au temps zéro, peut permettre de prévoir l'aptitude d'une poudre à sa conservation et que, dans le cas des poudres à simple base stabilisées à la diphénylamine, le vieillissement artificiel de 6 semaines à 50°C est bien représentatif de ce qui se passe en vieillissement naturel, alors que le vieillissement à température plus élevée (65,5°C) ne l'est pas.

6. - REFERENCES

[1] M. LEVEQUE : Epreuve de consommation de stabilisant à 50°C, mise au point de l'épreuve - Note technique (1980).

[2] M. LEVEQUE, O. RUAULT : Influence de l'humidité sur l'évolution des poudres à température ambiante, Proc 18 th Annual Conférence of I.C.T. (1983), 509.

[3] O. RUAULT : Epreuve à 50°C - Bilan après 12 ans d'utilisation et corrélation avec le vieillissement naturel, P.V n° 2268 (1987).

[4] M. LEVEQUE : Corrélation entre les résultats de l'épreuve de consommation de stabilisant à 50°C et le vieillissement naturel, Proc 8 th Symp Chen Probl Connected stabil Explo (1988), 125.

Paper Number: 19
Discussor's Name: Professor H. Schubert
Responder's Name: O. Ruault

Question: What are the conditions for "Natural Aging?" What was the life cycle of these powders?

Answer: The propellants were stored in an isothermal propellant storage where the temperature is about 15 plus or minus 2 degrees C. So there was no temperature cycle.

Paper Number: 19
Discussor's Name: Dr. G. Jenaro de Mencos
Responder's Name: O. Ruault

Question: Do you know if these conclusions are valid for double base and triple base propellants?

Answer: We don't have experience and data with triple base propellants.

For double base propellants we have different cases:
- Propellants with Diphenylamine (DPA): For these 65.5° C is too high of a temperature and 50° C seems not high enough to have a significant evolution. So 60° C is probably the best temperature.
- Propellants with centralite: The mechanisms seem to be the same at 50° and 65.5° C, but we have limited data.
- Propellants with 2-NDPA: 65.5° C is too high of a temperature and the results depend on the concentration of nitroglycerin. When the concentration of nitroglycerin is high (more than 30%) the decrease of stabilizer content is too rapid at 65.5° C.

Paper Number: 19
Discussor's Name: R. Pesce-Rodriguez
Responder's Name: O. Ruault

Question: Have you presented these results to STANAG? Are they receptive to the idea of changing the temperature at which accelerated aging tests are performed?

Answer:
- We presented the results at the beginning of our study to the STANAG 4117, but at that time (in 1990) we didn't have enough data to be sure of our conclusions.
- They are receptive to changing the temperature because other recent data with 2-NDPA and with double base propellant containing DPA prove that 65.5 Degrees C is too high of a temperature.

Ageing Behaviour of Propellants Determined by Mass Loss, Heat Generation, Stabilizer Consumption and Molar Mass Decrease

Fred Volk and Manfred A. Bohn

Fraunhofer-Institut für Chemische Technologie (ICT)
Postfach 1240, Joseph-von-Fraunhofer Str. 7
D-76318 Pfinztal, Germany
Fax: +49-721-4640-111

1. ABSTRACT

During the service life of nitric acid ester based propellants a consumption of stabilizer and a degradation of the mean molar (molecular) masses such as number average Mn, mass average Mw and Z-average Mz of the nitrocellulose occur due to decomposition reactions. Therefore the chemical and mechanical properties of the propellants are changed and the safe service life and the safe storage time, the so-called lifetimes, are limited. In order to predict the lifetimes one needs to measure properties P, which are changed by the decomposition reactions in the propellant and which can be determined with good accuracy as a function of time and temperature, if necessary also in dependence of further variables. For propellants consisting of nitric acid esters, stabilizer consumption, molar mass degradation and mass loss are very suitable properties. Heat generation measured by heat flux microcalorimeters is an assessment of the momentary reaction rate.

The stabilizer content was measured by reversed-phase high performance liquid chromatography (HPLC), the molar mass degradation by gel permeation chromatography (GPC), the heat generation was determined by a microcalorimeter and the mass loss with an analytical balance.

For the evaluation of the experimental data kinetic models are used. The molar mass decrease is reproduced very well by a model, which assumes a statistical chain scission by the decomposition of chain elements. Stabilizer consumption is described with two models, one is based on a reaction of first order, the other one is a combination of first and zero order reactions. With these kinetic descriptions lifetime predictions are made. This is done for single temperatures and for three temperature-time profiles, two from STANAG 2895 and one from the industry.

The mass loss and the heat generation measurements show the autocatalytic acceleration of the decomposition reactions for some gun propellants and for nitrocellulose and corresponding autocatalytic kinetic models are used for the mathematical description of the data. The pre-autocatalytic ageing can be evaluated by a reaction of zero order and results are given for the heat generation of a double and a trible base gun propellant The linear mass loss increase is compared between five German gun propellants (GP) and the energetic binder GAP. The gun propellants are: single base A5020, single base K503, single base (with DNT) CD5240 (US M6), double base L5460 (US JA2) and triple base KN6540 (US M30).

2. INTRODUCTION

The safe operational service life (safe use time) and the service life in storage (safe storage time) of propellants are limited by chemical decomposition reactions, which cause a loss in performance. A limiting factor also is the migration of burning catalysts, phlegmatizers (deterrents) and other surface treating agents, which influences the ballistic performance. In order to predict these service lives, one needs to measure properties P, which are related to the decomposition and migration processes, and which can be determined with high enough accuracy as a function of time and temperature. Such properties are:

- decrease of the mean molar (molecular) masses Mn, Mw and Mz (P = M)
- decrease of the stabilizer content (P = S)
- change in concentration of antioxidant, burning catalyst, deterrent (P = A, C, D)
- mass loss (P = ML)
- heat generation (P = Q)

Presented on the 87th Symp. of the Propulsion and Energetics Panel of the AGARD, Athens, Greece, 1996.

Paper presented at the AGARD PEP Symposium on "Service Life of Solid Propellant Systems" held in Athens, Greece, 10-14 May 1996, and published in CP-586.

- gas generation (P = G)

To make lifetime predictions at 20°C or with temperature-time profiles, one must accelerate the decomposition and migration processes by storing the materials at higher temperatures and describe the measured data mathematically. Storage temperatures between 50°C and 90°C are taken in the most cases. In spite of the small range, there can be a mechanistic change in the decomposition reactions. To be shure whether there is a change or not is a matter of much effort. Such mechanistic changes have a very pronounced effect on the prediction.

The mathematical description is achieved by so-called rate equations for the change of the property P = f(t,T,...). In the following only time t and temperature T as variables are taken. In some cases further variables are needed such as oxygen access and humidity. The rate equation separates the variables by introducing a rate constant $k_P(T)$ = f(T), which is only a function of temperature, eq.(1).

(1) $$\left(\frac{dP(t,T)}{dt}\right)_T = V_P = S \cdot k_P(T) \cdot f\left[P(t,T); g(t,T)\right]$$

$\left(\frac{dP(t,T)}{dt}\right)_T$	rate of change of property P(t,T)
$k_P(T)$	rate constant, only a function of temperature
$g(t,T)$	parameters and quantities, which influences V_P
$f\left[P(t,T); g(t,T)\right]$	specification of the kinetic formulation
S	= +1: P increases with time = - 1: P decreases with time

The temperature dependence of $k_P(T)$ is for chemical reactions and diffusion (migration) given by Arrhenius type equations, eq.(2):

(2) $$k_P(T) = Z_P \cdot \exp\left(-Ea_P / RT\right)$$

The Arrhenius parameters Z_P (preexponential factor) and Ea_P (activation energy) are determined from the experimental k_P values with eq.(2). The k_P values are determined from the measured data according to eq.(1) or the integrated form of eq.(1). The service lifetimes can now be calculated for any temperature by defining so-called degrees of degradation or degrees of change y_P of the property P, eq.(3).

(3) $$y_P = \frac{\text{limit value for P}}{\text{original value of P}} = \frac{P_L}{P(0)} = \frac{P(ty_P(T))}{P(0)}$$

The $ty_P(T)$ is the time at temperature T after which the limit value P_L is reached. These are the desired service lifetimes. P(0) is the value of P after manufacture or at the beginning of the ageing investigation. The value of y_P depends on the property P, the accuracy of the measured data, the safety factor. The times $ty_P(T)$ are reciprocal to $k_P(T)$ and one gets, with the proportionality constant d, eq.(4).

(4) $$ty_P(T) = \frac{d}{k_P(T)} = \frac{d}{Z_P} \cdot \exp(+Ea_P / RT) \quad \text{or} \quad \ln\left(ty_P(T)\right) = \ln(d / Z_P) + \frac{Ea_P}{RT}$$

To achieve a good prediction, it is very important to fulfill the following conditions:

- the suitable properties P must be selected
- the properties P must be measured with high accuracy
- the description according to eq.(1) must reproduce the measured data very well
- the description according to eq.(1) must extrapolate the data very well in the time axis
- the appropriate temperature dependence of $k_P(T)$ must be found
- the right temperature range for the accelerated ageing must be used.

For the temperature parameterization sometimes another type than of Arrhenius is applied. One form is eq.(5) and was used by W.Will /1/, but it is also associated with P.E.M. Berthelot.

$$(5) \quad \ln\left(k_P(T)\right) = a + b \cdot T \qquad \text{or} \qquad k_P(T) = c \cdot \exp(+b \cdot T)$$

From this follows eq.(6).

$$(6) \quad ty_P(T) = \frac{d}{c} \cdot \exp(-b \cdot T) \qquad \text{or} \qquad \ln\left(ty_P(T)\right) = \ln(d/c) - b \cdot T$$

After /2/ Berthelot used another form: $k_P(T) = a + b \cdot T$. It must be pointed out clearly that the correct form for the temperature dependence is eq.(2). If one can use eq.(5) or eq.(6), than there is very probably a change in the reaction mechanism with temperature. This will be shown in section 3.2.1 with an example. The reason to use eq.(6) can be also to have a high safety factor, because eq.(6) gives lower values for $ty_P(T)$ than eq.(4). This is especially true with a change in reaction mechanism. But the reliable way is, to determine the corresponding Arrhenius parameters correctly. However, this is at lower temperatures also a question of the expendable time for the investigation.

The rate equations to describe the quantities mass loss, heat generation, stabilizer consumption and molar mass degradation have been discussed in more detail in /3/ and therefore are only mentioned here.

3. LIFETIME PREDICTION WITH MOLAR MASS DECREASE AND STABILIZER CONSUMPTION

3.1 Molar mass decrease

The decomposition of nitrocellulose (NC) starts with the splitting off of NO_2 from CO-NO_2 - groups. This cannot be stopped. Stabilizers only can catch the NO_2. They prevent that the very reactive radical NO_2 attacks the cellulose backbone, which would further destroy the NC. The splitting off of NO_2 produces a radical at the backbone, which stabilizes itself in consecutive reactions, whereby small stable molecules are given off and at least one chain element of the NC is decomposed, that means a scission of the NC chain. This takes place with and without stabilizers and the mean molar masses of NC are lowered during the service life. The effect that stabilizers only slow down the ageing process is found also with HTPB-binder, which must be protected against the reaction with oxygen by the means of antioxidants. The decrease of the mean molar masses of NC can be measured precisely with gel permeation chromatography (GPC) /4/.

The equation used for the reproduction of the decrease of the mean molar masses Mn (number average), Mw (mass average) and Mz (Z-average) of nitrocellulose in propellants is given in eq.(7) for Mw. The quantity An is a conversion factor to convert relative Mn values from GPC to absolute ones /3/. The molar mass of one chain unit is m and D = Mw/Mn is the polydispersity.

$$(7) \quad \ln\left(1 + \frac{m \cdot D(t,T)}{An \cdot Mw(t,T)}\right) = \ln\left(1 + \frac{m \cdot D(0)}{An \cdot Mw(0)}\right) + k_M(T) \cdot t$$

The equation is based on a model, which assumes statistical chain scission by decomposition of chain elements /3, 5/. The number of chain elements decreases according to a reaction of first order. The lifetimes $ty_{Mn}(T) \approx ty_{Mw}(T)$ are calculated with eq.(8) by introducing $y_{Mn} \approx y_{Mw}$, which is expressed according to eq.(3) and eq.(7).

$$(8) \quad ty_{Mn}(T) = \frac{1}{k_M(T)} \ln\left(\frac{\frac{1}{y_{Mn}} + \frac{An \cdot Mw(0)}{m \cdot D(0)}}{1 + \frac{An \cdot Mw(0)}{m \cdot D(0)}}\right)$$

Reasonable values of y_{Mn} are between 0.6 and 0.9. Fig. 1 shows a part of the data for the molar mass degradation of nitrocellulose (NC) of the single base gun propellant A5020 (caliber 20mm). The stabilizer is diphenylamine (DPA) and the grains are surface treated with ethylcentralite (EC). The mean molar masses Mn, Mw and Mz were determined at 40°C, 50°C, 60°C, 70°C, 80°C, 90°C, 100°C and 110°C by GPC. The curves in Fig. 1 are eq.(7) fitted to the data with k_M as the only fit parameter. The Mw-values are back-calculated from eq.(7). The following start data were used: Mw(0) = 263.96 kg/mol, D(0) = 5.28, An = 0.8, m = 280.75 g/mol. The polydispersities D(t,T) were smoothed with polynomials of order one or two.

From the Arrhenius plot of the k_M-values, shown in Fig. 2, two distinct temperature regions can be recognized, with a transition at about 60°C. The corresponding Arrhenius parameters are listed in Table 1.

Table 1: Arrhenius parameters for the molar mass decrease of NC in GP A5020.

temp.range[°C]	Ea_M[kJ/mol]	Z_M[1/s]	lg(Z_M[1/s])	k_M-type
40-60	58.7	0.0741	-1.13	$k_{M2}(T)$
60-110	144.0	2.089 E+12	12.32	$k_{M1}(T)$
40-110	123.7	2.455 E+9	9.40	$k_{Ma}(T)$

$k_{Ma}(T)$ is the average over the whole temperature range. The storage times for the degrees of degradation y_{Mn} = 0.90, 0.75, and 0.60 at temperatures between 20°C and 100°C are given in Table 2. In the left hand columns of the main columns the values listed were calculated with $k_{M1}(T)$ (extrapolation from the upper temperature region), while in the right hand columns the values were calculated using $k'_M(T)$, which is formed according to the following equations:

$k'_M(T) \equiv k_{M1}(T) = Z_{M1}\exp(-Ea_{M1}/RT)$ from 70°C to 110°C

$k'_M(T) \equiv k_{M2}(T) = Z_{M2}\exp(-Ea_{M2}/RT)$ from 20°C to 50°C

$k'_M(T) \equiv k_{M1}(T) + k_{M2}(T)$ for 60°C

Table 2: Lifetimes ty_{Mn} for the molar mass decrease in GP A5020 at different degrees of degradation y_{Mn}.

	y_{Mn} = 0.90				y_{Mn} = 0.75				y_{Mn} = 0.60			
temp.	$ty_{Mn} = f(k_{M1})$		$ty_{Mn} = f(k'_M)$		$ty_{Mn} = f(k_{M1})$		$ty_{Mn} = f(k'_M)$		$ty_{Mn} = f(k_{M1})$		$ty_{Mn} = f(k'_M)$	
[°C]	[d]	[a]	[d]	[a]	[d]	[a]	[d]	[a]	[d]	[a]	[d]	[a]
20		534.8		9.5		1603.3		28.6		3202.8		57.1
30		76.2		4.3		228.4		12.9		456.2		25.8
40		12.3		2.1		36.8		6.1		73.6		12.3
50		2.2		1.0		6.7		3.1		13.3		6.1
60	162.1		88.2		486.0	1.3	264.3	0.7	970.9	2.7	527.9	1.5
70	35.6		35.6		106.8		106.8		213.4		213.4	
80	8.5		8.5		25.6		25.6		51.1		51.1	
90	2.2		2.2		6.6		6.6		13.2		13.2	
100	0.6		0.6		1.9		1.9		3.7		3.7	

With the data of both temperature regions, one obtains much shorter times compared with those calculated with k_{M1} only. The times in the right columns are more realistic. 28.6 years are predicted to reach a degree of degradation y_{Mn} = 0.75 at 20°C with k'_M, while with k_{M1} the extrapolation gives 1603.3 years.

The decrease in chain length of the NC by ageing reduces the compressive strength of the GP grains. This can shift the brittle - ductile transition to higher temperatures, which means that with ageing the danger of low temperature embrittlement increases /3/. Because of this loss in compressive strength, the impact pressure during the ignition can shatter the grains, which leads to an increase of the burning rate and this can build up gas pressure waves, which may destroy the gun by breech blow. The conclusion is that the safe lifetime may be limited by molar mass degradation with NC based GP.

3.2 Stabilizer consumption

3.2.1 Lifetimes for the GP A5020

As said above, stabilizer consumption and molar mass decrease of the NC are strongly correlated. From the way the stabilizer decreases a reaction of first order should be usefull to describe the consumption, eq.(9). This is called 'model 1' or 'exponential model'.

(9) $S(t,T) = S(0) \cdot \exp(-k_S(T) \cdot t)$

The lifetimes are given by eq.(10).

$$(10)\quad ty_S(T) = \frac{1}{k_S(T)} \cdot \ln\left(\frac{1}{y_S}\right)$$

The times $t_0(T)$ to reach the stabilizer content $S(t_0(T))=0$ are infinite, which is not the case with real propellants. A better reproduction of stabilizer consumption is achieved by a combination of the reactions of first and zero order /6/, called 'model 2' or 'exponential + linear model'. For this model eq.(11) gives S(t,T) and eq.(12) gives $ty_S(T)$.

$$(11)\quad S(t,T) = \left(S(0) + \frac{k_S^2(T)}{k_S^1(T)}\right) \cdot \exp\left(-k_S^1(T) \cdot t\right) - \frac{k_S^2(T)}{k_S^1(T)}$$

$$(12)\quad ty_S(T) = \frac{1}{k_S^1(T)} \ln\left(\frac{1 + \dfrac{k_S^2(T)}{S(0) \cdot k_S^1(T)}}{y_S + \dfrac{k_S^2(T)}{S(0) \cdot k_S^1(T)}}\right)$$

For $y_S = 0$ one gets from eq.(12) the $t_0(T)$-values to reach the stabilizer content zero. Both reaction rate constants are of Arrhenius type, whereby the two Ea_S and two Z_S have the corresponding indices. Model 2 has a much better extrapolation ability than model 1, see /3, 6, 7/, and therefore predicts more reliable lifetimes.

Some of the data of the diphenylamine decrease in GP A5020 (S(0)=0.67 mass%) are shown in Fig. 3. The broken lines are fitted with eq.(9), the solid curves are eq.(11). For comparison, a reaction of zero order is also shown, indicated as 'linear'. The best description is achieved with eq.(11). The Arrhenius plot of the $k_S(T)$-values from the evaluation with model 1 is presented in Fig. 4. As in the case of molar mass decrease, two distinct temperature dependencies of the k_S-values are found. The parameters are given in Table 3.

Table 3: Arrhenius parameters for the diphenylamine decrease in GP A5020, model 1 and 2. The x is a 'blank' for the parameters of model 1.

temp.range[°C]	Ea_S^x[kJ / mol]	Z_S^x[1 / s]	lg(Z_S^x[1 / s])	x	k_S^x - type
40-60	85.7	2.25 E+6	6.352		$k_{S2}(T)$
60-100	145.7	6.18 E+15	15.791		$k_{S1}(T)$
40-100	127.7	1.45 E+13	13.161		$k_{Sa}(T)$
60-100	138.3	3.078 E+14	14.488	1	$k_S^1(T)$
60-100	152.1	5.446 E+15)[1]	15.736	2	$k_S^2(T)$

)[1] The unit of $k_S^2(T)$ and Z_S^2 is 'mass%/s'.

The $k_{Sa}(T)$ is again the average over the whole temperature range. The two regions are also found with model 2. The data at 40°C have a to high y_S-value so that model 2 cannot be used. For the application of model 2 y_S must be at least 0.5 or smaller.

In Table 4 the calculated lifetimes are listed for y_S=0.005. In the first column the times are calculated according to eq.(10) with $k_{S1}(T)$, in the second column according to eq.(12), in the third column according to eq.(10) with $k'_S(T)$, which is formed analogously to $k'_M(T)$:

$k'_S(T) \equiv k_{S1}(T) = Z_{S1}\exp(-Ea_{S1}/RT)$ from 70°C to 110°C

$k'_S(T) \equiv k_{S2}(T) = Z_{S2}\exp(-Ea_{S2}/RT)$ from 20°C to 50°C

$k'_S(T) \equiv k_{S1}(T) + k_{S2}(T)$ for 60°C

In the fourth column the times are calculated according to eq.(13), which is obtained from eq.(6), lg means the decadic logarithm

$$(13)\quad \lg\left(ty_S(T)\right) = A - B \cdot T[°C]$$

Table 4: Lifetimes of GP A5020 with S(0) = 0.67 DPA, calculated for $y_S = 0.005$ according to model 1, model 2 and model 1 with low temperature data and model 1 with a 'linear extrapolation'.

temp. [°C]	$ty_S = -\ln(y_S)/k_{SI}$		$ty_S = f(k_S^1, k_S^2)$		$ty_S = -\ln(y_S)/k_S'$		$ty_S = 10^{(A-B\cdot T[°C])}$	
	[d]	[a]	[d]	[a]	[d]	[a]	[d]	[a]
20		2485.5		1096.0		139.1		495.1
30		346.0		157.4		43.6		121.0
40		54.6		25.5		14.7		29.6
50		9.7		4.6		5.3		7.2
60	692.9	1.9	335.5	0.9	359.0	0.98	644.2	1.8
70	149.6		73.3		149.6		157.4	
80	35.2		17.4		35.2		38.5	
90	9.0		4.5		9.0		9.4	
100	2.5		1.23		2.5		2.3	

The parameters A and B are determined in the following way. With the experimental k_S-values obtained from the measurements at at 60°C, 70°C, 80°C, and 90°C the corresponding times ty_S are calculated according to eq.(10). These are used in eq.(13) to obtain the parameters A and B, which have the values: A = 6.481 B = 0.0612 in 1/°C for ty_S in days. Then the numbers in Table 4 were calculated with eq.(13). This procedure works also with model 2. The values of the lifetimes depend on the type of determination. With model 1 and the high temperature data on gets at 20°C a lifetime of 2486 years, with model 2 1096 years. Using also the low temperature data, model 1 predicts 139 years, which is probably the best value obtainable from the determined data. If only data from the higher temperature range are available, the so-called 'linear extrapolation' predicts times, which are in the same order of magnitude as the values calculated with the full set of experimental data. At 20°C one gets 495 years.

3.2.2 Lifetimes determined with temperature-time profiles

In service GPs and RPs are exposed not to constant but to variing temperatures. For this situation representative temperatures-time profiles can be established, and for a reliable prediction in service they must be established. The above eq.(9) and eq.(11) can immediatly used for profile conditions, which is formulated for model 2 in eq.(14).

$$(14)\quad S(\Delta t_i, T_i) = \left(S(\Delta t_{i-1}, T_{i-1}) + \frac{k_S^2(T_i)}{k_S^1(T_i)} \right) \cdot \exp\left(-k_S^1(T_i)\cdot \Delta t_i\right) - \frac{k_S^2(T_i)}{k_S^1(T_i)}$$

$i = 1,2,3....n$ number of the profile step i

for $i = 1$ $S(\Delta t_{i-1}, T_{i-1})$ is equal to S(0) for the first profile cycle j=1, otherwise it is equal to the end value of profile cycle (j-1) for profile cycle j

Δt_i and T_i are the time intervall and the temperature of profile step i

The lifetime t_{PC} for one profile cycle is, eq.(15),

$$(15)\quad t_{PC} = \sum_{i=1}^{n} \Delta t_i$$

Eq.(14) is used in a loop until the given degree of stabilizer consumption y_S is reached. The entire lifetime adds up to $ty_S = j \cdot t_{PC}$, where j is the number of full profile cycles applied to reach y_S or a value just above y_S.

In Table 5 two examples are given. The lifetimes of the double base rocket propellant (RP) RLC 470/6A and GP A5020 for isothermal and profile stresses are calculated according to model 1 and model 2 with the corresponding Arrhenius parameters, which are for RP RLC 470/6A (S(0)=1.56mass% 2-nitro-diphenylamine) listed in Table 5. Two profiles have been taken from STANAG 2895 type M1 (maritime hot) and one profile is used by the automobile industry for airbag qualification, called Phoenix (very hot and dry).

The profiles STANAG - M1 - IDM and Phoenix - AMI include high temperatues. The time averaged mean temperature T_{tav} is 51.6°C and 37.7°C respectively. For these two profiles the lifetimes to reach $y_S = 0.1$ are nearly the same and not influenced by the low temperature region, as the results of GP A5020 show. The profile STANAG - M1 - EDM has not so high temperatures, they are below 50°C, T_{tav} is 32.5°C. The predicted lifetimes are significantly longer, but depend on the low temperature region. With the better extrapolating model 2 shorter lifetimes are calculated than with model 1.

Table 5: Lifetimes calculated for $y_S = 0.1$ in years for isothermal and temperature-time profile stresses.

	RP RLC 470/6A		GP A5020		
temp. stress	expon. 60°C - 90°C	expon.+ linear 60°C - 90°C	expon. 60°C - 90°C	expon. + linear 60°C - 90°C	expon. two regions
20°C	2408	930	1080	787	60.5
30°C	338	170	150	116	19
40°C	54	33.5	24	19.1	6.4
50°C	9.6	7.0	4.2	3.5	2.3
ST. - M1 - IDM	3-4	3	1-2	1-1.5	1-1.5
ST. - M1 - EDM	80	51	35	29	10
Phoenix - AMI	3	2-2.5	1-1.5	1-1.5	1-1.5

STANAG - M1 - IDM: maritime hot, induced daily maximum values in air;
$T_{max} = 69°C$, $T_{tav} = 51.6°C$
STANAG - M1 - EDM: maritime hot, environmental daily maximum values in air;
$T_{max} = 48°C$, $T_{tav} = 32.5°C$
Phoenix - AMI: profile of the automobile industry for airbag qualification;
$T_{max} = 80°C$, $T_{tav} = 37.7°C$
Calculations for GP A5020 with the corresponding Arrhenius parameters from Table 3.
For the double base RP RLC 470/6A the following parameters have been used:

$Ea_S = 145.0$ kJ/mol $Z_S = 2.080$ E+15 1/s
$Ea_S^1 = 123.7$ kJ/mol $Z_S^1 = 8.434$ E+11 1/s
$Ea_S^2 = 184.6$ kJ/mol $Z_S^2 = 5.580$ E+20 mass%/s

4. HEAT GENERATION

The heat generations $dQ(t,T)/dt = \dot{q}(t,T)$ of the German gun propellants L5460 and KN6540 (which are similar to the US Army types JA2 and M30) have been measured with a microcalorimeter (Thermometric, Sweden) between 65°C and 85°C. The heat generation is directly proportional to the reaction rate. One measures the netto flux of the decomposition heat. In Fig. 5 the heat generation of the two GPs are shown at 80°C, with newly weighed-in samples. At the beginning one has often a peak, that means a high rate, which decreases, until plateau values are reached after some days. The two samples of L5460 have only about half of the heat generation of KN6540. In Fig. 6 and Fig. 7 the heat generation is shown at 85°C and 75°C, measured with the same samples. Here no equilibration behaviour is to see, the heat generations rise directly to the plateau values. KN6540 has at all temperatures a higher heat generation than L5460. Table 6 lists the data measured together with the Arrhenius parameters, which were determined according to eq.(16).

(16) $\ln(\dot{q}(t,T)) = \ln(Z_Q) - Ea_Q/RT$

Table 6: Measured heat generation of GP L5460 and GP KN6540.

temp. [°C]	$\dot{q}$ [µW/g] L5460	$\dot{q}$ [µW/g] KN6540
85	18.15	44.17
80	9.88	25.43
75	5.12	13.61
70	2.43	5.37
65	1.3	2.8
Ea_Q [kJ/mol]	134.6 ± 2.2	142.8 ± 5.7
lg (Z_Q[1/s])	20.9 ± 0.3	22.5 ± 0.9

Table 7: Times ty_Q to reach $y_Q = 0.03$ (3% from Q_{ex}) for GP L5460 and GP KN6540.

temp. [°C]	L5460 $\dot{q}$ [µW/g]	L5460 ty_Q [d]	L5460 ty_Q [a]	KN6540 $\dot{q}$ [µW/g]	KN6540 ty_Q [d]	KN6540 ty_Q [a]
20	8.159 E-4		5480	1.145 E-3		3406
30	5.044 E-3		886.4	7.917 E-3		493
40	2.776 E-2		161.1	4.838 E-2		80.6
50	0.138		32.4	0.264		14.8
60	0.618		7.2	1.30		3.0
70	2.55	640		5.86	243	
80	9.69	168.4		24.2	58.8	
90	34.25	47.6		92.4	15.4	
100	113.1	14.4		328.5	4.3	
Q_{ex} [J/g]	4700			4100		

The activation energies are similar, the value for KN6540 is somewhat higher than for L5460. From these data one can calculate an energy loss lifetime ty_Q with the assumption that the dQ/dt data are independent of time, eq.(17). Table 7 lists the times to reach the energy loss of 3% from the total explosion enthalpy Q_{ex}, that means a degree of energy loss $y_Q = 0.03$.

(17) $ty_Q = y_Q \cdot Q_{ex}/\dot{q}$

The lifetimes are again very long at low temperatures. The value of 47.6 days at 90°C for L5460 seems to high, because the autocatalytic increase in mass loss starts already at about 21 to 24 days, see Table 9. With a $y_Q = 0.015$ the lifetimes agree more with the mass loss data of L5460.

5. MASS LOSS

The German gun propellants single base A5020, single base K503 ('ball-powder', with some nitroglycerine), single base (with DNT) CD5240 (US M6), double base L5460 (US JA2) and triple base KN6540 (US M30) are compared to each other and with the energetic binder GAP (glycidyle azide polymer). In Table 8 the typical composition of the GPs is given. In Fig. 8 the mass loss (ML) data of the five GPs at 90°C and of GAP at 110°C and 120°C are to see.

Table 8: Typical compositions of the investigated GPs (in mass%).

GP	NC (N-content)	stabilizer	blasting oil	plasticizer	deterrent	others
A5020	93 (13.15)	DPA 1.2	-	DBP 2	EC 2	1.8
K503	83 (13.2)	DPA 1.0	NG 9	-	EC 5	2.0
CD5240	84 (13.15)	DPA 1.0	-	DBP 3.5	DNT 9	2.5
L5460	59 (13.0)	AC II 0.7	NG 15 DEGN 25	-	-	0.3
KN6540	28 (12.6)	EC 1.5	NG 23	-	-	0.5 NQ 47

AC II: acardite II DBP: dibutylphthalate DEGN: diethyleneglycoldinitrate DPA: diphenylamine
DNT: dinitrotoluene EC: ethylcentralite NG: nitroglycerine NQ: nitroguandine

Initialy all samples show an offset, Fig. 9, which is due to volatile components like residual solvents, water and low molecular mass decomposition products. The L5460 and the K503 have a sharp increase in ML when compared with A5020 and CD5240. The ML of KN6540 increases steadily from the beginning without a transition to a pronounced increase in rate as with the other GPs. From the whole curve up to about 40% (≈55% to 60% is the plateau value at 100°C to 110°C for KN6540) one can conclude that the autocatalytic reaction starts nearly at the beginning of the storage, that means the ML rate increases steadily. This is found also in the heat generation for KN6540, Fig. 6, which is not exactly constant but increases slightly. To describe the ML behaviour quantitatively, an autocatalytic model was used (Riccati differential eq. for dMr/dt), which is discussed in /3/. In Fig. 10 the fit of the model to the data of K503, L5460 and KN6540 are presented. The offsets in ML have been omitted. The model cannot reproduce the very sharp onset of the autocatalytic induced increase of the ML rate for K503. The data of L5460 are described satisfactorily and the data of KN6540 are well described. In Table 9 the characteristic data of the ML curves and the rate constants k_1 and k_2 from the autocatalytic description are given.

The non-autocatalytic part of the ML increases linear with time, that means it is a reaction of zero order. The corresponding behaviour is a constant heat generation. From this part of ML the experimental reaction rate constants k_{ML} have been determined. Further data are the 'time to 2% ML' (without the offset), 'time to autocatalytic acceleration', 'time to 2% ML' from k_{ML}, and the ratios of the k_{ML} to the k_{ML} of the A5020. The decomposition of L5460 is about three times faster than of A5020. For the KN6540 the initial parts of the curves can be linearized and the rate constants are four to seven times greater than the k_{ML} of A5020.

The energetic binder GAP is used in new formulations of GP, RP and high explosives. GAP can split off molecular nitrogen from the azide group. The activation energy for this is not greater than the bond energy of the 'CN-NN' bond in the azide group, which is 170 kJ/mol, see e.g. /8/. The investigations done till now on GAP allow the

conclusion that the mass loss is nearly completely caused by nitrogen loss. Fig. 11 shows the mass loss data of GAP-N100 (GAP cured with Desmodur N100) between 90°C and 130°C. If one assumes only nitrogen loss from

Table 9: Kinetic data of gun propellants and of GAP from mass loss (ML) at 90°C.

gun propellant	time to 2% ML without offset [d]	time to autocatal. accele-ration [d]	k_{ML} [%/d]	time to 2% ML from k_{ML} [d]	$\frac{k_{ML}}{k_{ML} - A5020}$	autocatalytic model (Riccati diff. eq.)		data up to ML [%]
						k_1 [1/d]	k_2 [1/d]	
A5020	54.5	48	1.67 E-2	119.8	1	6.59 E-5 0.0057 E-5	5.96 E-2 19.8 E-2	4 11
K503	31.2	30	3.56 E-2	56.2	2.1	7.35 E-5	16.0 E-2	14
CD5240	48.3	48	3.87 E-2	51.7	2.3	5.94 E-5	6.78 E-2	8
L5460	24.7	21	4.83 E-2	41.4	2.9	4.93 E-5	20.8 E-2	8
KN6540						90.2 E-5	1.02 E-2	16
lower part	23.7	(~ 1)	7.07 E-2	28.3	4.2	-	-	-
upper part	-	-	12.2 E-2	16.4	7.3	-	-	-
GAP, uncur.	~ 400	-	0.460 E-2	435	0.28	-	-	-
GAP, cured	?	-	0.292 E-2	685	0.18	-	-	-

the azide groups, the maximum mass loss can be determined as 24% to 25% for cured GAP and about 29% for uncured GAP. Subtracting the offset from the data at 130°C one gets nearly this value, the mass loss plateau is for both about 2% - 3% higher. From the initial linear parts of the curves the reaction rate constants $k_{ML}(T)$ have been determined according to a reaction of zero order. The Arrhenius plot is shown in Fig. 12, the data have a high correlation coefficient. The parameters are:

	Ea_{ML} [kJ/mol]	Z_{ML} [%/s]	r	temp.range [°C]
uncured GAP:	134.0 ± 4	12.0 ± 0.5	0.9988	80 - 120
cured GAP:	141.7 ± 4	12.9 ± 0.5	0.9988	90 - 130

The reason for the significantly lower activation energy than the bond energy is unknown. Such a low activation energy was found from TGA measurements also /9/. The rate constants for uncured and cured GAP at 90°C are listed in Table 9 too. The rate of mass loss is not so much smaller than the rate of A5020. The advantage of pure GAP is the non - autocatalytic decomposition. But the limit is the energy loss of GAP, which is directly proportional to the number of decomposed azide groups. A loss of 3% of the azide groups corresponds to a mass loss of only 0.87%, which will be reached after 189 days at 90°C for the uncured GAP and 0.74% for the cured GAP, reached after 253 days. The mass loss behaviour of rocket propellants based on ammonium nitrate and a GAP binder has been evaluated with the autocatalytic model also /10/.

6. SUMMERY

The ageing behaviour of propellants is investigated in order to predict their safe service lifetimes at conditions of changing environmental stress. To achieve this, quantities of the propellants must be measured as function of time and temperature, which are connected to the ageing processes and which can be measured with a high enough accuracy. Such quantities are the mean molar (molecular) mass degradation of polymers, stabilizer consumption, heat generation, gas generation, mass loss, the decrease of antioxidant, burning catalyst and surface treating agent. The data must be described in a mathematical form in such a way that the reproduction of the data and the extrapolation in the time axis is at least good. This means the description must have an inherent extrapolation ability. This can be obtained with empirical and model-based rate equations. Further, the temperature dependence must be parameterized appropriately for a reliable prediction.

For the gun propellant (GP) A5020 lifetimes are predicted with molar mass decrease and stabilizer consumption. Both quantities are described with kinetic models, which have a good inherent extrapolation ability. The model for molar mass degradation is based on a statistical chain scission caused by the decomposition of chain elements. Stabilizer decrease is best reproduced by a kinetic formulation, which combines the reactions of first and zero order. With regard to safe storage, the stabilizer consumption is the best quantity for the assessment. To judge safe

operation in service, mean molar mass decrease of the nitrocellulose can be the dominant quantity, because with the degradation of mean molar mass Mw the mechanical properties decrease. The GP A5020 shows in molar mass decrease and stabilizer decrease two distinct temperature regions in the Arrhenius plots of the reaction rate constants. The calculation of the lifetimes is strongly influenced by this. An approximation in the calculation can be made with the so-called 'linear extrapolation in temperature'. The different prediction results are compared.

The real situation in service of GPs is the exposure to time - temperature profiles. Three examples are given. Two profiles were taken from STANAG 2895 (type M1, maritime hot) and one profile from the industry for the qualification of airbags. If the temperature stress includes higher temperatures, the resulting lifetime is determined by the higher temperature reaction rates. For storage and service in a temperature range between <20°C and 50°C, the lower temperature reaction rates determine the lifetime.

The heat generation measured by a flux microcalorimeter is directly proportional to the reaction rate. Results for the double base GP L5460 (US JA2) and the triple base GP KN6540 (US M30) are given and the times have been calculated to reach a preset loss in energy content. The heat generations of these GP rises to nearly constant values, which corresponds to a reaction of zero order.

The mass loss behaviour of five German gun propellants is compared: single base A5020, single base K503, single base CD5240, double base L5460, triple base KN6540. First of all, after an initial offset due to volatile components, a linear increase in mass loss is observed, which is followed by an acceleration of the rate by autocatalytic decomposition. The curves can be described with autocatalytic kinetic models. A satisfactory till good reproduction of the data is achieved by a model, which assumes a zero order reaction in combination with an autocatalytic part. The kinetic data are given and compared with the mass loss rate of uncured and cured GAP (glycidyle azide polymer). The mass loss rate of the GP A5020 is only about three times higher than the mass loss rate of uncured GAP.

7. REFERENCES

/1/ W. Will, *Mitteil. Zentralstelle wiss.-techn. Untersuch. 2, 12 (1900) and 3, 7 (1902).*

/2/ T. Urbanski, *„Chemistry and Technology of Explosives", Vol II*, Pergamon Press, London, 1965.

/3/ M.A. Bohn, *„Methods and Kinetic Models for the Lifetime Assessment of Solid Propellants"*, Proceed. 87th Symp. of the Propulsion and Energetics Panel of the AGARD, Athens, Greece, 1996.

/4/ F. Volk, G. Wunsch, *Propell. Expl. Pyrot. 10, 181 (1985).*

/5/ A. Pfeil, H.H. Krause, N. Eisenreich, *Thermochim. Acta 85, 395 (1985).*

/6/ M.A. Bohn, *Propell. Expl. Pyrot. 19, 266 (1994).*

/7/ M.A. Bohn, *„Modellierung des Stabilisatorverbrauchs in Treibmitteln", Paper 42*, Proceed. 25th Internat. Annual Conference of ICT, 1994. Fraunhofer-Institut für Chemische Technologie.

/8/ M.A. Bohn, F. Volk, *„Adiabatische Selbstaufheizung bei Treib und Explosivstoffen", Paper 8*, Proceed. 24th Internat. Annual Conference of ICT, 1993. Fraunhofer-Institut für Chemische Technologie.

/9/ Y. Oyumi, *Propell. Expl. Pyrot. 17, 226 (1992).*

/10/ M.A. Bohn, J. Böhnlein-Mauß, K. Menke, *„Lifetime Assessment and Stability of AN/GAP Propellants"*, Proceed. 87th Symp. of the Propulsion and Energetics Panel of the AGARD, Athens, Greece, 1996.

8. FIGURES

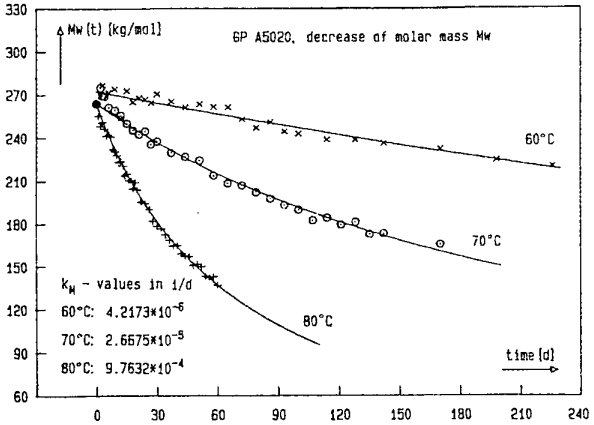


Fig. 1: Decrease of molar mass Mw of the NC in GP A5020. Lines are the model for molar mass decrease, eq.(7).

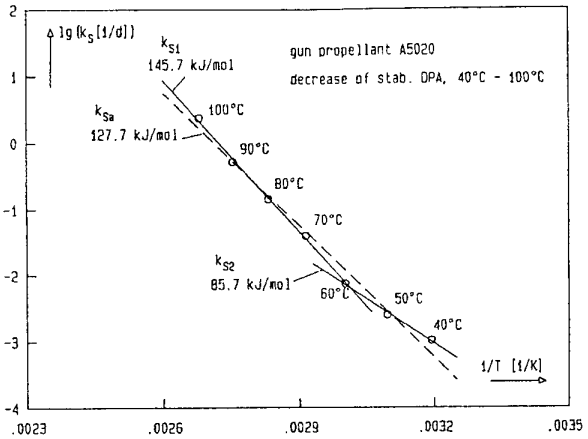


Fig. 4: Arrhenius plot of the reaction rate constants of the diphenylamine decrease in GP A5020.

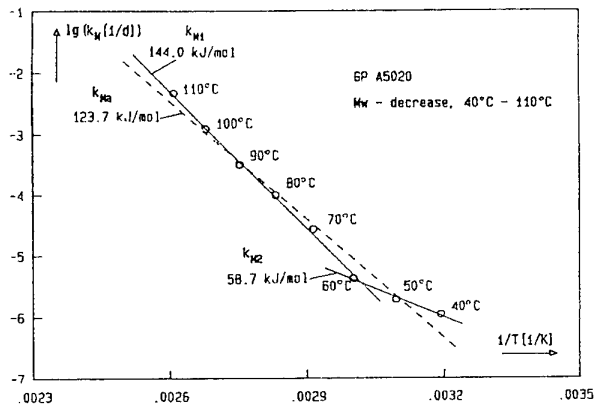


Fig. 2: Arrhenius plot of the reaction rate constants of molar mass decrease of the NC in GP A5020.

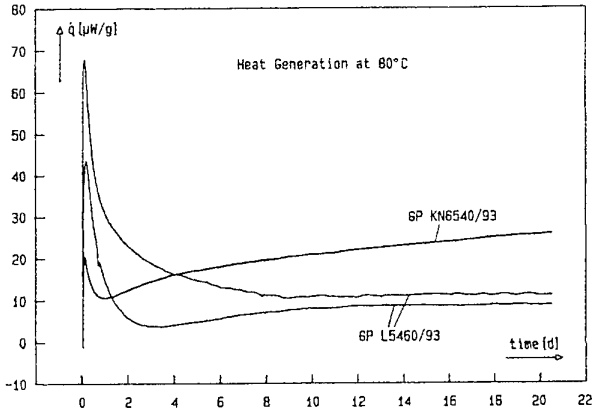


Fig. 5: Heat generation of GP L5460 and GP KN6540 at 80°C of newly weighed-in samples.

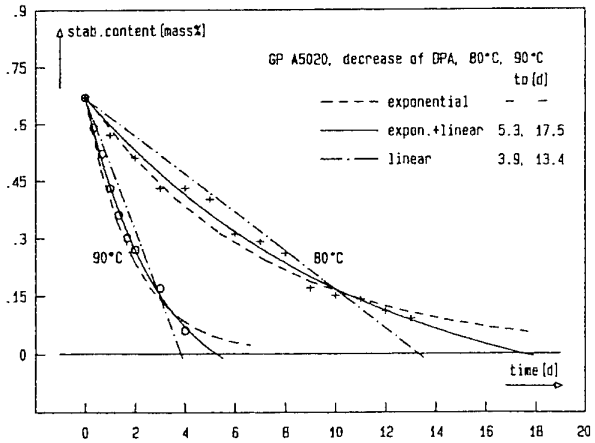


Fig. 3: Decrease of stabilizer diphenylamine (DPA) in GP A5020, part of the data. Evaluation with model 1 and 2 and a reaction of zero order.

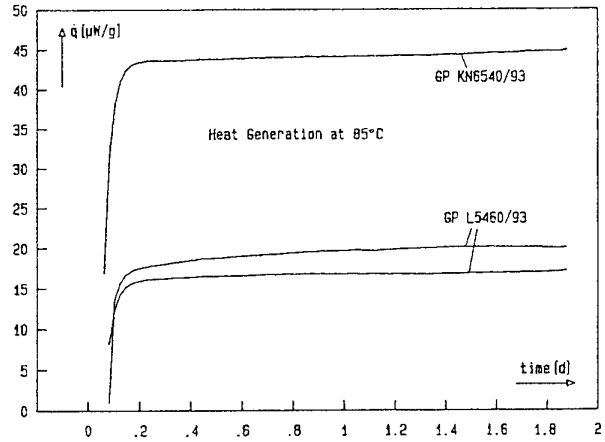


Fig. 6: Heat generation of the samples of Fig. 5 at 85°C. The curves show no inital equilibration as with newly weighed-in samples.

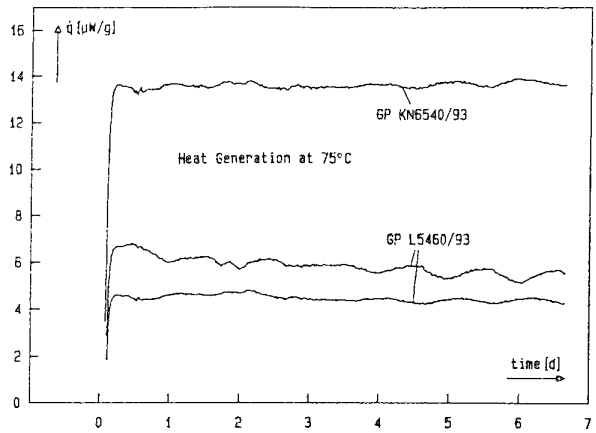


Fig. 7: Heat generation of the samples of Fig. 5 at 75 °C.

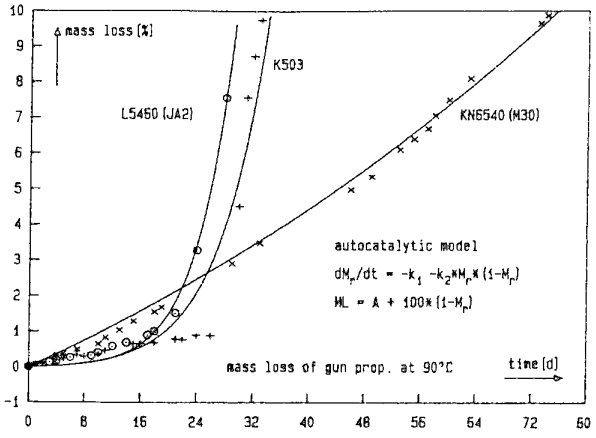


Fig. 10: Reproduction of the mass loss data (offset corrected) by an autocatalytic model /3/.

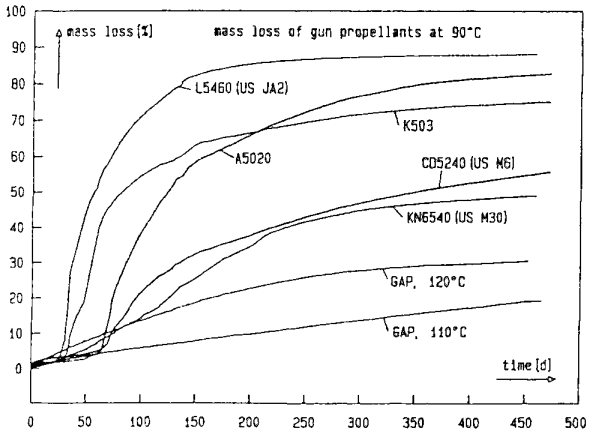


Fig. 8: Mass loss of five GPs at 90°C up to the plateau values and of GAP (uncured) at 110°C and 120°C.

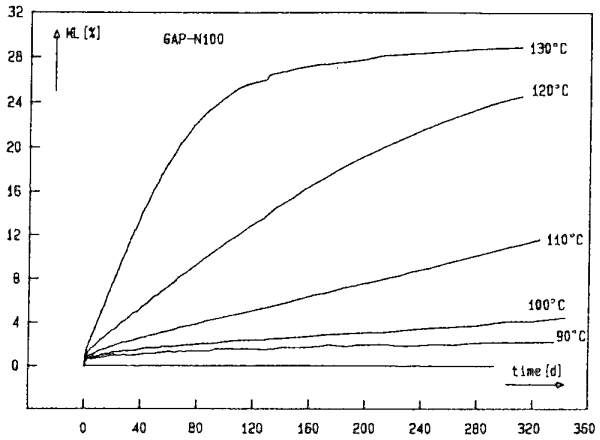


Fig. 11: Mass loss of cured GAP at temperatures between 90°C and 130°C. The curves show no autocatalytic behaviour.

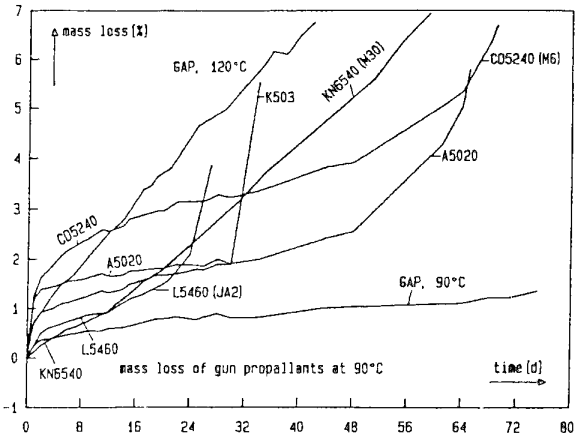


Fig. 9: Mass loss of five GPs at 90°C and of GAP (uncured) at 90°C and 120°C in the first part.

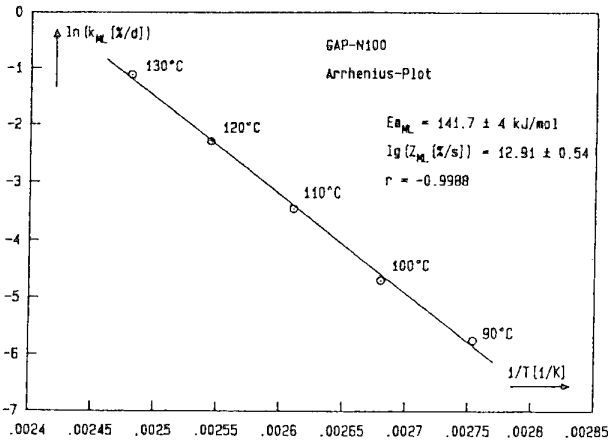


Fig.12: Arrhenius plot of the mass loss rate constants of the data of cured GAP, Fig. 11.

Paper Number: 20
Discussor's Name: Professor H. Schubert
Responder's Name: Dr. M. A. Bohn

Question: I have more of a philosophical question about the life time of propellants at normal conditions. May we really calculate some hundreds of years or more?
We are aware of a single base powder, which is now 80 years old and stable.
We are aware of double base propellants, from a sunken submarine, which are 40 years old and fulfill all ballistic conditions originally required. The question is, do we consider in our life time prediction of all possible influences on the stability? For instance: diffusion, evaporation, influences of inner surfaces, temperature cycling (day-night, summer-winter), etc. What is the influence on the lifetime of temperature cycling compared with constant temperature storage?

Answer: Your question addresses a point which can be formulated as 'What is the task of a prediction?' To answer this question, let me first show you with the following table, where prediction as a method to judge service life is located in the range of a degree of reliability as a criterion.

method to judge service life	used for	degree of reliability
assumption	planning the synthesis of a new energetic substance	low
estimation	planning a new propellant formulation	low to medium
prediction	assessment of safe service life	medium to high
surveillance	guarantee of safe service life	high

Surely, the best way is to observe the propellant over the whole period of its service life, this gives the highest reliability. A chemist with the task to synthesize a new energetic compound must judge it with regard to its thermal and chemical stability. From what is known already, he makes assumptions about the structure of the new compound. It is nearly a platitude to say but is a matter of fact that the real stability will be recognized after the substance has been synthesized. Therefore the degree of reliability is low in this situation. The

situation in planning a new formulation is somewhat better. One knows at least the stability of the single components quite well and can make an estimation about the stability and possible service life of the new formulation. The degree of reliability is now higher, but still relatively low.

The prediction as a method uses the change of one or more relevant property(ies) with time and temperature of a compound or a formulation to judge the time-temperature stability, which is determined for example with the vacuum stability test, the Dutch test, the Abel test and the Bergmann-Junk test. With this method one finds to what an extent the chemical reactions between the components of a formulation or the time and temperature effect on a single component limit the stability. It is the first method to judge the time-temperature behavior of an energetic substance in which moderate temperatures are used and which can give an answer of how long the lifetime can be. The method also indentifies the limiting processes and chemical reactions, and which indicate what can be done to stabilize the formulation. One part of the task of prediction is therefore to assess new compounds and new formulations with regard to their possible lifetime and to make suggestions for possible improvements.

Another part of the task is to make a prediction of service life for a known formulation which is already in field service. The standardized surveillance used by the armed forces does not allow a prediction. It is a continuous observation of the propellants. At this point the answer of the second part of the question starts. One can now even extend the question. Can surveillance done in the current way consider all the possible influences on service life, especially temperature cycling and the accompanying 'breathing' that changes the ambient atmosphere of the propellant grains? The answer to this part of the question is that we do not know the influence of all these parameters or variables. There have only been rare investigations until now. Mostly, only a type of global action of these parameters and variables has been included in the investigations, so in part the prediction contains these influences, but not as specified and separated variables.

As one has seen with the prediction of lifetime for the GP A5020 the predicted lifetime depends on the range of temperature from which the experimental data have been obtained and on the extrapolation method. The procedures work correctly. The more experimental data one determines the higher is the degree of reliability. But it is not the task of prediction to replace a necessary surveillance. The procedures developed to make a prediction can be used in surveillance. A procedure, which gives a very long lifetime is of value and suitable to judge the lifetime relatively. To predict service lifetime absolutely, one must determine the data corresponding to the condition in service.

LOVA Propellant Aging: Effect of Residual Solvent

R. A. Pesce-Rodriguez and R. A. Fifer
U.S. Army Research Laboratory
AMSRL-WT-PC, Aberdeen Proving Ground, MD 21005-5066
USA

1. SUMMARY:

An investigation of LOVA propellant aging was performed to identify the cause of stabilization periods in certain propellant lots. Two important observations were made: 1) the level of residual solvent in propellant grains slowly decreases while in storage; and (2) during the drying process and while the grains are in storage in storage, plasticizer "co-migrates" with solvent, resulting in plasticizer accumulation at grain surfaces. It was also observed that while in storage, residual solvent may be oxidized to generate organic acids. Based on these results, it is proposed that stabilization periods result from processes related to migration, evaporation, and oxidation of residual solvent.

Dans le but d'identifier la cause de la période de stabilisation pour certains lots de poudre, on a mené une étude du vieillissement des poudres LOVA. Deux observations importantes ont pu être effectuées : 1) le niveau de solvants résiduels dans les grains de poudre diminue lentement pendant le stockage ; et 2) pendant le séchage et le stockage des grains, le plastifiant « co-migre » avec les solvants, ce qui résulte en une accumulation de plastifiant à la surface des grains. On a également observé que, lors du stockage, les solvants résiduels peuvent s'oxyder pour donner naissance à des acides organiques. Sur la base de ces résultats, on peut avancer que la période de stabilisation est le résultat de processus de migration, d'évaporation et d'oxydation des solvants résiduels.

2. INTRODUCTION

The stimulus for initiating this investigation was the observation that certain nitramine-based propellants experience a "stabilization period". Stabilization periods can last as long as 20 weeks, and are characterized by measurements of breech pressure which gradually decrease before leveling-off at some constant value. Identification of the cause of the stabilization periods has been hampered by the absence of a coordinated ballistic, mechanical, and chemical testing program. The specific objective of this investigation was to examine the chemical aspect of the aging problem and, where possible, ascribe the results to potential variations in ballistic and mechanical properties.

To understand the propellant aging problem, the two following questions must be answered: 1) Which propellant component(s) is (are) responsible for the chemical and/or physical changes that occur during the stabilization period? 2) Why do formulations with identical formulations demonstrate different aging behavior? In our investigations, the most important observations made were those indicating a correlation between the migration of residual solvent and the migration (and accumulation) of plasticizer. Based on these observations, it is proposed that residual solvent is the source of the LOVA aging problem. A solution to the aging problem therefore appears to depend on the re-evaluation of the current drying processes, storage conditions, and standards for permissible residual solvent level.

As a bit of background regarding the effects of storage conditions and residual solvent content on propellant aging, the following information on propellant storage is provided: The volume of a typical storage drum (a *LEVER-PAC*) is approximately 75 liters, and is filled to approximately 20 cm from the top of the drum with 68 kg (150 pounds) of propellant. Drums are covered with a lid that is secured with a "snap-tight" ring. The volume occupied by the 68 kg of the propellant stored in the drum is approximately 40 liters. This leaves 35 liters of free volume in the drum, of which 20 liters is above the stored propellant, and 15 liters is in the space between the grains. In a drum that contains propellant with a residual solvent content of 0.25 wt-% (the US Military Specification limit for dried propellant of this type), there is approximately 170 g of solvent. Considering the vapor pressure of ethyl acetate (73 mm at 20°C) and the free volume available, approximately 12 g of solvent will be in the vapor phase. Of this, 7 g will occupy the space above the propellant, and 5 g will occupy the space between grains. The remaining 158 g of solvent will remain trapped in the propellant grains. If there is a leak in the drum, or if the drum is opened, solvent vapor will escape from the drum. Eventually, the propellant grains will be depleted of residual solvent.

3. EXPERIMENTAL

Three methods for the characterization of solid propellants were used in this investigation: micro-reflectance Fourier transform infrared spectroscopy[1,2] (FTIR-mic) and photoacoustic-FTIR[3-6] (PA-FTIR) spectroscopy for the nondestructive examination of chemical composition at propellant surfaces, and desorption-gas chromatography FTIR (D-GC-FTIR)[7] spectroscopy for the monitoring of desorption of volatiles such as residual solvent. PA-FTIR and FTIR-mic spectra were obtained on a Mattson Polaris FTIR spectrometer using First software (Kramers-Kronig transformations[8] were used to correct reflectance spectra). For PA analysis, a helium-purged MTEC Model 100 PA cell was used. The velocity of the moving mirror was 0.316 cm/sec. Carbon black (Norit-A) was used to obtain background spectra. FTIR-mic spectra were obtained using the Spectra-Tech IR-Plan® infrared microscope with a mercury-cadmium-telluride (MCT) detector. The microscope was operated in reflectance mode, and aluminum foil was used to obtain background spectra. For all spectra, 32 scans were collected with a

Paper presented at the AGARD PEP Symposium on "Service Life of Solid Propellant Systems" held in Athens, Greece, 10-14 May 1996, and published in CP-586.

resolution of 8 cm^{-1}. Desorption experiments were performed with a CDS Model 122 Pyroprobe® (coil probe, sample in quartz tube) connected via a heated interface chamber to the splitless injector of a Hewlett Packard GC-FTIR system (Model 5890 GC and Model 5965 IRD® with narrow band MCT detector). D-GC-FTIR conditions are provided in Table 1.

Table 1. Desorption-GC-FTIR Conditions

Pyroprobe conditions	
Pulse temperature:	100°C
Pulse duration:	20 sec.
GC Conditions	
Column type:	Quadrex capillary
Column dimentions:	0.32 mm x 25m
Stationary phase:	3μm OV-17 film
Temperature program:	50°C for 3 min
	50 → 200°C @ 10°/min
	200°C for 10 min
Injector temperature:	200°C
Interface temperature:	100°C
Light pipe temperature:	200°C
Transfer lines temp.:	200°C
FTIR conditions	
Sampling rate:	3 interferograms/sec
Resolution:	8 cm^{-1}

The composite propellant grains used in this investigation were cylinders having a length and diameter of approximately 1 cm. The four formulations examined in this investigation were all RDX/CAB/NC-based. Other additives include stabilizer, plasticizer, and a proprietary processing aid. Two different plasticizers (P1 and P2) were used; both are energetic materials with proprietary structures. Table 2 lists the plasticizer(s) used in each formulation. The other propellant ingredient are RDX (1,3,5-trinitro-1,3,5-triazacyclohexane), CAB (cellulose acetate butyrate) and NC (nitrocellulose). All propellant grains were processed using a mixture of ethyl acetate and ethyl alcohol.

Table 2. Plasticizers Used in Propellant Formulations

Formulation	Plasticizer
F1	P1 only
F2	P1 & P2 (2:1)
F3	P1 & P2 (1:1)
F4	P2 only

To examine the effect of grain geometry and drying conditions on plasticizer level, six specially processed sets of formulation F4 samples were used. Table 3 gives a description of these samples. Formulations F1, F2, and F3 were all processed under "standard" conditions. Except for "undried" F3, all grains were dried for 2 days at ambient temperature, then 2 additional days at 60°C, and then stored under ambient conditions prior to analysis. Analysis by FTIR-microscopy was initiated one week after completion of the 60°C drying process; samples were subsequently kept in unsealed vials during the 10 month examination period. Table 4 describes the storage conditions of samples analyzed by D-GC-FTIR (formulation F4 only).

Table 3. Description of Specially Processed F4 Samples

Sample	Perforations		Processing Conditions[a]
	No.	size (mm)	
A	0	---	---
B	1	3.0	---
C	19	0.38	---
D	19	0.38	t_{mix} = "std" + 1 hr
E	19	0.38	T_{mix} = "std" + 15°C
F	19	0.38	t_{dry} (@ 60°C) = "std" + 1 week

[a] other than proprietary "standard" conditions
T_{mix}: mixing temperature t_{mix}: mixing time

Table 4. Storage Conditions for F4 Samples Analyzed by Desorption-GC-FTIR

Set Number	Days stored in sealed bottle[a]	Days since removal from sealed bottle[a,b]
1	3	158
2	153	8
3	161	0

(a): all samples stored at ambient temperature, except for sample F (of each set), which was stored uncovered in a 60°C oven
(b): after removal from sealed bottle, samples were stored uncovered at ambient temperature

For analysis of plasticizer levels at interior "bulk" surfaces by FTIR-mic, grains were cross-sectioned by cleaving them lengthwise through the center row of perforations (see Figure 1). The surfaces examined did not come in contact with the blade used to cleave the grains. Measurements at the interior bulk surface and exterior "circumferential" surface were made on three different grains of each type and then averaged. The same 18 grains (3 grains of each of the 6 types) were analyzed during

the course of the FTIR-mic investigation. To aid in consistently analyzing the same area on these samples, measurements were made in the centers of small circles (approximately 1 mm in diameter) outlined with a pencil on each of the samples.

4. RESULTS & DISCUSSION

4.1. D-GC-FTIR Investigations.

Figure 2 shows chromatograms generated via FTIR detection of volatile components desorbed from the propellant samples; note that the data in set #1 was obtained approximately 22 weeks *after* the data in set #3. Identities of the peaks were determined by on-line searches of spectral databases, and are summarized in Table 5. Suspected sources of the observed peaks are also given in Table 5. Note that due to its low vapor pressure and vaporization rate, desorbed plasticizer is not observed in any of the chromatograms.

Table 5: Identity and source of peaks in Figure 2

Retention Time (min)	Identity	Suspected Source
5.2	ethyl acetate	processing solvent
10.1	acetic acid	oxidation of processing solvents
11.8	a carboxylic acid	oxidation of processing aid
13.6	isooctanol	solvent for processing aid
14.6	isooctanoic acid	oxidation of isooctanol

The chromatograms in Figure 2 indicate that compared to perforated grains (samples B through F), unperforated grains (sample A) retain more desorbable materials. This is the result of the longer distance through which the species must diffuse before reaching a surface from which they can evaporate. The effect of ambient aging is demonstrated by a comparison of the levels of the five desorbable species across a given row . Such a comparison indicates that when stored in an unsealed vial, most residual solvent escapes from the propellant grain. The only sample still possessing a significant level of residual solvent after 22 weeks in an unsealed vial is sample A, the unperforated grains. Considering that grains are usually kept in sealed drums during storage, it is suspected that the required time for complete loss of residual solvent would be relatively long, i.e. solvent must first evaporate from the propellant, and then escape from the drums. The consequences of trapping residual solvent in sealed containers is discussed below.

Although mechanical properties were not determined for the samples used in this investigation, it was observed that as the level of residual solvent dropped, the propellant grains tended to become more brittle, indicating the loss of plasticization by the solvent.

4.2. PA-FTIR Investigation:

Relative P1 levels for three propellant formulations were obtained from the PA-FTIR spectra (not shown) of three propellant formulations. This was accomplished by taking the ratio of the intensity of the P1 absorption at 2100 cm^{-1} to that of the CAB absorption at 1754 cm^{-1}. Unlike plasticizer P2, which does not appear to evaporate from propellant formulations (see Sect. 3.1, above), plasticizer P1 does evaporate. Furthermore, from a comparison of the slopes of the lines in Figure 3, it appears that the evaporation of plasticizer P1 is suppressed by the presence of P2. The effect of residual solvent is demonstrated by inspection of the data obtained for "dried" and "undried" samples formulation F3 (hereafter referred to as $F3_d$ and $F3_u$, respectively). The former had been subjected to the standard drying procedure (including cycles at 25°C and 60°C), while the latter was allowed to dry very slowly at ambient conditions in loosely capped vials. It is noted that formulation F3 generally experienced little or no loss of P1 over the course of the investigation. The exception to this generality occured for $F3_u$ during the first few weeks after processing. Initially the P1 level in $F3_d$ and $F3_u$ were nearly equal. After the third week, the P1 level in the $F3_u$ decreased slightly and then remained approximately constant for the remainder of the monitoring period. Two interpretations for this observation are offered. The first interpretation is that rapid drying made the extruded surface of $F3_d$ less permeable to plasticizer than did slow drying. The second interpretation is that although P1 appears to have little tendency to evaporate when in the presence of P2, P1 levels decreased as a result of "co-migration and co-evaporation" with solvent, i.e. solvent evaporation facilitated the evaporation of P1, and evaporation of P1 ceased after most of the solvent had evaporated. Both explanations are plausible, and both point to the potential importance of residual solvent.

4.3. FTIR-MIC Investigations.

The effect of ambient aging on plasticizer P2 levels was studied by monitoring the six types of grains described in Table 3. Typical FTIR-mic spectra (1500-1800 cm^{-1}) of bulk and extruded exterior surfaces of a F4 grain are shown in Figure 4. Absorptions assigned to RDX, CAB, NC, and P2 are labelled accordingly. Comparison of these spectra indicates that the composition of interior "bulk" material is significantly different from that of the extruded surface, i.e. the extruded surface is rich in polymeric binder and plasticizer P2. Scanning electron microscopy indicates that this binder-rich layer is several microns thick.[9] Figure 5 shows plasticizer levels for the interior bulk and extruded exterior surface of propellant grains as a function of time. Relative P2 levels were calculated by taking the ratio of the intensity of the P2 absorption band at 1570 cm^{-1} and that of the RDX absorption band at 1600 cm^{-1}. Two interesting observations can be made from these results. The first is that in all but the unperforated grains (sample F4/A), neither migration nor evaporation of P2 appears to occur to any significant extent during the time frame of this investigation. Migration in sample F4/A is evidenced by the increase in the "exterior" plasticizer level relative to the "bulk" plasticizer level at approximately 100 days. The plasticizer levels in samples B through F vary somewhat over time, but experience no net change. The possibility of a steady-state diffusion/evaporation process can be ruled out based on results of desorption experiments (see Section 3.1, above) which indicate no

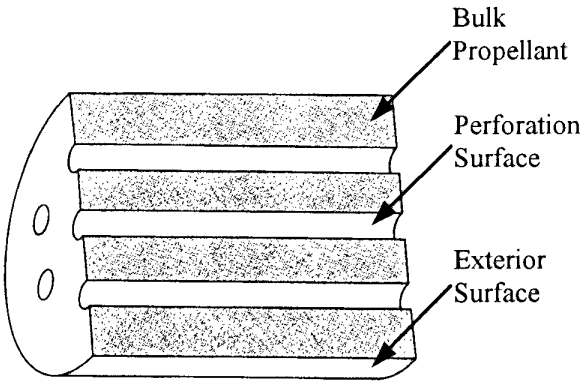


Figure 1: Cross -sectioned solid gun propellant grain

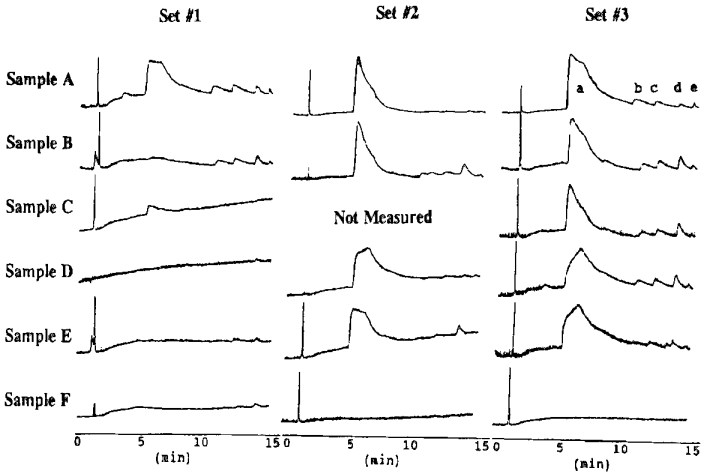


Figure 2: Desorption-GC-FTIR results, Sample F4. Relative IR response vs. retention time.
See Tables 3 and 4 for sample descriptions and storage conditions.
Peak identifications: (a) ethyl acetate; (b) acetic acid; (c) a carboxylic acid; (d) isooctanol; (e) isooctanoic acid.

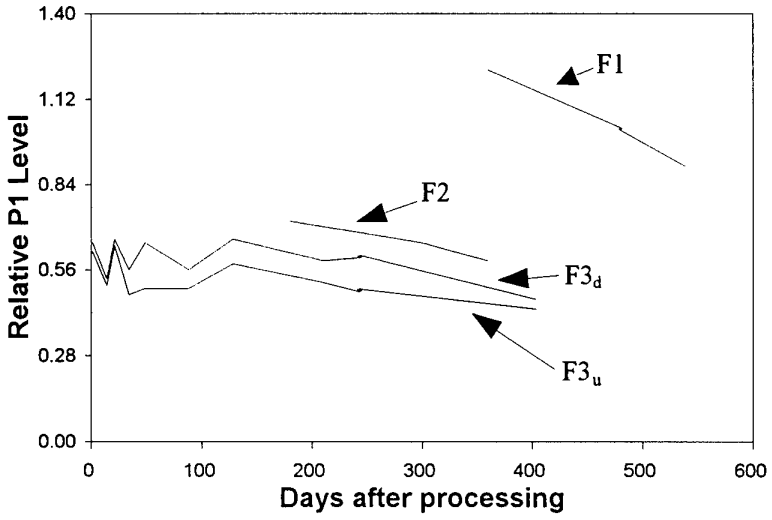


Figure 3: Relative levels of P1 in formulations F1, F2 and F3

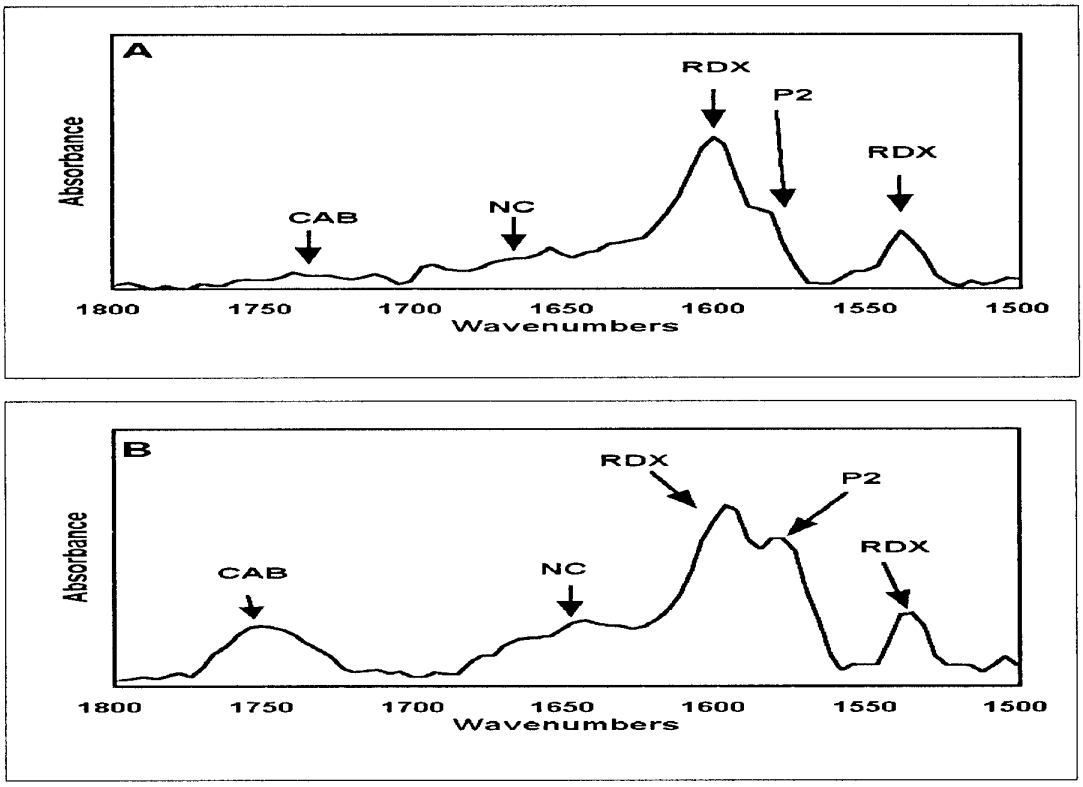


Figure 4: Typical FTIR-mic spectra of propellant F4 grain surfaces:
A) interior "bulk" surface of cross-sectioned grain; B) exterior extruded surface

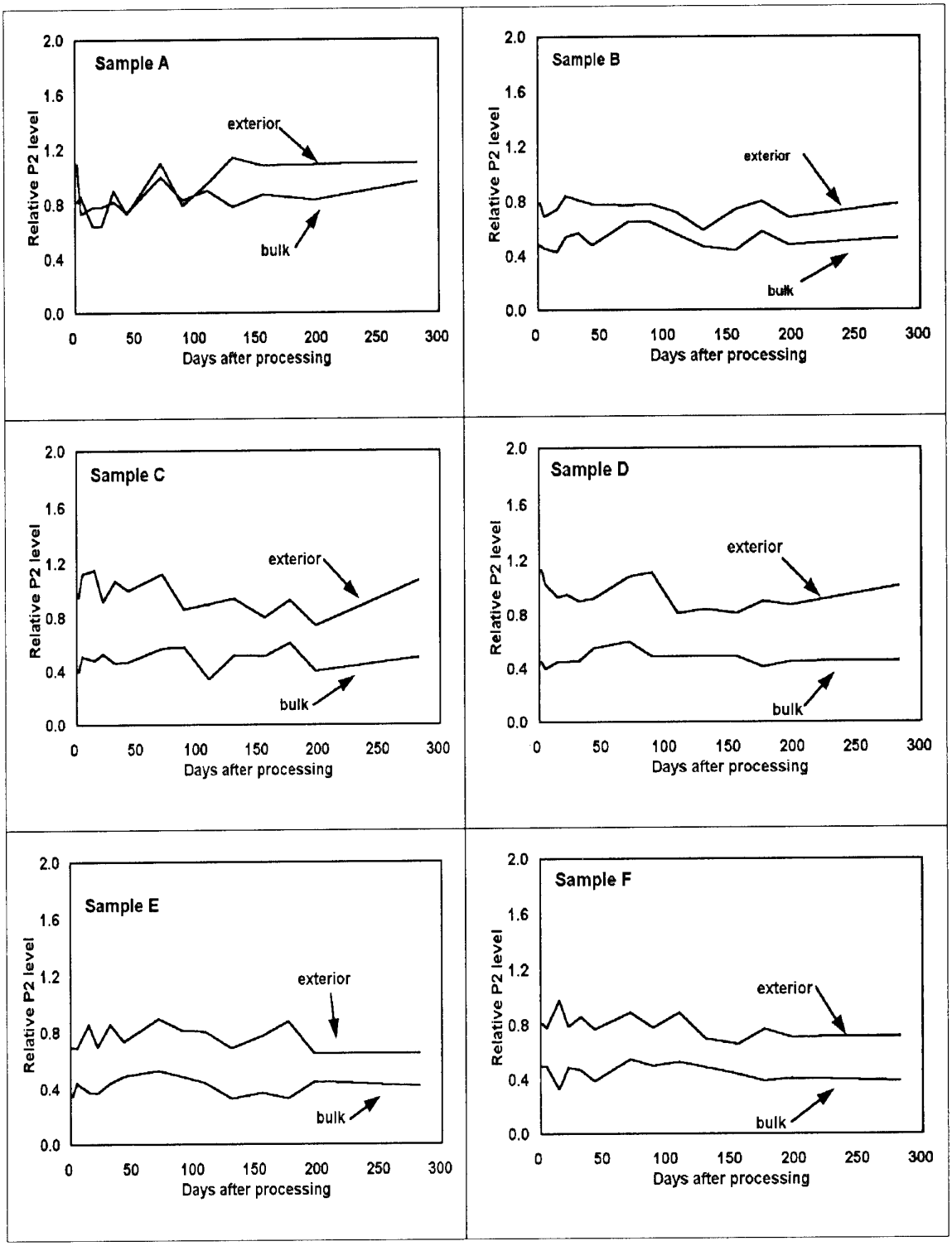


Figure 5: P2 levels at exterior extruded surface and interior bulk surface of F4 grains vs. time.

(See Table 2 for sample descriptions.)

evaporation of plasticizer even at temperatures as high as 100°C. The second observation that may be made from examination of Figure 5 is that the initial "bulk" plasticizer level for sample A is approximately twice that of samples B through F, i.e. 0.8 vs 0.4.

There are two new questions that must now be answered: "What characteristic of the unperforated grains makes them the only grains to experience significant plasticizer migration?", and, "Why is the initial bulk plasticizer level in unperforated grains so much higher than in perforated grains?". The answer to both of these questions appears to be related to the presence of residual solvent. The absence of perforations in sample F4/A restricts the evaporation of residual solvent (compare ethyl acetate levels in Figure 2, set #1). The observed increase in plasticizer level at exterior surfaces (i.e. at the "circumferential", perforation, and end surfaces) is the result of co-migration of solvent and plasticizer to those surfaces. Once at the surface, solvent evaporates and plasticizer accumulates. After all the residual solvent has migrated and evaporated, accumulation of plasticizer ceases. An explanation as to why unperforated grains have a relatively high level of plasticizer in the bulk is that since solvent cannot migrate to perforation surfaces, less plasticizer is transported away from the bulk.

To confirm that solvent actually can transport plasticizer through a propellant grain, the following experiment was performed: A dry, perforated propellant grain was placed in an atmosphere saturated with ethyl acetate vapor for several hours. As might be expected, exposure to the vapor resulted in a softening of the propellant grain, indicating the plasticizing ability of ethyl acetate. After cross-sectioning the grain, analysis was performed by micro-reflectance FTIR. The spectrum obtained from the bulk of the grain is presented in Figure 6d. Also shown in Figure 6 are typical spectra for bulk and exterior surfaces (circumferential and end) *before* exposure to ethyl acetate vapor. The spectra in Figure 6 indicate that solvent vapor permeates through the plasticizer-rich exterior of the dry grain, carrying plasticizer with it. The result is a redistribution of plasticizer throughout the entire grain. If the "solvent migration/plasticizer accumulation" theory is correct, then the only difference between the composition of the end and bulk surfaces before exposure to solvent vapor should be that the end surface, which is a non-extruded exterior surface, should be richer in plasticizer than the bulk as a result of plasticizer deposition during drying; the spectra should be identical after exposure to solvent vapor (and before re-evaporation of solvent) as a result of redistribution of plasticizer. A comparison of spectra b through d in Figure 6 confirms that both requirements are met.

The experiment described above indicates that the distribution of plasticizer in a propellant grain is controlled by solvent migration. Plasticizer is added to propellant formulations in such a way that it be uniformly distributed throughout the grain. Based on the results discussed above, it appears that this effort is defeated by co-migration of solvent and plasticizer to grain surfaces.

The following points have been discussed above, and are summarized here:

1) Residual solvent is oxidized to generate organic acids.
2) Residual solvent plasticizes propellant grain.
3) In the absence of solvent, plasticizer migration is insignificant.
4) Plasticizer migration occurs simultaneously with solvent migration.
5) Accumulation of plasticizer at the exterior surfaces of propellant grains is the result of co-migration with solvent.
6) In the presence of added solvent vapor, plasticizer accumulated at exterior surfaces of propellant grain will re- enter the bulk of the grain and be redistributed throughout the grain.
7) The rate of residual solvent evaporation is dependent on propellant storage conditions.

The next step in resolving the LOVA aging problem is to relate the findings summarized above to propellant stabilization times. Since ballistic and mechanical properties of the samples analyzed in this investigation were never made, it is difficult to directly ascribe "cause and effects". It is recommended that a concerted analysis of the chemistry, ballistics, and mechanical properties of solid propellants be undertaken to get to the root of the aging problem. For the present time, speculation as to the effects of residual solvent on propellant aging must suffice. Suggestions as to what these effects might be are as follows:

1) While in storage, trapped residual solvent may provide enough solvating effect to permit the relaxation of polymer chains experiencing stress induced by the mixing and extrusion processes.
2) Even after the relaxation of stresses, residual solvent can have plasticizing effects. The degree of plasticization will deteriorate as solvent evaporates and escapes from the grains' storage drum.
3) Migration of plasticizer *to* grain surfaces, and *away from* the bulk of the propellant, during drying and storage affects the propellant's physical properties, and therefore its ballistic properties.

Stated most generally, the cause of LOVA propellant aging appears to be the changes in propellant properties caused by the presence, the migration, and the evaporation, of residual solvent. The effect of solvent oxidation products (organic acids) on propellant aging is suspected to be of little significance.

A proposed solution to the propellant stabilization period problem is the development of a new drying cycle. For example, a drying cycle could be developed that removes all residual solvent before grains are put in storage. If such a cycle were adopted, is is likely that the composition, as well as the mechanical and ballistic properties, of the propellant should remain constant for the lifetime of the propellant (assuming that the propellant does not undergo "unusual" temperature cycling while in storage). While driving off all residual solvent may not result in propellant with *optimal* mechanical and ballistic properties, it should result in resultant propellant with more *predictable* properties than those of propellant dried and stored using current procedures. If it is true that physical and chemical changes occuring during the stabilization period result in a decrease in mechanical stresses induced by the mixing and extrusion processes, then it might be best to dry the propellant more slowly than is currently being done. To avoid the

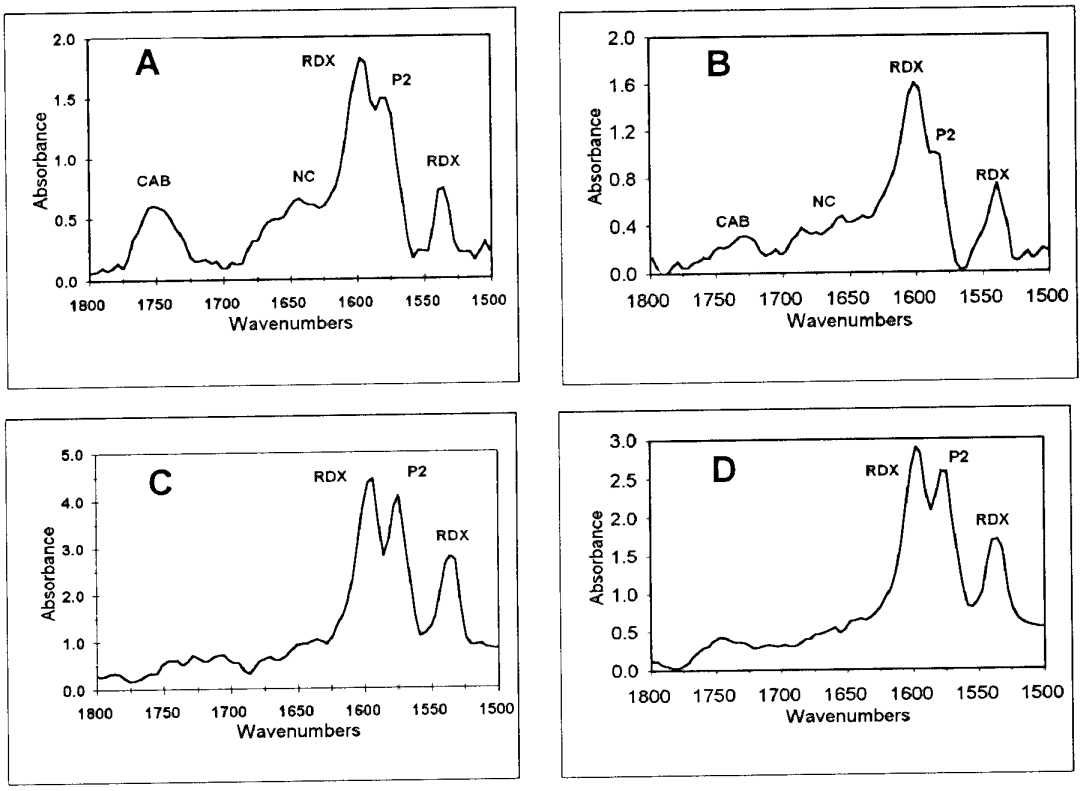


Figure 6. Microreflectance FTIR spectra of propellant grain
A) Exterior extruded surface; B) Interior "bulk" surface of cross-sectioned grain
C) End surface D) Interior "bulk" surface after exposing whole grain to ethyl acetate vapor

stabilization period, the slow drying cycle should probably be designed to be long enough to insure complete removal of residual solvent; the propellant that is eventually placed in storage should be free of residual solvent.

5. CONCLUSIONS

A study of the effect of residual solvent on LOVA propellant aging was conducted. The most significant finding of the study was that the distribution of plasticizer in propellant grains depends strongly on solvent content, i.e. in "wet" propellant, plasticizer is distributed relatively uniformly throughout the grain, in dry propellant, plasticizer is accumulated at the surfaces of the grain. In most of the samples examined, the residual solvent content was already quite low, such that little plasticizer migration was observed. It is proposed that "real" propellant grains do experience plasticizer migration while in storage. Furthermore, it is suspected that residual solvent trapped in grains during storage provides enough solvation, and therefore enough segmental mobility for polymeric binder, to permit the propellant to relax from stresses induced during mixing and extrusion. Based on the data obtained in this study, it is tentatively concluded that the LOVA stabilization period is a result of plasticizer migration and/or grain relaxation. To confirm these tentative conclusions, a concerted aging study including the analysis of the ballistic and mechanical properties, as well as the composition, of freshly processed propellant (stored under actual storage conditions) should be performed.

5. REFERENCES

1. F.J. Bergin, "Some Novel Applications of an Infrared Microscope" *Appl. Spectrosc. 43(3)*, 511, 1989.

2. *Infrared Microspectroscopy*, R.G. Messerschmidt & M.A.Harthcock, Eds., Marcel Dekker, NY, 1988.

3. J.A. Grahm, W.M. Grimm III, and W.G. Fateley, "Fourier Transform Infrared Photoacoustic Spectroscopy of Condensed-Phase Samples" in: J.R. Ferraro and L.J. Basile (eds) "*Fourier Transform Infrared Spectroscopy*", Vol. 4, Academic Press, New York, 1982, p. 345.

4. D.W. Vidrine "Photoacoustic Fourier Transform Spectroscopy of Solids and Liquids" in: J.R. Ferraro and L.J. Basile (eds) "*Fourier Transform Infrared Spectroscopy*", Vol. 3, Academic Press, New York, 1982, p.133.

5. J.F. McClelland "Photoacoustic Spectroscopy "*Anal. Chem. 55*, 89A, (1983).

6. R. A. Pesce-Rodriguez and R.A. Fifer, "Application of Fourier Transform Infrared Spectroscopy to Solid Propellant Characterization" *Appl. Spectrosc. 45(3)*, 417 (1991).

7. P.R. Griffiths & J.A. deHaseth, "*Fourier Transform Infrared Spectroscopy*", Wiley, NY 1986, p.604.

8. R.T. Graf, J.L. Koenig, and H. Ishida, "Optical Constant Determination of Thin Polymer Films in the Infrared", *Appl. Spectrosc., 39*, 405 (1985).

9. R.J Lieb, U.S. Army Research Laboratory, private communication.

Paper Number: 21
Discussor's Name: Professor H. Schubert
Responder's Name: R. Pesce-Rodriguez

Question: I would like to support your findings by other observations where the solvent is the transport vehicle. Examples are the crystallization of stabilizers and energetic substances on the surface (Ammonium perchlorate).

Answer: Thank you for bringing up these other examples of propellant ingredients that can migrate to the surface of a propellant with the assistance of residual solvents. An additional example is that of RDX, which dissolves in the nitrate ester plasticizer used in "JAX" (JA2+RDX) propellant and are transported to exterior surfaces of the grain (reference work of Heimer and Lieb proceedings of the Int'l Symposium on Ballistics, Israel, 1995).

EVALUATION COMPAREE DE LA DUREE DE VIE DE POUDRES COMPOSITES ET SIMPLE BASE

Mauricette RAT

S.N.P.E.

Division Préparation du Futur et Propulsion

Centre de Recherches du Bouchet, BP 2
91710 VERT-LE-PETIT
FRANCE

RESUME

Cette publication présente les travaux effectués par SNPE pour satisfaire aux spécifications (stabilité chimique et balistique à haute température, durée de vie) demandées lors du développement d'une munition moyen calibre pour application avion.

Le comportement des poudres industrielles a été amélioré en optimisant les caractéristiques de la matrice nitrocellulosique.

Cependant, cette solution est limitée par la stabilité chimique de la nitrocellulose. Aussi, SNPE a proposé des poudres composites à liant inerte ou actif, chargé en hexogène qui présentent des propriétés en température et de durée de vie nettement supérieures à celles des poudres simple base.

ABSTRACT

This paper presents the works carried out by SNPE to meet the specifications (chemical stability, ballistic stability at high temperature, lifetime) required for a medium caliber ammunition for aircraft.

The behaviour of industrial gun propellant has been improved by optimizing the properties of the nitrocellulosic matrix. Yet this solution is limited because of the chemical stability of nitrocellulose.

So, SNPE has proposed composite gun propellants based on an inert or energetic binder filled with nitramine (RDX). Their thermal properties and their lifetime will be discussed and compared to those of single base gun propellants.

1. INTRODUCTION

Au cours de leur vie, les poudres pour armes sont soumises à des contraintes d'environnements rencontrées lors de leur stockage, de leur transport et de leur utilisation. Ces contraintes sont très différentes suivant le lieu ou les conditions de stockage et suivant l'utilisation (emport sous avion, ...).

Aussi l'évaluation de leur durée de vie est complexe d'autant plus que deux aspects doivent être pris en considération, l'aspect sécurité lié à la stabilité chimique et l'aspect fonctionnement lié à la stabilité balistique. Les spécifications requises tendent à devenir de plus en plus sévères, par exemple les munitions embarquées sur avion en fonction des missions, peuvent subir des températures supérieures à 100°C.

SNPE a été amenée à mettre au point des poudres à tenue thermique améliorée. Deux voies d'amélioration ont été proposées :

- L'une conservant les poudres industrielles en optimisant les caractéristiques de la matrice nitrocellulosique.
- L'autre utilisant une nouvelle famille de poudres : les poudres composites (liant inerte ou actif contenant des charges énergétiques).

Cette communication présente les résultats obtenus dans ces deux voies et montre l'intérêt tout particulier des poudres composites vis à vis de la tenue thermique.

Paper presented at the AGARD PEP Symposium on "Service Life of Solid Propellant Systems" held in Athens, Greece, 10-14 May 1996, and published in CP-586.

2. POUDRES A BASE DE NITROCELLULOSE

Lors du développement d'une munition moyen calibre pour application avion, des spécifications de tenue en température ont été imposées en particulier la stabilité balistique après cycles simulant le vieillissement opérationnel tel que :

- Cycle emport avion représenté par 30 cycles de 26 heures à des températures montant par paliers de -40°C à +100°C.
- Cycle tir représenté par une montée en température jusqu'à 121°C durant 174 minutes.

A ces spécifications s'ajoutent celles définies par le STANAG 2895 (1).

Les premiers essais sur des poudres simple base candidates ont montré la difficulté de respecter de manière reproductible la stabilité balistique après les cycles avion. L'expertise a conduit à incriminer la tenue mécanique de la poudre après cyclages et donc d'orienter les études vers les caractéristiques de la nitrocellulose et tout particulièrement du taux de solubles. En effet, l'utilisation de nitrocellulose à fort taux d'azote pour atteindre le niveau de performances conduit à des taux de solubles plus faibles qui peuvent être à l'origine d'une moins bonne tenue mécanique de la poudre.

2.1. Plan d'expérience

- *Echantillons*

Des échantillons de poudres ont été fabriqués en choisissant les lots de nitrocellulose de telle manière que le taux de solubles de la poudre varie entre 22 % et 27 %.

Il est à noter comme l'indique la figure 1 que le taux de solubles a une influence sur les dimensions de la poudre finie avec à isofilière une diminution du diamètre des perforations et également une tendance à la réduction du diamètre du grain.

- *Conditions de vieillissement*

Pour simplifier les essais expérimentaux, les cycles "avion" ont été simulés par un vieillissement isotherme de 40 heures à 100°C.

- *Caractérisations*

Après vieillissement, les échantillons ont été caractérisés sous trois aspects :

- Comportement thermique : décomposition de la nitrocellulose à l'aide du taux d'azote.
- Comportement mécanique à l'aide du test canon à éclatement de chambre qui permet d'apprécier la tenue mécanique de la poudre soumise aux sollicitations de l'allumage.

  Le test consiste à éteindre le chargement de poudre par dépressurisation rapide pendant la phase d'allumage aux environs de 70 MPa, à recueillir la poudre et à étudier l'endommagement des grains de poudre par tamisage en différentes coupes granulométriques.
- Comportement balistique lors de tirs en moyen calibre.

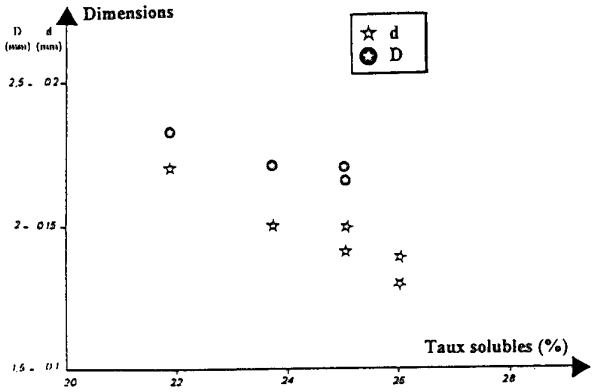


FIGURE 1

2.2. Résultats expérimentaux

- *Dénitration*

La figure 2 représente la dénitration en fonction du taux de solubles après 40 heures à 100°C.

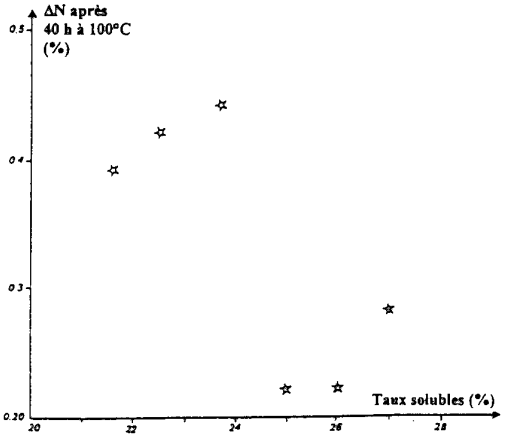


FIGURE 2

Deux population apparaissent :

- Taux de solubles > 24 % : dénitration faible
- Taux de solubles < 24 % : dénitration importante

• *Comportement mécanique*

La figure 3 représente la quantité de grains cassés pour la coupe granulométrique < 1,6 mm.

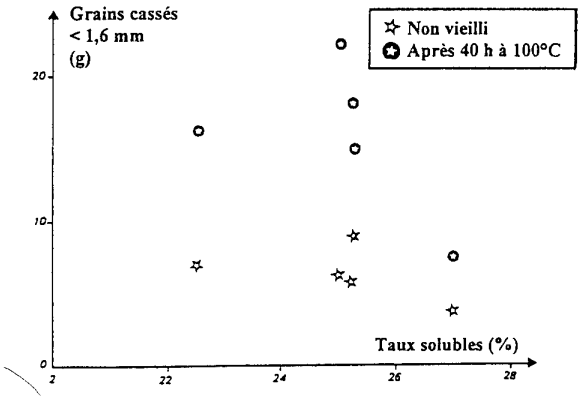


FIGURE 3

Après vieillissement 40 heures à 100°C, les poudres à 25 % et moins de solubles se révèlent très fragiles au test alors que les propriétés mécaniques de la poudre à 27 % de solubles évoluent peu.

• *Comportement balistique*

Les tirs en arme moyen calibre ont été réalisés entre -54°C et +100°C. L'influence du vieillissement est exprimée par l'augmentation de pression ΔP lors des tirs à 100°C, après vieillissement 40 heures à 100°C.

La variation du coefficient ΔP en fonction du taux de solubles est représentée sur la figure 4

L'augmentation du taux de solubles améliore la coefficient de vieillissement ΔP.

2.3. Commentaires

Ce plan d'expérience a montré que l'augmentation du taux de solubles des poudres améliore aussi bien leur comportement thermique que leur comportement balistique aux hautes températures. Ces améliorations s'expliquent probablement si l'on considère que les solubles jouent le rôle de plastifiant de la matrice nitrocellulosique.

Le meilleur état de gélatinisation de la nitrocellulose entraîne une meilleure tenue thermique ainsi qu'une meilleure tenue mécanique, ces deux paramètres étant essentiels pour le comportement aux cycles avion des poudres à base de nitrocellulose.

Il a fallu que les contraintes thermiques exigées soient plus contraignantes (100°C) pour montrer que le taux de solubles était un paramètre primordial.

En effet, les essais de vieillissements à température modérée (40 - 70°C) ne permettaient pas de mettre en évidence son influence sur la stabilité thermique et balistique de la poudre.

Cependant, le domaine d'utilisation de ces poudres sera toujours limité à cause de la décomposition intrinsèque de la nitrocellulose que l'on peut ralentir mais non supprimer (2).

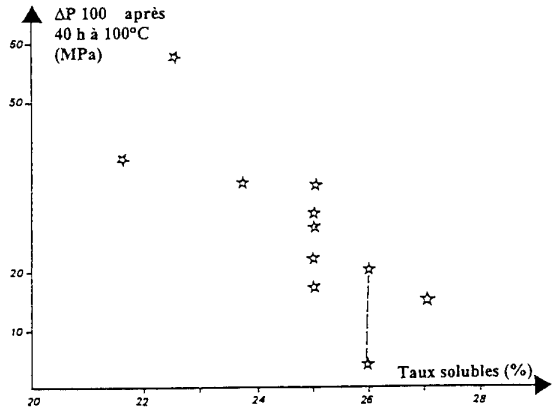


FIGURE 4

3. POUDRES COMPOSITES

En tant qu'industriel, SNPE recherche en permanence à améliorer les poudres en vue de répondre aux nouveaux besoins des munitionnaires. Aussi depuis quelques années, elle développe les poudres composites qui permettent d'accroître les performances balistiques tout en diminuant la vulnérabilité et en augmentant la durée de vie (3).

Elles se subdivisent en deux types :

- Poudres composites à liant thermoplastique (acétobutyrate de cellulose ou CAB) plastifié chargé à l'hexogène (RDX) jusqu'à des taux de 80 % en masse obtenues à l'aide d'un procédé à solvant. Ces poudres contiennent encore un faible pourcentage d'esters nitriques.

- Poudres composites à liant thermodurcissable soit inerte (polybutadiène ou PBHT), soit énergétique (polyazoture de glycidyle ou PAG, polymère fabriqué à la SNPE) chargé à l'hexogène à des taux pouvant atteindre 86 % en masse. Elles sont obtenues à l'aide d'un procédé sans solvant.

Par la nature même de leurs constituants, ces poudres composites présentent une meilleure tenue thermique que les poudres à base de nitrocellulose comme l'indiquent leurs températures d'inflammation ou de début de décomposition :

	NC	CAB RDX	PBHT RDX	PAG RDX
T_i (°C)	175	213	209	206

Cependant il est nécessaire de vérifier que leurs propriétés autres que thermiques n'évoluent pas au cours du temps (exemple : propriétés mécaniques).

3.1. Plan d'expérience

Deux types de vieillissement sont réalisés :

- Des vieillissements longs à température modérée (60°C) qui donneront accès à la durée de vie au stockage. Les poudres vieillies sont caractérisées à l'aide d'épreuves de laboratoire.

  Suivant le type de poudres considérées, les caractérisations seront :

  - Comportement thermique : dosage du stabilisant ou de l'antioxydant
  - Comportement mécanique : essais de compression sur cylindres (diamètre 10 mm, hauteur 10 mm).
  - Comportement balistique : tirs en bombe manométrique suivant le STANAG 4115 (4) qui permet de déterminer la force du produit (F), la vivacité (Ao) et la vitesse de combustion (V_{100} : vitesse mesurée à 100 MPa).

- Des vieillissements à haute température 100°C durant 40 heures simulant comme précédemment des cycles avion avec pour caractérisation des tirs en arme.

3.2. Résultats expérimentaux des vieillissements à 60°C

- ***Poudres à liant thermoplastique***

Ces poudres ont un faible taux d'esters nitriques aussi elles sont stabilisées à l'aide de la centralite (CNT).

La consommation de centralite en fonction du temps est linéaire et très faible : 2.10^{-5} % CNT/j.

Cette valeur est à comparer, dans le cas des poudres simple base stabilisées à la diphenylamine à ~ 5.10^{-3} % DPA/j, dans le cas des poudres double base stabilisées à la centralite à 1.10^{-3} % CNT/j.

- ***Poudres à liant thermodurcissable inerte***

Ces poudres contiennent un agent antioxydant pour éviter l'oxydation du PBHT :

- Taux d'antioxydant :

  Après 2 ans de vieillissement à 60°C, la consommation de l'antioxydant est de 0,03 % soit 27 %.

- Propriétés mécaniques :

  Les résultats sont rassemblés dans le tableau 1.

  Un léger durcissement apparaît au cours du temps.

	Sm (MPa)	E (MPa)	e (%)
0	2,4	11,0	34,2
1 mois	2,5	12,1	31,8
3 mois	2,6	14,4	38,2
6 mois	2,4	14,2	29,5
1 an	2,2	16,0	21,3
2 ans	2,3	17,9	20,8

TABLEAU 1

COMPRESSION SUR CYLINDRE

– Propriétés balistiques

Les résultats sont donnés dans le tableau 2.

	V100 (mm/s)	Ao (Hz)	F (MJ/kg)
0	67	136	1,121
1 mois	68	132	1,122
3 mois	69	132	1,123
1 an	64	130	1,155
2 ans	71	136	1,122

TABLEAU 2

BOMBE MANOMETRIQUE

Les caractéristiques balistiques n'évoluent pas de manière significative après deux ans de vieillissement.

- ***Poudres à liant thermodurcissable énergétique (PAG)***

– Propriétés mécaniques :

Les résultats sont rassemblés dans le tableau 3.

	Sm (MPa)	E (MPa)	e (%)
0	1,6	16	20
3 mois	1,6	17	17
6 mois	1,9	19	18
1 an	1,7	17	18
2 ans	1,9	23	15

TABLEAU 3

COMPRESSION SUR CYLINDRE

Après deux ans de vieillissement, les propriétés mécaniques n'évoluent que très peu. Il semble cependant apparaître après deux ans un léger durcissement de la composition.

– Propriétés balistiques

Les résultats sont rassemblés dans le tableau 4.

Après deux ans de vieillissement, les évolutions observées ne sont pas encore significatives.

En conclusion, les caractéristiques mécaniques et balistiques de ces poudres n'évoluent que très lentement lors de vieillissement à température modérée. Dans les mêmes conditions (60°C pendant 2 ans) une poudre simple base aurait consommé tout son stabilisant et par mesure de sécurité serait détruite ou utilisée prioritairement.

3.3. Résultats expérimentaux des vieillissements haute température (100°C - 40 heures)

- ***Poudres à liant thermoplastique (CAB)***

	V_{100} (mm/s)	Ao Hz	$F_{covl/B}$ (MJ/kg)	n
0	90	109	1,23	1,14
1 an	90	116	1,30	1,10
2 ans	95	119	1,30	1,10

TABLEAU 4

BOMBE MANOMETRIQUE

Des tirs en moyen calibre ont été effectués avant et après vieillissement dans le domaine de température -60°C, +100°C.

L'évolution des propriétés balistiques est évaluée comme dans le cas des poudres simple base par le coefficient de vieillissement ΔP qui correspond à l'augmentation de pression observée après vieillissement. Ce coefficient est pratiquement nul dans tout le domaine de température ce qui montre la parfaite stabilité balistique de ce type de poudre.

- ***Poudres à liant PBHT***

Des tirs en moyen calibre ont été réalisés dans les mêmes conditions que la poudre à liant CAB. Le coefficient de vieillissement ΔP est faible dans tout le domaine comme le montre les valeurs ci-dessous :

T°C (TIR)	-54	+20	+100
ΔP (MPa)	0	7	9

Cette poudre présente une bonne stabilité balistique.

3.4. Commentaires

Quel que soit le type de poudres composites considérées, leur comportement en température (chimique, mécanique, balistique) est très supérieur à celui des poudres à base de nitrocellulose. Aux températures modérées, leur durée de vie est plus importante car non limitée par la présence de nitrocellulose qui se décompose progressivement même à température ambiante. Aux températures élevées, grâce à leur meilleure tenue thermique, elles présentent une stabilité balistique excellente.

Ces poudres composites sont donc utilisables dans des domaines d'application plus étendus que les poudres à base de nitrocellulose en particulier en ce qui concerne la température. Cependant, elles nécessitent des travaux complémentaires dans le domaine du fonctionnement (allumage, combustion).

4. CONCLUSION

Les spécifications exigées de durée de vie des poudres pour armes (sécurité, fonctionnement) sont de plus en plus sévères notamment dans le cas d'emport sous avion.

Cette communication présente les solutions apportées par SNPE pour répondre à ces spécifications.

Dans le cas des poudres à base de nitrocellulose la stabilité chimique et la stabilité balistique en température ont été améliorées en choisissant des nitrocelluloses à fort taux de solubles, les solubles jouant le rôle de plastifiant. Cependant leur comportement aux températures élevées restera limité à cause de la stabilité même de la nitrocellulose.

Dans les environnements thermiques, plus contraignants il sera préférable d'envisager l'utilisation des poudres composites constituées d'un liant inerte ou énergétique et d'une charge énergétique stable, l'hexogène, qui sont en cours d'optimisation au niveau de leur fonctionnement balistique. En effet, ces poudres ne montrent aucune évolution chimique ou balistique lors de stockage longue durée à température modérée ou lors de cycles avion atteignant des températures de 100°C.

5. REFEREBCES

(1) STANAG 2895

Extrêmes climatiques et conditions dérivées à utiliser dans la définition des critères de conception et d'essai pour les matériels destinés aux forces de l'OTAN.

(2) Y. LONGEVIALLE - M. RAT

"Application de la chimiluminescence à l'étude de la stabilité des poudres". Proc. 7th symp. Chem. Probl. Connected Stabil. Expl. 1985, 43.

(3) B. MARTIN - A. LEFUMEUX - D. DEGANO

"Low vulnerability gun propellants manufactured with a solventless process", 3 rd. Australian gun propellant conference and seminar 25-27 oct. 88, MULWALA.

(4) STANAG 4115

"Definition and determination of ballistic properties of gun propellants".

Paper Number: 22
Discussor's Name: R. Couturier
Responder's Name: M. RAT

Question: 1. vous rappelez le role important du taux de NC soluble sur la gelatinization et par voie de consequence sur les termes mecaniques et balistiques des poudres a temperature elevee. Ne pourrait-on pas obtenir le meme resultat en jouant sur le pouvoir gelatinisant des solvants de fabrication (nature et taux)?

2. Concernant les poudres composites au PAG, avez-vous observe au cours de vos etudes de veillissement des pertes energetiques dues a des ruptures des fonctions azide (N_3)?

Question: 1. You recall the important role of the amount of NC solubles on the gelation (cross-linking) and consequently on the mechanical and ballistic properties of powders at elevated temperatures. Could we not obtain the same result by using the gelating power of solvents used in manufacturing?
2. With regard to composite powders in PAG, have you observed, during your aging studies, losses of energy due to the breaking of azide groups (N_3)?

Answer: 1. En effet il serait possible de jouer sur le pouvoir gelatinisant des solvants de fabrication. Mais pour des raisons industrielles il parait difficile d'envisager la modification de la nature de solvant. En ce qui concerne le taux d'arrosage, il est regle pour avoir de bonnes conditions d'extrusion de la poudre. Aussi les possibilites de reglage sont tres limitees.

2. Le PAG est parfaitement stable a 100° C. Il faut monter a des temperatures de 120° C--130° C pour observer une decomposition appreciable du PAG.

Answer: 1. In fact it would be possible to take advantage of the gelating power of solvents used in manufacturing. But, for industrial reasons it would seem difficult to visualize the modification of the nature of the solvent. Regarding the amount of solvent, this is determined by extrusion conditions for the powder and these possibilities are very limited.
2. PAG is entirely stable at 100°C. In order to observe any appreciable decomposition of PAG, the temperature must be raised to 120°C - 130°C.

THE CANADIAN GUN PROPELLANT SURVEILLANCE PROGRAM

by
L.S. Lussier and H. Gagnon
Defence Research Establishment Valcartier (DREV)
Department of National Defence
2459, Pie XI Blvd., North (P.O. Box 8800)
Courcelette, Québec, GOA 1R0
Canada

SUMMARY

This paper describes the work done at DREV to develop modern methods of monitoring the chemical stability and remaining safe life of gun powders stocked by the Canadian Forces (CF). It begins with the rationale behind the choice of high-performance liquid chromatography (HPLC), as well as the criteria the HPLC methods must meet. This is followed by a description of the development of two fast, reliable and efficient methods. Finally, the role of N-NO-DPA as a stabilizer and the sentencing criteria are discussed.

INTRODUCTION

Propellants stored in bulk (prior to filling) or in ammunition are among the biggest items in the DND inventory. These propellant formulations contain nitrate esters, such as nitrocellulose (NC) and nitroglycerine (NG), which tend to decompose with time, releasing nitrogen oxides. If not removed, these nitrogen oxides react catalytically to accelerate the nitrate ester's degradation and, as a result, heat is produced. Therefore, self-ignition may occur and several disasters that have occurred throughout the world bear testimony to this. To remedy this situation, stabilizers such as diphenylamine and ethylcentralite are added to gun propellant formulations. These stabilizers react easily with nitrogen oxides and prevent self-ignition from occurring. The reactions of these compounds are complex and many daughter products are formed. Some of these products act as stabilizers, but others do not and there is a depletion of the effective stabilizer level in the gunpowder with time. Therefore, an effective surveillance programme, that periodically monitors the stabilizer content of propellants, is essential for the maintenance of safety and the maximum use of resources.

Up to 1994 the Canadian gun propellant surveillance program was based on the Abel heat test and the colour test. These pass-or-fail-type tests are outdated and above all, under specific conditions, can lead to misleading results. Moreover, recent investigations with modern analytical instrumentation have given a more accurate description of propellant degradation and therefore, tests that were used twenty years ago have been replaced, in several countries, by more modern methods whose superiority over the older tests is generally accepted. Furthermore, the equipment in Canadian depots was old and in need of replacement. Therefore, this was the most opportune time to replace the Abel heat test and the colour test with a modern, efficient and reliable test.

In order to assess the chemical stability of a propellant, several propellant properties may be used. The methods can be classified into the following categories (1): production of oxides of nitrogen, spectroscopic properties of NC, molecular weight of NC, heat evolution, and stabilizer analysis. On the other hand, before selecting one of these methods, one must consider some important facts about propellant ageing.

As discussed above, during storage the stabilizer reacts with the nitrogen oxides and gives rise to several daughter products. Several studies have considered this chemical ageing process (2-8). All these studies have shown that the derivatives produced are mainly N-nitroso derivatives and C-nitro derivatives with ortho/para substitution. Moreover, not all the derivatives are produced at the same time, although the formation of the various daughter products is sequential. In others words, the older the propellant, the higher will be the level of nitro substitution of the daughter products produced. Therefore, the determination of residual stabilizer and its reaction products gives a quick snapshot of the propellant stability. Consequently the most appropriate methods for surveillance purposes would be those that can discriminate between the stabilizer and its reaction products. Therefore, gas chromatography (GC) and high-performance liquid chromatography (HPLC) are among the best methods because of their capability to resolve and quantify many components in a mixture. Moreover, GC and HPLC can easily be adapted to handle a large number of samples.

However, one drawback to GC is the thermal stress placed on the products in order to volatilize them. Indeed, the nitroso derivatives are thermally unstable and therefore GC is limited by its inability to separate DPA and N-NO-DPA (which is converted back to DPA). It is important to quantify N-NO-DPA since, because it is a stabilizer, it is included in the level of effective stabilizer considered when sentencing the DPA-

Paper presented at the AGARD PEP Symposium on "Service Life of Solid Propellant Systems" held in Athens, Greece, 10-14 May 1996, and published in CP-586.

stabilized propellants. This is why in countries that use GC and HPLC, the former is used firstly to screen the propellant but when the level of DPA reaches a certain limit, HPLC, which does not impose a thermal stress, is used in order to discriminate between DPA and N-NO-DPA. On the other hand, HPLC is slower than GC and therefore has higher running costs and lower sample throughput. However, the number of samples tested in Canada was determined to be about 200, much lower than the number of samples tested in countries like USA, UK or France. Consequently, this reduces the sample throughput and running cost drawbacks of HPLC. Furthermore, the current issue of NATO STANAG 4117 includes an HPLC alternative to the spectrophotometric method, but GC is not included for the reason mentioned above. Consequently, because there is no restriction on the use of HPLC and since this method has been selected by the NATO countries, we decided to select this widely-accepted method for implementation in the new Canadian gun propellant stability program.

OBJECTIVES

At this point, it must be stressed that the objective of this work was not to develop exhaustive and research-grade methods that produce a baseline separation of all the possible products; such methods have already been developed in Australia by Curtis et al (4,5). Instead, our objective was to develop methods that can be used on a routine basis and probably by personnel not necessarily having the chemist's knowledge of HPLC. Therefore, the objective of this work was to develop methods that could be used routinely and that were efficient, fast and reliable.

First, for the sake of reliability, the methods should be developed for bonded phase silica columns as opposed to unmodified silica columns. In fact, the former are generally viewed as superior to the latter in terms of reproducibility (9). Unmodified silica columns are less popular because of problems in maintaining a constant surface activity required for repeatable separation. For instance, retention with unmodified silica columns is more inconsistent because of their sensitivity to small concentrations of water in the sample or in the mobile phase (10). Among the various types of bonded phase silica columns, there are the reverse phase columns which are the most popular (11) primarily because of advantages such as short equilibrium time, separating capability for polar as well as non-polar solutes, and good reproducibility of retention times.

Secondly, a drawback of HPLC is its low sample throughput. In order to minimize this disadvantage, the methods should be not only able to separate the various components adequately but they should also do it in the minimum time possible (ideally <15 min). Consequently, the most appropriate methods are those using isocratic mobile phase as opposed to a mobile phase gradient which requires time to reach equilibrium between each injection. Also, the mobile phase should consist, ideally, of a binary mixture between either methanol (MeOH) or acetonitrile (ACN) with water. Tetrahydrofuran (THF) is unpleasant to work with, tends to form explosive peroxides and is more difficult to flush from the HPLC system than the other solvents. Consequently, all these drawbacks preclude the use of THF for a routine method.

Thirdly, all the gun powders stocked or used by the CF are either DPA- or EC-stabilized. In order to give an adequate picture of the state of ageing of a given sample of gunpowder, the methods must sufficiently resolve the stabilizer, its daughter products as well as the other ingredients present in the gunpowder formulation. Thus, the efficient methods are those that take into account all the possible products that either are present or that can be produced during the ageing process of the gunpowder formulations used by the CF. Furthermore, for the sake of reliability, completeness and in the eventuality that higher nitrated and/or nitrosated derivatives could be produced to a significant extent the methods must consider as many stabilizer daughter products as possible. The list of products that should be considered for the DPA-stabilized formulations are given in Table I, while those that should considered for the EC-stabilized formulations are given in Table II. With such an exhaustive list of products to consider, two methods should be developed: one for the DPA-stabilized gunpowders and a second one for the EC-stabilized gunpowders. Ideally, the two methods should use the same mobile phase and the same stationary phase in order to minimize the workload when switching between the two methods.

Finally, it would be almost impossible to obtain a baseline separation for all the products listed in Table I or II in less than 15 minutes with an isocratic mobile phase. However, these HPLC methods will be used for chemical stability surveillance purposes. However, not all the products listed in Tables I or II act as effective stabilizers, and as a consequence, it was only worthwhile to obtain baseline separations of products that acted as effective stabilizers and that would be considered to sentence the propellants. As will be discussed later, for DPA-stabilized propellants, depending on the country, effective stabilizers include the following products: DPA, N-NO-DPA, 4-NO_2-DPA and 2-NO_2-DPA. On the other hand, the EC-stabilized propellants are sentenced solely by using the concentration of EC.

In summary, our objectives were to develop or find in the literature two isocratic methods using the same stationary bonded phase, the same mixture of solvents for the mobile phase and a runtime of less than 15 min. In addition, the DPA method must give a baseline separation for DPA, N-NO-DPA, 4-NO_2-DPA and 2-NO_2-DPA with their respective peaks free of any interference from all the products listed in Table I, while the EC method must give rise to an EC peak baseline resolved and free of any interference from all the products listed in Table II.

TABLE I

List of products considered for the DPA method, their abbreviations and their retention times

Product name	Abbreviation	Retention Time (min.)
2,2',4,4',6,6'-HEXANITRO DIPHENYLAMINE	2,2',4,4',6,6' HNDPA	2.82
2,4',6-TRINITO DIPHENYLAMINE	2,4',6 TNDPA	5.31
2,2',4',6-TETRANITRO DIPHENYLAMINE	2,2',4',6 TNDPA	5.86
NITROGLYCERINE	NG	6.58 *
2,2',4,4',6-PENTANITRO DIPHENYLAMINE	2,2',4,4',6 PNDPA	6.6
2,2',4,6,6'-PENTANITRO DIPHENYLAMINE	2,2',4,6,6' PNDPA	6.78
2,2',4,4'-TETRANITRO DIPHENYLAMINE	2,2',4,4' TNDPA	7.49
DINITROTOLUENE	DNT Isomers	7.2 to 7.5
2,2',6,6'-TETRANITRO DIPHENYLAMINE	2,2',6,6' TNDPA	7.68
2,3',4,6-TETRANITRO DIPHENYLAMINE	2,3',4,6 TNDPA	7.68
2,2',6-TRINITRO DIPHENYLAMINE	2,2',6 TNDPA	8.19
4,4'-DINITRO DIPHENYLAMINE	4,4' DNDPA	8.28
2,2',4,6-TETRANITRO DIPHENYLAMINE	2,2',4,6 TNDPA	8.28
N-NITROSO-2,4'-DINITRO DIPHENYLAMINE	N-NO-2,4' DNDPA	8.28
2-NITRO-N-NITROSO DIPHENYLAMINE	2N-N-NO-DPA	8.49
2,4,6-TRINITRO DIPHENYLAMINE	2,4,6 TNDPA	8.49
2,6-DINITRO DIPHENYLAMINE	2,6 DNDPA	8.67
2,4,4',6-TETRANITRO DIPHENYLAMINE	2,2',4',6 TNDPA	8.77
2,4,4'-TRINITRO DIPHENYLAMINE	2,4,4' TNDPA	8.9
N-NITROSO-4,4'-DINITRO DIPHENYLAMINE	N-NO-4,4' DNDPA	8.96
2,2',4-TRINITRO DIPHENYLAMINE	2,2',4 TNDPA	9.25
4 -NITRO DIPHENYLAMINE	4 NDPA	9.59
4-NITRO-N-NITROSO DIPHENYLAMINE	4N-N-NO DPA	9.93
2,4'-DINITRO DIPHENYLAMINE	2,4' DNDPA	9.97
N-NITROSO DIPHENYLAMINE	N-NO DPA	10.38
2,2'-DINITRO DIPHENYLAMINE	2,2' DNDPA	10.75
2,4-DINITRODIPHENYLAMINE	2,4 DNDPA	11.05
DIPHENYLAMINE	DPA	11.51
DIAMYLPTHALATE	DAP	13.62
2-NITRO DIPHENYLAMINE	2 NDPA	13.92
DIPHENYLPHTHALATE	DPP	16.25
DIBUTYLPHTHALATE	DBP	22.62

* NG does not absorb at 254 nm. Its retention time was determined with the detector at 205 nm.

Many investigators have reported on the HPLC analysis of DPA, EC and their reaction products. However, in our opinion, none of these methods fulfilled the above-mentioned requirements. In fact, many of these methods either considered a limited number of derivatives or were sparse in detail regarding the other ingredients that are present in the gun propellant formulations used by the CF. On the other hand, the methods that are adequate in terms of the products considered either use unmodified silica columns, take more than 30 minutes for each sample or use gradient elution. Consequently, it was decided to develop new methods to meet the above-defined requirements.

TABLE II

List of products considered for the EC method, their abbreviations and their retention times.

Product name	Abbreviation	Retention Time (min.)
NITROGUANIDINE	NQ	1.94
4-NITRO PHENOL	4-N-P	3.2
4-NITRO ANILINE	4-N-A	3.2
2,4-DI NITRO ANILINE	2,4-DN-A	3.84
2-NITRO ANILINE	2-N-A	3.93
DINITROBENZENE	DNB	4.68
N-NITROSO 2-NITRO N-ETHYLANILINE	N-NO-2-N-NEA	4.40-4.95 #
NITROBENZENE	NB	5.13
4-NITRO N-ETYLANILINE	4-N-NEA	5.29
NITROGLYCERINE	NG	5.59 *
N-NITROSO-N-ETHYLANILINE	N-NO-NEA	5.69
N-NITROSO 4-NITRO-N-ETHYLANILINE	N-NO-4-N-NEA	6.22
METHYL CENTRALITE	MC	6.22
2,4,6 TRI NITRO-N-ETHYLANILINE	2,4,6 TN-NEA	7.12
2,2' DINITRO ETHYLCENTRALITE	2,2'-DN-EC	7.12
CAMPHOR	CPH	7.5
2-NITRO-N-ETHYLANILINE	2-N-NEA	8.02
4,4' DINITRO ETHYLCENTRALITE	4,4'-DN-EC	8.25
2,4' DINITRO ETHYLCENTRALITE	2,4'-DN-EC	8.52
TETRANITRO ETHYLCENTRALITE	TETRANITRO EC	9.08
2-NITRO ETHYLCENTRALITE	2-N-EC	9.12
2,2',4 TRI NITRO ETHYLCENTRALITE	2,2',4 -TN-EC	9.72
4-NITRO ETHYLCENTRALITE	4-N-EC	9.79
DIPHENYLAMINE	DPA	10.87
ETHYLCENTRALITE	EC	11.72
2,4 DI NITRO ETHYLCENTRALITE	2,4-DN-EC	13.12
DIPHENYLPTHALATE	DPP	13.09
DIAMYLPTHALATE	DAP	13.89
DIBUTYLPTHALATE	DBP	28.2

Gives rise to a double peak which became a single peak when the column was heated to 50 °C

* NG does not absorb at 254 nm. Its retention time was determined with the detector at 205 nm.

DEVELOPMENT OF HPLC METHODS

The development of an HPLC method follows well-defined steps and Drylab I/plus (LC Resources, Walnut Creek, CA) software was used to assist and facilitate this task. All the details concerning the development, the reproducibility and reliability of the two methods can be found in Ref. 12.

The conditions for the two methods developed are given in Tables III and IV. Figures 1 and 2 illustrate the chromatograms obtained for the two methods with the major derivatives of DPA and EC respectively. The retention times obtained for all the products considered are given in Tables I and II. It must be pointed out that retention times are not absolute and might change from column to column, even for columns from the

same manufacturer. They are given here to clearly demonstrate, with Figs. 1 and 2, that the two methods produced, for the above given lists of effective stabilizers, peaks that are well resolved and free of any interference.

Prior to HPLC analysis, the gunpowder is dissolved in ACN, an internal standard is added, and the NC is precipitated by the addition of 10 ml of water containing 2% of calcium chloride. This last step is needed in order to eliminate NC from the solution, thereby preventing the plugging of the HPLC column by NC. Indeed, NC is soluble in ACN; however, it is less soluble in a mixture of ACN and water. Consequently, if water is not added to the solution, the NC would be precipitated in the column by the mobile phase which consists of an ACN-water mixture. With time, this NC precipitation would plug the column and significantly reduce its lifetime. Moreover, this NC precipitation would raise the operating pressure during the analysis with the consequence of a higher wear rate for the various instrument components. This is why NC is precipitated prior to injection into the HPLC. However, it can be argued that, during the precipitation of NC, the stabilizer may coprecipitate, as was observed when NC was precipitated with water from a methanol solution (13).

TABLE III
Conditions for the DPA method

COLUMN	Lichrocart, RP-18e, 3µm 25 cm X 4.6 cm E. Merck
SOLVENT	71 % ACN + 29 % Water
FLOW	0.5 ml/min
COL. TEMP.	28 °C
WAVELENGTH	254 nm
VOLUME INJECTED	5 µL

TABLE IV
Conditions for the EC method

COLUMN	Lichrocart, RP-18e, 3µm 25 cm X 4.6 cm E. Merck
SOLVENT	58 % ACN + 42 % Water
FLOW	1.0 ml/min
COL. TEMP.	28 °C
WAVELENGTH	254 nm
VOLUME INJECTED	5 µL

On the other hand, a study (14) showed that when the NC is precipitated with an aqueous $CaCl_2$ solution from an ACN solution of the powder, there is no coprecipitation of DPA or EC. The same conclusion was reached among participating countries of an ad hoc group that prepared the revision of NATO STANAG 4117. Nevertheless, for the sake of completeness, we have also done some experiments to verify if there is coprecipitation of stabilizer during the NC precipitation (12). The results obtained showed no coprecipitation for DPA, EC, mono-nitro-DPA, mono-nitroso-DPA and even for mono-nitro-N-nitroso-DPA and di-nitro-DPA.

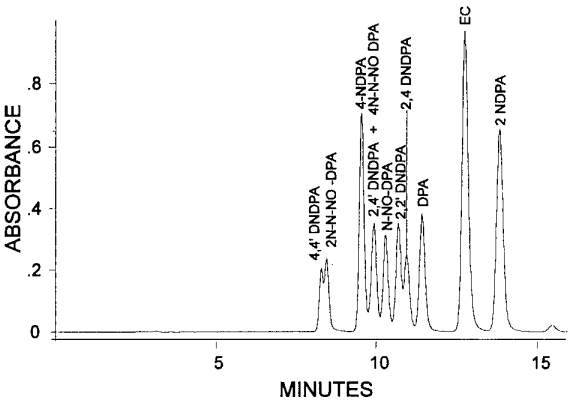


Figure 1- Chromatogram for the major DPA derivatives

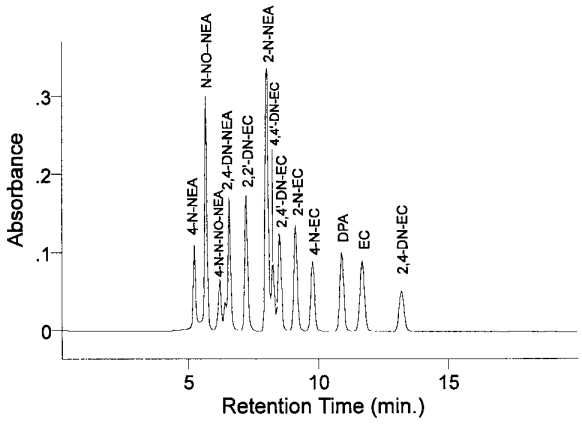


Figure 2- Chromatogram for the major EC derivatives

IS N-NO-DPA A STABILIZER?

Before setting up sentencing criteria, there is an important issue that must be investigated.

Up until 1987, N-NO-DPA was generally considered as a stabilizer. For instance, the studies of Davis (15), Alm (16), Mrzewinski (17) and Heemskerk (18) concluded that N-NO-DPA was an effective stabilizer. On the other hand, more recently, Curtis (4, 6) came to the opposite conclusion. The role of N-NO-DPA as a stabilizer is a very important issue from both an economic and a safety point of view. In fact, if the N-NO-DPA is not an effective stabilizer, this would imply that our current sentencing criteria are inadequate, with the resulting potential risks involved from unsafe gun powders sentenced as safe because of the inclusion of N-NO-DPA as an effective stabilizer. On the other hand, if N-NO-DPA is an effective stabilizer, its exclusion would result in a safe gun powder being unnecessarily destroyed and such a procedure could imply a large amount of money. Therefore, we undertook at DREV some experimental work in order to shed some light on this question, by comparing simulated normal storage temperature ageing with conventional accelerated ageing at temperatures higher than normal storage temperatures.

In order to study the order of appearance of the DPA derivatives, various studies were performed, based on the heating of a sample of a gun powder, contained in a loosely capped pyrex tube, at a specific temperature. At regular intervals of time, a sample was analyzed to determine the concentration of the stabilizer and its major derivatives. From this type of experiment, it was possible to build a concentration versus time profile, and the one illustrated in Fig. 3 being a typical example.

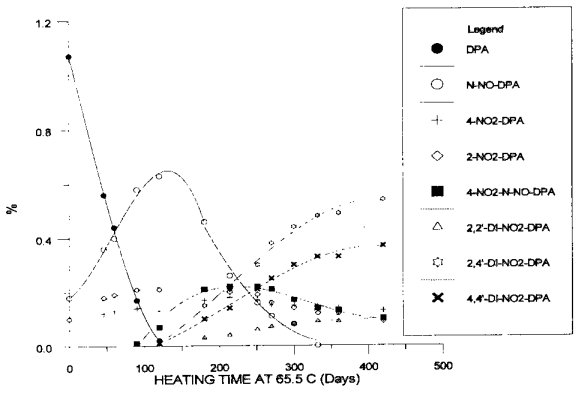


Figure 3-Concentration vs Time profile for a FNH powder aged at 65.5 °C

It is on the basis of such profiles that the authors in Ref. 4 stated that N-NO-DPA was not acting as a stabilizer because the mono-nitro-N-nitroso DPA derivatives did not appear concomitant with the mononitro DPA derivatives. Instead, they were only observed after large amounts of the mononitro DPA had already built up and began to appear after the same degree of ageing as the dinitro derivatives of DPA. In Ref. 6, although direct nitration of N-NO-DPA to form 4-NO_2-N-NO-DPA has been demonstrated for an experimental propellant, it was concluded that N-NO-DPA is a weak stabilizer and its direct nitration to produce 4-NO_2-N-NO-DPA is insignificant in propellants containing DPA and its unnitrosated nitro derivatives, which are more reactive towards nitrogen oxides. All these conclusions are based on concentration versus time profiles built for single base propellants such as an FNH gun powder aged at 80 °C. On the other hand, there was a study conducted at DREV in 1982 (19) where an FNH powder was aged at 65.5 °C and the samples used for this study have been conserved since that time in tightly capped vials in a DREV magazine.

The same samples where thus analyzed again, but this time with HPLC using a method which gave baseline separation for all the DPA derivatives considered (ACN 36%/MeOH 22%/H_2O 42%, flow of 0.7 ml/min). The concentration versus time profile obtained is illustrated in Fig. 3. Although the accelerated ageing of this powder was done 12 years ago and each of the samples has undergone natural ageing since then, it appears that this profile is very close to the one in Ref. 6. Of course, the time scale in our case is longer than the one in Ref. 6, which is normal since our ageing was done at 65.5 °C while in Ref. 6 it was performed at 80 °C. As observed in Fig. 3, the DPA is exhausted at the same time that N-NO-DPA has reached its maximum value, and after that maximum we observe a rapid rise in concentration for the same di-nitro derivatives as in Ref. 6. We also observe that 2-NO_2-DPA is formed in preference to 4-NO_2-DPA as in Ref. 6, although this difference is present for a longer period of time in the concentration versus time profile of Ref. 6. However, there is one striking difference between the FNH profile of Ref. 6 and our profile, and this is the fact that we do observe the formation of 4-NO_2-N-NO-DPA.

Now, if we analyze the profile of Fig. 3 with the one of Ref. 6, interesting conclusions can be drawn. Actually the two profiles are similar except for the appearance of 4-NO_2-N-NO-DPA in Fig. 3 which was absent in the profile of Ref.6. It must be stressed that the Fig. 3 profile represents a FNH powder which underwent accelerated ageing 12 years ago and has undergone ageing at normal storage temperatures since then. Consequently, the 4-NO_2-N-NO-DPA has been produced either during the accelerated ageing period or during the subsequent normal storage temperature ageing. If it were produced during the accelerated ageing, this would mean that the reaction pattern of the stabilizer evolution is temperature-dependent since the 4-NO_2-N-NO-DPA was absent in the 80 °C artificial ageing (6).

On the other hand, if the 4-NO_2-N-NO-DPA was produced during the normal storage aging period, this would also mean that the reaction pattern is temperature dependent since the derivative was not produced at 80 °C but produced at normal storage temperatures.

It appears from the above discussion that the set of reactions involved in stabilizer evolution is temperature dependant. This is also confirmed by the following experiment. N-NO-DPA and 4-NO_2-N-NO-DPA were weighed into capped vials and placed in ovens at 60 and 80 °C. At defined intervals of time, the vials were sampled and their contents analyzed by HPLC. In this way, the amounts of N-NO-DPA and 4-NO_2-N-NO-DPA as a percentage were monitored as a function of heating time. At 60 °C there was a weight percent loss for N-NO-DPA but the 4-NO_2-N-NO-DPA was scarcely reduced in weight percent. However, at 80 °C the weight percent loss for both derivatives was significant. The weight percent loss of N-NO-DPA is accompanied by an increase in weight percent of DPA, 2-NO_2-DPA, 4-NO_2-DPA and very low concentrations of dinitro derivatives as the heating time increases. In the case of 4-NO_2-N-NO-DPA, its weight percent loss is accompanied by an increase in the weight percent of 4-NO_2-DPA , 2,4'-di-NO_2-DPA and 4-4'-di-NO_2-DPA. These results could be explained by the denitrosation reaction.

Indeed, it is well known that the N-NO bond is thermally labile. For instance, N-NO-DPA is converted back to DPA in gas chromatography due to the hot environment encountered (20). Lilliott et al. (21) observed the formation of DPA from N-NO-DPA due to exposure to heat during the processing of a N-NO-DPA stabilized ball powder. Isler (22) has indeed noticed an important denitrosation of 4-NO_2-N-NO-DPA at 80 °C. Moreover, our results concerning N-NO-DPA are very close to the ones obtained for a similar experiment (23). In fact, in the case of N-NO-DPA, loss of the nitroso group yields DPA and nitrogen oxide (NO) which is easily oxidized (by the oxygen in air) to nitrogen dioxide (NO_2) and the latter will then react with the DPA which was produced to yield N-NO-DPA, 2-NO_2-DPA and 4-NO_2-DPA. Thus, with respect to N-NO-DPA, we are running in circles since N-NO-DPA produces DPA which produces N-NO-DPA by reacting with NO_2; however, there is a side reaction in which DPA reacts with nitrogen dioxide to yield mononitro derivatives which build up and eventually react with NO_2 to yield dinitro derivatives. On the other hand, in the case of 4-NO_2-N-NO-DPA, loss of the nitroso group yields 4-NO_2-DPA which by reacting with NO_2 will yield dinitro derivatives.

Therefore, the denitrosation reaction can explain our results and, as mentioned above, the occurrence of this reaction has been confirmed many times in the literature. It should be emphasized that the results obtained were strongly influenced by experimental conditions such as the air-tightness of vial caps and the amount of water and oxygen present. Therefore, these results should be taken as being qualitative and not quantitative. Nevertheless, they show that the N-nitroso derivatives of DPA can denitrosate to an extent and at a rate which are temperature dependent. Moreover, the denitrosation reaction and its temperature dependence can account for the build-up of mononitro derivatives and the appearance of mononitro-N-nitroso derivatives concomitant with the isomeric dinitro derivatives in the artificial ageing. Furthermore, it has been shown that if the mononitro-N-nitroso derivatives do not appear in artificial ageing, it does necessarily mean that the N-NO-DPA is not an effective stabilizer.

Actually, the answer concerning the role of N-NO-DPA as a stabilizer can only come from normal storage temperature ageing. However, nitrate ester decomposition is a slow process at normal storage temperatures and, for this reason, in most stability tests the powder must be heated to achieve a reasonable testing time interval. However, in the literature (24), there is an interesting approach which can be considered a type of accelerated ageing at normal storage temperatures.

It has been demonstrated by Alm (16) and Isler (22) that DPA and its first derivatives do not react with nitric oxide (NO) but do react with nitrogen dioxide (NO_2). Thus, the limiting reagent in stabilizer evolution during ageing is the production of nitrogen dioxide from the thermal decomposition of nitrate ester. Since the thermal decomposition of NC is slow at normal storage temperatures, the propellant is heated in order to accelerate the thermal decomposition and consequently the production of nitrogen dioxide. In a similar way, it is possible to simulate an accelerated ageing by the addition of known amounts of NO_2 at regular intervals of time. In this way, each addition of nitrogen dioxide corresponds to an increase in ageing and the concentration versus amount of NO_2 added profile should be equivalent to the concentration versus time of ageing profile obtained by accelerated ageing. However, if NC is used in this approach, the addition of nitrogen dioxide can accelerate the thermal decomposition of NC by autocatalysis and as a consequence, heat and nitrogen dioxide are produced. One way to circumvent this interference from the NC is to replace the latter with a similar polymer such as cellulose. In this way, the model will approach the actual system in the sense that we are working on an heterogenous medium (i.e. solid-solid phase contact with one reagent in the gas phase), ambient temperature, atmospheric pressure and nitrogen dioxide as the limiting reagent. Using this approach, we built a concentration versus amount of NO_2 added profile for a cellulose/DPA mixture and the results are illustrated in Fig. 4.

The most striking observation about Fig. 4 is that it is reminiscent of a typical concentration versus time profile obtained by accelerated ageing. There is, however, one obvious difference which is the concomitant appearance of mono-N-nitroso derivatives with the mono-nitro derivatives. Also, it appears that the formation of 4-NO_2-N-NO-DPA is favoured

over the formation of 2-NO_2-N-NO-DPA. It should also be pointed out that in this experiment, di-nitro-DPA derivatives, which are not included in Fig. 4 for the sake of clarity appear only after the addition of 70 ml of NO_2 and their concentration is small (below 3%). Comparison between Figs. 3 and 4 shows again that there is a difference in the stabilizer evolution between accelerated ageing and normal storage temperature ageing, and this difference can be accounted for by the denitrosation reaction as discussed above. Most importantly, even if the composition of the system in the normal storage temperature ageing is different from that of a gun powder , it has been shown that in a heterogeneous medium (solid-solid phase contact + gas phase), at ambient temperature, at atmospheric pressure, with nitrogen dioxide as the limiting reagent and while the denitrosation reactions are kept to a minimum, there is evidence that supports the stabilizing contribution of N-NO-DPA via direct reaction with nitrogen dioxide. However, one important point still remains to be discussed. Indeed, according to Refs. 6 and 25, the reaction rate for this reaction is much less than that of DPA or its mononitro derivatives.

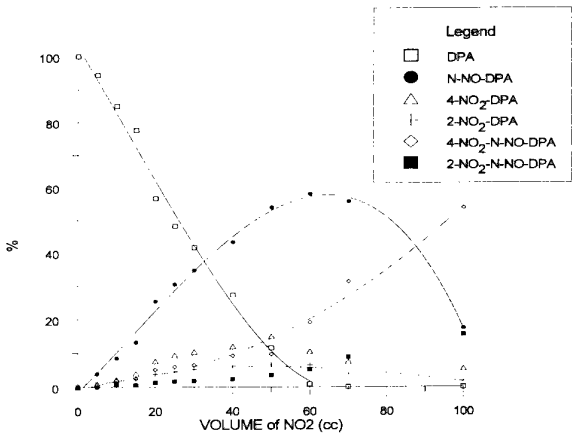
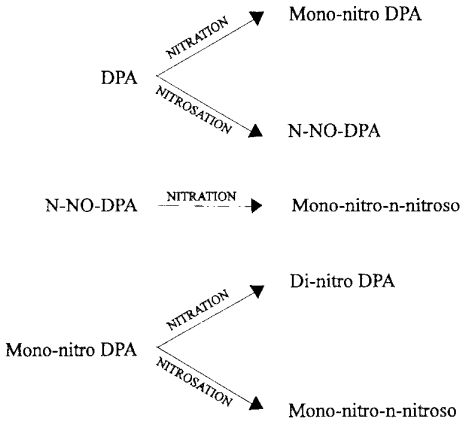


Figure 4- % of derivatives vs volume of NO_2 added profile for a DPA/cellulose mixture

In Ref. 25, various DPA derivatives were subjected to nitrogen oxide flow at 22 °C. The variations in the weight of the sample were continuously recorded since the reaction vessel was coupled to the balance arm of a thermal gravimetric instrument. The results showed that the rate of increase of N-NO-DPA to form 4-NO_2-N-NO-DPA is lower than the weight increase of DPA and its mononitro derivatives to form their respective nitroso derivatives. However, a later study by the same laboratory (18) concluded that the stabilizing effect of DPA and N-NO-DPA appears to be complementary. Alm (16) showed that the reaction rate of N-NO-DPA towards nitrogen oxide is greater than that of 2-NO_2-DPA. In addition, a chemiluminescence study (26) stated that the reactivity of N-NO-DPA is almost equivalent to that of DPA itself. On the other hand, Isler (22) stated that the mono-nitro-DPA derivatives are better stabilizers than N-NO-DPA at 25 °C. Thus, the best that can be said is that there is no general consensus in the literature concerning the reaction rate of N-NO-DPA with nitrogen dioxide.

Nevertheless, it may be interesting to see what the artificial ageing at ambient temperature approach can say about this question. Indeed, Fig. 4 can be of some help in comparing the relative reactivity of N-NO-DPA, 2-NO_2-DPA and 4-NO_2-DPA to nitrogen dioxide in an heterogenous medium (solid-solid phase contact + limiting reagent gaseous NO_2) at ambient temperature. As observed in Fig. 3, initially, nitrosation dominates over nitration and consequently the concentration of N-NO-DPA rises more rapidly than that of 2-NO_2-DPA or 4-NO_2-DPA. After this first period, the nitrogen dioxide molecule has the choice to react with DPA, 2-NO_2-DPA, 4-NO_2-DPA or N-NO-DPA according to the following scheme:



However, in Fig. 4, we also observe, at the initial period, small amounts of mono-nitro-N-nitroso derivatives but, since the latter can be formed, according to the above scheme, either from nitrosation of mono-nitro derivatives or nitration of N-NO-DPA, nothing can be said about their relative reactivity towards nitrogen dioxide. On the other hand, after the addition of 40 ml of NO_2, the increase in concentration of 4-NO_2-N-NO-DPA could not be reasonably accounted for only from the nitrosation of 4-NO_2-DPA, and moreover, the di-nitro-DPA derivatives (not shown in Fig.3) do not appear before the addition of 70 ml. Therefore, this clearly shows that the nitration of N-NO-DPA overcomes either the nitration or nitrosation of mononitro derivatives and consequently it appears that N-NO-DPA is a better stabilizer than the mononitro derivatives at normal storage temperatures. Furthermore, we can now attribute the early formation of mono-nitro-N-nitroso derivatives in Fig. 4 to the nitration of N-NO-DPA, and this means that the stabilizing effect of N-NO-DPA is similar to that of DPA at normal storage

temperatures. It is worth noting that the same observation was made in a cheminulescence study (26).

In order to double check the reactivity of N-NO-DPA towards nitrogen dioxide, a simulated normal storage temperature ageing for a N-NO-DPA/cellulose mixture was done. The results are

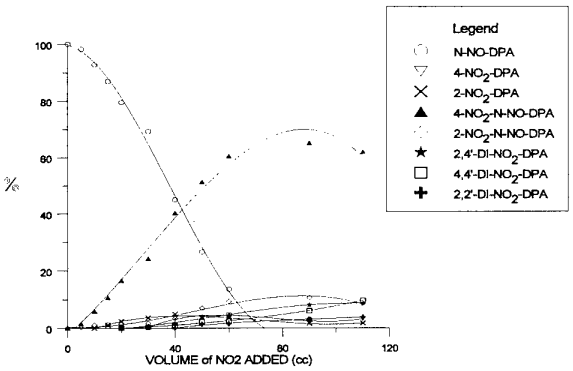


Figure 5- % of derivatives vs volume of NO_2 added profile for a N-NO-DPA/cellulose mixture

illustrated in Fig. 5. The results are in complete agreement with the above discussion and, moreover, it appears that the depletion of N-NO-DPA corresponds closely to the rise in concentration of 4-NO_2-N-NO-DPA, which is another argument in favour of the efficiency of reactivity of N-NO-DPA towards nitrogen dioxide.

Therefore, according to this investigation, N-NO-DPA reacts efficiently with nitrogen dioxide to produce mono-nitro-N-nitroso-DPA derivatives, and this to an extent and at a rate that allows one to consider N-NO-DPA as an effective stabilizer at normal storage temperatures.

SENTENCING CRITERIA

Countries such as France, the UK, the U.S. and Australia have developed their own sentencing criteria from observations and data collected over several years of gun powder chemical life testing. Therefore, they have acquired the data base, expertise, experience and history that allow them to set up appropriate sentencing criteria. On the other hand, no such expertise and data base have been acquired in Canada. Therefore, the only way to set up our sentencing criteria is to study those from other countries in order to determine if there is a general trend and from this, set up sentencing criteria to start with and adapt them according to the data base, experience and history that will be acquired over years of ageing of the gunpowder used by the CF.

Comparison of the different sentencing criteria from the UK (27), France (28), for the U.S. Navy (29) and in Australia (30) show that they are generally quite similar. In fact, the differences appear in the definition of the residual effective stabilizer (RES) and when the concentration of the residual effective stabilizer is low. However, it is still possible to set up sentencing critiria using those of the four aforementioned countries.

The sentencing criteria are given in Table V. For DPA-stabilized propellants, our definition of RES is the concentration of DPA plus the molecular-weight-corrected concentration of N-NO-DPA. For the EC-stabilized propellants, the RES is the concentration of EC. In fact, the RES definitions and the table were chosen in order to correspond roughly to the median of the sentencing criteria of the aforementioned countries. Nevertheless, we are confident that the criteria of Table V are strict enough to detect any powder with questionable chemical stability. Indeed, when the RES is less than 40%, the powder is considered to be uncertain and such a powder should be tested more frequently.

TABLE V

Sentencing criteria

% of original stabilizer remaining[1]	Years until next analysis
80-100	5
60-80	3
40-60	2
20-40	1[2]
<20	Retest +immediate disposal

1 Defined as the ratio of RES and the original amount of stabilizer in the propellant formulation.

2 These propellants must be used in priority.

Finally, as discussed above, these sentencing criteria are only a starting point, and will have to be adapted to the gunpowders used and stocked in Canada. In regard to this topic, the microcalorimetry technique should prove to be very useful. This is the technique of choice to extend the lifetime of energetic compositions and to make sound predictions about the remaining life. This technique can also prove to be essential for studies on predictive technology, a growing subject for the near future.

CONCLUSIONS

In this work, two efficient, fast and reliable HPLC methods which can be used routinely were developed. These methods take into acoount 32 products for DPA-stabilized propellants and 29 products for EC-stabilized formulations. They give

baseline resolved peaks for the products considered as effective stabilizers and these peaks are free of interference from the other products.

The preparation of the sample prior to HPLC analysis was investigated and the results obtained showed no coprecipitation for DPA, EC, mono-nitro-DPA, mono-nitroso-DPA, mono-nitro-N-nitroso-DPA and di-nitro-DPA when a 2% $CaCl_2$ water solution was added to the ACN solution of the gun powder.

In this study the role of N-NO-DPA as a stabilizer was investigated by comparing artificial ageing with normal storage temperature ageing. According to this investigation, N-NO-DPA reacted efficiently with nitrogen dioxide to produce mono-nitro-N-nitroso-DPA derivatives, and this to an extent and at a rate that allows one to consider N-NO-DPA as an effective stabilizer at normal storage temperatures.

Finally, the sentencing criteria for use as a starting point in the CF were established.

REFERENCES

1. Curtis, N.J. "The Chemical Basis for Gun Propellant Stability Testing", Fourth Australian Gun Propellant Conference, October 1990.

2. Schroeder, W.A., Malmberg, E.W., Fong, L.L., Trueblood, K.N., Landerl, J.D. and Hoerger E. "Derivatives of Diphenylamine formed in Double-Base Powders during Accelarated Aging", Industrial and Engineering Chemistry, Vol. 41, No. 12, pp. 2818-2827 (1949).

3. Schroeder, W.A., Wilson, M.K., Green, C., Wilcox, P.E., Mills, R.S. and Trueblood, K.N. "Derivatives of Centralite formed in Double-Base Powders during Accelerated Aging", Industrial and Engineering Chemistry, Vol. 42, No. 3, pp. 539-546 (1950).

4. Curtis, N.J. and Rogasch P.E. "Determination of Derivatives of Diphenylamine in Australian Gun Propellants by High Performance Liquid Chromatography", Propellants, Explosives, Pyrotechnics, Vol. 12, pp. 158-163 (1987).

5. Curtis, N.J. and Berry, P. "Derivatives of Ethyl Centralite in Australian Gun Propellants", Propellants, Explosives, Pyrotechnics, Vol. 14, pp. 260-265 (1989).

6. Curtis, N.J. "Isomer Distribution of Nitro Derivatives of Diphenylamine in Gun Propellants: Nitrosamine Chemistry", Propellants, Explosives, Pyrotechnics, Vol. 15, pp. 222-230 (1990).

7. Volk, F. "Determining the Shelflife of Solid Propellants", Propellants and Explosives, Vol. 1, pp. 59-65 (1976).

8. Volk, F. "Determination of the Lifetimes of Gun Propellants using Thin-layer Chromatography", Propellants and Explosives, Vol. 1, pp. 90-97 (1976).

9. Snyder, L.R., Glajch, J.L. and Kirkland, J.J. "Practical HPLC Method Development", Wiley, New York, 1988, Chap. 3.

10. Weiser, E.L., Salotta, A.W., Flach, A.M. and Snyder, L.R. "Basis of Retention in Normal Phase High Performance Liquid Chromatography with Cyano-propyl Columns", Journal of Chromatography, Vol. 303, pp. 1-12 (1984).

11 Majors, R.E. "Current Tends in HPLC Column Usage", LC-GC, Vol. 12, pp. 890-898 (1994).

12 Lussier, L.S. and Gagnon, H. "Development of Modern Methods for Determination of Stabilizers in Propellants", DREV-R-9511, April 1996, UNCLASSIFIED.

13 Haberman, J. "High Performance Liquid Chromatography of Propellants. Part 1 - Analysis of M1, M6 and M10 Propellants", ARDC Technical Report ARAED-TR-86017, U.S. Army Armament Research and Development Center, USA, May 1986.

14 Helama, H. and Kovero, E. "A Modern Method for Determining the Stability and Stabilizers in Solid Gun Propellants", Symposium on Chemical Problems Connected with the Stability of Explosives, Vol. 6, Part 2, pp. 285-303 (1982).

15 Davis, T.L. "The Chemistry of Powder and Explosives", Vol. II, Chapter 6, John Wiley and Sons, New-York, N.Y. 1943.

16 Alm, A. Chemical Problems Connected with the Stability of Explosives, Vol.I, pp.162-178 (1967).

17 Mrzewinski, T. "Change of Diphenylamine in Single Base Propellants", Chemical Problems Connected with the Stability of Explosives, Vol.6 , pp.317-327 (1982).

18 Heemskerk, A.H. "Stability of Nitrocellulose Propellant", in Chemical Problems Connected with the Stability of Explosives, Vol.8, pp. 137-148 (1988).

19 Asselin, M., Suart, R.D., Perreault, G. and Bédard, M. "GC/MS of DPA and its Derivatives : Validation of a TLC Propellant Stability Test", Chemical Problems Connected with the Stability of Explosives, Vol.6 , pp. 271-283 (1982).

20 Sopranetti, A. and Reich, H.U. "Possibilities and Limitations of High Performance Liquid Chromatography for the Characterization of Stabilizers and their Daughter Products in Comparison with Gas-Chromatography." , in Chemical Problems Connected with the Stability of Explosives, Vol.5 , pp. 163-181 (1979).

21 Lilliott, E.L., Mrazek, W.D. and Murray, T.A. "Comparative Studies of the Stabilizing Effect of the Diphenylamine and N-Nitrosodiphenylamine in Single and Double Base Experimental Ball Powder Propellants", Proc. of the Joint International Symposium on Compatibility of Plastics and Other Materials with Explosives, Propellants, Pyrotechnics and Processing of Explosives, Propellants and Ingredients, pp. 332- 338, San Diego, California, 22-24 April 1991.

22 Isler, J. " Etude du pouvoir stabilisant de la diphénylamine et de ses principaux dérivés", Note Technique No. 77/83 GERPy, Groupe d'Études et Recherches en Pyrotechnie, Direction des Constructions et Armes Navales de Toulon, Toulon, France (1983).

23 Bulusu, S., Cahill, S., Axenrod, T., Autera, J.R., Robertson, D. and Kansas, L. "Role of N-Nitrosodiphenylamine in the Stabilization of Nitrocellulose-based Propellants : A Preliminary Study using ^{15}N-NMR Spectroscopy", Proc. of the Vth International Gun Propellant & Propulsion Symposium, Picatinny Arsenal, N.J., pp. 498-508, 19-21 November 1991.

24 Moriarty, R.M., Richardson, A.C., Lee, D.,Patel, J., Liu, J. "Reaction of Diphenylamine and N-Nitroso Diphenylamine with NO_2 in Cellulose", Proc. of the Vth International Gun Propellant & Propulsion Symposium, Picatinny Arsenal, N.J., pp. 481-497, 19-21 November 1991.

25 Opschoor, J., Heemskerk, A.H., Verhoeff, J. and Pasman, H.J. "Stability of Nitrocellulose Propellants", 14th International Annual Conference of ICT, Karlsruhe, Fraunhofer-Institut für Treib und Explosivstoffe, pp. 495-507 (1983).

26 Wallace, I.G. and Westlake, S. "The Use of a Chemiluminescence NO_x Analyser to Study the Reactions of Propellant Stabilisers and their Derivatives", Chemical Problems Connected with the Stability of Explosives, Vol.7, pp. 19-41 (1985).

27 Dodds, J.S. "Current UK Procedures for Propellant Shelf-Life Determinations", Symposium on Chemical Problems Connected with the Stability of Explosives, Vol. 9, pp. 247-258 (1982).

28 Leveque, M. "Principe de l'étude et du contrôle de la stabilité chimique des propergols destinés aux armées françaises et de leur surveillance dans les stocks", Etablissement Technique de Bourges, Laboratoire des poudres et explosifs, Bourges, France, mai 1987.

29 Williams, D. "US Navy Gun Propellant Surveillance", TTCP W-4 held in US, 8-12 April 1991, Vol. V, Rocket and Gun Propellant Service Life, pp. 261.

30 Curtis, N.J. and Kempson, R.M. "A New Strategy for Service Safe-Life Surveillance Testing of Gun Propellants", WSRL-TR-49/89, Weapons Systems Research Laboratory, Australia, October 1989.

Paper Number: 23
Discussor's Name: Dr. M. A. Bohn
Responder's Name: S. Desilets

Question: Have you tried to separate the two reaction channels for the formation of 4-NO_2-N-NO-DPA? From the appearance with time of 4-NO_2-N-NO-DPA shown in the gun propellant data, one can conclude that this product originates from the nitrosation of 4-NO_2-DPA.

Answer: You are right. However, we do not attempt to separate the two reaction channels in a gun powder since accelerated artificial aging involves heat and consequently introduces a new reaction: the denitrosation. However, the competition between the denitrosation and nitration could explain why in figure 3, 4-NO_2-N-NO-DPA does not appear before about 100 days. In fact, the denitrosation reaction overcomes the nitration of N-NO-DPA and it is only when the concentration of N-NO-DPA is almost at its maximum that nitration of N-NO-DPA overcomes the denitrosation of 4-NO_2-N-NO-DPA. The denitrosation reaction could also explain the decrease in the concentration of 4-NO_2-N-NO-DPA after about 250 days. In fact, after 250 days the concentration of N-NO-DPA is decreasing and consequently the denitrosation of 4-NO_2-N-NO-DPA overtakes again the nitration of N-NO-DPA.
Actually, the answer can only come from a normal storage temperature aging. Our experiment with a mixture of DPA and cellulose (figure 4) can shed some light on this question since at low temperature the denitrosation reaction does not occur so it will be possible to compare the relative reactivity of N-NO-DPA and mononitro derivatives towards NO_2. In figure 4, the increase in the concentration of 4-NO_2-N-NO-DPA, after the addition of about 40 ml of NO_2, could not be reasonably accounted for only from the nitrosation of 4-NO_2-DPA. Therefore, this experiment shows that nitration of N-NO-DPA overcomes the nitrosation of mononitro derivatives and consequently it appears that the nitration of N-NO-DPA is the preferred channel for the formation of N-nitroso-mononitro derivatives.

SERVICE LIFE PREDICTION METHODOLOGIES ASPECTS OF THE TTCP KTA-14 UK PROGRAMME

G.S. Faulkner
British Aerospace Defence
Royal Ordnance Rocket Motors
Kidderminster, Worcs. DY11 7RZ
ENGLAND

D. Tod
Defence Research Agency
Fort Halstead
Sevenoaks, Kent TN14 7BP
ENGLAND

SUMMARY

At the 12th meeting of The Technical Cooperation Programme (TTCP) , Panel W-4, Propulsion Technology, participants from the United States and the United Kingdom jointly proposed a collaborative programme within TTCP. The aims of this programme were to improve experimental methods and attempt to validate current predictive service life methodologies. A decision was taken to evaluate solid rocket motor propellants containing HTPB propellants. All the participants fielded motors that were instrumented and then subjected them to agreed programmes of work. In September 1988, formal approval was received and the collaborative programme became Key Technical Area 14 (KTA-14). Canada, Australia, the UK and the US all fielded motors for the programme. This paper outlines some of the results from the work carried out in the United Kingdom by Royal Ordnance Rocket Motors and the Defence Research Agency Fort Halstead.

1. INTRODUCTION

At the start of the TTCP programme, service life prediction technology in the UK was centred on experimental methods where motors were tested to prove their ability to withstand an applied loadcase. If the motor failed the test, then a modification would be introduced. These methodologies relied strongly on past experience and design iteration. The cost and application of these methods was becoming increasingly prohibitive, especially as funding levels were reducing and cost-plus contracts were a 'thing of the past.' Improved design and analysis capability was required if cost and time schedules were to be met. In the aerospace and automotive industries, computer aided engineering (CAE) involving solid modelling and finite element analysis were proving to be valuable assets since candidate designs could be assessed prior to manufacture and an insight given as to likely problems. This approach was acceptable in terms of the geometrical design of a motor grain but the complexities of the solid rocket motor propellant behaviour did not readily lend themselves to analysis using small strain linear elastic codes. Specific rocket motor analysis codes such as 'Texgap' (Texas Grain Analysis Program) and derivatives were being used in some parts of the rocket motor industry (mainly in the US) but it wasn't until the mid-eighties that general purpose non-linear analysis codes became readily available. Geometrically complex finite element models could now be built and an ever-increasing analysis capability became available as both the hardware and software technologies advanced. Obviously, it was desirable to exploit the benefits of these new technologies. The TTCP collaborative programme has allowed rocket motor engineers from different countries, each with their own experiences, the opportunity to discuss both experimental and analysis techniques. The principal aims of the collaborative programme were:

(i) To upgrade analytical, instrumental and experimental methods, procedures and techniques.

(ii) To verify and validate state-of-the art stress analysis techniques

(iii) To determine the best method(s) for accurate service life predictions.

Data from the items outlined above were shared between all participants at progress meetings and through the final technical reports (1).

The KTA programme outline broadly took the form of motor trials, propellant rheology and finite element stress analysis. During the course of the collaborative programme, new methods for service life determination involving probabilistic methods emerged (2). The test motor submitted to the KTA programme by the UK was a case-bonded reduced-smoke HTPB propellant referred to as the 'Structural Test Motor', or STM. The charge configuration was a slotted-radial design, with four slots at the aft-end of the charge blending to a cylindrical section at the forward end via a highly stressed transition region. The four slots are positioned at angles of 90°to one another.

Instrumented variants of the motor contained thermocouples and Sensometrics bondline stress gauge, model 601511. Each one of the instrumented motors contained three stress gauges mounted in a line down the axis of the motor case.The instrumented motors were called 'STIMS'. Figure 1 shows a schematic drawing of the STIM charge and the positioning of the stress gauges. The figure shows that the motor was stress-relieved at the head end by means of a butyl boot. Although the STM was a research motor it was representative of a flightweight design. For the KTA programme motors were cast as detailed in Table 1.

2 MOTOR TRIALS

The bondline stress gauges were mounted flush with the inner lining material of the case and , in this motor, the diaphragm of the gauge was bonded to the propellant. Each one of the three stress gauges was held in place by special collars which followed the contour of the case. The collar had four retaining studs which secured the gauge.

Paper presented at the AGARD PEP Symposium on "Service Life of Solid Propellant Systems" held in Athens, Greece, 10-14 May 1996, and published in CP-586.

The general arrangement is shown in Figure 2. As the motor was temperature cycled below its stress-free temperature, the thermally induced stresses were measured as the propellant tried to separate from the case wall. These thermal stresses arise due to the different expansion coefficients of the steel case and propellant. The load acting on the gauge surface results in the generation of a voltage change in the activated gauge which can be converted to a stress value via prior gauge calibration work. All gauges were screened for hysteresis prior to calibration and installation in the motor. Further trials were carried out once the gauges were installed but prior to motor filling. The motor case and gauges were temperature cycled to determine the magnitude of any interaction between the components.

Instrumented motors were monitored during the cure process and during mandrel extraction. It was found that despite the use of a release agent, the propellant still bonded to the mandrel and an appreciable drop in the bondline stress was measured on mandrel extraction. An example of the stress gauge measurements pre-and post-mandrel extraction is shown in Figure 3.

STIM motors number 1 and 2 were the first of the motors to be instrumented using the Sensometric gauge. These motors were used for pre-cursor trials as the start of the KTA programme. The results of the trials are given in a separate paper (3). Trials on STIM3 are discussed in section 3.

Further instrumented STIM charges were subjected to a series of motor trials. The first trial that was carried out was arctic cycling using grain STIM4. This grain was accompanied by a non-instrumented sister motor. The nature of these trials was to induce mechanical damage as the propellant was strained on motor cooldown.

The results of the bondline stress measurements for an arctic cycling type of trial as shown in Figure 4 are discussed. One cycle is shown. Figure 5 shows the measured temperature-time profile for cycle number 1 for the arctic cycle trial. Figure 6 plots the measured bond line stress for the first of five temperature cycles. The results indicate that gauge 9F393 registered the highest level of stress. This gauge was nearest to the forward end of the charge. Stress relaxation effects can be seen as each gauge reaches the peak stress level. Repeated arctic cycling of STIM4 indicated a reduction in the stress levels as shown in Figure 7. The measured stress levels at 20°C and -20°C were found to be lower after storage at -45°C indicating that damage had occured. It should be noted that a sister motor, also subjected to this pattern of cycling, was subsequently successfully fired at -54°C.

STIM5, was subjected to a thermal shock load which consisted of repeated cycles between +60°C and -54°C. The instrumented motor was stored for 16 hours at 60°C before being rapidly transferred to an adjacent cold chamber where it was stored for 8 hours before being returned to hot storage. Eight hours was sufficient time for the propellant to reach thermal equilibrium. The results of the thermal shock trials are shown in Figure 8. After 5 cycles the datalogger malfunctioned and subsequent data was judged as un-reliable. The stress reductions on the first five cycles are appreciable and the results compared with those from the Canadian motor trials. The results are shown normalised as a percentage stress change. The UK and Canadian motors were of different diameters and hence the bond line stress levels were not directly comparable. The results indicate that after 5 cycles the stress levels have reduced by 27% in the case of the STIM and 24% for the Canadian motor. Trials on the Canadian test motor indicated that the damage increased to a 40% reduction in original stress levels by the fourteenth cycle when the test was stopped.

A programme of low temperature firing trials to determine the low temperature firing limit for the STM motor was carried out. Motors were instrumented with thermocouples to record the actual conduit temperature on ignition. Seven STM motors were fired as detailed in Table 2. Other designs of charge were also fired at low temperatures for comparison. The Ouzel II motor uses the same hardware as the STM but the grain design is a six-pointed star. The Ouzel III motor has the same grain configuration as the STM but the propellant is highly aluminised. The calculated safety factor based on maximum principal strain is shown. The strain levels were calculated using finite element analysis methods. The safety factor for each motor firing was calculated by the summation of both the thermal and pressurisation damage increment, Dt and Dp. The damage increments are calculated separately and then summed. The definition of the safety factor used within the UK is given below since it is known that each country has its own definitions (4).

The Safety Factor (SF) is defined

$$SF = \frac{1}{Dt + Dp}$$

Where Dt = the thermally induced strain / allowable strain for motor cooldown and Dp = the pressurisation induced strain / allowable for motor pressurisation . It is required that the safety factor is greater than unity throughout the life of the motor grain.

This work on the low temperature-high strain rate failure of propellant grains is to be used in the follow on TTCP KTA programme (5) to investigate failure criteria.

3 PROPELLANT RHEOLOGY

Propellant characterisation tests were carried out and fall into two categories. The first category consists of tests that are performed routinely to characterise the propellant, such as tensile tests to establish failure master curves, dynamic mechanical testing and stress relaxation tests.

The non-standard testing comprised a variation of the standard stress relaxation test. A sample was conditioned isothermally and then loaded to 3% strain level. The sample was allowed to undergo stress relaxation for a short period of time before being loaded to a higher level of strain. This procedure was carried out over a range of strains that the STIM3 motor would see as it was subjected to temperature cycling. The tests also encompassed the temperature range that the motor would see. The reasons

for this test are described below. Figure 9 shows a stress-relaxation curve as the sample was loaded in several strain increments. In this case the strain level reached was 23%, with the test being carried out at 20°C.

4 FINITE ELEMENT ANALYSIS

A 3D Finite element model of the grain was constructed and used to identify the region of highest strain in the grain. The region of highest strain is indicated in Figure 1. Subsequent temperature cycling of this design of motor leads to cracks in this zone of the charge. Because of the computing disc space requirements, large strain viscoelastic models were confined to 2D axisymmetric and plane strain analysis of the critical regions for bondline stress and failure prediction respectively. Correlation between the 2D models and 3D models was made on a strain level basis such that the maximum principal strain in the 2D plane strain model matched the elastic strain result from the 3D finite element analysis model.

Since the bondline stress gauges are located in the central, cylindrical region of the grain, the use of an axisymmetric model was deemed valid. Initial analysis indicated that the gauge at the head end of the grain would be subjected to the highest stress levels. This area of the grain would be the critical region in terms of bondline stress. The stress gauge measurements of the equilibrium stress levels of an instrumented grain cooled from 60°C to -50°C are shown in Figure 10. The ABAQUS finite element analysis code was used to predict the bondline stresses for the motor excursion described above. The viscoelastic material model option was used, with a nine term Prony series representing the propellant stiffness. Temperature shift factors were supplied using ABAQUS user subroutine, UTRS .

The linear viscoelastic stress predictions are also shown in Figure 10. It can be seen that the model under predicts the measured stress level. However, the simple test described above where a tensile test specimen was subjected to increasing strain levels has been used to correct the predictions as shown in Figure 10.

The method to obtain the stresses involved the derivation of correction factors by modelling tests carried out in the laboratory on a tensile test specimen as it was subjected to an increasing load (see section 3). A finite element model of the tensile test bar was modelled and displacement boundary conditions were applied to one end of the model to generate strain. Stress levels in the axial direction were computed for each strain level and plotted. An example is shown in Figure 11. Even in this controlled test it can be seen that the stress levels are generally lower than those measured. This implies that the effective modulus being supplied to the finite element code was too low. For each strain level , the factor by which the measured stress was greater than the predicted value was plotted . The procedure was carried out at several temperatures to provide the correction factor curves in Figure 12. Hence, to correct the linear viscoelastic predictions, one first determines the bore strain level and appropriate temperature. One then selects the correction factor from the appropriate curve for that particular temperature.

Although the method proved successful for STIM3, further work was carried out to establish if the method held good for other loading fractions of propellant. Four J-rounds (simple test vehicles), as shown in Figure 13 were cast using the same propellant used for the STM grains. Each grain had a different mandrel diameter. Charges with the smallest diameter conduit would generate the highest stress and strain levels on temperature cycling. The STIM motor had a grain diameter to bore diameter value of 3.0 (lambda=3.0). The J-rounds were chosen to yield lambda values of 3.0, 3.5, 4.0 and 5.0.

Figure 14 shows the measured stresses for the highest loading fraction charge with linear viscoelastic predictions and corrected stresses also marked. The results from the STIM3 motor reflect stresses measured in a motor with a relatively low lambda values whilst Figure 14 shows results for a relatively high lambda value. Results for other lambda values also show very good agreement.

5 DISCUSSION

Arctic cycling of the STIM4 motor indicated that after the first cycle the maximum bondline stress levels (measured at -45°C) had decreased by an average of 35% from those measured at 20°C .However , the stress levels measured at -20°C decreased by almost 45%. This indicates that the damage that was induced was more marked at the lower temperatures.

This repeated cycling trial indicated that the modulus of the propellant was decreasing. The occurrence of damage was expected and the same phenomenon can by seen in the laboratory with a tensile test bar loaded cyclically. The decrease in modulus through mechanical damage is a factor which needs to be considered in the service life determination. It is possible that the first mode of failure anticipated (which might have been grain cracking for example) may be replaced by grain deformation on ignition or under high axial acceleration. Grain cracking can of course be detected by inspection whereas the new primary mode of failure may occur on motor ignition and give rise to an over pressure and subsequent case failure.

The thermal shock trial indicated that the highest stress level was reached on the first shock loading and that the stresses after this first shock were less. After 5 cycles , the bondline stress measured at -54°C had decreased by 27% of its original value, that is, a decrease of 112 kPa.

In the case of the low temperature firings , the results of the stress analysis shown in Table 2 indicated that using maximum principal strain as a failure criterion for this and other designs of case bonded HTPB grains was a very conservative approach. The safety factor for each motor firing was calculated using the properties determined for the propellant fiilling batch. The results indicate that the factor of conservatism is almost two. The strain based criterion was deemed to be conservative in the prediction of the low temperature limit for a case bonded HTPB charge, even when the failure data was measured in uniaxial tension.

The problem of failure criterion for unflawed propellant grains is essentially based on stress or strain based criteria.

The advantage of the strain based methods are that one can measure the strain levels by many means ranging from bore strain measurement and X-rays, to in-situ strain gauges. Stress based criteria are more difficult since the stress levels in the grain are strongly rate and temperature dependent as well as being strain level dependent. Some of the non-linear viscoelastic properties of propellant are highlighted elsewhere (6).

The linear viscoelastic model has been shown to under predict bond line stress levels on motor cooldown. A method of correcting the stresses has been proposed but the technique was not handled directly within the finite element code.

Participation in the KTA programme has been beneficial to all countries involved. Areas of consensus of opinion and others of 'debate' arose. One area where there was no dissension was that there is still a lot to learned in the field of charge stress analysis and service life prediction. An important benefit from the programme has been the development of a reliable method of measuring and monitoring the thermally induced stress levels in the charge. Recommendations for future work involve the implementation of non-linear viscoelastic material models to account for some of the peculiarities of propellant behaviour such as cumulative damage and rehealing effects which are known to exist.

6 CONCLUSION

1 The methods and usage of stress gauge technology to measure stresses in case bonded charges have improved such that reliable data is now being obtained from motors.

2. Damage induced by temperature cycling proved to be real and was measurable by use of the bond-line stress gauges.Both thermal shock and Arctic cycling trials induced damage in the charges trialled.

3. A linear viscoelastic material model was found to underpredict the bond-line stress levels on slow cooling a STIM grain

4. A method has been proposed whereby the stress level predictions can be corrected to values very close to those measured during motor trials. The method makes use of test data which was both easy and relatively cheap to obtain in the laboratory.

5. The use of maximum principal strain as a failure criterion for the prediction of the low temperature firing limit for this motor was found to be a conservative approach.

7 RECOMMENDATIONS

Recommendations have been made and accepted for a follow on KTA to investigate low temperature failure on motor ignition. The programme will concentrate of the failure of motors during rapid pressurisation loading and assess current failure criteria prediction methods.

REFERENCES

(1) Rocket Motor Service Life Prediction Methodologies KTA-14 Final Report Volumes (I) to (X). (1994)

(2) A Multi-site Service Life Prediction Analysis for Solid Rocket Propellants. Volume VII, Annex E United Kingdom. Final Report - Analysis for Solid Propellant Rocket Motors Stored In Random Thermal Environments. 1994. Margetson,J. & Dickinson,M.

(3) Bondline Stress Gauge Measurements in a Case Bonded Charge. 16th Meeting TTCP-W4 paper. April 1991. Faulkner,G.S. & Buswell, H.J.

(4) AGARD working group 25 - final report to be published. Working group still current.

(5) KTA 4-24 Failure Analysis of Rocket Motors on Pressurisation . New TTCP collaborative programme to start in April 1996.

(6) Improvements in Rocket Motor Service Life Prediction. Buswell,H.J. & E.Francis,E. AGARD Paper 27 Service Life Of Solid Propellant Systems. Athens , Greece. May 1996.

ACKNOWLEDGEMENT

This paper was funded under DRA contract WSFH/E2096C Service Life Studies.

Serial Number	Trial
STIM1	initial datalogger trials
STIM2	initial datalogger trials
STIM3	slow cooldown equilib. stresses
STIM4	arctic cycle trial
STIM5	thermal shock
1	low temperature firing
2	low temperature firing
3	low temperature firing
4	low temperature firing
5	low temperature firing
6	low temperature firing
7	low temperature firing
8	fired to assess instability

Table 1. UK KTA-14 MOTORS

MOTOR TYPE	FIRING TEMP. (°C)	PREDICTED SAFETY FACTOR	RESULT
STM	-53	0.62	OK
	-53	0.62	OK
	-56	0.61	OK
	-57	0.61	OK
	-57.5	0.6	FAIL
	-58	0.6	FAIL
	-58	0.6	FAIL
OUZEL I	-53	1.23	OK
	-53	0.88	OK
	-58	0.66	OK
	-58	1.12	OK
	-60	1.07	OK
	-62	1	OK
	-68	0.76	OK
	-73	0.46	FAIL
OUZEL II	-58	0.66	OK
	-63	0.55	OK
	-66	0.54	OK
	-66	0.5	OK

Table 2. LOW TEMPERATURE FIRINGS OF CASE BONDED HTPB MOTORS.

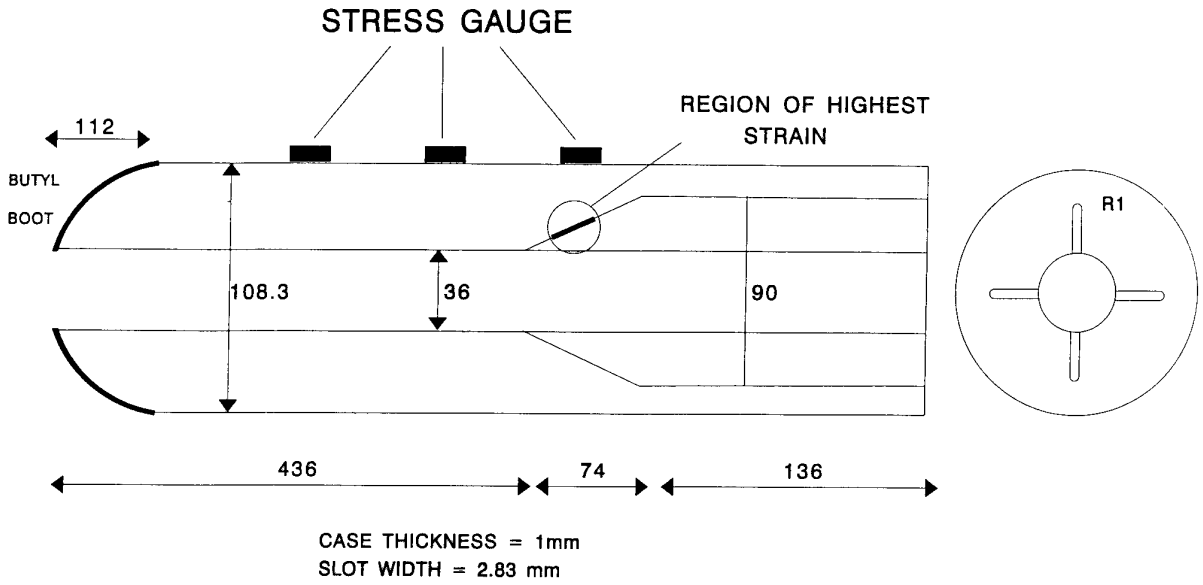


FIGURE 1 . STM/STIM MOTOR CHARGE (SCHEMATIC) SHOWING CHARGE DESIGN AND THREE STRESS GAUGES

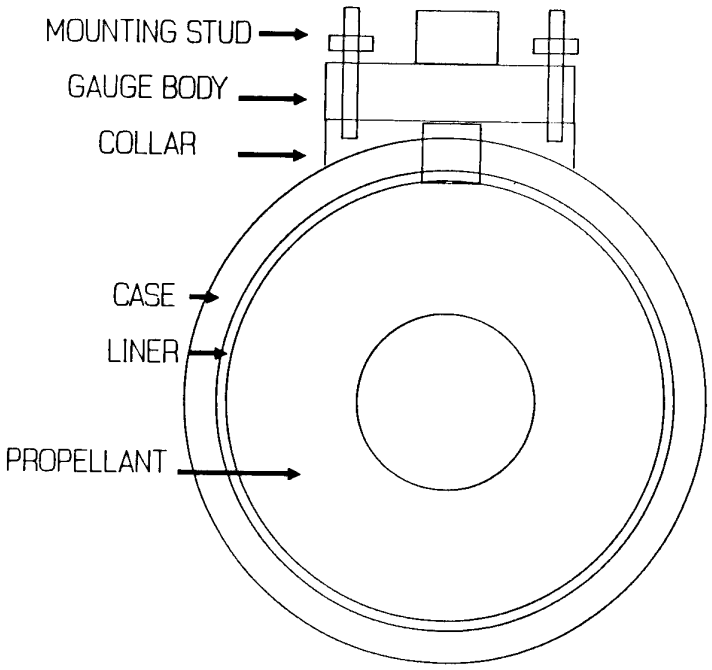


FIGURE 2 . STRESS GAUGE AND COLLAR MOUNTING (SCHEMATIC)

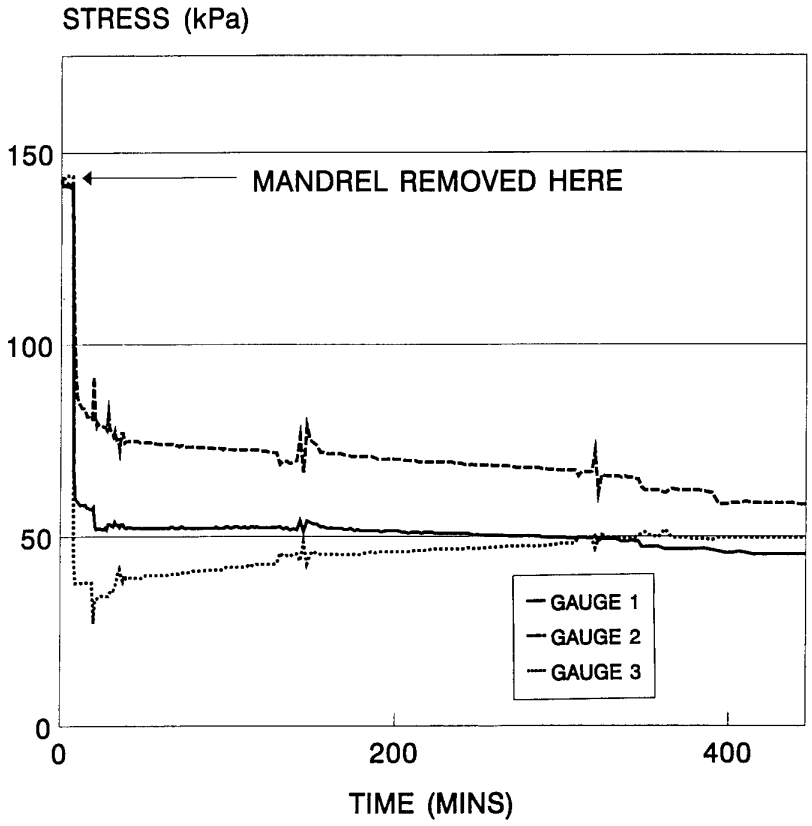


FIGURE 3. MANDREL REMOVAL AT AMBIENT . STRESS MEASUREMENTS BEFORE AND AFTER MANDREL REMOVAL

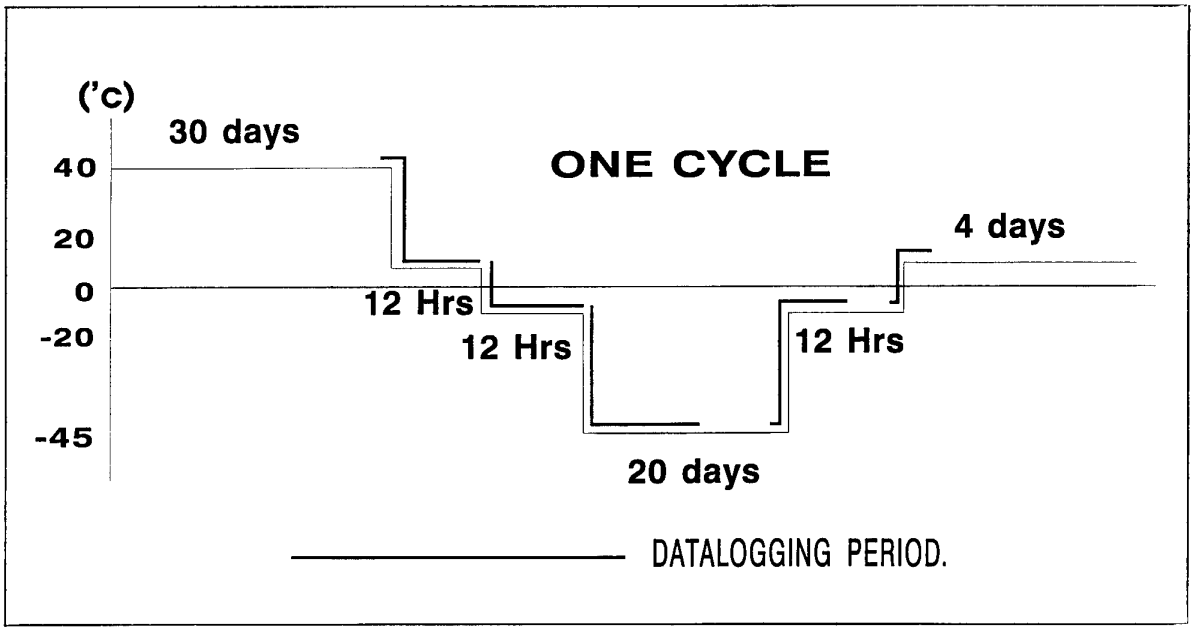


FIGURE 4. ARCTIC CYCLE PROFILE

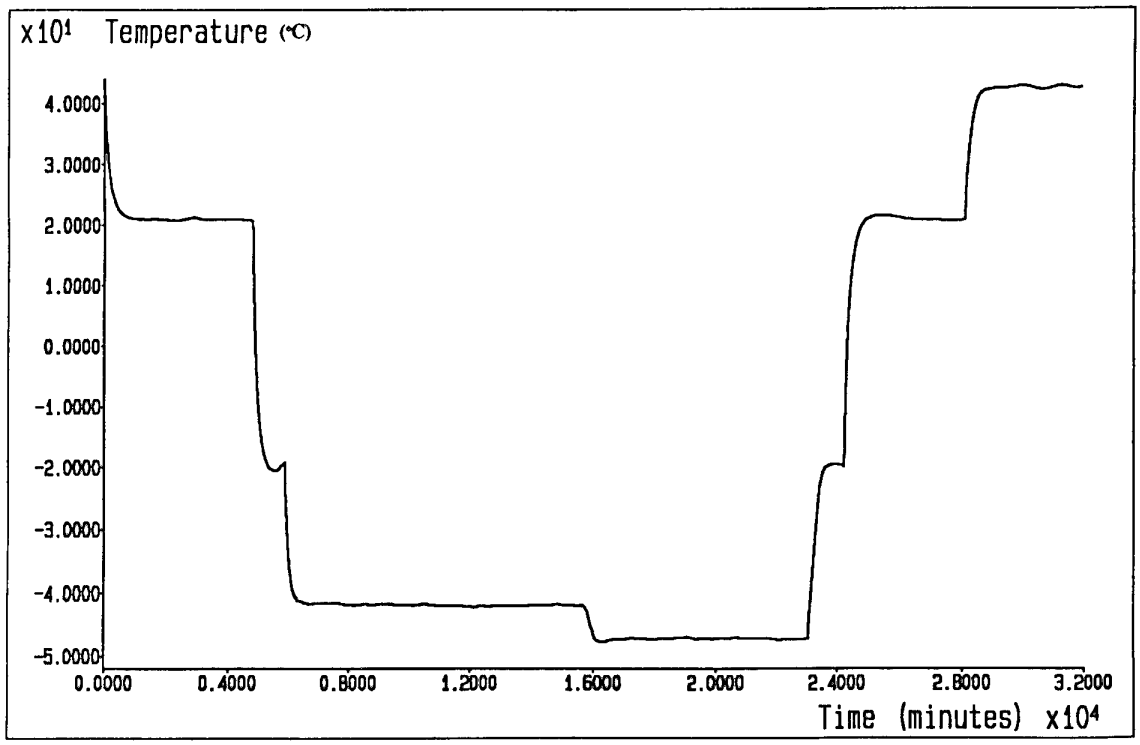


FIGURE 5. TIME-TEMPERATURE HISTORY FOR CYCLE #1 OF ARCTIC TEMPERATURE CYCLING

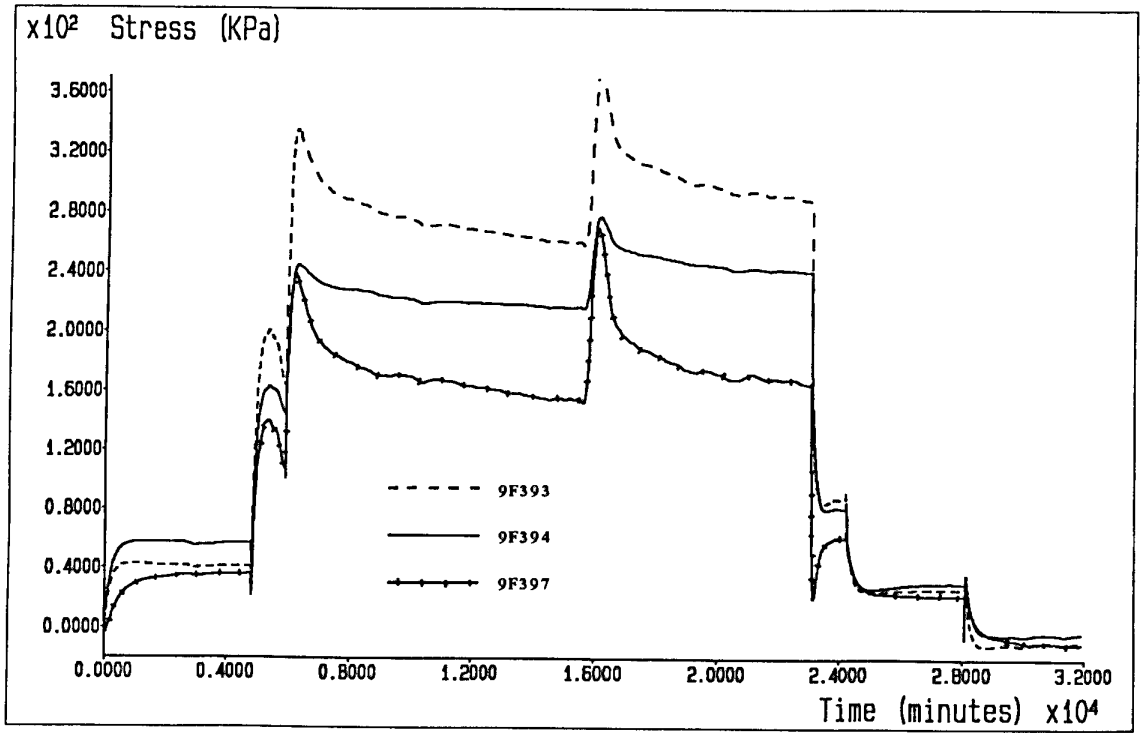


FIGURE 6. STRESS GAUGE MEASUREMENTS FOR ARCTIC CYCLE #1

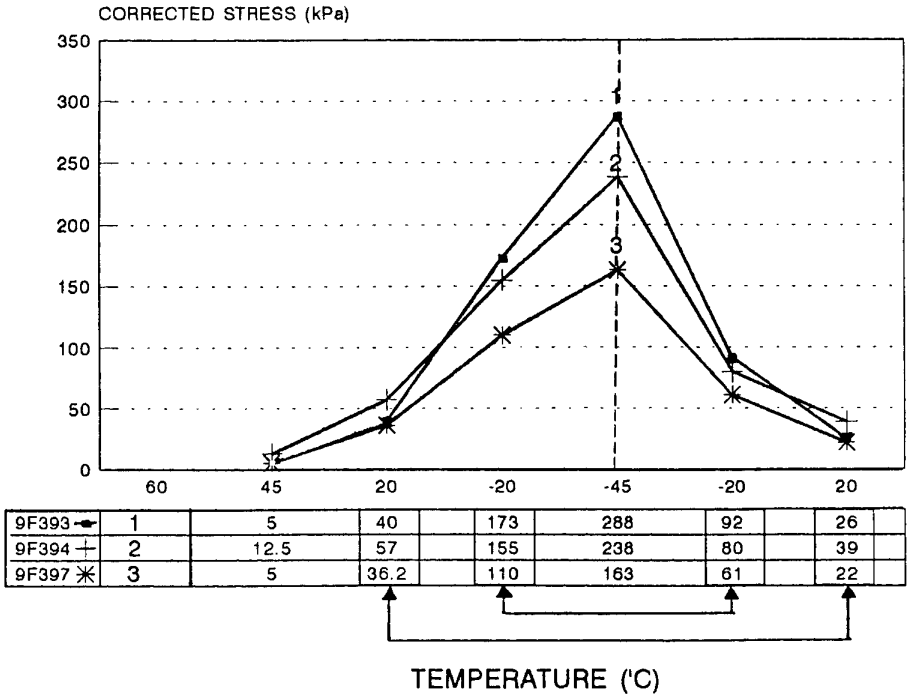


FIGURE 7. STRESS GAUGE MEASUREMENTS FOR ARCTIC CYCLE #1
HEATING & COOLING INDICATE DAMAGE HAS OCCURED.

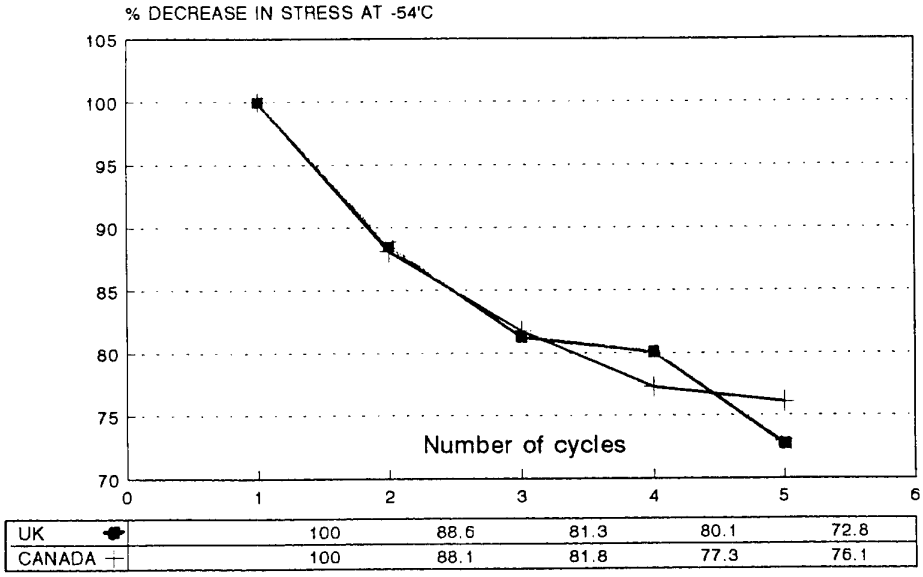


FIGURE 8. STRESS GAUGE MEASUREMENTS ON THERMAL SHOCK TRIALS
(UK AND CANADIAN RESULTS COMPARED)

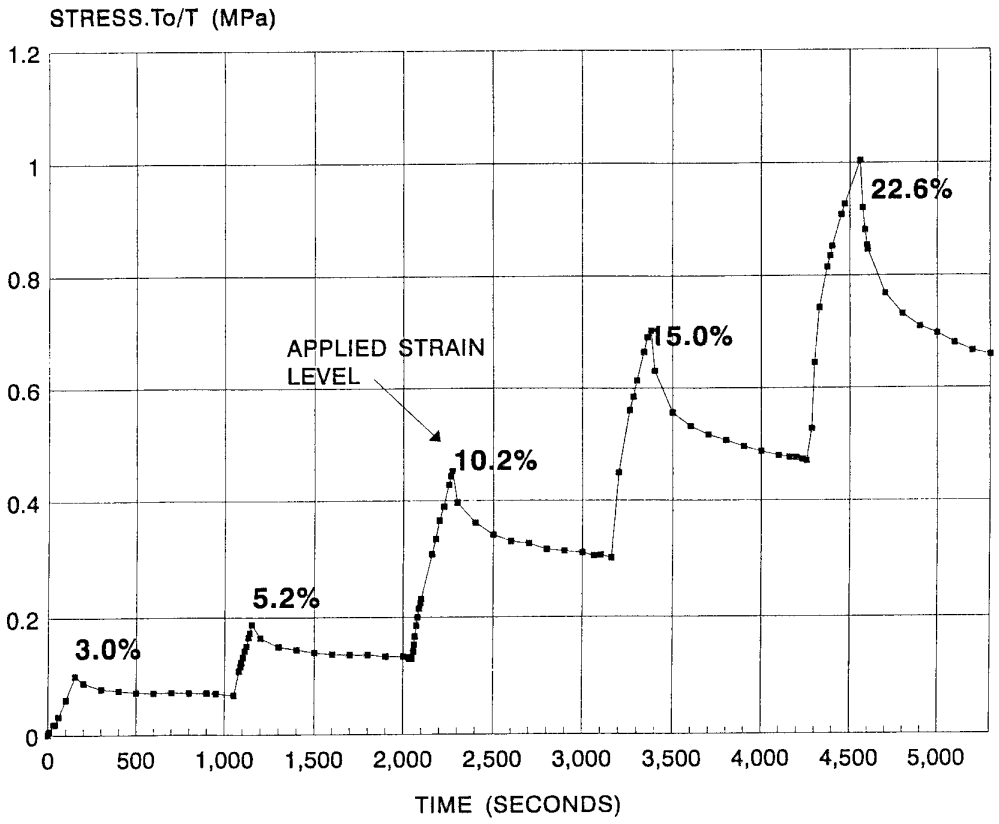


FIGURE 9. MULTI-STRAIN LEVEL STRESS RELAXATION TEST
(20°C TEST SHOWN)

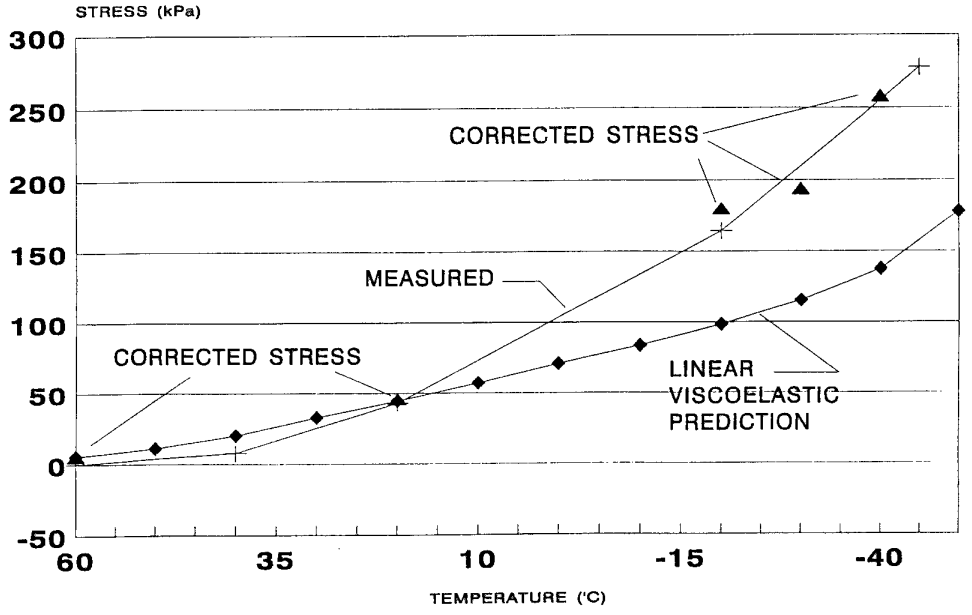


FIGURE 10. STRESS GAUGE MEASUREMENTS ON SLOW COOLDOWN OF A STIM CHARGE . GRAPH SHOWS FINITE ELEMENT ANALYSIS STRESS PREDICTIONS

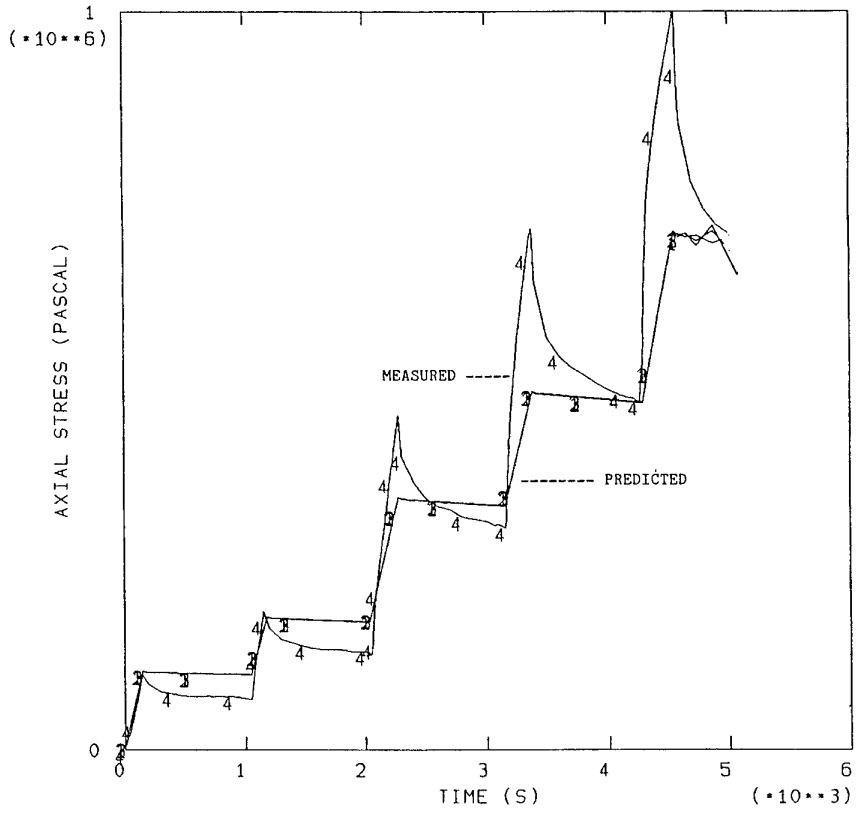


FIGURE 11. MEASURED AND PREDICTED STRESS LEVELS FOR MULTI-STRAIN LEVEL STRESS RELAXATION TEST SIMULATION

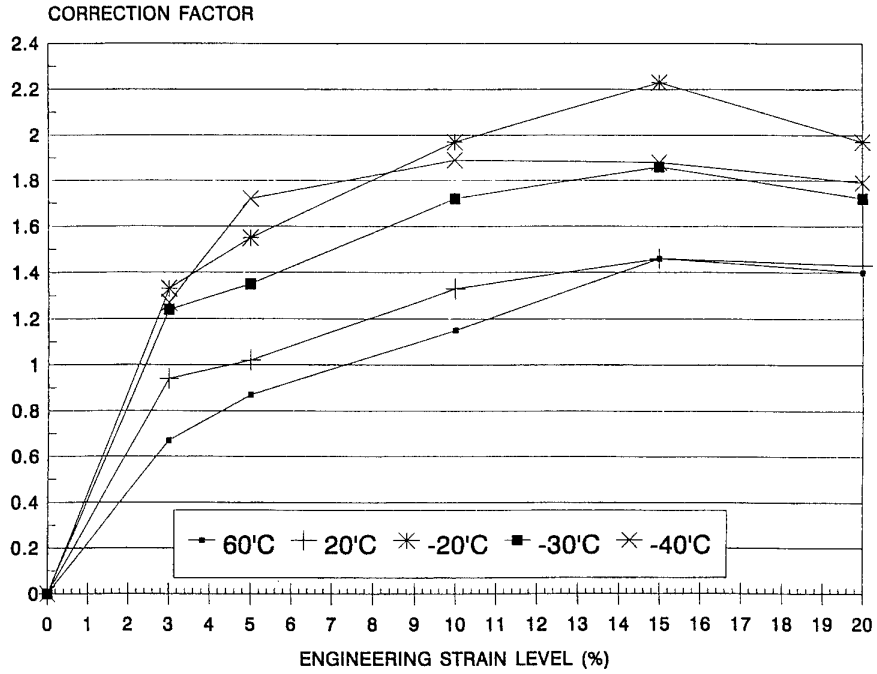
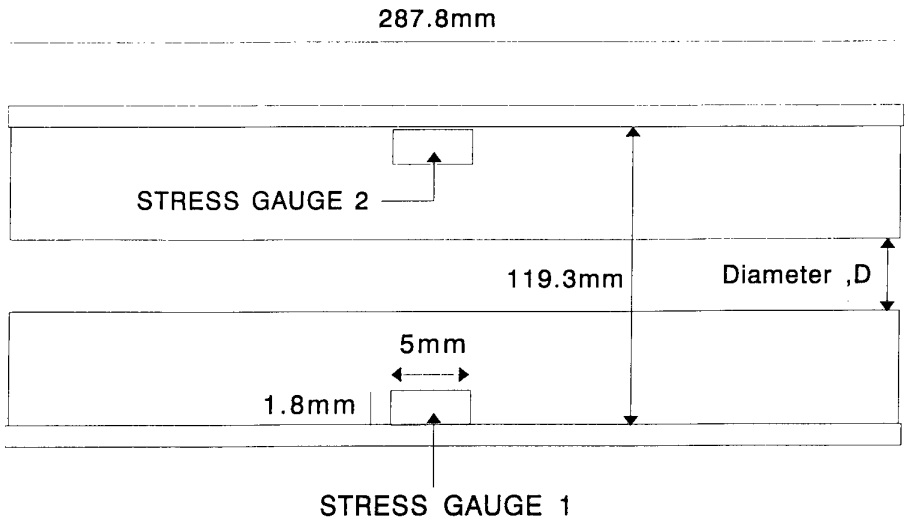


FIGURE 12. STRESS CORRECTION FACTORS DETERMINED FROM MULTI-STRAIN LEVEL STRESS RELAXATION TESTS



Mandrel Diameter (mm)	Lamda
39.75	3.0
34.07	3.5
29.81	4.0
23.85	5.0

FIGURE 13. J-ROUND TEST MOTOR WITH TWO STRESS GAUGES

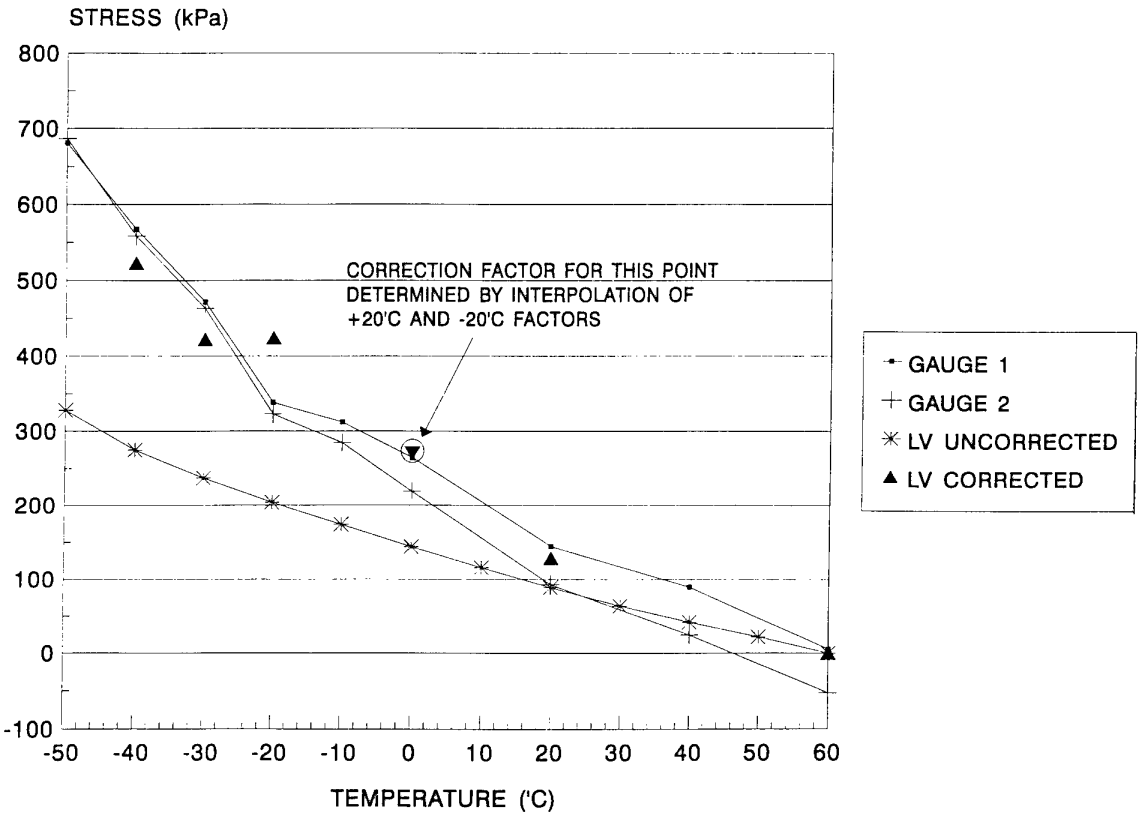


FIGURE 14. MEASURED AND PREDICTED BONDLINE STRESSES FOR J-ROUND (LAMBDA=5) ON COOLDOWN. GRAPH SHOWS LINEAR VISCOELASTIC PREDICTION (LV) AND CORRECTED LV PREDICTIONS

Paper Number: 24
Discussor's Name: D. I. Thrasher
Responder's Name: G. S. Faulkner

Question: What have you done to assess or correct for gage-grain interaction effects due to the gage installation (gage protruding through the insulator to the propellant)?

Answer: The interaction factor is calculated using finite element analysis. In the case of the STIM motor the factor was determined to be about 0.3% change in stress, a negligible amount. In the case of the Canadian motor (which has a smaller diameter) the interaction is larger and needs to be accounted for during subsequent analysis.

Paper Number: 24
Discussor's Name: D. I. Thrasher
Responder's Name: G. S. Faulkner

Question: Were transient thermal effects on the transducers significant during the shock loading tests?

Answer: In the case of the thermal shock trials, the large "through-the-case" gage does exhibit transients since it has a relatively large thermal inertia. It is for this reason that we have moved to using the new miniature gage. However, in the case of the thermal shock trials, we uniformly shock cycled the motor. The measured stresses should be used comparatively from shock load number 1 onwards (results were presented in a normalized manner).

Paper Number: 24
Discussor's Name: D. I. Thrasher
Responder's Name: G. S. Faulkner

Question: You showed that motor stresses under thermal loading can be under-predicted by a factor of 2. If this information produced a comment of "so what?" from an important customer, how would you respond?

Answer: This would depend on the predicted margin of safety. If we had a healthy margin, then maybe there isn't a problem. However, in terms of service life predictions, the customer may be perhaps more "impressed" if you were to say that this uncertainty may reduce the life of the motor and cost him money due to early motor replacement costs, i.e., one may need to translate M.O.S. to dollars.

Miniature Sensor for Measuring Solid Grain Rocket Motor Case Bond Stress

Herb Chelner
Micron Instruments
Simi Valley
CA93063

Dr J Buswell
Defence Research Agency
Fort Halstead
Sevenoaks
Kent TN14 7BP, England

1 INTRODUCTION

Solid propellant normal bond stress profiles are calculated and used in the predication of motor service and storage life. Bond stresses are calculated instead of measured due to the belief that making the measurement is difficult and available sensors too inaccurate. Recent developments in stress measurement technology and instrumentation has changed that situation completely. This reported work has resulted in the design of a miniature sensor with improved accuracy and stability and which is more easily installed in rocket motors with minimal effect on the grain stress distribution. The design goal for thermal hysteresis, when thermally cycled between -45°C to +65°C was 7 kPa (1 psi). Sensors with less that 3 kPa (±0.5 psi) were produced but the yield needs to be improved. The long term stability design goal of 7 kPa (1.0 psi) per year was exceeded. The average drift of all sensors tested was less than 5 kPa (0.7 psi) per year with many sensors drifting less than 2 kPa (0.25 psi) per year. For ease of installation the low flat miniature profile with a diameter of 7.6 mm and a 2.0 mm thickness fits easily into the motor lining or may be bonded to the case wall. A 1.0 mm hole is required for the 5 conductor cable which can be disconnected from the remote bridge completion package for installation and routing without soldering. The remote bridge completion housing comes complete with water seals on the cable, top cover and electrical connector.

2. SENSOR DESIGN

Earlier stress sensors used fixed edge circular diaphragms for the stress measurement member. Since most of the finite element analysis and actual testing was performed using[1] this transduction approach, the design described in this paper uses the same principles and diaphragm diameter to thickness ratios.

2.1 Mechanical Design Details

Sensor dimensions are shown in Figure 1. Two different materials have been used for the sensor body titanium 6AL4V and 17-4 PH CRES steel. Figure 2 shows the orientation of the semiconductor strain gages as they were bonded onto the diaphragm with epoxy. A five-conductor cable enters the sensor through the side wall hole and is soldered to the open bridge formed at the solder tabs. The other end of the cable is attached to a bridge completion and temperature compensation board. After the sensors have been computer tested over their temperature range in a temperature chamber, which defines the values and locations of the bridge completion balance and sensitivity resistors, the resistors are installed on the circuit board. These resistors bias the strain gages to force dynamic self thermal transient compensation. The cable has a 1.0 mm diameter. Routing the cable through the rocket motor casing would require a hole no bigger than clearance diameter for this small cable which minimize the damage and weakening of the rocket motor case and makes sealing much easier. A lid is bonded to the rear of the sensor after all electrical connections are made and the cable is bonded at the exit. A bridge completion package has been designed and this package consisting of resistors and soldered junctions can be miniaturized if required.

2.2 Measurement of Normal Stress

Homogeneous single crystal semiconductor strain gages are bonded to the inside surface of the diaphragm. Two gages are located in the centre of the diaphragm and two gages are located at the edge as close to the wall as possible. These gages are connected head to tail into an open bridge configuration. Special miniature 0.10 ohm cm boron doped gages 0.6 mm (0.026 inch) long were developed for this sensor. The gages have gold nickel pads and ball bonded 0.04 mm diameter 0.999 pure gold leads at each end. Nominal gage resistance at ambient is 500 ohms. Thermal coefficient of resistance is 17%/100°F and the gage factor is 150. The thermal coefficient of the gage factor is -13%/100°F. Due to crystal orientation and geometry, the gage is uni-directionally sensitive and therefore placed along the radius.
The radial stress (Sr) can be calculated as shown below[2].

$$Sr = \frac{3w}{8\pi mt^3}\left[(3m+1)\frac{v^2}{a^2} - (m+1)\right]$$

For a positive load or pressure on the diaphragm, the maximum radial tension is at the centre and compression is at the edge support. The gages in the centre of the diaphragm increase in resistance with tension and at the edge, decrease in resistance with compression. When the gages are connected into a bridge and properly excited, a linear and proportional electrical output is obtained with respect to pressure. Maximum deflection is at the centre of the diaphragm and is calculated by:

$$y = \frac{3W(m^2-1)a^2}{16\pi Em^2t^3}$$

With the modulus of elasticity of 126 GPa (18 million psi) for Titanium 6AL4V and 203 GPa (29 million psi) for 17-4PH steel, a normal bond stress measurement is expected to be better than 99 percent accurate with flush mounted

Paper presented at the AGARD PEP Symposium on "Service Life of Solid Propellant Systems" held in Athens, Greece, 10-14 May 1996, and published in CP-586.

sensors[3].

3. PERFORMANCE TESTING DETAILS

Since it is difficult to simulate bond stress, gaseous nitrogen pressure was used. The full scale range of the sensors is 700 kPa (100 psig). Errors or deviations are expressed in percent of full scale or psi. Detailed procedures for each test were established and followed. The quality control system requires all measurements to have recent calibration traceability and pressure standards are referenced to the NIST. The accuracy of pressure standard is better than 0.05% of reading.

3.1 Static Error Band

The static error band is comprised of the non-linearity, hysteresis and non-repeatability at ambient temperature. Design considerations of the sensor were initiated to meet the design goal of 2 kPa (±0.25 psi) and testing of 46 sensors produced an average error of 0.8 kPa (0.11 psi). Figures 3 and 4 show data for each of the materials used and show the static error band as a percentage of full scale. Also shown are the zero stress offset and full scale offset which are not considered errors. They are repeatable and can, therefore, be corrected during data analysis.

3.2 Balance Temperature Coefficient

The balance zero load electrical offset change with temperature is compensated for by shunting a gage with a resistor on the side of the bridge that is changing most rapidly. Since the resistor does not need to be subjected to the temperature change, it can be located remotely in the bridge completion external box. Although the four gages are computer matched for intercept at 26°C and between -45°C and 137°C for temperature coefficient, variations in diaphragm surface finish, epoxy bond thickness, etc. can effect performance. Passive resistor balance temperature compensation forces the bridge to be self-compensated. A high degree of thermal transient compensation is achieved. It is more important that the thermal balance temperature coefficient be repeatable, rather than just very low. The thermal hysteresis data is used for data correction of the gage output. Average balance coefficients for titanium sensors is 2.0% FS/100°F and steel 2.2% FS/100°F. The lowest value for titanium is 0.12% FS/100°F, given in Figure 3 and for steel is 0.35% FS/100°F as shown in Figure 4.

3.3 Sensitivity of temperature coefficient

The algebraic difference between the zero load electrical output and the 700 kPa (100 psi) electrical output is defined as the sensor sensitivity. The variation of the temperature coefficient is the change in this sensitivity with temperature. This change can either be a straight line or a more complex curved line function. Measured average values for titanium sensors was 1.15% FS/100°F with the lowest recorded sensitivity change being 0.05% FS/100°F. The average for steel sensors was 1.62% FS/100°F with the lowest recorded value of 0.16% FS/100°F.

3.4 Thermal Hysteresis

At zero pressure with the sensor properly excited, an output is obtained over the limits of its temperature compensated range. The curve thus obtained is called the balance temperature coefficient and is often expressed as percent of full scale per 100°F. This curve can be established by measuring the sensor output as it is changed from 65°C (+150°F) to -45°C (-50°F). If the balance curve obtained cooling from 65°C (+150°F) to -45°C (-50°F) is different from the curve obtained heating from -45°C (-50) to 65°C (150°F) then the difference is defined as thermal hysteresis. To minimize the thermal hysteresis the sensors are treated to processes which are known to optimize general performance such as heat treatment of metals after machining, thermal cycling to stabilize components, and specialized curing of epoxy. It is a design goal to obtain a thermal hysteresis of less than 7 kPa (1.0 psi) over the thermal range shown. For the curves shown in Figures 5 and 6, the temperature of the chamber containing the sensors was held constant for 120 minutes at each temperature shown. The complete thermal cycles were run over 110 hours and generated 55 data points. The curves produced from the data collected from the majority of sensor have similar signatures with the following characteristics:

1. For each sensor the temperature extreme end points repeated.
2. Increasing temperature data points between the limits were always more positive than the decreasing temperature points
3. The increasing temperature data points were repeatable.
4. The decreasing temperature data points were repeatable.

3.5 Long Term Stability

The sensors were put into a box to eliminate wind currents and subjected to slow ambient temperature changes. All sensors were tested for balance approximately twice per week. Each sensor's electrical output was measured by plugging its electrical connector into a mating connector wired to a constant current supply and digital readout. No attempt was made to compensate for temperature. Although the constant current power supply was always reset prior to collecting data and the current was recorded with each data point, no attempt to correct the data was made. It was assumed these small fluctuations of current would average out during the long test period. Some sensors required a stabilization lead time of up to 30 days whereas others require no stabilization lead time. After stabilization the changes were within the required 7 kPa (1 psi) for all the sensors with a small cyclic variation. It is believed that these long term cyclic changes shown in this data are due to long term room temperature seasonal changes. It was observed that these long term cycles are greater on sensors having the larger balance temperature coefficient. To check the accuracy of the long term stability measurement, a resistor bridge was assembled which simulates the sensor impedance. The resistors were metal film with 50 ppm temperature compensation and the results demonstrated that the measurement and power supply were of sufficient stability.

3.6 Thermal Burn-In

Before thermal hysteresis tests are run on production units, a

high temperature burn-in is applied to the sensor to age and stabilize any stresses in the material or wiring caused by fabrication and to further cure the epoxy bonds and seals. Sensors were subjected to 82°C (180°F) for 160 hours which is usually sufficient to stabilize the unit. However, if required a second burn-in at 88°C (190°F) for 190 hours has been shown to produce more stable units. Some sensors continued to show a small change after both thermal stress exposures. This drift may be long term stability drift accelerated by the higher temperature. These units are not considered stable enough for long term stress measurement.

3.7 High Pressure Testing

3.7.1 Experimental Method

By design, the bond stress transducer develops a low full scale pressure induced diaphragm stress level. This was the result of designing for a very high spring constant thereby minimizing interaction of the sensor with the propellant grain due to deformation of the sensor. A by-product of this design is the ability to withstand high overpressure without gage failure. To quantify this feature sensors were tested, individually, after being mounted into the standard calibration fixture. The sensor was excited with 4 mA constant current, the output signal is monitored by a six place digital voltmeter with ten microvolts resolution. The pressure is generated by an oil dead weight tester accurate to 0.1% of reading above 350 kPa (50 psi) and traceable to NBS. The power supply was checked frequently and proved to be stable. No adjustments were required. The data was recorded manually and stored for subsequent analysis.

3.7.2 Balance Shift with Overpressure

Since previous testing of overpressure showed little change below 3.5 Mpa (500 psi), i.e. a 5 x over-range test, the first overpressure was to this level. Electrical zero balance output was recorded before pressure was applied. There was a small zero shift when the sensor was installed in the test fixture. Pressure was applied using a dead weight tester which was allowed to settle before the full scale pressure electrical output was recorded. The pressure was reduced to zero and the zero output recorded. Typical results for a steel sensor is shown in Figure 7. Five sensors were tested and all gave very similar results. The accumulated zero shifts have been measured and could be used to correct gage readings if the units were used to measure high pressure.

3.7.3 Effects of Overpressure on sensor performance

A post 700 kPa (100 psi) calibration run was performed on the sensors and compared to the pre-run results as shown in Table 1.

No pre-cal test was performed on 13654 but thermal data was available and no post test has been run on 13656 at the time of this paper. The results are mixed and indicate no significant changes in performance at 700 kPa (100 psi).

After the post test calibration a linearity run was made on each type of sensor. The lowest resolution on the dead weight tester is 350 kPa (50 psi) so four steps of 800 psi were used on the steel sensor and five steps of 450 psi were used on the titanium sensors. The tests were repeated several times to test accuracy and the sensor output for the titanium gage is shown in Figure 8. After being exposed a second time to 3200 psi, the steel sensor zero reading shifted in the positive direction equivalent to 160 kPa (23 psi). This is considerably less than the accumulated shift of 315 kPa (45 psi) observed during the step pressure testing (see Figure 7). After subjecting the titanium sensor to step pressure ending at 2700 psi, the sensor electrical balance output also shifted positively to 357 kPa (51 psi), again significantly less than the accumulated shift. Assuming that the non-linear curves can be used to correct the data, the inaccuracy is determined mainly by the zero shift which for steel sensors after exposures to 22.4 MPa (3200 psi) was 190 kPa (27 psi) or 0.72% of 3200 psi. A titanium sensor tested to 16 MPa (2250 psi) ten times showed that with each cycle the full scale output decreased between 3 to 5 millivolts. 5 millivolts is equal to 80 kPa (11.5 psi). The uncertainty is 2 millivolts or 32 kPa (4.6 psi) or 0.20% of reading. By generating two over-range curves for the sensor and extrapolating, the above accuracy is obtained. This process does not correct the other system inaccuracies due to temperature etc., which need to be considered for overall accuracy prediction.

4. NORMAL BOND STRESS/TEMPERATURE DUAL SENSOR

Although the accuracy of the sensor over an extended temperature range is good, more accurate bond stress data could be obtained. Since the output change of balance and sensitivity is part of the data generated for every sensor, knowing the temperature permits correction of the data. Having the dual reading capability makes it possible to obtain temperature and bond stress data simultaneously. A silicon temperature element the same size as the strain gage has been developed and is bonded directly to the diaphragm as shown in Figure 9. This element has no significant strain sensitivity and will not be affected by pressure or case induced strains. It will have a rapid thermal transient response as it is small and low in mass. Only minor changes to the sensor mechanical design is required and no change in sensor performance is expected.

A single 4 mA constant current power source was used to excite both sensors in series. Two output signals are obtained, one for pressure and one for temperature, and can be data logged for later analysis. It was known that a series resistor can be selected to linearize the output curve. Testing was performed to determine the value of that resistor for optimized linearization over the temperature range -45°C to

65°C (-50°F to 150°F). Analysis of the data showed some non-repeatability at -45°C (-50°F) which may be due to the temperature chamber. A typical result is shown in Figure 10 and the maximum error is less than 1°C (±2°F).

5. SENSOR ENVIRONMENTAL AND OPERATIONAL USES

Some comments on the uses of the developed stress and temperature sensor are discussed below.

5.1 Safety Considerations

Safety is always an issue when working with solid grain rocket propellants. Any small spark is potentially dangerous. Installing electrical wires of any significant power inside rocket motors is not allowed. To minimize the potential of sparking, the sensor was designed to activate with only 4 mA constant current into a maximum bridge impedance at 71°C (160°F) of 320 ohms requiring 1.25 volts of excitation. The sensor impedance decreases with reducing temperature. The constant current source is limited to 6 mA maximum. If a gage fails, no current will flow through the bridge. The sensor housing is completely enclosed and the four strain gages are piezo-resistive with no other active components. It is very unlikely that a spark can be generated at 6 mA and less than 2 volts, the maximum of the signal conditioner. However, the gages are completely enclosed by the sensor housing and lid which is the most probable place for a potential open or short circuit. Safety fuses must also be incorporated into all circuits that connect to the rocket motor with full earth protection.

5.2 Measurement of Chamber Pressures

Design of the standard sensor is very conservative. The 700 kPa (100 psi) sensor has more than 30 X over-pressure capability and can be used to measure chamber pressure to 21 MPa (3000 psi). The titanium 6AL4V sensors operate to over 14 MPa (2000 psi). A number of sensors bonded inside the motor case can be used to establish the reactive pressure profile of the motor during operation until the flame front reaches the sensor[4]. The natural frequency of the sensor is approximately 150,000 Hz. Higher pressure range sensors with higher natural frequencies can be manufactured by increasing the diaphragm thickness.

The sensor diaphragm thickness determines the output. Increasing the diaphragm thickness to develop 40 millivolts of signal at the chamber pressure firing level, requires no re-calibration of the electronics. The output would be linear within 0.25% BFSL. If the sensor is used only to measure chamber pressure, much of the special processing can be eliminated and the cost of the sensor is significantly less.

5.3 Verification of Normal Bond Stress Calculations

Assuming that the sensor is functioning correctly and can be installed without affecting the normal bond stress, the data obtained can be used to quantify the stress analysis predictions[5,6]. If the actual stress does not agree with the theoretical stress, it signifies incorrect input material properties[7] or assumptions made during the margin of safety calculation.

5.4 Motor Health Monitor

If used to monitor rocket motors subjected to in-service loads valuable stress and temperature history records could be obtained. This sensor can also be used as a health monitor since it will detect grain cracks or propellant-to-case debond which may compromise motor operation[8]. It would also detect pressure build up due to motor operation.

Each motor design is different and the designer knows where the maximum normal stress regions should occur and what constitutes a change that would be considered dangerous. A rocket under the wing of a high speed jet is more of a problem if it misfires than one on a mobile ground launcher. It has already been shown that the sensor can sense cracks in a grain which shows as a drop in bond stress[8]. With the proven long term stability, the sensor is capable of measuring changes in stress level resulting from ageing, debonding or cracking of the propellant grain.

6. GENERAL DISCUSSION AND CONCLUSIONS

This paper describes a successful program of work to develop a miniature sensor for the measurement of normal bond stress and temperature in solid grain rocket motors. The transducer must be robust and capable of performing in demanding environments. The sensor must withstand high temperature during motor manufacture and then accurately measure the stress developed during cooling to room temperature. The sensor must record the temperature and stress level when the rocket motor is subjected to temperatures within the operating range of -50°C to 70°C. Motors can be stored for long periods before being used. Since many of the storage facilities are not air-conditioned and some are not insulated, the sensor must operate over a wide storage temperature range and over long periods of time with good accuracy. Motors are often cycled between -45°C (-50°F) and +65°C (+150°F) to determine their ability to withstand sudden thermal changes and as an accelerated life test. So that accurate measurements can be made during such testing, the sensor needs to be thermal transient temperature compensated and have low thermal hysteresis. To measure the bond stress accurately it is necessary for the sensor to have low compliance. Accuracy of the bond stress measurement is also determined by the way in which the sensor is installed in the motor.

Most designers of rocket motors use minimum case thickness since inert mass subtracts from the motor performance. Strain gage full bridge sensors with external bridge completion require five wires. An electrical cable containing these wires must be routed through the motor case. Therefore, an important design consideration is to reduce the size of the electrical cable thus requiring a correspondingly smaller hole through the case. This process minimize or may even eliminate the need for additional weighty reinforcement. There are two limiting factors affecting the degree of cable miniaturization. The first is cable strength. Working the cable under insulation and through the exit hole requires reasonable force, the cable strength should not fall below 20 Newtons (5 pounds) of pull. The second factor is line resistance. To eliminate line resistance changes which affect

sensitivity, constant current excitation is used which also compensate for most poor electrical connections.

Best accuracy is obtained when the sensor is flush with the inside surface containing the propellant so a design requirement is to make the sensor small. The height of the sensor needs be less than 2.5 mm (0.100 of an inch). A low mass stiff sensor with low compliance is also desirable.

The described sensor has the required properties and can be used to monitor temperatures and stresses induced during the life of a rocket motor. The use of this in-situ health monitor eliminates most of the uncertainty that currently exists in determining the true service life of tactical rocket motors.

REFERENCES

1 The Development of Improved Normal Stress Transducers for Propellant Grains, E.C. Francis, R.E. Thompson and W.C. Briggs (31 Jan 79).

2 See Noark's Formulas For Stress and Strain, Fourth Edition, Page 217, Example 6.

3. The Development of Improved Normal Stress Sensors for Propellant Grain, UTC/CSD Study 31 Jan 79 for AFRPL Edwards CSD2548-FR(D).

4 Improvements in rocket motor service life instrumentation, Eugene Francis et al, JANNAF Structures and Mechanical Behaviour Subcommittee Meeting, December 1995.

5 Service life prediction using stress gage technology and nonlinear viscoelastic analysis, F C Wong, Paper No 26.

6 Instrumented service life programme for the Pictor rocket motor, S Y Ho, Paper No 28.

7 Improvements in rocket motor service life prediction, E C Francis and H J Buswell, Paper No 27.

8 Stress Measurement in Solid Motors, H J Buswell et al, 18th Transducer Workshop, Range Commanders Council (June 1995).

ACKNOWLEDGEMENT

The work in this paper was supported by the UK Ministry of Defence as part of its applied research programme. The views expressed are those of the authors, and do not necessarily represent the policy of the MOD or Her Majesty's Government.
British Crown Copyright 1996/MOD.
Published with the permission of the controller of her Britannic Majesty's Stationery Office.

		Test psi	Sensitivity mV/100psi	SEB %FS	Bal Tc ±% FS -50 to 150°F	Sens Tc ±%FS -50 to 150°F
7625 (steel)	Pre Post	3200 3200	21.1 21.1	0.16 0.38	1.96 1.56	0.66 1.56
13656 (Titan)	Pre Post	2200 2200	48.6 48.0	0.08 0.07		
13654 (Titan)	Pre Post		46.4 46.4		2.15 2.74	1.53 0.68

Table 1

RESULTS FROM OVERPRESSURE TEST ON SENSOR PERFORMANCE.

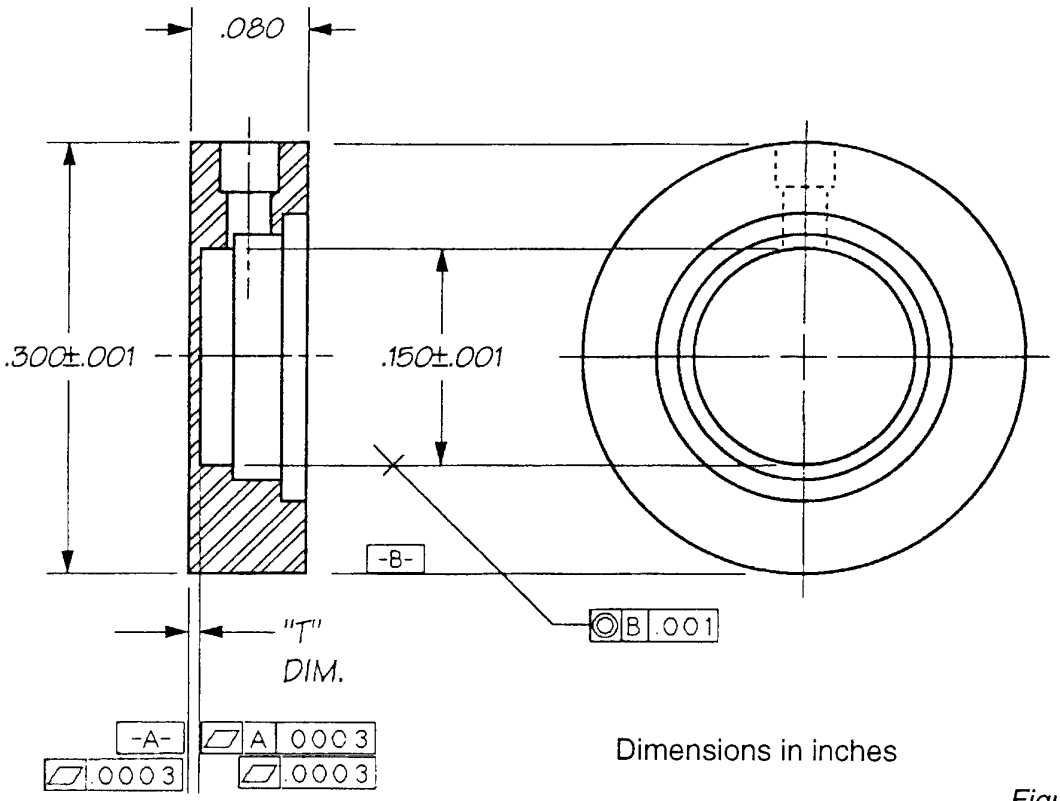
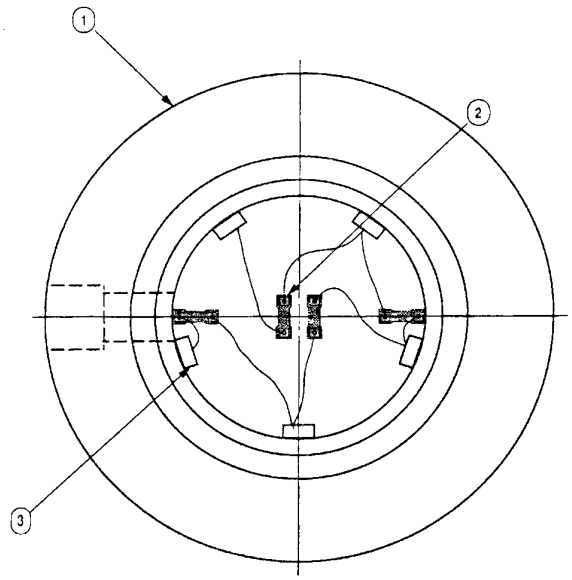


Figure 1
Stress transducer



3	5	MST035	Solder Tabs
2	4	SS-026-013-500P	Strain Gauges
1	1	440306 or 440312	Stress Sensor

Figure 2
Gauge installation

Model Number 140474 Serial Number 12236 Diaphragm Materials
Excitation 4.0 mA Type ◉ Constant Current ○ Constant Voltage Titanium
Pressure Range 100 PSI ○ Absolute ◉ Gage ○ Reference

AMBIENT PRESSURE CALIBRATION DATA Date Calibration Run: 27 Mar 95

Pressure	Increase (1)	Decrease	Increase(2)	Ideal	Linearity (%FS)	Hysteresis (%FS)	Repeatability (%FS)
0PSIG	-1.70 mV	-1.70 mV	-1.70 mV	-1.70 mV		0.0000%	0.0000%
20PSIG	6.33 mV	6.28 mV	6.33 mV	6.40 mV	0.1679%	0.1235%	0.0000%
40PSIG	14.39 mV	14.35 mV	14.40 mV	14.50 mV	0.2618%	0.0988%	0.0247%
60PSIG	22.51 mV	22.46 mV	22.50 mV	22.59 mV	0.2075%	0.1235%	0.0247%
80PSIG	30.64 mV	30.59 mV	30.63 mV	30.69 mV	0.1284%	0.1235%	0.0247%
100PSIG	38.79 mV		38.79 mV				0.0000%
SENSITIVITY	40.49 mV						

STATIC ERROR BAND ± 0.1309% FS

THERMAL CALIBRATION DATA Date Temperature Data Run: 20 Mar 94

	Low Temp.	Ambient	High Temp
Temperature	-50 °F	70 °F	150 °F
0 PSI	-0.29 mV	-0.36 mV	-0.26 mV
Full Scale	40.31 mV	39.92 mV	40.86 mV
Sensitivity	40.60 mV	40.28 mV	41.12 mV

	-50°F to 70°F	70°F to 150°F	AVERAGE
Thermal Balance Shift	-0.1729% FS	0.2470% FS	± 0.1235%FS
Thermal Sensitivity Shift	-0.7903% FS	-2.0746% FS	± 1.0373%FS

Figure 3
Pressure transducer calibration data

Model Number 140480 Serial Number 12253 Diaphragm Materials
Excitation 4.0 mA Type ◉ Constant Current ○ Constant Voltage Steel
Pressure Range 100 PSI ○ Absolute ◉ Gage ○ Reference

AMBIENT PRESSURE CALIBRATION DATA Date Calibration Run: 28 Mar 95

Pressure	Increase (1)	Decrease	Increase(2)	Ideal	Linearity (%FS)	Hysteresis (%FS)	Repeatability (%FS)
0PSIG	0.00 mV	0.00 mV	0.00 mV	0.00 mV		0.0000%	0.0000%
20PSIG	4.56 mV	4.54 mV	4.56 mV	4.58 mV	0.0699%	0.0874%	0.0000%
40PSIG	9.12 mV	9.11 mV	9.11 mV	9.15 mV	0.1399%	0.0437%	0.0437%
60PSIG	13.70 mV	13.69 mV	13.70 mV	13.73 mV	0.1224%	0.0437%	0.0000%
80PSIG	18.31 mV	18.29 mV	18.30 mV	18.30 mV	0.0262%	0.0874%	0.0437%
100PSIG	22.88 mV		22.89 mV				0.0437%
SENSITIVITY	22.88 mV						

STATIC ERROR BAND ± 0.0699% FS

THERMAL CALIBRATION DATA Date Temperature Data Run: 21 Mar 95

	Low Temp.	Ambient	High Temp
Temperature	-50 °F	70 °F	150 °F
0 PSI	-0.21 mV	-0.05 mV	-0.10 mV
Full Scale	22.63 mV	22.70 mV	22.68 mV
Sensitivity	22.84 mV	22.75 mV	22.78 mV

	-50°F to 70°F	70°F to 150°F	AVERAGE
Thermal Balance Shift	+0.6993% FS	-0.2185% FS	± 0.3497% FS
Thermal Sensitivity Shift	-0.3934% FS	+0.1311% FS	± 0.1967% FS

Figure 4
Pressure transducer calibration data

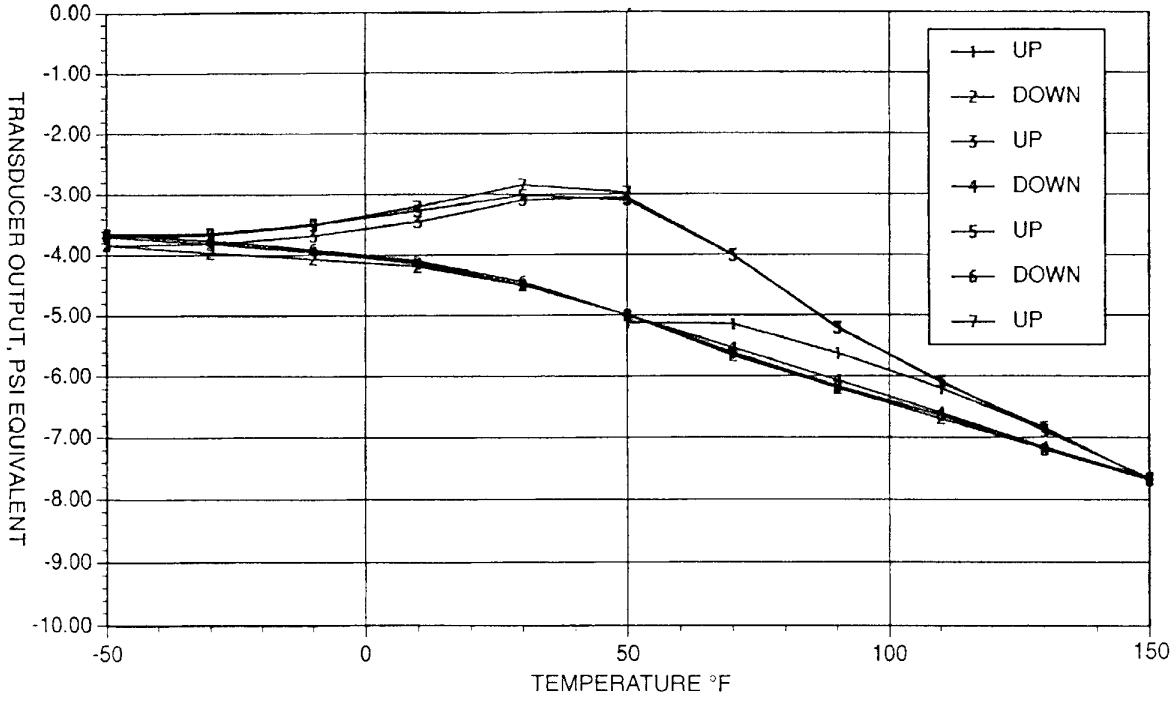


Figure 5
Thermal hysterisis data - steel

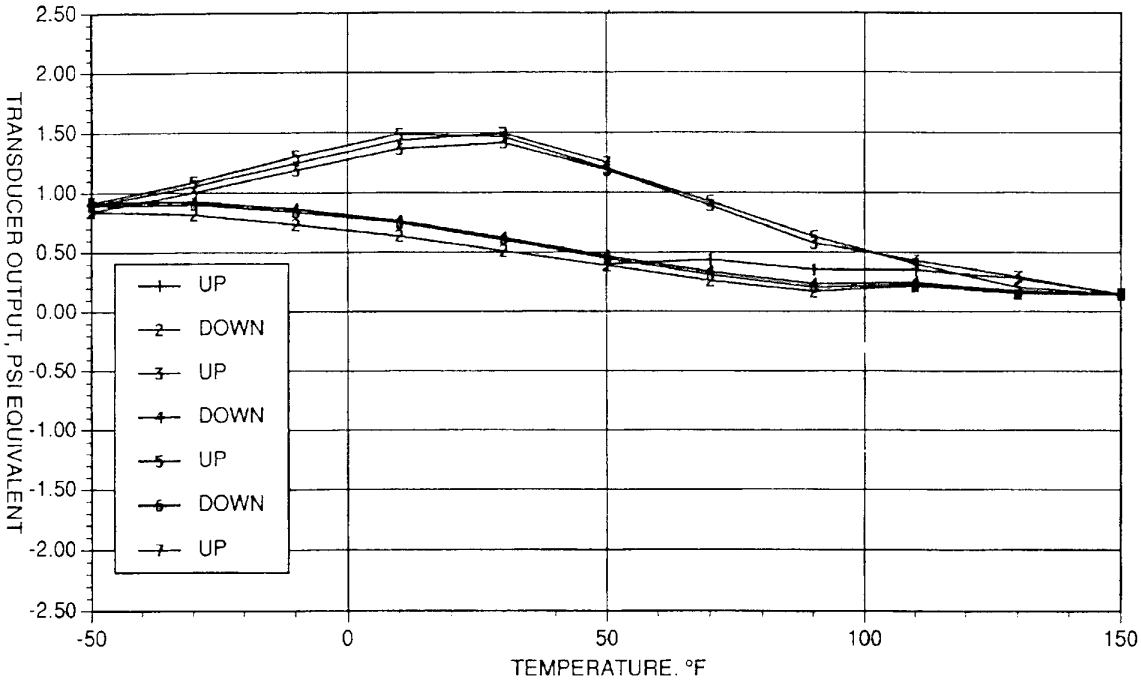


Figure 6
Thermal hysterisis data - titanium

Pressure Psi	Output mvdc	Return to Zero mvdc	Zero Change in Psi
0	-1.65		
500	100.98	-1.31	1.59
1000	198.00	-1.30	1.64
1500	287.00	-1.27	1.78
1600	304.00	-1.20	2.11
1700	320.00	-1.08	2.67
1800	336.00	-1.03	2.90
1900	350.00	-0.88	3.61
2000	365.00	-0.75	4.22
2100	380.00	-0.51	5.34
2200	391.00	-0.40	5.85
2300	406.00	-0.06	7.45
2400	419.00	0.28	9.04
2500	430.00	0.67	10.97
2600	440.00	1.34	14.00
2700	452.00	2.01	17.14
2800	462.00	2.68	20.28
2900	472.00	3.86	25.81
3000	481.00	4.91	30.73
3100	490.00	6.40	37.70
3200	498.00	7.89	44.68
Return to Zero	1/3/96	7.50	

Figure 7
Over pressure test - steel

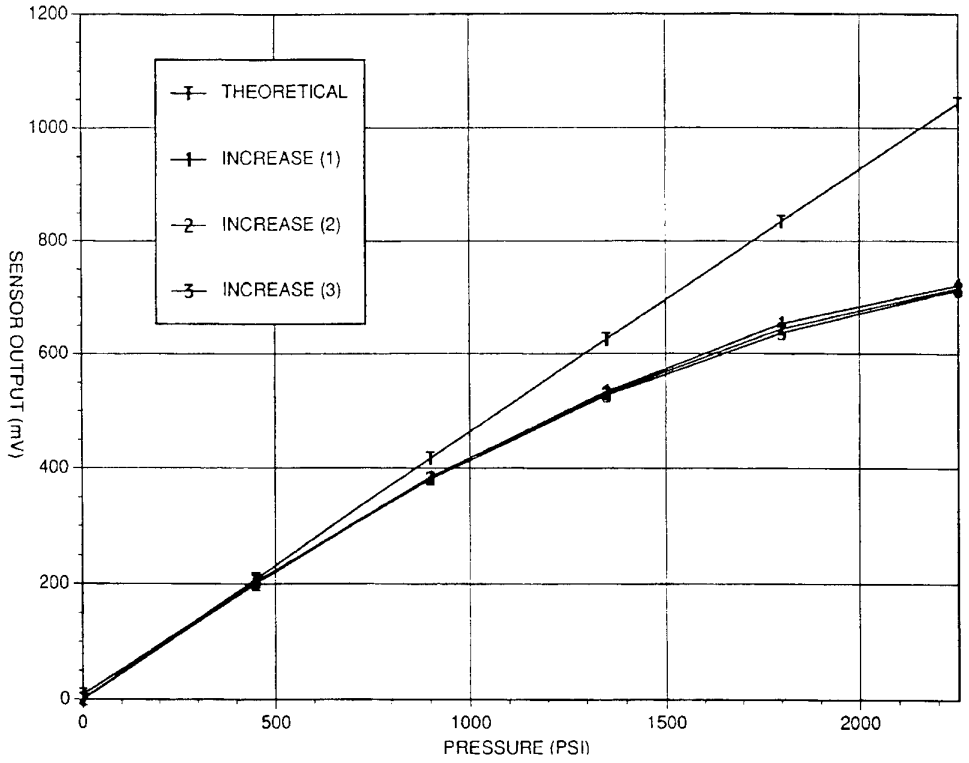
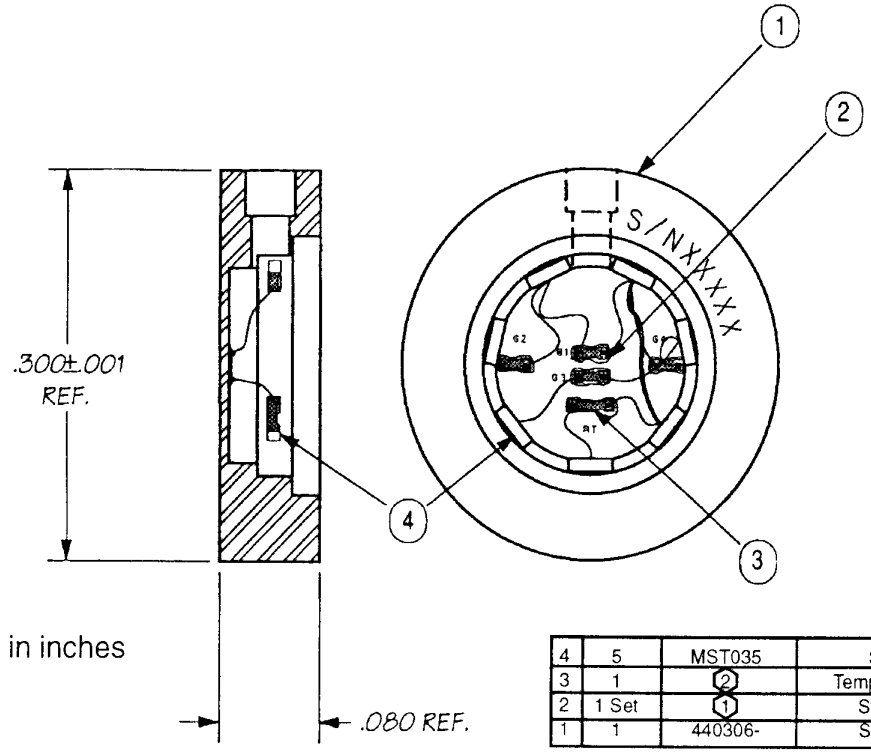


Figure 8
Overpressure test - titanium



Dimensions in inches

4	5	MST035	Solder Tabs
3	1	(2)	Temperature Sensor
2	1 Set	(1)	Strain Gauges
1	1	440306-	Stress Sensor

Figure 9
Stress and temperature sensor

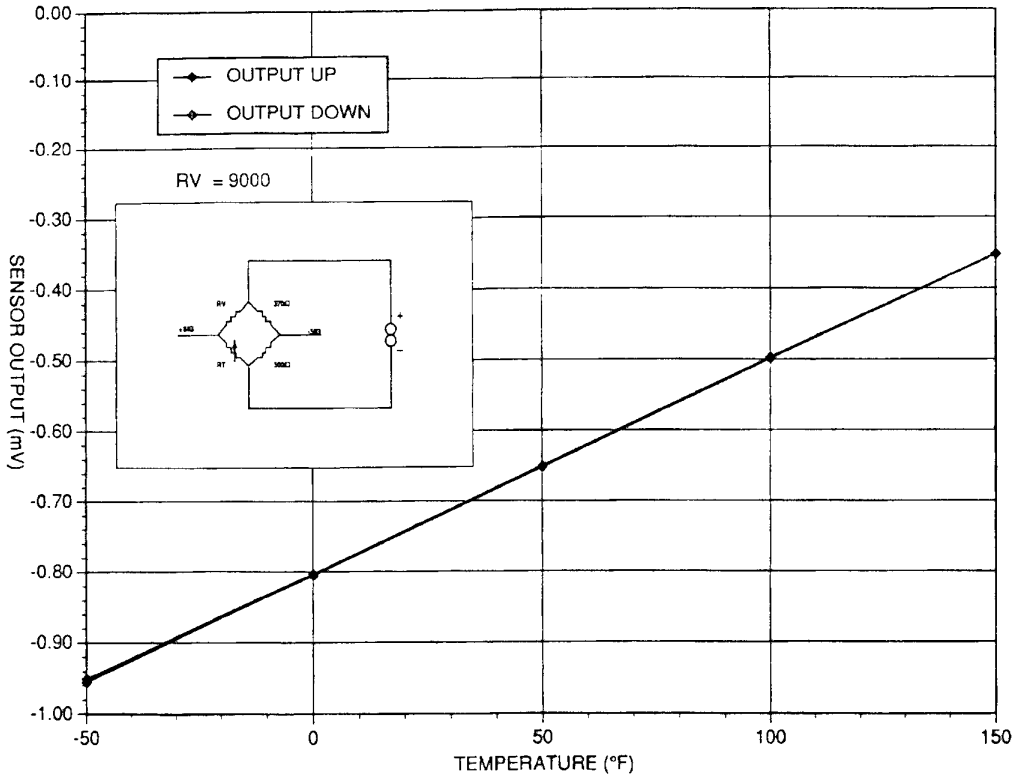


Figure 10
Temperature sensor output

Paper Number: 25
Discussor's Name: Professor J. Salva
Responder's Name: H. Chelner

Question: What can we expect about the future trend in this type of transducer?

Answer: Additional miniaturation of both the dual sensor and bridge amplification package is anticipated. Improvement in the sensor yield of high accuracy units and reduction of costs is being studied. Amplification of the signals to one or two volts full scale is also being considered. The use of the sensor as a health monitor and to measure chamber pressure has been proven to be feasible.

Paper Number: 25
Discussor's Name: E. C. Francis
Responder's Name: H. Chelner

Question: What processing changes were incorporated to eliminate the thermal hysteresis loop shown for the earlier transducers which has now disappeared for the newest miniature transducer?

Answer: The exact cause of the thermal hysteresis is not known. It is believed that a number of potential affecters are the cause. Since the epoxy is a viscoelastic substance with low yield (shear) stress at ambient conditions, it is the number one contributor.
Micron Instruments has taken steps to improve (reduce) the thermal hysteresis. Reduction of the cement thickness and slow step curing of the epoxy cement are two of the processing improvements. Should anyone wish to do a finite element analysis to prove the glue line effect on thermal hysteresis and grain sensor interface strain measurement accuracy, Micron Instruments will supply complete fabrication details.

Verification of the Swanson Nonlinear Thermo-Viscoelastic Model Using Stress Gage Technology

F. C. Wong
Defence Research Establishment Valcartier
P.O. Box 8800
Courcelette, Quebec
Canada, G0A 1R0

A. Firmin and **Y. C. Liu**
H. G. Engineering Ltd.
400 Carlingview Drive
Etobicoke, Ontario
Canada, M9W 6M8

SUMMARY

Solid propellants must function as a structural member as well as an energy source. They must deform without failing under thermal, acceleration and pressurisation conditions. Structural failure by cracking is usually catastrophic since the advancing flame front propagates into any exposed surface. Therefore, the ability to predict the stress-strain state of a propellant is critical to the establishment of a motor's operational limits. Stress prediction for propellants is complicated by the fact that this material exhibits nonlinear viscoelastic characteristics. This paper summarises the development of a modified Swanson constitutive model for use in the finite element program ABAQUS. Predictions of propellant behavior for three uniaxial test cases and one three-dimensional test case are made and compared to experimental results. The uniaxial test cases cover the propellant's stress response to straining-cooling and thermal shock environments. Measurements from an instrumented rocket motor placed in a thermal shock environment provide the data for evaluating the three-dimensional prediction capabilities of the ABAQUS implementation. It will be shown that the modified Swanson model can predict nonlinear viscoelastic behavior correctly but to be used for solid rocket motor service life methodologies, the model still requires some calibration using in-situ measurements from an instrumented rocket motor.

1. INTRODUCTION

Solid propellants are unique among materials in that the grain must function as a structural member as well as an energy source. The propellant in a solid rocket motor represents approximately 90% of the motor's total weight and must deform without rupture under thermal, acceleration and pressurisation conditions. Another unique feature of this material is that it exhibits nonlinear viscoelastic behavior. Structural failure by cracking is usually catastrophic since the advancing flame front propagates into any exposed surface. Therefore, an understanding of the propellant stress and strain state is critical to the establishment of basic design parameters and operational limits in solid rocket motors .

In the last two decades, several nonlinear viscoelastic models have been developed as a result of this need in the rocket industry. A comprehensive study of nonlinear models has been given by Francis et al. [1, 2]. Among the models examined in these references, the Swanson model [3, 4] with the use of a stress softening function, was reported to be the most suitable. By using characterisation data from three simple laboratory tests, a wide variety of complex uniaxial test histories was accurately predicted. These predictions included the stress and time response inside and outside the range of characterisation conditions. The validation of the Swanson model, however, has so far been confined to uniaxial or biaxial experiments. Evaluation of this model for a three-dimensional case has not been carried out.

This paper summarises the development of a modified Swanson model which is suitable for use in an ABAQUS user-defined subroutine. ABAQUS is a general-purpose finite element program written by Hibbitt, Karlsson and Sorenson Inc. [5]. Predictions of propellant behavior for three uniaxial test cases and one three-dimensional test case are made and compared to experimental results. The uniaxial test cases cover the propellant's stress response to straining-cooling and thermal shock environments. Measurements from an instrumented rocket motor placed in a thermal shock environment provide the data for evaluating the three-dimensional prediction capabilities of the ABAQUS implementation. It will be shown that the modified Swanson model can predict nonlinear viscoelastic behavior correctly but to be compatible with solid rocket motor service life methodologies, the model still requires some calibration using in-situ measurements from an instrumented rocket motor.

2. SWANSON CONSTITUTIVE MODEL

The Swanson model [4] has demonstrated that it can make stress predictions for undamaged propellants to within 10% of the measured data and for previously damaged propellant to within 15% [1]. The model was originally expressed as

$$\underline{S}' = g(\underline{E}) \int_0^t 2G(t-\tau)\phi(\tau)\frac{\partial \underline{E}'}{\partial \tau} d\tau \qquad (1)$$

where

$\underline{S}'$ are the deviatoric components of the second Piola-Kirchhoff stress,

$\underline{E}'$ are the deviatoric components of the Green strain,

Paper presented at the AGARD PEP Symposium on "Service Life of Solid Propellant Systems" held in Athens, Greece, 10-14 May 1996, and published in CP-586.

$g(\underline{E})$ is a softening function dependent on strain,
$\phi(\tau)$ is a function modifying the convolution integral for varying strain rates.

The model has the following features:

a) If only small strain and rotation is involved and function $\phi(\tau)$ is set to 1.0, eq. 1 reduces to a linear viscoelastic model.

b) If large rotations are involved and function $\phi(\tau)$ is influenced by changing strain rates, eq. 1 represents a model with geometrical and material nonlinearities.

c) If unloading and strain softening are involved, the softening function $g(\underline{E})$ can be modified to be a function of strain and temperature.

The variable τ is the reduced time and is defined by

$$\tau = \int_0^{t'} \frac{1}{a_T} dt' \tag{2}$$

The shift function a_T is based on the Williams-Landell-Ferry equation [6] and has the following form

$$\log a_T = -\frac{C_1(T - T_{ref})}{C_2 + (T - T_{ref})} \tag{3}$$

The function $\phi(\tau)$ correlates the behavior due changing strain rate with that due to changing temperature. It can be written generally as

$$\phi(\tau) = 1 + \gamma[f_c(\tau) - f(\tau)] \tag{4}$$

where

γ is an empirical parameter with $\gamma(0) = 0$,
$f(\tau)$ is the hereditary integral defined in eq. 1,
$f_c(\tau)$ is the hereditary integral under a constant strain rate.

The function $f_c(\tau)$ is calculated based on

$$f_c(\tau) = \dot{\underline{E}}' \int_0^{\xi} G(\xi - \tau) d\tau \tag{5}$$

where $\xi = \underline{E}'/\dot{\underline{E}}'$, $\dot{\underline{E}}'$ is the deviatoric strain rate at the current time and $G(\tau)$ is the shear modulus given by eq. 6 below. Equation 5 defines the response of the hereditary integral under a constant deviatoric strain rate. When the empirical parameter γ is equal to 0.0, $\phi(\tau) = 1$ so strain rate effects are not taken into account. When γ equals 1.0 in a multi-rate test, stress response jumps instantaneously from the level of the current rate to the level of the new rate. For γ between 0.0 and 1.0, the stress changes at a rate according to the magnitude of γ.

The implementation of the Swanson model into ABAQUS is not a straightforward matter because ABAQUS uses Cauchy stress ($\underline{\sigma}$) and logarithmic strain ($\underline{e}$) as objective pairs. Therefore, to avoid the additional complication of converting from one set of objective pairs to another within the UMAT subroutine, eq. 1 was coded using the ABAQUS compatible objective pairs instead of the ones proposed by Swanson [7]. The advantage of doing this was that the objective pairs were directly available from the ABAQUS internal ARRAYS and the Jacobian matrix arising from linear viscoelasticity model could be used. As a consequence, the modified form of the Swanson constitutive equation is suited for situations where the material experiences small motion, small strain and large rotation deformations.

The shear modulus in eqs. 1 and 5 was defined by a Prony series

$$G(\tau) = G_0 + \sum_{k=1}^{N} G_k \exp(-\tau / \tau_k) \tag{6}$$

For convenience, it was assumed that the function $\phi(\tau)$ operated on individual terms of the Prony series. Hence eq. 1 was re-expressed as

$$\underline{\sigma}' = g(\underline{e}) \int_0^t 2[G_0\phi_0 + \sum_{k=1}^{N} G_k \exp(-\tau/\tau_k)\phi_k] \frac{\partial \underline{e}'}{\partial \tau} d\tau \tag{7}$$

Since $\phi(0) = 1.0$, eq. 7 could be rewritten as

$$\underline{\sigma}' = g(\underline{e})[2G(\underline{e}^n - \sum_{k=1}^{N} \alpha_k \underline{e}_k^n)] \tag{8}$$

where

$$G = G(0) = G_0 + \sum_k G_k \tag{9}$$

$$\alpha_k = G_k / G \tag{10}$$

$$\underline{e}^n = \int_0^t \frac{\partial \underline{e}'}{\partial \tau} d\tau \tag{11}$$

$$\underline{e}_k^n = \int_0^t \exp(-\tau/\tau_k)\phi_k \frac{\partial \underline{e}'}{\partial \tau} d\tau \tag{12}$$

The recursive relationship for e_k at time t_{n+1} can be shown to be (eq. 13)

$$\underline{e_k^{n+1}} = [1-\exp(-\Delta\tau/\tau_k)]\underline{e^n} + \exp(-\Delta\tau/\tau_k)\underline{e_k^n} + [\Delta\tau - \tau_k[1-\exp(-\Delta\tau/\tau_k)]]\frac{\Delta\underline{e}}{\Delta\tau} - \int_m^{m+1}\gamma(f_{ck}-f_k)\exp(\tau'-\tau^{n+1}/\tau_k)\frac{d\underline{e}'}{d\tau'}d\tau' \quad (13)$$

The first three terms of eq. 13 are identical to the recursive relationship for linear viscoelasticity. The last term involving γ, f_{ck} and f_k accounts for the strain rate dependence. This term was calculated using the definition of $\phi(\tau)$ to give

$$\int_m^{m+1}\gamma\cdots d\tau' = \beta\exp(-\Delta\tau/\tau_k)\left[\frac{\Delta\underline{e}}{\Delta\tau}\tau_k[1-\exp(-\Psi/\tau_k)] - (\underline{e^n} - \underline{e_k^n})\right] \quad (14)$$

with $\Psi = \underline{\varepsilon'} / (\Delta\underline{e} / \Delta\tau)$.

The parameter β is an experimentally determined value which corresponds to γ in eqs. 4 and 13. It takes on a value ranging from 0.0 to 1.0. If β is set to zero, eq. 13 represents linear viscoelastic behavior with large rotations involved. The stress response rate due to changing strain rates increases as β increases. In practice, β is set to a constant for an analysis.

The tangent matrix of the deviatoric part $2G_T$ was derived by differentiating the increment of deviatoric stress $\underline{\sigma'}$ given in eq. 1 with respect to the deviatoric strain increment $\Delta\underline{e}$

$$2\frac{d(\Delta\sigma')}{d\Delta\underline{e}} = 2G_T = 2G(0)[1-\sum_{k=1}^{N}\alpha_i\frac{d(\underline{e_k^{n+1}} - \underline{e_k^n})}{d(\Delta\underline{e})}] \quad (15)$$

To handle incompressible materials, the formulation due to Herrmann [8] was used so that mean hydrostatic pressure is the only independent variation in the stress state. The increment in the pressure p may be stated as

$$\Delta p = -K\Delta e^{vol} \quad (16)$$

The bulk modulus K is assumed to be elastic.

The quantities calculated by eqs. 15 and 16 are passed to ABAQUS for assembly into an element total tangent matrix through the UMAT facility according to

$$\Delta\sigma_{ij} = g(\underline{e})[2G_T\Delta e_{ij} - K\Delta e^{vol} + \delta_{ij}K(\Delta e_{kk} - 3\alpha\Delta T)] \quad (17)$$

where α is the coefficient of thermal expansion and T is the temperature. The assembly of the element total tangent matrices and the application of the Newton-Raphson method for calculating the displacement vector which satisfies the set of linearized equations are taken care of by ABAQUS.

3. Experimental

Uniaxial tensile tests were carried out using non-aluminised HTPB/AP propellant cut into a stick-form measuring 12.7 mm x 12.7 mm x 125 mm long. The propellant sticks were bonded to phenolic/wood end tabs and tested on an Instron 4206 test machine equipped with a 100 kg load cell and a conditioning chamber. Propellant strain was calculated using crosshead displacement and a gage length of 125mm.

The CRV7 RLU-5002/B solid rocket motor was used as an instrumented test vehicle. The motor is part of an unguided air-to-ground weapon system manufactured in Canada. The motor casing is made from 7075-T8 aluminum alloy and measures 930 mm long with an outside diameter of 70 mm and an inside diameter of 66 mm. The motor is lined with a roll-formed insulant made up of asbestos and butadiene binder. An aluminum foil sheet is placed between the insulant and propellant to promote adhesion and to act as a chemical barrier. The motor is filled with a non-aluminised HTPB/AP propellant and has a cylindrical bore with an average diameter of 21 mm.

Motor instrumentation consisted of two Sensometrics (Simi Valley, CA) Thru-the-Case bond stress gages (P/N 601511-14), one bore strain transducer and six Type-T thermocouples [9, 10]. The bond stress gages were constructed from semi-conductor strain gages which were mounted in heat treated stainless steel bodies (Fig. 1). The bore strain transducer, fabricated by United Technologies - Chemical Systems Division, used conventional foil strain gages mounted on a beam assembly (Fig. 2). Temperature was measured in six locations. Two needle thermocouples were inserted into the propellant at the nozzle end, two "cement-on" thermocouples were installed on the casing and two needle-type thermocouples were used to measure air temperature.

Due to the large size of the sensing diaphragm, the bond stress gages were placed at a distance of 504 mm from the aft end of the casing to take advantage of the uniform bond stress field found in this portion of the motor. The bore strain

transducer was similarly placed 555 mm from the aft end to take advantage of the uniform bore displacement.

To obtain an accurate measurement of bondline stress and bore displacement, the gages' hysteresis behavior was measured and accounted for in the data reduction program. Hysteresis of the bond gages was evaluated by thermally cycling the mounted gages in an unfilled casing from $60^{\circ}C$ to $-54^{\circ}C$ using five complete thermal cycles. The bore gage was thermally cycled in a Plexiglas carrier tube using a similar temperature profile. As shown in Fig. 3 for bond gage OC518 and Fig. 4 for bore gage 09, hysteresis was present but more importantly, it was consistent from cycle to cycle. The hysteresis loop was split into an upper and lower curve and each curve was parameterized with a fourth-order polynomial. The data reduction program included a routine which determined whether the temperature was following the upper or lower portion of the hysteresis curve. By subtracting the calculated hysteresis from the measured hysteresis data, the inherent accuracy of the gage/casing combination could be assessed. An analysis of the zero offset measurements (see curve corresponding to the righthand axis of Figs. 3 and 4), showed that the accuracy of the bond stress data was ± 14 kPa and the accuracy of the bore gage was better than 0.2 mm or 1% strain. Typical bond gage sensitivities were in the range of 2 mV/100 kPa. For bore gages, it was 3 mV/mm.

4. Results and Discussion

4.1 Uniaxial Straining-Cooling - Swanson Test Case

To validate his constitutive model, Swanson compared his predictions with the measurements from a uniaxial straining-cooling test of TP H1011 propellant [4]. The air temperature started at $103^{\circ}F$, decreased at a rate of $0.432^{\circ}F$/min and finished at $-36^{\circ}F$. The sample was strained at 0.01305%/min up to 4.32%. Test duration was 320 minutes. In Ref. 4, the Prony series was defined in terms of tensile moduli and the shift factors were defined by a power law relationship. For this evaluation, Swanson's moduli were converted to shear moduli by dividing by 3 and the shifting function was converted to a WLF relationship by calculating the shift factors at various temperatures and then fitting them to the WLF equation. The Prony-series in terms of tensile moduli and the WLF constants are shown in Table I.

A uniaxial model was constructed with eight C3D20 brick elements. Using a $\beta = 0.5$ along with the Prony-series and the WLF constants, the same simulation was performed using the ABAQUS implementation of the Swanson model. Figure 5 shows that the ABAQUS results matched those obtained by Swanson. This demonstrated that the Swanson model was correctly coded into ABAQUS.

4.2 Uniaxial Straining-Cooling - DREV Test Case

A straining-cooling test was carried out using the same HTPB/AP propellant used in the CRV7 rocket motor. The air temperature started at $60^{\circ}C$, decreased at a rate of 0.2667 $^{\circ}C$/min and ended at $-52^{\circ}C$. The sample was strained at 0.02896%/min up to 12.83%. Test time was 440 minutes. These conditions simulated what the bore of the CRV7 motor would see in a thermal shock environment.

A linear viscoelastic and a nonlinear viscoelastic analysis was performed for this test. The finite element model used for the Swanson test case was also employed here. The Prony-series and WLF constants are shown in Table II. The calculated results are shown in Fig. 6. The linear viscoelastic analysis was carried out by setting the rate parameter $\beta = 0$ and the softening function $a_f = 1.0$. It can be seen that the linear viscoelastic predictions were clearly too low. By using a rate parameter of $\beta = 0.2$ and by keeping the softening function $a_f = 1.0$, the nonlinear model gave stress results which were half the measured stresses. Larger values for β were evaluated but convergence problems were encountered. The analysis did not make it out to 12% strain due to the same problem. This could probably be remedied by using smaller time increments.

A different approach was tried with Swanson model. Instead of accounting for the stress magnification through the rate parameter as Swanson proposed, it could be included through the softening function. If the linear viscoelastic form of the Swanson model was used, the softening function would act like a temperature-dependent correction function. This function was determined by calculating the magnification factor required to correct the linear viscoelastic solution as a function of temperature ie. $g(T) = \sigma_{meas} / \sigma_{lve}$. The correction function was linearly dependant on temperature

$$g(T) = -0.0346(T - 32.9) + 1.02 \qquad (18)$$

The function was only needed when the temperature dropped below $32.9^{\circ}C$; above this temperature $a_f = 1.0$. This was implemented in the ABAQUS user subroutine using an IF-THEN statement. Figure 8 shows that this approach worked well for this particular situation.

4.3 Thermal Shocking of a Uniaxial Test Specimen

In this test, a uniaxial specimen was strained to 11.5% at a rate of 11.5%/min and then allowed to relax. At the same time, the air temperature was held at $20^{\circ}C$ for the first 60 minutes and then rapidly lowered to $-54^{\circ}C$ and held there for the next 160 minutes. Figure 9 shows the experimental as well as the predicted results. The models used the Prony-series and WLF constants given in Table II. The temperature-time profile used in the analysis was obtained from the experimental measurements.

Using the finite element model for the Swanson test case, the linear viscoelastic model reproduced the stress history at $20^{\circ}C$ well. It failed miserably when the temperature

was changed. Using a $\beta = 0.5$ and $a_f = 1.0$, the nonlinear model gave a stress history which followed more closely the experimental results. The effect of the rate parameter can be seen. When the temperature changed, a spike occurred in the stress prediction because the model saw this as a near instantaneous effect. The appearance of the small spike and subsequent relaxation at 60 minutes was odd since one would expect the constantly changing temperature to give a constantly increasing stress. The second larger spike at 80 minutes looked more reasonable. The correction function approach gave a reasonable prediction of the peak stress but it missed altogether the relaxation at $-54^{\circ}C$.

4.4 Thermal Shocking of an Instrumented CRV7 Motor

The data for this comparison came from thermally shocking an instrumented motor between $-54^{\circ}C$ and $60^{\circ}C$ [11]. The test actually ran for 40 complete cycles, however in the interest of reducing analysis time, only the second cycle was analyzed because the first cycle contained a temperature dwell at $20^{\circ}C$ and $-17^{\circ}C$ (see Fig. 8). The data contained in the figure shows the bondline normal stress, the bore strain and the bulk propellant temperature. It can be seen that the peak bondline stress diminished on each successive cycle.

The CRV7 was modelled using 220 CAX4H axisymmetric elements with both z-faces restrained axially to simulate plane strain conditions. Linear viscoelastic and nonlinear viscoelastic models were run using the material properties from Table II. Nonlinearities were introduced either through the use of β or through the use of the correction function given in eq. 18. No attempt was made to determine a softening function which could be used in conjunction with β in order that the effects of each parameter could be seen. The temperature-time profile used in the analysis was obtained from the thermocouple data. If prediction of the stress response under multi-cycle loading (Fig. 8) was desired, both β and $g(\underline{e})$ would have to be considered simultaneously to get the proper form for $g(\underline{e})$.

Figure 9 shows a comparison between the measured and predicted bore hoop strains. It can be seen that permanent deformation had already occurred in the CRV7 motor. If this deformation was added to the predicted results, the predictions would have been within one percent of the measured bore hoop strains. This shows that prediction of hoop strains due to thermal loads would be fairly accurate as long as the rate of increase in the permanent deformation was known.

A summary of the bondline stress results from the different models is given in Fig. 10. The linear viscoelastic curve had the proper shape but the stress magnitude was quite a bit lower than that measured. The Swanson model using a rate parameter of $\beta = 0.5$ fared better but it was still four times lower than the measured peak stress. Using a rate parameter of $\beta = 0.8$ increased the stress magnitude but only by a fractional amount. The correction function approach gave a stress magnitude about 80% of that measured. In all cases, the predictions at the high temperatures were good. This could be expected since the stress-free temperature was set to $60^{\circ}C$.

Discrepancies between predicted and measured stresses may have been caused by the uncertainty in the measured stress relaxation data and the shift factors. Another cause of the discrepancies is most certainly related to the difference between the motor stress state and the stress state in the test specimens used for characterization. The bondline is actually under a triaxial stress state. The results suggest that the triaxial modulus may be much higher than the uniaxial modulus. Whether this is true or not is not known since, to the authors' knowledge, no one has ever carried out a stress relaxation test under triaxial tensile conditions. A comparison between biaxial relaxation moduli and uniaxial moduli shows, though, that uniaxial moduli must be multiplied by 4/3 to recover biaxial moduli [1]. Figure 11 shows what happens when the Prony-series has been multiplied by a factor of four. It can be seen that measured bondline stresses were predicted. However, the analysis ended prematurely because of convergence problems. Apparently, using $\beta = 0.5$ is too high of a value to get proper convergence. A lower β and a smaller time step would have resolved this problem.

These results show that while uniaxial characterization tests are suitable for use in predicting uniaxial tensile behavior, they are not adequate for predicting the behavior of the material in a three-dimensional stress state. If a propellant's relaxation modulus is higher and the relaxation times longer in triaxial tension then either new characterization methods must be developed or additional model calibration using data from instrumented motors is required. The additional calibration factors would compensate for the differences in propellant behavior under uniaxial tension and triaxial loading. With the proper softening function, β and calibration, this implementation of the Swanson model could be used for propellant structural analysis and rocket motor service life prediction.

5. CONCLUSIONS

A summary of the modified Swanson constitutive model has been presented. It was shown that this implementation for the ABAQUS finite element program gives, as a special case, the formulation for linear viscoelasticity. Nonlinear effects were introduced through a user-defined softening function $g(\underline{e})$ and an experimentally determined parameter β. Comparisons with uniaxial straining-cooling tests showed that linear viscoelastic results were clearly too low. Nonlinear predictions using only β reproduced the test results given by Swanson but underpredicted the stress response for in-house tests. Using a softening function dependent only on temperature gave good results for this particular test case. The uniaxial thermal shock results showed that β did account for the increase in stress

due to changing temperature. Comparison of predictions with measured bore strains and bond stresses showed that bore strains were accurately predicted but bondline stresses were underpredicted. This discrepancy was most likely due to the difference in propellant behavior under uniaxial tension and triaxial loading. With the proper softening function, β and calibration, this implementation of the Swanson model could be used for propellant structural analysis and rocket motor service life prediction.

ACKNOWLEDGEMENTS

F. Wong would like to thank the DREV management for their support in funding the theoretical work and the DREV technical staff for their assistance with the experimental portion of this program.

REFERENCES

1. Francis, E. C., Carlton, C. H., Thompson, R., Fisher, W. M. and Hufferd, W. L., "Solid Propellant Nonlinear Constitutive Theory Extension", AFRPL-TR-83-071, Chemical Systems Division, January 1984.

2. Francis, E. C. and Thompson, R. E., "Nonlinear Structural Modelling", AIAA/SAE/ASME, 20th Joint Propulsion Conference, AIAA-84-1290, June 11-13, 1984, Cincinnati, Ohio.

3. Swanson, S. R., Christensen, L. W. and Christensen, R. J., "A Nonlinear Constitutive Law for High Elongation Propellant", Proceedings of 1980 JANNAF Structures and Mechanical Behavior Subcommittee Meeting, CPIA Pub. 331, 1980.

4. Swanson, S. R. and Christensen, L. W., "A Constitutive Formulation for High Elongation Propellants", J. Spacecraft and Rockets, Vol. 20, No. 6, Nov.-Dec., 1983, pp. 559-566.

5. Hibbitt, Karlsson and Sorensen, Inc., ABAQUS Finite Element Program, Version 4.8, 1989.

6. Williams, M. L, Landel, R. F. and Ferry, J. D., "The Temperature Dependence of Relaxation Mechanisms in Amorphous Polymers and Other Glass-Forming Liquids", J. Am. Chem. Soc., Vol. 77, 1955, p. 3701.

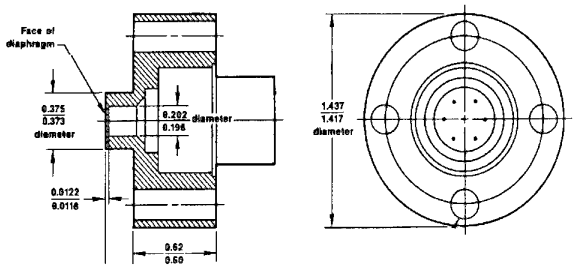
7. Firman, A. and Liu, Y. C., "A Nonlinear Thermo-Viscoelastic Finite Element Analysis Facility", DSS Contract No. W7701-8-0881/01-XSK, H. G. Engineering Ltd., Feb. 1991.

8. Herrmann, L. R., "Elasticity Equations for Incompressible and Nearly Incompressible Materials by a Variational Theorem", AIAA J., Vol. 3, 1965, p. 1896.

9. Wong, F. C., "Service Life Prediction Methodologies: Part 1 - Planning and Procedures", TTCP WTP4 KTA4-14 Rocket Motor Service Life Prediction Methodologies, Vol. III, Annex D, Nov. 1994.

10. Wong, F. C., "Service Life Prediction Methodologies: Part 2 - Preliminary Bondline and Bore Measurements", TTCP WTP4 KTA4-14 Rocket Motor Service Life Prediction Methodologies, Vol. IV, Annex D, Nov. 1994.

11. Wong, F. C., "Service Life Prediction Methodologies: Part 3 - Service Life Assessment", TTCP WTP4 KTA4-14 Rocket Motor Service Life Prediction Methodologies, Vol. V, Annex D, Nov. 1994.



Dimensions in inches

Fig. 1 Sensometrics Bond Stress Gage

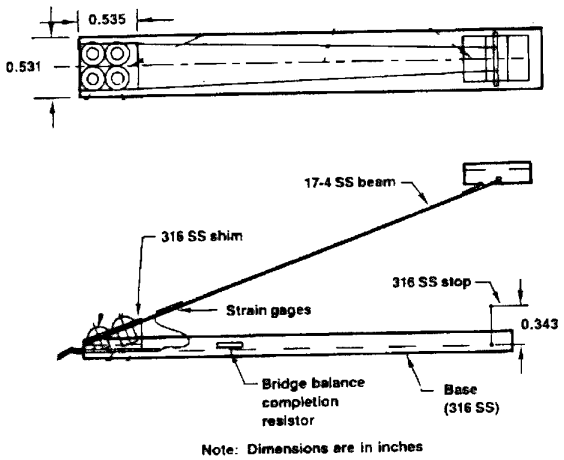


Fig. 2 Bore Displacement Gage

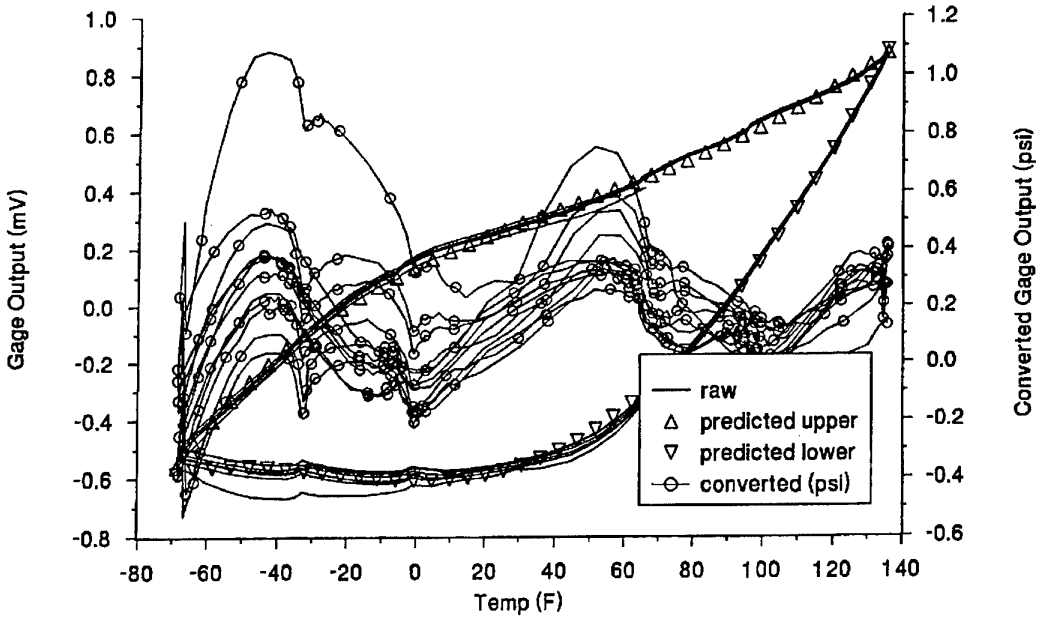


Fig. 3 Hysteresis Behavior of Gage OC518

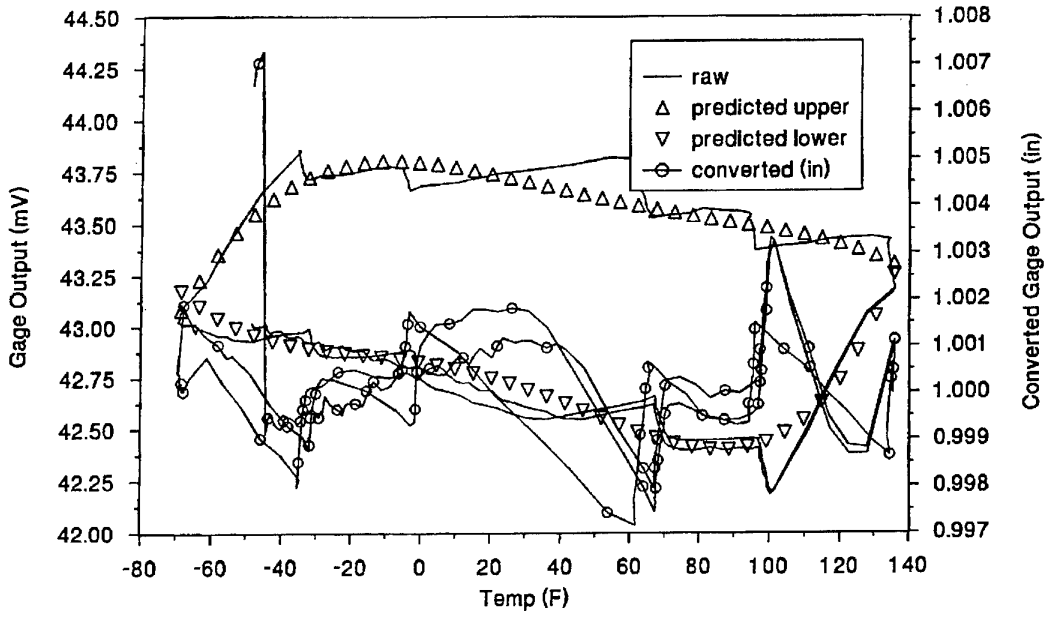


Fig. 4 Hysteresis Behavior of Gage 09

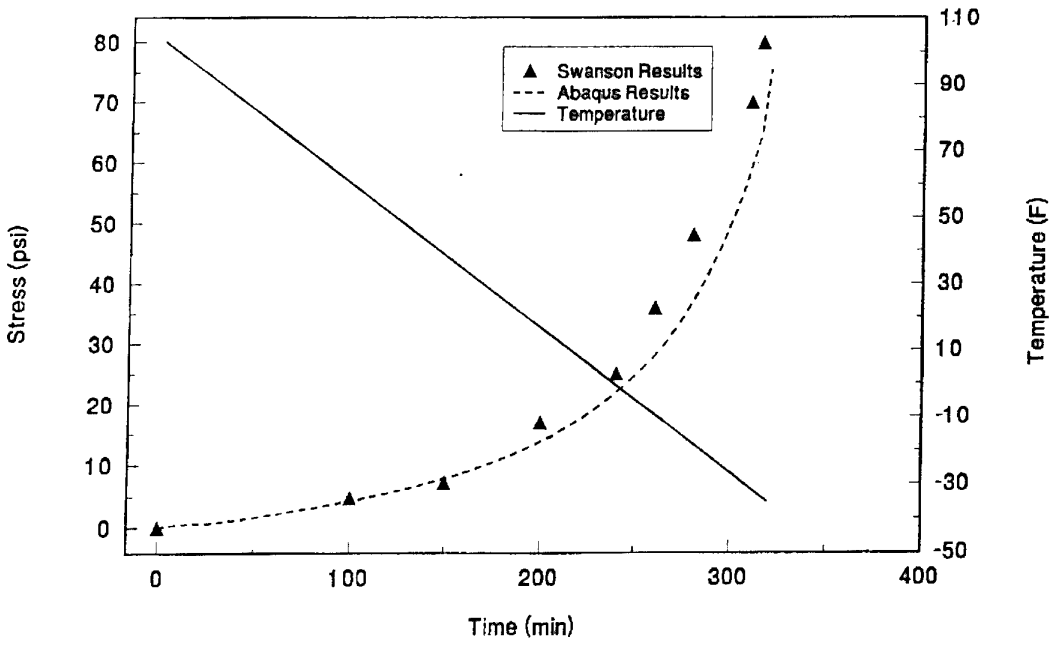


Fig. 5 Straining-Cooling, Swanson Test Case

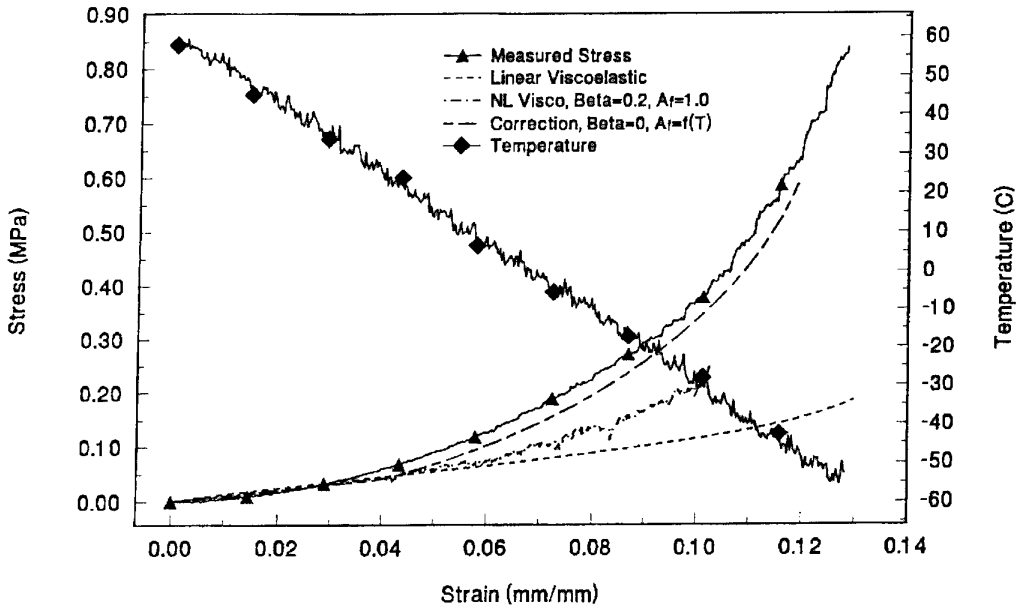


Fig. 6 Straining-Cooling, DREV Test Case

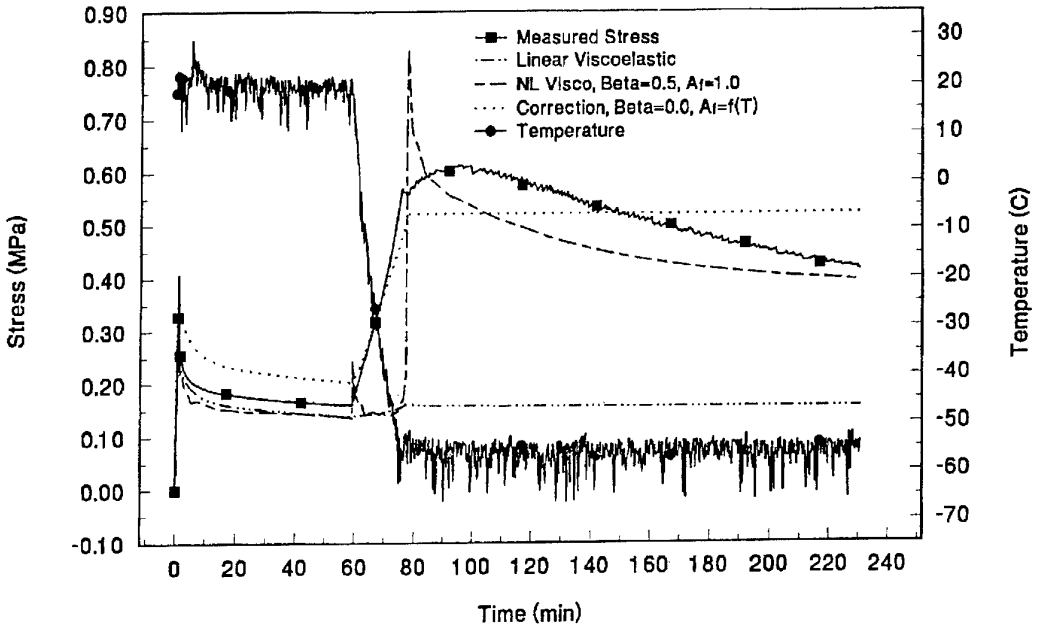


Fig. 7 Uniaxial Thermal Shock Test

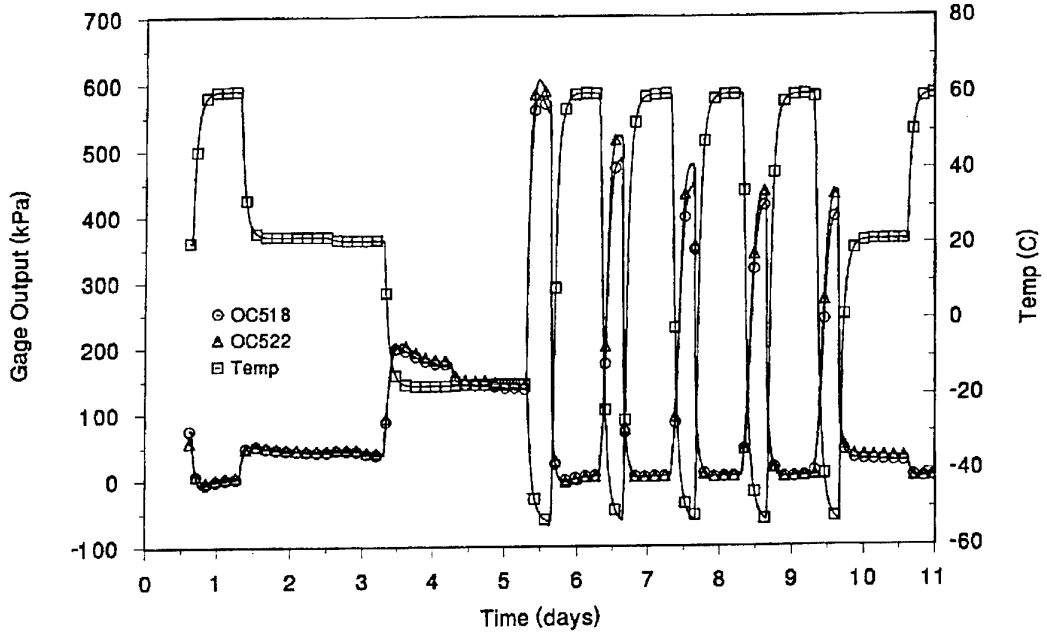


Fig. 8 Thermal Shock Cycling of a CRV7 Motor

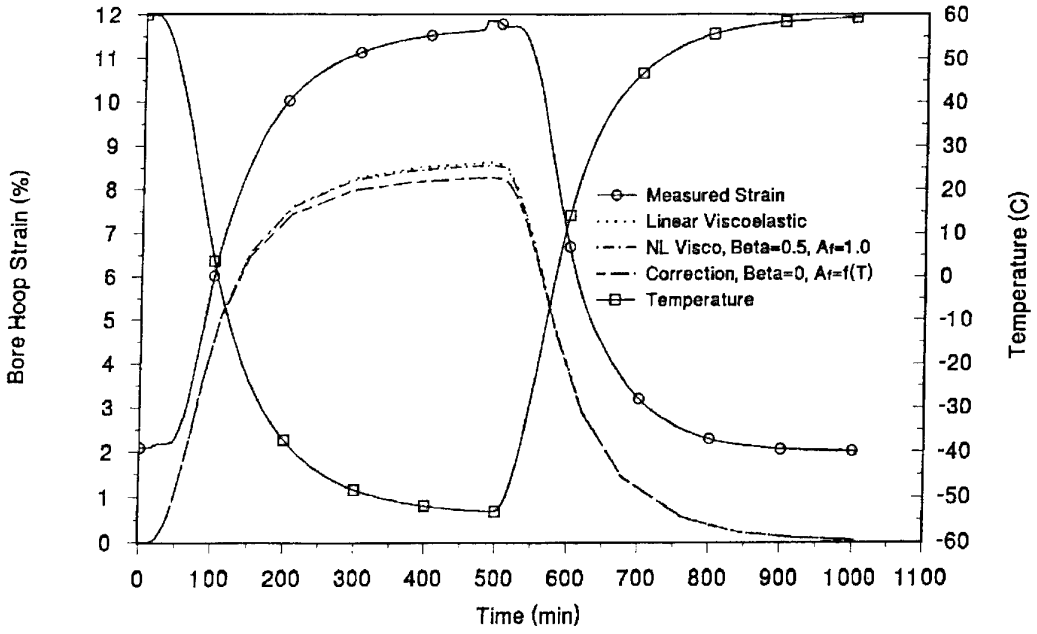


Fig. 9 Comparison of Bore Strain

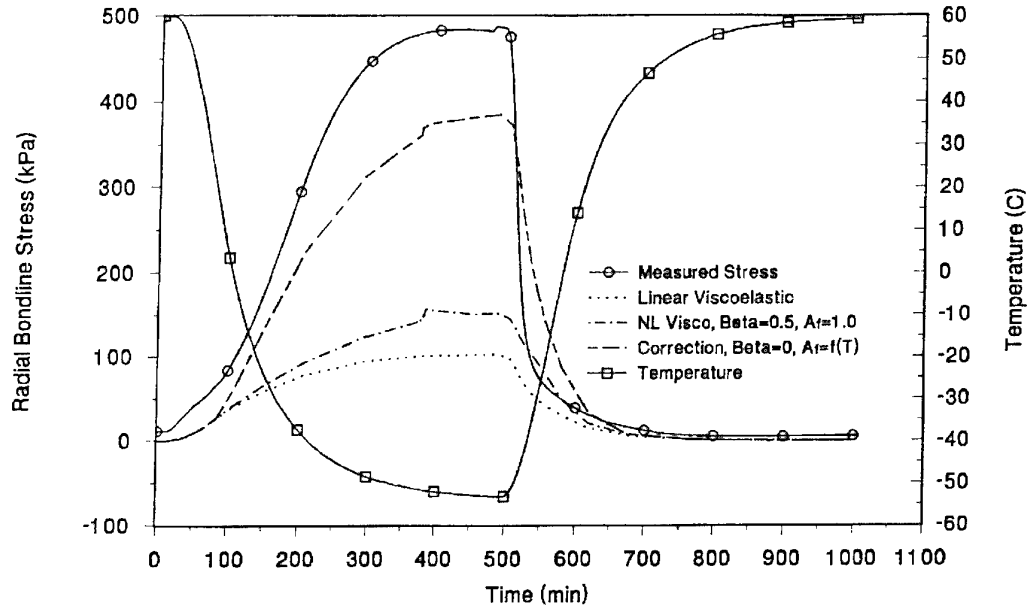


Fig. 10 Comparison of Bond Stress

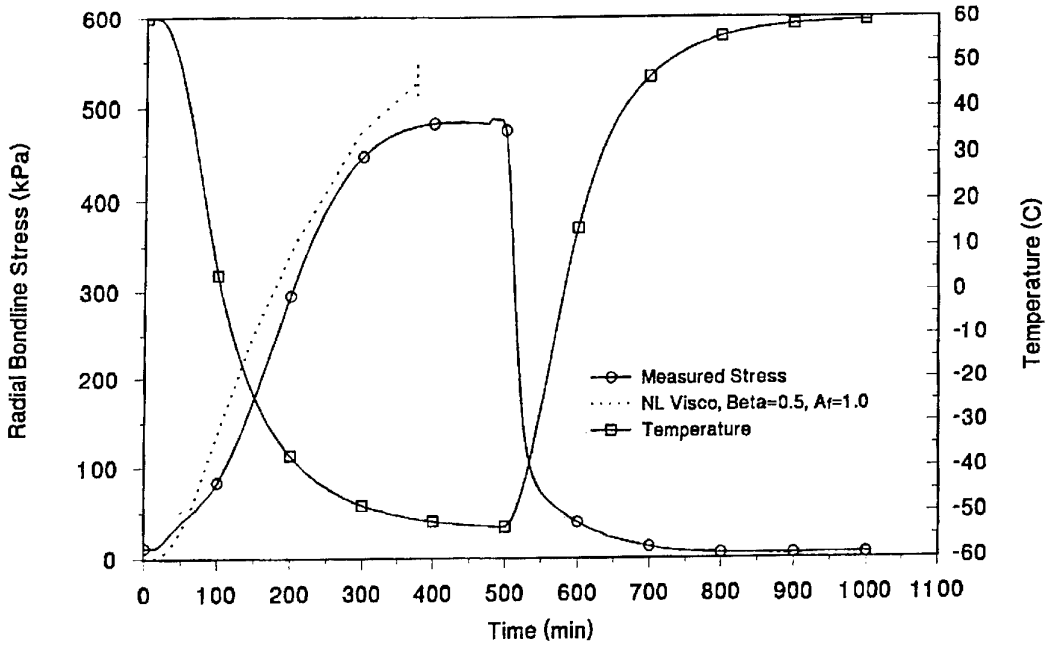


Fig. 11 Comparison of Bond Stress (Modulus x 4)

Table I - Prony series and WLF constants for TP H1011 Propellant

E_i (psi)		α_i (min^{-1})		WLF constants	
E_1	266.15	α_1	1e-7	C_1	9.2909
E_2	-116.14	α_2	1e-6	C_2	284.87
E_3	76.56	α_3	1e-5	T_{ref}	$76^\circ F$
E_4	5.23	α_4	1e-4		
E_5	45.03	α_5	1e-3		
E_6	54.05	α_6	1e-2		
E_7	74.30	α_7	1e-1		
E_8	186.68	α_8	1e-0		
E_9	200.22	α_9	1e+1		
E_{10}	420.82	α_{10}	1e+2		
E_{11}	506.24	α_{11}	1e+3		
E_{12}	1603.25	α_{12}	1e+4		
E_{13}	1893.33	α_{13}	1e+5		
E_{14}	5301.66	α_{14}	1e+6		
E_{15}	4409.99	α_{15}	1e+7		

Note: $E_{rel}(t) = \sum_{i=1}^{15} E_i \exp(-\alpha_i t)$

Table II - Prony series and WLF constants for HTPB/AP propellant

G_i (psi)		τ_i (min^{-1})		WLF constants	
G_1	1.96780	τ_1	1.8737e-2	C_1	1.126
G_2	1.31690	τ_2	1.9652e-1	C_2	98.8
G_3	0.64822	τ_3	1.7518e+0	T_{ref}	$20^\circ C$
G_4	0.45205	τ_4	1.4718e+1		
G_5	0.18765	τ_5	2.6242e+2		
G_6	0.10613	τ_6	2.8549e+3		
G_7	0.09532	τ_7	2.2022e+4		
G_8	0.16196	τ_8	7.3283e+5		

Paper Number: 26
Discussor's Name: D. I. Thrasher
Responder's Names: F. C. Wong

Question: You obtained a Swanson-model softening function that was a function of temperature from simultaneous straining-and-cooling tests. Was the softening function unique to those loading conditions, or does it also accurately predict response to mechanical loading under isothermal conditions?

Answer: I did not carry out any uniaxial or cyclic tests at different temperatures to see if the temperature dependant softening function/Swanson model could reproduce the results from these kinds of tests. It would be worthwhile to do this.

IMPROVEMENTS IN ROCKET MOTOR SERVICE LIFE PREDICTION

Mr Eugene C Francis
Viscoelastic Materials Services
5885 N. Calle Va12
Tucson, AZ 85715-1802, USA

Dr H J Buswell
Defence Research Agency
DRA Fort Halstead, Sevenoaks
Kent TN14 7BP, UK

1. SUMMARY

Rocket motor service life predictions have always been compromised by the nonlinear viscoelastic behaviour of the highly filled solid propellants. These nonlinearities include damage and rehealing which are dependent on the thermal loading histories and stress axialities in the grain. Recent work to eliminate some of these analytic uncertainties has led to the development of improved experimental stress analysis methods based on actual measured rocket motor bond stresses. A third generation of miniature bond line stress senors have been fabricated which have increased accuracy, stability and can be used for in-situ health monitoring of tactical motors. The use of these units in service life programmes has already measured the time dependency and nonlinearities which are exhibited in typical laboratory tests on solid propellants. These measurements can be used to correct the stress analysis output and hence lead to more accurate structural integrity calculations. The major objective of this new technology is the reliable prediction of safe service life giving a more cost effective missile replacement policy.

2. INTRODUCTION

Historically the structural reliability and service life projections of solid propellants grains have been defined in terms of margins of safety. However, many rocket motors with large calculated margins of safety have still malfunctioned because of grain bore cracking or case-liner-insulation-propellant debonds. Most structural margins of safety calculations are conducted using linear elastic or linear viscoelastic analysis techniques and material zero time properties and estimated ageing trends usually represented by knock-down factors. The current practice and recommended common procedures are under consideration by Working Group 25[1]. A major collaborative programme has also been conducted to acquire results from cast-in strain gauges and stress transducers, the results of which are reported in several papers at this conference[2,3]. This data-base will be used to compare predicted and measured stress and strains at various critical points in the propellant grain and relating this to observed failure. A full understanding not only reduces the risk of catastrophic failure on firing but will also prevent motors from being withdrawn prematurely from service.

The direct measurement of the induced stress by the currently available transducer technology[4] gives a technique to quantify the complex nature of the mechanical response of composite propellants, particularly on temperature cycling. It can also lead to the correction of stress analysis calculations based on inadequate mechanical data.

Recent advances in transducer technology has produced a smaller version of the bondline stress transducer which can be mounted on the inside of the rocket case wall[5]. The introduction of this miniature stress transducer into tactical rocket motors offers the potential of in-service health monitoring that would lead to a significant improvement in service life determination. It is also considered to be a major enhancement to the science of service life determination/prediction of composite propellant rocket motors with a corresponding large reduction in cost of ownership.

3. SERVICE LIFE CONSIDERATIONS

A solid propellant rocket motor service life analysis may be considered as a structural evaluation which is updated for material property changes as a function of age[6]. Figure 1 shows a typical modular representation of a structural evaluation. An essential component shown in Figure 1 includes the material properties for a stress analysis. These properties are required for the case, insulation, propellant and all other structural members. Grain geometry and loads are available based on the motor design and the motor specifications. The finite element analysis generates the stress and strain throughout the entire grain and bond system as function of the various loading conditions such as cure, cooldown, temperature cycling, vibration, pressurization, etc.. A failure analysis is next conducted by using the failure properties of the propellant and bond system as incorporated into appropriated failure criteria such as maximum stress or strain, cumulative damage, strain energy, etc.. By comparing the maximum predicted motor conditions with the corresponding allowable values, the grain margins of safety can be determined.

All of the above steps can now be included as part of the service life analysis. The primary item in the service life is inclusion of the age change of the material properties. The review must include all chemical and physical processes possible in both the grain and component/material interfaces that could have an influence on the system's service life. These property variations may require a combined experimental-analytical base to extend the prediction of properties beyond the experimental data range. An optional feature of service life analysis may be a verification activity which includes instrumented analog, subsale and full scale motor tests and over-tests with possible dissection of the devices. This verification provides another source of both the material properties and ageing properties as well as confirmation of the induced stress, strains and failure modes and limits.

Most stress analysis and service life analysis tends to utilize assumptions of material linearity and small strain linear elastic behaviour. However, some of the material nonlinearities are so large that neglecting these effects can introduce large uncertainties in service life predictions with the resulting possible failures of in-service motors.

Paper presented at the AGARD PEP Symposium on "Service Life of Solid Propellant Systems" held in Athens, Greece, 10-14 May 1996, and published in CP-586.

4. TYPICAL SOLID PROPELLANT NONLINEARITIES

Five of the more common known solid propellant material nonlinearities are briefly discussed in the following sections[7,8,9,10].

4.1 Strain Sensitivity

The nonlinear viscoelastic modulus of the propellant has a strain magnitude dependency as can be seen from Figure 2 which shows data over the strain range of 0.5 to 5.23% at 22° C. There is almost a 30% modulus change going from the high strain data to the small strain data at 0.1 minutes. Another set of modulus data (Figure 3) at -51° C shows strain sensitivity at low temperatures and strains up to 20%. Thermal strains in a rocket motor vary from almost zero at the case wall to 20% or higher at the bore regions (or star or slot tip regions). The effect of this strain variation is to induce large modulus changes from the case wall to the high strain motor regions at the bore. This modulus variation can cause deviations from expected stresses at critical bond or bore regions if not accounted for in the analysis.

4.2 Volume change/Dewetting

Solid propellants routinely exhibit volume change during testing such as illustrated in Figure 4. This volume change has been attributed to dewetting or breakdown of the oxidiser-binder bond. This may be partially responsible for the modulus sensitivity, but the largest modulus change occur before measurable uniaxial volume change is detected (less than 5% strain) as already shown in Figure 2. Although the exact mechanism is not known the effect on Poisson's ratio is critical. The value of Poisson's ratio has a direct impact on the results of any stress analysis, and these variations may account for much of the large variations between prediction and measurement.

4.3 Thermo-mechanical Coupling

Simultaneous straining and cooling such as occur in a rocket motor appears to generate larger stresses than predicted by linear viscoelastic theory. Test results for propellant tensile bars are presented in Figure 5 which show a 100% stress increase above the expected value. This phenomenon was originally predicted by Schapery[11] and later confirmed with laboratory and instrumented analogue tests[12]. Figure 6 compares predicted radial bond stress using a constant thermomechanical coupling coefficient with measured and linear viscoelastic predictions for slow thermal cooling of an analog motor. These results show that conventional linear viscoelastic analysis will under predict motor bond stress for the first cooldown loading

4.4 Axiallity effects

The stress axiallity in rocket motors is nearly always tri-axial instead of uniaxial. Tri-axial poker chip tests exhibit a much higher modulus than uniaxial or biaxial laboratory tests. The input of modulus values taking account of the axiallity of the stress state in complex geometries typical of rocket motors is a challenge to the stress analyst. Failure properties presented in Figure 7 show a significant drop off in triaxial strain capability (4% versus 30%) whereas an increase in failure stress is obtained. The affect of these allowables on predicted failure again lead to uncertainty.

4.5 Damage and rehealing effects

Solid propellant typically exhibit damage effects where unloading and reloading curves are significantly below the initial loading curve. Figures 8 and 9 show this effect for a bonded-end tensile bar exposed to a sawtooth strain history. Each time the strain history is reversed the stress (or modulus) response is only a fraction of the initial value. Each time the strain history exceeds the previous maximum strain level, the propellant tends to return to the virgin or undamaged curve. Some portion of this reduced modulus may be recovered if stored at an elevated temperature (Figure 10) or it may tend to become a permanent set if stored in the strained state for long time periods or the recovery time is short. This damage behaviour has been observed in instrumented solid propellant analogue motors where the first cooldown cycle shows the highest stress value, the subsequent behaviour depending on the dwell time at the temperature extremes as shown in a later section.

Paragraphs 4.1 to 4.5 show why solid propellants are not linear viscoelastic materials but exhibit highly nonlinear viscoelastic characteristics. These properties may also change significantly with age. All of the above nonlinear material factors contribute to uncertainties in motor structural analysis unless they are accounted for in the analysis. This is rarely done because of the major financial requirements to develop an extensive data base to cover all of these effects. These uncertainties also make it desirable to have an independent direct experimental measurement of bond stress values to bypass the analytical limitations in dealing with nonlinear viscoelastic properties of solid propellants. Actual measured values can then be used to correct or calibrate the stress analysis used in service life predictions.

5. STRESS TRANSDUCERS

The latest generation of solid propellant stress transducers is now available to provide these experimental measurements[5]. These new sensors have utilized design and fabrication procedures that avoid the major problems experienced with earlier transducers[13]. The mechanical and electrical stability of earlier sensors were poor because of the inadequate transducer structural design and fabrication procedures. Also, there was insufficient chemical protection for the electrical components from the corrosive propellant environment.

5.1 Stability and Chemical protection requirements

Long term stability is critical for embedded solid propellant stress transducers. Once a transducer is cast into the propellant grain, it cannot be removed nor can zero be reconfirmed. Any electrical drift of the transducer is interpreted as stress changes in the motor. In addition to the electrical problems experienced in field applications, any creep of the epoxy used to bond the semiconductor strain gauges would contribute to electrical drift. Very stable and low Tc temperature compensation and bridge completion resistors are used to insure electrical stability. The transducer body is sealed to ensure a chemical clean environment and a stable zero pressure output.

Typical solid propellants are highly filled elastomers containing solid oxidizers, powdered metal fuel and ballistic modifiers. Solid propellants therefore contain active chemicals which can attack the transducer materials. Stainless steel 17-4 is one of

the few metals to survive in this corrosive environment; epoxies and other adhesives cannot be exposed directly to the propellant. This problem is eliminated on current designs by having all critical parts of the circuit assembled and sealed at the factory where cleanliness and experimental procedures can be carefully controlled. The only field wiring is to attach excitation power and readout devices at a specially designed remote completion unit. Any potential field wire or contact resistance change problems are further eliminated by using constant current excitation.

5.2 Desirable Transducer Features

Some of the transducer features used to ensure accuracy and stability are listed below:

1) Transducer bodies are fabricated with 15-5 or 17-4 SS, or titanium 6AL4V to eliminate corrosion and provide a stable sensor material.
2) All metal components are stabilized after manufacturing with a special process to ensure stability of 1 micro-strain.
3) Four miniature semiconductor strain gauges are used with minimum length for optimal electrical output and strain matching.
4) The semiconductor epoxy adhesive is filtered and processed to provide a bond thickness of 0.02 mm or less.
5) A slope cure process (1°C/2 hours) starting at 70° C and finishing at 200° C is used to reduce the gauge zero stress temperature.
6) Bonded semiconductor gauges are screened by thermal shock eight times between -70° C and 150° C before final assembly.
7) The transducer structural design is optimized for stiffness and minimal stress disturbance and interaction with solid propellant.
8) Excitation is 4 to 5 ma constant current to avoid field contact resistance changes and minimize transducer self heating problem.
9) Transducer no-load out-put vs temperature is measured and used in all motor data analyses. This function must be repeatable, and is usually slightly nonlinear and unique to each transducer.
10) All transducers are screened for stability using temperature cycling tests before use. The range of these tests should exceed the temperature range over which the gauges are to be used.

Lead wire exits and any required safety features must be tailored to the specific motor requirements. Various transducer designs have been developed for specific application conditions. The current miniature design has been developed either to be bonded to the insulation/case and overcast with propellant or to be embedded in the insulation material. Two companies in the U.S. that can manufacture these miniature transducers with the required stability are Micron Instruments[5] in California and Kulite in New Jersey.

5.3 Transducer Interpretation Consideration

When these bond stress transducers are installed in a propellant environment the effect of the transducer on the propellant environment must be assessed. The three parameters which have to be evaluated to calculate accurate stresses from the electrical outputs are given in terms of analytic correction factors:

1) Stress distributions- propellant stress being measured is altered by the stress transducer.
2) Transducer propellant interaction- the diaphragm stiffness is affected by the rigidity of the solid propellant.
3) Non-uniform stress field- the measured stress and stress axiallity is not uniform in the measurement region.

The equation for calculating the stress and the analytic factor range is

$$Stress = \frac{(I_f)\,(D_f)\,(N_f)\,(Output - Offset)}{Sensitivity}$$

where I_f - Interaction factor from finite element analysis (for stiff transducer diaphragms)
D_f - Stress disturbance factor from finite element analysis (for correctly mounted transducers)
N_f - Non-uniform stress field factor from finite element analysis (for correct motor locations)

These factors are minimal for gauges buried in the insulation, a typical correction factor being less than 1.05, for the current miniature bond stress transducer because it has a rigid design and does not protrude into the propellant. However, these factors and design must be evaluated for any other transducer application to ensure accurate stress interpretation.

6. MEASURED MOTOR STRESS BEHAVIOUR

The stress response of two instrumented analogue motors from the same HTPB propellant batch are shown in Figures 11 and 12. The first motor was cooled from a soak temperature of 60° C to an isothermal temperature of -15° C (± 1°C) and stored for a period of five months (24 weeks) before being returned to 60°C. In that period the stress level relaxed to 25% of the original peak value of 650 kPa, whereas the measured uniaxial relaxation modulus, measured at the same strain level, reduced by a similar amount in just a few days. The second motor was subjected to a programme of temperature cycles +60° C to -15° C as shown in Figure 12. The effect on the stress level of the first three temperature cycles indicates the effect of damage which reheals during the April storage. Later temperature cycles gave the same peak value of induced stress with the mechanical properties of rehealed damaged material being less sensitive to repeated cycles of damage.

Similar results have also been observed during recent trials to demonstrate the use of stress transducers as in-situ health monitors of rocket motors. An instrumented motor with transducers mounted alonged its length was subjected to repeated temperature cycles[4]. The test sequence consisted of a long term, 30 day, soak at 40° C, then two cooling cycles down to -45° C with a 12 hour dwell at -20° C. At the low temperature the motor was again soaked for a prolonged period of 20 days and then returned to ambient temperature with two heating cycles. The dwell at -20° C during both cooling and heating cycles was designed to measure the relaxation modulus

in an attempt to assess any cumulative damage. The cycle was started with an uncontrolled heating back to 40° C before the sequence was repeated.

The recorded peak values of stress on the first cooldown to the low temperature was 350 kPa and this is at least 25% higher than the stress measured at thermal equilibrium. The equilibrium stress values are given in Figure 13 together with the corresponding values at the other temperatures in the cycle. The allowable stress level for the temperature of -45° C has been derived as 650 kPa. This implies that bondline separation is unlikely as a failure mode providing reasonable precautions have been taken during motor manufacture to ensure a good bond.

Even though bond failure is not predicted, it can be seen that the results do indicate some mechanical damage. The excursion to -45° C has caused a change in the apparent modulus since the equilibrium stress levels at both -20° C and 20° C during the heating part of the cycle are lower than those measured during initial cooling as can be seen in Figure 13. The stress level on returning to 20° C after the excursion has decreased on average by 35%. However, the stress levels at -20° C would appear to have decreased by an average of 47%. This implies that the amount of damage is dependent on the induced strain level, being 10% and 20% respectively. This behaviour illustrates the properties discussed in previous sections of this paper.

After a recovery period at 45° C the second cycle induced very similar stress levels. The recorded thermal equilibrium stresses at -45° C are given in Table A. Again the induced damage was not recovered during the low temperature storage. Between cycle 2 and subsequent cycles, a delay of several months was incurred due to malfunction of the data-logger equipment. The data-logger was returned to the manufacturer for repair with the loss of internal zero settings. Hence results for cycles 3, 4 and 5 are presented in comparative form with the stress values corrected so 2 and 3 correspond. As can be seen, the same pattern is repeated for all the cycles with the average values of the five cycles being the same as the actual values for the first cycle. The 30 day dwell period at the temperature of 45° C was sufficient to restore the propellant's initial properties. At the end of the trial the motor was visually inspected and found to be in good condition with no visible damage and no cracks apparent.

7. CONCLUSIONS

The measured stress magnitudes obtained from the temperature cycles described in this paper and other papers given at this Conference have demonstrated the usefulness of stress transducers as a health monitor. This work is continuing to compare the actual measured stress values in instrumented rocket motors and the results from the best available prediction techniques. The objective of current work is to obtain an estimate of time-to-failure of motors in service and a measure of remaining useful life.

It has been shown that stress changes in composite propellant rocket motors are complex. The ability to measure these stress magnitudes is an essential precursor to accurate structural integrity calculations. From this information an informed decision can be made about the state of the in-service instrumented rocket motor. Significant cost avoidance can be obtained using this possible extension of service life. However, no matter how sophisticated the measuring system the fact remains that the stresses in the motor situation are extremely complex. It still requires careful analysis of the data obtained to ensure validity of any of the readings. Even so, the progress made over the last few years in motor stress measurement has led to the possible validation of modelling techniques and to a significant improvement in rocket motor service life prediction.

REFERENCES

1. AGARD PEP Working Group 25 to report by end of 1996.
2. F C Wong "Service life prediction using stress gage technology and nonlinear viscoelastic analysis" Paper No 26.
3. S Y Ho etal "Instrumented service life program for the Pictor rocket motor" Paper No 28.
4. G S Faulkner etal "Service life prediction methodologies" Paper No 24.
5. H Chelner etal "Advances in in-situ stress monitoring instrumentation" Paper No 25.
6. F N Kelly etal "Elements of solid rocket service life prediction" AIAA Paper No 72-1085.
7. R B Beyer "Nonlinear mechanical behaviour of solid propellants" AIAA Paper No 65-159.
8. E C Francis etal "Some aspects of composite propellant nonlinear behaviour in structural applications", J of Spacecraft & rockets, Vol 6, No 1, 1969.
9. E C Francis etal "Considerations in the applications of nonlinear structural materials" Second Int. Conf on Mechanical Behaviour of Materials, Boston, MA, 1976 .
10. M E Gurtin etal "Simple rate independent model for damage", J of Spacecraft & rockets, Vol18, No 3, 1981.
11. R A Schapery "A theory of nonlinear thermovisoelasticity based on irreversible thermodynamics", 5th US National Congress of Applied Mechanics, 1996.
12. H J Buswell etal "Solid inclusion stress gauges in composite propellant charges", J of Spacecraft & rockets, Vol12, No8, 1975.
13. E C Francis etal "Bond stress transducer design for solid propellant rocket motors" J of Spacecraft & rockets, vol18, No5, 1981 .

ACKNOWLEDGEMENT

The UK Ministry of Defence supported this work which was conduced at Royal Ordnance Rocket Motors. The views expressed are those of the authors, and do not necessarily represent the policy of the MOD or Her Majesty's Government.
British Crown Copyright 1996/MOD.
Published with the permission of the Controller of Her Britannic Majesty's Stationery Office.

Corrected stress induced at -45°C /kPa /psi

Gauge # / Cycle	397	394	393	Average
1	163 23.6	238 34.5	288 41.8	230 33.3
2	146 21.2	226 32.8	296 42.9	223 32.3
3	(145) (21.0)	N/R	(300) (43.5)	223 21.5
4	(176) (25.5)	(267) (38.7)	(307) (44.5)	250 36.3
5	(215) (25.5)	(231) (38.7)	(248) (44.5)	231 36.3
Average	169 (24.5)	241 (34.9)	288 (41.7)	232 (33.7)

(numbers in parenthesis represent a span change)

Table A
Absolute stress variation with temperature cycle

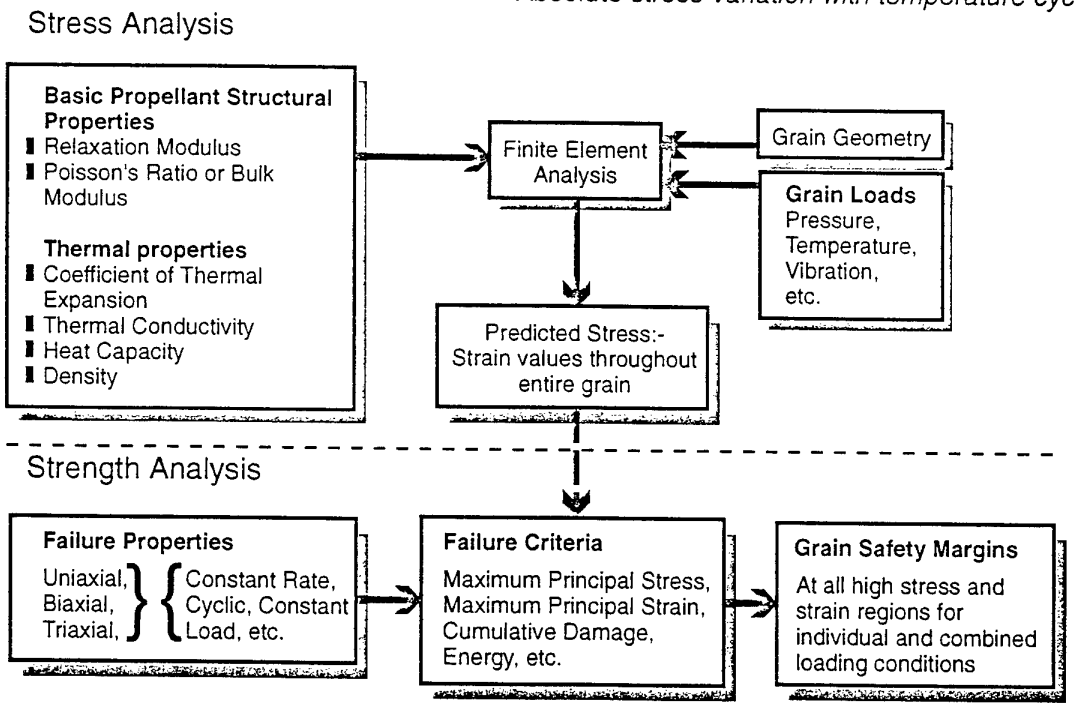


Figure 1
Solid propellant grain structural evaluation

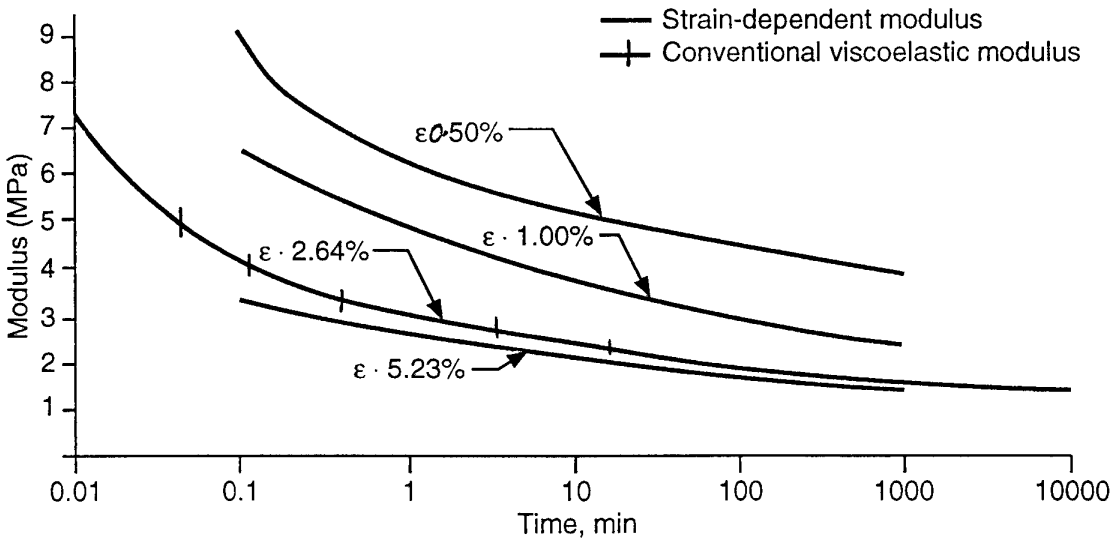


Figure 2
Conventional viscoelastic modulus data and strain dependent modulus for solid propellant at temperature 22°C

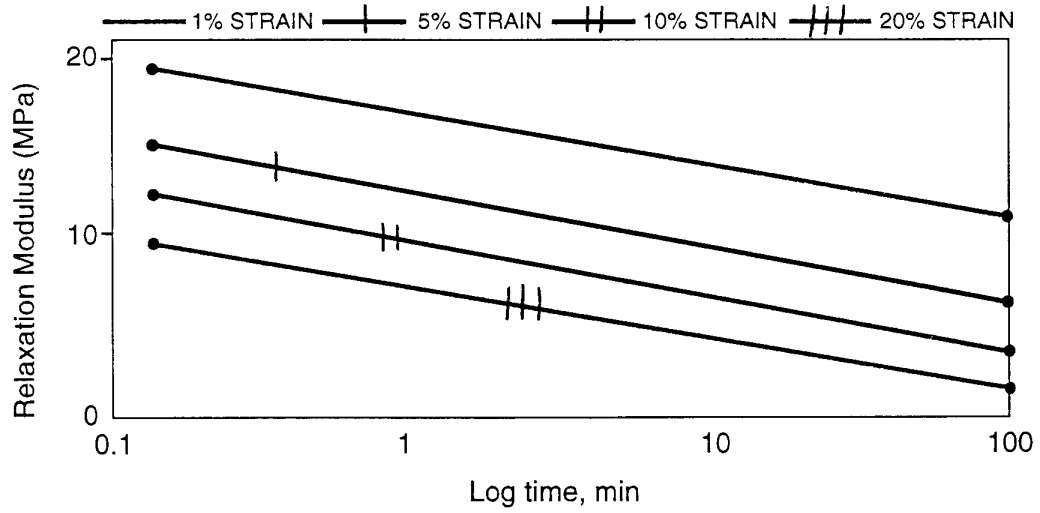


Figure 3
Solid propellant relaxation modulus data at different strain levels at temperature -50°C

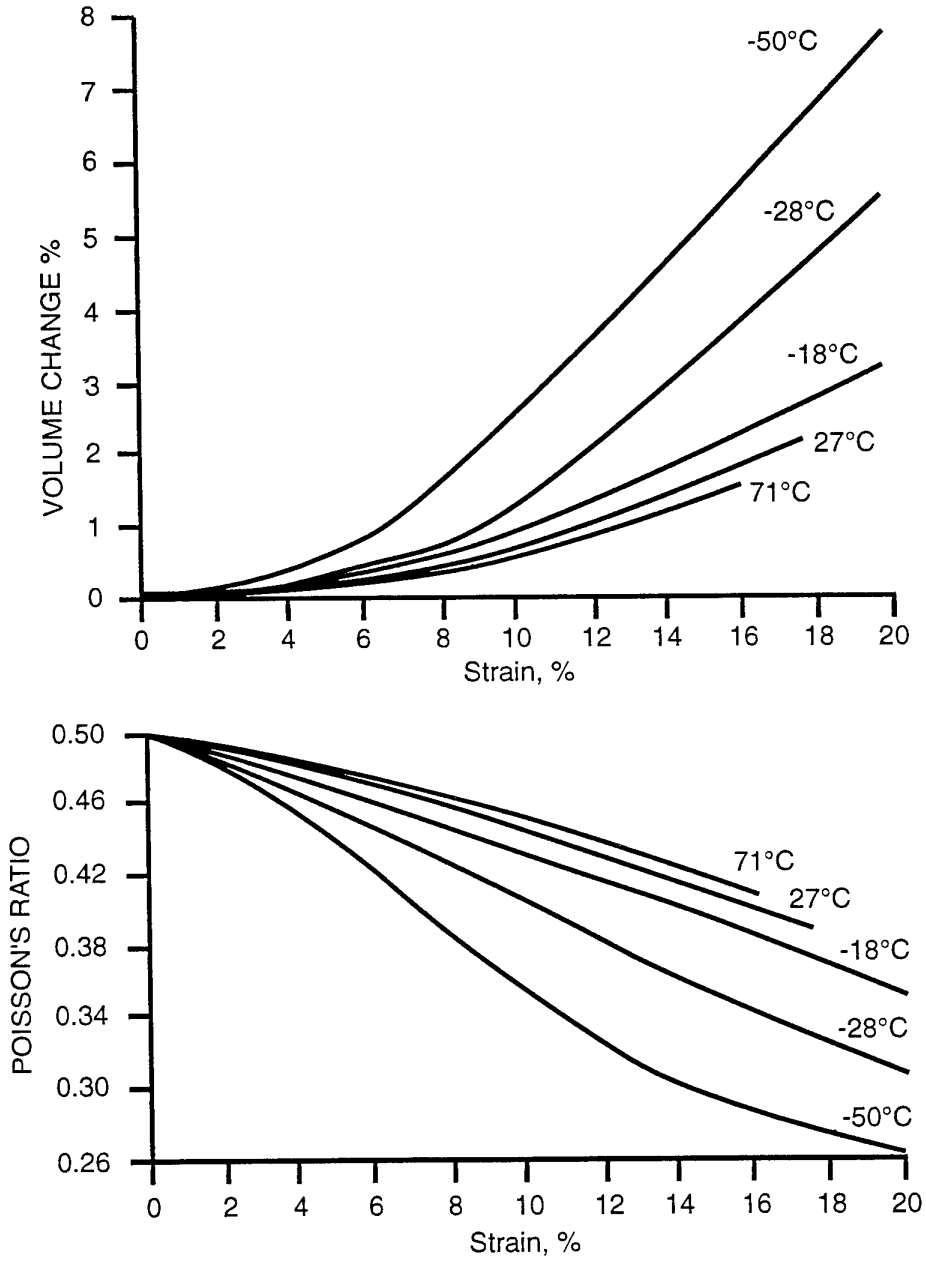


Figure 4
Volume change and Poisson's Ratio vs strain for various temperatures - rate 0.725 m/m/min

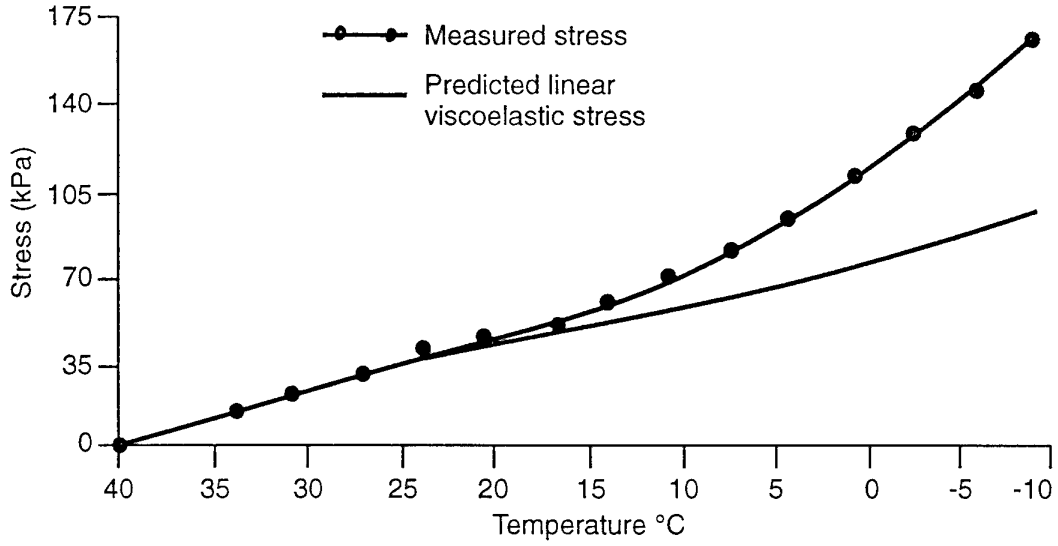


Figure 5
Comparison of measured and predicted stress for 64-hour simultaneous straining and cooling uniaxial bar

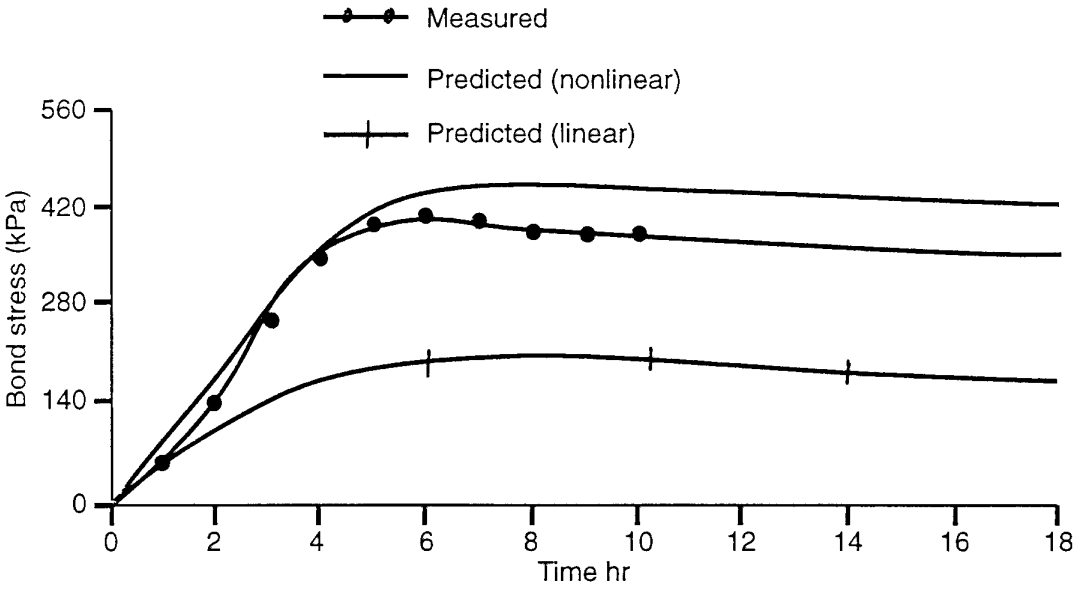


Figure 6
Comparison of measured and predicted radial bond stresses for cooling from 27°C to -18°C of analog motor

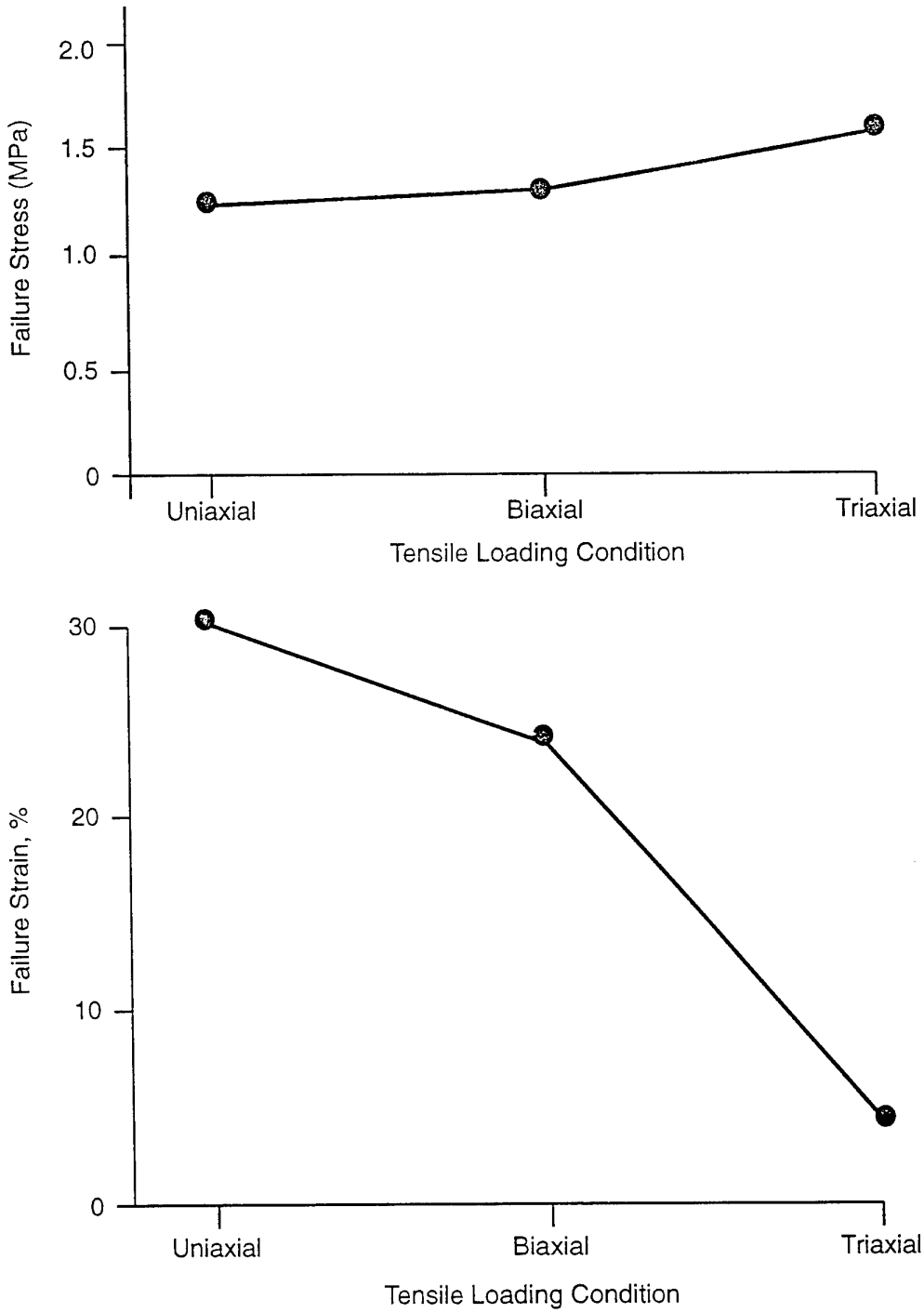


Figure 7
Comparison of typical propellant uniaxial, biaxial, and triaxial tension failure data

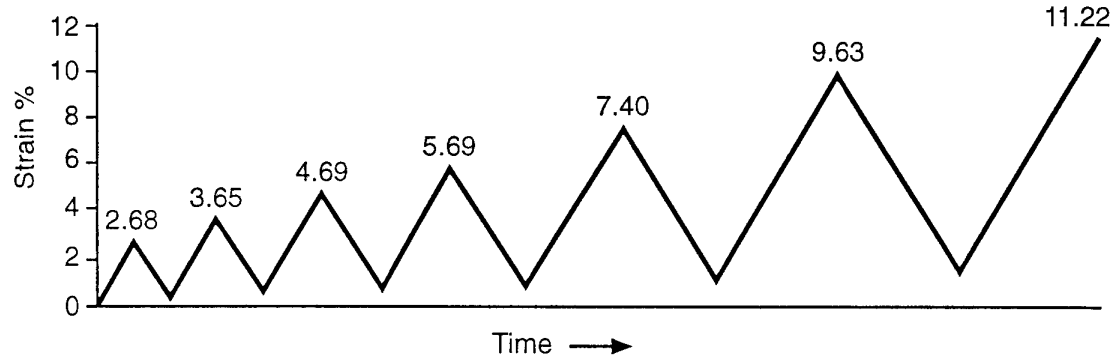


Figure 8
Saw tooth strain history

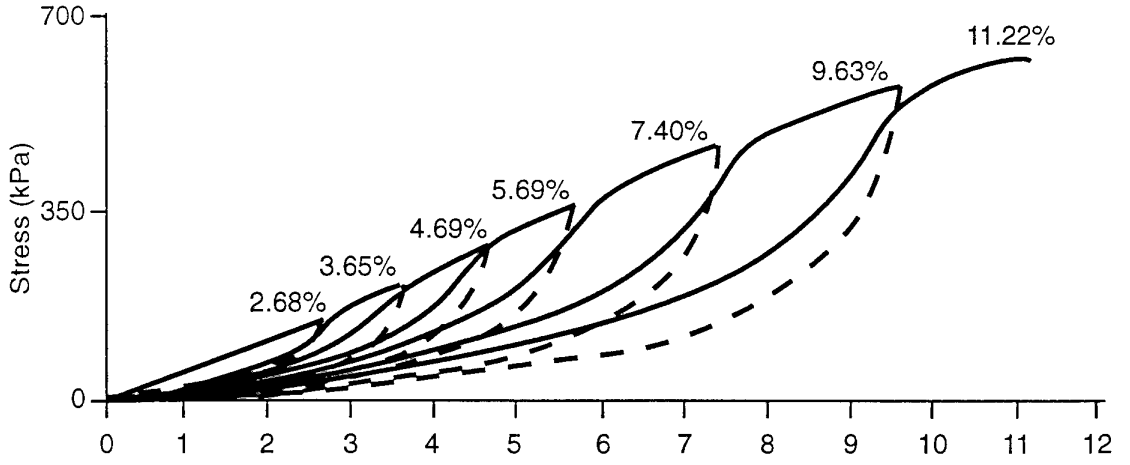


Figure 9
Propellant stress-strain response showing damage effects for saw tooth strain history

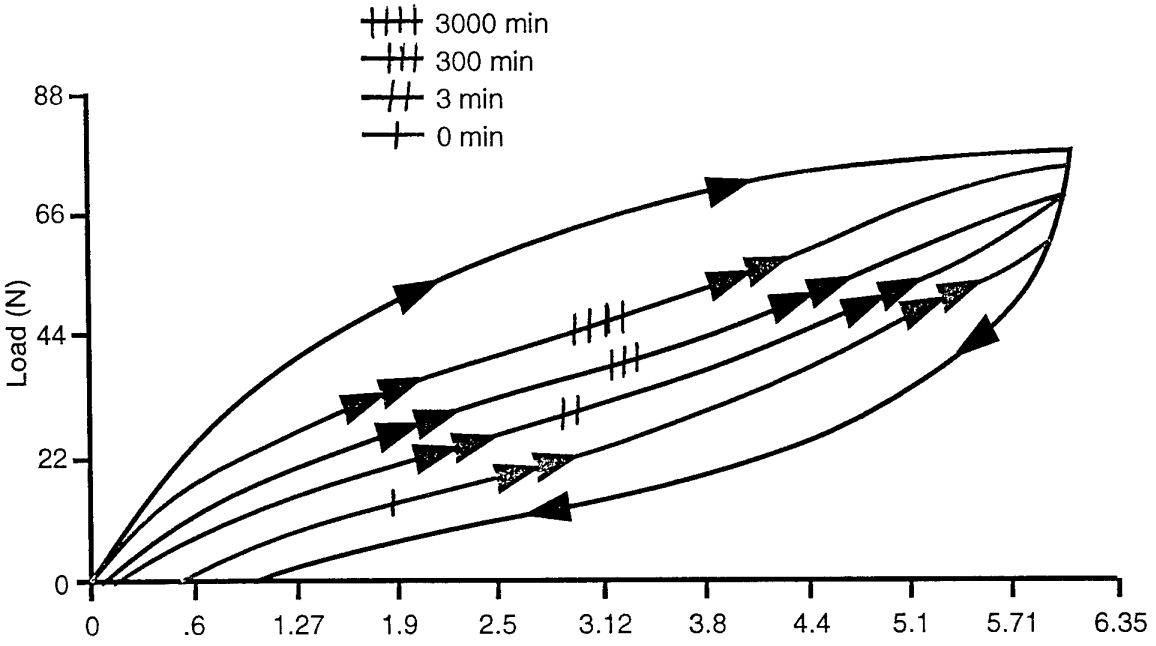


Figure 10
Healing curves for solid propellant

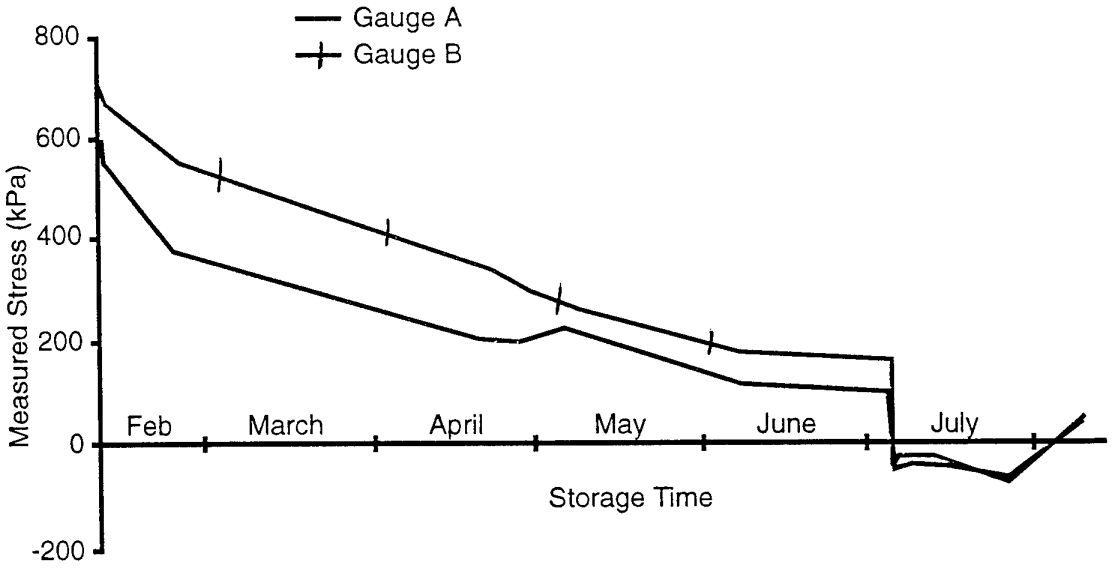


Figure 11
Absolute stress relaxation at -15°C

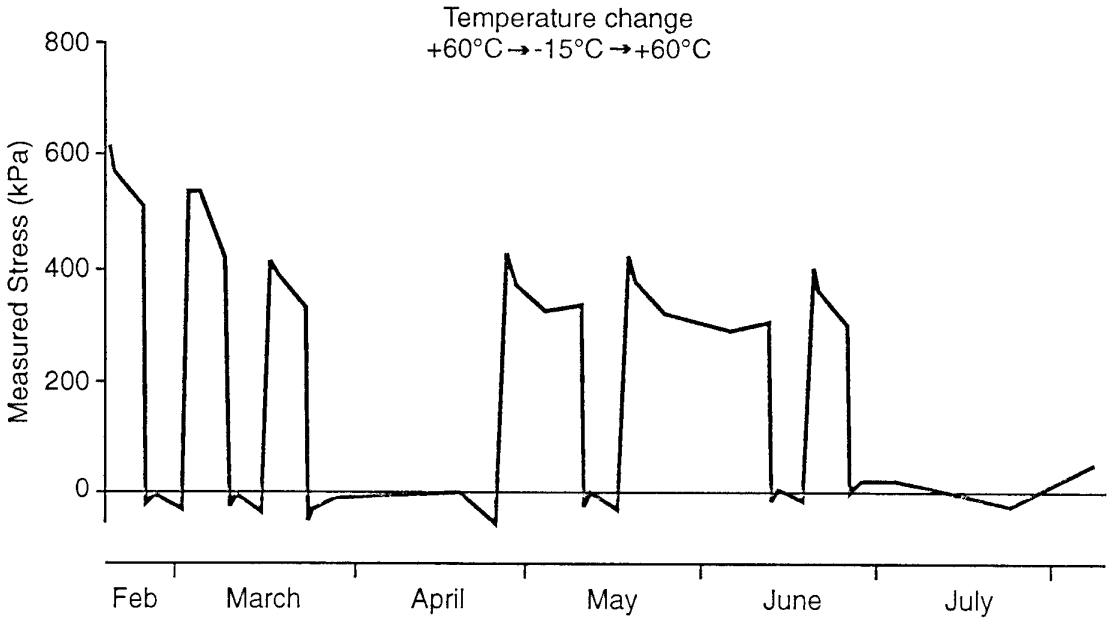
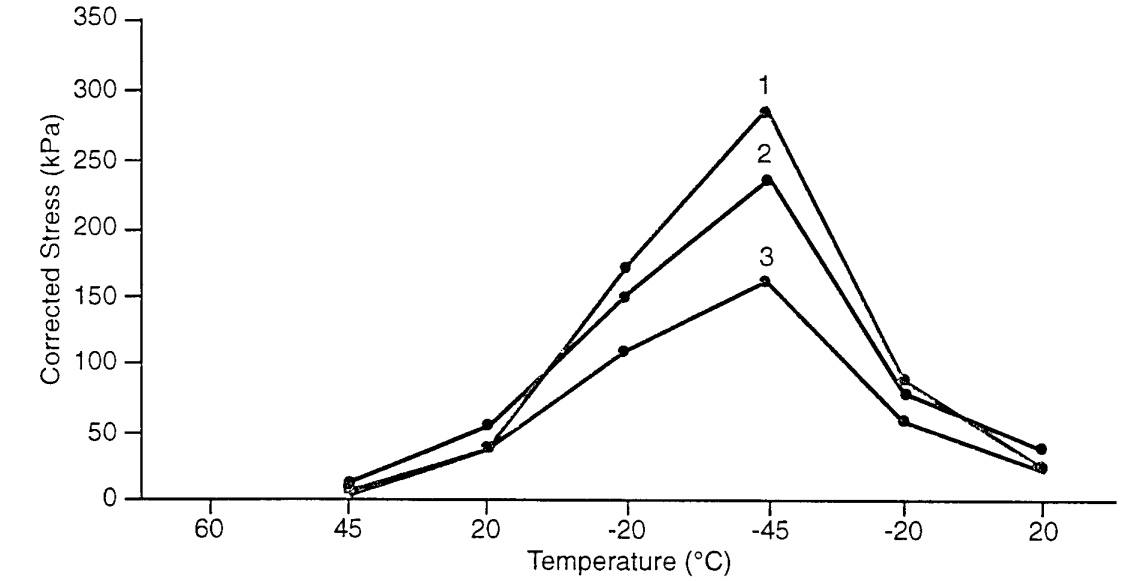


Figure 12
Absolute stress variation with temperature cycle



9F393 —	1	5	40		173	288	92		26
9F394 —	2	12.5	57		155	238	80		39
9F397 —	3	5	36.2		110	163	61		22

Figure 13
Arctic cycle: bond stresses - first cycle (data for cooling and heating)

Paper Number: 27
Discussor's Name: Professor J. Salva
Responder's Name: Dr. H. J. Buswell

Question: Are you planning to continue this experimental work or to extend this work to another type of propellant?

Answer: Most definitely YES. The international collaboration within TTCP will continue with KTA4-23 to investigate pressurization failure of motors using stress gages to measure flaw or debond criticality. The UK is also using gages in EMCDB propellant analog motors to investigate low temperature failure.

Paper Number: 27
Discussor's Name: Professor H. Schubert
Responder's Name: Dr. H. J. Buswell

Question: In practice, we also have dynamic stresses to take into account. Therefore, the uncertainty of prediction will increase. Do you have experience in this field?

Answer: No. The UK does not have any experience in testing instrumented motors under dynamic loads. The author suggests that gaged motors be used to obtain stress data under these transient conditions where non-linear effects may dominate.

Paper Number: 27
Discussor's Name: Dr. G. Hooper
Responder's Name: Dr. H. J. Buswell

Question: You mentioned the phenomenon of self-repair and recovery of propellant grains. Do you think that this phenomenon applies to classes of propellant other than those based on HTPB (for instance, new formulations based on energetic binders)?

Answer: Yes. The self-repair mechanism will apply to all types of composite propellants where solid particles are surrounded by a binder with an adhesive interface. The rate and magnitude of repair will of course depend on the storage environment and type of materials involved.

INSTRUMENTED SERVICE LIFE PROGRAM FOR THE PICTOR ROCKET MOTOR

S.Y. Ho, K. Ide and P. Macdowell
Weapons Systems Division
Aeronautical snd Maritime Research Laboratory
PO Box 1500, Salisbury, S.A. 5108
Australia

1. SUMMARY

This paper describes a Solid Propellant Rocket Motor Service Life program conducted at the Aeronautical and Maritime Research Laboratory/ DSTO, which combined a nonlinear viscoelastic analysis of an Australian R&D motor, Pictor, and used miniature embedded stress transducers to validate analysis and/or define the actual stresses in the rocket motor during various thermal loading conditions (thermal shock, thermal cycling, accelerated aging and ambient aging). The measured stresses during solid propellant rocket motor thermal cycling were obtained for comparison with linear elastic/viscoelastic and nonlinear viscoelastic finite element analysis. Measurements are in reasonable agreement with nonlinear viscoelastic analysis for most motor loading conditions. Capabilities for modified Fracture Mechanics and non-linear viscoelastic analysis were incorporated into a commercial general purpose finite element (FE) code, STRAND 6.1. The thermal stresses induced in the motors were modelled using this FE code. The code was also developed to calculate the critical crack length for propagation during thermal transients. Uniaxial and biaxial tension, and bond-in-tension tests were conducted for the failure analysis. Additionally, a modified Fracture Mechanics approach was used to obtain the fracture energy (G_c) as an alternative failure criterion and also to determine the critical crack length for propagation.

2. INTRODUCTION

Until recently, most service life programs for solid propellant rocket motors comprised of experimentally based methods such as qualification of testing and surveillance by scheduled material properties tests[1-3]. These conventional service life programs for rocket motors are wasteful and expensive, as they involve a large number of trial firings and dissection of several rocket motors to validate the service life of the remaining motors in the inventory.

Several new methods are available today for predicting the service life of solid propellant rocket motors, for example the structural analysis approach, cumulative damage model, the probabilistic approach, and using instrumented rocket motors. Currently no best method exists, as the method used would depend on the failure mode of the motor. However, regardless of the method used accurate stress predictions, under the expected environmental and operating conditions, are critical in developing a predictive service life analysis capability. In the past, the lack of analytical tools and confirmation with embedded stress transducer technology has led to gross errors in service life prediction. Solid propellants exhibit significant nonlinear viscoelastic response which challenges even the best finite element analysis and experimental stress analysis techniques[4-11]. Service life analysis remains further complicated by uncertainties in material ageing characteristics and failure criterion.

This paper presents a structural analysis approach for predicting the service life of rocket motors, using new miniature embedded stress transducer technology and recent developments in nonlinear constitutive models. The Pictor motor was selected for evaluating these new analytical and experimental techniques.

3. EXPERIMENTAL PROGRAM

The Pictor motor (Fig. 1) is an end burning design. The propellant grain is filled with a non-aluminized HTPB/AP propellant, inhibited with a tapered thickness beaker (inhibitor) of adiprene/TMP. This inhibited charge is case bonded at the head end with an epikote/versamid adhesive. The motor has a maraging steel case and is thermally insulated with EPDM which is spun cast in the case. There is a small air gap in the side wall of the motor between the inhibitor charge and the insulated case.

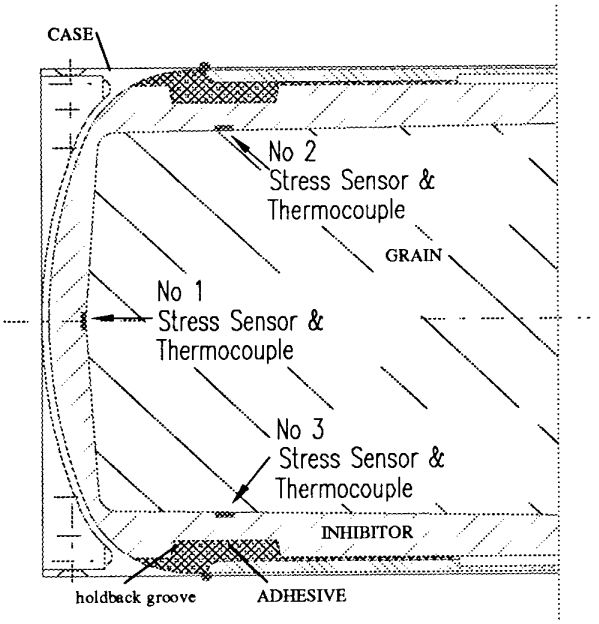


Fig. 1 Instrumented Pictor Motor

The Pictor motors were instrumented with Senso-Metrics miniature stress sensors and thermocouples (type T copper/constantan). The stress sensors (5 mm diameter by 1.5 mm thick) were used with 5 milliamp constant current excitation, and were flush mounted in the inhibitor tube at peak stress locations (Fig. 1) identified by early linear elastic analysis[7]. All data was collected on a Datataker 500 data logger with 10 differential input channels. The stress gauges

Paper presented at the AGARD PEP Symposium on "Service Life of Solid Propellant Systems" held in Athens, Greece, 10-14 May 1996, and published in CP-586.

and numerous thermocouples were monitored during motor processing and later cooldown and thermal cycling.
The zero offset of the transducers usually change after they are mounted in the propellant grain. Hence, it is important to measure the zero offset and hysteresis characteristics of the transducers after they are installed in the motor grain. The hysteresis and zero offset temperature response of the stress sensors were determined by step cycling the instrumented beaker (before propellant casting) from -60 to 55°C. Temperature zero offset coefficients were then obtained from a fourth order polynomial fit to each set of data for the different sensors.

In the initial stress calculations corrections have been made for the temperature zero offset of the transducers, obtained from a fourth order polynomial fit of the thermal offset vs. temperature data. However, corrections for the transducer-propellant interaction and stress disturbance of the gauges are insignificant (as indicated by a 2D-viscoelastic finite element model with the stress sensors) and have been neglected.

Thermal cooldown tests were conducted to determine the residual stresses at different temperatures[7]. Fig. 2 shows the equilibrium stresses as the charge was allowed to cool down from 60°C after the propellant had cured. A stress free temperature of 55°C was determined.

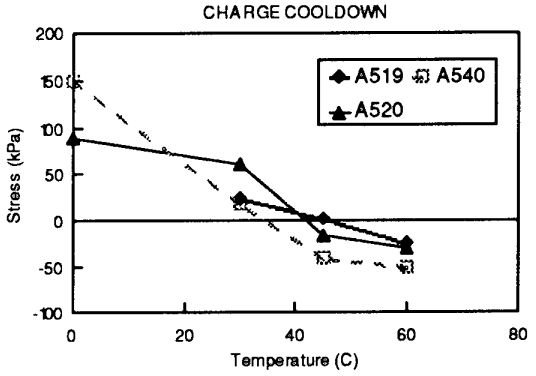


Fig. 2 - Residual Stresses at Different Temperatures

3.1 ENVIRONMENTAL TESTING

For the environmental testing, one instrumented and two uninstrumented motors were used for each of the tests presented in Table 1.

TABLE 1 - Environmental testing Program

Motors		Thermal Environment
1I, 2UI	Thermal shock	16 hours at -40°C and 16 hours at +50°C.
1I, 2UI	Thermal cycle	Minimum of 5 cycles of 30 days at 45°C and 20 days at -30°C.
1I, 2UI 2 sealed charges	Accelerated ageing	Minimum of 64 weeks at +60°C.
1I, 2UI	Ambient ageing	Storage at 22°C for at least 2 years.

The Pictor 2 motor was subjected to 13 thermal shock cycles. The bondline stresses and thermocouple temperatures for the heating and cooling cycles are shown in Fig. 3. The two sensors at the side of the motor showed the same trend. Relaxation was also observed and was more apparent in the cooling cycles. For both the heating and cooling cycles, the stresses decreased with each thermal shock cycle due to mechanical damage which was evident as a reduced compressive or tensile stress. In the cold cycle, the stresses decreased (95% reduction) very markedly after the 4th cycle, whereas in the hot cycle the damage was not apparent until the tenth cycle.

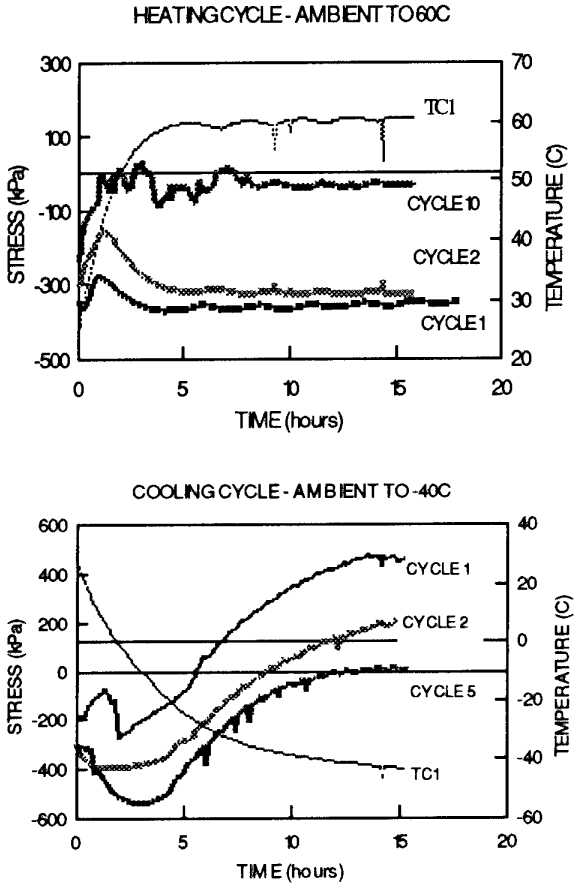


Fig. 3 - Thermal Shock Test

The reduction in the measured stresses may be due to debonding at the propellant-inhibitor interface. This was confirmed by radiographs (the motors were X-rayed after each hot and cold cycle) which showed a dark line, indicating a separation or debond, at the propellant/inhibitor interface adjacent to the holdback groove in the inhibitor, and is consistent with the critical stress areas predicted by FE models. The two uninstrumented motors also showed cracking in the propellant near the head end and adjacent to the holdback groove of the inhibitor after the first and second thermal shock cycles.

Fig.4 shows the bondline stresses of the Pictor 4 motor during ambient ageing over a period of 250 days. The two stress sensors at the side of the motor gave similar measurements. At the start of the test the measured stresses were 70 kPa

when the temperature was 15°C. After 5 days of storage at ambient temperature (22°C) the stresses decreased to 50 kPa and remained at this level during the 250 days of storage.

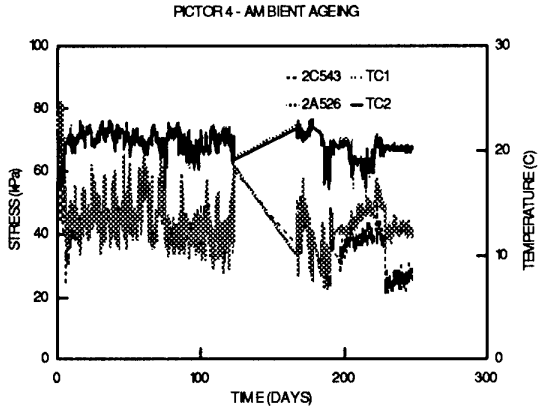


Fig. 4 - Ambient Ageing Test

Fig. 5 shows the bondline stresses for the thermal cycling test after one cycle of 30 days at +45°C and 20 days at -30°C. The equilibrium stresses from the sensors at the side of the motor were -10 and -92 kPa for the hot cycle and 305 and 105 kPa for the cold cycle. There were no measured changes in the bondline stresses after 6 complete thermal cycles. The uninstrumented motors have been subjected to 8 complete cycles and were radiographed at the end of each cold cycle. No cracks/damage were evident in the radiographs.

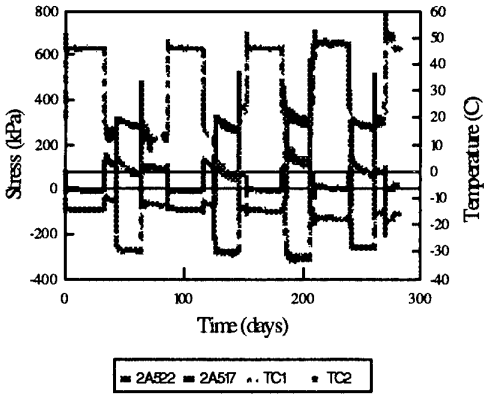


Fig. 5 - Thermal Cycling Test

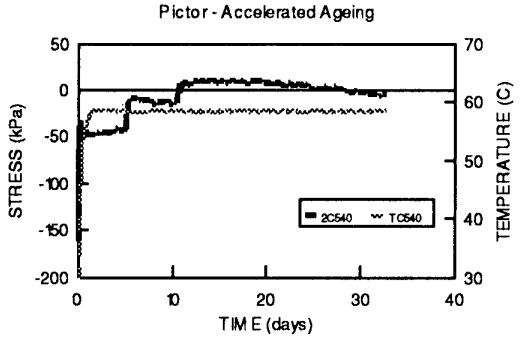


Fig. 6 - Accelerated Ageing Test

Fig. 6 shows the bondline stresses for the accelerated ageing test. Initially, the stresses from the two sensors at the side of the motor were around -50 kPa and changed to zero after ca. 10 days of ageing at 60°C. This indicates that the motor zero stress temperature has shifted to a higher temperature and is consistent with other previous work[15].

3.2 STRESS ANALYSIS

A commercial general purpose finite element program, STRAND 6.1 (developed by G+D Computing in Australia), was used for our stress analysis. AMRL/DSTO contracted and provided the theory and empirical constitutive equations to G+D Computing to incorporate nonlinear viscoelastic and Fracture Mechanics (based on strain energy release rates) capabilities[17] into the STRAND 6.1 code.

The viscoelastic analysis in STRAND 6.1 was carried out by a 3D interpolation of the relaxation modulus data (inputted in the form of a Prony Series) as a function of time, temperature and strain level. A 2D viscoelastic analysis of the Pictor motor was conducted using STRAND 6.1 for the upward (ambient to +47°C) and downward (+47°C to -23°C) thermal transients in the thermal shock test. The viscoelastic solutions assume that the motor begins in a state of zero stress and strain at the start of the thermal transient. Figure 7 shows the Von Mises stress contours in the Pictor motor from the nonlinear viscoelastic axisymmetric model for the upward thermal transient.

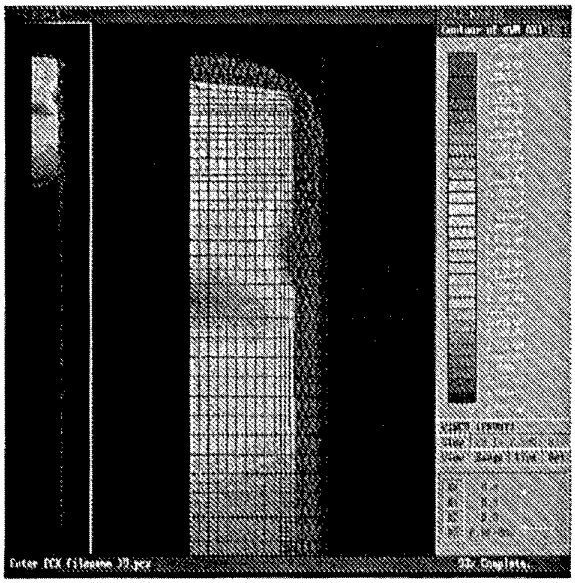


Fig. 7 - Von Mises Stress for Upward Thermal Transient

As expected, the high stresses in the propellant are concentrated at the head end of the motor and also at the side adjacent to the holdback groove of the inhibitor. In the upward thermal transient, the Von Mises stress in the propellant adjacent to the holdback groove of the inhibitor is around 130 kPa. The residual stress in the motor at 25°C is 48 kPa. After correcting for this, the predicted stress is ca. 180 kPa. This is in close agreement with the experimental values of 133 and 80 kPa. In the downward thermal transient (+47 to -23°C), the stresses in the propellant adjacent to the holdback groove of the inhibitor are ca. 400 kPa (see Fig. 8).

This compares with the experimental values of 500 and 380 kPa.

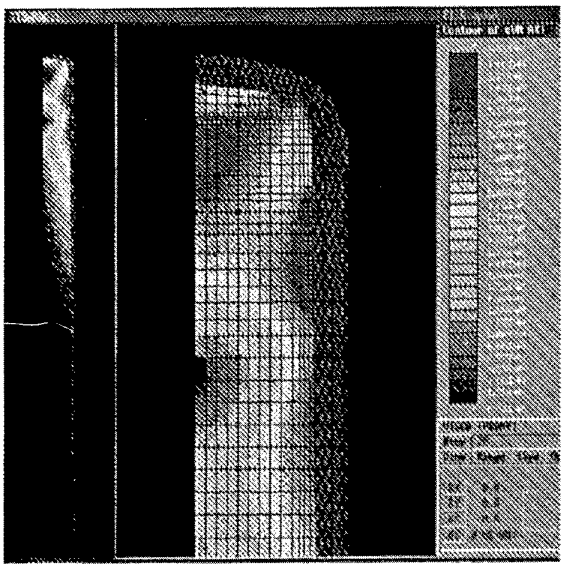


Fig. 8 - Von Mises Stress for Downward Transient

The analysis showed that the air gap, being a poor conductor of heat, had some effect on the predicted stress distribution. During the temperature heating transient the propellant and inhibitor expand into the air gap and during cooldown the air gap opens up. This has some effect on the magnitude and distribution of the stresses and strains during the transient. Fig. 9 shows the deformed shape of the strain contours in the motor at the upward thermal transient.

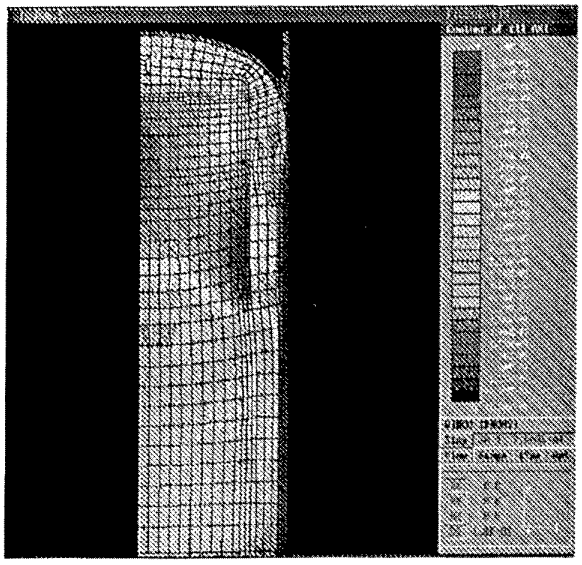


Fig.9 - Principal Strain for Upward Transient

The temperature distribution in a 3D model of Pictor for the upward transient is illustrated in Fig. 10. The motor was equilibrated at ambient temperature and step change to +47°C. It predicts that after 2 hours, the temperature differences between the motor case and propellant at the two different gauge positions, ie. at the head end and at the side adjacent to the holdback groove of the inhibitor, are 14 and 19°C respectively, as observed in the experiment. The model also predicts that thermal equilibrium is reached after 15 hours.



Fig. 10 - Temperature Distribution for Upward Transient

3.3 FAILURE ANALYSIS

The material characterization program is summarized in the table below, to provide the input data for the FE models and to obtain failure criteria for the service life analysis.

Table 2 - Material Properties Characterization

Response Properties	
1. Viscoelastic Modulus	-40 to +60°C; 0.5 to 2.5% strain;
2. Thermal Expansion Coefficient	-40 to +60°C;
3. Poissons Ratio	+20°C; 0.5 to 5.0 mm/min;
4. Specific Heat	-40 to +60°C;
Failure Properties	
5. Uniaxial tensile (Jannaf Class A)	-40 to +60°C; 0.5 to 50 mm/min;
6. Biaxial	-40 to +60°C; 0.5 to 1.5 mm/min;
7. Bond-in-tension	-40 to +60°C; 0.5 to 1.5 mm/min;
8. Fracture Energy	-40 to +60°C;

Constitutive equations were developed for the relaxation modulus as a function of time, temperature and strain level for input into the finite element analysis. Measurements were made on a RDA2 Rheometrics Dynamic Mechanical Thermal Analyser, using a rectangular torsion geometry, to measure shear relaxation modulus, G(t), and an Instron mechanical tester to measure Young's relaxation modulus, E(t). Fig. 11 shows G(t) and E(t) as a function of time, temperature and strain level.

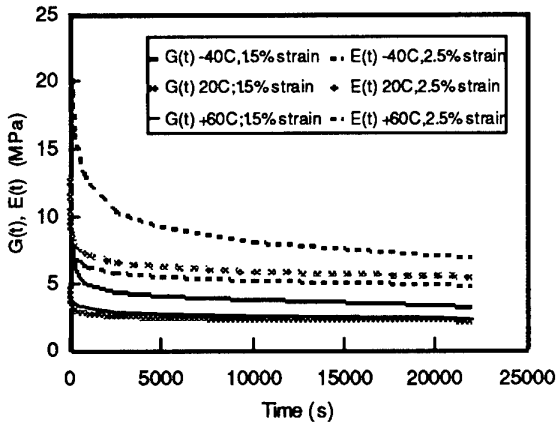


Fig. 11 - Relaxation Modulus of Pictor Propellant

The fracture energy (G_c) of the propellant, inhibitor and propellant-inhibitor bimaterial of the Pictor motor were determined using a modified fracture mechanics approach[17], where bulk inelastic behaviour is accounted for in the calculation of G_c. This is being used as an alternative failure criterion in the structural analysis. Because G_c indicates the energy required for crack extension, it may be a more appropriate failure criterion than criteria based on strain or stress capabilities alone. The modified fracture mechanics approach, for non-linear materials such as solid composite rocket propellants, also enables us to calculate the critical crack length for propagation when the rocket motor is subjected to a thermal load.

Figs.12 and 13 show the fracture energies and hysteresis ratios as a function of temperature for the unaged and aged propellants. The propellant samples were aged under the same conditions as for the motors (see Table 1). In general, an increase in the hysteresis ratio is refelected in a higher G_c value (ie. more energy is dissipated in the form of plastic deformation, microvoiding, etc. and consequently, less energy is available for cracking). This is consistent with previous studies[17,18]. It is interesting to note that G_c is higher at -40°C than at ambient temperature and 60°C. This can be explained by the higher hysteresis ratio at -40°C which arises from the presence of energy dissipation mechanisms operating at this temperature. This is supported by DMTA studies of this propellant which show a broad tan δ peak in the temperature range -40 to -20°C (see Fig. 14). Earlier studies[18,19] have shown that this transition is due to relaxation of the hard segments of the HTPB binder and the viscoelastic loss processes correlate with hysteresis energy loss and consequently, fracture resistance.

At ambient temperature and 60°C, the effect of ageing by thermal shock and thermal cycling is a decrease in the fracture resistance due to the propellant becoming more brittle as it ages (the maximum strain-to-failure decreased compared to the unaged propellant). However, at -40°C the fracture resistance of the samples which had been subjected to the thermal cycling and thermal shock tests were higher than that for the unaged propellant. Although the propellant had become more brittle with thermal cycling/shock and had lower hysteresis energies (see Fig. 13), it had a higher maximum stress and strain to failure at -40°C compared to the unaged propellant at the same temperature. Our earlier studies[17] found that high hysteresis energy is not the sole requirement for high crack resistance - some hard propellants with high modulus and high strength have low hysteresis energies but high fracture energies.

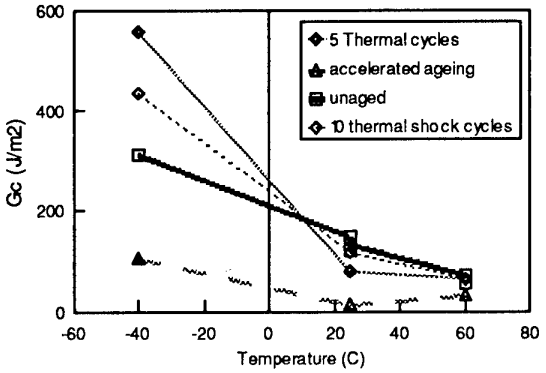


Fig. 12 - Fracture Energy vs. Temperature

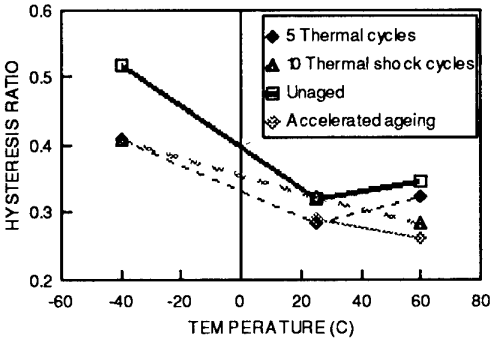


Fig. 13 - Hysteresis Ratio vs. Temperature

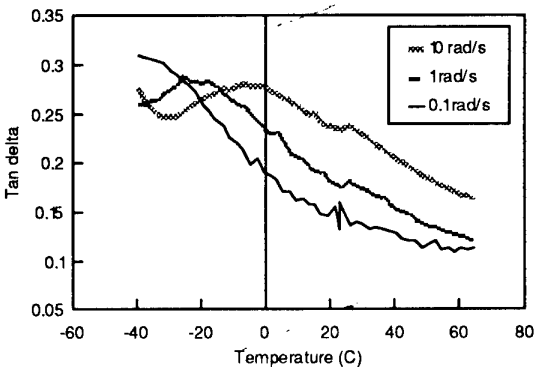


Fig. 14 - Viscoelastic Spectrum of Propellant

Uniaxial and biaxial tensile, and bond-in-tension tests were conducted over a range of temperatures, strain level and strain rates, as listed in Table 2. The majority of the bond test specimens failed cohesively in the propellant. The propellant/inhibitor bond strength corresponds closely with the tensile strength of the propellant under the same temperature and strain rate, indicating that the propellant strength was the limiting factor for the bond-in-tension test, ie. the propellant/inhibitor bond strength was equal to or exceeded the measured bond-in-tension value (the strength of the propellant).

4. SERVICE LIFE ASSESSMENT

4.1 STRUCTURAL ANALYSIS

A structural analysis approach was used for our service life assessment. In this study, grain safety margins were determined by comparing the predicted induced stresses with the measured failure criteria (where margin of safety = [capability-induced stress or strain]/induced stress or strain). No corrections (safety factors) were made for uncertainties in axiality, material properties, failure criteria, etc. For the thermal shock test, a comparison between the predicted stresses from the non-linear viscoelastic FE analysis with the measured maximum stresses at +50°C and -25°C gave grain safety margins of 2.8 and 0.4 for the hot and cold cycles respectively. This suggests that mechanical damage is likely to occur in the motor during the cold cycle in the thermal shock test. This was observed in the instrumented and uninstrumented motors subjected to the thermal shock test.

To date failure has not occurred in the motors subjected to the thermal cycling, accelerated ageing and ambient ageing tests.

4.2 BALLISTIC PERFORMANCE

The two uninstrumented motors which were subjected to the thermal shock test were radiographed at the end of the first and second thermal shock cycles and then after every two cycles. Long axial cracks were visible after the fourth cycle, consistent with the stress sensor measurements from the instrumented motor subjected to the thermal shock test. The two uninstrumented motors were left at ambient temperature for ca. 9 months and radiographed before static firing and dissection. The radiographs showed that the cracks have closed up during storage at ambient temperature. In order to determine whether permanent rehealing had occurred, these motors were conditioned at -40°C for 27 hours and radiographed at -40°C and also at ambient temperature. Cracks reappeared when the motor was conditioned at -40°C and remained opened when the motor was radiographed at 22°C, indicating that although the cracks closed up during storage at ambient temperature, they provided defect sites for cracks to initiate and propagate when the motor was conditioned at -40°C. One of the two uninstrumented motors (Pictor 12), where a long axial crack was present, was then statically fired at -40°C.

Fig. 15 shows a comparison of the pressure-time profile of the Pictor 12 motor, which had a long axial crack near the head end of the motor, with that for a motor (with a similar burning rate) without any cracks (Pictor 13) statically fired at the same temperature. There was a 15% increase in pressure and 10% increase in thrust due to the presence of the crack(s) and/or ageing. Although the crack was near the head end of the motor, the pressure increase occurred over most of the burn time. The increase in pressure during the early burning phase may be due to changes in propellant and/or bondline properties as a result of ageing. The increased thrust resulted in a corresponding decrease in the burning time of this motor. There was a 3-4% reduction in burning time compared to the motor without cracks fired at the same temperature (-40°C). Thus, although the increase in thrust due to the presence of the crack and/or ageing is below the maximum operational thrust limit of the motor, ie. the motor is still safe for firing, there was a reduction in burning time which can be highly critical to performance.

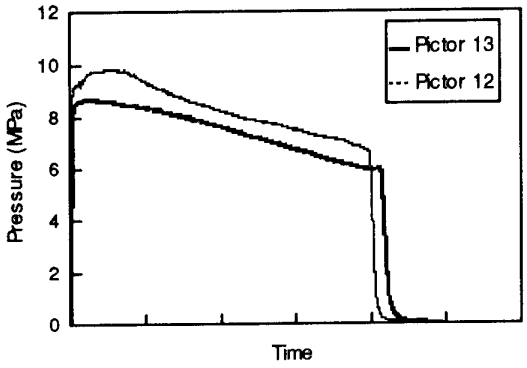


Fig. 15 - Pressure-Time Profile at -40°C

5. REFERENCES

1. F.N. Kelly and J.L. Trout, "Elements of Solid Rocket Service Life Prediction" AIAA Paper No. 72-1085, AIAA/SAE 8th Joint Propulsion Specialist Conference, New Orleans, Louisiana, Nov. 29-Dec.1 (1972).

2. " Tools Required for Meaningful Service Life Prediction", JANNAF Structural and Mechanical Behaviour Working Group Publication, March (1974).

3. E.C. Francis and J. Buswell, "Service Life Prediction and Testing of Composite Rocket Motors", 20th International Conference of ICT on Environmental Testing in the 90's, Karlesruhe, Germany, June (1989).

4. E.C. Francis, R.L. Peters, W.L. Hufferd, "Considerations in the Applications of Nonlinear Structural Materials", Second International Conference on Mechanical Behaviour of Materials, Boston, Mass., August (1976).

5. W.L. Hufferd and J.E. Fitzgerald, "Permanent Memory Effects in Solid Propellants", Proc. 1974 JANNAF SMBW and DSWG Meeting, CPIA Publications #253, July (1974).

6. E.C. Francis and C.H. Carlton, "Some Aspects of Composite Propellant Nonlinear Behaviour in Structural Applications", AIAA Paper 468-519 ICRPG/AIAA 3rd Solid Propulsion Conference, Atlantic City, New Jersey, June 4-6 (1968).

7. S.Y. Ho and E.C. Francis, "Instrumented Rocket Motor Service Life Program", Proceedings of the 36th AIAA/ASME/SME/ASCE/AHS/ASC Structures, Structural Dynamics, and materials Conference, New Orleans, LA, USA, April (1995).

8. R.B. Beyer, "Nonlinear Mechanical Behaviour of Solid Propellants", AIAA 6th Solid Propellant Conference, Paper 65-159, Washington, D.C., February (1965).

9. K.W. Bills, Jr., W.D. Hart and W.E. Holland, "Effects of Dewetting and Volume Change on the Tensile Behaviour of Solid Composite Propellants", JANNAF Physical Propulsion Panel, 20th Meeting Bulletin I, 61 (1961).

10. R.A. Schapery, "A Theory of Nonlinear Thermo-viscoelasticity Based on Irreversible Thermodynamics", Proceedings of the 5th U.S. National Congress of Applied Mechanics, 511-530 (1966).

11. M.E. Gurtin and E.C. Francis, "On a Simple Rate Independent Model for Damage", AIAA/ASME/SAE 16th Joint Propulsion Conference Paper #80-1176, Hartford, CT.

12. E.C. Francis and R.E. Thompson, "Normal Stress Transducer Behaviour", AIAA/SAE/ASEE Joint Propulsion Conference, Orlando, Fl, July 16-19 (1990).

13. E.C. Francis and R.E. Thompson", Bond Stress Transducer Design for Solid Propellant Rocket Motors", Journal of Spacecraft and Rocket, Vol. 18, No. 5, pp. 411-417, Sept-Oct. (1980).

14. E.C. Francis and W.E. Briggs, "Solid Propellant Stress Transducer Considerations", 26th International Instrumentation Symposium, Instrumental Society of America, Seattle, WA, May (1980).

15. E.C. Francis and W.E. Briggs, "Solid Propellant Stress Transducer Evaluation", 24th International Instrumentation Symposium, Instrumental Society of America, Albuquerque, N.M., (1978).

16. E.C. Francis and R.E. Thompson, "Subscale Motor Stress-Free Temperature Shift", JANNAF Structures and Mechanical Behaviour Conference, Pasadena, CA (1981).

17. S.Y. Ho and D.A. Tod, "Mechanical Failure Analysis of Rubbery Composite Propellants Using a Modified Fracture Mechanics Approach", 21st International Conference of ICT, Karlesruhe, Germany, July (1990).

18. S.Y. Ho, "Viscoelastic Response and Hysteresis Characteristics of Rubbery Composite and Thermoplastic Elastomer Propellants", Proceedings of the 16th TTCP WTP-4 (Conventional Weapons) Meeting, USA (1991).

19. S.Y. Ho and C.W. Fong, *J. Mater. Sci.* 22, 3023 (1987).

SOLID ROCKET MOTOR SERVICE LIFE PREDICTION USING NONLINEAR VISCOELASTIC ANALYSIS AND A PROBABILISTIC APPROACH

Gerald A. Collingwood
Michael D. Dixon
Thiokol Corporation
Mail Stop 254, P.O. Box 707
Brigham City, Utah 84302-0707, USA

Laurie M. Clark
Utah State University
Civil Engineering Dept.
Logan, Utah 84322-4110, USA

Eric B. Becker
University of Texas
Austin, Texas 787517, USA

ABSTRACT

Three critical factors were used to determine the Service Life Estimate for a solid rocket motor. First, the material property aging trends over time were evaluated. Second, an accurate structural analysis was performed. In this work, Nonlinear Viscoelastic (NLVE) analysis techniques were used to provide the most accurate assessment of propellant behavior. Finally, a probabilistic approach was applied, incorporating test data, aging trends, and variations of input parameters to obtain the service life. Development of the approach included an evaluation of various NLVE constitutive theories and their verification in laboratory tests using subscale motors. The approach was applied to a solid rocket motor using 3D NLVE analysis and the probabilistic service life estimate methodology.

LIST OF SYMBOLS

a_T	Viscoelastic time-temperature shift factor
C	Deformation tensor
dev	Deviatoric part of a tensor (also denoted by a bar over the symbol for the tensor)
F	Capability bias factor
G	Shear relaxation modulus
$\bar{I}_1$	Octahedral invariant
J	Ratio of material volume before and after deformation
K	Bulk Modulus
p	Pressure or mean normal stress
P_f	Probability of failure
S	Second Piola Kirchoff stress
t	Time
T	Temperature
U	Strain energy
α,β	Ozupek dilatation parameters
ε	Strain
$\dot{\varepsilon}$	Strain rate
ξ	Reduced time
ϕ	Normal Distribution function
σ	Standard deviation
τ	Integration variable for relaxation time

1. INTRODUCTION

Rocket motor service life can be predicted with a high degree of confidence using a probabilistic approach. This paper describes how the method was used to obtain the service life estimate for the rocket motors used in a missile system. First, an overview of the service life methodology is presented. Major components of service life methodology are discussed in detail. These include material testing and the evaluation of material aging trends, development and verification of NLVE constitutive models, the NLVE analysis of the full-scale motor, and finally, a detailed discussion of the probabilistic analysis that resulted in the service life estimate.

2. SERVICE LIFE METHODOLOGY

The most preliminary phase of the service life prediction program consisted of a failure modes and effects analysis. The most critical age sensitive failure modes for the motor were identified, and aging and surveillance efforts then focused on monitoring those critical failure modes. For the motor under consideration, cracking of the propellant grain in a transition area known as the "lip" was found to pose the greatest risk of failure for the system. Structural safety factors in the region were the lowest in the motor, and the propellant was extremely sensitive to the effects of aging.

In the next phase of the program, testing and analysis were completed to quantify the aging trends for age-sensitive materials. In our case, testing focused on the propellant grain and its associated bondlines. Material property tests of the propellant were designed to provide two different types of information about the propellant used in a solid rocket motor. First, the aging trends for the propellant were established. Degradation of the propellant capability over time is common, and some propellants may stiffen as they age. Second, sufficient property data was needed to fit propellant constitutive models used for the NLVE analysis. Once the data had been gathered, aging trends were assessed, and predictive equations for propellant modulus and capability were obtained. The evaluation of material aging trends is discussed in detail in Section 3.

Paper presented at the AGARD PEP Symposium on "Service Life of Solid Propellant Systems" held in Athens, Greece, 10-14 May 1996, and published in CP-586.

The next major task was to determine the induced loads that occurred in the motor under storage and operating conditions. Initially, our induced load assessments came from conventional linear elastic finite element analysis of the motor. However, the assessment was determined to be unduly conservative, and, when used for service life calculations, shortened the motor life to an unacceptable point. A more accurate nonlinear viscoelastic approach was employed to provide better induced load predictions for the service life estimate. This approach required additional effort to develop and calibrate appropriate NLVE constitutive models for the propellant. To validate the constitutive models, we compared analytical predictions with experimental results for several test specimens and subscale motors. Sections 4 and 5 describe the development and validation of our NLVE constitutive models, and the full-scale analysis is discussed in Section 6.

The final step in the service life prediction methodology was to develop a curve showing the probability of failure as a function of motor age. For this motor, the service life estimate was the point on the curve corresponding to a 2.5% probability of failure. The calculations incorporated the induced load predictions and material aging trends, as well as the variability of the material input properties, material capabilities, operating loads and environments. The approach is summarized in Section 7.

3. EVALUATION OF MATERIAL AGING TRENDS

To determine the aging trends for the solid rocket motor, propellant was excised from ten excise motors, one dissect motor, and propellant cartons. The dissect motor was a 28 year old motor from which detailed baseline material characterizations were completed. The excise motors, which covered a range of ages, provided propellant specimens for determining aging trends. Propellant was removed from the slotted section of the excise motors. The excise motors were carefully selected from the operational force to fulfill the requirements of the aging and surveillance program. Each motor was representative of the operational force in terms of age, and each had been exposed to a typical range of environments (e.g., storage temperatures and humidity) and loads (e.g., vibration due to transportation and vertical slump during storage). Some motors also had cartons available for testing, allowing us to determine the carton-to-motor bias for the propellant based on material property testing. A consistent bias between carton and motor data would allow the structural analyst to draw upon an extensive database of carton test results for material characterization.

Relaxation Modulus. Relaxation modulus testing provided the backbone for structural analysis of viscoelastic materials, governing the induced loads in the motor. The standard JANNAF Class A dogbone specimen was used for propellant relaxation modulus testing. The specimens were rapidly loaded to a strain level of 5% and held at that level while changes in the load were monitored. Tests were performed under ambient and 1000 psi pressure, over temperatures ranging from -40 to 130°F. Figure 1 shows the temperature shifted relaxation modulus data fit with a Prony Series for the propellant. The inset shows a shift function used to account for the viscoelastic time-temperature equivalence. The shift function relates log a_T to temperature, and is of the Williams-Landel-Ferry form.

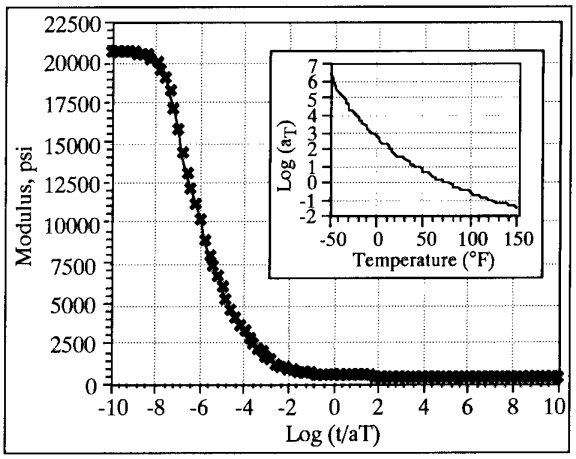


Figure 1. Prony Series Fit to Stress Relaxation Data. The Inset Shows the Time-Temperature Shift Function.

Aging evaluation of propellant relaxation modulus from the excise motors showed no significant trend. Linear regression of unpressurized relaxation modulus data at the time corresponding to the pressure rise time and 3% strain resulted in a very low correlation coefficient ($r \approx 0.14$). Analysis of the pressurized relaxation modulus data at the rise time and 3% strain showed similar results. Based on these results, the service life estimate assumed that the relaxation modulus for this propellant remained constant with age.

Propellant Capability Propellant failure properties, or capabilities, were derived from uniaxial tensile testing of propellant extracted from the 28 year old dissect motor, the excise motors, and the aged cartons. Testing was conducted at several rates and temperatures; and at ambient pressure and 800 psi pressure. The uniaxial data were acceptable to predict failure for this motor because the uniaxial and biaxial strain data compared closely with each other. This is an important result since for some propellants the strain capability of the propellant is affected by the stress field (e.g., the stress field at a motor bore is biaxial).

The strain at maximum true stress was selected as the failure criterion for propellant cracking. This assumption was conservative, since beyond the point of maximum true stress on the uniaxial tensile stress-strain curve, the strain will increase until failure occurs without additional load.

Comparison of the propellant uniaxial tensile data from the six excise motors and the associated cartons showed a very

consistent bias. The maximum stress data showed that the carton data was approximately 15 to 20 psi higher than the motor data. The strain at maximum stress data showed that the carton data was approximately 2 to 3% higher than the motor data. This information was very useful because it would enable us to utilize carton data for predicting grain failure if necessary.

The strain capability master curve was derived from pressurized uniaxial tensile testing with material from the dissect motor. The testing conditions included four temperatures and three strain rates at 800 psi. The strain at maximum stress was plotted as a function of the temperature shifted strain rate ($\dot{\varepsilon}a_T$). (See Figure 2). The average of four different areas was calculated for each data point.

$$\varepsilon_{capability} = -0.783\ (\log \dot{\varepsilon}a_T)^2 + 0.709\ (\log \dot{\varepsilon}a_T) + 30.988 \quad (1)$$

Each strain data point was temperature shifted according to the corresponding maximum stress data. The temperature shift factor ($\log a_T$) is plotted as a function of temperature. The resulting linear regression was:

$$\text{Log}(a_T) = 3.919 - 0.0505T \quad (2)$$

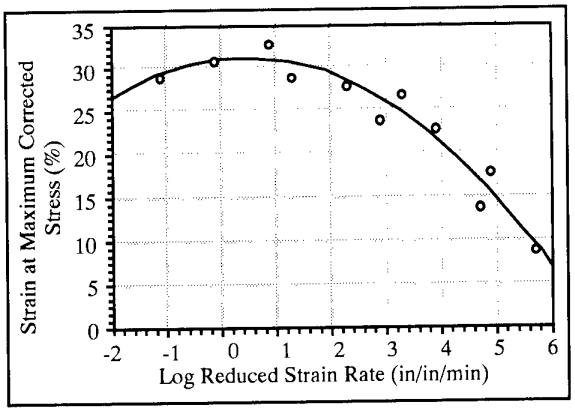


Figure 2. Propellant Strain Capability as a Function of Strain Rate.

The equation used to calculate the strain rate was:

$$\dot{\varepsilon} = \frac{\varepsilon_{induced}}{t_{rise}} \quad (3)$$

In Equation 3, $\varepsilon_{induced}$ was the maximum induced strain in the propellant grain at maximum chamber pressure due to the pressure and acceleration load (in/in), and t_{rise} was the time to achieve maximum chamber pressure (in minutes).

The aging trend for the strain capability curve was derived from excise and dissect motor pressurized uniaxial tensile testing at 77°F and 20 ipm since the temperature and strain rate are similar to the motor grain ignition conditions. A linear regression was fit to the ten excise motor and two dissect motor points. (See Figure 3)

$$\varepsilon_{capability} = 49.39 - 0.428\ t \quad (4)$$

where time is expressed in years, and strain capability is in percent.

The 28-year point on the excise motor linear regression line (Equation 4) was reduced by a bias factor, F, to account for the differences between the temperature and strain rate at critical operating conditions and those occurring during capability testing. The equation used to determine the factor was:

$$F = \frac{\varepsilon_{capability}(\text{Operating Temperature, Critical } \dot{\varepsilon})}{\varepsilon_{capability}(\text{Ambient Temperature, Test } \dot{\varepsilon})} \quad (5)$$

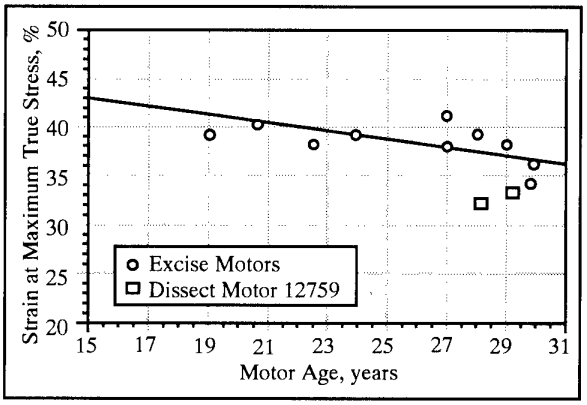


Figure 3. Aging Trend for Propellant Strain Capability

Strain capability at the 28-year point was calculated to be 37.38% using Equation 4. The F factor was calculated as (28.92%/31.00%) or 0.933. Therefore, strain capability at the 28-year point was reduced (0.933 x 37.38%) to 34.88%. Also, the slope of the excise motor linear regression was reduced by the same factor (0.933 x 0.428) to 0.399% per year. The Y-intercept for the 0.399%/year slope was calculated as 46.06%. The new strain equation was generated using the new slope and Y-intercept:

$$\varepsilon_{capability} = 46.06 - 0.399\ t \quad (6)$$

The new strain capability equation was used to calculate strain capability for the propellant under pressurized conditions at the critical strain rate and temperature. The failure properties of the propellant at ignition conditions decrease at the rate of 0.399% strain per year. The baseline strain capability was 46.06%.

4. DEVELOPMENT OF NONLINEAR VISCOELASTIC CONSTITUTIVE MODELS

Although the nonlinear viscoelastic (NLVE) behavior of solid propellants has been acknowledged for many years, only recently has an NLVE analysis approach become computationally feasible. Using test specimens and subscale motors, we applied some NLVE models currently

available in two commercial finite element codes. Several different constitute theories were evaluated for the propellant by analyzing test specimens and subscale motors. By comparison of analysis results with experimental data, the validity of the models was assessed, and areas for constitutive model improvement were identified.

All of the models referenced in this paper were evaluated using the TEXPAC finite element code developed by Dr. Trent Miller at Mechanics Software, Inc. The TEXPAC codes descended from the TEXGAP family of codes that were recommended by the Chemical Propulsion Information Agency (CPIA) for use in the analysis of solid propellants. The TEXPAC codes offer several hyperelastic models such as the Mooney-Rivlin, Rivlin polynomial, Ogden, Peng-Landel, and variations of Peng. Viscoelasticity may be incorporated into all of these hyperelastic models by combining them with a stress relaxation function. In addition, TEXPAC also provided damage functions to incorporated damage effects into the nonlinear viscoelastic models. These included the Swanson damage model, the Simo damage model, and the Ozupek damage and dilatation model.

Each of the NLVE models used strain energy density functions to describe the elasticity of the material together with a single relaxation function to describe the rate dependence of the response. The viscoelastic materials are assumed to behave entirely elastically in bulk; the rate dependence applied only to the deviatoric part of the response.

The stress-strain equations are written using the material description. Separating deviatoric and bulk terms gives:

$$S = 2J^{-\frac{2}{3}}\,\mathrm{dev}\left[\frac{\partial \bar{U}}{\partial \bar{C}}\right] + pJC^{-1} \tag{7}$$

where:

- S is the second Piola Kirchoff stress.
- $\bar{U}$ is the deviatoric part of the strain energy function.
- $\bar{C}$ is the deviatoric part of the deformation tensor.
- J is the ratio of volumes of a material after and before deformation.
- p is pressure or mean normal stress.

Assuming that the deviatoric part of the stress relaxes in proportion to the relaxation function, the full viscoelastic model is written as:

$$S(t) = 2J^{-\frac{2}{3}}\,\mathrm{dev}\left[\int_0^t G\left(\xi(t)-\xi(\tau)\right)\frac{\partial}{\partial\tau}\,\mathrm{dev}\left[\frac{\partial \bar{u}}{\partial \bar{C}}\right]d\tau\right] + pJC^{-1} \tag{8}$$

The reduced time, ξ, is used to account for shifts in the time scale due to temperature changes.

Hyperelastic Models. A number of hyperelastic models, including Mooney Rivlin, Rivlin polynomial, Ogden, and Peng were evaluated in conjunction with these studies. [1] However, because they did not account for damage effects, they did not adequately model the behavior of this propellant. During our preliminary evaluation of test specimens and subscale motors, it became apparent that we needed to modify the hyperelastic constitutive models to fully account for damage effects.

Basic Damage Models. The TEXPAC finite element codes (2-D and 3-D) have two damage functions available that may be incorporated with any NLVE constitutive model. These damage functions, which were developed for use in propellant analysis, are the Simo and Swanson models. [2,3]. Each uses a single relaxation function together with a constitutive model for finite strain elasticity. Our best results were obtained using the Simo model, discussed below.

Simo. For the Simo model any form of the strain energy density function, such as a polynomial in the deformation invariants or Ogden's principal stretch model, can be used. The model contains a damage functional inside the hereditary integral that modifies the deviatoric stress. The argument of the damage functional is the maximum distortional energy over history. The model assumes near (or complete) incompressibility. Simo's constitutive equation for a NLVE material with damage is:

$$S = J\frac{\partial U^0}{\partial J}C^{-1} + J^{-2/3}\,\mathrm{dev}\left\{\int_0^t G(t-\tau)\,\tilde{g}\frac{\partial}{\partial\tau}\,\mathrm{dev}\left[2\frac{\partial \bar{U}}{\partial \bar{C}}\right]d\tau\right\} \tag{9}$$

In Equation 9, the strain energy:

$$U = U^0(J) + \bar{U}(\bar{C}) \tag{10}$$

is a separable function of the dilatation J (i.e., the determinant of the deformation gradient), and the volume-preserving part of the right deformation tensor.

This energy is typically augmented with a constraint to treat nearly incompressible materials. For example, for incompressible materials the constraint, J - 1 = 0, is introduced into the strain energy by means of a Lagrange multiplier and at equilibrium, this constraint is satisfied to within some prescribed tolerance.

For nearly incompressible materials (i.e., materials with high Poisson's ratio), the constraint, $J = \hat{J}$, is enforced and the energy depends explicitly upon $\hat{J}$. For example:

$$U = \frac{K}{2}\left(\hat{J}-1\right)^2 + \bar{U}(\bar{C}) \tag{11}$$

The scalar damage functional may evolve in a variety of ways, though care must be taken to provide a symmetric tangent stiffness tensor. The notation dev[**A**] for some symmetric tensor **A** is defined by:

$$\mathrm{dev}[A] = A - A{:}C\,C^{-1} \tag{12}$$

and is the appropriate form of the deviator in the reference configuration.

Ozupek Dilatation Model. The Ozupek dilatation model [4] is a modification applicable to either the Swanson or Simo model. It includes a constraint on the dilatation coupled to the distortion:

$$\hat{J} - 1 = \frac{p}{K} + \alpha e^{[\beta p]\bar{I}_\gamma} \tag{13}$$

Where p is the mean stress, K is the bulk modulus, and $\bar{I}_\gamma$ is the octahedral invariant of $\bar{C}$. The octahedral invariant is as follows:

$$\bar{I}_\gamma = \frac{1}{3}\left(2\,\bar{I}_1^2 - 6\,\bar{I}_2^2\right)^{1/2} \tag{14}$$

The material parameters A and B determine the extent of the dilatation due to distortion and the sensitivity to pressure, respectively. The model referred to as Ozupek is actually the Ozupek dilatation model and was applied as an extension of the basic Simo model.

To develop the Ozupek model, pressurized dilatation data was obtained for the propellant. A gas dilatometer was used to monitor the volume change of a modified JANNAF Class C specimens subjected to uniaxial loading applied at a constant rate of 2.0 inches per minute. Volume dilatation measurements were made at test pressures ranging from 0 to 1000 psig crosshead speed of 2.0 inches per minute. Figure 1 shows the marked effect that an applied pressure of 100 psi has on the measured stress and volume dilatation for this propellant. Except at low strain, these data showed that the propellant increased in volume when specimens were strained under pressure. (See Figure 4) This phenomena, which may be attributed to damage, is not accounted for by any of the other constitutive models.

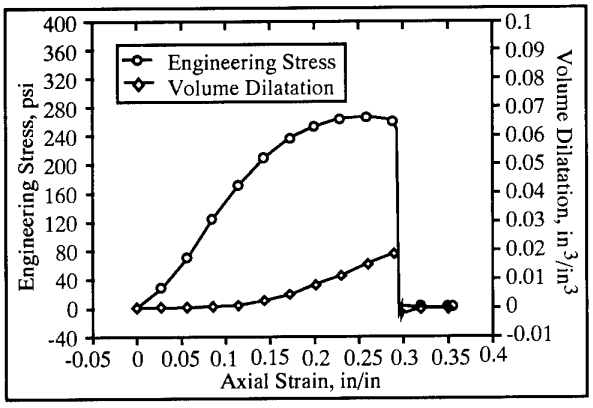


Figure 4. Propellant Dilatation Data Showing How Damage Causes an Apparent Increase in Volume under Uniaxial Tensile Loading

5. VALIDATION OF NLVE CONSTITUTIVE MODELS

The NLVE analyses of the test specimens and subscale motors demonstrated that the approach was both feasible and accurate. [1] Comparison of analysis results and experimental data allowed a relative ranking of the constitutive models, and we determined that, overall, the Ozupek model provided the best predictions, followed by Swanson, and Peng. Among the models evaluated, the Rivlin and Ogden models provided the least accurate predictions. Although the Peng model appeared to do an excellent job of describing the behavior of the test specimens, the Ozupek and Swanson models were both more accurate for subscale motor analysis, which more closely approximates actual motor conditions. Application of different damage functions might improve the analytical predictions, but it was evident from the results of thermal cooldown loading on a subscale that a dilatation model, such as the one incorporated in Ozupek's model, is necessary.

6. NLVE ANALYSIS OF THE FULL-SCALE SOLID ROCKET MOTOR

The NLVE analysis of the full-scale motor provided the induced loads for the service life estimate. The 3D loaded motor model included the case, liner, insulation, inhibitor and propellant. A single computer run was required to model the load history of the motor, which included storage environments (thermal history and vertical slump loads), and operational loads (the ignition pressurization curve and launch acceleration).

Storage loads, including vertical slump and thermal cooldown of the motor from its stress free casting temperature to the minimum storage and operating temperature was modeled in five equal increments of a time of 10,000 minutes. This time scale corresponded to the time at which the equilibrium modulus was predicted by the Prony series, and thus approximated the long-term storage condition at low temperature.

Pressurization of the motor was approximated by the piecewise linear function shown in Figure 5. Pressure loads were applied to the surface of the propellant in a total of nine increments. The first 0.1 seconds of pressurization was modeled in three increments as the pressure load was ramped for 0 to 590 psi. Between 0.21 and 0.35 seconds, induced loads were calculated at three increments as the pressure was held at a constant level of 590 psi. Finally, between 0.35 and 0.5 seconds, the pressure was ramped from 590 to 900 psi in three increments.

The 3D NLVE analysis predicted that the maximum induced strain was 25.16%, occurring in the lip region of the propellant grain.

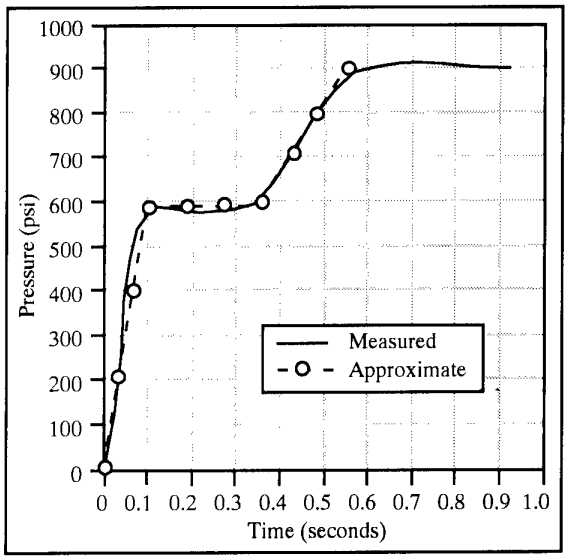


Figure 5. Comparison Between Actual Motor Chamber Pressure and Approximate Pressure Used for NLVE Analysis

History plots showing the deviatoric stress component and the maximum principal strain at the propellant lip during the ignition transient are shown in Figure 6. Although the strain response is proportional to the input loading, the stress response is highly nonlinear.

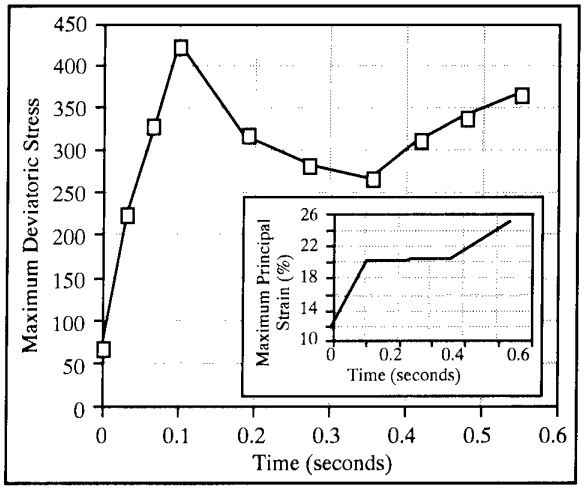


Figure 6. Deviatoric Stress Occurring at the Propellant Lip during the Ignition Transient. The Inset Shows the Corresponding Maximum Principal Strain

7. SERVICE LIFE PREDICTION

A probabilistic approach was used to obtain the service life prediction rather than the margin of safety and or factor of safety calculation. The probabilistic approach implies a factor of safety of 1, where the predicted induced loads are equal to the material capability. A statistical model was developed that incorporated the induced strain (calculated) and strain capability (measured), as a function of age, and used the corresponding standard deviations of these values. The probability of a grain crack as a function of age was calculated from this statistical model. The induced strain value included induced strain due to thermal cooldown, vertical slump, pressurization, and flight acceleration. Other variables incorporated into the service life prediction were the statistical variations of modulus, pressure, ignition rise rate, coefficient of thermal expansion.

The equation used to calculate the probability of a grain crack as a function of age was of the form:

$$P_f = \text{Probability}(\varepsilon_{capability} < \varepsilon_{induced}) \tag{15}$$

$$P_f = 1 - \phi\left[\frac{\varepsilon_{capability} - \varepsilon_{induced}}{\left(\sigma^2_{capability} + \sigma^2_{induced}\right)^{1/2}}\right] \tag{16}$$

ϕ, the cumulative normal distribution function, is evaluated using statistical tables to determine the area under the normal distribution curves. $\sigma_{capability}$ and $\sigma_{induced}$ represent the standard deviations of age-dependent material strain capability and induced strain.

Variability of Applied Loads. The induced strain term included the induced strain due to the thermal cooldown, vertical slump, acceleration, and pressure load. The $\sigma_{induced}$ term accounted for the standard deviation of the material properties and applied loads that are input to the finite element codes. Variability in maximum pressure and rise rate was included in $\sigma_{induced}$. The standard deviation in maximum pressure standard, $\sigma_{maximum\ pressure}$ was calculated to be ± 21 psig. The max pressure variation caused the induced strain at the propellant lip to vary at ± 0.30% strain. The rise rate standard deviation, $\sigma_{rise\ rate}$, was assumed to be ± 0.033 seconds which caused the induced strain to vary at ± 0.025% strain. The variability of the strain free temperature, σ_{SFT}, was assumed to be 3.3°F. The strain free temperature variability caused the induced strain due to thermal cooldown to vary at ±0.52% strain.

Variability of Propellant Input Properties. The relaxation modulus used to analyze the effects of thermal cooldown, vertical slump, acceleration, and pressure was found to be constant with age. The standard deviation of the relaxation modulus data, $\sigma_{relaxation\ modulus}$, was ± 134 psi. The relaxation modulus variation caused the induced strain at the propellant lip to vary at ± 0.18% strain. The coefficient of thermal expansion (CTE) was also found to remain constant with age. If thermal expansion characteristics had shown aging effects, the service life estimate would not change significantly, although the slope of the reliability curve would become slightly steeper causing the force to age out at a higher rate. A coefficient of variation of 5% was

assumed for CTE which resulted in a $\sigma_{thermal}$ of ± 0.315 in/in/°F or ± 0.71% strain.

The standard deviation of the induced strain was calculated according to the following equation:

$$\sigma_{induced} = \pm(\sigma^2_{maximum\ pressure} + \sigma^2_{rise\ rate} + \sigma^2_{relaxation\ modulus} + \sigma^2_{thermal} + \sigma^2_{SFT})^{1/2} \quad (17)$$

$$\sigma_{induced} = \pm(0.30^2 + 0.025^2 + 0.18^2 + 0.71^2 + 0.52^2)^{1/2}$$

$$\sigma_{induced} = \pm\ 0.95\ \%\ strain$$

Motor Induced Loads. The maximum induced strain occurring in the motor, 25.16%, was obtained from the structural analysis. It included the combined effects of thermal cooldown, vertical slump, acceleration, and ignition pressure. Because modulus, coefficient of thermal expansion, and Poisson's ratio for propellant did not age, induced strain remained constant with age.

$$\varepsilon_{induced} = 25.2\ \%\ strain$$

Propellant Capability. The strain capability of the propellant was highly age-sensitive, and the following relationship was derived:

$$\varepsilon_{capability} = 46.1 - 0.40\ t$$

The derivation was presented in the section on evaluation of material aging trends. The standard deviation of propellant capability about the excise motor regression line (Equation 5) was calculated to be:

$$\sigma_{capability} = \pm\ 2.5\%\ strain$$

This calculated standard deviation, $\sigma_{capability}$, was assumed to be the variability of the propellant strain capability at the critical ignition conditions. The standard deviation of the strain capability translated to a coefficient of variation of approximately 5 percent, which is typical for propellant failure data. This value can be directly input to Equation 16 for the calculation of the probability of grain failure.

Probability of Failure. The probability of failure at the propellant lip was calculated by substituting the induced strain, strain capability, and variability into Equation 16:

$$P_f = 1 - \phi\left(\frac{(46.1 - 0.40\ t) - 25.2}{(2.5^2 + 0.95^2)^{1/2}}\right)$$

$$P_f = 1 - \phi\left(\frac{20.9 - 0.40\ t}{2.67}\right)$$

Figure 7 shows the resulting curve. For this system, the service life estimate was determined to be 39 years, the age at which 2.5% of the motors were predicted to exhibit grain cracking.

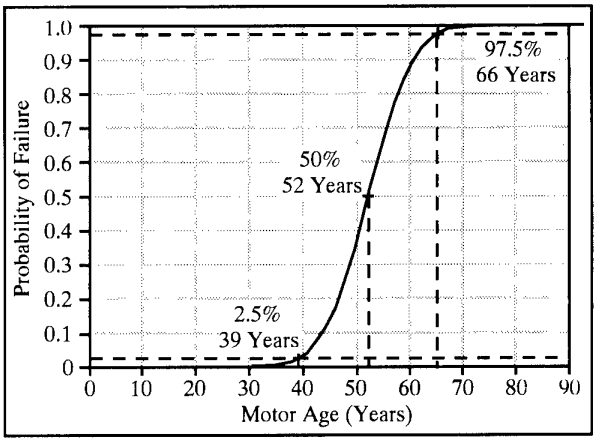


Figure 7. Probability of Propellant Grain Failure as a Function of Motor Age

8. CONCLUSIONS

The approach presented in this paper provided a rigorous approach to the service prediction for the solid rocket motor involved. Once an acceptable risk of failure is identified, the service life estimate for the motors can be taken directly from the probability of failure curve resulting from the analysis. As is evident from the probability of failure curve, the service life estimate for this motor is 39 years. The authors have high confidence in the service life estimate due to our incorporation of accurate 3-D NLVE analysis methods, our improved understanding of propellant aging trends, and the statistic foundation of the probabilistic approach.

9. REFERENCES

[1] "Evaluation of Nonlinear Viscoelastic Constitutive Models by Analyzing Test Specimen and Instrumented Subscale Motors," Gerald A. Collingwood, Michael D. Dixon, Laurie M. Clark, J. David Becker and Eric B. Becker, *1995 JANNAF Propulsion and Subcommittee Joint Meetings*, Chemical Propulsion Information Agency Publication No. Pending, December 1995.

[2] "On a Fully Three-Dimensional Finite-Strain Viscoelastic Damage Model: Formulation and Computational Aspects," J.C. Simo, *CNAME*, Vol. 60, pp. 153-173, 1987.

[3] "A Constitutive Formulation for High Elongation Propellants," S.R. Swanson and L.W. Christensen, *J Spacecraft and Rockets*, Vol 20, pp. 559-566, 1983.

[4] "Constitutive Equations for Solid Propellants," Sebnem Ozupek, Ph.D. Dissertation, University of Texas at Austin, 1995.

Paper Number: 29
Discussor's Name: I. H. Maxey
Responder's Name: G. A. Collingwood

Question: For the dilatation tests, would you advise that it was necessary to go to the higher pressures, e.g., 1000 psi for individual tests.

Answer: The dilatation tests should be run up to the highest pressure the motor will experience on ignition.

Paper Number: 29
Discussor's Name: D. I. Thrasher
Responder's Name: G. A. Collingwood

Question: 1. Did the propellant relaxation data corresponding to Figure 1 actually show the glassy response (implied in the figure) between 10 E -8 and 10 E -10 on the log (t/a_T) scale?
2. Could you comment on the lack of chemical approaches in the "Methodologies and Techniques for Predicting Service Life" session?

Answer: 1. No. The glass transition temperature was not measured.
2. I believe that Dr. I. Lee Davis (Thiokol) micro-constitutive theory incorporates the chemical aging mechanism and could produce the input material properties for the non-linear viscoelastic analysis codes. Also, when motors stored at high temperature are dissected and properties measured the chemical effect is accounted for but the actual mechanisms are not understood. There should be more interfacing and working together of the two groups.

Intrinsic Strength of Solid Propellant Bond Systems

Stress-Strain Behavior of Rectangular Bit-in-Tension With Rubber Materials

Sandra H. Slivinsky
Kirtland AFB
PL SXP, 3550 Aberdeen SE, NM, 87117-5776
USA
H. Peter Kugler, Harry Drude
Fiedler Optoelektronik GmbH
Oetzscher Weg 6
D-06686 Lützen
Germany

ABSTRACT
The deformation of bonded rubber samples is studied through use of an opto-electrical system, consisting of electronics, optics, and software. The system makes it possible to determine the stress-strain behavior of specimens tested in a tensile tester. Measurements are unique in that detailed localized information becomes available so that particular deformation behavior can be studied. The test series being reported was performed as a design of experiments so that a statistical analysis of variance could be applied to the results. The parameters studied were rubber flexibility, thickness, and order of sample stacking. Sample test data and the complete analysis of variance are presented, resulting in generalized equations for the parameters tested.

INTRODUCTION
An opto-electrical system has been used to study the deformation of a series of rubber samples in an effort to determine the detailed deformation occurring at bonded interfaces between both similar and different types of materials. The opto-electrical system was designed at Fraunhofer Institute in Pfinztal, Germany and then improved and manufactured by Fiedler Optoelektronik GmbH of Lützen, Germany. It consists of electronics and optical equipment coupled to a computerized data analysis package, which makes it possible to determine the stress-strain behavior of specimens tested in conventional configurations in a tensile tester. The unique particular contribution of this system in making these types of measurements lies in the detailed information which becomes available as to the deformation of regions of the sample being tested. Through application of reflective paint to the material and local integration of the reflected signal during the test cycle, a complete deformation history is obtained. This is beyond the capabilities of conventional testing and data acquisition systems.

BACKGROUND
The work discussed in this paper came about as a result of performing the testing under a Foreign Comparative Testing Program, begun in September, 1993. The objective of the "Bondline Energy Measurement System" program was to use the data from the tests to learn more about the local deformations in bonded stressed systems, so as to eventually lead to a calculation of the energy required to make a good bondline in solid rocket motors. The accurate evaluation and characterization of the propellant/liner/insulation bondline system in these motors is essential for assessing the structural integrity and margins of safety. A variety of analog specimens have been used to generate failure data for service-life predictions. However, while such samples continue to provide stress/strain data, there is very little agreement in the solid propulsion industry as to which design and testing criteria are best. There is a need to produce an accurate model to simulate bondline stresses. Through the use of the data obtained from the measurement technique reported on here, a new generalized approach may be realized. As it will be shown later in the paper, the desired output of the data obtained in the program is to yield data which provides information as to the contributions of the various deforming layers in any given sample configuration, to the overall fracture force.

For some portion of the program, inert propellant samples were tested. These samples consisted of some which had been especially constructed for the testing within this program, in various configurations and some which had been previously constructed for another purpose. These samples, when tested were subject to a large number of end-tab failures and the results were somewhat mixed. In addition, results from propellant samples are normally somewhat varied, since they have inherent differences (such as batch-to-batch variations due to mixing procedures).

Consequently, it was decided that a more consistent approach was required to correctly perform evaluations of the system in a timely manner, and to confine ourselves to solving the bondline problem with the opto-electrical system, avoiding the additional complications arising from using the propellant materials. This clearly led to the use of rubber materials, which could be counted on to provide consistent and repeatable results.

EXPERIMENTAL DESCRIPTION
A schematic of the system is shown in Figure 1. The output of the measurement is to the distribution of the longitudinal elongation. As is indicated by the figure, a collimated beam of a semiconductor laser in cw-mode is directed centrically onto a rotating mirror. The deflected beam scans the surface of the test specimen along a fixed scanning length or angle. The power of the laser is in the range of several milliwatt and the wavelength is 670 to 830 nm. At preselected areas of interest on the sample highly reflective contrasting fringes are applied. The technique for these consists of using a faint black primer, followed by a white or silver metallic coating through an adhesive masking foil. Diffuse scattering of the scanning laser light occurs at these fringes. The scattered light is collected by a lens and converted into an electrical

Paper presented at the AGARD PEP Symposium on "Service Life of Solid Propellant Systems" held in Athens, Greece, 10-14 May 1996, and published in CP-586.

signal via a photodiode. The signal is subsequently amplified and formed into a digital pulse train after passing through a complex constant fraction trigger unit. The time information within this pulse train, which corresponds to a scanning length of the sample is measured by a multi-stop-counter which has been specifically developed as a plug-in unit in a personal computer. In addition, the angular velocity of the scanning system is permanently captured and used to normalize the pulse train data as a definite measure of scanning length. The reference length between single stripes for the unstressed sample are recorded at the beginning of the experiment. As the sample is placed under load, the distance between the fringes and the corresponding time pattern in the electrical pulse train changes as the test proceeds. This change of the time pattern is analyzed on-line and subsequently transformed into strain values between the fringes on the sample.

Using these principles, the measurement system is self-calibrating. Long-term stability is achieved through the simultaneous measurement of the angular velocity of scanning. The precision of the measurement is a function of the scanning length, degree of contrast, scattering of the constant fraction trigger, scanning speed, short term scanning stability, noise in the laser output, and resolution of the multistop counter. The optimization of the counter occurs with an internal clock of 40 MHz and a depth of 16 bits.

For this system, the following parameters were achieved. The scanning length at the sample is 160 mm with a measurement accuracy of 3.5 micron, an active scanning time of about 1.5 msec, with a minimum fringe distance of 1 mm. The software evaluation of the measured data documents the principle statistical error of the measurement. The latter aids in the optimization of the scanning parameters. The average deviatation of the mean value for unstressed samples is 0.005% for a reflective length of 80 mm. The number of fringes used in these experiments was generally 16. The fringe thickness was 1 mm, with a minimum distance between fringes of 1 mm.

An additional feature of the system is that it is possible to change the data rate during the scanning process. Through the software, a selection can be made of the number of scans registered. This control can be accomplished either by a fixed time choice or by the dynamics of the measured data. For any given data set, consisting of a set of angular measurements for discrete stripes seen by the scanner, the analogue values of the force on the sample, the contraction, and the absolute time are stored. In this manner it is possible to combine discrete measurements in long-term creep experiments and observe cyclic loading for previously observed starting conditions. Details of the scanning system, detection of the optical signal, and signal processing have been previously discussed.[1]

As an intricate part of the experimental procedure, it was decided to use the design of experiments approach in determining the best set of samples to test. The design of experiments approach employs statistics and is sometimes called the 'Taguchi Method.'[2]. It is a powerful technique for deducing information from the results of a carefully designed sample group, while avoiding the testing of every possible combination of the materials. The method uses orthogonal arrays, in which design parameters are given different values (or factor levels). The focus of the technique is on the average effect that occurs as other conditions change. There is a pair-wise balancing property in that the parameter choice for each variable occurs with the parameter choice for all other factors the same number of times. Experiments using orthogonal arrays minimize experimental runs while maintaining this property. Such a technique results in a powerful form of planned experimentation which leads to information about alternatives. In the application of this technique to this work, a generalized equation in the tested parameters is the end result. This equation is reached by applying a statistical analysis of variance (ANOVA) to the experimental designs.

The rubber materials (polyethylene) used in this experimental design were chosen to be thick enough to provide interesting results and flexible enough to provide different results from specimen to specimen. It was also intended to keep the test matrix as simple as possible, while exercising the opto-electrical system. Accordingly, the test matrix was made up of 8 orthogonally independent specimens (called an L8) and three parameters were tested. These three parameters were: (1) the flexibility of the material (given by the durometer of the rubber), (2) the thickness of the samples, and (3) the assembled order of the rubber components.

A typical sample is shown in Figure 2, where the thickness stacking order of 1/8", 1/2", 1/2", 1/8" with the 1/2" material being 20 durometer. All of the 1/8" rubber material was of 60 durometer, since its purpose was to simulate a thin, rigid material; while the thicker material was either 10 or 20 durometer, simulating a pliable material. An epoxy based adhesive was used to attach the rubber components to each other and the aluminum end-tabs to the test samples. The complete test matrix is shown in Table 1. The results of a complete testing sequence can provide a quantitative expression for the variables tested as defined in the original test matrix. The physical construction of the samples was made to be that close to the types of samples known as rectangular bits-in-tension, which are used in testing in the United States to test the characteristics of the bondline.

TYPES OF DATA POSSIBLE WITH SYSTEM

Since the data obtained with this system is unique, it is important to discuss the various types of data plots which can be obtained by coupling the system with a tensile tester and applying a physical force across the samples. The first, overall stress vs. strain, is of the type which is routinely collected from tensile testing. Examples of such data are shown in Figure 3. If this were the only result from use of the system, it would not be especially interesting.

The results become considerably more interesting to view, if the data are broken down from painted stripe to painted stripe. These data are collected as part of the process, and the software provides the integrated results that have just been shown. What this system makes possible, is the view of the contribution of each portion of the specimen to the overall distortion or subsequent failure, and further definition of the failure site location. This possibility is demonstrated in Figure 4. What is seen in these figures are the strain vs. time plots for each pair of painted stripes. Additionally, the data can also be displayed as three dimensional plots of strain vs. zone vs. scan number, as shown in Figures 5 and 6. The zone refers to a pair of painted lines, where the zone number refers

to the stripes on either side. For example: zone 1 refers to the region between stripe 1 and stripe 2. A view may be plotted which shows strain vs. time. This type of plot is shown in Figure 7.

As the test proceeds, the number of laser scans continues to increase, following the detailed trajectory of the sample distortion. The sample tensile test rates can be controlled, as they can in conventional tensile testing procedures. (It would be ideal to follow the distortions, in weaker types of samples, through to failure.) The rubber samples were not taken to failure, since that would required very large extensions and it was more interesting to preserve the samples and reproduce the results for verification purposes. The samples were strained to a value of 15 - 20 % and then relaxed back to zero.

Using the detail provided by this technique, it is possible to determine the portion of the fracture force which is directly applicable to distorting or breaking the bond. Considering the problem, it becomes clear that only a portion of the force normally measured in conventional testing actually distorts or breaks the bond. If this small fraction of the force can be measured, it becomes possible to determine the intrinsic energy at the bondline. This is not possible by conventional methods, since only the overall or average result is obtained as a measured number.

RESULTS

For sample E, the full set of possible data plots are shown here in Figures 8-10. From the general character of the data, two maxima were observed for each data run and a single minimum. Since the data were observed over some period of time, there was some thought that a general statement could be made about the time dependence of the maxima and minimum. Accordingly, an analysis of variance was made on 2 levels of maximum strain, minimum strain, and for the (highest) maximum at 60, 120, and 180 seconds. For simplicity of presenting the calculations, the data tables contain a value of -1 for the lower of two values tested and 1 for the higher: in the case of durometer -1 = 10 durometer, 1 = 20 durometer; in the case of thickness, -1 = 1/2", 1 = 3/4", in the case of order -1 = thicker material outside of 1/8" (for example 1/2", 1/8", 1/8", 1/2"), 1 = thicker material inside the 1/8" (for example 1/8", 1/2, 1/2", 1/8"). The measured responses are the "Y" values and the ANOVA results are shown in each data table. The data are shown in Tables 2 - 7. Each table includes the equation for the expected response in a similar type of experiment in the variables tested. The desired result is for the overall strain to be the maximum possible, that is, the material should be as stretchable (or pliable) as possible, without breaking (in particular, at the bondlines). Accordingly, the choice for this result is that the durometer and thickness be minimum values, while the order should be the conventional one: thinner material external to the thicker material. The resulting equations are shown in Table 8. These equations can now be used to predict results at durometers and thickness not specifically tested in this series.

In the course of performing the experiments of the non-conventional order (of thickness), an apparent anomaly was observed. It is generally expected that wherever a layer of glue exists, that materials in the neighborhood should stretch more than the layer containing the glue, at least for our flexible materials. It was observed that this was not the case for this group of sample tests. That is, the observed maxima (% elongation) were in the zone of the glue layer. Since this was contrary to what was expected, a small subset of experiments were performed to determine the cause of this anomaly. A video camera set up in an opposite direction to that of the laser viewing side, that is, behind the sample, with similar markings or strips, was employed as an additional aid to determining the cause. It was observed that the maxima were caused by the flexible rubber material, literally wrapping itself around the glued or restrained regions. Once this was understood, the experimental test matrix, as described above, was completed and these data and calculations are included in the tables

CONCLUSION

It has been demonstrated that consistent local effects can be observed in rubber bonded materials with the opto-electrical system described above. The results can be generalized to samples other than those specifically tested in this series through the use of the design of experiments approach and the use of a statistical analysis of variance (ANOVA) applied to the types of observations during these tests. This work has set the foundation for using this experimental apparatus in the difficult problem of predicting failure modes in bondlines in any arena where materials are joined.

An especially interesting result arises from the unexpected observations made at glued surfaces. This is information about behavior at the bondline, which would not even be indicated in normal measurement techniques, since only the average behavior over the entire sample is measured. It is the detailed information about local effects which will lead to understanding the behavior at the bondlines in diverse types of materials.

REFERENCES

1. N. Eisenreich, C. Fabry, R. Fischer, A. Geissler, H.P. Kugler, and F. Sinn, (1987) Propellants Explos. Pyrotech. 12, 101

2. S. R. Schmidt, R. G. Launsby, (1989) "Understanding Industrial Design Experiments," CQG Ltd. Printing, Longmont, Colorado, USA

TABLE 1. SAMPLE TEST MATRIX

SAMPLE	RUN	DUROMETER	THICKNESS (IN)	ORDER
A	1	10	1/2	1/2, 1/8, 1/8, 1/2
E	2	10	1/2	1/8, 1/2, 1/2, 1/8
C	3	10	3/4	3/4, 1/8, 1/8, 3/4
F	4	10	3/4	1/8, 3/4, 3/4, 1/8
B	5	20	1/2	1/2, 1/8, 1/8, 1/2
Z	6	20	1/2	1/8, 1/2, 1/2, 1/8
D	7	20	3/4	3/4, 1/8, 1/8, 3/4
G	8	20	3/4	1/8, 3/4, 3/4, 1/8

IN ANALYSIS OF VARIANCE COEFFICIENTS, WHERE -1 IS LOWER VALUE, INVERSE ORDER

SAMPLE	RUN	A	B	C
A	1	-1	-1	-1
E	2	-1	-1	1
C	3	-1	1	-1
F	4	-1	1	1
B	5	1	-1	-1
Z	6	1	-1	1
D	7	1	1	-1
G	8	1	1	1

TABLE 2. MAXIMUM 1 STRAIN, RESPONSE MATRIX

SAMPLE	RUN	Y1	Y2	Y3	$\overline{Y}$	S.S
A	1	16	16.2	16.1	16.1	0.01
E	2	19.2	18.9	18.9	19	0.03
C	3	13.1	13	13.1	13.07	0.0034
F	4	15.5	15.7	15.7	15.63	0.0134
B	5	15.5	15.6	15.7	15.6	0.01
Z	6	16.5	17.4	17.9	17.27	0.5034
D	7	12	12	12	12	0
G	8	13.8	13.9	13.8	13.83	0.0034

AVERAGE $\overline{Y}$ = 15.31, SUM S.S = 0.5736

COEFFICIENTS CALCULATION:

	A	B	-A.B	C	-A.C	-B.C	A.B.C
AVERAGE -	15.95	16.99	15.23	14.19	15.07	15.29	15.25
AVERAGE +	14.68	13.63	15.39	16.43	15.56	15.33	15.38
DIFFERENCE	-1.27	-3.36	0.16	2.24	0.49	0.04	0.13

$\tilde{Y}$ = 15.31 - 0.64A - 1.68B + 1.12C - 0.08 (AxB) - 0.25 (AxC) - 0.02 (BxC) + 0.07 (AxBxC)

TABLE 3. MAXIMUM 2 STRAIN, RESPONSE MATRIX

SAMPLE	RUN	Y1	Y2	Y3	$\overline{Y}$	S.S
A	1	16.8	16.5	16.6	16.63	0.0234
E	2	17.4	17.1	17.1	17.2	0.03
C	3	12.6	12.7	12.6	12.63	0.0034
F	4	12.2	12.3	12.4	12.3	0.01
B	5	15.3	15.4	15.4	15.37	0.0034
Z	6	16	16.5	16.5	16.33	0.0834
D	7	11.5	11.5	11.4	11.47	0.0034
G	8	12.5	12.6	12.5	12.53	0.0034

AVERAGE $\overline{Y}$ = 14.31, SUM S.S = 0.1604

COEFFICIENTS CALCULATION:

	A	B	-A.B	C	-A.C	-B.C	A.B.C
AVERAGE -	14.69	16.38	14.46	14.03	14.53	14.21	14.18
AVERAGE +	13.93	12.23	14.16	14.59	14.08	14.41	14.43
DIFFERENCE	-0.76	-4.15	-0.3	0.56	-0.45	0.2	0.25

$\tilde{Y}$ = 14.31 - 0.38A - 2.08B + 0.28C + 0.15 (AxB) + 0.23 (AxC) - 0.1 (BxC) + 0.13 (AxBxC)

TABLE 4. MINIMUM STRAIN, RESPONSE MATRIX

SAMPLE	RUN	Y1	Y2	Y3	$\overline{Y}$	S.S
A	1	1.32	1.36	1.32	1.32	0.0016
E	2	3.36	4	4	3.79	0.1366
C	3	1.28	1.28	1.28	1.28	0
F	4	6.6	6.6	6.6	6.6	0
B	5	2.88	3.52	3.36	3.25	0.1110
Z	6	5.52	5.76	5.6	5.63	0.0015
D	7	3.36	3.28	3.44	3.36	0.0064
G	8	4.8	4.9	4.9	4.87	0.0034

AVERAGE $\overline{Y}$ = 3.76, SUM S.S = 0.274

COEFFICIENTS CALCULATION:

	A	B	-A.B	C	-A.C	-B.C	A.B.C
AVERAGE -	3.25	3.50	3.34	2.31	3.28	4.01	4.23
AVERAGE +	4.28	4.03	4.22	5.22	4.25	3.51	3.30
DIFFERENCE	1.03	0.53	0.88	2.91	0.97	-0.5	-0.93

$\tilde{Y}$ = 3.76 + 0.52A + 0.27B + 1.46C - 0.44 (AxB) - 0.49 (AxC) + 0.25 (BxC) - 0.47 (AxBxC)

TABLE 5. STRAIN AT 60 SECONDS, RESPONSE MATRIX

SAMPLE	RUN	Y1	Y2	Y3	$\overline{Y}$	S.S
A	1	6.6	7.8	7.5	7.3	0.39
E	2	7	9	8.75	8.25	1.186
C	3	5.3	5.3	5.3	5.3	0
F	4	6.24	6	6	6.08	0.0192
B	5	6.2	6	6	6.07	0.0134
Z	6	6	6.13	6.25	6.13	0.0157
D	7	5	5	4.5	4.83	0.0834
G	8	5.8	6	6	5.93	0.0134

AVERAGE $\overline{Y}$ = 6.24, SUM S.S = 1.7211

COEFFICIENTS CALCULATION:

	A	B	-A.B	C	-A.C	-B.C	A.B.C
AVERAGE -	6.73	6.94	6.58	5.88	6.17	6.35	6.04
AVERAGE +	5.74	5.54	5.59	6.60	6.31	6.13	6.39
DIFFERENCE	-0.99	-1.4	-0.99	0.72	0.14	-0.22	0.35

$\tilde{Y}$ = 6.24 - 0.5A - 0.7B +0.36C + 0.5 (AxB) - 0.07 (AxC) + 0.11 (BxC) + 0.18 (AxBxC)

TABLE 6. STRAIN AT 120 SECONDS, RESPONSE MATRIX

SAMPLE	RUN	Y1	Y2	Y3	$\overline{Y}$	S.S
A	1	15	15.5	16	15.5	0.25
E	2	17	18	17.75	17.58	0.2709
C	3	11	11	13	11.67	1.333
F	4	10.75	12.25	12.25	11.75	0.75
B	5	14	13.8	13.8	13.87	0.0134
Z	6	14.75	15.13	16	15.29	0.4107
D	7	11	11	10.5	10.83	0.0834
G	8	12.15	12.5	12.5	12.38	0.0409

AVERAGE $\overline{Y}$ = 13.61, SUM S.S = 3.152

COEFFICIENTS CALCULATION:

	A	B	-A.B	C	-A.C	-B.C	A.B.C
AVERAGE -	14.13	15.56	14.08	12.97	13.71	13.38	13.34
AVERAGE +	13.09	11.66	12.39	14.25	13.51	12.18	13.88
DIFFERENCE	-1.04	-3.9	-1.69	1.28	-0.20	-1.2	0.54

$\tilde{Y}$ = 13.61 - 0.52A - 2.0B + 0.64C + 0.85 (AxB) + 0.10 (AxC) + 0.6 (BxC) + 0.27 (AxBxC)

TABLE 7. STRAIN AT 180 SECONDS, RESPONSE MATRIX

SAMPLE	RUN	Y1	Y2	Y3	$\overline{Y}$	S.S
A	1	9.4	9	8.8	9.07	0.0934
E	2	11.25	10.25	10.25	10.58	0.3334
C	3	9.8	9.5	9.5	9.6	0.03
F	4	11.5	11	11	11.17	0.0834
B	5	8.9	8.8	9	8.9	0.01
Z	6	10.5	11	11.25	10.92	0.1459
D	7	7.4	7.4	7.5	7.43	0.0034
G	8	8.65	8.62	9	8.76	0.0447

AVERAGE $\overline{Y} = 9.55$, SUM S.S = 0.7442

COEFFICIENTS CALCULATION:

	A	B	-A.B	C	-A.C	-B.C	A.B.C
AVERAGE -	10.10	9.87	8.96	8.75	9.59	9.47	9.65
AVERAGE +	9.00	9.24	9.78	10.36	9.52	9.63	9.13
DIFFERENCE	-1.1	-0.63	0.82	1.61	0.07	0.16	-0.52

$\tilde{Y} = 9.55 - 0.55A - 0.32B + 0.81C - 0.41\ (AxB) + 0.04\ (AxC) - 0.08\ (BxC) - 0.27\ (AxBxC)$

TABLE 8. ANALYSIS OF VARIANCE EQUATIONS

MAXIMUM STRAIN 1 (A,B = -1, C = + 1 FOR MAXIMUM)

$\tilde{Y} = 15.31 - 0.64A - 1.68B + 1.12C - 0.08\ (AxB) - 0.25\ (AxC) - 0.02\ (BxC) + 0.07\ (AxBxC)$
$15.31 + 0.64 + 1.68 + 1.12 - 0.08 - 0.25 + 0.02 - 0.07 = 18.37$

MAXIMUM 2 STRAIN (A,B = -1, C = +1 FOR MAXIMUM)

$\tilde{Y} = 14.31 - 0.38A - 2.08B + 0.28C + 0.15\ (AxB) + 0.23\ (AxC) - 0.1\ (BxC) + 0.13\ (AxBxC)$
$14.31 + 0.38 + 2.08 + 0.28 - 0.15 - 0.23 + 0.1 - 0.13 = 16.64$

MINIMUM STRAIN (A,B = - 1 FOR MINIMUM)

$\tilde{Y} = 3.76 + 0.52A + 0.27B + 1.46C - 0.44\ (AxB) - 0.49\ (AxC) + 0.25\ (BxC) - 0.47\ (AxBxC)$
$3.76 - 0.52 - 0.27 + 1.46 - 0.44 + 0.49 - 0.25 - 0.47 = 3.76$

STRAIN AT 60 SECONDS

$\tilde{Y} = 6.24 - 0.5A - 0.7B + 0.36C + 0.5\ (AxB) - 0.07\ (AxC) + 0.11\ (BxC) + 0.18\ (AxBxC)$
$6.24 + 0.5 + 0.7 + 0.3 + 0.5 + 0.07 - 0.11 + 0.18 = 8.44$

STRAIN AT 120 SECONDS

$\tilde{Y} = 13.61 - 0.52A - 2.0B + 0.64C + 0.85\ (AxB) + 0.10\ (AxC) + 0.6\ (BxC) + 0.27\ (AxBxC)$
$13.61 + 0.52 + 2.0 + 0.64 + 0.85 - 0.10 - 0.6 + 0.27 = 17.22$

STRAIN AT 180 SECONDS

$\tilde{Y} = 9.55 - 0.55A - 0.32B + 0.81C - 0.41\ (AxB) + 0.04\ (AxC) - 0.08\ (BxC) - 0.27\ (AxBxC)$
$9.55 + 0.55 + 0.32 + 0.81 - 0.41 - 0.04 + 0.08 - 0.27 = 10.59$

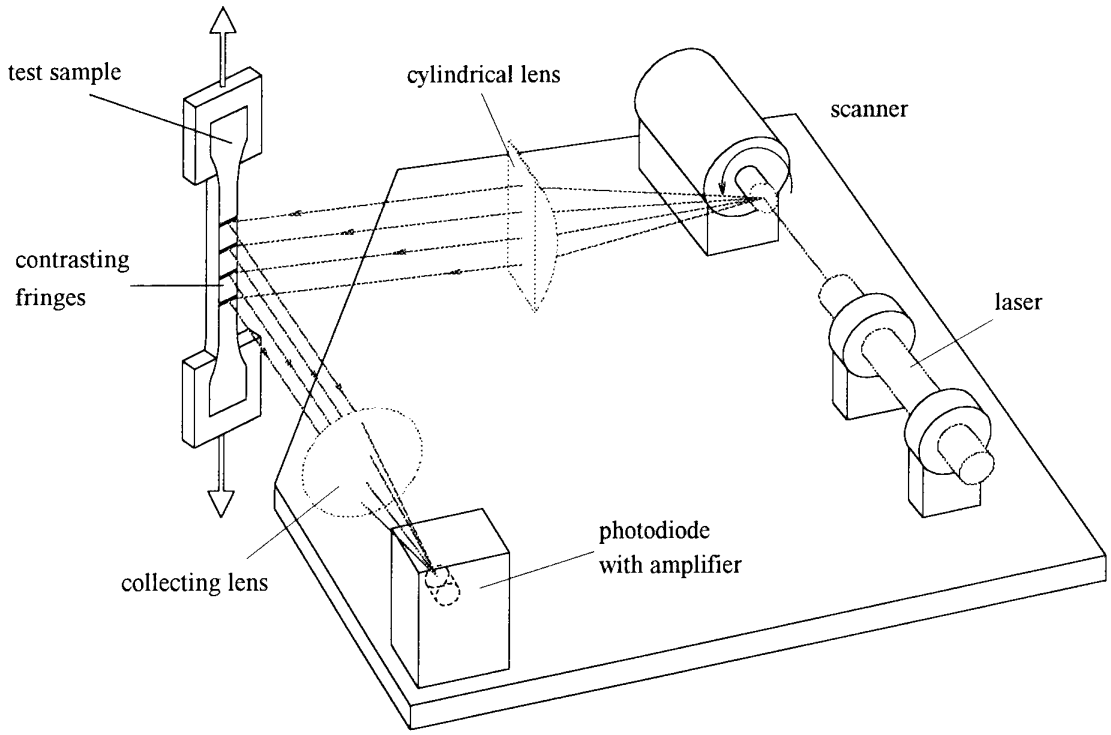


fig. 1: Schematic of the system

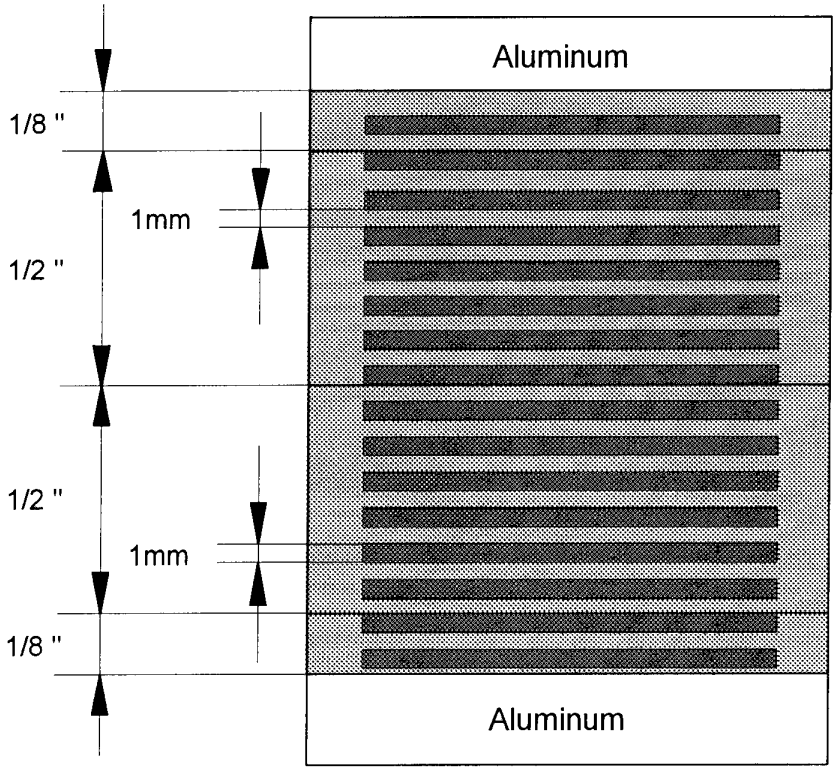


fig. 2: Typical sample schematic (F-type)

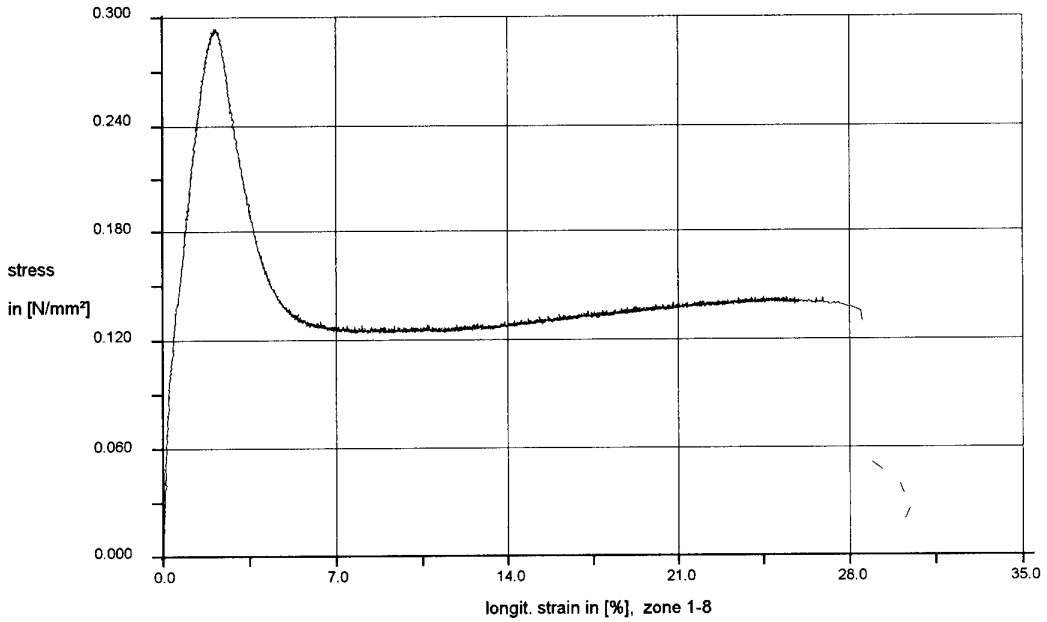
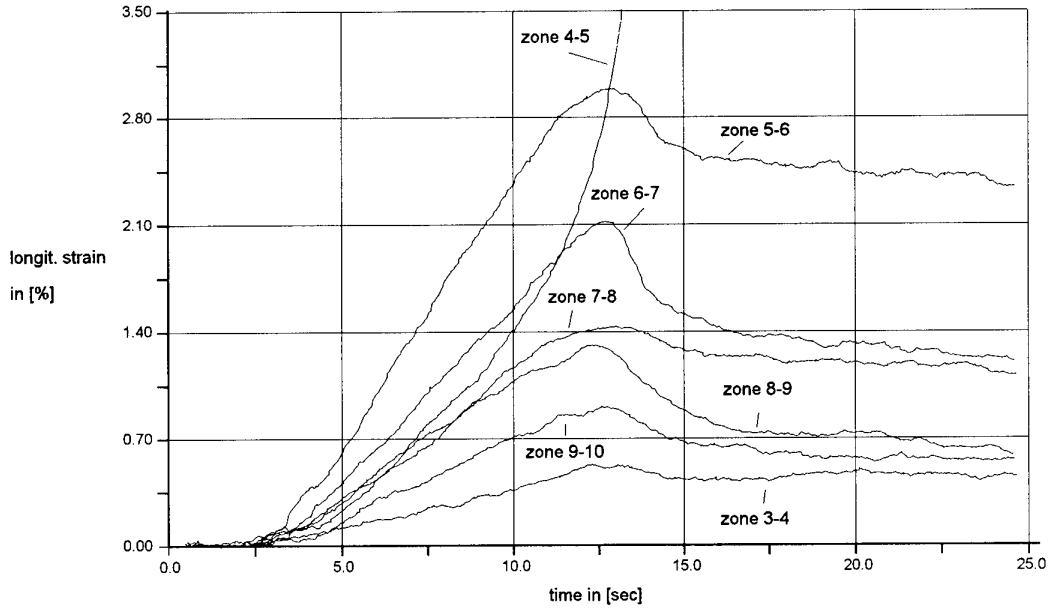


fig. 3: stress vs. strain for representative sample (SBITG.001)



fig, 4: Stress vs. strain for each strip pair (HERCRZ.001)

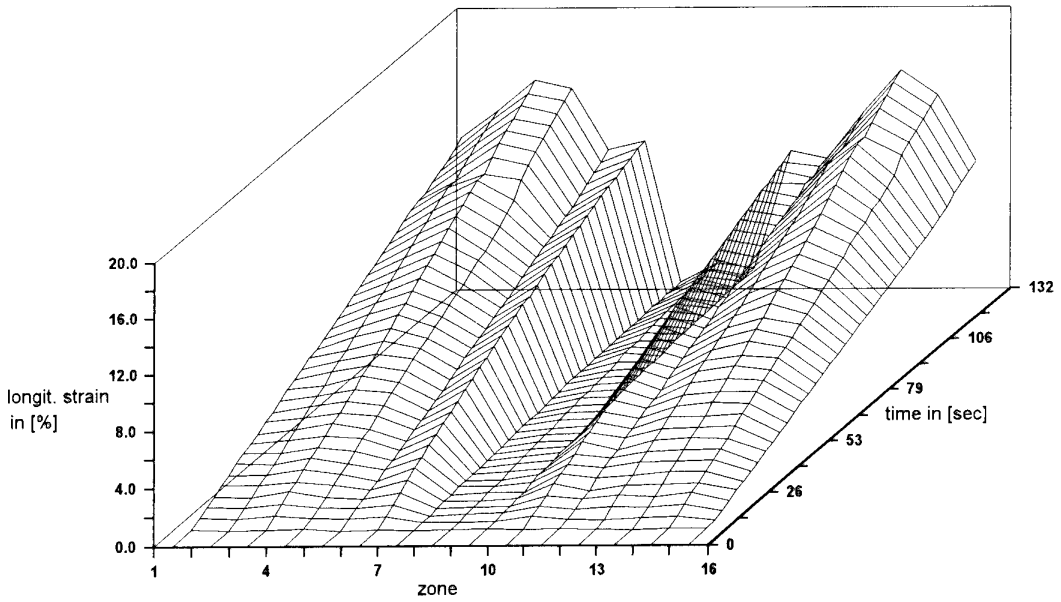


fig.: 5: Strain vs. zone vs. time (A1940829.001)

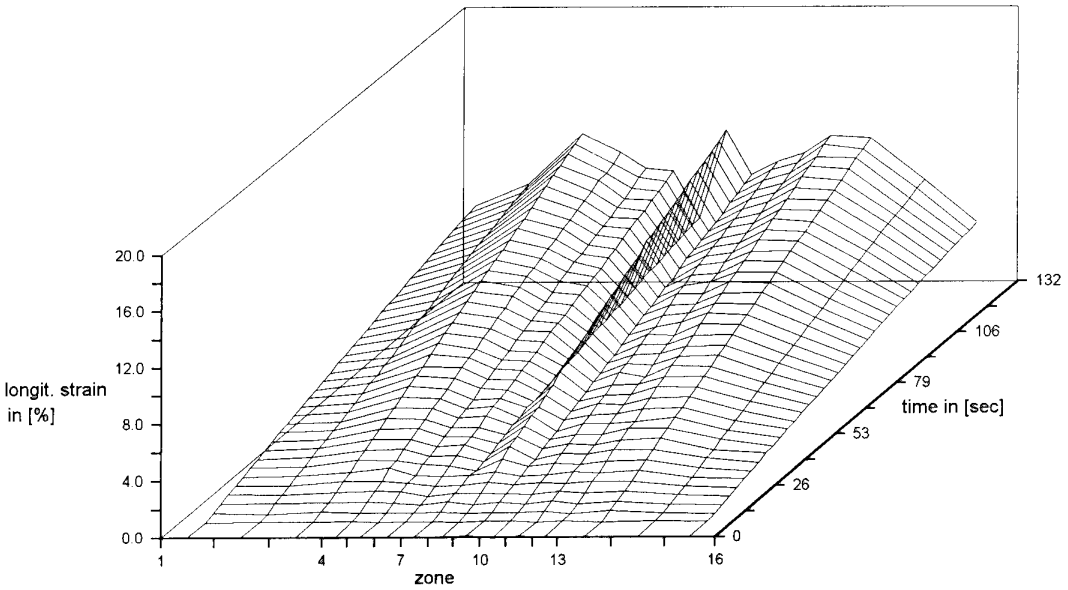


fig. 6: Strain vs. zone vs. time (G4940526.002)

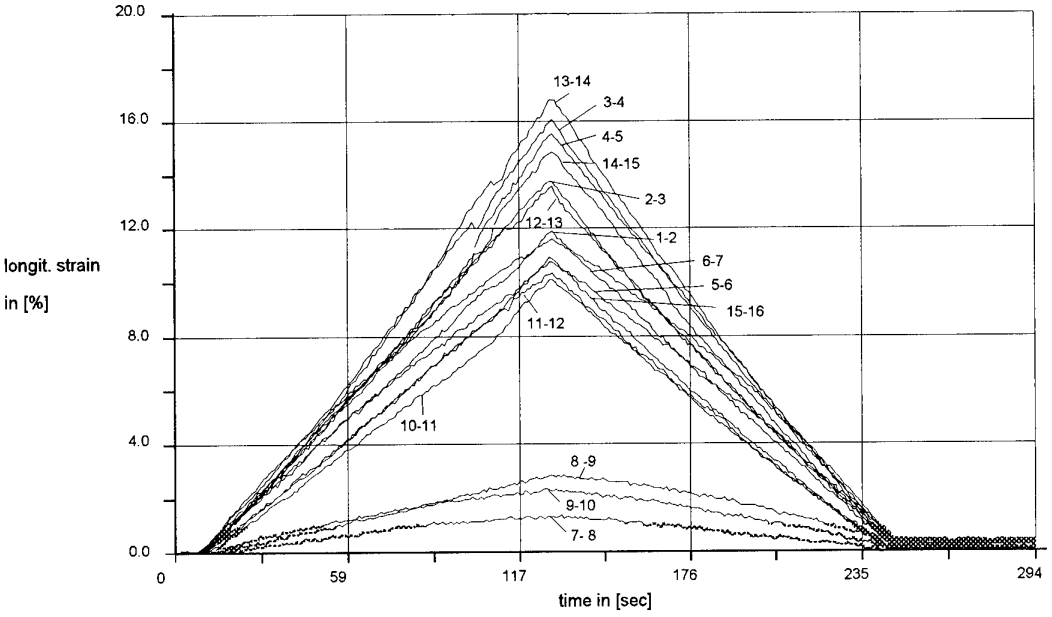


fig. 7: Strain vs. time (A1940829.001)

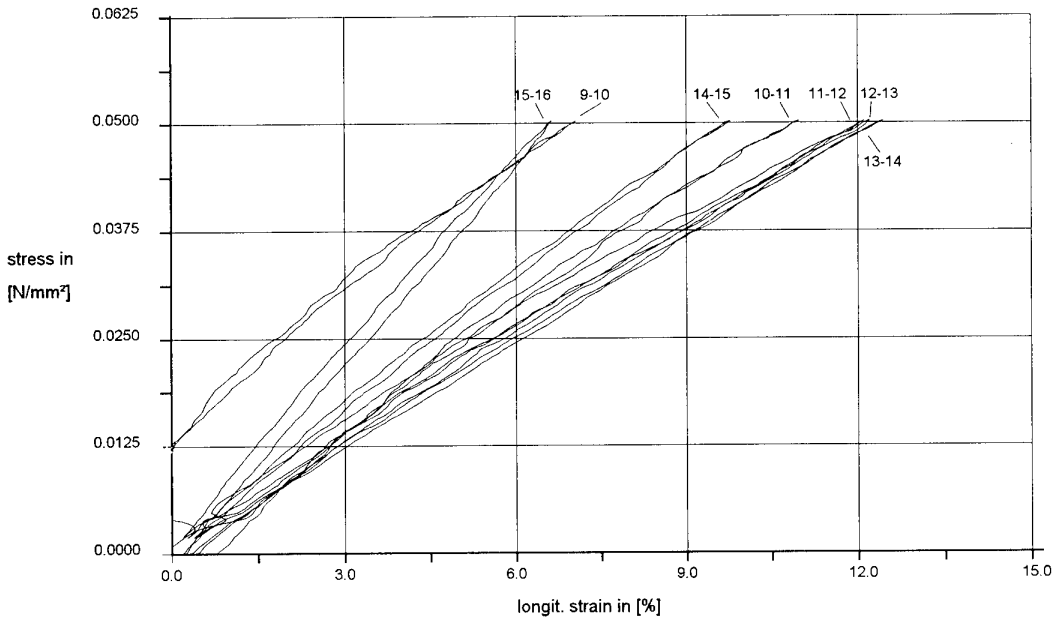


fig. 8: Stress vs. strain (F1940901.001)

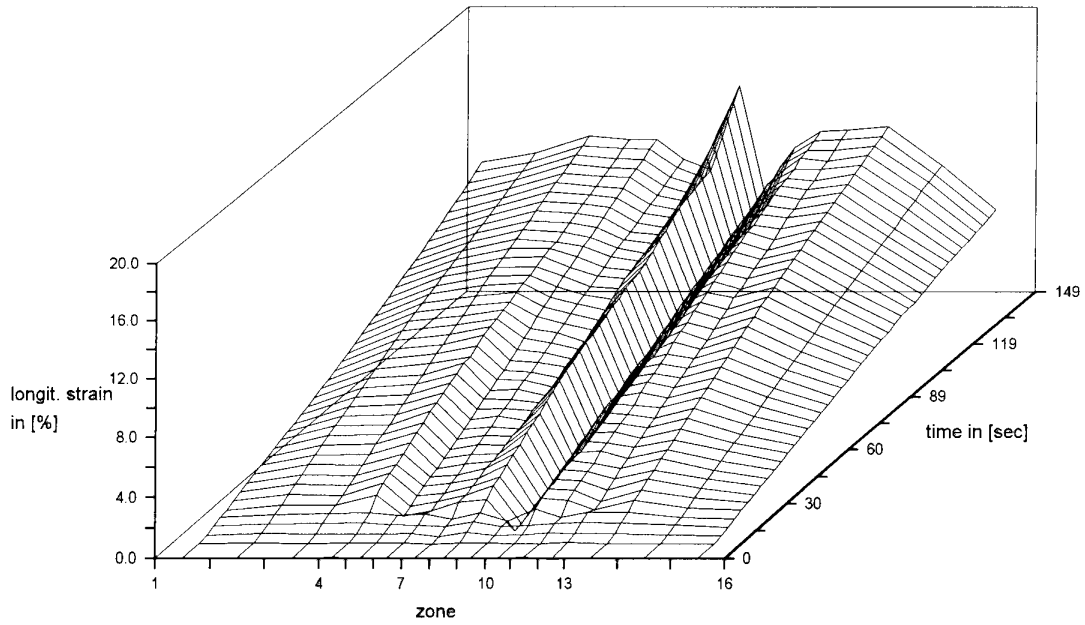


fig. 9: Strain vs. zone vs. time (F1940901.001)

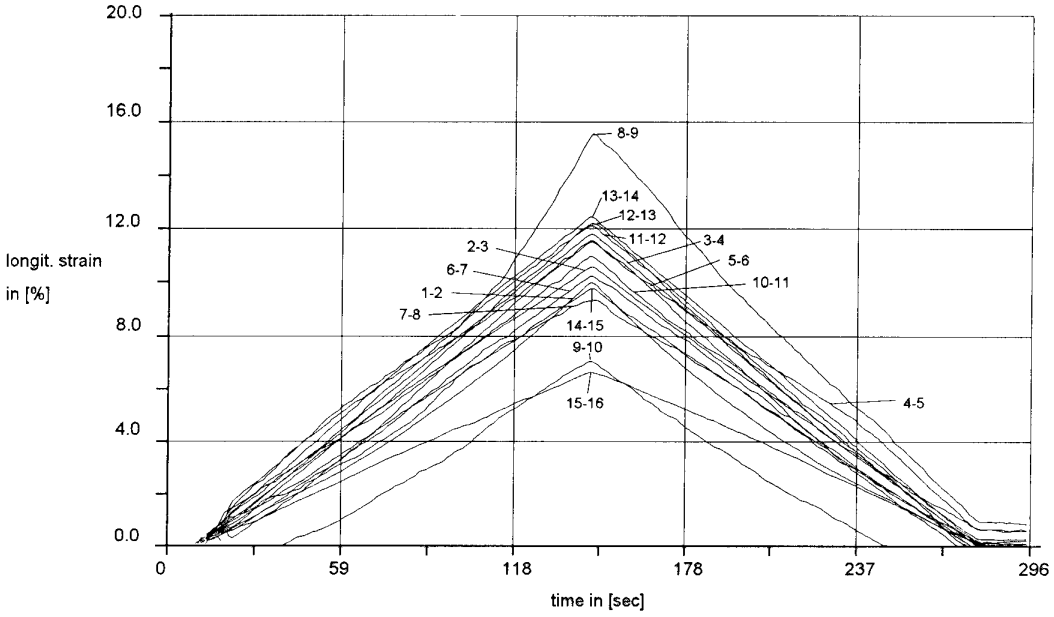


fig. 10: Strain vs. time (F1940901.001)

Paper Number: 31
Discussor's Name: Dr. A. Davenas
Responder's Name: I. H. Maxey

Question: Ten or fifteen years ago an Arctic cycle (cycling between -10 and -40 degrees C) was applied to some motors. It seems today that this type of cycle is less and less applied for characterization. Is that your observation and what is, in your opinion, the reason for this trend?

Answer: Arctic cycling can and often is applied but either:

A. The C1 or C2 1% climatic category conditions are used or
B. System specific conditions (eg, +63 to -51° C, i.e., hot takeoff to high altitude conditions) are applied for the operational phase. Although the older cycle was used for colloidal propellant problems (crystallization), its modern equivalents are still necessary to look at composite motor problems. The STANAG'S or Environmental testing referred to in my paper all specify the need to carry out low temperature tests using the cold climatic conditions and I think they are useful in life assessment testing as well.

STRUCTURAL SERVICE LIFETIME MODELLING FOR SOLID PROPELLANT ROCKET MOTORS

H.L.J. Keizers, J.R. Miedema
TNO Prins Maurits Laboratory
Lange Kleiweg 137, P.O. Box 45
2280 AA Rijswijk, The Netherlands.
Fax +31 15 284 39 58.
Phone +31 15 284 33 78

1. SUMMARY

An approach of the structural service lifetime problem of solid propellant rocket motors is presented, based on a combination of experimental and theoretical techniques. It includes propellant aging research, monitoring and non-destructive testing of life motors, dissectioning of motors, testing of the propellants, accelerated aging techniques, static firings and computer modelling incorporating aging effects. Typical aging results regarding chemical and mechanical aging of composite propellants are shown. Preliminary lifetime prediction models are used to give insight in the available rest life of a rocket motor. For an accurate lifetime prediction it is important to have insight in the initial propellant properties, aging characteristics, motor design and environmental history of the motor.

2. INTRODUCTION

The degradation of solid propellant properties is generally the limiting factor in the service lifetime of rocket motors. Aging of composite propellants mainly results in a change in mechanical properties, eventually resulting in a loss of the structural integrity of the grain design. Assessment of the aging behaviour of the propellant is therefore essential.

Aging may originate from different type of processes:

- chemical (i.e. oxidation, chain chissioning, incompatibilities),
- mechanical (i.e. thermally induced stresses, vibrations, shock loads),
- physical (i.e. migration of liquid propellant components).

Although the extent of these processes can partly be anticipated during design and development, the actual aging behaviour is shown during in service use. Surveillance of rocket motors in combination with aging research on material level of rocket components (propellant, seals, etc.) is necessary for an optimal use of rocket systems in terms of safety, effectivity and life cycle costs.

The lifetime problem has gained much interest over the last number of years. Due to worldwide budget cuts, military forces are forced to look for possible means of costs reductions. Extending the lifetime of the current missile stock is very attractive in this context. Lifetime extension requires available safety margins to be accurately known in order to use them up to their maximum possible extend.

3. EXPERIMENTAL TECHNIQUES

Several techniques are in use to determine the service lifetime of rocket motors. The status of a rocket motor can be assessed based on tests on material level and modelling of the overall motor performance (structural analysis, ballistic performance). Material tests include mechanical, ballistic and safety tests on materials extracted from life motors. By correlating the motors tested to the total missile population, predictions can be made regarding the structural service life of all motors within this population. In addition the status of a number of motors should be tested on system level to verify the obtained results. This is done by means of non-destructive evaluation techniques and static firings.

Non-destructive evaluation

Non-destructive tests give an indication of the quality of rocket motors, without the necessity to reduce the number of operational motors. Techniques used in The Netherlands include:

- visual inspection to assess status external motor parts (dents, corrosion),
- endoscopy to asses status grain bore (cracks, recrystallisation, decolorisation),
- X-ray to identify possible cracks within the propellant grain,
- ultrasonic evaluation to asses the propellant-liner-casing bond properties.

Motor dissectioning

When assessing the status of rocket propellants after a certain period of field use, it is necessary to dissect the rocket motor and retrieve the propellant from the casing. This has been done successfully for rocket motors ranging from 40 - 400 kg with aluminum and high strength steel casings. Large motors can be cut by means of specially developed mechanical sawing equipment (Figure 1).

After slicing of the rocket motor, propellant from motor segments is machined on a numerically controlled milling machine into the required test items for material characterisation testing.

Paper presented at the AGARD PEP Symposium on "Service Life of Solid Propellant Systems" held in Athens, Greece, 10-14 May 1996, and published in CP-586.

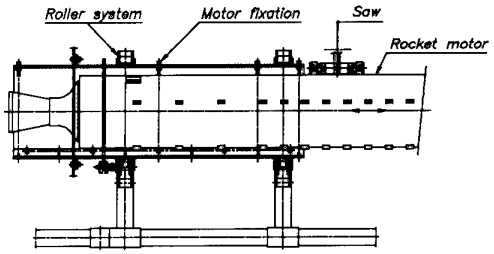


Figure 1. Sawing equipment for motor dissectioning

Material testing

Aging of composite propellants mainly manifests itself as a change in mechanical properties, thereby endangering the structural integrity of a rocket motor. Therefore a large number of test methods are in use to determine these properties (uniaxial tensile tests, biaxial tests, bond tests, peel tests, strain energy tests, hardness, etc.).

Tensile tests and bond tests are generally performed, since they provide direct information in the assessment of the structural service life of a motor. The tests are performed at relevant test temperatures and strain rates (see for example Figure 2). Based on the time-temperature superposition principle, results are related to the structural requirements (strain capacity, strength and modulus) for the propellant under relevant motor conditions.

By performing mechanical tests after different periods of (accelerated) aging, aging trends can be deduced, from which the remaining life time and the age-out mechanism can be determined. Figure 3 shows the typical effect of aging on the material properties of an AP/HTPB propellant extracted from a 14 year old air-to-air missile. Aging resulted in a hardening of the propellant with time.

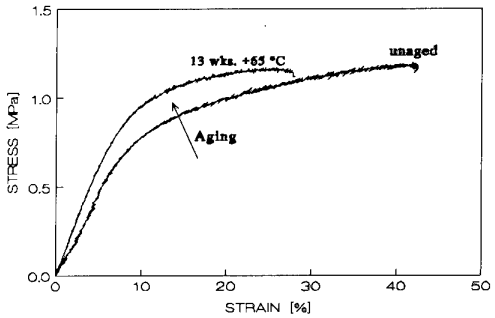
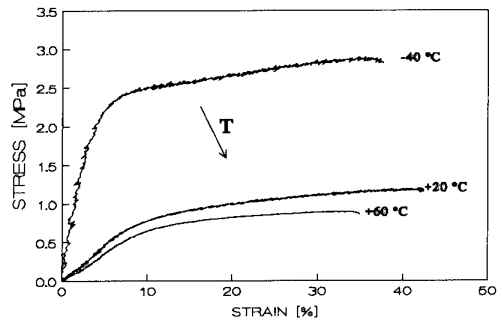
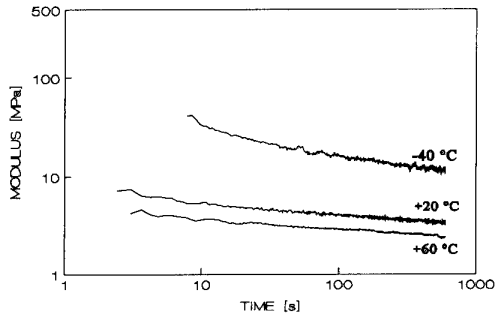


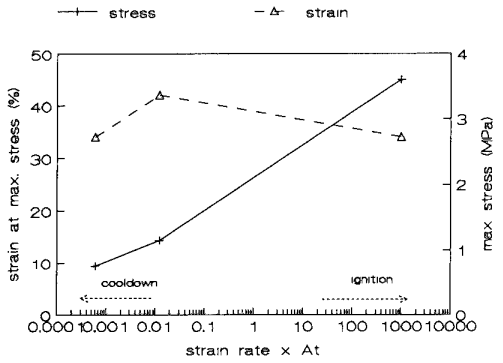
Figure 3. The effect of aging on the mechanical properties of an AP/HTPB propellant (20 °C, 50 mm/min)



a. Tensile tests (50 mm/min)



b. Relaxation tests



c. Mechanical properties as a function of shifted strain rate (note: only results shown in Figure 2 a are included).

Figure 2. Typical mechanical properties of an AP/HTPB propellant from an air-to-air missile after dissectioning (age 14 years)

By testing propellant extracted from different geometrical positions within a motor, possible gradients in mechanical properties can be determined. Gradients which were absent in freshly produced motors are indicative for aging mechanisms originating at the grain inner bore as for example atmospheric oxidation or migration of propellant components (plasticiser, liquid burn catalysts).

Small scale ballistic test motors are in use as a characterisation test to determine possible effects of aging on the ballistic properties of the propellants.

Besides mentioned characterisation tests a number of analytical techniques are used in order to determine the occurring aging mechanisms (sol/gel analysis, IR-spectometry, iso-thermal storage tests, etc.). Insight in occurring aging mechanisms is essential since it determines whether specific aging processes are possible for the actual motor application.

As an example, the atmospheric oxygen consumption for pure HTPB in an air-tight sealed volume is shown in Figure 4. Oxidation of the HTPB backbone is generally stated as one of the main aging mechanisms. After 2 weeks storage at 60°C, the available oxygen had been consumed. Relatively to the performed experiment, a multiple amount of grams HTPB per ml air is available in an actual motor. Aging caused by oxidation from atmospheric oxygen will end after a relatively short period of time or will become dependent up on the diffusivity of oxygen through the seals. The latter would change aging from a pure propellant property into a system dependent property.

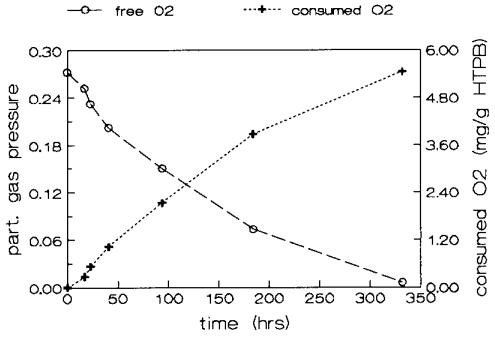


Figure. 4 Atmospheric oxygen consumption for HTPB. Oxygen content is determined by means of Gas-Chromatography

Static firings

Static firings of rocket motors at operating temperature extremes can show changes in motor performance as a function of aging time. By testing a number of motors after storage at elevated temperatures (accelerated aging on system level) and after thermal cycling (additional mechanical damage) an indication of the remaining lifetime of the motors can be obtained. However, static firings might still indicate acceptable motor performance, whereas the lifetime might very well have ended from a safety point of view (unacceptable low, or negative safety margins). When used in combination with the results of accelerated aging trials on material level and analysis of the structural integrity of the motor, static firing can be used to justify a potential lifetime extension on system level.

4. ACCELERATED AGING

Since aging is an intrinsically slow process, accelerated aging trials are performed to obtain information about aging characteristics in a relatively short period.

Chemical and physical aging

Chemical and physical aging processes can be accelerated by increasing the storage temperature of the propellant. By performing accelerated aging trials at a number of temperatures, predictions can be made about the long term behaviour under nominal operating conditions. Under the assumption that identical aging mechanisms are activated at the storage temperatures, the aging rate at different temperatures is related through the Arhenius equation (k aging rate factor A pre-exponential constant, E_a activation energy, R gas constant, T temperature).

Arhenius:

$$k = Ae^{\left(\frac{-E_a}{RT}\right)} \qquad [1]$$

Accelerated aging trials are performed at moderate temperatures (up to approximately 70 °C). Too high values might activate mechanisms which are not present under normal operating conditions.

The effect of accelerated aging conditions on the aging rate of an AP/HTPB propellants is shown in figure 5. For this propellant plasticiser depletion was found to be the dominant aging process. The aging behaviour could very well be described by the Layton model in combination with the Arhenius description for the acceleration factor (equation 2, P is a specific propellant property, t is time). The activation energy of the processes involved was approximately 30 KJ/mol, which is of the same order of magnitude as activation energies as found by several authors for the (oxidative) aging process of rocket propellants [i.e. 3, 4].

Layton [1]:

$$P = P_0 + k \ln \frac{t}{t_0} \qquad [2]$$

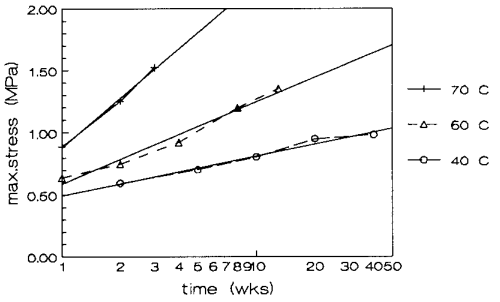


Figure 5. Accelerated aging at three aging temperatures

Applied environmental storage conditions during accelerated aging (available oxygen, possibility of plasticiser transport) can largely influence the aging rate. It is necessary to either apply storage conditions as representative as possible or to be able to account for system dependent effects on the aging rate. Otherwise a large error in the predicted remaining lifetime for the propellant in the actual motor might be obtained.

Mechanical aging

Mechanical aging or damage is the effect of a change in mechanical properties upon repetitive mechanical loading. For case-bonded motors, such loads will mainly occur during thermal cycling, due to the differences in thermal expansion coefficient of the propellant and motor casing. In figure 6 the effect of mechanical damage is shown for a ground-to-air missile. The stress-strain curve as determined after dissectioning indicates that this propellant had been loaded up to approximately 4-5 % strain. This was in accordance to the strain level as determined by means of structural analyses for this specific motor position.

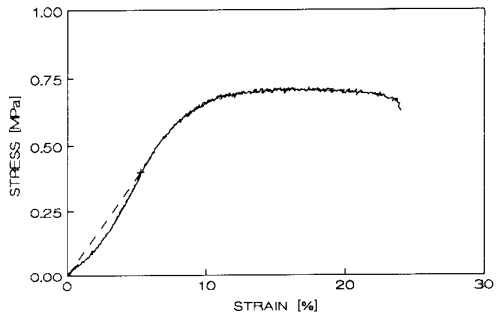
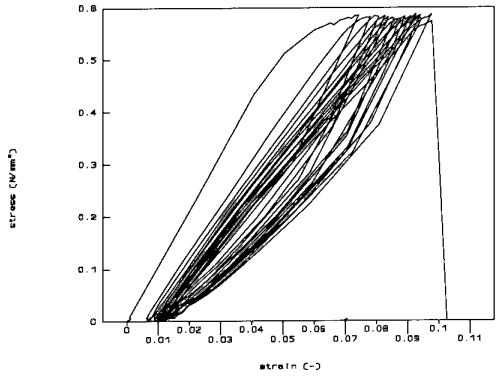


Figure 6. Stress-strain curve of a composite propellant extracted from a 400 kg rocket motor of a ground-to-air missile

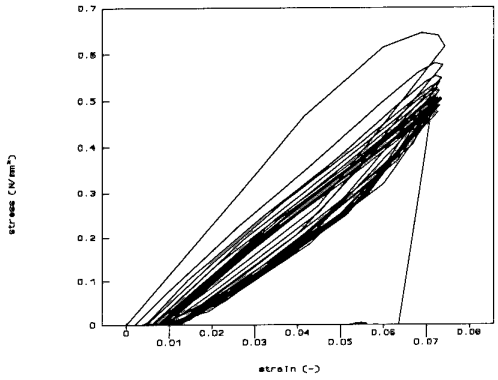
Test methods to accelerate mechanical aging and to determine the sensitivity of specific propellants for mechanical damage include mechanical tests on material samples with known stress-time histories (i.e. creep-tests, stress-cycle tests, strain cycle tests, Load-Unload-Load tests etc.). The response of an experimental composite propellant in a stress-cycle and a strain-cycle test is shown in figure 7. In the stress cycle test, the strain increases, whereas in the strain cycle test, the stress level at a specific strain level reduces, as a result of the damage induced.

Damage of composite propellants may be described by the Linear Cumulative Damage technique (LCD) [2]. With this method the damage, D, induced is proportional with the time, t_i, a specific stress level is applied, divided by the required time to failure at that stress level, t_{Ri}. P(n) is a statistical parameter accounting for the variability in material properties.

$$D = \frac{1}{P(n)} \sum_{i=1}^{N} \frac{\Delta t_i}{t_{Ri}} \qquad [3]$$



a. Stress-cycle



b. Strain cycle

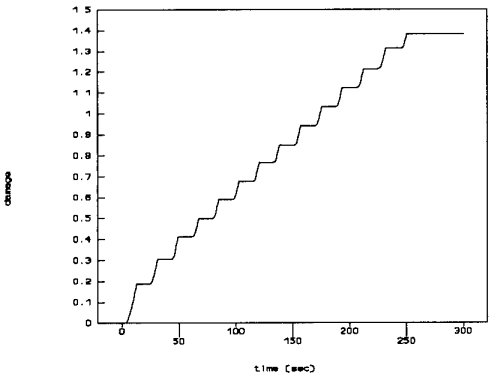
Figure 7. The effect of damage on the response behaviour of a composite propellant for two typical load cases

Based on LCD the total damage can be described as a direct function of the stress-time history encountered by the propellant. A possible method to describe the damage for infinitesimally small time increments, and considering specific material behaviour of composite propellants, is described by equation [4] (C and B are material specific damage parameters, a_T shift factor, σ_i induced stress):

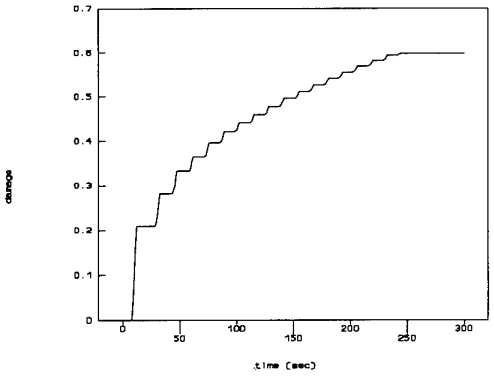
$$D(t) = \frac{1}{C}\left[\int_0^t \sigma_i(t)^B \frac{dt}{a_T}\right] \qquad [4]$$

The increase in damage for the stress/strain histories of Figure 7 are shown in Figure 8. The performed tests indicate that the increase in damage induced during strain cycle test flattens with successive test cycles. This cyclic straining can be compared to the cyclic strains at the grain inner bore during thermal cycling of the motor. In stress cycle tests the damage

increases with the same amount with successive cycles. Further tests are planned to examine these effects in more detail.



a. Increase in damage according to eq. 4 in a stress-cycle test



b. Increase in damage according to eq.4 in a strain cycle test

Figure 8. The increase in mechanical damage for the tests shown in Figure 7.

By using LCD in combination with laboratory scale tests to determine the material specific damage parameters, the damage and the lifetime of a propellant can be calculated instead of being tested by experimentally loading the propellants with the actual load-time spectra (which would be more labour and time intensive). LCD is based on the assumption that damage can be added in a linear fashion. Therefor it is likely that tests in which propellant is ramp-loaded up to failure underestimates the actual mechanical resistance against damage. Creep tests or low frequency stress cycle tests up to normally encountered stress level will probably yield more accurate results (albeit at the cost of increased testing times).

5. SERVICE LIFETIME MODELLING

Accelerated aging, mechanical tests on propellant samples, modelling of the structural behaviour of the propellant grain and knowledge about the environmental conditions give the possibility to predict the remaining service lifetime of rocket motors. In addition effects of different storage conditions on the lifetime can be assessed, which gives the possibility of optimising the storage conditions with respect to maximum service life.

A computer code, LARM (Lifetime Assessment Rocket Motors) is currently under development which uses the input of chemical and mechanical aging characteristics, as determined by the methods discussed previously. The used logic is shown in Figure 9.

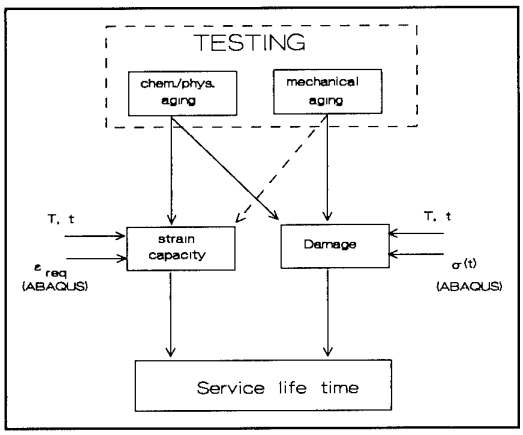


Figure 9. Service lifetime prediction logic (schematically).

Linear and logarithmic chemical aging models are currently included in the code. If required, other models can easily be implemented. Since chemical aging effects the response properties of the propellant, there is a direct link between chemical aging and structural lifetime as determined based on LCD. Mechanical damage is generally considered to have only limited effect on the failure properties up to high values of damage. Since such high damage values are normally considered unacceptable, the interference of mechanical damage on the strain capacity during chemical aging will remain limited (dotted line in Figure 9).

Inputs to the LARM code are the operational conditions (temperatures, handling and storage loads), mechanical properties of the propellant, aging characteristics and grain geometry. Mechanical strains and stresses are determined by the Finite Element code ABAQUS. Maximum strain capacity (during the motors lifetime) is compared to the minimum required strain as calculated. The amount of damage is deduced from calculated visco-elastic stress levels. End of lifetime is reached when either of these two conditions indicate insufficient safety margins.

Stress levels based on linear visco-elastic material models can

be considered as state of the art technology. However, composite propellants generally exhibit non-linear material response when loaded up to relatively high strain levels (i.e. Mullins effect). More refined damage calculations will require the introduction of non-linear material models in the future. Since non-linear material models will yield lower stress levels, damage calculations based on visco-elastic material models and using equation 4 will yield conservative results.

In figure 10, the effect of a hypothetical temperature-time history on the strain capacity for propellant from an air-to-air missile is shown. This propellant was aged under atmospheric conditions, to examine the effect of worst case aging conditions (i.e. broken weather seals). End of structural lifetime is reached when the lower 3-sigma level of the strain capacity falls below a system dependent value (arbitrarily set at 25 % in Figure 10).

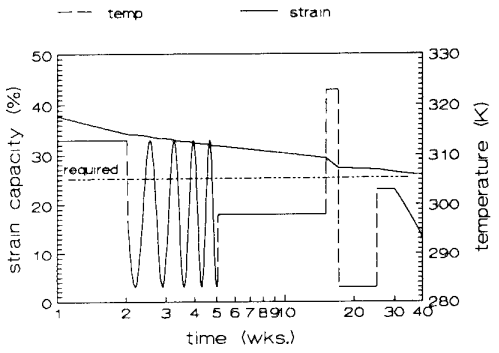


Figure 10. The calculated effect of chemical aging on the strain capacity of an AP/HTPB propellant (propellant was aged under free atmospheric, low rh., conditions).

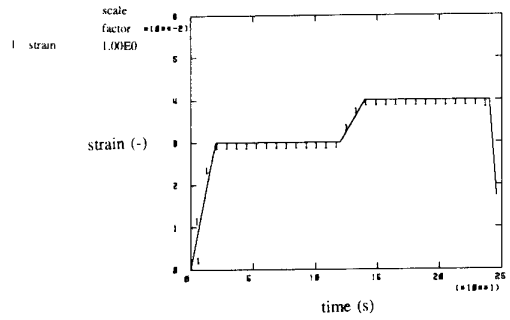
In Figure 11, the increase in damage for a typical load case is shown. Due to the assumed visco-elastic nature of the propellant, damage increases mostly directly after the up-going loading realm. Stress-relaxation reduces the additional amount of damage during comparable time periods there after. The damage induced by total stress-time history of motors can be determined in this manner. Structural lifetime has ended as soon as the damage has grown above a (user defined) damage level.

5. CONCLUSIONS

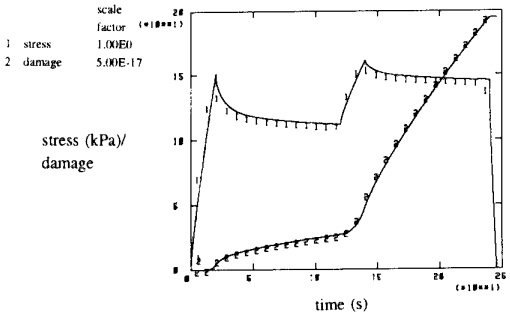
A number of techniques have been discussed, which are in use to asses the structural service life of composite rocket motors.

For optimal lifetime assessment a combination of material scale tests and system scale tests is required.

Based on the chemical, physical and mechanical aging characteristics of a propellant, the structural service life time can be predicted.



a. strain-time profile



b. Stress-time and damage time

Figure 11 The increase in damage as a function of a typical stress-strain history

A methodology based on material level aging experiments in combination with computer modelling is presented. Besides assessing the service lifetime, this method enables determination of the effect of different storage conditions on the remaining lifetime. Therefore this code can be used as a tool to optimise the service lifetime in terms of safety and life cycle costs.

The rate of certain aging processes can largely be effected by system dependent aspects of the motor (quality seals, liners used, etc.). Including such aspects as part of the lifetime modelling methodology will be part of further study.

ACKNOWLEDGEMENTS

Presented work is supported by the Dutch Ministry of Defense.

SYMBOLS

a_T	shift factor
A	pre-exponential coefficient
B, C	damage properties of a propellant
D	cumulative damage
E_a	activation energy
i	various elementary loads
k	chemical aging rate, dependent on temperature
σ	stress
R	gas constant
Δt_i	time spend under elementary loads i
t_{Ri}	failure time corresponding to the elementary load i
T	temperature
P(n)	statistical distribution parameter

AP	Ammonium Perchlorate
FE	Finite Element
HTPB	Hydroxyl Terminated PolyButadien
LARM	Lifetime Assessment Rocket Motors
LCD	Linear Cumulative Damage

REFERENCES

1 Christiansen, A.G., Layton, L.H., Carpenter, R.L., HTPB propellant aging, AIAA 80-1273, 1980

2 Bills, K.W., Campbell, D.M., Steel, R.D., McConnnell. J.D., Applications of cumulative damage in the preparation of parametric grain design curves and the prediction of grain failure on pressurization, Final report, Report 1341-26F, 1970

3 Layton, L.H., Chemical structural aging effect, AFRPL-TR-74-77 1974

4 Bunyan, P., Cunliffe, A.V., Davis, A., Kirby, F.A., The degradation and stabilisation of solid rocket propellants, Pol. Degradation and Stability 40, 1993

Paper Number: 32
Discussor's Name: Professor R. A. Heller
Responder's Name: Dr. H. L. J. Keizers

Question: Did chemical aging produce reduction or increase in modulus and strength, while mechanical aging resulted in reduction in modulus and strength?

Answer: Both modulus and strength increased due to chemical aging but only modulus decreased due to damage. Strength did not change unless significant damage occurred.

Paper Number: 32
Discussor's Name: G. S. Faulkner
Responder's Name: Dr. H. L. J. Keizers

Question: The aging trial results that you showed indicated severe aging at +70° C. Is this a typical result for an HTPB/AP propellent?

Answer: It is a typical result for a plasticized AP/HTPB propellant under free atmospheric conditions at low relative humidity. In an actual motor application, the aging rate will be reduced due to the sealing of the motor.

Paper Number: 32
Discussor's Name: Dr. J. Margetson
Responder's Name: Dr. H. L. J. Keizers

Question: I can understand how you use the Layton model to modify the strain capacity to account for chemical aging. It was not clear how you modify the strain capacity to account for mechanical damage.

Answer: We only use the Layton model for chemical effects. We currently do not use a model for mechanical damage. We regard this as a small effect if applied loading conditions are not severe.

Aging Studies on HTPB Propellants by Dynamic Mechanical Analysis

Carlos Schüller and José Luis de la Fuente

Department of Rocket Motors, Division of Energy and Propulsion.
Carretera de Ajalvir Km 4
I.N.T.A. 28850 Torrejón de Ardoz. Madrid. Spain.

1. SUMMARY

Aging studies on hydroxyl terminated polybutadiene (HTPB) propellants have been carried out. The change in the mechanical properties have been measured using a Dynamic Mechanical Analyzer DMA operating in two different modes: frequency scan and temperature scan. This technique allows evaluation of the actual state of a propellant grain with a small sample and an easy measurement.

2. INTRODUCTION

Since solid propellants are composed of a large percentage of energetic ingredients, it would be expected that prolonged storage might result in deterioration. Chemical aging may be the result of thermal, oxidation or hydrolytic reactions. The changes observed may be softening, hardening, swelling, discoloration, and gas evolution. Various ingredients may interact with each other or with the atmosphere to produce irreversible changes which can seriously affect both ballistic and mechanical properties.

Athough many chemical and physical analysis techniques have been used in aging studies of solid propellants, the one most applied has been the measurement of changes in some prominent mechanical properties such as Young's modulus or tensile strength at various temperatures. These observed changes have been explained on the basis of chemical reaction ocurring between the ammonium perchlorate and polymeric binder. The main techniques used for aging studies of propellants are summarized in Table 1

The studies to evaluate and charaterize the aging behavior of composite propellants have attracted considerable attention in recent years[1-5]. However the most efficient investigations have been reported by Layton and co-workers[6-9] and Kishore et al[10-21], who correlated the structure with changes in mechanical and ballistical properties in PBAN, CTPB and HTPB propellants.

Detailled investigations on the aging of hydroxyl terminated polybutadiene (HTPB) propellants have been carried out in this laboratory. These formulations, selected for continued aging evaluation, have been developed under the Capricornio Program conducted by I.N.T.A. (Instituto Nacional de Técnica Aeroespacial, Spain).

Capricornio will be a launch vehicle with three solid rocket motors designed to place small satellites in LEO through dedicated lauches, without secondary payload limitations. The Capricornio will allow a low cost launch, following simple procedures and paying dedicated attention to the satellite(s).

In the present paper, experimental dynamic mechanical properties were used to study aging behaviour of the composite propellant chosen.

Table 1. Techniques for Aging Studies

Characteristic studied	Technique
Chemical structure and changes in composition.	Spectrocopic methods (NMR, IRFT, UV, etc.)
Appearance of crystalline degradation product.	X-Ray diffraction, microwave.
Surface cracks, migration products, roughness, accumulation of degradation products, oxidizer concentration owing to moisture, and localized dewetting.	Visual observation, miniatured TV, microscope, etc.
Slump, liner separation, subsurface voids, surface cracks.	Profilometer, ultrasonic.
Porosity voids (due to dewetting), cracks.	X-Ray.
Propellants modulus and relaxation rate changes caused by chemical changes or compositional changes owing to migration or absorption.	Hardness and hardness relaxation.

3. DYNAMIC MECHANICAL MEASUREMENTS.

Dynamic Mechanical Analyzer (DMA) provides the necessary performance capabilities for the caracterization of a broad range of materials, from soft samples such as elastomers and thin films to hard samples like composites and ceramics. DMA measures changes in mechanical behaviour, such as modulus and damping, as a function of temperature, time, frequency, stress or combinations of these parameters.

The practical advantages of the DMA techique are:

- This technique can be accommodated to a broad range of sample types and test geometries.
- Because the tests are non-destructive and use small test specimens.
- The broad modulus range provides full characterization capabilities and certifying accurate and reproducibility in every mode of operation.

Dynamic mechanical test measures the response of a material to a sinusoidal or another periodic stress. Since the stress and the strain are generally not in phase, two quantities can be determinated:

- A modulus
- A phase angle or a damping term.

If the material under test is completely elastic there will be no phase. The two sinusoidal motions can be expresed as follows:

$$\text{strain} \quad \varepsilon = \varepsilon_o \sin(\omega t)$$
$$\text{stress} \quad \sigma = \sigma_o \sin(\omega t + \delta)$$

Paper presented at the AGARD PEP Symposium on "Service Life of Solid Propellant Systems" held in Athens, Greece, 10-14 May 1996, and published in CP-586.

where ω is the angular frequency, t the time and δ the phase angle.
The equation for the stress may be expanded to give:

$$\sigma = \sigma_o \sin(\omega t) \cos(\delta) + \sigma_o \cos(\omega t) \sin(\delta)$$

As can be seen, the stress would be considered to consist of two components, one in phase with the strain and the other which is ninety degrees out of the phase with the strain.
By resolving the stress and the strain components it is possible to determinate two moduli, one in phase with the strain (E') and the other ninety degrees out of phase (E'').

$$E'(\omega) = \sigma_o/\varepsilon_o \cos(\delta)$$

$$E''(\omega) = \sigma_o/\varepsilon_o \sin(\delta)$$

The complex modulus E^* is defined by:

$$E^* = E' + iE''$$

E' is the storage modulus and is an indication of a materials ability to store mechanical energy. E'' is the loss modulus or the amount of energy lost to viscous dissipation (such as heat). The ratio of energy dissipated to energy stored in the material during one cycle of oscillation is the tangent delta:

$$\tan \delta = E''/E'$$

4. EXPERIMENTAL.

All dynamic mechanical measurements were carried out on a Perkin-Elmer DMA 7 Analyzer. The measuring system was a parallel plate of stainless steel with 5 mm of diameter. Propellant samples used in these studies were generally prepared in the form of rectangular bars of 6 mm x 10 mm cross-section and 2 mm of thickness. In order to observe possible changes in mechanical properties between different areas from the propellant grain, surface and core samples of the grain were tested.
HTPB propellants containing 86% solids loading, 68 % ammonium perchlorate, 18% aluminium and 14% binder were selected for this work. The differences between these formulations were based on the composition of the binder. The binder composition involved 2% of plasticizer (dioctyl adipate, DOA) and different percentages of aziridinyl bonding agent.
Although the Analyzer DMA 7 can be operated in up to six different modes, only two were employed. The *temperature scan mode*,by far the most routinely used mode in DMA testing, was used for characterizing temperature dependent behavior such as modulus and tan delta. When the temperature scan mode was utilized the single frequency point of 1 Hz was chosen and a low heating rate of 3 °C/min was programmed. Thermal transitions were determinated by measuring viscoelastic dissipation as a function of temperature, and estimated from the point at which there is a maximun in the value of the tan delta and a descent in the value of storage modulus. The *frequency scan mode*, also an important routine testing mode, allowed the characterization of the moduli and tan δ dependence with the rate or frequency when the propellant samples were exposed to a stepped changing frequency. The viscoelastic properties were determinated through three decades of frecuencies. The frequency scan range was from 50 to 0.01 Hz. The static and dynamic stresses applied in all experiences and in both operating modes were $1.0\ 10^4$ and $8.33\ 10^3$ Pa respectively.
The propellant samples were aged for over 5000 hours at the temperatures of 40, 60 and 80 °C. The dynamic mechanical properties were periodically measured during the aging period by operating on frequency and temperature scan modes.

5. RESULTS AND DISCUSSION.

The characterization of the unaged propellant under observation was first carried out by means of variations of the storage modulus and tangent delta with frequency and temperature.Through isothermal variations of E' versus frequency a typical behaviour of composite materials is observed. Data were collected over three decades of logarithmics of frequency and temperatures ranging from 60 °C to -10 °C. Storage modulus E' increases in a regular fashion with increasing frequency or decreasing temperature, suggesting that time-temperature superposition of these data may be possible. These curves can be observed in Figure 1. It is possible to obtain the master frequency curve shown in Figure 2 from the different isotherms by a shift operation in the horizontal axis towards the reference curve selected to equal 22 °C. The horizontal shift factors a_T used to superpose the data are the following:

a_T (60° C) = 0.0832
a_T (40° C) = 0.3162
a_T (0° C) = 14.4544
a_T (-10° C) = 42.6580

Due to the important information that the variation of tan delta with temperature brings, especially about the various thermal transitions owing to the different movements of the macromolecular chain segments (transitions α,β,γ, etc), it has been considered suitable to examine this variable in the aging process of a composite propellant. The damping peaks are associated with the partial loosening of the polymer structure so that groups and small chain segments can move. In Figure 3 the storage modulus and tan delta for unaged samples of the HTPB propellant is shown as a function of temperature and α and β transitions can be observed at 25 and -65 °C respectively. The beta transition is very close to T_g. At temperatures below to T_g the damping can be small, nearly all the energy stored in deforming the material is quickly recovered when the stress is removed since molecular slipping and other motions are frozen in.

A very important factor to take into account in any aging study of a propellant grain is the effect of external (surface) or internal (core) sampling in the intensification of the aging process. This work has intensively attended to this effect. Thus Figures 4-9 show this influence by testing external and internal samples after various aging time periods (850, 2500 and 5000 hours) at aging temperatures, above mentioned. As expected, the storage modulus of propellant samples increased with time and with rising aging temperature. An increase in E' indicated that the material was becoming more brittle or glasslike. The importance of superficial phenomenon can be observed in these figures, mainly when the aging tenperature is higher than 60 °C. For example, in external samples, E' takes a nearly constant value of 50/80 MPa at an aging temperature of 80 °C all over range of frequency (at aging

time higher than 850 hours approximatily). However in the case of a core sample the increase of the storage modulus is minor and keeps the tendency of the reference curve (unaged propellant curve).

Tangent delta and storage modulus versus temperature are represented through Figures 10-17. These being measured during heating from -110 to 100 °C. In these curves a great difference behaviour is also observed between the external and internal samples of aged propellant. The series of curves of tan delta show that the area under the curve decreases with the increasing aging, showing that the ability to absorb energy decreases with consequent material embrittlement. Also it can be observed that on increasing the aging time, the damping peak of the transition alpha tends to decrease while the peak corresponding to transition beta increases. On the other hand, when the external samples, aged during 2500 hours at 80 °C were tested, a dramatic descent appears in the damping curve, taking values near zero. This result indicates that the samples have experimented a high degree of descomposition. Data of the E' as a function of temperature show the same dependence found in the scan frequency tests realized.

6. CONCLUSIONS.

The following conclusions can be derived from the work presented in this paper:

1) The *surface factor* is very important when sampling a propellant grain for carring out a dynamical mechanical study based on aging process.

2) The testing procedure based on temperature scan (fixed frequency) provides great information about the aging state of the propellant under study. Tan delta data are an excellent way to determine the service life of a propellant, thus samples with values of tan δ near zero all over temperature range can be considered out of service. On the other hand, the frequency scan procedure turns out to be a less accurate method to aging study.

3) At aging temperature of 80 °C and higher an remarkable increase effect is observed in the kinetic of the aging process and a high chemical degradation is produced.

4) The DMA technique allows the evaluation of the actual state of a propellant grain with the help of small samples and a quick and easy procedure, compared with traditional aging studies.

These conclusions are in agreement with the results reported by Husband[4]. However superficial effects of propellant samples obtained from rocket motors are very important and must be taken into account.

References

1. Francis, E.C. and Ho, S.Y. Instrumented Rocket Motor Service Life Program. *AIAA Paper*, N° 95-1455 (1995).

2. Villeneuve, S. and Lessard, P. Correlation of Tensile and Dynamic Mechanical Analysis Results in Ageing Studies of Rocket Propellants. *Int. Annu. Conf. ICT*, pp. 15-1 to 15-13 (1994).

3. Liu, D. and He, N. Investigation on the Storage Life and its Reliability of Composite Propellant. *Journal of Propulsion and Technology*, N° 6, 63 (1993).

4. Husband, D.M. Use of Dynamic Mechanical Measurements to Determine the Aging Behavior of Solid Propellant. *Propellants, Explosives and Pyrotechnics*, N° 17, 196 (1992).

5. Bilgin, F; Sage, T; Orbey, N. and Guven, O. Lifetime Prediction of Carboxyl-Terminated Polybutadiene (CTPB). *Journal Applicate Polymer Science*, Vol. 42, N° 1, 153 (1991).

6. Layton, L.H. Chemical Aging Studies on ANB-3066 and TP-H1011 Propellants. *AFRPL-TR-74-16* (1974).

7. Christiansen, A.G.; Layton, L.H. and Carperter, R.L. HTPB Propellant Aging and Service Life. *AIAA Paper,* N° 80-1273 (1980)

8. Layton, L.H. Chemical Structural Aging Effects. *AFRPL-TR-74-77* (1974).

9. Layton, L.H. Chemical Structural Aging Studies on an HTPB Propellant. *AFRPL-TR-75-13* (1975).

10. Kishore, K.; Pai Verneker, V.R.; Gayathri, V.; Shubha, K.R. and Sridhara, K. Aging Studies on Carboxyl Terminated Polybutadiene (CTPB) Binder and Propellant. *Journal Spacecraft Rockets,* Vol 20, N° 4, 371 (1983).

11. Kishore, K. and Prasad, G. A Survey of Solid Propellant Aging Studies. *Journal of Spacecraft Rockets,* Vol 15, N° 5, 261 (1978).

12. Kishore, K.; Pai Verneker, V.R. and Prasad, G. Effect of Storage Temperatures on the Mechanical Properties of the Composite Solid Propellants. *Combustion Science Technology*, Vol 19, N° 3-4, 107 (1979).

13. Kishore, K.; Pai Verneker, V.R.; Vencatesh, R. and Prasad, G. Storage Stability of Solid Rocket Fuel-2. Effect of oxidizer Loadings. *Fuel,* Vol 57, N° 1, 22 (1978).

14. Kishore, K; Sankaralingam, S. and Begum, A.S. Studies on the Aging Behavior of Poly(vinyl chloride)/Ammonium Perchlorate Composite Solid Propellant. *Fuel,* Vol 68, N° 11, 1476 (1989).

15. Kishore, K; Sankaralingam, S. and Begum, A.S. Changes In the Calorimetric Value and Ignition Temperature of Composite Solid Propellants During Ageing. *Defence Science Journal*, Vol 36, N° 4, 425 (1986).

16. Kishore, K.; Prasad, G. and Mohandas, K. Some Observation on the Ageing of Composite Solid Propellants. *Fuel,* Vol 59, N° 6, 451 (1980).

17. Kishore, K. and Prasad, G. Review on Aging of Composite Solid Propellants. *Journal of Scientific and Industrial Research,* Vol 38, N° 8, 414 (1979).

18. Kishore, K; Pai Verneker, V.R. and Prasad, G. Mechanism of the Oxidative Degradation of Binder During the Aging of Composite Solid Propellants. *Journal of Applied Polymer Sciences,* Vol 24, N° 2, 589 (1979).

19. Prasad, G.; Kishore, K. and Pai Verneker, V.R. Mechanism of Ballistic, Thermal and Chemical Changes During the Aging Composite Solid Propellants. *CONFERENCE Proc.-Natl. Conf. I. C. Engines Combust.* PC4, Vol. 2, 7 (1978).

20. Pai Verneker, V.R.; Kishore, K. and Varadaraju, U.V. Chemical Changes During the Aging and Decomposition of Composite Solid Propellants. *Combustion and Flame*, Vol 45, 137 (1982).

21. Kishore, K. and Prasad, G. Mechanism of Aging Composite Solid Propellants. *Combustion and Flame*, Vol 36, 79 (1979).

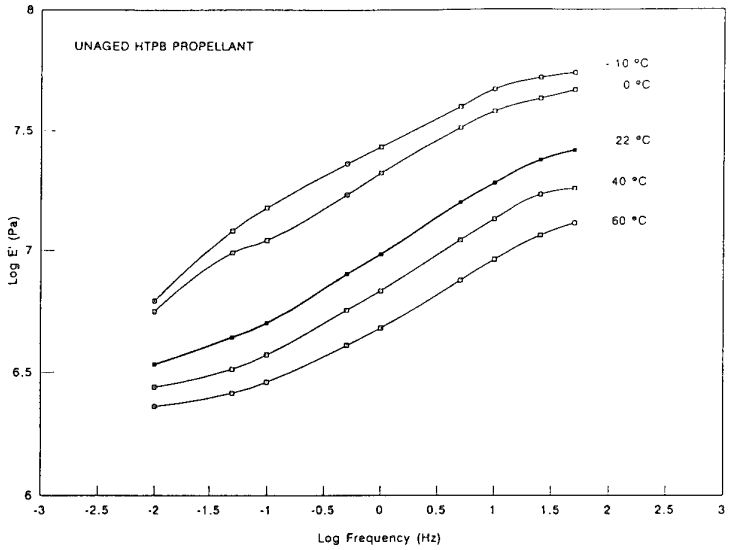


Figure 1. Logarithm Storage Modulus E' plotted against logarithm frequency for a HTPB propellant at various temperatures. Reference temperature T_0= 22 °C.

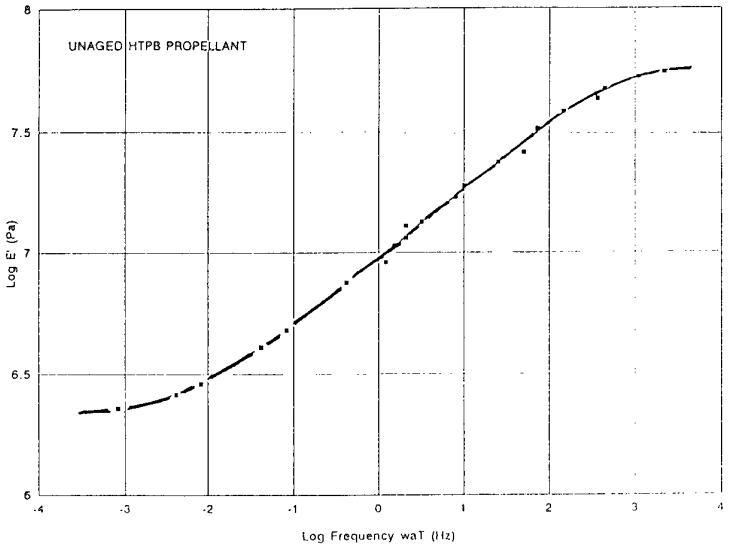


Figure 2. Log of Storage Modulus E' for a HTPB propellant displayed as a function of the log of ωa_T. Master Curve.

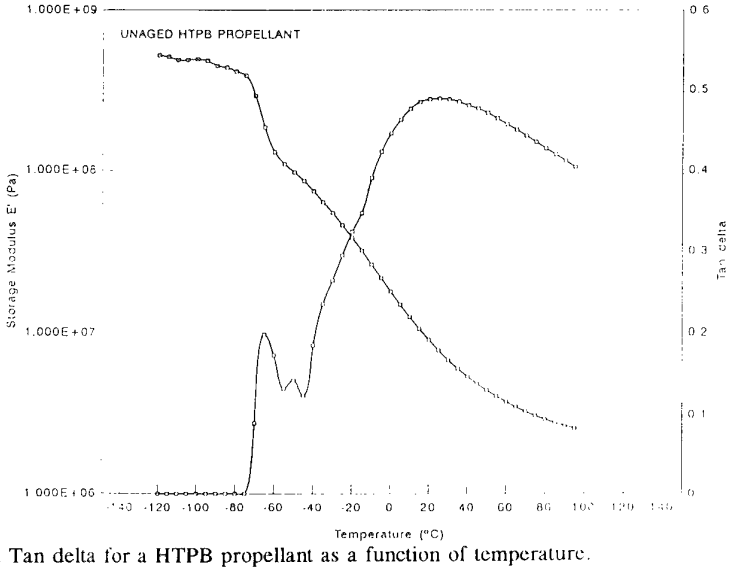


Figure 3. Storage Modulus E' and Tan delta for a HTPB propellant as a function of temperature.

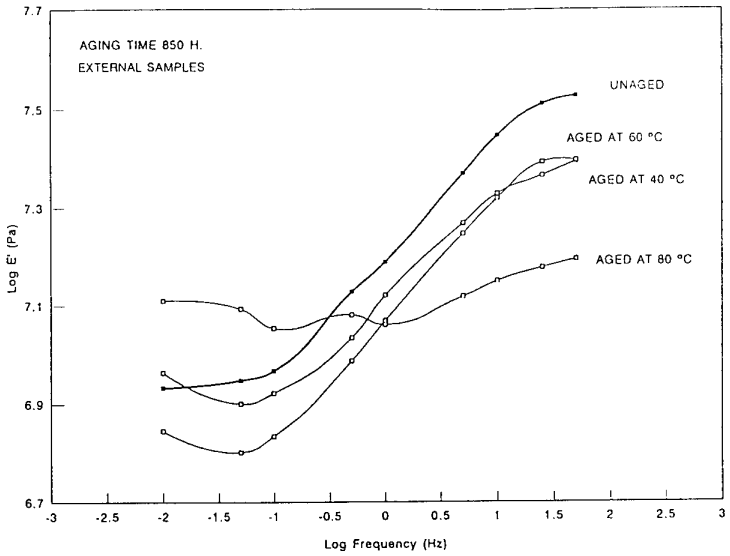


Figure 4. Log Storage Modulus E' as a function of the log frequency for rocket motor samples (external) aged at 40 °C, 60 °C and 80 °C after 850 hours of aging.

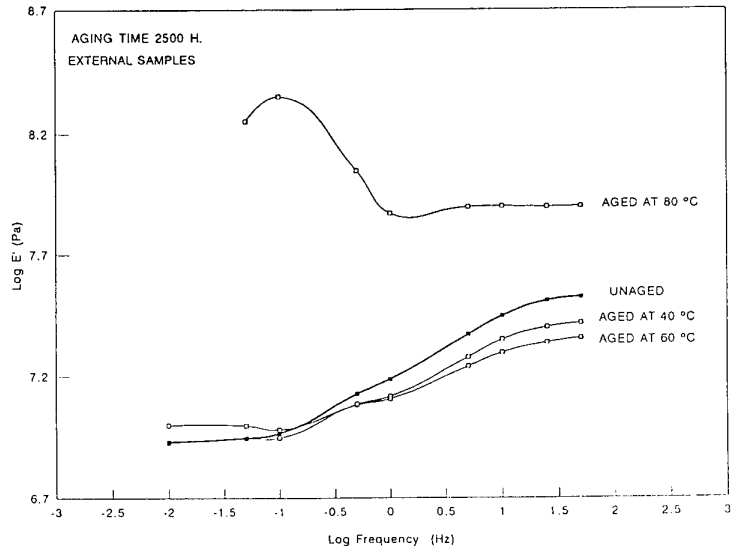


Figure 5. Log Storage Modulus E' as a function of the log frequency for rocket motor samples (external) aged at 40 °C, 60 °C and 80 °C after 2500 hours of aging.

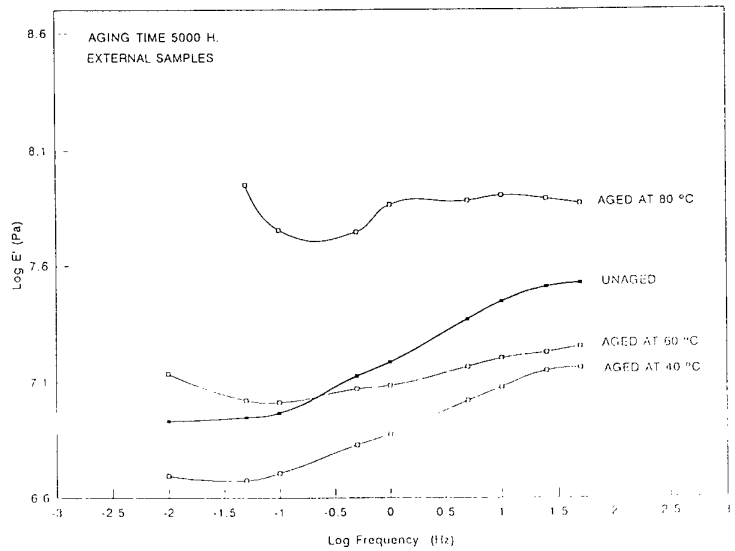


Figure 6. Log Storage Modulus E' as a function of the log frequency for rocket motor samples (external) aged at 40 °C, 60 °C and 80 °C after 5000 hours of aging.

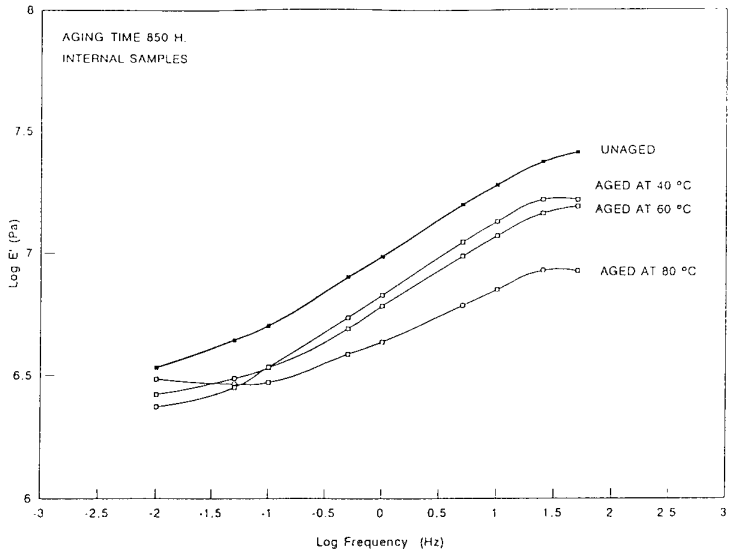


Figure 7. Log Storage Modulus E' as a function of the log frequency for rocket motor samples (core) aged at 40 °C, 60 °C and 80 °C after 850 hours of aging.

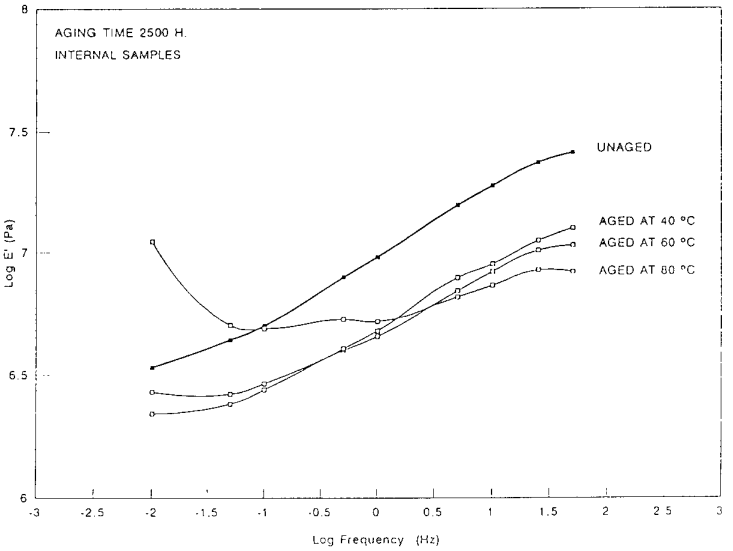


Figure 8. Log Storage Modulus E' as a function of the log frequency for rocket motor samples (core) aged at 40 °C, 60 °C and 80 °C after 2500 hours of aging.

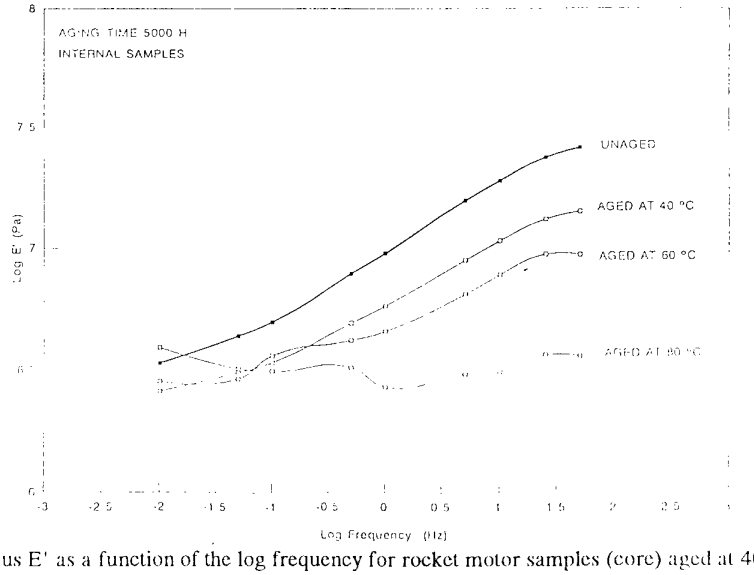


Figure 9. Log Storage Modulus E' as a function of the log frequency for rocket motor samples (core) aged at 40 °C, 60 °C and 80 °C after 5000 hours of aging.

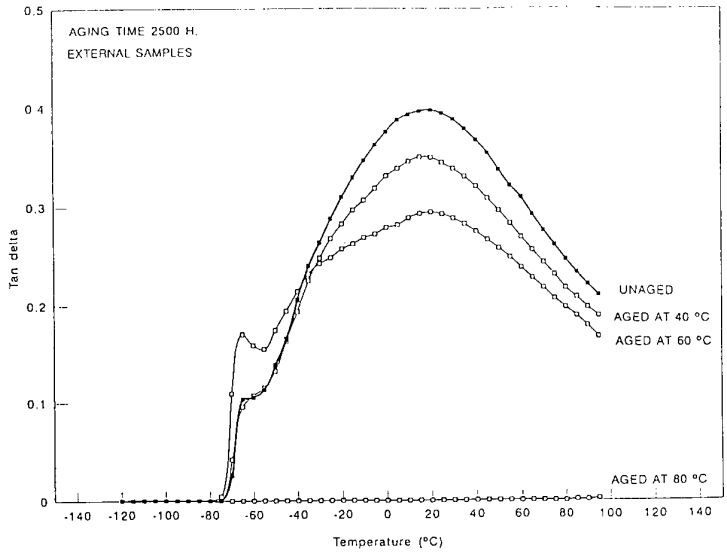


Figure 10. Tan delta as a function of temperature for rocket motor samples (external) aged at 40 °C, 60 °C and 80 °C after 2500 hours of aging.

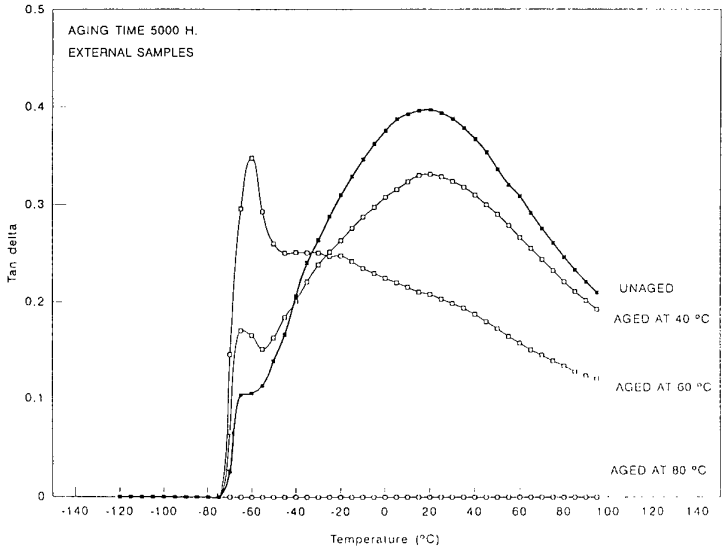


Figure 11. Tan delta as a function of temperature for rocket motor samples (external) aged at 40 °C, 60 °C and 80 °C after 5000 hours of aging.

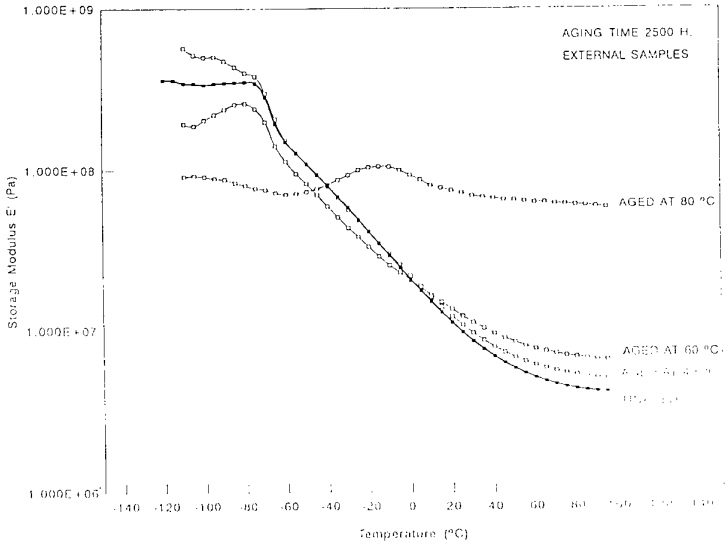


Figure 12. Storage Modulus as a function of temperature for rocket motor samples (external) aged at 40 °C, 60 °C and 80 °C after 2500 hours of aging.

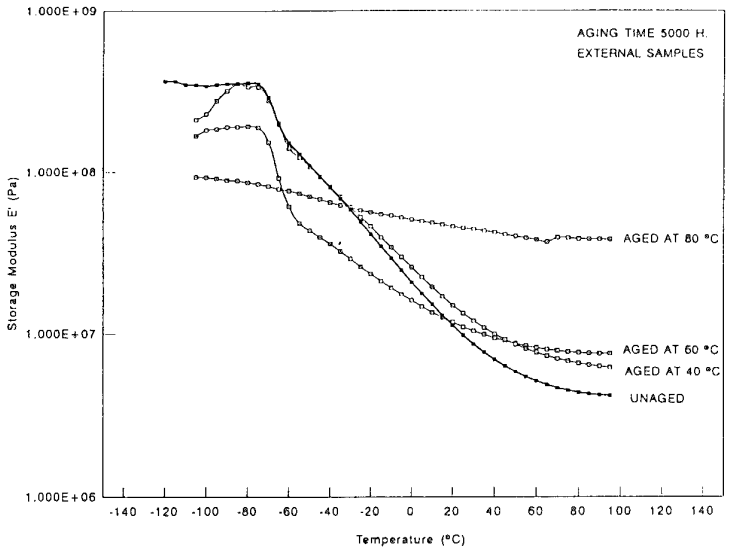


Figure 13. Storage Modulus as a function of temperature for rocket motor samples (external) aged at 40 °C, 60 °C and 80 °C after 5000 hours of aging.

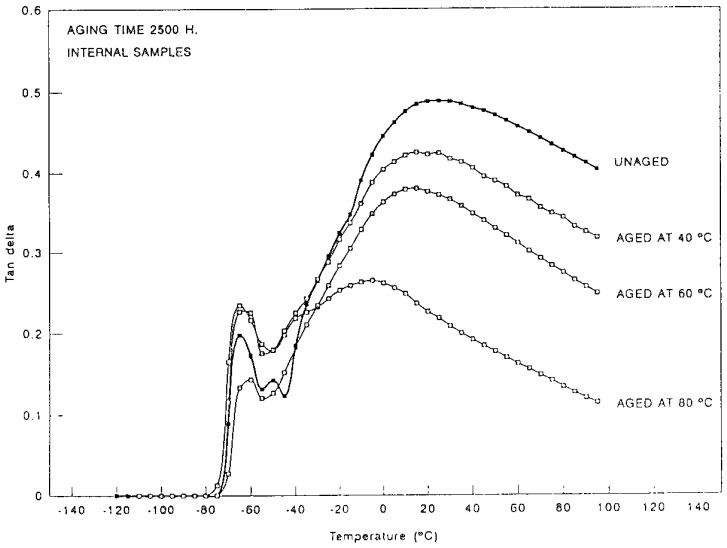


Figure 14. Tan delta as a function of temperature for rocket motor samples (core) aged at 40 °C, 60 °C and 80 °C after 2500 hours of aging.

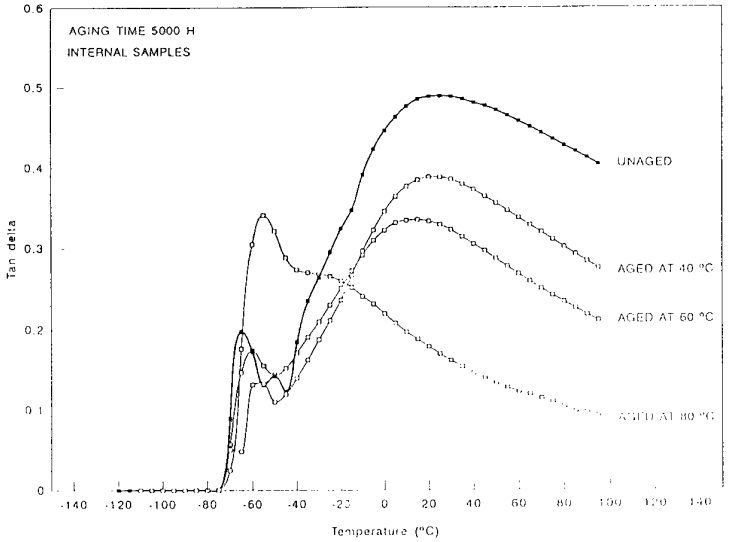


Figure 15. Tan delta as a function of temperature for rocket motor samples (core) aged at 40 °C, 60 °C and 80 °C after 5000 hours of aging.

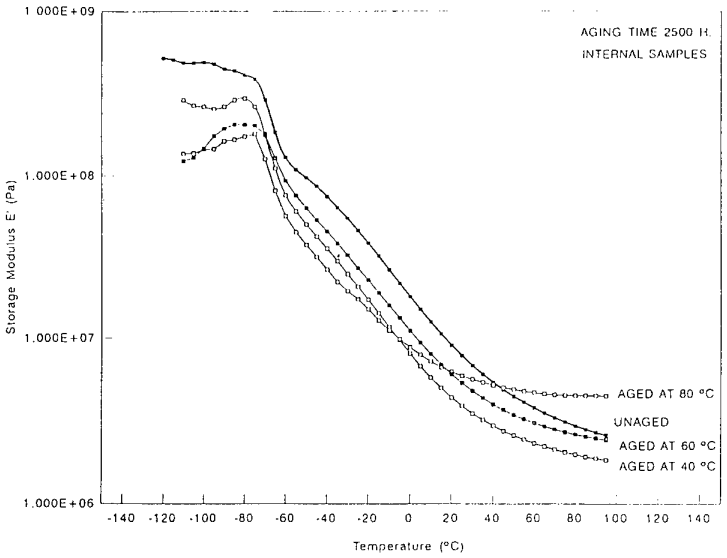


Figure 16. Storage Modulus as a function of temperature for rocket motor samples (core) aged at 40 °C, 60 °C and 80 °C after 2500 hours of aging.

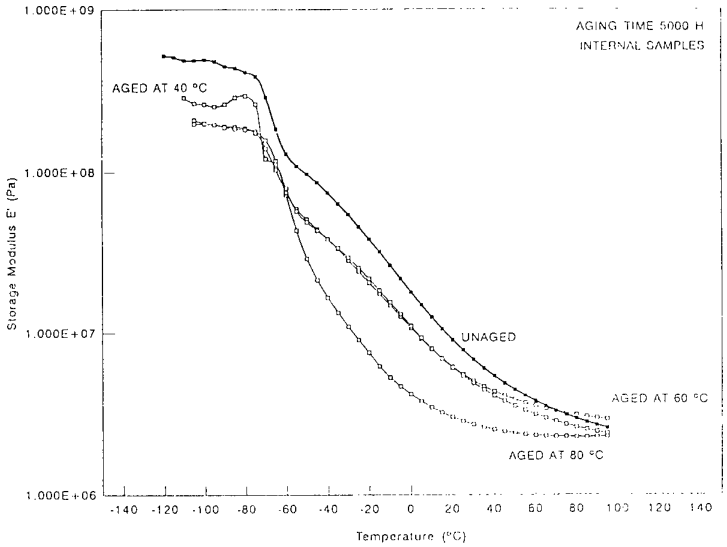


Figure 17. Storage Modulus as a function of temperature for rocket motor samples (core) aged at 40 °C, 60 °C and 80 °C after 5000 hours of aging.

Paper Number: 33
Discussor's Name: G. S. Faulkner
Author's Name: C. Schuller

Question: I was surprised by conclusion #3 (Frequency Scan Mode is a less accurate method in aging studies). This mode of operation is the one that is used by the stress analyst. Have you a comment on this?

Answer: Only, that when trying to get regular trends over a broad frequency range, the frequency scan mode appears to be less accurate.

Paper Number: 33
Discussor's Name: Dr. H. L. J. Keizers
Responder's Name: C. Schuller

Question: Do you know what causes the softening of your AP/HTPB propellant (even at moderate temperatures)?

Answer: Figures 12 and 13 of the paper show an increase of storage modulus with aging temperature i.e., the propellant becomes more brittle. On the other hand, figures 4, 5 and 6 (storage modulus versus frequency) show a decrease of storage modulus with aging temperature (softening) in the high frequency region. This is why I believe that Frequency Scan Mode is, in my opinion, less accurate when trying to obtain trends over a broad range of frequency.

Probabilistic Service Life Prediction for Solid Propellant Motors Subjected to Environmental Thermal Loads

R. A. Heller, S. Thangjitham
Virginia Polytechnic Institute and State University
Blacksburg, VA 24061-0219, USA

and

I. M. Janajreh
Currently at Michelin America
Greenville, SC 29600, USA

1. SUMMARY

Tactical solid propellant rocket motors stored under field conditions are subjected to environmental temperature variations and, as a consequence, to variable thermal stresses. These stresses may, during the service life of the motor, exceed the cumulatively damaged strength of the propellant resulting in cracks that could induce failure upon firing. Because both temperature and material properties are random variables, service life calculations should be based on probabilistic considerations, i.e., motor life is to be terminated when the progressive probability of failure which increases with elapsed time exceeds a predetermined value.

2. INTRODUCTION

Solid propellant motors consist of a granular oxidizer in a polymeric binder bonded, with several layers of interface materials, to a metallic or composite case. The propellant (oxidizer and binder) is a visco-elastic material while the case may, for most practical purposes, be considered elastic.

Long-term storage under environmental temperature conditions will produce chemical aging resulting in changed mechanical and thermal properties as well as variable thermal stress-induced cumulative damage.

The statistical variations of initial properties and of the thermal input require probabilistic analyses, in order to predict the safe service lives of such motors.

In this paper for the purpose of thermal stress analysis, solid propellant motors are modeled as long, concentric, layered cylinders consisting of a hollow propellant layer bonded to a thin steel case as shown in Fig. 1. Both layers are assumed to be isotropic materials.

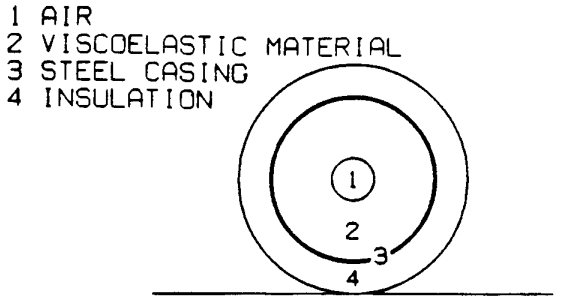


Fig. 1. Motor configuration.

Transient Fourier heat-conduction equations are used together with an elastic (case) and visco-elastic (propellant) stress analysis. First Order Second Moment (FOSM) reliability methods are applied and a progressive probability of failure is calculated as a function of time.

The analysis was carried out for three storage locations with arctic, desert and moderate climates, respectively.

3. THERMAL STRESS ANALYSIS

Air temperature is considered as a random process. The average weather conditions accounting for the mean and typical seasonal and daily variations can , for a given location, be predicted with fair accuracy. The superimposed random noise results from the change

Paper presented at the AGARD PEP Symposium on "Service Life of Solid Propellant Systems" held in Athens, Greece, 10-14 May 1996, and published in CP-586.

in weather conditions such as local cloud formation and weather front movements. Figure 2 shows typical hourly air temperatures at Phoenix, Arizona. The temperature input is characterized here as[1,2]

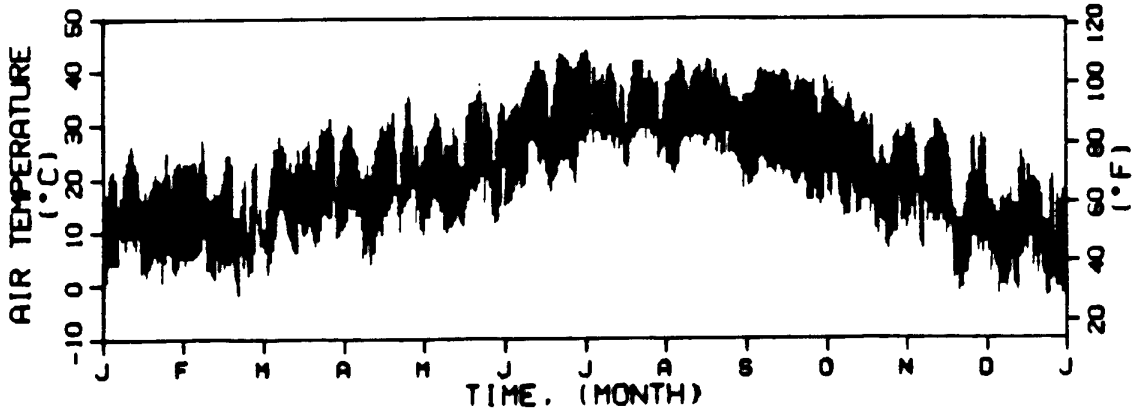


Fig. 2. Temperature variations in Phoenix, AZ.

$$T(t) = T_m + A_y \sin(\omega_y t + \phi_y) + A_d \sin(\omega_d t + \phi_d) \tag{3.1}$$

with

T_m = long term mean temperature

A_y, A_d = mean annual and daily amplitudes

ω_y, ω_d = annual and daily frequencies

ϕ_y, ϕ_d = annual and daily phase angles

These parameters are listed in Table 1, together with the coefficients of variation, δ, of the two statistically varying amplitudes for three locations: Barrow, AK, Phoenix, AZ and Nashville, TN[2].

The Fourier heat conduction equation for the j^{th} layer of a system of long cylinders, with no input variation along the length and without the presence of heat source, is written as[3]

$$\nabla^2 T_j(r,t) = \frac{1}{\gamma_j} \frac{\partial T_j(r,t)}{\partial t} \tag{3.2}$$

Table 1. Temperature Parameters

	Point Barrow, AK	δ	Nashville, TN	δ	Phoenix, AZ	δ
Mean Temperature $T_m(C°)$	-12.6	-	14.7	-	23.1	-
Yearly Amplitude $A_y(C°)$	17.1	0.10	11.5	0.10	10.7	0.10
Daily Amplitude $A_d(C°)$	0.9	0.10	4.2	0.10	6.4	0.10
Yearly Frequency $\omega_y(rad/hr)$	$2\pi/8760$	-	$2\pi/8760$	-	$2\pi/8760$	-
Daily Frequency $\omega_d(rad/hr)$	$2\pi/24$	-	$2\pi/24$	-	$2\pi/24$	-
Yearly Phase $\phi_y/\omega_y(hrs)$	5088	-	4871	-	4920	-
Daily Phase $\phi_d/\omega_d(hrs)$	15	-	16	-	16	-

where ∇^2 indicates the Laplacian operator, $T_j(r,t)$ is the temperature distribution function, γ_j is the thermal diffusivity, and r and t are the radial coordinate and time, respectively.

For an axially symmetric sinusoidal surface temperature input, the solution of Eq. (3.2) is sought in the following form:

$$T_j(r,t) = \bar{T}_j(r,\omega)e^{i\omega t} \qquad (3.3)$$

where $\bar{T}_j(r,\omega)$ is the complex frequency response function for the temperature within the jth layer and is given as

$$\bar{T}_j(r,\omega) = C_1^j Br(a_j r) + C_2^j Kr(a_j r) \qquad (3.4)$$

where $a_j = \sqrt{\omega/\gamma_j}$, ω is the loading frequency, C_1^j and C_2^j are the complex constants which must be determined by imposing the appropriate boundary and interface conditions, and Br$(\cdot)$ and Kr$(\cdot)$ are Kelvin functions of zero order[5].

For a plane stress problem, the elastic compatibility equation for the jth layer can be expressed in terms of a stress function $\phi_j(r,t)$ as

$$\nabla^2\left[\nabla^2\phi_j(r,t) + 2\beta_j\Delta T_j(r,t)\right] = 0 \qquad (3.5)$$

where $\beta_j = \alpha_j E_j/2(1-\nu_j)$ and α_j, ν_j, and E_j are the linear coefficient of thermal expansion, Poisson's ratio, and modulus of elasticity for the jth layer, respectively. Their numerical values are listed in Table 2. $\Delta T_j(r,t)$ in Eq. 3.5 is the temperature difference between the stress-free temperature, T_f, at which the propellant was cast, and the environmentally induced temperature, $T_j(r,t)$ of Eq. 3.1.

Because the input temperature on the surface of the cylinder consists of harmonic components, the following form of stress function is assumed[1].

$$\phi_j(r,t) = f_j(r,\omega)e^{i\omega t} \qquad (3.6)$$

where $f_j(r,\omega)$ is the complex frequency response for the stress function.

For an axisymmetric heating problem, the response function is given as

Table 2. Geometric, Thermo- and Elastomechanical Properties

Layer	1	2	3
Radius, r mm	48	109	112
Aging parameters for modulus	$A_E = 4 \times 10^5$	$B_E = 5 \times 10^3$	
Aging parameters for strength	$A_R = 1 \times 10^{11}$	$B_R = 9 \times 10^{13}$	
Damage parameters	$C = 2 \times 10^{51}$	$B_d = 9$	$\delta_c = 0.20$
Stress-free temperature	$T_f(C^\circ)$	73	
Conductivity, κ $(W/m -^\circ K)$	0.02508	1.4315	25.25
Diffusivity, γ (cm^2/hr)	685.672	28.064	316.308
Modulus of elasticity, E, E_∞ (N/m^2)		1.9433×10^6	2.068×10^{11}
Coefficient of thermal expansion, α $(cm/cm/^\circ C)$		3.31×10^{-5}	1.17×10^{-5}
Poisson's Ratio, ν		0.49	0.25

$$f_j(r,\omega) = K_1^j + K_2^j \ln(r) + K_3^j r^2 + K_4^j r^2 \ln(r) + 2\beta_j \left[\int^r \bar{T}_j(\rho,\omega)\rho \ln(\rho) d\rho - \ln(r) \int^r \bar{T}_j(\rho,\omega)\rho d\rho \right] \quad (3.7)$$

where $K_i^j; i$ = 1,2,3,4 are complex integration constants which are evaluated by imposing the appropriate boundary and interface conditions on stresses and displacements.

In terms of the resulting stress function, the radial and tangential stress components, $\sigma_{rr}^j(r,t)$ and $\sigma_{\theta\theta}^j(r,t)$, within the jth layer are readily calculated by the following relations:

$$\sigma_{rr}^j(r,t) = s_{rr}^j(r,\omega)e^{i\omega t} = \frac{1}{r}\frac{\partial f_j(r,\omega)}{\partial r}e^{i\omega t} \quad (3.8)$$

$$\sigma_{\theta\theta}^j(r,t) = s_{\theta\theta}^j(r,\omega)e^{i\omega t} = \frac{\partial^2 f_j(r,\omega)}{\partial r^2}e^{i\omega t} \quad (3.9)$$

where $s_{rr}^j(r\omega)$ and $s_{\theta\theta}^j(r,\omega)$ are the complex frequency response functions for the radial and tangential stress components, respectively.

For the cylinder with circular bore the tangential component at the bore is significantly greater than the radial stress at the bond line and consequently the bore tangential stress and its effects will be considered in the following.

because the propellant is a visco-elastic material, the elastic-visco-elastic correspondence principle may be applied.

For harmonic stresses it is expedient to replace the visco-elastic relaxation modulus of the propellant, E_2, with the frequency dependent complex modulus[6]

$$E(T,\omega) = E'(T,\omega) + iE''(T,\omega) \quad (3.10)$$

with

$$E'(T,\omega)_{RE} = E_\infty + \sum_{i=1}^{8} \frac{E_i \omega^2 a_t^2 \tau_i^2}{1 + \omega^2 \tau_i^2 a_i^2}$$

and

$$E''(T,\omega)_{IM} = 2\pi \sum_{i=1}^{8} \frac{E_i \omega a_t \tau_i}{1 + \omega^2 \tau_i^2 a_t^2} \quad (3.11)$$

where E_∞ is the rest modulus, E_i and τ_i are moduli and relaxation times of parallel Maxwell elements (see Table 3) and a_t is the time-temperature shift function:

Table 3. Prony constants for complex modulus

i	Modulus, E_i (N/m^2)	Relaxation time, τ_i, hour
1	1.3644×10^8	3.3333×10^{-12}
2	5.5088×10^7	3.3333×10^{-10}
3	1.7378×10^7	3.3333×10^{-8}
4	7.9472×10^6	3.3333×10^{-6}
5	5.0648×10^6	3.3333×10^{-4}
6	1.4975×10^6	3.3333×10^{-2}
∞	1.9433×10^6	

$$\log a_t = \frac{C_1(T - T_o)}{C_2 + (T - T_o)} \tag{3.12}$$

with $C_1 = -7$, $C_2 = 150°K$ and $T_o = 300°K$.

Using Eqs. 3.1, 3.5-3.12 the tangential stress at the bore may be expressed as

$$\begin{aligned}\sigma^2_{\theta\theta}(r_2,t) = T_f s^2_{\theta\theta}(r_2,0) \\ - \big[T_m s^2_{\theta\theta}(r_2,0) \\ + A_y \sin(\omega_y t + \phi_y) s^2_{\theta\theta}(r_2,\omega_y) \\ + A_d \sin(\omega_d t + \phi_d) s^2_{\theta\theta}(r_2,\omega_d)\ \big]\end{aligned} \tag{3.13}$$

4. STRENGTH, AGING AND CUMULATIVE DAMAGE

4.1 Strength

At temperatures below the stress-free temperature, T_f, the bore tangential stress is tensile. Consequently the ultimate tensile strength of the visco-elastic propellant is of interest. This time-and-temperature dependent strength may be given as[2]

$$R(T,t) = R_o \left(\frac{t}{4a_t}\right)^{-n} \tag{4.1}$$

where $R_o = 675\ KPa, n = 0.0857$ and time is measured in hrs.

4.2 Aging

The polymeric binder of the propellant is subject to chemical aging that is accelerated at higher temperatures.

Both the strength and the modulus are affected by this process. For the material considered here, both of these mechanical properties are reduced as functions of time. The aging parameter, $\eta(T,t)$, is the ratio of the mechanical property at time, t, to its value at $t = 0$ and is of the form[7]

$$\eta(T,t) = 1 - \beta(T)\log t \tag{4.2}$$

where β is an exponentially decreasing function of the temperature

$$\beta(T) = Ae^{-B/T} \tag{4.3}$$

The constants, A and B, which are different for strength and modulus, are listed in Table 2.

Consequently, the aged strength becomes

$$R(T,t) = \eta_R(T,t) R_o \left(\frac{t}{4\alpha_t}\right)^{-n} \tag{4.4}$$

Under variable temperature conditions an equivalent time t' is introduced

$$t'_1 = t_1^{\frac{\beta_1}{\beta_2}} \tag{4.5}$$

where β_1 and β_2 refer to the temperatures T_1 and T_2, before and after the change, respectively. If aging is continued at the second temperature for a period, Δt, the total aging time becomes

$$t_2 = t'_1 + \Delta t \tag{4.6}$$

Because aging is a rather slow process, it is not effected by daily temperature variations and only the annual cycle needs to be considered.

4.3 Cumulative Damage

According to the linear cumulative damage rule, the damage produced in a unit of time spent at a particular stress level S_i is inversely proportional to the time t_{fi} required to produce failure in the material at that stress level[7]

$$d_i = \frac{1}{t_{fi}} \tag{4.7}$$

and when a mixture of n stress levels is present each for a time t_i, the total damage D becomes equal to

$$D = \sum_{i=1}^{n} \frac{t_i}{t_{fi}} \tag{4.8}$$

A power function will describe the relationship between applied constant stress and reduced time to failure,

$$\frac{t_f}{a_t} = CS^{-B_d} \tag{4.9}$$

where C and B_d are material parameters listed in Table 3, and S is the stress, adjusted for aging and viscoelastic effects. Because of the statistical nature of the damage process, C is considered to be a statistical variable.

If the total time, under a random set of stresses is denoted by t_d, of which a fraction f_i is spent at stress level S_i, Eq. 4.8 may be rewritten as

$$D = \sum_{i=1}^{n} \frac{f_i t_d}{t_{fi}} \qquad (4.10)$$

For continuously varying stress levels the summation is replaced by integration and the fraction f_i becomes the probability density function $f_S(s)$ of random stresses. Substituting Eq. (4.9) into Eq. (4.10)

$$D = t_d \int \frac{f_S(s)ds}{a_t C S^{-B_d}} = t_d \times \Delta \qquad (4.11)$$

results with the integral denoted by Δ.

The initial strength of the material is a statistically variable property. Under the influence of damaging stresses this strength is gradually reduced as shown in Fig. 3. The reduced strength adjusted for aging may be written as[8]

$$R(T,t) = \eta_R(T,t) R_o \left(\frac{t}{4a_t}\right)^{-n} (1-\Delta) \qquad (4.12)$$

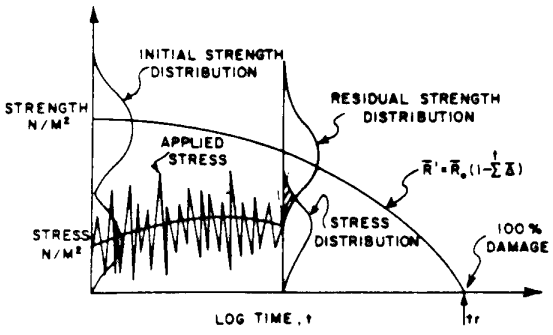


Fig. 3. Applied stress and damaged strength distributions.

5. FAILURE ANALYSIS

5.1 Instantaneous Probability of Failure

All of the mechanical and thermal properties of both motor-case and propellant are statistically variable as is the ambient temperature, and therefore, the resulting thermal stress.

Though it would be desirable to know the statistical distributions of these parameters, such distributions are seldom available. Consequently approximate methods are used in the analysis of failure.

Here the First Order, Second Moment (FOSM) technique will be used[9]. For this type of analysis only the first two moments, mean and variance of a variable are required.

The probability of failure may be expressed in terms of the applied stress, s, and the strength, R, of the material as

$$P_f = P\left[R \leq S\right] = P\left[(R-S) \leq 0\right] \qquad (5.1)$$

Because both strength and stress are functions of other statistical variables, such as temperature, modulus, etc.. The difference, $R - S$ is expressed as a function, G, which for failure is equal to zero.

$$G = G(X_1, X_2, \ldots, X_n) = 0 \qquad (5.2)$$

The variables X_1, X_2, ..., X_n are first normalized with respect to their means and standard deviations

$$x_i = \frac{\bar{X}_i - \mu_{x_i}}{\sigma_{\bar{X}_i}} \qquad (5.3)$$

The new function

$$G = G(x_1, x_2, \ldots, x_n) = 0 \qquad (5.4)$$

is the limit state function. A safety index, β, is defined as the shortest vector that connects the limit state function to the origin, therefore

$$\beta = \sqrt{x_1^2, x_2^2, \ldots, x_n^2} \qquad (5.5)$$

its direction cosines are calculated as

$$\alpha_i = \frac{\frac{\partial G}{\partial X_i^*}\sigma_{x_i}}{\sqrt{\sum_{i=1}^{n}\left(\frac{\partial G}{\partial X_i^*}\sigma_{x_i}\right)^2}} \qquad (5.6)$$

where the starred values of the variables denote the end point of the vector, β, on the limit state boundary.

The starred values of the variables are related to the safety index as

$$X_i^* = \mu_{X_i} - \alpha_i \beta \sigma_{X_i} \qquad (5.7)$$

when these are substituted into the G function, the value of β may be calculated. The process is iterative. New values of X_i^* are obtained in each cycle after initial, assumed, values until β converges.

If the variables are uncorrelated and normally distributed, the probability of failure is obtained from the safety index, β as

$$P_f = \Phi(-\beta) \qquad (5.8)$$

with Φ the area of the standardized normal distribution to the left of -β.

For correlated and non-normal variables[9] transformations are performed to uncorrelate them and to establish pseudo-normal distributions for them. It should be noted that the direction cosines, α_i, are used as measures of sensitivity. , When an α_i is small compared to others it is an indication that the corresponding variable needs not to be considered to have statistical significance and should be incorporated at its mean value.

5.2 Progressive Probability of Failure

A common approach for assessing the time dependent reliability problem is through the use of the failure rate function, $\lambda(t)$, defined in terms of the probability density, $f(t)$, and the reliability, $L(t)$, functions[1] as

$$\lambda(t) = \frac{f(t)}{L(t)} = -\frac{dL(t)}{dt}\frac{1}{L(t)} \qquad (5.9)$$

In this case, $\lambda(t)dt$ is interpreted as the conditional probability that a component that has survived to time t will fail in the next short time interval dt. Hence, the reliability of the component at time t may be evaluated by integrating the failure rate function

$$L(t) = \exp\left[-\int_0^t \lambda(\tau)d\tau\right] = \exp\left[-\Lambda(t)\right] \qquad (5.10)$$

where $\Lambda(t)$ is the cumulative failure rate up to time t.

For the problem in which the instantaneous probabilities of failure are defined over a specific time interval (e.g., daily probability of failure), the cumulative failure rate, $\Lambda(n)$, after n time intervals have passed is obtained by replacing the integral with a summation up to the n^{th} interval and the time increment dt with the interval duration Δt. Thus

$$\Lambda(n) = \sum_{k=1}^{n} \frac{P_f(k)}{L(k-1)}\Delta t \qquad (5.11)$$

with $L(0) = 1$ and $P_f(k)$ is the daily probability of failure calculated in Section 5.1.

Consequently, the progressive probability of failure in the n^{th} interval, $P_f(n)$, becomes

$$P_f(n) = 1 - L(n) = 1 - \exp\left[-\Lambda(n)\right]. \qquad (5.12)$$

6. SERVICE LIFE CALCULATIONS

6.1 Stress and Strength

Motors with geometric, mechanical and thermal properties listed in Tables 2 and 3 are subjected to the temperature variations of Phoenix, AZ, Nashville, TN, and Barrow, AK. The temperature parameters are presented in Table 1.

First the variations of thermal-stresses, calculated with the aid of the Eqs. of Section 3 are determined[10]. The aging effects of modulus degradation (Section 4.2) are also considered. The resulting tangential stresses are plotted in Fig. 4. It is seen that the viscoelastic nature of the modulus is reflected in the sinusoidal variations of these stresses. Largest amplitudes are observed at arctic conditions because the complex modulus is most sensitive at low temperatures.

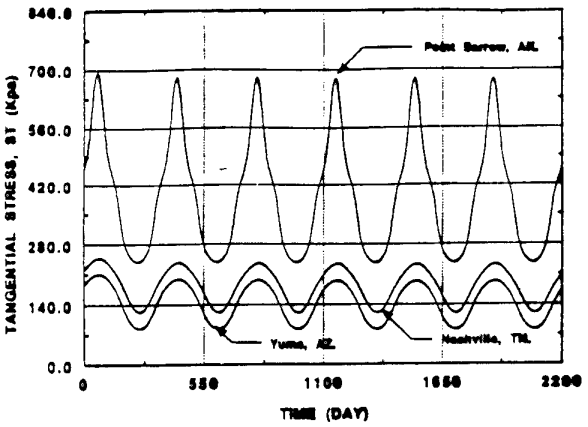


Fig. 4 Variations of tangential bore stresses.

Next the aged and damaged visco-elastic strength of the propellant is determined based on Eq. 4.12 and is presented in Fig. 5.

Cumulative damage reduces the propellant strength quite rapidly under arctic conditions.

6.2 Probability of Failure

Of the many variables, those deemed statistically significant based on sensitivity analyses (Eq. 5.6) are the diurnal and annual amplitudes of the temperatures, the modulus of the propellant and case, the initial strength of the propellant and the cumulative damage parameter, C.

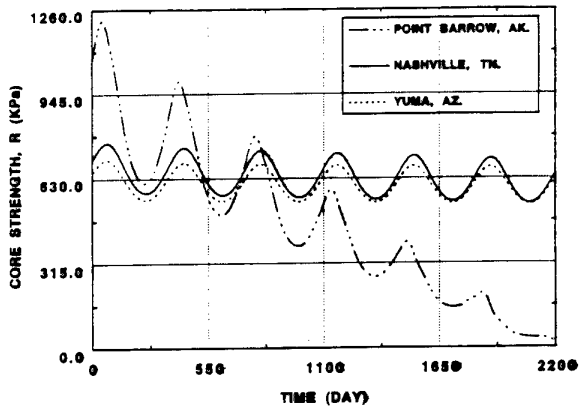


Fig. 5 Variations of aged and damaged propellant strength.

It has been assumed in the probabilistic analysis that the strength and the modulis of the propellant are independent and follow two parameter Weibull distributions:

$$L_X(x) = e^{-\left(\frac{x}{x_c}\right)^m} \tag{6.1}$$

where m is the Weibull shape parameter, $m \doteq 1.2/\delta$ (δ = coefficient of variation) and x_c, the characteristic value that is related to the mean as

$$\bar{x} = x_c \Gamma\left(1 + \frac{1}{m}\right) \tag{6.2}$$

with $\Gamma(\cdot)$ the tabulated gamma function.

The coefficient of variation for strength and modulus were taken as $\delta_R = .1$ and $\delta_E = .05$. The other variables were assumed to be normally distributed.

Utilizing the methods described in Section 5, the progressive probabilities of failure have been calculated and are presented in Fig. 6.

At Point Barrow, AK, this probability increases rapidly and indicates that motors should be removed from storage after about a year. At moderate climate sites motor safety remains high for considerably longer periods.

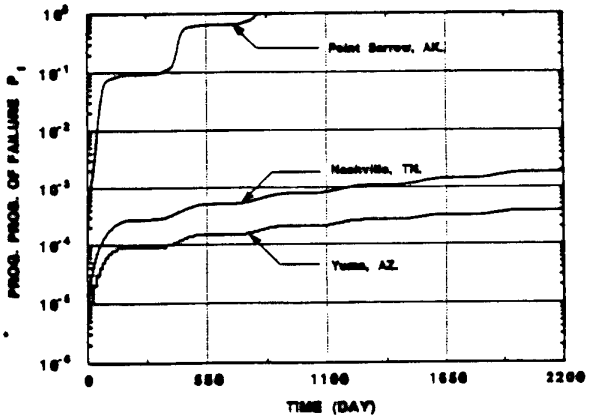


Fig. 6 Progressive probabilities of failure.

6.3 Correlated Strength and Modulus

It is frequently observed that the strength and the modulus of propellant materials are correlated variables, that is a stronger material also possesses a higher modulus.

Such correlations are characterized by the correlation coefficient, ρ that may vary between -1 and 1

$$-1 \leq \rho \leq 1 \tag{6.3}$$

$\rho = \pm 1$ indicates that the variables are linearly related (positively or negatively), i.e.,

$$R = \pm CE \tag{6.4}$$

while $\rho = 0$ when the variables are independent of each other as assumed in Section 6.2

For fractional values of the correlation coefficient, the variables are not perfectly correlated.

In the present analysis various ρ values have been considered for the conditions at Nashville, TN.

The results plotted in Fig. 7 indicate that the progressive probability of failure is significantly reduced when the variables are correlated. Because both strength and modulus are visco-elastic and are affected in the same direction by temperature changes, such correlations definitely exist and should be considered in safety analyses.

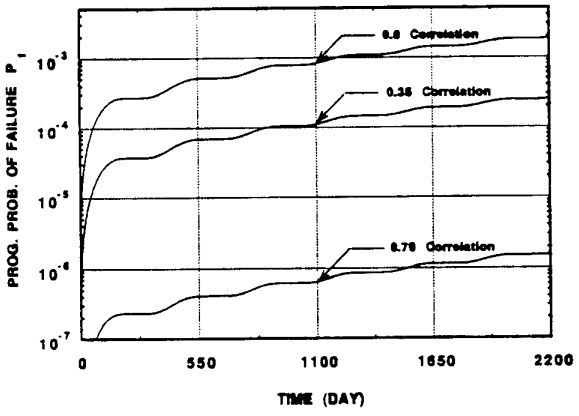


Fig. 7 Progressive probability of failure; strength and modulus are correlated.

7. CONCLUSIONS

A service life analysis methodology based on stress-strength interference has been presented. Such a technique may be used to estimate the safe life of rocket motors and offers a rational approach for motor replacements.

The effects of correlation between variables implies a possibility of extending the service life of motors that have been evaluated without such considerations.

8. REFERENCES

1. Heller, R. A., and Thangjitham, S., "A Survey of Probabilistic Service Life Prediction Methods for Structures,"IUTAM Symposium on Probabilistic Structural Mechanics. Ed: Spanos, P. D. and Wu, Y. T. Springer, New York, 1993. pp. 237-267.

2. Janajreh, I. M., Heller, R. A., and Thangjitham, S., "Safety Index Approach to Predicting the Storage Life of Rocket Motors,"J. Spacecraft and Rockets, V.31, No. 6, 1994, pp. 1072-1078.

3. Boley, B. A. and Weiner, J. H., "Theory of Thermal Stresses,"Wiley, New York, 1960.

4. Abrammowitz, M., and Stegum, I. A., "Handbook of Mathematical Functions,"Nat. Bureau of Stds. Applied Math, Series 55, Washington, 1964.

5. Christensen, R. M., "Theory of Viscoelasticity," Academic Press, New York, 1961.

6. Cost, T. L., "Service Life Predictions for Thermal Loads Using Viscoelastic Finite Element Simulation Models,"U.S. Army Missile Command, Final Rep., Contract DAAH01-76-C-1069, USAMICOM-CR-79-3, Huntsville, AL, Dec. 1979.

7. Bills, K. W., Jr. and Wiegand, J. H., "The Application of an Integrated Structural Analysis to the Prediction of Reliability,"Annals of Reliability and Maintainability, Feb. 1970, pp. 514, 526.

8. Heller, R. A., and Singh, M. P., "Thermal Storage Life of Solid Propellant Motors,"Journal of Spacecraft and Rockets, Vol. 20, No. 2, 1983, pp. 144-149.

9. Ang, A. H. S., and Tang, W. H., Probability Concepts in Engineering Planning and Design, Vol. II, Wiley, New York, 1984.

10. Heller, R. A., Thangjitham, S., and Janajreh, I., "User's Guide to the Safety Index Calculation Program ROCKT2,"U.S. Army Missile Command, CR-RD-PR-91-2, Redstone Aresenal, Huntsville, AL, Sept. 1991.

Paper Number: 34
Discussor's Name: Dr. M. A. Bohn
Responder's Name: Professor R. A. Heller

Question: Can you describe the influence of temperature cycling on gun propellant grains with this approach?

Answer: Sorry but I have no experience with gun propellants.

Paper Number: 34
Discussor's Name: Dr. H. L. J. Keizers
Responder's Name: Professor R. A. Heller

Question: What do you expect will be the effect of chemical aging on the damage parameters? Should this possible effect be included in the predictions?

Answer: If it can be measured, it could be included. I would be interested if anyone has such experience.

Paper Number: 34
Discussor's Name: I. H. Maxey
Responder's Name: Professor R. A. Heller

Question: Do you think the optimistic prediction of the progressive probability of failure for the hot regions is due to the limitations of the model in accounting for the significant variations from mean temperature in these regions. Can the model take these into account?

Answer: The model illustrated in the paper has only two thermal cycles included. We have in past analyses included several other harmonics and have also followed hourly variations. The spikes mentioned can be accounted for if the thermal history is followed. It is only a question of computer time.

Paper Number: 34
Discussor's Name: Dr. H. J. Buswell
Responder's Name: Professor R. A. Heller

Question: The true service life is less than your analysis would indicate due to the damage induced during motor firing. How would you handle this extra damage?

Answer: We have so far not included damage due to firing pressures. The way we look at it, one would have to have a partially damaged motor to start with. An initial crack could be propagated by firing pressures.

Paper Number: 34
Discussor's Name: C. P. Daykin
Responder's Name: Professor R. A. Heller

Question: With the increase of worldwide policing operations, the majority of air-to-air rocket motors have been subjected to many hundreds of air carriage hours, typically seeing temperature ranges of +30° C to -50° C. Have you considered modifying the equations to take into account the significant effect of air carriage hours?

Answer: Yes. Given a temperature history, the effects can be incorporated. We have, however, found that short duration temperature variations do not have significant effects on bore stresses, though bondline stresses may be affected. The air heating and vibration loads should also be considered.

Methodology and Techniques for Determining Service Life of Solid Rocket Motors

Richard K. McCamey, Edmund K. S. Liu
GenCorp Aerojet
P.O. Box 13222
Sacramento, CA 95813-6000, USA

ABSTRACT

One methodology in common use today for evaluating service life is based on chemical kinetic models quantified by the rate theory of Eyring and the Arrhenius relationship. Techniques employed to accomplish this task may include mechanism studies as well as kinetic evaluation of material property changes. Verification of aging trends and models may be accomplished through motor dissections, plug motors, and excised samples. This methodology and associated techniques will be discussed in depth.

INTRODUCTION

Service life determination of solid rocket motors is a broad terminology that is applied to a variety of techniques employed in the industry. The complexity of the technique often depends on the service life goals specified for the motor system. Some systems may require an actual end-of-life prediction with considerable lead time desired, while others may only specify a finite number of years for the service life requirement. The funds available are also a key factor in designing an adequate service life assessment program. Additionally, some techniques are considered predictive while others are essentially a static use-test.

The later technique, by itself, does not determine service life and often employs motor firing, nondestructive testing, and dissections to determine if the motor still meets performance specifications. This type of activity, although quite common, should be classified as surveillance and ideally used for the verification phase of a predictive program.

Of the predictive methodologies, two stand out because of their frequent use within the industry; the cumulative damage approach and the chemical kinetic approach. The cumulative damage approach is primarily used in situations where aging changes are anticipated to be a result of mechanical and thermal loads. This applies largely to tactical motors where thermal loads during storage and operation are often quite broad and mechanical loads can be severe. These loads result in damage to the motor that accumulates as a function of age. A damage function calculated at various times increases to unity, the defined service life of the motor. The chemical kinetic approach is most often applied to motor systems where diffusion phenomena and concurrent or sequential chemical reactions control the aging process. The service life of strategic motors or other large boosters is often evaluated using this methodology since thermal and mechanical loads are presumed to be minimal for these types of motors. The chemical kinetic approach has been used for numerous tactical systems as well, since chemical changes are quite common. In reality, both chemical and mechanical aging occur simultaneously. The feasibility of combining these two methods has been evaluated through several techniques including the PAL[1], and Predictive Surveillance[2] techniques. These techniques typically utilize a time-compressed aging/damage cycle which is designed to accelerate the motor's chemical and mechanical aging while maintaining thermal exposure very close to specification requirements. Following the accelerated aging, the motors are structurally overtested, usually by thermal cycling.

Considerable work has been performed in the wide variety of methodologies available for predictive service life assessment, however, the chemical kinetic approach has provided a large experience base and demonstrated success in several motor systems. This predictive approach will be illustrated utilizing the results from a specific motor system with emphasis on the verification phase.

GENERAL APPROACH

It is important from the overall view to bear in mind that the integrity of the solid rocket motor depends primarily upon its ballistic performance. From a service life standpoint, factors influencing ballistic performance may involve changes in combustion properties directly, changes in structural integrity of the propellant grain or other components, and changes in hazard characteristics of the propellant or system. To evaluate these changes, the general service life prediction approach depicted in Figure 1 is typically followed.

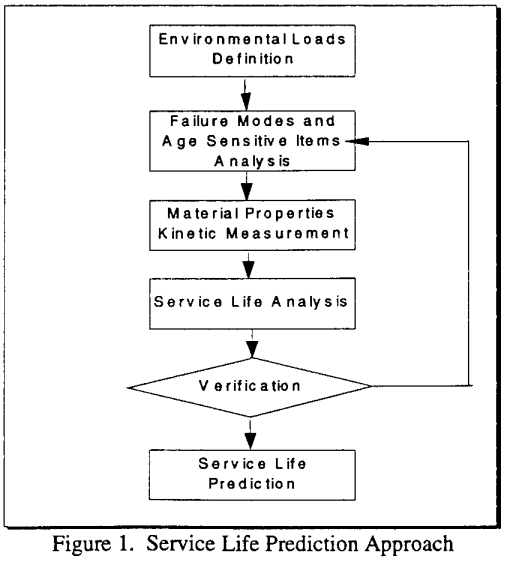


Figure 1. Service Life Prediction Approach

Paper presented at the AGARD PEP Symposium on "Service Life of Solid Propellant Systems" held in Athens, Greece, 10-14 May 1996, and published in CP-586.

Environmental loads placed on the system are key parameters that must be considered but are often poorly defined in any service life prediction study. Such loads include transportation, ground handling, operational, thermal storage, short-term thermal excursions, pressure, and exposure to environmental contaminants. During motor design and development, the anticipated loads and associated statistical definition of load history should be used. Later in a program, this item should be reviewed to establish realistic statistical definition of loads and environmental exposure. This may require use or development of comprehensive models to account for these sources of uncertainty.

An in-depth analysis to identify and define all the credible potential failure modes is then performed for each component of the system. The failure modes analysis provides the basis for subsequent analysis of failure mechanisms. A key consideration for each potential failure mode and mechanism is the age sensitivity of all components, materials, and phase boundaries. One method commonly employed is to initially evaluate all potential diffusion phenomena within the system. Subsequent or concurrent potential reactions may be considered based on theoretical chemistry and experience with other systems. Screening studies are often performed at this point to validate expected age-induced changes.

Based on the prioritized summation of failure modes, failure mechanisms, age sensitivity and anticipated aging mechanisms, an accelerated aging program is designed. Individual diffusion or reaction mechanisms are characterized kinetically and often validated with actual composite material. Appropriate test parameters, both chemical and mechanical, are selected to quantify aging changes. The individual processes are then combined into analytical or empirical kinetic models unique to either specific components or locations within the motor. Failure criteria are established and a preliminary service life assessment can be made based on the intersection of the kinetic projection with statistical consideration and the failure criteria.

Finally, the aging and preliminary service life analysis must be validated prior to the final useful life prediction. The preliminary service life assessment is often based on sub-scale samples or analogs. It is next to impossible to simulate accurately all motor locations or loading conditions. Further, it is unrealistic to expect that the motor will be built with the precision, accuracy and environmental control that is possible in the laboratory. Experience has shown that the differences between motors and laboratory assets are considerable and that simple tests conducted on materials from motors may be more meaningful than results of sophisticated tests that require use of laboratory samples. The motor itself should serve initially as a guide for the design of laboratory analogs and ultimately as a basis for verification of aging trends and service life. This phase of the program may include verification through overtest (testing of full-scale motors under loading conditions in excess of operational loads), characterization of material properties from dissected motors, evaluation of aging trends using techniques like plugging, excising, or even accelerated aging of motors.

DIFFUSION/REACTION MECHANISMS

Solid rocket motors are composed of a variety of polymeric materials such as propellant, liner, insulation and adhesives. Each of these materials consist of potentially mobile chemical species that also may be chemically reactive. These species include inert and energetic plasticizers, curatives, catalysts, stabilizers, bonding agents as well as non-crosslinked binder fractions. In addition to internal species, most motors must consider interactions with environmental contaminants. There is typically a gas phase interface at the bore surface which serves as a source or sink for various volatile species including water vapor and oxygen.

The design of the motor system studied in this work incorporates a non-permeable case with a booted configuration on both ends of the motor. The boot gap as well as the inner bore surface is essentially open to the environment since the motor itself had no form of environmental protection at the nozzle. The system is stored in a relatively controlled temperature environment of 60 to 80°F with an estimated mean of 70°F. The humidity environment however, is totally uncontrolled with indications of humidity exposures to very high levels.

A preliminary review of the chemistry for this system was undertaken to evaluate potential failure modes, age sensitive items, and the theoretical aging mechanisms that could lead to failure. The primary potential diffusion processes were identified as illustrated in Figure 2.

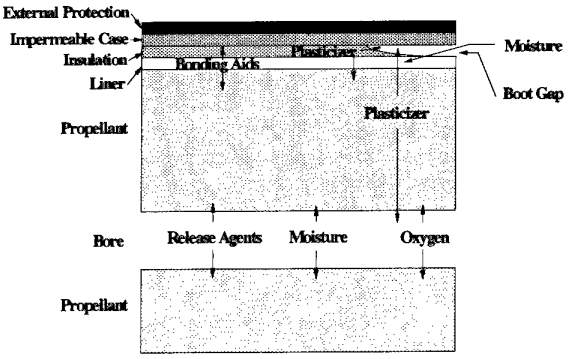


Figure 2. Evaluation of Diffusion Phenomena

In the bond region, moisture present in the boot gap diffuses through the insulator into the liner and ultimately the propellant. Propellant plasticizer (inert) diffuses through the liner, insulation and can ultimately volatilize from the insulation surface. Insulation plasticizer (inert) will volatilize from the surface and diffuse into the liner and propellant. The change in concentration of these diffusing species can, at a minimum, result in material property changes. Additionally, the aziridine cured liner can undergo hydrolytic degradation.

At the bore surface, oxygen and moisture can both diffuse into the propellant while the inert propellant plasticizer will

volatilize off the propellant surface. Loss of the propellant plasticizer results in hardening of the surface while moisture absorption partially counteracts the hardening with a softening mechanism. Subsequent oxidative crosslinking reactions of the propellant polymer can also harden the propellant and reduce strain capability. These potential failure mechanisms are summarized in Table 1.

Table 1. Key Failure Modes

Failure Mode	Aging Mechanism
Inner Bore Cracking	-Net decrease in strain capability Oxidative crosslinking Loss of propellant plasticizer Absorption of moisture
Bond Separation	-Hydrolytic liner degradation -Influence of insulation plasticizer diffusion -Influence of propellant plasticizer diffusion

The potential aging mechanisms and failure modes identified for this system are associated with the structural integrity of the grain. Potential changes in ballistics properties and hazard characteristics, typical in some systems, were considered minor for this system.

Laboratory studies were initiated to evaluate the potential aging mechanisms. The ability of the propellant polymer to oxidatively crosslink at the bore surface was evaluated through oxygen absorption measurements and polymer viscosity increases. The reaction was found to be catalyzed by trace concentrations of iron. Continued experimentation verified the reaction and diffusion mechanisms at the bore surface. However, the importance of this aging process became secondary to the aging mechanisms in the bond region and is not discussed further.

The hydrolytic liner degradation mechanism was verified using model compounds to simulate the liner polymer network. These were prepared by forming esters from the liner aziridine curatives. Aging under various environments coupled with measurement of molecular structural changes by NMR and IR analysis identified the hydrolytic attack on the amide linkages. The severity of the degradation mechanism indicated this to be the primary aging mechanism that could limit service life. Consequently, an accelerated aging program was initiated to quantify and model the aging process.

ACCELERATED AGING

Once the possible mechanisms leading to aging changes were identified, the kinetics of the individual processes were measured in storage tests over a range of temperatures from 110 to 180°F and humidity from 10 to 100 %RH according to the matrix presented in Table 2. Humidity were maintained using saturated salt solutions.

Table 2. Accelerated Aging Matrix

Humidity, %RH	10	30	50	80	100
Temperature, °F					
180	x	x	x	x	
165	x	x	x	x	
150	x	x	x	x	x
135	x	x	x	x	x
125		x	x	x	x
110		x	x	x	x

Initial attempts to begin the accelerated aging experiments provided data that indicated unanticipated results. Crosslink density of liner and composite bond strength both initially increased before any signs of degradation were observed. Apparently, the liner and bond analogs were not fully cured following the standard production cure cycle. Consequently, it was necessary to isolate the two individual mechanisms, postcure and hydrolytic degradation, by first assuring that materials for hydrolytic degradation kinetic measurement were fully cured.

To assure that the kinetics of the degradation process were as accurate as possible, two techniques for measuring property changes were employed. The first, considered the more accurate, was the determination of neat liner polymer crosslink density calculated from swelling ratio and gel filler fraction measurements using the Flory-Rehner equation. This provides a direct measurement of the degradation mechanism while minimizing the influence of other variables. Figure 3 illustrates the typical results with a specific temperature and humidity condition. The degradation process could be modeled, as expected from the chemical mechanism, as a first order reaction (ln property vs time). The correlation coefficient (0.993) was excellent for this kinetic fit.

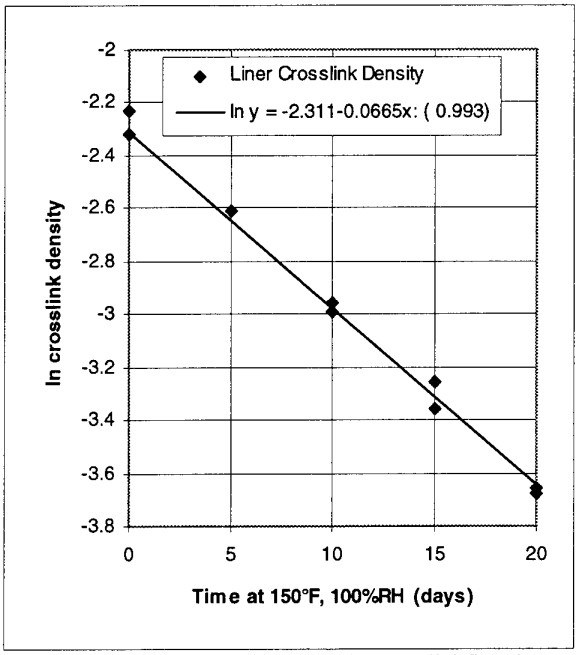


Figure 3. Degradation Measured by Crosslink Density

The critical property from a structural integrity viewpoint, however, is propellant-liner-insulation bond strength. Consequently, analogs were prepared that simulated the bond interface and stored isothermally at the same humidity conditions as the neat liner. Bond strength as a function of time was measured after the analogs had been fully cured. Changes in bond tensile strengths as a function of storage time were empirically fit with a first order treatment of the rate constants providing the best fit. This is illustrated in Figure 4 for the same temperature/humidity aging condition as that used in the neat liner study. The rate data for the two curves are nearly identical over the time span evaluated. This relationship validates the use of mechanical properties in place of, or in addition to, crosslink density in determining the kinetics of aging. As expected, the variability (correlation coefficient = 0.85) for this measurement is not as good as experienced for crosslink density. Bond strength measurements are dependent on additional variables such as specimen geometry variations and material properties of both the insulation and adjacent propellant.

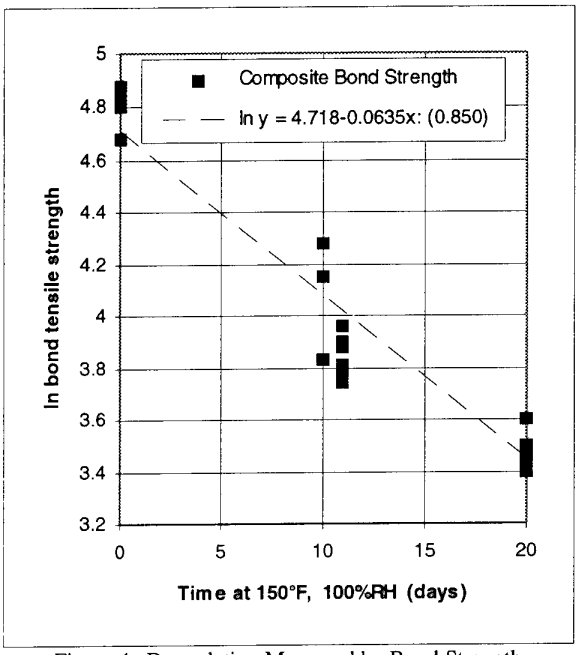


Figure 4. Degradation Measured by Bond Strength

From the accelerated aging studies, rate constants using first order reaction kinetics are determined. Plots of regression lines relating rate constant to relative humidity are drawn for each temperature (Figure 5).

These changes can then be quantified by the kinetic rate theory of Eyring and the Arrhenius relationship:

$$k = Ae^{-Ea/RT}$$

where k is the rate constant, A is the pre-exponential factor, Ea is the energy of activation, R is the gas constant and T is the temperature in °K. A plot of ln k against 1/T will then be linear with a slope proportional to the activation energy provided another reaction has not become dominant at elevated temperature.

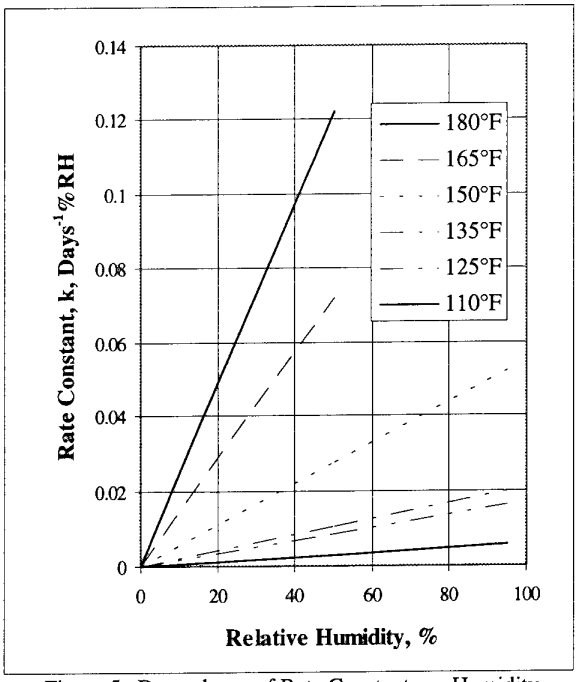


Figure 5. Dependence of Rate Constants on Humidity

A weighted Arrhenius plot (Figure 6) was constructed to obtain a mean activation energy of 19.3 kcal/mole and a humidity dependent rate constant at any desired temperature. One can then project an effective property over any aged time.

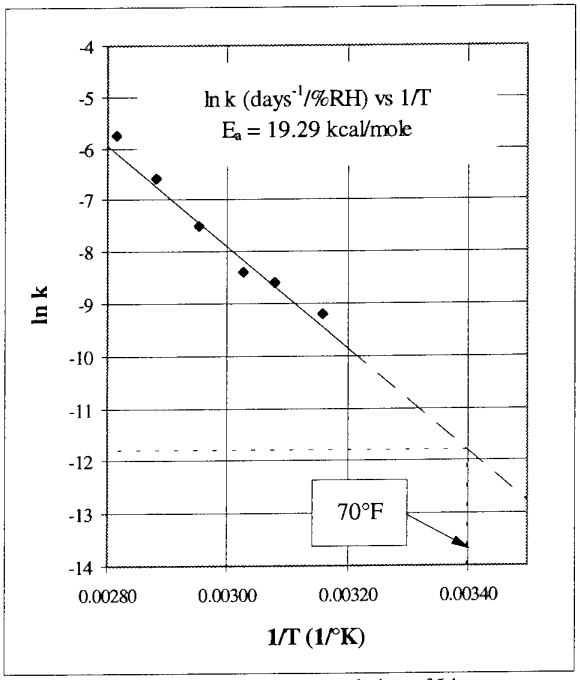


Figure 6. Hydrolytic Degradation of Liner

An often mentioned problem associated with the chemical kinetic approach is the potential for alternate mechanisms with high activation energies that are insignificant at nominal storage temperatures but dominate at elevated temperatures. At extreme temperatures, a lower activation energy reaction which may control the behavior at nominal conditions could be completely obscured. This scenario results in a non-linear Arrhenius relationship in which multiple reactions are being accelerated at different rates. The incorporation of six different accelerated aging temperatures rather than the theoretical minimum of three temperatures in our study assures that this potential problem is not significant.

The postcure mechanism was kinetically modeled separately using the same process as that illustrated for hydrolytic degradation. In this case, propellant-liner-insulation bond interface analogs were aged at three elevated temperatures of 110, 135, and 150°F under dry conditions. The increase in bond strength was monitored until it leveled off. Property change rates were modeled kinetically assuming a first order reaction. Results indicate a rate constant of 0.507 months^{-1} at 70 °F with an activation energy of 11.7 kcal/mole.

Diffusion processes are also typically accelerated by increased temperature. Permeation and diffusion rates are obtained at multiple temperatures and kinetically treated using the Arrhenius relationship. Since moisture was the key contributor to the hydrolytic degradation process, transport properties of moisture through the insulation were measured. The permeability coefficient was kinetically determined using the cup method to be:

$$1.55 \times 10^{-6} \text{ g-inch/(day)(inch}^2\text{)(\%RH) at 70°F}$$

with an activation energy of 11.94 kcal/mole. The solubility coefficient is approximately independent of temperature on a %RH basis.

PREDICTIVE MODELING

A predictive aging model can be developed by combining the kinetic data from all the pertinent individual aging mechanisms. For some motor systems, the number of processes may be few and the aging mechanisms relatively simple. In this case, a model may be constructed manually by combining individual rate equations in either consecutive or simultaneous fashion.

For complex systems, a computer code to combine and model all the simultaneous chemical kinetic and diffusion processes is required. Such codes exemplified by the 2D-axisymmetric TEXCHEM[3] code or DIAL[4] code can handle both diffusion and chemical kinetic processes.

Utilization of such codes for predictive service life assessment requires characterization of all significant chemical reactions as well as diffusion and volatility related changes. Characterization includes experimentally determining kinetic reaction rates, diffusion coefficients and their activation energies. Activity coefficients must also be determined from specie solubility data as a function of temperature and concentration. Additionally, the chemical species concentration changes must be correlated with the appropriate age-related mechanical property changes in the case of structural life-limiting mechanisms.

The aging model for the specific system studied here is relatively simple. The primary aging mechanism that impacts service life was identified (hydrolytic liner degradation) and the kinetics of the degradation process characterized (Figure 6). Correlation of liner crosslink density with bond strength was made so that the model would be based on the critical structural property. Other aging mechanisms directly involved in this failure scenario include moisture diffusion and post cure, both of which were kinetically modeled. The post cure reaction opposes the hydrolytic softening process (both first order reactions) and can be modeled as consecutive competing reactions. The model becomes:

$$B = A_o(k_1/k_2-k_1)(e^{-k_1 t}-e^{-k_2 t}) + B_o e^{-k_2 t}$$

where B is the bond strength (or liner crosslink density) at any time, B_o is the initial bond strength (or liner crosslink density), A_o is the fully cured bond strength - B_o, k_1 is the post cure rate constant, k_2 is the hydrolytic degradation rate constant and t is the time.

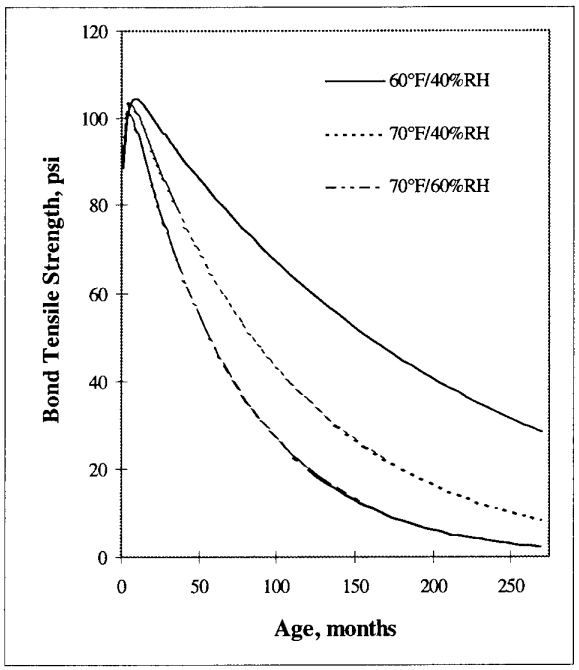


Figure 7. Kinetic Projection

Moisture diffusion through the relatively thin insulator was not included in this model since moisture was readily available at the critical location (liner) by the time the postcure mechanism was complete. Diffusion, however, was included in another application where the presence of a much thicker material layer significantly delayed the infiltration of moisture into the liner. The model is illustrated in Figure 7 with variations in humidity and temperature.

Predictions of material properties can then be made for specific known environmental conditions or for population means with appropriate variability factors.

Predictive models are only as good and useful as the data obtained. It is important to periodically update the predictive models as additional data is collected and analyzed. This is particularly important as discussed in the verification portion of this paper. As the database increases with input from actual motors after long-term storage or varied environmental exposure, the baseline predictive model may change.

AGE-OUT CRITERIA

Service life prediction of a solid rocket motor is based on a comparison of some aspect of the motors capability with a failure criteria. The age-out criteria may be as simple as comparison of appropriate material properties with their specifications or as complex as the propagation of an induced flaw that results in catastrophic motor failure. The most widely used, however, is the point at which material capability equals a calculated structural requirement.

In this motor system, the established predictive model addresses the change in bond capability. However, another aging mechanism, boot shrinkage, influences structural requirements by generating bond normal and shear stresses at the boot nipple (end of boot near igniter). Boot shrinkage is controlled by a net loss of diffusible species from the insulation material. In reality, this net loss represents an interchange of mobile chemical species between all three components of the bond interface as well as with the atmosphere in the boot gap.

Shrinkage of the rubber was measured by aging composite bond samples with degraded liner as well as undegraded liner at 110, 135, and 150°F. A simple first order kinetic equation (volumetric shrinkage = $5(1-e^{kt})$) was used in curve fitting the data. The Arrhenius relationship provided a rate constant of 3.9×10^{-4} days^{-1} at 70°F with an activation energy of 16 kcal/mole and a maximum volumetric shrinkage of 5%. No significant effect in shrinkage or rate was observed with the degree of liner degradation. Consequently, the liner degradation mechanism and the boot shrinkage mechanism can be treated separately.

Structural analysis of this region indicated that a 5% shrinkage of the insulation will produce a tensile stress of approximately 2 psi at a long-term storage condition (reduced time ~ 10^6 min). Bond strengths below this level will result in boot nipple lifting (separation) and is defined as the failure point. Of course, bond strength at long-term storage conditions must be converted to a bond strength that would be measured at the same test conditions (constant rate, ambient temperature) used for the predictive model (reduced time ~ 10^{-1} min).

The service life of the motor may then be estimated by determining the point at which the nominal capability or the lower 3σ limit of liner degradation equals the calculated induced bondline stress.

VERIFICATION

Up to this point, laboratory and subscale analogs are often used to develop the aging models and predictive equations. It is during the verification phase of the program (which may or may not be the same as the long-term surveillance program) that full-scale assets are used. It is through the full-scale assets that the validity of the models developed are verified, updated and modified. This process is generally an iterative one, which could change failure modes and models. This is a very important part of the process in that actual motor data is used and as more data becomes available, the accuracy of the model increases.

Translating the results of analog accelerated aging to full-scale motor conditions assumes the two types of assets are identical. In fact, there are significant differences between analogs and motors. First, the state of stress in the two configurations during both cure and aging are often completely different. Secondly, material thickness, size and consequently paths for thermal and specie diffusion may be different. Finally, a significant bias has been observed in material properties between motors and smaller analogs.

To verify the entire aging process, a 62-month-old motor was dissected. Dissection of full scale motors is an ideal technique to establish motor/analog bias for all pertinent material properties. The quantity of material available is adequate to evaluate variability of properties within the motor as well as unique differences that are a function of location within the motor.

From this asset, material response properties of the propellant, insulation and liner were measured to verify the structural analysis used to calculate the induced stress in the boot nipple region. The bias between motor data and analog data can result in significant errors in service life prediction. Bulk propellant modulus determined for the full-scale motor was significantly higher than that obtained from analogs (motor/analog = 1.4). Additionally, there was a hard modulus layer near the liner surface resulting from diffusion and reaction phenomena. A reevaluation of the induced stress using the updated material properties obtained during this verification phase resulted in an increase of the calculated normal stress to 6 psi for the long-term storage condition.

To verify the hydrolytic degradation mechanism, bond strengths were measured as a function of axial location along the bond interface. The results depicted in Figure 8 are consistent with expectations.

Bond strengths are considerably lower in the boot region than in the case bonded sidewall of the motor. Moisture diffuses readily from the boot gap through the 0.06-in.-thick boot insulation into the liner but can only diffuse laterally along the bond interface in the case bonded region. Numerical values in the booted region (~60 psi) are also consistent with projected

values based on the motor's age of 62 months. Bond strengths in the case bonded region are typical for the fully postcured liner (~ 105 psi).

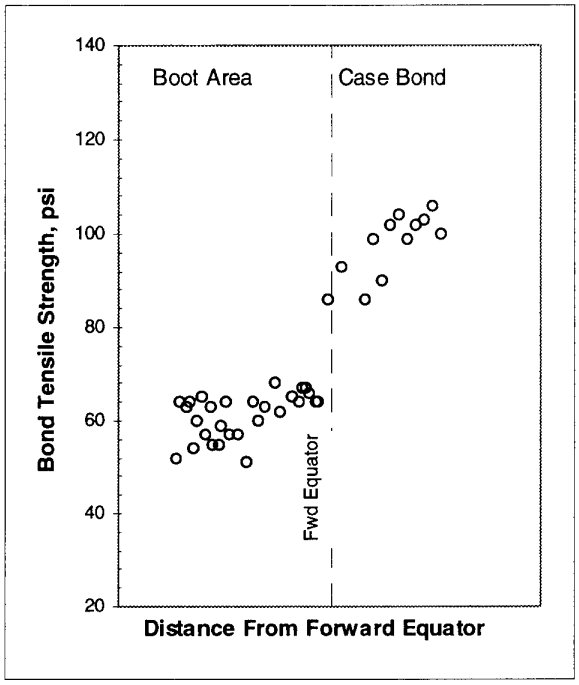


Figure 8. Bond Strengths from a Dissected Motor (62-mo.)

Motor dissection, however, is best described as characterization for a "slice in time". Dissection will relieve any stresses in the motor and expose the remnants to different environmental conditions so that attempts to further age dissected sections of the motor result in an unrealistic aging condition. Additionally, many motors would be required to validate the predictive aging model. This limitation can be overcome through use of plug motors or excised samples from motors. Excised samples are more appropriate in this case since they are typically used for booted or flapped regions while plugging provides critical information from the case bonded region.

Consequently, samples were excised at the end of the boot from numerous motors with a wide range in age. The excised sampling technique was considered nondestructive since the removal site was repaired and the motors returned to service. Bond strengths were measured and added to the plot of the predictive model in Figure 9.

The points are actual motor data obtained at the various ages after the kinetic projections were made. The scatter in data points represents variability indicative of material lot variability and the uncertainty in environmental storage conditions (temperature and humidity). The preliminary service life assessment based on laboratory analogs assumed an environmental storage condition of 70°F and 50% RH. Since storage temperature is the only environmental parameter that is monitored, the updated predictive model assumes the same temperature and varies only the humidity. It is clear from Figure 9 that an actual mean storage humidity is probably closer to 40% RH.

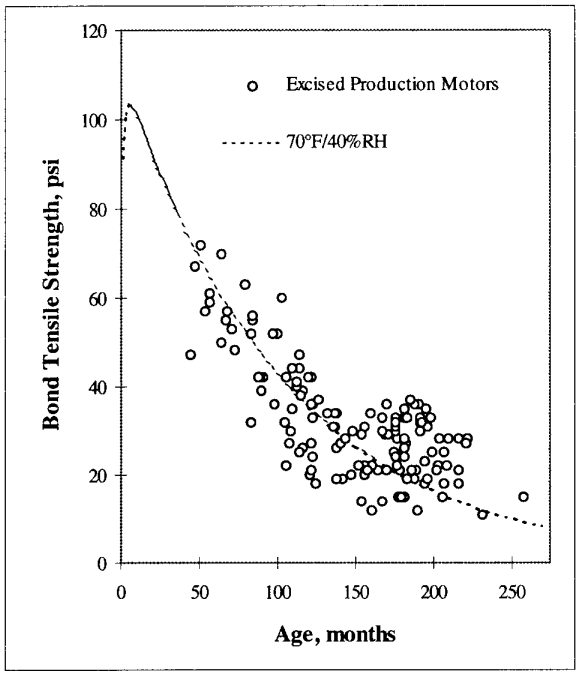


Figure 9 Bond Degradation from Excised Motors

Considering the strong dependence of service life on primarily a single degradation mechanism, it seemed likely that placing a hermetic weatherseal in the nozzle throat could lengthen service life, or at the very least, minimize extremely high humidity exposure and reduce variability. Such a modification to the motor would provide additional verification of the service life predictive model.

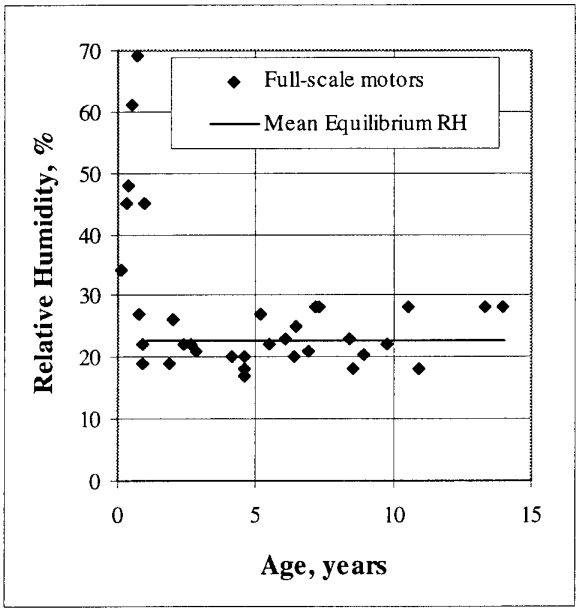


Figure 10. Moisture in the Bore of Sealed Motors

Weatherseals were then placed into motors. Periodically, the humidity in the bore cavity of the sealed motors was measured by sampling the air using a hypodermic needle. The results of bore RH measurements are summarized in Figure 10. Initially, moisture content is quite variable with a mean relative humidity of approximately 50%. Within a year, however, the bore cavity RH decreased to a mean value of 22.5% RH. This value is consistent with laboratory measurement of the equilibrium moisture content of the propellant.

Excised samples were then removed from weathersealed motors and tested to verify that the predictive model could successfully validate the humidity change. Data summarized in Figure 11 verify that sealed motors are now aging at a lower humidity very close to the expected value.

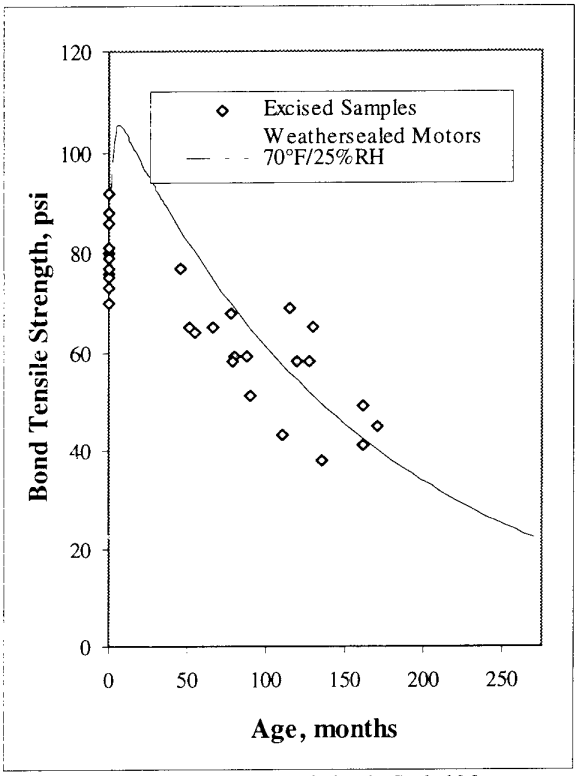


Figure 11. Predicted Degradation in Sealed Motors

CONCLUSION

The chemical kinetic approach can obviously be used with chemical degradation processes. Aging studies have shown that the same kinetic treatment is equally applicable to the rate of change induced by non-chemical processes such as diffusion. Predictive aging models can then be developed by combining kinetic data from pertinent individual processes. The approach can model multiple simultaneous chemical and physical changes, including diffusion of both inert and of reactive species.

Verification of established models using full-scale motors is a key step in determining the service life of solid rocket motors. Characterization of material properties can be obtained from dissected motors while aging trends are best evaluated using plug motors and excised sample. Excised samples also provide critical information on field population variability.

REFERENCES

1. Prototype Age Life Program; Vol. I-IV - Reduced Smoke Maverick, AFRPL-TR-81-86, Contract F04611-77-C-0029, Thiokol Corp. (Huntsville)

2. Predictive Surveillance Techniques, Vol. I, AFRPL-TR-82-097, Contract F04611-79-C-035, Aerojet Solid Propulsion Company

3. TEXCHEM User's Manual, PL-TR-91-3063, Aerojet Propulsion Division

4. DIAL, Lockheed-Martin Computer Code

Paper Number: 35
Discussor's Name: Professor H. Schubert
Responder's Name: R. K. McCamey

Question: What is the real aim of your investigation? We learn from long time experience that a rocket motor with a composite propellant has to be sealed.

Answer: The motor system studied was in fact not sealed because its mission at development was such that environmental load conditions were considered moderate and initial service life requirements were only 3 years. The investigation was designed to predict ultimate service life of an existing system and provide adequate lead time for replacement.

Paper Number: 35
Discussor's Name: D. I. Thrasher
Author's Name: R. K. McCamey

Question: Based on your experience with the rocket motor discussed, what is your assessment of the chance of correctly identifying the true age-out mode of a brand new propulsion system through the initial Failure Modes Effects and Criticality Analysis process?

Answer: I believe formalized emphasis on FMEA has resulted in a higher probability of correctly identifying age-out modes. Experience is a large contributor to successfully completing this task. Increased familiarity with failure experience would also be beneficial to those who develop new propulsion systems.

Service Life Prediction of Solid Rocket Propellant Motors Stored in a Random Thermal Environment

J Margetson
Defence Research Consultancy
Westcott
Aylesbury
Buckinghamshire HP18 ONZ
England

F C Wong
Defense Research Establishment
Valcartier
PO Box 8800
Courcelette
Quebec GOA 1RO
Canada

SUMMARY

A service life prediction analysis is developed for solid propellant rocket motors which are stored under statistically varying environmental conditions. Monitoring devices are used to measure the statistically varying stresses and strains which are induced as a result of the statistically varying diurnal and seasonal thermal cycles. A failure probability analysis is used to determine the probability that the statistically varying time dependent stress (strain) exceeds the statistically varying strength (strain capacity) of the propellant. A time dependent failure probability growth relationship is used to determine the time taken for the failure probability to increase to a specified unacceptable level. This time denotes the service life. The probabilistic service life prediction analysis is applied to an instrumented rocket motor stored at the environmental site at Valcartier, Canada.The results are compared with the service life predictions derived from a deterministic structural analysis approach.

1. INTRODUCTION

Tactical missiles using solid rocket motors are either stored under controlled thermal conditions or deployed at geographical locations where the thermal environment varies both diurnally and seasonally. Because the stress/strain free temperature of solid propellant cast in a rocket motor is substantially higher than storage temperatures, motors are subjected to cyclically varying thermal induced stresses and strains that can cause the propellant grain to fail. For the service life prediction of environmentally stored missiles it is necessary to have a statistical description of the long-term cyclic temperature environment that the rocket motors will be subjected to during their storage and field deployment. The statistically varying temperature will in turn induce statistically varying stresses and strains within the rocket motor and an accurate description of these quantities are essential inputs into the service life prediction analysis. The service life prediction analysis also requires statistical models of the propellant strength and strain capacity. In most cases these material properties are obtained from laboratory tests during the production of the propellant. Uniaxial tensile specimens are prepared from batches of the propellant and the maximum stress and maximum strain levels are usually recorded. However, these tests invariably show that there is significant variability associated with these strength measurements particularly when performed at the lower temperature range. Appropriate statistical models need to be considered in order to extend the strength distributions from the measured data range into the lower probability regions. During storage the propellant may be subjected to an environmentally induced thermal stress history. These time dependent stresses will induce damage into the propellant which in turn will result in a degradation of strength. In addition to this mechanically induced degradation the strength will also be affected by chemical aging.

The service life prediction analysis requires an accurate determination of the stress and strain response resulting from storage under controlled and statistically varying environmental thermal conditions. It is unfortunate that with the currently available viscoelastic structural analysis procedures it is not possible to accurately predict the stress response theoretically for the highly non-linear viscoelastic solid propellants used in solid rocket motors. In the service life prediction analysis the quantities usually required are the strain at the bore and the bond stress at the interface between the solid propellant and rocket motor case. For both these regions monitoring devices can be used to directly measure these quantities. Ideally the field trial data should be

Paper presented at the AGARD PEP Symposium on "Service Life of Solid Propellant Systems" held in Athens, Greece, 10-14 May 1996, and published in CP-586.

recorded over a period of a year so that the underlying seasonal trend and statistically varying diurnal cycle can be accurately determined. However, if this is not possible then a reduced monitoring schedule can be considered, for example one where the measured data is spread evenly throughout the year, which can still yield an accurate characterisation of the environmental variation.

Once the stress and strain response recorded from an instrumented rocket motor has been analysed and the strength and strain capacity distributions determined, specialised probabilistic mechanics techniques can be used to perform the service life prediction calculations. Using these procedures the statistically varying temperatures, stresses and strains can be incorporated into a time dependent propellant strength/load interaction analysis. This yields the failure probability as a function of time from whence the failure probability growth can be determined. The service life corresponds to the time required for this probability to exceed a specified unacceptable level.

2 SERVICE LIFE PREDICTION ANALYSIS

2.1 Probabilistic Loading Analysis

When a rocket motor is stored in a random thermal environment the temperature exhibits a seasonal sinusoidal variation about some mean temperature level with a superimposed random daily or diurnal fluctuation. On this basis it has been suggested that a suitable mathematical form for the peak daily temperature is

$$T(t) = T_m + T_y a(t) + T_d \qquad (2.1)$$

In the above equation T_m is the mean yearly temperature, T_y is the yearly amplitude and T_d is the amplitude of the peak diurnal temperature. The yearly and diurnal amplitudes T_y and T_d are statistically varying quantities taken from some distribution. The quantity $a(t)$ is given by

$$a(t) = \sin\left(\frac{2\pi}{w}(t - t_o)\right) \qquad (2.2)$$

and defines the underlying sinusoidal seasonal variation. In the above equation w denotes the frequency of the seasonal cycle (w = 365 days), t is the time measured in days and t_o denotes the start of the yearly temperature fluctuations.

The above random temperature variations will induce similar randomly varying stresses and strains in the rocket motor. Although the stress and strain response will be out of phase with the temperature cycle it is nevertheless reasonable to assume that the mathematical variation of the peak daily stresses and strains will be of the form

$$\sigma(t) = \sigma_m + \sigma_y b(t) + \sigma_d \qquad (2.3)$$

$$\epsilon(t) = \epsilon_m + \epsilon_y c(t) + \epsilon_d \qquad (2.4)$$

where

$$b(t) = \sin\left(\frac{2\pi}{w}(t - t_1)\right) \qquad (2.5)$$

$$c(t) = \sin\left(\frac{2\pi}{w}(t - t_2)\right) \qquad (2.6)$$

In the above equations $(\sigma_m, \sigma_y, \sigma_d)$ and $(\epsilon_m, \epsilon_y, \epsilon_d)$ respectively denote the mean, seasonal amplitude and diurnal amplitude of the stress and strain response and their respective starts to the annual cycle are denoted by t_1 and t_2. Since the thermal amplitudes (T_y, T_d) are assumed to be statistically varying quantities it follows that the stress amplitudes (σ_y, σ_d) and strain amplitudes (ϵ_y, ϵ_d) are also statistically varying quantities. Because the thermal strain and stress response are identical in form it is convenient to express their time dependent variation through the single equation

$$s(t) = s_m + s_y \sin\left(\frac{2\pi}{w}(t - t_o)\right) + s_d \qquad (2.7)$$

Henceforth $s(t)$ will be used to denote the thermal strain and stress histories.

If the statistical variation of the thermal amplitudes T_y and T_d satisfy certain distributional relationships then it is reasonable to assume that the same type of probability distributions will apply to s_y and s_d. For example, if T_y and T_d are random variables taken from Weibull distributions then s_y and s_d will also be random variables belonging to Weibull distributions. Clearly the parameters of the respective distributions will in general all be different. In this analysis it will be assumed that the thermal amplitudes (T_y, T_d) and stress and strain amplitudes (s_y, s_d) vary statistically according to the two parameter Weibull distribution [1]. Thus the probability density functions for s_y and s_d are respectively given by [1]

$$f_y(s_y) = \left(\frac{\alpha}{s_{oy}}\right)\left(\frac{s_y}{s_{oy}}\right)^{\alpha-1} \exp\left\{-\left(\frac{s_y}{s_{oy}}\right)^{\alpha}\right\} \quad (2.8)$$

$$f_d(s_d) = \left(\frac{\beta}{s_{od}}\right)\left(\frac{s_d}{s_{od}}\right)^{\beta-1} \exp\left\{-\left(\frac{s_d}{s_{od}}\right)^{\beta}\right\} \quad (2.9)$$

In the above equations α and β are the Weibull modulus values and s_{oy} and s_{od} are the normalising factors which have the same dimensions as s_y and s_d. The Weibull modulus α is an inverse measure of scatter and can be approximately related to the coefficient of variation through the relationship [2]

$$\alpha = \frac{1.2}{CV} \quad (2.10)$$

The quantity s_{oy} approximately equals the mean strength s_{my} or is more precisely given by the approximate relationship [2]

$$s_{oy} = s_{my}\left(1 + \frac{0.57}{m}\right) \quad (2.11)$$

The cumulative probability distributions are given by the integrals

$$P_y(s_y) = \int_o^{s_y} f_y(s_y)\, ds_y \quad (2.12)$$

$$P_d(s_d) = \int_o^{s_d} f_d(s_d)\, ds_d \quad (2.13)$$

which simplify to

$$P_y(s_y) = 1 - \exp\left\{-\left(\frac{s_y}{s_{oy}}\right)^{\alpha}\right\} \quad (2.14)$$

$$P_d(s_d) = 1 - \exp\left\{-\left(\frac{s_d}{s_{od}}\right)^{\beta}\right\} \quad (2.15)$$

2.2 Probabilistic Strength Analysis

In the service life prediction analysis of case bonded solid rocket propellants two failure models are usually considered. One is a strength based criterion which relates the induced tensile stress at the case propellant bondline to the tensile strength properties of the propellant. This implies that the expected failure is a cohesive failure in the propellant rather than an adhesive failure between the propellant and insulant. This induced tensile stress component occurs at all temperatures lower than the cure temperature. The other failure model is a strain based criterion which relates the maximum tensile strain at the bore of the propellant to the strain capacity of the propellant. Both failure criteria depend on a number of factors such as temperature, loading rate, cumulative damage and chemical aging. It is usual to determine both the maximum strength and strain capacity properties from a uniaxial tensile test experiment. The tests are normally carried out for a range of temperatures and strain rates. In the service life prediction analysis the temperature dependent strength properties normally used are those associated with the slowest measured strain rate. From these uniaxial tensile tests, performed over a range of temperatures, a temperature dependent strength relationship of the following form can be derived

$$S(T) = F(T)\, S(T_o) \quad (2.16)$$

In the above equation $F(T)$ defines a temperature dependent factor which relates the strength at temperature T to the strength at the reference temperature T_o. At the reference temperature T_o the quantity $F(T_o)$ is unity.

For solid rocket propellants there is an inherent statistical variability associated with its strength (strain capacity) properties and this variability is particularly apparent at the low temperature range. To account for this statistical variability it is assumed that the propellant strength S is distributed according to the three parameter Weibull distribution [1]

$$P(S) = 1 - \exp\left\{-\left(\frac{S - S_T}{S_o}\right)^{m}\right\} \quad (2.17)$$

where m is the Weibull modulus, S_o is the characteristic strength and S_T is the threshold strength below which no failures are observed. The strength characteristics m, S_o, S_T are determined from a maximum likelihood estimation analysis of the fracture data [1].

Once the strength parameters have been evaluated at the reference temperature T_o their values at any other temperature T follows from the relationships

$$m(T) = m(T_o) \tag{2.18}$$

$$S_o(T) = S_o(T_o)\,F(T) \tag{2.19}$$

$$S_T(T) = S_T(T_o)\,F(T) \tag{2.20}$$

In the above equations $F(T)$ is the temperature dependent strength factor defined by equation (2.16). It is also worth noting that the Weibull modulus is assumed to be independent of temperature. This is consistent with the assumption that the strength variability is assigned a particular value for the entire temperature range (this is a conservative assumption).

The above discussions have been applied to a bond strength analysis of the solid rocket propellant. However, the methodology for modelling strength can equally well be used to model the strain capacity. In this respect a strain capacity temperature dependent relationship can be defined and expressed in the form

$$\epsilon(T) = G(T)\,\epsilon(T_o) \tag{2.21}$$

To account for the statistical variability of propellant strain capacity ϵ a three parameter Weibull distribution can be adopted

$$P(\epsilon) = 1 - \exp\left\{-\left(\frac{\epsilon - \epsilon_T}{\epsilon_o}\right)^m\right\} \tag{2.22}$$

where m is the Weibull modulus, ϵ_o is the characteristic strain capacity and ϵ_T is the threshold strain capacity below which no failures are observed. Once the strain capacity parameters have been evaluated at the reference temperature T_o their values at any other temperature T follows from the relationship

$$m(T) = m(T_o) \tag{2.23}$$

$$\epsilon_o(T) = \epsilon_o(T_o)\,G(T) \tag{2.24}$$

$$\epsilon_T(T) = \epsilon_T(T_o)\,G(T) \tag{2.25}$$

In the above equation $G(T)$ is the temperature dependent strain capacity factor defined by equation (2.21). As before the Weibull modulus is assumed to be independent of temperature and is assigned a value for the entire temperature range.

It is implied in the above temperature dependent strength (strain capacity) relationships that there is no degradation in strength (strain capacity) as a function of time, temperature and stress loading history. For solid rocket propellants it is well known that degradation effects do occur and must be taken into account in the service life prediction analysis. Modelling degradation effects in solid rocket propellants have been the subject of considerable research and continues to be an important issue presenting many unresolved problems. In a recent study by the author some progress was made in the development of strength and strain capacity degradation models which were appropriate for use in the service life prediction analysis [3]. It was shown that cumulative damage and crack propagation concepts could be used to develop a strength degradation model [3]. It was also shown that a strain capacity degradation model could be developed using a propellant aging analysis [3].

For the strength degradation model it was shown that the strength $S(t, T)$ at any time t and temperature T was related to the initial temperature dependent strength $S(O, T)$ by the relationship [3]

$$S(t,T) = S(0,T)\left\{1 - D(t) + \left(\frac{\sigma_f}{S(0,T)}\right)^{\beta-2} D(t)\right\}^{\frac{1}{\beta-2}} \tag{2.26}$$

where $D(t)$ is the cumulative damage function defined by

$$D(t) = \frac{1}{\sigma_f^{\beta} t_f}\int_o^t \sigma^{\beta}\,\frac{dt}{a_T} \tag{2.27}$$

In the above equation β denotes the cumulate damage index, σ_f and t_f respectively denote the failure stress and time to failure of the propellant fractured under uniaxial endurance test conditions whilst a_T denotes the WLF shift factor.

For variable temperature aging a strain capacity degradation model was developed which was an extension of Layton's aging model for constant temperature aging [3,4]. For variable temperature conditions it was shown that the strain capacity $\epsilon(t, T)$ at time t and temperature T could be related to the initial strain capacity by an equation of the form [3]

$$\epsilon(t, T) = \epsilon(0, T)\,\eta(t, T) \qquad (2.28)$$

Here $\eta(t, T)$ is an aging factor defined by the recurrence relationship [3]

$$\eta(t_K, T_K) = 1 - \beta_K \ln\left\{\exp\left(\frac{1-\eta(t_{K-1}, T_{K-1})}{\beta_K}\right) + \frac{\Delta t_K}{t_r}\right\} \qquad (2.29)$$

where

$$\beta_K = A \exp\left\{-\frac{B}{T_K}\right\} \qquad (2.30)$$

$$t_k = \sum_{i=1}^{k} \Delta t_i \qquad (2.31)$$

$$\Delta t_i = t_i - t_{i-1} \qquad (2.32)$$

In the above equations A and B are material constants which are determined experimentally from appropriate aging tests and t_r is a reference time for which the aging factor $\eta(T, t)$ is unity (ie no aging occurs for time $0 < t < t_r$).

2.3 Service Life Prediction Study

For a solid rocket motor stored under environmental conditions the induced stress and strain response will depend on the applied temperature. For environmentally stored locations the temperature will vary statistically and this in turn will induce a statistically varying stress (strain) response of the form

$$s(t) = s_m + s_y \sin\left(\frac{2\pi}{365}(t - t_o)\right) + s_d \qquad (2.33)$$

In the above equation s_m, s_y, s_d and t_o respectively denote the seasonal mean, yearly amplitude maximum peak daily value and start of the seasonal cycle. For the service life prediction analysis the variables s_d and s_y are assumed to be statistically varying quantities with respective probability density functions $f_d(s_d)$, $f_y(s_y)$. The propellant strength (strain capacity) also varies statistically and has an associated probability density function denoted by $f_S(S)$. There is also the added complexity that the mean strength and strain capacity values together with their associated coefficients of variation are temperature dependent. Thus at any instant of time there is the probability that the induced stress and strain response will exceed the strength or strain capacity of the propellant. This gives rise to a complex strength load interaction analysis which can be expressed in terms of the general probability integral relationship

$$P_f^{(i)} = P(S < s) = \int_{-\infty}^{\infty}\int_{-\infty}^{\infty}\int_{-\infty}^{\infty} f_d(s_d) f_y(s_y) f_S(S)\, dS\, ds_y\, ds_d \qquad (2.34)$$

where S is the strength (strain capacity) and s is the induced stress (strain). Now the above triple integral can be integrated with respect to the strength variable S to yield the double integral representation

$$R_f^{(i)} = \int_{-\infty}^{\infty}\int_{-\infty}^{\infty} P_S(s_m + s_y b(t)\, s_d) f_d(s_d) f_y(s_y)\, ds_d\, ds_y \qquad (2.35)$$

where $P_S(S)$ is the cumulative probability strength distribution. If it is also assumed that the yearly amplitude s_y is deterministic and the only source of statistical variation in the stress and strain components are associated with the diurnal cycle s_d then it follows directly from the above equation that

$$P_f^{(i)} = \int_{-\infty}^{\infty} P_S(s_m + s_y b(t) + s_d) f_d(s_d)\, ds_d \qquad (2.36)$$

To evaluate the above integral expressions economised numerical quadrature algorithms are required to reduce the computational requirements of the calculations.

The reliability of a solid rocket propellant when subjected to repeated diurnal load applications can be calculated assuming successive diurnal load applications are statistically independent events. This assumption leads to marginally conservative results because it does not take into account the conditional probability that the solid propellant has survived the previous load applications. Alternatively a more refined analysis can be developed which takes into account the survival of the propellant when the propellant is subjected to a previous loading history. In this alternative approach a hazard analysis can be used to yield the following expression for the failure probability after n diurnal load applications

$$P_f(t_m) = 1 - \exp\left\{-\sum_{i=1}^{n} \frac{P_f^{(i)}}{R^{(i-1)}}\right\} \qquad (2.37)$$

where $R(t_n)$ is the reliability function

$$R(t_n) = \exp\left\{-\sum_{i=1}^{n} \frac{P_f^{(i)}}{R^{(i-1)}}\right\} \qquad (2.38)$$

The service life is the time taken for the time dependent failure probability $P_f(t)$ to exceed a specified maximum probability level P_f^{max}.

3. APPLICATION STUDY

3.1 Data Monitoring Procedure

Data was obtained using CRV7 rocket motors instrumented with Sensometrics Model 601511 thru-the-case bond stress gauges, custom-built bore displacement gauges and Type T thermocouples. The bond gauges were fabricated like a pressure transducer where semi-conductor strain gauges are mounted on a metallic diaphragm. Bore gauges were constructed by mounting foil strain gauges on the fixed end of a cantilever beam. Any changes in bore diameter were registered as changes in strain on the top and bottom surfaces of the beam.

Two bond stress gauges were mounted 500 mm from the nozzle end at right angles to each other in order to measure bondline stresses at a location where stress gradients were low. One bore displacement gauge was located 525 mm from the nozzle end to measure bore displacements at a location where they were large. Thermocouples were located in the propellant, on the motor casing and beside the motor. Bond stress, bore displacement and temperature were acquired with a Hewlett-Packard 3852 data acquisition system and downloaded to a personal computer at five minute intervals.

Before temperature cycling began, the instrumented motors were packed in a regulation CRV7 packing crate and loaded onto the top row of a storage test pallet. Correspondence between the thermal mass of the test pallet and a regular CRV7 storage pallet was maintained by filling unused packing crates with sand-filled motor tubes. The test pallet was placed on-site at DREV in Valcartier, Quebec and oriented such that the longitudinal axis of the motors were pointed in an east-west direction. Temperature and bondline monitoring took place between June 1992 and May 1993 with an interruption between November 1992 to January 1993.

Bondline stresses were recovered from the raw bond gauge voltage values through a data reduction program which took into account temperature-induced zero-offset variations, gauge sensitivity, gauge disturbance and barometric pressure variations. Filtering routines within the reduction program eliminated anomalous temperature and bond gauge readings.

3.2 Service Life Prediction

The recorded temperature, bond stress and bore strain, respectively, depicted in Figs 3.1 to 3.3, were analysed using a non-linear least squares algorithm to determine the time dependent and statistically varying response of these three quantities. From this analysis the thermal characteristics (T_m, T_y, T_d), bond stress characteristics $(\sigma_m, \sigma_y, \sigma_d)$ and bore strain characteristics $(\epsilon_m, \epsilon_y, \epsilon_d)$ were established. The Weibull parameters detailed in equations (2.8) and (2.9) which are associated with the yearly and diurnal probability distributions were evaluated as part of this analysis.

The statistical failure characteristics for the strength and strain capacity were first evaluated at the reference temperature of 23°C. This was achieved using a methods of moments analysis which is particularly appropriate when only the mean and coefficient of variation are known for the probability distribution under consideration. For the application of this method a coefficient of variation of 11% was assumed for both the strength and strain capacity. This coefficient of variation magnitude was assigned to all temperature levels. The mean strength value of 390 KPa and mean strain capacity value of 28% were used in the calculations (see Table 3.1). The temperature dependent strength and strain capacity Weibull distribution parameters were then respectively evaluated using equations (2.18) to (2.20) and equations (2.23) to (2.25). The temperature dependent functions F(T) and G(T) appearing in these equations were evaluated from Table 3.1 using a cubic spline interpolation procedure to calculate the functions at the non-tabulated values.

For the bond stress data recorded at the Valcartier site the service life was predicted using equations (2.34) to (2.38). The service life prediction calculations were carried out assuming $P_f^{max} \approx 10^{-3}$. Thus the service life based on bond stress was calculated as the time taken for the failure probability given by equation (2.37) to increase to $P_f^{max} = 10^{-3}$. The results of these calculations are shown in Fig 3.4. It is apparent from Fig 3.4 that the daily failure probability varies approximately sinusoidally over a period of 365 days from a minimum value of 10^{-7} to a

maximum value of $10^{-6.4}$. This pattern is repeated every year due to the fact that the strength is a function of temperature and the temperature varies sinusoidally each year. The time dependent failure probability increases with time in accord-ance with equation (2.87) from the minimum failure probability value of 10^{-7} to the assigned maximum failure probability level of 10^{-3}. The time taken for this failure probability growth is 7280 days (20 years). If strength degradation was included in this analysis it is anticipated that these daily failure probabilities would be modified towards the end of the service life. However, at the time of performing these computations no strength degradation of strain capacity chemical aging data was available.

Service life prediction calculations for the Valcartier site were also carried out for a strain based failure analysis assuming failure originated at the bore. For the service life prediction analysis based on the bore strain measurements a maximum failure probability of $P_f^{max} = 5 \times 10^{-1}$ was assigned. Computations showed that the daily probability of failure varied sinusoidally over a period of 365 days from a minimum value of 10^{-8} to a maximum of $10^{-5.7}$. The time dependent failure probability growth increased from an initial failure probability level of approximately 10^{-8} to the assigned $P_f^{max} = 5 \times 10^{-3}$ value in 12.22 years (see Fig 3.5).

The probabilistic service life prediction analysis discussed so far is appropriate for making long term life predictions once the missile system is in service. If a surveillance program is in place to monitor the degradation of propellant properties then a complimentary methodology based on a deterministic structural analysis approach may be used. This kind of approach was used in a Canadian service life study of the CRV7 motor [5].

The Canadian study predicted service life by extrapolating historical propellant strength data to various motor ages. The extrapolation was based on an exponential law as opposed to a logarithmic law as originally proposed by Christiansen [6]. This was used to give a more conservative estimate of service life. The most likely mode of failure for the CRV7 was found to be bore cracking. This type of failure was defined analytically as the stress-strain state which exceeded the limits given by the Smith failure envelope [7]. Although the method was deterministic, probabilistic effects were included in the definition of the failure envelope through the use of B-basis allowables [8]. This allowable is defined as the 90th percentile survival probability and accounts for data scatter and the number of specimens tested.

Figure 3.6 shows the relationship between the predicted worst case motor stresses and strains for a motor aged 12 years and the measured failure envelopes at various motor ages. The projected failure envelope at an age of 12 years is also shown. The motor stresses and strains were calculated using a time-shifted equilibrium modulus to account for the gradual hardening seen in the propellant [6]. Table 3.2 shows the margin of safety based on bore hoop stresses and strains at different age times for the case of thermal cool-down under storage conditions. The margin of safety (MS) was defined as the vertical or horizontal distance between the motor stress-strain state and the failure envelope. As shown in Table 3.2, a negative MS was predicted at a motor age of 20 years when considering strain capacity. In terms of stress capacity at 20 years, the MS was 0.3. With the uncertainties in the analysis, a minimum acceptable MS in terms of stress or strain was set at 0.4. Thus, according to Table 3.2, the service life of the CRV7 motor was limited by its strain capacity. The life of the motor was determined to be 12 years.

A comparison of the results obtained from the probabilistic approach and the deterministic structural analysis approach showed that the two methods arrived at similar conclusions. In both cases, for the minimum P_f's and MS's chosen if service life was based on a bore strain criterion, the motor life would be set at 12 years. If the motor life was based on a stress criterion, the motor life would be set at 20 years. It should be noted here that the probabilistic approach examined bondline stresses while the structural analysis approach examined bore hoop stresses. Both approaches arrived at the same conclusion for the stress criterion because the bondline stresses and bore hoop stresses were roughly the same order of magnitude in a CRV7. These results provided a measure of confidence that the predictions based on the probabilistic methodology were reasonable.

It is evident that the selection of minimum P_f or minimum acceptable MS plays an important role in determining the safe life of a motor. The service life of a motor could be conceivably extended an order of magnitude in life if one was willing to accept a higher risk or a lower margin of safety. The level of risk that one is willing to accept depends largely on the quality of the data used in the analysis. Therefore, it is imperative that the data sets used for service life analysis be statistically significant and that they cover the entire range of conditions seen by the rocket motor.

4. CONCLUSIONS

A service life prediction analysis was presented for solid propellant rocket motors which are stored under statistically varying environmental conditions. For this analysis it was assumed that

monitoring devices were located at selected positions within the rocket motor (i.e. at the bondline interface between the propellant and rocket motor case and at the bore conduit) and used to measure the statistically varying stresses and strains which are induced as a result of the statistically varying diurnal and seasonal thermal cycles. Probabilistic techniques were used to analyse this data and hence determine the time dependent statistical variation of the peak stress and strain response. A Weibull analysis was used to characterise the strength (strain capacity) variability which was both temperature and strain rate dependent. Theoretical models were presented for predicting the degradation in strength and strain capacity as a function of the thermal stress loading history. The strain capacity degradation model was based on a generalisation of the Layton aging model for time dependent thermal conditions. The strength degradation model was developed from a propellant fracture mechanics analysis which was originally proposed by Schapery. A failure probability analysis was used to determine the probability that the statistically varying time dependent stress (strain) exceeds the statistically varying strength (strain capacity) of the propellant. A time dependent failure probability growth analysis was developed which was based on a probability hazard model to determine the time taken for the failure probability to increase to a specified unacceptable level. The time taken to reach this probability level defined the service life of the propellant. The service life prediction analysis capability was demonstrated by predicting the time dependent failure probability growth, and hence service life, for an instrumented rocket motor stored at the environmental site at Valcartier, Canada.

A comparison of the results obtained from the probabilistic approach and the deterministic structural analysis approach showed that the two methods arrived at similar conclusions. In both cases, if service life was based on a strain criterion, the rocket motor service life was estimated to be 12 years. If the rocket motor service life was based on a stress failure criterion, the service life was estimated to be 20 years. These results provided a measure of confidence that the predictions based on the probabilistic methodology were reasonable.

5. REFERENCES

1 Bury, K V
Statistical Models in Applied Science
John Wiley, New York, 1975

2 Margetson, J
A Statistical Theory of Brittle Failure for an Isotropic Structure Subjected to a Multiaxial Stress State
AIAA paper No 76-632, AIAA/SAE 12th Propulsion Conference, Palo Alto, California, July 1976

3 Margetson, J
Characterisation Procedures for Solid Rocket Propellant Strength and Strain Capacity Degradation Models
DRC Technical Report prepared for DRA

4 Layton, L H
Chemical Aging Studies on ANB-3066 and TP-H1011 Propellants
US Air Force Report AFRPL-TR-74-16,1974

5 Wong, F C
Service Life Assessement of the CRV7 RLU-5002/B Rocket Motor
DREV R-4679, 1992, Unclassified

6 Christiansen A G, Layton L H and Carpenter R L
HTPB Propellant Aging
J Spacecraft, Vol 18, No 3, May-June 1981, pp 211-215

7 Engineering Materials Handbook Vol 1 - Composites, ASM International, Metals Park, Ohio, 1987, p 304

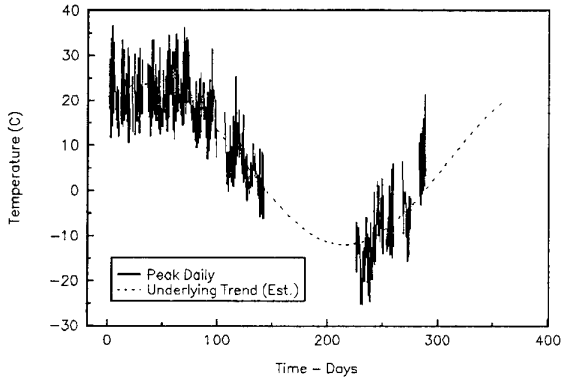


Figure 3.1 Measured peak temperature variations for the Valcartier location

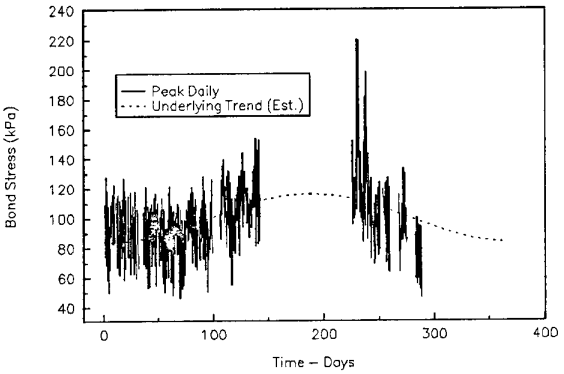


Figure 3.2 Measured peak bond stress variations for the Valcartier location

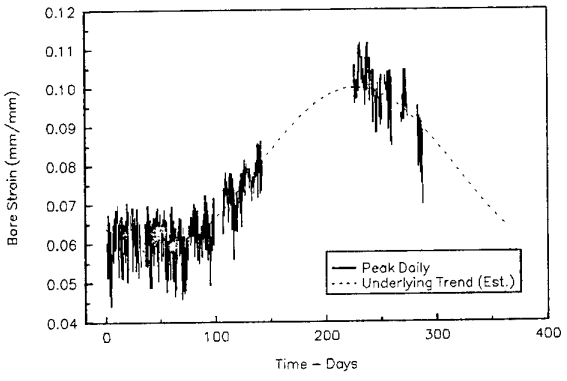


Figure 3.3 Measured peak bore strain variations for the Valcartier location

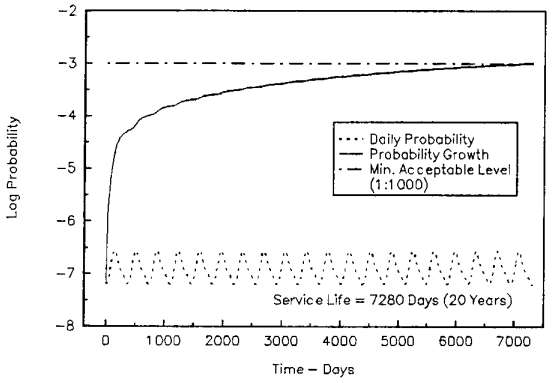


Figure 3.4 Service life prediction for Valcartier site showing failure probability growth and daily failure probability variation (bond stress analysis)

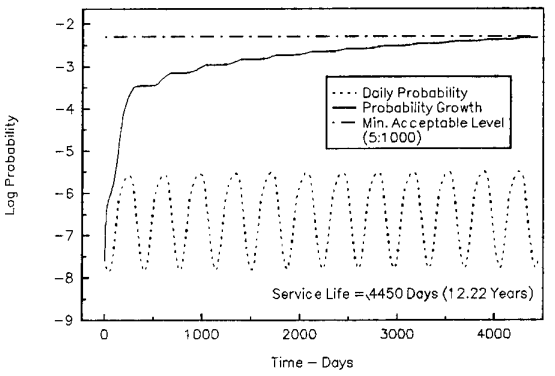


Figure 3.5 Service life prediction for Valcartier site showing failure probability growth and daily failure probability variation (bore strain analysis)

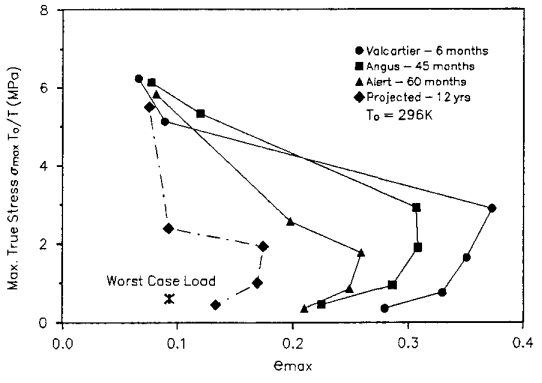


Figure 3.6 Service life prediction of CRV7 using a deterministic structural analysis approach (bore cracking analysis)

Temperature (°C)	Strain at Max Load		Stress at Max Load	
	Mean (%)	COV (%)	Mean (kPa)	COV (%)
60	27.41	8.32	316.6	2.34
23	28.66	1.98	390.8	2.82
0	27.94	2.88	496.0	2.20
-17	31.23	1.15	562.9	0.20
-40	27.30	4.13	756.7	0.93
-54	17.82	1.87	883.8	11.30

Table 3.1 Strength and strain capacity characteristics of CRV7 HTPB propellant

Age (yr)	Predicted		Allowable		Margin of Safety	
	Stress (MPa)	Strain (%)	Stress (MPa)	Strain (%)	Stress	Strain
10	0.432	9.3	4.24	15.0	8.8	0.62
12	0.479	9.3	2.38	13.5	4.0	0.45
15	0.530	9.3	2.20	11.3	3.1	0.21
20	0.594	9.3	0.80	8.4	0.3	-0.10
Note: Margin of safety = (allowable - predicted)/predicted						

Table 3.2 Margin of safety for hoop stress and strain at different age times

Paper Number: 36
Discussor's Name: Professor R. A. Heller
Responder's Name: DR. J. Margetson

Question: Do you not consider the variability of the modulus in your analysis?

Answer: No. This is only required if the stress and strain response is being calculated theoretically. In this service life prediction methodology these quantities are measured directly using appropriate monitoring devices.

Paper Number: 36
Discussor's Name: Dr. H. J. Buswell
Responder's Name: Dr. J. Margetson

Question: Has your 12 year predicted life been experimentally verified?

Answer: Realistically that is not possible because the estimated failure after 12 years is one in a million.

Paper Number: 36
Discussor's Name: E. Nicol
Responder's Name: Dr. J. Margetson

Question:
- The different methods and studies presented speak about thermal environmental conditions only.
- Do you think that mechanical environments like transport vibrations, shocks, etc., can have an influence on the results of your analysis and likely change the estimation of service life?

Answer: The load response can be measured and the stress response at the bondline and bore strain can be measured. Then the current algorithms will be able to analyze for the reliability. For vibrational loads, monitoring a random response, this would not be possible with current methodology. Shock loads would result in "step jumps" in the failure probability (instantaneous response) and also the failure probability growth.

Paper Number: 36
Discussor's Name: L. G. Meyer
Responder's Name: Dr. J. Margetson

Question: What confidence do you have in the stress and strain measurements that were used in the analysis?

Answer: The confidence is very high based on other experience with the gages.

Paper Number: 36
Discussor's Name: D. I. Thrasher
Responder's Name: F. C. Wong

Question: What procedures were used to determine the as-installed no load response of the bond stress transducers?

Answer: The stress gage measurements are dependent on temperature, so calibration of the no-load response of the gages must take this into account. In unfilled casings, the installed gage/motor case combination is temperature cycled over the range of interest. The gage readings are recorded and used to generate a correction curve to adjust all readings from this test to give zero load at any temperature. In filled casings, a further correction is usually necessary to ensure zero load at cure temperature after the motor has been cast. This correction is in the form of an offset value and is obtained by reheating the gage/motor combination back up to cure temperature. At cure, the bondline stress and bore diameters should be in the reference no load condition. If the temperature corrected gage reading gives anything other that zero load, then this offset value must be included in the data reduction equation.

Prediction of the Shelf Life of Munitions: Ballistic and Chemical Properties.

Jenaro de Mencos,G.; Hernandez Tamayo, J.
Laboratorio Químico Central de Armamento (LQCA)
P.O.Box 1105, 28080 Madrid
SPAIN

SUMMARY

A correlated experiment between stabilizer consumption in the propellant and ballistic properties of a solid rocket motor -which include the same propellant- has been performed. Results have showed that ballistic properties can change substantially before the stabilizer has been consumed.

Previously propellant was analysed and compared with other propellants. These are four homogeneous rocket propellants which were tested to find out stabilizer consumption during two years artificial ageing at 50°C. All propellants had a previous natural ageing of between 10 and 27 years.

Ballistic properties were measured during a series of firings in rocket motor test stand.

Propellant samples and solid rocket motor have been subjected to the same ageing test.

The prediction of shelf life of this type of rocket motor is shown below.

1. INTRODUCTION

This paper is concerned with the relationship between the chemical evolution of the propellant and ballistic properties of a solid rocket motor.

In particular it deals with double base propellants where the binder is mainly nitrocellulose plasticised with nitroglycerine.

Service life of an ammunition can be shortened either by changes in tactical missions that can make it obsolete or by chemical degradation of main propellant and pyrotechnic compositions.

We have experience of different cases, for example: one type of solid rocket motor in which the igniter had been degraded to the extreme of being inert; another, where the pyrotechnic mix of the tracer had evolved and made the whole anmunition unusable; and finally others -gun propellants- that have lost chemical stability.

For this reason, samples of guns and rocket propellants periodically undergo stability tests.

The "Laboratorio Químico Central de Armamento" (LQCA) is the Spanish National Authority with regard to service classification and Surveillance Tests of ammunitions, warheads and rockets.

Shelf life has been defined as the time in which all functions of an ammunition remain intact within given tolerances -although some ageing processes have already taken place-. Shelf life as defined above can be considered under the following three aspects[1,2,3]:

Chemical shelf life
Physico-mechanical shelf life
Ballistic shelf life

The chemical shelf life covers the period of time during which the ammunition can be safely stored and does not represent any hazard to its environment. The end of the chemical shelf life is reached when the danger of an autocatalytic decomposition of the propellant becomes apparent.

The ballistic shelf life is the period of time during which all ballistic requirements remain fulfilled.

The physico-mechanical shelf life is the interval during which the ammunition can be handled and used without danger.

Of course the three above mentioned shelf lives can not be considered separately and any of them can limit the service life of the ammunition.

Paper presented at the AGARD PEP Symposium on "Service Life of Solid Propellant Systems" held in Athens, Greece, 10-14 May 1996, and published in CP-586.

The chemical stability properties can be determined by measuring the consumption of the stabilizer and the byproducts of the stabilizer conversion [3, 5].

Moreover, heat production permits to appraise the chemical shelf life [4]. But, what about the ballistic shelf life?. How long does an ammunition fulfill the ballistic requirements? Is there any relationship between the loss of the stabilizer and the ballistic properties of the ammunition?

Two parallel experiments have been performed; in one of them several samples of propellants have been tested to register the depletion of stabilizer content. The other experiment consists of the artificial ageing and subsequent test firing of several motors. Both -samples and motors- had the same previous natural ageing.

The experimental data of residual stabilizer contents versus time has been analysed and correlated with results of the firing in Solid Rocket Motors Test Stand. These analyses have permitted us to find relations between chemical and ballistic shelf life.

2. THEORETICAL BACKGROUND

It is well known that single and double base propellants decompose even in room temperature, evolving oxides of nitrogen.

To avoid the autocatalysis and possible self ignition of the propellant, stabilizers are added during the manufacturing process.

Several methods have been used for the determination of the stability and service life of the propellant.

Stability tests have traditionally been classified in three groups (Tranchant [6], Wallace [7]):

-Those measuring the gas evolution of the propellant, for example the quantity of gas produced after heating or the time taken to evolve a known quantity of nitrogen oxides.

-Those evaluating the consumption and evolution of the stabilizer.

-Those following the variation of the physico-chemical properties of the polimer.

Techniques such as the study of nitrogen oxides evolution by chemiluminiscence [7] or measurement of stabilizer contents by thin layer chromatography (TLC) [8], gas chromatography (GC) [9] and high pressure liquid chromatographic (HPLC) methods [10] have been used in the last decade. All these tests are routinely used in our Laboratory.

During the development of this work the measurement of residual stabilizer content versus time has been used as the criterium for propellant deterioration, moreover data of calorimetric values complete the study of one of the propellants.

3. EXPERIMENTAL WORK

Rocket propellant samples (see compositions and natural previous ageing in Table 1) were subjected to artificial ageing at 50° C over a two year period; moreover propellant DB1 has been subjected to ageing at 65° C and 95° C with the purpose of obtaining a better characterization. The HPLC method has been applied.

Stabilizer consumption, calorimetric values and physico-mechanical properties have been measured at different ageing times.

Rocket motors type E3 were designed by LQCA and manufactured by Military Industries (nowadays E.N. Santa Bárbara) in Spain 31 years ago. This rocket has been in service in the Army during 20 years.

Ballistic properties of E3 Rocket Motor have been measured during static tests at LQCA Facilities. The composition of the E3 motor propellant is the same as composition DB1 shown in Table 1. This motor with a 27 years natural ageing completed has been exposed to an artificial ageing test at 65 °C.

E3 rocket motor consists of seven propellant cylinders inhibited by their endings, 19 small nozzles, and the case of steel.

4. ANALYSIS OF RESULTS

4.1 Preliminary analysis: chemical stability

The objective of the preliminary analysis was the characterization of the 27 year old propellant DB1 from the chemical point of view and to obtain a classification with regard to the stability.

Propellant DB1 samples were taken from an E3 rocket motor and studied according to the following aspects:

a) chemical analysis: stabilizer content and explosion heat.
b) stability test at 50° C for a two-year period and comparison with other propellants.

Chemical analysis showed that the 27 year old DB1 propellant has its levels of stabilizer content and calorimetric values within manufacturing tolerances.

Ageing test at 50° C and fixed humidity allows an estimation of the propellant stability [11, 16 and 17]. This stability test was applied to several propellants. All of them had a previous natural ageing that oscilated between

11 years (DB3) and 27 years (DB1), and in these periods of time the propellants lost small quantities of stabilizer.

Figures 1 and 2 show the depletion of stabilizer versus time at 50° C for the five compositions of Table 1. The application of the stability criterium (Table 7) provides Table 2 results. See that the loss of stabilizer was slower in the propellant DB1 than in the other propellants. Therefore we can conclude that propellant DB1 presents very good stability.

Since the loss of stabilizer in natural ageing periods is almost a straight line, the results obtained after 27 years of natural ageing and ageing test at 50° C allow us to conclude that from the chemical point of view, shelf life of propellant DB1 would be in excess of 100 years.

4.2 Ballistic results after 27 years of natural ageing.
A serie of four rocket motors (rounds 1 to 4)type E3 has been fired in test Stand after conditioning during 24 hours at 20° C.

Results are presented in Figure 4 and Table 3. Three typical ballistic properties of a solid rocket motor are (a)total impulse, (b)maximum thrust and (c)burning time.

Table 3 summarizes the results. It is easy to notice that the differences with the nominal values of this type of motor are small; in fact, of less than 1% in total impulse; of less than 1% in maximum thrust with respect to the average value and slightly larger in burning time.

Figure 4 presents the thrust-time history of the firings. It can be seen that there are no odd peaks; levels of thrust are similar in all the firings and the shape of the trace is good.

Our conclusion is that 27 year old motors are in perfect condition from the ballistic and chemical point of view. Round 9 shows an odd peak in the thrust-time history, this motor belongs to a different lot and is one year older.

4.3 Chemical characterization of the DB1 propellant
DB1 rocket propellant samples were subjected to artificial ageing at 65° C over a 12 week period, and at 95° C for a 5 day period. All propellant samples have been handled with the same preparation procedure and HPLC analysis conditions.

These tests have been performed with the quantitative analysis of centralite changes at specific time intervals, so that it is possible to extrapolate it to lower ageing temperatures. The results allow us to apply the kinetic Analysis and therefore obtain conclusions about the behaviour of DB1 propellant.

Two methods have been applied. The first is the Bohn first order method [13] and the second is Berthelot's law of the deterioration phenomena, a law already used by several other authors [12].

Figure 3 shows the consumption of stabilizer at different ageing temperatures, and Table 5 the theoretical prediction of the life time of the propellant from the chemical point of view, the values for coefficients a and b, and the constant rate for propellant deterioration at any ageing temperature.

Figure 7 gives the curves at three stages during propellant deterioration, corresponding to 25, 50 and 75% of stabilizer loss.

Figure 8 presents the reduction in explosion heat and % of nitrogen in nitrocellulose (NC).

It was found that the shelf life of this propellant stored at 20° C would be longer than 100 years.

4.4 Ballistic results after artificial ageing at 65° C
Rocket Motors E3 with even 28 years of natural ageing in depot have been exposed to artificial ageing at 65° C for a 12 week time period and fired at different levels of ageing.

We have accepted that with respect to chemical ageing the continuous storage of the rocket motor at 65° C for 3 months is equivalent to 15 years at 20° C; similar values have been proposed by other authors [14].

After the ageing test, motors were revised and no evidence of cracking was found.

Firing results are summarized in Table 4 and Figures 5 and 6. Figure 9 presents the total impulse and maximum thrust of the motors versus ageing time at 65° C.

The examination of the thrust-time histories shows that larger ageing times imply the appearance of larger peaks of maximun thrust in addition to non-homogeneus results, even although the stabilizer amount is sufficient to guarantee several years more of chemical life (Figure 10).

Maximum pressure (and then maximum thrust) must not exceed a defined value because of the danger of explosion. In fact maximum thrust in motor E3 must be less than 53464 N. Table 4 shows that this value is exceeded in rounds number 5, 7, 8 and following. That is, these motors do not fulfill the ballistic requirements.

These data therefore, lead us to the conclussion that ballistic shelf life of rocket motor E3 is less than chemical shelf life (Figure 10).

This tendency to irregular and larger peaks could be a consequence of the degradation -molecular weight loss- of the nitrocellulose, as shown by Ammann [1] in a gun propellant; or perhaps by the migration of nitroglicerine (NG) to the external surfaces of the propellant. Other possible causes for the initial peak in the thrust-time history are igniter deterioration, and degradation of physico-mechanical properties of the propellant.

We have elaborated an exact reproduction of the igniter without ageing and interchanged it with the original one of a motor. The firing with the new igniter in the aged motor (round 12) is presented in Figure 6; note that initial peak of thrust is very large, more than permitted values for this type of motor. Therefore, igniter is not the cause of this thrust peak.

Regarding the physico-mechanical properties of the propellant, see Table 6 with the original (after manufacturing) compression properties and the same properties after natural plus artificial ageing. The results show that these properties have changed in the ageing time, the propellant has hardened and evolutioned towards a more brittle material.

With respect to the migration of NG to the external surfaces of the propellant, see Table 8 with chemical analysis results. This table shows the quantities of nitroglicerine, centralite and other components, and heat of explosion at different layers of the propellant. Results confirm that external layer have lost small quantities of nitroglicerine and EPU. In our opinion the cause of the peaks lies in the chemical changes in the external layer of the propellant.

As was expected, total impulse decreases slightly with ageing time, but this has small significance. With these results it seems that service life of motor E3, from the ballistic point of view, is about 30 years, and from the chemical point of view is in excess of 100 years.

4.5 Stability criterium and service life prediction

Results obtained show that ballistic aspects must be taken into account in the service life asessment of a solid rocket motor. Failure can appear in the igniter, propellant, inhibitor and other.

For these reasons we propose the following steps in the service life asesssment of ammunitions:

A) To apply the ageing test at 50° C as defined by Leveque [11] and M. Rat [16] to the propellant. We have chosen this type of test because several authors [15] have proved that the asesssment of the stability by the decrease of the stabilizer should be carried out at temperatures not higher than 65° C.

B) To obtain an estimation of the minimum chemical shelf life and of the degradation of the nitrocellulose. Kinetic Analysis Methods are applied.

C) To check periodically the ballistic properties.

5. FINAL CONCLUSIONS

This paper has presented ballistic results of two series of solid rocket motors firings in static test stand.

The first series of motors were at least 27 years old, and results were very close to the nominal results.
The second serie of motors, with 27 years natural ageing plus artificial ageing at 65° C, showed problems in ballistic properties although motors were in good condition from the chemical point of view.

The influence of ageing over the main ballistic properties of a solid rocket motor has been evaluated.

A relative stability criterium has been proposed by comparing the slopes of stabilizer content loss of several propellants at 50° C.

It has been shown that ballistic properties can limit the service life of the motor, even if the chemical stability properties are good.

6. REFERENCES

1. R. Amman, "Ballistic Shelf Life Prediction of the Gewehrpatrone 90 (GP 90)", 8th Symp. Chemical Problems Connected with Stability of Explosives, Stromstad, Sweden, 12-16 June, 1988.

2. Bronniman, E; Sopranetti, A; "A Universal Test Procedure to Predict the Shelf Life of Propellants", 7th Symposium on chemical problems connected with stability of explosives, Sweden, 1985.

3. F. Volk, "Determination of the shelf life time of solid rocket propellants", Propellants and explosives, 1, 59-65, 1976.

4. M. A. Bohn and F. Volk; "Aging Behavior of Propellants Investigated by Heat Generation, Stabilizer Consumption and Molar Mass Degradation", Propellants, Explosives, Pyrothecnics 17, 171 (1992).

5. F. Volk, "Determination of the Life time of Gun Propellants Using Thin-Layer Cromatography", Propellants, Explosives, Pyrotechnics 1, 90 (1976).

6. J. Tranchant; "Internal Mechanism of the Chemical Evolution of Nitrocellulose Propellants "6th Symposium on chemical problems connected with stability of explosives, Sweden, 1982.

7. Wallace, I. G.; Powell, R. J.;Downes, B. J.; "A Chemiluminiscence Study of Oxides of Nitrogen Evolved from Propellants", Symposium on chemical problems connected with stability of explosives, Sweden, 1979.

8. Volk, F.; "Probleme bei der Ermittlung der Levensdauer von Festtreibstoffen", Jahrestagung 1971, Germany.

9. A. Sopranetti; H. U. Reich; "Simultaneous Analysis of Stabilizers and their Decomposition Products by Gas Chromatography, Applications of the New Method for the Judging of Propellants by 65.5°C Surveillance Test", 4th Symposium on chemical problems connected with stability of explosives, Sweden, 1976.

10. H. Helama; E. Kovero; "A Modern Method for determining the Stability and Stabilizers in Solid Gun Propellants", 6th Symposium on chemical problems connected with stability of explosives, Sweden, 1982.

11. M. Leveque, "Correlation entre les Resultats de L,epreuve de Consummation de Stabilisant a 50°C et le Vieillissement Naturel", 8th Symp. Chemical Problems Connected with Stability of Explosives, Stromstad, Sweden, 12-16 June,1988.

12. M. H. Sammour, "Stabilizer Reactions in Cast Double Base Rocket Propellants. Part V: Prediction of Propellant Safe Life",. Propellants, Explosives, Pyrotechnics 19, 82 (1994).

13. M. A. Bohn, "Prediction of Life Times of Propellants-Improved Kinetic Description of the Stabilizer Consumption" Propellants, Explosives, Pyrotecnics 19, 266 (1994).

14. G. I. Evans and J. F. Binghan; "Propellant gas cracking in solid propellant rocket motors", 18th International Annual Conference of ICT, July 1-3 1987, Karlsruhe, Germany.

15. A. Sopranetti and H. U. Reich, "Comparisson of high temperature stability-tests with studies of the conversion of stabilizers in single-basse propellants", Symposium On Chemical Problems Connected with Stability of Explosives, may 28-30, 1979, Bastad, Sweden.

16. M. Rat, "Evolution du stabilisant des poudres a simple base an cours d'un vieîllissement a basse temperature (50 °C), Resultats experimentaux", Symposium On Chemical Problems Connected with Stability of Explosives ,6th, 1982, Sweden.

17. M. Dreyfus and M. Leveque, "The chemical stability control on French propellants", Symposium On Chemical Problems Connected with Stability of Explosives, 6th, 1982, Sweden.

TABLE - 1

PROPELLANTS COMPOSITION

DB 1	DOUBLE BASE WITH CENTRALITE, EPU, DPU AND POTASSIUM SALTS.
DB 2	DOUBLE BASE WITH 2NDPA AND DIETHYL PHATALE
DB 3	DOUBLE BASE WITH CENTRALITE, TRIACETIN, DIETHYL PTHALATE AND COPPER SALTS.
DB 4	DOUBLE BASE WITH DINITROTOLUENE AND DPA
DB 5	DOUBLE BASE WITH DINITROTOLUENE AND DPA

TABLE - 2

RESULTS OF AGEING TEST AT 50ºC (42 DAYS)

PROPELLANT	STABILIZER LOSS(%)	SLOPE VALUE 10^{-4} (% / day)	CLASSIFICATION	TYPE
DB 1	0,037	8,8	VERY GOOD	I
DB 2	0,08	19	VERY GOOD	I
DB 3	0,067	15,9	VERY GOOD	I
DB 4	0,12	28,5	GOOD	II
DB 5	0,18	42,8	GOOD	II

TABLE - 3

SUMMARY OF EXPERIMENTAL RESULTS OBTAINED IN TEST FIRING WITH MOTORS TYPE E-3 AFTER NATURAL AGEING OF 27 YEARS

	NOMINAL VALUES	TEST Nº				
		1	2	3	4	9
PRODUCTION YEAR	1965	1965	1965	1965	1965	1967
TEST DATE	-	30-JUNE-92	1-JULY-92	2-JULY-92	3-JULY-92	16-MARCH-95
TEMPERATURE (ºC)	20	20	20	20	20	20
TOTAL IMPULSE (N.S.)	52091	51983	52246	51988	51901	52085
BURNING TIME (s)	1,35	1,30	1,42	1,34	1,37	1,43
MAX. THRUST (N)	< 53464	48935	46667	48775	47502	46672

TABLE - 4

SUMMARY OF EXPERIMENTAL RESULTS OBTAINED IN TEST FIRING WITH MOTORS TYPE E-3 AFTER NATURAL AGEING AND ARTIFICIAL AGEING (AT 65º C)

	NOMINAL VALUES	5	6	7	8	10	11	12	13
PRODUCTION YEAR	1965	1965	1967	1967	1967	1967	1967	1967	1967
LOT		5-129	5-69	5-79	5-35	5-90	5-31	5-15	5-46
AGEING TIME	-	29 YEARS 70 H AT 65ºC	27 YEARS 336 H AT 65ºC	27 YEARS 480 H AT 65ºC	27 YEARS 576 H AT 65ºC	28 YEARS 720 H AT 65ºC	28 YEARS 888 H AT 65ºC	28 YEARS 1224 H AT 65ºC	28 YEARS 1680 H AT 65ºC
TEST DATE	-	25-OCT-94	11-NOV-94	30-NOV-94	3-DIC-95	12-JAN-96	15-JAN-96	2-FEB-96	21-FEB-96
TEMPERATURE (ºC)	20	20	20	20	20	20	20	20	20
TOTAL IMPULSE (N.S)	52091	51901	51617	51439	50338	51166	50843	50676	51301
BURNING TIME (s)	1,35	1,35	1,38	1,36	1,35	1,36	1,38	1,40	1,34
MAX. THRUST (N)	< 53464	61479	52705	61314	70091	74709	71080	71190	90211

TABLE - 5

PREDICTION OF THE CHEMICAL SHELF LIFE OF THE PROPELLANT DB1 BY KINETIC ANALYSIS

BERTHELOT LAW OF THE DETERIORATION PHENOMENA.

$\log t = 17{,}3 - 0{,}0458 \cdot T$ ..... Stabilizer Loss of 20 %
$\log t = 20{,}08 - 0{,}053 \cdot T$ ..... Stabilizer Loss of 50 %
$\log t = 21{,}05 - 0{,}055 \cdot T$ ..... Stabilizer Loss of 75 %

Chemical shelf life estimation at 20°C > 100 years

BOHN LAW.

$s = 2{,}41 \cdot \exp(-0{,}00172 \cdot t)$ ..... T = 323° K
$s = 1{,}77 \cdot \exp(-0{,}00656 \cdot t)$ ..... T = 338° K
$s = 1{,}76 \cdot \exp(-0{,}1812 \cdot t)$ ..... T = 363° K

Chemical shelf life estimation at 20°C >> 100 years

$k_s = 6{,}05 \cdot 10^{15} \cdot \exp(-13863 \cdot 1/T)$

NOTE: The stabilizer consumption curve has two zones, the former is linear, the latter is exponential. The obtained values have been fitted in the exponential zone.

t = time (days)
T = temperature (°K)
s = % of stabilizer content

TABLE - 6

COMPRESSION PROPERTIES OF PROPELLANT DB1 AT 20°C (according with spanish norm NM - P - 2359 (EMA))

	AFTER MANUFACTURING	AFTER 27 YEARS (NATURAL AGEING) PLUS 6 WEEKS (1176 HOURS) AT 65°C
COMPRESSIVE MODULUS (MPa)	708	762
COMPRESSION STRENGTH (MPa)	37,8	62,4
STRAIN AT BREAK (%)	39,8	44,2

TABLE - 7

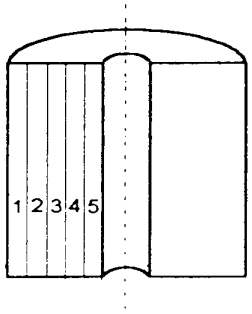
RELATIVE STABILITY CRITERIUM

SLOPE VALUE $x \cdot 10^{-4}$ (% / DAY)	TYPE	CRITERIUM
20	I	VERY GOOD
35	II	GOOD
50	III	MEDIUM
60	IV	MEDIUM
80	V	MEDIUM
100	VI	BAD

TABLE - 8

RESULTS OF CHEMICAL ANALISIS AT VARIOUS PROPELLANT LAYERS, PROPELLANT HAS NATURAL (27 YEARS) AND ARTIFICIAL (1176 HOURS AT 65 °C) AGEING.

	NITROGLICERINE(%)	CENTRALITE(%)	EPU(%)	EXPLOSION HEAT (cal/g)
LAYER 1	24,82	1,35	3,94	829,7
LAYER 2	27,39	1,27	3,90	829,4
LAYER 3	26,98	1,33	4,08	845,6
LAYER 4	26,54	1,39	4,27	837,5
LAYER 5	25,68	1,28	3,75	831,1



THRUST VS. TIME

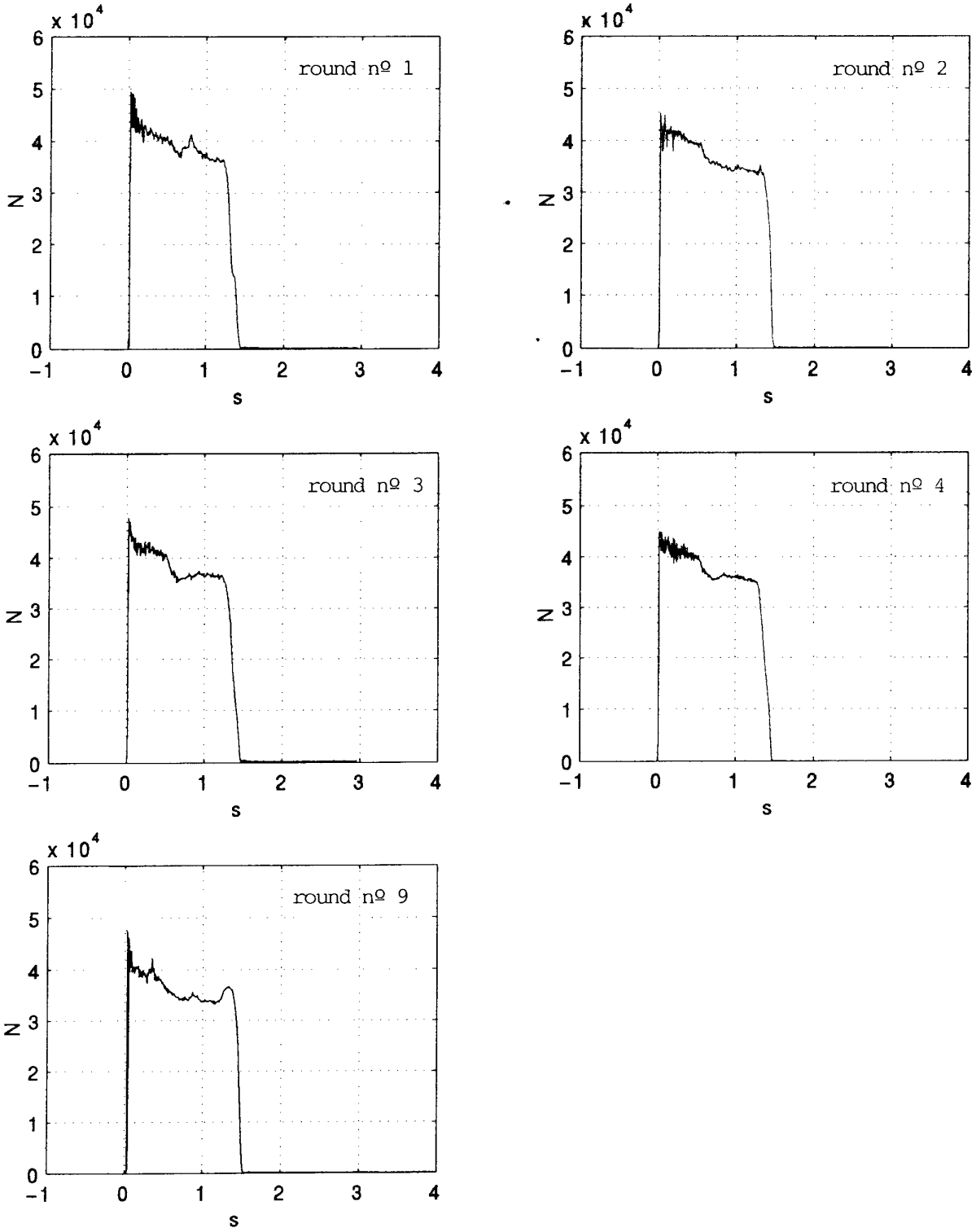


Figure 4. Rocket type E-3. Results obtained in four firings in Test Stand: rockets are 27 years old.

THRUST VS. TIME

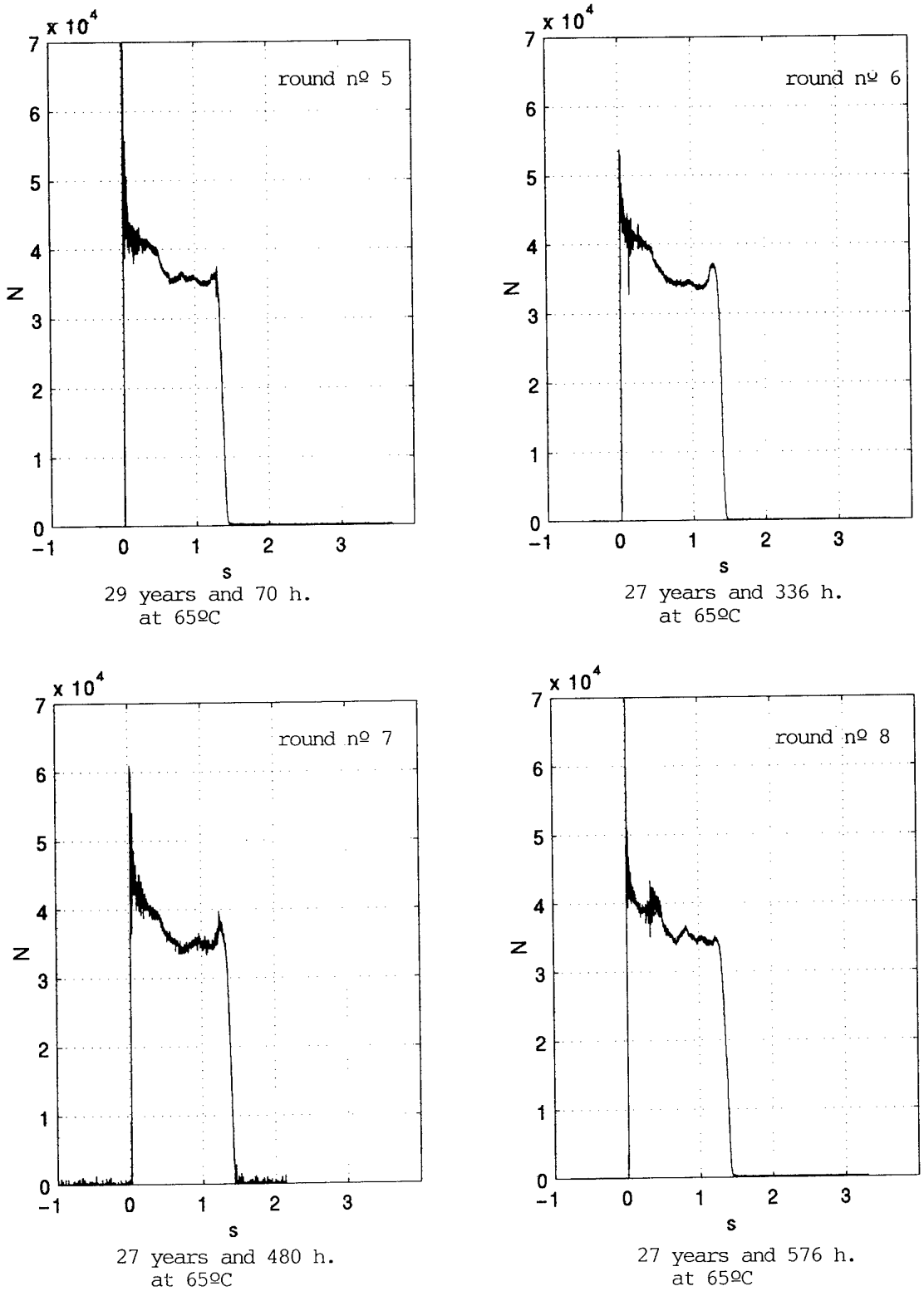
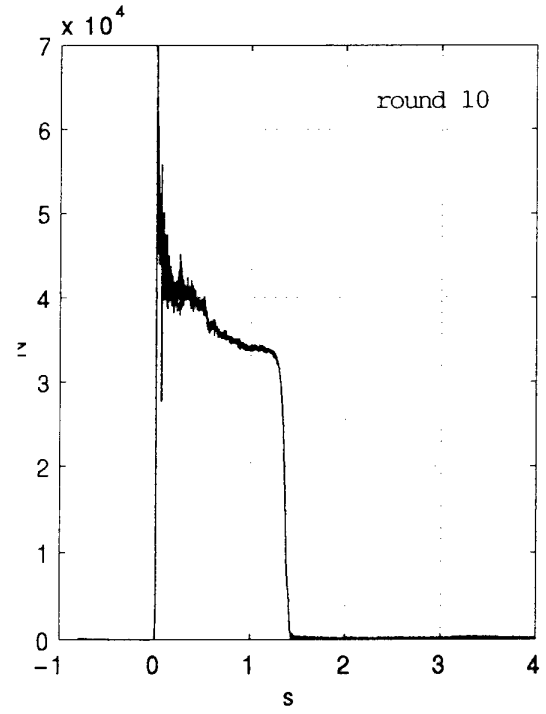
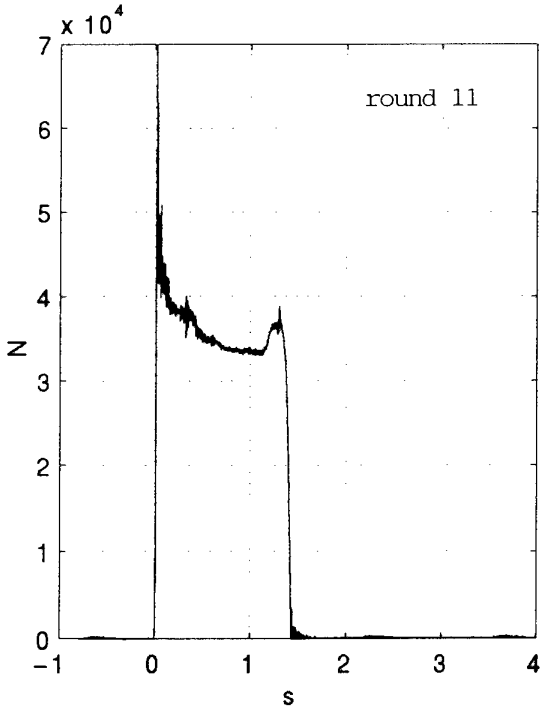


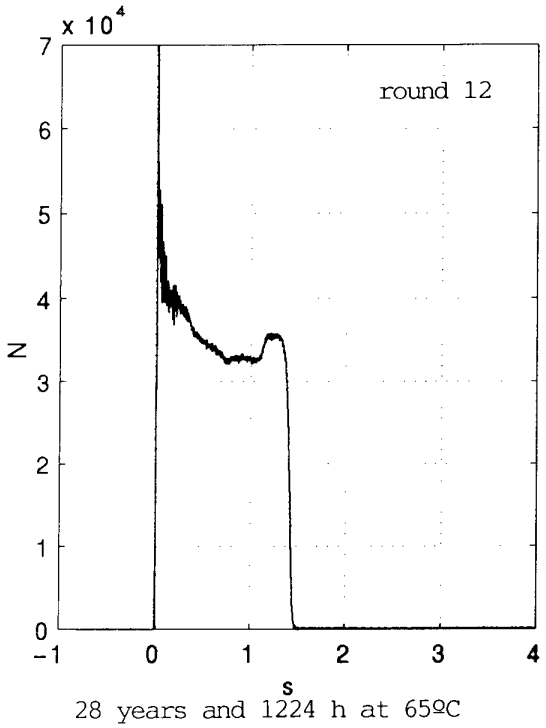
Figure 5. Measured thrust histories of Rocket type E-3 with natural and artificial ageing.



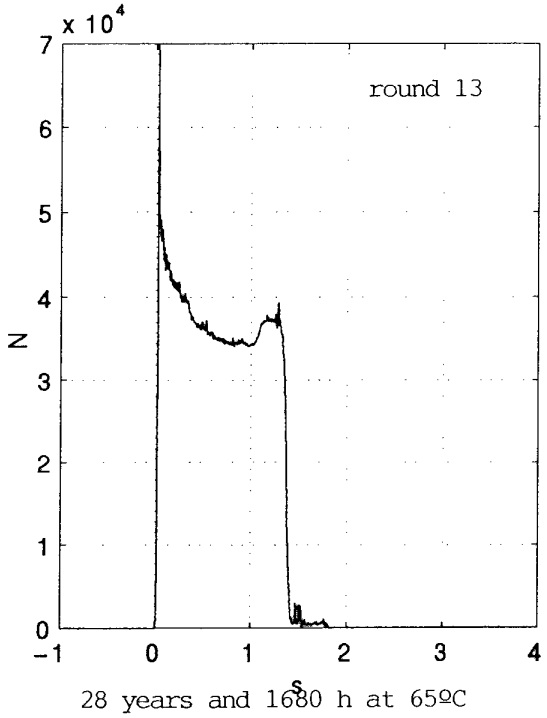
28 years and 720 h at 65ºC



28 years and 888 h at 65ºC



28 years and 1224 h at 65ºC



28 years and 1680 h at 65ºC

FIGURE 6: Measured thrust-time histories of rocket type E3 with natural and artificial ageing.

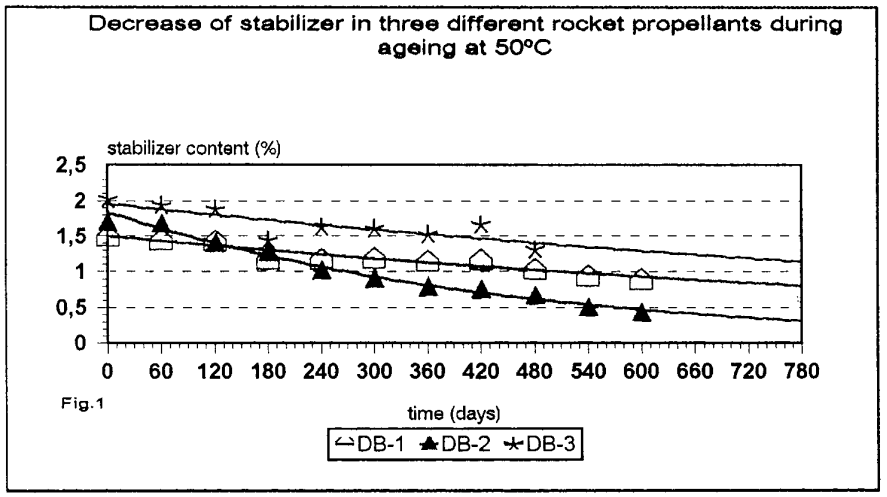


Fig.1

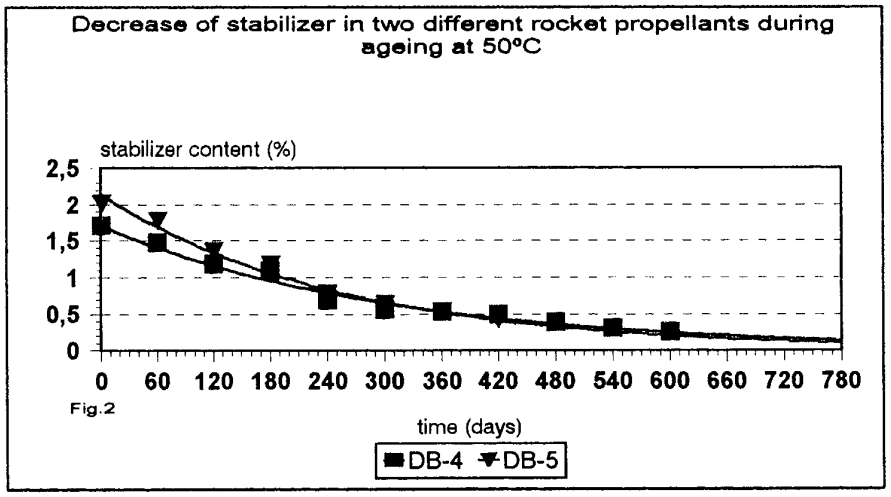


Fig.2

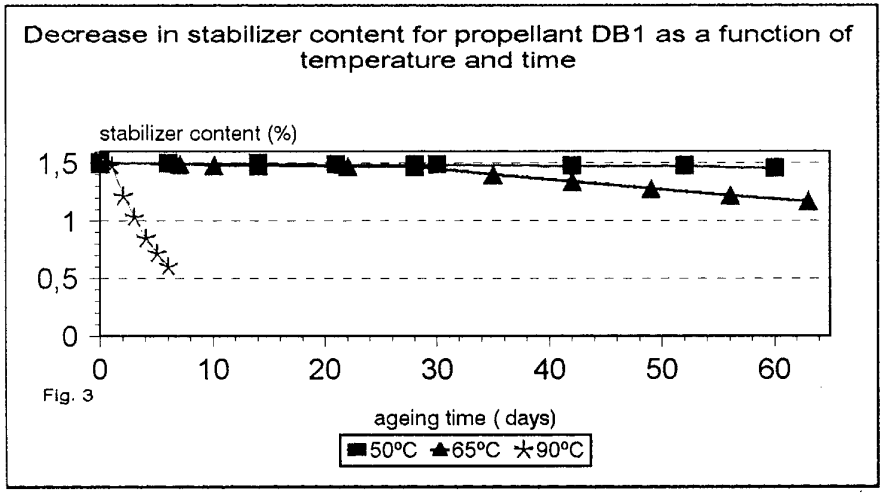


Fig. 3

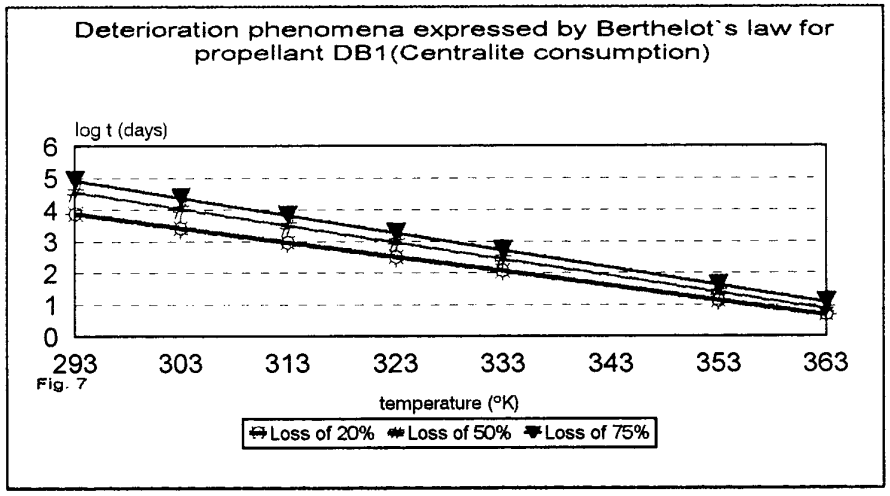
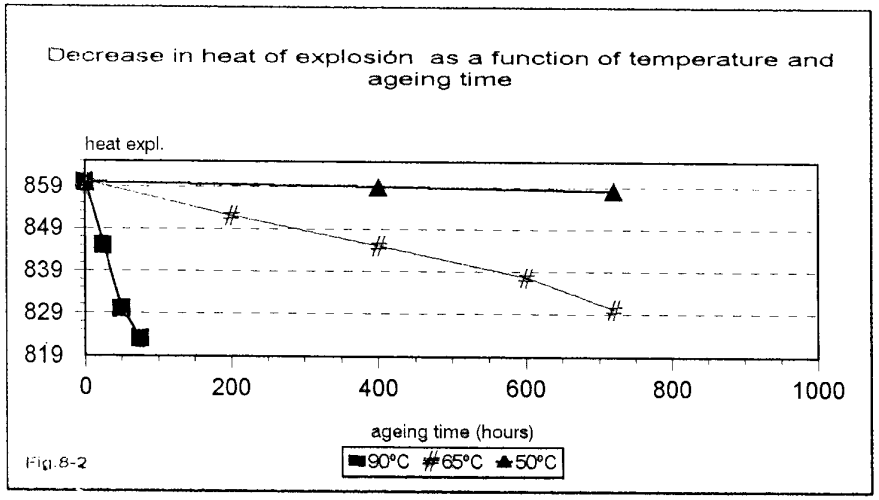
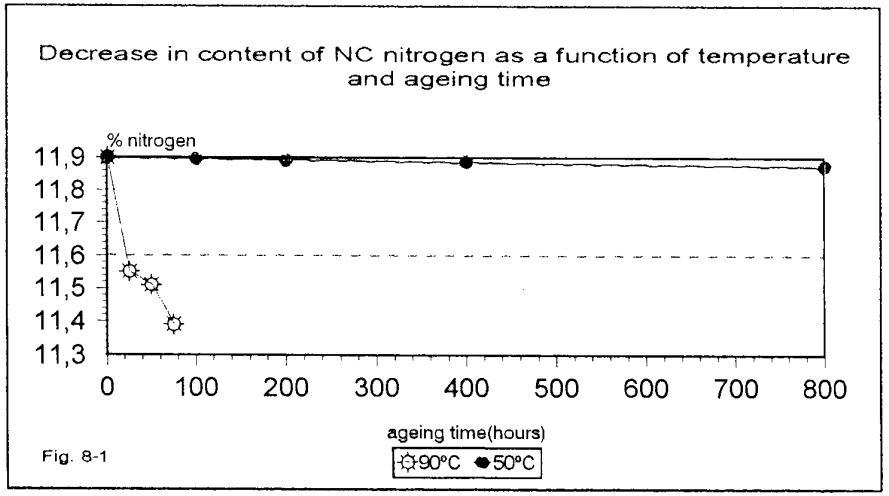
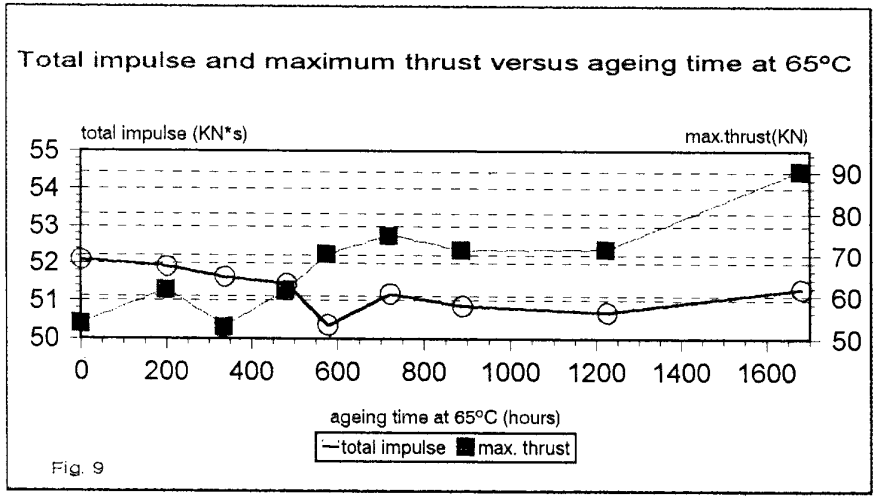
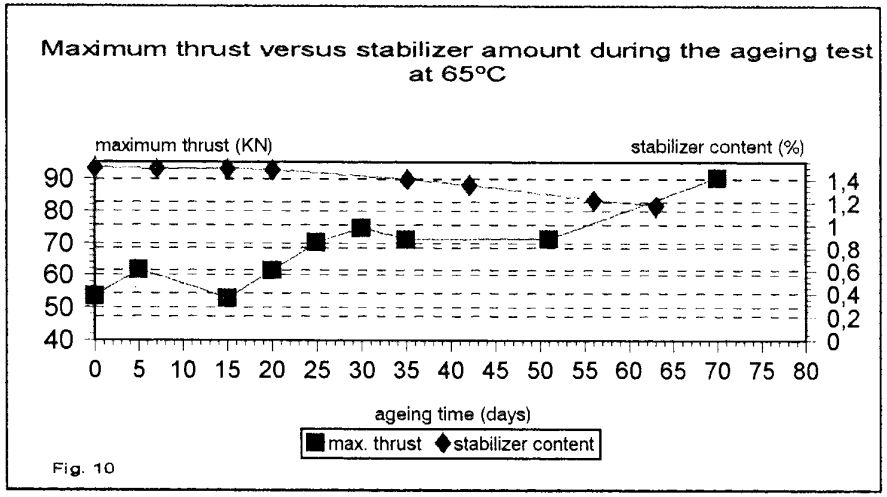


Fig. 7


Decrease in heat of explosión as a function of temperature and ageing time
heat expl.
859
849
839
829
819
0
200
400
600
800
1000
ageing time (hours)
90°C
65°C
50°C
Fig.8-2


Decrease in content of NC nitrogen as a function of temperature and ageing time
% nitrogen
11,9
11,8
11,7
11,6
11,5
11,4
11,3
0
100
200
300
400
500
600
700
800
ageing time(hours)
90°C
50°C
Fig. 8-1


Total impulse and maximum thrust versus ageing time at 65°C
total impulse (KN*s)
max.thrust(KN)
55
54
53
52
51
50
90
80
70
60
50
0
200
400
600
800
1000
1200
1400
1600
ageing time at 65°C (hours)
total impulse
max. thrust
Fig. 9


Maximum thrust versus stabilizer amount during the ageing test at 65°C
maximum thrust (KN)
stabilizer content (%)
90
80
70
60
50
40
1,4
1,2
1
0,8
0,6
0,4
0,2
0
0
5
10
15
20
25
30
35
40
45
50
55
60
65
70
75
80
ageing time (days)
max. thrust
stabilizer content
Fig. 10

Paper Number: 38
Discussor's Name: L. G. Meyer
Responder's Name: Dr. G. Jenaro de Mencos

Question: Do you see any degradation in the restrictor at the ends of the propellant grain, i.e., such as separation?

Answer: No.

Paper Number: 38
Discussor's Name: Dr. M. A. Bohn
Responder's Name: Dr. G. Jenaro de Mencos

Question: Have you looked for an increase of porosity on the inner bore surface of the aged rocket propellant, E3? By a decrease of the molecular mass of NC this can happen.

Answer: This phenomenon is being studied. Data have not been available until now.

Paper Number: 38
Discussor's Name: R. Pesce-Rodriguez
Responder's Name: Dr. G. Jenaro de Mencos

Question: How long after the artificial aging process were the data in table 8 obtained? I suspect that the observed reduction of NG at grain surfaces might not be significant. We have observed that diffusion of NG in NC is fairly rapid, and that it is difficult to obtain a concentration gradient. Equilibrium should be established fairly quickly.

Answer: The data of table 8 were obtained several days (less than one week) after the artificial aging process, whereas the rocket motor firings in a static test stand were performed 24 hours after the artificial aging process. As you know, it could be that the artificial aging is not representative of the natural aging because of the different diffusion coefficients at several temperatures.

Environmental Data for Rocket Motor Service Life Assessment

IH MAXEY
Defence Research Agency
Fort Halstead
Sevenoaks
Kent TN14 7BP, UK

SUMMARY

Descriptions are given of the various NATO standards and specifications for the environmental aspects in the service life cycle. Details are given of the differing climatic and mechanical loads related to the individual elements in the manufacture-to-target sequence within the life cycle of the rocket motor for tactical missiles. Aspects concerning the use of extreme conditions and measured data are related to the storage and operational use phases in the differing life cycles of land, sea and air forces' tactical missiles. The main considerations and limitations during environmental testing programmes are discussed. The use of modern methods of data capture and analysis are recommended.

INTRODUCTION

1. The influence of the physical environment experienced for a motor is a most difficult and significant problem facing those involved with life assessment. The complete life history of a particular motor is almost impossible to predict, even with present levels of In-Service monitoring, due to the various climatic and induced loading environments experienced in the wide range of ship, ground and flight conditions. It is a fundamental issue that, at both the time of initial development and during the designed, and often extended, life of a rocket motor, a definition of the total service environment that the motor will be subjected to is required, so that those concerned with its life assessment can then model, and assess the effects of, the environment.

2. Most methods of life prediction have a crucial dependence on the accurate and complete identification of the thermal and mechanical loads which the rocket motor is required to meet. However, the many papers on assessment methods refer only briefly to how these loads are defined. The loadings are not always known accurately enough, so design analysis and environmental test programmes for safety and life assessment purposes are nearly always based on extreme conditions.

3. For a motor in service use, the designer would wish the maximum use of good-quality storage with predicted conditions, and a minimum of exposure to extremes. The problem arises in that the motor may experience a range of conditions in widely different locations at any time in its life cycle. The Service User staffs have an excellent understanding of their munitions' use, and obviously are aware of the costs and consequence of their failure. In general, they require an assessment of the service life, ie. that covering both storage and operational use in the specified Service environment. The different elements in the service life cycle and types of environments that affect a motor's life need to be detailed sufficiently to allow realistic design analysis, and appropriate life assessment models and test procedures to be created. Those involved in these aspects could use the extensive knowledge available on the Service conditions to better effect.

4. After a long and varied involvement with the service use and life assessment aspects of guided weapons, the Author has noted that there is sometime a lack of knowledge as to how the elements in the service history are defined and used. To be able to do so leads to the concept of describing the history of the motor in its service life cycle as it progresses in the sequence from first production to engaging the target - defined in NATO as the Manufacture-Target Sequence (MTS). The main aim of this paper is to describe how the elements of the service life cycle in the MTS for a tactical missile can be considered in relation to service life assessment of the rocket motor.

NEED FOR ENVIRONMENTAL DATA

5. The current trend is to make tactical missiles increasingly more complex but demand higher performance especially from the motor. For the motor such factors as higher kinematic performance at longer ranges, and a need for aircraft to carry greater munition payloads, require more energetic and densely packed propellants inside smaller and lighter motor structures. The use of new propellants and higher load fraction charges will bring a new set of uncertainties to the analysis and assessment process of the safety of new motors. Meanwhile, in most fields of defence procurement there is an increasing emphasis on - and greater legislation for - improving the safety aspects of munitions on both risk and cost grounds of the expensive launch platforms and for the personnel involved. This will mean it will become necessary for risk assessments reasons to analyse and test motors more thoroughly and give an improved quality of prediction.

6. Structural integrity analysis of the grain is a key activity for risk assessment during the Design and Development phases in a motor project. It involves reviewing the critical areas with respect to the intended life cycle to determine critical conditions and the risk of failure during use. The analysis process for a solid propellant grain is being reviewed by NATO AGARD WG25 *[1]*. The Working Group has already established that the process must begin with a review of all loading conditions that will apply in storage and use of the motor. The quantitative assessment of the loading conditions can then be compared to mechanical and chemical failure criteria and required performance objectives. Although WG25 has decided not to concentrate on service life aspects in any detail, it is clear that the information generated in the structural analysis will provide the baseline on the environmental effects on grain's properties needed for the extended review process throughout the lifetime of the motor.

7. A great deal of work has been conducted on chemical and thermo-mechanical effects of the long term storage of motors and various models for storage life assessment have been developed. There are a great number of models for ageing, cracking, cumulative damage, etc. that can be used. Most are derived for and suited to the damage that occurs from typical ground use and storage conditions. Without doubt there is now a need for a systematic approach, to bring the many well developed aspects of life assessment together, such as those shown in the various papers at this Conference *[2,3,4,5,6]* covering work in the joint US/Australia/Canada/UK TTCP programmes on tactical rocket motors. Nonetheless, as well developed as these aspects have become after numerous years of effort, the different approaches all require a knowledge of the thermal history of important elements

Paper presented at the AGARD PEP Symposium on "Service Life of Solid Propellant Systems" held in Athens, Greece, 10-14 May 1996, and published in CP-586.

in the life of the motor, but this is not yet available in a practical way for any particular system. Moreover, there is as well a lower level of effort being applied to the operational use aspects in the MTS, especially for determining the combined thermo-mechanical damage in tactical carriage. For these reasons the predictions arising from the existing models are still not sufficiently robust to give Service staffs anything near the definitive answers on motor service life they require.

8. The more precise the definition of the Service environment, the more realistic can the models become and allow analysis be conducted and trials be arranged to ensure the motor will survive all elements in the MTS. In addition, repeatable and accurately set procedures to define the environment in the conduct of service life assessment are essential in International procurement projects to provide read-across between different motor programmes, analysts and users. Meanwhile, best value must be gained from environmental and life testing programmes. The long lead times in determining a realistic service life for a motor, the high costs involved and the continuing contraction - yet need for their increased use - of research and testing assets are the main drivers in seeking to improve such test programmes. Increased efforts have been made in recent years to improve the dialogue and co-operation - between interested nations, organisations and individuals - to help in the formulation of the most suitable methods of determining motor life.

STANDARDS AND REQUIREMENTS

9. General Aspects. It is normal to define two different classes of environments: a Natural Environment, wherein the conditions are generated by the forces of nature; and an Induced Environment, wherein the conditions are either man made or generated by the material. The safety and/or suitability for service of a motor will be influenced by both the Natural and the Induced environment effects within the whole life cycle. During the past 10 years there has been considerable international and national effort, particularly within NATO, to reach agreement and publish the various philosophies, standards, test methods and results documentation for environmental aspects. Some details in open literature were given by Herb Egbert *[7]*; further descriptions of the continuing process can be gained from individual Countries' representatives to the respective NATO groups described later. This paper will not to attempt to review the massive efforts being undertaken by the various NATO specialist bodies to produce growing volumes of publications on conditions and testing but will confine itself to describing the primary sources of information and how they are useful for service life assessors.

10. NATO Standards. The two main forums in NATO have been in Groups AC/301 and AC/310. AC/301 concentrates its efforts in these areas into a Working Party on Allied Environmental Conditions and Test Procedures (AECTPs), whilst AC/310 has a particular Sub-Group (SGIII) who deal with Environmental matters. Each Group publishes agreements on principles and procedures in Standardisation Agreements, STANAGs. SGIII also provide technical support to the Working Party on AECTPs. In the last 5 years the AECTP working group have progressed the issue of a supporting set of AECTPs to NATO STANAG 4370 *[8]*. The AECTPs being issued comprise the 100, 200, 300, 400 & 500 series to cover, respectively, the 5 main areas of: General Requirements, Definition of Environments, and Climatic, Mechanical and Electrical Test Procedures. These will primarily incorporate the current principles given in the American MIL-STD-810, the French GAM-EG-13 and the British Defence Standards (DEFSTANs) 07-55 and 00-35. The definition of the climatic and mechanical environments that NATO munitions may be exposed to are detailed, respectively, in STANAG 2895 *[9]* and STANAG 2914 *[10]*. There are also a number of generic system-related STANAGs that define the testing requirements and whole life cycle test procedures for munitions, eg. 4325 for Air-launched and 4337 for Surface-launched guided weapons, which provide much useful information for service life testing *[11,12]*.

11. UK Standards. In the UK, attention has always been paid to continuing efforts to rationalise and publish Nationally and Internationally agreed environmental definitions and testing requirements. UK National defence standards (DEFSTANs) are prepared, in consultation with industry, and published by the Department of Standardisation; this, together with the Ordnance Board, is now in the new Directorate General of Technical Support area in the UK MOD PE. The primary design requirements for guided weapons are promulgated in DEFSTAN 08-5 *[13]* and those on environmental criteria are given in DEFSTAN 00-35 *[14]*, the latter replacing DEFSTAN 07-55. DEFSTAN 08-5 includes 2 important aspects for all those involved in life or structural integrity analysis to note. The first is the requirement for overall system structural assessment, which includes the need to generate a structural design record (SDR) of all structural components of the missile. The procedures for compilation of a SDR are given; for environmental aspects they specify that a `Design Cases and Load Factors' document be produced. The other aspect is that mandatory design verification and test requirements, as well as advice, is given for all aspects of missiles, including the hardware and the overall motor. DEFSTAN 00-35 describes a variety of environmental data and a range of tests for the Natural and Induced environments, to reproduce the conditions and mechanisms in the MTS of any munition. In the UK, it implements NATO STANAGs 2895 and 2914. The UK has previously specified DEFSTANs 00-35/07-55 for environmental criteria and testing but is increasingly moving to use the STANAGs and the AECTPs for future, and many existing, projects' environmental criteria, definitions and tests; mirroring in some way the US move away from a plethora of National standards being quoted in the specifications.

12. Project Environmental Requirements. In the UK, a formal means for setting out the MTS and patterns of use to permit analysis of the requirements for each Project was set up by mandating the completion of an Environmental Questionnaire - titled the Ordnance Board Form 41 (OB F41). This was introduced primarily to enable discussion between the MOD Project Sponsors and Managers with the OB, and to provide a defined record for all to use, on every aspect of use needed for assessment of a munition. The OB F41 was then included in the first edition of NATO Allied Ordnance Publication (AOP) 15 *[15]*, promulgated by STANAG 4297. These NATO documents are now being further updated by AC/310 SGIII, to define all aspects of safety and suitability assessment of munitions, including the system safety planning requirements given in US MIL-STD-882 and various UK DEFSTANs.

DEFINITION OF ENVIRONMENT

13. General Definition. Much of the effort in the use of environmental data for life assessment of a missile needs to go into defining the individual conditions that can apply to any individual missile at each element in the service life cycle. It is normal to consider that the environmental effects acting on the munition are either climatic (ie. Natural) or mechanical (ie. Induced), which can act either separately or in combination (eg. thermo-mechanical) to degrade its condition.

14. Climatic Conditions. Climatic conditions throughout the world vary considerably. In an ideal procurement policy, the Service Users would wish that their munitions should be designed so that it can be stored and operated anywhere in the world for indefinite periods but without increased risk or cost of purchase. Some 25 years ago, recognising that this was impractical and in an effort to review the climatic testing requirements for Army guided weapons, the UK OB sponsored a Working Party to consider revising the defined normal and extreme conditions of temperature, humidity and solar radiation to which missiles could be exposed. A great deal of historical data was used to be able to describe and replicate these climatic conditions, their probabilities of occurrence in the various parts of the world, including conditions at differing altitudes. The culmination of this, together with information from other countries, formed the diurnal cycle tables and other weather conditions (eg. sun, wind, sand, ice) relevant to a munitions' storage or use conditions which are nowadays set out in STANAG 2895/DEFSTAN 00-35. For simplification the world's land and sea masses were sub-divided into fourteen general climatic categories. In general these Climatic Categories describe conditions in areas that are either hot (A1 - A3), humid (B1 - B3) or cold (C0 - C4) as well as 3 deep-sea marine areas (M1 - M3). Figures 1 & 2 show example conditions.

15. Extreme Conditions. Study of STANAG 2895 will show the rationale for using the normal and extreme conditions in design and in testing. It describes the likelihood that there are a small number of occasions in each month, some 7 - 8 hours or 1%, in which the seasonal temperature conditions are likely to be exceeded. In preparing the STANAG it was accepted that, when considering the risk of exposure to the 1% condition, there is need for a compromise between the operationally desirable and the economically practicable. However, the STANAG (as well as US & UK standards) sets out that the 1% probability of temperature and humidity levels for the storage and use conditions should be used when conducting the Qualification and Proof Testing of stores containing explosives or propellants. The use of 1% conditions is considered necessary to provide assurance that munition safety will not be compromised throughout the whole MTS. This has been particularly required for ensuring the safety requirements for tactical missiles are met - where the general design criterion is that 99.9% of units, at a 95% confidence level, shall remain safe after exposure to all possible service conditions - despite limited numbers of missiles generally being made available for testing to achieve a high reliability. In most respects for service life assessment purposes, the use of the 1% conditions is thought to lead to an underestimate of the life of the stockpile, especially for units that have been held in more benign conditions in service. However, although they are a worst case assumption, their use ensures an appropriate safety factor which allows each tactical missile to survive extreme conditions that may arise in the ever changing, more extensive Service use that inevitably occurs. For service life assessment, it is worth noting that the NATO, US & UK standards make the point that these 1% conditions can be redefined by the use of more specific thermal data, gathered from the munitions' actual Service conditions, and accurate determination of the life cycle.

16. Modelling of Climatic Conditions. A great amount of work has been carried out in the USA and UK on the derivation of models for temperature and solar radiation. In the general case, air temperature is considered as a long term mean value with superimposed harmonic components (seasonal & diurnal) and additional random noise from local weather. This can be used to generate a probabilistic damage function from the induced thermal stress/strain. Continuing programmes are being undertaken by Dr Jim Margetson, sponsored in the UK by the OB and DRA, and in Canada by DREV. It has been shown that temperature monitoring need not be continuous, as an estimate of the seasonal thermal effects can be made from small samples, avoiding a criticism raised by any service user to demands for more temperature records. Extensive records from the UK Met Office of sites around the world have been used as the input load conditions for use in damage effects programmes on service motors *[16]*. Some aspects are shown in Figures 3 & 4. Meanwhile, a very comprehensive effort to characterise the typical conditions in South West Asia, particularly in the Gulf States, was undertaken by the US following the deployment of munitions to that area during the Gulf War. The UK Services haves also carried out a similar, but smaller, programme of work for this area. The situation for solar radiation thermal effects is also reasonably well defined, albeit with some simplifying assumptions being necessary for the general case in the absence of measured data; STANAG 2895 has some typical levels, as seen in Figure 2. Where the solar radiation level is greater than 1000 w/m^2, it is generally assumed that a 20° C increment to the Met Condition (screen) air temperature occurs; indeed the tables in STANAG 2895 uses such a figure, together wih the use of standard values for the absortivity of covering materials, to produce the general Storage & Transit conditions. The temperature increment may be even higher than 20° C when in standby conditions, especially for stores with highly absorptive qualities (eg. dark paint) or where reflective surfaces (eg. metals and concrete) add an extra component of radiation to the incident radiation.

17. Determining Mechanical Conditions. For mechanical conditions, the environment can be defined in terms of the parameters that constitute the energy input. These include intensity (eg. levels of shock, drop heights or amplitudes, rates of precipitation, etc.), the type of impulse (in terms of waveform, eg. sine wave, sawtooth, etc. or random vibration) and the duration. Several typical and most often used mechanical conditions are published in STANAGs 2914 & 4370, DEFSTAN 00-35 and MIL-STD-810. These publications, like those for climatic conditions and tests, represent a great deal of efforts to describe standard conditions that have been experienced in the long use of military stores. In general, various forms of acceleration loads occur during storage, transportation, and during operational use, ie. at launch and manoeuvre. Handling and movement of the munition and its storage medium (eg. Ship magazines) generally apply acceleration levels of 2 - 4g, whilst the long term effect of gravity may affect larger motors, especially those with low modulus propellants. Logistic and Tactical transportation loads will include shock pulses (sometimes of 9g) or drops, frequent load reversals of +/-3g, and vibration of differing levels and characteristics from the ground, sea or air transportation vehicle. Dependent upon the method of firing (eg. ejection or rail launcher) the launch shocks can be as high as 35g in a sharp pulse. For ship based aircraft, catapult launch and retardation may be 9g, again in a sharp pulse shape. Additionally, operational carriage will include severe acoustic, airflow or pressure shock conditions, particularly when adjacent weapon firing takes place, as well as significant levels of random vibration. These all cause high energy inputs which need to be defined in terms of magnitude, type and frequency or duration for each particular system being assessed. The publications give guidance on the type of loads although all state that the specifications should only be used if more appropriate measured data is not available.

18. Thermo-Mechanical. In a real service life cycle of a tactical missile, a combination of the thermal and mechanical loads are mostly found to be the cause of greatest damage. In the motor, the grain and bond to the insulation are inevitably damaged through a fatigue mechanism caused by these thermo-mechanical loads. As

is well known, motors are invariably at a temperature below the stress-free temperature of the propellant so that stresses and strains arise due to differences in coefficients of thermal expansion of the propellant and the motor case causing contraction or expansion of the case and propellant. Typically, the coefficient of expansion for propellants, liners and insulation materials are an order of magnitude larger than that of case materials and thermally induced stresses and strains in the grain occur due to restrained shrinkage. In storage or standby conditions these thermal loads are cyclic in day or season *[16,17]*, thus stress/strain is a cyclic loading which leads to cumulative damage. In the Tactical phase of the motors' life, the high levels of thermo-mechanical stress induced by rapidly changing conditions can also be coupled with the vibration energy that arises from operational carriage to cause a further degree of cumulative damage. Where high levels of thermal and mechanical energy are coupled, eg. due to the air-carriage heating and vibration effects, a motor will experience considerable viscous dissipation over the wide range of temperatures involved. However, it would not be correct to assume these worst-case conditions occur in every operational period; if they were it would be practically impossible to provide long storage and operational lives on a motor without excessive weight penalties. For service life assessment, therefore, it is important to gain a knowledge of both the magnitude and duration, as well as frequency of occurrence, of the complex set of thermo-mechanical loading conditions which can apply to a tactical motor throughout its service life cycle, especially for those subjected to the extremely hostile operational condition. The wide variety of these loading conditions, as well as the system-specific response and dynamic nature of the cause and effect on a particular system, make the thermo-mechanical loads the most difficult to determine *a priori*, and representative conditions are not well documented in National and International standards. Even given measured data, it is still not easy to apply it. The normal situation appears to be that the expected design load cases are established, during the Design Phase by the Contractor, from the storage and operational environmental profiles given in the system specifications and are then passed down to the motor design team as a set of load conditions to be survived. However, it seems to be rare that this continues into a resolution of the load conditions for specific use in service life programmes, leading again to the use of somewhat extreme conditions, and without a good knowledge of their frequency throughout the service life cycle.

SERVICE LIFE CYCLE

19. General Specification. The expected usage conditions and required life for a missile will originally be set by the Services' Operational staff in the Staff Target or Requirement. This information is most often then taken as the basis for an environmental and usage section included in the Technical Requirements or Cardinal Point Specifications created by the Project Manager. The defined environment and use pattern for the missile in these specifications often may need to be modified as necessary at the Project Definition stage; essentially these details must be fully agreed in time to set the design and determine the planned Test and Evaluation stages needed during the motor's Development and Qualification phases. Most NATO countries now follow the Integrated Logistics Support (ILS) route in procurement and ILS staffs are being incorporated into modern munitions' Project Management offices. The ILS staffs, responsible for the In-Service logistics and useage aspects and oversight of Test and Evaluation plans, will then produce a Use Study document and various forms of Equipment Policy Statement to meet ILS requirements. These will also contain valuable environmental topic areas and reflect the more detailed usage pattern that the store will see, rather than the outline detail given in the Requirement Specifications. For mature projects, which in the UK pass from MOD PE project management to the In-Service Manager of the particular store, there may be revisions to the Use and Equipment Policy Statements to consider as the Service Users expand their employment or alter the policies. The Contractor will most often have been required to produce, and have concurred by the customer's Project Manager, some form of Environmental Design or Load Data Book (eg. the UK's Design Cases and Factors document in DEFSTAN 08-5). It was this variety of sources for environmental information that the OB Form 41/AOP-15 was designed to address; its use is highly recommended for any Nation not already using the system. The aim in service life assessment must be to ensure that the actual use and environments of the motor throughout its service can be determined accurately and compared with the original defined condition, so that the service life programme analysts, test managers and trials agents can be provided with the most precise description possible of the likely loads at all stages in the Manufacture-to-Target sequence (MTS). Thus, the task of the users in the environmental description process is to ensure that all possible data sources are complete, accurate and consistent, whilst the designers need to consider how the data and definitions apply to their stores.

20. MTS Elements. To gain an understanding of the life cycle, it is useful to resolve the MTS into a typical sequence of elements. In general terms, for a tactical missile, there will be 2 phases: the Logistic phase, undergoing Storage or Transport as either components or as an All-Up-Round; or a Tactical phase, either on Standby or in Operational Use. In the Standby condition, the missile may be either on the ground or launch platform - ie. being loaded to its launch platform, held in temporary storage adjacent to the launcher or held fitted on the launcher. In the Operational Use condition, the missile will be moving on its launch platform, ie. captive- carried on a ship, ground vehicle or aircraft launch platform.

21. Logistic Conditions. The elements in the Logistic Phase will, typically, involve logistic transportation (broadband vibration & bounce), storage (hot & cold diurnal cycling), tactical transportation by vehicles or helicopters (broadband random vibration with peaks generated by the rotors or track patter), handling (drop & shock) in both packaged & unpackaged state, as well as servicing and testing. The range of these will depend upon the Services' operating policy. Perhaps the most important of these to consider in life assessment of the Logistic phase is the storage policy.

22. Storage Policy. The storage policy for a missile is set normally at the procurement stage by the Service Sponsors' operational and engineering branches, and is then adjusted by the Project or Service managers at appropriate points in the procurement or in-service phases of the munitions' life cycle. It is normal for the Services to obtain a stockpile of weapons so as to hold the majority, if not all, of its wartime requirement under its own control and as near to any possible point of use as possible. The stockpile of tactical missiles is sometimes described as being of 2 portions: the majority being held as In - Store stock, either remaining in their packages or - to avoid the long preparation time in the confused and busy time of wartime - being partially or fully assembled; and a minority held as Ready-Use stock, which are built-up, mostly out of their packages, and thus immediately available whenever required. There are a number of major considerations for the motor that result from the adoption of such a `Dual Inventory' policy. For the In-Store motors, these include whether they are held in high quality component packages - sometimes called `Deep-Stored' - or are held in environmentally

sealed All-Up-Round containers; in both these conditions the packages can greatly moderate the storage environment and the storage conditions can be optimised to provide long life. For In-Use missiles, the periodicity and duration that the motors are removed from store, and the conditions they will then experience - which will cause exposure to water, temperature, direct radiation, wind, etc. - are major factors affecting life. The differences in storage policy, conditions and durations need careful and accurate definition in the OB Form 41/AOP-15 and Use documents for the service life assessor to use.

23. Storage Method. The manner of storage may differ between nations, or in the Services of each nation. For tactical missiles, the greatest divergence in method arises from whether the In-Store stocks are held in either magazines at static bases - ie. for most of the Army or Air Forces' use - or on board ships at sea - ie. for Naval Forces' use. The former method is generally more benign, as, with the magazines mostly being high-mass structures, it is easier to control the temperature and humidity, provide alleviation of the external weather and maintain stable conditions, and where, being static, the stores are not subjected to vibration until transported. As it is well established that the deterioration of explosives and propellants is directly linked to exposure to higher temperatures, it has been UK policy for some years to store Air Forces' missiles wherever possible in magazines at 5 to 15°C, though without air-conditioning applied. UK Ships' magazines have been found *[18]* to be mostly held constant at around 20°C in Northern waters and at around 30°C in hotter marine areas; they often have some form of humidity control. Naturally, Ship storage does additionally provide some seaborne vibration and shock, although for most missiles this will be reduced by good packaging or racking and often further reduced by packaged missiles being placed onto shock mattresses.

24. Tactical Use. In the Tactical period, the effects of both temperature change and radiation - either the heat from direct and reflected solar radiation or exposure to ultraviolet light - may be significant. As the conditions may be so varied at different sites, and indeed across a site itself, despite extensive data capture efforts already undertaken there are only general definitions available in standard specifications. It is normal policy to minimise the times for which live missiles are exposed on Standby outside storage; often they are limited to a set period, eg. 56 days exposure, before maintenance is needed. In Tactical use, Army missiles may be fully exposed on their launchers, eg. for many SAMs, or enclosed within the launch tube, eg. anti-tank and area denial missiles. Typically, Air Forces' tactical missiles are held on Standby, either next to or on the aircraft, within reasonably sized ready-use store buildings such as open sided barns or fully protected, enclosed aircraft shelters. For Naval shipborne missiles, sometimes shading can be provided when in weapons parks on deck or by the launch canister, though enclosed conditions can vary considerably dependent on position or local wind conditions *[18]*. In sheltered but open standby situations, exposure can be less severe as natural ventilation provides cooling of the motor; and the STANAG 2895 data on wind should always be considered to determine thermal effects. For example, a number of sources have noted that stores in open sided shelters or even when unshaded can experience lower temperatures in hotter areas than in enclosed magazines *[17,18]*; quite naturally the opposite will occur in cold climate winter conditions. Again the conditions need to be monitored accurately for use in service life assessment.

25. Airborne Operations. To help avoid mishaps and preserve safety in peacetime at as high a level as possible, fully functional, armed missiles are generally only carried on aircraft for operations where hostilities may break out. There are 3 differing ways to carry the missile: internal carriage, inside a protected, enclosed bay; conformal carriage, semi-buried in the fuselage; and, external carriage, mounted on a wing ejector pylon or rail launcher. The aggressive effects of the air-carriage environment are generally felt increasingly more by externally carried stores, although conformally carried stores may suffer greater effects if the aircraft engines transmit sufficient heat and vibration, whilst missiles in open bomb bays will experience heavy buffet conditions. However, the situation is difficult to predict, and, more so than in any other part of the MTS, there is no substitute in service life work to gathering measured data for each condition.

26. Data for Air-Carriage. There has been in the past some extensive efforts to quantify load conditions for particular systems, which have then been translated into certain National standards as design cases. The US and Australia carried out a series of F-4 aircraft flight trials with instrumented fuselage and wing-mounted missiles *[19]* that provided a basis for many years of the typical air-carriage temperatures seen by such missiles, and the US has continued to monitor air-carriage temperature and vibration levels on a number of aircraft/missile combinations at intervals since then. The UK has similarly carried out series of flight tests, when needed to verify US missiles' Qualification levels on UK aircraft or to validate requirements for new missiles. From these sources, it is generally taken that the worst-case captive-flight profile on a modern air-carried missile during an interception mission can subject the motor, within a few minutes after takeoff, to a maximum temperature of 120 - 150° C on the case - with the propellant/insulator interface typically at around 30° C lower - whilst undergoing random vibration of high amplitude/low frequency (short-term, buffet) and medium amplitude/high frequency (longer duration, nonbuffet) conditions The most severe carriage conditions are generally experienced during flight profiles of the interceptor aircraft types, so these are often set as the design criteria for a missile which is used on different types of aircraft. In some situations though, the ground attack type of aircraft experience very different and ocasionally more severe conditions, especially under high dynamic pressure, eg. fast speed, low altitude flight. It is though a difficult exercise to determine in advance of design, or to apportion during the subsequent life assessment, the length of time a missile will experience a particular sortie profile or flight condition, so generalisations are inevitably needed and pessimistic designs or life assessment results. Whilst a considerable amount of data measurement has been conducted for air-carried munitions, most of this is used to determine the structural integrity of the overall munition, ie. the airframe fatigue and strength characteristics. Obviously, this data can then be put through flight simulation and transient heat transfer analysis programmes to determine the conditions likely to be experienced by the motor, and the data used to refine the grain structural integrity calculations. Perhaps the biggest challenge to be faced for an air launched motor is in being able to determine the complex loads experienced in air-carriage and their duration during the life cycle so as to then use such measured data to generate appropriate simulated accelerated life test programmes and also obtain an analysis of the effects of this environment for use in the overall cumulative damage models of any systematic, meaningful service life assessment programme.

27. Air-Carriage Effects. Air-carriage involves extremely complex subject areas, with cross-coupling of thermal and mechanical energies on a wide range of materials, and the system specific response makes the effects too specialised for any significant treatment in this paper. It is also very costly to gather data, using instrumented missiles, on the actual environments and energy levels experienced over the wide range of flight conditions.

There are 2 particular areas of concern for the motor: aerodynamic heating, particularly during conformal and external carriage; and the levels of energy imparted by acoustic and air pressure (change and shock) and random vibration. Aerodynamic heating can cause grain structural problems when a motor which has been held in store at a low temperature, say at -51°C in C3 Climatic Category, or externally carried attached to a high-flying aircraft for a length of time sufficient to allow the major portion of the propellant grain to reach equilibrium, is then subject to the thermal barrier which results from the supersonic dash of the aircraft. The temperature of the boundary layer and that of the missile skin is raised appreciably because of the dissipation of energy generated in the boundary layer at high speeds and the shearing work done on the fluid by the viscous stresses within the boundary layer at high speeds *[20]*. Since the major portion of the grain does not have time to react to the thermal gradient caused by the aerodynamic heating, bond stresses in addition to those already present are induced. The levels of acoustic (sound) and dynamic pressure the munition may experience in captive carriage are considerable. The response to adjacent gun-firing on munitions during air-carriage is not particularly well established, especially on aged stores; although the conditions are only seen for a small amount of time in the air-carried life, the hammer shock they induce on a motor may be the cause of the critical failure in terms of conduit cracks or liner disbonds. The air-carriage environment remains most difficult to assess yet it has been considered that the damage from air-carriage can be 1000 times the rate of an equivalent period in ground storage. Indeed, the UK are practically alone in setting an operational life for its missiles based on air-carriage hours; most Nations only carry out surveillance of whether damage has occurred in the whole life (ie. storage and operational elements) or do not record flight hours. A great reliance is placed on initial environmental testing, with surveillance of missiles that are considered 'fleet leaders'. As far as is possible to see, little has been published on the unique effects of air carriage causing end of life of the charge. The result is that there is a pressing need to examine what damage does occur to the propellant charge from the application of the overall thermo-mechanical loads in air-carriage, especially on aged propellants and bonds.

ENVIRONMENTAL TESTING

28. General Requirements. All tactical motors provided for NATO Forces use are required to undertake an Environmental Test Programme, as given in such standards as STANAGs 4325 and 4337. These are based on interpretation of the specified Service conditions, laid out for example in the AOP-15, and are intended to simulate the life cycle of the motor. They can be used to determine the motor is able to withstand an initial period of service life, with the test schedule parameters adjusted to suit the life duration required. The fundamental need in these test programmes is to establish ways of quantitatively accelerating the processes leading to the failure modes of the motor, but without creating unrepresentative failures, such that an authoritative opinion can be developed of how a motor of a given age will react to its environment long before that age is reached. To gain best use of any forced ageing regime needs an accurate and positive identification of the damage mechanisms that degrade the material and failure modes that act to end the life. This can only be achieved in practice by a systematic and iterative process of analysis of the modes and mechanisms of failure caused by the environmental conditions and then testing the validity of the forced life regime that has been used in the assessment.

29. Test Durations. In general, and in increasing length of likely durations in the MTS, the total ground or ship-based cycle will comprise periods in the operationally ready state, in transit and in storage. In the first period, the motor is likely to be exposed to the full climatic effects, especially when fitted to the launcher. Usually this will only be for a short period in its total life and deterioration during this process can best be determined from real-time, simulated real-life trials which use standard combined climatic and mechanical conditions. In the transit period, duration is again relatively short and it's effect can also be evaluated by similar real-life trials using measured data taken from the transport vehicles response to differing transport conditions. However, in both these above cases the durations for which the dynamic aspects of the mechanical environment may be present in the whole life cycle can preclude the adoption of real time trials, and so acceleration of the trials, eg. by enhancing the amplitude of stressing within the design limits, may be needed to yield substantial economies in time. The remaining life of the motor which is spent in storage is nearly always required to be many years - up to 20 years is quite normal - but it would require real-time trials of unacceptably long duration; so a method of accelerating the storage period is especially needed.

30. Environmental Acceleration - Storage Life. The main method of acceleration of storage time is by the principle of high temperature causing forced ageing; this is based on the assumption that a long period of storage at a relatively low temperature can be simulated by a shorter period at a higher temperature. The application of Arrhenius-based acceleration, using extreme diurnal temperature and humidity cycle regimes, is well known and has been described in many papers here and at other symposiums. It is though appropriate to reflect on some of its aspects.

31. Use of Arrhenius. The main limitation of the Arrhenius equation for use in life assessment is that it is only valid when ageing is determined solely by first-order reaction rates. The activation energy of the reaction, ie. ageing, can be determined experimentally, given the knowledge of what is the damage mechanism for the material; more often in setting out test parameters for an initial life assessment programme empirical values are used. A basic precondition is that no material changes occur within the temperature range between natural and accelerated ageing. It is also only valid if the difference between test and operational temperatures is small, so that the activation energy can then be regarded as independent of the temperature. Where a system comprises components with different activation energies, some components be will be under or over tested dependent upon which component activation energy is chosen for use in the Arrhenius equation. Normally the lowest value from among the components assessed to have a limiting effect on storage life is the one selected. Meanwhile, using solely activation energies, it is difficult to take into consideration synergistic effects induced by, for example, moisture, oxygen, and corrosive gases. Sometimes the effects of diffusion and various types of stress can be at least as limiting. Nonetheless, the use of Arrhenius-based acceleration is a valuable method to reduce testing time, providing forcing is not too dramatic, and it is used extensively by many nations. The UK apply it to a diurnal cycling test regime to achieve acceleration of the storage life *[21]*, rather than by different periods of constant temperature cycling as in the US Type-Life approach, and generally use the hot-humid Climatic Category cycles. The diurnal regime is considered by the UK to be more representative of the climatic conditions seen by a store, and it also causes the required stress of seals and bonds to replicate real life conditions. However, due to the various limitations described above, the UK limit the confident prediction of life from solely accelerated ageing testing to a maximum of 10 years.

32. Acceleration - Standby/Operational Life. During the Development and Qualification of a motor, Proof-level environmental tests are mostly conducted for the Tactical phase, ie. the Standby and Operational periods. As the reliability required may be 0.9999 at 95% confidence, the programme will need to necessarily overtest to suit the worst case and most aggressive examples of the environment. However, as the conditions to be applied are often derived from limit or extreme cases then it is essential to check that motors are not subjected during testing to levels of stress more severe than the design limits. There is a general lack of standard reference works for use in obtaining suitable parameters and the methods of conducting realistic testing of the Service Life for the Tactical phase. Additionally, there are few established or quantified ways of accelerating thermo-mechanical effects without causing unrepresentative failures. The thermal damage effects during the Standby period are generally simulated through low and high temperature testing, often using the extreme conditions diurnal cycle method, and sometimes with additional radiation from lamps. The wavelength of natural solar radiation differs from that generated by the typical radiant lamps used in many test programmes (Figure 5), and it is difficult to apply the correct heat flux to simulate solar radiation in Standby conditions. Mechanical damage to a motor in Standby or Operational use is considered primarily to be caused by vibration, particularly for air-carried stores but also in ship or tracked vehicle carriage. Thermo-mechanical effects are mostly simulated by discrete tests, such as thermal shock or altitude/temperature change, and by conditioning to extremes before each test. Acceleration of vibration time is though extensively used, sometimes with additional heat input during the test.

33. Service Life Acceleration Methods. Miner's Rule, although developed for fatigue of metals, is generally used as the basis for the acceleration method for vibration. The hypothesis is that a reduction in test time can be achieved by increasing the stressing level using a power law. For sinusoidal vibration the stress is the acceleration level, whereas for random vibration the stress intensity is the acceleration spectral density, ASD. For the latter case, as applies for example in air-carriage, to obtain acceleration from real-life to stressed-life, with R_1 as the real and R_2 the test intensities in ASD terms of g^2/Hz, and the times as T, the following empirical relationship has been most often used in the past:

$$T_2 = T_1 \times (R_1/R_2)^{2.5}$$

The correctness of the exponent is being reviewed but the method has up to now formed a reasonable approximation for air-carriage acceleration. A typical test for air-carried life will use as the basis for the real intensity the enveloped vibration spectra obtained from the induced spectra monitored in air-carriage *[22]* and then try to arrange for the accelerated load to be inputted such that the levels are distributed in a representative manner across the store. It is not easy to simulate the full service life environment in ground test facilities. Many simplifying assumptions are used in various aspects of testing because of the difficulties, and it is generally necessary to simulate individual parts of the environment separately. For example, when a missile is being vibrated under typical test conditions, it may only be possible to apply some simulated aero-heating and not the acoustic and pressure effects when cross-coupled with the random vibration. Testing and modelling for other aspects such as gun-shock or acoustic energy is also a rather difficult area. Gun pulses result in a deterministic response on the store and they cannot be easily represented in an ASD mode *[23]*. The present limitations of control technology do not allow translations between ASD levels and the monitored acceleration/time functions without separate and specialised conversion. The tests for gun-firing effects are not well established as difficulties exist as to the spectrum to be represented and the test method to be used. Acoustic simulation for representative operational use conditions is another less well defined aspect *[24]*. Moreover, there are few acoustic energy test facilities in the world that will take explosive stores and very little advice on deriving suitable test parameters for whole-life simulations. Additionally, whilst the various tests in the Development and Qualification stages will have provided adequate structural clearance for safety at entry to service, there is a difficulty in applying results from these tests to aged stores. This deficiency is overcome in part at present only by surveillance exercises where missiles that have seen real operational life are selected for critical examination. However, the type of conditions they have experienced are rarely known with any degree of accuracy, leading to wide assumptions as to where damage may have taken place. Overall, the Tactical phase is the most difficult overall to test with any degree of certainty that real life has been simulated either correctly or for a sufficient duration. As it is likely to be the most damaging for a tactical missile then it is clear that more work is needed to determine the conditions and obtain a better understanding of the combined load conditions to be tested in service life assessment programmes.

CONCLUSIONS & RECOMMENDATIONS

34. Extensive work has been carried out in NATO and National programmes over a long time to define the expected climatic conditions and to make available standards that incorporate a good set of definitions of the climatic and induced environments. The specified service life cycle can be translated into general environmental models for use in design analysis and testing tasks in service life programmes. However, it is still necessary to make a number of conservative assumptions because of the limitations of obtaining measured data for all the different elements in the missile's Service life. Often the worst case extremes have to be used in the models and tests as the actual environmental exposure of the munition is not known.

35. The determination, and subsequent feedback, of accurate and reliable data on the climatic and mechanical environment in service is recognised as an increasingly important element in achieving the maximum safe service life for a munition. An accurate record of the condition a motor experiences in its life cycle can enable quantified data to be used rather than extremes. This allows the analyst to set and refine the service life calculations from measured data and the test engineer to set specifications with realistic parameters. Feedback meanwhile enables the models and assumed degradation or damage to be verified *[25]*. In this way a systematic method of providing the required assurance on service life is enabled.

36. Regrettably, the Service users cannot afford to record all the environmental data for periods of storage and use, nor are there systems in place to do so for the operational conditions, and the User has great difficulty in establishing the durations every missile spends in each different condition. Recording of the temperature and humidity for groups of, or even individual, motors in storage and standby conditions is however possible through modern data logging systems. There is as well a great deal of information from Met Office records that can be used to characterise storage and standby sites around the world, as was shown in the post-Gulf war work of the US and UK Services. For operational conditions, the UK is intending to continue the development and use of miniature stress gauges *[26]* to incorporate temperature readout, and such systems may reach fielded status in the next few years.

Nonetheless, the rocket motor lags behind its air-breathing cousin, the aircraft powerplant, which is hooked up to a variety of recording and monitoring systems. Health monitoring is already being used also on other systems; it would be a considerable improvement if one were developed for Service use on a motor.

37. One present deficiency is it is not yet possible to record and take into account the thermo-mechanical loads and the cross coupling effects that arise in the Tactical phase of the life cycle. This leads to an inability to be able to assess the damage that the high levels of input energy can cause, particularly within the operational life elements. As many aspects of the operational environment are difficult to model and test simultaneously, these general difficulties lead to a rather broad and general approach to what is a most damaging part of the Service Life cycle. Moreover, Life cycle testing of the operational elements for a tactical missile is a somewhat crude process due to a general difficulty inherent in using available trials facilities to replicate the complex nature of the environmental elements.

38. The increasing use of microprocessor based data logging systems and fast computers would allow huge amounts of environmental data to be gathered and processed more readily than in the past. With recent advances in modelling and analysis of the effects of the environment on propellants, there is now becoming available a rationale for providing such data. The reason for doing so is an increasing need to more accurately specify the loads for suitable structural analysis of the charge and to set reasonable parameters for service life cycle testing.

39. If such data collection can be applied hand in hand with refined models of rates of degradation and cumulative damage, then the Service User can be given more confident predictions, and even increases, in service life of their motors. This is particularly true where a 'dual inventory' approach has been used as selective parts of the inventory may be extended if they have not experienced the predicted average or extremes of conditions but some lower level. A combination of recording and feedback of environmental data with established ageing and damage models could rapidly provide an improvement which outweighs the cost of implementing such a policy and give enhanced confidence in the safe life of service motors. Certainly, the users would welcome it!

LIST OF FIGURES

1. Example Climatic Conditions.
2. STANAG 2895 Climatic Category A1.
3. Reduced Monitoring
4. Thermally Induced Strain
5. Solar Radiation - Natural and Artificial.

REFERENCES

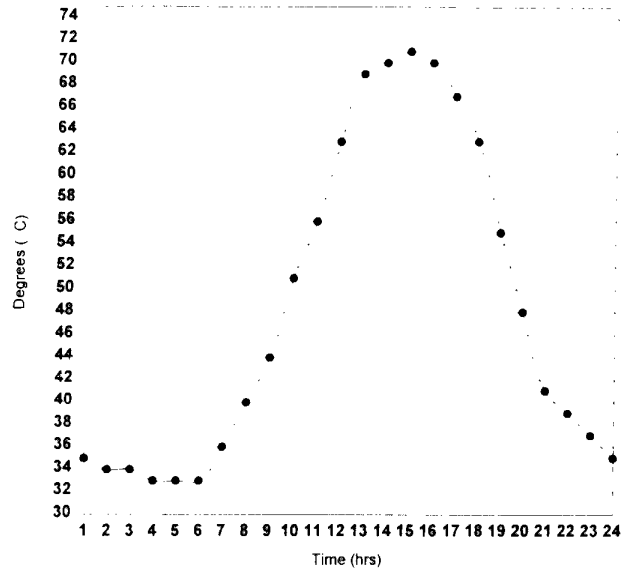
1. AGARD Working Group 25 to report by end of 1996.
2. Marsh, B., "Service Life Analysis ", Paper No 38.
3. Buswell, H.J. & Francis, E.C., "Improvements in Rocket Motor Service Life Prediction", Paper No 27.
4. Faulkner, G.S. & Tod, D.A., "Service Life Prediction Methodologies", Paper No 24.
5. Margetson, J & Wong, F.C.,"Service life Assessment in a Random Thermal Environmental", Paper No 36.
6. Ho, S.K. etal, "Instrumented Service Life Program for the Pictor Rocket Motor", Paper No 28.
7. Egbert, H.W., "International Standardisation of Environmental Testing", Paper No 44 in "Jahrestagung 1989", FICT, (1989).
8. Standardization Agreement (STANAG) 4370, "Environmental Testing of Munitions", NATO, 1992.
9. STANAG 2895, "Extreme Climatic Conditions and derived Conditions for Use in Defining Design/Test Criteria for NATO Forces' Materiel", NATO, 1990.
10. STANAG 2914, "Mechanical Environmental Conditions Affecting NATO Stores and Materiel", NATO, 1990.
11. STANAG 4325, "Standard Environmental & Safety Tests for Air Launched Munitions", NATO, 1991.
12. STANAG 4337, "Surface Launched Munitions, Appraisal, Safety & Environmental Tests", NATO, 1994.
13. Defence Standard 08-5/1, "Design Requirements for Guided Weapon Systems", Ministry of Defence, 1984.
14. Defence Standard 00-35/1, "Environmental Hanbook for Defence Materiel", Ministry of Defence, 1987.
15. Allied Ordnance Publication AOP-15, "Guidance on the Assessment of the Safety & Suitability for Service of Munitions for NATO Armed Forces", NATO, 1985.
16. Margetson, J., "Programme Report - Service life Prediction Application Study", Unpublished Paper for UK Ordnance Board/DRA, 1996.
17. Heller, R.A., Singh, M.P. & Zibdeh, H., "Environmental Effects on Cumulative Damage in Rocket Motors", J.Spacecraft, Vol 22, No 2, pp 149-155, (1985).
18. Barnes, P., Hanning, H.S., & Kidson, D., "UK Experience with Munitions in South West Asia, Part II", Paper at ADPA 3rd Predictive Technology Symposium, 22-24 June 1993.
19. Schafer, H.C. & Murphy, B.J., "Measurement of Missile Thermal Response During Captive Flight at High Altitudes", Report No. NWC TP5365/RAAF TN-ARM-18, NWC China Lake, (1973).
20. Kapp, R., Mathaeur, H. & Rieger, H., "Aerodynamic Heating of Missiles", Paper 10 in AGARD Report 75, (1988).
21. Cottle, L., & Rudman,C., "Principles of UK Life Assessment Testing of Munitions", Paper presented at ADPA 2nd Predictive Technology Symposium, 13-14 November 1991.
22. Dreadin, W.O., "Amraam Vibration Spectrum Definition Using Flight Test Data", in Proceedings 8th JAC Group on Aircraft/Stores Compatibility Study, 23-25 Oct 1990, Fort Walton Beach, Fla, (1990).
23. Brevan, J.P., "Aircraft Gunfire Vibration: Standardisation and Experience", J. Env Sciences, Jul/Aug 1988, pp 15-19, (1988).
24. Sims, D., "Acoustic Simulation of the Flight Vibration Environment", J.Socy of Env Engrs, March 1979, pp 27-29, (1979).
25. Bunyan, P., Cunliffe, A.V., Davis, A, & Tod, D.A., "Input Data for Predictive Models for Lifetimes of Propellants", Paper Presented at ADPA 3rd Predictive Technology Symposium, 22-24 June, 1993.
26. Buswell, H.J. & Chelner, H., "Miniature Sensor for Measuring SRM Case Bond Stress", Paper No 25.

ACKNOWLEDGEMENT

This paper was supported by the UK Ministry of Defence as part of its Research Programme.
The views expressed are those of the author, and do not necessarily represent the policy of the MOD or Her Majesty's Government.
British Crown Copyright 1996/MOD.
Published with the permission of
the Controller of Her Britannic Majesty's Stationery Office.

STANAG Category	GENERAL DESCRIPTION	TYPICAL LOCATIONS	TEMPERATURES °C (Air)	(Surface/Store)	DIURNAL VARIATIONS	HUMIDITY	OTHER CONDITIONS
A - 1	Hot Arid Desert Regions	N & S Africa, Arabia/Iran, C Australia, S USSR	+ 50 hot season - 10 cold season	+ 75	40°C normal, rapid fall in evening.	10 % day, rise at night (2 - 18 g/m^3)	Intense solar radiation, High winds, Sand/Dust storms
A2 - A3 B - 1	Temperate Zones	Extends between 40° - 65° N & S of Equator Europe, SCanada E. America	+ 21 to + 35 max - 14 to - 4 min	+ 50 max	Up to 20°C in evenings	Warmer regions 2- - 40 % day, up to 85 % night (2 - 18 g/m^3)	
B - 3 B - 2	Humid & Semi-Humid Tropical	W, C & E Africa, C America S & SE Asia N Australia	+ 50 B-3 + 40 B-2	+ 70 - 80	Small var'n, 10°C fall in evening	75 - 100 % High at night (15 - 35 g/m^3)	High Rainfall, especially in monsoon season
C - 1 C - 2 C - 3 C - 4	Cold Arctic Extreme Cold - N of 60°N, S of 60°S	Norway, Sweden N Canada, Alaska, N & E USSR	- 20 C-1 - 35 C- 2 - 50 C-3 - 55 C-4	5 ° Colder, winds make more cold	Small Some none	Approaching Saturation (3 - 10 g/m^3)	Ice, Snow, High winds

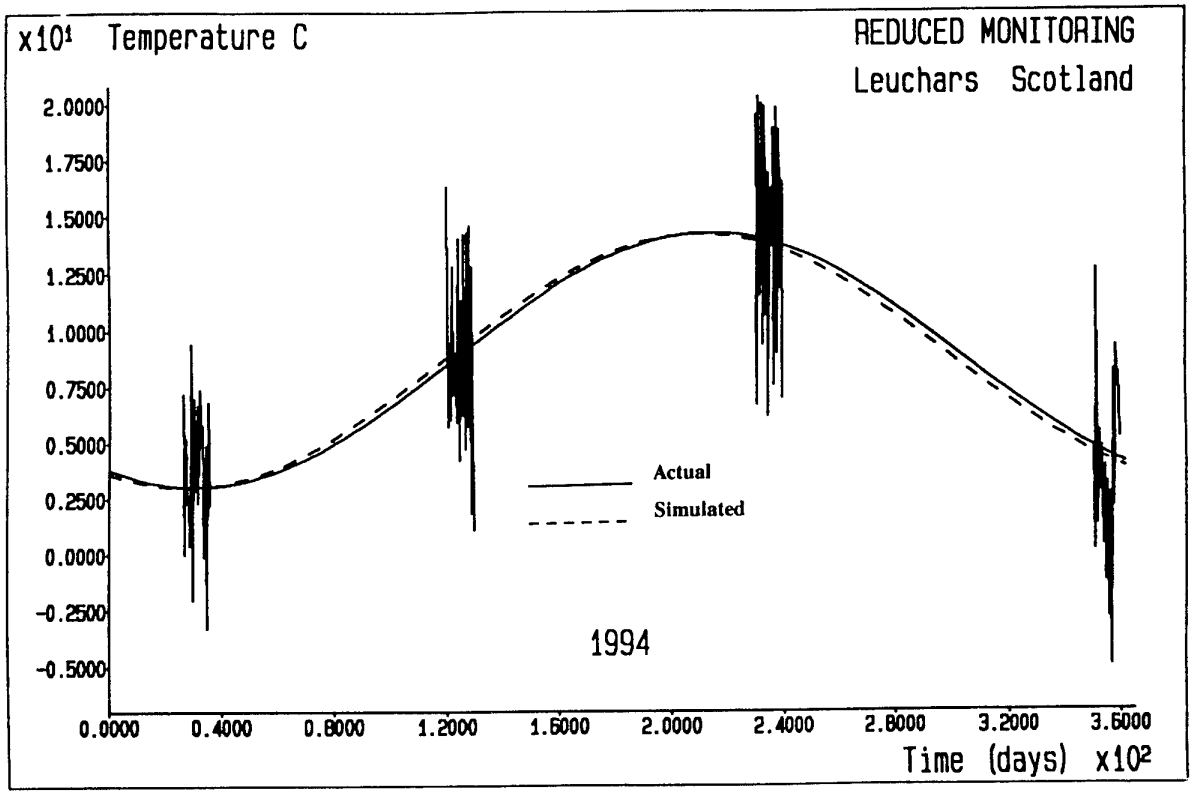
FIGURE 1: EXAMPLE CONDITIONS IN WORLDWIDE CLIMATIC CATEGORIES

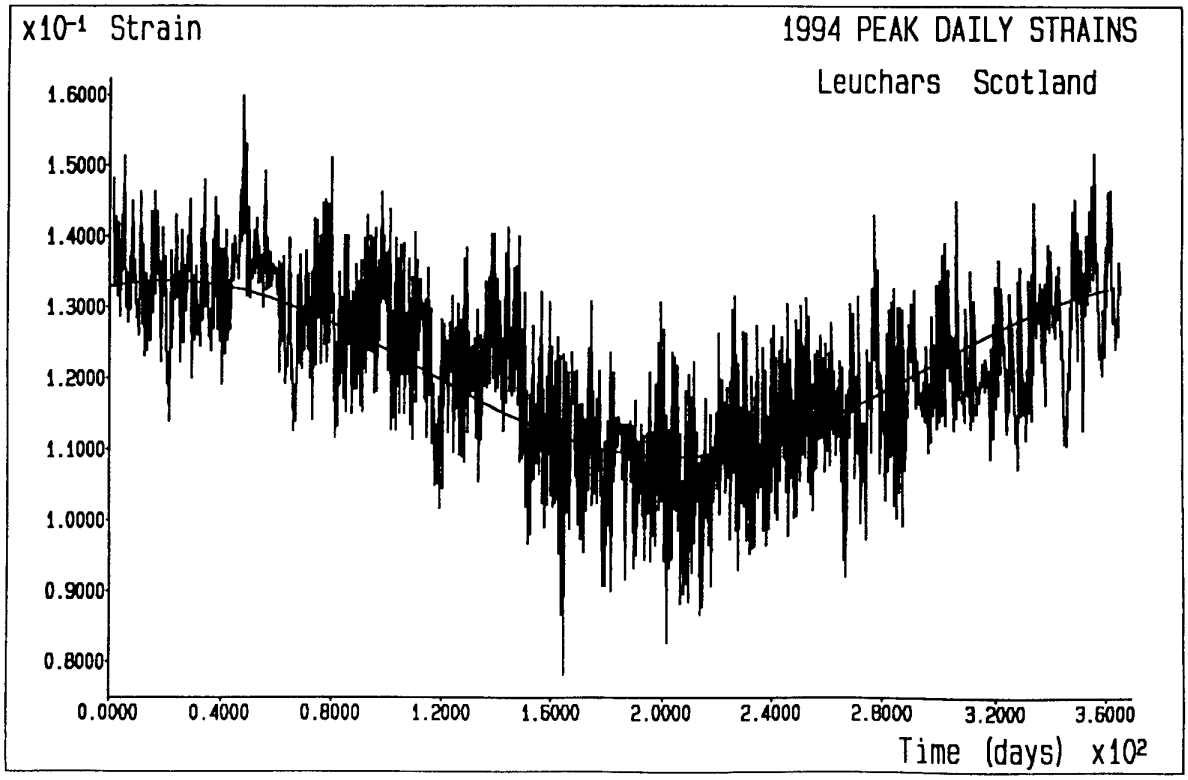


A1 Storage & Transit Temperature

TIME	METEOROLOGICAL			STORAGE & TRANSIT	
	Air Temp °C	Relative Humidity %	Solar Radiation W/m²	Induced Air Temp °C	Relative Humidity %
0000	37	6	0	35	
0300	34	7	0	34	Too
0600	32	8	55	33	
0900	38	6	730	44	Variable
1200	44	4	1120	63	
1500	48	3	915	71	to
1800	48	3	270	63	
2100	41	5	0	41	Quote

FIG 2: STANAG 2895 - CLIMATIC CATEGORY A1





FIGURES 3 & 4: REDUCED MONITORING AND PEAK DAILY STRAINS

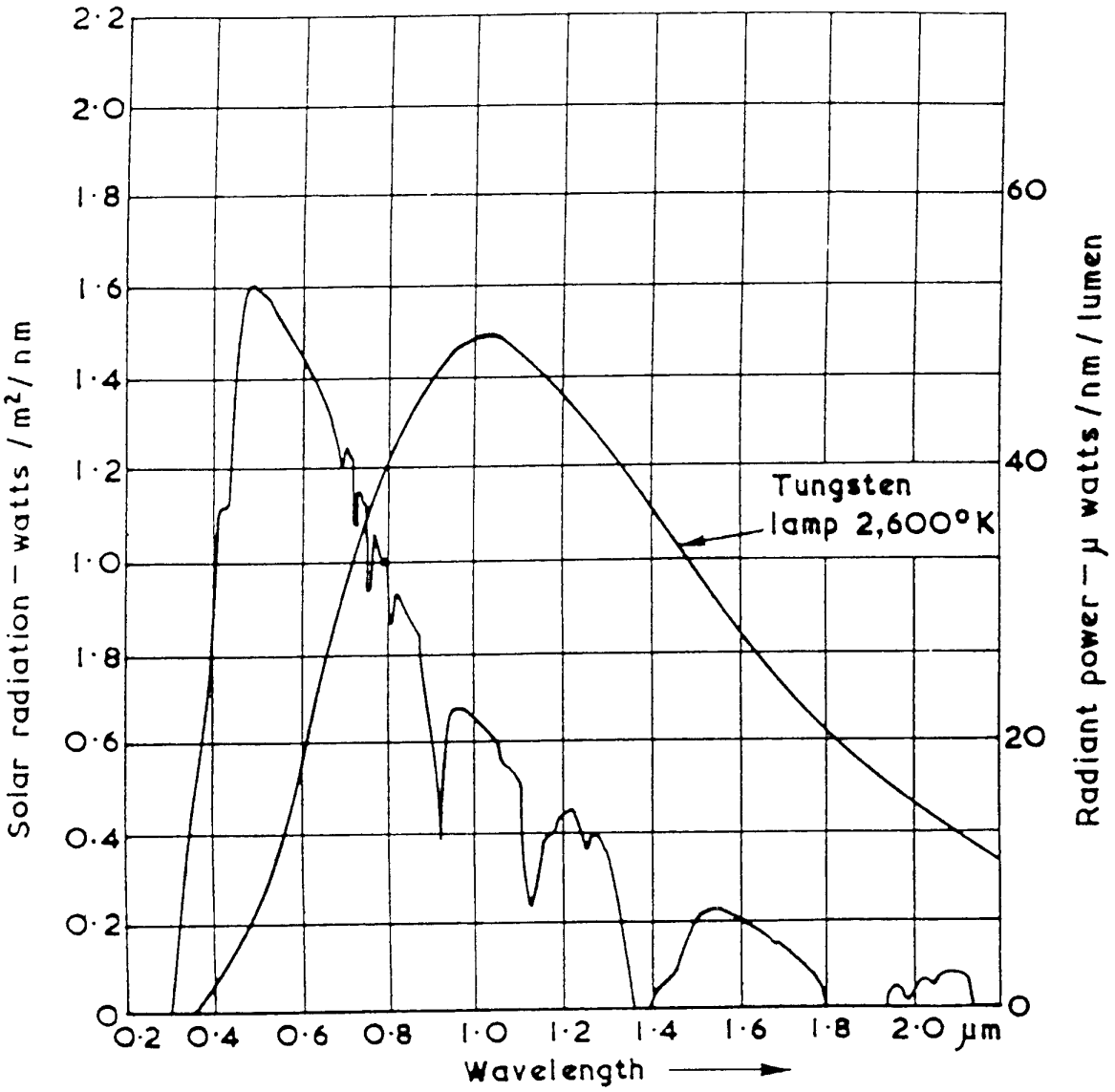


FIGURE 5: SOLAR RADIATION & RADIANT LAMPS

Paper Number: 39
Discussor's Name: C. P. Daykin
Responder's Name: I. H. Maxey

Question: You have highlighted the lack of consideration of air carriage effects on service life in contemporary research, a concern that I share. You state that rocket motors may age 1000 times quicker whilst being subjected to air carriage. A number of rocket motors with a 12 year life have accrued 400 air carriage hours, equivalent to 45 years using the x1000 factor. Should we be concerned about the safety of using or storing such items?

Answer: It is good that you are able to discriminate your stockpile so well, with an operational life policy in place. From your records you should be able to select motors with high age and cumulative damage to determine degradation which has actually taken place. Of course, tactical carriage will have been at different levels with individual sorties containing segments that may range from a damage rate of 100 to 1000 times a benign storage rate. So arbitrary calculation of environment storage time is not so easy. This is where either better records of sortie profiles the missiles see in their individual life cycles or automatic recording such as the planned stress and temperature gages will be of benefit to decide if the motors have reached critical life.

Paper Number: 39
Discussor's Name: L. G. Meyer
Responder's Name: I. H. Maxey

Question: Why is the induced cold temperature lower than the ambient temperature?

Answer: The difference is caused by the temperature of the ground surrounding the ordinance.

EVALUATION DE LA DUREE DE VIE DES MOTEURS TACTIQUES

B. Herran et J.C Nugeyre
CELERG
B.P n° 21
33165. SAINT-MEDARD EN JALLES Cedex
France

RESUME

Deux méthodes sont proposées pour l'évaluation de la durée de vie d'un moteur d'engin tactique :

- la première méthode, dite de vieillissement naturel simulé (V.N.S.), consiste à évaluer les effets du vieillissement sur des moteurs complets en simulant les phases de stockage longue durée et d'utilisation opérationnelle avant de vérifier les caractéristiques et les performances du moteur,

- la seconde méthode s'appuie sur les résultats obtenus à l'issue d'un programme de vieillissement naturel simulé, réalisé sur des maquettes représentatives du moteur considéré, pour calculer une fiabilité en fonction du temps et en déduire une durée de vie.

Cette seconde méthode n'est applicable que si le facteur principal de vieillissement a bien été identifié et si une modélisation de l'influence de ce facteur est envisageable.

SUMMARY

This paper presents two different methods for tactical service life prediction.

In the first approach, called Simulated Natural Aging (S.N.A), the evaluation of aging effects on physical properties and performances of Rocket Motor is performed through specific short time aging programs, simulating long term storage and field conditions.

In the second approach, S.N.A programs are conducted on case bonded Rocket Motors analogs. Dissections provide convenient results used in reliability predictions as a function of aging time. The comparizon with reliability requirements makes possible the Rocket Motor service life prediction.

The second approach can be used if the main aging risk is identified and if the modelisation is possible.

1. INTRODUCTION

Un moteur de missile ou de roquette à ergol solide présente la particularité de ne fonctionner qu'une seule fois et à une date à priori indéterminée ; il n'en reste pas moins que l'utilisateur souhaite le voir fonctionner en toute sécurité et conformément à la prévision, c'est à dire qu'il délivre un certain niveau de poussée pendant un temps donné, et ce, à tout moment de la durée prévue d'utilisation de la munition : il est donc indispensable de se doter d'une méthodologie d'évaluation prévisionnelle de la durée de vie de ces moteurs pour l'appliquer le plus tôt possible avant la mise en service de la munition.

Deux approches sont possibles :

- l'une, essentiellement expérimentale, consiste à évaluer les effets du vieillissement sur des moteurs complets tout en cherchant à réduire le coût et la durée du programme d'évaluation,

- l'autre, plus fiabiliste, vise à déterminer la durée de vie par le calcul de l'évolution d'un coefficient de sécurité à partir de données obtenues sur des maquettes ayant fait l'objet d'un programme de vieillissement.

La seconde méthode paraît bien adaptée aux moteurs à chargements moulés collés à la structure pour lesquels la défaillance majeure, l'éclatement du propulseur, est liée à une rupture mécanique du propergol lors de cycles thermiques, ou lors de la montée en pression à l'allumage : dans ces cas là, une modélisation de la tenue du chargement au cours du temps est réalisable à partir des seules données de propriétés mécaniques obtenues sur des maquettes vieillies représentatives du moteur considéré.

La première méthode sera quant à elle utilisée dans tous les cas de moteurs pour lesquels on ne sait pas bien modéliser les phénomènes mis en jeu, soit faute de données, soit parce que la modélisation est trop complexe et donc incertaine. Elle sera notamment utilisée pour les moteurs à chargements libres qui subissent des contraintes mécaniques pouvant provoquer des évolutions de géométrie dont les conséquences sur le fonctionnement sont difficiles à prévoir. Ajoutons à cela que ces chargements, généralement réalisés avec des propergols double base, sont sujet en vieillissement à des évolutions de nature physico-chimique susceptibles de modifier de façon non négligeable les caractéristiques de balistique interne du moteur (survitesses, affaiblissement des collages, perte de masse.....) : une évaluation de la durée de vie sur objets réels devient alors indispensable.

Paper presented at the AGARD PEP Symposium on "Service Life of Solid Propellant Systems" held in Athens, Greece, 10-14 May 1996, and published in CP-586.

2. EVALUATION DE LA DUREE DE VIE PAR UN PROGRAMME DE VIEILLISSEMENT DE MOTEURS

Trois types de méthode expérimentale d'évaluation de la durée de vie peuvent être envisagés :

• Le vieillissement naturel (V.N.)

Cette méthode consiste à mesurer périodiquement les performances des moteurs en stockage jusqu'à constat d'une dégradation inacceptable des dites performances. Cette façon de procéder est longue et coûteuse et présente l'inconvénient majeur de ne pouvoir prédire une durée de vie avant la mise en série et la mise à disposition des utilisateurs des munitions. Elle n'est donc pratiquement jamais utilisée pour estimer une durée de vie mais plutôt pour assurer une surveillance du stock opérationnel ayant vieilli dans des conditions parfois mal définies. Elle présente cependant l'avantage pour le concepteur de pouvoir comparer les résultats de sa prévision à la réalité, à condition bien sûr qu'il ait pu prendre connaissance de ces résultats. Ce contrôle périodique des performances s'accompagne d'expertises qui présentent un grand intérêt pour le concepteur qui, généralement, y participe activement.

• Le vieillissement accéléré isotherme (V.A.I.)

Dans ce cas, on suppose vérifiée une équivalence temps/température et on estime une durée de vie à partir de données acquises sur des durées courtes en faisant vieillir le matériel à 50°C ou 60°C. Cette méthode, largement utilisée dans le passé, est jugée aujourd'hui peu représentative du vieillissement naturel parce qu'elle ne prend notamment pas en compte les effets des cycles thermiques subis par les munitions. Elle n'est plus utilisée aujourd'hui que pendant la phase de développement pour valider le choix des matériaux constitutifs du moteur en vérifiant leur aptitude au vieillissement ainsi que celui des assemblages par collage et ce dans une configuration plus réaliste que les essais réalisés en amont, sur éprouvettes, à l'échelle du laboratoire.

• Le vieillissement naturel simulé (V.N.S.)

La méthode empirique de prédiction de durée de vie décrite ci-après est le résultat du constat des insuffisances des méthodes consistant soit à observer de manière attentiste la lente dégradation des performances au cours du temps sans pouvoir prédire de durée de vie (V.N.), soit à tirer des conclusions hâtives après quelques mois de vieillissement accéléré isotherme (V.A.I.) en affichant une durée de vie qui sera bien souvent mise en défaut par insuffisance de représentativité.

2.1 Données nécessaires à l'élaboration d'un programme de vieillissement naturel simulé (V.N.S.)

La méthode de prédiction de durée de vie par vieillissement naturel simulé (V.N.S.) nécessite une bonne connaissance :
- des conditions réelles d'environnement thermique et mécanique des munitions de façon à bâtir un programme de vieillissement aussi représentatif que possible,
- des vitesses de réaction des mécanismes de vieillissement les plus importants de façon à réduire la durée du programme en utilisant une loi d'équivalence temps/température.

Il est aussi bien sûr extrêmement souhaitable d'avoir préalablement validé la méthode par comparaison des résultats obtenus en V.N. et en V.N.S. pour un type de moteur donné (moteur à chargement libre en propergol homogène ou moteur à chargement moulé-collé en propergol composite par exemple).

Les données relatives aux conditions réelles de vieillissement et aux mécanismes de dégradation ayant été rassemblées, il est alors possible d'établir le programme pour lequel on distinguera deux phases : le stockage longue durée et l'utilisation opérationnelle des munitions.

2.2 Simulation du stockage longue durée

La phase de stockage longue durée est simulée par une succession de cycles thermiques représentatifs chacun d'une année. Il convient au préalable de préciser :
- le climat de stockage, en se référant par exemple aux zones climatiques du STANAG 2895,
- la durée du stockage, pour déterminer le nombre de cycles à appliquer.

On considérera pour ce qui suit que les munitions sont stockées à l'abri de l'influence du flux solaire et que les températures retenues pour établir les cycles thermiques sont les températures de l'air ambiant.

Le cycle thermique simulant une année de stockage sous un climat donné est défini selon les principes suivants :
- choix des températures maximale, minimale et intermédiaire du cycle ; par souci de simplification, la température intermédiaire retenue sera de 20°C,
- succession de paliers aux trois températures simulant les variations saisonnières du climat considéré,
- contraction du temps par augmentation de la durée de maintien à la température maximale ; pour ce faire, on utilise l'équivalence temps/température de la loi d'Arrhénius qui décrit la sensibilité à la température du mécanisme de vieillissement le plus significatif (par exemple, oxydation des polymères, consommation de stabilisant ou migration de certaines espèces),
- les durées de maintien aux températures intermédiaire et minimale seront, en règle générale, limitées au temps juste nécessaire pour la mise en équilibre de l'ensemble du propulseur à la température considérée.

Des exemples de cycles thermiques sont présentés sur les figures 1 et 2 pour un moteur de taille limitée et une énergie d'activation de la loi d'Arrhénius de l'ordre de 60 kJ/mole. Sont considérées comme négligeables les variations de température diurne/nocturne compte tenu de ce qu'elles sont :
- toujours inférieures ou égales à 20°C à l'abri de l'influence du flux solaire, et ce quel que soit le climat considéré,
- amorties par la structure d'enceinte du lieu de stockage et par l'emballage des munitions

2.3 Simulation de la phase d'utilisation opérationnelle

Sont pris en compte pour la simulation de cette phase :
- les chocs et vibrations dues aux manutentions et au transport,
- les variations de température induites par les emports aériens (le cas échéant) et le stockage de courte durée sous abri léger ou sous flux solaire direct.

La définition de ces épreuves a généralement été faite pendant le développement du moteur et on se contentera alors de les reprendre in extenso pour la simulation de cette phase qui sera réalisée sur des moteurs en configuration opérationnelle, soit des munitions nues, soit en emballage dit "tactique".

Un exemple de cycle thermique représentant un stockage sous abri léger de courte durée est présenté sur la figure 3.

2.4 Simulation combinée des phases de stockage et d'utilisation opérationnelle

Pour certaines applications (ex. : missile air/air), les phases de stockage alternent presque toujours avec des missions opérationnelles ; une année de vieillissement pourra alors être simulée comme indiqué sur la figure 4 avec :
- un cycle thermique représentant une année de stockage dont une partie en climat chaud et l'autre en climat froid (A2 + C1),
- un choc thermique, avec 2°C/mn, simulant une mission.

2.5 Principes d'établissement du programme de vieillissement naturel simulé

• Les essais réalisés sur moteurs pendant la durée du programme de vieillissement naturel simulé seront les suivants :
- contrôle non destructif par endoscopie et examen aux rayons X (ou au tomographe) pendant les passages à 20°C des cycles thermiques,
- expertise physico-chimique complète du moteur (propergol, matériaux d'aménagement interne, allumeur....),
- tirs à différentes températures.

• Ces essais seront répartis dans le temps de manière à apprécier avec suffisamment de précision l'évolution des caractéristiques et des performances du moteur en vieillissement : ainsi, pour un programme d'une durée simulée visée de 15 ans, les tirs et expertises pourront être effectués à to et après 8, 12, 15 et 18 ans de vieillissement simulé. Les dates d'essais seront choisies en fonction de l'objectif fixé de durée de vie et des connaissances acquises sur le vieillissement de moteurs de conception voisine.

• La durée totale du vieillissement simulé sera supérieure à celle de l'objectif de durée de vie de façon à évaluer la marge disponible et à prendre en compte l'imprécision relative de la méthode due notamment au fait qu'on ne teste qu'un faible nombre de moteurs tous issus d'un lot unique.

• Quelques moteurs supplémentaires seront mis en vieillissement simulé pour constituer une réserve et pouvoir être testés à tout moment du programme en cas de difficulté particulière d'interprétation des résultats obtenus avec les autres moteurs affectés aux différents essais prévus dans le programme.

• Enfin, les phases de simulation du stockage et de l'utilisation opérationnelle devront être réparties dans le temps conformément au profil de vie "type" de la munition.

Un exemple de programme de vieillissement naturel simulé, dans lequel le stockage longue durée n'est pas interrompu par les phases d'utilisation opérationnelle, est présenté sur la figure 5. Sur cet exemple, la durée de vieillissement simulé est de 18 ans pour un objectif de durée de vie de 15 ans minimum : on montre que la simulation est réalisée sur une durée réelle de 3 ans avec une quinzaine de moteurs qui seraient testés à 8, 12, 15 et 18 ans simulés.

Il est également envisageable de réaliser un programme de V.N.S. sur des propulseurs vieillis naturellement pour déterminer quelle extension de durée de vie paraît possible.

Concernant l'utilisation de cette méthode, il convient pour finir d'indiquer qu'un tel type de programme a déjà été réalisé sur des moteurs actuellement en série, mais la comparaison avec les résultats de vieillissement naturel, et donc la validation de la méthode, n'a pu être effectuée à ce jour : les tirs et expertises de moteurs vieillis naturellement devraient cependant être réalisés dans les toutes prochaines années.

3. DETERMINATION DE LA DUREE DE VIE D'UN PROPULSEUR DE MISSILE TACTIQUE PAR UNE APPROCHE FIABILISTE

3.1 Introduction

La fiabilité, associée à un niveau de confiance, d'un moteur tactique est sa probabilité de bon fonctionnement ou capabilité instantanée. Celle-ci doit être assurée au niveau spécifié pendant toute la durée de vie du système d'arme, constituée de stockages et de transports pendant lesquels les moteurs subissent des sollicitations thermiques et mécaniques, puis le tir.

La principale défaillance vis à vis de la sécurité d'un moteur à propergol solide est liée à la tenue mécanique du chargement. La rupture du propergol, ou des liaisons aux collages, se traduit par une augmentation de la surface de combustion et donc de la pression de fonctionnement, conduisant le plus souvent à l'éclatement du propulseur.

Le problème consiste à évaluer, avec un modèle approprié, l'évolution de la tenue mécanique et la fiabilité associée du chargement pendant la vie du moteur. La comparaison des valeurs obtenues aux valeurs spécifiées permettra alors une estimation de la durée de vie du moteur.

3.2 Méthodes d'analyse (1)

Le problème à résoudre en mécanique est l'évaluation du risque d'apparition d'une rupture dans le propergol, pour les sollicitations mécaniques les plus pénalisantes subies par le chargement.

La méthode consiste à déterminer deux grandeurs caractéristiques :

- **la capacité du propergol (C)**
- **la sollicitation maximum (S)**

♦ La **sollicitation (S)** maximum au **point critique** du chargement est une grandeur (contrainte ou déformation) fonction du champ de contraintes et de déformations, en général tridimensionnel, existant en ce point.
La position du **point critique** et le **niveau de sollicitation** sont déterminés par des méthodes numériques de calcul par éléments finis. Un critère approprié, Von-Misès ou Stassi, permet de passer d'une grandeur tridimensionnelle à une grandeur uniaxiale équivalente.

♦ La **capacité (C)** est la charge mécanique à laquelle il faut soumettre le propergol pour qu'il y ait rupture. Cette grandeur est déterminée par traction d'éprouvettes uniaxiales pour des valeurs variables de température, de vitesse de traction et de pression.
Les éprouvettes à tractionner sont prélevées sur un moteur disséqué, ou une maquette, ou un bloc de contrôle, représentatifs des propriétés mécaniques du propergol du moteur. Le résultat est présenté sous la forme de courbes maîtresses (figure 6). La capacité mécanique du chargement est déterminée par la lecture, sur ces graphes, des valeurs des contraintes et allongements au temps réduits de l'épreuve (tir, choc thermique.....).

♦ Le **coefficient de sécurité** en mécanique est défini par le rapport : **K = C/S**.

Si K > 1 il n'y a pas de rupture
Si K ≤ 1 il y a rupture

♦ Les valeurs de **Capacité** et **Sollicitation** ne sont pas des grandeurs exactes et on admet que ce sont des variables aléatoires de distribution gaussienne (2). La **fiabilité mécanique** peut alors s'exprimer comme étant la **probabilité** pour que :

- le **coefficient de sécurité K = C/S soit supérieur à 1** ou
- la **capacité soit supérieure à la sollicitation C > S** ou
- la **marge de sécurité M = C-S soit supérieure à 0**

Ce qui s'exprime par :

F = Prob (K > 1) ou Prob (C > S) ou Prob (M > 0)

M = C-S étant une variable gaussienne (figure 7) avec :

moyenne $\bar{M} = (\bar{C} - \bar{S})$

écart type $\sigma M = \sqrt{\sigma c^2 + \sigma s^2}$

En introduisant la variable centrée réduite de M (figure 8) :

$u = (M-\bar{M}) / \sigma M = [(C-S)-(\bar{C}-\bar{S})] / \sqrt{\sigma c^2 + \sigma s^2}$

On peut écrire qu'à la rupture :

$C = S \Rightarrow M = 0 \Rightarrow u = u0 = -(C-S) / \sqrt{\sigma c^2 + \sigma s^2}$,

ce qui entraîne :

défiabilité = Prob $(S \geq C) = \Phi(u\,0) = \dfrac{1}{\sqrt{2\pi}} \displaystyle\int_{-\infty}^{uo} e^{-\frac{t^2}{2}} dt$

fiabilité = Prob $(C > S) = 1 - \Phi(u0) = \Phi(u0^+)$

avec $\Phi(u0^+) = \dfrac{1}{\sqrt{2\pi}} \displaystyle\int_{-\infty}^{uo+} e^{-\frac{t^2}{2}} dt$

et

$u0^+ = (\bar{C}-\bar{S}) / \sqrt{\sigma c^2 + \sigma s^2} = (\bar{K} - 1)\sqrt{\bar{K} Cvc^2 + Cvs^2}$

L'utilisation de tables statistiques permet de déterminer facilement $\Phi(u0^+)$ en connaissant les coefficients de variation sur la capacité et sur la sollicitation définis par les valeurs suivantes :

$Cvc = \sigma c/\bar{C}$ $\quad Cvs = \sigma s/\bar{S}$ $\quad$ et $\bar{K} = \bar{C}/\bar{S}$

pour un taux de confiance de 60 %

Si $\bar{K} = 1$ à la rupture, $u0^+ = 0$ $\Rightarrow$ $\Phi(u0^+) = 0,5$
il y a une chance sur deux de rupture

Ce type d'analyse convient pour l'étude des moteurs à chargements moulés-collés pour lesquels l'analyse mécanique peut être simple. Le comportement des chargements libres est beaucoup plus complexe à analyser pour les états transitoires dimensionnant : à l'allumage, en cycles thermiques et en environnements mécaniques. On préfère pour ce type de moteur, réaliser des analyses de type AMDEC ou les programmes de vieillissement décrits paragraphe 2.5.

3.3 Application à un moteur de missile tactique de type air-air

3.3-1 Description du moteur et de sa vie

Le moteur étudié figure n° 9 possède une structure métallique en maraging et un chargement moulé-collé en propergol butalane faiblement aluminisé, de forme finocyle. Cette architecture supprime les problèmes liés aux calages, aux évolutions de géomètrie en cyclages thermiques et vieillissement et la plupart des problèmes liés aux environnements mécaniques, vibrations, chocs, accélération.... Un calcul préalable a permis de déterminer que le cas de charge le plus dimensionnant pour le moteur considéré était le **tir à - 45°C**.

La fiabilité mécanique requise est F = 0,999 pour toute la durée de vie du moteur : 15 ans requis, 20 ans souhaités.

La vie de la munition est constituée de phases de stockage longue durée et d'utilisation opérationnelle incluant des missions d'emport. Ce type de vie a été décrit au paragraphe 2.5 ainsi que la méthode permettant de simuler, sur une durée réduite de deux mois, un an de vie, à l'aide de cycles et de chocs thermiques décrits figure n° 4.

3.3-2 Détermination de la fiabilité avant et après vieillissement

3.3-2.1 Capacité du propergol avant vieillissement

Les propriétés mécaniques du propergol du moteur ont été établies par traction d'éprouvettes JANAF prélevées sur le moteur, sur des blocs de contrôle et sur une maquette représentative du point de vue mécanique du moteur et définie figure n° 10.

Il a été montré que les propriétés mécaniques de ces trois objets étaient identiques et que l'on pouvait, dans ces conditions, utiliser, d'une part, les blocs de contrôle pour suivre les propriétés mécaniques au cours des fabrications et, d'autre part, les maquettes de coût réduit pour connaître l'évolution des propriétés mécaniques en vieillissement du moteur.

On trouve, figure n° 6, les courbes maîtresses du propergol obtenues sur les trois types d'objets, hors vieillissement.

3.3-2.2 Capacité du propergol après vieillissement

Plusieurs maquettes ont subi les cycles et chocs thermiques définis figure n° 4, paragraphe 2.5, pendant des durées de 1 et 2 ans simulant les durées de vie de 6 ans et 12 ans du système d'arme. Une maquette, dont le canal a été maintenu sous atmosphère d'azote, a subi 2 ans de vieillissement pour évaluer l'intérêt d'un stockage sous gaz inerte. Après ces épreuves, les maquettes ont été disséquées pour mesures des propriétés mécaniques.

On trouve figure n° 11, les courbes maîtresses du propergol obtenues après épreuves de vieillissement.

3.3-2.3 Calcul des sollicitations au tir à - 45°C

Pression d'allumage	10,4 Mpa
Temps d'allumage	12 ms
Déformation structure vide	0,027 %/Mpa

Un calcul par éléments finis a permis de déterminer :
- que le point critique était en pied d'ailette du chargement (figure n° 9)
- que les valeurs des sollicitations au tir étaient :

$\sigma 0$ = 4,3 Mpa hors vieillissement
$\sigma 6$ = 5,35 Mpa après vieillissement simulé 6 ans
$\sigma 12$ = 6,1 Mpa après vieillissement simulé 12 ans
$\sigma 12$ = 5,2 Mpa après vieillissement simulé 12 ans sous azote

3.3-2.4 Calcul des coefficients de sécurité au tir à - 45°C

Le temps réduit pour le tir à - 45°C du moteur est de 10^{-8} mn en utilisant le facteur d'équivalence temps-température de at = $10^{4,4}$ mn pour ce propergol. Les valeurs de la capacité (Sm) lues sur les courbes maîtresses, en tenant compte d'une amélioration due à la pression de 1,45 (validé par des tirs durcis ayant entrainé la rupture du propergol), sont :

Sm = 8,85 Mpa hors vieillissement
Sm = 9,4 Mpa après vieillissement simulé 6 ans
Sm = 9,9 Mpa après vieillissement simulé 12 ans
Sm = 9,4 Mpa après vieillissement simulé 12 ans sous azote

Les coefficients de sécurité au tir à - 45°C, $K = Sm/\sigma 0$, sont alors :

K0 = 2,04
K6 = 1,76
K12 = 1,62
K12 = 1,8 pour un stockage sous azote

L'évolution de ces coefficients est reportée sur le graphique figure n° 12.

3.3-2.5 Calcul de la fiabilité au tir à - 45°C

Les travaux menés au cours du développement ont permis d'évaluer les variabilités sur les propriétés mécaniques (capacité Sm mesurée sur différentes coulées) et sur les sollicitations (déformations de la structure et pression d'allumage).

Les valeurs obtenues pour les coefficients de variation sont les suivantes :

Cvc = 11,5 %

Cvc = coefficient de variation de capacité sur le Sm

Cvs = 3,5 % $\qquad Cvs = \sqrt{Cv^2st + Cv^2Pall}$

Cvs = coefficient de variation de sollicitation (st : déformation de la structure, Pall : pression allumage)

Le nombre de maquettes vieillies n'a pas permis d'établir des variabilités après vieillissement. On a considéré ces valeurs comme constantes alors que des évolutions sont probables : par exemple, les dispersions sur la pression d'allumage, liées à la vitesse de combustion, peuvent évoluer avec les migrations du catalyseur balistique ou du plastifiant.

Ces valeurs et les coefficients de sécurité obtenus permettent, en utilisant la méthode décrite au paragraphe 3.2, d'obtenir les valeurs suivantes de fiabilité associées à un taux de confiance de 60 % :

F0 = 0,999994
F6 = 0,9999
F12 = 0,9995
F12 = 0,99993 sous azote

Ces valeurs ont été reportées sur le graphique 13 et extrapolées pour les durées supérieures à 12 ans.

La comparaison avec la valeur spécifiée de 0,999 permet alors d'estimer la durée de vie de ce moteur à 15 ans.

Un stockage sous azote permettrait de porter cette valeur au delà de 20 ans.

3.3-2.6 **Observations et limites de la méthode**

La démarche que nous avons proposée ici nécessite une validation expérimentale qui peut être réalisée à l'aide de tirs durcis et expertises de moteurs en retour de dotation.

Elle s'appuie sur l'étude du point critique du chargement mais ne prend pas en compte la totalité des éléments du moteur (allumeur, protection thermique....) pouvant générer des défaillances. D'autre part, elle ne traite pas de fiabilité balistique et serait difficilement applicable aux chargements libres. Cette méthode permet cependant d'avoir, avant la fin du développement et à l'aide d'un programme de coût réduit, une idée précise du vieillissement du propergol retenu et de la durée de vie du moteur.

4 CONCLUSION

Ce document a proposé deux types de méthodes d'évaluation de durée de vie :
- la réalisation de programmes de vieillissement sur moteurs,
- une évaluation basée sur l'évolution de la fiabilité mécanique.

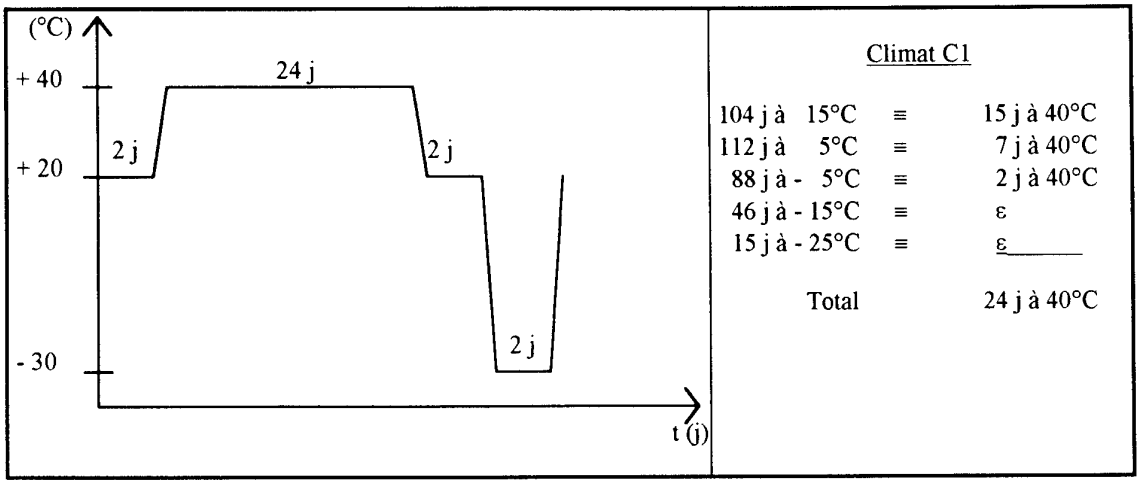
La première méthode est bien adaptée à tous les types de moteurs mais elle reste relativement coûteuse et ne peut être appliquée qu'à la fin du développement. La validation des cycles appliqués reste à faire à l'aide de programmes en cours de réalisation et de matériels en retour de dotation.

La deuxième méthode, plus simple, convient aux moteurs à chargements moulé-collés. Moins coûteuse, elle est basée sur l'application de cycles thermiques simplifiés sur maquettes dont la représentativité doit être validée. Elle peut être étendue à l'étude de la fiabilité balistique et elle permet d'avoir une bonne évaluation de la durée de vie prévisionnelle d'un moteur sans prétendre donner une réponse apportant toutes les garanties nécessaires, parce que, d'une part, la vie réelle des munitions n'est pas toujours conforme au profil de vie pris en compte au départ, et parce que, d'autre part, elle n'est appliquée qu'à l'élément du moteur jugé le plus critique, et qu'elle est basée sur une méthode d'analyse mécanique, certe éprouvée et permettant d'étudier la plupart des cas, mais aujourd'hui en cours d'amélioration.

BIBLIOGRAPHIE

(1) Technologie des propergols solides - A DAVENAS et collaborateurs

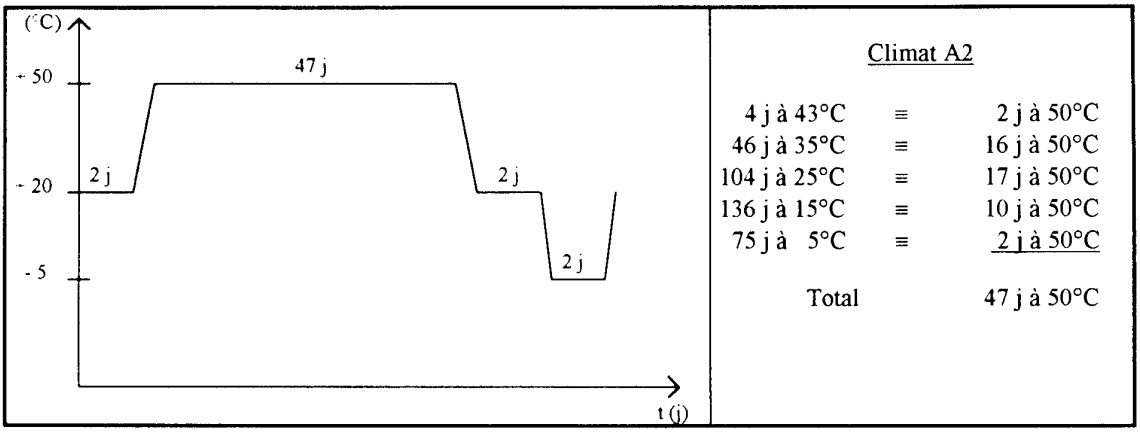
(2) European Safety and Reliability Conference 92.
RISO COPENHAGEN
10/12 JUNE 1992
Relation between capability and reliability -
GOLIGER - NAHON - PARADIS



Climat C1

104 j à 15°C	≡	15 j à 40°C
112 j à 5°C	≡	7 j à 40°C
88 j à - 5°C	≡	2 j à 40°C
46 j à - 15°C	≡	ε
15 j à - 25°C	≡	ε
Total		24 j à 40°C

Figure 1 - **Simulation d'une année de stockage - Climat C1**



Climat A2

4 j à 43°C	≡	2 j à 50°C
46 j à 35°C	≡	16 j à 50°C
104 j à 25°C	≡	17 j à 50°C
136 j à 15°C	≡	10 j à 50°C
75 j à 5°C	≡	2 j à 50°C
Total		47 j à 50°C

Figure 2 - **Simulation d'une année de stockage - Climat A 2**

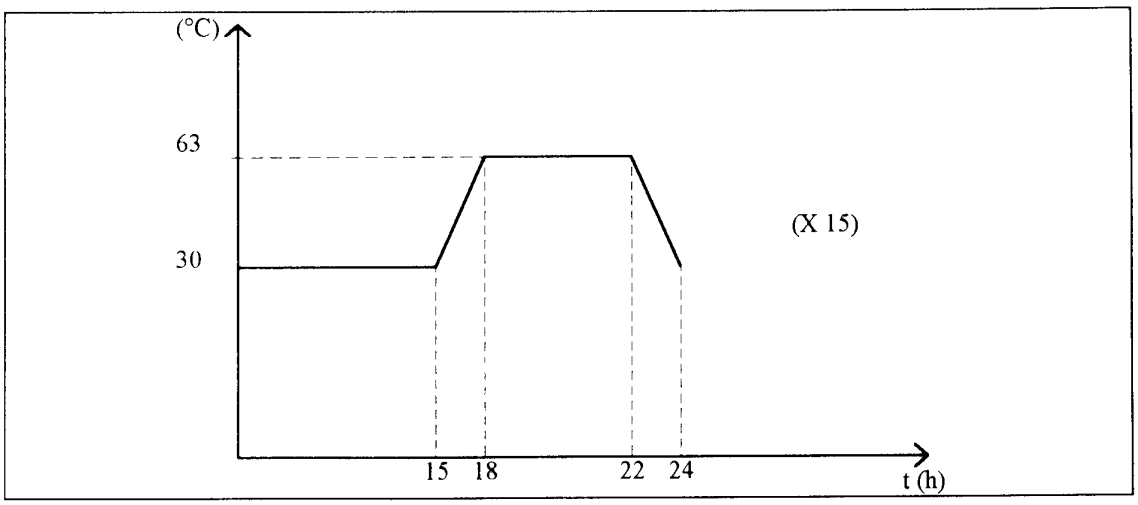


Figure 3 - **Cycles thermiques de la phase d'utilisation opérationnelle Climat A 2 - Propulseur de missile anti-char**

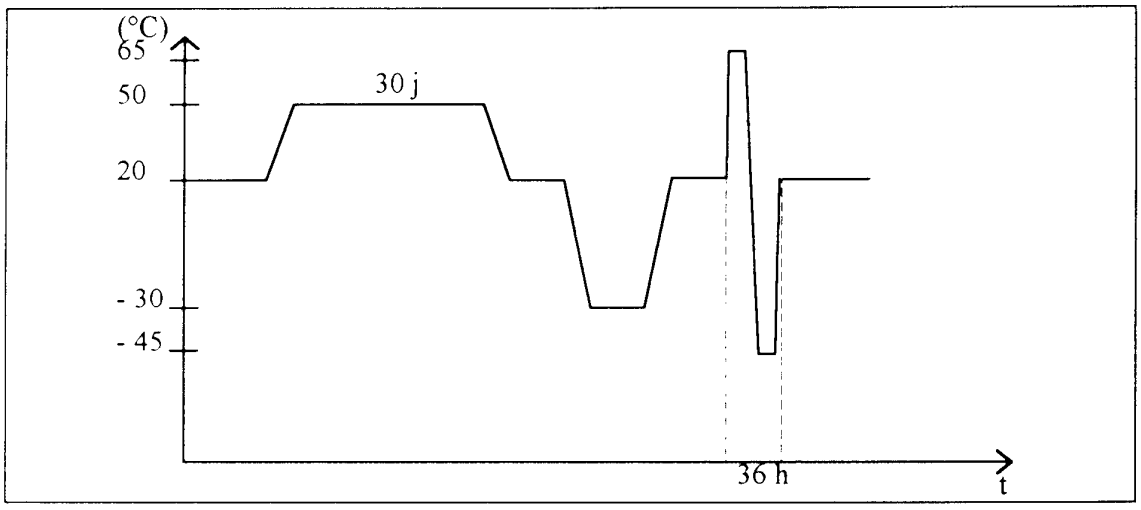


Figure 4 - **Simulation d'une année de vieillissement - Climat "A2 + C1"**
Moteur de missile air/air avec chargement moulé-collé en propergol composite
Eact ≃ 60 kJ/mole (oxydation du PBHT)

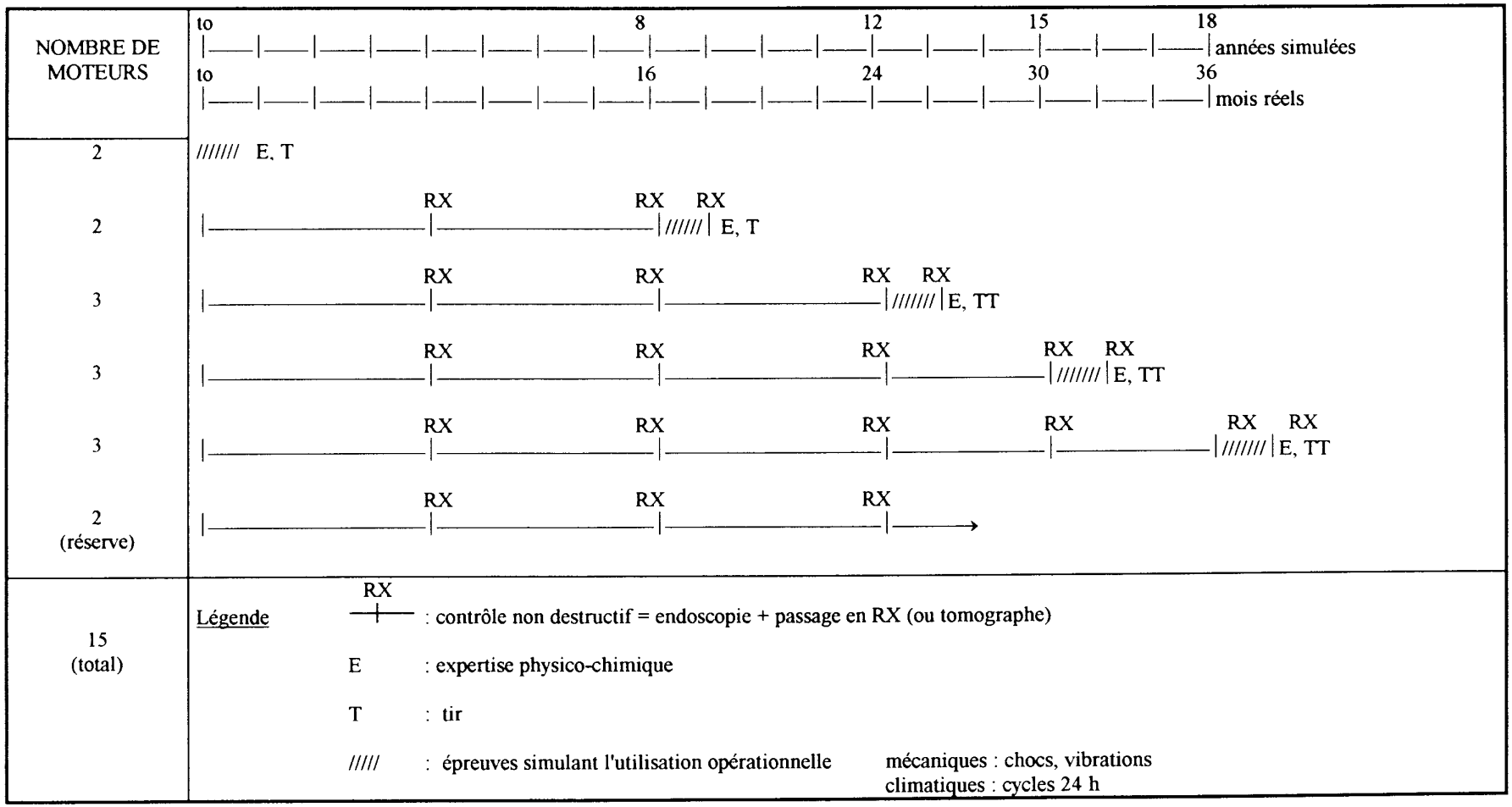
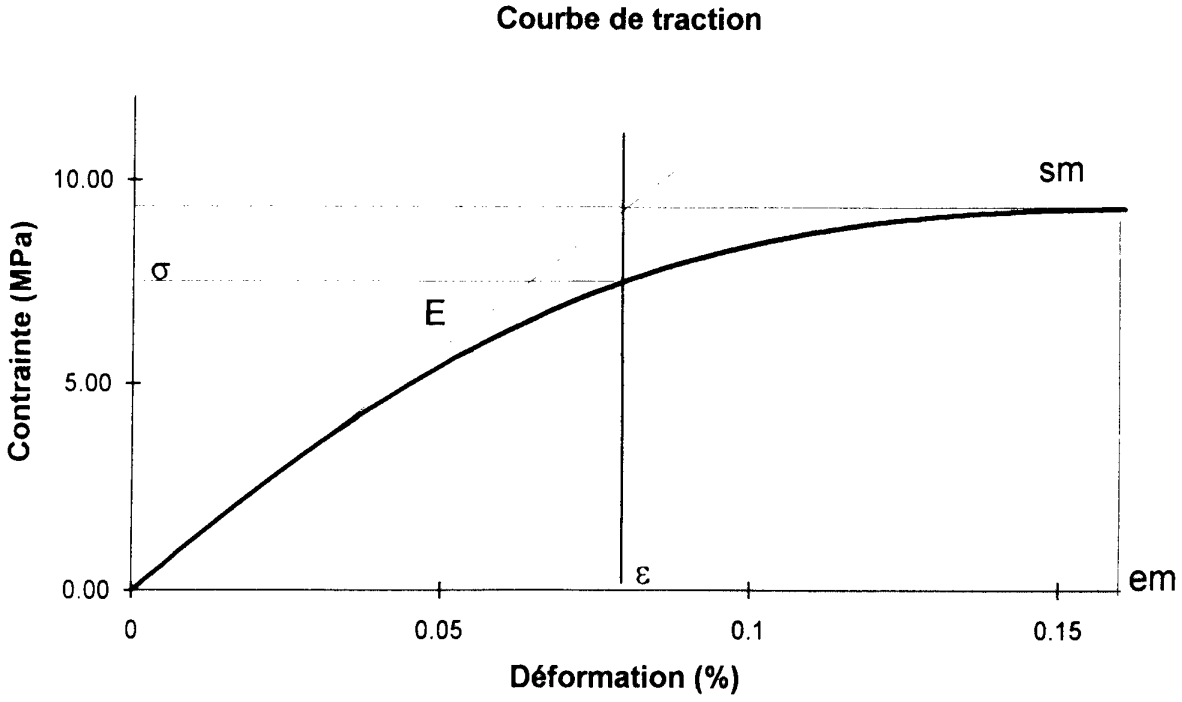
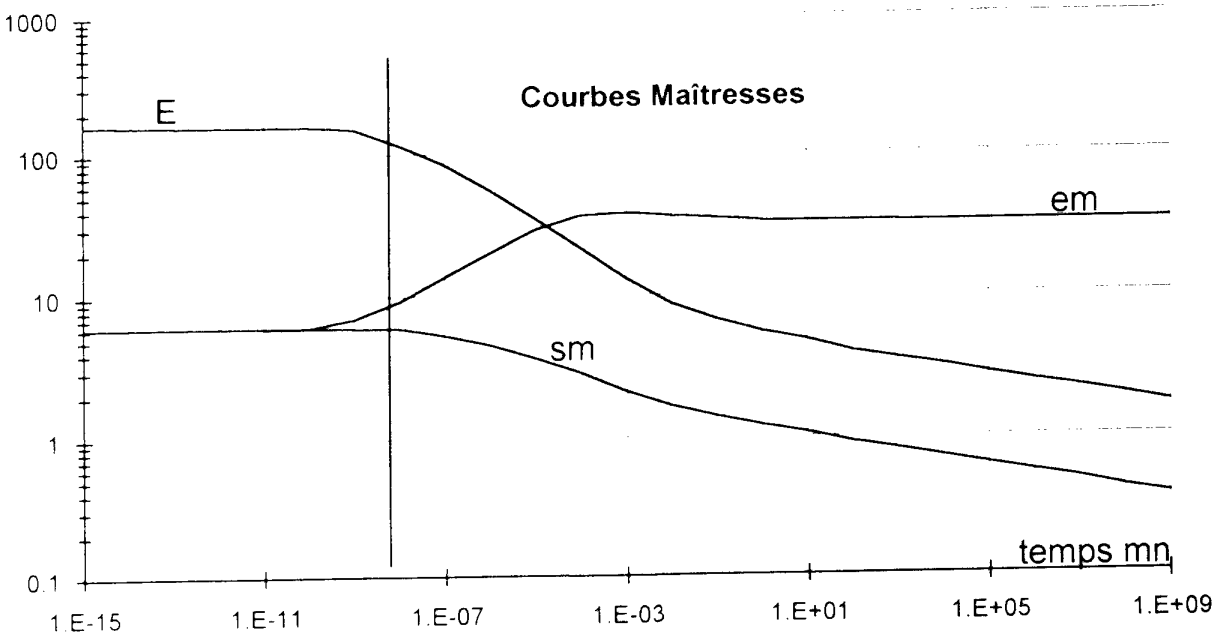


Figure 5 - **Exemple de programme de vieillissement naturel simulé**





Figures 6 - **Courbes maîtresses de propriétés mécaniques**

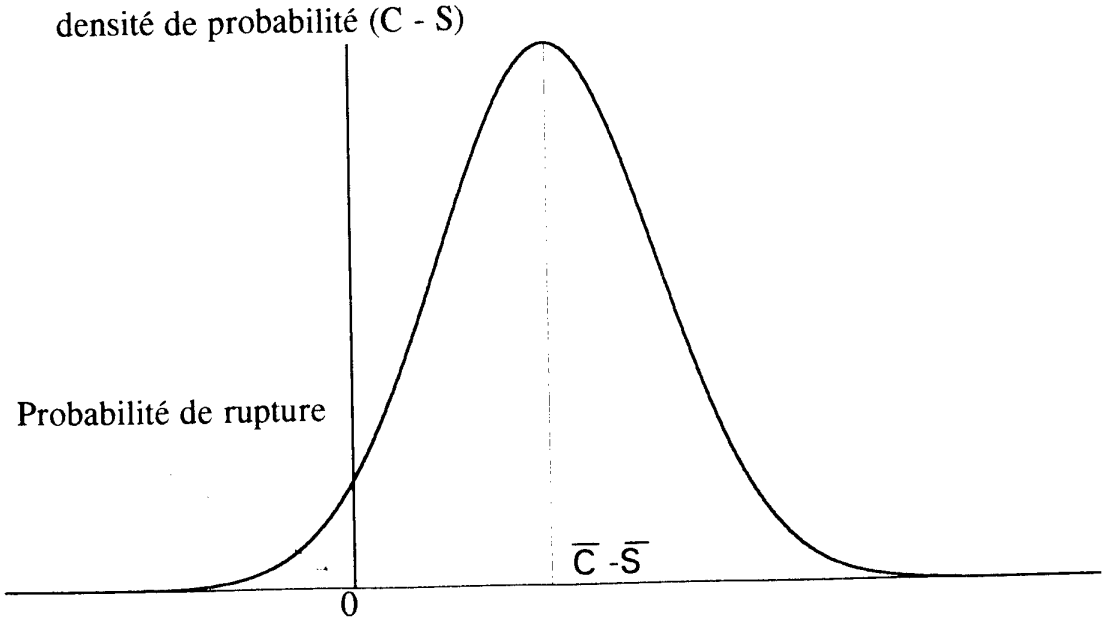


Figure 7 - **Distribution de la variable C-S**

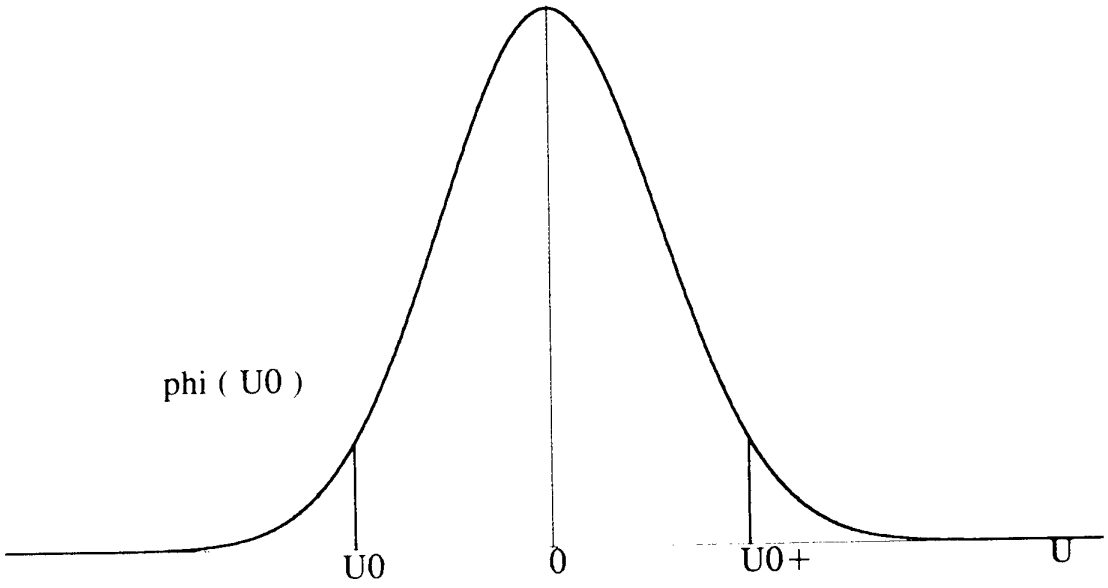


Figure 8 - **Variable centrée réduite de C-S**

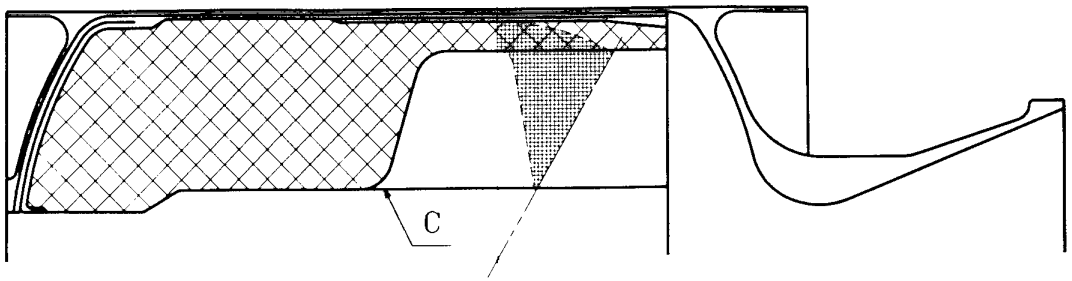


Figure 9 - **Schéma du moteur étudié**

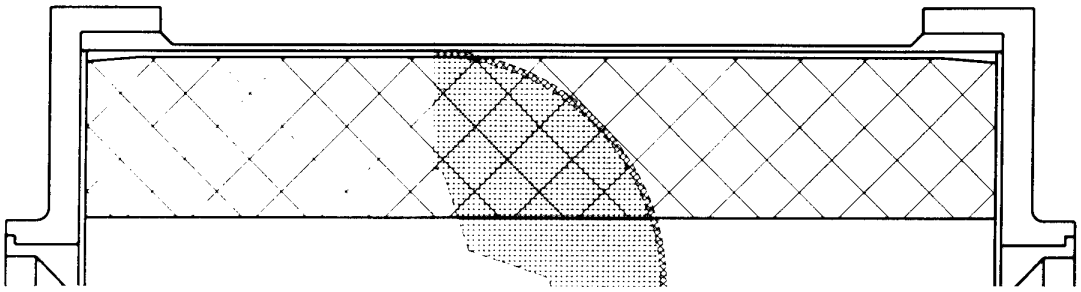


Figure 10 - **Maquette pour mesure des propriétés mécaniques**

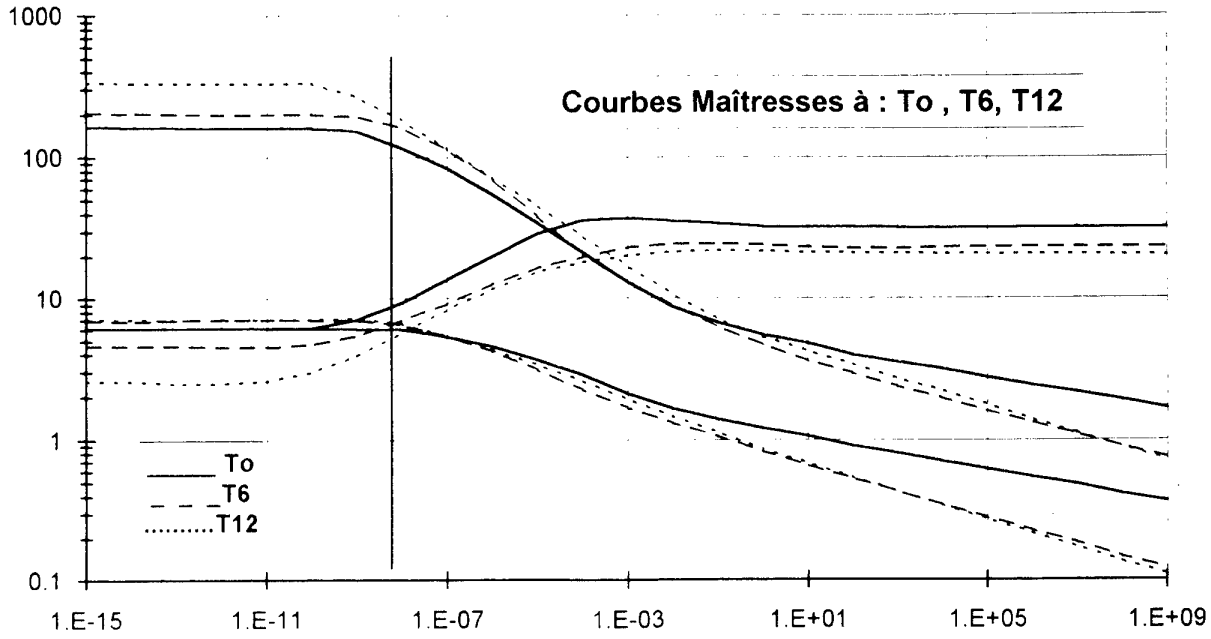


Figure 11 - **Courbes maîtresses après vieillissement**

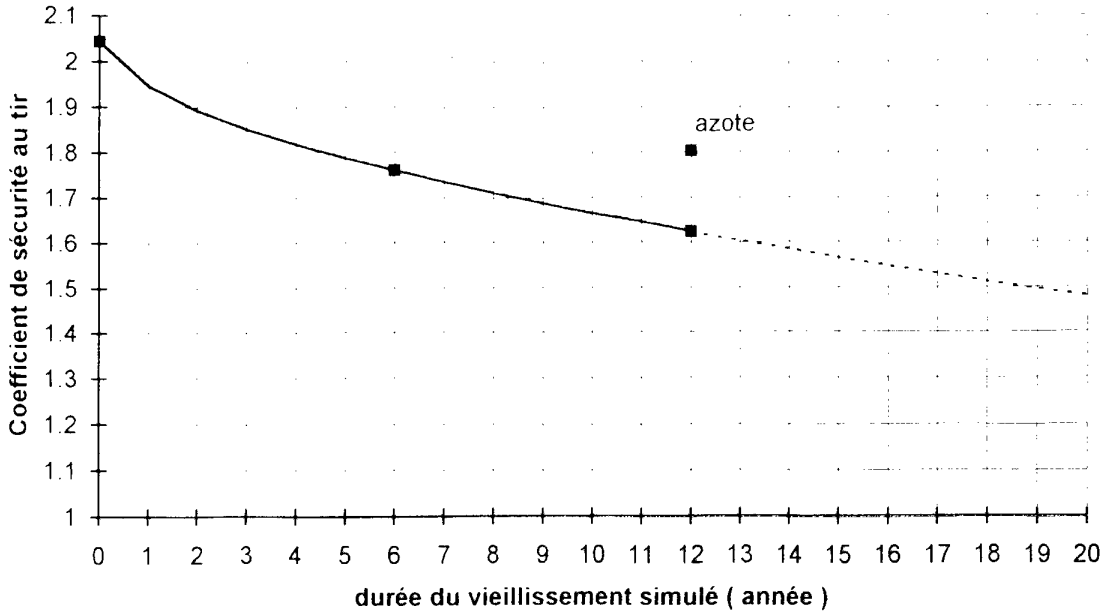


Figure 12 - **Coefficient de sécurité après vieillissement**

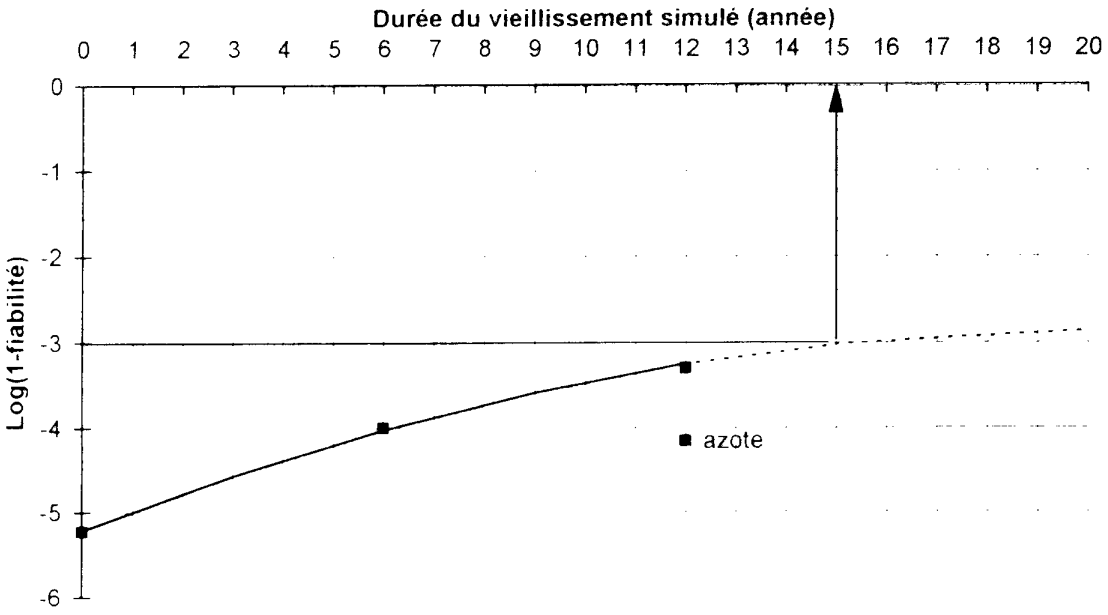


Figure 13 - **Fiabilité après vieillissement**

Service Life Determination of Rocket Motors by Comprehensive Property Analysis of Propellant Grains

Hiltmar Schubert, Klaus Menke
Fraunhofer-Institut (ICT)
Postfach 1240
Joseph-von-Fraunhofer Str. 7
76327 Pfinztal
Germany

1. SUMMARY

Over three decades ICT and the first author of this paper were engaged in research of the aging behaviour of propellants and the life time prediction of rocket propellant grains. In the context of these R + D activities test methods were created or known procedures were improved for special application.

These methods were used to predict the service life determination of rocket motors, which were in service for many years in NATO countries.

Starting with some definitions about life time the most important physical and chemical aging phenomena for the different propellant types and their influence of the life time of the grain were described and their effects discussed.

The knowledge of the time depending on aging behaviour will be the fundament of the simulation procedure to evaluate the predicted life time of a system.

To safe expenses and time, for the investigations to predict life time a tailoring principle is used.

This method collects all stresses which the weapon system has to overcome during the whole future life time, including all pretreatments.

Outgoing from these data a tailored simulation will be performed to fix the predicted service life time.

KEYWORDS
Sevice Life Determination
Aging Behaviour
Solid Propellants
Rocket Propellants
Life Time Prediction

2. INTRODUCTION

The service life of a rocket motor ends when the reproducibility of performance and function within the prescribed limits cannot be guaranteed longer. The duration of the service life of a rocket motor depends mainly on the behaviour of the rocket propellant and its mutual effects with the motor itself. Therefore, the investigations of testing the life time of the rocket motor start with the inspection of the motor itself.

In most cases the lifetime of a motor will be influenced by the propellant, its chemical composition, size of the propellant charge, type of use, storage temperature, temperature fluctuations, moisture, mechanical stress and the prescribed operational conditions. Rocket propellants generally have a shorter service life than gun propellants: In some cases only 12 - 15 years.

The service life time of a propellant charge depends on the chemical stability of the propellant itself and on the changes of the mechanical properties of the propellant charge during the life cycle of the rocket motor.

2.1 Motor Inspection

To get an overlook about the condition of the motors, the investigations start with a non-destructive material test. By this means knowledge can be gained about the condition of the igniter and booster, influences of humidity, bending of the isolation, cracks and voids in the charge etc.

2.2 Chemical Aging

Depending on the chemical components of the propellant, chemical aging influences on the lifetime in different ways. Energetic components like nitrate esters or organic components with nitro- or nitramino groups decompose in different ways, forming thermally instable products which influence more or less on the stability of the whole propellant. The decomposition process of nitrate esters is the most important one, well known and can be reduced by stabilizers.

Polymeric compounds like nitrocellulose but also polymeric binders like polybutadiene (HTPB, CTPB) and other binders decrease their chain length during the life cycle or increase their network by remaining curing agents.

In case of composite propellants with a high percentage of filling material like ammonium perchlorate, HMX, RDX or aluminium powder, we may observe dewetting between filler and the polymeric matrix by temperature changes or mechanical stresses. During aging, plasticizers may separate from the polymeric matrix and emigrate to the propellant surface or penetrate into the isolator or liner. This process may deteriorate their functions.

Paper presented at the AGARD PEP Symposium on "Service Life of Solid Propellant Systems" held in Athens, Greece, 10-14 May 1996, and published in CP-586.

All these chemical reactions or physical processes can be more or less measured by testing mechanical properties during the life cycle of the rocket propellant. Many investigations over decades of years have shown that the determination of the mechanical properties of a propellant is the most sensitive method of all these chances during the lifetime, provided that a stable propellant was produced.

2.3 Mechanical Properties

Propellant charges are subjected to mechanical stresses that depend on the missions of the rocket motor and the shape, size and form in which the propellant is used. Since propellants mainly consist of polymers, their mechanical properties also depend on the temperature and stress rate. During the whole service life the propellant has to produce values of mechanical properties which are high enough to fulfill all stresses during the life cycle, according to transport, storage and mission.

The thermoplastic double-base propellants generally have a high tensile strength and a relatively low elongation at break. They are therefore used as cartridge case propellant charges. The temperature range is limited due to embrittlement in the low temperature range (ca. -30°C) and softening above +70°C

Viscoelastic composite propellants generally have a high elongation at break and a relatively low tensile strength. Composite propellants are therefore almost always used as case-bonded propellants, the large expansion capacity of the propellant absorbs the chamber movement as a result of temperature cycling. The tensile strength needs only be sufficiently large to ensure stability of the propellant under load. The larger the diameter and length of the propellant charge, the greater must be its elongation at break.

During the service life of a solid propellant the mechanical properties change in varying degrees. With composite propellants the elongation at break can deteriorate resulting in embrittlement, caused by postcuring effects. Softening can also occur as a result of depolymerization, and leads to deterioration of the tensile strength.

The mechanical properties are also greatly affected by adhesion between the filler and binder. Moisture, frequent temperature variations and vibration can cause dewetting of the filler from the binder, resulting in a decrease of the mechanical properties. In nitrocellulose the mean molecular weight decreases during aging, which likewise negatively affects the mechanical properties.

Surfaces of rocket propellants that are not meant to burn for internal ballistic reasons are provided with firmly adhering insulation layers, made of polymers that are compatible with the propellant (e.g., ethylcellulose for double-base propellants and PVC or HTPB for composite propellants). The insulation layers may also contain inert fillers and plasticizers. The mechanical properties of the propellant and/or insulation can also change due to mutual migration of their constituents, and may result in malfunctions.

3. SERVICE LIFE DETERMINATION OF A TWO-STAGE ANTI-AIRCRAFT ROCKET MOTOR

3.1 Problems and Test Schedule

In order to determine the service life of anti-aircraft rocket motors which were produced under license by two companies in Europe between 1975 and 1979, a trial programme had been predetermined.Several of the specifications described in this programme had to be modified thanks to experiences ICT gained during many years of research work in this field. The test programme started in 1982 and was carried out in two stages depending on test results which were gained during the test procedure. The second stage was finished in 1987. For the first stage 26 motors have been furnished for testing purposes. For the second stage additional 10 motors were delivered.

For the prediction of service life time a severe problem had to be taken into consideration: Because of legal circumstances no data about the properties of the propellant after manufacturing were available.

The test procedure was also enlarged by a wider control programme to detect irregularities by faulty manufacturing operations.

The ammonium perchlorate, nitroguanidine composite propellant consists of an internal booster-sustainer star burner.

3.2 Test Procedures

3.2.1 Non-Destructive Tests

The motor inspection is divided in four groups:

- visual inspection
- sonic inspection
- X-ray inspection at room temperature
- ultra-sonic inspection

3.2.1.1 Visual Inspection

This inspection refers to the outer and inner state of the motor. Especially the forward and the ignition opening was examined by an endoscope with 240° view angle, one light source coupled with a fibre optic bundle, registration was done with an Olimpic Camera on contoured solids. The container of the drying agent was weighed and exposed to humidity. The difference in weight is a measuring value to find out if the motor case has been sealed during the whole storage time.

The grade of crystallization is defined in the following table:

Grade	with ammonium perchlorate crystals covered area of propellant surface in %
0	no crystallization
1	< 10
2	10 to 30
3	39 to 60
4	60 to 100
5	more than one layer of crystals

Result:
The examination has shown nearly no irregularities but more or less friction points and corrosion spots and the evidence that the motor cases were sealed. AP-crystals were found on the propellant surface which covered up to 30 - 40 %. The content of water was on average: booster 0.06 %, sustainer 0.10 %.

3.2.1.2 Sonic and Ultrasonic Testing
Goal of the test was to inspect the binding between motor case and liner. For the sonic inspection the motors were jacked up and positioned on rollers. For the test a silver coin was used and the sound was acoustically observed by the tester. It was a surprise that all separations of the liner, apart from small improper bindings, were found by this rather simple method.

By ultrasonic means best results were obtained with the damping of the back wall echo. The acoustic impulse is coupled into the motor and the temporal damping of the multi-echo is measured. The most clear results we got with a frequency of 4.65 MHz and a pulse duration of 0.6 µs. The tests were performed at -31°C.

Result:
In many cases a separation was found near the after end.

3.2.1.3 X - Ray
With the help of x-ray test debonding, voids and separations of the propellant in the system should be detected.

Voids and cracks can be localised. Debonding between motor case and liner could be found by both, sonic and ultra-sonic inspection, but the x-ray testing did not point out anything.

An optimum exposure was found to be 250 kV, 3 mA and 7.5 min. Recording is done by a x-ray film AGFA Strukturix D7 Pb. The film focus distance was 1.2 m.

Processing is done according to the instructions of the producer.

The igniter is x-rayed with 100 kV, 6 mA and 4 min. The other data are the same as above.

The tests were performed at room temperature.

Result:
In some motors we found small cavities and in very few examples cracks at forward and after end. The largest cavity had 8 mm ∅.

3.2.2 Conditioning and Preloading of the Rocket Motor
The conditioning and temperature cycling programme is executed in climate chambers and the temperature control is done automatically by a computer programme. The temperature cycling programme is shown in Fig. 1. The motors were exposed to 10 temperature cycles. The time at the extreme temperatures was extended to six hours.

3.2.3 Motor Dissection
It is well known that the dissection of case bonded propellants in single sections is a problem. Extremely critical is the interface from metal to propellant.

An additional difficulty is, that the motor case of the ground to air missile is not ideally round but shows a polygonal structure. Fig. 2 shows the schematic structure of the saw, used for the cutting of the motor in segments. A sensor follows the contour of the rotating motor thus controlling the support that the saw blade will not be in contact with the propellant.

The rocket itself is positioned on a jack and rotated one time per 10 min. against the saw blade. The cutting of the case is done in three steps.

The insulation is cut with a sharp knife. The propellant itself is sliced by a steel wire of 9 mm diameters, weighted with 187 kg. The separation of the propellant from the motor case is done also with a steel wire whereat the cutting is done into the liner. The dissection is done under remote control and monitored by a TV system.

The specimens for determination of the propellant property are produced by machining and cutting techniques.

3.2.4 Mechanical Properties
For testing of mechanical properties following methods are used:

- tensile test
- relaxation test
- creep test
- shear test

- crack propagation test
- torsional pendulum test
- hardness test

3.2.4.1 Uniaxial Tensile Test
This test with standard probes (JANAF) is done according to the German TL 1376-701 with a constant rate of 50 mm/min. and at 8 temperatures between - 40°C and +74°C. Some samples were also tested with a high rate of 1.22 m/s between -32°C and +52°C. Before testing the probes were conditioned over 4 weeks at ≤ 5 % rh and 23°C. The samples were machined and cut out of the propellant material (sustainer and booster separate and in combination). Two cutting examples are shown in Figs. 3 and 4. The probes were taken from the forward and after end of the propellant. Sample productions have a strong influence on the result and all test parameters must be identical. Because of the failure of data after manufacturing the propellant charge was cut in 3 sections. Two of these were artificially aged, one for 12 weeks at a temperature of +50°C and the other for 6 weeks at 70°C.

Result:
It was found that all data do not show exceptional results.

3.2.4.2 Relaxation Test, Creep Test
The results of the relaxation and creep test allow to deduct the long-term behaviour and the aging estate of the solid propellants.

Both experiments lead to a concurrent mode in the case of linear viscoelastic behaviour. This mode is a base for a structure analytical calculation, but composite solid propellants show neither linear elastic nor linear viscoelastic behaviour; that means relaxation and creep tests lead to different results.

From each propellant two specimens were investigated and the relaxation mode versus time and the time-temperature shift factor were calculated. In the creep test with a constant strain < 3 % the creep compliance was measured.

Result:
The propellants show similar relaxation behaviour. But the propellants display a minor bonding strength between binder and filler as a function of time. Also the creep tests show that the bonding strength between filler and binder decreases with time.

3.2.4.3 Shear Test
For the measurement of the bonding strength between liner and propellant or liner and motor case poker chip tensile and shear test are used.

The shear test is limited to samples taken from the nozzle side. The areas of interest should be extended to the wing area of the motor.

The poker chip shear test at a constant rate of 0.085 m/s was realized at temperatures of -32°C and +52°C. Also a poker tensile test was performed with a constant rate of 5 mm/min.

Result:
A dependence of the storage time for tensile and shear strength cannot be found. Different motors allowed the isolation to be removed quite easily (Fig. 5).

3.2.4.4 Crack Propagation
The crack propagation test was carried out in accordance with DIN 53363. The sample consisting of sustainer and booster propellant is provided with a notch in the middle of its longitudinal side. The draw-off speed was 5 mm/min at temperatures like in the tensile tests.

Result:
Two samples are tested under the same test conditions. There are broad variations between test results and no definite tendency is to be seen.

3.2.4.5 Torsional Pendulum Test
The torsional test will provide information on the dependence on temperature of the mechanical properties of the isolation (puddle). The test will be performed in accordance with DIN 53445. The values of shear mode and loss mode as a function of temperature will be recorded.

Result:
All materials become rigid beyond -40°C.

3.2.4.6 Hardness Test
This test was accomplished by a Shore A Hardness Tester at distinct position points of the sustainer propellant and puddle at a temperature of 25°C.

Result:
The variations of the values of all motors were disregarding small.

3.2.5 Burning Rate
The burning rate is measured using the Crawford method. The execution follows the German TL 1376-70.

The method induces larger errors at slow burning rates (sustainer). Significant for the judgement of the estate of the propellants are the data measured during static firing. The Crawford data serve for the comparison and for the detection of tendencies limited by the systematic and statistical error.

Result:
The measured linear burning rate did not show any differences higher than the mean deviation, except from propellant samples with higher burning rates (~ 10 %) out of the forward end perpendicular to the axis and adjacent to the puddle of the booster phase of some charges.

3.2.6 Static Firing

The test stand is constructed to withstand a rocket thrust up to 140 kN. The heavy mass containing the rocket fixation is positioned on spring elements to insure that the existing thrust is always vertical to the load cell. This fixation allows the rocket motor to move freely in thrust direction, while it is being held on two sides in the vertical position, which means this is a statically defined system (Fig. 6).

Fig. 7 shows the arrangement of the thermocouples on the outside of the motor case. They are evenly distributed, so that unregular high temperatures can be regionally detected.

Static firing is recorded visually by a high speed camera; this was done since in the first campaign one motor showed a misbehaviour during firing. Using this method it is possible to detect unregularities optically. The thrust is measured by a load cell. The thrust-time-diagram is multiple recorded by different transient recorders (10 bit resolution, 0.1 % linearity) and a visicorder.

5 motors were fired at +52°C and -31°C after 10 times cycling between +60°C and -31°C. 10 motors were fired at -31°C and 5 motors after preloading 30 days at 70°C and -31°C.

Result:
All values of the motor firings are inside the specification of MIS 16424D with the following deviations:

2 x sustainer impulse too low (~ 2 %)
3 x booster impulse too low (~ 2 %)
1 x booster impulse too high (1.2 %).

Two motors with these divergent values were fired at 52°C without preloading and 4 motors with divergent values were preloaded and fired at -31°C.

One motor bursted - the after end section was torn off directly after ignition. This motor had been preloaded and fired at -31°C. It is assumed that the misfire of this motor was caused by a lack of shear strength between liner and motor case and not due to aging.

A second motor nearly bursted during firing, caused by debonding of the insulator from the motor case at the after end.

The exterior chamber temperature, measured 50 sec. after ignition, was in 2/3 of all motors lower than 50°C. The temperatures of the other motors decrease up to 130°C. In some cases hot spots on the chamber were registered.

3.2.7 Chemical Investigations for Determination of Service Life

Because of the high stability of ammonium perchlorate and nitroguanidine and also due to the absence of nitrate ester, chemical stability is beyond any doubt. If the polymerization of the binder is not completed during manufacturing, an aftercuring may occur during storage. Investigations like IR spectroscopy and gelpermeationschromatography have shown that the polymerization during manufacturing was completed.

4. CONCLUSION

The evaluation of the test results according to the service life determination of this rocket motor resulted in prolonging the life time of the propellant to twelve years at least as a result of the mechanical and interior ballistic investigations.

The maximum stress and strain are significant for the estimation of the aging process of the propellants. As an indication for the bonding strength of the sustainer-booster boundary the stress at break is taken. As an outcome of these investigations aging could not be detected.

The internal ballistic behaviour has shown that nearly all values were inside the specification, also after preloading. Therefore, no restrictions could be seen for prolonging the life time of the propellant itself.

In contradiction the debonding of the insulator from the motor case seems to be a severe restriction. There is the risk that when firing these motors at low temperatures the flames are able to contact the case at the after end. The shrinkage of the grain at low temperatures causes debonding along the inner motor case as consequence of the bad shear strength. This effect could be traced back to a former production series in both companies and was to be attributed to a manufacturing defect and not to aging.

The outcome of this investigation confirms the practical knowledge that very often the service life of a rocket motor is determined by misfunction of the liner or the insulation rather than by the propellant itself.

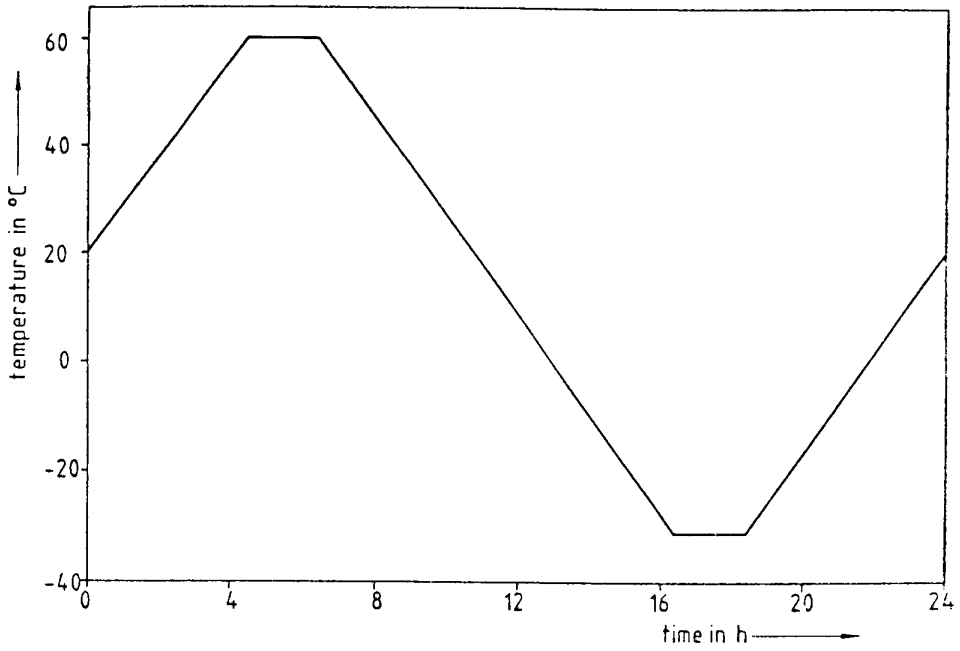


Figure 1: Programme for temperature cycling

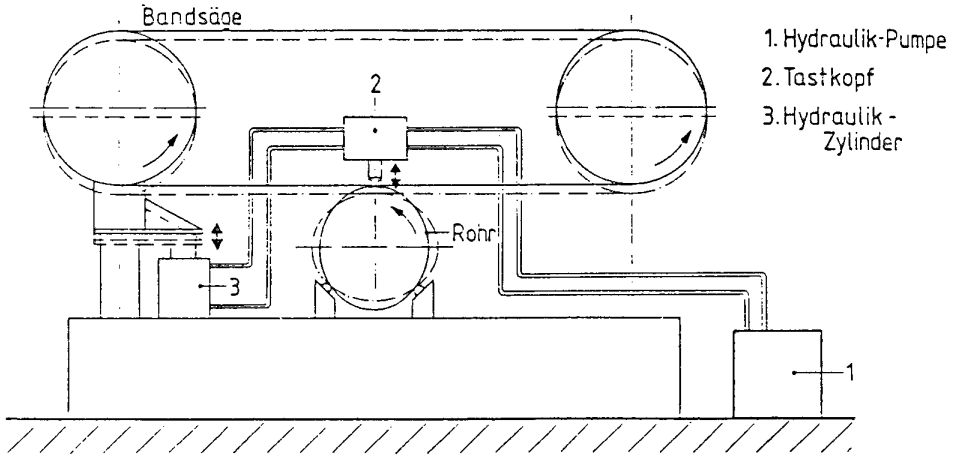


Figure 2: Schematics of motor dissection

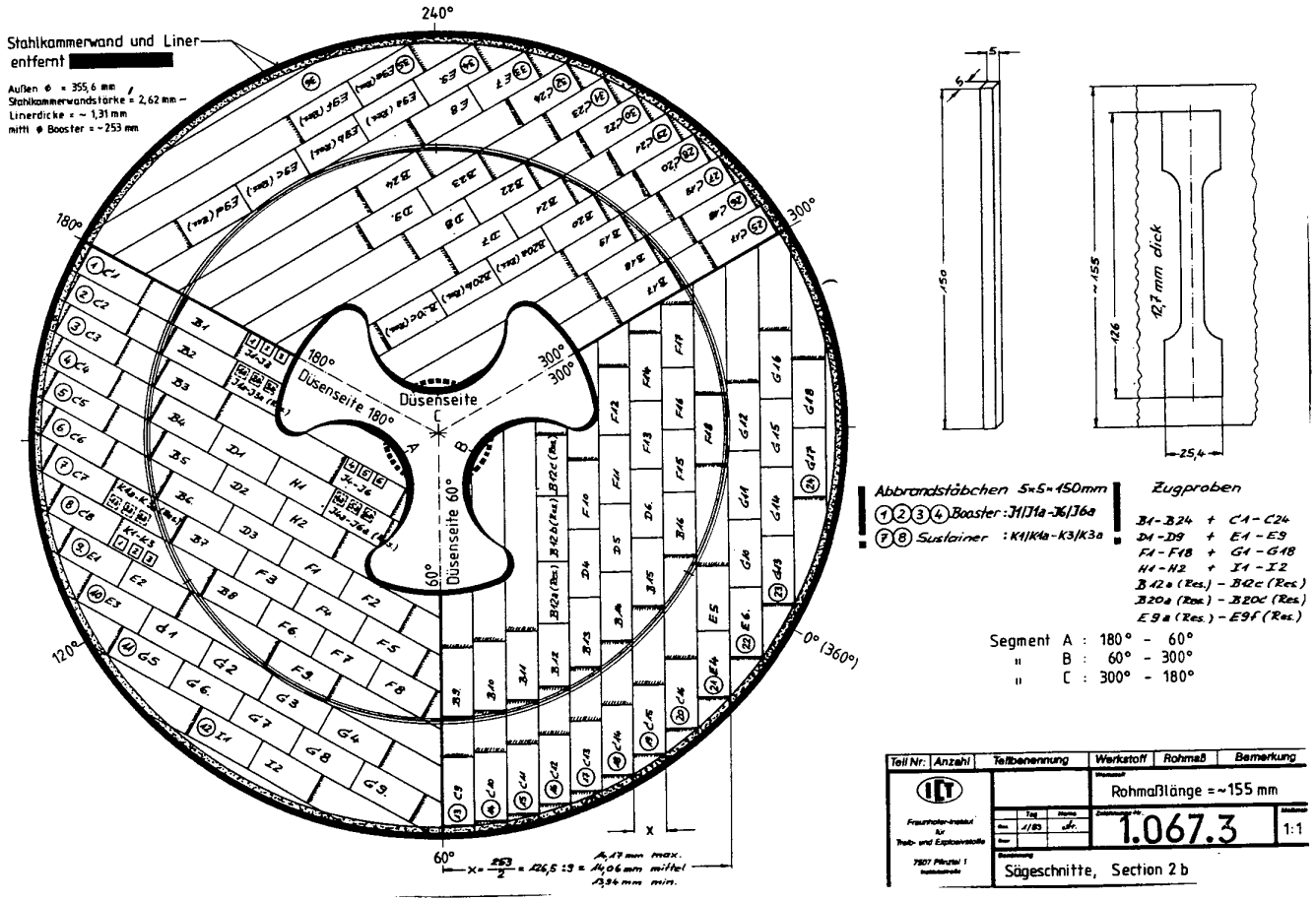


Figure 3: Example for the division of the propellant charge for testing mechanical properties

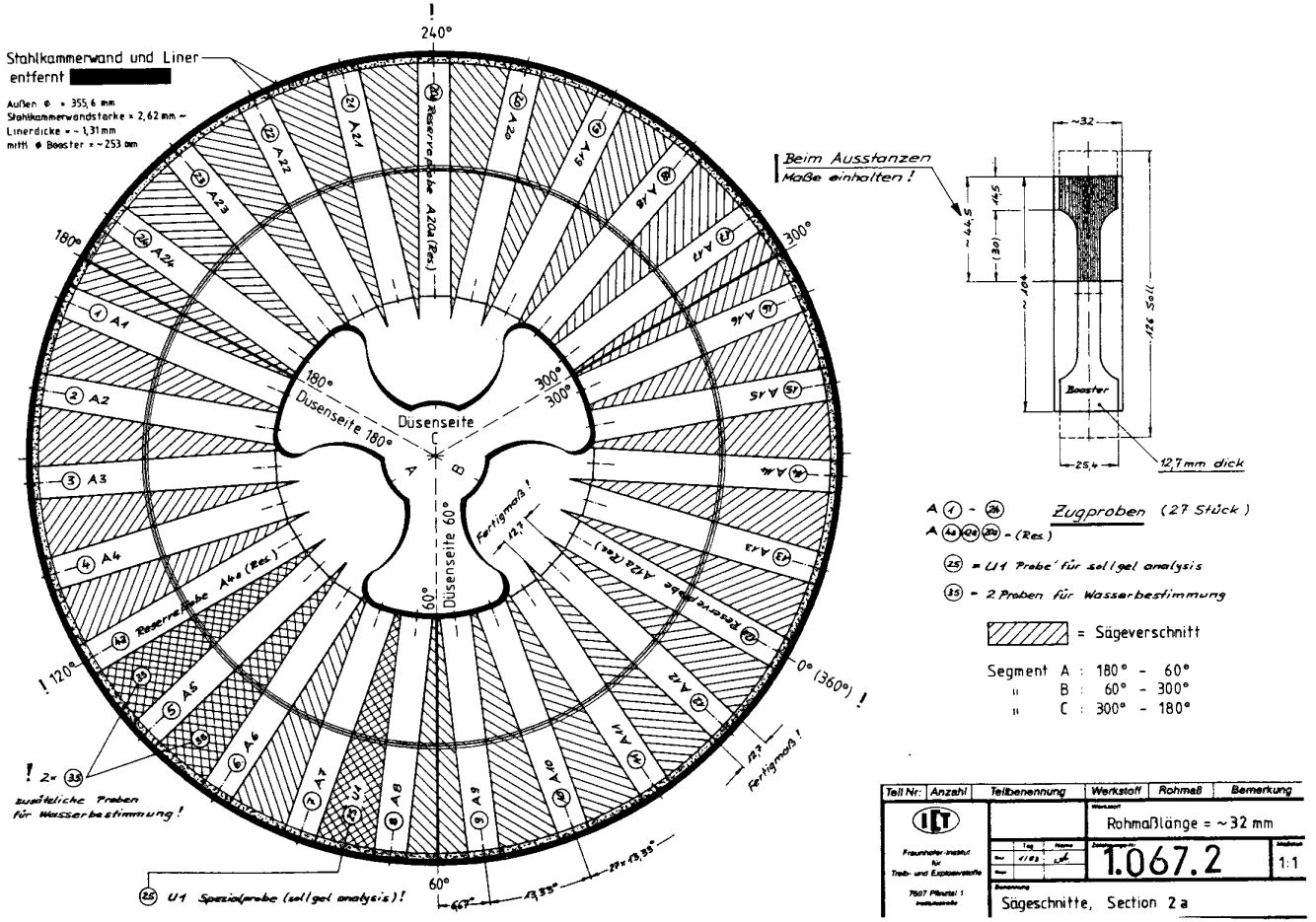


Figure 4: Example for the division of the propellant charge for testing mechanical properties

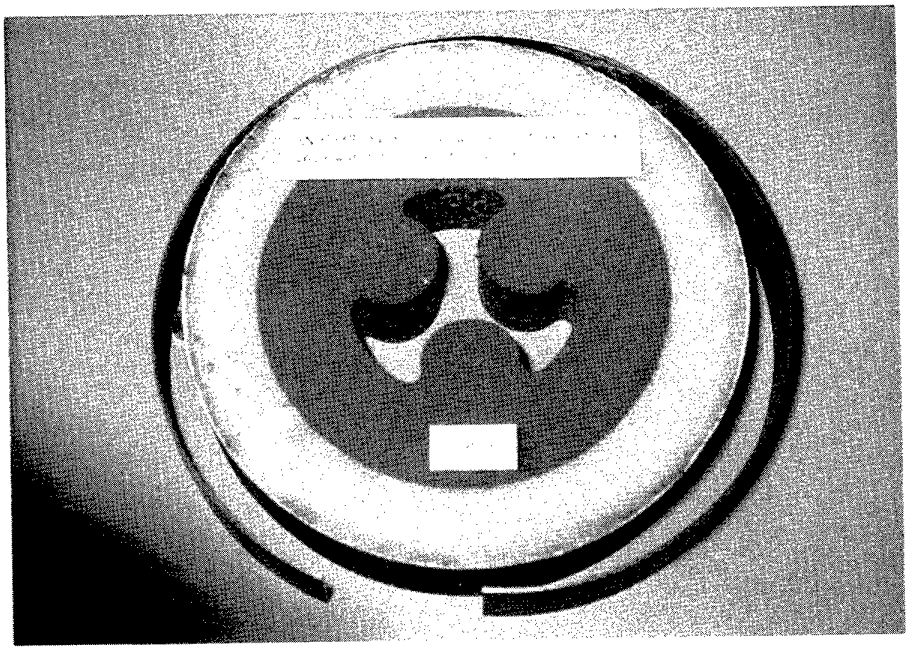


Figure 5: Unbonding between case and insulator

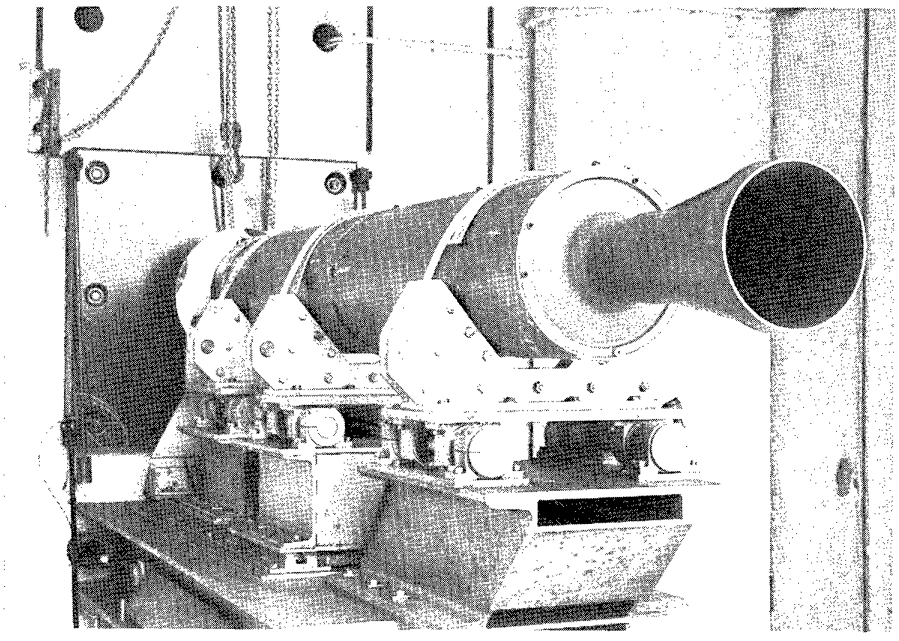


Figure 6: Static test loading fixture

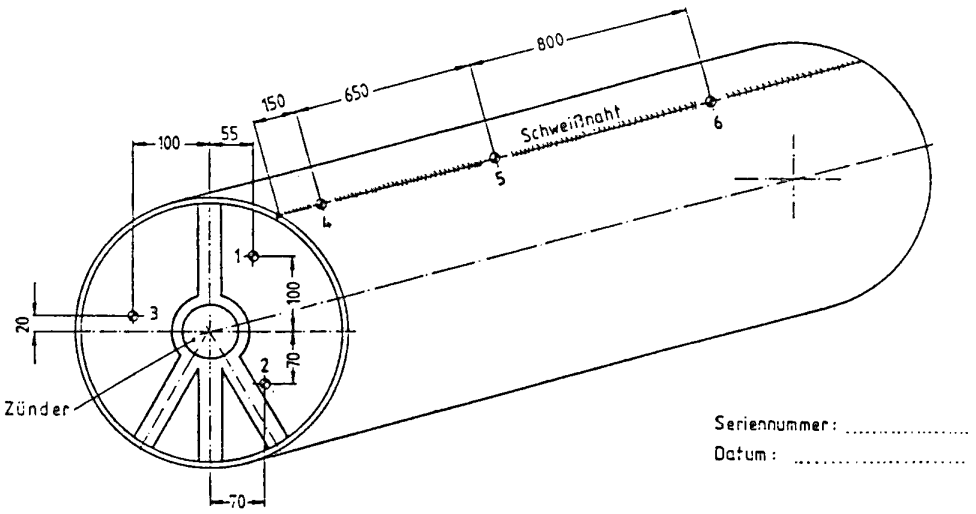


Figure 7: Arrangements of thermocouples

Paper Number: 41
Discussor's Name: L. G. Meyer
Responder's Name: Professor H. Schubert

Question: What do you consider the limiting factor in age out of the motor somewhere beyond 12 years.

Answer: The motor will probably age-out due to the chemical degradation.

Paper Number: 41
Discussor's Name: D. I. Thrasher
Responder's Name: Professor H. Schubert

Question: Were the debonds which caused "near failure" known to exist before the test firings?
How did you verify that no aging effects were involved in these bond failures?

Answer: Before firing, we had no information about the debonding. Debonding was not an aging effect for we found this situation after dissection of motors which had not experienced any preloading or temperature cycling.

Paper Number: 41
Discussor's Name: Professor R. A. Heller
Responder's Name: Professor H. Schubert

Question: What values did you obtain for Poisson's ratio?

Answer: The values depend on the stresses. Values of 0.48 - 0.40 and lower were observed.

STRUCTURAL/BALLISTIC INSTABILITY AGEOUT MECHANISM IN THE SPARROW MARK 52 SRM

D. I. Thrasher
OL-AC Phillips Laboratory
4 Draco Drive
Edwards Air Force Base, CA 93534

P. R. Empleo
Sparta, Inc.
244 E. Avenue K-4
Lancaster, CA 93535
USA

SUMMARY
A three dimensional finite element analysis and a one dimensional incompressible flow model were used to investigate the interaction between the internal ballistics and the structural grain deformations for the Sparrow Mark 52 rocket motor. The results confirm earlier investigators' conclusions (based on two dimensional structural analysis) that a mechanism exists for pressure spiking driven by choking of the gas flow within the bore cavity due to grain structural deformations. Significant differences were found between the 2D and 3D results, however; the 3D analysis requires a higher propellant modulus to prevent choking under the same analysis conditions.

INTRODUCTION
The Sparrow Mark 52 rocket motor had a history of occasional "pressure spikes" during the ignition transient in test firings at 71 °C. The Mark 52 motor (see Figure 1) was characterized by a 5-lobed star grain configuration and a relatively constrained flow passage.

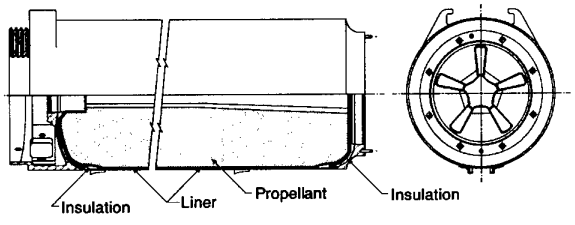


Figure 1. Motor Geometry

Previous analyses of the Sparrow Mark 52 motor had indicated that the anomalies were caused by an interaction between the flow field and the motor structural response, coupled through the pressure/grain deformation relationship. The nonlinear interaction between the two processes can become unstable in these motors if the propellant modulus is low enough, causing the flow to choke near the end of the grain and causing the pressure spike. At the time this analysis was conducted, the frequency of occurrence of pressure spikes in Mark 52 test firings was increasing with motor age, so we were concerned about this phenomenon as a potential ageout mechanism for the motor. Since accelerated aging of the propellant showed a tendency to soften with age, (see Figure 2) it appeared that the tendency for pressure spiking should be age dependent.

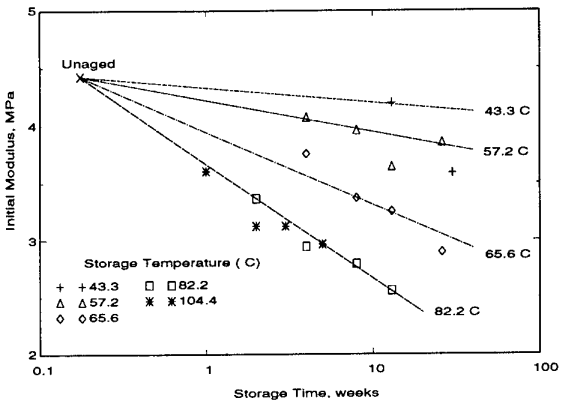


Figure 2. Propellant Accelerated Aging Data

The purpose of the work reported here was to verify previously reported analyses of the problem with an important improvement: while the earlier analyses used axisymmetric ("2D") structural models to represent the propellant grain, we used the TEXGAP-3D program to generate a detailed three-dimensional structural model of the motor.

ANALYSIS PROCEDURE
Figure 3 shows the overall approach that we used to model the structural/ballistic interaction problem. The key parts of the overall model are the geometry model (composed of a burnback model and a structural deformation model) and the flow model. As indicated in Figure 3, the original motor geometry is altered to a burnback configuration by the burnback model. The geometry is further modified by the structural deformation

Paper presented at the AGARD PEP Symposium on "Service Life of Solid Propellant Systems" held in Athens, Greece, 10-14 May 1996, and published in CP-586.

model to account for the structural deformations (which are defined in terms of a deformation amplitude and the motor head end pressure). The final modified geometry and head end pressure are then fed into the flow model, which computes the pressure distribution. The structural deformation model within the geometry model is a set of empirical relationships based on results from the TEXGAP-3D analysis and other structural analyses.

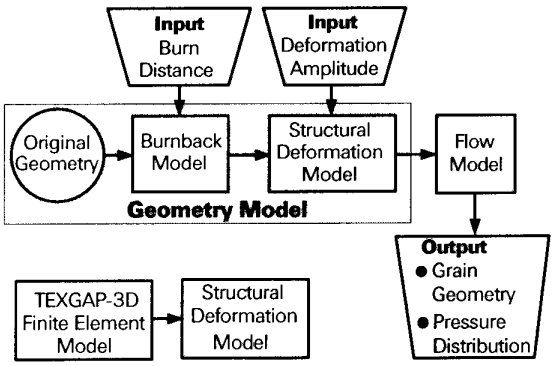


Figure 3. Modeling Approach

Details of the modeling approach are discussed later in this paper.

ASSUMPTIONS

The major assumptions we made are listed separately below for the two main parts of the analysis: the structural analysis and the flow analysis.

Structural Analysis Assumptions

1. All materials in the motor behave either elastically or in a quasi-elastic manner, characterized by effective viscoelastic moduli for the propellant grain, liner, and insulation and by constant values of the bulk modulus of compressibility for these materials.

2. Linear superposition applies for all structural deformations; furthermore the net area change from all contributions (including burning) can be determined by linear superposition of the components of area change.

3. The structural deformations calculated for the original geometry are valid for the burnback geometry.

Flow Analysis Assumptions

1. Friction is negligible.

2. The gas flow is steady and one-dimensional.

3. The gas can be treated as an incompressible fluid.

4. The mass generation rate per unit of undeformed surface area is independent of pressure and location within the propellant grain.

5. Area changes due to structural deformation do not change the mass flow rate per unit of undeformed surface area.

STRUCTURAL ANALYSIS

We used a number of different structural analysis tools in the course of this analysis. The structural models used, and their roles in the overall analysis, are discussed below.

TEXGAP-3D Model

We made a detailed TEXGAP-3D analysis of the motor under the pressure loading shown in Figure 4.

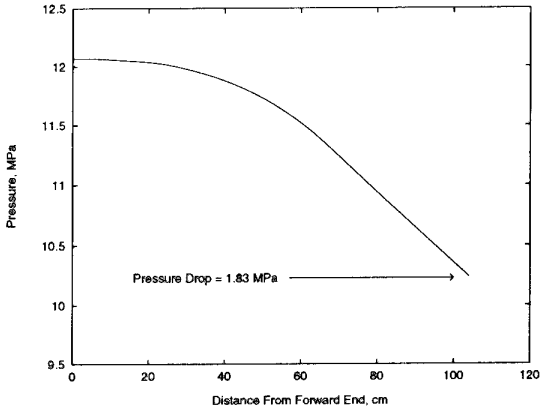


Figure 4. Applied Pressure Load.

The analysis used a total of 492 quadratic-displacement elements to model a basic-symmetry section (a 36-degree wedge) to capture the 5-point slotted geometry of the motor. The elements used to model the insulator, liner, and propellant were the reformulated elements designed for nearly incompressible materials. In addition to the internal pressure load, the boundary conditions included the nozzle ejection load and the igniter ejection load. The deformed geometry of the aft portion (containing 159 elements) of the 3D model is shown in Figure 5.

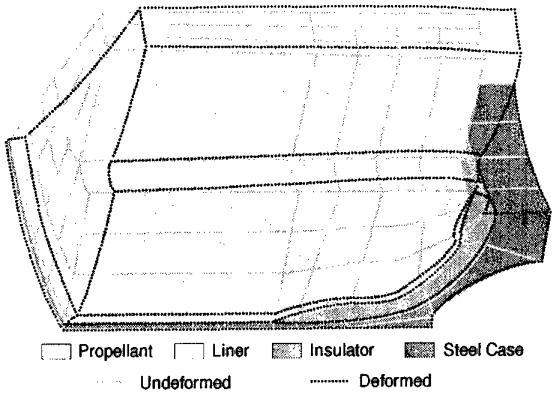


Figure 5. Aft End of TEXGAP-3D Motor Model

Figure 5 shows a primary feature of the grain deflection of the Sparrow Mark 52 motor under the pressure loading of Figure 4; the propellant grain is forced against the aft dome, causing it to bulge inward and constrict the cross sectional area available for gas flow. The constriction of the flow area is evident in Figure 6.

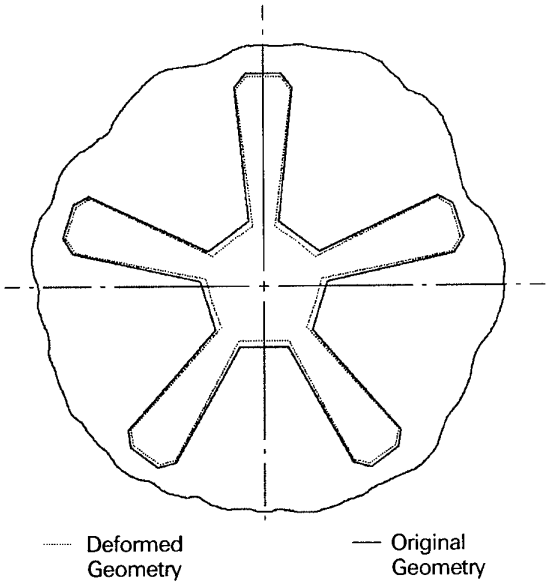


Figure 6. Deformation of Motor Bore

The low modulus of the liner material (white layer in Figure 5), permitting a large shearing deformation of the liner layer, is a key factor in this behavior.

TEXGAP-2D/Approximate-3D Models

We used the TEXGAP-2D/Approximate-3D finite element code to link our analysis to earlier investigations which used two dimensional models. Two geometry models were generated, an axisymmetric equivalent cylinder model (basically the 3D geometry with all material between the slot valleys removed) and an approximate 3D model using slot elements to model the slotted region of the grain. Figure 7 shows the Approximate-3D finite element model.

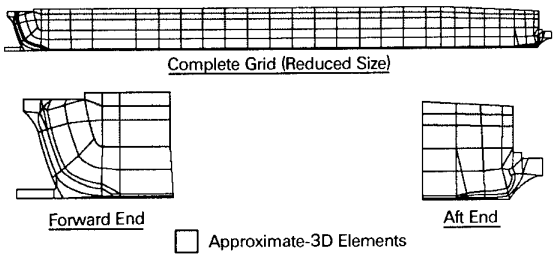


Figure 7. Approximate-3D Finite Element Model

These models used 153 and 237 elements respectively, mostly quadratic-displacement isoparametric elements. Reformulated elements were used for the propellant, insulation, and liner. Both models were subjected to the same boundary conditions as the 3D model.

"QUICK-LOOK" Code Models

The Phillips Laboratory "QUICK-LOOK" code is an upgraded version of a programmable calculator Lamé-cylinder structural analysis program [1] which was ported to the Hewlett-Packard HP-85 microcomputer. The "QUICK-LOOK" code was used to model an equivalent cylinder for the slotted grain as well as the short forward circular port section of the grain which surrounds the igniter. These models were analyzed under generalized plane strain conditions for the thermal and uniform pressure loads.

Material Properties Used

The material properties we used in the various structural analyses are shown in Table 1. The properties used for the nominal analysis (i.e. propellant modulus of 1.55 MPa) are essentially the same as those used by Aerojet in their analysis of the spiking problem. The properties for the propellant, insulation, and liner were considered to represent the lower limits of modulus for these materials. The lower and higher propellant modulus values (0.689 MPa and 3.45 MPa) for pressurization were included to allow scaling of the results for different propellant modulus values. The modulus values used in the "QUICK-LOOK" analyses were based on effective modulus calculations for a specific set of propellant data discussed later in this paper.

Table 1. Mechanical Properties Used in Structural Analyses

	TEXGAP-3D	TEXGAP-2D APPROX-3D	QUICK LOOK
PROPELLANT			
E, MPa	1.55	0.689, 1.55, 3.45	0.35, 1.55*
$\beta^{\dagger}$, MPa	517	517	517
LINER			
E, MPa	0.14	0.14	N/A
$\beta^{\dagger}$, MPa	6894	6894	N/A
INSULATION			
E, MPa	6.895	6.895	N/A
$\beta^{\dagger}$, MPa	10300	10300	N/A
CASE			
E, MPa	200000	200000	200000
ν	0.32	0.32	0.32

* Used for thermal deformation only:
used $\alpha = 3.6x10^{-6} cm/cm/^{\circ}C$. $\Delta T = -6.6^{\circ}C$

† Poisson's ratio $(\nu) = 0.5 - E/(6\beta)$
where β is the Bulk Modulus of Compressibility

Application of Structural Analysis Results

The primary result from the 3D model was the radial deflection at the bottom of the slot valley under the pressure load. These results are shown in Figure 8.

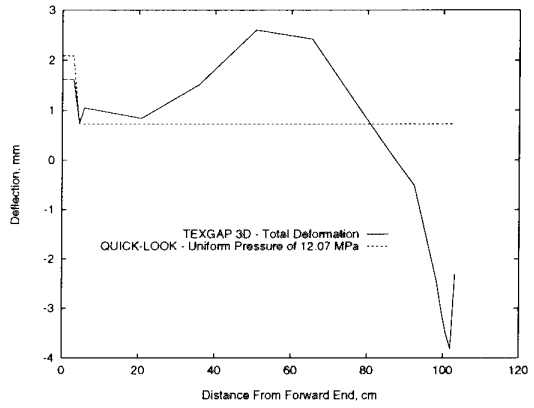


Figure 8. Radial Deflection at Slot Bottom from TEXGAP-3D Analysis

In addition, the deflections at nodal points on the bore surface output by the TEXGAP-3D post processor were analyzed using a specially written microcomputer code to determine the area change under the pressure load.

We used the axisymmetric equivalent cylinder results only for comparison with TEXGAP-3D and the Approximate-3D model. The parameter of interest is the radial deflection, shown in Figure 9.

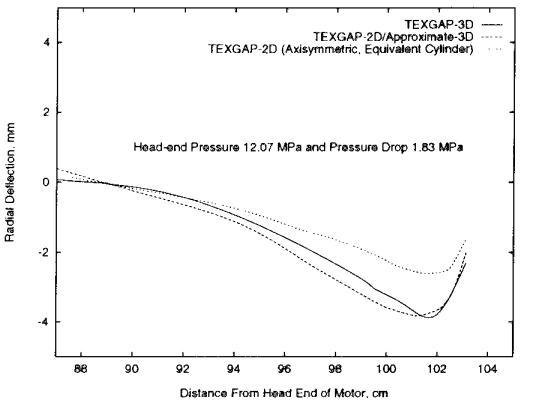


Figure 9. Comparison of 2D and 3D Analysis Results

We used the Approximate-3D model results for comparison with TEXGAP-3D and also (in conjunction with the "QUICK-LOOK" models for uniform pressure) to develop an empirical relationship between the propellant modulus and the radial deflections. As shown in Figure 9, the radial deflection determined by the Approximate-3D model very closely matches the TEXGAP-3D results in the aft end of the motor, while the axisymmetric model's radial deflection is approximately 50% smaller than the 3D model's deflection. These results emphasize the need for a 3D grain analysis.

We used the "QUICK-LOOK" analysis results in two ways: (1) to define the grain response to the thermal load; (2) to provide the uniform pressure component of the radial deflection at the slot bottom so that it could be subtracted from the 3D deformations under the total pressure and thus determine the pressure drop component of the this deflection (see Figure 8). The same procedure was applied to the peak deflection from the Approximate-3D model to determine the relationship between the propellant effective modulus and the pressure drop component of the deflection. The resulting empirical relationship is

$$(\Delta r_{\Delta p})_{max} = [2.1234 + (3.684/E)](\Delta p/1.827) \qquad (1)$$

where $(\Delta r_{\Delta p})_{max}$ is the maximum value of radial deformation, in mm, at the slot bottom with the uniform pressure contribution subtracted out, E is the effective elastic modulus of the propellant in MPa, and Δp is the pressure drop in MPa applied to the grain. This empirical equation fits the Approximate-3D results (and the single 3D result) with a maximum error of 1.2%.

THE GEOMETRY MODEL

The geometry model modifies the motor internal geometry to account for the effects of propellant burning, structural deformation under thermal load, and structural deformation under pressure load. The cross sectional flow area calculated by the geometry model at the nominal analysis conditions (p_0 = 12.07 MPa, Δp = 1.83 MPa, T = 71 ^{o}C, and *burn distance* = 0.45 *mm.*) is shown in Figure 10. The relative magnitudes of the various effects are evident in the figure. (The alternative calculations for total deformation–"3D" and "Rigid Fin"–are explained below.

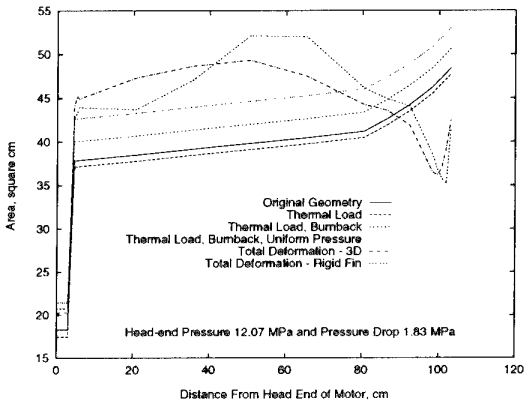


Figure 10. Area Variation Along Motor Length

Overall Geometry Calculations

The geometry model calculates two motor geometry parameters which are needed by the flow model. These parameters are the effective radius of the burning perimeter

at each axial station and the cross-sectional flow area at each axial station.

The burning perimeter, P, is represented in terms of an effective radius, $a(z) = P/(2\pi)$. The effective radius calculation is part of the burnback model. The cross-sectional flow area is:

$$A(z) = A_0(z) + \Delta A_B + \Delta A_T + \Delta A_{p_o} + \Delta A_{\Delta p} \quad (2)$$

where $A_0(z)$ is the original flow area, $\Delta A_B(z)$ is the change in flow area due to burnback, and the remaining three terms are the structural deformation components due to thermal load, uniform pressure, and pressure drop, respectively. The detailed models used to generate the individual geometry change components are discussed below.

The Burnback Model

The burnback model consists of the following two equations:

$$a(z) = a_0(z) + x \quad (3)$$

$$\Delta A_B = \pi\left\{\left[a(z)\right]^2 - \left[a_0(z)\right]^2\right\} \quad (4)$$

where $a_0(z)$ corresponds to the original burning perimeter and x is the burn distance, which is specified as an input variable.

The Structural Deformation Model

The structural deformation model computes three structural components of area change: the thermal load component, the uniform pressure component, and the pressure drop component.

Thermal Load Component

The area change due to the thermal load on the motor (temperature soak) is estimated from

$$\Delta A_T = \pi {r_0}^2\left[(1+\epsilon_T)^2 - 1\right] - 2\alpha\Delta T A_0 \quad (5)$$

where ϵ_T is the hoop strain in an equivalent-cylinder plane strain model of the motor cross section, r_0 is the linear coefficient of thermal expansion of the propellant and ΔT is the difference between the soak temperature and the motor's stress-free temperature. The $\alpha\Delta T$ term arises because the computed strain is the "stress-producing strain," i.e., $\epsilon_T = \Delta r/r_0 - \alpha\Delta T$. The strain level was found to be nearly independent of the modulus over the range considered.

Uniform Pressure Component

The area change due to a uniform pressure equal to the motor head-end pressure is calculated from

$$\Delta A_{p_0} = \pi r_0^2\left[(1+\epsilon_{p_0})^2 - 1\right] \quad (6)$$

where ϵ_{p_0} is the hoop strain in an equivalent-cylinder plane strain model of the motor cross section and r_0 is defined as in the thermal load case above. Based on our plane strain analysis, the strain level is nearly independent of the modulus over the range considered.

Pressure Drop Component

The area change due the pressure drop through the motor bore is calculated from the TEXGAP-3D analysis results and the uniform pressure plane strain analyses described above. the specific relationship used for this calculation is

$$\Delta A_{\Delta p} = \pi\left[r_0(z) + \Delta r_{\Delta p}(z)\right]^2 - \left\{\pi\left[r_0(z)\right]^2 - a_0)z) + \Delta A_{p_0}\right\}\left[1 + f(z)\Delta r_{\Delta p}(z)\right] \quad (7)$$

where $\Delta r_\Delta p(z)$ is the change in radial displacement at the bottom of the slot valley due to $\Delta p(z)$; $r_0(z)$ and $A_0(z)$ are as previously defined; and ΔA_{p_0} is given by Equation (6). The empirical function f(z) accounts for the effect of grain fin cross-section deformations, and was determined from the deformed and undeformed geometries using the TEXGAP-3D results at each axial station. As used in the structural model, $\Delta r_\Delta p(z)$ was calculated from

$$\Delta r_{\Delta p}(z) = \left[\Delta r_0(z)\right]\frac{(\Delta r)}{\left[\Delta r_0(z)\right]_{max}} \quad (8)$$

where $\Delta r_0(z)$ is the TEXGAP-3D radial deformation with the uniform-pressure component $\Delta r(z)|_{p=p_0}$ subtracted out, and Δr is the input strain amplitude.

Previous analyses of the Sparrow Mark 52 pressure spiking problem were based on axisymmetric ("2D") structural models which were incapable of providing the three-dimensional deformed shape of the propellant grain. As a result the analysts were forced to rely on an assumption termed the "rigid fin" assumption. According to this assumption, the fin cross-section does not deform, but simply translates toward or away from the motor centerline to conform to the radial deflection of the equivalent-cylinder 2D model. We used the rigid fin assumption implicitly in our thermal load and uniform pressure models, where we expected the resulting error to be small due to the essentially plane strain boundary conditions. We considered using the assumption for the pressure-drop component model as well, since it would have simplified the calculations. To determine whether a rigid fin assumption was acceptable, a "rigid fin" model was obtained from our 3D model by setting $f(z) = 0$ in Equation (10). The results (see Figure 10) show that the "rigid fin" assumption does not provide an accurate area determination. We therefore retained the empirical $f(z)$ representation of the ΔA-to-Δr relationship.

THE FLOW MODEL

The theoretical flow model we used was originally derived by Schapery [2] and was applied (in a somewhat simplified version) in earlier analyses of the Sparrow Mark 52 pressure spiking problem.

Based on the assumptions stated earlier along with the conservation of mass and momentum, the pressure drop

equation was found to be

$$\Delta p = p_0 - p = C_2 \left[0.5 \left(\frac{\overline{a}}{A} \right)^2 z^2 + \int_0^z a \frac{\overline{a}}{A^2} z dz \right] \quad (9)$$

where

$$C_2 = C_1 \left[\frac{A_t}{(L\overline{a}_L)} \right]^2 \quad (10)$$

$$C_1 = \frac{1}{\rho} \left(\frac{\dot{m}}{A_t} \right)^2 = p_0 \gamma \left[\frac{2}{(\gamma - 1)} \right]^{\left(\frac{\gamma+1}{\gamma-1} \right)} \quad (11)$$

and

$$\overline{a} = \frac{1}{z} \int_0^z a dz; \quad \overline{a}_L = \frac{1}{L} \int_0^L a dz \quad (12)$$

As before, a is the effective radius of the burning perimeter and p_0 is the motor head end pressure. The other variables are L = motor length, A_t = nozzle throat area, ρ = gas density, $\dot{m}$ = total mass flow rate, and γ = ratio of specific heats for the gas, the gas being the propellant combustion products. Note that if we assume the variation in the burning perimeter with axial distance to be negligible, we can set $a = \overline{a} = \overline{a}_L$, and Equation (9) simplifies to

$$\Delta p = C_1 \left[0.5 \left(\frac{A_t}{A} \right)^2 \left(\frac{z}{L} \right)^2 + \left(\frac{A_t}{L} \right)^2 \int_0^z \left(\frac{z}{A} \right)^2 z dz \right] \quad (13)$$

Equation (13) is the simplified version used by Schapery and other previous analysts. We compared the results using Equation 13 with those using Equation (9) and found them to be in close agreement except that the simplified model produces an abrupt "dip" in the pressure at the sudden expansion in the forward end of the grain, while the pressure calculated by the more complex model varies smoothly.

We implemented Schapery's model (Equations (9) to (12)) in our flow model by assuming a piecewise-linear variation with z for both a and A. At zero burnback distance, the flow analysis results show a reasonable agreement with the original Aerojet flow analysis results (labeled "Assumed Pressure" in Figure 11).

By repeating the flow analysis with different geometries, we were able to show that the difference between the Aerojet results and our zero-burnback results were caused by Aerojet's approximation of the motor port geometry as a constant-area duct.

Figure 11 shows that the expected burnback of 0.45 mm at a burn time of 0.36 ms produces a significant change in the pressure distribution, indicating that burnback must be included in a realistic analysis of the pressure spiking.

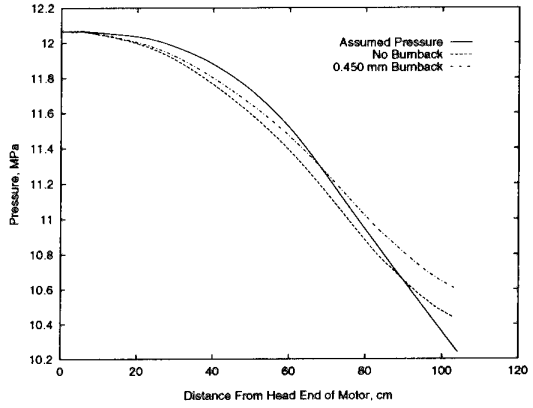


Figure 11. Initial Flow Analysis Results

Figure 12 shows the effects of area changes due to thermal load, uniform pressure, and pressure drop on the calculated pressure distribution for the nominal analysis conditions. From Figure 12, it is evident that the final calculated pressure distribution has a different shape from the assumed distribution, which violates one of our original assumptions. While we did not directly assess the impact of this lack of closure, we think it is minor.

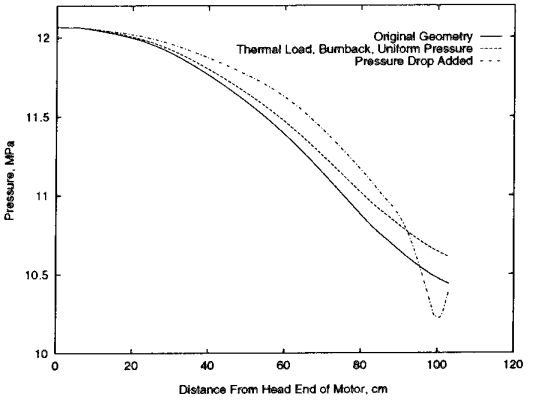


Figure 12. Flow Analysis Results at Nominal Analysis Conditions

RESULTS

Taking the maximum pressure drop from Figure 12 as the relevant parameter to compare to the nominal pressure drop in the original 3D structural model, we were able to attempt a solution of the nonlinear problem that defines the equilibrium pressure drop for the motor. The method used here was based on that used by Glick, Caveny, and Thurman [3] to evaluate the stability of a slotted-tube propellant grain using results from a water-table flow simulation and a propellant grain structural analysis. The method used was to first plot pressure drop as a function of the maximum value of the Δp component of radial displacement, as defined by the flow analysis. We then plotted the maximum Δp component

of radial displacement versus pressure drop, as determined by the structural model (i.e., Equation (1)), and determined where the curves intersect. Failure of the curves to intersect corresponds to an unstable condition that would lead to very large deformations and choked flow at the minimum-area point. This condition would produce a pressure spike.

Incorporation of Actual Mechanical Properties

The process described above is carried out in Figure 13 for a specific set of propellant modulus values based on data from a dissected Mark 52 motor.

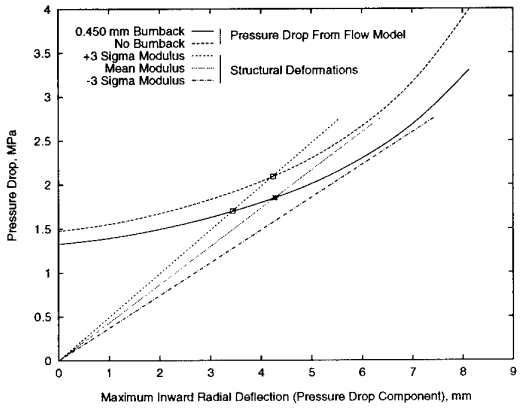


Figure 13. Analysis Results for Ignition at 71 ° C (Head-End Pressure = 12.07 MPa)

The propellant from this dissected motor was very soft. The modulus values were less than half the normally expected values over the entire relaxation spectrum. However, since this propellant (ANB-3109-2) softens with age, the modulus data from this motor (SN 3600646) was selected to obtain a conservative evaluation of the pressure spiking problem. A modified power law relaxation modulus function was determined from the relaxation modulus data using a curve fitting technique. Using this relaxation modulus function, the effective elastic modulus was calculated by carrying out the linear viscoelastic convolution integral for a strain history proportional to the motor pressure during a 71 °C ignition pressurization with a 36-ms duration. The procedure used is described in detail in Reference 4. The resulting modulus values (accounting for the error estimate produced by the curve fit) were

$$+3\ Sigma: \quad E = 2.35 MPa$$

$$Mean: \quad E = 1.76 MPa$$

$$-3\ Sigma: \quad E = 1.32\ MPa$$

Equation (1) is plotted in Figure 13 for the three different modulus values. As shown in Figure 13, the analysis would predict unstable deformations for the mean modulus value if burnback were ignored. However, for the burnback geometry, the analysis predicts only a small chance of instability (i.e., the modulus must be at or near the lower 3-sigma value to cause instability).

CONCLUSIONS

This analysis confirmed the potential for failure of the Sparrow Mark 52 rocket motor through large bore deformations leading to choked flow at the aft end of the propellant grain, supporting the results obtained previously by other investigators. The following specific conclusions are drawn based on our results:

(1) For the motor operating conditions and propellant properties used in this analysis, the structural deformation is marginally stable. Lower propellant modulus or higher burn rate (producing a higher head-end pressure) could trigger unstable deformation. A lower liner modulus would also increase the potential for instability.

(2) Because of the significantly higher deformations, the three-dimensional structural model leads to a substantially lower margin of stability than would be obtained with a two-dimensional structural model.

(3) The TEXGAP-2D/Approximate-3D computer code closely approximated the radial deformations obtained in the aft end of the motor from the TEXGAP-3D code. This result both corroborates the TEXGAP-3D results and shows the usefulness of the Approxi- mate-3D feature of TEXGAP-2D for analyses involving three-dimensional geometry.

REFERENCES

1. Leighton, R., "Quick-Look Structural Analysis Techniques for Solid Rocket Propellant Grains", AFRPL-TR-81-80, Air Force Rocket Propulsion Laboratory, Edwards AFB, CA May 1982.

2. Schapery, R. A., Texas A&M University, Private Communication, September 1983.

3. Glick, R. L., Caveny, L. H., and Thurman, J. L., "Internal Ballistics of Slotted-Tube, Solid-Propellant Rocket Motors," *j. Spacecraft,* Vol. 4, No. 4, April 1967.

4. Thrasher, D. I., and Corbett E., "An Analysis of a Solid Propellant Transient Viscoelastic Response under Motor Ignition Conditions", AFRPL-TR-81-80, Air Force Rocket Propulsion Laboratory, Edwards AFB, CA, January 1982.

Paper Number: 42
Discussor's Name: Dr. H. J. Buswell
Responder's Name: D. I. Thrasher

Question: Did you establish a minimum value in mechanical properties for the onset of ballistic spike on hot firing?

Answer: The lower three-sigma value given in the paper (1.32 MPa) would be a reasonable lower acceptable value for the effective modulus at peak ignition transient pressure at 160 degrees F. However, this is a computed value based on the relaxation modulus function and the propellant strain history during motor ignition. Further calculation would be required to relate this modulus value to another measure of the modulus (e.g., constant-rate initial modulus).

Paper Number: 42
Discussor's Name: G. S. Faulkner
Responder's Name: D. I. Thrasher

Question: Is it possible to avoid this age-out mechanism (and extend service life) by counter boring (slight amount of propellant removed) the aft-end of the charge?

Answer: This is a possible solution. In fact, this solution has been applied in several motors which encountered SBI during design and development, including Castor IV and the Titan IV solid rocket motor upgrade (SRMU). If the geometry were axisymmetric, the conservative fix would be to remove any propellant that intrudes (in the deformed condition) inboard of the undeformed flow channel surface. With the star cross-section, you'd remove an appropriate amount of propellant from the fin tips.

Paper Number: 42
Discussor's Name: Dr. H. J. Buswell
Responder's Name: D. I. Thrasher

Question: Have you measured the pressure drop along the motor bore?

Answer: Not on the Sparrow motor.

Chemical Safe Life Predictions for Cast Double Base Rocket Propellants

M.P. Sloan, S. J. Salsbury and G. M. Keeton
British Aerospace Defence
Royal Ordnance Rocket Motors
Kidderminster, Worcs. DY11 7RZ
U K

SUMMARY

The chemical stabiliser depletion rates of a number of Cast Double Base (CDB) propellants have been investigated by ageing at elevated temperatures. New values for the activation energy for para-nitro-N-methylaniline (pNMA) degradation have been calculated for formulations containing both lead and copper based ballistic modifier systems. These have been used to generate predictions of depletion during natural storage of service motors. These predictions were accurate within the limits imposed by the absence of detailed thermal history for the test rounds. Suggestions for future study are made.

1.0. GENERAL INTRODUCTION

The service life of double base rocket propellants is determined largely by the efficiency of the chemical stabiliser systems present in these formulations. The NO/NO_2 molecules produced by homolytic cleavage of the $CO\text{-}NO_2$ moiety, react with the chemical stabilisers rather than with other nitrate ester molecules. In the absence of chemical stabilisers, thermal stressing produces porosity followed by gas-cracking in double base propellants. If the thermal environment is severe or sufficiently prolonged, propellant combustion will be initiated. To ensure this cannot happen under manufacturing or service conditions a range of chemical stabiliser systems has been developed. The concentration of these materials, which are generally aromatic amines, can be easily monitored and the safe life of a propellant is often judged to be the time taken for the stabiliser content to fall to a given proportion of their initial value. A great deal is known about the detailed reaction mechanisms of chemical stabilisers [1,2] and the chemical kinetics of some systems have been studied extensively to enable accurate prediction of safe chemical life [3,4]. Such is the success of amine stabiliser systems that their use would generally prevent simple chemical stability from being the life limiting factor for a solid rocket propellant. It is more often the case that ballistic characteristics change during life, ultimately leading to deviation outside acceptable performance limits. This process can be related to the reactions of nitrate ester degradation products with ballistic catalysts and by this means propellant ballistic life may be influenced by the chemical stabiliser system employed.

Clearly any propellant formulation proposed for service should be demonstrated as possessing satisfactory safe chemical life. Whilst a number of alternative methods, such as differential scanning calorimetry and vacuum stability are available, stabiliser depletion is generally considered the most useful method. By measurement of depletion rates at different temperatures kinetic parameters can be calculated and used to generate life predictions. It has been proposed in the STANAG 4527 [see note 1] that a standardised test procedure be adopted for assessing the stabiliser consumption characteristics of nitrocellulose propellants. It is intended that this protocol should serve as a common method of chemical safe life prediction. The work described within this paper is aimed at determining the usefulness of the proposed general method for the range of CDB propellants.

1.1. CAST DOUBLE BASE PROPELLANTS; CHEMICAL STABILISER CHARACTERISTICS

The chemical stabiliser system used in CDB propellants is largely determined by the particular method by which this type of propellant is manufactured. A batch of casting powder is manufactured by solvent incorporation followed by extrusion. Casting powders produced by Royal Ordnance Rocket Motors (RO RM) generally contain the stabiliser para-nitro-N-methylaniline (pNMA) which is added in crystalline form to the incorporators at the start of manufacture. The finished casting powder batch is blended to give optimum compliance with the ballistic specification before being cast into the required rocket motor configuration by flow of casting liquid (desensitised nitroglycerine) followed by thermal cure. Another chemical stabiliser 2-nitrodiphenylamine (2NDPA) is added via the casting liquid.

The two stabilisers used serve different purposes in the propellant through its service life. The slow reacting 2NDPA is often considered to be the primary stabiliser [2] though in the presence of pNMA it is generally depleted at a low rate even in extreme thermal conditions. Indeed 2NDPA depletion is only significant where pNMA has been excluded from the formulation or has been fully depleted by accelerated ageing. The pNMA is sometimes considered to be the secondary stabiliser and there is evidence of it showing preferential stabilisation of reactions associated with insoluble gases [5]. Its inclusion does serve to reduce the level of gas evolution of CDB formulations as measured by Vacuum Stability Testing. In addition to the dual chemical stabiliser system described above, CDB propellants generally contain ballistic catalysts and rate modifiers. These are typically lead salts of hydroxy-substituted aromatic carboxylic acids though aliphatic salts or metal oxides of lead and/or copper may also be used. The precise combination in any given formulation is determined by the ballistic requirements of the application. It is known [5] that these materials can modify chemical stability and thereby the rate of chemical stabiliser depletion depending on the nature of the metal and the organic ligand present.

2.0. PROPELLANT COMPOSITIONS TESTED

A range of propellant samples covering both historic and current RO RM projects are being assessed as part of a private venture chemical stability research programme. This includes CDB/EMCDB (Elastomer Modified Cast Double Base) and EDB (Extruded Double Base) based on a range of nitrocellulose levels and nitrogen contents. An assessment of the effect on degradation rates produced by ballistic modifiers is included as an essential part of the investigation. The propellant types referred to in this paper are shown in Table 1.

Paper presented at the AGARD PEP Symposium on "Service Life of Solid Propellant Systems" held in Athens, Greece, 10-14 May 1996, and published in CP-586.

These samples are being subjected to prolonged storage at a range of elevated temperatures to enable calculation of rate constants and thereby activation energies. This data can then be used to predict in-service stabiliser depletion rates which can be checked against motors returned from service for surveillance programmes or for the purposes of disposal at the end of life.

3. EXPERIMENTAL

Propellant samples for calculation of kinetic parameters were manufactured using fully proofed batches of each formulation. The test pieces were stored in the form of a 100mm by 50mm by 10mm monolithic block which was tightly wrapped in aluminium foil to reduce surface plasticiser loss. All samples for chemical analysis were extracted from the bulk of the propellant block rather than from the surface. All materials met existing product specifications and were fully analysed initially to confirm compositional requirements. Samples for service life examination were recovered from disassembled motors and care was taken to ensure sample position was fixed for each test configuration. Motor history sheets relating to manufacture were used to determine the precise date of manufacture and dispatch. Service history including storage regimes were supplied by the respective service organisation. These records were of varying quality but in no case were they either specific enough for the round being examined or accurate enough for use in calculation of thermal history.

All ovens used for sample storage were regulated to within +/-0.2°C and all analysis was carried out using a Waters Ltd. Millennium HPLC unit; UV detector; C18 Radial Nova-pak column, running reverse phase.

4. RESULTS

4.1. CDB PROPELLANT STABILISER DEPLETION; GENERAL CHARACTERISTICS

A typical stabiliser content depletion profile for a lead modified propellant is shown in Figure 1. The depletion of the pNMA is matched quantitatively by the increase in its degradation product N-nitroso-pNMA (NO-pNMA). This increases steadily until the pNMA content falls below a detectable level. It is therefore possible to monitor the course of this reaction either by quantifying the loss of pNMA or the increase in its degradation product.

As the point of pNMA exhaustion approaches the depletion of the 2NDPA becomes more significant. Throughout the wide range of dual stabiliser CDB propellants manufactured at RO RM this sequence of reactivity is found, however the actual rate of stabiliser depletion is dependant on the detailed formulation.

4.2. CDB PROPELLANT STABILISER DEPLETION; THE EFFECT OF NITROGLYCERINE CONTENT

To obtain the mechanical properties required for particular applications it is possible to formulate CDB propellants having nitrocellulose to nitroglycerine ratios of anywhere between 2:1 for stiff, cartridge loaded applications and 1:3 for Elastomer Modified CDB propellants suitable for case bonding. Given the lower chemical stability of nitroglycerine (NG) compared with nitrocellulose [5] it might be expected that increasing nitroglycerine content would increase the rate of chemical stabiliser depletion. Two sample propellants (Compositions B and C) containing respectively the maximum and minimum NG content consistent with useful mechanical properties and sharing the same concentration of a standard aromatic lead ballistic modifier system were analysed during 60°C storage. The resultant pNMA depletion profiles are shown in Figure 2. The rates of pNMA consumption are similar with the higher NG propellant reacting slightly more slowly for much of the trial. It can be concluded that NG content is not a primary determinant of stabiliser depletion rate for CDB propellants of this type.

4.3. CDB PROPELLANT STABILISER DEPLETION; THE COMPARISON OF LEAD AND COPPER BALLISTIC MODIFIERS

The characteristics of a copper modified formulation (Composition D) are shown in Figure 3. This particular formulation was selected for study as the high burn-rate ballistic modifier combination used is considered the extreme in terms of general chemical stability of RO RM solid rocket propellants. The initial NO-pNMA content actually matches that of pNMA due to more significant degradation taking place during the manufacturing process than was the case for Composition A. Storage at an equivalent temperature produces very much more rapid pNMA consumption than the lead modified system, though again 2NDPA depletion becomes significant only when pNMA is no longer present. Once 2NDPA depletion does begin it is again faster than the lead based propellant but less dramatically so than was the case for pNMA. These differences are quantified in Table 2 and illustrated for pNMA depletion only in Figures 4 and 5. The large differences in consumption rates may relate to an earlier observation that different decomposition product gases are evolved depending on the ballistic modifiers used [6]. It has been proposed that copper may enable an alternative degradation pathway possibly via a copper (I) intermediate, though it should be noted that the copper complex used in this work was different [7]. Attempts to identify and isolate intermediate complexes have been unsuccessful so far and only the kinetic measurements attempted will be discussed in this paper.

4.4. KINETIC CALCULATIONS FOR TEST PROPELLANTS

The draft STANAG 4527 details the method of analysis recommended in accordance with the equation (1)

$$(1) \qquad k = \ln(a/(a-x))/t$$

where k = rate constant, t = reaction time, a = initial concentration of stabiliser, and x = the amount converted after time t. Should first order or pseudo first order kinetics be appropriate for the reaction in question then the plot of t against ln(a/(a-x)) should yield a straight line of slope -k. The

variation of k with temperature is described using the Arrhenius equation (2)

(2) $k = A \exp(-Ea/RT)$

where A = frequency factor, R = Gas constant, T = temperature and Ea = the activation energy for the reaction. A plot of ln k against the reciprocal of temperature should yield a straight line of gradient Ea/R. This has been done using the data generated across the temperature range between 40 and 80°C. Figures 6 and 7 show plots of pNMA consumption against time at 65.5°C for compositions A and D and for these data sets reaction rate constants could be calculated with an r^2 error of around 2%. At lower temperatures the degree of error was greater and it is not possible to be certain whether this reflected non-first order kinetic behaviour or the greater relative error in these analyses. It had been intended that analysis of NO-pNMA would serve to verify the kinetic data calculated from pNMA loss though the reaction rate constant plots, a typical one is shown in Figure 8, were not generally straight lines and consequently were not suitable for analysis. Again it is not clear whether this was a result of experimental inaccuracy or alternatively that a more complex reaction mechanism prevails and the assumption of first order kinetics is invalid. Arrhenius plots are shown derived from pNMA analyses in Figures 9 and 10. For the propellants under discussion the extent of 2NDPA depletion was insufficient across the range of test temperatures for meaningful calculation. It is intended that our continuing programme of ageing studies shall make this possible in the future.

5.0. COMPARISON OF PREDICTION WITH MEASURED DEPLETION RATES

The Arrhenius plots shown in Figures 9 and 10 were extrapolated to give a series of lower temperature rate constants for lead and copper modified propellants. These could then be compared with measured data derived from accelerated or natural life ageing. The storage of Compositions B and C for 84 days at 60°C resulted in a pNMA residual content of 62% of the original level. This compares well with a predicted residual of 64% using the 60°C rate constant extrapolated from Figure 9. Given that Compositions A, B and C use the same ballistic modifier system it is not surprising that a reasonably accurate prediction is possible. It should be noted the historic practice for double base propellants has been to use an activation energy of 86 kJ/mol for rate constant calculation whatever the detailed formulation.

It was originally expected that the choice of aliphatic or aromatic ligands would be a major determinant of pNMA depletion rate due to possible competition reactions involving ring nitration of aromatic modifiers by nitrate ester decomposition products. In fact use of the Composition A derived kinetic data led to reasonably accurate predictions for all the lead modified formulations tested. A very much more limited database exists for copper modified propellants and only one comparison was made. This is discussed in section 5.2.

5.1. ANALYSES OF CDB MOTORS RETURNED FROM SERVICE; GENERAL CONSIDERATIONS

The most significant use of the degradation rate constants extrapolated from the test propellants is in prediction of stabiliser depletion and thereby safe chemical life for service propellants. These predictions can then be compared with actual levels recovered from natural aged rocket motors returned from service for the purpose of in-service surveillance or at the end of service life. Unfortunately use of information derived from returned motors is not straightforward for reasons associated with actual munition life cycles and, more specifically the detailed nature of cast double base propellants. The most significant general factor is the lack of adequate thermal history of rocket motors during service. Even where magazine storage records are available for specific rounds these are rarely sufficiently accurate for meaningful analysis. The CDB process also introduces particular uncertainties regarding the actual initial stabiliser levels for a given round. The most significant of these are:

1. The thermal environment required for casting powder manufacture and propellant cure produces a significant depletion of pNMA. The precise extent of this is largely determined by the ballistic modifier combination employed.
2. Depending on detailed composition the casting powder may be saturated in pNMA which, when subjected to the casting liquid flow may be redistributed through the grain. The quantitative effect of this is low but not consistent throughout the grain.
3. The ratio between pNMA and 2NDPA present in each charge will vary slightly depending on the precise casting powder to casting liquid ratio produced by the casting.

All three of these effects are negligible for general purposes, however as it is not possible to sample each round entering service, a degree of uncertainty exists as to the exact stabiliser content after manufacture is complete. When a round is returned from service at the end of life or for surveillance it is a straightforward task to sample the propellant and measure the residual stabiliser content. However for actual service, as opposed to accelerated regime, absolute depletions hare been found to be low and the error induced by uncertainty over initial stabiliser content may be significant.

To overcome these problems RO RM have developed a protocol involving full analysis of degradation products at a number of points in manufacture. This enables calculation of accurate baseline data for use during service surveillance and at the end of service life for any given motor. In turn this allows predictions of accelerated trials to be verified or where predictions are significantly inaccurate may point to possible temperature dependence of degradation mechanisms.

5.2. ANALYSES OF MOTORS RETURNED FROM SERVICE; RESULTS

Compositions E to I were returned from service and analysed for residual stabiliser content. The results obtained are shown in Table 3. Their measured pNMA levels can be compared

with projections using the kinetic values calculated for Composition A. Projections obtained using the historic 86kJ/mol activation energy with original proof data are also shown. These compositions used lead based modifier systems as shown in Table 1. Composition J, a mixed copper and lead modified type, was removed from a temperature controlled RO RM facility and for this motor there is accurate knowledge of thermal history. It will be seen for all propellant types that there is a reasonable match between actual pNMA levels and those predicted for 10 and 20°C storage during service. Lack of accurate thermal history prevents more detailed comparison though the two temperatures selected are typical of UK storage and it is considered unlikely that the rounds E1,E2 and F/G saw any significant excursions outside this temperature range. The round containing propellants H/I spent the majority of its service life in an A2 climatic environment in an uncooled facility. Consequently it is thought that this round has experienced significant excursions beyond 20°C and this may explain the underestimate of pNMA depletion The absolute loss of pNMA was low for all the lead based propellants. After 14.5 years service, motor E was still compliant with the original specification value for a fresh propellant batch (0.75% minimum pNMA). Such a low rate of loss may indicate storage at low temperature for part of the missile life. It is considered unlikely that loss of chemical stabiliser would be the life limiting factor for the rocket motors E to I. Depending on detailed application, ballistic ageing or plasticiser migration/loss are more likely to produce deviation from specification before the standard RO RM minimum level, 30% of the initial total (pNMA + 2NDPA) is reached. For the copper modified composition J pNMA loss was more rapid though a high residual 2NDPA content remains. At this point no analyses are available to confirm pNMA levels over more extended periods of natural storage for this propellant and it is considered that further research on the detailed mechanism and reaction kinetics of copper modified systems should be carried out. For all the propellant types recovered from service the predictions made on the basis of the measured kinetic data were superior to the historic predictions.

6.0. CONCLUSION

It is clear that the safe chemical lives of pNMA stabilised CDB propellants using lead based modifier systems are long and are likely to be in considerable excess of fifteen years. Whilst the reaction rate constants derived experimentally match those produced by accelerated and natural storage programmes, the thermal history of propellants returned from service is not sufficiently known for a more detailed comparison to be justified. For copper based systems it is likely that a different reaction mechanism to that of lead modified propellants is taking place. It is certainly the case that pNMA depletion is much more rapid for these propellants. Whilst an experimentally derived depletion prediction was accurate for the single long term storage copper modified propellant tested it is not known whether the predictions will prove as generally useful as those for lead modified propellants. The activation energies measured, 102 kJ/mol and 115 kJ/mol for lead and copper modified systems respectively, are greater than the historically used 86kJ/mol standard but do yield accurate pNMA depletion predictions. It is considered that use of the experimental activation energies should replace the historic figure for lead and copper modified CDB propellants respectively. The origin of the current standard is not fully clear at present and it may relate to alternative grades of nitrocellulose to the 12.6% nitrogen used for RO RM CDB propellants. Experiments being carried out at present should determine whether or not this is the case.

REFERENCES

[1] J.M. Bellerby and M.H. Sammour "Stabiliser Reactions in Cast Double Base Rocket Propellants. Part I" Propellants, Explosives, Pyrotechnics 16, 235 (1991).

[2] A.J. Bellamy, M.H. Sammour and J. M. Bellerby "Stabiliser Reactions in Cast Double Base Rocket Propellants. Part IV" Propellants, Explosives, Pyrotechnics 18, 223 (1993).

[3] M.A. Bohn "Prediction of Life Times of Propellants" Propellants, Explosives, Pyrotechnics 19, 266 (1994).

[4] M.A. Bohn and F Volk, "Ageing Behaviour of Propellants Investigated by Heat Generation, Stabiliser Consumption and Molar Mass Degradation" Propellants, Explosives, Pyrotechnics 17, 171 (1992).

[5] D.G. Davies, "Chemistry of Propellant Stabilisers", PERME Technical Report 2 (1977).

[6] J.M. Bellerby and M.H. Sammour etc., "The Effect of Ballistic Modifiers on Gas Evolution from CDB Propellants" Symp. Chem. Probl. Connected Stabil. Explos, 9th 309 (1992).

[7] M. H. Sammour, Ph.D. Thesis, Royal Military College of Science, Shrivenham, Wilts., U. K. (1993).

[Note 1] STANAG 4527 serves to replace first draft STANAG 4480 'PROCEDURE FOR ASSESSMENT OF CHEMICAL LIFE AND TEMPERATURE DEPENDENCE OF STABILISER CONSUMPTION RATES FOR NITRO-CELLULOSE BASED PROPELLANTS".

TABLE 1

CDB PROPELLANT COMPOSITIONS

Composition	NC:NG	Ballistic Modifier Combination
A	1:2.4	4% aromatic lead (complex 1)
B	1:3.2	4% aromatic lead (complex 1)
C	1:1.3	4% aromatic lead (complex 1)
D	1:1.1	6% copper (complex 1)
E	1:1.08	3.3% lead 50/50 aromatic/aliphatic (complex 2)
F	1:2.4	2.2% aromatic lead (complex 3)
G	1:0.97	3.5% lead 50/50 aromatic/aliphatic (complex 2)
H	1:1.03	2.8% aromatic lead (complex 1)
I	1:1.5	3.2% lead 50/50 aromatic/aliphatic (complex 2)
J	1:0.4	4.55% lead/copper complex

TABLE 2

COMPARISON OF LEAD AND COPPER BALLISTIC MODIFIER DEGRADATION REACTION RATES

COMP.	pNMA DEPLETION FACTOR (% per day)				
	80°C	70°C	65.5°C	51.5°C	40°C
A	0.011	0.0075	0.0043	0.00075	0.00033
D	0.08	0.022	0.015	0.0027	0.00067
COMP.	**NO-PNMA DEPLETION FACTOR (% per day)**				
	80°C	70°C	65.5°C	51.5°C	40°C
A	0.012	0.0095	0.006	0.00083	0.00039
D	0.077	0.021	0.018	0.0033	0.00056
COMP.	**2NDPA DEPLETION FACTOR (% per day)**				
	80°C[1]	70°C[1]	65.5°C	51.5°C	40°C
A	0.0034	0.0023	[2]	[2]	[2]
D	0.0046	0.0037	[2]	[2]	[2]

[1] As measured after point of pNMA exhaustion
[2] No significant 2NDPA depletion recorded

TABLE 3

COMPARISON OF PREDICTED AND ACTUAL SERVICE PROPELLANT STABILISER DEPLETION

Composition	Age (Years)	Initial Stabiliser Content pNMA %	Initial Stabiliser Content 2-NDPA %	Final Stabiliser Content pNMA %	Final Stabiliser Content NO-pNMA %	Final Stabiliser Content 2-NDPA %	Calculated pNMA Content Storage Temperature % at 10°C	Calculated pNMA Content Storage Temperature % at 20°C	Calculated pNMA Content Storage Temperature % at 10°C	Calculated pNMA Content Storage Temperature % at 20°C
							Ea=102kJ/mol		Ea=86kJ/mol	
E MOTOR 1	14.5	0.83	0.30	0.79	0.08	0.32	0.80	0.69	0.74	0.53
E MOTOR 2	14.5	0.87	0.30	0.83	0.08	0.30	0.83	0.72	0.78	0.53
F BOOST	4.9	0.58	0.28	0.53	0.09	0.31	0.57	0.54	N/A	N/A
G SUSTAIN	4.9	0.60	0.28	0.53	0.11	0.31	0.59	0.56	N/A	N/A
H BOOST	11.3	0.67	0.32	0.52(2)	0.14	0.33	0.65	0.58	0.59	0.40
I SUSTAIN	11.3	0.64	0.31	0.51(2)	0.13	0.28	0.61	0.55	0.58	0.44
							Ea=115kJ/mol		Ea=86kJ/mol	
J (Cu type)	6.7	0.61	1.01	0.42	0.22	0.96	0.57	0.43(1)	0.30	0.00

Using Ea = 102 kJ/mol (as calculated for lead- modified CDB) (1) Actual storage temperature known to be 16-21°C
Using Ea = 115 kJ/mol (as calculated for copper- modified CDI(2) Service life in A2 climate
N/A; Directly comparable kinetic data not available

FIGURE 1, 70°C STORAGE
LEAD MODIFIED CDB DEPLETION CHARACTERISTICS

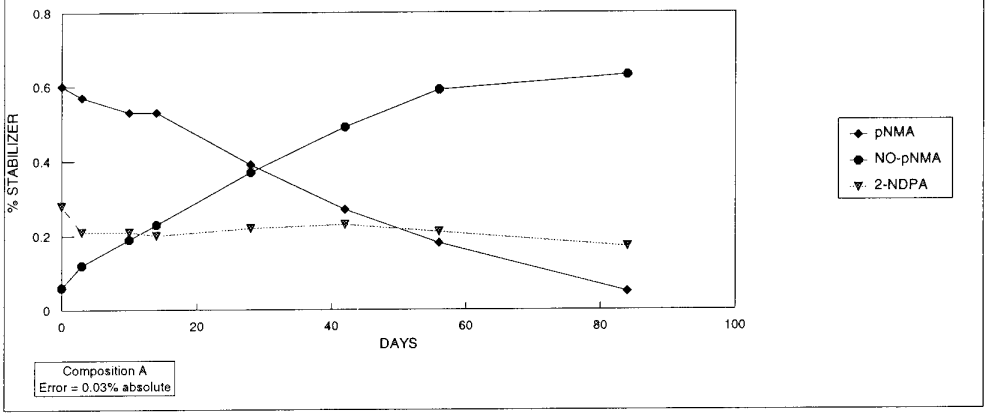


FIGURE 2
THE EFFECT OF NG CONTENT ON PNMA DEPLETION

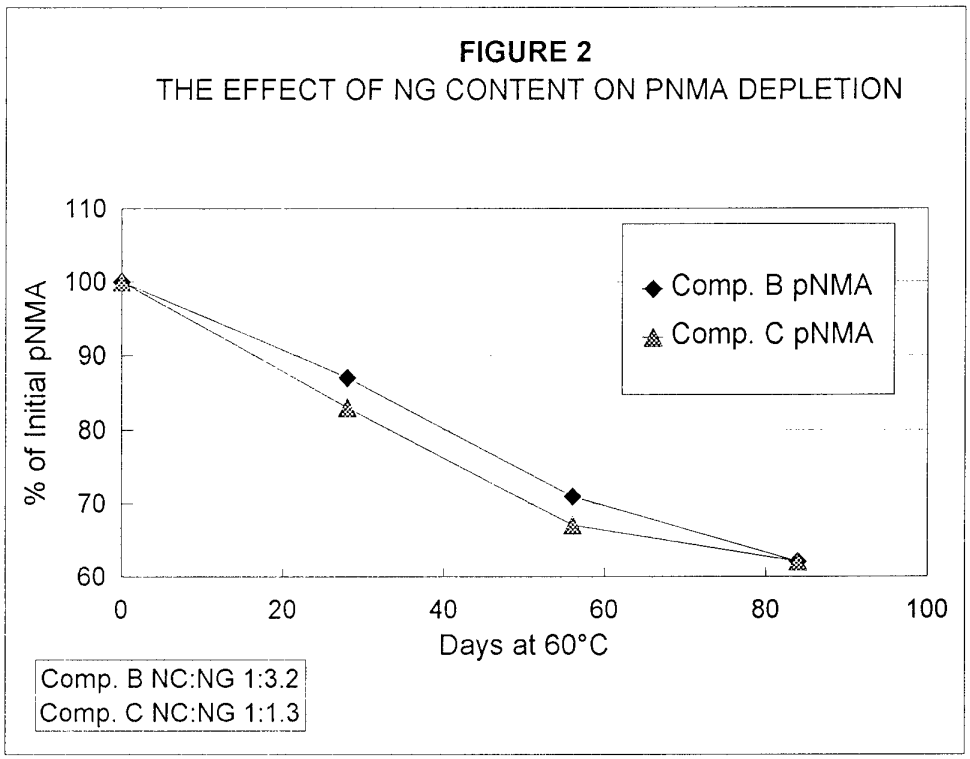


FIGURE 3, 70°C STORAGE
COPPER MODIFIED CDB DEPLETION CHARACTERISTICS

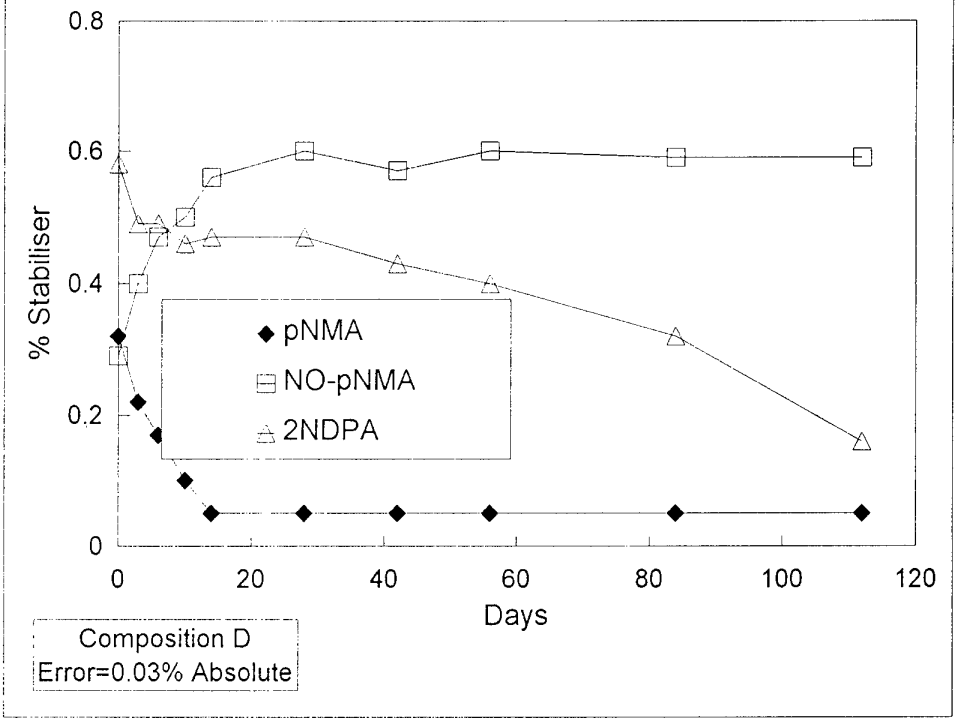


FIGURE 4

PNMA DEPLETION IN PROPELLANT A

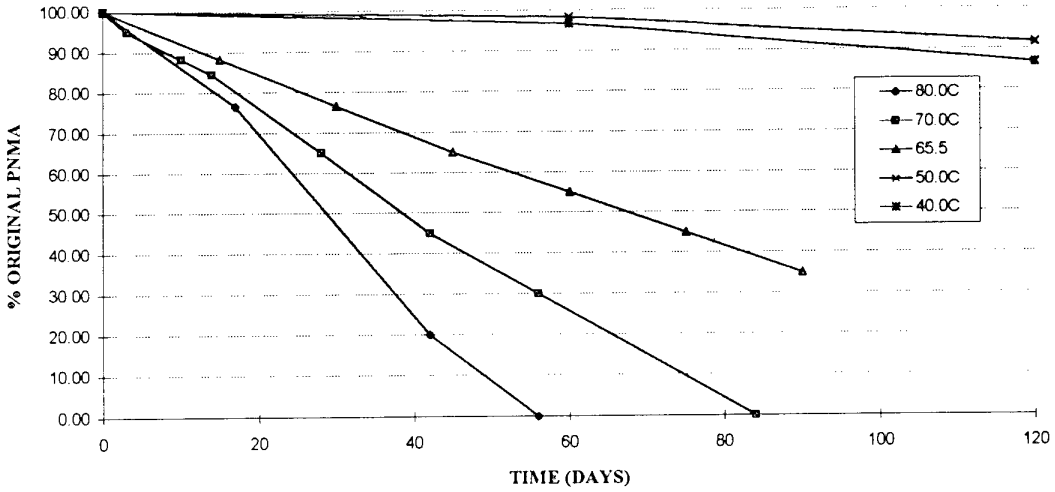


FIGURE 5

PNMA DEPLETION IN PROPELLANT D

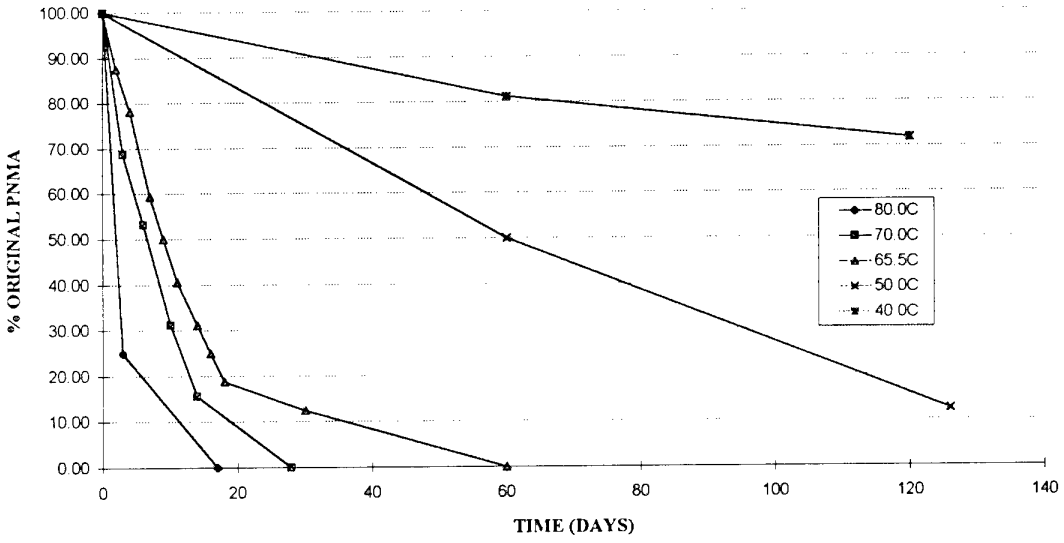


FIGURE 6

pNMA DEPLETION AFTER STORAGE AT 65.5°C

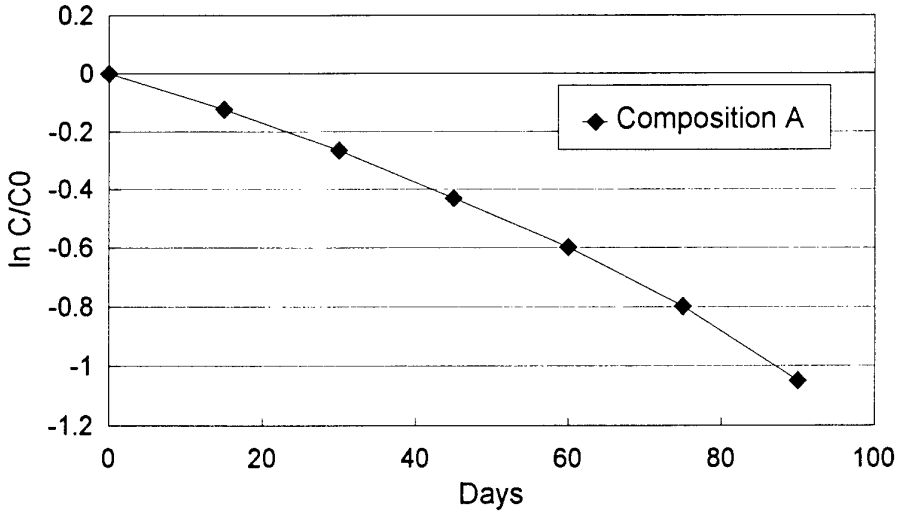


FIGURE 7

pNMA DEPLETION AFTER STORAGE AT 65.5°C

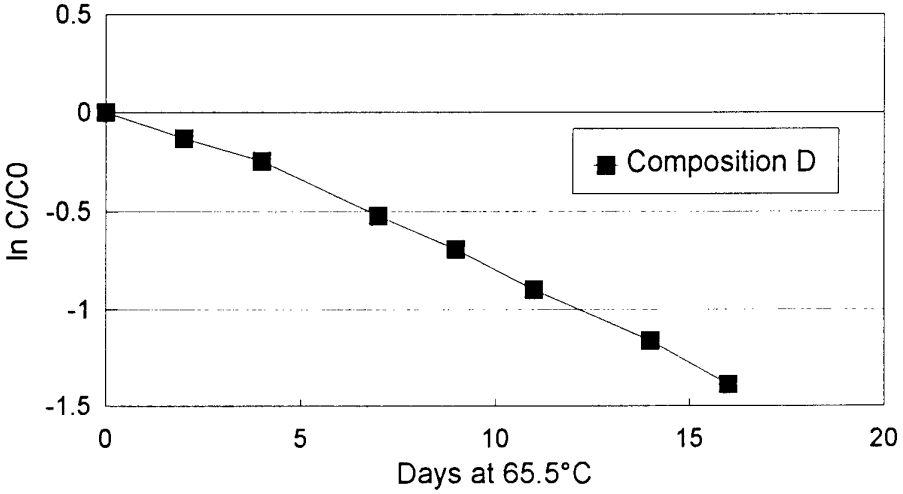


FIGURE 8
INCREASE IN NO-pNMA WITH STORAGE AT 65.5°C

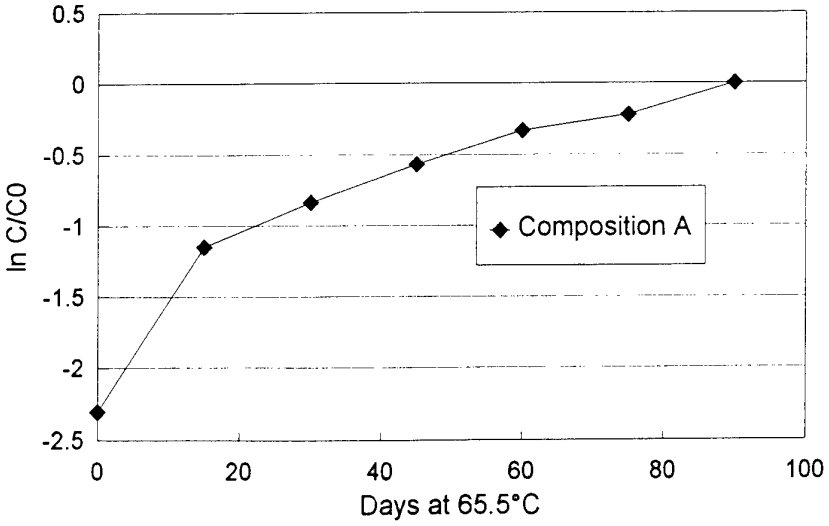


FIGURE 9
ARRHENIUS PLOT FOR pNMA DEPLETION

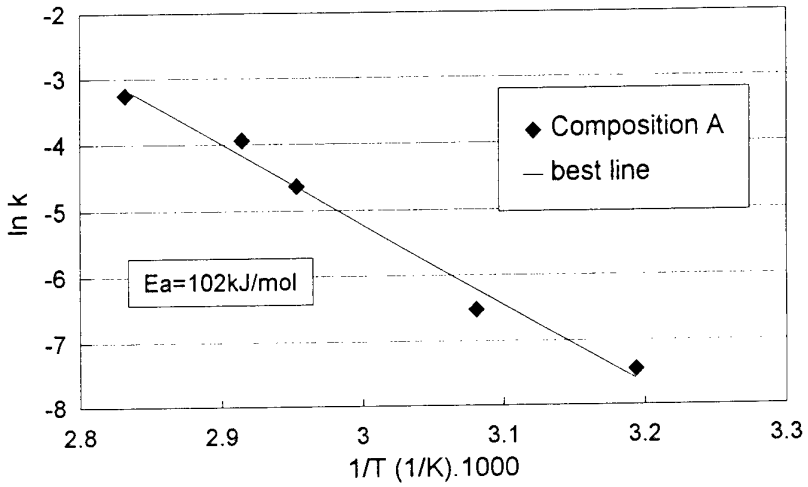
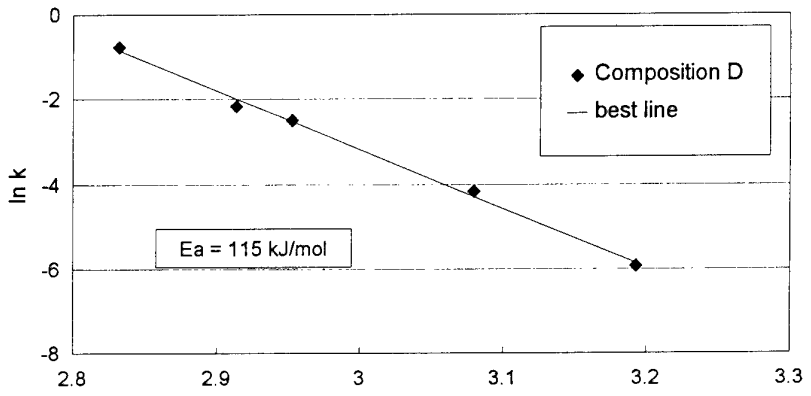


FIGURE 10
ARRHENIUS PLOT FOR pNMA DEPLETION



Contraintes opérationnelles et durée de vie des systèmes propulsifs pour missiles tactiques Particularités des propulseurs à structure composite

Norbert Laurençon
Société Européenne de Propulsion
Le Haillan - BP 37
F33165 Saint Medard en Jalles Cedex
(France)

1. RESUME

Entre 1970 et 1980 la SEP a réalisé de nombreux essais permettant de caractériser et de tester l'emploi des matériaux composites sur les systèmes propulsifs utilisés pour les missiles stratégiques, préstratégiques et tactiques.

Entre 1980 et 1988 la SEP a d'autre part réalisé les développement des propulseur des missiles S530D et Mistral. Elle a ainsi acquis une bonne expérience concernant les contraintes enregistrées lors de la vie opérationnelle des propulseurs des missiles tactiques. Leur prise en compte dans les développements des moteurs a ainsi permis d'améliorer et d'adapter les performances des matériaux et des architectures pour les systèmes propulsifs.

Dans cette communication nous présentons tout d'abord la méthode d'assemblage structural utilisée pour la réalisation des propulseurs S530D et Mistral compte tenu de ses particularités et de son influence potentielle sur le vieillissement des systèmes propulsifs utilisant des structures bobinées verre, kevlar et carbone.

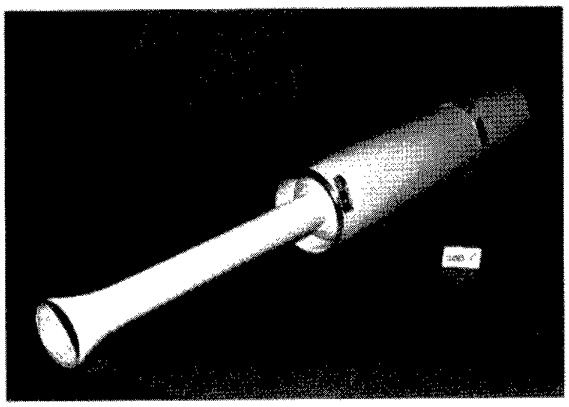
Les particularités liées aux propulseurs à structures composites bobinées et les risques spécifiques encourus au cours de la vie opérationnelle seront également présentés. Les actions préventives mises en place au niveau de la conception et les résultats connus sont résumés.

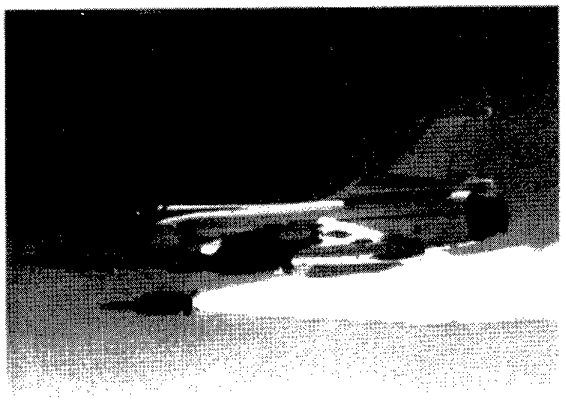
La méthodologie et les techniques utilisées en cours des développements des propulseurs pour garantir l'absence de problème seront également développées avec les résultats obtenus.

Enfin les simulations réalisées pour obtenir le plus vite possible une première approche des mécanismes de vieillissement des matériaux composites font l'objet de la dernière partie de cette communication. On insistera tout particulièrement sur la nature des essais mis en oeuvre et sur les méthodologies utilisées.

2. INTRODUCTION

C'est en 1978 que la SEP a obtenu un contrat pour développer le moteur du missile air-air S530D (Photo 1).



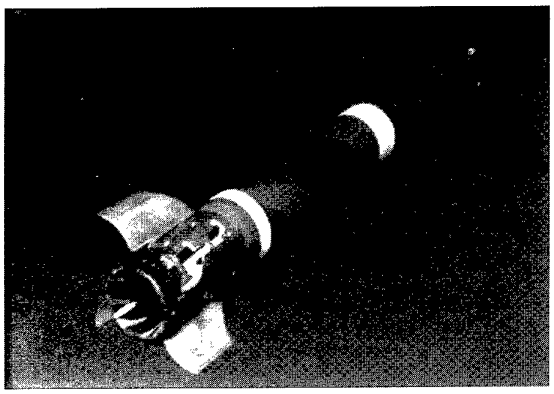


Tir en vol du missile S530D

L'obtention de ce contrat faisait suite à plusieurs démonstrations réalisées pour tester l'utilisation des matériaux composites sur les parties structurales des moteurs de missiles tactiques.

Deux années plus tard, en 1980, les spécifications émises pour le développement du missile Mistral (Photo 2) particulièrement contraignantes en ce qui concerne la masse de l'ensemble propulsif ont également conduit SEP à proposer avec succès, l'utilisation de matériaux composites bobinés pour la réalisation de la structure du moteur principal de ce missile.

Paper presented at the AGARD PEP Symposium on "Service Life of Solid Propellant Systems" held in Athens, Greece, 10-14 May 1996, and published in CP-586.



Propulseur MISTRAL



Tir en vol du missile MISTRAL

Le développement de ces deux systèmes propulsifs et leur qualification (obtenue en 1986 pour le moteur du S530D, et en 1988 pour celui du Mistral) ont confirmé que les matériaux composites permettaient d'obtenir des gains de performances significatifs pour les moteurs des missiles tactiques et possédaient les qualités nécessaires pour bien répondre aux contraintes opérationnelles prévues au cours de la vie de ce type d'engin.

Dix années plus tard, le suivi réalisé sur les missiles en opération confirme également que l'emploi des matériaux composites bobinés est bien adapté pour une utilisation dans ce domaine.

Cette note présente :

- l'architecture des propulseurs ainsi que les protections choisies pour garantir l'absence de dégradation des systèmes propulsifs au cours de la vie du missile.
- les principaux essais réalisés en développement et depuis le début de la fabrication de ces moteurs pour garantir l'absence d'incident majeur.
- les méthodes d'essais employées pour démontrer la qualité des matériaux choisis et des technologies utilisées.

3. ARCHITECTURE ET METHODE DE FABRICATION DES MOTEURS S530D ET MISTRAL - EXAMEN DE LEUR INFLUENCE POTENTIELLE SUR LA DURÉE DE VIE DU PROPULSEUR

Dans les technologies habituellement employées pour la fabrication des moteurs à propergol solide on réalise tout d'abord le corps de propulseur chargé (CPC) en coulant le propergol dans la structure protégée. Puis on termine l'assemblage du propulseur par la mise en place de l'allumeur et de la tuyère sur ce CPC.

L'assemblage structural modifie cette séquence classique et permet d'enchaîner les opérations de fabrication de la façon suivante :

- réalisation d'une protection thermique,
- coulée du chargement à l'intérieur de cette protection thermique maintenue par des outillages spécifiques nécessaires pour cette opération,
- réalisation de la structure bobinée autour du chargement protégé.

Les étapes sont les suivantes (voir schémas 1 et 2 et tableau 1)

L'emploi de matériaux composites bobinés (structure carbone/kevlar/époxy) et la technologie d'assemblage structural présentée ci-dessus ont constitué deux innovations importantes pour ces deux programmes.

Ainsi tout au long du développement le vieillissement du propulseur, sa résistance aux conditions opérationnelles spécifiées ont constitué un souci constant et pour lequel des essais préalables ont été effectués.

3.1 Analyse des opérations d'assemblage structural

L'assemblage structural comporte des étapes dont l'enchaînement est susceptible de modifier le comportement du propulseur au cours de sa vie opérationnelle.

Le tableau 2 montre comment ces étapes ont été analysées ainsi que les principales conclusions obtenues.

3.2 Analyse de l'emploi des matériaux composites et précautions prises en développement

L'emploi de matériaux composites bobinés avait fait l'objet, avant leur utilisation pour le développement du S530D et du Mistral, de caractérisations détaillées, dans le cadre de leur emploi pour les engins de la force stratégique française.

Des caractérisations complémentaires ont toutefois dû être effectuées pour prouver que les conditions opérationnelles des missiles tactiques (domaines de température et d'hygrométrie, agressions externes différenciées par rapport aux missiles stratégiques) n'affectaient pas la durée de vie des moteurs.

Etapes	S530D	MISTRAL
1	Fabrication de la protection thermique élastomère et mise en place de cette dernière dans un outillage de maintien	Fabrication de la protection thermique structurale et équipement de celle-ci avec les outillages nécessaires pour la coulée.
2	Réalisation du chargement	Réalisation du chargement
3	Collage du fond rallonge sur le chargement protégé et mise en place de l'axe de bobinage	Collage du fond avant et du fond arrière sur la protection thermique chargée.
4	Bobinage de la structure sur le chargement équipé, assemblage des jupes équipées des cadres, puis polymérisation	Bobinage de la structure sur le chargement équipé puis polymérisation
5	Contrôle en pression (MEOP)	Contrôle en pression (MEOP)
6	Assemblage de la tuyère, de l'allumeur et finition du propulseur (opérations de contrôle et de peinture)	Assemblage des parties AR, de l'allumeur, et finition du propulseur (opérations de peinture et de contrôle)

Tableau 1

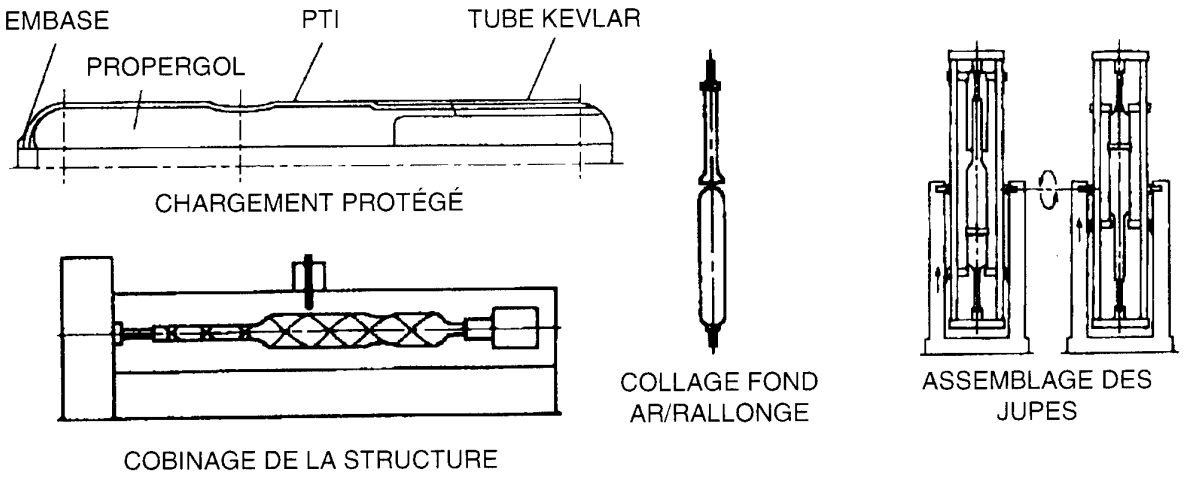


Schéma 1 : Réalisation Moteur S530D

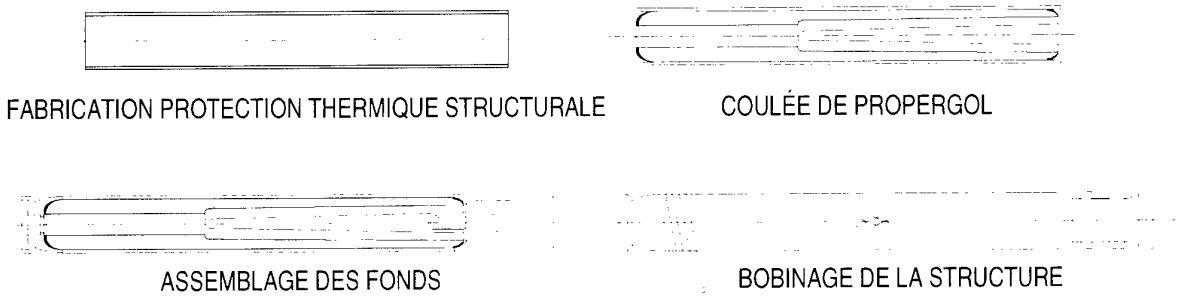


Schéma 2 : Réalisation du MISTRAL

Analyse des opérations d'assemblage structural

Risque	Analyse ou essais réalisés	Situation - conclusions
Risque lié à la coulée du propergol dans une protection thermique libre (non liée à la structure)	• Dossier de calcul réalisé au début du développement • Suivi du propergol lors des essais de vieillissement réalisés.	Facteur plutôt favorable à un bon vieillissement du propergol. En effet les possibilités de relaxation de contraintes lors du refroidissement après cuisson sont facilitées par cette configuration.
Risque de dégradation du propergol lors du bobinage ou de l'assemblage	• Radiographie des liaisons et du propergol • Endoscopie unitaire du canal central • Examen détaillé du propergol et de ses caractéristiques lors des essais de vieillissement • Travail en hygrométrie contrôlée • Radiographies détaillées avant et après mise en pression du chargement	Aucune dégradation ou évolution anormale des propriétés du propergol et des propulseurs n'a été enregistrée - au cours des opérations de vieillissement accéléré - au cours des tirs réalisés après 3 à 6 ans de durée de vie opérationnelle
Mise en pression (MEOP) du propulseur terminé (avec propergol) lors du contrôle final du moteur	• Dossier de calcul permettant de justifier l'absence de dégradation • Découpes d'éprouvettes dans le chargement et vérification de leur propriétés après mise en pression	Mêmes observations que ci-dessus

Tableau 2

3.2.1 Essais préliminaires réalisés en cours du développement sur le S530D et le MISTRAL

Au tout début du développement nous avons lancé des essais de vieillissement accéléré sur les propulseurs (conditionnement 3 et 6 mois à 50 °C).

Pour les S530D un premier essai a montré la nécessité de protéger le propergol PBCT de toute pollution (humidité par exemple) susceptible de provenir de dégazage de matériaux des parties AR.

Après correction de ce problème aucune anomalie n'a été détectée lors des tirs au banc réalisés aux températures extrêmes (-45 °C + 60 °C) sur les propulseurs ayant subi des épreuves de vieillissement en température.

On notera que tout au long des épreuves les variations d'hygrométrie et de pression ont été enregistrées grâce à un outillage spécifique développé par SEP.

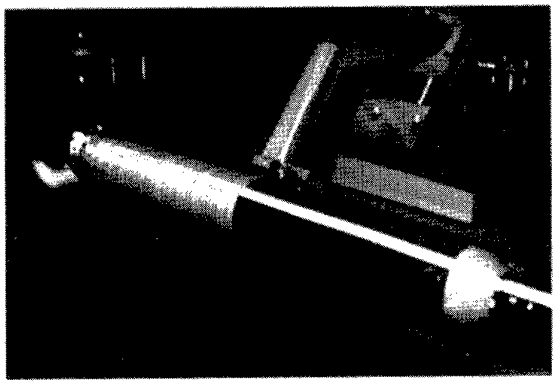
3.2.2 Expérience SEP et précautions prises lors de la conception

Notre expérience, ainsi que les essais réalisés sur éprouvettes avaient montré la nécessité de protection contre l'humidité des matériaux utilisant du kevlar, du carbone ou du verre.

Dans ce cadre, bien que les spécifications aient été peu différenciées le propulseur du missile S530D accroché sous avion présentait plus de risque potentiel que celui du Mistral dont la vie opérationnelle est prévue en tube.

Sur les deux propulseurs les précautions suivantes ont été prises lors de la conception afin d'éviter toute évolution anormale en vieillissement pour le propergol et l'ensemble des matériaux composites employés :

- mise en place d'obturateurs à l'arrière et de joints à l'avant, permettant de protéger le propergol contre l'humidité et contre toute pollution pouvant provenir du dégazage des matériaux employés sur les parties AR ou des conditions d'environnement du missile.
- mise en place sur la partie virole au cours de la réalisation de la structure bobinée d'un feuillard d'aluminium permettant une barrière efficace contre l'humidité (voir photo 3).
- mise en place, après l'opération de mise en pression (opération 5 tableau 1), d'un vernis "VE 10" formulé spécifiquement par SEP permettant de colmater toutes les craquelures de la matrice époxy susceptibles de se produire pendant cette opération de mise en pression.
- mise en place d'une peinture extérieure permettant d'obtenir la couleur souhaitée mais jouant également un rôle dans la protection contre l'humidité.
- mise en place de produits d'interposition du type isolant entre les parties métalliques et les matériaux composites à base de carbone pour éviter tout couple galvanique.



Structure bobinée d'un feuillard d'aluminium

4. ESSAIS REALISES PERMETTANT DE VALIDER LA CONCEPTION ET LES MATERIAUX EMPLOYES POUR LES PROPULSEURS

Le cas du S530D étant, comme expliqué ci-dessus, le plus pénalisant nous présentons ci-après les essais réalisés sur ce propulseur.

Les essais ont été réalisés en ambiance durcie. La majorité de ceux-ci sont issus des conditions décrites dans le GAM T13. Leur application au S530D a fait l'objet d'une procédure spécifique fournie par le maître d'oeuvre missile.

4.1 Description des méthodologies d'essais

Ces essais sont décrits dans les planches 1 et 2 ci-jointes.

4.2 Essais et résultats obtenus

4.2.1 Au cours du développement une structure inerte a été soumise à l'ensemble des essais décrits sur les planches 1 et 2

L'hygrométrie et la pression interne étaient enregistrées tout au long des essais.

L'absence de dégradation des propriétés a été démontrée par la pression de rupture de cette structure identique à la moyenne des essais réalisés pour la démonstration du bon dimensionnement.

Aucune variation d'hygrométrie significative n'a été décelée au cours des suivis, garantissant ainsi l'absence de risque de dégradation du propergol et des liaisons.

4.2.2 Au cours de la qualification un propulseur a également subi l'ensemble des essais décrits planches 1 et 2

Les observations dimensionnelles et radiographiques réalisées après les épreuves et les résultats nominaux du tir au banc ont confirmé la qualité satisfaisante du propulseur.

5. VIEILLISSEMENT ACCELERE PERMETTANT DE VALIDER UNE DURÉE DE 6 ANS SUR LE PROPULSEUR S530D

Trois essais successifs ont été réalisés pour simuler 6 ans de durée de vie et vérifier la qualité du propulseur à l'issue des épreuves.

5.1 Cycle retenu pour réaliser le vieillissement accéléré

Ce cycle a été choisi en fonction de l'expérience de nombreux intervenants dans le programme. (responsables opérationnels, laboratoires étatiques, services techniques de la DGA, MATRA et SEP).

Il comprend les épreuves du type suivant enchaînées et reconnues pour simuler un an de durée de vie :

- épreuve en température (partie haute du domaine d'emploi),
- cycles thermiques avec conditions d'hygrométrie permettant de simuler le givre à froid et la chaleur humide à chaud,
- brouillard salin.

5.2 Contrôles réalisés pendant les essais

L'utilisation d'un outillage spécifique réalisé par SEP pendant le développement a permis de vérifier l'évolution de l'hygrométrie dans le propulseur tout au long des épreuves. De même après chaque épreuve des contrôles visuels et/ou radiographiques permettaient de noter toute évolution du propulseur.

5.3 Principaux résultats obtenus

Trois essais réalisés pour simuler 6 ans de durée de vie :

- un premier propulseur a subi des cycles d'essais permettant de simuler 3 ans de durée de vie. Les contrôles (visuel, dimensionnel, radiographique) ainsi que le tir au banc nominal ont confirmé l'absence de dégradation des performances du propulseur,
- un deuxième propulseur ayant subi des cycles d'essais permettant de simuler 6 ans de durée de vie a également été tiré au banc avec des résultats nominaux,
- un troisième propulseur a été expertisé après les mêmes épreuves simulant 6 ans de durée de vie.

La méthode d'expertise, mise au point en développement, a consisté à découper le propulseur dans des zones où le coefficient de sécurité calculé donne des résultats minimum.

Après découpe des éprouvettes ont été réalisées (voir photo 4) pour vérifier :

- la bonne tenue de l'ensemble des liaisons (à l'intérieur du composite, entre composite et protection thermique et au niveau du chargement),
- le contrôle des propriétés mécaniques du propergol et la vérification du coefficient de sécurité du chargement en fonction des caractéristiques obtenues.

La comparaison des résultats obtenus pendant le développement avec ceux obtenus au cours de cet essai a montré qu'il n'y avait pas d'évolution importante des caractéristiques et que les coefficients de sécurité restaient supérieurs aux valeurs spécifiées.

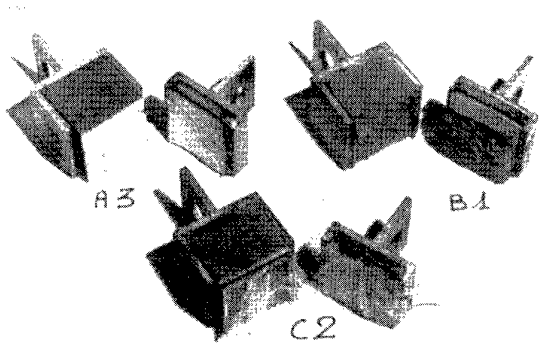


Photo 4

6. CONCLUSION

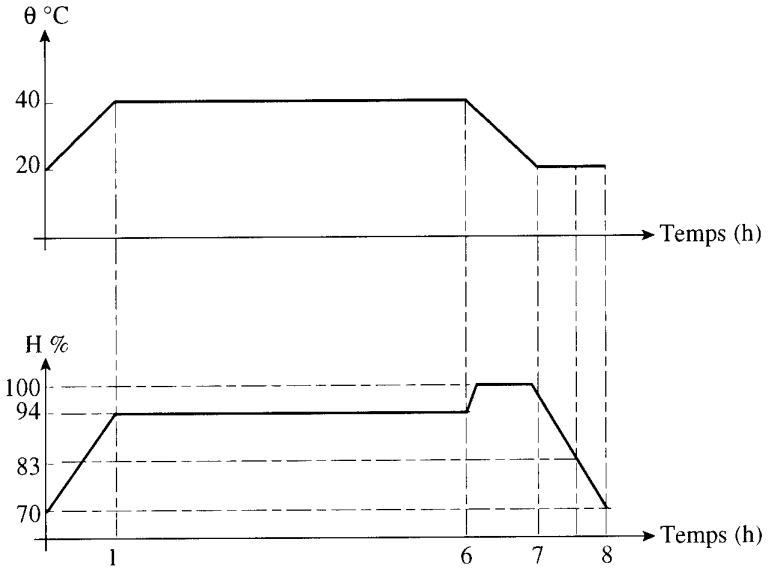
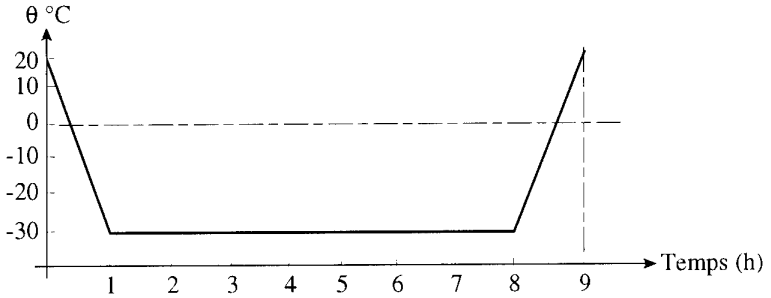
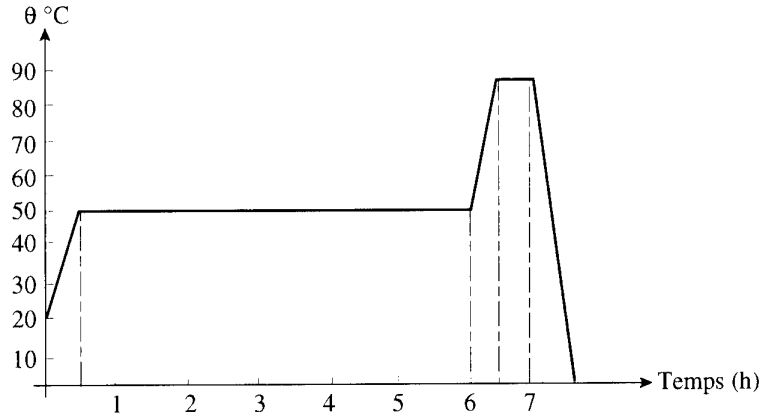
Au cours de leur développement les propulseurs des missiles S530D et Mistral ont fait l'objet d'essais permettant de valider l'architecture composite utilisée et de prouver l'absence de dégradation importante des performances en vieillissement.

Les épreuves de vieillissement trois et six mois en température réalisées en tout début de développement ont permis de lever les risques majeurs.

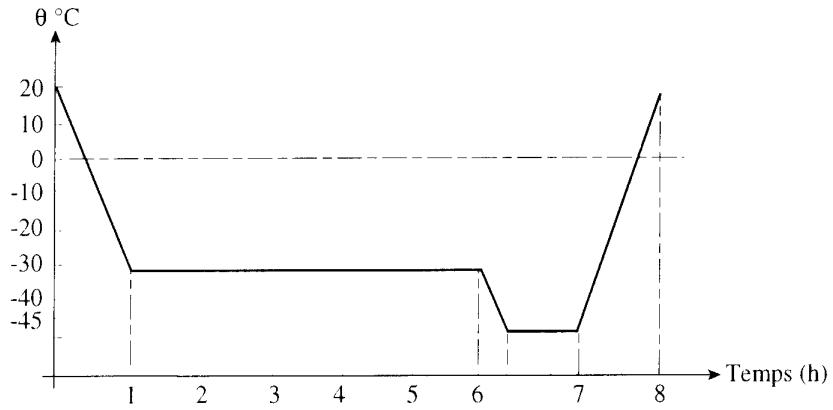
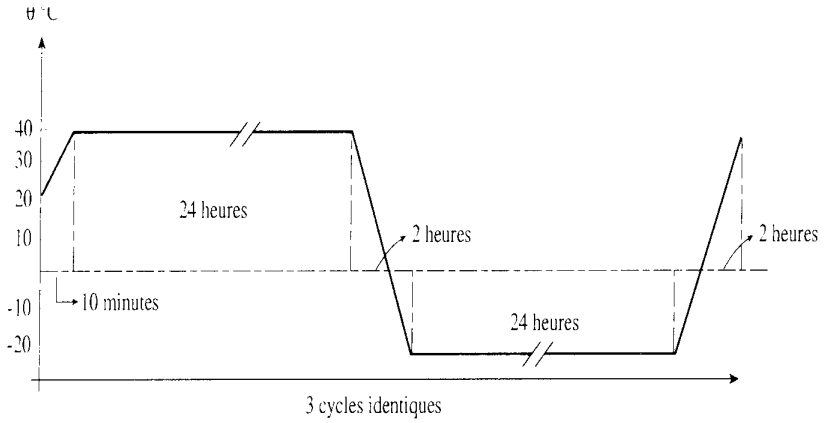
Les épreuves spécifiques faites en qualification ou par la suite en vieillissement accéléré avec épreuves combinées ont confirmé les résultats initiaux.

Les renseignements obtenus auprès du maître d'oeuvre MATRA ainsi qu'auprès des services techniques et opérationnels confirment que l'emploi du missile dans les forces n'entraîne pas de contraintes ou de difficultés particulières, ce qui, plus globalement, permet de bien valider les matériaux et les technologies choisies pour la propulsion.

Essais d'environnement climatique et thermique
Planche 1

Essai	Description
Chaleur humide	
Epreuve d'altitude	
Brouillard salin	144 heures à 35 °C concentration Nacl 5 %
Pluie artificielle	Aspersion au jet d'eau pendant 2 minutes sur chacune des 4 génératrices
Exposition chaud	

Essais d'environnement climatique et thermique
Planche 2

Essai	Description
Exposition froid	
Contamination par fluide et vent de sable	- Fluides : Huile moteur Antigel Huile hydraulique Kérosène Chlorure de Méthylène Graisses Aspersion des propulseurs avec successivement les fluides ci-dessus, puis séjour de 48 heures à 50 °C. Un nettoyage au White Spirit était réalisé avant aspersion avec le fluide suivant. - Vent de sable : 3 heures sur chaque axe ; vitesse de l'air 3 à 10 m/s ; sable 60 g/m^3
Chocs thermiques	

Programme général d'essais de vieillissement Application à un missile Air-Sol

Alain CHEVALIER
AEROSPATIALE Missiles
2 à 18, rue Béranger - BP 84
92322 Châtillon Cedex - France
et
Jean Marie LAURENT
CELERG
381, avenue du Général de Gaulle
92142 Clamart Cedex- France

1 . RESUME

Le but des essais de vieillissement est de procéder à une surveillance régulière de l'évolution des performances et caractéristiques du système d'arme dans le temps, de manière à pouvoir garantir, pendant toute la durée de vie du système, les performances et les disponibilités contractuelles, en permettant le déclenchement suffisamment tôt de mesures conservatoires éventuellement nécessaires (recyclage, fabrication de matériels neufs) au cas où certains matériels arriveraient à péremption avant le délai prévu.

Trois grandes catégories d'essais de vieillissement peuvent permettre cette surveillance :

- les essais de vieillissement accéléré,
- les essais de vieillissement naturel réel,
- les essais de vieillissement naturel simulé.

Cet exposé présentera les choix réalisés ainsi que les principes et le contenu du programme d'essais retenu dans le cadre de l'accélérateur d'un missile Air Sol.

2 . ABSTRACT

The purpose of the ageing tests is to perform a regular monitoring of the development of the weapon system's performances and characteristics in the course of time in order that performances and the contractual availabilites during the whole lifetime of the system can be guaranteed so as to initiate early enough preservation actions which might become necessary (recycling, manufacture of new equipement) in case life of some equipement should expire before the planned time limit.

Three important test and ageing categories can make the above monitoring possible :

- accelerated ageing tests,
- real natural ageing tests,
- simulated natural ageing tests.

This conference presents the choice made as well as the principles and the content of the test programme considered for the accelerator of an air to surface missile.

3 . GENERALITES

Pour tous nos missiles se pose le problème de la détermination de la durée de vie. Il s'agit du temps, à partir de la livraison du matériel à l'utilisateur, pendant lequel le matériel conserve ses caractéristiques spécifiées, en particulier la sécurité, dans les conditions d'emploi de l'utilisateur.

Il y a donc lieu de vérifier la tenue de nos matériels soumis à ces conditions d'emploi qui normalement sont définies dans les spécifications techniques du système d'arme.

La vie opérationnelle des missiles peut se décomposer en trois phases principales :

Phase 1 :
Le transport de l'usine de production au lieu de stockage de l'utilisateur. Il peut être routier, ferroviaire, aérien ou maritime. Il s'effectue par des moyens conventionnels, le missile étant dans son emballage logistique ; sa durée est courte : on peut considérer pour un transport maritime de l'ordre de un mois.

Phase 2 :
Le stockage de longue durée. Il peut atteindre des années. Le missile est toujours dans son emballage logistique.

Phase 3 :
La mission opérationnelle. Elle est propre à chaque type de missile, elle peut être définitive (tir en fin de mission) ou mission d'alerte, ou mission annulée.

4 . BUT ET NATURE DES ESSAIS DE VIEILLISSEMENT

Le but des essais de vieillissement est de procéder à une surveillance régulière de l'évolution des performances et des caractéristiques des matériels du système d'arme dans le temps, de manière à pouvoir garantir, pendant toute la durée de vie du système, les performances et la disponibilité contractuelle, en permettant le déclenchement suffisamment tôt de mesures conservatoires éventuellement nécessaires (modifications, recyclage, fabrication de matériels neufs) au cas où certains matériels arriveraient à péremption avant le délai prévu.

Paper presented at the AGARD PEP Symposium on "Service Life of Solid Propellant Systems" held in Athens, Greece, 10-14 May 1996, and published in CP-586.

Trois grandes catégories d'essais de vieillissement peuvent permettre cette surveillance :

- les essais de vieillissement accéléré, (V.A.),
- les essais de vieillissement naturel réel, (V.N.),
- les essais de vieillissement naturel simulé, (V.N.S.).

Le problème consiste donc à définir les essais de vieillissement les plus représentatifs selon le matériel considéré.

5 . PRESENTATION DETAILLEE DES DIFFERENTS TYPES DE VIEILLISSEMENT

5.1. Essais de vieillissement accéléré (V.A.) Voir tableau 1

Le principe consiste à accélérer le vieillissement des matériels en les stockant pendant un temps fonction de la durée de vie à simuler, à une température supérieure à celle prévue pour le stockage opérationnel (correspondant pratiquement au maximum du domaine d'emploi, soit en général entre + 50°C et + 60°C).

On réalise en final un essai de fontionnement après avoir effectué des contrôles périodiques plus ou moins appronfondis (examens visuels et radiographiques) et éventuellement un environnement thermomécanique.

Un vieillissement isotherme à température élevée accélère les phénomènes chimiques et permet donc de se faire en un temps court une idée de l'évolution des propriétés mécaniques et surtout des propriétés balistiques.

Ce type d'essai s'applique surtout aux propergols pour lesquels il a été estimé des équivalences entre durée de vie réelle et durée de vie simulée en fonction de la différence de température appliquée en stockage.

Mais d'une manière générale, de tels essais ne sont cependant pas suffisants pour avoir une connaissance précise de l'évolution réelle des matériels dans le temps et à fortiori pour déterminer leur délai de péremption.

Il donne cependant des indications précieuses sur l'aptitude d'un matériel à vieillir et peuvent ainsi permettre de se fixer des objectifs réalistes de durée de vie, ce qui est particulièrement intéressant lorsqu'on utilise des produits ou technologies sur lesquels on manque d'expérience.

Pour cela, les essais de vieillissement accéléré doivent être effectués très tôt en développement.

Exemple :

Entre isotherme et accéléré, on constate dans certains cas un comportement différent sur l'évolution de la capacité du collage propergol/inhibiteur.

5.2. Essais de vieillissement naturel réel (V.N.) Voir tableau 2

Il s'agit dans ce cas, de laisser vieillir les matériels dans leur environnement opérationnel normal, et de les prélever au fur et à mesure qu'ils atteignent l'âge prévu pour les tests de comportement.

En pratique, on choisira les plus vieux des matériels en service, ou ceux ayant été les plus sollicités .

5.3. Essais de vieillissement naturel simulé (V.N.S.) Voir tableau 3

Il s'agit de laisser vieillir en usine les matériels dans des conditions aussi proches que possible des conditions opérationnelles (et même en général un peu plus sévères pour disposer d'une marge).

Ces conditions comprennent les agressions mécaniques, climatiques,... subies par les matériels opérationnels ; sauf cas particulier, celles-ci sont simulées (vibrations, cycles thermiques,...) périodiquement (par exemple annuellement).

Ce type d'essai n'est intéressant que s'il s'applique à des matériels plus agés que les plus vieux des matériels opérationnels d'une valeur égale au cycle de fabrication correspondant (ou de recyclage), augmenté de la périodicité des essais de vieillissement .

6 . PRINCIPES RETENUS POUR L'ETABLISSEMENT DU PROGRAMME GENERAL D'ESSAIS

Compte tenu d'un certain nombre d'éléments de choix, on définira le programme général des essais basé sur les principes suivants :

Principe 1 :
Se fixer pour chaque matériel un dispositif raisonnable de durée de vie, compte tenu de l'état actuel de nos connaissances et définir un programme adapté à cette durée.

Remarque :
Cet objectif doit-être, soit la durée de vie totale envisagée pour le système (x ans), soit un sous multiple de celui-ci de manière à ce que les derniers matériels de renouvellement aient une durée de vie opérationnelle sensiblement identique à celle des matériels précédents. Sauf cas particulier, on prendra dix ans pour les matériels pyrotechniques et vingt ans pour les autres matériels.

Principe 2 :
Ne prévoir des essais de vieillissement accéléré que lorsqu'on n'a pas ou peu de données sur la durée de vie possible du matériel ou pour vérifier la compatibilité d'un assemblage de matériaux. Les résultats de ces essais à faire très tôt dans le développement (même sur une définition non parfaitement représentative) permettront de recaler éventuellement les objectifs fixés dans le principe 1.

Principe 3 :
N'effectuer des essais de vieillissement naturel simulé que sur les matériels " monocoups " (*voir paragraphe 7.2.*) pour lesquels aucun contrôle n'est possible en service.

Remarques :
Les matériels correspondants doivent être fabriqués en développement, avec une avance suffisante pour éviter, si possible la mise en place de rechanges destinées à supprimer toute indisponibilité des matériels en service en cas de péremption avant la durée objective fixée. Pour la même raison, on appliquera une périodicité multiple de un an pour la réalisation des essais de performances. La définition de ces matériels doit être représentative de la définition série (au moins conforme à la définition qualifiée).

Principe 4 :
Effectuer des essais de vieillissement naturel réel pour tous les autres matériels pour lesquels les contrôles périodiques normaux et les réparations apportent déjà des précieux renseignements sur leur évolution éventuelle. La périodicité applicable à ces essais pourrait être de deux ou trois ans.

Remarques :
Si ,au cours des contrôles périodiques ou des réparationss,des évolutions inquiétantes des performances étaient détectées, elles entraîneraient l'avancement des essais de vieillissement pour confirmation des résultats et le lancement de mesures conservatoires avant péremption. Il pourra malgré tout être prévu un minimum de rechanges à titre de sécurité.

Principe 5 :
Appliquer à la fin de chaque période de vieillissement des tests de performances au niveau de la qualification technique (tenue ou fonctionnement aux limites du domaine des conditions normales d'emploi).

Principe 6 :
Appliquer, pour le vieillissement naturel simulé, des épreuves annuelles simulant la vie opérationnelle légèrement durcie, de manière à disposer d'une certaine marge par rapport au vieillissement réel et pour tenir compte d'une certaine incertitude sur la représentativité des épreuves choisies.

Principe 7 :
Effectuer pour tous les matériels de grande précision un suivi particulier pour surveiller l'évolution de leurs performances.

7 . APPLICATION A L'ACCELERATEUR INTEGRE D'UN MISSILE AIR SOL

7.1. Principes retenus

Principe 1 :
Objectif dix ans.

Principe 2 :
Ne faire du V.A. que si l'on a peu de données sur la vie possible du matériel --> à faire tôt dans le développement pour recalages éventuels.

Principe 3 :
V.N.S. uniquement sur les matériels nonocoups.

Principe 4 :
V.N. réel pour les autres matériels dont les contrôles périodiques normaux et les réparations apportent de précieux renseignements.

Principe 5 :
Application à la fin de chaque période de vieillissement de tests de performances du niveau de la qualification aux limites du domaine de conditions normales d'emploi.

Principe 6 :
Pour le V.N.S., réaliser des applications d'épreuves annuelles, simulant la vie opérationnelle, légèrement durcies.

Principe 7 :
Pour les produits pyrotechniques : produits connus, d'où V.N.S. seulement. Si produit nouveaux (composition d'accélérateur nouvelle ou/et liaison poudre liner nouvelle), V.A. + V.N.S.

7.2. Programme proposé

Il est proposé des essais de vieillissement accéléré (V.A.), des essais de viellissement naturel simulé (V.N.S.) et des essais de vieillissement naturel (V.N.), basés sur un objectif de durée de vie de dix ans.

Les essais prévus couvrent le suivi du propergol, la protection thermique et tous les matériels monocoups de l'accélérateur intégré (dispositifs d'allumage accélérateur, contacteurs à pression, mano-contacts, cordeau découpeur de tuyère,...) pour lesquels il n'est pas prévu d'essais particuliers.

7.2.1. Essais de vieillissement accéléré sur accélérateur complet

Le programme comporte :
- simulation d'un vieillissement de six ans (stockage neuf mois à + 50 °C),
- simulation d'un vieillissement de dix ans (stockage quinze mois à + 50°C).

A l'issu de cette période de stockage, on procédera dans l'ordre à :
- des contrôles non destructifs (aspect, radiographie, endoscopie),
- des cycles climatiques et des vibrations représentatifs de la vie simulée et cumulée,
- à nouveau des contrôles non destructifs,
- des tirs aux températures limites d'utilisation (- 30 à + 50°C).

Remarques :
Par ailleurs, à l'occasion de chaque coulée, des éprouvettes témoins de propergol seront stockées et serviront à réaliser éventuellement des essais de vieillissement accéléré complémentaires.

7.2.2. Essais de vieillissement naturel simulé sur accélérateur complet

Le programme comporte le stockage d'accélérateurs complets qui seront stockés à une température comprise entre + 5 et + 25°C, dans la même position que les accélérateurs opérationnels, auxquels on fera subir chaque année :

- des cycles thermiques et des vibrations représentatifs de la vie opérationnelle annuelle,
- des contrôles non destructifs (aspect, radioscopie, endoscopie,...).

Il sera effectué un tir au bout de cinq et neuf ans de stockage, alternativement à - 30°C et + 50°C.

Remarques :
Avant tir, il sera simulé des épreuves mécaniques et thermiques représentatives de la vie opérationnnelle temps de crise et de guerre, jusqu'au tir. Un accélérateur sera mis en réserve pour servir à confirmer les résultats si nécessaire .

7.2.3. Essais de vieillissement naturel sur accélérateur et simulé sur éprouvettes de poudre et protection thermique

Le programme sera identique au précédent avec des tirs au bout de sept et dix ans (plus une réserve).

En ce qui concerne les éprouvettes, on effectuera un suivi de l'évolution des propriétés mécaniques et physiques du propergol, de la protection thermique et du collage.

Pour cela, on effectuera une coulée spécifique d'éprouvettes en quantité suffisante pour couvrir l'ensemble des besoins.

Ces éprouvettes seront mises à vieillir à 20°C $\pm$ 5°C d'une part et à - 30°C et + 50°C d'autre part.

On procédera tous les deux ans et jusqu'à dix ans à des mesures comparatives (densité, fluage, traction, cisaillement) permettant d'effectuer des calculs de fiabilité et d'estimer les coefficients de sécurité.

8 . SANCTION DES EPREUVES FINALES

Toute anomalie ou défaillance rencontrée au cours des épreuves donnera lieu à la convocation d'une commission d'expertise qui, après examen et analyse appronfondis du défaut classera celui-ci soit :

- cas d'espèce relevant du taux normal de défaillance,
- cas de vieillissement caractérisé,
- cas douteux.

Dans le premier cas, ainsi que si les résultats sont corrects, le calendrier prévisionnel des essais sera poursuivi comme prévu.

Dans le deux derniers cas, il sera lancé sans délai, des essais de confirmation ainsi que des mesures conservatoires en vue d'un renouvellement anticipé éventuel.

9 . DOCUMENTS A ETABLIR

9.1. Programme général

9.2. Programmes détaillés d'essais

Après accord du programme général, le titulaire établira les programmes détaillés des essais relatifs à chaque matériel concerné pour accord final.

Remarques :
Les programmes détaillés de vieillissements naturel réel seront par contre établis ultérieurement au cours de la série.

9.3. Comptes Rendus

Les épreuves finales donneront lieu à l'établissement de comptes rendus détaillés. Les épreuves annuelles relatives au vieillissement naturel simulé donneront lieu à l'établissement de comptes rendus succincts.

En cas de défauts (voir paragraphe 6), des comptes rendus particuliers d'expertise seront établis.

10 . CONCLUSION

Dans l'état actuel de notre expérience à AEROSPATIALE MISSILES et à CELERG, la méthodologie utilisée nous paraît être actuellement la meilleure possible, à condition d'être vigilant sur les conditions réelles de son application en regard des spécifications réelles justifiées (et non d'estimations qui constituent fréquemment une amplification du strict besoin).

Il semble ainsi que l'on puisse éviter des erreurs du passé liées à une méthode trop sommaire.

La simulation du vieillissement est maintenant modulée en fonction des thèmes d'emploi possibles les plus significatifs, retenus en accord avec le Client.

Ceci doit se traduire finalement par une meilleure efficacité et une confiance accrue dans la validité de l'interprétation des résultats obtenus, sur le plan des performances, de la fiabilité et de la sécurité.

Tableau 1

AVANTAGES	INCONVENIENTS
* Simulations peu coûteuses sur des durées courtes. * Déduction d'une durée de vie présumée par " age équivalent à + 20°C " $t_{acc} = \frac{t_{naturel}}{k.(\theta_{acc} - \theta_{nat})}$ θ_{acc} = 50 à 60 °C θ_{nat} = 20 °C 0,25 < k < 0,26 Exemples : t_{acc} = 9 mois => t_{nat} = 72 mois t_{acc} = 15 mois => t_{nat} = 120 mois	* Méthode insuffisante : - L'absence de cycles thermiques est minorante (contraintes liées au calage), - La présence de hautes températures est pénalisante (dégradations chimiques moins sévères à 20°C) - Cinétique de décomposition pénalisante à haute température (accumulation de produits de décomposition)

Tableau 2

AVANTAGES	INCONVENIENTS
* Vieillissement entièrement représentatif des matériels en service (si conditions de stockage identiques). * Définition conforme à celle des matériels en service. * Coûts des essais limités aux essais finaux de comportement	* Résultats optimistes non représentatifs, si différences importantes dans la vie des matériels livrés. * Certaines vérifications régulières seulement possibles en usine (radiographies,...) * Nombre important de matériels périmés en service, si péremption avant délai de renouvellement. Problème du remplacement avant arrivée du matériel nouveau. * Rechanges inutiles si les matériels tiennent toute la durée de vie prévue.

Tableau 3

AVANTAGES	INCONVENIENTS
* Pas de risque de matériel périmé en service * Pas de rechange à fabriquer en anticipation (préavis suffisant à lancer plus tôt que prévu) * Bonne garantie sur les résultats obtenus en durcissant les conditions de stockage et les épreuves simulant les agressions mécaniques et thermiques). * Surveillance régulière tout au long de la période.	* Frais de stockage et d'épreuves importants. * Définition des matériels de vieillissement pouvant être légèrement différente de celle des matériels opérationnels.

Paper Number: 45
Discussor's Name: I. H. Maxey
Responder's Name: A. Chevalier

Question: How does your program cover:
a. Cumulative damage from thermo-mechanical cycling or long range storage and operational life elements?
b. The high and low temperatures of the storage and use conditions in the life cycle?

Answer: a. Lors des essais de viellissement on annule les effets thermo-mécaniques du stockage, les cycles thermiques et les vibrations représentatifs de la vie opationelle annuelle, ainse que les memes epreuves représentatives de la vie operationelle temps de crise ou de guerre. (voir 721-722-723)

b. Les cyclages représentatifs des variations des températures journalieres n'ont pas été effectués dans ce programme.

Answer: a. During the aging tests, we simulate the thermo-mechanical effects of storage, the thermal cycle and vibrations corresponding to the yearly operational life, as well as the same conditions corresponding to operational life in times of crisis or war (see 721-722-723).

b. The cycles corresponding to daily temperature variations were not studied in this program.

Paper Number: 45
Discussor's Name: N. Laurencon
Responder's Name: A. Chevalier

Question: Le programme viellissement presenté pour le programme Air-Sol est très complet. Aussi on ne peut pas l'isoler de son cout. Avez-vous une idée du cout de ce programme de viellissement par rapport au cout total du developpement du moteur?

Question: The aging program given for the Air-Sol program is very complete, and cannot be separated from its cost. Have you an idea of the cost of this aging program relative to the total cost of motor development?

Answer: Le cout associé à ce programme est en effet assez élevé, mais il faut prendre en compte le haut niveau de varieté et de fiabilité specifié.

Answer: The cost associated with this program is in fact rather high, but we must consider the high level of variance and reliability which are specified.

Service Life Assessment For Space Launch Vehicles

William L. Hufferd[1]
The Johns Hopkins University
Chemical Propulsion Information Agency
10630 Little Patuxent Parkway, Suite 202
Baltimore, Maryland 21044-3200, USA

1. SUMMARY

This paper describes a test program conducted by United Technologies Chemical Systems to improve the understanding of propellant aging behavior and establish failure characteristics in motor-like test conditions. The data obtained provide a basis for assessing the storage service life of large solid rocket motor components.

2. INTRODUCTION

The critical loads and the particular failure modes for solid rocket motors are system dependent. The critical loading conditions for large SRM boosters, such as the Titan, SRMU, RSRM or Ariane 5, are thermal cooldown and storage, including horizontal or vertical storage with a 1-g gravity load, segment stacking (destacking/restacking), and combined flight loads. The combined flight loads include thermal storage loads, accelerations, pressure, pressure differentials along the grain length and across the grain web, and local joint rotations near propellant grain terminations. The critical combined flight loading condition may not necessarily occur at ignition, but it may instead occur for some burnback configuration. Degradation due to aging is an additional requirement which is imposed on these loading conditions.

In the case of the Titan IV SRM, the minimum structural margin of safety is associated with long term storage of the forward closure in flight attitude with a 1-g slump load. The critical failure mode is bore surface cracking. Traditional storage service life analysis methods for this failure mode are overly conservative when applied to large solid rocket motors such as the boosters for the Arianne V, the Space Shuttle and the Titan IV. This conservatism stems, in part, from the fact that these motors are generally subjected to very benign storage environments and mechanical strains are induced prior to propellant aging. In particular, the motor components experience very minor temperature excursions following completion of cure and initial cooldown to ambient temperature. Thus, the induced thermal stains associated with cooldown and storage are essentially "locked-in" prior to propellant aging. Service life assessments, on the other hand, are typically based on propellant data obtained from cartons cast with the components which are aged in a stress and strain free environment. These data are not representative of the behavior of loaded components subjected to the same storage and aging environment. A testing program was conducted to separate the effects of loading and environment during aging.

The scope of the test program consisted of real-time and accelerated aging tests of bulk propellant samples and subscale analog motors in order to assess:

- the differences between first mechanically loading the propellant and then aging, versus aging the propellant prior to mechanical loading,
- the failure criteria used in computing margins of safety, and
- the effects of storage pre-strains on motor ignition capabilities.

Particular attention was given to establishing strain endurance aging behavior (i.e., aging factors).

3. TEST PROGRAM

Replicate testing was conducted from multiple production batches of propellant to establish aging trends and the statistical variability of strain endurance and aging factors. The test program included tests of samples aged under load and assessed the effect of aging on stress axiality factors. Accelerated aging tests were conducted in order to confirm long term aging trends.

Subscale analog motor aging was conducted to confirm propellant bulk sample aging behavior and to validate storage life estimates. Analog motors were cast from multiple production batches of propellant, aged and periodically temperature cycled to demonstrate structural margins of safety.

Appropriate analyses of the aging data collected was conducted for the purpose of correlating bulk sample aging data with analog motor aging results.

Bulk sample propellant aging was conducted to evaluate propellant aging factors, axiality factors, aging behavior under strain and batch-to-batch aging variability. Propellant samples were cast from 12 production batches of propellant, 2 each from 6 different components, and aged according to the schedule shown in figure 1. Fifteen standard cartons and 15 biaxial blocks were cast from 7 batches of propellant, and 30 cartons and 30 biaxial blocks were cast from the remaining 5 batches of propellant. Figure 2 shows the propellant sample configurations for the biaxial blocks and cartons.

The tests conducted consisted of standard JANNAF constant rate tests, biaxial constant rate, uniaxial and biaxial strain endurance, and pre-strained JANNAF constant rate tests as shown in figure 1. All testing was conducted at 70 °F with the standard number of replicate tests. The aging was accomplished at 70, 120 and 140 °F for the times noted in figure 1.

Subscale analog motors, also known as Strain Evaluation Cylinders (SEC) (see figure 2), were cast, aged and periodically temperature cycled in order to confirm propellant bulk sample

[1] Formerly Manager, Engineering Analysis and Propulsion Sciences, United Technologies Space Propulsion Operations, Chemical Systems Division, San Jose, California, USA.

Paper presented at the AGARD PEP Symposium on "Service Life of Solid Propellant Systems" held in Athens, Greece, 10-14 May 1996, and published in CP-586.

Test Type	Aging Time (Months)				
	1	2	3	5	11
JANNAF Constant Rate	12ABC	5ABC	5A	5ABC	12ABC
Uniaxial Strain Endurance	12ABC	5ABC	5A	5ABC	12ABC
Biaxial Constant Rate	12A	5A	5A	5A	12A
Biaxial Strain Endurance	12A	5A	5A	5A	12A
Pre-Strained Uniaxial Constant Rate ($\frac{1}{4}$, $\frac{1}{2}$, and $\frac{3}{4}$ of ε_{end})	3AB	3B	3A		3A

Notes: Number indicates number of batches; i.e., 5ABC = 5A, 5B, 5C
Letter indicates aging temperature; A = 70 °F, B = 120 °F and C = 140 °F

Figure 1 Propellant Sample Aging Plan

aging behavior, validate shelf life estimation procedures and demonstrate structural factors of safety. Twenty 4-in. by 24-in. SECs with cylindrical bores were cast from each of 4 production batches of propellant, yielding a total of 80 analog motors. The selected batches were common with aging samples processed above. The 20 motors per propellant batch had 5 different bore diameters (4 each), which were selected so as to experience a bore cracking failure at a temperature less than 20 °F, and at 20, 40 and 60 °F, as shown in figure 3. Aging was conducted at 70, 120 and 140 °F as shown in figure 3. The analogs were cooled to the temperatures noted in figure 3 at each aging withdrawal time. Bore strain measurements and borescope inspections were made at 20 °F intervals during the temperature conditioning. The analogs designed to fail below 20 °F were temperature cycled following 1, 5 and 11 months of 70 °F aging. All other test conditions were single point tests with thermal cooldown proceeding until bore cracking was observed, or a temperature of 20 °F was reached. Figure 4 shows the analog motor test matrix. The numbers refer to the number of different bore diameters tested at each aging condition.

Statistical analyses of the bulk propellant sample aging data generated were conducted to establish the cast components service life. Kinetic parameters for strain endurance aging were established using the accelerated aging test data in an Arrhenius relationship. Specific aging parameters evaluated consisted of aging factors and their variability, aging characteristics of the axiality factor and batch-to-batch aging variability.

Statistical analyses of the analog motor aging data were conducted to assess aging trends in a motor-like geometry, confirm the service life model and validate shelf life estimation procedures.

Failure temperatures and failure strain levels from the thermally cycled analog motors were analyzed to determine the structural margins of safety demonstrated by the failure testing.

4. SERVICE LIFE ANALYSIS METHODOLOGY

A typical approach to service life assessment is shown in figure 5. The approach is best visualized in terms of the computation of a structural margin of safety:

$$MS = \frac{\varepsilon_{all} \times Axiality \times Aging \times Variability}{\varepsilon_{induced} \times Factor\ of\ Safety} - 1$$

where,

MS = Margin of Safety

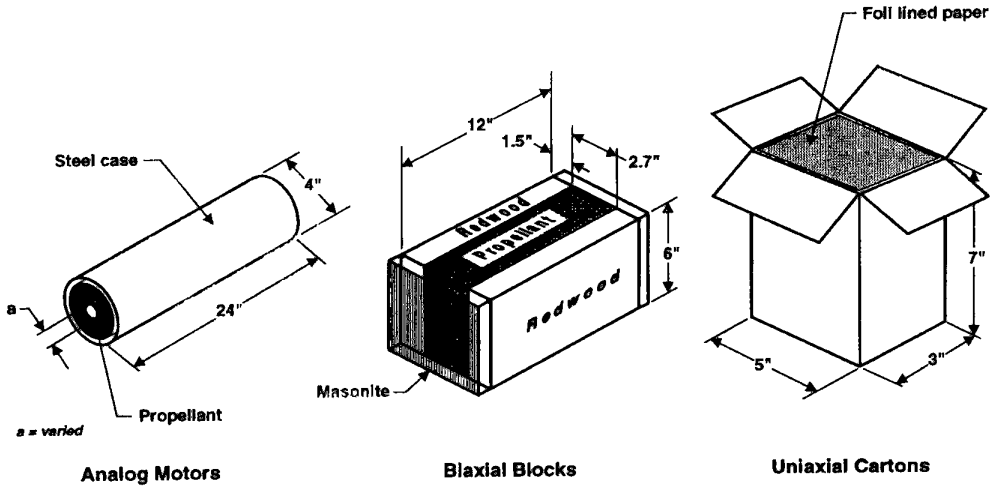


Figure 2 Propellant and Analog Motor Sample Configurations

Quantity	Bore Diameter	Induced Biaxial Hoop Strain at 60 °F	Design Failure Temperature (°F)	Aging Time (Months)				
				1	2	3	5	11
4	0.625 in.	20%	80 °F	A			A	A
4	0.750 in.	15%	60 °F	A			A	A
4	0.875 in.	12%	40 °F	A			A	A
4	1.000 in.	9%	20 °F	A	B,C	A	A,B,C	A,B,C
4	1.125 in.	7%	<20 °F	A			A	A

Notes: Letter indicates aging temperature; A = 70 °F, B = 120 °F and C = 140 °F.

Figure 3 Subscale Analog Motor Aging Conditions

ϵ_{all} = Allowable Uniaxial Endurance Strain

Axiality = Ratio of Biaxial Strain Endurance to Uniaxial Strain Endurance

Aging = Aging Degradation Factor

Variability = Batch-to-Batch Variability

$\epsilon_{induced}$ = Induced Bore Hoop Strain

Factor of Safety = Prescribed Design Safety Factor

Propellant Batch	Aging Time	Aging Temperature		
		70 F	120 F	140 F
11859	1 Month	4		
	2 Month		3	
	3 Month	3		
	5 Month	2	3	2
	11 Month	3	2	2
11886	1 Month	5		
	2 Month		3	3
	3 Month	3		
	5 Month		3	3
	11 Month	3	2	2
11902	1 Month	5		
	2 Month		3	3
	3 Month	3		
	5 Month	2	4	1
	11 Month	2	2	2
11918	1 Month	4		
	2 Month		2	3
	5 Month	3	3	2
	11 Month	2	2	1

Figure 4 Analog Motor Test Matrix

The ultimate strain shown in figure 5 represents the product of the induced strain and a prescribed design factor of safety. Uniaxial strain endurance tests establish the propellant strain capabilities as a function of time under load. The uniaxial capability is degraded to account for propellant batch-to-batch variability, aging degradation and the fact that the induced motor hoop strain at the bore surface is a biaxial strain in a 2:1 biaxial stress field.

The difficulty in assessing service life stems from the fact that the induced strain is applied during the initial cooldown of the motor segment following propellant cure. At this time in the life of a component, significant strain endurance capabilities exist. Aging then occurs under a fixed strain. Previous laboratory investigations have shown that this loading environment results in what has been called a "permanent set" or "stress-free temperature" shift, with the result that the ultimate capability of the propellant is only slightly reduced. The propellant testing conducted in this investigation quantitatively assessed this effect.

5. TEST RESULTS

5.1 Laboratory Test Results

Figures 6 through 8 show the aging trends for JANNAF uniaxial properties. The initial modulus, maximum stress and strain at maximum stress all show that this propellant continues to post-cure for about 11 months and then undergoes no further significant change or aging. Figure 9 tabulates the aged and unaged strain endurance for 5 years storage at 70 °F. Figure 10 shows a plot of the five year endurance strain capability versus aging time. Figure 11 shows all of the uniaxial endurance strain data with the nominal curve fit and the lower 90% confidence level, 95% data. The extrapolated lower bound is 8% strain for seven years storage at 60 °F. Figure 12 compares uniaxial and biaxial strain endurance.

Additional testing was conducted to assess the effects of prestrain on subsequent JANNAF strain capabilities. Samples were strained to 4, 8 and 12% strain and then aged at 70 and 120 °F. Figure 13 compares the JANNAF total strain (i.e., including pre-strain) at maximum stress with the baseline unstrained data as a function of age. It may be seen that the total strain capability is in fact improved for the more highly prestrained samples. This observation is in agreement with previous investigations, including high-rate tests in a pressurized environment, and is attributed to polymer chain scission in a strained state and reformation of the chains in a stress/strain free state. This phenomena has often been referred to as "healing", and is, in part, the justification for treating storage and ignition pressurization loading conditions as separate events in margin of safety computations.

5.2 Subscale Analog Motor Test Results

Figure 14 shows the aged analog motor failure strain data. Data

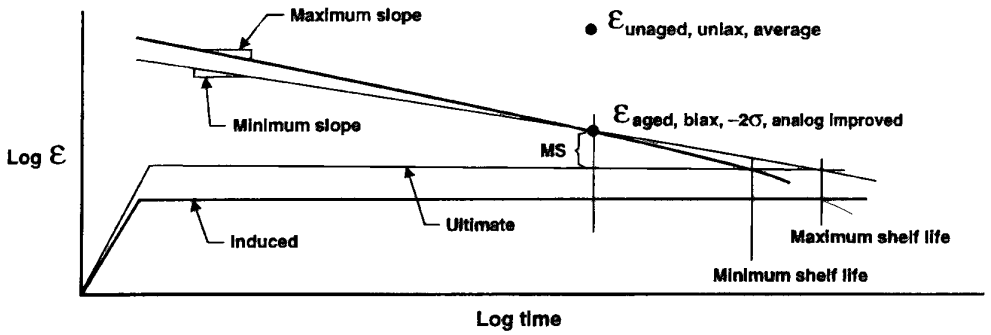


Figure 5 Schematic of Storage Life Margin of Safety Determination

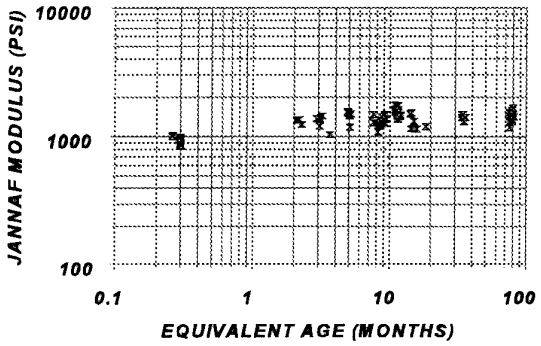


Figure 6 Aging Trends of JANNAF Uniaxial Modulus

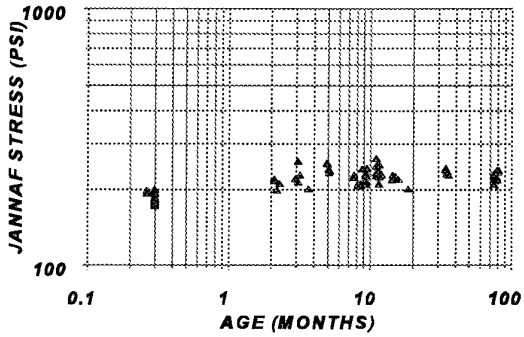


Figure 7 Aging Trends of JANNAF Uniaxial Stress

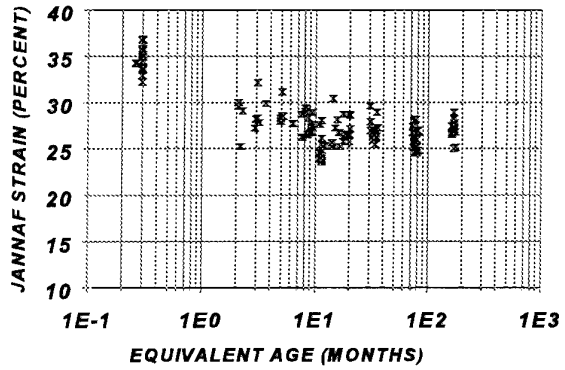


Figure 8 Aging Trends of JANNAF Uniaxial Strain

are presented for the highest strain level for which no failure was observed and the lowest strain level for which failure was observed. The aged uniaxial strain endurance data, corrected for biaxiality using figure 12, are also shown in figure 14; as well as the "analog adjustment factor", derived from the ratio of induced analog motor strain to aged uniaxial strain endurance capability.

Measurements of the analog motor bore strain and temperature were also used to investigate the variability of the propellant cure shrinkage and the linear coefficient of thermal expansion, α. Propellant cure shrinkage is expressed in terms of an equivalent strain free temperature; that is the temperature at which the measured bore diameter is equal to the casting mandrel diameter. Figure 15 shows the distribution of the computed strain free temperatures. The arithmetic mean is 157 °F. All propellant samples were nominally cured at 150 °F ± 5 °F. Thus, some of the variability may be associated with slight differences in cure temperature. Also, no attempt has been made here to attribute any differences to the different web fractions used in the analog motor testing.

Poisson's ratio, ν, and the coefficient of linear thermal expansion, α, both affect volumetric response. By comparing measured bore strains in strain evaluation cylinders of different web fractions, with the analytically predicted bore strains, one can determine the best combination of α and ν (in a least squares sense) for the propellant. For small web fraction motors (e.g., 50 to 70%), plots of α versus ν usually intersect at the best choice of α and ν. Poisson's ratio is typically close to 0.499. Figure 16 shows the distribution of the linear coefficient of thermal expansion for ν = 0/499 for the 80 analog motors tested. The arithmetic mean is 56.2×10^{-6} in/in/°F.

Batch	5 Year Endurance at 70 °F		Aging Factor
	Unaged	Aged	
11857	14.1	9.9	0.702
11859	14.6	10.4	0.712
11884	12.4	11.1	0.895
11886	13.5	8.7	0.644
11894	14.5	9.2	0.634
11900	11.7	9.3	0.795
11902	12.9	7.4	0.574
11910	14.2	6.8	0.479
11916	12.5	7.9	0.632
11918	13.0	8.9	0.685
11932	14.6	9.6	0.658
11934	14.5	10.3	0.710
11948	10.6	9.7	0.915
11950	13.4	8.3	0.619
Average of Batches	13.3	9.1	0.690
Standard Deviation	0.976	0.949	0.0846

Figure 9 Comparison of Aged and Unaged Uniaxial Strain Endurance for 5 Years Storage at 70 °F

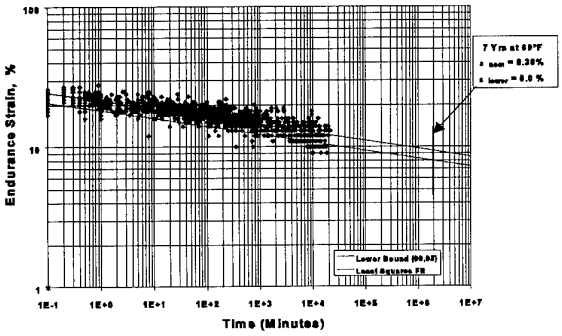


Figure 11 Uniaxial Strain Endurance

6. EVALUATION OF AGING FACTORS

Statistical analyses of the propellant data were conducted to establish the one-sided 95th percentile of the data with a 90% confidence level. Figure 17 compares the aged and unaged uniaxial and biaxial strain endurance, aging factors, axiality factors and the analog motor augmentation factor. The results indicate little difference in aging characteristics of uniaxial and biaxial sample configurations, and a significant effect from application of the storage induced strains prior to aging. As a consequence, evaluation of aging structural margins of safety may be sign ificantly underestimated if this effect is not accounted for.aging structural margins of safety may be significantly underestimated if this effect is not accounted for.

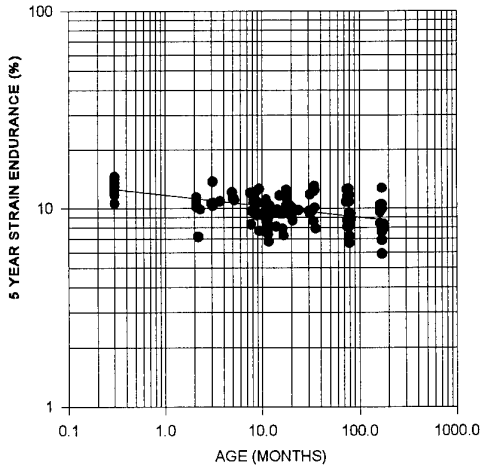


Figure 10 Five Year Endurance Strain Capability As a Function of Aging Time

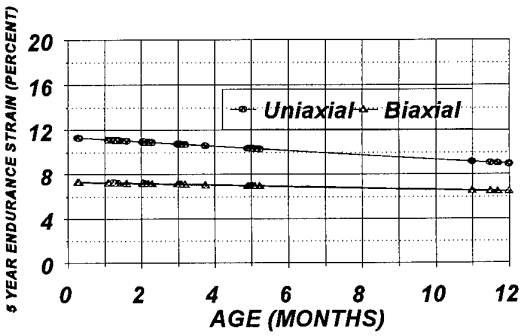


Figure 12 Comparison of Uniaxial and Biaxial Strain Endurance

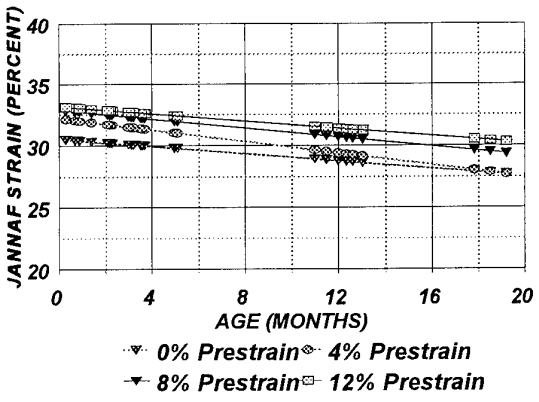


Figure 13 Aging Under Strain Does Not Degrade Total Strain Capability

Batch	Age (Months)	Temp (°F)	Analog Motors		Uniaxial Endurance	Analog Adjustment	
			Non-Fail	Fail	(%)	Non-Fail	Fail
			(%)	(%)			
11859	1	70	15.5	17.5	13.4	1.157	1.306
	5	70	9.6		10.6	0.906	
		120	8.6		10.6	0.811	
		140	8.9		10.9	0.817	
	11	70	11.7		9.0	1.300	
		120	8.6		9.2	0.935	
		140	8.9		8.6	1.035	
11886	2	120	12.5	14.5	9.6	1.302	1.510
		140	13.0	14.5	9.3	1.398	1.559
	5	70	10.7		9.7	1.103	
		120	13.4	15.8	10.0	1.340	1.580
		140	7.8		9.9	0.788	
	11	70	10.8		8.3	1.301	
		120	7.9		8.3	0.952	
		140	7.7		9.6	0.802	
11902	2	120	12.5	14.0	9.3	1.344	1.505
		140	11.5	13.0	8.8	1.307	1.477
	5	70	10.5		9.9	1.061	
		120	12.3		9.0	1.367	
		140	8.0		8.7	0.920	
	11	70	8.2		7.7	1.065	
		120	8.0		9.0	0.889	
		140	8.0	9.2	8.0	1.000	1.150
11918	1	70	14.0	13.8	12.5	1.120	1.104
	2	120	12.3	14.2	9.6	1.281	1.479
		140	12.4	14.3	10.2	1.216	1.402
	5	70	8.5	11.3	9.6	0.885	1.177
		120	8.7	11.0	10.2	0.853	1.078
		140	6.4		10.6	0.604	
	11	70	8.7		8.3	1.048	

Figure 14 Analog Motor Failure Data Compared to Aged Uniaxial Strain Endurance

7. CONCLUSIONS

The results of this test program demonstrate that the conventional approach for evaluating the service life of large solid rocket motors for bore surface cracking is overly conservative. The induced strains following the completion of propellant cure and initial cooldown to ambient temperature occur when the propellant typically has its maximum strain capability. Inasmuch as launch vehicles experience only small temperature excursions, subsequent aging of the prestrained propellant causes very little further degradation of strain capabilities.

Acknowledgments

This aging program was conducted while the author was at the United Technologies Space Propulsion Operations Chemical Systems Division under prime contract number GD5-161551 to the Lockheed Martin Corporation Astronautics Division (formerly Martin Marietta Astronautics). The author gratefully acknowledges the efforts and support of Mr. Harold J. Zitzer, Jr., Mr. Steven Perkins and Mrs. Susan Houghton in conducting the tests and summarizing the test data.

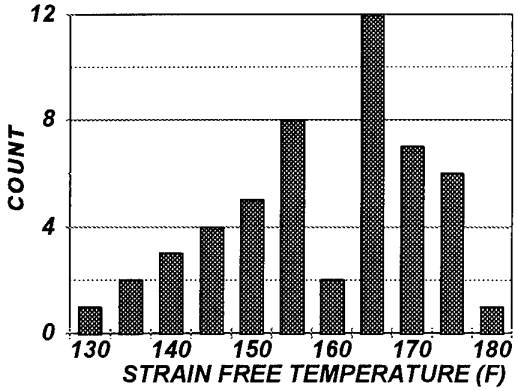


Figure 15 Distribution of Strain Free Temperatures From Analog Motor Bore Strain Measurements

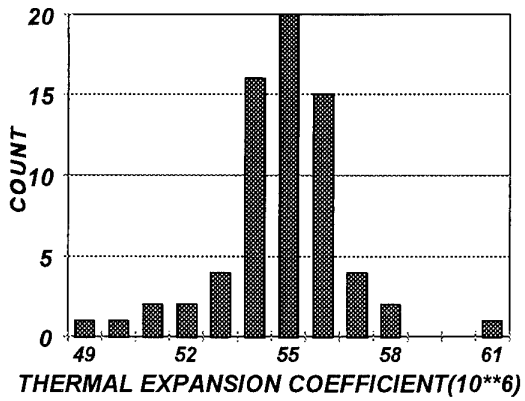


Figure 16 Distribution of Linear Thermal Coefficient of Expansion From Analog Motor Bore Strain Measurements

Test Type	Unaged	Aged	Aging Factor	Axiality Factor	Analog Motor Adjustment
Uniaxial	13.3%	9.1%	0.69	0.64	1.36
Biaxial	8.5%	5.9%	0.62	1.00	1.36

Figure 17 Summary of Uniaxial, Biaxial and Analog Motor Aging Test Data

Paper Number: 46
Discussor's Name: D. I. Thrasher
Responder's Name: Dr. W. L. Hufferd

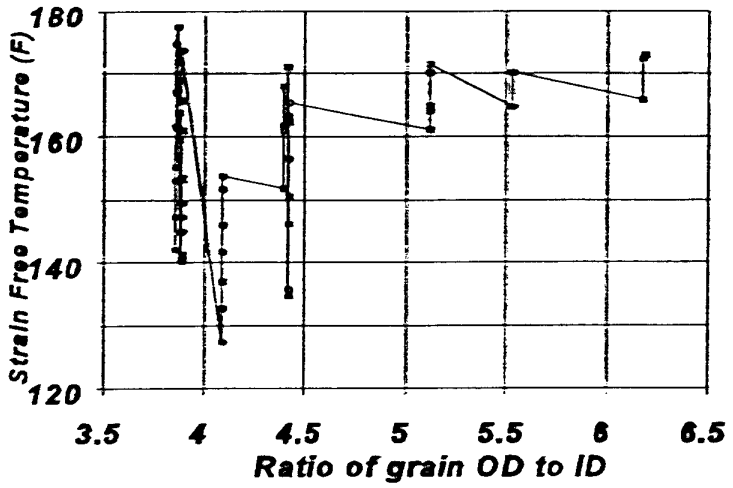
Question: How do you determine a 5 year strain endurance for a propellant age of less than a year?

Answer: A master curve is established using time-temperature superpositon and the curve is extrapolated to the time and temperature of interest; typically $1^1/_2$ to 2 decades as shown in Figure 11.

Paper Number: 46
Discussor's Name: Dr. H. J. Buswell
Responder's Name: Dr. W. L. Huffered

Question: a) Did you find a relationship between strain free temperature and λ (i.e., b/a), the induced strain magnitude?

Answer: No. The graph below shows a plot of strain free temperature, derived from measured analog motor strains versus the b/a ratio. There is no apparent correlation.



Question: b) Comment on the difference between strain free temperature and stress free temperature.

Answer: Stress is an a priori parameter related to the primitive concept of force. Strain, on the other hand, is a derived parameter related to an arbitrary, but specified reference configuration (e. g., the initial length of an

undeformed line segment). In a rocket motor, hoop strain is defined relative to the mandrel dimension for convenience, and is a deterministic quantity. That is, hoop strain in an axisymmetric configuration can be corrupted by simply comparing the measured change in bore diameter to the original measured mandrel diameter. The computation of stress, on the other hand, requires knowledge of a constitutive, or stress-strain law relating material properties (i.e., Poisson's ratio and Young's modulus) to the measured displacements or strains.

The cure process for propellant transforms the propellant from a viscous fluid to a viscoelastic solid. During this polymerization process, the propellant shrinks and cross-links are formed as the propellant solidifies. These cross-links form in a stress-free state since the propellant as a fluid cannot sustain loads. Since the greatest majority of the cure shrinkage occurs prior to propellant gel, there is very little build-up of additional stress following gel due to further propellant shrinkage. The result is that the initial stress-free temperature, immediately following completion of propellant cure, is very nearly the same temperature as the cure temperature.

Since hoop strains are primarily determined by the motor geometry and propellant shrinkage (due to the fact that Poisson's ratio = 0.5), there is no fundamental relationship between strain-free temperature and stress-free temperature.

REPORT DOCUMENTATION PAGE

1. Recipient's Reference	2. Originator's Reference	3. Further Reference	4. Security Classification of Document
	AGARD-CP-586	ISBN 92-836-0036-3	UNCLASSIFIED/ UNLIMITED

5. Originator Advisory Group for Aerospace Research and Development
North Atlantic Treaty Organization
7 rue Ancelle, 92200 Neuilly-sur-Seine, France

6. Title
Service Life of Solid Propellant Systems

7. Presented at/sponsored by
the AGARD PEP Symposium held in Athens, Greece, 10-14 May 1996.

8. Author(s)/Editor(s)	9. Date
Multiple	May 1997
10. Author's/Editor's Address	**11. Pages**
Multiple	494

12. Distribution Statement There are no restrictions on the distribution of this document. Information about the availability of this and other AGARD unclassified publications is given on the back cover.

13. Keywords/Descriptors

Shelf life
Solid rocket propellants
Gun propellants
Propellant Storage
Non-destructive testing
Reliability
Tests
Cost engineering
Records
Service life
Aging tests (materials)
Life (durability)
Propellant handling
Gas generator propellants
Methodology
Safety
Aging (materials)

14. Abstract

The Propulsion and Energetics Panel Symposium on Service Life of Solid Propellant Motors was held from 10-14 May 1996, in Athens, Greece. It dealt with the methods of extending and predicting service life of solid propellant systems for rockets, gas generators and guns. It also dealt with shelf life under varying conditions. This defence-specific symposium was aimed at improving system reliability, safety and cost. There were five sessions (43 papers) and a keynote address:

— Chemical and Physical Aging Mechanisms (9);
— Non-Destructive Test Methods (6);
— Gun Propellants (7);
— Methodologies and Techniques for Determining Service Life (11);
— Application of the Service Life Methodology and Techniques to Rocket Motor Systems (10).

AGARD

NATO OTAN

7 RUE ANCELLE • 92200 NEUILLY-SUR-SEINE

FRANCE

Télécopie 0(1)55.61.22.99 • Télex 610 176

DIFFUSION DES PUBLICATIONS

AGARD NON CLASSIFIEES

Aucun stock de publications n'a existé à AGARD. A partir de 1993, AGARD détiendra un stock limité des publications associées aux cycles de conférences et cours spéciaux ainsi que les AGARDographies et les rapports des groupes de travail, organisés et publiés à partir de 1993 inclus. Les demandes de renseignements doivent être adressées à AGARD par lettre ou par fax à l'adresse indiquée ci-dessus. *Veuillez ne pas téléphoner.* La diffusion initiale de toutes les publications de l'AGARD est effectuée auprès des pays membres de l'OTAN par l'intermédiaire des centres de distribution nationaux indiqués ci-dessous. Des exemplaires supplémentaires peuvent parfois être obtenus auprès de ces centres (à l'exception des Etats-Unis). Si vous souhaitez recevoir toutes les publications de l'AGARD, ou simplement celles qui concernent certains Panels, vous pouvez demander à être inclu sur la liste d'envoi de l'un de ces centres. Les publications de l'AGARD sont en vente auprès des agences indiquées ci-dessous, sous forme de photocopie ou de microfiche.

CENTRES DE DIFFUSION NATIONAUX

ALLEMAGNE
Fachinformationszentrum Karlsruhe
D-76344 Eggenstein-Leopoldshafen 2

BELGIQUE
Coordonnateur AGARD-VSL
Etat-major de la Force aérienne
Quartier Reine Elisabeth
Rue d'Evere, 1140 Bruxelles

CANADA
Directeur - Gestion de l'information
(Recherche et développement) - DRDGI 3
Ministère de la Défense nationale
Ottawa, Ontario K1A 0K2

DANEMARK
Danish Defence Research Establishment
Ryvangs Allé 1
P.O. Box 2715
DK-2100 Copenhagen Ø

ESPAGNE
INTA (AGARD Publications)
Carretera de Torrejón a Ajalvir, Pk.4
28850 Torrejón de Ardoz - Madrid

ETATS-UNIS
NASA Center for AeroSpace Information (CASI)
800 Elkridge Landing Road
Linthicum Heights, MD 21090-2934

FRANCE
O.N.E.R.A. (Direction)
29, Avenue de la Division Leclerc
92322 Châtillon Cedex

GRECE
Hellenic Air Force
Air War College
Scientific and Technical Library
Dekelia Air Force Base
Dekelia, Athens TGA 1010

ISLANDE
Director of Aviation
c/o Flugrad
Reykjavik

ITALIE
Aeronautica Militare
Ufficio del Delegato Nazionale all'AGARD
Aeroporto Pratica di Mare
00040 Pomezia (Roma)

LUXEMBOURG
Voir Belgique

NORVEGE
Norwegian Defence Research Establishment
Attn: Biblioteket
P.O. Box 25
N-2007 Kjeller

PAYS-BAS
Netherlands Delegation to AGARD
National Aerospace Laboratory NLR
P.O. Box 90502
1006 BM Amsterdam

PORTUGAL
Estado Maior da Força Aérea
SDFA - Centro de Documentação
Alfragide
2700 Amadora

ROYAUME-UNI
Defence Research Information Centre
Kentigern House
65 Brown Street
Glasgow G2 8EX

TURQUIE
Millî Savunma Başkanliği (MSB)
ARGE Dairesi Başkanliği (MSB)
06650 Bakanliklar-Ankara

Le centre de distribution national des Etats-Unis ne détient PAS de stocks des publications de l'AGARD.

D'éventuelles demandes de photocopies doivent être formulées directement auprès du NASA Center for AeroSpace Information (CASI) à l'adresse ci-dessous. Toute notification de changement d'adresse doit être fait également auprès de CASI.

AGENCES DE VENTE

NASA Center for AeroSpace Information
(CASI)
800 Elkridge Landing Road
Linthicum Heights, MD 21090-2934
Etats-Unis

The British Library
Document Supply Division
Boston Spa, Wetherby
West Yorkshire LS23 7BQ
Royaume-Uni

Les demandes de microfiches ou de photocopies de documents AGARD (y compris les demandes faites auprès du CASI) doivent comporter la dénomination AGARD, ainsi que le numéro de série d'AGARD (par exemple AGARD-AG-315). Des informations analogues, telles que le titre et la date de publication sont souhaitables. Veuiller noter qu'il y a lieu de spécifier AGARD-R-nnn et AGARD-AR-nnn lors de la commande des rapports AGARD et des rapports consultatifs AGARD respectivement. Des références bibliographiques complètes ainsi que des résumés des publications AGARD figurent dans les journaux suivants:

Scientific and Technical Aerospace Reports (STAR)
publié par la NASA Scientific and Technical
Information Division
NASA Langley Research Center
Hampton, Virginia 23681-0001
Etats-Unis

Government Reports Announcements and Index (GRA&I)
publié par le National Technical Information Service
Springfield
Virginia 22161
Etats-Unis
(accessible également en mode interactif dans la base de
données bibliographiques en ligne du NTIS, et sur CD-ROM)

Imprimé par le Groupe Communication Canada Inc.
(membre de la Corporation St-Joseph)
45, boul. Sacré-Cœur, Hull (Québec), Canada K1A 0S7

AGARD

NATO OTAN

7 RUE ANCELLE • 92200 NEUILLY-SUR-SEINE

FRANCE

Telefax 0(1)55.61.22.99 • Telex 610 176

DISTRIBUTION OF UNCLASSIFIED

AGARD PUBLICATIONS

AGARD holds limited quantities of the publications that accompanied Lecture Series and Special Courses held in 1993 or later, and of AGARDographs and Working Group reports published from 1993 onward. For details, write or send a telefax to the address given above. *Please do not telephone.*

AGARD does not hold stocks of publications that accompanied earlier Lecture Series or Courses or of any other publications. Initial distribution of all AGARD publications is made to NATO nations through the National Distribution Centres listed below. Further copies are sometimes available from these centres (except in the United States). If you have a need to receive all AGARD publications, or just those relating to one or more specific AGARD Panels, they may be willing to include you (or your organisation) on their distribution list. AGARD publications may be purchased from the Sales Agencies listed below, in photocopy or microfiche form.

NATIONAL DISTRIBUTION CENTRES

BELGIUM
Coordonnateur AGARD — VSL
Etat-major de la Force aérienne
Quartier Reine Elisabeth
Rue d'Evere, 1140 Bruxelles

CANADA
Director Research & Development
Information Management - DRDIM 3
Dept of National Defence
Ottawa, Ontario K1A 0K2

DENMARK
Danish Defence Research Establishment
Ryvangs Allé 1
P.O. Box 2715
DK-2100 Copenhagen Ø

FRANCE
O.N.E.R.A. (Direction)
29 Avenue de la Division Leclerc
92322 Châtillon Cedex

GERMANY
Fachinformationszentrum Karlsruhe
D-76344 Eggenstein-Leopoldshafen 2

GREECE
Hellenic Air Force
Air War College
Scientific and Technical Library
Dekelia Air Force Base
Dekelia, Athens TGA 1010

ICELAND
Director of Aviation
c/o Flugrad
Reykjavik

ITALY
Aeronautica Militare
Ufficio del Delegato Nazionale all'AGARD
Aeroporto Pratica di Mare
00040 Pomezia (Roma)

LUXEMBOURG
See Belgium

NETHERLANDS
Netherlands Delegation to AGARD
National Aerospace Laboratory, NLR
P.O. Box 90502
1006 BM Amsterdam

NORWAY
Norwegian Defence Research Establishment
Attn: Biblioteket
P.O. Box 25
N-2007 Kjeller

PORTUGAL
Estado Maior da Força Aérea
SDFA - Centro de Documentação
Alfragide
2700 Amadora

SPAIN
INTA (AGARD Publications)
Carretera de Torrejón a Ajalvir, Pk.4
28850 Torrejón de Ardoz - Madrid

TURKEY
Millî Savunma Başkanliği (MSB)
ARGE Dairesi Başkanliği (MSB)
06650 Bakanliklar-Ankara

UNITED KINGDOM
Defence Research Information Centre
Kentigern House
65 Brown Street
Glasgow G2 8EX

UNITED STATES
NASA Center for AeroSpace Information (CASI)
800 Elkridge Landing Road
Linthicum Heights, MD 21090-2934

The United States National Distribution Centre does NOT hold stocks of AGARD publications.
Applications for copies should be made direct to the NASA Center for AeroSpace Information (CASI) at the address below. Change of address requests should also go to CASI.

SALES AGENCIES

NASA Center for AeroSpace Information
(CASI)
800 Elkridge Landing Road
Linthicum Heights, MD 21090-2934
United States

The British Library
Document Supply Centre
Boston Spa, Wetherby
West Yorkshire LS23 7BQ
United Kingdom

Requests for microfiches or photocopies of AGARD documents (including requests to CASI) should include the word 'AGARD' and the AGARD serial number (for example AGARD-AG-315). Collateral information such as title and publication date is desirable. Note that AGARD Reports and Advisory Reports should be specified as AGARD-R-nnn and AGARD-AR-nnn, respectively. Full bibliographical references and abstracts of AGARD publications are given in the following journals:

Scientific and Technical Aerospace Reports (STAR)
published by NASA Scientific and Technical
Information Division
NASA Langley Research Center
Hampton, Virginia 23681-0001
United States

Government Reports Announcements and Index (GRA&I)
published by the National Technical Information Service
Springfield
Virginia 22161
United States
(also available online in the NTIS Bibliographic
Database or on CD-ROM)



Printed by Canada Communication Group Inc.
(A St. Joseph Corporation Company)
45 Sacré-Cœur Blvd., Hull (Québec), Canada K1A 0S7

ISBN 92-836-0036-3